MECHANICAL FAILURE OF BONE AND ANTLER:

THE ACCUMULATION OF DAMAGE

Volume one, of two volumes

Andrew James Sedman

Thesis submitted for the degree of Doctor of Philosophy
Department of Biology, University of York
September 1993

degree awarded June 1994.

THESIS CONTAINS

VIDEO

ABSTRACT

Many aspects of bone's tensile loading response are well documented. However, the processes that cause this response are poorly understood. The nomenclature commonly used to describe this response includes the terms *elastic*, *plastic*, *yield* and *Young's modulus*. This nomenclature implies that bone is considered to be an elastic-plastic material, and that the knee in the loading curve is due to yielding. In many published studies of its time-dependent mechanical behaviour bone is viewed as a viscoelastic material. However, a few workers have attributed the creep and failure of bone to another process: damage accumulation. This thesis extends this latter approach.

To gain a better understanding of bone's mechanical behaviour and the associated processes, a comparative study has been conducted. Two bones with different mechanical responses were used: bovine bone (mostly femoral) and antler (from red deer and reindeer). Only tentative suggestions of the cause of this difference are found in the literature. The results of impact, tension, creep and notch sensitivity tests on these materials are described. In some cases the rate-dependence of these results is examined. During many of these tests optical changes that are indicative of damage were observed and recorded. It is concluded that damage accumulation is the main controlling process of the mechanical behaviour for both materials. Anelasticity and fracture also contribute to the mechanical response. The relative importance of these three processes depends on a number of factors, those considered are: the material in question, the aspect of the response examined, and the loading rate. The difference between the mechanical response of bovine bone and that of antler is attributed to the different rates at which these materials accumulate damage. It is concluded that bone fails by a *damage related fracture* process, and antler by a *damage coalescence process*.

That the Theory of Physic has been much improved, and many truths discovered by the industry of the Moderns, of which the Ancients were intirely ignorant, is a position nobody, I believe, will dispute. But that a great many more relating to every branch of this useful Art lie still buried in obscurity, is equally certain. And what is yet more to be lamented than real ignorance itself, is, false maxims and positions are many times introduced as facts, and assumed as Data, whereon to build future inquiries. Anatomy itself, tho' it has been more cultivated, and received greater improvements, than any other branch, as lying most obvious to our senses, is not free from this error, no not even the largest vessels; what then shall we think of such as are more remote?

The fatal spring from whence most of the errors in the Theoretical part of physic have flowed, is, the deducing general conclusions from a few particular Experiments, and on this foundation erecting some pompous plausible Hypothesis, which like Descartes's Vortices may indeed shew how the one would have framed the Universe, and the other the Animal body; but give us very little light into the real structure of either.

This can only be obtained by a laborious search, and the strictest examination imaginable, and that too by a vast variety of Experiments; as any one may be convinced by the few methods of trial here made use of, wherein only the different Densities, Strengths and Thicknesses of some few of the Solids are considered; but much more so, if he will give himself the trouble of such a variety of Experiments, as are requisite fully to illustrate any branch of this complicated Machine, or thoroughly explain any one particular Secretion; wherein it is impossible to advance one step without error, unless we be supported by undeniable matters of Fact.

Wintringham, C. (1740)

An Experimental Inquiry on some parts of the Animal Structure

TABLE OF CONTENTS

Volume I

LIST OF ACCOMPANYING MATERIAL

This thesis is comprised of two volumes and a VHS video tape, of about 7 minutes in duration. This video formed part of a paper presented at the Eighth Meeting of the European Society of Biomechanics. A description of the video images is given in appendix 11.

AUTHOR'S DECLARATION

Some of the material within this thesis was presented at the Eighth meeting of the European Society of Biomechanics, June 21-24, Rome, Italy. This material is given in appendix 11 and on the accompanying video tape. A short abstract of this presentation has now been published (Sedman *et al.* 1993). I would like to declare my co-authorship with John Currey and Marianne Mauch of the paper presented in appendix 6. This paper is reviewed within this thesis. However, the experiments and results on which the paper is based are not presented as part of this thesis. This is because the experimental work was conducted by Marianne Mauch.

ACKNOWLEDGEMENTS

I would like to express my gratitude to the people who, through their encouragement or direct assistance, have enabled me to complete this thesis. To describe their contributions I shall use the analogy of a juggling act, with myself as the performer and this thesis as the act; an act composed of various tricks or experiments.

I am indebted to Professor John Currey for giving me the opportunity to perform my various routines. I also thank him for his help and guidance in improving the individual tricks, while subtly directing the whole act, and helping me to polish-up this public performance of it. (The rough edges that remain are a result of my lack of practice.) I am grateful to those who supplied the skittles and balls (or the antler and bone), especially Dick Youngson[1] and Batters Butchers. This performance would be far poorer without the props (or equipment) produced with the assistance of John Hoggarth and Les Turner of the mechanical workshop, and Brian Adamson and Tom Broxup of the electrical workshop.[2] I am also grateful to Pete Goodyer of SERC for the loan of a whole bag of tricks (the high speed video equipment), and to John Aldworth,[3] for editing the video that accompanies this thesis. A large section of this performance was inspired by Dr Peter Purslow,[4] who kindly showed me the details of a trick he devised. Thanks also go to Dave Coulthard,[5] for his efficient and enthusiastic assistance when I wanted to try a new routine (the detection of damage cracks by using X-rays).

I appreciate of the support given by the other members of this laboratory and department: Peter, Richard, Peggy, Julie, Kevin, Roland, Paul, Amy, Marianne, - the list is almost endless. Their comments have been invaluable; when juggling, it is sometimes difficult to appreciate what the performance looks like. They have also made the whole performance an enjoyable event. Special thanks go to Anne who has so generously tolerated my endless hours of practice, and has helped me pick up the skittles when I dropped them.

Juggling is not possible without first learning to catch, for which I thank all my previous teachers in Lymington, Brockenhurst and at the Universities of Reading and Strathclyde. I am also most grateful to my family who have given me a great deal of encouragement throughout all of my formal education. I thank the Science and Engineering Research Council for funding my research - throwing some coins in my cap.

---

[1]Red Deer Commission, Inverness.
[2]Department of Biology, University of York.
[3]Audio-visual unit, University of York.
[4]Muscle and Collagen Research Group, University of Bristol.
[5]Department of Physics, University of York.

1

THE FUNCTION, GROWTH, STRUCTURE AND MECHANICAL PROPERTIES OF BONE AND ANTLER

The engineering designer requires the device he is creating to meet certain design criteria and be manufactured at the lowest possible cost. He therefore wants to select those materials that will best meet these requirements.

Felbeck, D. K. and Atkins, A. G. (1984)
Strength and Fracture of Engineering Solids.

1.1. INTRODUCTION

An investigation of the function, growth and structure of bone and antler is not the main aim of this thesis. However, the mechanical response and ultimate failure of bovine bone and antler are not independent of these factors. When such biological materials are examined we must recognise that 'nature' has to balance the costs and benefits of a structure in a similar way to the engineering or industrial designer. In the case of bone this design process can be divided into at least two levels: that of the individual (short term modifications) and that of the species (evolution).

At the individual level the design (or the interrelationship of function and structure) of bones is in constant flux. Such changes are often referred to as *functional adaptation*. The ability of an individual's bones to remodel or change their size, shape and structure according to the mechanical demands placed on them is often summarised by reference to 'Wolff's law'. However, as Roesler (1987) says in his historical review of bone biomechanics, Wolff's (1892) monograph is 'often quoted, hardly read'. Roesler's paper continues with a critical evaluation of the impact of Wolff's work. Here it is adequate to say that bone will grow where increased strength is required and it can be resorbed in regions where it is not required.

Evolutionary pressures drive the long term development of a biological material or structure (such as an antler) throughout the history of a species. The direction of this development is not towards some ultimate goal, but is in response to what was cost effective in previous generations. I will leave a thorough consideration of the evolution of bone and antler to others. I will simply introduce the materials, so the mechanical test results described below may be viewed in the context of the natural material and the original structure from which it came. However, to justify a comparative study of the mechanical properties of these materials the antler specimens were not tested in their physiological state. Thus extrapolation to the natural state should consider this fact.

There is a considerable body of published literature on the function, growth and structure of bone. Much of this literature concerns human bone. In this chapter I concentrate on the accounts relating to bovine bone, especially femora. (The majority of bovine bone specimens used in this thesis were obtained from femoral bone, the remainder from tibiae.) For the same reason when discussing antler, I draw more heavily from published works on red deer and reindeer than works on other species.

After introducing the function, growth and structure of bone and antler, I give some mechanical test results. These test results show that there is a considerable difference between the mechanical response of the two materials, reflecting their

different functions. I then summarise some of the factors that can affect the results obtained from mechanical tests of these materials.

1.2. THE FUNCTION, GROWTH AND STRUCTURE OF BONES

In the conclusion to his paper *What is bone for? Property-Function relationships in Bone*, Currey (1981) entreats those working on bone to adopt a particular train of thought

> First, to think, always, what bones are for. Second, to assume, unless the facts ineluctably forbid it, that natural selection has produced the best possible compromise between the various pressures acting on the design, whether these pressures be of metabolic cost, conflicting mechanical requirements, physiological function or the mob of other factors that may be of great, or little, importance.

In the first part of this section I consider what bones are for, concentrating on their mechanical function. In section 1.4 I show that the mechanical properties of bone are those expected for a material that aims to fulfil these mechanical functions.

1.2.1. THE FUNCTION OF BONES

Currey (1981) points out that the mechanical properties of skeletal materials must be a compromise between competing functions. The basic functions fulfilled by, and associated with, the skeletal system have been listed by Tortora and Anagnostakos (1987) as;

a) Support: the skeletal system is the framework formed by bones, which provides support for, and spatial organisation of, the soft tissues.

b) Protection: the skeletal system helps to protect the internal organs from mechanical damage. An obvious example is the cranial bones.[1] Some bones combine the job of protection with other functions, such as the ribs that protect the heart and lungs but also play an important role in respiration.

c) Movement: bones act like levers, converting the contraction of muscles into usable movement. With the addition of ligaments, for example the anterior and posterior cruciate ligaments of the knee joint, they also enable this motion to be repeatable and stable.

d) Mineral storage: bones are a repository of several minerals, principally calcium and phosphorous; when required these minerals are distributed to other parts of the body.

---

[1]These take the form of a sandwich construction, of dense outer shells and a foam like core. Their structure and properties are examined by Wood (1970 and 1971).

An example of this is antler growth, which (as noted below) demands considerable amounts of minerals. Goss (1983) reports that during antler growth 'there is an increase in the rate of turnover in skeletal elements'. The minerals obtained from the diet are deposited in the body's skeleton before being resorbed and redeposited in the growing antler.

e) Blood Cell Production: red marrow within the main cavities of certain bones is capable of producing red blood cells, some white blood cells, and platelets. Red marrow consists of blood cells in immature stages, fat cells, and macrophages.

In this thesis it is the response of bone (and antler) to mechanical loading that is of primary importance. Thus some of the other functions of bone may appear irrelevant. The production of blood cells has no obvious bearing on the mechanical properties, apart from the requirement of connecting spaces between the medullary cavity and the external tissues. Compliance with this requirement affects the structure of the bone as a whole. However, the functions are interrelated, for example the mineral storage function can be viewed as a result of the mechanical requirements, but it also has an important role in homeostasis.

In his book *The Mechanical Adaptations of Bone*, Currey (1984a) points out that the ability of bones to fulfil their mechanical functions requires them 'to be stiff enough; and not to break under either static or dynamic loading'. If it is too flexible, a bone will not act as an efficient lever, or as an adequate supporting structure. Three factors determine the deformation of a loaded structure: the stiffness of the material, the shape of the structure and the load placed on it. This is an area where metabolic cost and mechanical requirements interact.

1.2.2. THE MACROSTRUCTURE OF BONES

Bones are generally classified by their overall shape. There are *flat bones* that have two fairly thin plates of *compact*, or dense bone, normally separated by a foam like construction of bone, referred to as *cancellous* bone. There are bones that are more cubic in shape, *short bones*, such as the carpals and tarsals. Bones like the femora used in this work, and the other main limb bones, are described as *long bones*.

A long bone, essentially consists of a closed tube that has an articulating surface at both ends. The surface of the tube wall may possess other processes, or surface irregularities, due to muscle, or other connective tissue insertion points. The articulating surfaces are covered in cartilage, and beneath this there is a thin shell of compact bone. The joint forces are transmitted through this shell to the underlying cancellous bone,

which distributes the load. The widened ends of the bone are called the *epiphyses*. As the distance from the articulating surface increases, the density of the cancellous bone structure decreases. Simultaneously the shell thickness increases until a reasonably thick walled tube is obtained (figure 1.001b). This central region of the bone is referred to as the *diaphysis*. The surfaces of the diaphysis are covered in a fibrous and osteogenic layer: the internal one is called the *endosteum* and the outer the *periosteum*. (Diagrams are provided later, and some relevant photos are given in appendix 2, which describes the preparation of specimens.)

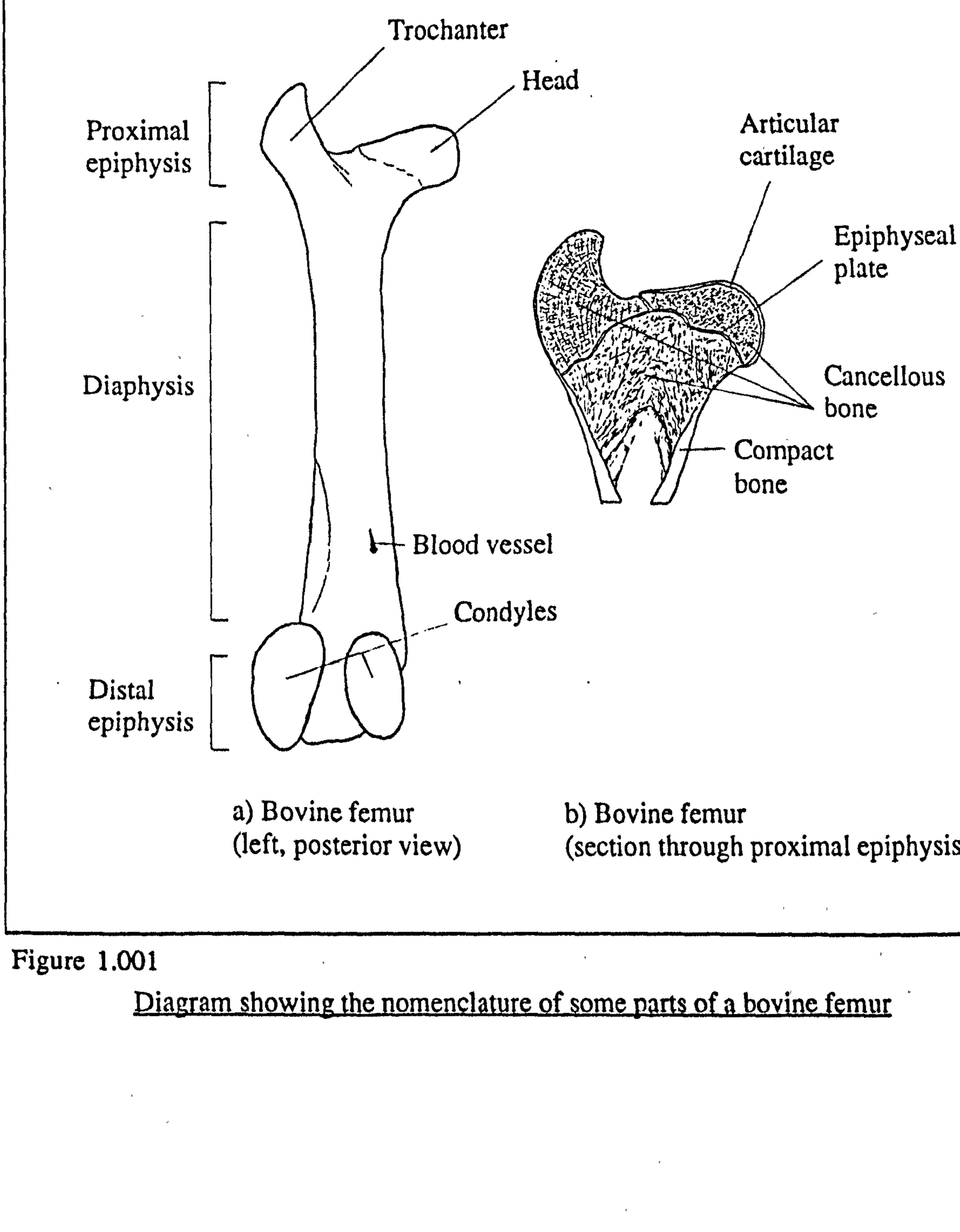

a) Bovine femur (left, posterior view)

b) Bovine femur (section through proximal epiphysis)

Figure 1.001

Diagram showing the nomenclature of some parts of a bovine femur

1.2.3. THE GROWTH AND DEVELOPMENT OF LONG BONES

A mammalian embryo possesses a precursor (or template) skeleton, composed of fibrous membranes and hyaline cartilage. These are similar in shape to bones and provide the medium for ossification. Ossification begins at a relatively early stage of embryonic life (at around the sixth or seventh week in the case of humans). Throughout life there is a constant process of construction, removal and replacement of bone, referred to as *remodelling*. Un-remodelled bone is referred to as *primary bone*, and that due to remodelling as *secondary bone*. Two types of ossification that form primary bone, *intramembranous* and *intracartilaginous* ossification, are described below.

1.2.3.1. INTRAMEMBRANOUS OSSIFICATION

Intramembranous ossification is the formation process of bones such as the surface skull bones and the clavicles. Osteoblasts group together in the fibrous membrane that makes up the template skeleton of the embryo, forming a so-called *centre of ossification*. The osteoblasts secrete intercellular substances, including collagenous fibres that quickly form a framework, in which calcium salts are deposited. When a cluster of osteoblasts is surrounded by the calcified matrix, it is called a *trabecula*. As other adjoining clusters also form trabeculae, they fuse to produce the open lattice, or foam like, structure that is characteristic of cancellous bone. As successive layers of bone are laid down some osteoblasts become entombed in small almond shaped cavities, or *lacunae*. These entombed cells lose their ability to form bone and are called *osteocytes*. The original connective tissue that surrounds the growing mass of bone then becomes known as the *periosteum*. The external surfaces of the cancellous bone are reconstructed into compact bone. This whole bone is continuously remodelled to meet the demands placed upon it.

1.2.3.2. INTRACARTILAGINOUS OSSIFICATION

Intracartilaginous, or endochondral, ossification is characteristic of the development of long bones. Early in embryonic life, a miniature cartilage template of the future bone is produced. This is covered in a membrane called the *perichondrium*. As the embryo develops, a blood vessel penetrates the perichondrium, midway along the shaft of the template. This stimulates the cells in the internal layer of the perichondrium to enlarge and form osteoblasts. Thus a ring of compact bone is formed in this region. Therefore the perichondrium is henceforth referred to as *periosteum*. The cartilage in the centre of the diaphysis also changes with the penetration of the blood vessel. The cells

hypertrophy and burst, increasing the alkalinity of the extracellular substance. According to Tortora and Anagnostakos (1987) this causes mineral deposition, or calcification. This calcification forms a barrier to the nutrients needed by the cartilage cells, which consequently die. With the degradation of the intercellular substance, large cavities form in the central core of the cartilage template, permitting the growth of blood vessels within the structure. Thus the process extends over a greater length of the bone. The central voids unite to form the medullary cavity. During this process the periosteum deposits more layers of bone, thickening the walls of the structure, and the cartilage template continues to grow, thus increasing the prospective bone's length.

Near the end of this ossification process, the blood vessels enter the epiphyses, and secondary ossification centres appear: these lay down cancellous bone.[2] After the two secondary ossification centres have formed, bone tissue completely replaces cartilage, except for two regions: the articulating surfaces and the *epiphyseal plate*, which lies between the epiphysis and the diaphysis. Epiphyseal plates are zones of active bone growth, which remain cartilaginous until the adult size is reached, whereupon they also ossify.

1.2.3.3. WOVEN AND LAMELLAR BONE

Currey *et al.* (1981) state that mammalian bone comes in two basic types.[3] First, *woven bone*, in which the direction of the collagen fibrils is random over distances of more than 1 μm or so, and where the apatite is not uniformly oriented along the line of the collagen fibrils. Woven bone is different from other forms of bone in one important aspect: it can be formed *de novo*. In contrast other types of bone can only be deposited on a pre-existing bone structure. The second type of bone is *lamellar bone*, in which the fibres are arranged in more regular layers, or lamellae, about 5 μm thick. Currey *et al.* say that the fibrils in any particular lamella are in small *domains*, typically 30 - 100 μm across. The orientation of the fibrils changes somewhat from domain to domain. However, nearly all the fibrils are oriented in the plane of the lamellae, with a preferred orientation within any one lamella.

Woven and lamellar bone may exist independently or in combined states to form more complex structures. In adults woven bone is associated with pathological skeletal processes. The most common example of this is callus formation following a fracture.

---

[2]In the human tibia, one secondary ossification centre develops in the proximal epiphysis soon after birth. The other, in the distal end, develops in the child's second year.
[3]The work by Currey *et al.* (1981) introduces the properties of bone (cartilage and synovial fluid). It is a mixture of secondary and primary source material. I do not include the primary references here.

The function of woven bone is primarily mechanical. It can rapidly provide temporary strengthening and a structure upon which lamellar bone may be deposited (Martin and Burr, 1989). Lamellar bone can be found in circular rings around the endosteal and periosteal circumference of a long bone. This lamellar bone can be very dense, having few vascular channels or other discontinuities.

1.2.3.4. PRIMARY BONE

Woven and lamellar bone may combine in a number of ways to produce more complex structures. Woven bone generally contains irregular shaped vascular spaces with osteoblasts on the surrounding bone surface. These osteoblasts deposit successive layers, lamellae, of new bone, and thus progressively diminish the calibre of the vascular spaces. The resulting structure is usually parallel to the long axis of the bone and is referred to as a *primary osteone.*

Another form of primary bone common to the femora of cattle is *laminar*, or plexiform, bone. This is constructed from a series of laminae between which there is an almost planer network of blood vessels, like a sandwich. In bovine femoral bone the laminae are about 0.18 mm thick (Currey, 1960). This construction is itself sandwiched between layers of woven bone. The demarcation between successive laminae is indicated by a layer of heavily calcified woven bone. This is the so-called bright line. The canaliculi of the osteocytes do not pass across this region, and thus nutrients have to be derived from the adjoining vascular network. (A description of the blood supply is given in Currey's (1960) paper.)

Remodelling of a bone's structure occurs during the whole of its life. This adaptation is achieved by the removal of old bone material. This removal is followed by the production of new bone, in the form of Haversian systems. It has been suggested (Currey, 1984a) that the introduction of these systems could reorientate the grain of the bone or possibly repair micro-cracks. This new bone is referred to as secondary bone.

1.2.3.5. SECONDARY BONE

Remodelling of the primary bone structure begins with osteoclastic erosion of bone around blood vessels. Osteoblasts on the surface of these cavities then deposit successive layers of new bone with an orderly fibre orientation. By this method the diameter of the cavity is reduced until it is the same size as the blood vessel that it contains. The whole structure, which is called a *Haversian system*, or secondary osteone,

is oriented with respect to the blood channels. Haversian systems are generally oriented in line with the long axis of a long bone. The outer limit of the Haversian system is marked by a cement line, a sheath of calcified mucopolysaccharide from which the collagen seems to be absent (Currey *et al.* 1981). The introduction of a Haversian system into laminar bone can disrupt the vascular supply to the surrounding bone. The resulting cell necrosis can initiate the production of more Haversian systems. Thus the process continues, the number of Haversian systems in a volume of bone increasing. The volumes of bone between secondary osteones are called *interstitial bone*. This consists of the remnants of the bone that previously occupied that region, whether woven, lamellar, primary osteones or even previous secondary osteones.

1.2.3.6. GROWTH, MATURATION AND REMODELLING OF BOVINE BONE

As an animal matures, a mechanism is required to permit growth of the skeleton without disrupting its function. Elongation of long bones occurs by the replacement of the diaphysis surface of the epiphyseal plate with bone. Simultaneously the epiphyseal plate grows on its epiphysis surface. Thus the distance between the epiphyseal plates increases. During this process the osteoblasts produced from the periosteum are also producing bone, thus further increasing the diameter of the bone shaft. The overall shape of the bone is maintained by the action of osteoclasts that erode redundant bone. Much of the original cancellous bone of the main section of the diaphysis is also resorbed. The region where this growth occurs is generally referred to as the *metaphysis*. Finally, when the bone has reached its definitive size, the animal has reached adulthood, generation of cartilage at the epiphyseal plate ceases, and what remains is replaced by bone. In this way the epiphysis finally fuses to the diaphysis. Thus inspection of these plates can be used as an indication of the maturity and structure of the bone. The specimens of bovine femoral bone used in this thesis (that were so examined) were obtained from bones in which the epiphyseal plate within the head of the femur had not fused (see appendix 2). Thus the bone examined in this thesis is probably laminar, rather than Haversian, bone.

Carter *et al.* (1976) describe the maturation of bovine compact bone.[4] They give a schematic representation of the maturation of bovine compact bone (adapted from Smith, 1960); this is redrawn in figure 1.002. They say that at birth a transverse section contains only woven-fibered bone and primary osteones (figure 1.002a). Rapid growth occurs by subperiosteal deposition of woven-fibered bone, in which primary osteones are rapidly incorporated (figure 1.002b). During a slower growth phase, circumferential

---

[4] They also examine human bone, attributing the structural differences between these materials to the faster maturation rate of the bovidae. Cows are fully grown in two years.

lamellar bone may form on the endosteal and periosteal aspects (figure 1.002c). When rapid growth is re-initiated, the endosteal surface bone is eroded to widen the medullary cavity. The periosteum, however, begins to form woven-fibered bone directly on the periosteal surface. In this manner one or more thin layers of circumferential lamellar bone may become trapped within the woven-fibered bone, which contains primary osteones (figure 1.002d). Secondary Haversian bone often first appears near the endosteal surface (figure 1.002e), but may be diffuse throughout the cortex. Remodelling continues through adult life and may eventually result in secondary Haversian bone across the whole section of the cortex. Circumferential lamellar bone may also be deposited on the periosteal and endosteal surfaces (figure 1.002f).

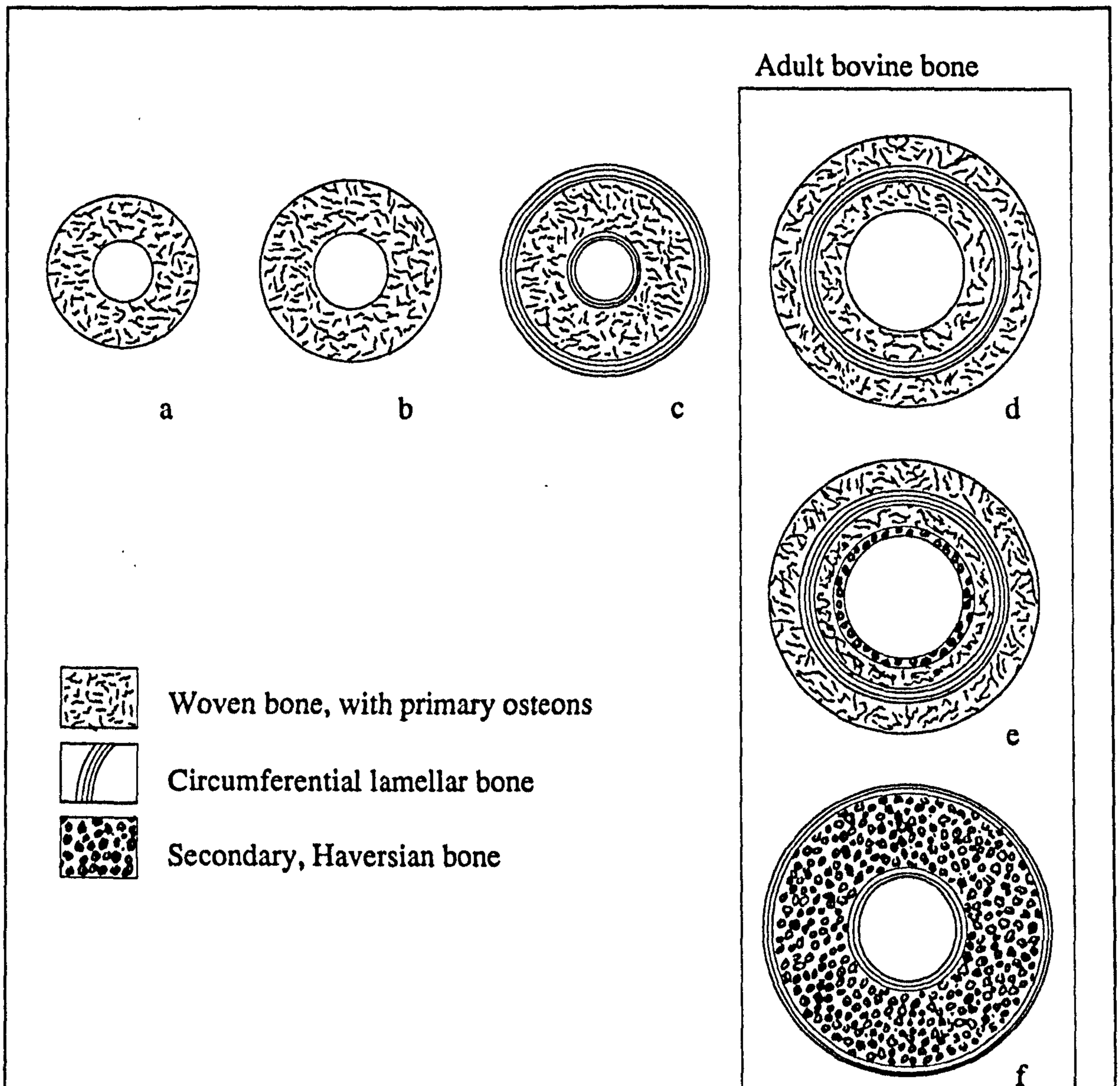

Figure 1.002 After Carter *et al.* (1976)

Schematic representation of the maturation of bovine compact bone

1.2.4. THE MICROSTRUCTURE OF COMPACT BONE

Most of the microstructural constituents of compact bone have been described in the above sections; there is no point in repeating their description here. However, some indication of the relationship of these structures is shown in figures 1.003 and 1.004, and some of their dimensions are given in table 1.001. When the sizes quoted in table 1.001 are examined, it is noticeable that the dimensions of the Haversian system are inconsistent. I consider this to be due to the different definitions used by the different workers. It appears that some workers have used what could be referred to as an internal diameter (canal) while others have used an external one (system). I suggest that the diameter given by Cartwright (1975) is an internal diameter and that given by Martin and Burr (1989) an external one. The values from Pope and Outwater are perhaps the best guide as they give three dimensions; 'the osteone [Haversian system] is about 20 mm long, 250 μ dia. and contains the Haversian canal which is about 70 μ in dia'.

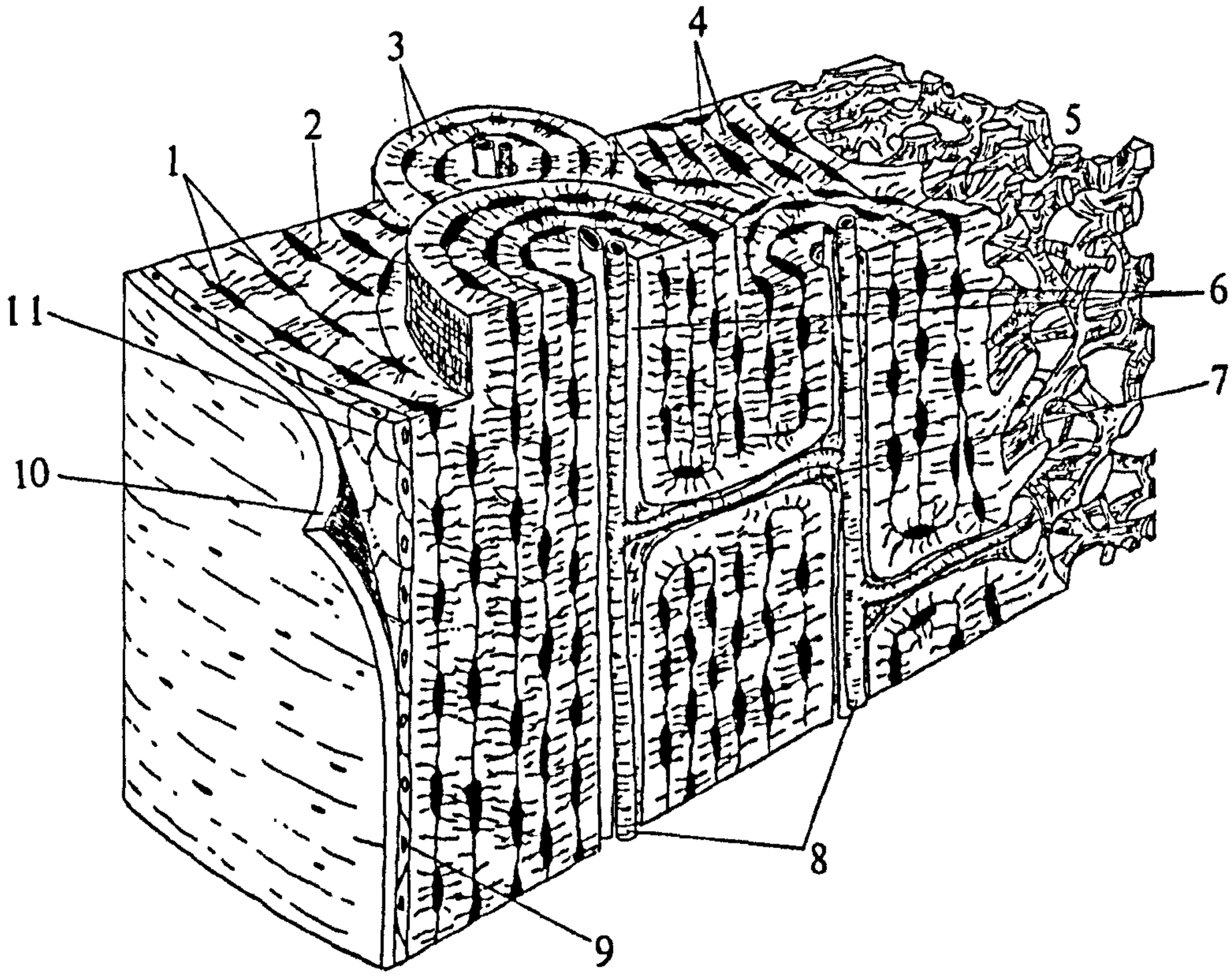

1) Osteocyte lacunae
2) Canaliculi
3) Concentric lamellae
4) Interstitial lamellae
5) Cancellous bone
6) Haversian canals
7) Volkmann's canal
8) Blood vessels
9) Osteoblast
10) Periosteum; outer fibrous layer
11) Periosteum; inner osteogenic layer

Figure 1.003 After Tortora and Anagnostakos (1987)

Representation of some of the structure within a normal mammalian long bone

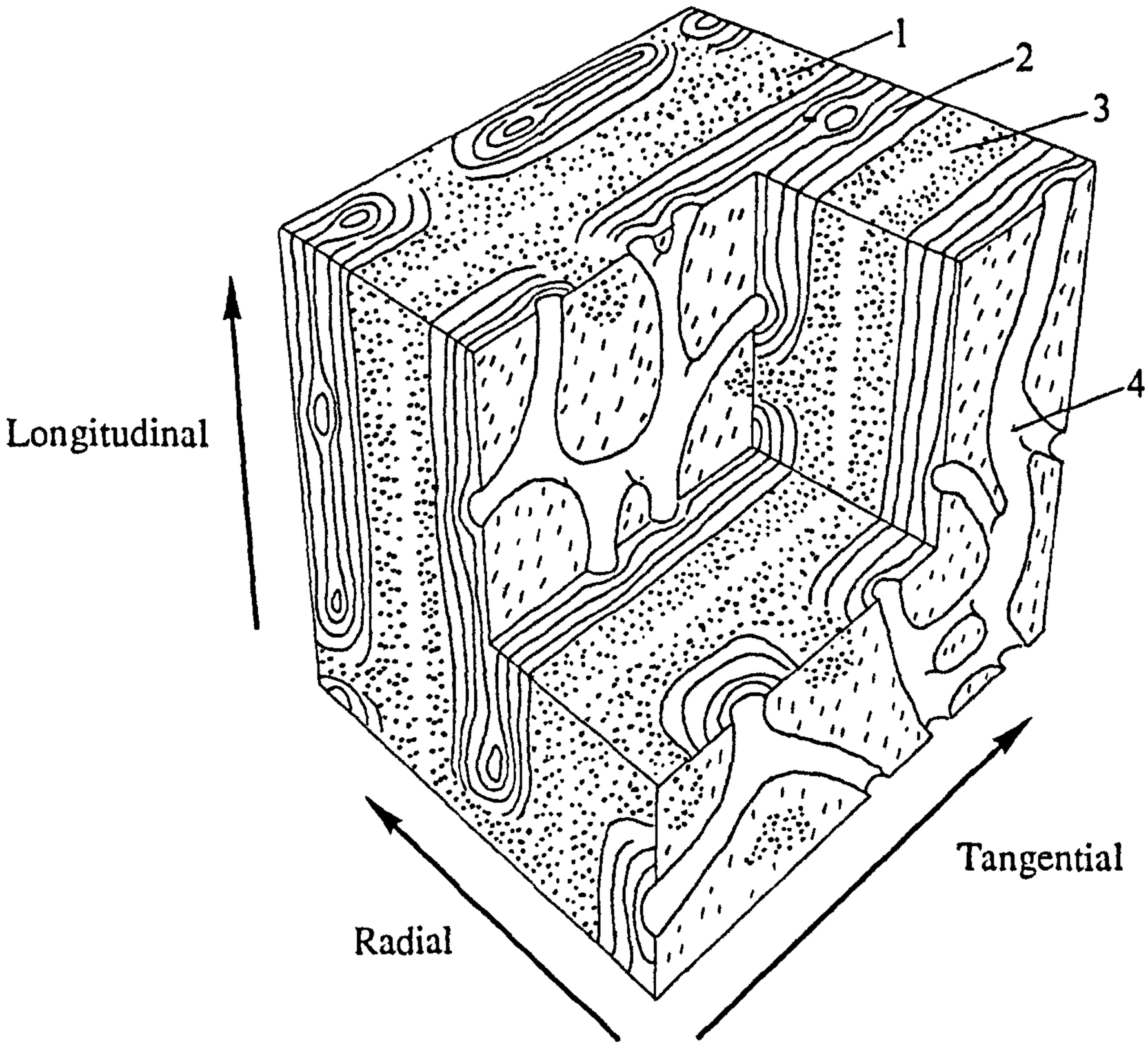

1) Woven bone
2) Lamellar bone
3) Bright line
4) Vascular network

Figure 1.004 After Currey (1960)

Diagram of section of laminar bone showing two laminae and the related vascular system

Bone Structure and Species	Measurement	Dimension	Reference
Whole bone, bovine femur	Overall length	0.4 m	This study (used to produce specimens in data set CB1)
Whole bone, bovine femur	Width at mid diaphysis	42 to 46 mm (not circular)	This study (used to produce specimens in data set CB1)
Mid diaphysis, bovine femur	Wall thickness	20 mm (not uniform)	This study (used to produce specimens in data set CB1)
Haversian canal, bovine tibia	Diameter	17±4 μm	Lees (1982)
Haversian canal, generic	Diameter	50-90 μm	Martin and Burr (1989)
Haversian system, Human	Diameter	up to 20 μm	Cartwright (1975)
Haversian system, generic	Diameter	200-300 μm	Martin and Burr (1989)
Haversian system ('osteone'), generic	Length	20 mm	Pope and Outwater (1972)
Haversian system ('osteone'), generic	Diameter	250 μm	Pope and Outwater (1972)
Haversian canal, generic	Diameter	70 μm	Pope and Outwater (1972)
Cement line, generic	Thickness	3-7 μm	Martin and Burr (1989)
Lamellae, generic	Thickness	3-7 μm	Martin and Burr (1989)
Lamina, generic	Thickness	200 μm	Currey (1984a)
Collagen fibres in woven bone	Diameter	0.1 μm	Currey (1984a)
Collagen bundles in lamellar bone	Diameter	2-3 μm	Currey (1984a)
Mineral crystal	Length	35-40 nm	Currey (1984a)

Table 1.001

Dimensions of various bone structures

1.2.5. THE ULTRASTRUCTURE OF COMPACT BONE

At the ultrastructural level, bones are basically a composite of three materials: an organic phase, a mineral phase and water. The organic material consists predominantly of collagen fibrils combined to form bundles. The inorganic material accounts for about 70% of the dry mass of bone, and about 60% for wet bone (Viano, 1986). The mineral is believed to be a crystalline calcium phosphate compound based on the structure of hydroxyapatite. However, it is not stoichimetric with respect to the pure material, $Ca_{10}(PO_4)_6 OH_2$. The departure from the pure material is mainly due to the substitution into the hydroxyapatite lattice of several types of ions. This affects the morphology of the crystals within the bone (Hodgskinson, 1991).

The amount of mineral present in a certain mass of bone depends on a number of factors. The data presented by Currey (1988a) shows that one very important factor is the species from which the bone was obtained. The anatomical position of the bone and the type of material from which it is constructed also affects the degree of mineralisation. The ratio of mineral to organic material is usually higher in lamellar bone than in woven bone (Currey *et al.* 1981). The amount of mineral contained within the bone affects its response to mechanical loading. This important aspect of mineral content is outlined below when the properties of bone and antler are examined.

A large amount of literature has been published on the way the organic and mineral components are combined and arranged to form such structures as Haversian systems. One such study on bovine bone was conducted by Green (1986). His thesis contains an examination of the orientation of the collagen fibres in Haversian systems of bovine tibial bone. Briefly, the experimental method he used was to polish a section of bone, then etch it with collagenase. The angles of the holes produced by removing the fibres were then measured relative to the axis of the Haversian system. Green found the same basic structure of alternating fibre directions in all the specimens he studied (figure 1.005). He noted that the angle of the more aligned lamellae to the axis, of about 20°, varied. The extreme cases of this variation were 8° and 35°. He says that it is reasonable to assume that the variation in the angles of the collagen fibres is in some way linked to the local mechanical environment. That Green obtained only one basic form of structure, when others are described in the literature could, he postulates, be explained by the fact that most of the previous work was conducted on human femoral bone.

One investigation into the distribution of the inorganic component of bone is contained within Turner's doctoral thesis (Turner, 1981). In which she says that the mineral is in a contiguous form. However, I do not know enough about the technique of ion etching which Turner used to prepare the bone specimens (for later examination by

scanning electron and transmission electron microscopy) to express an opinion on the significance or validity of this statement. Relevant to the present study are some comments from her summary:

> From the mechanical point of view the ultrastructural detail revealed does not contribute greatly to our understanding of the fracture mechanisms found in bone at the level of the microscopic elements. These seem to depend mainly on the local architecture of the bone which, as we have seen, can be very variable.

Therefore, I will finish this description of bone here. There appears to be no benefit, to this thesis, of examining the literature on the smaller scale features of bone.

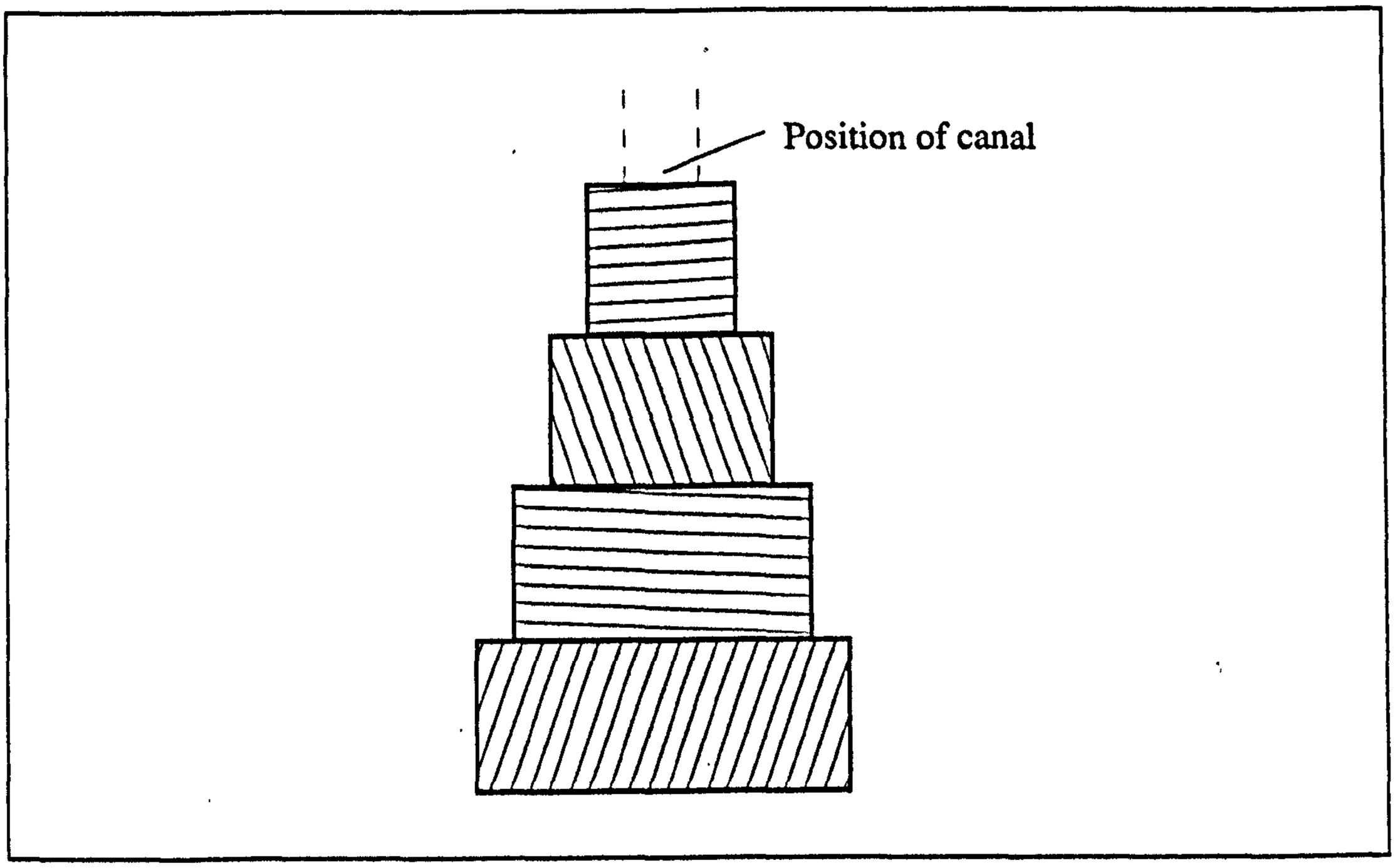

Figure 1.005 After Green (1986)

The orientation of the collagen fibres in bovine tibial Haversian systems (secondary osteones), as determined by Green (1986)

1.2.6. CLOSING REMARKS ON THE FUNCTION, GROWTH AND STRUCTURE OF BONE

In the preceding sections it has been suggested that the main mechanical function of bone is to be stiff. The process of bone growth was also outlined, as was the structure. One of the most interesting features of bone is that it is able to remodel itself, unlike engineering materials. This enables it to fulfil the changing demands placed upon it, or simply to repair damage. (It is possible to argue that this ability to repair damage reduces the safety factor required in the design of bones. If damaging events are far enough apart the cumulative effect of any damage will be reduced.) The design of whole bones and

the material from which they are made is determined by a large number of factors. It must not be assumed that the resulting material is the one that will best fulfil the mechanical functions. However, it is reasonable to assume that bone is the best compromise between these competing functions and the methods of manufacture available.

Bone and bones have been described as composite structures at each of the levels examined above. At the largest scale bones are a composite of solid and foam-like materials, compact and cancellous bone. At the finest scale bone is a composite of mineral crystals and organic fibres. This composite structure has led a number of workers, perhaps most notably Katz (1971, 1980a and 1981), to propose composite models to explain the properties of Haversian bone. The model is based on the assumption that bone can be considered as a fibre-reinforced composite, the Haversian systems being the fibres. The literature on composite models of bone has recently been reviewed by Bundy (1989). I do not examine these works here because I consider these models to be outside the study of this thesis.

1.3. THE FUNCTION GROWTH, AND STRUCTURE OF ANTLERS

Antlers should not be confused with horns. Horns are continually growing keratinous structures, whereas antlers are deciduous and made of bone. Antlers emanate from bony protuberances on the skull of the males in most species of deer. Antlers are, generally, considered to be a secondary male sexual characteristic. Reindeer are the only species of deer in which the female also produces antlers. Some of the smaller species of deer do not produce antlers: Chinese water deer and three species of musk deer.

All experiments, conducted on antler for this thesis, used the appendages of red deer *Cervus elaphus* and reindeer *Rangifer tarandus*. Therefore the following sections on the structure and function of antlers concentrate on those belonging to these two species.

1.3.1. THE FUNCTION OF ANTLERS

It is now accepted that antlers fulfil two main functions, both having the same aim. These functions are as display organs and, if necessary, weapons between males. The aim is to obtain dominance and thus access to females during the rut (Putman, 1988; Goss, 1983; Lincoln, 1992).

1.3.1.1. ANTLERS AS DISPLAY ORGANS

The use of antlers as display organs is one explanation for their size and complexity being greater than that required by structures used solely as weapons. There is some controversy over the view that as antlers evolved into more complex and larger structures, their function shifted from being simply a weapon to become a purely display organs (Putman, 1988). However, Currey (1979a) points out that if the antlers are only used for display, their mechanical properties are 'irrelevant - waterproof cardboard would suffice'.

The importance of antlers as display organs is demonstrated by their deterrent effect in prospective violent encounters. Clutton-Brock *et al.* (1979) describe the course of events that occur when a red deer stag challenges another that has a harem. When the challenging stag is within 200 to 300 m of the harem-holder the stags start to roar at each other. This roaring lasts for several minutes, after which the intruder usually withdraws. If this vocal contest proves insufficient to resolve the question of dominance, or if the challenging stag approaches his opponent, both deer will start a *parallel walk.* The stags pace along parallel paths, separated by five to ten meters, displaying the size of their antlers to each other. Frequently such displays are decisive enough to settle the challenge. In less decisive cases, either stag might invite combat by turning to face his opponent and lowering his antlers. This invitation is usually accepted, the opponent turns and animals lock antlers.

1.3.1.2. ANTLERS AS WEAPONS

The sharp tips of the antler tines are effective weapons capable of inflicting serious injury. However, the junctions between the tines and the main beam of the antlers form pivots that interlock with the opponent's antlers.[5] In red deer, once the antlers are locked together, the conflict takes the form of a vigorous pushing match, in which the stags attempt to twist the opponent off balance. The fight continues until one of the pair is pushed rapidly backwards. At which point this animal will break contact and attempt to escape without sustaining further injury.

Some idea of the forces to which the antlers are subjected when used as weapons can be formed when the size of the animals is considered. Clutton-Brock and Albon (1980) give mean values of shoulder high and antler length for a number of species. For red deer these were approximately 1.2 m and 0.9 m respectively, and for reindeer 1.2 m

---

[5]Bubernik (1983) reports that roe deer, which have simple spike type antlers, have been found with pierced skulls.

and 1.2 m. The body mass of male red deer increases throughout life until they no longer take part in the rut (Kitchener, 1991). Kitchener (1991) provides a plot that shows the changes in body mass with age (using data obtained from other sources). This plot indicates a body mass of more than 120 kg for a mature red deer stag. Lincoln (1992) provides a series of photographs that demonstrate the various stages of a combat between two red deer. These photographs give the impression that there is a considerable amount of violence involved in this fighting.

Goss (1983) points out (with reference to work by others), that antlers are in jeopardy of sustaining major damage and that analysis has confirmed they are designed to sustain considerable abuse. The success, in mechanical terms, of antlers as weapons can be assessed in terms of the failure rate of the structure itself. Henshaw (1971) estimates that less than 5% of shed antlers from caribou and moose exhibit evidence of any breakage. He continues 'in observations of approximately a quarter of a million cervids of nine species I have recorded only one instance of breakage to the main beam itself and only two of breakage to the palm'. This is an extraordinarily low occurrence of failure. However, Henshaw gives no details about these deer; were they all stags and was it a time of year when they might have been in combat? Even if this latter statistic is only reasonably accurate it still adds to the evidence that antlers, in the natural state are, as Currey (1979a) showed, superior to the 'waterproof cardboard' already mentioned above. Alexander (1982) reports that a study of red deer on the Isle of Rhum showed that the probability that a branch of a particular antler would be broken during a season was about 0.2. He points out that the failure of an antler is probably less costly than the failure of a leg bone (which, he estimated, has a probability of failure in a lifetime of 0.02).

1.3.2. THE MACROSTRUCTURE OF MATURE ANTLERS

The overall shape of a mature antler depends on a number of variables, primarily the species of deer. An obvious manifestation of this is the palmate antlers of moose or fallow deer compared with branching structure of red deer or reindeer antlers. Normally a set of antlers is symmetrical, or nearly so. Reindeer and caribou are the main exception to this, having a single palmate brow tine. Another determining factor of the size and complexity of the antler is the age, and condition of the deer. This complexity is not achieved by adding new material to a pre-existing antler, but by the complete removal, *casting*, of the old antler and the growth of a new structure in its place. Time series showing the overall size and shape changes of the antlers from a red deer, over a number of years, are given by Putman (1988) and Lincoln (1992). The antlers change from simple un-branching spikes in the stag's second year, to larger structures with a number of branches, or tines (see figure 1.006).

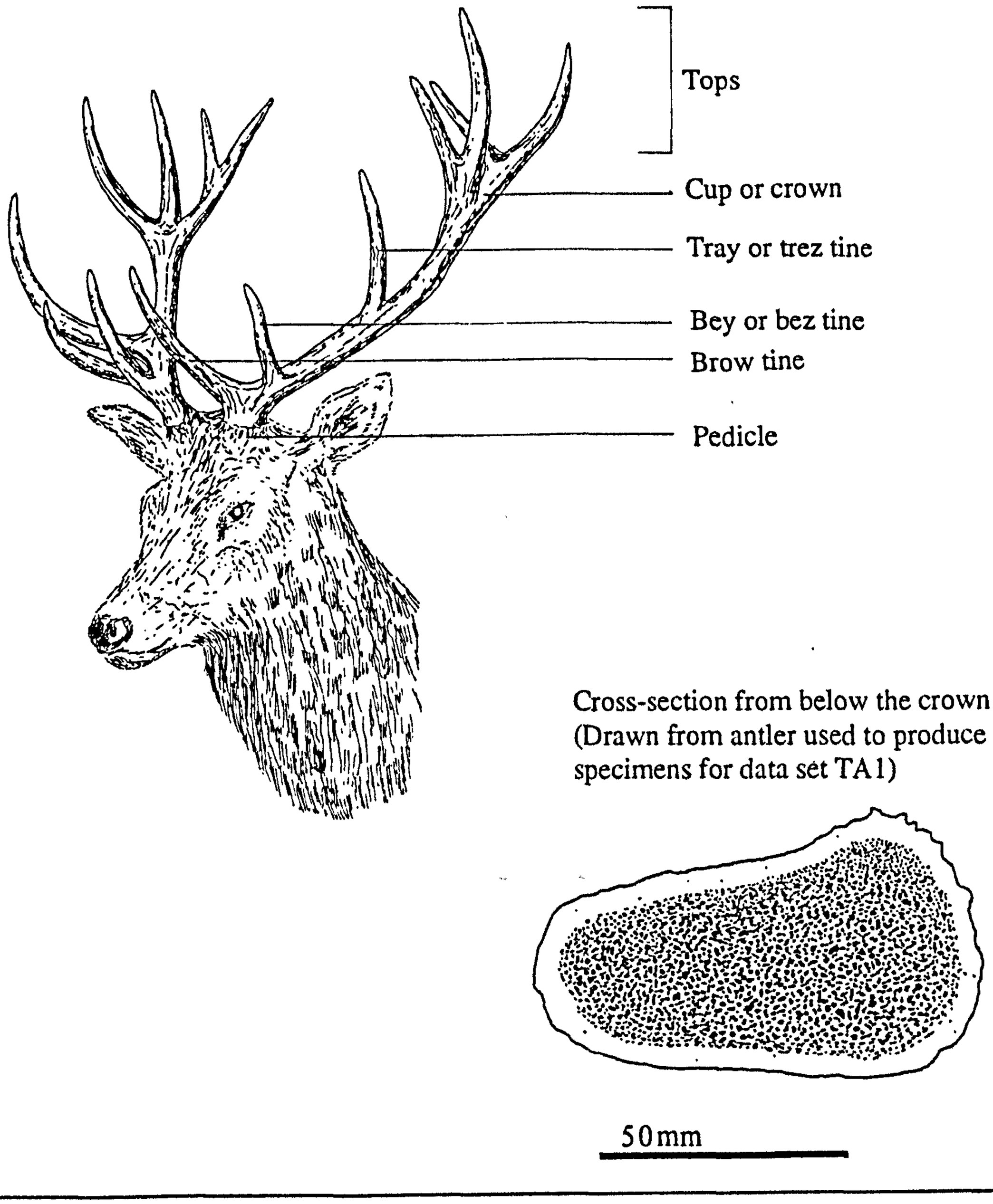

Figure 1.006 Figure 1.006a after Goss (1983) with some additions

Red deer antlers and the associated nomenclature

1.3.3. THE GROWTH AND DEVELOPMENT OF ANTLERS

One major work on the growth and development of antlers is that by Goss (1983).[6] As mentioned above, antlers are grown and cast annually by the males of most species of deer. During the period in which they are used for fighting the antlers are completely dead. Antlers grow and mature in about 100 days. Thus animals with large

---

[6]This is in the form of chapter 7 of his book *Deer Antlers: Regeneration Function and Evolution*, from which most of the information here comes.

antlers produce new tissue at a surprisingly high rate (see figure 1.007). It has been estimated that a bull moose will generate 417 g of antler tissue a day in June when his antlers are growing maximally (Van Ballenberghe, 1983).

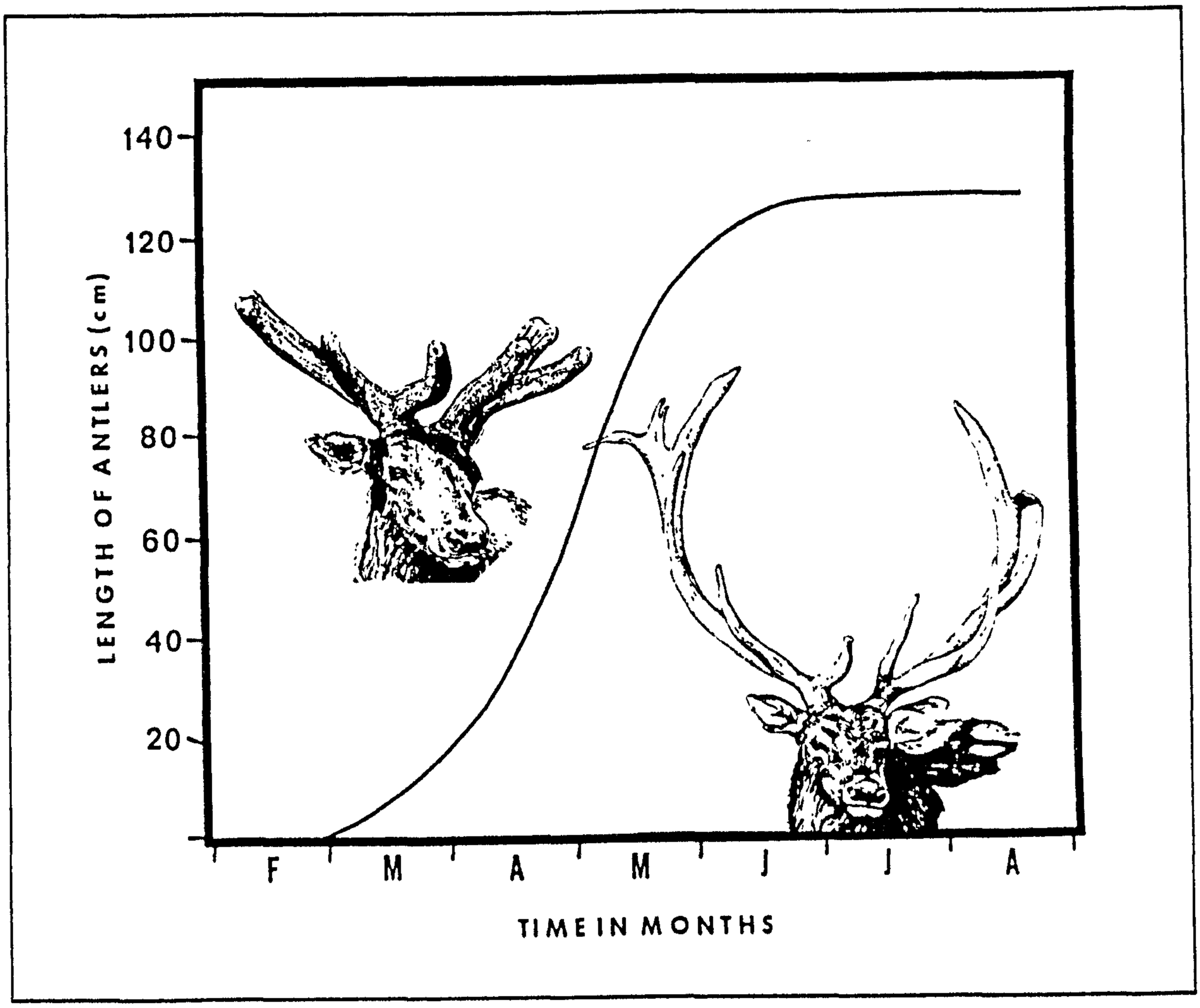

Figure 1.007 Reproduced from Goss (1983)

Antler growth of a wapiti (a North American relative of red deer)

The cycle of antler growth starts and ends with the antlers being cast and then the wound, thus produced, healing. The important features of this process will now be briefly described.

1.3.3.1. ANTLER GROWTH: WOUND HEALING AND VELVET

As soon as the old antlers are cast, skin migrates over the stump of the pedicle. A layer of epidermal cells is then formed between the scab and the underlying viable tissue (Goss 1983). Unlike wound healing in other regions of the body no scar tissue is formed, instead a bud, or blastema, is produced. The growing antler is covered in a richly vascularised and innervated type of hair covered skin known as velvet.

1.3.3.2. ANTLER GROWTH: ZONES OF DIFFERENTIATION

Goss (1983) says that during antler development there are persistent growth zones at the tips of the antler. Elongation continues for as long as the proliferation of cells at the apex surpasses the differentiation of these cells into the various components of the antler in the subapical region. (In some ways this is similar to the extension of long bones at the epiphyseal plate described above.) A longitudinal section through the growing antler reveals spatially the time course of events (figure 1.008). These events are continuous so their spatial representation is not discrete.

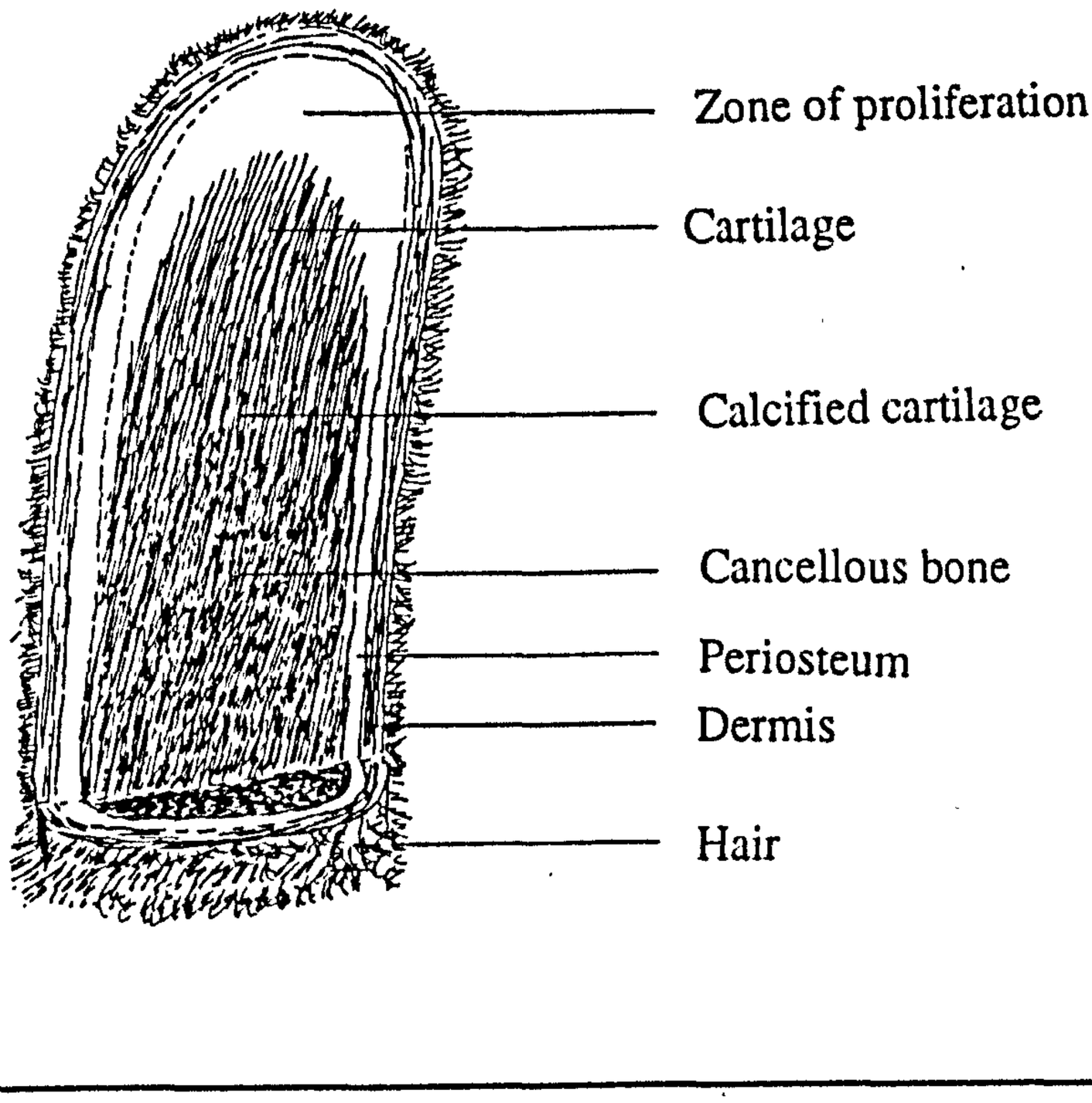

Figure 1.008 After Goss (1983)

Cross-section of a growing antler

Beneath the envelope of the epidermis and dermis lies a hyperplastic layer of perichondrium, few of whose cells show signs of differentiation. However the deeper (and thus older) cells are recognisable as chondroblasts (Goss, 1983). This layer of perichondrium is continuous peripherally with the more proximal periosteum that surrounds the shaft of the antler immediately inside the dermis of the velvet. (As in the description of normal mammalian bone formation, the nomenclature changes due to the change in the underlying material.) The perichondrium is rich in collagen fibres, some longitudinal and some circumferential. Goss also says this region is highly vascularised by the cascade of vessels that drain blood from the growing tip. The moving cap of

perichondrium produces a zone of cartilaginous trabeculae which as time passes becomes calcified, forming a type of cancellous bone in the central locations and more compact bone peripherally. Continuing ossification leads to the formation of increasingly solid bone in more proximal, older, regions. This operation moves distally along the antler as it elongates.

1.3.3.3. ANTLER GROWTH: OSSIFICATION

The method by which ossification occurs is not unanimously agreed, but Goss (1983) reports 'the current consensus favours endochondral [intracartilaginous] ossification as the dominant mechanism by which antler bone is formed'. The cartilaginous trabeculae, described above, become calcified and eroded by chondroclasts. Simultaneously, osteoblasts begin to lay down a bone matrix on the surface of the trabeculae remnants. It is by the appositional deposition of bone that ossified trabeculae are formed, replacing their cartilaginous precursors. The maturation of the antler occurs by the appositional ossification on the surfaces of these trabeculae. The thickening of the trabeculae gradually reduces the vascular spaces, thus reducing the blood flow, especially in the outer sections of the antler. The central core remains more porous, permitting some residual blood flow even after the velvet is shed. Eventually the outer sections of the antler becomes converted into almost solid bone, by which time the blood flow is fully shut off and the antler is totally dead.

When the growth of antler is considered, it is obvious that the stage of development of the region from which a specimen is obtained will affect its mechanical properties. All the antlers used in this thesis were free from velvet and thus assumed to be mature. Some of the antlers had been cast while others were sawn from culled animals.

1.3.3.4. ANTLER GROWTH: CONTROL OF THE GROWTH CYCLE

As secondary sex characteristics, the driving force behind the timing of the growth cycle is hormonal change. Like other animals native to the temperate zone, deer undergo annual cycle of fertility and sterility. A rising level of testosterone results in the slowing down of antler growth, an increase in ossification and eventually, the shedding of the velvet. After the rutting season the decrease in the production of testosterone is responsible for the casting of antlers, which occurs in early winter in many species. Male reindeer are notable in showing the shortest period in hard antler. This is associated with a very short rutting season and period of fertility (Lincoln, 1992).

1.3.4. THE MICROSTRUCTURE OF MATURE ANTLER

Some of the microstructural features of antler have been described above. The compact part of antler is composed of what Watkins (1987) refers to as 'osteate bone'. These osteones were reported by Rajaram and Ramanathan (1982) as being predominantly primary osteones. However they do report some difficulty in differentiating between primary and secondary osteones in some cases. In the limited number of observations I have made I did not recorded any osteones that are, indisputably, secondary. Contrary to this, Lees (1982) says that

> The extensive osteonal system is indicative of intensive remodeling when it is noted that the deer antler attains full growth within a few months and is discarded within a year.

Lees later states that

> The large Haversian canals may facilitate rapid remodeling to repair the microfracture in a bone without major blood vessels.

I find both of Lees comments to be questionable. First, the lack of observed secondary osteones implies a lack of remodelling. (Lees uses the term 'Haversian canals' in such a way that it is unclear if he referring to primary or secondary osteones.) Second, when the antler is living it is well supplied with blood, through the velvet and internal blood vessels. Moreover as the antler is not loaded while it is growing,[7] the occurrence of microfractures in the living structure would seem unlikely. When antlers are used in combat they are completely dead, and thus repair and remodelling is not possible. Therefore, this lack of secondary osteones could simply be because they are not required in this structure.[8] Rajaram and Ramanathan's finding is used by Martin and Burr (1989) as evidence to support the theory that the existence of primary osteones is directly related to body size and rapid growth.

1.3.5. THE ULTRASTRUCTURE OF MATURE ANTLER

The organisation of the fibres within the osteones and surrounding matrix of antler from several species of deer is described by Watkins (1987). He examined fracture surfaces and found that the angle of the fibres in the lamellae of the osteones was about 30 to 35° to the osteone axis. He also observed that the fibre orientation may alternate between neighbouring layers, but that this is not always so. The region between the

---

[7]Goss (1983) reports that when in velvet the antlers are very sensitive, touching them 'elicits a vigorous avoidance reaction on the part of the deer'.

[8]This could be tested by examination of antlers damaged during the velvet stage of development. Goss states that if during this stage an antler is cracked fracture healing follows. This may therefore stimulate remodelling in the form of Haversian systems.

osteones has circumferential fibres. He provides a model of these findings (figure 1.009), but he admits that this is an over-simplification as the fibre direction can, and does, change locally within a lamella.

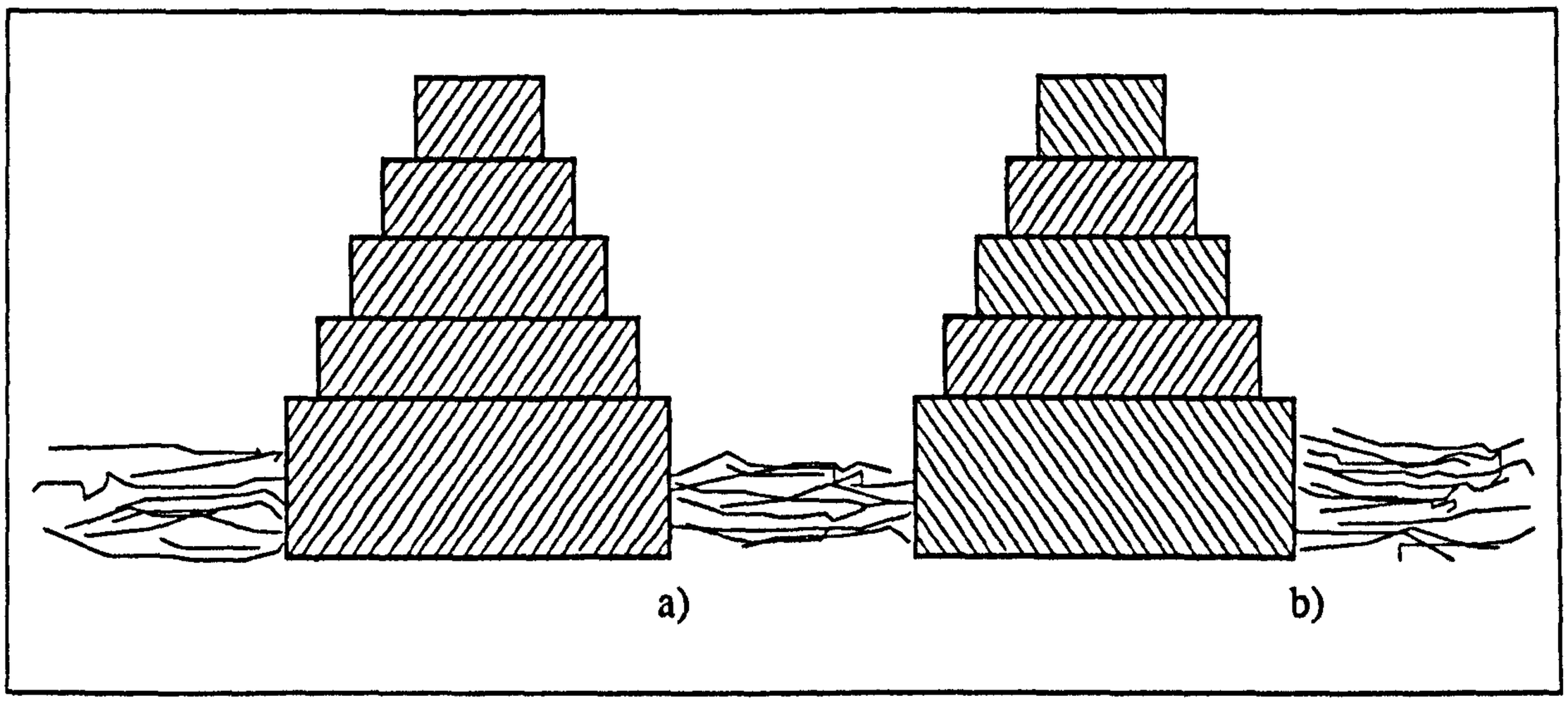

Figure 1.009 After Watkins (1987)

Watkin's proposed models for the orientation of collagen fibres in antler osteones.

The smallest structural units that Watkins identified were fibres roughly 100 to 200 nm in diameter. He says they were visible on almost all the antler fracture surfaces. (These were not observed during his study of bone fracture surfaces.) Watkins indicates that these fibres and their structure play an important role in the microscopic mechanical properties of antler:

> The difference in the mineral contents of antler and bone is most likely what controls the fracture process, it is postulated that in antler most or all of the mineral is contained within the fine, 100 to 200 nm diameter fibres. The antler fibres, although strong and probably quite brittle, are not bonded together, this has the effect of allowing many toughening mechanisms to be employed particularly the fracture and pullout of many thousands of calcified collagen fibres.

While underlining the role of mineral content in determining the mechanical response of bones, this statement clearly contrasts the assertion made about bovine bone by Turner (1981) (section 1.2.5). However, Watkins gives no evidence in support of his statement, nor is this area of research pursued in this thesis. I will end this description of the ultrastructure of antler here. This brief section has only scratched the surface of a whole field of continuing research.

Bone Structure and Species	Measurement	Dimension	Reference and comments
Whole antler, reindeer	Overall length	0.76 m	This study (used to produce specimens in data set CA1)
Whole antler, red and reindeer	Width	variable along length	This study
Section of antler, red and reindeer	Wall thickness	Up to 15 mm distally	This study. At the extreme distal end the antler is essentially solid bone.
'Haversian canal', mule deer	Diameter	37±4 μm	Lees (1982). (About twice the value he gives for bovine bone.)
Osteone, red deer	Diameter	100-150 μm	Unpublished study from Professor Currey's laboratory

Table 1.002

Dimensions of various antler structures

1.3.6. CLOSING REMARKS ON THE FUNCTION, GROWTH AND STRUCTURE OF ANTLER

The two main functions of antlers are as display organs and as weapons. It is reasonable to assume that the use of antlers as weapons has had a greater influence on the evolution of the material from which they are made. (Both functions probably played an important role in the evolution of the shape of the antlers.) The antlers of mature stags of red deer and reindeer are both about a metre long, and the mass of the animals is about 100 kg. When used in combat the antlers, and thus the material from which they are made, can sustain impact loading. This may be followed by a period of bending and twisting of the structure as the deer try to push each other off balance. To be effective antlers have to withstand such treatment. There are a number of variables in the design. One of these variables is the overall shape and structure, for example the use of tines that interlock, and the use of a foam-like structure internally covered in a hard shell. Another variable, the one of interest here, is the mechanical response of the material that this shell is made from. This material needs to sustain impact loading and needs to be relatively stiff. However, these two variables are not independent. It is possible to construct a stiff strong structure using a flexible and weak material, and *vice versa*. It can be assumed that there are a number of factors that influence the balance between shape and material. The most important of these is metabolic cost. Another is the simple practicality of building the structure: it may be stronger without the holes for blood vessels running through it, but without them how would it be constructed? As suggested in the introduction, like the engineering designer, nature has to meet certain criteria, and this

may involve compromise. Therefore, although the compact bone of antlers has been designed to sustain impact loading it may not be the most effective material nature could produce for this task. However, it is reasonable to assume that if the costs and benefits were fully examined it would be found to be the most efficient. The metabolic cost of producing antler, and normal bone, is beyond the scope of this thesis. Henceforth, bone and antler will be examined as materials, their biological functions being referred to mainly as a reason for their possession of certain mechanical properties.

1.4. THE MECHANICAL PROPERTIES OF BONE AND ANTLER: A SHORT REVIEW AND SOME RESULTS

In the following sections I will mention a few important papers that have advanced the analysis of the mechanical properties of bone. This is not an extensive review, for that would be a considerable study in itself. In reviewing these papers I introduce some of the mechanical properties of bone and antler, and how these properties have been interpreted or described. I expand the description of certain of the mechanical properties with the inclusion of some of my own experimental results. These experiments concentrate on the factors that have been deemed important from the consideration of the function of femoral bones and antlers (above); stiffness and impact strength. In the last part of this section I list some of the factors that can affect the measured value of various of the mechanical properties.

1.4.1. IMPORTANT DEVELOPMENTS IN THE STUDY OF BONE'S MECHANICAL PROPERTIES

Burstein *et al.* (1973) view the study of the mechanical properties of bone as passing through several plateaux. They consider the first to be the work of Messerer (1880). However Roesler (1987) states that

> The first systematic investigation into the material properties of bone was made by Rauber (1876). Rauber mentioned his predecessor Wertheim (1847), who had measured strength of bones and elasticity, respectively, but he regarded their experiments as unreliable because they reported to have had difficulties with the specimen holders.

Roesler reports that Rauber conducted tension, compression, shear and torsion tests on specimens of cortical and cancellous bone. Whereas, Messerer (1880)[9] examined the

---

[9]By this time the well-known engineers I. K. Brunel and W. Fairburn had both died (Brunel in 1859 and Fairburn in 1874). Eaton Hodgkinson (1789-1861) had conducted a

failure behaviour of whole bones. He discovered characteristic failure patterns for various types of loads. Roesler (1987) says this may be considered as the first attempt to introduce fracture mechanics into bone biomechanics. However, as will become clear in chapter 5, Messerer's work predates the development of *fracture mechanics* by some forty years. Burstein *et al.* (1973), when referring to Messerer, state that these early investigations treated bone tissue as a linear elastic material.

The second plateau in the study of bone (implied by Burstein *et al.* (1973)) was the recognition of bone as an anisotropic material, although still considered elastic. This finding they credit to Evans (1958). (Again Roesler cites the earlier work of Rauber (1876)).

The third plateau of research defined by Burstein *et al.* (1973) is marked by the work of McElhaney and Byars (1965) who according to Burstein *et al.* 'recognised that bone was a viscoelastic material'. A viscoelastic material is one particular form of time-dependent material. Some aspects of the time-dependent properties of bone are described and experimental evidence presented in later chapters. At this stage it is sufficient to say the more rapidly a viscoelastic material is loaded the stiffer it appears to be.

Another aspect of bone mechanics that Burstein *et al.* deem noteworthy is the consideration of its structure as that of a composite material. These authors include references to the work of Currey (1964) and Katz (1971). In this thesis the composite structure of bone and antler is considered to be a controlling factor in the failure process, and analogies will be drawn with composite materials at various stages. However, (as suggested in section 1.2.6) I make no attempt to construct a composite model for bone, although this is a direction in which this study may be extended.

An important development in the study of bone occurred only 3 years before the publication of the work by Burstein *et al.* They simply state 'recently Piekarski (1970) examined crack propagation and energy of fracture of bone tissue'. This is an area of research that expanded dramatically, especially with the contribution of many papers by Bonfield and his co-workers. This type of study, the fracture mechanics of bone, will not be discussed here as it is examined in depth in later chapters.

---

series of experiments on the bending of cast iron beams, which showed that as the load increased the neutral axis changed its position. He also found the properties of cast iron where different in tension and compression. Using this information he optimised a cast iron I beam, the flange in tension being several times the size of that in compression (Timoshenko, 1958). Thus it appears that material science and biomechanics were developing in together, but industrial engineering was in the driving seat.

The next plateau is due to the work of Burstein *et al.* (1972). Until the publication of their paper the mechanical response of bone was viewed as being that of a brittle material. The tensile load-deformation plots obtained were essentially a straight line up to the point of failure. (Although this is generally true there are exceptions, such as the work of Sedlin (1965), reproduced here as figure 3.008.) In their 1972 paper entitled *The Ultimate Properties of Bone Tissue: The effects of Yielding*, Burstein, Currey, Frankel and Reilly report a different shaped loading curve. After the initial straight region the curve bends over, a greater amount of elongation is then obtained per increment in load. The authors report, that 'there was more than twice as much deformation produced after the initial yielding as there was in the elastic zone'. They also say 'our findings showing the large amount of plastic strain in bone tissue are probably the result of keeping the bone surface wet during testing'. The nomenclature these authors used; elastic, yield and plastic have remained within the literature. Burstein *et al.* (1973) present a figure showing loading-unloading cycles of a specimen of bone. They use this figure as evidence that the 'behaviour is truly plastic'. However, they also note a reduction of the specimen's stiffness between successive loading cycles. It will be shown later that this observation contradicts their description of the process as plastic deformation. This observation is related to what I consider to be the next plateau in the description of the mechanical properties of bone.

It is my opinion that the next, and most recent, important advance in the research of the mechanical properties of bone is the application of the theory of damage accumulation to bone. This idea was first applied to the mechanical testing of bone by Carter and Caler (1983). This theory is reviewed in chapters 2 and 3 and features prominently in this thesis. The concept of damage accumulation is based on the idea that the material fails as a result of the continual degradation of its mechanical properties, caused by an increasing density of voids or cracks, rather than due to the flow of material as in plasticity.

1.4.2. SOME ILLUSTRATIVE RESULTS OF THE MECHANICAL AND CHEMICAL PROPERTIES OF BONE AND ANTLER.

This section contains the results from some of the experiments that I have conducted that clearly illustrate a number of the points made in the previous sections. Some of the mechanical properties of bovine bone are presented first. This is followed by a comparison of the properties of bone and antler, concentrating on tests that would be expected to reflect the different mechanical properties needed to fulfil the functions as described above.

1.4.2.1. TENSILE LOAD-DEFORMATION CURVES OF BOVINE FEMORAL BONE.

Figure 1.010 contains the load-deformation plots, normalised to stress and strain, for two specimens of bovine femoral bone tested as part of this study.[10] The values of the various quantities obtained from these plots are examined in chapter 4. These curves display some of the features explained above. The shape of curve 'b' bears a considerable similarity to the load-deformation trace of bovine bone given by Burstein *et al.* (1972). (It has an even greater similarity to the loading curve presented by Burstein *et al.* in 1973.) The initial region of the curve is relatively straight. There is then a sharp transition, or knee, to a region where the deformation increases more rapidly relative to the increases in the applied load. The deformation that occurs after the knee in the curve, or what Burstein *et al.* called yield, is several times greater than the deformation that occurs before the knee.

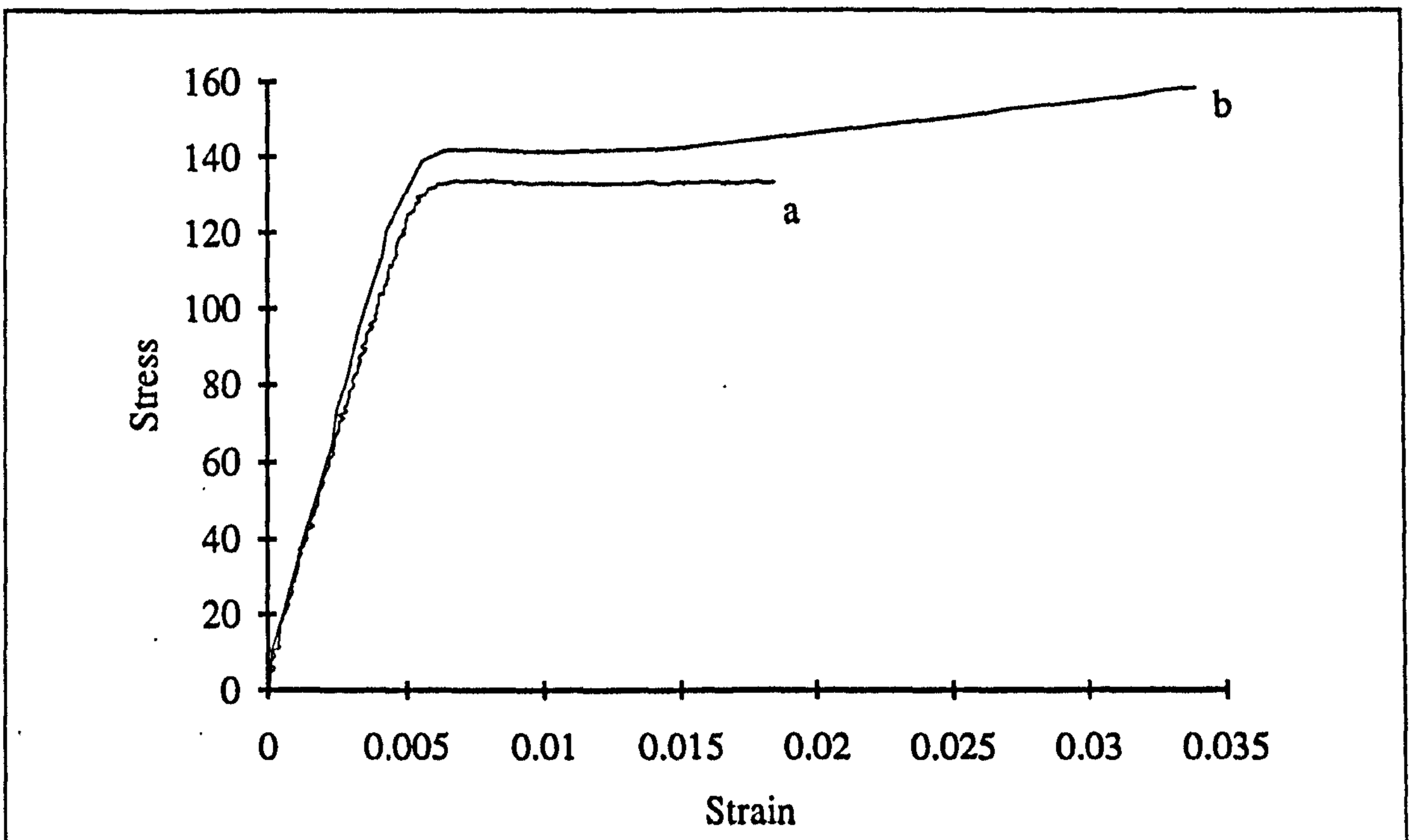

Units:
Stress, MPa.
Comments:
Curve 'a' was obtained from a test using a cross-head speed of 8.33×10^{-5} m s^{-1} (specimen 01/11/91/32), and curve 'b' from one at 8.33×10^{-4} m s^{-1}(specimen 01/11/91/50).

Figure 1.010

Tensile stress-strain (load-deformation) plots for bovine femoral bone

---

[10]The process of this normalisation, and the definitions of stress and strain are explained in chapter 2.

The two curves in figure 1.010 are from tests conducted at different rates. In the test from which curve 'a' was obtained the cross-head was moved at a rate of 8.33×10^{-5} m s^{-1} [5 mm min^{-1}], while in that for curve 'b' the rate was 8.33×10^{-4} m s^{-1}. The more quickly loaded specimen is stiffer, and maintains a linear loading line to a higher load. This observation agrees with the idea that the material is time-dependent. The data from just two results are no proof of such time dependence; a more thorough statistical analysis is conducted in chapter 4.

Figure 1.011 shows the stress-strain response obtained for a specimen of bovine femoral bone that was loaded and unloaded several times (the time intervals were not regular). The figure is similar to that shown by Burstein *et al.* (1973). However, here I have emphasised the reduction in stiffness during successive cycles by redrawing the loading section of the curves (figure 1.011d). The loading and unloading curves are not superimposed as would be the case for a material whose deformation was a function of load only. It is reasonable to assume the loop is caused by a time-dependent, or energy dissipating, effect.

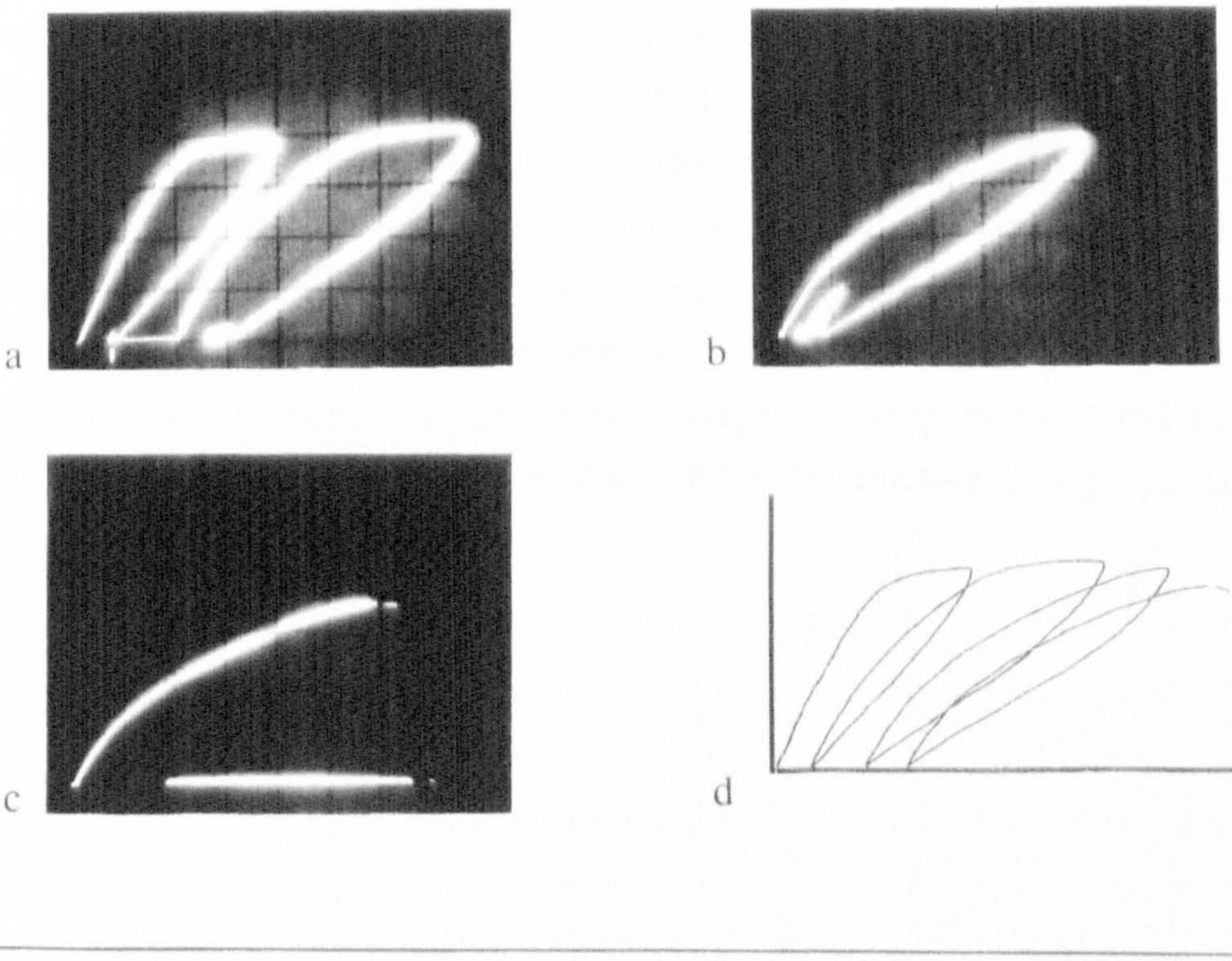

Figure 1.011

Stress-strain plots from tensile loading-unloading test of bovine femoral bone

A loading-unloading test was also performed on a similarly shaped specimen of aluminium alloy. In the post-knee region the metal's unloading-loading curves were almost linear with only a very limited loop (about the thickness of the trace). Thus the reduction in stiffness and the existence of a hysteresis loop shown in the test of the bone specimen is due to the specimen, and not due to the testing equipment.

This experimental technique, loading and un-loading, was not exploited in this thesis for a number of reasons. First, the test machine available for this work had no feed-back control or other facility for true cyclic loading. Second, the time available for experimental work was more than consumed by the tests described in this thesis. However, I consider that an extensive study of the behaviour of bone (both bovine and antler) under cyclic loading would be an informative exercise.[11]

1.4.2.2. TENSILE LOAD-DEFORMATION CURVES OF BOVINE FEMORAL BONE AND ANTLER.

Figure 1.012 displays the stress-strain response for specimens of bovine femoral bone (the same as figure 1.010) and red deer antler. The antler specimens appear to exhibit a greater rate dependence than the bone specimens. However, the main feature is the difference between the mechanical response of these materials. Antler does not display the initial stiff region exhibited by the bovine bone. Antler exhibits far higher strain at every stress and especially at failure. (The strain values obtained here indicate that a specimen of antler initially 10 mm long will be more than 11 mm long when it fails.) The higher stiffness of the bovine bone was predicted when its function as a lever was considered above. There is no obvious advantage in having very stiff antlers. However, antlers are required to be sufficiently stiff to be effective during a pushing match.

---

[11]There are many variables that can be studied. For example, how is the shape of the reloading curve affected by the time spent at the zero load level between cycles, or what is the effect of cycling at different stress (or strain) levels? Some studies of these areas are available in the literature, but they are not extensively drawn on here.

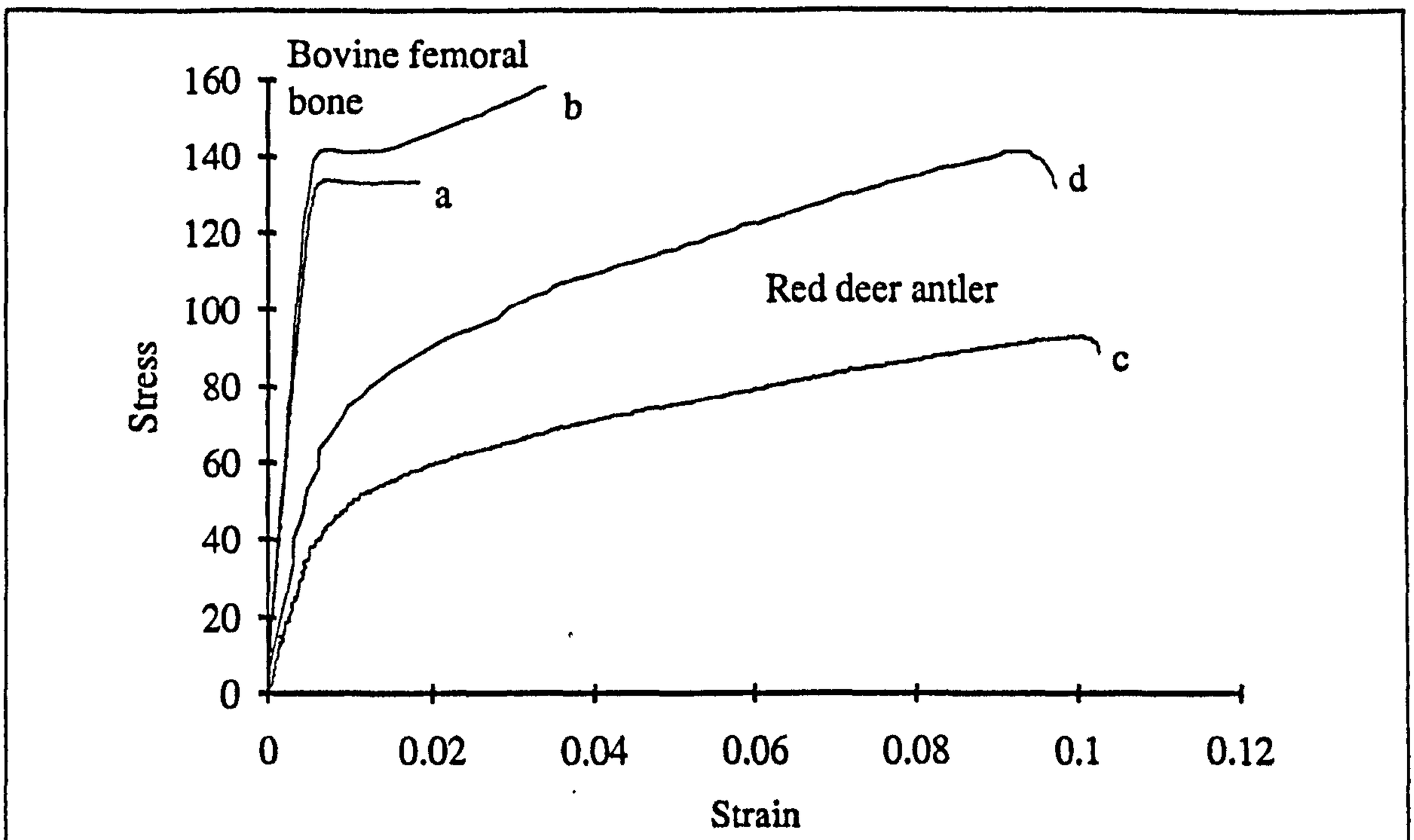

Units:
Stress, MPa.
Comments:
Curves 'a' and 'c' was obtained from tests using a cross-head speed of 8.33×10^{-5} m s^{-1}, whereas curves 'b' and 'd' are from ones at 8.33×10^{-4} m s^{-1}. (Specimens: 'a' 01/11/91/32; 'b' 01/11/91/50; 'c' 10/11/91/105 and 'd' 10/11/91/51)

Figure 1.012

Tensile stress-strain relationship for specimens of bovine femoral bone and red deer antler tested at two cross-head speeds (under the same conditions)

1.4.2.3. IMPACT TESTING OF BOVINE FEMORAL BONE AND RED DEER ANTLER

In the preceding section it was shown that bone was stiffer than antler, as predicted by the examination of their functions. When the function of antlers was examined it was noted that the material must be able to tolerate impact loading. This means it must to be able to absorb or store large amounts of mechanical energy without failing. A stag with antlers that snapped off the first time he used them in combat would not obtain dominance, and hence would not breed. In chapter 9 I present what I consider to be the consequences that fulfilment of this requirement to absorb energy has on the tensile failure and other mechanical properties of antler. In this section the impact strength of the materials is examined directly.

The equipment used for these tests was an adapted Charpy impact tester (manufactured by Hounsfield). The standard machine was adapted to enable images of the specimen to be recorded on video tape. The impact hammer that is normally used

consists of a slender pendulum arm supporting a **C** shaped mass. When an impact test is conducted the pendulum is released from a known height. At the bottom of the pendulum's swing the arms of the **C** shaped mass pass above or below the specimen, then upright section of the **C** hits the middle of the specimen. The mass of the impact hammer I used was contained in one essentially rectangular block that swung below the specimen. Thus permitting the specimen to be viewed from above. The specimen was hit by the round bar supporting this mass. The experimental arrangement is shown in figure 1.013. The amount of energy consumed by fracturing a specimen can be determined, by recording the height to which the hammer rises after fracturing the specimen, and then calculating the difference in potential energy between the start and end of the swing. This is simplified by a dial and pointer, calibrated so the value is obtained more directly (once the mass of the hammer and the distribution of this mass has been calculated). When this value is obtained it can be divided by the cross-sectional area of the specimen (or approximately the surface area of one fracture face) to obtain a normalised quantity.[12]

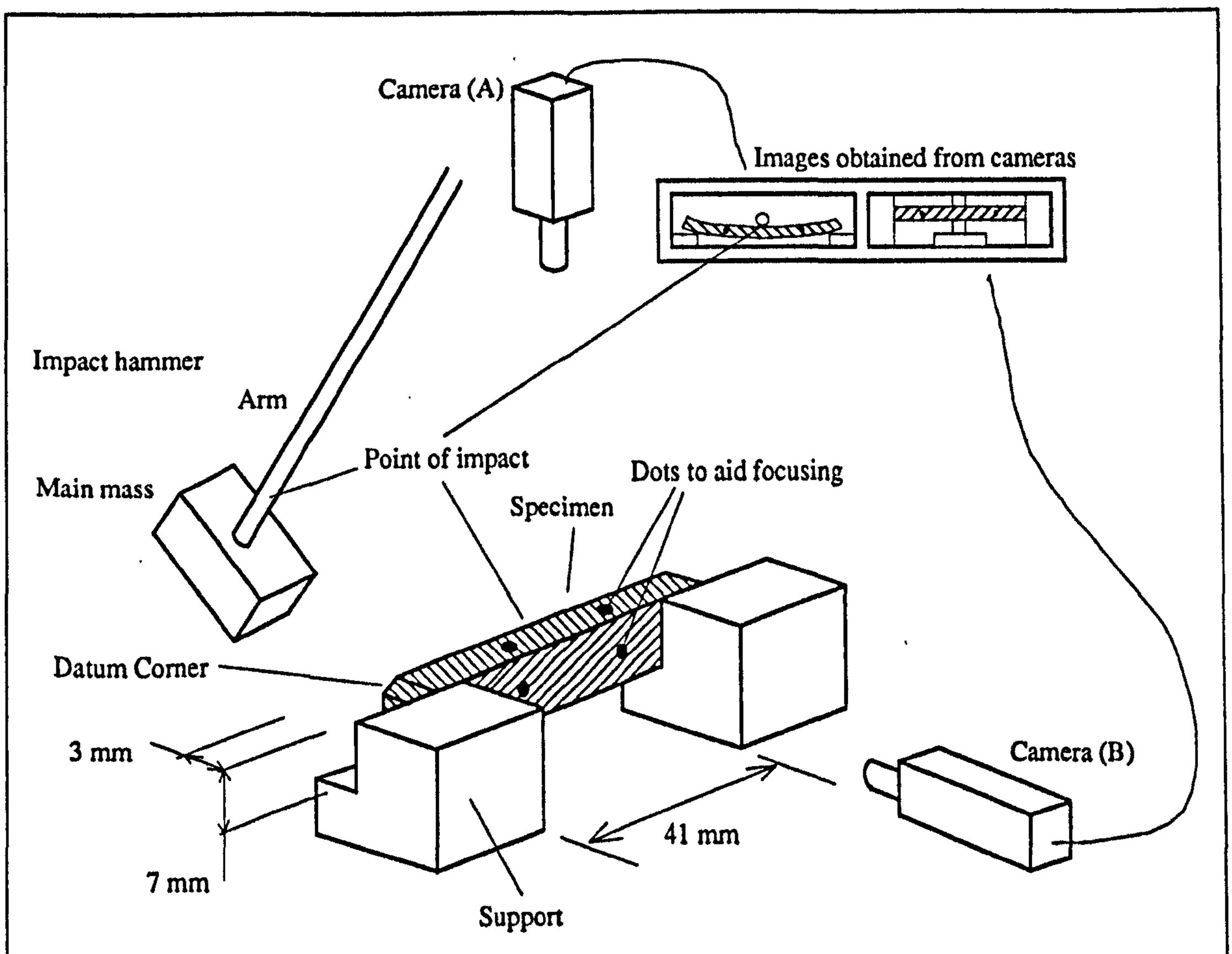

The datum corner permitted a consistent specimen orientation (see section 4.2.3).

Figure 1.013

The arrangement of the specimen and cameras, showing how the images where obtained

[12]In chapter 5 and 6 there are further references to impact tests. Other comments in those chapters raise the question, should the normalising area be once or twice the cross-section. In engineering standard specimens are used so the energy is quoted directly.

Specimens of red deer antler and bovine femur were prepared in similar manner to that described in appendix 2. However, in this case the specimens were rod shaped, approximately 55 mm long by 7 mm wide by 3 mm thick. The long axis of the specimens was the same as that of the bone from which they were cut. The specimens were machined, stored and tested wet.[13] They were positioned (using the datum corner) on the impact rig so that the tensile surface (seen by camera B in figure 1.013) was that which had been nearer the external surface of the original bone.

The data obtained from these impact tests are given in table 1.003. The data sets are referred to as IA1 and IB1 (signifying impact data from antler specimens set one and impact data from bovine bone set one).[14] The bovine bone specimens failed in a manner that would be expected for a brittle material: they consumed only a small amount of energy and some specimens produced a large number of fragments. The fragments produced ranged in size from almost a dust, to fragments with dimensions similar to those of the sides of the specimen. None of the antler specimens fractured in two; the fractures that did occur did not traverse the whole cross-section. Some of the antler specimens eventually bent so much that they were pulled between supports of the test rig. Other antler specimes slowed, stopped and then reversed the direction of the impact hammer without fracturing. No quantitative results were obtained from these two groups of specimens and they are not included in the data set. However, this observation clearly shows the ability of antler to sustain impact loads that would smash normal bone.

Examination of the shape of the specimens shown on the video tape recordings implies that the bone specimens failed at a low value of strain. Due to the apparently uniform curvature along the length of the specimen it can be assumed that the strain on the tensile surface is approximately uniform. The antler specimens display different behaviour; their deformation is huge compared to that of the bovine bone specimens. The curvature of the antler specimens is not uniform. Near the time of maximum deflection, or just prior to fracture, nearly all the curvature is concentrated at the point of impact, the sections either side being relatively straight. This combined with only a limited amount of permanent deformation implies that a localised failure process has occurred, which has permitted the antler to absorb the impact energy without failing. In the case of the 5 unfractured antler specimens, which bent to about 90°, they all returned to within 15° of a straight bar again. Most of this recovery was almost instantaneous, but some further recovery occurred with time. This recovery implies that a damage process occurs within these impact specimens of antler; not a *plastic* or flow process.

---

[13]The material stiffness the specimens was determined before they were tested in impact.
[14]Due to the number of specimens tested and the different quantities measued in each type of test the presentation of the amassed data sets would require a considerable number of pages. Thus the data sets are not included within this thesis, but I am happy to supply them on computer disk or in printed format (see appendix 4).

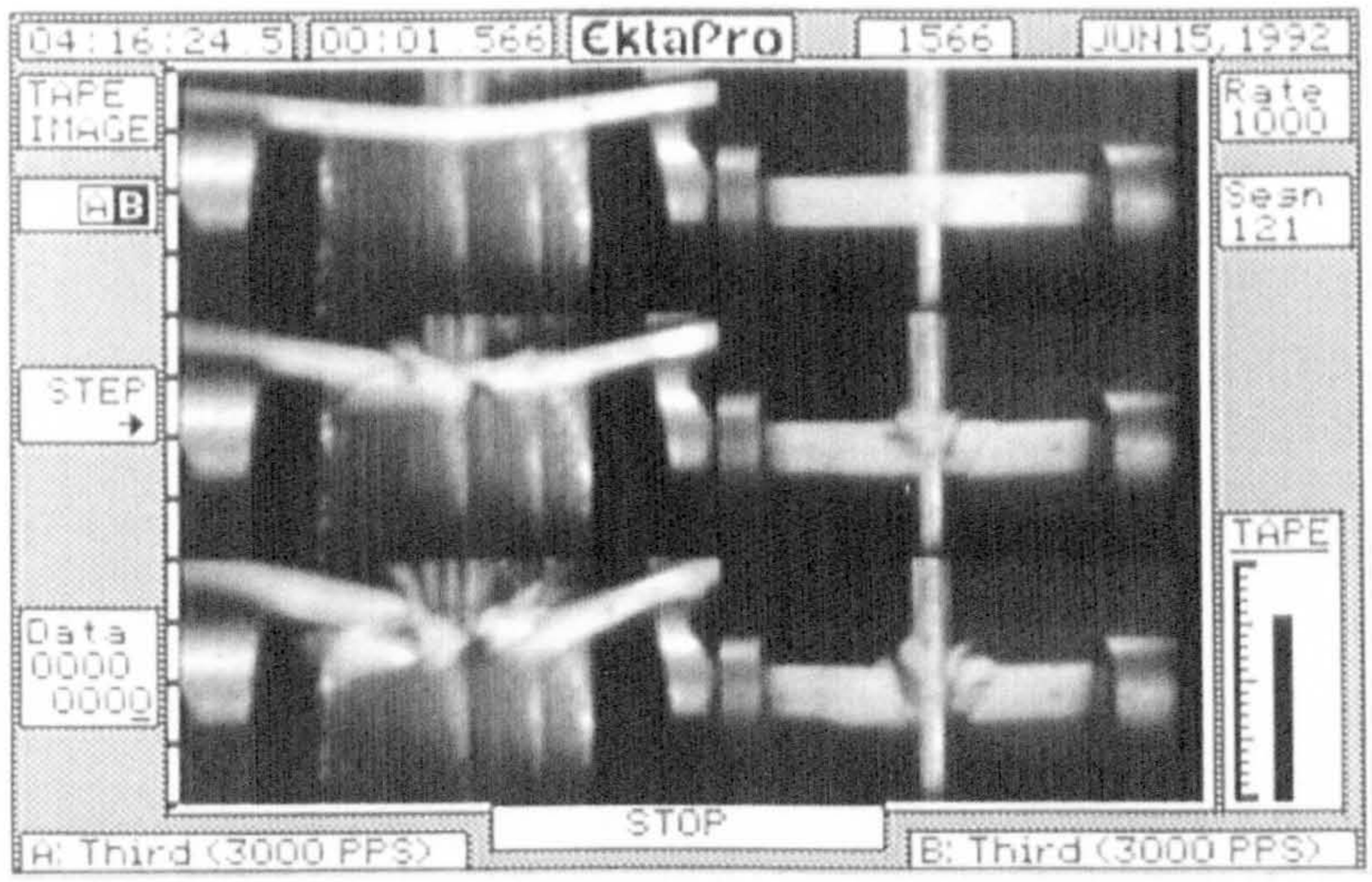

1

2

3

Specimen 13/06/92/03

Each image 1, 2, 3 and so on is 1/3000 of a second apart

Figure 1.014

Images of impact test of bovine bone

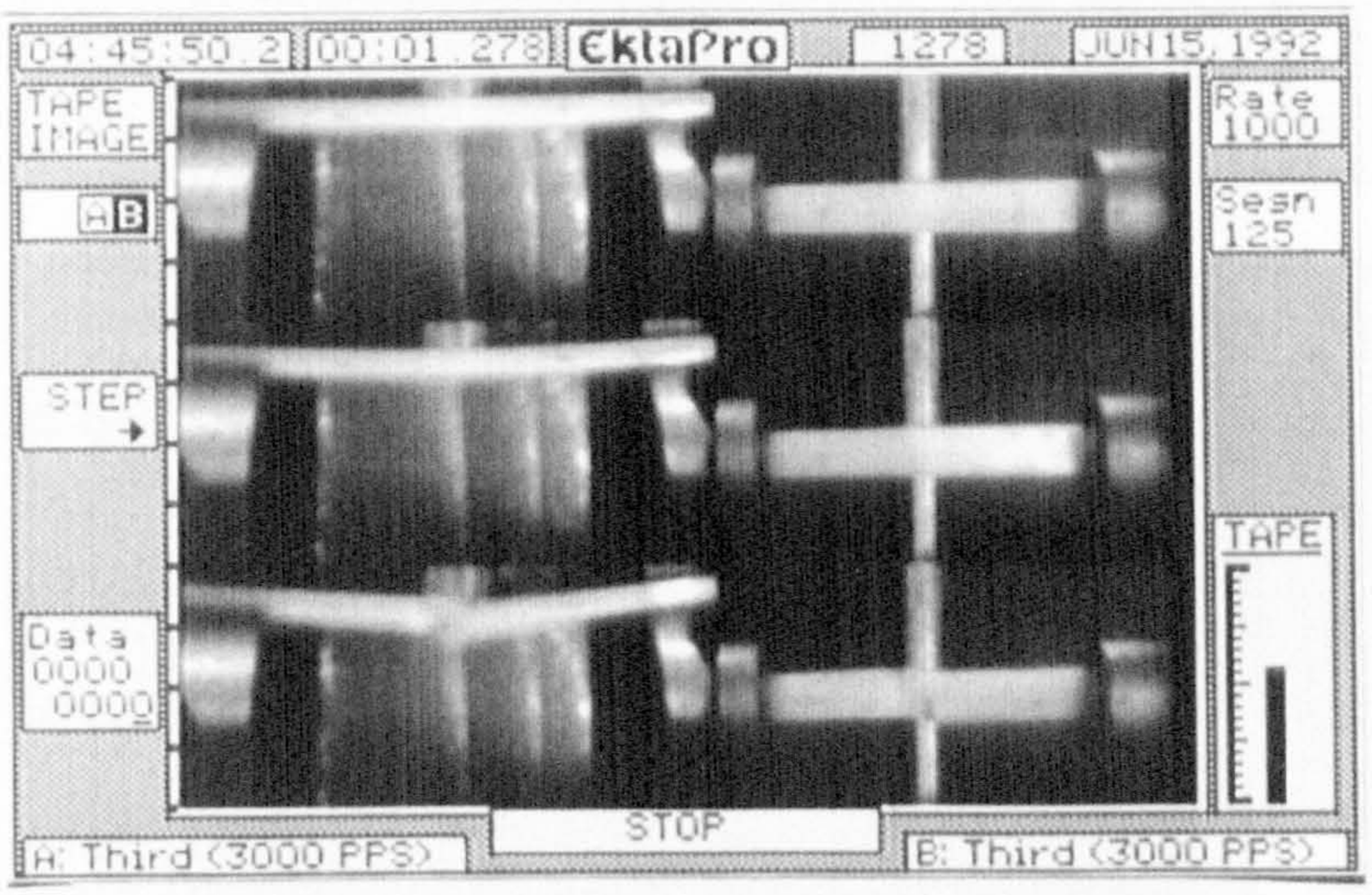

1

2

3

Specimen 13/06/92/06

Each image 1, 2, 3 and so on is 1/3000 of a second apart

Figure 1.015

Images of impact test of bovine bone

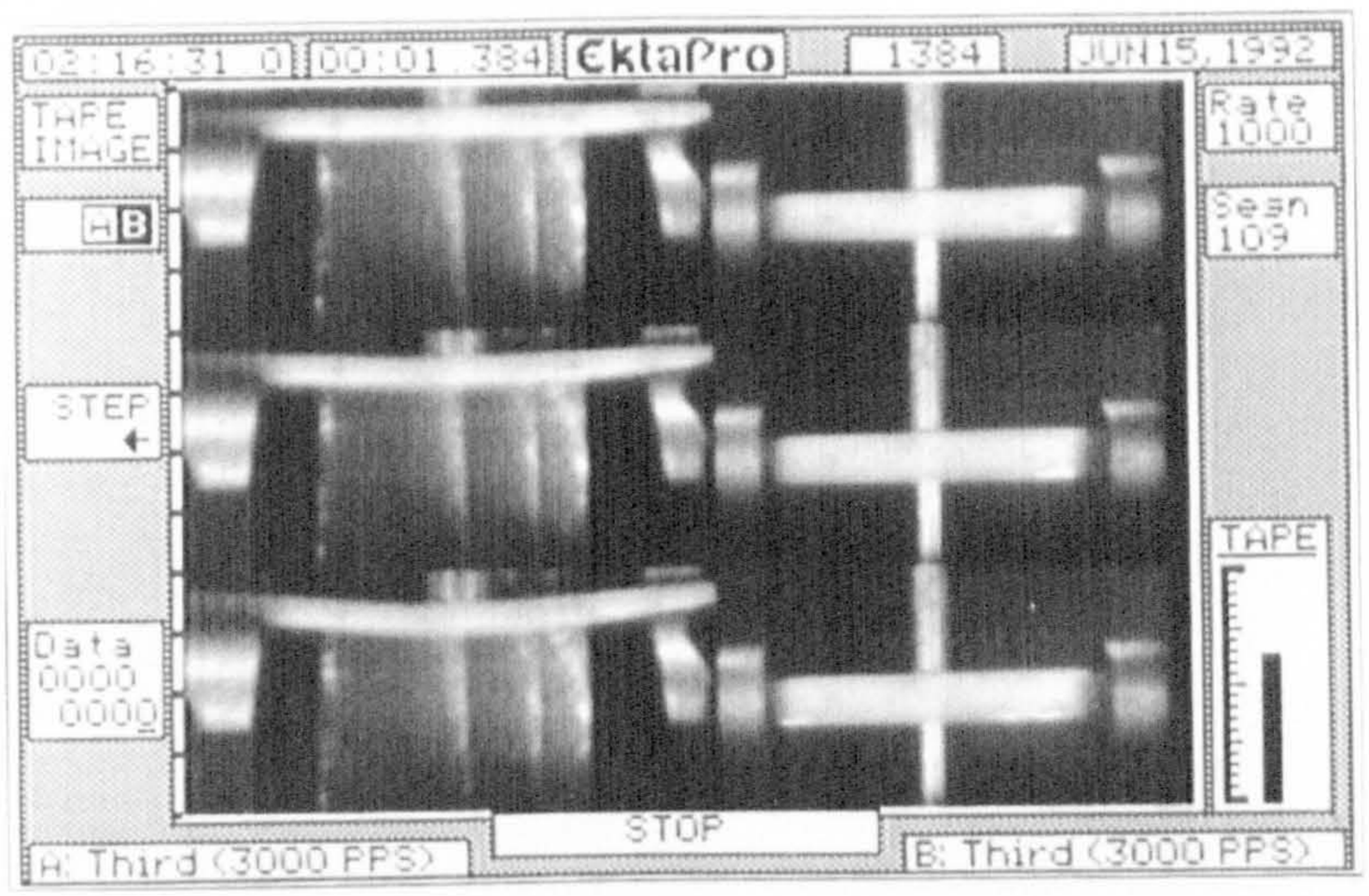

1

2

3

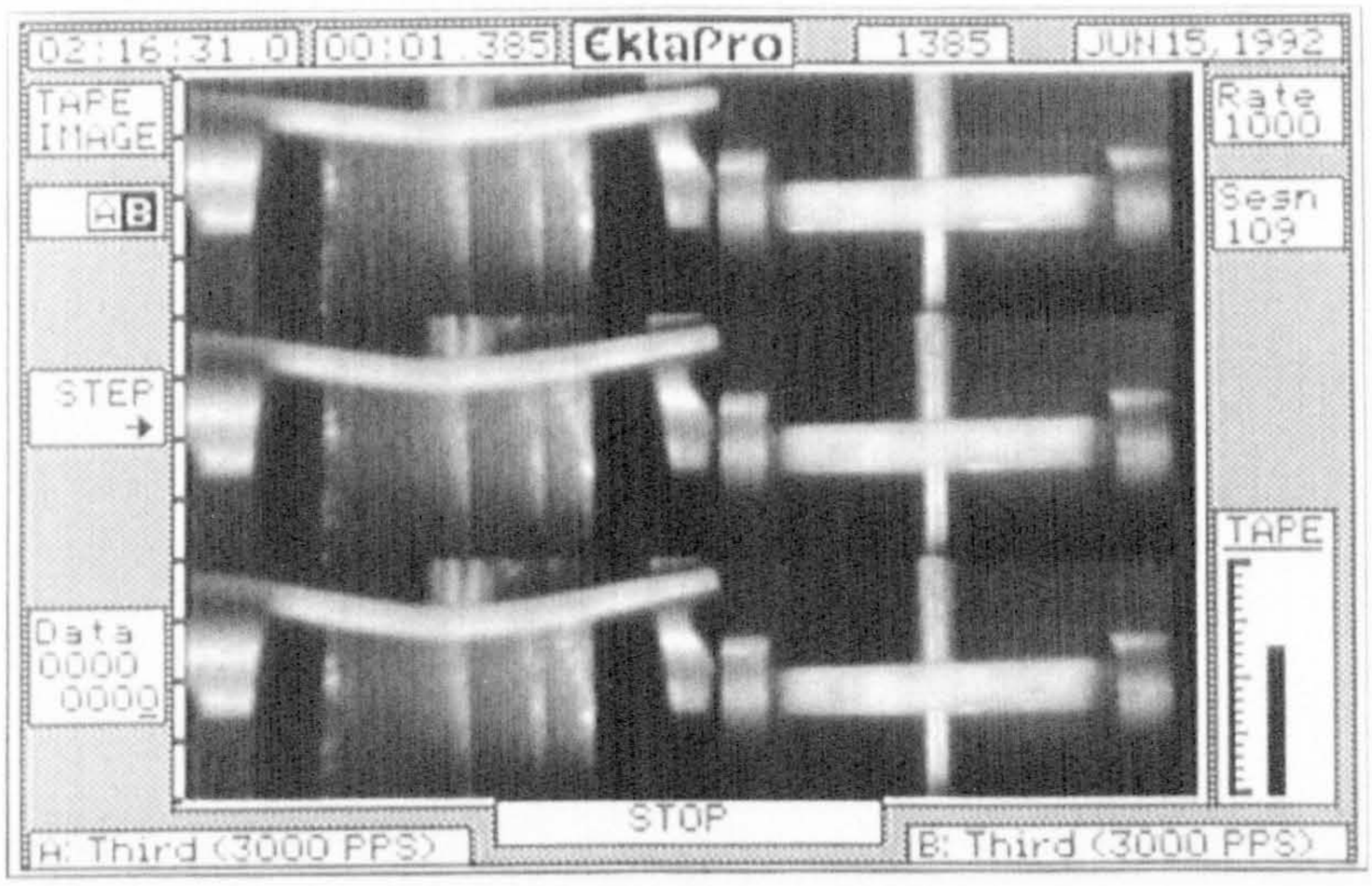

4

5

6

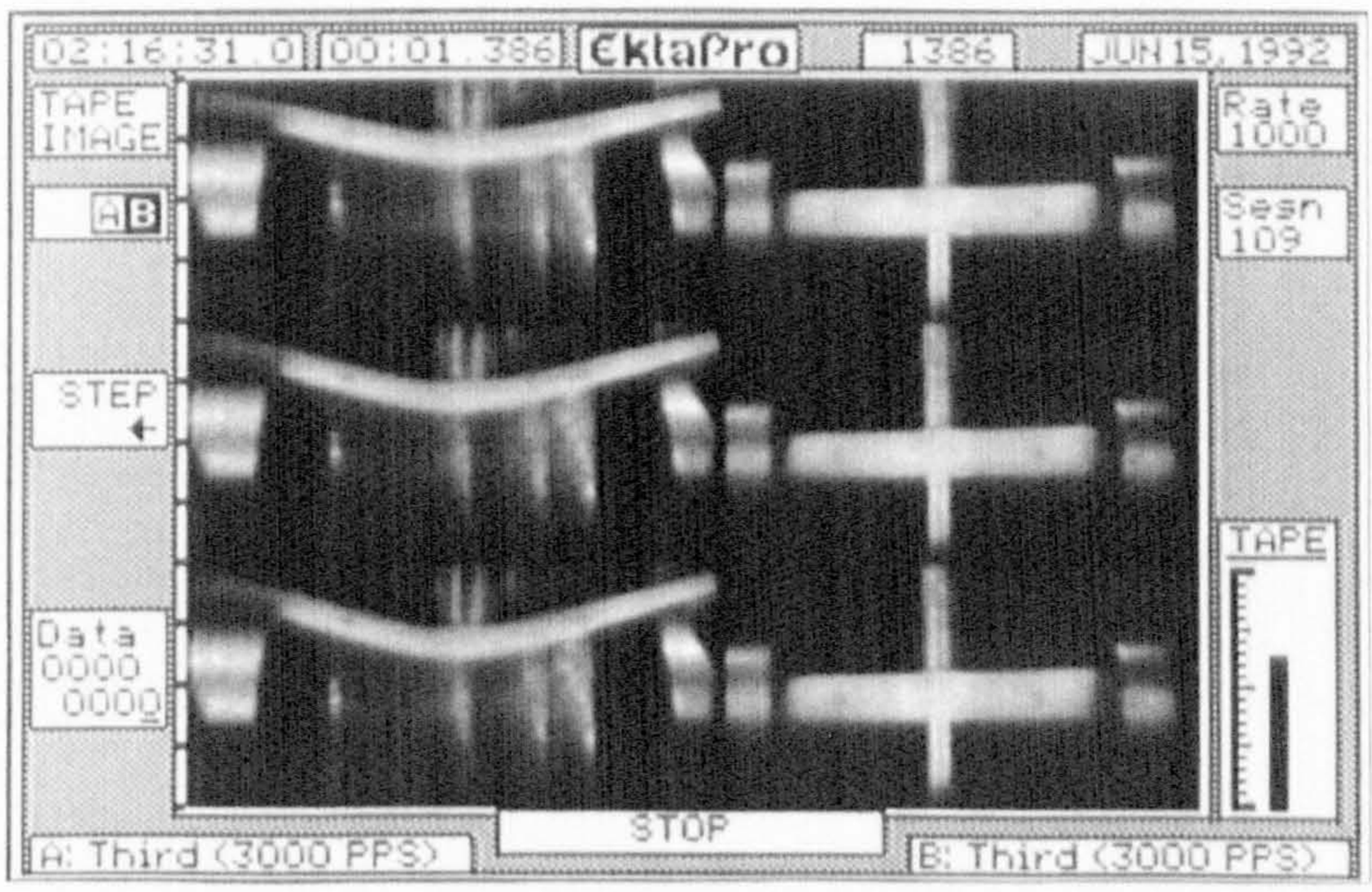

7

8

9

Specimen 13/06/92/15

Each image 1, 2, 3 and so on is 1/3000 of a second apart

Figure 1.016 Continued in figure 1.017

Images of impact tests of an antler

10

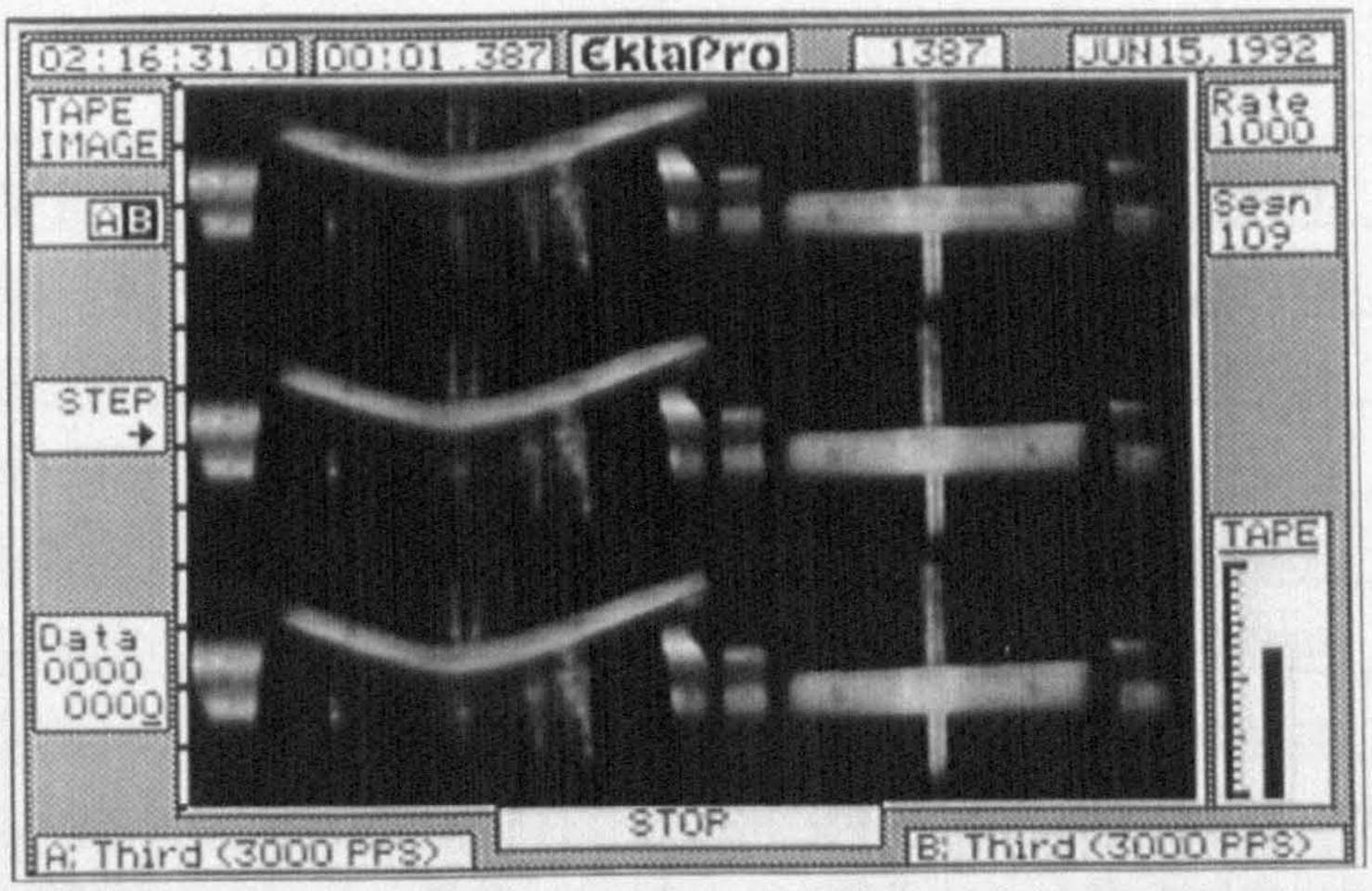

11

12

13

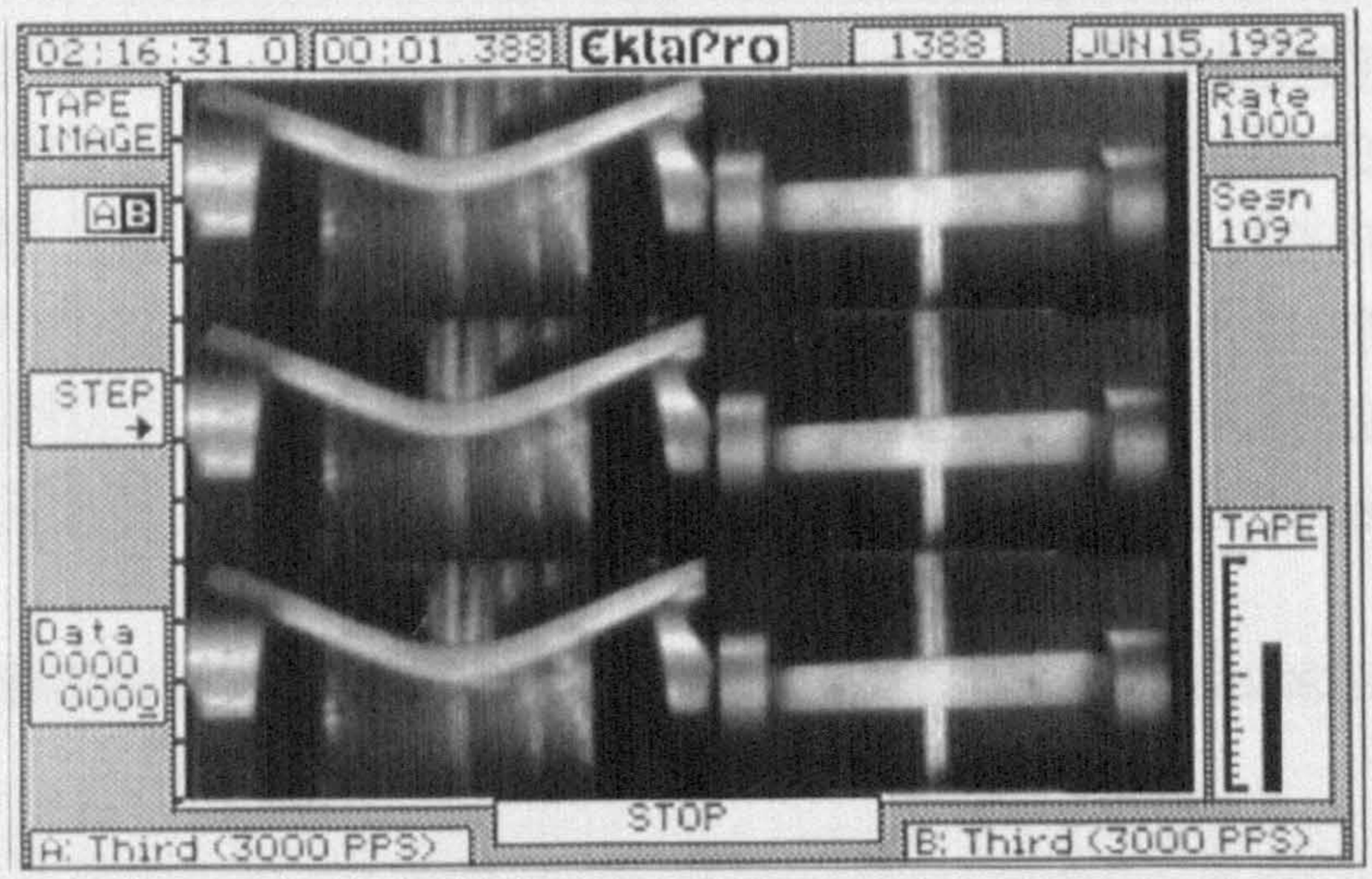

14

15

16

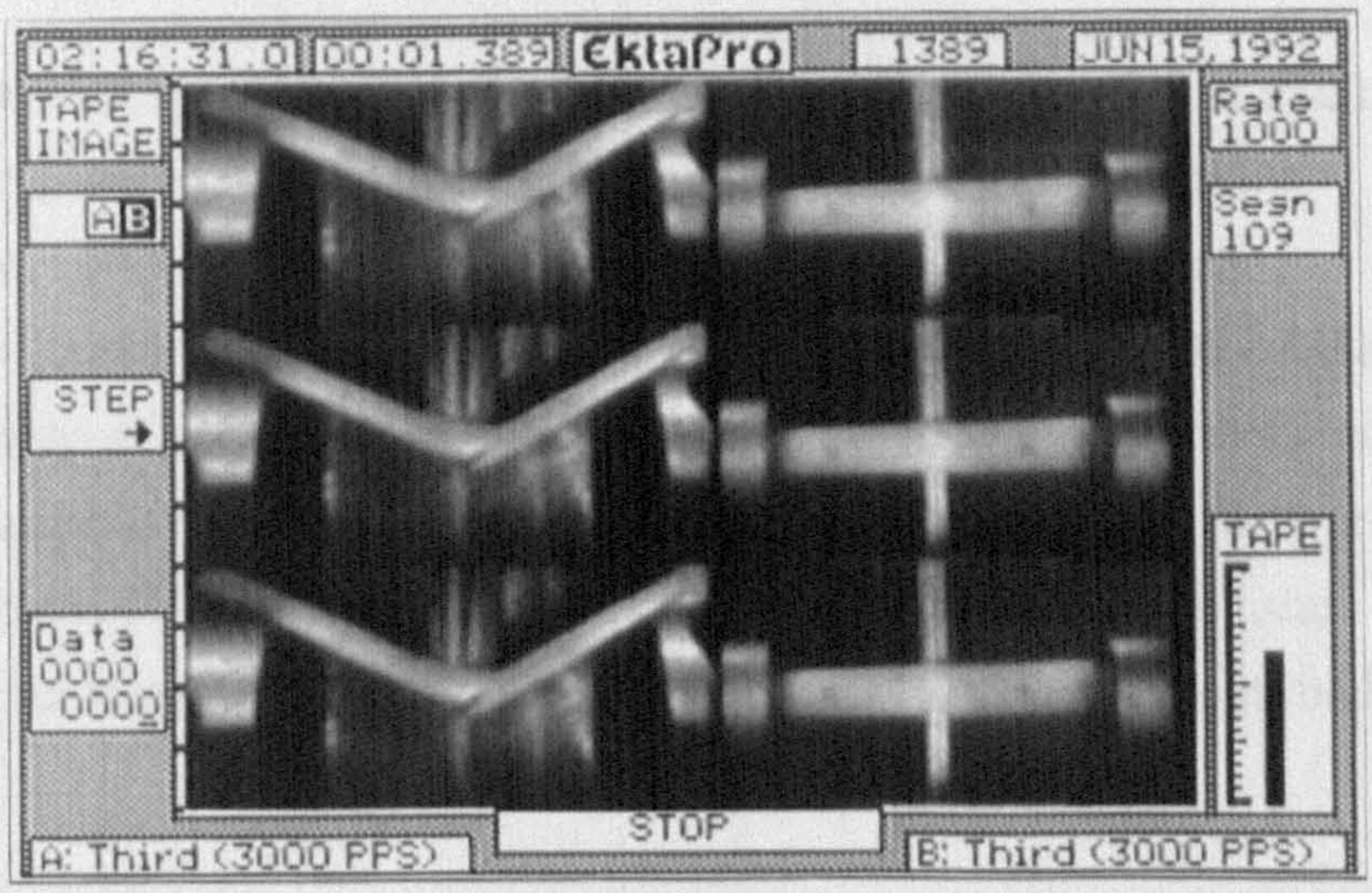

17

18

Specimen 13/06/92/15

Each image 10, 11, 12 and so on is 1/3000 of a second apart

Figure 1.017 Continued from figure 1.016

Images of impact tests of an antler

Bone	Specimen number	Bending stiffness, GPa	Impact energy, kJ m^{-2}	Type of failure
Bovine femur	13/06/92/01	8.9	7.6	2 fragments
Bovine femur	13/06/92/02	11.7	23.0	5 fragments
Bovine femur	13/06/92/03	12.9	36.3	6 fragments
Bovine femur	13/06/92/04	11.5	35.5	5 fragments
Bovine femur	13/06/92/05	11.1	38.1	6 fragments
Bovine femur	13/06/92/06	14.2	10.2	3 fragments
Bovine femur	13/06/92/07	11.8	5.2	2 fragments
Antler	13/06/92/14	-	100.4	Partial fracture
Antler	13/06/92/15	7.8	90.7	Partial fracture
Antler	13/06/92/16	7.0	92.0	Partial fracture
Antler	13/06/92/17	7.1	110.7	Partial fracture
Antler	13/06/92/21	6.8	113.1	Partial fracture
Antler	13/06/92/22	6.2	100.2	Partial fracture
Antler	13/06/92/23	6.4	117.5	Partial fracture
Antler	13/06/92/24	5.5	118.9	Partial fracture

Table 1.003

Data obtained from impact tests of specimens of bovine femoral bone and red deer antler (part of data sets IB1 and IA1)

The results presented in table 1.003 show that the antler specimens that exhibited some degree of fracture absorbed about three times as much energy as the bovine specimens without completely failing. This difference should be viewed as an underestimate, because 5 other antler specimens were able to resist the impact loading without showing any signs of a fracture. Antler is clearly able to sustain impact loads far greater than those sustainable by normal bone. This finding is supported by the work of Currey (1979) and Watkins (1987). This finding is also in full agreement with the differences in mechanical response suggested by the materials functions (as outlined above).

When the data and the specimens were examined in more detail I noticed that the energy consumed by the fracture of the bovine bone specimens appeared to be related to the number of reasonably sized fragments produced. Due to the almost explosive nature of the failure of the bone specimens I had been unable to collect all the fragments after some tests. Therefore I examined the video recordings, noting the number of fragments visible. Due to the resolution of the images, as shown in the figures above, only the larger fragments were observed. (Observations were made easier by viewing the moving

video images.) The data obtained in this way is plotted in figure 1.017. The correlation is easily explained if it is considered that a fixed amount of energy is required to fracture a unit area of the bone. The more fragments there are, the larger the surface area will be, and thus the larger the amount of energy consumed.[15] This finding suggests that a better value of the normalised impact energy may be obtained by substituting two fragments into the regression equation. In this way the area through which the fracture passes is more closely approximated by the cross-sectional area. This procedure gives a result of 5.3 kJ m^{-2}, which is about twenty times smaller than the value of the energy consumed by the antler specimens. These findings imply that the difference between these materials could be far greater than the values obtained here: antler is a considerably more impact resistant material.

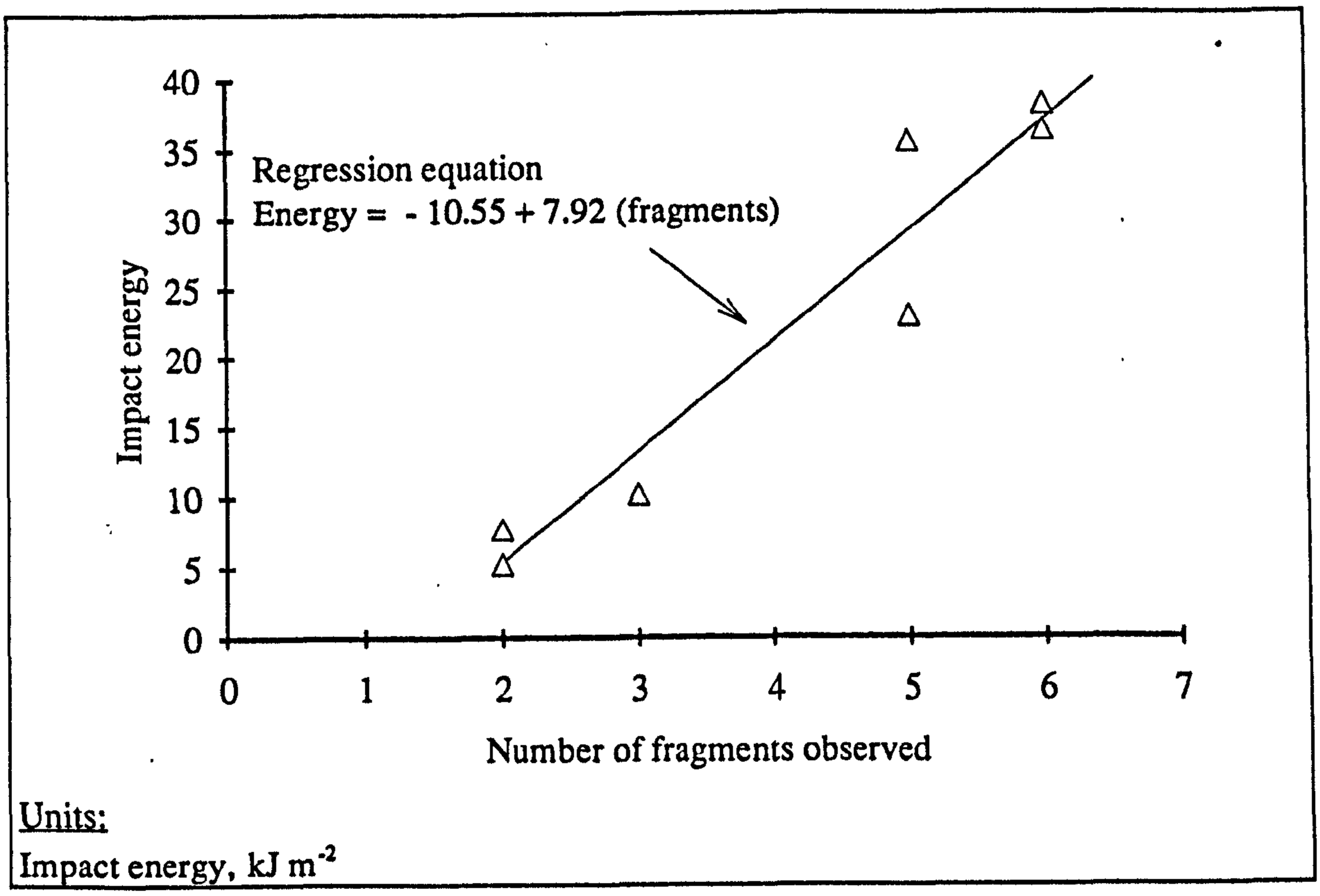

Figure 1.018

The relationship of the number of fragments and the impact energy of bovine bone.

---

[15]In an investigation of the changes in the impact energy absorption of human bone with age, Currey (1979b) used an estimated ratio of fracture length to specimen width. He points out that this ratio will be greater if there are more fragments or if the fracture takes a more tortuous (or indirect) route across the specimen. He found that the higher impact energies were associated with the higher values of this ratio, and thus larger fracture surfaces.

1.4.3. THE CALCIUM CONTENT OF BOVINE FEMORAL BONE AND ANTLER

In a previous section it was stated that the material from which antlers are constructed is bone of lower than normal calcium content. I use the term calcium content as that is the quantity determined by the tests I conducted. The exact nature of the mineral component in antler is not known. However, it can be assumed that it is not too dissimilar to that in normal bone so the differences in calcium content should reflect the overall differences in mineral content. The importance of the difference in mineral content of these two materials has been remarked on by Watkins (1987), among others. He says that

> Antlers are grown from bone which is known for being fairly brittle, yet antlers are relatively tough. Given that antlers are bone, deer have made the best of a bad situation, they have toughened the material by altering the mineral content but not the structure.

I question the assertion that the structures are the same, for normal bone can (as reported in section 1.2.3) take several different forms. (In another section Watkins equates the structure of antler with that of Haversian bone.) However, Watkins underlying theme is reinforced by a number of works published on the relationship of the mechanical properties of bone, in most cases from different species, to the calcium content. Examples of these are Currey (1988a) *The Effect of Porosity and Mineral Content on The Young's Modulus of Elasticity of Compact Bone* or Currey (1990) *Physical Characteristics Affecting The Tensile Failure Properties Of Compact Bone*. In the former paper Currey shows that for specimens from a range of species the material stiffness is strongly positively related to mineral content. The findings of his second paper are best expressed in his own words:

> The principal findings were that the ultimate strain and work under the stress-strain curve declined sharply with mineralisation, as did the stress and strain appearing after the specimen has yielded. Ultimate tensile strength was not simply related to any combination of the possible explanatory variables, but some relatively poorly mineralised bones, notably antlers, had high stresses at failure. These high strengths were allowed by a great increase in stress after the bones had yielded at quite low stresses.

As the data presented in this thesis comes from, essentially, only two types of bone, the difference in the calcium content of the types of material cannot be used to explain the differences in mechanical properties of these materials in such a definite way. The difference in calcium content may only identify that the materials are different, and with only two sets of data it would not be reasonable to try and determine the degree to which this variable is responsible for the difference in mechanical properties. An analogy can be based on the speed of certain cars. Suppose a group of red cars was found to be faster than a group of black ones. The conclusion appears obvious the red cars are faster.

This is true, but the reason may be the red ones are sports cars and the black ones London taxis. Similarly, the difference in mechanical properties of bovine bone and antler is correlated with calcium content, but it could be due to other differences between bone and antler, such as structure, and thus mode of failure. However, a reduction in toughness and an increase in material stiffness as the proportion of mineral in the material increases appears to be a reasonable progression. This argument is supported by consideration of a more extreme material, such as tympanic bulla, the more highly mineralised and more brittle bone of the ear (Currey, 1979a). If there were also such a trend within each material this argument would be strengthened.

The method used to determine calcium content of bone, expressed as mg of calcium per g of dry de-fatted bone, is essentially the same as the colourimetric method used by Currey (1988a). The method is explained in appendix 3. The results for each section of antler shown in figure 1.019 are the means of the values for the specimens produced from that section.

Only some of the specimens tested in this work were analysed for calcium content. Specimens from a reindeer antler, a red deer antler and a bovine femur were analysed. The data from each bone are contained in separate data sets (MA1, MA2 and MB1, respectively. For more information see appendix 4). Some of these data are also contained in other data sets, where they are available as an explanatory variable for use in later analysis. (For example, they are used in section 7.4.3.3.) Here I will present only the overall mean values and a diagrammatic presentation of the distribution of the calcium content in various regions of a red deer antler. (This antler was used to produce the specimens described in section 7.4.)

Type of bone (data set)	Number of specimens tested	Calcium content, calculated from the mean value for each specimen. $mg\ g^{-1}$	
		Mean	s.d.
Reindeer antler (MA1)	78	213.89	5.80
Red deer antler (MA2)	110	228.77	6.88
Bovine femur (MB1)	37	254.75	5.66

Table 1.004

The calcium content of reindeer and red deer antler and bovine femoral bone

The values of calcium content given in table 1.004 are in general agreement with the values given by Currey (1988a). (His results were: reindeer antler 225.3 and 212.8, red deer 208.3 and 211.5, bovine femur 255.7 mg g^{-1}.) Clearly the calcium content of the bovine bone is greater than that of both types of antler. When the development of antler was described, it was stated that the mineralisation process moved with the growing tip. If additional calcification occurs it is logical to assume that the older, more distal, antler may have a greater mineral to organic ratio. This was not found to be the case for either the reindeer or red deer antlers that were examined. The distribution of the calcium between the various sections cut from the red deer antler are show in figure 1.019.

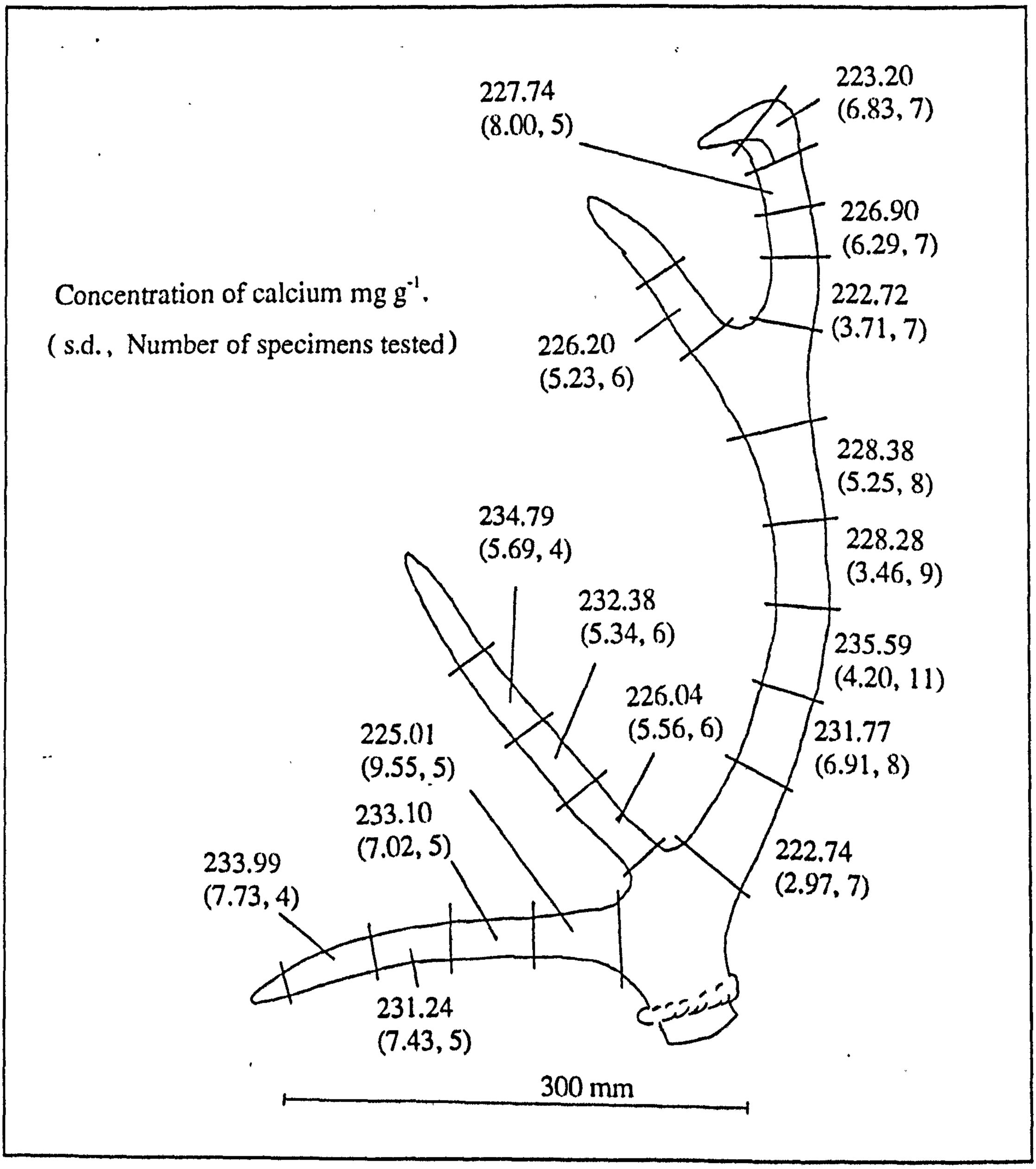

Figure 1.019 (data set MA2, mechanical data in NA3)

The distribution of the calcium in a mature, but un-cast, red deer antler

1.4.4. SOME FACTORS THAT AFFECT THE MECHANICAL RESPONSE OF BONE AND ANTLER.

There are a great number of factors that affect the mechanical response of bone and antler specimens. Clearly there are additional ones that affect the mechanical response of whole bones, such as size and shape. The factors that determine the mechanical properties of whole bones have been reviewed by Martin (1991). The factors that affect bone as a material can be broadly divided into two categories, internal factors and external factors. By internal factors, I am referring to the type of bone and its structure, while external factors are things such as the test conditions. I will briefly outline a number of these factors, and refer to works where more information can be obtained.

1.4.4.1. SOME INTERNAL FACTORS

Type of bone: there is some variation between the mechanical responses of different types of compact bone. Bone may be classified as being of a different type by virtue of its anatomical position, species from which it is obtained or both. (There is also a degree of variability between individuals.) This thesis demonstrates the combination of these factors. To reduce the variability in the results obtained in this study most of the experiments on bovine bone were restricted to tests on specimens obtained from femora. However, some tibial bone was used. Likewise the majority of tests on antler used material obtained from red deer. (Due to availability reindeer antler was used for the creep tests described in chapter 4.)

Age and structure: it has been shown that the structure of bone changes with age, due to the process of remodelling. This structural remodelling affects the properties of bone. Evans (1973) presented a review of the effect that age has on the mechanical properties of human compact bone. Since his review, other papers have been published, for example one by Currey (1979b) entitled *Changes in the Impact Energy Absorption of Bone with Age*. In this study Currey found that 'the impact energy absorption of human femoral cortical bone decreases by a factor of about three between the ages of three and ninety'. Another of his statements connects age with another internal factor 'the decrease is associated with, and partially caused by, an increased mineralization of the bone'. As mentioned above, the structure of the bone within a specimen affects its mechanical properties. Cartwright (1975) examined the effect of structure on the tensile strength of compact bone. His study mainly examined human bone. However, the study also contains some results and comments on bovine bone. Cartwright found a positive correlation between tensile strength and the percentage of primary bone. The proportion

of secondary to primary bone within the specimens tested for this thesis has not been determined. To reduce the age related (and hence structure related) variation of the mechanical properties of the specimens examined in this study, all the bovine specimens came from immature animals, and all the antler specimens from antlers that had shed their velvet.

Calcium content: the effect that changes in calcium content have on the mechanical properties of bone is reviewed above. This variable is interrelated with the other factors highlighted here.

Porosity: Martin (1991) says that 'it can be argued that the primary determinant of the mechanical properties of bone tissue is its porosity'. In making this statement he is considering the full range of bone, both compact and cancellous. Clearly cancellous bone contains many more voids, and thus has a greater porosity than compact bone. Currey has published a number of studies on the effects of porosity on the mechanical properties of compact bone. For example in one paper (Currey 1988a) he examined the effect of porosity (and mineral content) on the 'Young's modulus of elasticity'. In this case *volume fraction* (also called apparent density, Currey 1990), the complement of porosity (1-porosity), was the variable examined by regression analysis. The data came from 23 tensile and 80 bending specimens, obtained from 18 species. Currey found that 'Young's modulus has a roughly cubic relationship with both calcium content and volume fraction'. He presented his data in two tables: one for the bending specimens and one for the tensile ones. The data relevant to this thesis is repeated here in table 1.005. To ascertain the porosity of his specimens Currey (1988a) used a point counting method where 4356 points were scored as either lying over a cavity or not. He defined a cavity as including blood channels and erosion cavities, but not osteocyte lacunae or canaliculi. The published works on the effect of porosity will not be discussed further, as this quantity was not determined for the specimens used in this thesis.

Type of bone	Number of specimens and test	Volume fraction	
		Mean	s.d.
Bovine tibia	7 (bending)	0.948	0.015
Bovine femur	1 (tension)	0.956	-
Red deer antler	8 (bending)	0.807	0.095
Red deer antler	6 (tension)	0.866	0.072
Reindeer	4 (bending)	0.766	0.094
Reindeer	2 (tension)	0.824	0.023

Table 1.005 After Currey (1988a)

The calcium content of reindeer and red deer antler and bovine femoral bone

1.4.4.2. SOME EXTERNAL FACTORS

Specimen geometry and size: the variation in the geometries and sizes of specimens used to determine the tensile load-deformation of bone is considerable. It appears that many groups of workers or research centres use a specific design. A number of examples are shown in figure 1.020.

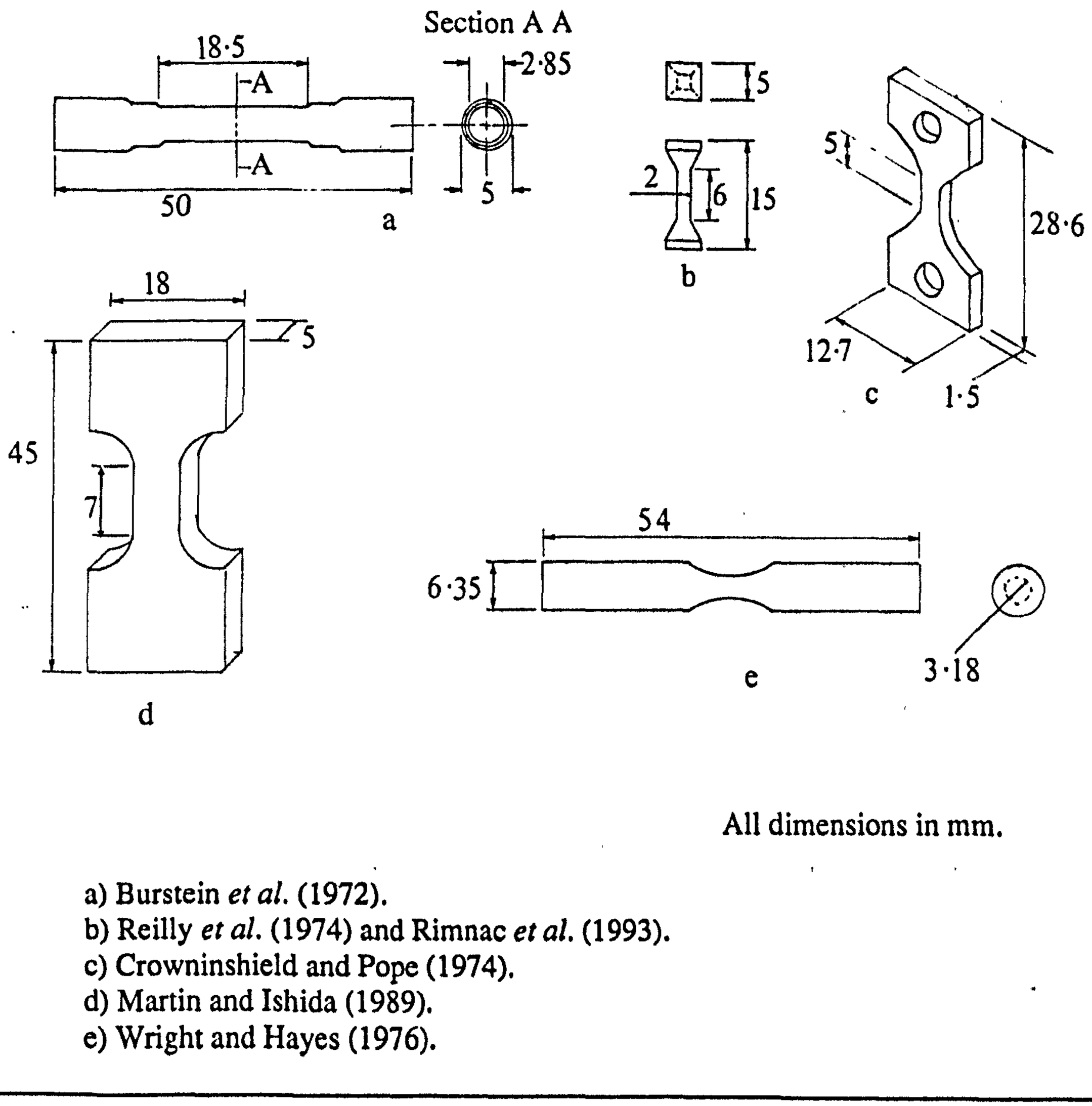

All dimensions in mm.

a) Burstein *et al.* (1972).
b) Reilly *et al.* (1974) and Rimnac *et al.* (1993).
c) Crowninshield and Pope (1974).
d) Martin and Ishida (1989).
e) Wright and Hayes (1976).

Figure 1.020 Redrawn or traced from diagrams given in the original papers

Examples of the geometry and sizes of tensile specimens of bone used by various workers

An important result of a specimen's geometry is the effect on the stress field within the specimen. The ideal for a tensile specimen is to obtain a uniaxial stress field within the gauge length of the specimen. This is normally achieved by using cylindrical

specimens. (Thus the strains and stresses perpendicular to the long axis of the specimen, are uniform at all angles around the axis.) Another important feature is the way load is transferred to the gauge length. Specimens are normally gripped by way of widened ends. The increase in cross-section of the specimen is aimed to reduce the loading induced stress in these regions, so that additional stresses, or damage induced by gripping the specimen, do not result in the failure occurring outside the gauge length. The radius of curvature that merges the widened ends of the specimen with the gauge length is clearly important as a sharp corner will result in a stress concentration and initiate failure in that region. In this study the specimen sizes and geometries were developments of those previously used in the same laboratory. These specimens were essentially flat plates, the central section of which had a reduced width. The basic geometry is shown in figure 4.001. There were two main reasons for choosing this shape. First, increasing the area of two of the faces produced a larger surface for the examination of optical changes. Second, the thickness of the cortical bone of antler restricted the thickness of the specimens that could be produced.

The stress field within a specimen is not only determined by the specimen geometry, but also by the mechanical properties of the material. A large cylindrical specimen may include regions of compact (stiff) and cancellous (more compliant) bone. This heterogeneity would clearly result in bending.[16] Such effects are not avoided if only compact bone is tested, for, as Currey (1984a) points out, bone (like many real materials) is anisotropic. Therefore, even if the specimen is symmetrical about its long axis the strains perpendicular to this axis may not be. The anisotropy of bone introduces another external factor that can affect the experimentally obtained mechanical properties of bone: specimen orientation.

Specimen orientation: Evans (1983) reviewed the directional differences of bone. He opened his chapter on the subject with the following words:

> Because bone is an anisotropic material, the values obtained for its mechanical properties depend upon the direction, with respect to the various axes of the intact bone, in which the specimen is loaded. The axes of the specimen itself also influence the values obtained for its mechanical properties.

Evans says that Hülsen (1896) was the first to investigate directional differences in the tensile strength of standardised specimens of compact bone. Hülsen's specimens of ox tibia had a greater tensile strength when they were aligned with the long axis of the bone than when they were perpendicular to it. Reilly and Burstein (1975) examined the properties of human, and bovine, femoral bone at various angles to the long axis of the

---

[16]Heterogeneity was cited as the cause of the dependence of bone's work-of-fracture on the specimen size found by Rogers and Moyle (1988). They did not find a similar dependence for specimens made from aluminium or Plexiglas®. (See section 6.3.1.)

bone. They found that the ultimate tensile stress of bovine laminar bone in the tangential direction is about a third of that in the longitudinal direction. For bovine Haversian bone the decrease was less dramatic. An approximate halving of the material stiffness accompanied these reductions in strength. In this study the effect of the specimen orientation on the recorded mechanical properties was avoided, or at least minimised. This was achieved by using the same orientation for the production and testing of each specimen. The preparation of the specimens is described in appendix 2.

State of saturation: in section 1.4.1 it was reported that Burstein *et al.* (1972) attributed the attainment of high values of tensile failure strain to the maintenance of a wet specimen surface. Knets and Melnis (1982) examined the effect of water content on the tensile properties of human tibial bone. Amongst other findings they noted that specimens that had been stored in water produced a curve whose 'character is similar to the typical stress-strain curve of elastic-plastic material with a strongly marked yield point'. The effect of drying on the mechanical properties of bone is summarised by Currey (1988b) in the following way:

> Drying increases the modulus of elasticity, increases the tensile and bending strength, and makes bone much more brittle and less tough. It reduces the strain at failure.

Similar findings were made by Rajaram and Ramanathan (1982) in their tests on dry and wet antler. From the description of antler given above it is not clear what degree of saturation of the specimens should be used to reflect the natural situation. However, as the basis of this study is a comparison of the properties of bovine bone and antler, all tests were performed under the same conditions of saturation. This was achieved by testing the specimens while they were immersed in a water tank. The exceptions to this arrangement were the impact tests and the loading-unloading test shown in figure 1.011, all of which were conducted while the surfaces of the specimen were wet.

Temperature: like many other materials, the mechanical properties of bone are dependent on the temperature at which they are measured. One study that has examined the impact energy absorbed by specimens of bone at different temperatures is that of Bonfield and Li (1966). They tested notched and un-notched, transverse and longitudinal specimens of bovine femoral and tibial bone. The temperature range they used, –196°C to 900°C, takes these specimens far outside the range of physiological temperatures. The results obtained for the two orientations of specimens were different. However, all sets of specimens showed that at temperatures below and above those that may be normally expected *in vivo*, or *in vitro* without temperature control, the energy absorbed was lower. In a recent paper Rimnac *et al.* (1993) reported the effect of temperature on the creep of bovine femoral bone at 25, 37 and 43°C. They found a positive, significant association between the steady-state creep rate and the absolute temperature. This paper is discussed

in more detail in section 3.3.3. For the experiments reported in this thesis the effect of temperature on the mechanical properties was reduced by conducting most of the tests at a standard temperature. This was achieved by maintaining the temperature of the water in the test tank to within 1°C of 37°C. (The impact and three-point-bending tests were conducted at room temperature.)

Loading or testing rate: in section 1.4.2.1 it was reported that the rate at which a tensile specimen of bone is loaded affects its mechanical response. This effect is the main concern of chapters 2 to 4. In this thesis the rate of loading of different specimens was approximately consistent, unless it was the effect of this variable that was being examined. The reason the rate is only approximately constant between specimens, and may vary during the testing of an individual specimen is explained in appendix 7.

In this section a number of factors both internal and external to the specimen have been outlined. It was partly these factors that determined the methods of specimen preparation, specimen size, specimen geometry and the test conditions used for the majority of the tests described in the following chapters.

1.5. SUMMARY

In this chapter some features of the function, growth, structure and mechanical properties of bone and antler have been outlined. This information can be used to place the results of the mechanical tests presented below into the context of the natural situation for these materials.

One of the most important features of the two materials studied in this thesis is that they are both bones. (Within this thesis I generally use the term *bone* to refer to those contained in the normal skeletal system, and *antler* for the appendages of deer.) As in the case of engineering materials bones and antlers are designed to meet certain criteria, these are many, complex and interrelated. If only the mechanical functions of long bones and antlers are considered it is clear that the materials from which they are made are required to have different mechanical properties. Bone should be stiff and antler resistant to impact loading. When tested using the appropriate technique, this was found to be the case; the bovine bone specimens were stiffer, and the antler specimens considerably more resistant to impact loading.

In the previous sections a number of the variables that can affect the value of the quantities measured during mechanical testing have been outlined, as have the methods used to limit their effect on the results presented in this thesis. (Some of these methods,

for example testing antler under water at approximately 37°C, separate the test conditions from the natural ones.) Due to the limited time available for this study some of these variables, such as porosity and structure have not been determined for the specimens tested. The variability due to these factors was limited by reducing the variability of other factors, such as age and source of the bone and antler material tested.

One of the internal variables that is considered, in the literature, to be important in determining the mechanical properties of bone is the mineral content. It has been shown here (and in published works) that the mineral content of antler is less than that of bovine bone. I have quoted two researchers on the structure of the mineral within bone and antler. Turner (1981) states that the mineral is in a contiguous form in bovine bone, while Watkins (1987) say that it is in a discontinuous form in antler. I am uncertain of the validity of these statements (due to my lack of knowledge of the techniques used), but if they are true they could contain the explanation for the difference in the mechanical properties of these materials. The possible effect of a continuous or discontinuous mineral phase can be visualised if the materials are considered to be a fibre composite, with collagen fibres and a mineral matrix.

2

TIME-DEPENDENT PROPERTIES OF BONE AND ANTLER: A THEORETICAL BACKGROUND

"I thought," said Piglet earnestly, "that if Eeyore stood at the bottom of the tree, and if Pooh stood on Eeyore's back, and if I stood on Pooh's shoulders--"

"And if Eeyore's back snapped suddenly, then we could all laugh. Ha ha! Amusing in a quiet way," said Eeyore, "but not really helpful."

"Well," said Piglet meekly, "I thought--"

"Would it break your back, Eeyore?" asked Pooh, very much surprised.

"That's what would be so interesting, Pooh. Not being quite sure till afterwards."

Milne, A. A. (1928)
The House at Pooh Corner.

2.1. INTRODUCTION

It was shown above (section 1.4.2), and has been reported in published studies, that bone is not the elastic-brittle material it was once considered to be. I also reported that some mechanical properties of bone and antler exhibit a degree of time-dependence. Two examples are the increase in material stiffness associated with an increase in the rate of loading and the gradual extension of a specimen when subjected to a constant load. As a result of these and related observations, some workers have classified bone as a viscoelastic material. However, viscoelasticity only models some of the time-dependent properties exhibited by bone. It can not explain features such as the knee (or so-called *yield* region) in the tensile loading curve. Therefore other approaches have been applied. One such approach is the concept of damage accumulation, or the degradation of material properties. An examination of the application of this approach to bone and the consequences of such a mechanism forms a major part of the thesis. The concept of damage accumulation has already been applied to the failure processes of bone and to a lesser degree antler, most notably by D. R. Carter, W. E. Caler and co-workers. The significance of this approach is twofold: not only can it be used to model the mechanical response, but it also has a physical basis, (whereas, viscoelasticity is merely phenomenological, as it is based on observed mechanical behaviour). Furthermore, this physical basis: degradation of the material due to an increasing density of small voids or cracks, has been shown to occur in bone and antler (see chapter 8).

In this thesis I examine some aspects of the time-dependent mechanical behaviour of bone and antler. This task is accomplished in three stages, presented in this and the two subsequent chapters: first, in this chapter, some theoretical background to the modelling of time-dependent behaviour is given. (Due to the theme of this thesis there is some bias towards creep testing and the theory of damage accumulation.) Second, I will introduce some published works on the time-dependent properties of bone and antler. Third, I will present a chapter describing my own experiments and then analyse their results. This third chapter (chapter 4) uses the concepts and equations given in the earlier chapters.

2.2. TIME-DEPENDENT MECHANICAL BEHAVIOUR: VISCOELASTICITY

The theory of viscoelasticity and the terminology that accompanies it are widely used to describe time-dependent materials and their properties. The use (or perhaps I should say abuse, for it is sometimes used for situations and behaviour that appear to be outside its realm of applicability) of this term is widespread within the published

literature on bone. Initially, I too was guilty of this error; at the start of this research I was very willing to attribute all of bone's time-dependent properties to viscoelasticity. To clarify the meaning of some of the viscoelastic terms that will appear later and to enable comparisons to be drawn with other models, this section contains an introduction to the theory of linear viscoelasticity.

The description of a material as viscoelastic is related to comparisons with two well-known idealised materials, the *linear-elastic solid* and the *Newtonian fluid.* To make such a comparison requires knowledge of some basic engineering concepts and quantities. These are concepts such as *stress* and *strain.* (Full derivations and explanations of these quantities were avoided in the previous chapter.) Other concepts more specific to time-dependent materials will also be introduced, for example *creep.*

2.2.1. MATERIAL CLASSIFICATIONS, FORCE-EXTENSION RELATIONSHIPS AND MODELS

In the following sections methods commonly used to model some mechanical responses of viscoelastic materials are introduced. However, I will start with a few of the basics of material classification and force-extension relationships. I will exclude many areas. For example, I give little consideration to mechanical behaviour that is non-linear with respect to variables other than time.

2.2.1.1. THREE IDEALISED MATERIALS: THE LINEAR-ELASTIC SOLID, THE NEWTONIAN FLUID AND THE ELASTIC-PLASTIC SOLID

Materials may be placed in two idealised groups, on which a great deal of classical materials theory is based: first, *linear-elastic solids* (or Hookean materials); and second, *Newtonian fluids.* A third group of materials will be introduced below, the *elastic plastic solids* (or Prandtl bodies). These materials exhibit linear-elastic behaviour up to a certain load and then flow indefinitely. Although this last group of materials is not relevant in a strict theoretical outline of viscoelasticity, it has some bearing on the work presented in the following chapters.

The first material listed above, and perhaps the most commonly understood, is the linear-elastic solid. The amount a linear-elastic solid deforms is directly proportional to the load placed upon it (this is normally accompanied by the caveat that the deformations are infinitesimal). If the load is maintained, so is the resulting deformation; there is no time-dependent behaviour (figures 2.001b and 2.001c). For a uniform rod of this

material, where the load is acting in the line of the rod axis, normalising the load by the area over which it is acting results in a quantity called *stress*.[1] This is conventionally represented by

$$\frac{P}{A_0} = \sigma \qquad (2.001)$$

where P = load (or force), A_0 = initial area and σ = nominal stress. Thus stress will have the units of force per area. (In this study SI units are used and the values of stress are normally expressed in MPa.)

A similar procedure to that applied to load is used for normalising the deformation. In this case the normalising factor is the original length of the rod; this normalisation results in a dimensionless quantity called *strain*,

$$\frac{L - L_0}{L_0} = \varepsilon \qquad (2.002)$$

where L_0 is the initial length of the rod, L is the instantaneous length of the rod (under tensile loading $L > L_0$) and ε is the nominal, or engineering, strain.[2]

The constant of proportionality in the load-deformation relationship can also be normalised. For a linear-elastic solid this quantity is a material property, and is referred to as the *Young's modulus*. This is conventionally given the symbol E defined by the following equation.[3]

$$\frac{\sigma}{\varepsilon} = E \qquad (2.003)$$

The load-deformation response of a linear-elastic solid is a straight line that is retraced exactly on loading, unloading and reloading (figure 2.001d). Thus the energy used to deform the material is totally recovered on unloading. The gradient of this line reflects the value of the material stiffness (from equation 2.003). Materials exhibiting these characteristics are commonly modelled as a *perfect spring*. *K* is usually used to signify the stiffness of such a spring model. Many materials, especially metals subjected to only small strains, behave in a fashion that is adequately modelled by linear-elasticity.

---

[1]When the initial area is used, the quantity is more correctly called the nominal or engineering stress. If the specimen's actual area while loaded is used in the calculation, the value obtained is called the *true stress*, σ_{true}.

[2]So-called *true strain* is expressed as $\delta\varepsilon_{true} = \delta L/L$, and thus $\varepsilon_{true} = \ln(L/L_0)$.

[3]In this thesis I will use the symbol E (sometimes with a sub or super-script) to represent the *material stiffness*, expressed as the ratio of stress to strain. This *material stiffness* should be referred to as Young's modulus if, and only if, the material is a linear elastic solid. However, this nomenclature cannot be avoided when reviewing papers.

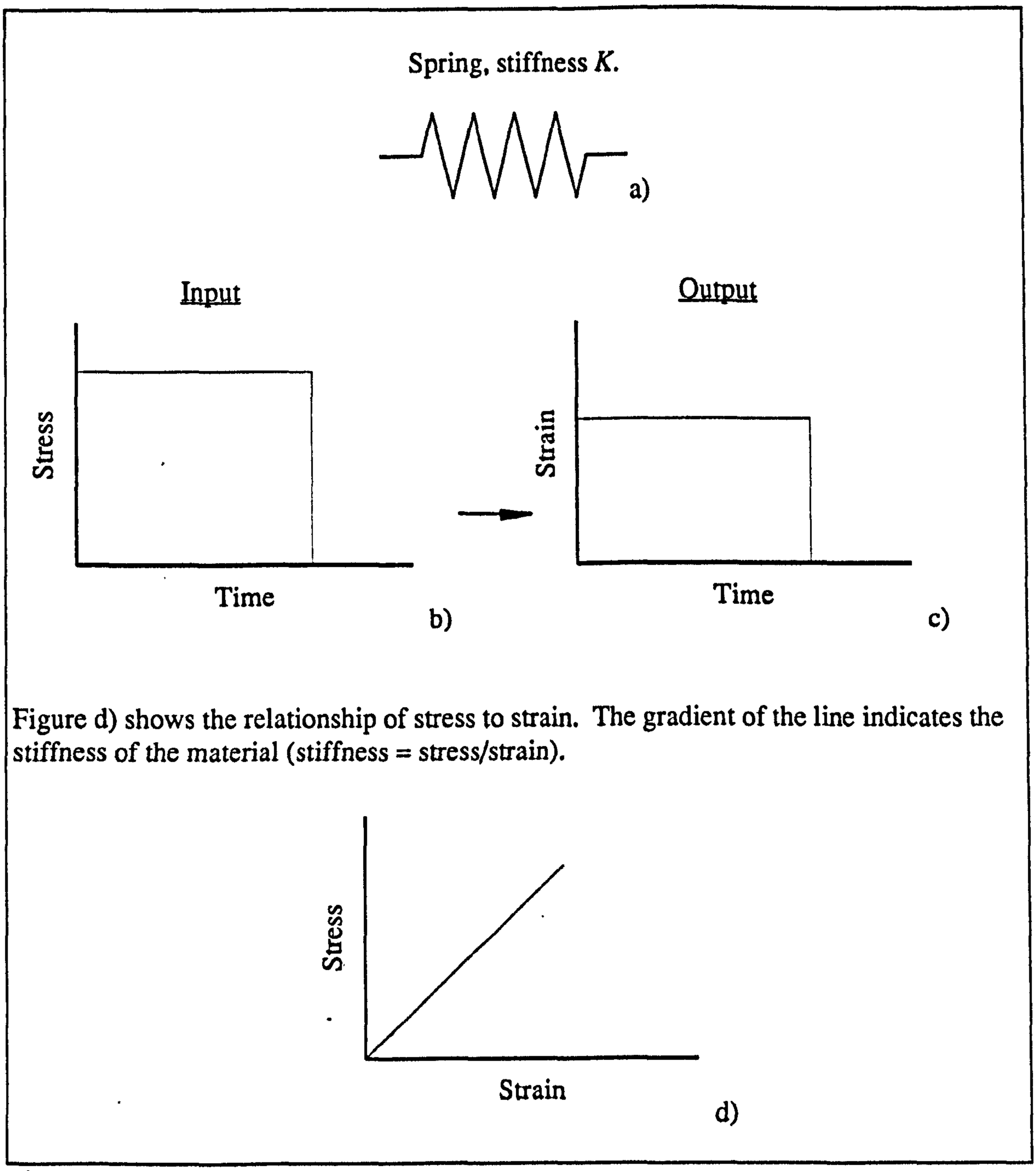

Figure 2.001

The mechanical response of a linear-elastic solid

The second idealised material mentioned above is the Newtonian fluid. For this material, stress is dependent only on the rate of strain, with respect to time, and not on the magnitude of the strain. This relationship is described by the following equation

$$\sigma = \eta \dot{\varepsilon} \qquad (2.004)$$

where σ is the stress, ε is the strain (as defined above) and η is the viscosity. Using standard nomenclature, the strain rate with respect to time is expressed as $\dot{\varepsilon} = d\varepsilon/dt$. The energy used in deforming this material is not recovered on unloading, and restoring the material to its original shape will also consume energy. The mechanical response of

such a material is analogous to that of a dashpot: a cylinder and piston containing a viscous fluid. (This is analogous to filling and emptying a syringe that has its nozzle immersed in water; the quicker you move the plunger, the more force is required.) Figure 2.002 shows the response of such a model to constant stress and strain inputs. For a constant stress input, the response is a constant strain rate $\dot{\varepsilon} = \sigma_0/\eta$, where η represents the viscosity of the element (figure 2.002b and 2.002c). It must be emphasised that η does not represent the viscosity of the fluid in the dashpot (or any physical structure within a material modelled using such dashpot elements) it is used simply to mathematically model the mechanical response. (The graphical representation of the material as a dashpot is simply a tool to aid our understanding of its behaviour.) The element's response to a constant strain is shown in figure 2.002d and 2.002e. In this case the stress response is the product of the viscosity, the strain and a Dirac delta function, $\sigma = \eta\, \varepsilon_0\, \delta(t)$.[4]

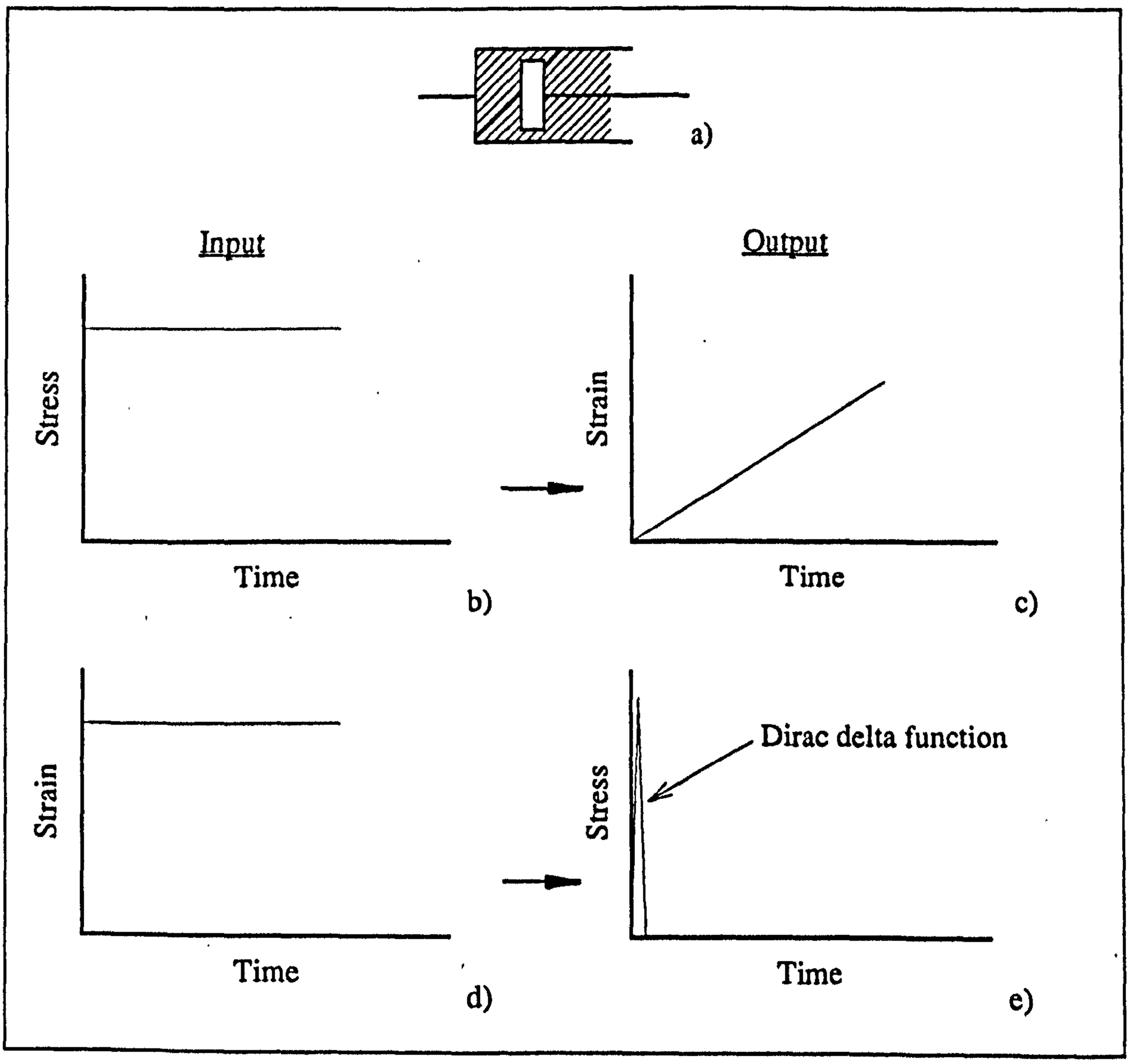

Figure 2.002

The mechanical response of a Newtonian fluid

[4]The Dirac delta function $\delta(t)$ is defined as zero when $t \neq 0$, and infinite for $t = 0$.

Unfortunately real materials do not conform to the two classical descriptions given above. Therefore, other descriptions have been introduced and modifications to the existing ones made. For example some materials may appear to behave like a linear-elastic solid on loading, showing a linear load-deformation response, but on unloading they may not retrace the same line. This demonstrates that they are not elastic. Alternatively a material's mechanical response may depart from its initial linear relationship. A material model that clearly falls into this second category (and thus the first) is the elastic-plastic, or Prandtl, body. This material is not directly related to a study of viscoelasticity. However, its properties are used in modifications to viscoelastic models, for example by Sedlin (1965). Like the two previous idealised materials, the elastic-plastic solid can be interpreted using a mechanical analogy. This analogue uses two elements in series, a spring and a Saint-Venant body. The properties of the spring have been explained above. The Saint-Venant body on its own can be described as a rigid plastic material. When loaded the Saint-Venant body resists deformation until a certain load is reached. At this load it exhibits no further resistance to deformation. This mechanical response is symbolised by a weight resting on a flat surface. The addition of a spring to this model results in a linear load-deformation plot, up to the point of unrestrained deformation. This deformation is described by the following equations:

$$\begin{aligned} &\sigma < \sigma_Y ; \qquad \varepsilon = \frac{\sigma}{E} \\ &\sigma > \sigma_Y ; \qquad \varepsilon \quad \text{indeterminate} \end{aligned} \tag{2.005}$$

where σ_Y is the stress at which the material *yields*, or becomes *plastic*. This representation of a perfectly plastic material is also an idealisation, but is a considerable aid in the representation of many materials, especially metals. Clearly, if the material is loaded and unloaded at levels below that at which plasticity occurs it behaves exactly like a linear-elastic material.

There are other types of behaviour exhibited by real materials. For example they may exhibit some form of time-independent non-linear-elasticity, where the strain is not proportional to the applied stress. Many materials exhibit a degree of time-dependence in their force-extension relationships that falls between that of the linear-elastic solid and the Newtonian fluid. A sub-group of these materials, which are commonly referred to as viscoelastic, is considered in the next section.

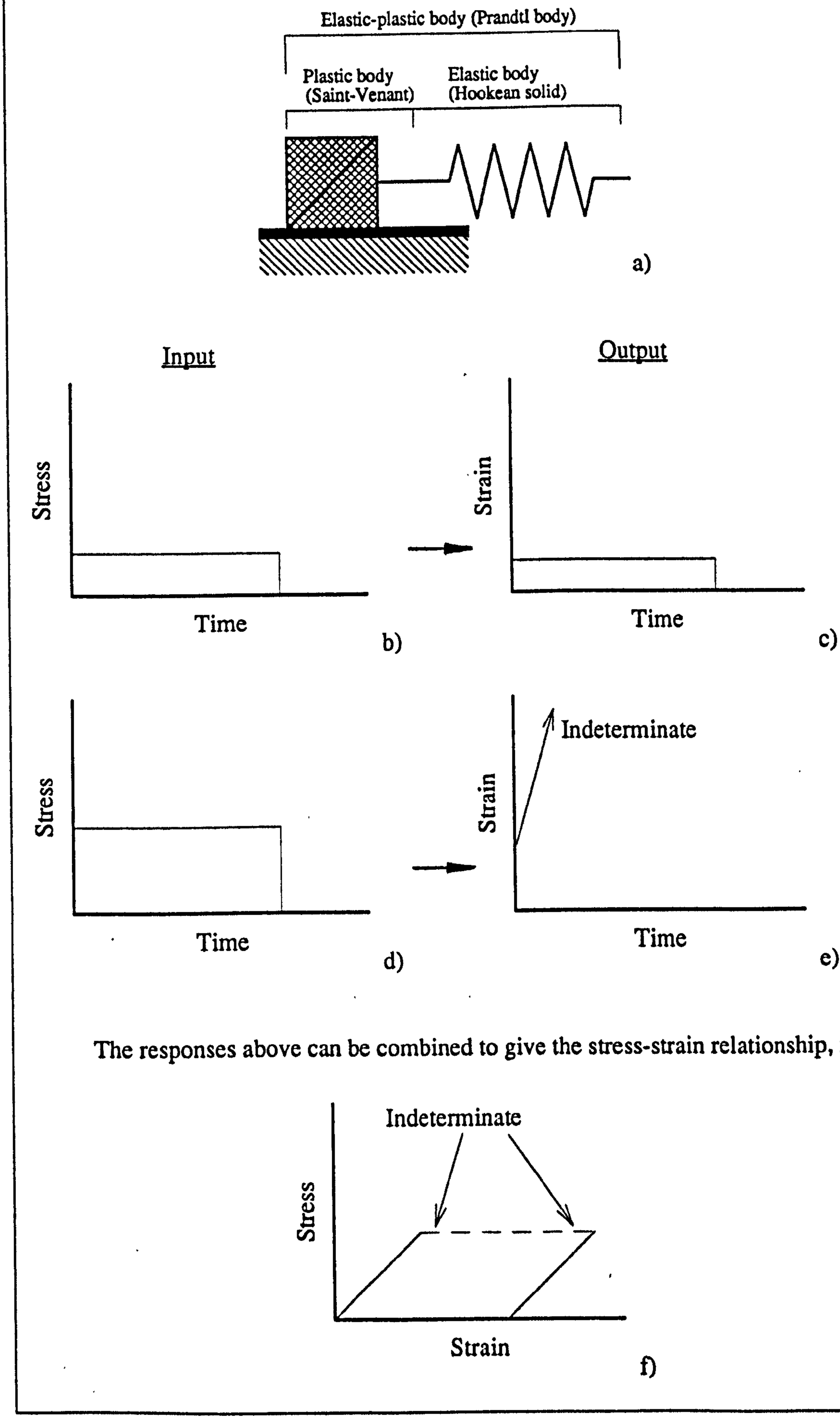

Figure 2.003

The mechanical response of an elastic-plastic, or Prandtl, body

2.2.1.2. MECHANICAL BEHAVIOUR AND STRESS-STRAIN RELATIONSHIPS OF VISCOELASTIC MATERIALS.

In this section I consider viscoelastic materials. These materials can be viewed as falling between linear-elastic solids and Newtonian fluids. Viscoelastic materials deform in a manner that is dependent on both; the magnitude of the applied load and also the rate of its application.

Findley *et al.* (1989) list some phenomena that are common to many viscoelastic materials. This list (with added descriptions) is given below and illustrated in figure 2.004:

a) Instantaneous elasticity: when loaded rapidly the resulting deformation is a function of the applied load only. (Figure 2.004, I.)

b) Creep under constant stress: if the load is maintained, the material exhibits some deformation in addition to the instantaneous one. The extra deformation is dependent on the size and duration of the applied load application. (Figure 2.004, II.)

c) Stress relaxation under constant strain: the load required to maintain a constant deformation decreases with time. (Figure 2.004, III.)

d) Instantaneous recovery: on removal of the load there is an instantaneous decrease in the deformation. The proportion of the total deformation restored depends on how much of the deformation is due to creep. (Figure 2.004, IV.)

e) Delayed recovery: on removal of the load the deformation that remains (after the instantaneous recovery) decreases with time. (Figure 2.004, V.)

f) Permanent set: some deformation is not recovered. (Figure 2.004, VI.)

The deformation of viscoelastic material can be described using functions of stress (or strain) and time. These deformations can be linear or non-linear with respect to stress. For reasons of brevity I concentrate on linear viscoelasticity. In linear viscoelasticity the deformation is directly proportional to the applied stress. However, unlike linear-elasticity, the deformation is also a function of time. Again for reasons of brevity, and relevance, I do not include a description of the effects of viscoelasticity under cyclic loading, or conditions other than those of uniaxial stress.

As in the case of a linear-elastic material, the ratio of stress to strain of a viscoelastic material is a property of that material. However, for viscoelastic materials the period that has elapsed since the application of the load and the type of loading must be considered. It is normal to use one of two quantities to express the changing stress-strain relationship with respect to time. In the first, a step input of stress is assumed to have been applied and in the second, a step input of strain (see figure 2.004). These

relationships are referred to as the *creep compliance* and the *stress relaxation modulus* respectively and defined are below.

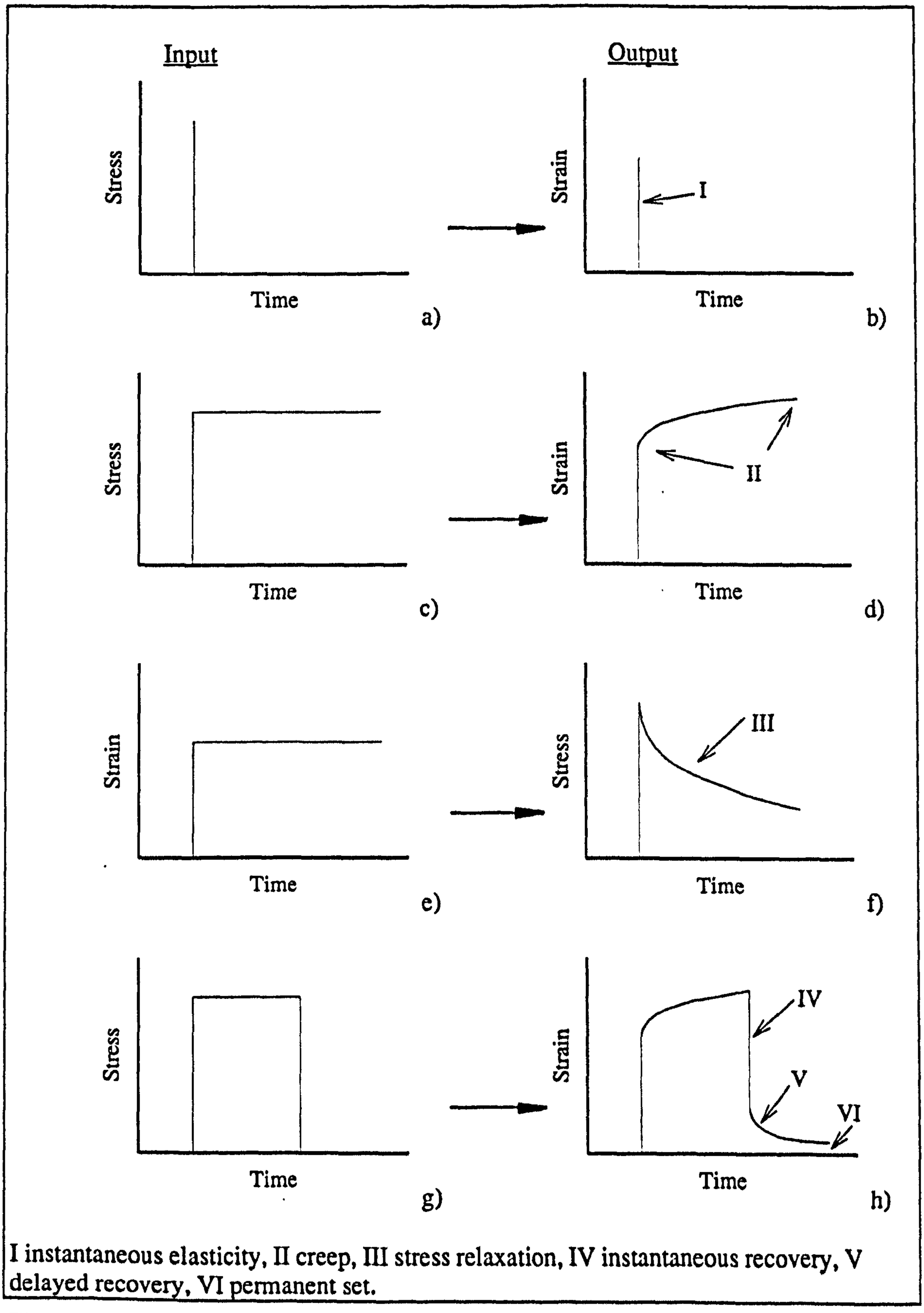

I instantaneous elasticity, II creep, III stress relaxation, IV instantaneous recovery, V delayed recovery, VI permanent set.

Figure 2.004

Phenomena common to many viscoelastic materials

Creep compliance, J(t): when a specimen that has not previously been loaded is subjected to a step input of stress σ_0 H(t), which is maintained over the time under consideration, the ratio of strain to stress is the creep compliance.[5] As viscoelastic materials generally continue to extend under such circumstances the value of the creep compliance increases with time. This can be expressed mathematically as $J(t) = \varepsilon(t)/\sigma_0$, the origin of time being the instant the load was applied.

Relaxation modulus, Y(t): this is the ratio of stress to strain for a specimen subjected to a step increase in nominal strain that is then maintained, ε_0 H(t). At increasing times since the application of the change in length, the load needed to sustain the length change decreases. Thus the ratio of stress to strain decreases with time. A mathematical representation of the quantity is $Y(t) = \sigma(t)/\varepsilon_0$.

2.2.1.3. LINEAR VISCOELASTICITY: SPRING AND DASHPOT MODELS

It was mentioned above that viscoelastic materials fall between the classical linear-elastic solid and Newtonian fluid. Therefore the mechanical response of a viscoelastic material is commonly modelled by combining the models of these two idealised materials: the spring for the linear-elastic material and the dashpot for the Newtonian fluid. The response of these two basic elements to mechanical loading is shown in figures 2.001 and 2.002, above. These two types of element can be combined in various ways in an attempt to mimic the observed mechanical behaviour of viscoelastic materials (as listed above). The simplest models use one of each of the elements arranged either in series or in parallel. The former is the Maxwell (or Voigt) and the latter the Kelvin model. These are illustrated in figures 2.005 and 2.006. Spring and dashpot models do not bear any more than a coincidental relationship to the actual structure of the real material.

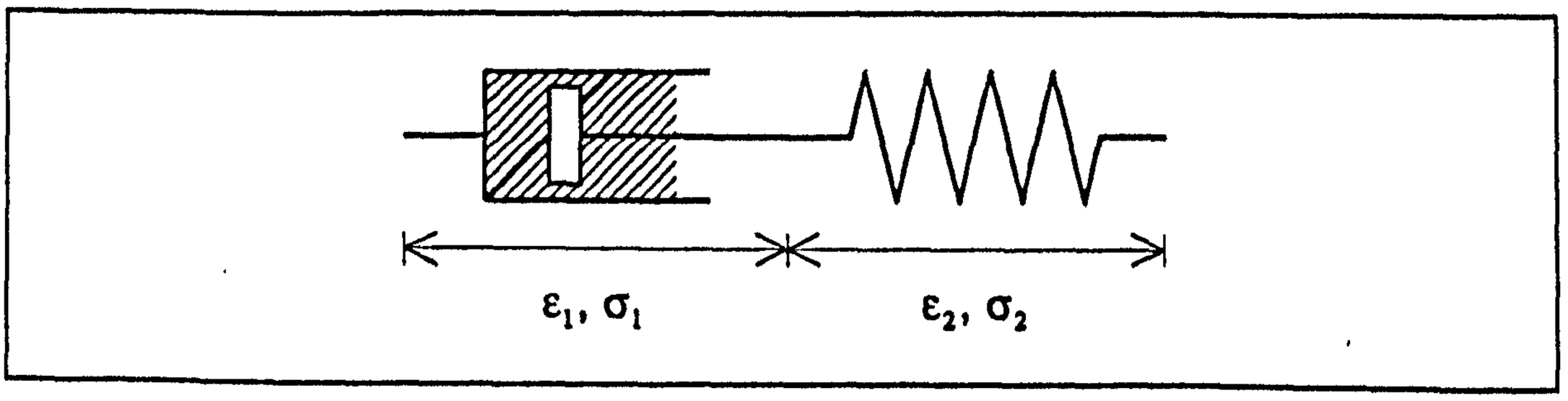

Figure 2.005

The Maxwell model

---

[5] σ_0 H(t) is a method of expressing a step stress input, of magnitude σ_0, applied at t = 0. H(t) is a unit or Heaviside step function. This is more rigorously defined in the glossary.

The mechanical response of the Maxwell model can be deduced by examining the model as a whole and in parts. As the elements are in series the stress applied to the model is expressed as[6]

$$\sigma = K\ \varepsilon_2 = \eta\ \dot{\varepsilon}_1 \qquad (2.006)$$

where K is the stiffness of the spring and η is the viscosity of the dashpot element of the Maxwell model (K and η do no represent any physical component of the real material). The overall strain is the sum of the strain in the two elements[7]

$$\varepsilon = \varepsilon_1 + \varepsilon_2 \qquad (2.007)$$

and the strain rate is

$$\dot{\varepsilon} = \dot{\varepsilon}_1 + \dot{\varepsilon}_2 \qquad (2.008)$$

This equation can be used to establish a relationship of stress and strain (or strain rate) by substituting into it the equations for the individual elements

$$\dot{\varepsilon} = \frac{\dot{\sigma}}{K} + \frac{\sigma}{\eta} \qquad (2.009)$$

From examination of equation 2.009 and the equivalent mechanical model it can be seen that the strain rate, $\dot{\varepsilon}$, under conditions of constant stress (a creep test) will be a constant determined by the stress and the viscosity of the damping element.

From equation 2.009 the strain resulting from a constant stress σ_0, applied to the Maxwell model at $t = 0$ can be derived.

$$\varepsilon(t) = \int \dot{\varepsilon}\, dt = \int \left(\frac{\dot{\sigma}}{K} + \frac{\sigma}{\eta} \right) dt = \frac{\sigma_0}{K} + \frac{\sigma_0}{\eta}\, t \qquad (2.010)$$

This equation indicates that the strain exhibited by the model material will show an instantaneous extension on the application of a load. This extension is due to the elastic

---

[6]The symbol σ will (generally) be used in place of $\sigma(t)$ to represent the stress at time t. This form of symbolism will also be applied to strain, strain rate, stress rate, etc. Values at specific times will be noted by a subscript.

[7]Expansion of this equation, using the definition of $\varepsilon = \Delta L/L_0$, appears to show a possible source of conceptual error. The addition of two strains of 0.01 (one experienced by each element) can not result in an overall strain as large as 0.02, whereas the deformations are additive. So this model should not be interpreted too literally. I have not found an explanation or clarification of this point in the literature.

element. If this load is maintained (a creep test) the value of strain will increase as the time since the application of the load increases. This time-dependence is due to the fluid element. On removal of the load, only the strain due to the elastic element will be recovered. This model is therefore considered to be a poor approximation to the response of many real materials. Recovery of the initial length on removal of the load is modelled by another mechanical analogy, the Kelvin model. This model uses the same elements as the Maxwell model, but in this case they are arranged in parallel. This arrangement is shown in figure 2.006.

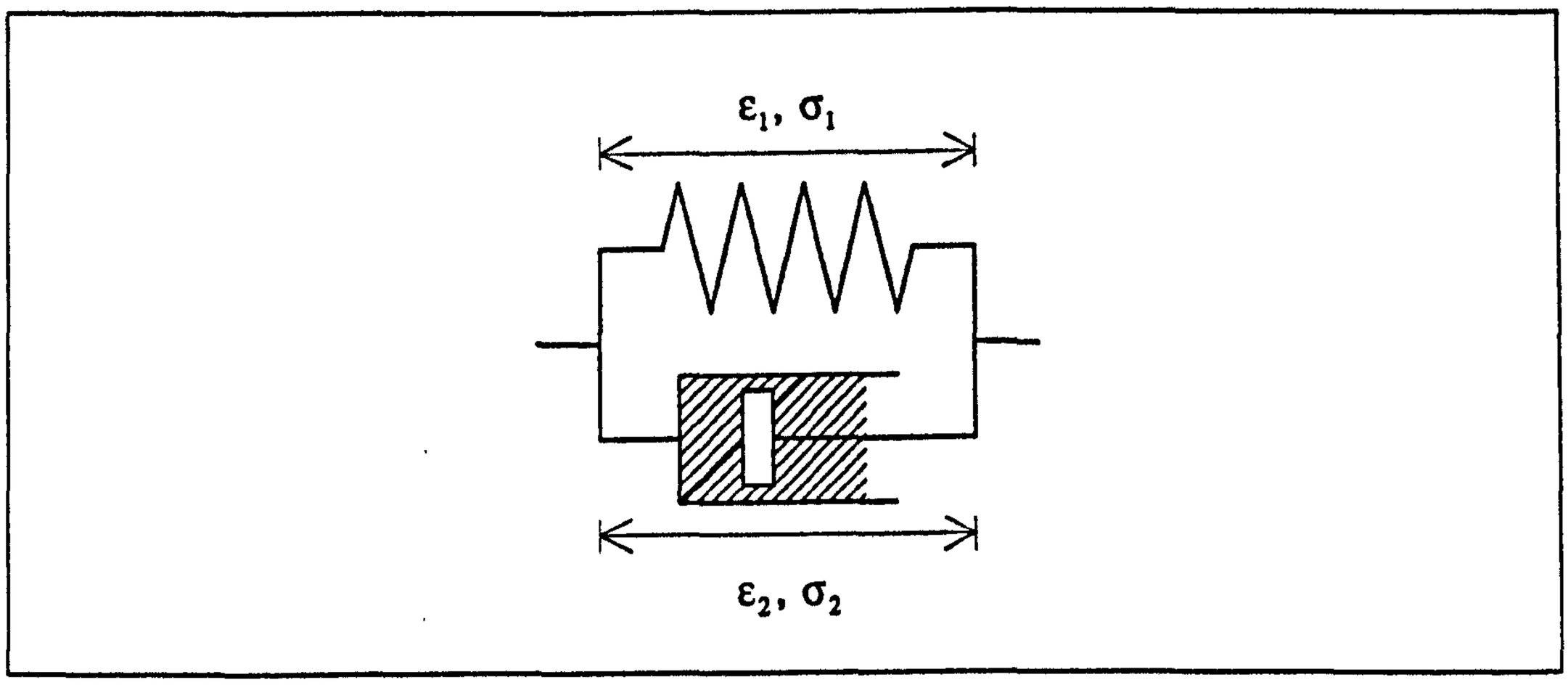

Figure 2.006

The Kelvin model

The mechanical response of the Kelvin model can, like that of the Maxwell model, be simply deduced from examination of the system as a whole and in parts. This time the elements are in parallel, thus their strain is the same as that of the whole model and the stress is divided in some indeterminate way between the elements

$$\sigma = \sigma_1 + \sigma_2 \tag{2.011}$$

By substituting the relationships for the individual elements into this equation a more applicable form is obtained

$$\sigma = K\varepsilon + \eta\dot{\varepsilon} \qquad \text{or} \qquad \dot{\varepsilon} + \frac{K}{\eta}\varepsilon = \frac{\sigma}{\eta} \tag{2.012}$$

Equation 2.012 can be solved for the condition of a creep test (by the method of Laplace transforms outlined in appendix 5) to give

$$\varepsilon = \frac{\sigma_0}{K}\left(1 - e^{-tK/\eta}\right) \tag{2.013}$$

When this model material is subjected to constant load, the strain, ε, will increase, but the rate of this increase, $\dot{\varepsilon}$, decreases until, as t tends towards infinity, the strain tends towards σ_0/K. The strain rate during a creep test can be expressed by differentiating the above equation.

$$\dot{\varepsilon} = \frac{\sigma_0}{\eta} e^{-tK/\eta} = \frac{\sigma_0}{\eta e^{tK/\eta}} \qquad (2.014)$$

The Maxwell and Kelvin models do not exhibit all the features of a viscoelastic material, as listed above. An improvement in the modelling of these features is provided by the Burgers (or four element model). The Burgers model is based on a combination of a Maxwell and Kelvin model in series. The total strain at time, t, will be the sum of the strain in the three elements, where the spring and dashpot in the Kelvin model are considered as one element. The strain response to a step load applied at t = 0, which is then removed some time later, is similar to that shown in figure 2.004h. Obviously there is a multitude of other possible combinations of springs and dashpots.

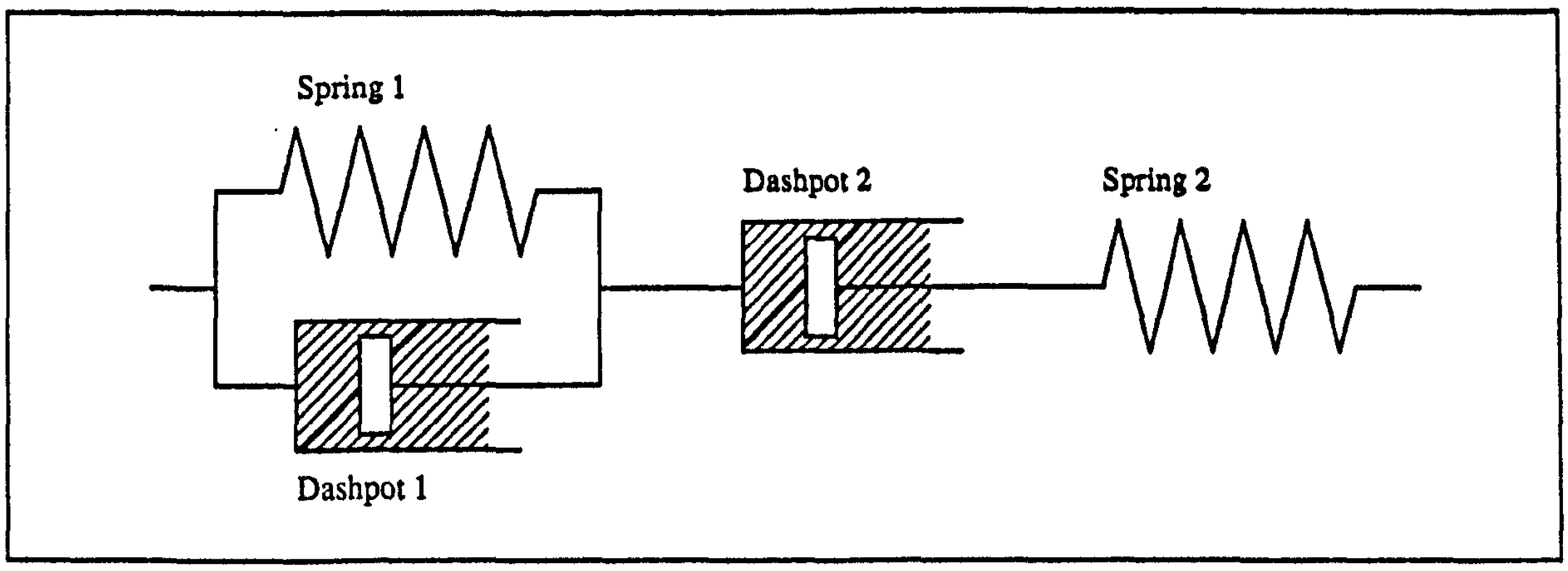

Figure 2.007

Burger's model

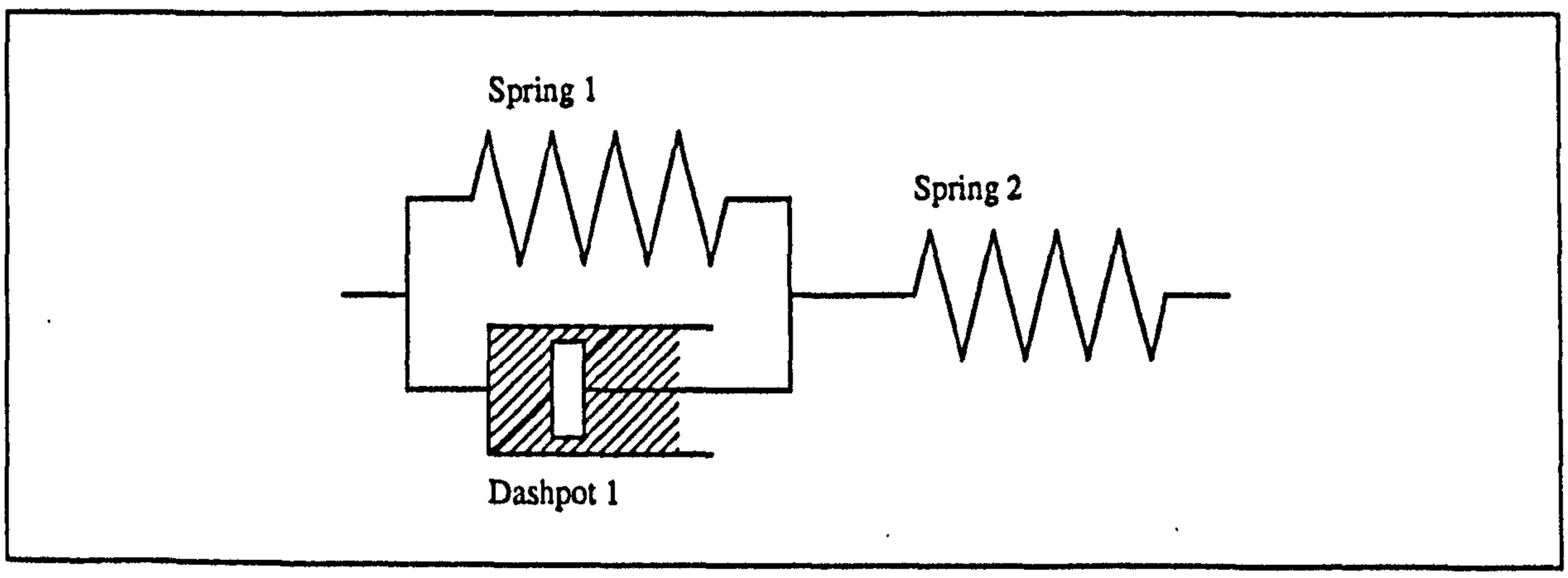

Figure 2.008

The three-element model

A mechanical analogue that has been used by a number of authors to describe or model the behaviour of bone is the three-element solid (sometimes called a Bingham body).[8] This is a Burger's model without the second dashpot. Thus the three-element solid shows no permanent deformation, and attains a constant extension under load. The three-element model is represented in figure 2.008 (above).

Viscoelastic materials were described above as those that exhibit behaviour somewhere between a fluid and a solid. The distinction of a material as a fluid or a solid is based on the material's behaviour under constant load. If the extension of the specimen becomes (or tends towards) a constant value, it is considered to be a solid. However, if the material continues to extend and the rate of this extension becomes constant, then the material is considered a fluid. Thus the two basic models above are commonly referred to as the Kelvin solid and the Maxwell fluid. Likewise the Burger's model is a fluid and the three-element model a solid. The three-element model is often referred to as the standard viscoelastic solid.

The representation of viscoelastic materials by mechanical models, especially the graphical forms, is a considerable aid to understanding the concepts of viscoelasticity. However, the mechanical models need to be interpreted mathematically to enable relationships of stress, strain and time to be determined and solved for the specific loading conditions and time under consideration. This was done for the simple Maxwell and Kelvin models for the conditions of a creep test (equations 2.009 and 2.010; 2.012 and 2.013). Once this has been done the stress-strain response of the model can be compared with that of the real material and the coefficients in the equation (for example K and η) can be determined. These coefficients although not related to any specific components in the real material help to characterise it and differentiate it from other materials. However, for the more complicated models, which may be needed to describe a real material, such graphical representation is more cumbersome and a more direct and generally applicable mathematical approach is required. Such an approach is described in the next section.

---

[8]This has been used to model bone by a number of workers. For example: Sedlin (1965), Tennyson *et al.* (1972) and Tanabe *et al.* (1991a, b and c).

2.2.1.4. REPRESENTATION OF LINEAR VISCOELASTICITY BY MATHEMATICAL METHODS: CONSTITUTIVE EQUATIONS AND THEIR LAPLACE TRANSFORMS.

A numerical representation of linear viscoelastic behaviour for multiple step or non-step changes in stress or strain may be obtained by a number of mathematical approaches. One of these is based on the solution of the constitutive equations, giving the stress-strain-time relationships for step changes in stress or strain (creep compliance and stress relaxation functions). These are then combined using Boltzmann's superposition principle. This approach enables the stress-strain-time relationship to be determined for a material subjected to a number of step changes, or differentiable non-step changes, of stress or strain. Another method is to obtain the solution of the equations for the relevant loading conditions directly. The application of this second approach is relatively easy for a limited range of loading conditions. The solution of the equations for step changes in stress or strain (as required by Boltzmann's superposition principle) and ramp changes by this second approach is briefly outlined below. Further explanation of these approaches can be found in appendix 5 and in books such as that by Findley *et al.* (1989). Boltzmann's superposition principle is not outlined in this thesis; because the relationships for the loading conditions of interest here are obtained directly.

The constitutive equation of a linear viscoelastic material may be expressed as a linear function of stress, strain and their time derivatives (as in equations 2.009 and 2.012). This can be represented by the following general expression, where $\sigma = \sigma(t)$ (the variation of stress with time) and $\varepsilon = \varepsilon(t)$ (the variation of strain with time). The dots indicate the derivatives with respect to time.

$$f(\sigma, \dot{\sigma}, \ddot{\sigma}, \dddot{\sigma}, \ldots ; \quad \varepsilon, \dot{\varepsilon}, \ddot{\varepsilon}, \dddot{\varepsilon}, \ldots) = 0 \tag{2.015}$$

This is commonly expressed in the more compact form of

$$P\sigma = Q\varepsilon \tag{2.016}$$

where P and Q are linear differential operators, with respect to time. These can be expressed as

$$P = \sum_{r=0}^{a} p_r \frac{\partial^r}{\partial t^r} , \qquad Q = \sum_{r=0}^{b} q_r \frac{\partial^r}{\partial t^r} \tag{2.017}$$

The differential operator form of this equation is expressed in the following way

$$P\sigma = p_0\sigma + p_1\dot{\sigma} + p_2\ddot{\sigma} + \ldots + p_a\frac{\partial^a\sigma}{\partial t^a}$$

$$= q_0\varepsilon + q_1\dot{\varepsilon} + q_2\ddot{\varepsilon} + \ldots + q_b\frac{\partial^b\varepsilon}{\partial t^b} = Q\varepsilon \qquad (2.018)$$

There is no loss of generality if $p_0 = 1$. Taking the Laplace transform of the above equation results in the following equation.[9]

$$\hat{P}(s)\,\hat{\sigma}(s) = \left(p_0 + p_1 s + p_2 s^2 + \ldots + p_a s^a\right)\hat{\sigma}(s)$$

$$= \left(q_0 + q_1 s + q_2 s^2 + \ldots + q_b s^b\right)\hat{\varepsilon}(s) = \hat{Q}(s)\,\hat{\varepsilon}(s) \qquad (2.019)$$

where s is the transform variable. From this equation a more simple form of relationship can be expressed as follows

$$\frac{\hat{Q}(s)}{\hat{P}(s)} = \frac{\hat{\sigma}(s)}{\hat{\varepsilon}(s)} \qquad (2.020)$$

For the linear case p_r and q_r are, by definition, independent of stress and strain. By substituting the correct values into these terms a description of the idealised viscoelastic properties can be obtained. If the relationship of strain to some stress input (for which there is a Laplace equivalent, for example the step stress input of an ideal creep test) is required the equation is arranged as an expression of strain in the functional domain. The Laplace equivalent of the stress input is then substituted into the equation. The penultimate stage is to rearrange the equation so that an inverse Laplace transformation can be performed. This inverse transformation will produce a function relating stress to strain in the normal time domain, for the specific input considered. The stress, or strain, inputs that can be examined using this method are limited, but include ramp, step, sinusoidal, impulse and exponential functions. In this thesis the step and ramp functions are the most relevant. Some stress-strain relationships of the three-element solid, commonly used to model bone, that have been obtained by the method of Laplace transforms are presented below. In appendix 5 the method of Laplace transforms is

---

[9]The application of a Laplace transform moves the differential equation from the time domain into a functional domain, in which it is expressed as an algebraic relationship. Use of algebraic manipulations permit the application of an inverse transformation, which returns the problem to the time domain, but in such a way that the original differential equation has been solved.

explained in more depth, and examples of the solution methods used for the three-element solid are given together with more general solutions.

The following expression is for the strain exhibited by a three-element solid during a creep test. The creep stress, σ_0, is applied by a step function at t = 0.

$$\varepsilon(t) = \sigma_0 \left[\frac{1}{q_1} \left[\frac{q_1}{q_0} \left(1 - e^{-q_0 t/q_1} \right) \right] + \frac{p_1}{q_1} e^{-q_0 t/q_1} \right] \qquad (2.021)$$

Consequently the creep compliance, $\varepsilon(t)/\sigma_0$, is expressed as

$$J(t) = \left[\frac{1}{q_0} \left(1 - e^{-q_0 t/q_1} \right) + \frac{p_1}{q_1} e^{-q_0 t/q_1} \right] \qquad (2.022)$$

or

$$J(t) = \frac{1}{q_0} \left[1 + \frac{q_1 - p_1 q_0}{q_1} e^{-q_0 t/q_1} \right] \qquad (2.023)$$

The procedure by which equation 2.023 was obtained is given in appendix 5. A similar procedure can be used to find the relaxation modulus. That process results in the following equation

$$Y(t) = \left[q_0 - q_0 e^{-t/p_1} + \frac{q_1}{p_1} e^{-t/p_1} \right] \qquad (2.024)$$

The creep compliance and relaxation modulus are related, being two manifestations of the same behaviour. Their relationship is explained in more depth in appendix 5. However, in this thesis the behaviour under constant load is of more interest than that under constant deformation.

If, instead of a step input, stress is applied at a constant rate $\dot{\sigma}$ the stress at any time is described by $\sigma(t) = \dot{\sigma} t$, where t is the time measured from the start of the load application. This situation describes one form of idealised tensile test. In this case the strain response, again determined by using Laplace transforms is

$$\varepsilon(t) = \dot{\sigma} \left[\frac{t}{q_0} + \left(\frac{p_1}{q_0} - \frac{q_1}{q_0^2} \right) \left(1 - e^{-q_0 t/q_1} \right) \right] \qquad (2.025)$$

or

$$\varepsilon(t) = \frac{\sigma(t)}{q_0} + \dot{\sigma} \left(\frac{q_0 p_1 - q_1}{q_0^2} \right) \left(1 - e^{-q_0 t/q_1} \right) \qquad (2.026)$$

Clearly for a fixed stress rate the deviation from the time-independent linear response, $\varepsilon(t) = \sigma(t)/q_0$, increases with time. (The value of the term in the extreme right hand parentheses changes from 0 at $t = 0$, to 1 at $t = \infty$.) Similarly if some value of stress is considered, σ_1, then the strain exhibited by this solid on reaching this stress level is dependent on the stress rate, in the following way,

$$\varepsilon_1 = \frac{\sigma_1}{q_0} + \dot{\sigma}\left(\frac{q_0 p_1 - q_1}{q_0^2}\right)\left(1 - e^{\beta}\right) \qquad (2.027)$$

Where $\beta = {}^{-q_0 \sigma_1}\!/_{\dot{\sigma} q_1}$ (by virtue of $t = \sigma_1/\dot{\sigma}$). As the stress rate increases the term within the extreme right hand parenthesis of equation 2.027 will tend towards zero. Thus at high stress rates the viscoelastic component of the deformation is very small. Obviously the exact proportion of the deformation that is time-dependent under such fixed conditions will be governed by the relative magnitude of the constants p_n and q_n.

The Laplace transform approach can be used to obtain the stress response of a three-element solid under the conditions of another idealised tensile test, in which the strain is applied at a constant rate. During such a test $\varepsilon(t) = \dot{\varepsilon}\, t$.

$$\sigma(t) = \varepsilon(t)\, q_0 - \dot{\varepsilon}\,(q_0 p_1 - q_1)\left(1 - e^{-t/p_1}\right) \qquad (2.028)$$

In this case the higher the strain rate, the closer the relationship is to the time-independent one. Statements regarding the departure from linearity, similar to those made for the constant stress rate test above, can also be applied to this equation.

2.2.2. CLOSING REMARKS ON VISCOELASTICITY

In section 2.2.1.1 three idealised materials were introduced, the elastic solid, the Newtonian fluid and the elastic-plastic solid. Their force-extension relationships were then described. By using combinations of the first two materials, models of the behaviour of linear viscoelastic material were produced. This was done both graphically and mathematically. Mathematical models approximating the loading conditions used for the experiments described in chapter 4 were provided for a three-element solid.

The rationale behind the graphical and mathematical models should be considered when applying them. They only describe the observed mechanical response of the material. They do not provide any information on the processes involved. The spring and dashpot models are only an aid to comprehension. They should not (generally) be identified with structures within the material.

One important aspect of a more realistic force-extension relationship that viscoelasticity does not model is failure of the material. The models given above contain no upper time, stress or strain limit. Thus they imply that a material could reach an infinite length if loaded for an infinite time and still support the load regardless of its magnitude. This lack of failure behaviour reduces their ability to describe real materials. Another implication of viscoelasticity is that, given time, a material will regain its original mechanical properties. This similarly reduces viscoelasticity's ability to describe some real materials. Therefore, an area of study has developed around the time-dependent failure and mechanical deterioration of materials. When a specimen is subjected to constant load such failure is referred to as *creep-rupture*. This topic and the related one of *damage*, or deterioration of the material, are examined in the next section.

2.3. TIME-DEPENDENT BEHAVIOUR: CREEP-RUPTURE

Creep-rupture is the name given to failures that occur under conditions of prolonged constant load. There are few common domestic occurrences of this type of failure. However, one example could be the failure of blu-tack™: under certain conditions an object, such as a poster mounted on a wall by means of blu-tack™, may fall down. The material may fail internally leaving one part attached to the poster and one to the mounting-surface.

In this section I introduce some approaches used to analyse creep-rupture failures. First, I introduce an approach based on the examination of the correlations between measured quantities relating to the creep behaviour. I then introduce an approach that has evolved over the last 35 years: *continuum damage mechanics*.

2.3.1. CREEP-RUPTURE: GENERAL CORRELATION APPROACHES

In the opening lines of a chapter on creep-rupture analysis Conway (1967) states:

> Since rupture represents the terminal point on a creep curve and hence must be considered as one of the component parts of the overall creep process it is not too illogical to consider that the rupture point must be related to various preceding portions or characteristics of the creep curve.

Conway says that much thought has been given to the identification of such relationships. According to Conway one of the most common of these relationships is one of inverse proportionality between the time-to-rupture, t_R, and the secondary creep rate. Figure 2.009 shows a generalised creep curve and the nomenclature used in this thesis.

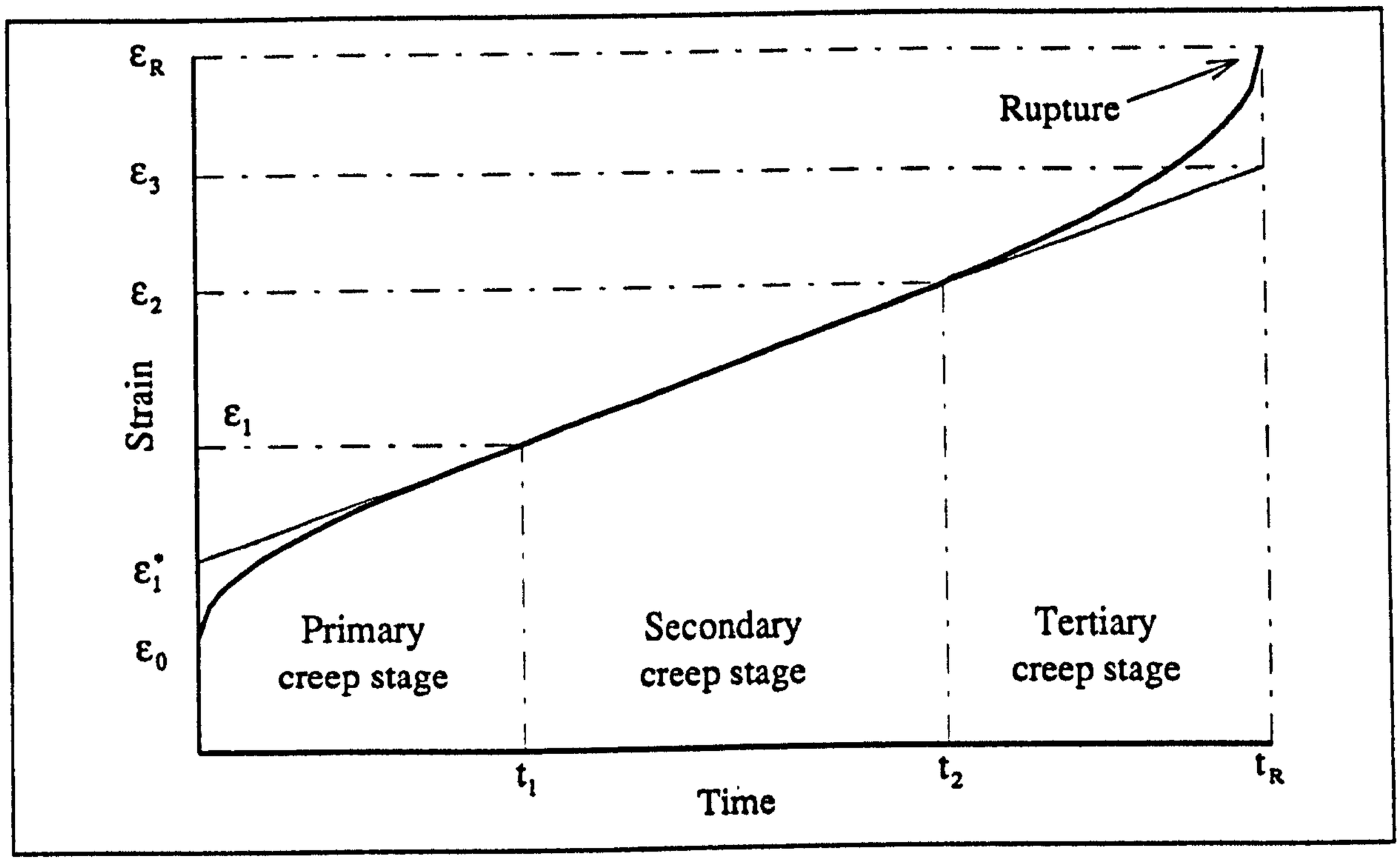

Figure 2.009

A generalised creep-rupture curve and accompanying nomenclature

The creep rate during the secondary stage, $\dot{\varepsilon}_{1^*\rightarrow 3}$, can be expressed in various ways, one of which is

$$\dot{\varepsilon}_{1^*\rightarrow 3} = \frac{\varepsilon_3 - \varepsilon_1^*}{t_R} \qquad (2.029)$$

Conway says if the quantity $\varepsilon_3 - \varepsilon_1^*$ remains constant for tests conducted using different levels of stress, the time-to-rupture is inversely proportional to the creep rate during the second stage of the process. This relationship can be expressed in logarithmic form as follows

$$\ln(\dot{\varepsilon}_{1^*\rightarrow 3}) = \ln(\varepsilon_3 - \varepsilon_1^*) - \ln(t_R) \qquad (2.030)$$

Thus a plot of this relationship will exhibit a linear line of slope minus one. From the references Conway cites it appears that such a relationship had been observed for iron and some steels by 1931. Conway refers to other relationships that have been found on the examination of experimental data. His work also contains a table of suggested correlations for use with stress rupture data. This is reproduced here, and his recommendations are followed in the analysis of my own data.

In the following sections (especially 2.3.3) I will examine some approaches to analysis of creep-rupture data that have some theoretical basis rather than the almost random search for a correlation displayed here.

Ordinate	Abscissa	Remarks	
Log (stress)	Log (time-to-rupture)	at constant temperature	*a*
Stress	Log (time-to-rupture)	at constant temperature	*b*
Log (stress)	Log (elongation at rupture)	at constant temperature	*c*
Elongation at rupture	Log (time-to-rupture)	at constant temperature or at constant stress	*d*
Log (stress)	Log (secondary creep rate)	at constant temperature	*e*
Log (stress)	Log (average creep rate)[10]	at constant temperature	*f*
Log (time-to-rupture)	Log (average creep rate)	at constant temperature	*g*
Temperature	Log (time-to-rupture)	at constant stress; should be linear	*h*
Stress	Temperature	Isochronal plot with time-to-rupture as a parameter	*i*
Log (time-to-rupture)	Reciprocal of absolute temperature	at constant temperature	*j*

Table 2.001 After Conway (1967)

Commonly used correlations of creep rupture data

2.3.2. CREEP-RUPTURE: PARAMETRIC APPROACHES

Conway (1967) discusses three parametric approaches to the correlation of creep-rupture data. These are the Larson and Miller, the Dorn, and the Manson and Haferd parameters. These will not be examined here as their derivation is dependent on data obtained at different temperatures. Conway states that

> The basis of the Larson-Miller parameter is a series of linear but non-parallel constant stress lines on a plot of log t_R versus (1/T). Further these lines have a common point of intersection at a value of (1/T) equal to zero. On the other hand the Dorn parameter is based on these same constant stress lines being linear and parallel with of course no point of intersection. And finally the development of the Manson-Haferd parameter is founded on the fact that these isostress lines are linear, or nearly so , on a plot of log t_R versus T. Also these lines are non-parallel and have a common point of intersection at some value of T but not necessarily at T = 0.

Conway points out that all three of the above functional relationships cannot be exhibited by a material simultaneously under the same test conditions. Such an approach would be of little value in the study of (normal) bone, as properties are only significant at one temperature.

---

[10]Conway describes the average creep rate as 'rupture elongation/rupture time'.

2.3.3. CREEP-RUPTURE: THE CONCEPT OF DAMAGE

It is widely agreed that it was Kachanov (1958) who introduced the concept of *damage* in the study of creep (Leckie and Hayhurst; 1974, Lorrain and Loland; 1983 and Krajcinovic, 1984). However, some authors report that this approach is similar to previous theories. In this section I concentrate on this concept's relevance to creep-rupture under uniaxial stress conditions, its importance in other situations is examined later. There is a large body of literature and a considerable area of study built on the original concept. A great deal of this research is concerned with composite materials, notably fibre composites and particulate ones, such as concrete.

Kachanov's 1958 paper entitled *Time of the Fracture Process Under Creep*, and the appropriate sections of two of his later books *The Theory of Creep* (1960) and *Introduction to Continuum Damage Mechanics* (1986) appear to use the same approach and nomenclature.[11] I use Kachanov's approach as explained in *The Theory of Creep*, as the basis for my explanation, because it has some advantages over the more common method of explanation used in more recent literature (which normally start with the idea of damage accumulation). However, I have altered some of Kachanov's original nomenclature. For example his use of F for area will be changed to A, and I will generally refer to failure under creep conditions as rupture and the associated process as the rupture process. Some other forms of explanation, and the application of this approach to the study of bone and antler will be discussed later.

Kachanov presented his ideas in four sections; 'life to rupture', 'failure as a result of unlimited flow', 'life to failure in the presence of crack formation' and 'the failure localisation effect'. The first part points out that creep-rupture can take a number of forms. For example, the elongation at rupture can be large with the failure occurring at a neck, indicating a large degree of flow. Kachanov (in translation) refers to such a rupture process as being 'viscous' in character. At the other end of the spectrum the elongation may be small, indicating a brittle rupture process. Many materials fall into the region of behaviour between these two extremes. Kachanov states that the mode of failure can vary for the same material at the same temperature, according to the stress level. To help distinguish between the theory of purely brittle rupture process and that for a combination of brittle and ductile failure, I examine them separately. I will now present his theory for a ductile, then brittle, and finally a combined rupture process. I have attempted to emphasise those points that will be used later in the analysis of my creep data.

---

[11]The original paper is in Russian, so was *The Theory of Creep*. However the book was later translated into English by Bishop and edited by Kennedy.

2.3.3.1. RUPTURE AS A RESULT OF UNLIMITED FLOW

Kachanov points out that the ideas he uses to form a model of the time-to-rupture by an idealised ductile process are not original, but follow those of Hoff (1953). Similarly the approach given here is not mine but an explanation of that used by Kachanov. The main concept is one of unlimited creep flow in a rod subjected to a constant tensile force, P. Rupture occurs when the cross-sectional area of the specimen is reduced to zero under a constant load. Because the creep strains are large, Kachanov says the elastic strains can be disregarded. The condition of incompressibility expressed by the following equation, is assumed.

$$A\,L = A_0\,L_0 \tag{2.031}$$

where;

A_0 = Initial cross-sectional area (at time t = 0)

L_0 = Initial length (at time t = 0)

A = Instantaneous cross-sectional area (at time t)

L = Instantaneous length (at time t)

Kachanov says the strain rate, $\dot{\varepsilon}$, can be expressed by equation 2.032. This expression, when integrated, produces what is normally referred to as the true strain, thus I will use the symbol $\dot{\varepsilon}_{true}$.

$$\dot{\varepsilon}_{true} = \frac{1}{L}\,\frac{dL}{dt} \tag{2.032}$$

(At this point the explanations in the two books (Kachanov (1960) and (1986)) diverge, but merge again at the solution to equation 2.037.) Kachanov (1960) states that 'in problems of this type, strains accumulated in the primary stage, can usually be ignored'. He then gives the following equation

$$\frac{1}{L}\,\frac{dL}{dt} = B_1\left(\frac{P}{A}\right)^m \tag{2.033}$$

where P is the load and A the area of the rod at the time considered. Thus the quantity in the parentheses is the stress. This stress is normally called the true stress, σ_{true}, as the area used in its calculation is the cross-sectional area possessed by the material at the time considered. (Equation 2.033 can also be expressed as $\dot{\varepsilon}_{true} = B_1\,\sigma_{true}^{\,m}$.) By substitution of equation 2.031 into equation 2.033 the following relationship is obtained.

$$\frac{1}{L}\,\frac{dL}{dt} = B_1\left(\frac{P\,L}{A_0\,L_0}\right)^m \tag{2.034}$$

Thus

$$\int \frac{1}{L^{m+1}} \, dL = \int B_1 \left(\frac{P}{A_0 L_0} \right)^m dt \tag{2.035}$$

This in turn gives the following equation

$$\frac{-1}{m L^m} = B_1 \left(\frac{P}{A_0 L_0} \right)^m t + C \tag{2.036}$$

Substitution of the initial conditions; $L = L_0$ at $t = 0$ and using the definition of the initial stress $\sigma_0 = P/A_0$ (as load is constant in a creep test), results in the following relationship,[12]

$$B_1 \sigma_0{}^m m t = 1 - \left(\frac{L_0}{L} \right)^m \tag{2.037}$$

The time-to-rupture, t_1, is defined as the time when the cross sectional area has been reduced to nothing, and therefore the material has no strength. Because in this analysis local effects such as necking are ignored and incompressibility is assumed, this definition of rupture is equivalent to the length becoming infinite, $L \rightarrow \infty$. Thus the term on the right hand side of the equality sign (in equation 2.037) tends towards unity, resulting in the following condition at rupture,

$$t_1 = \frac{1}{m B_1 \sigma_0{}^m} \tag{2.038}$$

where t_1 is the time-to-rupture by this idealised ductile mode. This equation can be rearranged to give,

$$B_1 \sigma_0{}^m = \frac{1}{m t_1} \tag{2.039}$$

Kachanov (1986) points out that the left hand side of the equation can be expressed as the initial creep strain rate, $\dot{\varepsilon}_0 = B_1 \sigma_0{}^m$. It must be remembered that the primary creep stage is not considered, (thus I interpret this 'initial' creep stain rate to be that in the secondary creep stage) so $t_1 = 1/(m \dot{\varepsilon}_0)$. This equation is akin to equation 2.029 above. Equation 2.039 implies that the time-to-rupture is inversely proportional to the initial strain rate under constant load. Thus plotting such a relationship on a graph with logarithmic axes will produce a slope with a gradient of -1 (in the same way as equation 2.030). The higher the initial creep rate, the shorter the time that the material can sustain the applied load without failing.

---

[12]The translation contains a typographical error in this equation L being represented as 1.

Having obtained a value of time-to-rupture for this process, some predictions of the material's behaviour before rupture can be obtained. Substitution of the right hand side of equation 2.039 into equation 2.037 results in the following relationship

$$\frac{1}{m\,t_1}\,m\,t = 1 - \left(\frac{L_0}{L}\right)^m \qquad \text{or} \qquad 1 - \frac{t}{t_1} = \left(\frac{L_0}{L}\right)^m \tag{2.040}$$

Due to the assumption of incompressibility (equation 2.031) this can be re-written in terms of the ratio of the instantaneous to the initial cross sectional area of the specimen.

$$\frac{A}{A_0} = \left(1 - \frac{t}{t_1}\right)^{1/m} \tag{2.041}$$

If m > 1 the rate of change of the cross-sectional area will tend towards infinity as the specimen approaches rupture. Kachanov represents this in a diagram that is reproduced here as figure 2.010. As the value of m increases a greater majority of the decrease in the specimen's cross-section occurs in a later and shorter period of the specimen's life.

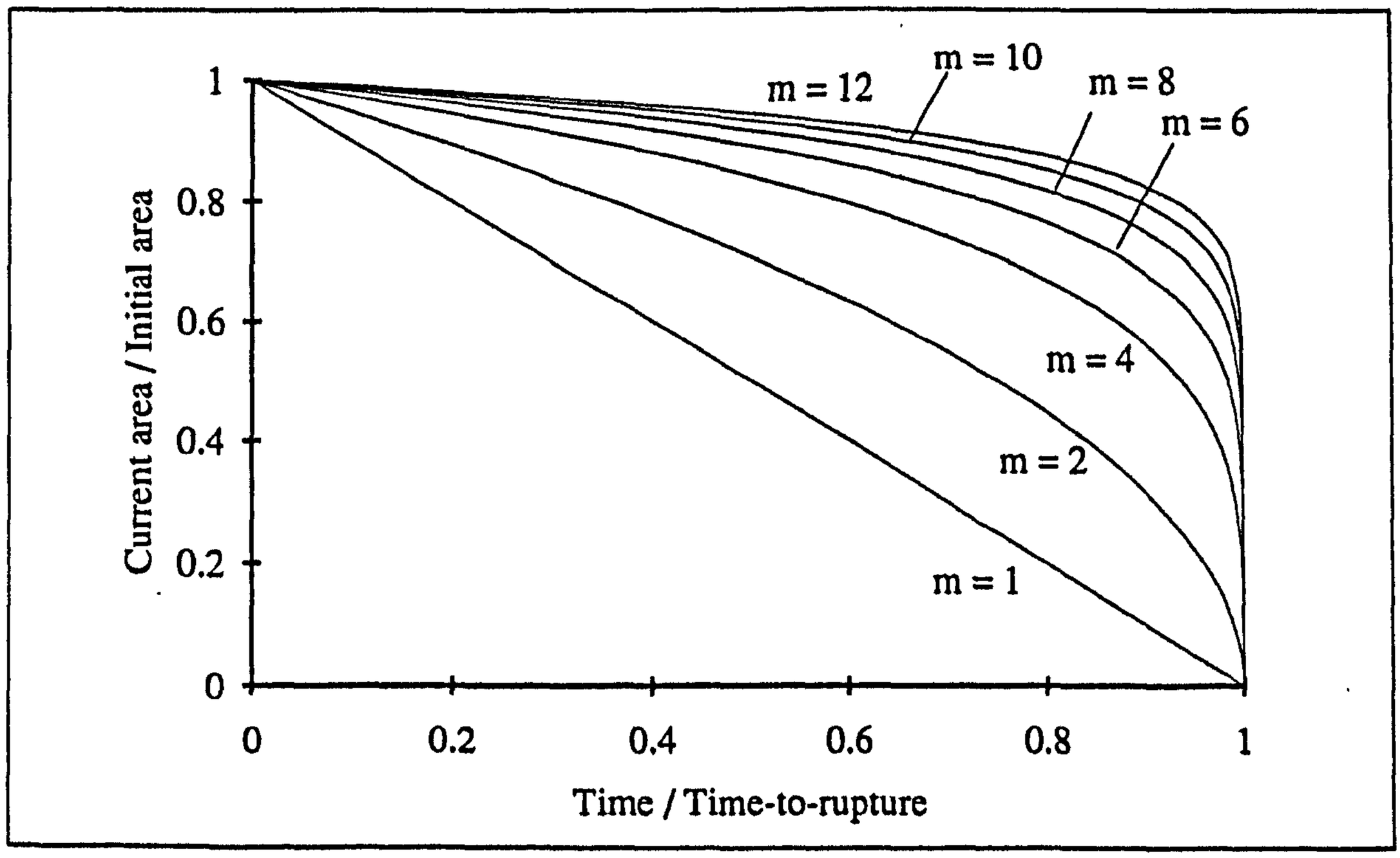

Figure 2.010 After Kachanov (1960). (Substituted of m into equation 2.041)

The variation of the relationship of normalised specimen area and normalised time-to-rupture for the conditions of *viscous* creep

I would like to point out that the above graph can be interpreted in a different way by considering the implications of the assumption of incompressibility. Rearranging equation 2.031 gives

$$\frac{A}{A_0} = \frac{L_0}{L} = \frac{1}{\varepsilon + 1} \tag{2.042}$$

This equation can also be expressed as

$$\varepsilon = \frac{A_0}{A} - 1 \qquad \text{or} \qquad \varepsilon + 1 = \lambda \tag{2.043}$$

where $\lambda = L/L_0$. Thus the nominal strain and nominal strain rate change: both approach infinity as the material approaches rupture. (This is observed to a limited extent experimentally in the tertiary stage of some creep tests.) Extending my interpretation, the equations presented here suggest that as the value of m increases the difference between the secondary and tertiary creep stages become more marked. If m = 1 there is no difference in the creep rate throughout the test. However, an extremely high value of m would indicate a low initial creep rate and a sharp transition to a high creep rate just before failure.

In the next section I return to Kachanov's work, and examine his model for failure by a purely brittle process.

2.3.3.2. TIME-TO-RUPTURE IN THE PRESENCE OF CRACK FORMATION: THE PURELY BRITTLE CASE

Kachanov (1960) points out that the ideas based on flow, given above, do not cover the full range of failures experienced in practice. He describes his equivalent of this section as an attempt to determine the theoretical time-to-rupture, allowing for embrittlement. The argument is based on the development of faults, or flaws, in the material. (Kachanov was considering metals in his work.) He states that 'it can be assumed that the development of crack formation is initiated immediately on loading'. He also states that two stages of progressive failure can be distinguished, these he describes as a 'gradual crack propagation (stable stage)' and a 'significantly accelerated (unstable) failure'. Kachanov continues by stating that the stable stage usually covers most of the life of the specimen. He interprets the rupture process as 'one of crack formation, superimposed on a background of increasing creep strains'.

Kachanov assumes that the propagation of cracks does not, on average, influence the creep strain. He puts forward two supporting arguments for this. The first is based on the granular structure of metal, and in the second he points out that 'if the cracks exert any influence on creep, the creep curves, upon which the creep equations are based, reflect the overall effect'. The introduction of a variable to represent these cracks is performed in the following way.[13]

---

[13]Kachanov used the symbol ψ_0 for continuity at failure I have changed this to ψ_R, to remove possible confusion with the nomenclature for conditions at t = 0.

> We shall characterize the damage by some scalar factor ψ, which can take the value $1 \geq \psi \geq 0$; this will be referred to as the soundness. Initially, in the absence of damage, the soundness $\psi = 1$; as time t passes, soundness ψ decreases. At low ψ values the random nature of the damage becomes unstable and major cracks arise in weak areas. From this point of view the moment of failure should be regarded as occurring at some value $\psi_R > 0$; let us then agree to speak of the failure localisation effects. In the basic variant of the theory we shall assume that at the moment of brittle failure $\psi = 0$. In other words, localisation of crack formation in the final stages of failure is not considered (similarly, in Hoff's theory the appearance of a neck is disregarded).

The quantity signified by ψ is now more commonly referred to as *continuity* (and $(1 - \psi) = D$, or ω, as damage). Kachanov continues by introducing the following equation,[14]

$$\frac{d\psi}{dt} = - B_2 \left(\frac{\sigma_{true}}{\psi} \right)^n \tag{2.044}$$

where $B_2 > 0$, $n \geq 0$ are constants. The ratio σ_{true}/ψ can be interpreted as an *effective stress* (the load divided by the apparently undamaged cross-sectional area). If there is no creep in the bar the measured cross-sectional area will be constant $A = A_0$ and thus $\sigma_{true} = \sigma_0$. The next stage is to integrate equation 2.044:

$$\int \psi^n \, d\psi = - \int B_2 \, {\sigma_{true}}^n \, dt \tag{2.045}$$

$$\frac{\psi^{n+1}}{(n+1)} = - B_2 \, {\sigma_{true}}^n \, t + C \tag{2.046}$$

The initial conditions, $\psi = 1$ at $t = 0$, give a value of $C = 1/(n + 1)$. As this is the purely brittle case, $\sigma_{true} = \sigma_0$, this results in the subsequent prediction of the time-to-rupture, at which point $\psi_R = 0$.[15]

$$t_2 = \frac{1}{B_2 \, (n+1) \, {\sigma_0}^n} \tag{2.047}$$

Where t_2 is the time-to-rupture by this idealised purely damage, or brittle, process. Equation 2.047 is very similar to equation 2.038, the equation for an idealised ductile process.

The situation described above is, like the purely ductile process, an unrealistic one for many materials. However, it approximates to many situations (in a similar way to how Young's modulus is used to describe a material's stiffness).

---

[14]Kachanov (in translation) uses the symbol σ_{max}, but states that when the bar is under tension $\sigma_{max} = P/A$.

[15]This is equivalent to $D = 1$. In a later section I will examine a suggestion within more recent literature that failure occurs at a lower level of damage.

2.3.3.3. TIME-TO-RUPTURE IN THE PRESENCE OF CRACK FORMATION: COMBINED DUCTILE AND BRITTLE FAILURE

In this section the rupture of a material by the brittle processes will be examined again, but in this case the possibility of its coexistence with creep deformation is considered. The time-to-rupture in this situation will be expressed as a function of the time-to-rupture by both the idealised ductile and brittle failure processes, t_1 and t_2. This more general case where creep occurs and thus the cross sectional area changes, is obtained by use of equations 2.041 and 2.044, which are shown in the appropriate form below.

$$\frac{A}{A_0} = \left(1 - \frac{t}{t_1}\right)^{1/m} \qquad \text{and} \qquad \frac{d\psi}{dt} = -B_2 \left(\frac{P}{A\psi}\right)^n \tag{2.048}$$

Thus by substitution

$$\frac{d\psi}{dt} = -B_2 \left(P \Big/ \left(A_0 \left(1 - \frac{t}{t_1}\right)^{1/m} \psi\right)\right)^n \tag{2.049}$$

Alternatively this can be expressed as

$$\frac{d\psi}{dt} = -B_2 P^n A_0^{-n} \psi^{-n} \left(1 - \frac{t}{t_1}\right)^{-n/m} \tag{2.050}$$

This results in the following expression

$$\int \psi^n \, d\psi = \frac{\psi^{n+1}}{(n+1)} = \int -B_2 P^n A_0^{-n} \left(1 - \frac{t}{t_1}\right)^{-n/m} dt + C \tag{2.051}$$

To enable its solution the above equation can then be expressed as

$$\frac{\psi^{n+1}}{(n+1)} = \int -B_2 P^n A_0^{-n} U^{-n/m} \frac{dt}{dU} \, dU + C \tag{2.052}$$

where

$$\left(1 - \frac{t}{t_1}\right) = U \qquad \text{and thus} \qquad \frac{dU}{dt} = -\frac{1}{t_1} \tag{2.053}$$

so equation 2.052 becomes

$$\frac{\psi^{n+1}}{(n+1)} = \frac{-B_2 P^n A_0^{-n} \left(1 - \frac{t}{t_1}\right)^{1-\frac{n}{m}}}{\left(1 - \frac{n}{m}\right)} (-t_1) + C \tag{2.054}$$

This may be written in a slightly different form as

$$\psi^{n+1} = \frac{t_1\, m\, (n+1)\, B_2\, P^n\, A_0^{-n} \left(1 - \frac{t}{t_1}\right)^{\frac{m-n}{m}}}{(m-n)} + C \qquad (2.055)$$

Using the initial conditions $\psi = 1$ at $t = 0$, (remembering t_1 is a constant derived in equation 2.038) gives

$$C = 1 - \frac{t_1\, m\, (n+1)\, B_2\, P^n\, A_0^{-n}}{(m-n)} \qquad (2.056)$$

Thus

$$\psi^{n+1} = \frac{t_1\, m\, (n+1)\, B_2\, P^n\, A_0^{-n} \left(1 - \frac{t}{t_1}\right)^{\frac{m-n}{m}}}{(m-n)} - \frac{t_1\, m\, (n+1)\, B_2\, P^n\, A_0^{-n}}{(m-n)} + 1 \qquad (2.057)$$

As $B_2\, (n+1)\, P^n\, A_0^{-n} = B_2\, (n+1)\, \sigma_0 = 1/t_2$ equation 2.057 above can be rearranged such that

$$\psi^{n+1} = \frac{t_1\, m \left(1 - \frac{t}{t_1}\right)^{\frac{m-n}{m}}}{t_2\, (m-n)} - \frac{t_1\, m}{t_2\, (m-n)} + 1 \qquad (2.058)$$

If it is assumed that at rupture the soundness or continuity of the material is zero, $\psi = 0$, the time-to-rupture by a combination of ductile and brittle processes, t_3 can be calculated:

$$-\, t_2\, (m-n) = t_1\, m \left(1 - \frac{t_3}{t_1}\right)^{\frac{m-n}{m}} - t_1\, m \qquad (2.059)$$

Equation 2.059 may be rearranged to give the following equation

$$\left(\frac{-\, t_2\, (m-n) + t_1\, m}{t_1\, m}\right)^{\frac{m}{m-n}} = 1 - \frac{t_3}{t_1} \qquad (2.060)$$

Hence

$$\frac{t_3}{t_1} = 1 - \left(1 - \frac{(m-n)}{m}\, \frac{t_2}{t_1}\right)^{\frac{m}{m-n}} \qquad (2.061)$$

where

t_1 = time-to-rupture by a purely ductile creep process

t_2 = time-to-rupture by a purely brittle creep process

t_3 = time-to-rupture some combination of ductile and brittle creep processes.

Kachanov then uses the condition that $t_3 \leq t_1$ to obtain an upper limit of the stress range for which this equation should be considered valid. The expression he gives for this upper limit can be obtained in the following way. The first step is to substitute the equations for the time-to-rupture under the brittle and ductile processes back into equation 2.061, so that it contains only stress terms on the right hand side and time on the left:

$$\frac{t_3}{t_1} = 1 - \left(1 - \frac{(m - n)}{m} \frac{m B_1 {\sigma_0}^m}{B_2 (n + 1) {\sigma_0}^n}\right)^{\frac{m}{m-n}} \tag{2.062}$$

As $t_3 \leq t_1$ (and thus $t_3/t_1 \leq 1$) the above equation can be expressed as

$$1 \geq 1 - \left(1 - \frac{(m - n)}{m} \frac{m B_1 {\sigma_0}^m}{B_2 (n + 1) {\sigma_0}^n}\right)^{\frac{m}{m-n}} \tag{2.063}$$

Therefore

$$0 \leq \left(1 - \frac{(m - n) B_1 {\sigma_0}^m}{B_2 (n + 1) {\sigma_0}^n}\right)^{\frac{m}{m-n}} \tag{2.064}$$

Taking the values of the initial stress in the numerator and the denominator together and removing the power term (outside the parentheses), this becomes

$$0 \leq \left(1 - \frac{(m - n) B_1}{B_2 (n + 1)} {\sigma_0}^{m-n}\right) \tag{2.065}$$

Subtracting 1 from each side of this equation, then multiplying both sides by -1 (and changing the inequality sign accordingly) results in the following equation:

$$1 \geq \frac{(m - n) B_1}{B_2 (n + 1)} {\sigma_0}^{m-n} \tag{2.066}$$

This may also be expressed in the following way:

$$\sigma_0 \leq \left(\frac{B_2 (n + 1)}{(m - n) B_1}\right)^{1/(m-n)} = \bar{\sigma}_0 \tag{2.067}$$

This equation (2.067) can be viewed as giving the upper bound of the range of stresses for which some degree of brittle fracture will occur and the lower bound of the stress range where specimens will exhibit only ductile rupture. Using evidence from experimental data, Kachanov says that $m \geq n$, and produces a pictorial description of the time-to-rupture at various stresses. The solid line represents the solution to equation 2.061. This diagram is redrawn in figure 2.011. Above a certain stress level, $\bar{\sigma}_0$, purely ductile rupture occurs. In that case the stress level and time-to-rupture relationship is represented in figure 2.011 by line *AB* (equation 2.038). Kachanov points out that embrittlement becomes increasingly important at lower stresses, and the curve

approaches the straight line *DE*. The constants B_2 and n (which describe the line *DE* via equation 2.047) can be determined experimentally from creep-rupture tests performed at low stresses.

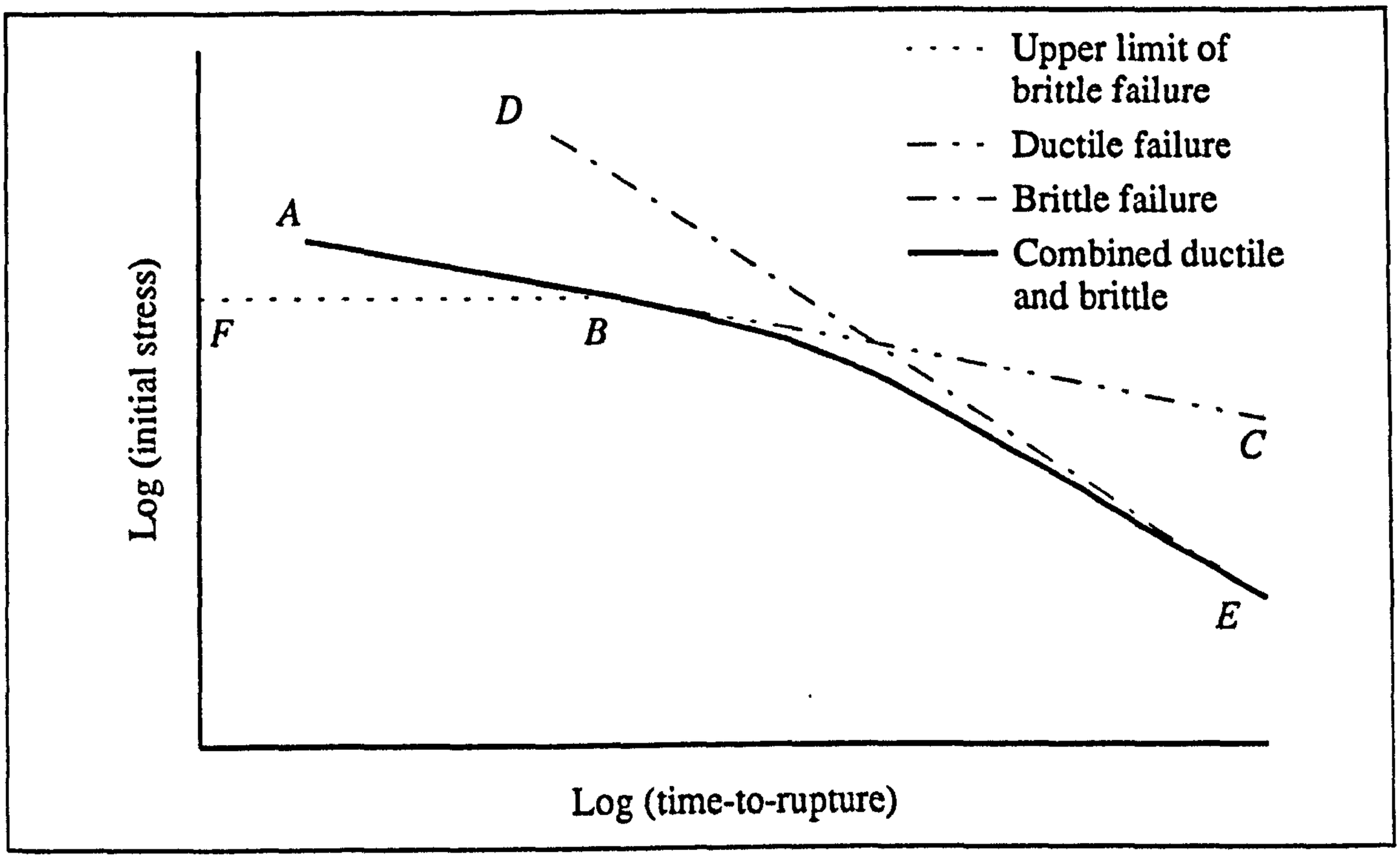

Figure 2.011 After Kachanov (1960)

The predicted time-to-rupture for a specimen subjected to a constant load

Returning to equation 2.050, if n = m then the equation can be expressed in the following way:

$$\frac{d\psi}{dt} = - B_2 P^n A_0^{-n} \psi^{-n} \left(1 - \frac{t}{t_1}\right)^{-1} \qquad (2.068)$$

Kachanov moves straight to equation 2.076. However, I will include some stages of the calculation. Using the same approach as above equation 2.068 can be expressed as

$$\frac{\psi^{n+1}}{n+1} = \int - B_2 P^n A_0^{-n} \left(1 - \frac{t}{t_1}\right)^{-1} dt + C \qquad (2.069)$$

which after integration and multiplying both sides by (n + 1) gives

$$\psi^{n+1} = (n + 1)\, t_1\, B_2\, P^n\, A_0^{-n} \ln\left(1 - \frac{t}{t_1}\right) + C_2 \qquad (2.070)$$

The condition that the continuity is unity at zero time permits the evaluation the constant. The logarithmic term becomes zero giving

$$1^{n+1} = 0 + C_2 \qquad (2.071)$$

Thus at rupture ($t = t_4$) where the continuity is zero, $\psi_R = 0$, and the expression is

$$0 = (n + 1)\, t_1\, B_2\, P^n\, A_0^{-n} \ln\left(1 - \frac{t_4}{t_1}\right) + 1 \qquad (2.072)$$

This equation is simplified using equation 2.038 (with n = m):

$$0 = \frac{t_1}{t_2} \ln\left(1 - \frac{t_4}{t_1}\right) + 1 \qquad (2.073)$$

which can be re-expressed as

$$-\frac{t_2}{t_1} = \ln\left(1 - \frac{t_4}{t_1}\right) \qquad (2.074)$$

So

$$e^{-\frac{t_2}{t_1}} = 1 - \frac{t_4}{t_1} \qquad \text{or} \qquad t_4 = t_1\left(1 - e^{-\frac{t_2}{t_1}}\right) \qquad (2.075)$$

Kachanov gives the expression in the non-simplified form, also stating that the expression enclosed by the parentheses is less than or equal to unity:

$$t_4 = t_1\left(1 - e^{-\frac{B_1 m}{B_2 (m+1)}}\right) \qquad (2.076)$$

where t_4 is the time-to-rupture under creep conditions if n = m. Kachanov says that in this case the rupture is always brittle, for it is determined by the condition $\psi = 0$ and occurs at the same strain.

The prediction that the failure strain is constant if n = m can be shown by manipulation of Kachanov's equations. The method I have used is as follows. First equation 2.040 can be rewritten to give the relationship between the length at rupture and the time-to-rupture, given here as

$$L_4 = L_0\left(1 - \frac{t_4}{t_1}\right)^{-1/m} \qquad (2.077)$$

Equation 2.076 can be rearranged to give the ratio of time-to-rupture in this specific case of a combined ductile and brittle process where m = n, and substituted into 2.077:

$$L_4 = L_0\left(1 - \left(1 - e^{\frac{-B_1 m}{B_2 (m+1)}}\right)\right)^{-1/m} \qquad (2.078)$$

This equation simplifies to

$$L_4 = L_0\, e^{\frac{B_1}{B_2 (m+1)}} \qquad (2.079)$$

Using the equation for nominal strain I thus obtained the relationship

$$\varepsilon_4 = \frac{L_4 - L_0}{L_0} = \frac{L_0 e^{\frac{B_1}{B_2 (m+1)}} - L_0}{L_0} = e^{\frac{B_1}{B_2 (m+1)}} - 1 \qquad (2.080)$$

Kachanov says, when referring to metals, that if m = n, the metal is stable; the experimental curve of log(initial stress) and log(time-to-rupture) (figure 2.010) does not sharply change its direction. This statement appears to be almost stating the obvious, if the logarithmic forms of equations 2.038 and 2.047 are considered. The examination of these equations in logarithmic form, when n = m, also suggests that $B_1 m = B_2 (n + 1)$. I base this statement on the simple logic that as the lines have the same slope, these equations will have to be equal for a combined process to exist. If they are not equal the specimen will fail at the time predicted by the occurrence of a single process.

2.3.3.4. THE FAILURE LOCALISATION EFFECT

So far it has been assumed that $\psi = 0$ at rupture ($\psi_R = 0$). However, if $\psi_R > 0$, the time-to-rupture by a purely brittle process would be shorter. Kachanov expresses this shorter time as

$$t_5 = \left(1 - \psi_R^{n+1}\right) t_2 \qquad (2.081)$$

He continues by giving a modified form of equation. This is not considered relevant here for Kachanov says (in translation)

> For the problem of a bar in uniform tension, the localisation effect is of no interest, since it is essentially equivalent to the choice of another value for coefficient A [B_2 in the nomenclature of this thesis].

By localisation Kachanov appears to be drawing comparisons with the necking seen in the tensile tests of ductile metals. If this is the case, it suggests that damage is concentrated in one region of the specimen. This would result in a lower overall average measure of damage (or a higher measure of continuity). Thus there could be an argument for regarding continuity as being greater than zero at the time of failure. This argument is considered in section 2.3.3.8.

2.3.3.5. COMMENTS ON KACHANOV'S APPROACH: ODQVIST'S CORRECTION

In the early stages of the mathematical model (section 2.3.3.1) Kachanov made the assumption that the strain accumulated during the primary creep stage could be ignored. Odqvist (1966) presents an amended form of Kachanov's theory, in which he takes account of this extension. Kachanov (1986) says 'the agreement with the experimental data is better'. The log(stress) versus log(time-to-rupture) plot Odqvist gives is very similar to Kachanov's original plot, but it is slightly displaced towards the time axis. Thus the amended theory predicts the earlier occurrence of rupture. I will derive my explanation of *Odqvist's correction* mainly from Kachanov's (1986) version, as this is more easily related to what I have presented above.

The strain accumulated during the primary creep stage is taken into account, by using the 'instantaneous plastic strain':

$$\varepsilon_{pri} = B_3 \sigma^p \tag{2.082}$$

Both the constant and the power terms are greater than zero. The secondary creep rate is described by the following equation (it is basically the same as equation 2.033, although expressed in another form. The nomenclature has been changed to avoid confusion.)

$$\dot{\varepsilon}_{sec} = B_4 \sigma^q \tag{2.083}$$

Thus, the total strain rate exhibited by the material is

$$\dot{\varepsilon} = \frac{d}{dt} B_3 \sigma^p + B_4 \sigma^q \tag{2.084}$$

Kachanov (1986) then says that according to experimental data, as a rule, $q > p$. He changes the variable in the equation and then 'after some transformation' obtains equation 2.096. I will include some stages of this operation. The first stage is to rearrange equation 2.084 into the following form.

$$B_4 = \sigma^{-q} \left(\dot{\varepsilon} - \frac{d}{dt} B_3 \sigma^p \right) \tag{2.085}$$

Since the quantity σ_0 is a constant the initial strain rate is expressed by

$$\dot{\varepsilon}_0 = B_4 \sigma_0^q \tag{2.086}$$

Equation 2.085 can be expressed, by multiplying both sides by σ_0^q, as

$$\dot{\varepsilon}_0 = \sigma_0^q \sigma^{-q} \left(\dot{\varepsilon} - \frac{d}{dt} B_3 \sigma^p \right) \tag{2.087}$$

There are a number of relationships that are needed to convert this equation into the desired form. These are given below (some of them have appeared previously):

$$\frac{\sigma}{\sigma_0} = \lambda \tag{2.088}$$

$$\dot{\varepsilon} = \frac{1}{L}\frac{dL}{dt} = \frac{1}{\lambda}\frac{d\lambda}{dt} \tag{2.089}$$

$$\frac{d}{dt}\left(B_3 \sigma^p\right) = \left(p B_3 \sigma^{p-1}\right)\frac{d\sigma}{dt} \tag{2.090}$$

This last differential term in equation 2.090 can be rearranged (due to equation 2.088) to give

$$\frac{d\sigma}{dt} = \sigma_0 \frac{d\lambda}{dt} \tag{2.091}$$

Equation 2.088 can be rewritten as

$$\sigma^{p-1} = {\sigma_0}^{p-1} \lambda^{p-1} \tag{2.092}$$

Thus equation 2.090 can be restated as

$$\frac{d}{dt}\left(B_3 \sigma^p\right) = \left(p B_3 {\sigma_0}^{p-1} \lambda^{p-1}\right)\sigma_0 \frac{d\lambda}{dt} \tag{2.093}$$

or

$$\frac{d}{dt}\left(B_3 \sigma^p\right) = \left(p B_3 {\sigma_0}^p\right)\lambda^{p-1} \frac{d\lambda}{dt} \tag{2.094}$$

Substituting equations 2.088, 2.089, 2.090, 2.091 and 2.092 into equation 2.087 gives

$$\dot{\varepsilon}_0 = \lambda^{-q}\left(\lambda^{-1}\frac{d\lambda}{dt} - p\,\varepsilon_0\,\lambda^{(-1+p)}\frac{d\lambda}{dt}\right) \tag{2.095}$$

where $\varepsilon_0 = B_3 {\sigma_0}^p$, or the 'instantaneous plastic strain' at $t = 0$.[16] Equation (2.095) is the same as

$$\dot{\varepsilon}_0\, dt = \left(\lambda^{-q-1} - p\,\varepsilon_0\,\lambda^{(-1+p-q)}\right) d\lambda \tag{2.096}$$

Kachanov (1986) then integrates this equation with the initial condition $\lambda = 1$ at $t = 0$, and arrives at the formula

$$\left(1 - \lambda^{-q}\right) - \beta\left(1 - \lambda^{-q+p}\right) = \frac{t}{t_1} \tag{2.097}$$

---

[16] $\varepsilon_0 = B_3 {\sigma_0}^p$ is the same as equation 2.082 when $\sigma = \sigma_0$. I have used the same nomenclature, ε_0, in figure 2.009 and consider the quantities to be comparable, although in this section true strain is considered and in the figure nominal strain.

where the $\beta = \left(\frac{q\,p}{q-p}\right)\varepsilon_0 \geq 0$ and recalling that $t_1 = (m\,\dot{\varepsilon}_0)^{-1}$ (section 2.3.3.1)[17]

The time-to-rupture under purely ductile conditions predicted by this method (which contains Odqvist's correction for the primary creep stage[18]), t_{1P}, can be derived by assuming that the material becomes infinitely long at rupture. Taking $\lambda \rightarrow \infty$ reduces equation 2.097 to the following one:

$$t_{1P} = t_1\,(1 - \beta) \tag{2.098}$$

Due to the condition placed on β it can be seen that the inclusion of the primary creep stage has reduced the predicted rupture time from that predicted by Kachanov's original theory, $t_{1P} < t_1$.

The next case considered is that of combined ductile and brittle rupture. For this condition I will return to equation 2.044, and again it will be integrated. However, in this case the stress term is not independent of time.[19]

$$\frac{d\,\psi}{d\,t} = -\,B_2\left(\frac{\sigma_{true}}{\psi}\right)^n \tag{2.099}$$

This can be rearranged to give

$$\int \psi^n\,d\,\psi = -\int B_2\,\sigma_{true}{}^n\,d\,t \tag{2.100}$$

Remembering that in equation 2.100, $\sigma_{true} = f(t)$, so the integration of the right hand side can not be immediately solved. Using the initial conditions that continuity $\psi = 1$ at $t = 0$, the following equation is obtained

$$\frac{1 - \psi^n}{n + 1} = -\,B_2 \int \sigma_{true}{}^n\,d\,t \tag{2.101}$$

Recalling that $\lambda = \sigma_{true}/\sigma_0$ this can be rearranged as

$$\frac{1 - \psi^n}{n + 1} = -\,B_2 \int (\lambda\,\sigma_0)^n\,d\,t = -\,B_2\,\sigma_0{}^n \int \lambda^n\,d\,t \tag{2.102}$$

When fracture occurs, the continuity becomes zero and $t = t_R$; thus the above equation becomes

---

[17]In his book Kachanov (1986) gives this equation in a confusing, if not incorrect way, as (in his nomenclature) $\beta = mm_0/m - m_0\,\varepsilon_{00} \geq 0$.

[18]Hence I will use the subscript *P*.

[19]When this equation was previously used it was in the context of a purely brittle failure where no reduction in area was considered.

$$\frac{1}{(n+1)\,B_2\,\sigma_0^{\,n}} = -\int_0^{t_R} \lambda^n \, dt \qquad (2.103)$$

The left hand side of this equation is the same as that used to quantify the time-to-rupture under a brittle process when the primary creep stage was neglected, t_2, (equation 2.047).

So equation 2.103 can be re-expressed as

$$t_2 = -\int_0^{t_R} \lambda^n \, dt \qquad (2.104)$$

Equation 2.104 and 2.096 can then be equated to give

$$t_2 = \int_1^{\lambda_R} \lambda^n \, \frac{\lambda^{-q-1} - p\,\varepsilon_0\,\lambda^{-1+p-q}}{\dot{\varepsilon}_0} \, d\lambda \qquad (2.105)$$

which in turn gives

$$t_2 = \frac{1}{q\,\dot{\varepsilon}_0}\left[\frac{q\,\lambda^{n-q}}{n-q} - \frac{q\,p\,\varepsilon_0\,\lambda^{n+p-q}}{n+p-q}\right]_1^{\lambda_R} \qquad (2.106)$$

The q terms were added inside and outside the brackets to enable further simplification of equation 2.106, by reference to previous ones (for example by equation 2.048).

$$\frac{t_2}{t_1} = \frac{q\left(\lambda_R^{\,n-q} - 1\right)}{n-q} - \frac{(q-p)\,\beta\left(\lambda_R^{\,n+p-q} + 1\right)}{n+p-q} \qquad (2.107)$$

The value of λ_R found from this equation (2.107) can then be substituted in to equation 2.097 to determine the time-to-rupture t_{3P}.

I would like to suggest that if λ at rupture is considered to be a constant for the range of stresses used, equation 2.097 can be viewed as a relationship between the time-to-rupture, the secondary creep rate and the 'instantaneous plastic strain'. This equation would be of the form $C_1/\dot{\varepsilon} + (C_2\,\varepsilon_0)/\dot{\varepsilon} = t_{3P}$. This equation can easily be applied to creep data. However at this stage, the accuracy of the assumption that λ is a constant is unknown for bone and antler.

2.3.3.6. COMMENTS ON KACHANOV'S APPROACH: IS CREEP DEFORMATION INDEPENDENT OF THE DAMAGE PARAMETER?

Kachanov (1986) comments on the assumption that the creep deformation is independent of the damage parameter (section 2.3.3.2). He says that creep acceleration in the tertiary period cannot be fully attributed to the decrease in cross-sectional area. Damage resulting from the development of micro-cracks and micro-voids can also lead to

creep acceleration. He thus introduces a damage parameter into a generalised creep equation as follows:

$$\dot{\varepsilon} = f(\sigma, \omega) \tag{2.108}$$

$$\dot{\omega} = g(\sigma, \omega) \tag{2.109}$$

The damage parameter can be viewed as the complement of continuity, $\omega = 1 - \psi$. The symbol 'D' is also widely used to signify the scalar (isotropic) form of the damage parameter. Equations of this form have been developed for both uniaxial and multiaxial creep by Hayhurst and others (according to Dunne *et al.* 1990). Specific forms of these equations have been applied to 2½ Cr-Mo, Alloy 800H and cast copper by Dunne *et al.* (1990). I will not discuss this approach here, but I examine its application to bone and antler in section 4.3.9.

2.3.3.7. COMMENTS ON KACHANOV'S APPROACH: RELATED IDEAS AND OTHER FORMS OF EXPLANATION

A number of workers have extended the concept of damage accumulation under creep loading to other loading conditions. The application of the concept of damage accumulation to tensile tests forms a major part of chapter 4. I will briefly introduce some other ways of describing the damage approach that are more easily visualised. The amount of damage (or loss of continuity) within a material can be expressed as a change in the effective cross-sectional area.[20] Many of the damage theories can be explained from this viewpoint. For example Kraus (1980), in his book *Creep Analysis*, starts a section on the damage concept with the following phrase:[21]

> We define the damage in terms of the net area A_{eff} of a cross-section that remains to carry the load in a member as a result of some internal flaw distribution
>
> $$D \equiv 1 - \frac{A_{eff}}{A_0} \qquad 0 \leq D \leq 1$$
>
> Here A_0 is the initial area and A_{eff} is the area after some damage has occurred.

These ideas can also be expressed graphically. Figure 2.012 shows three images of a specimen a, b and c. In the first image the specimen is in an undamaged state. In the second it has sustained some damage. The final image shows a specimen of undamaged material that possesses a mechanical response (force-extension) that is the same as the

---

[20]For example, this expression has been used by Lorrain and Loland (1983), Kraus (1980) and Murakami (1990).

[21]Kraus used A_R to signify the undamaged area remaining I use A_{eff} to avoid confusion.

damaged specimen. The third specimen has a smaller cross-sectional area than the original one. This reduced cross-section is the *effective cross-section* of the damaged material, A_{eff}. Clearly, assumed changes in cross-sectional area and the area of voids or cracks within the material are not simply related. The exact form the damage takes (for example inclination, shape or size of a crack) will affect this relationship, and such considerations have led to a number of different non-scalar damage parameters.

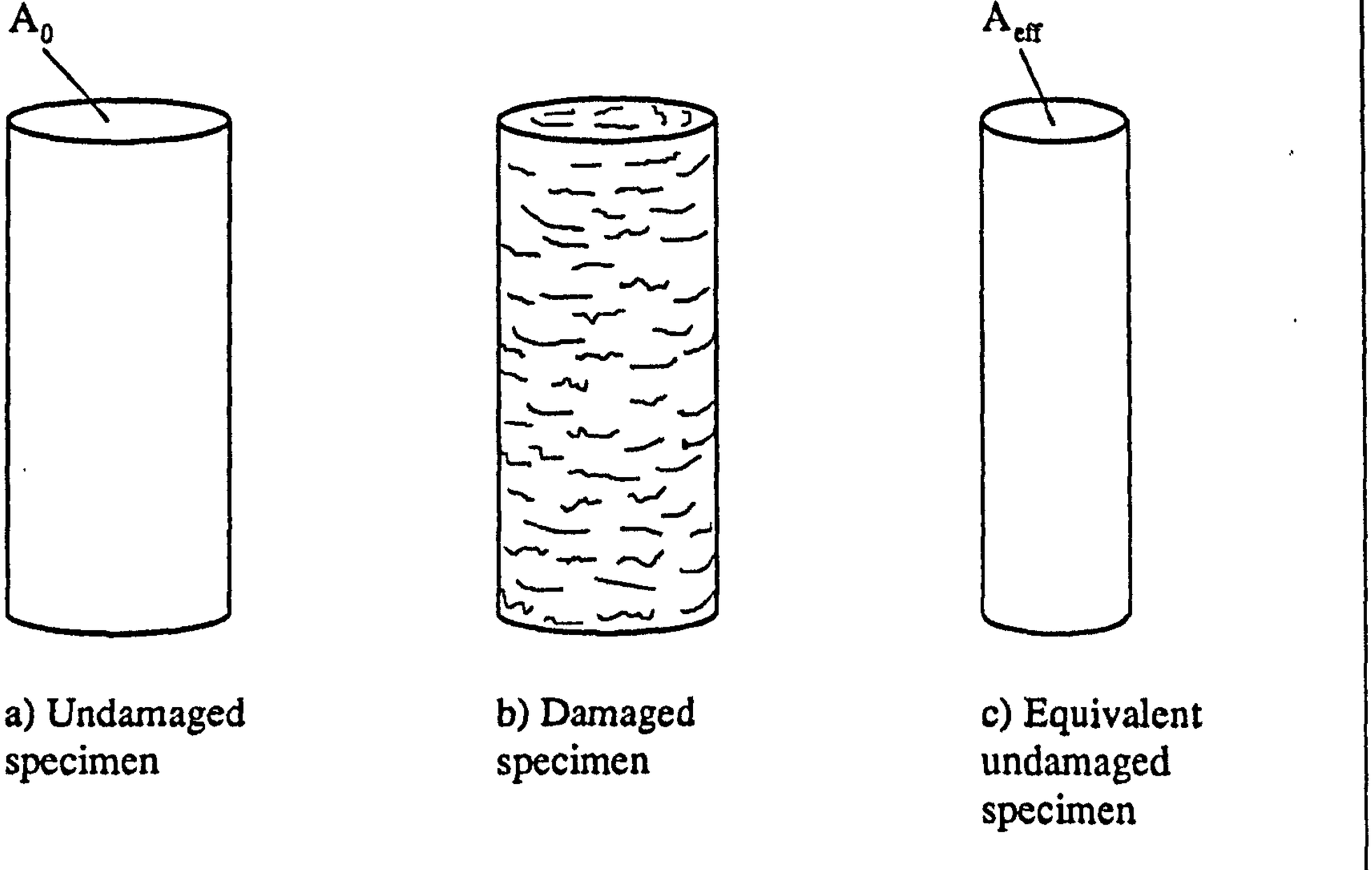

a) Undamaged specimen

b) Damaged specimen

c) Equivalent undamaged specimen

Figure 2.012
Graphical representation of undamaged, damaged and equivalent undamaged specimens

Another closely related form of approach to (or explanation of) damage is based on the observed reduction in material stiffness. For example, in the case where the load on the specimen is constant, if the specimen sustains *damage* its *effective area*, A_{eff}, is reduced. Thus the stress in the remaining, equivalent undamaged, material increases. This stress is referred to as the *effective stress*, σ_{eff}:[22]

$$\sigma_{eff} = \frac{\text{Load}}{A_{eff}} \tag{2.110}$$

As more damage occurs, the effective cross-sectional area will decrease, and thus the effective stress will increase. This process is accompanied by an increase in strain. The

---

[22]If damage has occurred, the value of the effective stress, σ_{eff}, will be more than the stress calculated using the initial area, σ. As the damage is internal, σ_{eff} will also be greater than the stress calculated using the actual cross-section of the specimen σ_{true}.

reduction in the material's integrity has resulted in a reduction of the specimen's stiffness. Therefore, damage can be expressed in terms of a reduction in the measured stiffness of the specimen. This can be demonstrated using the following argument.

$$E_U = \frac{\sigma_{eff}}{\varepsilon} = \frac{P}{A_{eff}\,\varepsilon} \tag{2.111}$$

The stiffness of the undamaged material, E_U, remains constant. Using the ideas introduced above this stiffness may be expressed as the ratio of the effective stress to the measured strain, or the load divided by the effective area of undamaged material and the strain exhibited by the specimen. The same specimen when damaged will have a smaller measured stiffness, E_M, (using nominal stress and strain). This is due to the measured stress, σ, being less than the effective stress:

$$E_M = \frac{\sigma}{\varepsilon} = \frac{P}{A_0\,\varepsilon} \tag{2.112}$$

Rearranging equations 2.111 and 2.112 gives

$$A_{eff} = \frac{P}{E_U\,\varepsilon} \qquad \text{and} \qquad A_0 = \frac{P}{E_M\,\varepsilon} \tag{2.113}$$

These equations when substituted into $D \equiv 1 - (A_{eff}/A_0)$ yield the following equation

$$D = 1 - \frac{E_M}{E_U} \tag{2.114}$$

This equation has been used by a number of workers to quantify the amount of damage within a material as it was loaded. This procedure may be conducted in a number of ways, two of which are mentioned here: first it may be assumed that the material when unloaded will return to its initial length (zero strain) by a linear stress-strain relationship. This is similar to the idealised case shown in figure 2.012b. Second, the material can be mechanically tested using a loading and unloading regime, and a true value of stiffness can thus be obtained. In the case of the elastic-damage material, the initial slope of the loading line is E_U and the dotted unloading lines are various values of E_M. It has already been shown that the stiffness of bone decreases after the yield region has been entered or exceeded (figure 1.011). These procedures have been used by Newaz and Walsh (1989) on particulate composites, and the application of such an approach to concrete is reviewed by Lorrain and Loland (1983).

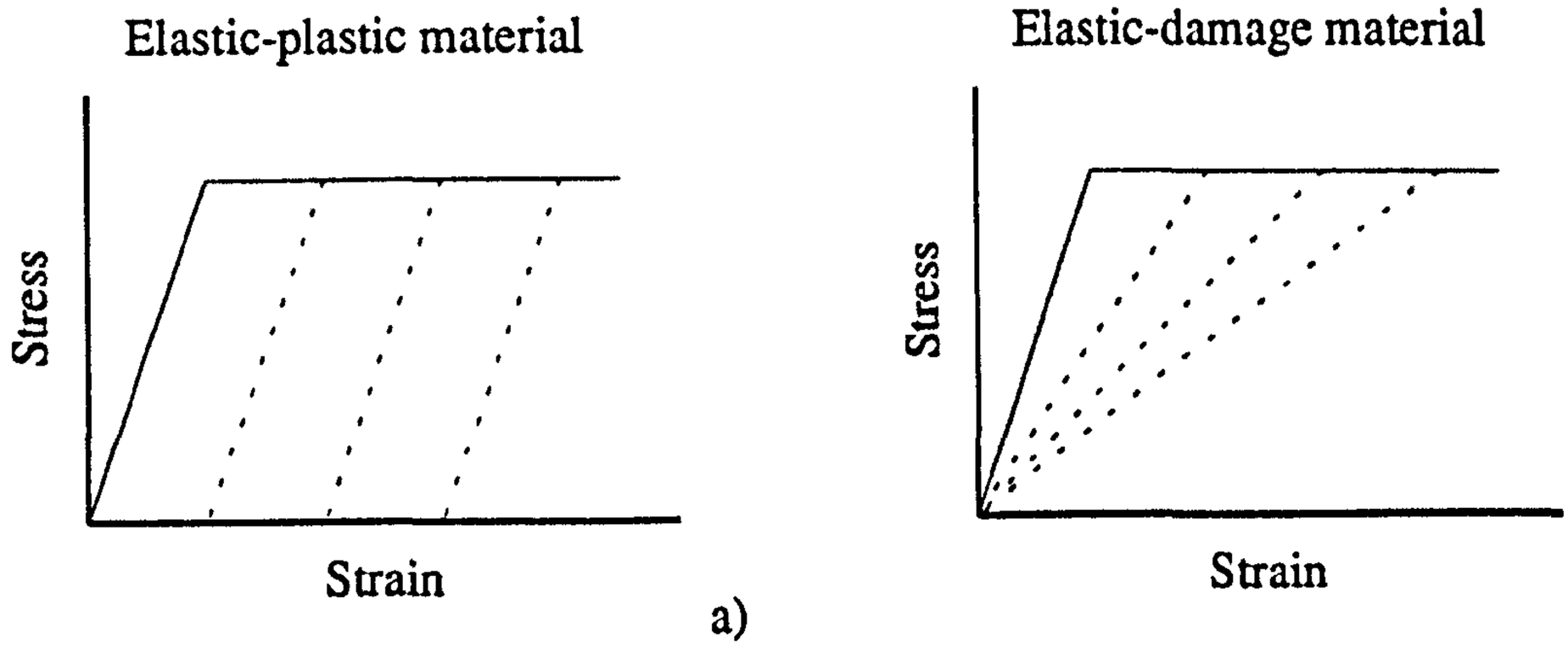

The solid line shows the stress-strain response of the idealised material when subjected to a continuously increasing strain (the same in both cases). The dotted line shows the relationship when the specimen is unloaded and reloaded from various strains.

Figure 2.013

Stress-strain relationships for idealised elastic-plastic and elastic-damage materials

Figure 2.013 shows two idealised materials, one fitting the description *elastic-plastic* and the other *elastic-damage*. Both materials departure from elastic behaviour at a single value of stress (or strain). Such a sharp transition is not seen in real materials. For example; metals, although they are described as elastic-plastic exhibit a more gentle transition between these two behaviours. In metals this is referred to as the *yield* region. Another idealisation is that of the linear loading-unloading paths. For some damage materials the loading unloading lines do not coincide, but form a loop. Such behaviour is similar to that shown by bone in figure 1.011 and may be due to some form of time-dependent behaviour. (At this stage I will not claim that bone is an elastic-damage material. However, this is a strong indication that the properties of bone may have more in common with the ideal elastic-damage material that the elastic-plastic one.)

2.3.3.8. COMMENTS ON KACHANOV'S APPROACH: IS CONTINUITY ZERO AT FAILURE?

In section 2.3.3.4 the idea that continuity may not be zero at failure was raised. Kachanov dismissed the importance of this idea for creep tests. However, I consider that this idea should be examined or at least not dismissed if other forms of testing are employed, as in this study. One form of logic for assuming that the continuity may be greater than zero at the instant before failure is based on a consideration of the effective stress. If the measured damage increases to one without a (mathematical) discontinuity then the effective stress increases to infinity. Likewise the strain would increase to infinity, clearly not a realistic situation.

The factors that determine the level of damage, or effective stress, at which the material fails are considered in later chapters. Here it is sufficient to say that failure occurs when the remaining material can no longer sustain the stresses to which it is subjected. (However, the assumption of zero continuity, or D = 1, at failure is used as a first approximation in the following analysis.)

2.3.3.9. COMMENTS ON KACHANOV'S APPROACH: CAN A SINGLE SCALAR QUANTITY FULLY DESCRIBE DAMAGE IN BONE AND ANTLER?

The answer to the question 'can a single scalar quantity fully describe damage in a material like bone and antler?' is no, but I consider that the scalar quantity is sufficient for the present study. Ascertaining which possible alternative to use would be a very complex task for the biological materials considered here.

The reason for using other damage variables becomes clear if the damage is envisaged as cracks. The orientation of these cracks to the stress field will have a considerable influence on the amount of measured damage in that direction. In this thesis uniaxial stress has been assumed in all cases and likewise damage has only been considered in the same direction. Therefore a scalar representation of damage is sufficient. A review of some of the damage variables in the published literature and their comparative advantages is provided by Krajcinovic (1984). He points out that a vector representation can be used for damage in the form of flat planar microcracks, the vector's direction being normal to the plane of the crack. He then points out that this takes no account of the effect of the crack's shape. He continues:

> The somewhat restricted amount of information which can be stored in a vector variable, coupled with the traditional infatuation of the continuum mechanics community with tensors, spawned a veritable maze of tensorial models. The gamut runs from an eight-order tensor . . . down to the variety of second-order tensors . . .

I expect that a more accurate description of the damage cracks in bone, would only be worthwhile if it is accompanied by a more accurate description of the material, which is not homogeneous before the development of damage. In this thesis I assume conditions of uniaxial stress in all the tensile and creep experiments and I consider damage as a scalar quantity only. I have had no time to examine the exact geometry of the damage cracks in bone. (Although a co-worker in this laboratory, Dr Peter Zioupos, is now under-taking such an examination.) For the reasons given above, I consider that a scalar measure in sufficient and practicable for my purposes.

2.3.4. CONCLUDING REMARKS ON THE DAMAGE APPROACH

In the preceding sections I have used the (almost) original source of the theory of continuum damage mechanics, Kachanov (1960), which contains a number of equations that can be used to predict the time-to-rupture during a creep test, accounting for whether the failure is ductile, brittle or some combination of these. It is shown in the next chapter that such data for bone has been fitted to one of these equations. In chapter 4, I examine the fit of my own data to a number of these equations. I shall also examine the predictive power of these concepts when applied to creep and tensile tests rather than just fitting data to equations of the same form.

The theory of continuum damage mechanics as explained above has produced a number of equations that may be fitted to the data obtained from creep tests. Some of the important ones are repeated in table 2.002.

Equations	Type of model	Source and equation
$t_1 = \frac{1}{m B_1 \sigma_0^{\,m}}$	Time to creep rupture by idealised ductile mode	Kachanov (2.038)
$t_1 = 1/(m \dot{\varepsilon}_0)$	Time to creep rupture by idealised ductile mode	Kachanov
$t_2 = \frac{1}{B_2 (n + 1) \sigma_0^{\,n}}$	Time to creep rupture by idealised brittle mode	Kachanov (2.047)
$\frac{t_3}{t_1} = 1 - \left(1 - \frac{(m - n)}{m} \frac{t_2}{t_1}\right)^{\frac{m}{m-n}}$	Time-to-rupture by a combined ductile and brittle process.	Kachanov (2.061)
$t_4 = t_1 \left(1 - e^{-\frac{B_1 m}{B_2 (m+1)}}\right)$	n = m, always brittle ruptures at same strain	Kachanov (2.076)

Table 2.002

Some equations for predicting the time-to-rupture by various processes

2.4. SUMMARY

In this chapter I have introduced two theories that are used to model, or even explain, many of the time-dependent properties of materials. The first, viscoelasticity, can be used to model the stress-strain relationships of such a material with respect to time. Some simple models of time-dependent materials were introduced and some stress-strain relationships under various loading conditions were given. It was reported that such a model had no way of accounting for the failure of materials. Thus the concept of damage was introduced, which deals specifically with the failure of materials. In the form in which it was introduced here, this failure was that occurring during creep by a ductile, brittle or combined process. The extension of the material was attributed to the combination of plastic flow and damage. Brittle failure was considered to be due to the degradation of the material. This degradation was modelled mathematically, and attributed to physical damage in the form of micro-crack or void formation within the material.

In the next chapter I will examine a number of published works, in which some of the ideas and methods explained within this chapter have been applied to bone and antler.

3

TIME-DEPENDENT PROPERTIES OF BONE AND ANTLER: PUBLISHED STUDIES

3.1. INTRODUCTION

In this chapter I review some published works on the time-dependent properties of bone and antler. I restrict this discussion to papers that either demonstrate an approach, method of analysis, or explanation that is either widely used or is comparable with those of the preceding chapter. This restriction results in the exclusion of many studies, for example those that involve torsional testing. In the following chapter some of the approaches reported here (along with others) will be used to examine the data that I have obtained from tensile and creep-rupture tests of bovine bone and antler.

The order in which the papers are considered reflects that in which the approaches or ideas they contain are explained in the previous chapter. Thus I will start with a brief section on viscoelasticity and the time-dependence of some mechanical quantities. In the later sections I discuss papers that use the concept of damage accumulation.

3.2. VISCOELASTICITY, CREEP AND OTHER RELATED TESTS

Katz (1980b) said that 'it is only in recent years that serious consideration has been given to examining the time-dependent properties, i.e. viscoelastic properties of bone'. He mentions a number of workers who have reported the strain rate dependence exhibited by some of bone's mechanical responses. Time-dependence of the behaviour of antler has been reported, by Currey (1989). In this section I review a number of papers that report such effects for both bone and antler.

3.2.1. HIGH STRAIN RATE TESTS: THE SPLIT-HOPKINSON BAR TECHNIQUE

Tennyson *et al.* (1972) used the split-Hopkinson-bar technique to obtain data on the material stiffness of bovine femoral bone in compression.[1] The strain rates they used were in the range of 10 to 450 s^{-1}. These strain rates are higher than those I used in the experimental section of this study. They are also greater than those encountered in

[1]The specimen is placed between, and in contact with, two metal bars. The whole arrangement has the same axis. Strain gauges are placed on the bars near to the specimen. One bar is struck by a projectile so that an elastic strain pulse is propagated along the bar. Some of this pulse passes through the specimen and into the second bar, where it is detected by the strain gauge. The signals from the strain gauges are used to obtain values of strain, strain rate and stress.

normal physiological loading.[2] However, I consider a review of the results obtained with this equipment is useful because the authors explain their results using viscoelasticity. The authors include the following statement:

> Due to the apparent viscoelastic behavior of beef-femur bone, it was decided to determine if, in fact, the material could be characterized by a classical linear viscoelastic solid described by the general equation
>
> $$P\sigma = Q\varepsilon$$
>
> where P and Q are polynomials with constant coefficients in the operator (d/dt).

The latter part of this statement is clearly the same as that given in section 2.2.1.4 above. Tennyson *et al.* performed their experiments on specimens at different times post-mortem. The authors decided that because there was only a small degree of non-linearity in the response curve their results could be represented by an equation having the following form (Tennyson *et al.* use other nomenclature for the derivatives).

$$p_0 \sigma + p_1 \dot{\sigma} = q_0 \varepsilon + q_1 \dot{\varepsilon} \qquad (3.001)$$

This equation is the same (allowing $p_0 = 1$) as equation 2.018 above, and can, as the authors point out, be interpreted physically as the three-element model (figure 2.008). On the basis of observations that the stress rate during the test was almost constant, and comparison of their dynamic tests with static ones, they concluded that p_1 is very small, and assume it to be zero. Thus they used the following model (expressed in my nomenclature)

$$\sigma = K\varepsilon + \eta\dot{\varepsilon} \qquad (3.002)$$

The authors point out that this equation describes a Kelvin (or Voigt) solid. They convert this equation to one giving the compressive modulus as follows.[3]

$$E_c = K + \eta \frac{\dot{\varepsilon}}{\varepsilon} \qquad (3.003)$$

They used their results of E_c obtained from specimens tested at various times after death to obtain estimates of the values of the stiffness and viscosity terms at the time of death. These they give as $K \approx 21$ GPa [$\approx 3\times10^6$ psi] and $\eta \approx 0.55$ MPa s [≈ 8 psi-sec]

---

[2]Lanyon *et al.* (1975) measured the strain rate on the anteromedial aspect of the tibial midshaft of an active 35 year old man, using strain gauges. During running the peak strain rate was 1.3×10^{-1} s^{-1}.

[3]This relationship is poorly defined, the modulus being the ratio of stress to strain, but by definition this is not constant for a viscoelastic material. At one point the quantity E_c is even referred to as 'the compressive modulus of elasticity'.

These tests were compression tests. The exact environmental conditions of the specimen are unclear; it appears that most of the specimens were wet during testing. However, the authors state that

> Many tests were conducted for a range of PMA [post-mortem ages] varying from 1 to 38 days, including a set at 240 days in which the specimens were allowed to dehydrate in a refrigerated environment.

The authors do not state if these specimens were re-hydrated, nor do they give any indication of the temperature of the specimens during testing. Therefore, the changes in mechanical response the authors recorded are more likely to be due to a departure from physiological conditions, than simply the time since the animal was butchered.

The split-Hopkinson-bar technique has also been used by Tanabe in conjunction with various co-workers to examine the mechanical properties of bovine femoral bone (Tanabe *et al.* 1991a, b and c). One aim of their papers is to establish the influence of loading rate on the anisotropy of compact bone. To model the higher material stiffness under conditions of a higher loading rate (the methods used were ultrasound, impact loading and quasi-static loading) the authors adapted the three-element model. At high loading rates they depict the dashpot as being rigid, and thus the stiffness of the material is that of the spring 2 in figure 2.008. At intermediate rates the dashpot acts as a true dashpot so the overall material stiffness is a rate dependent variable. Whilst at low loading rates Tanabe's model shows the dashpot as a slider, in this case the material stiffness is due to the two spring elements in series. This interpretation of the three-element model exaggerates the effect of the, rate-dependent, dashpot element. However, it is a useful way to interpret its properties, and simplify the modelling of the mechanical properties at high and low strain rates.

3.2.2. LOW STRAIN RATE TESTS: STANDARD TENSILE TESTS

The dependence of bone's material stiffness on the strain (or loading) rate during tensile tests has been reported in a number of papers. These studies are generally at lower strain rates than the split-Hopkinson-bar technique. Some examples of these studies are those by Crowninshield and Pope[4] (1974), Currey (1975) and Wright and Hayes (1976). The only such study of antler that I am aware of is one by Currey (1989). Normally the approach is simply to plot the results or look for relationships between various explanatory variables. The latter process usually involves some form of regression analysis. Some of the resulting equations published in the literature are presented below. In the following chapters these equations are compared with the predictive equations

---

[4]These workers only give the relationship graphically, reproduced here in figure 3.001.

resulting from the various concepts outlined in chapter 2 (viscoelasticity and damage accumulation) and my own results.

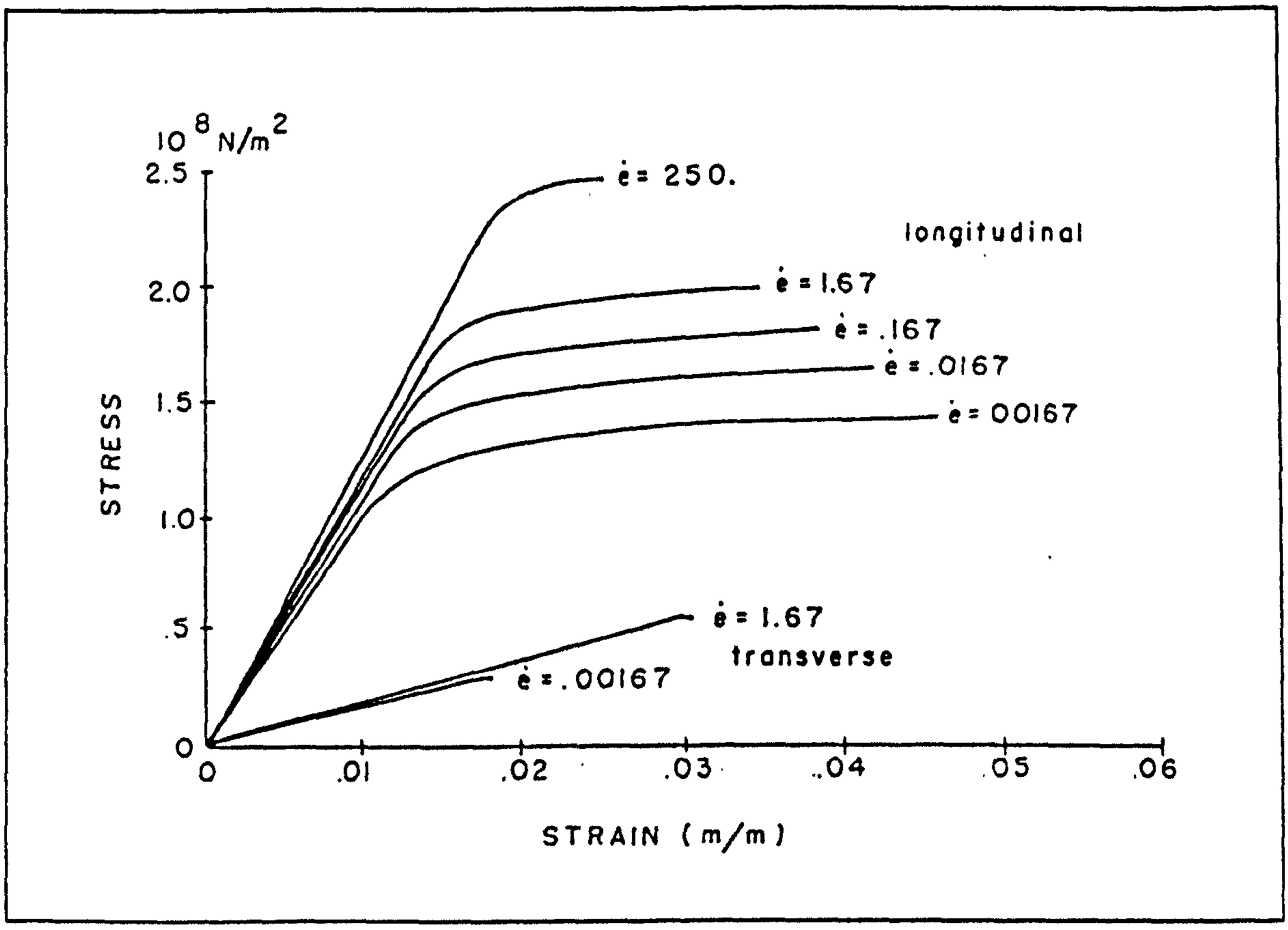

Figure 3.001 Reproduced from Crowninshield and Pope (1974)

Mean stress-strain curves for tensile specimens of bovine bone

Figure 3.001 reproduces the results of Crowninshield and Pope (1974). It will become clear later that although these results are qualitatively correct I consider them to be quantitatively inaccurate. To obtain their estimate of strain within the specimen Crowninshield and Pope measured the relative motion of the two specimen grips, and assumed that 'all the measured displacement occurred in the .005 m gauge length of the specimen'. I suggest this assumption results in an overestimate of the strain, due to deformations outside the gauge length. The existence of deformations outside the gauge length also makes the values that they quote for strain rate questionable. To obtain these values the authors used a slightly different method; they say 'the value of strain rate for a specimen was calculated to be the crosshead speed of the loading device divided by the specimen gauge length'. Thus this estimate will include errors due to the deformation of the machine. (The reasons for differences between the estimates of strain and strain rate and the true values are examined in appendix 7.)

I will now briefly examine the papers by Currey, and that of Wright and Hayes, which contain numerical results. Currey (1975) examined 35 specimens of wet bovine

femoral bone, at room temperature. These were stretched at a number of cross-head speeds in an open loop tensile testing machine. The strain rate was calculated from 'the strain at yield divided by the time taken to yield'.[5] The mechanical quantities he reported were 'yield stress, ultimate tensile stress, modulus of elasticity and strain at yield'. He also examined the degree of reconstruction of the specimen and its mineral content (by ashing). The data for each mechanical variable was analysed using multiple regression analysis on strain rate and reconstruction or strain rate and ash content. However, Currey also provides a full listing of his data. This has permitted me to reanalyse the mechanical properties in relation to strain rate alone and in combination with the material stiffness. I have thus made them more comparable with my own results and the form of analysis that I use for my own data, and with the equations presented in this and the theoretical chapter, above.[6] These results are reproduced in figures 3.002 to 3.005. The regression equations I obtained are given in tables 3.001 and 3.002.

Bovine specimens	Regression equations and t values, from my reanalysis of the data published by Currey (1975).	R^2 %	
35 femoral	$\sigma_{ult} = 115 + 306\,\dot{\varepsilon}$ t: 18.17 2.79	16.6	*a*
35 femoral	$\sigma_{ult} = -0.9 + 197\,\dot{\varepsilon} + 5.25\,E$ t: -0.04 2.43 5.67	57.1	*b*
35 femoral	$\sigma_{y} = 110 + 308\,\dot{\varepsilon}$ t: 18.63 3.00	19.0	*c*
35 femoral	$\sigma_{y} = -6.5 + 198\,\dot{\varepsilon} + 5.29\,E$ t: -0.36 2.86 6.67	65.1	*d*
35 femoral	$\varepsilon_{y} = 0.00503 + 0.00801\,\dot{\varepsilon}$ t: 29.89 2.74	16.1	*e*
35 femoral	$\varepsilon_{y} = 0.00469 + 0.00769\,\dot{\varepsilon} + 0.000016\,E$ t: 5.96 2.52 0.45	14.0	*f*
Units: σ_y, MPa. σ_{ult}, MPa. $\dot{\varepsilon}$, s^{-1}. E, GPa			

Table 3.001

The relationship of various mechanical properties to strain rate exhibited by the data published by Currey in 1975

[5]Discussion of this aspect of the experimental procedure is contained in appendix 7.
[6]During the analysis of this data a typographical error in the paper became apparent. On consultation of the original laboratory notebooks it was found that the one strain rate quoted in the paper as 0.0011 s^{-1} should be 0.00011 s^{-1}.

Bovine specimens	Regression equations and t values, from my reanalysis of the data published by Currey (1975); using the logarithmic value of strain rate.	R^2 %	
35 femoral	$\sigma_{ult} = 179 + 10 \ln(\dot{\varepsilon})$ t: 18.32 6.09	51.5	*a*
35 femoral	$\ln(\sigma_{ult}) = 5.26 + 0.0881 \ln(\dot{\varepsilon})$ t: 57.61 5.72	48.2	*b*
35 femoral	$\ln(\sigma_{ult}) = 2.43 + 0.869 \ln(E) + 0.0633 \ln(\dot{\varepsilon})$ t: 5.40 6.36 5.70	76.4	*c*
35 femoral	$\sigma_y = 171 + 9.55 \ln(\dot{\varepsilon})$ t: 18.58 6.13	51.8	*d*
35 Bovine femoral	$\ln(\sigma_y) = 5.21 + 0.0867 \ln(\dot{\varepsilon})$ t: 57.42 5.65	47.7	*e*
35 femoral	$\ln(\sigma_y) = 2.22 + 0.920 \ln(E) + 0.0605 \ln(\dot{\varepsilon})$ t: 5.44 7.42 6.00	80.2	*f*
35 femoral	$\varepsilon_y = 0.00669 + 0.000260 \ln(\dot{\varepsilon})$ t: 25.21 5.81	49.0	*g*
35 femoral	$\ln(\varepsilon_y) = -4.97 + 0.0528 \ln(\dot{\varepsilon})$ t: - 88.93 5.58	47.0	*h*
35 femoral	$\varepsilon_y = -4.86 - 0.036 \ln(E) + 0.0538 \ln(\dot{\varepsilon})$ t: - 11.74 - 0.28 5.25	45.5	*i*
35 femoral	$E = 26.1 + 0.623 \ln(\dot{\varepsilon})$ t: 15.76 2.23	10.4	*j*
35 femoral	$\ln(E) = 3.26 + 0.0285 \ln(\dot{\varepsilon})$ t: 41.5 2.15	9.6	*k*
Units: σ_y, MPa. σ_{ult}, MPa. $\dot{\varepsilon}$, s^{-1}. E, GPa			

Table 3.002

The relationship of various mechanical properties to logarithm of strain rate exhibited by the data published by Currey in 1975[7]

[7]Some of these equations are similar to those of Currey (1989) when he reanalyses this data, but in his work they are in base ten logarithms and one erroneous strain rate value has been used.

Tables 3.001 and 3.002 show that all the mechanical quantities reported by Currey (1975) display some dependence on the strain rate. This dependence is at least statistically significant.[8] The material stiffness displays the smallest dependence on strain rate. This could be considered as ironic, for it is such an increase in material stiffness that is normally used (by other workers) as a justification for applying a viscoelastic model or viscoelastic terminology. However, those properties that are shown here to display a greater time dependence cannot be modelled by viscoelasticity. This point is made by Currey:

> The effect on measured E can be considered simply as the result of bone being a viscoelastic material. The effect on yield strength and breaking strength could not be predicted directly from the viscoelasticity of bone without making use of some further assumptions or facts.

This paper (Currey, 1975) will be discussed further later, and the analysis of the data it provides referred to.

Wright and Hayes (1976) examined a number of mechanical quantities of bovine femoral bone, with respect to strain rate, micro structure and density. They machined 100 specimens to the dimensions shown in figure 1.020. Of these specimens 10 specimens were tested at each of 'seven displacement rates (from 0.013 to 5850 mm/s)'. 'Five additional specimens were instrumented with strain gauges . . . and tested to establish the relation between specimen displacement and strain'.[9] All tests were performed at room temperature. These workers found the 'ultimate strength' and the 'modulus of elasticity' increased with strain rate. The mean values (for the sets of 10 specimens) quoted in the paper are plotted in figures 3.002 and 3.003 along with the data from Currey (1975). Wright and Hayes report that these quantities 'varied linearly with the logarithm of the strain rate'.

The data provided by Currey (1975) and Wright and Hayes (1976) can be combined to obtain a larger data set (when the mechanical quantity is provided in both cases). Obtaining regression equations from this data set is not a fully justifiable process as the values given in the later paper are the mean values for groups of ten specimens. However, the general trend can be seen in the following plots.

---

[8]I have choose three levels of significance for this thesis. In these regressions there are either 33 or 32 degrees of freedom. Thus the significance can be conservatively estimated by assuming 30 degrees of freedom, as follows.
$t \geq 3.646 \Rightarrow p \leq 0.001 \Rightarrow$ Very highly significant
$t \geq 2.750 \Rightarrow p \leq 0.01 \Rightarrow$ Highly significant
$t \geq 2.042 \Rightarrow p \leq 0.05 \Rightarrow$ Significant. (For a more extensive table see appendix 12)

[9]It is shown in appendix 7 that their statement that 'because the displacement rate is constant during a test, the load/displacement behaviour relates directly to the stress-strain behaviour' is erroneous.

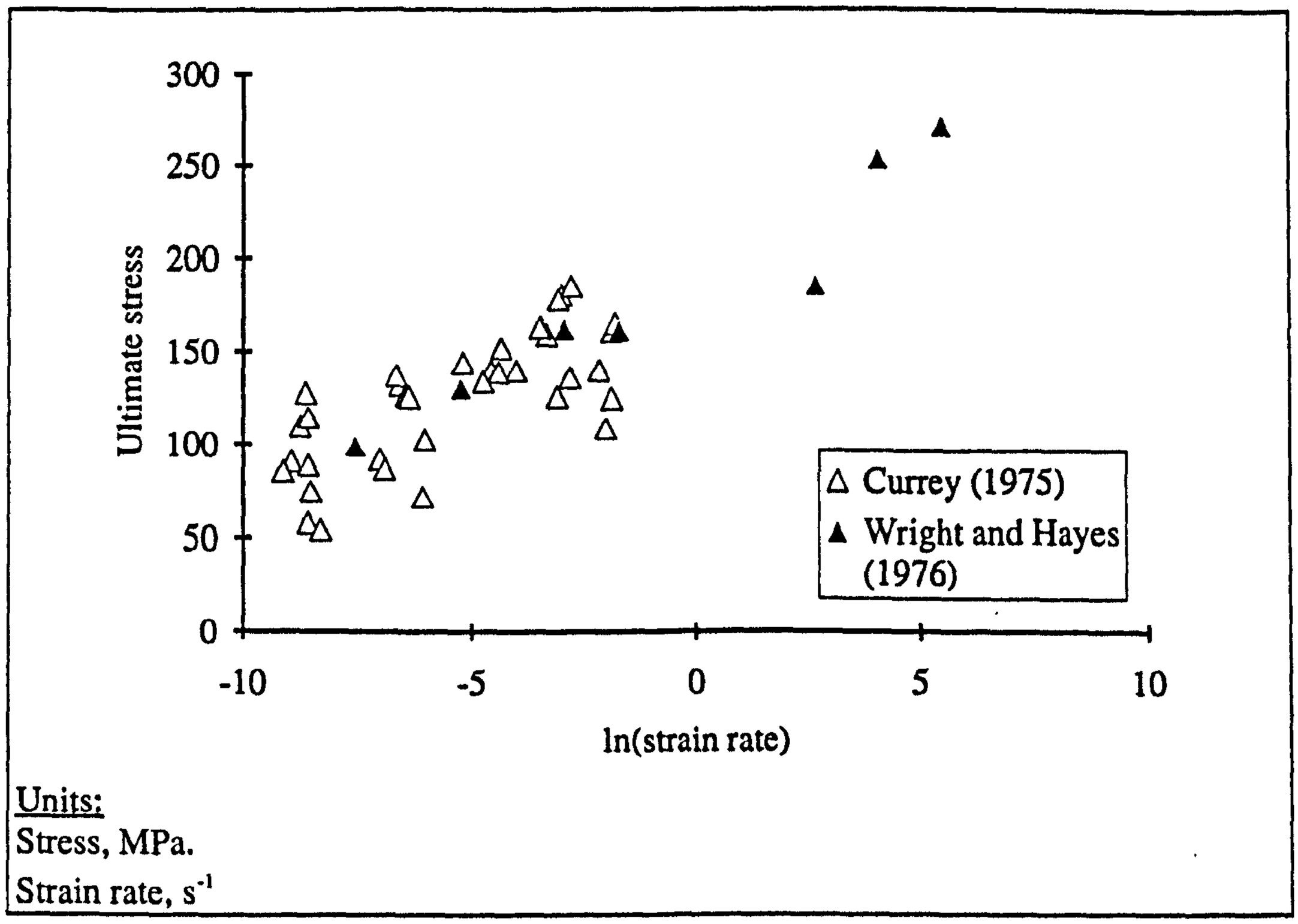

Figure 3.002 Data from Currey (1975) and Wright and Hayes (1976)

The variation of ultimate stress with respect to strain rate

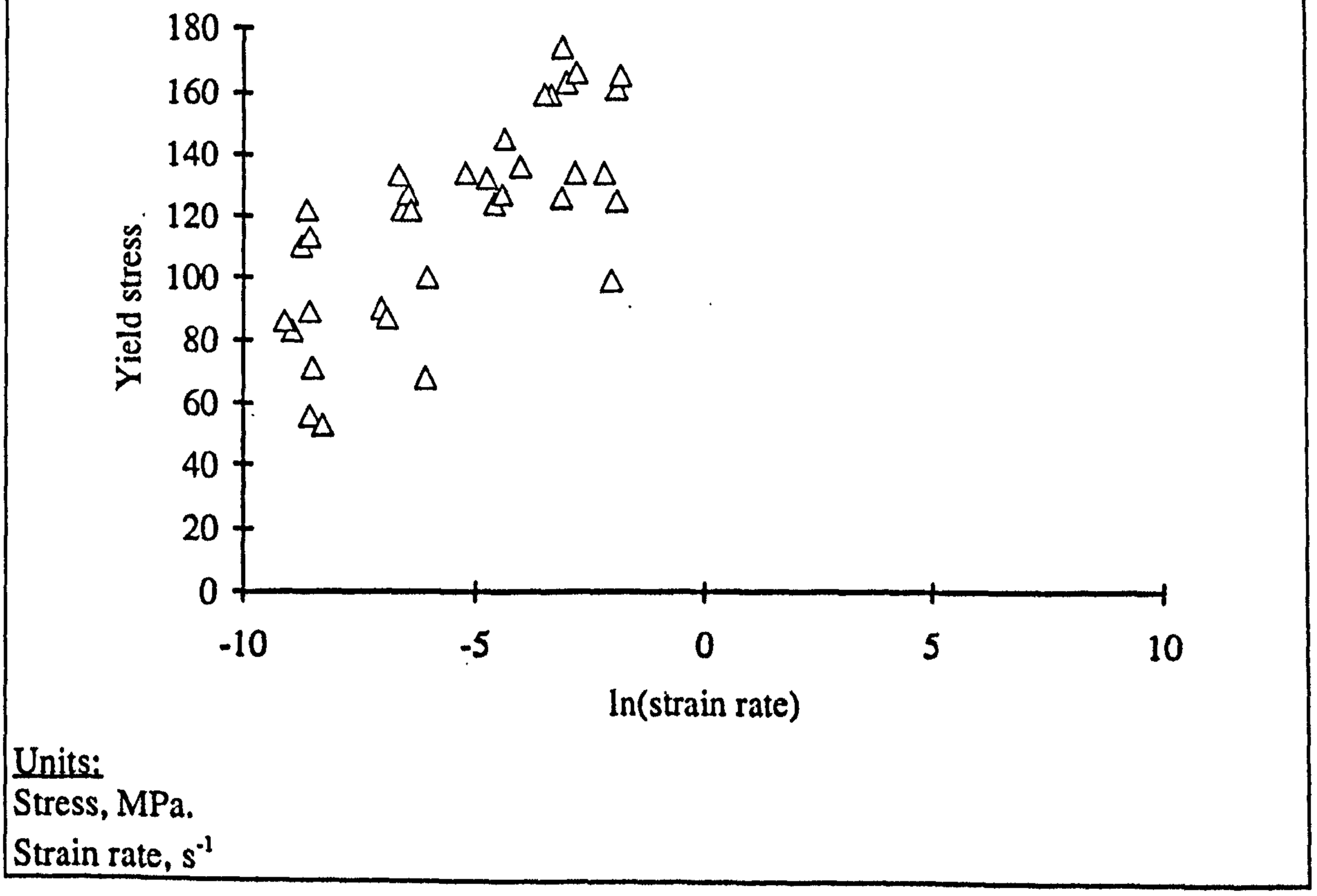

Figure 3.003 Data from Currey (1975)

The variation of 'yield' stress with respect to strain rate

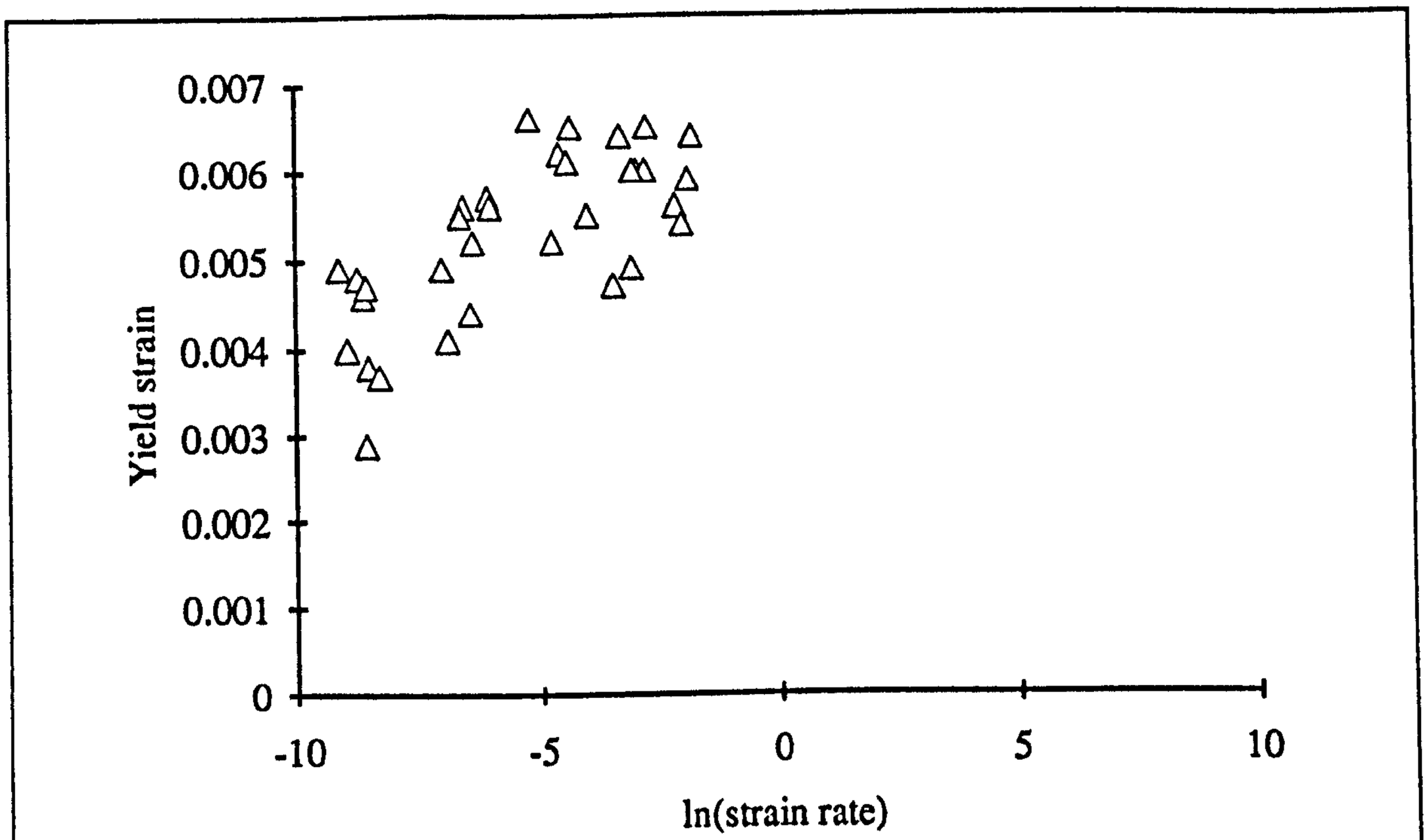

Units:
Strain, unitless.
Strain rate, s^{-1}

Figure 3.004 Data from Currey (1975)

The variation of 'yield' strain with respect to strain rate

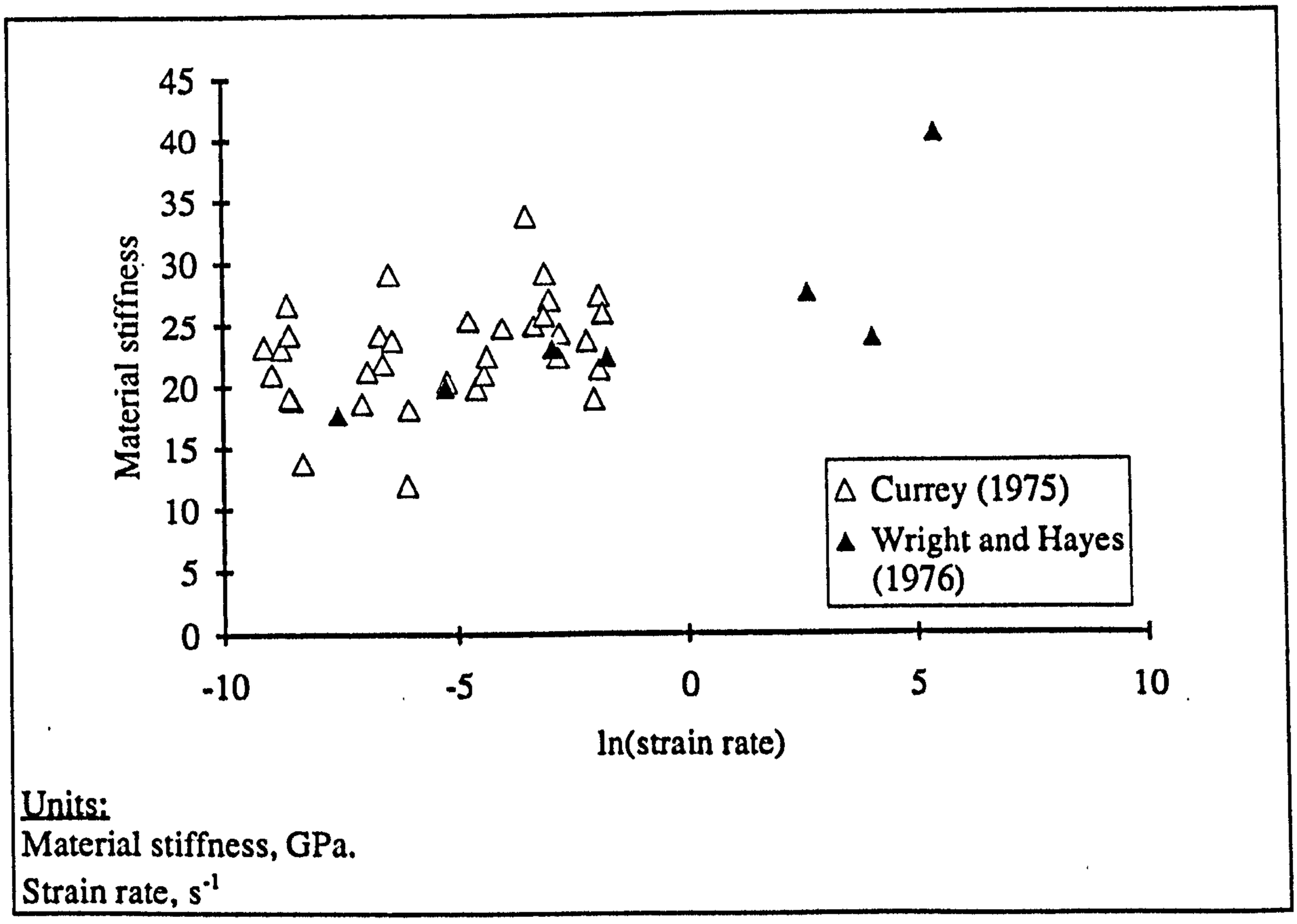

Units:
Material stiffness, GPa.
Strain rate, s^{-1}

Figure 3.005 Data from Currey (1975) and Wright and Hayes (1976)

The variation of material stiffness (Young's modulus) with respect to strain rate

As mentioned above, the strain rate dependence of various mechanical properties of reindeer antler is examined by Currey (1989). This paper is referred to again later, as the investigation had two aims: first, to see if antler is rate dependent and second to examine this data with reference to Carter and Caler's TDF model. (The second aim is the concern of section 3.3.3.) In this paper Currey reports the results of tensile tests on 28 specimens of reindeer (*Rangifer tarandus*) antler. The specimens were tested using an Instron 1122 materials testing machine. Their extension was monitored by a 10 mm gauge length extensometer. The loading curve was stored using a storage oscilloscope. The specimens were kept wet during machining and testing. Currey reports that the specimens were tested at room temperature at various strain rates from 7.6×10^{-5} to $1.59\ s^{-1}$ (a larger range than that used for his bovine tests reported above).[10] From the load deformation curve he obtained a number of properties, 'Young's modulus of elasticity, yield stress, yield strain, fracture stress, fracture strain, the stress and the strain occurring after yield, the final slope, and final stiffness'. Figure 3.006, reproduced from the paper, shows how these values were derived. Other variables were determined, such as porosity and calcium content. The first variable gives rise to 'bone volume fraction' (1 - porosity) and the second to an estimate of the 'mineral volume fraction'. As reported in chapter 1, I have not determined these two quantities for the specimens examined in this study. Therefore this aspect of the paper is not examined.

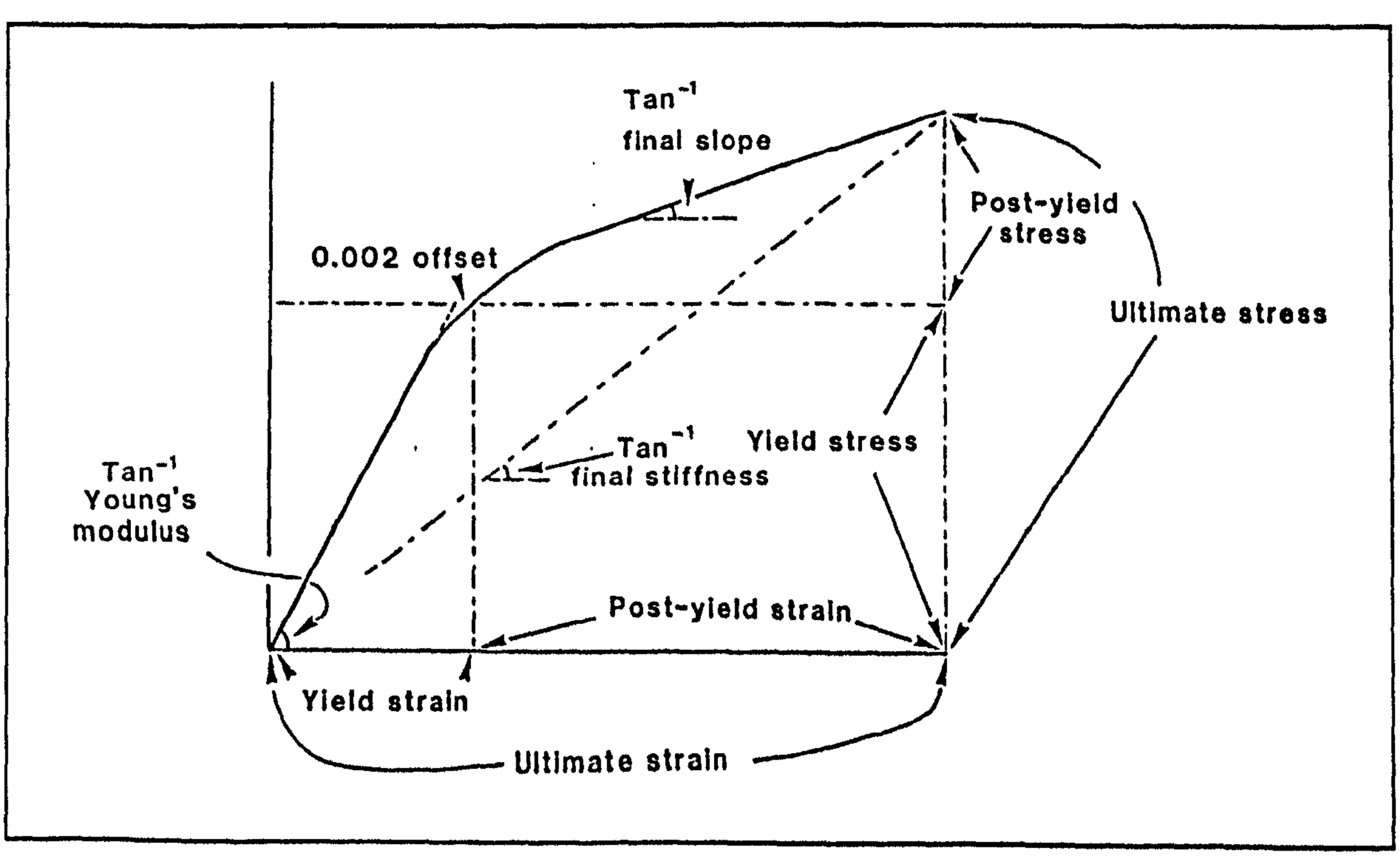

Figure 3.006 Reproduced from Currey (1989)

The derivation of the various mechanical variables examined with respect to strain rate by Currey (1989)

---

[10]The method used to determine these strain rates is criticised in appendix 7. Here it is sufficient say they contain an error. However, this will only have a slight effect (if any) on the exponent of the strain rate.

The data Currey obtained from the specimens of reindeer antler were analysed using multiple least-squares linear regression using two types of equation:

$$M = B_1 + B_2 \ln(\dot{\varepsilon}) + B_3 (BVF) + B_4 (MVF) + B_5 E \qquad (3.004)$$

where

BVF = bone volume fraction

MVF = mineral volume fraction

E = Young's modulus of elasticity

The second form of equation (which was regressed in logarithmic form) is

$$M = C_1 \times (\dot{\varepsilon})^{C_2} \times (BVF)^{C_3} \times (MVF)^{C_4} \times E^{C_5} \qquad (3.005)$$

where $M = \sigma_y, \sigma_{py}, \sigma_{ult}, \varepsilon_y, \varepsilon_{py}, \varepsilon_{ult}$, slope, work or stiffness.

Currey presents his results (for the untransformed and logged forms of analysis) in tabular form. Included in his table are the results for the explanatory variables that improve the value of the R^2 only. I will not reproduce this table here (although later I will compare my results with them), for Currey highlights the important points, some of which I will repeat here. Of the untransformed data he says that

> Young's modulus showed no significant relationship with any of the explanatory variables, or any combinations of them. In the case of the other variables to be explained, strain rate was always a significant explanatory variable, and Young's modulus itself added significantly to the amount of variance explained in the case of six of the nine mechanical variables.[11]

He then reports that bone volume fraction and mineral content have significant explanatory power in some cases. He continues, stating that

> For each mechanical variable, except final stiffness, variation in strain rate has more effect than variation in the other explanatory variables.

Currey (1989) reports that, although of a different form, the pattern of results for the logarithmic equations is very similar. He provides a table containing the exponents of strain rate in the various equations relating this quantity to the various dependent variables, using logged values, when the other variables (in equation 3.005) are held constant. This table is reproduced below. Currey found the relationship of E, the stiffness, to strain rate was not significant (NS). (In this paper Currey defined a significant variable as one that improved the overall predictive power of the regression equation. This, as he points out, does not mean the variable is significant in the more

---

[11]This paper is also reviewed in section 3.3.3, where the relationship of this statement to the TDF and NTDF models of Carter and Caler (introduced below) is highlighted.

formal statistical meaning of the term.) The exponents of strain rate are presented in table 3.003.

Dependent variable	Exponents of strain rate, $\dot{\varepsilon}$
E, Young's modulus	0.015 (NS)
ε_y, yield strain	0.063
ε_{ult}, ultimate strain	0.044
ε_{py}, strain in the post yield region	0.040
σ_y, yield stress	0.063
σ_{ult}, ultimate stress	0.050
σ_{py}, stress in the post yield region	0.032
Slope: final slope	0.094
Work: area under the stress-strain curve	0.093
Final stiffness	0.006 (NS)

Table 3.003 After Currey (1989)

The exponents of strain rate in the equations relating it to the various dependent variables for tensile tests of reindeer antler

Currey (1989) reports that for his antler specimens 'there is apparently no dependence of Young's modulus on strain rate'. He cites other workers as having found such a relationship in normal bone then states that 'no explanation for this difference is offered'. I consider that the strength of any such relationship that may exist will not be fully expressed in Currey's experimental results due to his use of an open loop test machine. If the material is time-dependent, a higher cross-head speed would be expected to induce a stiffer response from the specimen. However, due to the open loop control a stiffer response will result in a lower strain rate. This will produce a slight uncoupling the relationship of strain rate to stiffness. Therefore the observation that there is such an effect in these tests, albeit non-significant, may be stronger evidence for its existence than the statistical analysis would imply. This interaction is modelled in appendix 7, and evidence for its existence in my own work is given in section 4.2.5 and 4.2.6.3.

The rate dependence of the mechanical properties (such as material stiffness) of bone and antler demonstrates that they should not be described as an elastic material or even an elastic-plastic material, because such descriptions imply rate-independent behaviour. An elastic material when subjected to a constant load displays a constant deformation. This is not the case with bone or antler. This aspect of their behaviour is considered next.

3.2.3. CREEP TESTS

As noted above there are two forms of static experiment commonly used to examine viscoelastic materials, or materials that are considered to be viscoelastic: *stress relaxation* and *creep* tests. As creep tests are the most important of the two I will only consider these. The two tests are related and I have observed a phenomenon akin to stress relaxation in a number of specimens. These specimens were stretched in the materials testing machine, the cross-head of which was then stopped. The load experienced by the specimen was seen to fall as in a stress relaxation test. However, due to the machine used, the specimens also extended; see appendix 7. I will describe a few studies that assume a viscoelastic, or viscoelastic like, nature for bone. Then some studies that use the concept of damage accumulation will be examined.

A paper by Currey (1965) on the time-dependent behaviour of bone (and echinoderm skeletons) is associated with the word *creep* by Katz (1980b) and Lakes and Katz (1984). However, Currey included neither term in his paper. Instead he used the term *anelasticity*. This he defines as 'a recoverable strain appearing over a period of time'. This initial definition is broader, than that of viscoelasticity. However, Currey then narrowed his definition (to essentially that of viscoelasticity) with the inclusion of the statement quoted below. With hindsight (and perhaps excessive reading between the lines) this statement appears to imply that Currey gave consideration to the accumulation of damage, expressed as a reduction in material stiffness. However, he has assured me that the idea of damage accumulation was not in his mind at the time.

> If a piece of material is loaded for a long time and shows an extra deflexion beyond the initial one. there are in general three things that could have brought this about: (a) irrecoverable plastic flow; (b) a decrease in the stiffness of the material; (c) anelasticity. These effects could, of course, be all present together. If the extra deflexion is produced solely by plastic flow, then the piece would show a permanent set when the load is removed. If the extra deflexion is caused solely by a decrease in stiffness of the material, then the piece will immediately recover *all* the extra deflexion.
>
> If, therefore, we wish to exclude the first two possibilities, we must show that all the deflexion is recoverable, that on unloading the bone will immediately recover the initial deflexion, but not the extra deflexion, and that the elastic properties are unaltered.

Currey performed creep tests in bending, using the deflexion of the beam as an indication of the strain. The specimens were tested wet at room temperature. (The effect of drying and a range of test temperatures and loads were also investigated.) Currey said that care was taken not to load the bone specimens into the 'plastic-range'. He found 'good agreement' between the results obtained in the initial and repeated test for the same sample of bone. The author states that the maximum difference in the deflexions was

only 5% initially and became less as the test continued. From his tests Currey concluded that

> at least the greater part of the considerable extra deflexion caused by prolonged loading is indeed true anelasticity, and is not plastic flow nor is it caused by a change in the elastic properties of the bone.

Thus Currey (1965) examined the bone for a reduction in material stiffness, which as noted above is an indicator of mechanical damage. He reports that no such change occurred. Therefore it appears that the bone he tested did not accumulate a measurable degree of damage. This is evidence for the viscoelastic approach and against the damage theory, at the loads used. Unfortunately, Currey gives no indication of the size of the loads he used in relation to that which would cause the material to yield or fail, only that they were 'well below the elastic limit'. Currey points out in his summary that the rate at which the anelastic deflexion appears is proportional to the applied stress. This would support the idea of linear viscoelasticity.

Currey (1965) highlights the temperature dependence of bones mechanical response (already outlined in section 1.4.4.2). He reports that the rate at which this deflexion appears increases with increasing temperature (tested over the range 2 to 50°C). This shows that for bone (as with most materials) the test conditions, including temperature, should be consistent during testing and stated when publishing the results.[12]

3.2.4. THE MECHANICAL MODELLING OF BONE: SEDLIN'S MODEL

In the previous sections I reviewed a number of papers that report the time-dependence of various properties of bone and antler. Some of these papers report that the materials, or certain aspects of them, can be modelled using viscoelasticity, while others, including those by Currey, either avoid such a comparison or highlight its limitations in describing certain behaviour. In this section I concentrate on these limitations, and the methods that have been used to extend the viscoelastic approach to encompass such behaviour.

The most widely cited model of bone's time-dependent mechanical properties (that I am aware of) is that of Sedlin (1965). It will become clear that this is not a truly viscoelastic model, so it will be referred to (in Sedlin's words) as a *rheological model.* Sedlin's study is based on the results from tests that he performed in a variety of ways upon '663 samples of human femoral cortex obtained from 43 autopsy subjects ranging in

---

[12]BS 4618 (1970) a specification for plastics testing, requires the temperature to be controlled to ±1°C of nominal and the humidity to ± 2% r.h. of nominal, unless it has no effect on the creep behaviour.

age from 14-91 years'. All the bending tests (considered here) were conducted at 37°C in Ringer's solution. The tensile tests appear to have been conducted at room temperature 21 ± 1°C and at a relative humidity of 66 ± 2%. The conditions used for the creep tests are unclear. Within Sedlin's paper these tests are placed under a number of headings. I will briefly comment on each of these sections, to put Sedlin's model into context.

The first section of Sedlin's work I consider is what he entitles 'the behavior of bone under a constant deformation'. These tests initially appear to be the same as a stress relaxation test, and if the deformation was indeed held constant, they are identical. The so-called constant deformation was obtained by stopping the cross-head of the materials testing machine.[13] Thus I suggest that Sedlin falsely assumed that his test machine and fixtures were infinitely rigid. As explained in appendix 7, an open loop test machine is not rigid, and a reduction in load will result in an increase in the specimen length, contradicting the basis of a stress relaxation test. Such an observation in my own work was reported in section 3.2.3. Sedlin (1965) subjected a number of specimens to such constant deformation tests, some in cantilever bending, 16 in tension, 25 in three-point-bending, 5 complete femurs in longitudinal compression and 15 blocks in compression. The deformation used was that obtained at 25 % of the estimated failure load. Sedlin says that

> The *qualitative* result was *identical* in all specimens from all subjects. When deformation become constant (i.e. loading stopped), a decrease in stress occurred with 50-60 % of the decrease being apparent at 30". . . The curves all were asymptotic to some new level, but none tended to zero.

From this Sedlin concluded that these tests 'demonstrate that stress relaxation is a phenomenon present in bone and that bone has a relaxation time as a material property'.

Sedlin's next series of tests investigate the 'changes in the deformation of bone at different rates of deformation up to a constant load'. The different deformation rates were achieved by using different cross-head speeds. As in the stress relaxation type tests different forms of loading were used. The cross-head speeds used were limited by the rate of response of the chart recorder. The specimens were loaded to a constant level rather than to failure so that the same specimen could be retested at the different speeds. The specimens were then re-tested the next day, the order of the speeds being reversed. From these rather restricted tests Sedlin concluded that

> the results for cantilever bending and tension demonstrate that bone deforms less with rapid loading conditions than with slower conditions. . . It is thus evident that deformation of bone is some function of the rate of deformation and that the modulus of elasticity of bone is, in reality, a range of values.

---

[13]In the description of the Instron TT-CM tensile test machine used, Sedlin says 'one can run the [chart] recorder while cross-heads are stopped, thus obtaining a direct record of the behavior of stress over time under constant deformation'.

The third section of Sedlin's paper considers the 'behavior of bone during loading and unloading at different constant rates'. A number of different specimens were tested in a number of different ways: 25 cantilever, 5 blocks in compression, 15 three-point-bending and 10 in tension. Again only a very limited range of test speeds was used. Sedlin reports that the general shape of the hysteresis loops differed according to the type of loading. However, in all tests a loop was described and the findings were similar. The inclination of the loop was greater at the higher testing speeds, as would be expected from the results mentioned above. Sedlin also found that the residual deformation at zero stress was greater for the more slowly loaded specimen. He concludes 'these hysteresis loops thus indicate that more energy is dissipated in this type of testing with a slow rate as compared to a more rapid rate'.

The final set of experiments investigated 'the characteristics of bone deformation under a constant load - creep studies'. Five tensile specimens were loaded using a dead weight loading device. Sedlin states that 'readings of deformation were accurate to 0.0005 mm'. The specimens had a reduced central section of $2 \times 3 \times 25$ mm. Loading was performed in a successive manner, with loads of 5, 10, 20 and 30 kg loads for two specimens and 10, 20 and 30 kg for the others. The load was applied for 30 minutes, then released. The test was deemed to be complete when the specimen returned to its original length or when 30 minutes had passed. The results are summarised in figure 3.007. Under the lower loads the maximal deformation was reached almost immediately after the application of the load. In the case of the higher loads the maximum deformation occurred some time after their application. When he describes the creep tests that used the 20 kg load Sedlin says that

> all specimens showed progressive deformation up to 30'. With removal of the load, only one specimen regained original length within 30'.

This deformation was even more pronounced in the case of the 30 kg load.

Sedlin (1965) reports a number of features common to all creep tests. The initial deformation was attained as rapidly as the specimens could be loaded (10 to 15 seconds) with the equipment used, while the initial recovery length was attained as rapidly as they could be unloaded (1 to 2 seconds). From these observations Sedlin concludes that bone possesses both instantaneous elasticity and a time-dependent deformation under load.

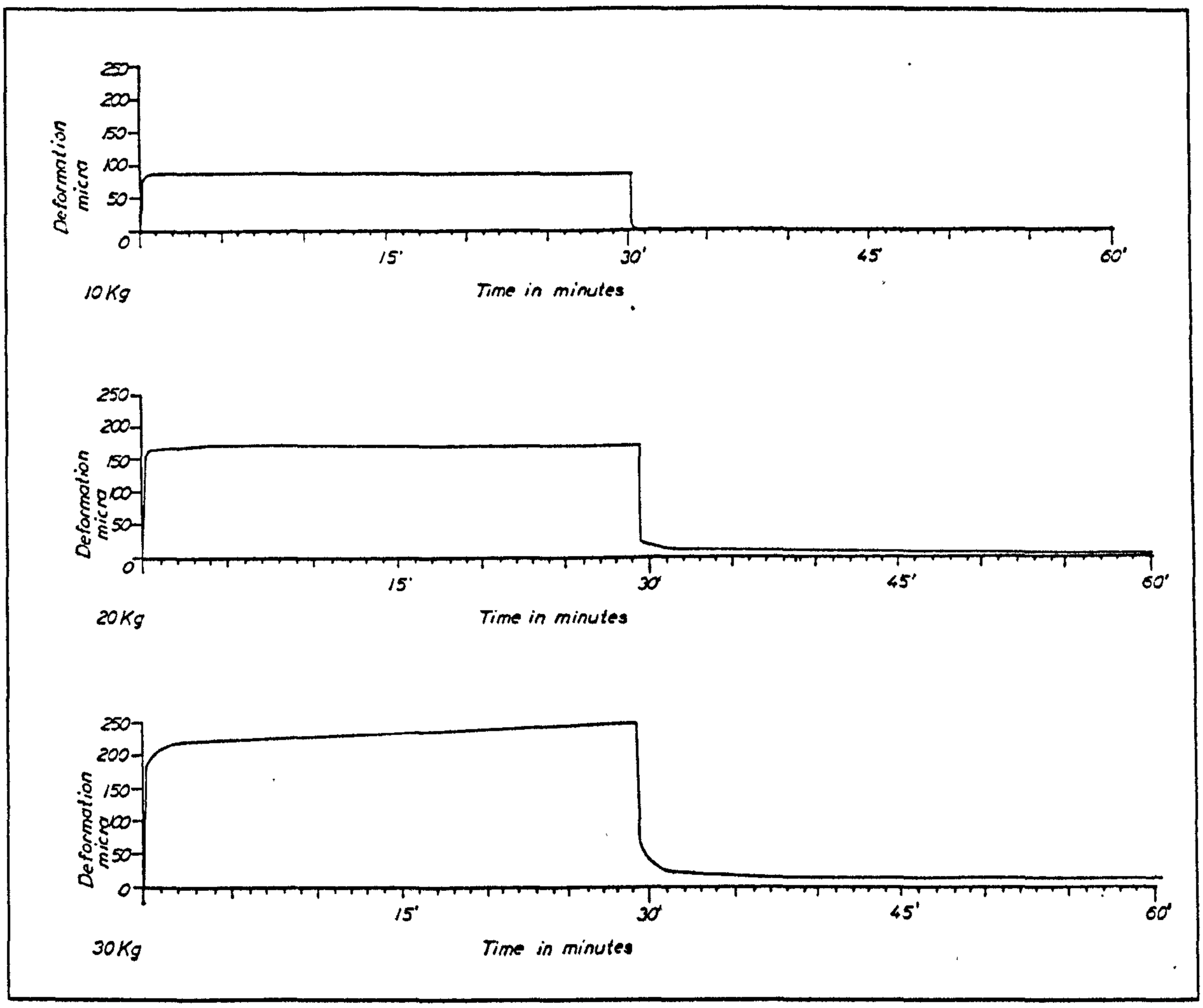

Figure 3.007 Reproduced from Sedlin (1965)

The deformation of human bone during creep tests conducted at different load levels

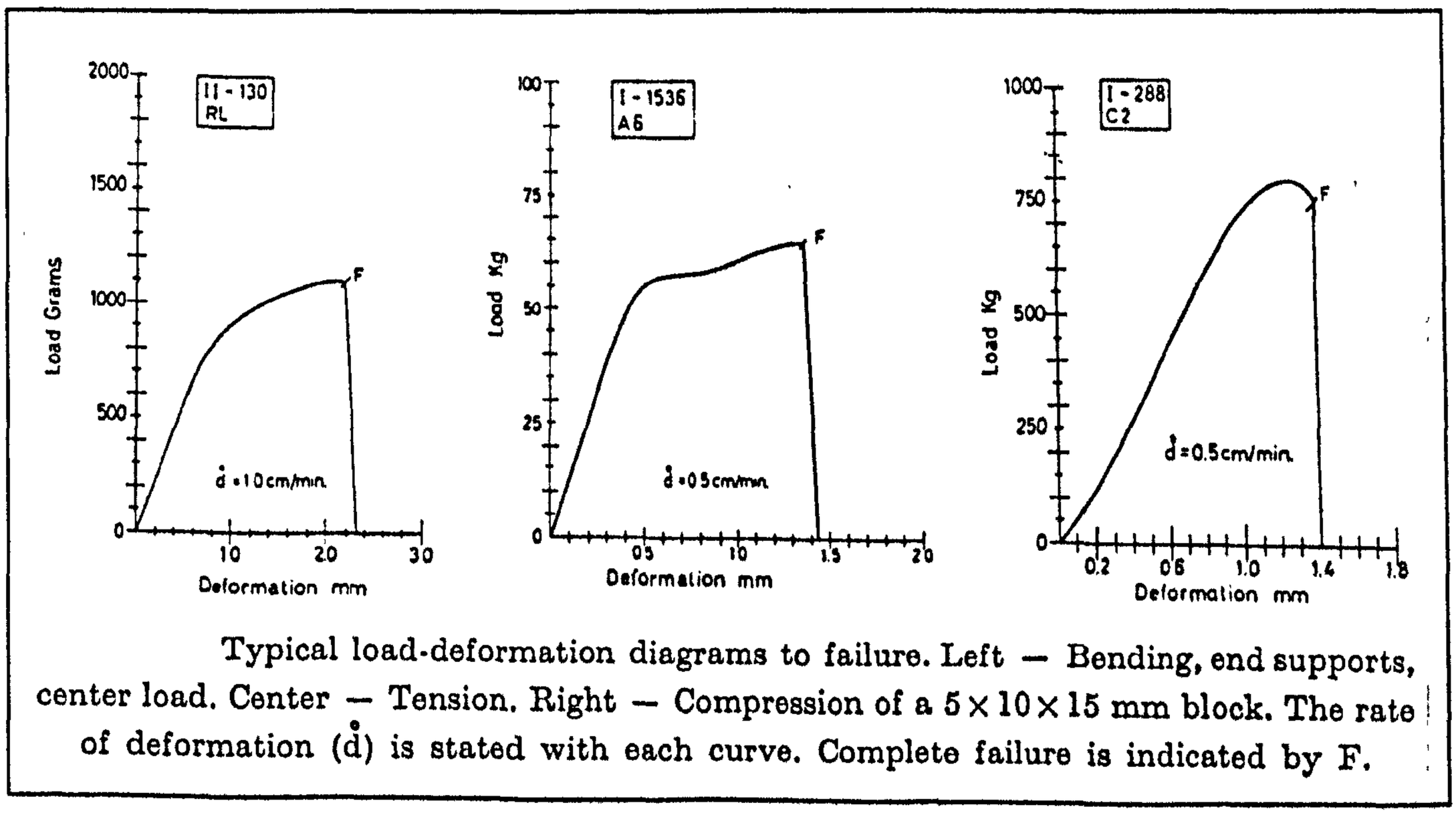

Typical load-deformation diagrams to failure. Left — Bending, end supports, center load. Center — Tension. Right — Compression of a $5 \times 10 \times 15$ mm block. The rate of deformation ($\dot{d}$) is stated with each curve. Complete failure is indicated by F.

Figure 3.008 Reproduced from Sedlin (1965)

Load deformation plots of human femoral bone

Sedlin (1965) reports that the strain-time curves for all subjects, taken individually, showed a good fit to the following equation, for the loading portion of the experiment:

$$\varepsilon(t) = A\left(1 - e^{-Bt}\right) \qquad (3.006)$$

where A and B are constants. If it is assumed that the constant A contains the stress term (a valid assumption as the specimens were examined individually) this equation is the same as that for a strain of a Kelvin solid during a creep test (equation 2.013).

Sedlin conducted additional creep tests on five specimens, in these cases a load of 30 kg was maintained for 24 hours and the recovery was recorded for another 24 hours. He reports that two specimens attained a constant deformation within the loading period, two others continued to deform for the entire period, and one specimen failed after one hour. Of the three specimens for which a recording of the unloading was obtained, all exhibited some residual deformation at the end of the test. Sedlin says that

> it can be concluded from this phase of the experiment that bone will attain a constant deformation under a constant load or will fail. If the load is of sufficient magnitude, permanent deformation will result.

This statement initially appears to support the use of a viscoelastic solid, rather than a viscoelastic fluid, as a model. However, it also introduces failure, thus indicating one of the limitations of such a model. The final point in the statement indicates some degree of plasticity or some other irreversible process.

It is upon the above results and load deformation tests that Sedlin constructs his model of the time-dependent behaviour of bone. Sedlin (1965) reports that inspection of the load-deformation curves revealed one common feature for all types of loading used: 'there were no straight lines'. (His loading curves are reproduced in figure 3.008.) He says this feature therefore 'eliminated the perfectly elastic body', by which I assume he means a linear-elastic body. The existence of a progressive increase in stress until failure of the specimens likewise eliminated the perfect plastic and rigid plastic bodies as suitable models. The simple Newtonian liquid could also be eliminated from the search for a suitable model. However, the presence of viscous damping is implied by four factors; the time-dependent deformation under constant load, the existence of stress relaxation, the hysteresis loop and the strain rate dependence of the material stiffness. Sedlin thus proposed a working model that appeared to account for the behaviour at small load levels. This model was a spring in series with a Kelvin solid. (This model, the three-element solid, has already been described in section 2.2.1.4.) Sedlin then compared the theoretical response of this model with the results of his experimental work. I summarise his findings in table 3.004.

Property or experiment	Does Sedlin (1965) consider a three-element solid is consistent with his experimental results	Comments
Loading-unloading constant strain rate	Yes	
Increased stiffness and narrower hysteresis loop at higher strain rates	Yes	
Stress relaxation	Yes	
Creep test	Yes, during the period the load is applied, but not during the recovery period.	In the model all creep strain is recovered on unloading, this was not observed in the experiments conducted at the higher loads.
Monotonic loading	No	Sedlin did not examine this specifically in relation to this model, but used information from these tests to determine the type of modifications required.

Table 3.004

Sedlin's consideration of using a three-element solid to explain his experimental results

As a result of the areas of disagreement between the model and his experimental findings, Sedlin introduces another element into his three-element model. This element is composed of a number of Saint-Venant bodies in series. Thus its inclusion signifies a departure from a truly viscoelastic model. Sedlin says that the addition of such a group of elements, in series with the three-element model, accounts for all but one aspect of the experimental data. During the creep tests he noted that there was no sudden increase in the deformation after the initial load was applied. If the friction elements were acting in an undamped fashion, Sedlin says there would be sudden increases at various phases of the strain-time diagrams as different yield stresses were passed. He therefore added a damping element to the model, in parallel to the friction elements. This model was then rearranged into the form shown in figure 3.009.

Sedlin concludes the section on his rheological model with the following statement:

> This model thus explains all of the observations, and answers the requirement of being the simplest model that was compatible with the available data. It consists of a

Hooke body linked in series to a unit consisting of a Newton body in parallel with a modified Prandtl body. No attempt should be made to ascribe anatomical elements to the components of the model.

It is interesting to contrast Sedlin's statement with that of Lakes and Katz (1984). The latter workers report that a variety of mechanisms have been proposed to account for the mechanical energy losses associated with viscoelasticity. These elements range from lamellar motions to stress-induced fluid motion. However, there is a considerable difference between proposing a mechanism to account for viscoelasticity and associating physical structures with the elements of a spring and dashpot model. Viscoelasticity is a mathematical representation of time-dependent behaviour. The spring and dashpot models are only an analogue of the mathematics and an aid to understanding. Such models have no obvious structural basis, although this behaviour may be due to structural features.

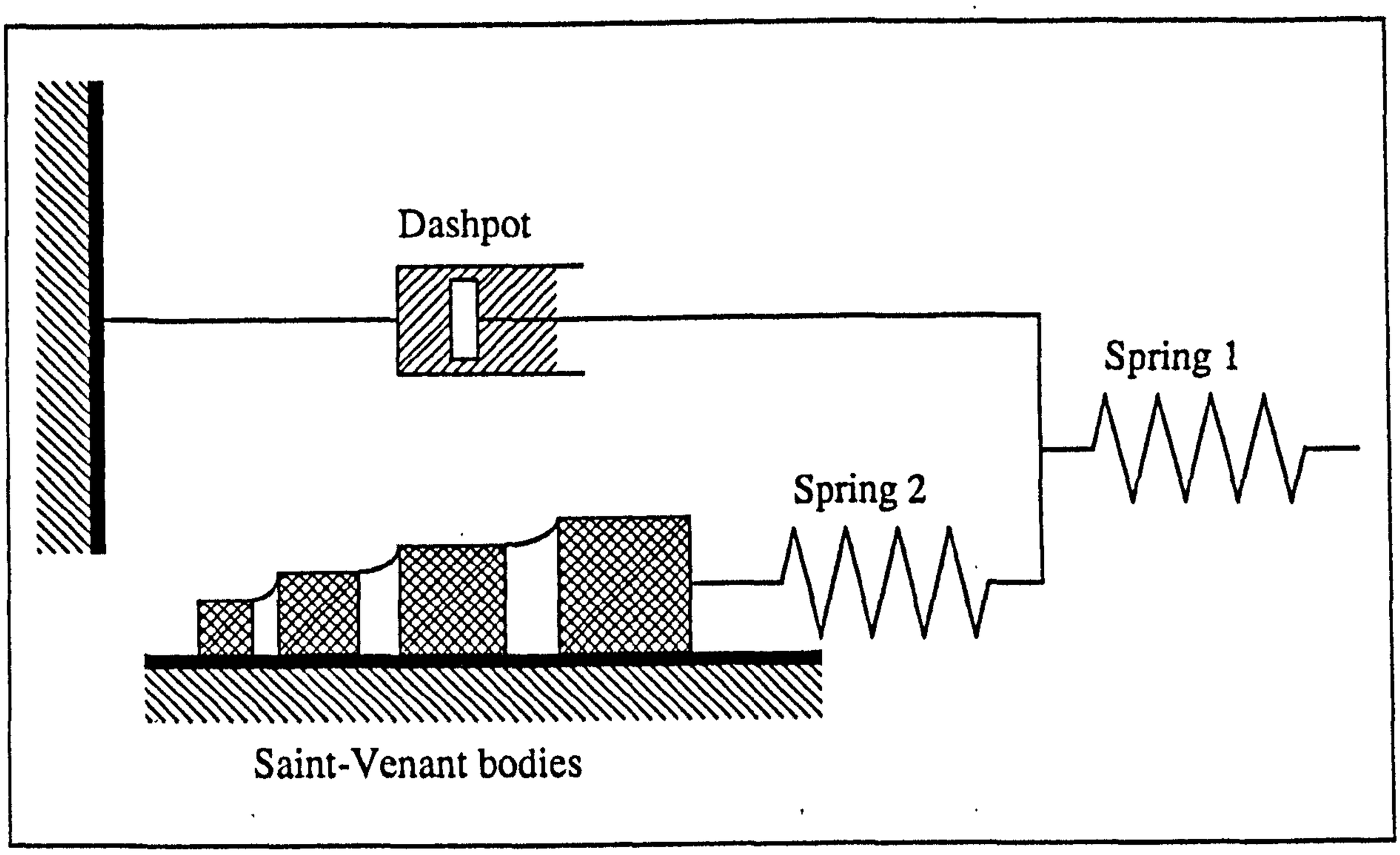

Figure 3.009

Sedlin's rheological model for cortical bone

3.2.4.1. COMMENTS ON SEDLIN'S MODEL

Sedlin's model is an adaptation of a viscoelastic model to account for the knee in the loading curve of bone. If the applied stress is below that at which the Saint-Venant bodies start to move, this model is the same as a three-element solid. As reported above when the stress on a Saint-Venant body reaches a set value it starts to move. This motion produces a sharp knee in the stress-strain curve. A chain of such elements has a smoothing effect. This arrangement is able to model another aspect of bone's behaviour:

the increase in the value of the stress at which the knee occurs when a faster loading rate is used. (This is an aspect of the model that was not reported by Sedlin.) The ability of Sedlin's model to mimic the rate dependence of the knee stress is explained by the rate-dependent response of the dashpot: the faster it is loaded the more resistance it exhibits. Thus the faster the whole model is loaded the greater is the proportion of the load exerted on the dashpot. This results in the Saint-Venant bodies experiencing proportionally less load. Thus the model predicts a higher value of knee-stress at higher loading rates. The extreme case of this is akin to the models proposed by Tanabe *et al.* (1991a) where the dashpot is modelled as a slider or a rigid element at the extremes of strain rate. In the first case all the load is transmitted to the Saint-Venant bodies, and in the latter no load is transmitted to them.

The arrangement of elements proposed by Sedlin (1965) appears to model many aspects of the behaviour of bone. However, this model still lacks a process of final failure. It also implies that the deformation is not recovered. On the other hand the initial mechanical properties of the material are recovered with time. Currey (1965) found that the deformation was recoverable, and the mechanical response remained unaltered below the knee region while I have provided evidence (figure 1.011) that there is a change in the mechanical response of bone after the knee region. These responses can not be mimicked by Sedlin's modification to viscoelasticity, a modification based on plasticity.

Piekarski (1978) suggests that reversing the order of the Saint-Venant bodies and connecting them with springs 'may allow the possibility that in cyclic loading some reversible plastic deformation can occur'. He also modifies the spring and dashpot arrangement, as shown in figure 3.010. (If spring a is stiffer than spring b, this change in arrangement of the springs is only of cosmetic value.)

Piekarski does not extend his analysis beyond the statement I have quoted. Consideration of the model shows that the nature of the unloading path is dependent on the viscosity of the dashpot. It is not clear if the unloading path predicted by this model is that demonstrated by bone. The manner in which the force in the Saint-Venant bodies will decrease during unloading depends on the viscosity of the dashpot. The force on these bodies determines when and where they stop, and thus the changes in stiffness of the body. As with Sedlin's original model, Piekarski's model does not contain a failure mechanism.

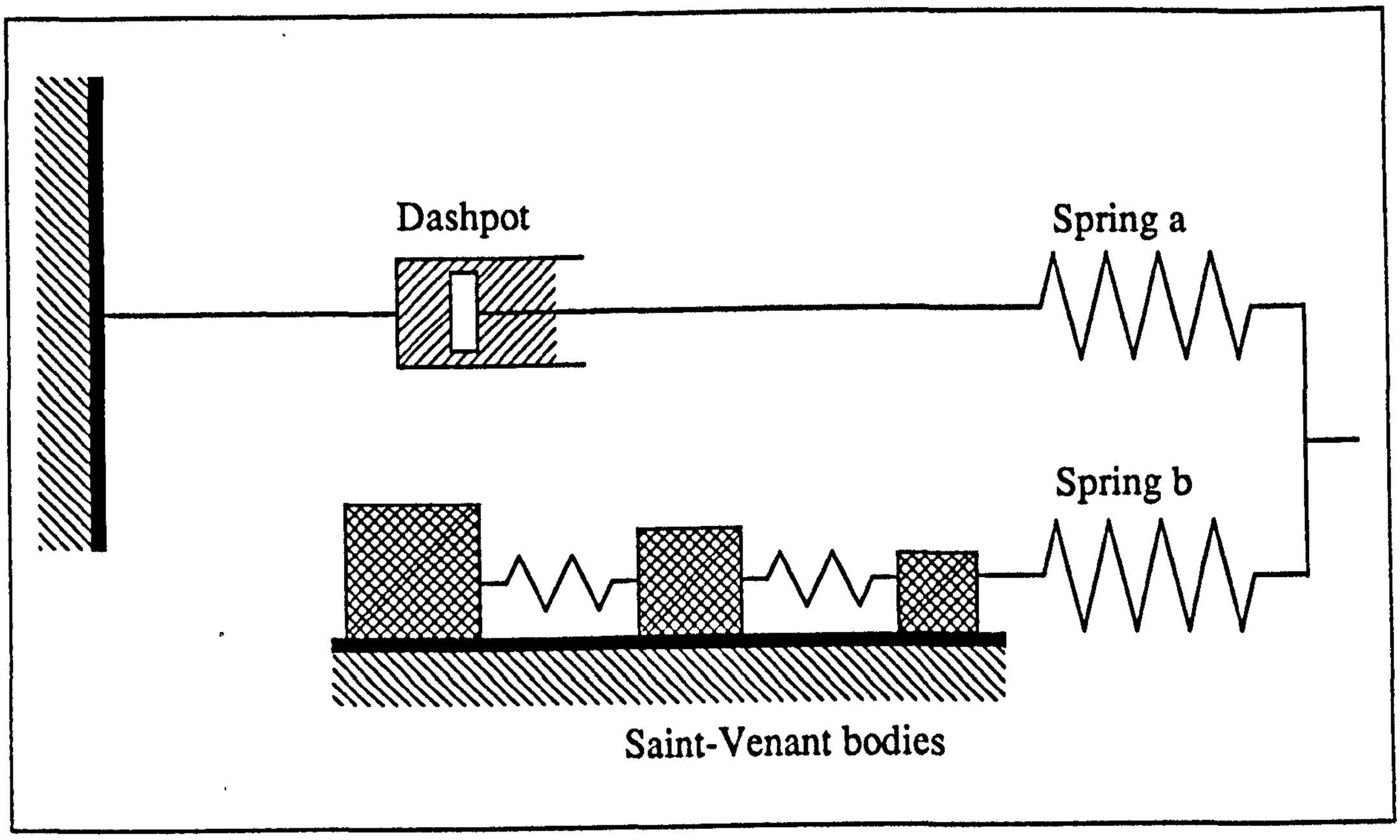

Figure 3.010 After Piekarski (1978)

Piekarski's proposed rheological model for bone

In the next section I examine another approach to modelling bone's behaviour: damage accumulation. As stated above, this may be viewed as the failure of small elements within the bone. This results in a change in the specimen's mechanical properties. This approach, almost by definition, also contains a criterion for final failure.

3.3. CREEP-RUPTURE AND THE CONCEPT OF DAMAGE

The first published application of the theory of damage accumulation to bone that I am aware of is that of Carter and Caler (1983).[14] However, their earlier work shows a progression towards the application of the damage approach.

Carter and Caler, in some cases in association with other people, have published a series of papers on damage accumulation and related subjects. These include Carter and Caler (1983), Carter and Caler (1985), Caler and Carter (1989) and Pattin *et al.* (1990). Before their 1983 paper, Carter and Caler (again individually or in association with others) had published a number of papers in which they examined time-dependent properties and fatigue. (These earlier papers include Carter and Hayes, 1976; Carter and Hayes, 1977a; Carter and Hayes, 1977b; and Carter *et al.* 1981a and b.) However, in

---

[14]It is possible to argue that the clinical literature on *stress fractures* has been concerned with this problem for several more decades.

these papers the results were not analysed by using the damage concept. Almost all the previously mentioned papers deal with the mechanical response of bone in two situations: creep testing and fatigue testing.[15] They also investigate the interaction between these two situations. I will concentrate on the creep aspect of their work here.[16]

Carter and Caler's (and co-workers) application of the theory of damage accumulation to bone appears to have occurred in the reverse order to the development of the original theory. The original theory was developed to explain observed mechanical behaviour, and evidence for a physical explanation was gathered later. In their early work Carter and Caler used the ideas of crack formation and damage. However, it is only in their more recent papers that they use the theory of damage accumulation to explain some aspects of bone's mechanical behaviour.

Carter and Caler's 1983 paper contains the background to their application of the concept of damage. They refer in their introduction to the work of Carter and Hayes (1977a) entitled *Compact Bone Fatigue Damage: A Microscopic Examination.* This earlier paper is closely related to another one by the same workers (Carter and Hayes, 1977b) entitled *Compact bone Fatigue Damage: I Residual Strength and Stiffness.* In the second paper the authors subject bone specimens to a variety of tests, the results of which Carter and Hayes (1977) summarise in the following way:

> These studies show that repeated loading of bone can cause a progressive loss of stiffness and ultimate strength. A similar fatigue behavior is seen in composite materials and is attributed to cumulative microcracking, debonding, void growth, and fibre breakage. . . These results further suggest that bone yielding observed in monotonic loading to failure is caused by diffuse structural damage such as microcracking and debonding.

In the introduction of Carter and Hayes (1976) there is another general reference to fatigue damage. Carter and Hayes point out that the stress to which bone is normally subjected is less than that required to cause fracture. They continue, stating that 'repeated loading of bone in everyday activities or prolonged exercise, however, may lead to microscopic damage'. When behaviour such as that described in the above quotations is observed in an engineering composite (such as a combination of fibres and a matrix or a material like concrete) it is commonly explained, or modelled, by the concept of damage accumulation based on Kachanov's theory.

---

[15]A fatigue failure is one that occurs due to a larger number of repeated stress cycles, below the level that results in a change in the mechanical response of the material in monotonic loading, for example below the yield stress in metals.
[16]In chapter 9 some papers that discuss aspects of the physical basis of the damage concept in relation to the structure of bone are reviewed.

3.3.1. CARTER AND CALER'S TIME-DEPENDENT FAILURE (TDF) MODEL

As I have pointed out above, it is not until their paper in 1983 that Carter and Caler apply the damage approach to bone. This section contains an examination of that paper and the development of the model of failure that it contains.

The test material described in Carter and Caler's 1983 paper is human bone, from the mid-diaphyses of the femurs of two males and one female. The specimens were oriented with the long axis of the bone. The specimens were turned on a lathe to produce a central section of 3 mm and a gauge length of 10 mm. The bone was not allowed to dry at any time during preparation. The specimens were stored at -20°C prior to testing. Mechanical testing was conducted in a high humidity environmental chamber with an ambient temperature of 37°C.

Carter and Caler (1983) describe their 'time-dependent failure', TDF, model in the following way: first, they assume that damage accumulation is related to 'the time (t) history of the stress magnitude' only, and second, they assume that failure will occur at time t_{fail} when the following equation is satisfied[17]

$$\int_0^{t_{fail}} \frac{1}{t_R\,[\sigma(t)]}\,dt = 1 \qquad (3.007)$$

where

t_{fail} = time-to-fail

$\sigma(t)$ = the stress history

$t_R\,[\sigma]$ = the time-to-rupture in a creep test, with stress level σ.

The authors point out that to apply such an equation the function $t_R\,[\sigma]$ must be determined from constant stress creep-rupture tests. They state that a power law relationship fitted their experimental data better than an exponential one. They use a power law relationship of the form

$$t_R\,[\sigma] = B\,\sigma^{-n} \qquad (3.008)$$

where B and n are empirically determined constants. Carter and Caler continue, saying that these two equations provide a creep-rupture model equivalent to the brittle-fracture model proposed by Kachanov (reviewed in chapter 2). The values that Carter and Caler

---

[17]As I use some of their letters and symbols elsewhere, I have changed their nomenclature to avoid confusion.

(1983) give for the constants B and n are 3.02×10^{35} and 17.95, when the time is in seconds and the stress is expressed in MPa. Thus equation 3.008 can be represented as

$$t_R = 3.02\times10^{35}\ \sigma^{-17.95} \qquad (3.009)$$

According to this equation an increase in stress will severely reduce the time-to-rupture in a creep test. The relative size of this decrease in time-to-rupture will become larger at higher stresses. For example a stress of 60 MPa will result in a rupture time of 3649 seconds and a 1% increase to 60.6 MPa will give a rupture time of 3052 seconds, while a stress of 90 MPa gives 2.52 seconds and 90.9 MPa, 2.11 seconds. The equation predicts that a 1% increase in the level of the stress will result in a 16.4% decrease in the time-to-rupture.

In making a comparison with the work of Kachanov, Carter and Caler appear to be referring to the equivalent of equation 2.047. These two equations have a slightly different form. As I am conducting a study of two materials, bovine bone and antler, it may be better to use the original form of Kachanov's equation, in which the constants are not combined. I have therefore repeated equation 2.047 below (3.010), and then rearranged it into a form comparable with equation 3.009. The values of the constants are then substituted into it.

$$t_2 = \frac{1}{B_2\,(n+1)\,\sigma_0^{\,n}} \qquad (3.010)$$

$$t_2 = \left(\frac{1}{B_2\,(n+1)}\right)\sigma_0^{\,-n} \qquad (3.011)$$

When compared to Caler and Carter's equation (3.008) and their this data implies

$$t_2 = \left(\frac{1}{1.75\times10^{-37}\,(17.95+1)}\right)\sigma_0^{\,-17.95} \qquad (3.012)$$

If an equation of the form of 3.012 is used in place of 3.009, it is possible to examine the values of B_2 for each material. This may give more insight than the value of B alone; as the above equation implies that B is a function of n. I will return to this expanded form of equation later; before I do so I will continue with Carter and Caler's approach.

Carter and Caler (1983) say that combining their equation relating the time-to-rupture and the creep stress (represented here as equation 3.008) and their assumed model of damage accumulation (3.007) 'provides a creep-fracture model equivalent to the brittle-fracture creep model proposed by Kachanov'. I question their logic, as an inspection of the other equations given by Kachanov shows that the equation for a purely ductile failure (equation 2.038) is also of the same form as their equation. Clearly the

creep-rupture (or more general failure) of bone is not a purely ductile process, due to its limited extension at failure. However, this is an aspect of Kachanov's work that is not questioned or commented on by Carter and Caler. If their equation is assumed to be equivalent to equation 2.038 (that which gives the time-to-rupture by a purely ductile process) then the high exponent of stress, 17.95, suggests that the extension of specimens of human bone during a creep test is strongly concentrated in the period just prior to failure. (This is shown by substituting 17.95 into equation 2.040, or comparing this value with those of m in figure 2.10.)

Carter and Caler (1983) then use their TDF model to predict some aspects of the mechanical response of two other stress histories. I will consider one of these - the case of loading at a constant stress rate until failure. Carter and Caler (1983) refer to this situation as 'monotonic failure at a constant stress rate'. The authors use equation 3.013 and another based on equation 3.008 to produce a predictive model of the ultimate tensile strength, σ_{ult}, for any stress rate, $\dot{\sigma}$. For such a constant stress rate the stress history $\sigma(t)$ is expressed as.

$$\sigma(t) = \dot{\sigma}\, t \tag{3.013}$$

From equation 3.008 it follows that

$$t_R\,[\sigma(t)] = B\,[\dot{\sigma}\, t]^{-n} \tag{3.014}$$

Substituting equation 3.014 into equation 3.007 gives

$$\int_0^{t_{ult}} \frac{1}{B\,[\dot{\sigma}\, t]^{-n}}\, dt = 1 \tag{3.015}$$

and

$$\int_0^{t_{ult}} \frac{1}{B}\,[\dot{\sigma}\, t]^n\, dt = \frac{\dot{\sigma}^n}{B} \int_0^{t_{ult}} t^n\, dt = \frac{\dot{\sigma}^n}{B}\left[\frac{1}{n+1}\, t^{n+1}\right]_0^{t_{ult}} = 1 \tag{3.016}$$

This equation can be expressed in a more concise way as

$$\frac{\dot{\sigma}^n}{B}\left[\frac{{t_{ult}}^{n+1}}{n+1}\right] = 1 \tag{3.017}$$

Equation 3.017 can then be rearranged to give the relationship between the, stress rate (which is constant) and ultimate stress by using the relationship, $\sigma_{ult} = \dot{\sigma}\, t_{ult}$. First the equation is rearranged into an appropriate form:

$$\dot{\sigma}^n\, {t_{ult}}^{n+1} = B\,(n+1) \tag{3.018}$$

which is the same as

$$\frac{\dot{\sigma}^{n+1} t_{ult}^{n+1}}{\dot{\sigma}} = B(n+1) \tag{3.019}$$

Next the substitution of equation 3.031 is made

$$\frac{\sigma_{ult}^{n+1}}{\dot{\sigma}} = B(n+1) \tag{3.020}$$

This can be rearranged to give

$$\sigma_{ult} = \left(B\,\dot{\sigma}\,(n+1)\right)^{1/(n+1)} \tag{3.021}$$

Which may be expressed in logarithmic form as

$$\ln(\sigma_{ult}) = \frac{1}{n+1}\left(\ln(B(n+1)) + \ln(\dot{\sigma})\right) \tag{3.022}$$

Equation 3.022 may more simply be expressed as

$$\ln(\sigma_{ult}) = C_1 + C_2 \ln(\dot{\sigma}) \tag{3.023}$$

Using the above equation (3.023) and the values of the constants that they derived from the creep tests, Carter and Caler (1983) produced the following prediction for the ultimate stress in monotonic loading:

$$\sigma_{ult} = 87\dot{\sigma}^{0.0528} \tag{3.024}$$

where the stress is measured in MPa and the rate is in units of MPa s^{-1}. The value of the coefficient is similar to those in the literature. (For example Currey (1975), see table 3.002.) Carter and Caler manipulated their equation for monotonic loading to give an expression in terms of the strain rate, $\dot{\varepsilon}$. This they achieved by using a, previously, experimentally determined relationship of the material stiffness to the strain rate:

$$E = C\,\dot{\varepsilon}^{m} \tag{3.025}$$

Considering that during the linear portion of the stress-strain curve E is constant and thus $\dot{\sigma} = E\,\dot{\varepsilon}$, Carter and Caler combined equation 3.025 with the relationship of stress to time during a constant stress rate loading, $\sigma = \dot{\sigma}\,t$, to give

$$\sigma = \left(C\,\dot{\varepsilon}^{m}\right)\dot{\varepsilon}\,t = C\,\dot{\varepsilon}^{m+1}\,t \tag{3.026}$$

Therefore

$$\dot{\sigma} = C\,\dot{\varepsilon}^{m+1} \tag{3.027}$$

And by substitution into equation 3.021

$$\sigma_{ult} = \left(B \left(C \dot{\varepsilon}^{m+1}\right) (n + 1)\right)^{1/(n+1)} \tag{3.028}$$

This may be rearranged as

$$\sigma_{ult} = \left(B C (n + 1)\right)^{1/(n+1)} \dot{\varepsilon}^{(m+1)/(n+1)} \tag{3.029}$$

Carter and Caler (1983) again supply empirically obtained values of the constants from which they obtain the relationship

$$\sigma_{ult} = 147 \dot{\varepsilon}^{0.055} \tag{3.030}$$

where the stress is measured in MPa and the strain rate is in units of s^{-1}. The comparison of these predictions of ultimate stress with experimental data is the subject of a few published papers. Such comparisons are more direct in the case of the constant strain rate equation because tensile tests are normally conducted at constant (or assumed to be constant) strain rates.

I would like to suggest that another equation (not given by Carter and Caler) can be derived using the same approach. This derivation starts with the relationship $\dot{\sigma} = E \dot{\varepsilon}$ and equation 3.021

$$\sigma_{ult} = \left(B E \dot{\varepsilon} (n + 1)\right)^{1/(n+1)} \tag{3.031}$$

Equation 3.031 may also be expressed in logarithmic form as

$$\ln(\sigma_{ult}) = \frac{1}{n + 1}\left(\ln(B (n + 1)) + \ln(E) + \ln(\dot{\varepsilon})\right) \tag{3.032}$$

where E is the material stiffness measured during the test, which is conducted at a constant strain rate. The stress and the material stiffness are in MPa and the strain rate is in reciprocal seconds. It should be remembered that this equation and that of Carter and Caler are based on a stress-strain relationship that assumes linearity. (If this assumption is correct, this equation (3.032) is identical to equation 3.022 above.) It can therefore be assumed that a departure from such linear behaviour will detrimentally affect the predictive power of the equations I have developed.

Carter and Caler (1983) also examine the case of a specimen subjected to a haversine loading history.[18] I will not consider that situation here, instead moving on to a more recent study.

---

[18]In this case the loading history was defined as $\sigma(t) = (1/2)\,\Delta\sigma\,(1 + \sin(2\,\pi\,\omega\,t))$.

Carter and Caler (1985), in a paper entitled *A Cumulative Damage Model for Bone Fracture*, present a 'theoretical analysis and interpretation of previously published experimental work'. In this paper they analyse the interaction of creep and fatigue damage, and consider the overall damage to comprise three-elements: damage due to creep, damage due to fatigue and damage due to the interaction of creep and fatigue. This they express as

$$D_S = D_C + D_F + D_I$$

where

D_S = the damage due to 'generalized' stress

D_C = the damage due to creep

D_F = the damage due to fatigue

D_I = the damage due to the interaction

The analysis of their creep data is essentially the same as in their 1983 paper. Similar ideas of summating the damage due to different causes, but also including the reduction in damage due to repair, have been presented by a number of workers. For example; this idea was presented by Nash (1966) for general self healing structures and by Martin (1992) for 'osteonal bone'.

Carter and Caler (1985) do not comment on one aspect of their results, which I consider could be important in the interpretation of their results by Kachanov's approach. This is a graphical representation of some of their earlier (1983) results for fatigue testing. Two sets of results are presented graphically; first, specimens that were cycled between zero stress and a tensile stress, and second those that were cycled between a compressive and tensile stress. What I consider to be noteworthy is the similarity between the plot of these results (reproduced as figure 3.011) and that of Kachanov's theoretical predictions (figure 2.011). Carter and Caler's 'fatigue damage' line could be considered as having some correlation with Kachanov's 'brittle failure' line, and their 'creep damage' line with his 'ductile failure' line. Due to the reversals in load, the creep component of the fatigue line is taken to be negligible, and it could thus be viewed as damage occurring within the material without the material as a whole deforming. However, drawing comparisons between fatigue and brittle failure under creep conditions is (I admit) a questionable procedure. It should also be noted that in their paper Caler and Carter (1989), when referring to the models contained in figure 3.011, say that

> A transition point for cyclic loading, from creep dominated failure at high stress to fatigue dominated behavior at low stress, was predicted. . . The stress levels we have tested so far have shown no evidence of a transition.

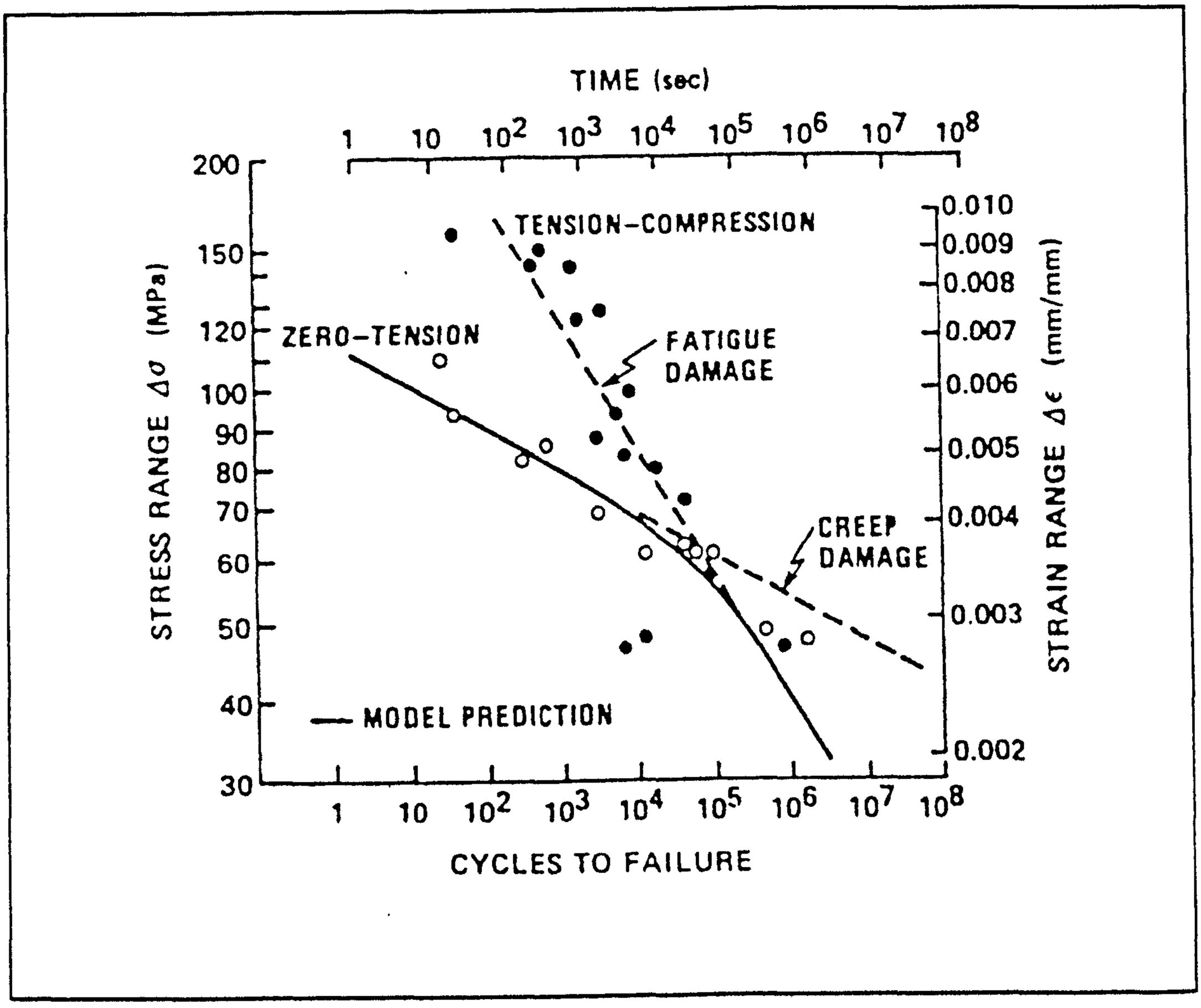

Figure 3.011 Reproduced from Carter and Caler (1985)

Graphical representation of experimental data from Carter and Caler (1983) compared to their creep-fatigue model predictions

3.3.2. CALER AND CARTER'S NORMALISED TIME-DEPENDENT FAILURE (NTDF) MODEL

In their 1989 paper, (entitled *Bone Creep-Fatigue Damage Accumulation*) Caler and Carter modified their relationship of time-to-rupture and the stress level during a creep test by the inclusion of a normalisation. This results in the following equation[19]

$$t_R [\sigma] = B_N (\sigma/E_N)^{-P} \qquad (3.033)$$

E_N is the value of the tensile material stiffness. This value of stiffness, expressed in MPa, is used to normalise the stress level. Therefore, it was measured under standard conditions at a stress rate of 28 MPa s^{-1}. The peak stress they applied to find this value

---

[19]I use E_N in place of Caler and Carter's E^*, the latter symbol is used elsewhere. Other slight changes in nomenclature and forms of expression have also been incorporated to make this section (3.3.2) more consistent with that describing their 1983 paper (3.3.1).

was 14 MPa. For this equation I have adopted the subscript 'N' and the power term 'P', as these quantities will differ from those of equation 3.008. I will refer to this model as the *normalised time-dependent failure* or NTDF model. Caler and Carter (1989) give values of the constants in equation 3.033. These were determined from a linear regression of the experimental data the results are given for 11 specimens as follows

$$B_N = 1.45\times10^{-36}\ \text{s} \qquad P = 15.81 \qquad R^2 = 95\%$$

The above constants can be substituted into equation 3.033 to give

$$t_R[\sigma] = 1.45\times10^{-36}\,(\sigma/E_N)^{-15.81} \tag{3.034}$$

As a result of including the material stiffness in the equation the value of the first constant decreases. (In fact B_N is approximately the reciprocal of B.) It should be noted that the power term also changes. Caler and Carter (1989) continue with an examination of fatigue damage. However, using the same approach as above (equation 3.014 onwards), a new model of failure stress can be produced. This I have done, as follows

$$t_R[\sigma] = B_N\,(\sigma/E_N)^{-P} = B_N\,E_N{}^P\,\sigma^{-P} \tag{3.035}$$

E_N is a specimen dependent constant and not a function of time. Thus, the ultimate stress obtained under conditions of constant stress rate, can be interpreted as

$$\sigma_{ult} = \left(B_N\,E_N{}^P\,\dot{\sigma}\,(P+1)\right)^{1/(P+1)} = E_N{}^{P/(P+1)}\left(B_N\,(P+1)\right)^{1/(P+1)}\,\dot{\sigma}^{1/(P+1)} \tag{3.036}$$

Equation 3.036 can also be expressed in logarithmic form, as

$$\ln(\sigma_{ult}) = \ln\left(E_N{}^{P/(P+1)}\right) + \ln\left(\left(B_N\,(P+1)\right)^{1/(P+1)}\right) + \ln\left(\dot{\sigma}^{1/(P+1)}\right) \tag{3.037}$$

which as the same as

$$\ln(\sigma_{ult}) = \frac{P}{P+1}\ln(E_N) + \frac{1}{P+1}\ln(B_N\,(P+1)) + \frac{1}{P+1}\ln(\dot{\sigma}) \tag{3.038}$$

In the same order of presentation this can be simplified, by combining the constants, to give

$$\ln(\sigma_{ult}) = C_1\ln(E_N) + C_2 + C_3\ln(\dot{\sigma}) \tag{3.039}$$

Due to the form of equation (3.039), expressing the value of the normalising material stiffness and the stress in different units will only alter the value of the constant C_2. (In

the literature it is quite common to use GPa for stiffness and MPa for stress.) However, Carter and Caler express their normalising stiffness in MPa, thus giving a direct ratio. The equivalents of equations 3.029 and 3.032 can be obtained in the same way and are given below. The first stage (of the derivation of the equivalent of equation 3.029) is to use the equation $\dot{\sigma} = C\,\dot{\varepsilon}^{m+1}$ (3.027) again. Thus equation 3.038 becomes

$$\ln(\sigma_{ult}) = \frac{P}{P+1}\ln(E_N) + \frac{1}{P+1}\ln\left(B_N\,(P+1)\right) + \frac{1}{P+1}\ln\left(C\,\dot{\varepsilon}^{m+1}\right) \tag{3.040}$$

Equation 3.040 is the same as

$$\ln(\sigma_{ult}) = \frac{P}{P+1}\ln(E_N) + \frac{1}{P+1}\ln\left(B_N\,(P+1)\right) + \frac{1}{P+1}\ln(C) + \frac{m+1}{P+1}\ln(\dot{\varepsilon}) \tag{3.041}$$

This may be simplified to give

$$\ln(\sigma_{ult}) = C_1\ln(E_N) + C_4 + C_5\ln(\dot{\varepsilon}) \tag{3.042}$$

I would like to suggest an alternative approach; using the relationship $\dot{\sigma} = E\,\dot{\varepsilon}$ as in the TDF model. In this case equation 3.038 becomes

$$\ln(\sigma_{ult}) = \frac{P}{P+1}\ln(E_N) + \frac{1}{P+1}\ln\left(B_N\,(P+1)\right) + \frac{1}{P+1}\ln(E\,\dot{\varepsilon}) \tag{3.043}$$

or

$$\ln(\sigma_{ult}) = \frac{P}{P+1}\ln(E_N) + \frac{1}{P+1}\ln\left(B_N\,(p+1)\right) + \frac{1}{P+1}\ln(E) + \frac{1}{P+1}\ln(\dot{\varepsilon}) \tag{3.044}$$

Remember that E is the stiffness of the specimen measured during the test and that E_N is the measure of stiffness used to normalise the data. Clearly if these two quantities are the same, then

$$\ln(\sigma_{ult}) = \ln(E) + \frac{1}{P+1}\ln\left(B_N\,(p+1)\right) + \frac{1}{P+1}\ln(\dot{\varepsilon}) \tag{3.045}$$

It should be remembered that the value of the material stiffness used as a normalising factor and that obtained during the tensile test may be different. (The size of this difference is dependent on the degree to which the test conditions vary between the two tests.) These equations (3.041, 3.042 and 3.045) can also be compared with the experimentally derived ones presented previously in table 3.002. These equations will also be compared with these derived from the data obtained for this thesis (see chapter 4).

The applicability of Carter and Caler's initial assumptions and equations should be considered when examining their TDF and NTDF models. Their first assumption (Carter and Caler, 1983) was that 'damage accumulation is related only to the time (t) history of the stress magnitude'. The second assumption or equation was that the time-to-rupture during a creep test is modelled by $t_R [\sigma] = B \sigma^{-n}$. It was then assumed that this equation could be used to predict the time-to-fail (and thus ultimate stress) under other loading conditions. They later adapted this model by the introduction of a measure of the material stiffness to normalise the stress level (Caler and Carter, 1989). This modification invalidates the application of their first assumption to bone as a material. The accumulation of damage is no longer modelled as simply a function of time and stress, but also of material stiffness. (However, Carter and Caler's first assumption is valid if the material stiffnesses are constant, and it therefore appears to be true for a single specimen.) This modification also produces a considerable gulf between their equations and those of Kachanov. Caler and Carter's second model can be viewed as one based on strain not stress. However, there are two factors to be considered when taking this view-point. First, the strain is a pseudo-strain produced by the normalising effect of the material stiffness, and therefore its relationship to the strain experienced by the specimen is not necessarily direct. Second, the data on which the model is based came from creep tests, not stress relaxation tests. Thus I consider that it remains a stress dependent damage model, the normalisation accounting for some of the material's variability. Material variability was not a factor considered by Kachanov. In engineering situations such material variability (for example the slight anisotropy induced by the rolling of steel) is small and more predictable.

I would like to suggest that the change from the TDF to the NTDF model may have analogies in the theoretically determined models. As noted above, the TDF model has an almost direct relationship to the model of creep-rupture proposed by Kachanov. It was noted in section 2.3.3 that Kachanov's derivation ignored primary creep. Odqvist's correction, which accounted for primary creep (section 2.3.3.5), made Kachanov's theoretical model more consistent with experimental data. I suggest that the change from the TDF to the NTDF model may be analogous to this correction. My thoughts are based on the assumption that the primary creep behaviour will have a large influence on the stiffness of the material. The earlier models (Kachanov's and the TDF) ignored the initial response, while in their adapted form they include this behaviour. This analogy is not a straightforward one. I therefore suggest that this as an area of further investigation.

The predictions of the failure stress of bone during a constant strain rate test (based on the ideas of Carter and Caler) raise a number of points. First, how reliable are the relationships $E = C \dot{\varepsilon}^m$ and $\dot{\sigma} = C \dot{\varepsilon}^{m+1}$ on which these predictions are made? Second, the first relationship is based on the initial section of the loading curve and the

latter one was derived from it assuming a constant stress rate. However, when the specimen passes the knee in the loading curve, the relationship of stress to strain will change. If a feed-back controlled test machine is used, the specified rate (stress or strain) will remain constant. In tests conducted using an open loop machine both rates will change (see appendix 7). Therefore it may be more reasonable to consider the (so called) yield stress as the failure stress of the material. This would appear to be justifiable for normal bone, but questionable for antler. The ultimate strength of antler is considerably higher than its so-called 'yield' stress. Some aspects of this conundrum are examined by Currey for the TDF model in a paper reviewed in the next section.

3.3.3. APPLICATION OF CARTER AND CALER'S TDF AND NTDF MODELS

Currey has published two papers (1988c and 1989) in which he examines the ability of Carter and Caler's 1983 model to explain the variation in the mechanical response of bone, and antler, subjected to tensile tests at different strain rates. In the first paper he applies their model to pre-existing data from bovine bone specimens (from Currey (1975) already reviewed in section 3.2.2). In the second paper he applies the model to data from specimens of reindeer antler. These papers are therefore of particular importance to the investigation presented in this thesis. (Their importance is twofold: first they are relevant to the materials and the tests that I have conducted for this thesis. Second, they form the historical background to my own research in the same laboratory.) Both papers pre-date the NTDF model of Caler and Carter (1989). However, in both papers Currey finds that the inclusion of another material property improves the predictive power of this type of model. In the first paper he finds mineral content is an important factor. In the second he finds that the Young's modulus measured during the test is important. This second finding is very significant considering the normalisation used by Caler and Carter in their 1989 paper (and equations that I have derived such as 3.045). I will now consider Currey's papers in more detail.

In his 1988 (c) paper Currey re-examines some data he had published in 1975. (I have reanalysed his original data and presented the results in tables 3.001 and 3.002, above.) The data was obtained from 35 specimens of bovine femoral bone, tested in a wet condition at room temperature, using various strain rates from 1.1×10^{-4} s^{-1} to 1.6×10^{-1} s^{-1}. The stress rate was calculated as strain rate × Young's modulus.[20] His new analysis was conducted in a way that was more conducive to comparisons with Carter

---

[20]The method used to measure strain rate is reviewed in appendix 7. Such a method may help to explain why 'the value of Young's modulus is barely if at all dependent on loading rate' Currey states that this finding is 'surprising'.

and Caler's initial model and to answering a number of questions. An outline of these questions is given below.

a) Do Currey's (1975) data in general support the model for the conditions of monotonic tensile loading?

b) The original model considered only ultimate tensile strength. 'Does the model hold when applied to the yield stress?'

c) Carter and Caler's relationship between stress rate and strain rate was based on a constant value of *Young's modulus*. Currey's data contained a value of *Young's modulus* of each specimen. These values exhibited 'considerable variation'. 'To what extent does this vitiate a simple movement from stress rate to strain rate?'

d) Currey's data also include mineral content of widely different values. 'To what extent does ignoring or including these differences vitiate the model?'

e) What further information, if any, about the cause of fracture can be obtained by knowledge of the *Young's modulus* and yield stress?

In order to answer his questions Currey uses his data to produce 20 equations of the following 5 forms

$$M = C_0 \times Min^{n_0} \tag{3.046}$$

$$M = C_1 \times \dot{\varepsilon}^{n_1} \tag{3.047}$$

$$M = C_2 \times \dot{\sigma}^{n_2} \tag{3.048}$$

$$M = C_3 \times Min^{n_3} \times \dot{\varepsilon}^{n_4} \tag{3.049}$$

$$M = C_4 \times Min^{n_5} \times \dot{\sigma}^{n_6} \tag{3.050}$$

where $M = \sigma_{ult}$, σ_y , ε_y or E. Some of these equations will be referred to, but Currey's equations will not be reproduced here in full.

After Currey points out that his test materials and conditions are different to those used by Carter and Caler, he answers the first question (do the data in general support the model?) by saying that 'when the effects of mineralisation are excluded, the effects of loading rate are similar'. He substitutes the median value of mineral content into his equation (of the form of 3.049) with $M = \sigma_{ult}$ to obtain

$$\sigma_{ult} = 177\ \dot{\varepsilon}^{0.067} \tag{3.051}$$

He compares the exponent of this equation with that of Carter and Caler's equation (3.030). Currey reports that statistically the exponents from these two equations 'can not be taken to be different'. In answer to the second question, he points out that the yield stress and strength values are 'always similar, and the equations describing them. . . are virtually identical'. In answer to the question regarding the possible degradation of the results due to the inference of strain rate from stress rate, Currey states that

> The present data produce virtually identical exponents for both strain rate and stress rate, and we can conclude that inferring strain rate from stress rate is perfectly satisfactory given the range of Young's modulus likely to be encountered in practice.

However, for an open loop test machine, like that used by Currey, the strain rate is not constant. When the specimen passes into the post-knee region of the loading curve, it is less stiff. Therefore in this region the strain rate is higher. Thus inferring strain rate from stress rate by assuming a direct and constant relationship is a dubious procedure. (This aspect of materials testing is explained in more depth in appendix 7.)

In answer to the question of ignoring mineral content Currey concludes with the observation that

> calculated relationships between mechanical properties and strain rate will be secure only if mineral content is taken into account or if there is little variation in mineral content.

The final question, (can further information be obtained from Young's modulus and yield strain?) is answered in the following way. First, Currey points out that the higher strengths occurring at higher strain rates are associated with higher yield stresses. He then asks if this accords with the model of Carter and Caler (who did not consider yield strain). He gives a very affirmative answer to this, using the logic that because materials stiffness is little effected by strain rate, the stress in a specimen is effectively proportional to strain: higher stress implies higher strain.

The overall findings of this paper (Currey, 1988c) can be summed up by the first two sentences of his conclusion:

> The object of this study was to test the cumulative damage model of Carter and Caler for bone fracture insofar as it applies to monotonic loading. The model survives the test well, in that most of the findings reported here are consonant with what would be expected according to the model.

My reanalysis of his results, and my extension of the NTDF model have produced a variety of interesting results, which relate Currey's remarks on strain rate (quoted above) to the model developed later by Caler and Carter. One result is that the experimental equation (table 3.002*c*), and the predicted equation (3.045) are very similar. These equations are rearranged and repeated below.

$$\ln(\sigma_{ult}) = 0.869 \ln(E) + 2.43 + 0.0633 \ln(\dot{\varepsilon}) \qquad (3.052)$$

$$\ln(\sigma_{ult}) = \ln(E) + \frac{1}{P+1} \ln(B_N (p+1)) + \frac{1}{P+1} \ln(\dot{\varepsilon}) \qquad (3.053)$$

The exponent of the material stiffness is predicted to be unity and is found to be 0.869. (The agreement is greater if the experimental equation for 'yield stress' (table 3.002*f*) is used instead.) I return to this equation when I consider my own results in the next chapter.

In a later paper (already reviewed above) Currey (1989) applies the TDF model to results obtained from the tensile testing of 28 reindeer antler specimens. In this case the data were fitted to similar equations to those of his 1988 (c) paper. (The equations from Currey (1989) have already been given as equations 3.004 and 3.005.) Currey's findings concerning the effect of strain rate on the various mechanical quantities were reported previously (section 3.2.2). Here I will examine his findings in relation to the TDF model.

Currey (1989) points out that due to the high power of stress in the TDF model an increase in stress to 1.3 times the yield value implies a 146 times increase in the damage rate, compared to that at yield. This prompts the question, how is it that antler can sustain such an increase in stress, and accommodate the associated damage rate? Currey suggests that 'it might be that antler has a remarkable ability to absorb damage', but he considers this unlikely. In way of justification of this second supposition he cites the fact that the final stiffness is still quite high for antler, and states that this stiffness is a measure of the damage accumulated. However, I do not consider that this fact supports his second supposition. One interpretation of the observation that the final stiffness of antler is less than that of bone is that it indicates a greater degree of damage. Damage can be expressed using the reduction in the stiffness of a specimen (section 2.3.3.7). It is possible that damage has a less detrimental effect on the strength of antler. The larger area contained within the stress-strain plot of antler (compared to bone) suggests that it requires the input of more energy before failure. These two points are complementary. Currey (1989) concludes with the statement that

> it is possible that creep tests on antler might resolve this question. It is also possible that 'yield' in antler is a different kind of phenomenon from that in more highly mineralised bone.

Although published without knowledge of Carter and Caler's NTDF model, Currey's 1989 paper (on reindeer antler) clearly shows the importance of the material stiffness as a predictor of other mechanical variables. Due to the form of the equations comparisons can be drawn between his regression equations and some the equations derived from the NTDF model. For example, equation 3.045 predicts a logarithmic relationship between ultimate stress, material stiffness and strain rate. In his logarithmic analysis Currey produces such a relationship (having found that bone volume fraction and mineral volume fraction did not improve the predictive power of the relationship). However, unlike the prediction made in equation 3.045 he found the exponent of material stiffness to be between 0.3 and 0.4, depending on whether the ultimate stress or the 'yield'

stress was the variable considered. (Clearly the agreement between the theoretical and experimental value of this exponent is less in the case of antler than it has been shown to be for bovine bone.)

I mentioned above that Currey's 1988 (c) and 1989 papers had some bearing on the theme of my thesis. Another paper that had a considerable influence over the initial stages of my research is that of Mauch, Currey and Sedman (1992). This paper is presented in full (with an erratum) in appendix 6, and reviewed briefly below. It is included within this review section rather than in chapter 4 as the experimental work was performed by Marianne Mauch, an undergraduate student, within the same laboratory as my own work. My main contribution was the design and construction of the test equipment (later adapted for my own tests) as well as criticisms and suggestions during the preparation of the manuscript.

Mauch *et al.* (1992) describe creep-rupture tests of bovine bone and antler specimens. (Also included in the paper is an analysis of Caler and Carter's 1989 results using information that they did not publish, but that they kindly supplied.) The bovine test material was from the mid-shaft of two ulnae that had been deep frozen. The antler specimens came from the tip and base of a 'normal hard antler' of a red deer, which had been stored dry. Specimens were kept wet during machining and testing. Before being subjected to a creep test, the bending stiffness of each specimen was measured. During creep testing a predetermined load was gradually applied over a period of about 6 seconds. This was accomplished by raising the cross-head (of the Instron 1122 materials testing machine) under which the specimen (wrapped in water soaked tissue) was clamped. This in turn raised a predetermined mass, by way of a lever. When the mass and level were supported only by the specimen (and pivot), the cross-head was stopped. The load remained constant. To account for the loading period, the time recorded as the time-to-rupture was that from the moment that the final load was reached to rupture plus one second. The results were analysed using Carter and Caler's TDF and NTDF models. In the second case the normalisation was achieved by using the bending stiffness. The main findings of this analysis will be outlined below.

Analysis using the TDF model showed no overall relationship between time-to-rupture and the stress level. When the results for the different materials were analysed, only those for the antler base had a significant relationship between t_R and σ. However, there was a clear difference in the region of the graph over which the specimens of bovine bone and antler were distributed. The bone specimens fell in a region that indicated that they would be able to sustain a certain level of stress for a longer time than a specimen of antler. An example is given in the paper of hypothetical creep tests performed using a stress of 100 MPa. For such a test the experimental data predict that a

specimen of bovine bone would rupture in 1260 s, one from the base of the antler in 63 s and one from the tip of the antler in 8 s. (The value of 1260 s for bovine ulna was erroneously given as 12.6×10^6 s in the paper, see appendix 6.)

Analysis using the NTDF model improved the ability to predict when rupture would occur. In the NTDF model the predictive relationship is between t_R and σ/E_N. The results are shown in figure 3 of the paper (appendix 6). A test for homogeneity of slope gave no evidence that the slopes are different. In this case the results show that if specimens of bone and antler were subjected to the same normalised stress the bone would fail first. The example of a value of $\sigma/E_N = 0.006$ is given: bovine bone would rupture in 320 seconds, antler tip in 260 days, and antler base in 29,000 years. This normalisation appears to have produced a greater separation between the results for each material, and not brought them closer together as may be expected. We stated that

> since the data of Caler and Carter for human bone, and our own data for each separate type of bone, show that there is indeed a clear relationship between time to fracture and σ/E_N (which is effectively some measure of the initial strain) the problem is: why is there no relationship *overall?* At the moment there is no answer to this.

In a recent paper, Rimnac *et al.* (1993) examined bone using creep-rupture tests. Their paper is initially concerned with the relationship of creep rate, applied stress, degree of remodelling and temperature. In the later sections of the paper an assumed relationship of time-to-rupture and creep rate is combined with the TDF and NTDF models of Carter and Caler, to obtain another relationship of creep rate and stress. The exponents of these two relationships are then compared.

Rimnac *et al.* supply the results from creep tests of 117 specimens bovine femoral bone. These specimens were tested wet at three temperatures of 25, 37 and 43°C, using stresses between 71 and 115 MPa. The authors analyse their results by fitting them to an Arrhenius relationship. It will become clear in my review of this paper that I do not consider that the use this relationship is fully justifiable. However, the inclusion of the raw data within the paper has permitted me to reanalysis some of their data using the theories and relationships I propose in this chapter. This enables a degree of cross-checking of my own data. For example see figure 4.051. The Arrhenius relationship assumes that the secondary creep rate is a thermally activated process. The authors say that this has been found to be the case for both single crystal and polycrystalline material. Rimnac *et al.* clearly view bone as such a polycrystalline material. In their discussion section they hypothesise that the 'permanent deformation during creep is primarily due to damage mechanisms in the hydroxyapatite.' They continue by saying that 'the classic creep strain verses time curve for compact bone, similar to that found for crystalline

materials, supports this hypothesis'. In a previous section (2.3.3) I presented a method of modelling creep, based on the accumulation of damage. It was implied that this damage was in the form of cracks, and thus (more probably) an intergranular rather than intragranular process as proposed by these authors. (Intergranular damage in copper is clearly shown in a paper by Leckie and Hayhurst (1974). The presence of microcracks in fatigue specimens of bone, have been reported by Carter and Hayes (1977).) Rimnac *et al.* fit their data to their model and obtain an R^2 of 41%; the equation is

$$\dot{\varepsilon}_s = 5.6 \times 10^{-9}\, e^{4.6F}\, \sigma^{5.2}\, e^{-5330/T} \qquad (3.054)$$

where $\dot{\varepsilon}_s$ is the secondary creep rate in s^{-1}, F is the volume fraction of secondary Haversian bone, σ is the creep stress in MPa, and T is the temperature in Kelvin. It can be seen that increasing the temperature will increase the creep rate (such an effect was reported by Currey in 1965). The authors point out that the estimated creep rate would be nearly one hundred times faster for a specimen with a fully secondary Haversian microstructure than one with a fully lamellar microstructure. The authors then refer to the models of Carter and Caler and the paper by Mauch *et al.* among others. They quote the relationship (using B in place of C shown here)

$$\ln(t_R) + m \ln(\dot{\varepsilon}_s) = C \qquad (3.055)$$

They say this relationship is an empirical one used by other workers in 1956, for several metal alloys for which $0.77 < m < 0.93$. Rimnac *et al.* then combine equation 3.055 with each of Carter and Caler's relationships for the time-to-rupture and stress during a creep test, which expressed in my nomenclature are $t_R = B\,\sigma^{-17.95}$ and $t_R = B_N\,(\sigma/E_N)^{-15.81}$. (Presumably this is done in a similar way to that shown in equations 3.056 to 3.062.) From this combination they produce two predictions of the steady state creep rate, $\dot{\varepsilon}_s$. The first is a function of stress, and the second a function of normalised stress. The exponent of stress they obtain in the first case is 19 and that in the second is 17. They point out that the equivalent exponent in their study, obtained from experimental observations, is 5.2 (equation 3.054). The authors suggest that their exponent would be higher if a normalisation by material stiffness were used. (They repeat the combination of equations, this time using the equations for specimens of bovine ulna presented in Mauch *et al.* (1992), which for the un-normalised case gives an exponent of 4.5 and for the normalised case one of 18.) Because the regression equation associated with the un-normalised equation for Mauch *et al.* was not significant, this argument may be unsound.

I would like to examine another possibility for the difference between the results of Rimnac *et al.* and those obtained from other published studies. In combining the equations Rimnac *et al.* assumed that m = 0.93, the upper limit from a study of metal

alloys. However, as they supply their data it is possible to obtain the actual value of m. (They give no reason why they do not do this themselves.) For this I have examined the data from tests conducted at 37°C only. First I will manipulate the equations, starting with equation 3.055

$$\ln(t_R) + m \ln(\dot{\varepsilon}_s) = C \tag{3.056}$$

and

$$t_R = A_1 \sigma^{-17.95} \tag{3.057}$$

combine to give

$$\ln(A_1 \sigma^{-17.95}) + m \ln(\dot{\varepsilon}_s) = C \tag{3.058}$$

or

$$\ln(A_1) - 17.95 \ln(\sigma) + m \ln(\dot{\varepsilon}_s) = C \tag{3.059}$$

Thus, combining the constants this becomes

$$\ln(\dot{\varepsilon}_s) = C_1 + \frac{17.95}{m} \ln(\sigma) \tag{3.060}$$

Which in non-logarithmic form is

$$\dot{\varepsilon}_s = C_2 \sigma^{\frac{17.95}{m}} \tag{3.061}$$

In the case of the normalised relationship this process will result in

$$\dot{\varepsilon}_s = C_3 \left(\frac{\sigma}{E_N}\right)^{\frac{15.81}{m}} \tag{3.062}$$

Thus a smaller value of m will result in a larger exponent. Regression analysis of their data produced a value of m = 1.08 (R^2 = 78%). The exponents thus obtained are 16.6 and 14.6. (The same process performed on the data from Mauch *et al.* for the normalised equation, reduces the exponent from 18 to 15.5.) These values are still higher than that in equation 3.054. The authors state that 'it is possible, . . that the exponent would have been higher [in equation 3.054] had stress been normalized by elastic modulus'. This proposition will be examined later using my own data (creep tests on bovine femoral bone), for which I have a measure of material stiffness.

To reiterate Rimnac *et al.* examined the relationship of creep stress and creep rate for specimens of bovine femoral bone. The main aim was to fit the data thus obtained to the Arrhenius equation. They also used an equation relating secondary creep rate to time-to-rupture. (In this way they connect their work to the equations used by Carter and Caler (1985) and Caler and Carter (1989), which are supposedly based on the damage approach.) However, Rimnac *et al.* did not fit their data to such creep-rate time-to-rupture relationships. In chapter 4 I examine the fit of the data I have obtained from

creep tests on bovine femoral bone and antler to the relationship of creep-rate and time-to-rupture and other equations. I consider that the relationship of stress to time-to-rupture, stress to creep-rate and the relationship of creep rate to time-to-rupture are three facets of the same behaviour.

In the next section I review another paper on creep exhibited by specimens of bone. However, in this case the tests are of a shorter duration and the creep rate, rather than the time-to-rupture, is the variable of interest.

3.3.3.1. PSEUDOPLASTICITY: ANOTHER WORD FOR DAMAGE?

As the title of this section implies, the nomenclature used to describe material properties is at times ambiguous. This is especially the case when new ideas are being applied. In this section I will examine a paper by Fondrk *et al.* (1988) entitled *Some Viscoplastic Characteristics of Bovine and Human Cortical Bone.* This paper is concerned with the post-knee behaviour of bone and is closely related to the approaches of viscoelasticity (Sedlin's rheological model) and damage reported above. However, the authors use another form of nomenclature, and thus a different interpretation could be intended. Fondrk *et al.* say in their abstract that their tests 'enabled total strain to be decomposed into elastic, linear viscoelastic, creep and permanent plastic components'. However, they confuse matters by using the terms yield and damage.

Fondrk *et al.* (1988) start their introduction by pointing out that biological materials cannot be understood in an engineering context until equations describing the mechanical properties are obtained. They report that these have not been obtained for the post-yield behaviour of bone. They point out that simple monotonic loading tests show that there is a significant deviation from a straight line stress-strain response. However, Fondrk *et al.* also point out that because such tests do not include unloading these tests cannot fully illuminate the nature and mechanisms behind the inelastic material response. Fondrk *et al.* use the examples of classical plasticity and what they refer to as pseudoplasticity or damage plasticity. Their definition of pseudoplasticity is consistent with the description of damage given above. Their paper contains a figure (similar to figure 2.013, above) showing the loading and unloading of these two idealised materials, both show the same ⌜ shaped loading curve, but they differ in their stress-strain response during unloading.[21] These they describe by saying that

---

[21]Fondrk *et al.* refer to a classical plastic material, but the gently curving ⌜ shaped stress-strain response of their diagram implies some concession to reality.

> the classical plastic material unloads along a straight line with the same slope as its elastic modulus, while the pseudoplastic material unloads along a straight line back to the origin. The two materials also follow these respective unloading paths back up to the yield point when a second load is applied. The yielding process, therefore, has a softening effect on the subsequent preyield elastic properties of the pseudoplastic material, while the elastic modulus of a classical plastic material remains unchanged.

The authors then state that different post-yield constitutive equations would apply for the pseudoplastic material, and that these equations would have to reflect some form of continuous damage model. (Clearly they are using the term yield to describe the curve not the process.) They then point out that both the classical plastic and the pseudoplastic materials are rate independent. They cite a number of references to the rate dependence of bone, pointing out that these studies do not include an examination of the unloading behaviour. Fondrk *et al.* state that it is consequently unclear whether this time dependence is due to rate dependent plasticity or rate dependent pseudoplasticity. The aim of their paper is to clarify this aspect of the material's mechanical response.

The test material used by Fondrk *et al.* (1988) consisted of fresh and frozen bovine metatarsal bone and some human femoral bone. The specimens were of the rectangular waisted type, machined under continuous water irrigation. Tests were conducted using an Instron dynamic testing machine (Model 1230).[22] Extensions were measured over a 10 mm gauge length using an Instron 10% extensometer. The data were recorded on an IBM PC based data acquisition system. The basic testing cycle consisted of a one second ramp-up in load, a 60 second hold at constant load (referred to as a 'stress hold'), a one second ramp-down and a 60 second hold at zero load. This sequence was repeated several times using progressively higher loads. One group of specimens were taken through two sets of load cycles. The first set was performed in the normal manner but, instead of continuing to rupture, it was stopped after the first cycle that produced significant creep. Each specimen was then taken through a second set of load cycles, starting at the lowest load and continuing to rupture.

---

[22]From the description of the experiment it would appear that the machine was used in closed-loop stress control.

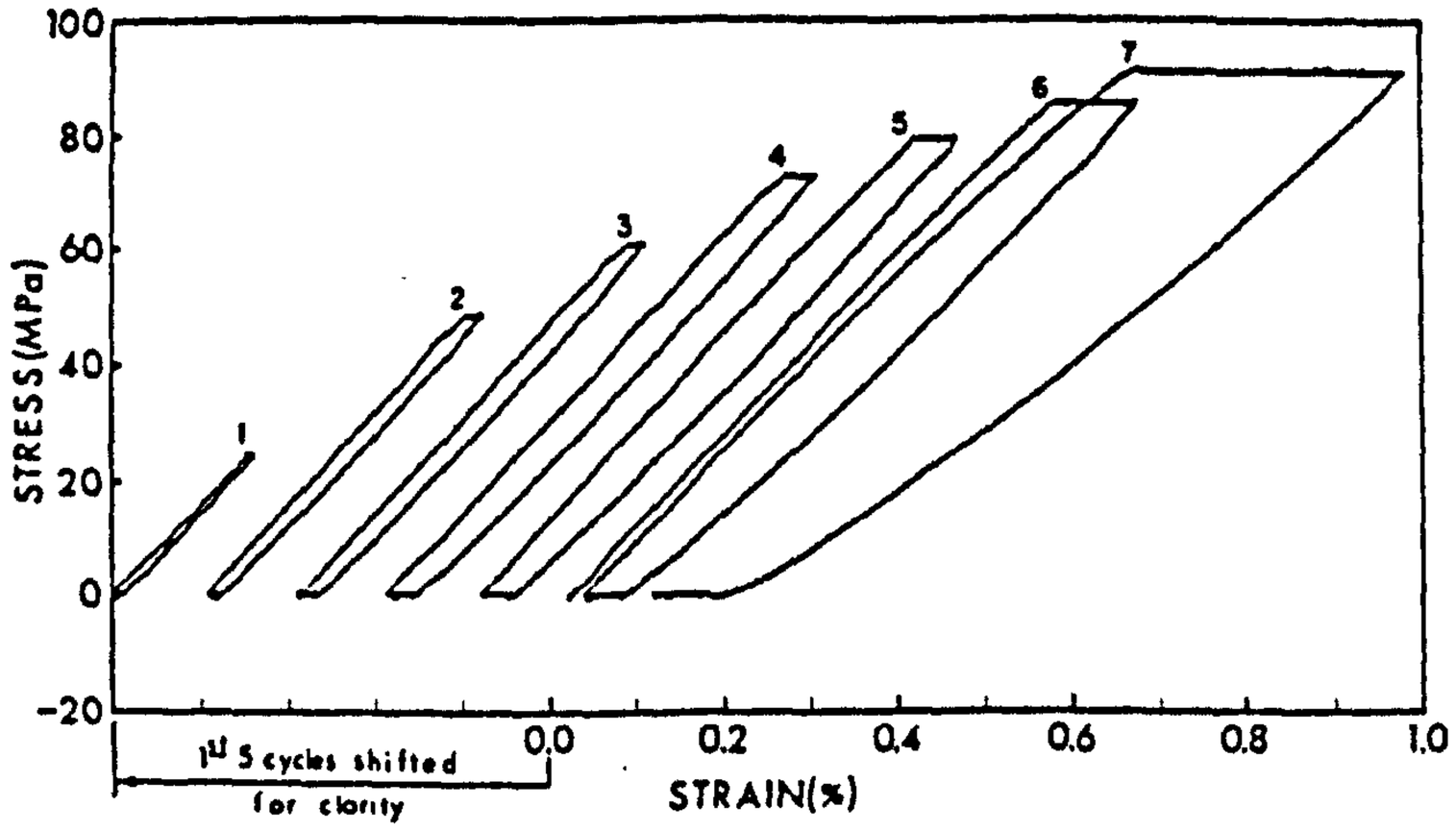

Fig. a. The stress–strain curves produced by applying seven load cycles to a human specimen. (Note that the first five cycles have been artificially shifted to the left for the sake of clarity, i.e. the lower left apices of the actual unshifted curves lie at the origin.)

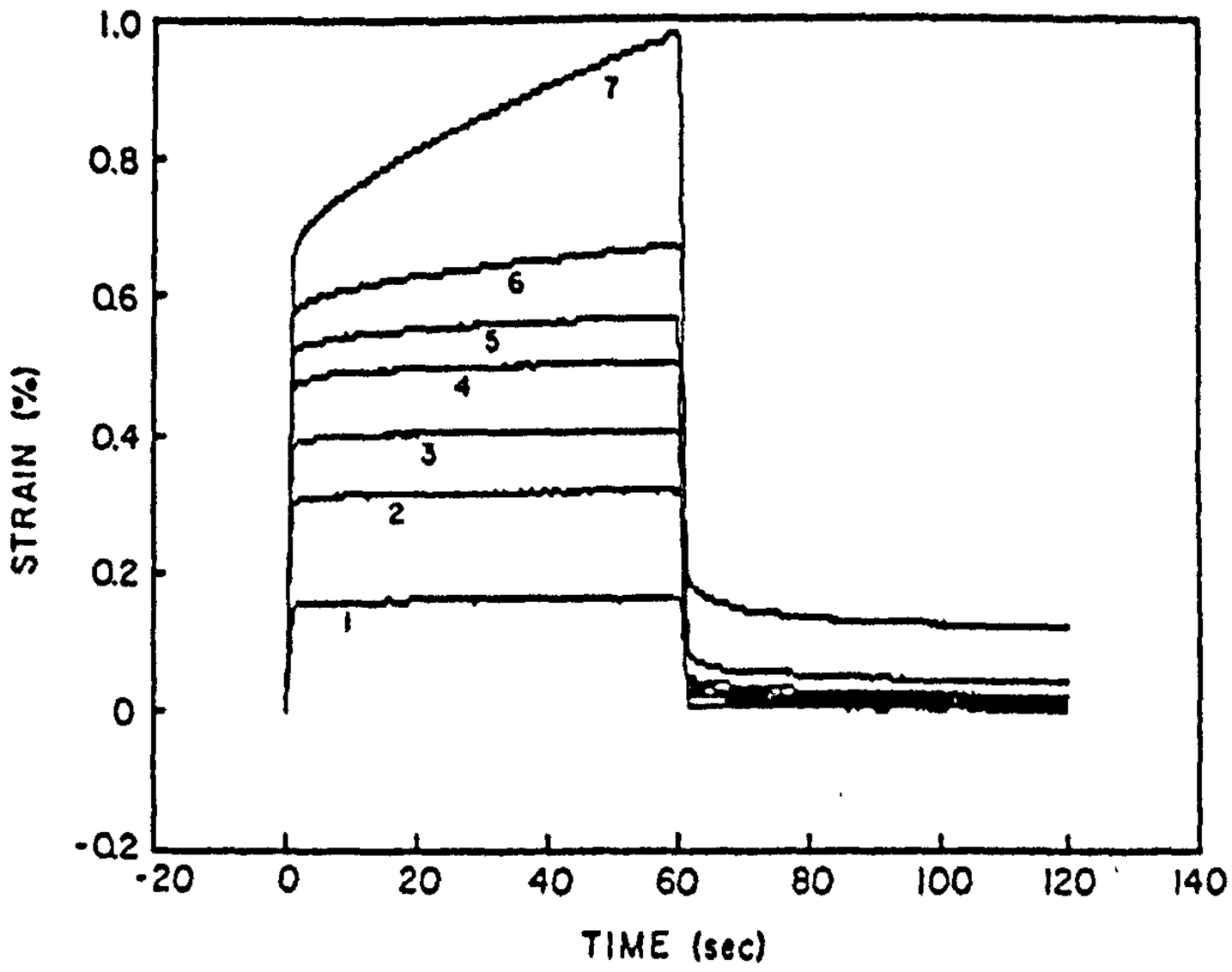

Fig. b. The strain–time curves produced by the same seven load cycles that are shown in Fig. a.

Figure 3.012 Reproduced from Fondrk *et al.* (1988)

Stress-strain and strain-time response of a cyclically loaded specimen of human bone

Figure 3.012a and 3.012b are reproduced from Fondrk *et al.* (1988) and show the stress-strain and strain-time behaviour for a typical specimen of human bone. The authors state that the first five load cycles produced closed stress-strain loops and strain-time curves that, during the period of constant stress, stabilised to an equilibrium strain. They say these two attributes are indicative of a viscoelastic solid. They also say that the strain response of the first five cycles is linear with respect to load, 'indicating that the behavior is linear viscoelastic'. However, the later cycles show a proportionally larger

deformation. For example, the authors say that during the stress hold on cycle 7, a strain of 0.003 developed, which is six times the strain produced during the hold on cycle 5 even though the load was only 1.13 times greater. The later cycles (6 and 7) also displayed different strain-time behaviour: instead of the strain reaching an equilibrium value, a steady creep strain rate developed. This rate was determined for each cycle by linear regression of the data from the last 40 seconds of the creep loading period. A creep-rate of greater than 5 micro-strain per second were recorded during 57 cycles.

Having identified two types of behaviour the authors propose a boundary between them. This they call the creep threshold, which is the level of stress that results in a steady state creep rate of 10 micro-strain per second (10 $\mu\varepsilon\, s^{-1}$). The creep threshold stress obtained for these two test materials were 73 MPa (s.d. 5 MPa) for human bone and 117 MPa (s.d. 10 MPa) for the bovine. (Even though the bones are of different types, this difference between species may be comparable to the longer creep-rupture time for bovine bone compared to human bone noted by Mauch *et al.* (1992).) I will now present the equations given by Fondrk *et al.* (1988). These authors examined the relation of stress level to creep rate and say it is of the following form:[23]

$$\sigma_0 = F_1 \log(\dot{\varepsilon}) + F_0 \qquad (3.063)$$

Fitting this equation to the data for the bovine specimens that had at least three data points at creep rates above 5 micro-strain per second, gave R^2 values of over 0.90 in all cases. However, for the pooled bovine data this fell to $R^2 = 0.57$, and gave the equation

$$\sigma_0 = 15.1 \log(\dot{\varepsilon}) + 191 \qquad (3.064)$$

where creep rate is in reciprocal seconds and stress in MPa. The result was similar for the human data: for the data from the six specimens analysed individually $R^2 > 0.95$, while for the pooled data $R^2 = 0.47$. The equivalent of equation 3.064 for the human bone is

$$\sigma_0 = 10.4 \log(\dot{\varepsilon}) + 126 \qquad (3.065)$$

The authors also fitted their data to the Bailey-Norton equation which relates the creep rate to the applied stress in the following way

$$\log(\sigma_0) = F_2 \log(\dot{\varepsilon}) + F_3 \qquad (3.066)$$

The fit of this equation was about the same as the previous one, being poorer for most of the individual specimens (but still over 0.9 in each case). For the pooled data the

---

[23]In conversions from these equations I will assume $\log(y) = \log_{10}(y) \neq \ln(y)$

predictive power is again lower: $R^2 = 0.56$ for the bovine specimens and 0.48 for the pooled human data. The equations of the pooled data are

$$\log(\sigma_0) = 0.053 \log(\dot{\varepsilon}) + 2.32 \qquad (3.067)$$

for the bovine, and in the case of the human bone

$$\log(\sigma_0) = 0.058 \log(\dot{\varepsilon}) + 2.16 \qquad (3.068)$$

These equations can be rewritten in a non logarithmic form. First, that for bovine bone:

$$\log(\sigma_0) = 0.053 \log(\dot{\varepsilon}) + 2.32 \quad \Rightarrow \quad \dot{\varepsilon} = 0.00479\ \sigma_0^{18.9} \qquad (3.069)$$

and second, that for human bone:

$$\log(\sigma_0) = 0.058 \log(\dot{\varepsilon}) + 2.16 \quad \Rightarrow \quad \dot{\varepsilon} = 0.00692\ \sigma_0^{17.2} \qquad (3.070)$$

The exponents are approximately 19 for bovine bone and 17 for human bone. These are similar values to those derived by Rimnac *et al.* (described above).

Fondrk *et al.* (1988) also examined the amount of strain remaining after each loading-unloading cycle. This they compared with the amount of creep strain. They say that about 70%, of the inelastic strain was recovered when the specimens were unloaded, and that this 'is consistent with a damage theory of inelastic deformation'. They continue:

> the fact that 30% of the inelastic deformation was permanent can be explained, as pointed out by Rabotnov (1980) for polymer materials, by incomplete closure of submicroscopic cracks associated with damage.

The authors make another important statement regarding damage. (A statement that is intrinsic in the work of Carter and Caler, reviewed above, but should not be overlooked.) The statement is that 'creep strain is produced at a constant rate, indicating that damage is not instantaneous, but requires time to accumulate'.[24] One implication of the constant creep rate, that the authors, mention is the effect on the shape of the stress-strain response of a constant strain rate test.

> It implies that a test performed at a constant strain rate should, at some load level above the creep threshold, produce a flat (zero slope) stress-strain curve.

This remark is important because it demonstrates a relationship between creep tests and tensile tests. (Fondrk *et al.* refer to the works of Crowninshield and Pope (1974) and

---

[24]It should be noted that they were examining the last sections of short term tests and thus primary and tertiary creep are not considered. Changes in the creep strain rate throughout the period of a test is an aspect of this behaviour that I consider in my own work.

Currey (1975) for evidence of such a flat region.) However, I consider that this relationship can be extended, and may (in a phenomenological way) explain the rate dependence of some of the mechanical responses of bone during a standard tensile test. The model I have derived from this idea is presented in the next section.

3.3.3.2. TENSILE TEST MODEL: THE CREEP ANALOGY

In this section I consider some of the implications of the remark made by Fondrk *et al.* (1988) (quoted above) in which they suggest that a material displaying a constant creep rate (during a creep test) will exhibit a flat post-knee region during a tensile test conducted at constant strain rate. It is possible to examine the significance of this observation by use of some idealisations. The first idealisation is that the creep strain rate (which I will refer to as $\dot{\varepsilon}_{P1}$) for an otherwise elastic specimen subjected to a certain nominal stress, P1, is constant during the whole creep test and that no creep occurs at stresses below P1. At stresses above P1, the material creeps at a higher rate. This is shown diagrammatically in figure 3.013. In this idealisation it is supposed that a tensile specimen of the same material is loaded at a constant strain rate identical to the creep rate produced by the load P1. On reaching the load P1 the specimen will therefore creep at the same rate as that at which it is being extended. Therefore the load will remain constant and the specimen will extend until it fails. (This will result in the production of a flat post-knee region.) Any variations that are induced in the post-knee load will be counteracted by the system. If the load is increased, the creep rate will become greater than the machine extension rate and thus the load applied to the specimen will be reduced. If the load is reduced below P1 the material will stop creeping. The specimen will thus be stretched by the test machine until the stress reaches P1 again, and the process continues.

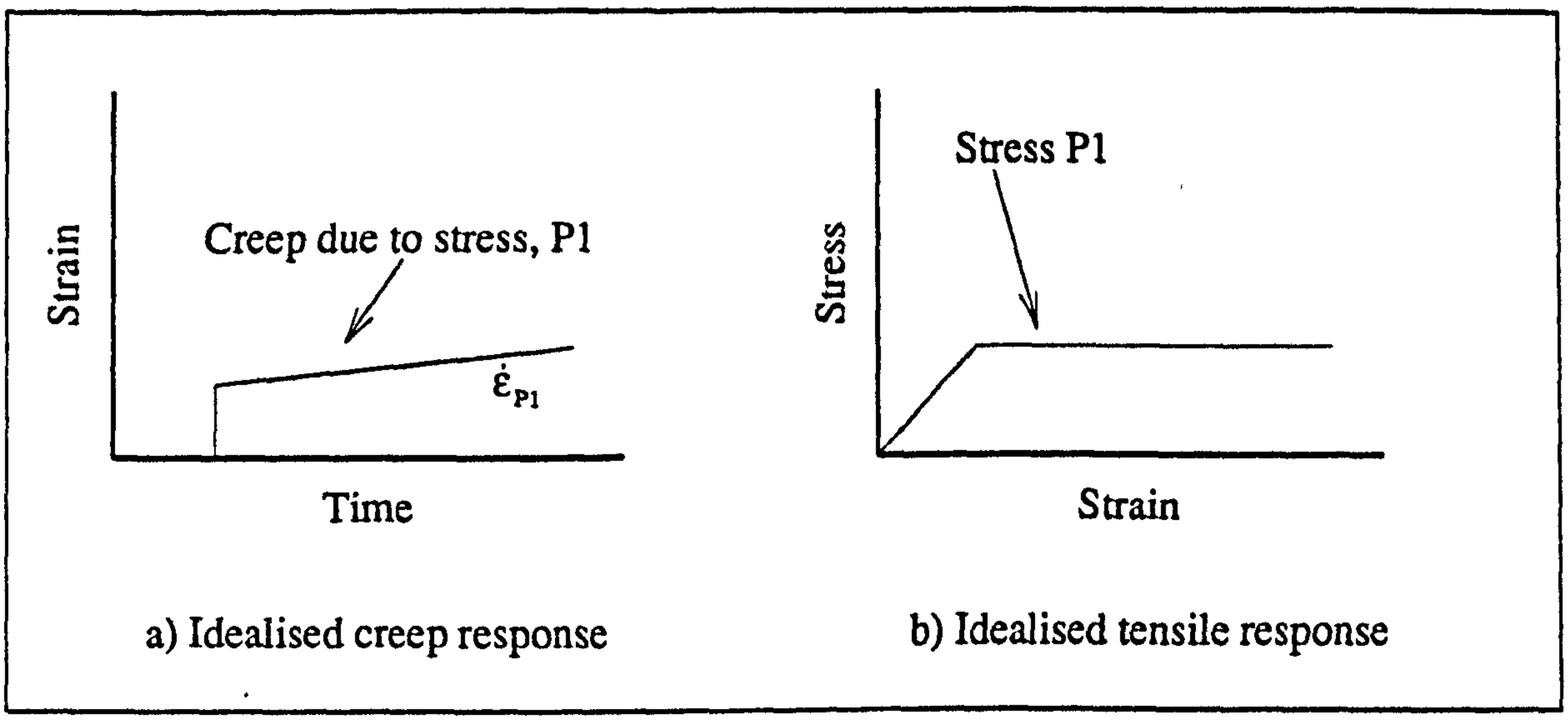

a) Idealised creep response

b) Idealised tensile response

Figure 3.013

Model of tensile response of an idealised material that is elastic up to a certain load at which it then creeps at the same rate that it is being extended

Other factors can be included in the idealisation presented above to increase the level of reality in this model. As noted above, the creep strain rate is greater if a greater creep loading is applied. This is shown in figure 3.014 for a number of discrete stresses of increasing value P1, P2, P3 and P4 and with the associated creep rates. Previously I used the assumption that the test was conducted at the lowest creep rate of the material. This assumption can be modified by examining the effect of several distinct creep rates. Using the same approach as above it can now be shown that the maximum stress reached during a tensile test will depend on the rate at which the specimen is deformed. The greater the extension rate, the greater the stress that would be needed to provide the same extension rate in a creep test. The form of the relationship between the applied load and the creep rate will determine the sharpness of the knee in the loading response during a tensile test.

There appears to be (at least) one problem with the idealisations I have used to relate creep tests to tensile tests. The idea that when the creep rate and extension rate during a tensile test are equal the applied load becomes a constant, relies on the creep rate under that load being constant. It is unlikely that this is true for bone and antler, although the curves provided by Fondrk *et al.* suggest it is a reasonable assumption for bone. Bone also displays an almost flat post-knee region as in the idealisation. However, it has already been reported that antler specimens do not exhibit such a plateau in their loading curves. If this is related to their creep behaviour, the idealised model would suggest that the creep rate of antler under constant load decreases with time. Thus to obtain a constant creep rate an increasing load is required. By similar logic, the accelerated creep rate during the tertiary period, may explain the slight reduction in loaded sometimes

observed just prior to failure during a tensile test. These speculative ideas can be investigated by performing creep tests on antler.

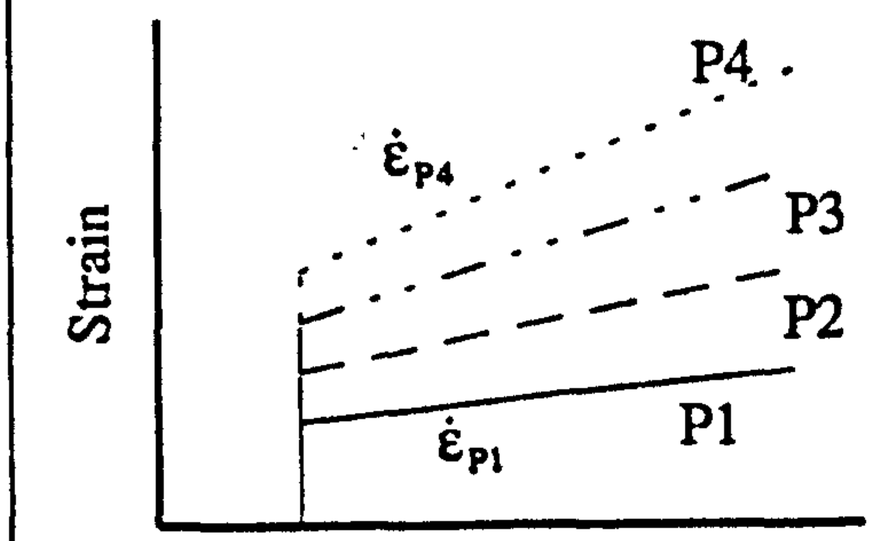

a) Idealised creep responses for loads P1, P2, P3, P4

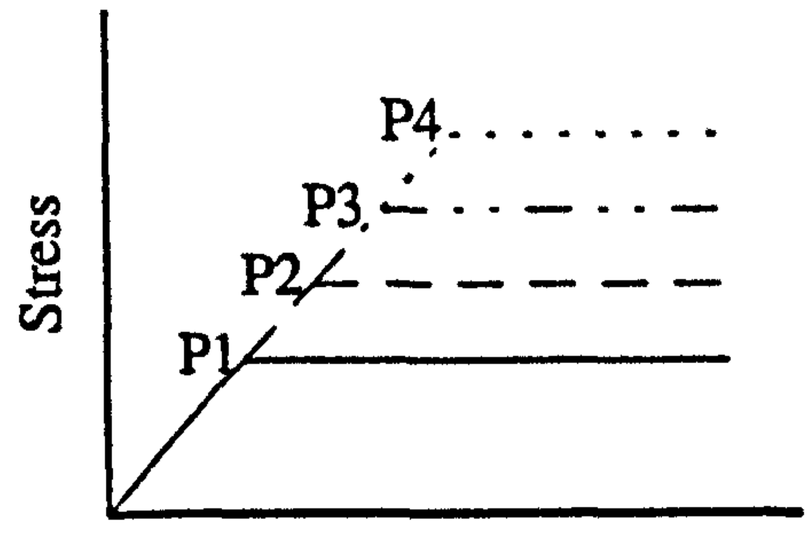

b) Idealised tensile responses for extension rates $\dot{\varepsilon}_{P1}$, $\dot{\varepsilon}_{P2}$, $\dot{\varepsilon}_{P3}$ and $\dot{\varepsilon}_{P4}$

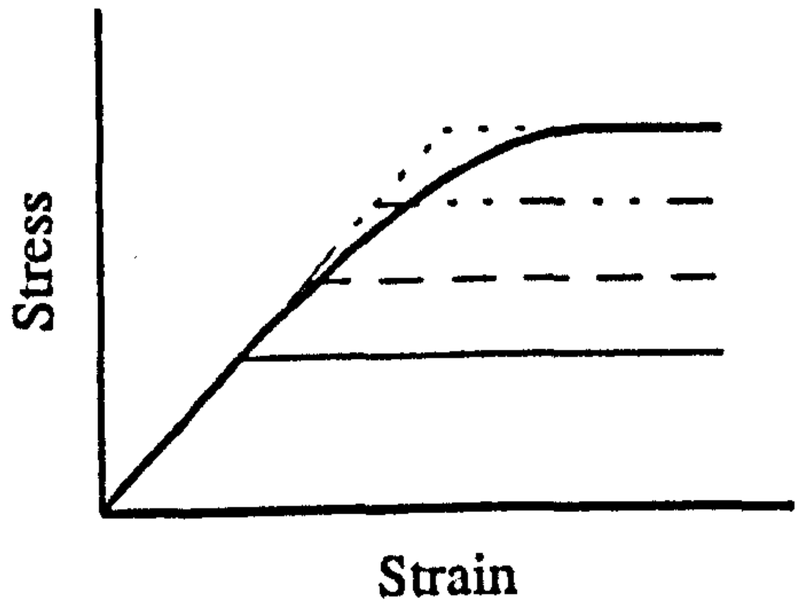

c) Idealised tensile response for extension rate $\dot{\varepsilon}_{P4}$, when the creep at lower loads is considered

Figure 3.014

Model of tensile response of an idealised material that is elastic up to a certain load at which it then creeps at a constant rate (the rate depends on the applied stress)

3.3.3.3. DAMAGE MODEL FOR CORTICAL BONE

In this section I examine a 'simple constitutive model for cortical bone' proposed by Krajcinovic *et al.* (1987). To form this model these workers apply the damage concept in a very straight forward way. Their paper contains a large number and verity of assumptions and idealisations, nor is there any consideration of the time dependence of such a damaging process. Thus I suggest that it may be better to view it as another explanation of damage and not an explanation of how bone fails. However, the general approach is one I will return to later.

The authors state that the objective of their study was to propose a constitutive theory for damage induced irreversible changes in Haversian cortical bone. These authors view the material as a fibre composite, the fibres being the Haversian systems. They consider that it is the failure of the bonding of these fibres, as a result of microcracking, which results in the failure of the material as a whole. They assume that

> the microcracking is the only (or at least the dominant) mode of inelastic rearrangement of the mesostructure of a long cortical bone, the microcracks always occur along the cement line, and that, consequently, the tensile strength of a haversian bone is gradually degraded during loading by the sequential pull-out of the osteons traversing the path of a macrocrack perpendicular to the tensile stress.

They also make some idealisations for convenience, such as all the osteones being mutually parallel and geometrically identical. The authors apply 'the loose bundle tensile model, proposed originally by Krajcinovic and Silva (1982)' in this they say they are 'guided by the fact that the tensile strength of haversian bone is provided, at slow loading, by the pull-out strength of the osteons'. I consider that this fact is open to a considerable degree of question. They then give a list of premises on which their model is based. These appear to increase the gulf between their model and reality. I give these premises in list form below.

> The entire tensile load is carried by the osteons.
>
> All the osteons traversing the macrocrack equally share in transmitting the externally applied tensile force F (i.e. macro stresses).
>
> All osteons have the same stiffness K/N (and, therefore, same elongation).
>
> The ability of an osteon to transmit the tension is controlled solely by its embedding length (i.e. the osteons will neither yield nor rupture).

The stiffness term K/N represents, the stiffness of the whole material, K, and the number of osteones, N. The authors say that as the embedded length is a random variable so is the strength. They assume all the osteones to be the same length, l. Hence the embedded length ranges from l/2 to 0. Again using assumptions in this case 'disregarding the finer points of the shear stress distribution along the osteon-cement line interface'[25] they express the pull-out strength for a single osteon as

$$F_{RI} = 2 \pi r \tau_b L_I \qquad (3.071)$$

where:

F_{RI} is the pull-out, or failure, strength of the I-th osteon.

---

[25]The stress required to pull a fibre, or osteon, from a matrix increases with fibre length, but at some *critical length* the stress needed to pull the fibre out is the same as its failure stress. The failure mode thus changes and increasing the fibre length no longer results in a stronger material. Further information is given by Hull (1981)

τ_b is the ultimate shear strength of the cement line.

r is the radius of the osteon.

L_I is the embedded length of the I-th osteon. Thus $2 \pi r L_I$ is the embedded area of the I-th osteon.

Krajcinovic *et al.* (1987) say that the probability density function for the pull-out strengths is band limited and uniform. The limit is imposed by the maximum length l/2, and the uniformity is due to the assumption of a perfectly random length distribution. (The probability density function would become skewed, if the critical length of the osteon was less than l/2.) The authors say that in the case where the osteons are not all of the same geometry (a more realistic model) 'the determination of the pull-out strength would merely get more complicated since it would involve the determination of joint probability functions'.

The authors consider two situations uniaxial tension and pure bending. I will concentrate on the uniaxial case. The force experienced by the I-th osteon is expressed as the result of multiplying the osteon's stiffness by its elongation, x.

$$F_I = \frac{K x}{N} \quad \text{if} \quad 0 < K x < F_{RI} \tag{3.072}$$

and

$$F_I = 0 \quad \text{if} \quad K x > F_{RI} \tag{3.073}$$

Due to the assumptions the authors have made regarding the properties and distribution of the osteons, the load is shared equally by all the embedded osteons. Krajcinovic *et al.* use this idea to produce an equilibrium equation, between the external force and the internal situation.

$$F = \sum_{I=N+1}^{N} F_I = K x \left(1 - \frac{\overline{N}}{N}\right) \tag{3.074}$$

where $\overline{N}$ is the number of osteons that are already pulled out. The authors introduce a variable (for which I will use the symbol 'D' to obtain consistency with the previous chapter) equal to the ratio of number of pull-out osteons to total number of osteons.

$$D = \frac{\overline{N}}{N} \tag{3.075}$$

Thus

$$F = K x (1 - D) \tag{3.076}$$

The quantity D expressed in the form given in equation 3.075 is, due to the restraints placed on the geometry of the osteons, identical to the expression of damage using the idea of reduction in effective area already given in section 2.3.3.7.

Krajcinovic *et al.* (1987) then assume that the number of osteons is very large and re-express equation 3.074 in an integral form, which includes the probability density function of the pull-out strength of the osteons. From this they obtain an integral expression of the damage and finally arriving at a prediction of the failure conditions. These are that the product of the materials initial stiffness and its maximum strain is twice the value of the maximum stress.

I consider that this paper, although it presented (in the author's words) a 'one-dimensional constitutive theory for cortical bone with haversian structure [that] satisfies two basic conditions: simplicity and accuracy', should not be used as a direct explanation for the failure of bone. I consider that this approach is similar to that of using the theory of viscoelasticity to explain a material's behaviour while attributing the springs and dashpot to structural elements. However, as I shall show in later chapters a damaging process does occur in bone. Thus adaptation of this model may be a fruitful area for further work.

3.4. SUMMARY

In this chapter I have reviewed a number of papers that have considered some of the time-dependent properties of bone and, to a lesser degree, antler. I divided the papers roughly into two groups: those that take a viscoelastic type approach and those that take a damage approach.

The application of viscoelasticity to the modelling the mechanical response of bone is normally based on an examination of the material's stiffness. It must be remembered that this is all viscoelasticity can do: providing equations that will model the stress-strain relationship as it changes with time. Such an approach is unable to model other aspects of the material's behaviour such as the knee in the loading curve or final failure.

Sedlin (1965) introduced a modification to the viscoelastic model enabling it to describe the knee in the tensile loading curve. His model was able to do this by incorporating an element that essentially failed at a certain load, thus reducing the overall material stiffness. Therefore his model and the concept of damage accumulation (as introduced in chapter 2) have common features. However, in Sedlin's case the change in

mechanical properties is not permanent, as it is in the case of damage. I showed that the rate at which Sedlin's model was extended affected the load at which the knee occurred. It was also shown that the ultimate stress predicted by the damage approach increased with strain rate.

In this chapter I introduced and extended two damage models developed in a series of papers by Carter and Caler. These I referred to as the TDF and NTDF models. The first is a time-dependent failure model, which is based on the time-to-rupture being a function of the creep stress alone. The second is a normalised time-dependent failure model. In this second case the time-to-rupture is a function of the creep stress and the material stiffness. I reviewed papers that support the use of the TDF model for bone and antler. I also showed that a predictive equation based on the NTDF model closely resembled one derived from Currey's experimental data.

In the final section of the chapter I considered two papers that have examined the creep rate of bone specimens. (The creep rate may be considered to be related to the damage rate.) Based on a comment made by Fondrk *et al.* (1988), I developed a simple model to explain the relationship between creep and tensile tests. (The physical mechanism that causes creep was not considered in this model.) The model assumed that creep strain was accumulated uniformly, with respect to time. (The same assumption was made in the TDF and NTDF models.) I suggested that it may be a variation in this creep-rate (primary, secondary and tertiary creep stages) that is responsible for the differences in the slope of the stress-strain curves of bone and antler, in the post-knee region. This hypothesis is one of the topics examined in more depth in the following chapter.

4

TIME-DEPENDENT PROPERTIES OF BONE AND ANTLER: EXPERIMENTAL RESULTS

4.1. INTRODUCTION

This chapter contains the results of some experiments I have conducted to examine the time dependent mechanical behaviour of specimens of femoral bone and antler. The antler specimens come from two species of deer, reindeer (*Rangifer tarandus*) and red deer (*Cervus elaphus*). The bone specimens were obtained from the femora of immature cattle. This chapter is divided into two main sections. The first section contains an examination of the results from standard tensile tests conducted at four different rates (cross-head speeds). The second section contains an analysis of the results of creep-rupture tests.[1]

4.2. TIME-DEPENDENT BEHAVIOUR: TENSILE TESTS.

The reason for conducting tensile tests at different cross-head speeds is to identify how this variable effects the mechanical response of the bone and antler specimens examined here. If the mechanical properties of these materials are dependent on the rate at which they are tested, a full description of their mechanical response must contain some function of time, or at least the rate at which they are derived should be given. For example it will be shown that the material's strength and stiffness should not be quoted as if these were material properties. The existence, or lack of existence, of a relationship between cross-head speed and a mechanical quantity may also provide an insight of the processes that determine the nature and scale of that mechanical response. It is reasonable to assume that if the events occurring before failure are rate dependent, then so is the process of failure. Thus a study of the earlier events may provide an insight to the final destructive events.

I reported in the previous chapter that certain features of the mechanical response of antler and bone are rate-dependent. However, I am not aware of any published study that compares the nature of this effect in these two materials.

The tests presented here form part of a larger data set that enables comparisons to be drawn between notched and un-notched specimens tested using the same four values of cross-head speed. In addition these specimens provide some data on the relationship between the optical changes and mechanical response. However, in this chapter I will only consider the tests of un-notched specimens conducted at different rates. The results

---

[1]Notch sensitivity tests have also been conducted at different cross-head speeds. These are described in chapter 7. Likewise the optical changes that were observed during these tensile tests display some rate-dependence (see chapter 8).

of these tests are examined with reference to the equations and theories outlined in the previous two chapters.

4.2.1. EXPERIMENTAL AIMS AND DESIGN

The experimental design was determined, to a large extent, by the desire to produce a data set for un-notched specimens that could be directly compared to that for notched specimens. The specimens for both types of test came from the same bones. (This was done as an attempt to reduce the variability of the material examined in these tests.) Both types of test were conducted at four cross-head speeds (8.33×10^{-7}, 8.33×10^{-6}, 8.33×10^{-5} and 8.33×10^{-4} m s^{-1}) on specimens of two widths (nominally 4 and 5 mm). The specimens were produced from either bovine femoral bone or red deer antler. The maximum justifiable testing speed was determined by the maximum sampling rate of the data acquisition equipment. The maximum size of specimen was determined by the range of the load measuring system used (1000 N) and by the estimated failure stress of the material at the fastest testing rate. The dispersion of specimens (for which a full set of data is available) between these test groupings is shown in table 4.002 and 4.003. The information needed for the comparisons with the notched data are: the failure, or ultimate, stress of the material at each cross-head speed and some normalising variable. The normalising variable used was the material stiffness in bending measured before the final shaping of the specimen. This quantity is available for both notched and un-notched specimens. However, other mechanical quantities were also determined from the stress-strain curves. This enables a more extensive comparison to be made between the behaviour of bovine bone and antler. These data also enable the experimentally observed behaviour to be compared with that predicted by the various models and theories explained in the preceding chapters.

4.2.2. TEST MATERIAL

The source of the specimens examined here is given in table 4.001. The range of identification numbers given in the table indicate all the specimens cut from an individual bone. These numbers are assigned at the earliest stage of preparation. The numbers are composed of the date on which the bone was first sectioned, or cleaned, and the number of the specimen. The number in parentheses indicates how many of those specimens are contained in the data sets examined statistically in this section. There is some degree of variation between the number of specimens initially cut and the number examined. The greater proportion of these missing specimens were used for notch sensitivity tests and are analysed in chapter 7. However, some specimens were rejected during preparation,

and others were rejected because they had an incomplete data set associated with them (due to failure of the experimenter or experimental equipment). The 'data sets' column, of table 4.001, gives the name assigned to the data set. For example the first set of antler tensile data is TA1. Further information on each data set, and how the raw data may be obtained is given in appendix 4. The data sets in parenthesis are those in which specimens from the same antler or bones also appear. These other data sets contain data on the specimens that were notched (see chapter 7).

Bone type	Comments	Identification numbers (Data used)	Data Sets
Red deer antler	The proximal end of the antler was sawn off. This implies it was not cast. No velvet was attached and it appeared fully calcified and normal.	10/11/91/01 - 10/11/91/104 (27)	TA1 (NA4) (NA5)
Femur	Approximately 18 months old, epiphysis un-fused. Collected fresh from butcher, then stored in freezer for 4 days before it was cut into slabs.	28/10/91/01 - 28/10/91/39 (3)	TB1 (NB4) (NB5)
Femur	Approximately 18 months old, epiphysis un-fused. Collected fresh from butcher, then stored in freezer for 8 days before it was cut into slabs.	01/11/91/01 - 01/11/91/52 (27)	TB1 (NB4) (NB5)

Table 4.001

Source, storage and usage of the test material

4.2.3. SPECIMEN PREPARATION FOR THE TENSILE TESTS

The specimens were prepared in a similar way for both materials. The only difference was that the initial preparation of the antler was done in the *as received* dry state whereas the bovine bone was kept wet (or frozen) during all stages of the operation. After the initial sectioning, the antler test material was kept wet during all subsequent stages of preparation, storage and testing. Appendix 2 contains a complete description of the preparation technique used for both the antler and bone specimens. However, in this section I will review most of the important points. Rectangular slabs of bone or antler, roughly 7 mm × 1.25 mm × 45 mm, were obtained from the whole bone by cutting and grinding. These rectangular slabs were oriented so that their long axis was parallel to the long axis of the cylinder of bone, or antler from which they were cut. The large flat surfaces were cut and ground so they were approximately parallel to the external surface of the original structure. One corner of the slab was ground off to indicate its orientation in the bone from whence it came. This will be referred to as the *datum corner* and the

end containing it the *datum end*. If the slab is viewed, so that its long axis is vertical and the datum corner is that at the bottom left hand side, then the large surface seen is that closest to the periosteal, or external, surface of the original structure. This orientation is similar to that in the original structure (see the figures of appendix 2) and will be referred to as the *natural* orientation. For the antler specimens this (datum) end was closest to the base of the antler (or for specimens cut from tines closest to the main beam), and is thus proximal, while in the bovine bone the datum end is the more distal one. The datum corner enabled every specimen to be positioned consistently during each machining or testing stage. The purpose of this was to reduce a possible source of variance and highlight any errors in the preparation method. (Thus such errors may have been expressed by the tensile specimens failing preferentially at one end. This was not observed.)

The rectangular slabs of material were tested in three-point-bending using an Instron 1122 machine. The aim of this test was to obtain a value of material stiffness under standard conditions for each specimen. The slab to be tested was positioned so that it straddled a machined cavity in a metal block. The block was mounted on an Instron compression load cell, with the hole positioned centrally. The slab was totally immersed in tap water. The compression surface was that which had been closest to the external surface of the original bone or antler. They were centrally loaded to approximately 2 N, using a cross-head speed of 8.3×10^{-6} m s^{-1} [0.5 mm min^{-1}]. The load was recorded on the Instron's chart recorder. The straight portion of the loading curve (after the so-called *bedding-in* section, or initial non-linearity) was extrapolated to give the total deflection due to a load of 2 N. This deflection is the sum of the deflection of the specimen being tested and the deflection of the loading equipment. To account for the *machine deflection*, the system was loaded without a specimen and the deflection (assumed to be due to the machine only) was recorded. The deflection due to the machine was subtracted from the total measured deflection in each test before the calculation of *material stiffness* was undertaken.[2] To calculate the material stiffness the equation describing the *Young's modulus* of a uniform rectangular beam of elastic material in three-point-bending was used (this is provided in appendix 2).

After testing in three-point-bending, the rectangular sections of test material were machined into the familiar *dog-bone* shaped specimens. The waisted sections of the specimens were 4 or 5 mm in width. This operation was performed using an engraving machine with a milling tool. The tool is guided by a manually operated jig follower. Thus with different jigs specimens of different shapes can be accurately replicated.

---

[2]The effect of disregarding the machine deflection is demonstrated by the mean values of bending stiffness for data sets TB1 and TA1. First bone, 20.5 GPa (s.d. 2.6 GPa) when the deflection is accounted for and 19.9 GPa (s.d. 2.4 GPa) when it is not. In the case of the antler specimens these values were 11.3 GPa (s.d. 1.7 GPa) and 11.1 GPa (s.d. 1.6).

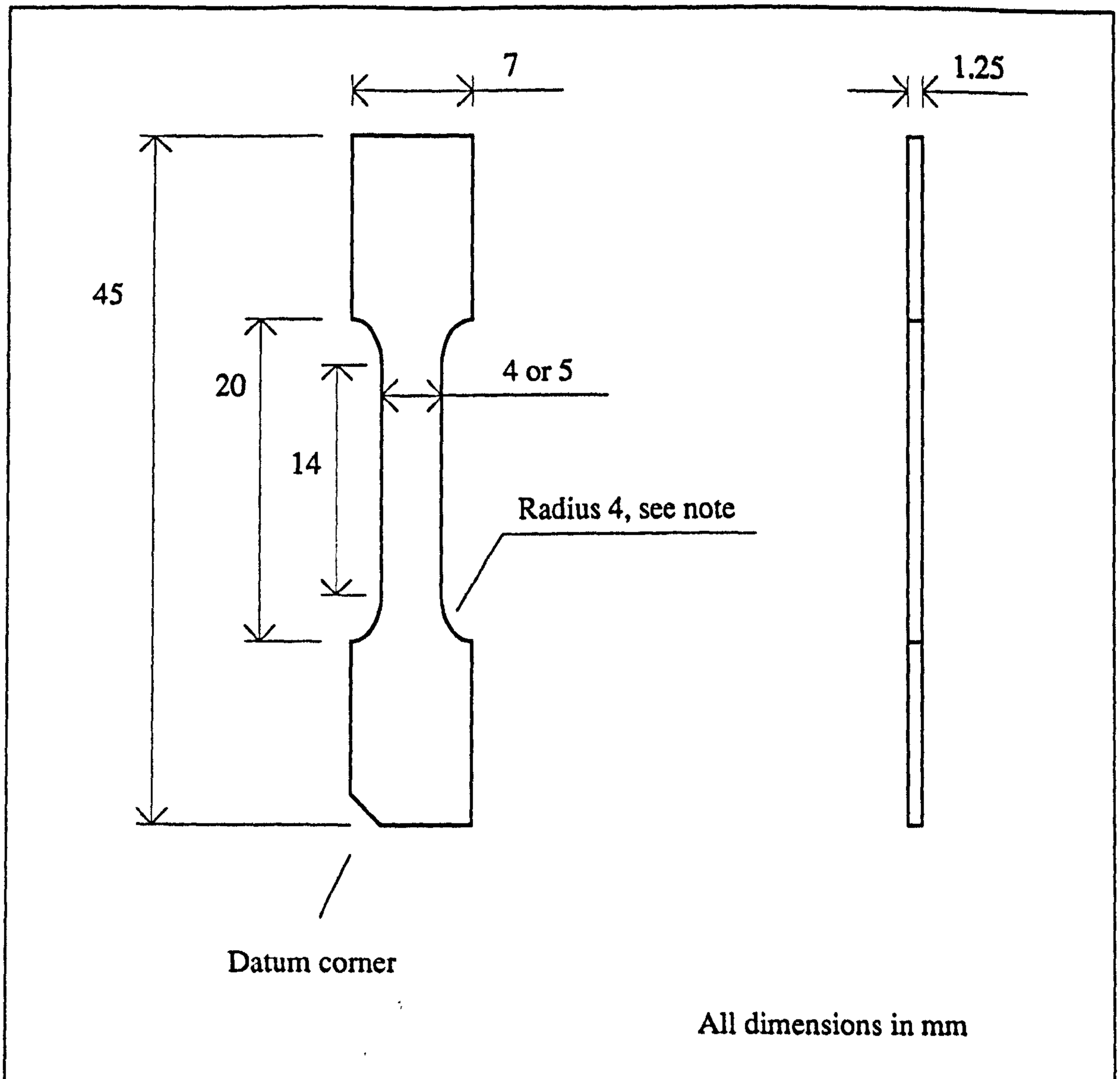

Note: This is not a true radius, as the flare at the reduced cross-section is more gradual. The specimen is viewed in its *natural* orientation, the largest surface seen here was that closest to the surface of the original bone.

Figure 4.001

The basic shape and nominal dimensions of the tensile specimens

The specimens were assigned to the various test groupings by examination of their stiffness in three-point-bending. The aim was to obtain an even distribution of specimens within each group. This distribution has been affected to some degree by the failure to obtain results from a number of specimens. Tables 4.002 and 4.003 demonstrate the distribution of the specimens

Cross-head speed	Nominal specimen width 4 mm			Nominal specimen width 5 mm		
		s.d.	n		s.d.	n
8.33×10^{-7} m s^{-1}	w = 3.94	0.02	4	w = 4.78	0.01	3
[0.05 mm min^{-1}]	E_b =12.19	0.85	4	E_b = 11.18	0.30	3
8.33×10^{-6} m s^{-1}	w = 3.90	0.03	4	w = 4.78	0.03	3
[0.5 mm min^{-1}]	E_b = 11.39	1.56	4	E_b = 13.21	0.50	3
8.33×10^{-5} m s^{-1}	w = 3.90	0.01	6	w = 4.76	0.01	2
[5.0 mm min^{-1}]	E_b = 10.73	2.03	6	E_b = 8.9	2.06	2
8.33×10^{-4} m s^{-1}	w = 3.89	0.03	3	w = 4.76	0.03	2
[50 mm min^{-1}]	E_b = 10.39	1.65	3	E_b = 11.84	1.83	2
Units:						
E_b Material stiffness in three-point-bending, GPa.						
w Specimen width, mm.						

Table 4.002

Various mechanical and geometrical properties of the antler specimens, in each of the test groupings (Data set TA1)

Cross-head speed	Nominal specimen width 4 mm			Nominal specimen width 5 mm		
		s.d.	n		s.d.	n
8.33×10^{-7} m s^{-1}	w = 3.87	0.03	3	w = 4.75	0.04	3
[0.05 mm min^{-1}]	E_b = 21.54	1.29	3	E_b = 20.46	4.09	3
8.33×10^{-6} m s^{-1}	w = 3.89	0.014	4	w = 4.72	0.04	4
[0.5 mm min^{-1}]	E_b = 19.50	0.88	4	E_b = 17.86	3.03	4
8.33×10^{-5} m s^{-1}	w = 3.88	0.03	6	w = 4.74	0.01	3
[5.0 mm min^{-1}]	E_b = 19.32	2.11	6	E_b = 22.54	1.00	3
8.33×10^{-4} m s^{-1}	w = 3.87	0.02	2	w = 4.72	0.02	5
[50 mm min^{-1}]	E_b = 22.81	0.42	2	E_b = 22.33	2.66	5
Units:						
E_b Material stiffness in three-point-bending, GPa.						
w Specimen width, mm.						

Table 4.003

Various mechanical and geometrical properties of the bovine bone specimens in each of the test groupings (Data set TB1)

4.2.4. PROCEDURE USED FOR TENSILE TESTING

A standard test procedure was used for all tensile specimens, the main features of which are outlined below.

a) The same mechanical test machine, an Instron 1122, was used in all tests.

b) The load transducer was an Instron tensile load cell, rated at 100 kg full scale.

c) The strain (or more correctly extension) transducer was either a 10 or a 50% static extensometer produced by Instron, both of which had a nominal 10 mm gauge length. The actual length was measured in each case (at both edges of the specimen and an average of these was used). The extensometers were waterproofed using a combination of a bicycle inner-tube, to contain the body of the extensometer and connecting wire, and a thin piece of plastic sheet around the arms of the extensometer. To avoid restricting the movement of the extensometer arms the plastic sheet was folded in a concertina fashion. The extra mass produced by this waterproofing was offset by the buoyancy of the arrangement. The extensometer was attached to the specimen using orthodontic elastic bands. (This arrangement is shown in figure 4.002.)

d) The values of stress, strain and time were recorded using the AJS/BBC data collection system that is described in appendix 1.

e) All specimens were clamped in the same jaws. These were originally developed for creep testing. The jaws were made of two roughened aluminium sections. These sections were clamped, sandwiching the specimen between them, by tightening two nuts. The bottom jaw was fixed to the base of the test machine, and was contained within a temperature controlled water tank.

f) All specimens were tested while completely submerged in tap water. The water was maintained at a temperature within one degree of 37°C.

g) The orientation of the different specimens was kept consistent, by positioning them in the *natural* orientation.

h) These tensile tests were recorded on high-speed video tape. This involved a few additional steps in the test procedure. After the specimen was clamped in the jaws, the video recorder was started. This was followed by starting the data collection system and then the Instron at a pre-selected speed.[3] The reverse of this procedure was used after the test.

i) The high speed video was then down loaded at 30 frames per second onto standard VHS video tape.

---

[3] 8.33×10^{-7}, 8.33×10^{-6}, 8.33×10^{-5} or 8.33×10^{-4} m s^{-1}.

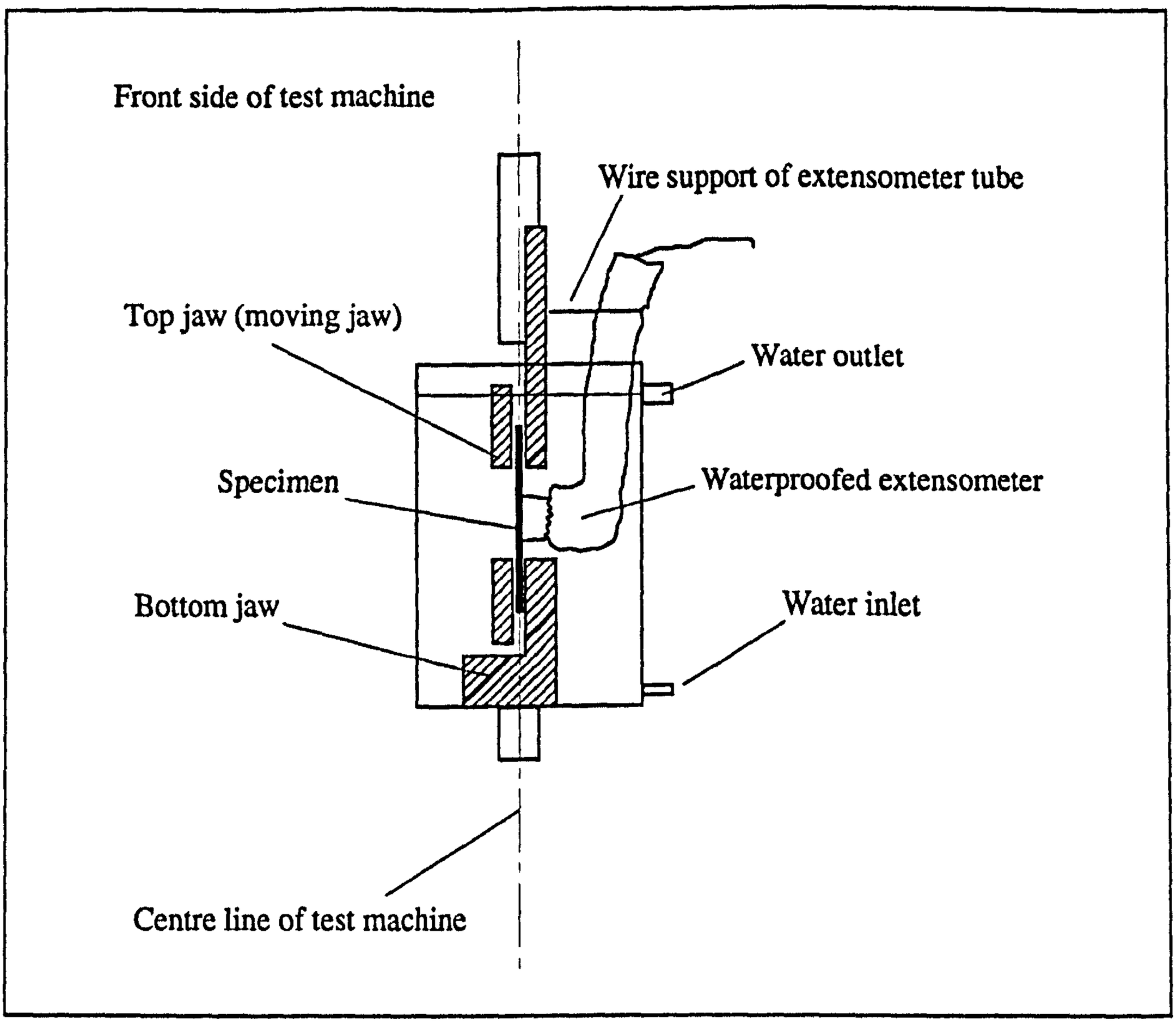

Figure 4.002

The arrangement of the specimen, extensometer, jaws and environmental chamber used during tensile testing.

4.2.5. RESULTS: NON-CONSTANT TESTING RATE, RESULTING FROM A MACHINE-SPECIMEN INTERACTION

Within this chapter I have (so far) referred to the rate dependence of bone and antler being tested by the application of different cross-head speeds. I have reported that similar studies in the literature are referred to as investigations into the effects of strain rate. I doubt if such a reference is true in a considerable number of cases, and I know it to be false in some. Many of the papers that I reviewed in chapter 3 rely on the use of different cross-head speeds to attain different testing rates and estimate the strain rates thus produced. In most cases this error arises from the assumption that the test machine (all structures outside the gauge length) is infinitely rigid. Only under this condition will the extension rate of the specimen be independent of its own stiffness, unless a closed-

loop control system exists.[4] I will refer to this lack of independence as the *machine-specimen interaction*. The machine used for the experiments presented in this thesis, an Instron 1122 material testing machine, works in open-loop control. Some of the implications of this interaction are considered in following sections.

As a simple example I will expand on my criticism of Sedlin's tests to investigate 'the behavior of bone under a constant deformation'. It was noted above (section 3.2.4) that Sedlin (1965) appears to have assumed his test machine was rigid. I suggested that this was an erroneous assumption and procedure. The deflection of the test machine would result in an extension of the test specimen as the stress upon it relaxed with time. A simple analogue of this situation can be made, consisting of two springs in series: one spring is the test machine and the other is the specimen. This system is stretched so that when the specimen-spring reaches some set length the extension of the system is fixed. Because the load is applied to both springs the machine-spring has also extended. The extension of the whole system is the sum of these two extensions. If the stiffness of the specimen-spring decreases with time, the load it exerts also decreases (stress relaxation). Because the load on each spring must be equal, that on the machine-spring also declines, due to its higher stiffness its extension lessens. The ends of the system are fixed; therefore contraction of the machine spring results in an extension of the specimen spring. (The changes in length are determined by the need to maintain the forces in equilibrium.) Thus the assumption of constant specimen length is invalidated.

The use of a spring analogue for the machine-specimen interaction is presented in more detail in appendix 7. In that appendix other situations are considered, such as the effect of machine-specimen interaction on strain rate. Essentially, if the specimen is very stiff its deflection will be a smaller proportion of the overall deflection of the whole system. Therefore if the loading system is extending at a set rate, a stiffer the specimen will have a smaller extension rate, and thus a smaller strain rate. This is demonstrated by the change in strain rate that occurs when a tensile specimen starts to display a knee in its stress-strain curve (indicating that it has become less stiff). Plots of stress against strain, stress against time, and strain against time are given in figure 4.003. Figure 4.003c clearly shows that there is a change in the strain rate associated with the knee region, or the reduction in stiffness of the specimen.

The observation that the extension rate of a specimen is dependent on its own stiffness, has implications when examining time-dependent properties. It was noted above (in section 3.2.2) that one of the properties of bone that has been used as a basis of

---

[4]In a closed-loop, or feed-back, control system the deformation rate is measured, using an extensometer for example. The measured rate is compared with the required rate. The machine then speeds-up or slows-down according on the error between these two values.

a description of its visco-elastic nature is the observed increase in material stiffness with strain rate. However, with the machine specimen interaction described here, such an increase in material stiffness will result in a lower strain rate. Thus the true increase in stiffness with increased testing rate is likely to be greater than the one observed using such an open-loop machine. The specimen-machine interaction also opens a debate on what measure of testing rate should be used. This is considered in more detail in following sections.

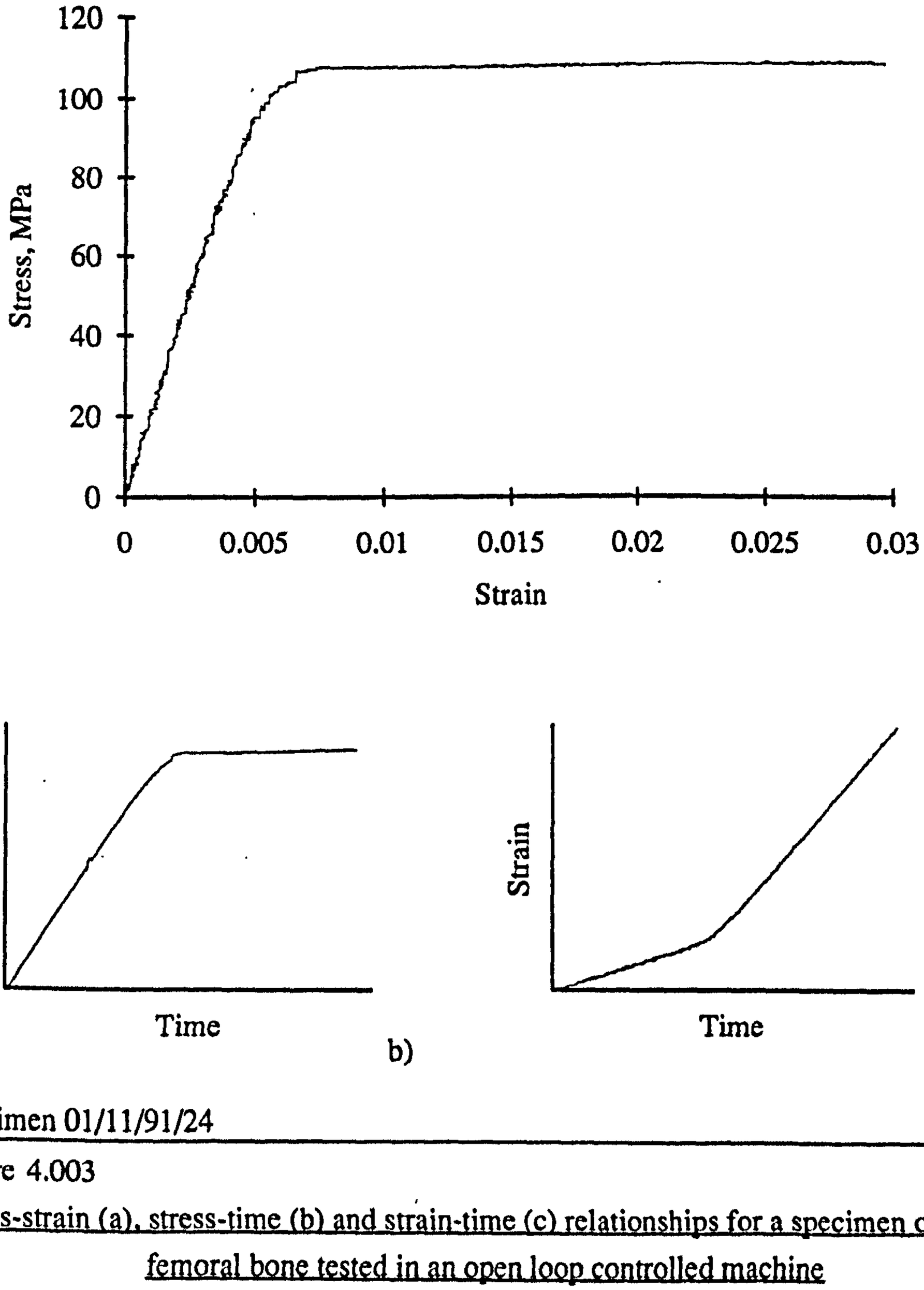

Figure 4.003

Stress-strain (a), stress-time (b) and strain-time (c) relationships for a specimen of bovine femoral bone tested in an open loop controlled machine

Figure 4.003 clearly shows that the strain rate changes when the specimen stiffness changes. (This plot shows one of the more extreme cases, where the reduction in the specimen's stiffness is quite severe.) This result shows that it is incorrect to assign a single extension, loading or strain rate to such a test conducted on an open-loop machine. The change in strain rate may also affect the shape of the knee region. From examination of the model I constructed based on a statement made by Fondrk *et al.* (section 3.3.3.2) the effect of the non-constant strain rate on the shape of the knee region can be postulated. As the strain rate increases, on the specimen entering the knee region, the load required to attain a creep rate that is equivalent is slightly increased. This may produce a more gentle curve.

In this section I have stated and shown that the open loop test machine used in this study does not produce a constant stress or strain rate during a test in which the specimen exhibits an increase in compliance. I have also presented a model to explain this fact, which is expanded in appendix 7. In a later section I will consider the size of this effect in my own work and the problems that this may cause in interpretation of the results.

4.2.6. RESULTS OBTAINED FROM TENSILE TESTS ON BONE AND ANTLER (DATA SETS TB1 AND TA1)

In this section I consider the results obtained from tensile tests I conducted on specimen of bone and antler at four cross-head speeds. The analysis is based on the use of regression equations. The form of these equations has been chosen to enable comparisons with previously published results, reviewed above, and with various model-based predictions. However, before this analysis is presented, I shall explain how the various quantities considered were derived from the stress, strain and time data. I will also explain what considerations were taken into account when deciding which measure of testing rate to use.

4.2.6.1. DEFINITION OF THE MECHANICAL PROPERTIES STUDIED

Following the examples given in tables 3.001, 3.003 and figure 3.006, I have derived a number of quantities from the stress-strain data of each specimen. (Some of the stress-strain plots from which this data set was derived are shown in figures 1.010 and 1.012, and another in figure 4.003a.) The relationship of some of these quantities to such a loading curve is shown in the idealised plot in figure 4.004. (A number of other quantities were also derived to show specific points. How these were obtained will be explained at the relevant place.) I have not adopted the nomenclature normally used in

the literature, because some of those terms refer to processes that do not occur in bone or antler. I have attempted to use wording that describes the observed behaviour without suggesting its cause. For as Herbert Spencer (1820-1903) said 'how often misused words generate misleading thoughts'. The nomenclature I use is as follows:

a) E_t, *Material stiffness in tension* (this is also referred to as material stiffness measured in tension or tensile material stiffness): this quantity was determined by fitting a least-squares linear regression line to the data in the initial region of the loading curve.

b) S, *Final slope:* this was determined by fitting a least-squares regression line to the data in the post-knee region. This nomenclature I have adopted from Currey (1989).[5] The slope of the post-knee region has also been referred to by nomenclature borrowed from metals testing. For example Reilly and Burstein (1975) clearly refer to it as the 'strain hardening modulus' saying it is 'a term borrowed from the engineering description of metallic behavior'. I wish to avoid using such terms that are not only associated with some measure of the stress-strain response but are also associated with a description of the material or the process it is undergoing.

c) σ_K, *Knee stress:* this is the value of stress at which the regression lines of the material stiffness in tension and the final slope intersect. The method used to find this point was to solve these regression lines as a pair of simultaneous equations. If the post-knee region was too short to fit a regression line the maximum value of stress was substituted into the regression equation for E_t.

d) σ_{ult}, *Ultimate stress:* this is the maximum value of the nominal stress attained during the test. (There was a slight reduction in stress just prior to the failure of some bovine specimens.)

e) ε_K, *Knee strain:* the value of nominal strain obtained by solving the regression equations of the material stiffness in tension and the final slope for strain.

f) ε_{ult}, *Ultimate strain:* the maximum value of the nominal strain obtained during the test.

g) W, *Work:* this value of work, or area under the curve, can be viewed as the energy supplied per unit volume to the gauge length of the specimen up to the point of failure. The proportion of this energy that is stored in the specimen and how much of it is consumed by the failure process is indeterminate in such a test. The numerical value of this quantity was obtained by using the trapezium rule on each successive pair of data points for the whole loading curve.

---

[5]Currey's nomenclature was presented in figure 3.006.

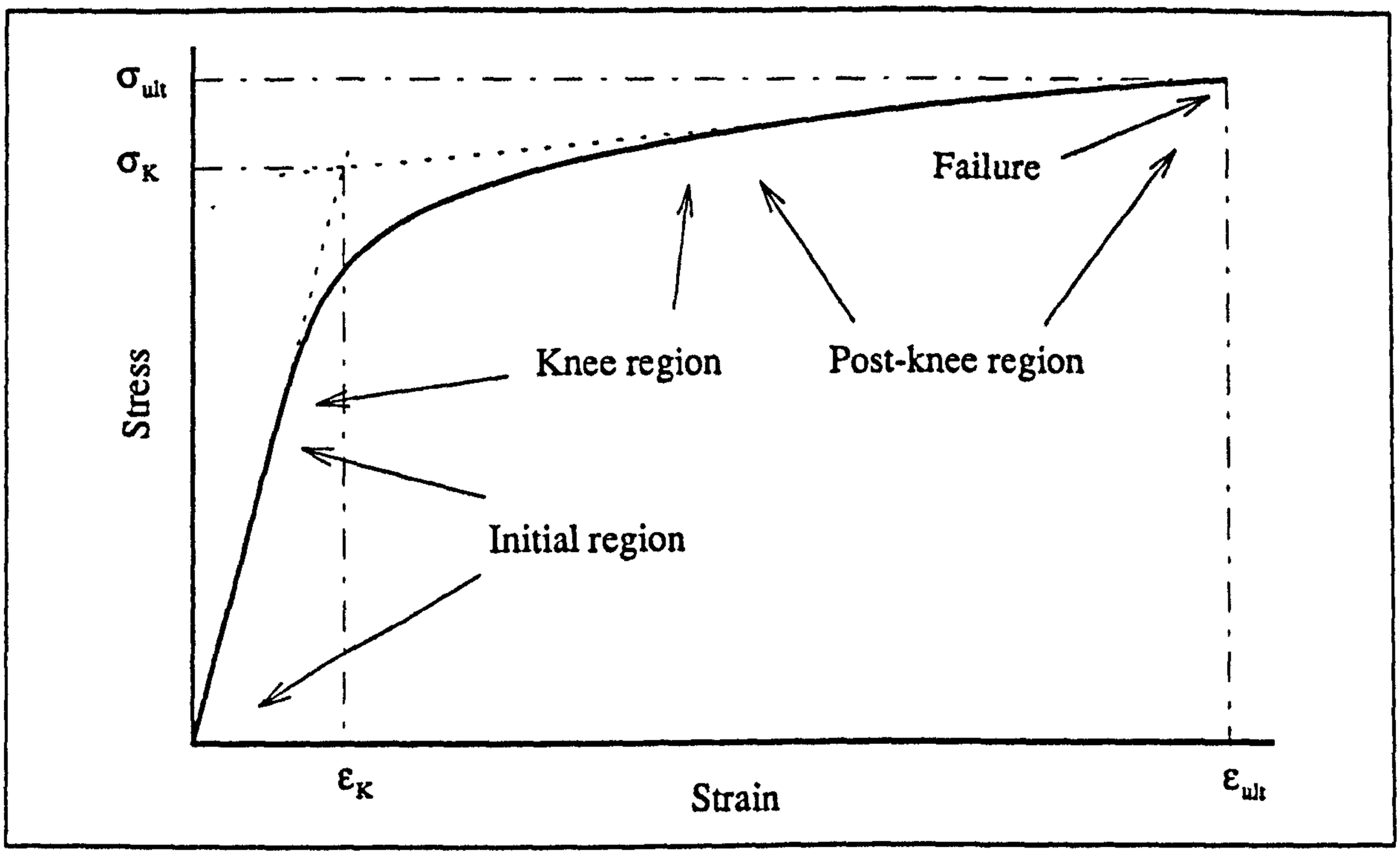

Figure 4.004

Idealised plot showing how various quantities were derived, and the nomenclature used to describe the loading curve

The derivation of some of the above quantities are the same as those used by Reilly and Burstein (1975) for bovine and human bone[6] and by Currey (1975) for bovine bone. However, I use different terminology denoting the transition region of the curve as the *knee* rather than the *yield* region. This is because the term yield can be interpreted as describing the process that produces such a knee. However, the term *knee* has no association with a specific process. Clearly the derivation of knee stress is different to the derivation of 'yield stress' given by Currey (1989). The method of calculation used here has a closer resemblance to the knee stress and knee strain for an idealised stress-strain response (see figure 2.013). The point at which a metal yields, or starts to show plastic deformation, is of great importance to engineers. Thus in engineering it has become necessary to define a stress that corresponds to a defined amount of permanent deformation in such engineering materials. This is commonly referred to as the proof stress, and is defined as the stress at which the deviation from the linear response has reached the defined amount of deformation (Higgins, 1983). Thus the so-called *yield stress* defined by Currey (1989) maybe expressed more accurately as the 0.2% proof stress. This assumes the nomenclature is transposable, and the unloading line has the

---

[6]When referring to the intersecting slopes method, Reilly and Burstein (1975) report that 'this method was convenient and gave repeatable results for the yield point which represented approximately the same value as a 0.2% offset strain method.'

same slope as the loading one.[7] The choice of the deformation limit is arbitrary, but Higgins when discussing metals says that 'proof lengths are commonly 0.1% and 0.2% of the gauge length depending upon the type of alloy'. I suggest that applying such an engineering design procedure to the stress-strain relationship of bone or antler has no more biological significance than the method I use. The case against using the proof stress method can also be argued by referring to the value of idealised damage associated with such a measure. In section 2.3.3.7 an equation relating material stiffness and damage was given:

$$D = 1 - \frac{E_M}{E_U} \qquad (4.001)$$

Assuming the material to be an elastic-damage one, the damage at 2% proof stress, $\sigma_{2\%}$, can be expressed as

$$D = 1 - \frac{\sigma_{2\%}\,\varepsilon_U}{(\varepsilon_U + 0.002)\,\sigma_{2\%}} = \frac{0.002}{\varepsilon_U + 0.002} \qquad (4.002)$$

where ε_U is the strain that would be associated with the stress if the material showed no deviation from its initial linear stress-strain relationship. Equation 4.002 shows that the degree of damage associated with the 2% proof stress is dependent on the strain that the material would have exhibited had it not become damaged. In other words it is dependent on the initial stiffness and the stress level. Therefore the proof stress does not give a consistent (idealised) measure of damage for materials of variable stiffness such as bone and antler. However, the method of intersecting slopes gives the point at which the damage would start if the material was an ideal elastic damage one. From the damage viewpoint, the method of intersecting slopes is therefore more consistent. Due to these points I consider that the knee stress is a more justifiable quantity. Coincidentally, it is very easy to determine knee stress (as defined above) for discrete data considered here.

4.2.6.2. DIFFERENT MEASURES OF TESTING RATE: WHICH ONE SHOULD BE USED?

The tensile tests described in this chapter are intended, in part, to demonstrate whether certain mechanical properties of the bone and antler are rate-dependent. I have reported that the testing rate is not constant during the testing of a single specimen, and that it will vary from specimen to specimen. This produces a problem: what measure of testing rate should be used in this study? A number of possibilities exist. Some of these

---

[7]Unless the material is unloaded it will not be known if this deviation is permanent or if the curvature was due to non-linear elastic behaviour for example. Metals, for which the proof stress is defined, behave in an almost elastic-plastic fashion.

have been used within published papers. I will consider five of the possibilities that are available in this study:

a) The estimated strain rate (the division of cross-head speed by the gauge length).

b) The value of the knee-strain divided by the time taken to reach that strain.

c) The directly measured strain rate during the initial stage, for all analysis.

d) The directly measured strain rate during the stage being analysed.

e) The cross-head speed of the machine.

The first method is only correct if everything outside the gauge length is rigid. This method was used by Crowninshield and Pope (1974). They say that the relative motion of the gripping devices was measured using a resistive displacement transducer. They assumed that all of this displacement was the result of strain occurring in the gauge length of their specimen. However, due to the design of their specimens (figure 1.020) I consider that a certain amount of this displacement will be a result of deformations occurring outside the gauge length. When they refer to the calculation of strain rate the authors say that 'the value of strain rate for a specimen was calculated to be the crosshead speed of the loading device divided by the specimen gauge length'. The deformations outside the gauge length would result in this calculated quantity being an exaggeration of the true strain rate. The lack of compensation of the machine-specimen interaction could explain the low values of material stiffness obtain by these workers (about 11 GPa). It is reasonable to assume that the strain rates calculated by Crowninshield and Pope are greater than those truly experienced by the specimen gauge length.

The method of estimating strain rate from cross-head speed and gauge length was used by Currey (1989). No reference to this method is made in the paper. This information was provided by Professor Currey's technician Kevin Brear. Mr Brear stated that the value was obtained by dividing the cross-head speed by the length of the specimen over which the extensometer was attached. This is less than the reduced section of the specimen. Currey (1989) gave these lengths as nominally 10 and 14 millimetres. In appendix 7 it is shown that a more accurate estimate would have been obtained if the length of the reduced section of the specimen had been used. Thus it appears that a more accurate estimate of strain rate in Currey's tests is 70% of the value quoted. However, it should be remembered that strain rates are normally logged before they are used in regression analysis. Therefore, such a multiplication error will only change the value of the constant in the regression equation not the coefficient (i.e. the exponent in the normal form).

The second of the methods listed above was used by Currey in his 1975 paper. This would appear to be a more accurate measure of the strain rate than the first method. This is because the value of strain used can (as it was in Currey's paper) be measured

directly thus removing the error in the value of strain due to the machine deflection.[8] Currey does not present a similar calculation for the post-knee region. If he had done this calculation I suggest the difference between the strain rates in the pre and post-knee regions would have become apparent.

The third method for determining a measure of testing rate is available for the tests described in the present work, as time was recorded as well as stress and strain. Thus the gradient of a strain-time plot (for example figure 4.003c) can be measured. I have done this by fitting a least-squares regression line to the data of the initial region. Wright and Hayes (1976) used the measured value of strain rate from a few instrumented specimens (fewer specimens than the number of cross-head speeds they used). These workers did not consider the effects of different specimen stiffnesses. As they only considered one quantity related to the post-knee region the effect of changing specimen compliance is not very important. (The quantity that may be affected is the 'energy absorption capacity', presumably area under the curve. However, it is not clear how this was calculated.)

The measured strain rate changes as the specimen enters the knee and post-knee region. This observation suggests the use of the fourth method. (For other purposes I have obtained the strain rate in the post knee-region of the loading curve by fitting a regression line to the strain-time data.) I do not consider that the use of the post-knee strain rate is justifiable, even for the analysis of the post-knee behaviour. This is because it is a reasonable assumption that the mechanical properties in the post-knee region are not independent of the material's mechanical response in the pre-knee region. Therefore this method is not as simple as it first appears.

The last method listed above is to use the cross-head speed of the machine. This clearly has draw-backs as stated above. However, it is the only measure that is independent of the specimen being tested. Clearly, its exact relationship to the strain rate is complex. However, the use of cross-head speed avoids confusion between viewing the results as being from a test where the strain rate is measured, or from a test where the rate is imposed on the specimen.

---

[8]Clearly the use of direct measurement gives the correct value of strain but it does not avoid the effect that the specimen-machine interaction has on the strain rate.

4.2.6.3. DIFFERENT MEASURES OF TESTING RATE: RESULTS AND SOME EVIDENCE FOR THE FAILURE PROCESS.

I will now examine my experimental results for evidence of an effect on strain rate due to the material and specimen stiffness. For this I will use the values in data sets TA1 and TB1. First, I will take the material stiffness measured in three-point-bending and the strain rate, measured by way of an extensometer, during the initial region of the loading curve.

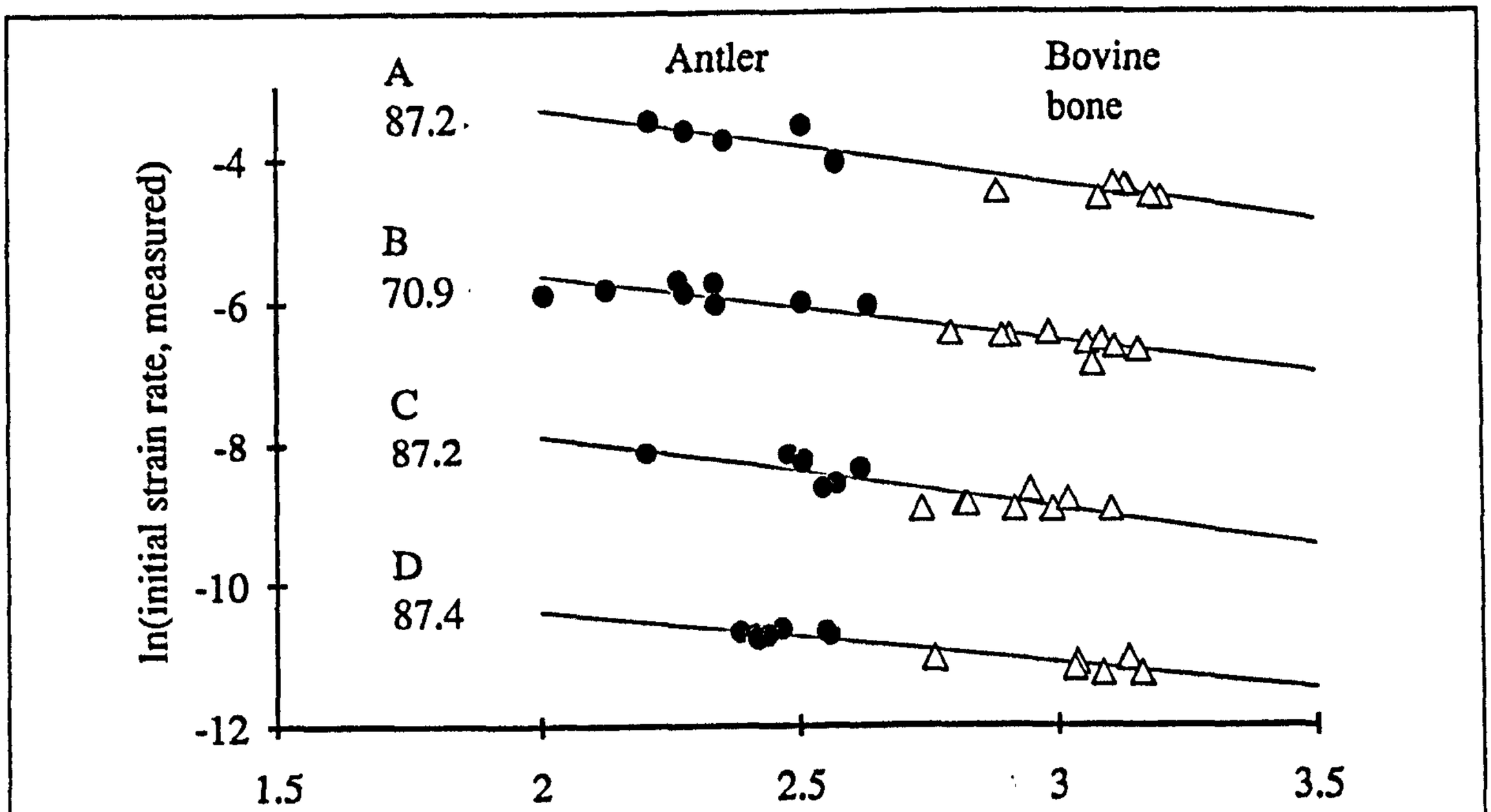

Units:

$\dot{\varepsilon}_i$ Strain rate measured during the initial region of the loading curve, s^{-1}

E_b Material stiffness in three-point-bending, GPa.

Comments:

The cross-heads speed of the test is indicated by; A 8.33×10^{-4}, B 8.33×10^{-5}, C 8.33×10^{-6} and D 8.33×10^{-7} m s^{-1}. The accompanying numbers are the R^2% of the regression lines, also shown.

Figure 4.005

The effect of material stiffness on the strain rate, as measured with an extensometer, at four cross-head speeds

There is a very highly significant relationship between the material stiffness and the measured strain rate, at each of the cross-head speeds used. The p values associated with the stiffness variable was less than 0.001 in every case. This supports the comments made above (section 4.2.5), and the models proposed in appendix 7. However, the stiffness of a specimen is also dependent on its cross-sectional area as well as on the

material it is made from. In these tests two nominal specimen widths were used (4 or 5 mm). Therefore, there can be a considerable difference between the stiffness of the specimens. This can be accounted for by multiplying the material stiffness by the specimen's cross-sectional area. The result of such a multiplication is shown in figure 4.006.

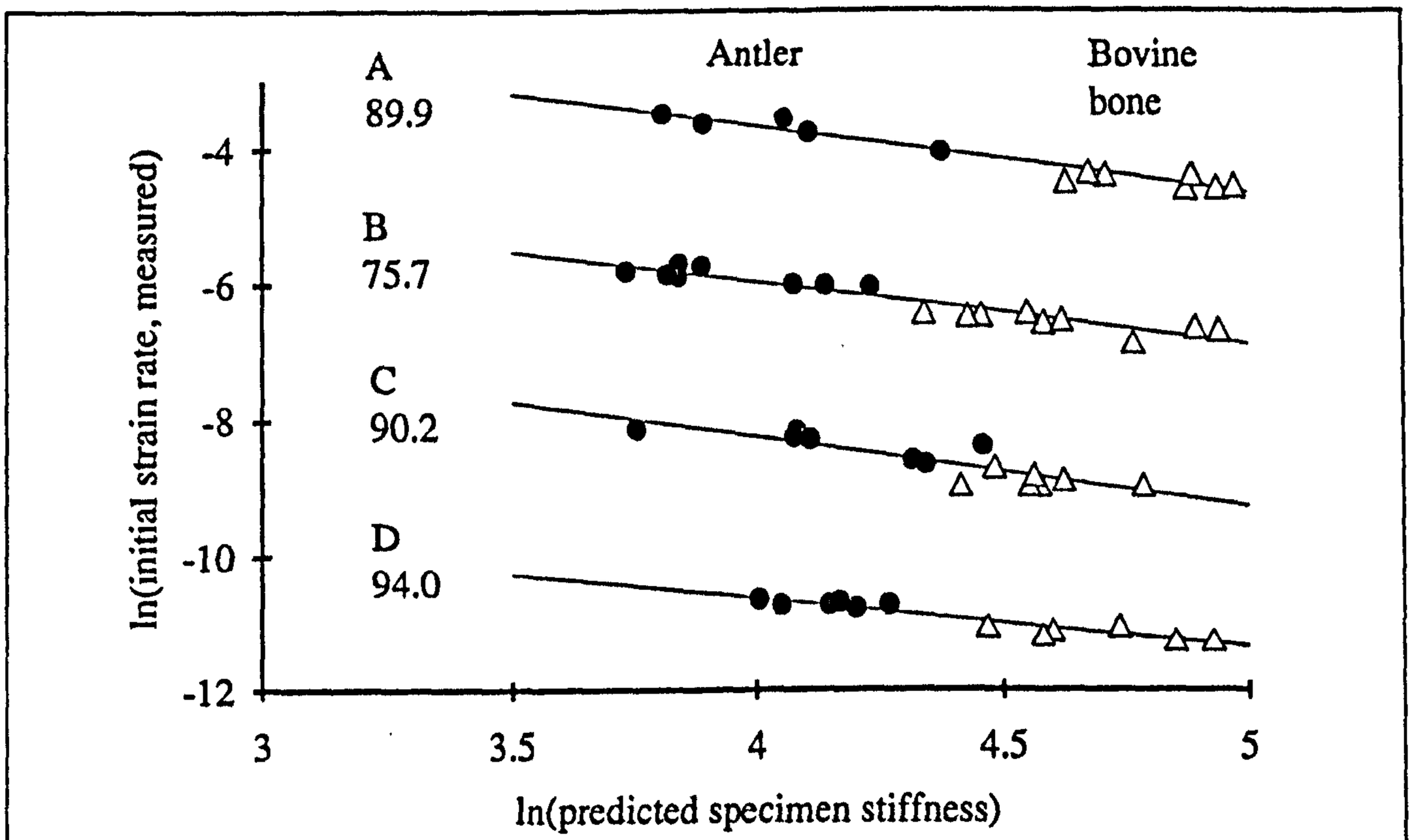

Units:

$\dot{\varepsilon}_i$ Strain rate measured during the initial region of the loading curve, s^{-1}

K Predicted specimen stiffness, MN.

Comments:

The cross-heads speeds are indicated by: A 8.33×10^{-4}, B 8.33×10^{-5}, C 8.33×10^{-6} and D 8.33×10^{-7} m s^{-1}. The solid circles represent antler specimens and the triangles those of bovine bone. The regression lines for each speed and their R^2% values are also shown.

Figure 4.006

The effect of specimen stiffness on the strain rate measured with an extensometer during the initial region of a stress-strain curve at four cross-head speeds

The relationship of measured strain rate to the stiffness of the specimen is shown clearly in figure 4.006. The lines shown are the least-squares regression lines for the data at each cross-head speed. The power of the regression equations has been increased by a few percentage points at each cross-head speed. This increase may appear to be small, but in every case it reduces the unexplained variation by more than 15% and in one case by more than 50%. In figure 4.006 (as in figure 4.005) there is a division between the antler (solid circles) and the bovine bone specimens (open triangles), but this has become blurred in figure 4.006. This blurring is due to the ability of a 5 mm wide antler specimen to be stiffer than 4 mm wide bone one. The antler specimens, which are

generally more compliant than the bone ones, display a higher strain rate at the same cross-head speed. This is shown numerically in table 4.006. The effect of material stiffness on strain rate, although noticeable, is still far smaller than the effect of changing the cross-head speed over the ranges used here. However, if intermediate speeds had been used, this machine-specimen interaction could have produced anomalies: a faster cross-head speed would not necessarily produce a higher strain rate.

The relationship of measured strain rate to the cross-head speed is shown in figure 4.007. Table 4.004 contains the regression equation for the antler and bovine bone data shown in that figure.

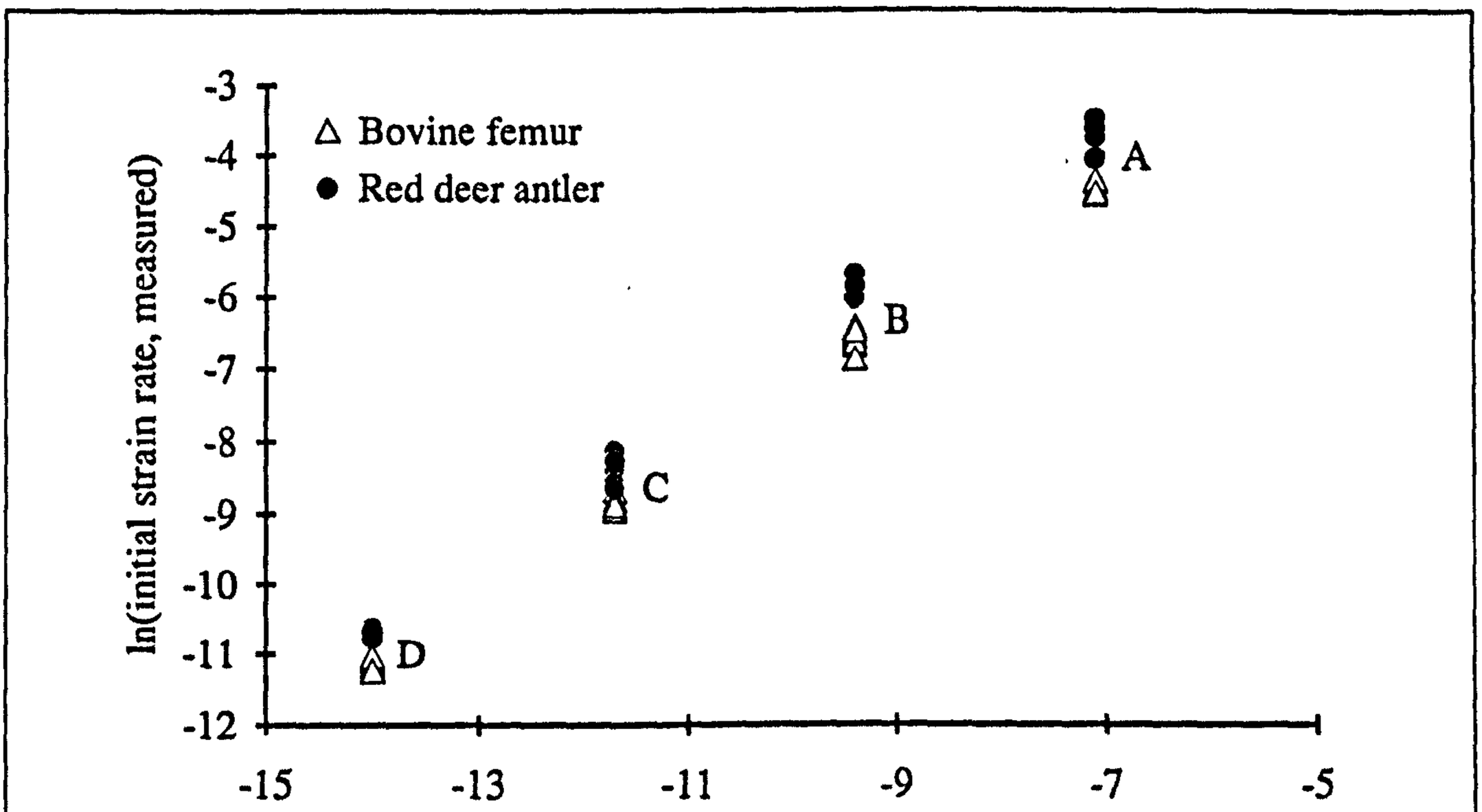

Units:

$\dot{x}$ Cross-head speed, m s^{-1}

$\dot{\varepsilon}_i$ Strain rate measured during the initial region of the loading curve, s^{-1}

Comments:

Different cross-head speeds are indicated by A, B, C and D, these are the same groupings as used in figure 4.006

Figure 4.007

Strain rate during the initial stage of the tensile test and the cross-head speed

Type of specimens	Regression equations and t values, obtained from the analysis of the data shown in figure 4.007. (Data sets TA1 and TB1)[9]	R^2 %	
27 antler	$\ln(\dot{\varepsilon}_i) = 3.64 + 1.02 \ln(\dot{x})$ t: 25.60 79.33	99.6	*a*
30 bone	$\ln(\dot{\varepsilon}_i) = 2.48 + 0.971 \ln(\dot{x})$ t: 25.65 107.01	99.7	*b*
Units: $\dot{\varepsilon}_i$, s^{-1}. $\dot{x}$, $m\ s^{-1}$.			

Table 4.004

The relationship of the strain rate during the initial stage of the tensile test and the cross-head speed of that test

The equations given in table 4.004 can be re-expressed in exponential form. Equation *a* can be rewritten as

$$\dot{\varepsilon}_i = 38.09\ \dot{x}^{1.02} \qquad (4.003)$$

This equation can be made more comparable with the ideas explained above (and in appendix 7) by converting the cross head speed into millimetres per second (using the symbol $\dot{X}$) This results in the relationship

$$\dot{\varepsilon}_i = \frac{\dot{X}^{1.02}}{30} \qquad (4.004)$$

Thus if the strain rate was estimated by dividing the cross-head speed by the gauge length of the specimen (the reduced section being about 14 mm long or the length over which the strain was measured being less than that) the estimate of the strain rate would be about twice the actual value. Similarly for bovine bone

$$\dot{\varepsilon}_i = 11.94\ \dot{x}^{0.971} \qquad (4.005)$$

which on converting to millimetres per second becomes

$$\dot{\varepsilon}_i = \frac{\dot{X}^{0.971}}{66} \qquad (4.006)$$

In this case an even larger error will be introduced. This agrees with the model given above, as the bone specimens are stiffer than antler ones.

A similar procedure can be used for the post knee strain. This is represented in figure 4.008 and table 4.005.

---

[9]Relationships of t and *p* values are given in appendix 12.

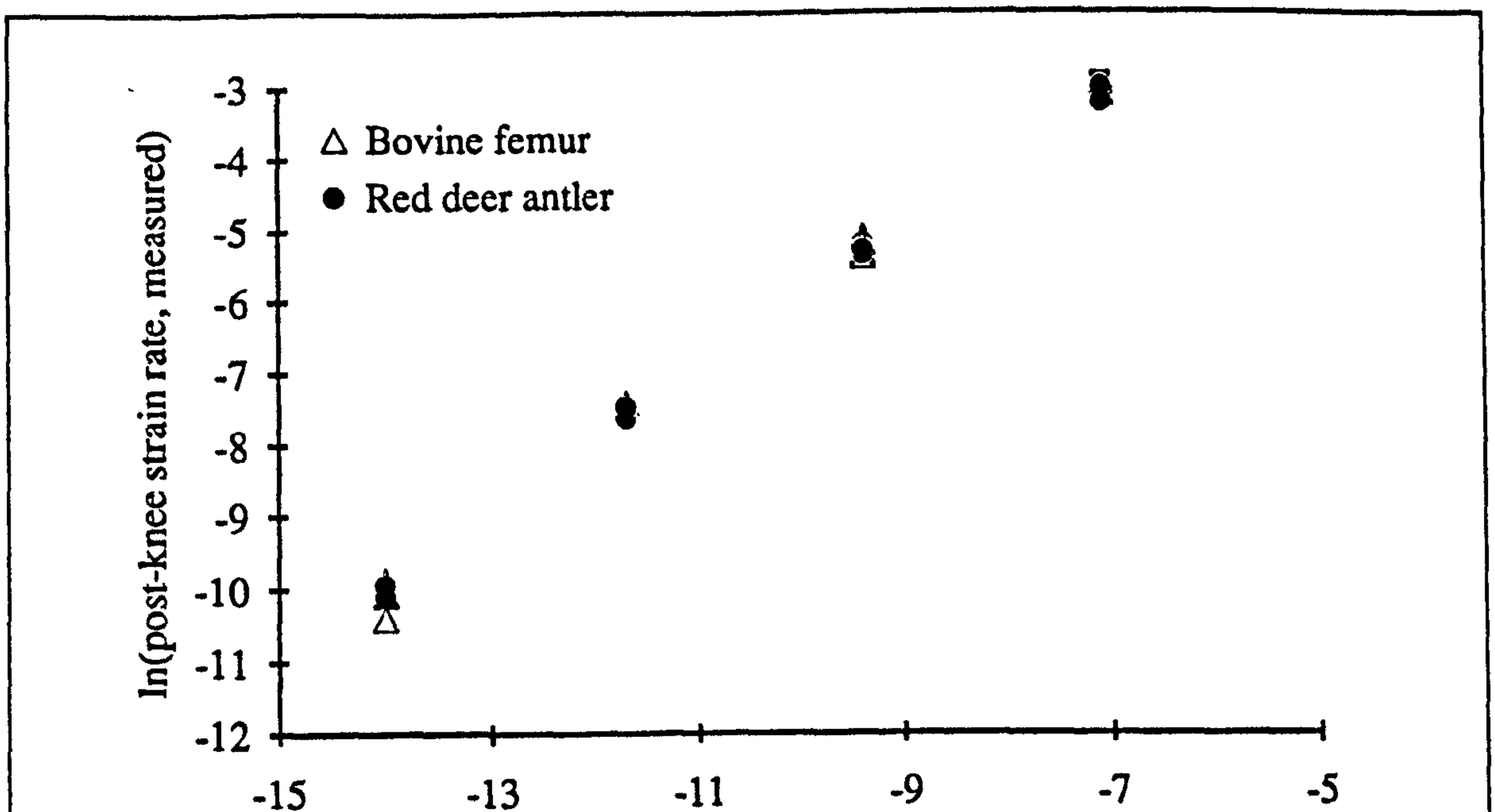

Units:

$\dot{x}$ Cross-head speed, m s^{-1}

$\dot{\varepsilon}_{pk}$ Strain rate measured during the post-knee region of the loading curve, s^{-1}

Figure 4.008

The strain rate measured in the post-knee region and the cross-head speed used

Type of specimens	Regression equations and t values, obtained from the analysis of the data shown in figure 4.008. (Data sets TA1 and TB1)	R^2 %	
27 antler	$\ln(\dot{\varepsilon}_{pk}) = 4.23 + 1.02 \ln(\dot{x})$ t: 58.27 154.48	99.9	*a*
17 bone	$\ln(\dot{\varepsilon}_{pk}) = 4.31 + 1.02 \ln(\dot{x})$ t: 26.91 66.38	99.6	*b*
Units: $\dot{\varepsilon}_{pk}$, s^{-1}. $\dot{x}$, m s^{-1}.			

Table 4.005

The regression equations of the relationship of the strain rate measured in the post-knee region and the cross-head speed of the testing machine

The same form of treatment that was applied to the strain rates in the pre-knee region (see above) can be applied to those in the post-knee region. Equation *a* in table 4.005, can be expressed as

$$\dot{\varepsilon}_{pk} = 68.72\ \dot{x}^{1.02} \tag{4.007}$$

or when the cross-head speed is expressed in mm s^{-1} as

$$\dot{\varepsilon}_{pk} = \frac{\dot{X}^{1.02}}{17} \tag{4.008}$$

Similarly for the second equation in the table, which expresses the relationship of measured strain rate to cross-head speed for a limited number of bone specimens. These were the specimens that achieved a post-knee region that was of a size comparable to that of the pre-knee region

$$\dot{\varepsilon}_{i} = \frac{\dot{X}^{1.03}}{15} \tag{4.009}$$

These equations (4.008 and 4.009) imply that if the machine were infinitely rigid, the length of the compliant specimen is 17 or 15 millimetres.

As the load is almost constant in the post-knee region of a tensile test of bovine bone, the machine can be considered to be rigid. Therefore, by the logic of the spring models, this implies that the process that results in the increase in compliance of the specimen has occurred, over the whole length of the reduced section of the specimen. This implication is only possible because the length over which the strain rate was measured is less than the length of the reduced cross-section. If a localised failure (like necking in metals) had occurred the extension rate measured by the extensometer would be the same as the machine's. Thus the strain rate would be a function of the cross-head speed and the extensometer gauge length (10 mm). If the gauge length was the same as the length of the reduced cross-section, a localised or uniform failure process would result in the same regression equation.

A similar approach can be used to examine the results for antler (equation 4.008). However, in this case the load on the machine increases in the post-knee region. Thus the assumption of a rigid machine is not as justifiable. This may account for the apparent compliant length being longer than the reduced cross-section of the specimen. Visual examination of the fracture surfaces produced during a tensile test (of both materials), shows no evidence of a reduced cross-section in the region of the failure (as may be observed in a metal that has yielded). This provides no evidence for a localised failure process, (akin to localised necking in plastically deformed materials). Evidence that the increase in compliance is indeed due to a widespread failure process, especially in antler, is provided in chapter 8.

A summary of the values of measured strain rate for both materials at the various cross-head speeds used is given in table 4.006. I have provided an approximate value of

the natural logarithm of the cross-head speed as this is the value used in the plots and many of the regression equations that follow.

Cross-head speed, $\dot{x}$, m s^{-1}	Mean value of measured strain rate in the initial region, $\dot{\varepsilon}_i$		Mean value of measured strain rate in the post knee region, $\dot{\varepsilon}_{pk}$	
	Antler	Bovine bone	Antler	Bovine bone
8.33×10^{-7} $\ln(\dot{x}) = -14.0$	0.00002	0.00001	0.00004	0.00004
8.33×10^{-6} $\ln(\dot{x}) = -11.7$	0.00024	0.00014	0.00050	0.00059
8.33×10^{-5} $\ln(\dot{x}) = -9.39$	0.00281	0.00142	0.00496	0.00531
8.33×10^{-4} $\ln(\dot{x}) = -7.09$	0.02522	0.01156	0.04978	0.04954

Table 4.006

The relationship of strain rate measured in the initial and post knee regions of the tensile loading curve to cross-head speed used for the test

4.2.6.4. METHOD USED FOR THE PRESENTATION OF THE EFFECT OF DIFFERENT CROSS-HEAD SPEEDS ON VARIOUS MECHANICAL QUANTITIES

In the previous sections I have highlighted the problems associated with the use of an open loop test machine to study rate-dependent mechanical quantities. I will now consider the results that I have obtained from such a machine. These results will be presented in the following way. First a plot of the data will be presented. (More information on the data sets and how they may be obtained can be found in appendix 4.) As well as the data points, each plot contains lines that link the mean and median values for both materials at each cross-head speed. An example of such a plot, with a full key, is given in figure 4.009. All subsequent plots in this chapter use the same symbols unless otherwise stated, but do not contain a full key. The data were analysed by least-squares linear regression, using Minitab (release 7) a statistical computer package. The R^2 values quoted have been adjusted for the degrees of freedom. The variable under consideration has been regressed against the natural logarithm of the cross-head speed, $\ln(\dot{x})$ (expressed in meters per second). Then a second variable, material stiffness measured in three-point-bending, E_b, was added. The logic behind this was that such a quantity, measured under standard conditions (described above), would have some normalising effect. This was envisaged as removing some of the scatter due to the material's variability. The two regressions were then repeated in logarithmic form. Other forms of regression equations,

suggested by the equations in the two preceding chapters, have also been used. Perhaps the most notable of these is the inclusion of the material stiffness measured during the initial state of the tensile test, E_t. All the regressions were repeated with the addition of another variable that simply indicated if the specimen was nominally 4 or 5 mm wide. The R^2 values of these repeat regressions are presented in parenthesis below that of the other regressions. All the regressions were repeated using two other measures of testing rate, the initial measured strain rate and the cross-head speed divided by the specimen gauge length, no noticeable improvement in explanatory power was generally observed, the values being slightly higher in one equation but then lower in another (the regression equations are not given in this thesis). This result is not unexpected as it has already been shown that the logarithms of the measured strain rate and the cross-head speed are very closely related by way of an almost linear equation.

To reduce the disruption of the text caused by the inclusion of figures and tables, the relationships are only shown graphically here. This representation has also been limited to graphs of the main two quantities studied. The tables of the associated regression equations are presented in appendix 9. To avoid excessive repetition I will assume that the reader has ready access to these tables. I apologise for any frustration this arrangement causes the reader. A summary of the results from these tests is given in tabular form (table 4.007) in section 4.2.7. Within that section I also examine the overall impression gained from the information provided from the examination of the individual quantities. Based on this impression I propose a mechanical analogue to describe the rate dependence of the tensile behaviour of bovine bone and antler.

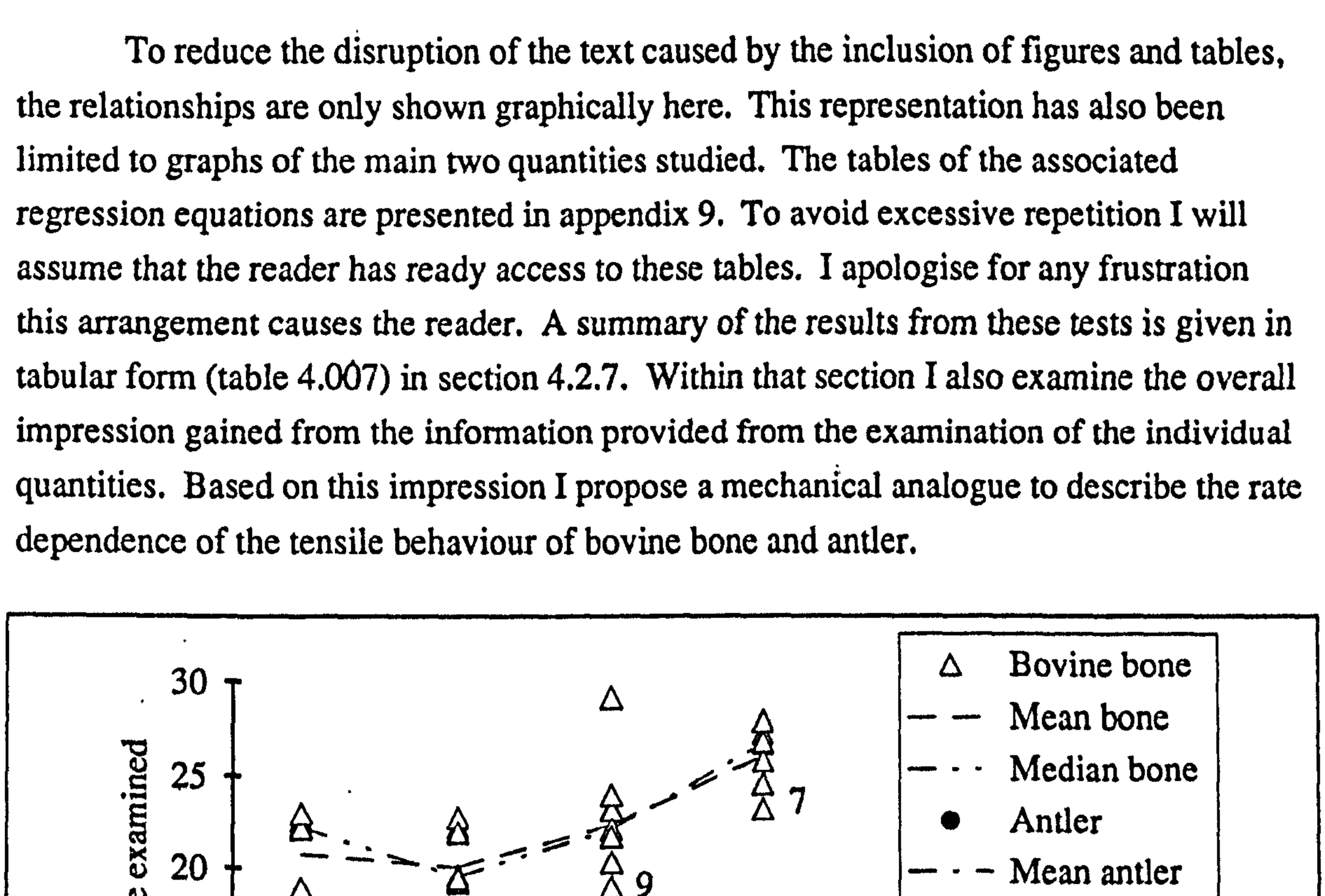

Figure 4.009

Diagram showing the symbols that are used in subsequent graphs

4.2.6.5. RESULTS: THE EFFECT OF CROSS-HEAD SPEED ON MATERIAL STIFFNESS

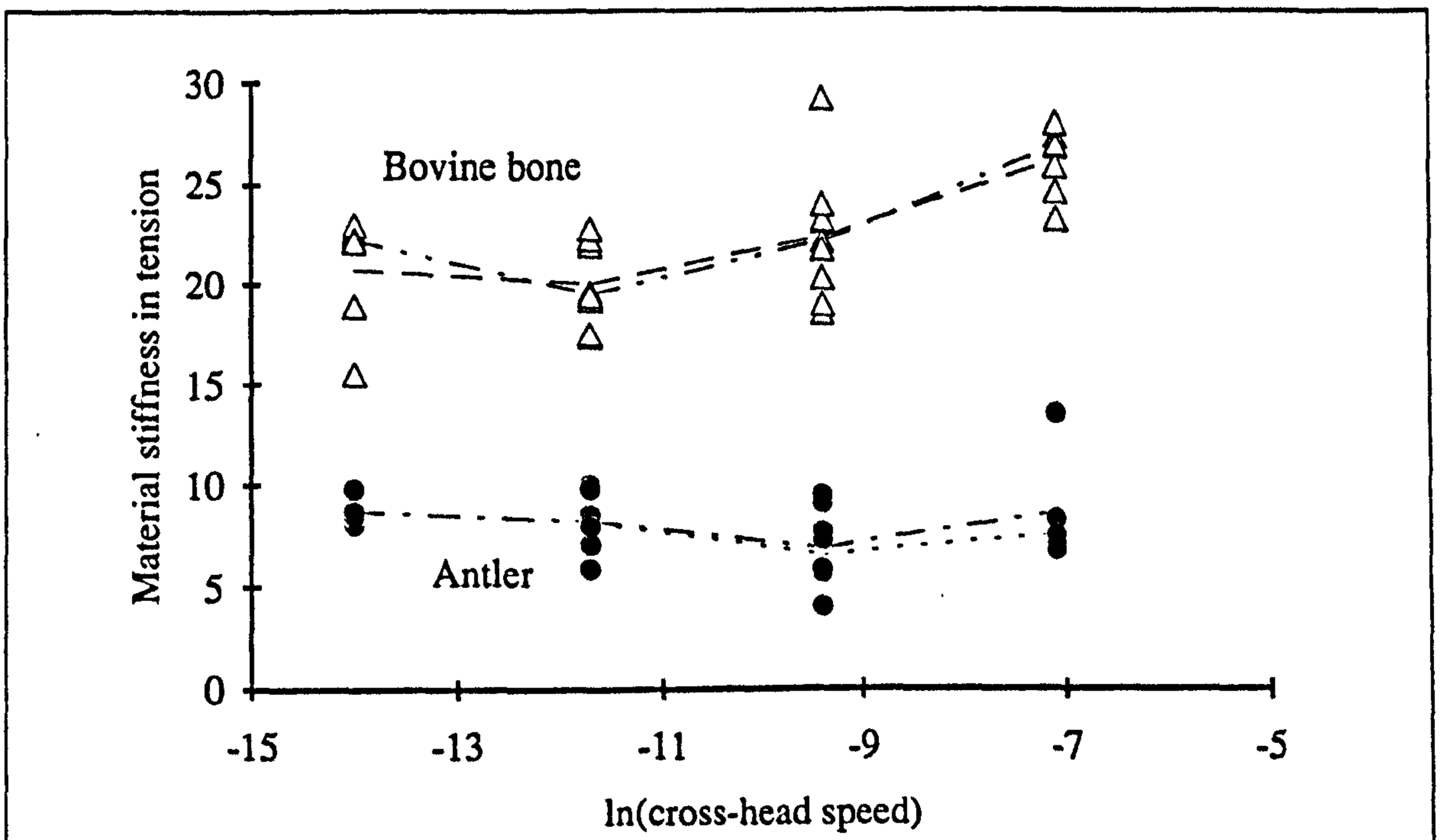

Units:

E_t Material stiffness in tension, GPa

$\dot{x}$ Cross-head speed, m s^{-1}

Comments:

For full key see figure 4.009

Figure 4.010

The material stiffness and cross-head speed for specimens of bovine bone and red antler

Table A9.001 of appendix 9 contains the regression equations of the data shown in figure 4.010. These regression equations show that the material stiffness measured in tension, E_t, has a lower dependence (indicated by the Student's t values) on the cross-head speed than it has on the material's bending stiffness, E_b (measured under standard conditions). (See equations *b* and *d* for antler and *f* and *h* for bovine bone in table A9.001.)

In the logarithmic equation that relates E_t to $\dot{x}$ and E_b for the antler data, the effect of cross-head speed is non-significant (*d* table A9.001). However, in the same regression equation, the material stiffness in bending is a very highly significant explanatory variable. Minitab quotes the *p* values associated with the cross-head speed and the bending stiffness variables as 0.784 and 0.000 respectively.[10] Equations *a* and *c*

[10]The *p* values quoted by Minitab as 0.000 will be given as < 0.001. To describe the level of significance of a variable or constant I use: *very highly significant* ($p \leq 0.001$), *highly*

show that an increase in cross-head speed is related to a (non-significant) decrease in predicted material stiffness is opposite to that expected for a visco-elastic material. When the material stiffness in bending is used as another explanatory variable (equation *b* and *d* of table A9.001), the relationship of material stiffness to cross-head speed is more like that expected for a viscoelastic material, but it is still non-significant.

The dependence of the measured stiffness of bovine bone on cross-head speed is greater than it is for antler. This is clearly shown by the coefficients of the rate term in equations *b* and *f* of table A9.001; that for bone is approximately ten times larger than that of antler. Thus indicating a similar change in testing rate will have an effect on bovine bone that is ten times the effect exhibited by antler. The results also show that the statistical significance of the rate term as a predictor of material stiffness is weaker in the case of antler. This may be shown by comparing the significance of this term in equation *d* (antler) with that in equation *h* (bovine bone). The values for the former equation are given in the preceding paragraph. In the same order as those given in the previous paragraph for equation *d* the *p* values of equation *h* are 0.001 and <0.001. Thus in regression *h* the cross-head speed is shown to be a very highly significant explanatory variable of bovine bone's material stiffness, whereas it is non-significant for antler.

The observation that the testing rate significantly affects the stiffness of bovine bone but not that of antler mirrors those reviewed in the previous chapters. For example see table 3.002 for Currey's (1975) data and table 3.003 from Currey (1989). The various coefficients (and exponents) can be compared with those obtained from published data. For example, the value of 0.0365 in equation *g* can be compared with that of 0.0285 obtained from Currey's data (Currey, 1975) re-analysed in section 3.2.2 (equation *k* table 3.002). Similarly the value of 0.0036 in equation *d* can be compared to his value of 0.015 (Currey 1989). The last comparison should be treated with caution as in both cases the variable is non-significant. Also these comparisons are not direct ones due to differences in the other explanatory variables used, and dissimilar environmental and test conditions.

The main conclusion to be drawn from the statistical analysis of the data presented in this section is that the effect of cross-head speed on material stiffness measured in these tests is small and statistically non-significant in the case of antler. However, in each of the equations for the bovine bone data the cross-head speed was found to be very highly significant, (although still of less significance than the bending stiffnesses in equations *f* and *h)*.

---

significant ($p \leq 0.01$), *significant* ($p \leq 0.05$) and *non-significant* ($p > 0.05$). (See appendix 12.)

I have already stated that the observed effect of cross-head speed on material stiffness may be less than the true effect of strain rate due to the machine-specimen interaction. Although the specimen-machine interaction has a marked effect at a particular cross-head speed (as shown in figure 4.005), it is unlikely to have such a profound effect over a range of four magnitudes of rate as used here. The effect of the specimen-machine interaction can be clouded by the use of two sizes of specimen. This is because a 4 mm wide specimen with a high material stiffness can have a lower specimen stiffness than a 5 mm wide specimen made of a more compliant material. Thus using two sizes of specimens will, to a limited extent, decouple the relationship of actual strain rate to the material stiffness. This decoupling is shown in figure 4.005 and 4.006, where the measured strain rate is shown to be less dependent on the material stiffness than it is on the specimen stiffness. However, in both cases the relationship was very highly significant at each cross-head speed. Assessing this evidence, I conclude that the difference in the effect of cross-head speed on the material stiffness measured in tension of bovine bone and antler, reported here is a true account of this relationship and not an artefact of the testing technique.

There are a number of possible causes for the time dependence of the material stiffness of bone. In the next few pages I will discuss some of these. First, I examine the application of a visco-elastic equation. Such an equation suggests that the initial region is not linear but curved. However, a curved initial region does not imply visco-elasticity. Thus I examine the possibility that the observed curvature could be an artefact of the definition of stress and strain used in this study. However, if the curvature could be attributed to such definitions the rate dependence can not be similarly attributed. Finally I examine the possibility that the rate dependence and the curvature of the initial region in a tensile test of bovine bone could be due to the accumulation of damage.

In the previous chapters the use of a visco-elastic theory to model the rate dependence of bone's stiffness was discussed. Particular attention was given to the three element solid. The relationship of stress to strain during a constant strain rate test was given above and is repeated here

$$\sigma(t) = \varepsilon(t)\, q_0 - \dot{\varepsilon}\,(q_0\, p_1 - q_1)\,(1 - e^{-t/p_1}) \qquad (4.010)$$

In section (3.2.1) a paper by Tennyson *et al.* (1972) was reviewed. These workers suggested that their value of p_1 was small enough to permit them to assume $p_1 = 0$. (They used compression tests at very high strain rates.) This implies that a simplified form of equation (4.010) could be used as a first approximation

$$\sigma(t) = \varepsilon(t)\, q_0 - \dot{\varepsilon}\,(-\, q_1) \qquad (4.011)$$

This equation is that of a Kelvin solid. However, equation (4.011) predicts that the relationship of stress to strain is a linear one, with an offset. The size of this offset is dependent on the strain rate. Clearly the situation implied by this equation at the instant after t = 0 is unrealistic. Thus the full equation must be used. This equation can be re-expressed as

$$\sigma = A\,\varepsilon - B\,\dot{\varepsilon}\left(1 - e^{-t/p_1}\right) \tag{4.012}$$

If it assumed that the strain rate for each specimen tested at one cross-head speed is the same then this may be re-expressed as

$$\sigma = A\,\varepsilon - C\left(1 - e^{-t/p_1}\right) \tag{4.013}$$

Where C will depend on cross-head speed and A is the slope that forms a tangent with the stress strain curve at its origin. The data collection system used provides time data as well as stress and strain data. This permitted the data from the tests on bovine bone specimens to be fitted to equation 4.013. To assess the accuracy of the fit of the data to the equation the process was conducted using Minitab. (This was seen as a speculative study that would be followed by other methods of curve fitting if these appeared to be worthwhile.) The equation was fitted to a range of data: from the start of the loading period up to 75% of the knee stress. A range of values of p_1 was used so that the quantity in parenthesis could be calculated for each set of stress and strain points. For example

$$\omega = \left(1 - e^{-t/p_1}\right) \tag{4.014}$$

The value of p_1 under consideration is substituted into the equation together with the appropriate values of time. The values of time used are those for which a stress and strain value have been recorded. (Zero time coincides with the start of loading.) This produces a set of values for ω that correspond with the set of stress and strain values obtained at the same time. Linear regression can now be used to find the best fit equation to

$$\sigma = A\,\varepsilon - C\,\omega \tag{4.015}$$

Various values of p_1 were used; my idea was to use an iterative process to find an estimate of the true value of p_1 and C. I assumed these values would correspond to the highest value of R^2 obtained for the range of p_1 values used. I found this form of equation could be used to improve the R^2 value (for the data sets that were tested) from that of a simple linear relationship of stress and strain (C = 0). However, the determination of the values of p_1 and C was not possible. This was because Minitab quoted R^2 of 100% for a large range of p_1 values. As p_1 was changed there was a

corresponding change in C and the significance of each variable in the regression changed. (With hindsight an examination of the significance of the variables may have been a more fruitful approach.) No conclusions about the fit of the stress-strain data to the three element solid can therefore be made. However, the improvement in R^2 shows that the initial region of the tensile stress-strain relationship of bovine femoral bone is slightly curved. If the material is truly visco-elastic, this curvature will start on the first application of the load and no part of the initial region of the loading curve will be truly straight.[11]

A possible source of curvature in the stress-strain plots is the use of nominal stress and nominal strain values, in the place of true stress and true strain. (These quantities are defined above.) It is reasonable to assume that as the specimen gets longer it also gets narrower. (A number of values of Poisson's ratio, for different bones, are quoted by Duck (1990). Most of these values are in the region of 0.2 to 0.4.) Thus the true stress is greater than the nominal stress. So using nominal stress values induces a bend in the stress-strain curve: producing a slight ⌜ shape. (This is especially noticeable in the yield and post-yield regions of ductile metals.) Similarly the effects of nominal strain (in place of true strain) can be demonstrated as producing a slight ⌜ shaped curve.

$$\varepsilon_{nom} = \frac{\Delta L}{L} \tag{4.016}$$

and

$$\varepsilon_{true} = \ln\left(\frac{L}{L_0}\right) = \ln\left(\frac{L_0 + \Delta L}{L_0}\right) = \ln(1 + \varepsilon_{nom}) \tag{4.017}$$

thus

$$e^{\varepsilon_{true}} - 1 = \varepsilon_{nom} \tag{4.018}$$

Therefore if the true strain is 0.001 the nominal strain is 0.0010005, and if the true strain is 0.01 the nominal strain is 0.01005. Using nominal stress and strain in place of true stress and strain could be responsible for some of the curvature observed in the initial region of the stress-strain curve. The curvature that results from the use of nominal stress and strain will depend on the ratio of those quantities and the properties of the specimen. The above calculation shows that there is only a 0.5% error between the true and nominal strain in a strain of 0.01 (which is greater than that associated with the knee region of the curve). Therefore, it is unlikely that the difference between the true and nominal stress

---

[11]The lack of linearity in the pre-knee region has been reported in a number of papers, for example Bonfield and Li (1967), Bonfield and O'Connor (1978) and Bonfield and Datta (1974). These workers report the existence of a *microscopic yield stress*. This quantity is defined as 'the stress to produce a non-elastic strain of 2×10^{-6}'. I consider that this measure of yield strain has no more validity than the 2% proof-stress.

and strain values can account for the observed curvature in the initial region of the stress-strain response.

There is another possible cause of the curve in the initial section of the loading curve: damage. A high power relationship between the time-to-rupture and normalised stress during a creep test of human bone has been observed by Caler and Carter (1989). It may be that this observation can be used as a basis of an explanation for the initial curvature in, and strain rate dependence of, the initial stress-strain relationship of bone. First, I have assumed that there is no lower threshold to this behaviour. This implies that as soon as the stress increases from zero damage starts to accumulate. The effect of this damage would be imperceptible at first. However, as the stress approached the value the knee stress the damage would be detectable. Damage can be expressed as a reduction in material stiffness, and thus alternatively as a greater strain under the same load (equation 2.114). Therefore if damage occurs, the additional damage-induced strain would result in a curved stress-strain response. As damage is time-dependent the curvature of the line (and consequently the measured stiffness) depends on the rate at which the bone was stretched. Thus the damage concept may model and explain a feature of bone previously modelled by visco-elasticity.

To examine the validity of the damage explanation of the non-linearity and rate dependence of the initial region of the tensile stress-strain curve, I have assumed that such an approach can be based on the damage equations of Caler and Carter. By taking one of the intermediate stages between equations 3.035 and 3.036 (used to derive the failure stress of bone in a constant stress rate test by a method akin to equations 3.014 to 3.017) and representing the damage as a variable, rather than the value of unity assumed at failure, the following equation can be derived

$$\frac{1}{B_N E_N^{\,P} (P + 1)} \frac{\sigma^{P+1}}{\dot{\sigma}} = D \qquad (4.019)$$

Using equation 3.136 this can be re-expressed as

$$\frac{1}{B_N E_N^{\,P}} \frac{\sigma^{P+1}}{\dot{\sigma}} = 1 - \frac{E_M}{E_U} \qquad (4.020)$$

If it is assumed that there is no residual strain, the measured unloading stiffness is the ratio of the stress to the strain. The value of the undamaged material stiffness is a constant. Thus

$$1 - \frac{E_M}{E_U} = 1 - \frac{\sigma}{E_U \varepsilon} \qquad (4.021)$$

So equation 4.020 can be re-expressed as

$$\left(\frac{E_U}{\sigma} - \frac{E_U}{B_N E_N{}^P (P+1)} \frac{\sigma^P}{\dot{\sigma}}\right) = \frac{1}{\varepsilon} \qquad (4.022)$$

This equation is clearly of a form that can model a curved stress-strain response: a linear relationship with a modification for damage. An increase in the stress rate will result in decrease in the size of this modification. (The modification is negative due to the reciprocal expression of strain.) By use of a further assumption, that the undamaged stiffness and the normalising stiffness are the same, equation 4.022 can be simplified to give

$$\left(\frac{E_N}{\sigma} - \frac{\sigma^P}{B_N E_N{}^{P-1} (P+1) \dot{\sigma}}\right) = \frac{1}{\varepsilon} \qquad (4.023)$$

This equation can be converted to one based on strain rate rather than stress rate by using the relationship $\dot{\sigma} = E_N \dot{\varepsilon}$. Some of the drawbacks of such an equation have already been mentioned (section 3.3.2). However, this relationship permits equation 4.023 to be expressed as

$$\left(\frac{E_N}{\sigma} - \frac{\sigma^P}{B_N E_N{}^P (P+1) \dot{\varepsilon}}\right) = \frac{1}{\varepsilon} \qquad (4.024)$$

By using the data from Caler and Carter (1989) for human bone (section 3.3.2) this can be expressed as

$$\left(\frac{E_N}{\sigma} - \frac{\sigma^{15.81}}{2.437\times10^{-35} E_N{}^{15.81} \dot{\varepsilon}}\right) = \frac{1}{\varepsilon} \qquad (4.025)$$

Without I hope falling in the trap of erecting what Wintringham (1740) called 'some pompous plausible Hypothesis', I have used equation 4.025 to determine a number of stress strain curves at different strain rates. For this I have assumed a value of 25 GPa for the material stiffness, E_N. Due to the formulation of the equation the value that is substituted into it is the stiffness in MPa. The curves I obtained by this substitution are presented in figure 4.011. The length of the axes and strain rates have been chosen so that the plot can be compared with those obtained experimentally by Crowninshield and Pope (1974) from test on bovine bone reproduced in figure 3.001. It will be remembered that their values of strain were considered to be an over estimate, and that the basis of the predicted results here is data from human bone published by Caler and Carter (1989) along with a number of assumptions. When these factors are taken into account, visual comparison shows the curves to be very similar. However, unlike Crowninshield and Pope's curves (and my results), the predicted ones shown in figure 4.011 display no obvious variation in the initial slopes with testing rate. The plots also highlight a problematical aspect of the damage approach that was noted in chapter 2. This aspect is that the assumption that the numerical value of damage changes from 0 to 1 results in the

material having an infinite length (and thus strain) at failure. This aspect of the model is returned to in section 4.2.6.9.

From examination of figure 4.011 it would appear that this extension of the NTDF model predicts little if any reduction in stiffness in the initial region. At the rates examined no difference is visible until a stress of 100 MPa is reached. This can be examined by repeating the substitution of this stress and the stiffness of 25000 MPa into equation 4.025.

$$\left(\frac{25000}{100} - \frac{(100)^{15.81}}{2.437\times10^{-35}\ (25000)^{15.81}\ \dot{\varepsilon}}\right) = \frac{1}{\varepsilon} \qquad (4.026)$$

Equation 4.026 can be simplified to give

$$\left(\frac{25000}{100} - \frac{1}{2.437\times10^{-35}\ (250)^{15.81}\ \dot{\varepsilon}}\right) = \frac{1}{\varepsilon} \qquad (4.027)$$

which is approximately the same as

$$\left(250 - \frac{1}{1987\ \dot{\varepsilon}}\right) = \frac{1}{\varepsilon} \qquad (4.028)$$

Manipulation of equation 4.028 shows that a 1% increase in the strain at 100 MPa, over that predicted by the material stiffness of 25 GPa, will only be achieved at strain rates of less than 0.0002 s^{-1}.[12] Therefore, I suggest that the accumulation of damage at different strain rates as modelled here will not noticeably affect the pre-knee material stiffness in the tests on bovine bone examined here. This is due to the relative sizes of P and B_N in the model. The lack of evidence supplied by this model in support of the idea that damage accumulation is responsible for the rate dependence of material stiffness, should not be taken as evidence to reject such a suggestion. It could be that the simple model used here is incapable of accurately describing the development of damage at low stresses. However, attributing the rate dependence of the stiffness to a visco-elastic type of effect still appears to be the most plausible explanation. Visco-elasticity could also model the loops formed during the unloading and reloading of specimens of bone and antler. This phenomenon has been reported in both the pre and post-knee behaviour. An example of the latter case is shown in figure 1.011. This is clearly an important aspect of the material's behaviour, but due to the changes in material stiffness, one that could be considerably affected by the machine-specimen interaction (examined in appendix 7).[13]

---

[12]Table 4.006 shows that this value of strain rate falls between that obtained at the two lowest cross-head speeds used in this study. Figure 4.012 shows that at these rates 100 MPa is similar to the values obtained for the knee stress.

[13]In this section it has been assumed that the materials unload linearly to their original length. See section 7.4.3.1 and 7.7.1.1 for some details of the real behaviour.

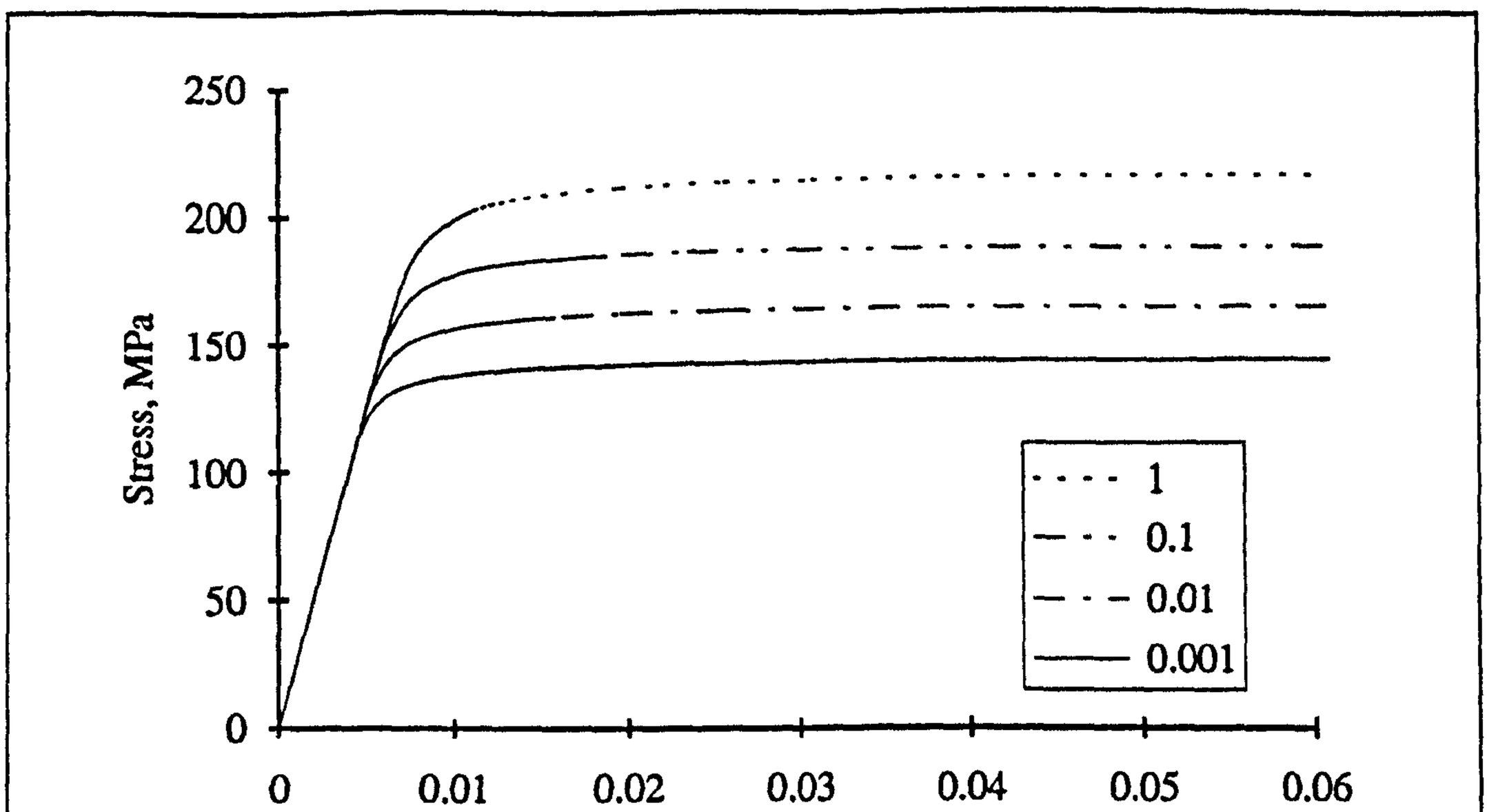

Values obtained from an equation based on my extension of Caler and Carter's (1989) NTDF model and their data for human bone assuming a stiffness of 25 GPa.

Figure 4.011

The predicted stress-strain response of bone at four strain rates

An examination of the regression equations of material stiffness and cross-head speed (table A9.001) reveals another result relevant to the TDF and NTDF models and my treatment of them. The equation with the highest explanatory power for each material is that which has the form

$$\ln(E_t) = A + B\ln(\dot{x}) + C\ln(E_b) \qquad (4.029)$$

which in the same as

$$E_t = A\,\dot{x}^B\,E_b^C \qquad (4.030)$$

This is an important result because when the TDF model was converted from one that predicted failure under conditions of constant stress rate, to one that predicts failure under conditions of constant strain rate Carter and Caler used an equation of the form $E_t = A.\dot{x}^B$ ($E = C\,\dot{\varepsilon}^m$ equation 3.025). If they had used an equation of the form of 4.030, it would have resulted in equation 3.029 also containing a material stiffness term. Thus it would have a similar form to the comparable equation for the NTDF model. Clearly the adoption of the equation containing the normalising material stiffness would also effect the comparable conversion of the NTDF model. I will not pursue this

particular point any further here, but would like to suggest that it could be investigated in some future project.

An interesting result is obtained from the regression analysis where specimen width was added as an additional variable. This variable improves the explanatory power of each of the relationships for the equations relating to antler. However, size has no apparent effect on the explanatory power for, and thus properties of, the bone specimens. When the effect of specimen size on strain rate, and in turn strain rate on stiffness is considered, this inconsistency is unexpected. I comment on the effect of the specimen size on the various quantities examined in these tests in section 4.2.6.13.

The main conclusion to be drawn from the tensile material stiffness results is that the range of cross-head speeds used here had no significant effect on the material stiffness of the antler specimens. On the other hand, the effect of cross-head speed on the material stiffness of bovine femoral bone is very highly significant. The main determining factor of the material's tensile stiffness is some structural or physical characteristic that also expresses itself when the material is measured under standard conditions. Examination of the initial (pre-knee) stress-strain relationship suggests that of the models proposed thus far, a visco-elastic rather than a damage approach gives the more plausible explanation of the observed variation in stiffness with rate for the bovine bone. I consider that a more definite statement to this effect would require more work, both experimental and analytical. Perhaps this would be done over a wider range of rates using a closed-loop machine, with the inclusion of some cyclic loading in the pre-knee region.

4.2.6.6. RESULTS: THE EFFECT OF CROSS-HEAD SPEED ON KNEE STRESS

Comparison of figures 4.012 and 4.010 shows that the relationship of knee stress to cross-head speed is more apparent than that for material stiffness to cross-head speed examined above. This observation is supported by the statistical analysis presented in table A9.002. The cross-head speed is a very highly significant variable in all the equations shown in table A9.002, except equation *c* where $p = 0.003$ (still highly significant). As in the case of tensile stiffness, the material stiffness measured in bending is an important predictor of the knee stress for both materials. The inclusion of material stiffness in the regression equations approximately halves the unexplained variability (equations *a* and *b*, *c* and *d*, *e* and *f*, *g* and *h*). However, in this case the significance of the cross-head speed and the normalising material stiffness are about equal.

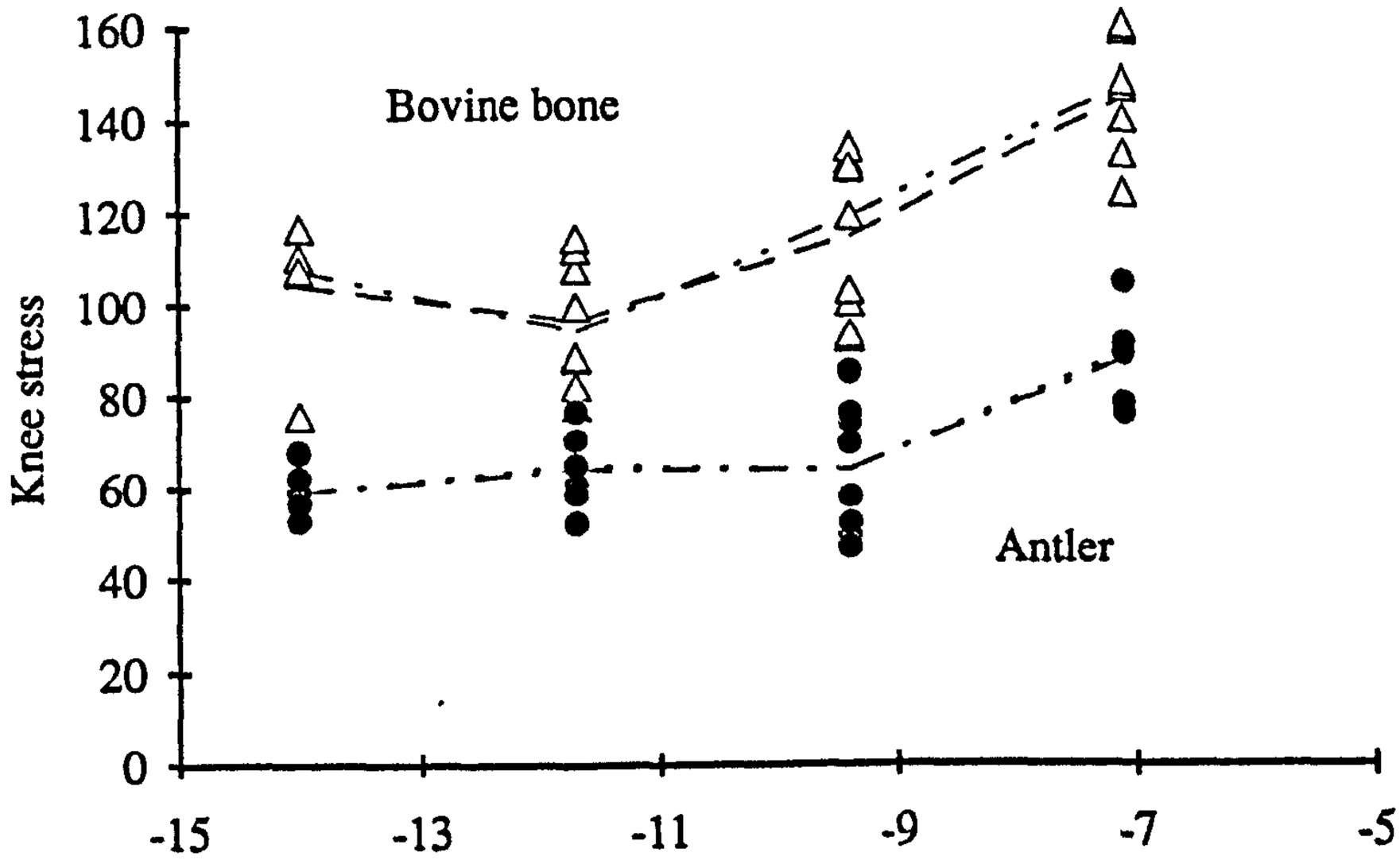

Units:

σ_K Knee stress, MPa

$\dot{x}$ Cross-head speed, m s^{-1}

Comments:

For full key see figure 4.009

Figure 4.012

The relationship of the knee stress to the cross-head speed for bovine bone and antler

The exponent of the cross-head speed obtained by analysis of the data from the antler specimens can be compared to the exponent of strain rate obtained by Currey (1989). Here I obtained a value of 0.0623, while Currey obtained a value of 0.063. Likewise the bovine results can be compared with his 1975 results (table 3.002) the most directly comparable are 0.0527 from equation *g* above and 0.0867 for his data. The prediction made by Carter and Caler (1983) (using the TDF model) of the exponent of strain rate in an equation modelling failure stress of human bone was 0.055, my extension of their NTDF model (equation 3.045) using their data gave a value of 0.059. There is only a slight difference between the failure stress and knee stress of in this model, and the same is true experimentally, for normal bone. Thus a general comparison can be drawn between these two measures of stress. Such a comparison shows my results to be in broad agreement with those previously obtained or implied by other workers. However, it should be pointed out that the value of the exponent of rate in my regression equation changes between the case where the cross-head speed is the only variable and that where the bending stiffness is also considered. This suggests at least two possibilities. First, there was an uneven distribution of specimen stiffness in the test grouping. Regression analysis of the material stiffness in bending and the logarithm of the cross-head speed for

the bovine specimens demonstrated a non-significant relationship, $p = 0.136$. Second, it could be the effect of material stiffness on the strain-rate, resulting from the machine-specimen interaction. If the second case were true the arguments presented above would suggest that the inclusion of a *size* variable would account for more of the unexplained variation. This is not shown to be the case in the regressions presented in table A9.002.

When I analysed Currey's 1975 data for bovine bone (section 3.2.1) I used the material stiffness in tension as an additional variable. I also used this quantity as a variable in an adaptation of the damage models produced by Carter and Caler equations 3.032 and 3.045. Equations 3.032 and 3.045 were formulated on the basis that the failure stress, was the maximum stress the specimen could sustain. However, these equations are also based on the idea of a constant stress (and in the initial region strain) rate. I have shown that for my tests the strain rate changes as the specimen enters the knee region. The initially constant strain rate, and the similarity between the knee and ultimate stresses, supports the approach used by Currey (1989)[14] of analysing the value of the knee stress using the same model. Figure 4.011 shows that the NTDF model would predict the occurrence of the knee stress and ultimate stress at very similar levels for human bone (the constants used in that case), similar to the experimentally observed behaviour of bovine bone.[15] Thus in table A9.003 I present the analysis of my results using the stiffness measured during the test as an additional variable. In the previous section it was shown that the material stiffness of antler did not alter greatly with strain rate, while the variation of the stiffness of the bovine bone was very highly significant (table A9.001). Thus the material stiffness in tension is not an independent variable. Comparing equation *c* of table A9.003, obtained for bovine bone with that from Currey's data (*f* table 3.002) shows that the exponent of material stiffness is similar (0.968 and 0.920), but that for cross-head speed or strain rate is different (0.0173 and 0.0605). This difference in exponents of the testing rate variable may be explained by a number of factors. The main candidate is the environmental conditions. The dependence of some of the time-dependent properties of bone on temperature was reported in section 1.4.4.2. Another factor could be the differences in specimen geometry. Different specimen shapes and sizes would effect the machine-specimen interaction. These geometrical effects are not quantified here, but I consider them to be relatively small. Despite these differences, in each case the exponent of material stiffness is almost one. This value fits that predicted by my extension of the NTDF model (equation 3.045) very well.

Equation 3.045 also predicts that the exponent of the strain rate would be $1/(P + 1)$. My data implies a value of $P = 56.8$ compared to Caler and Carter's value of

---

[14]Reported in chapter 3.

[15]This statement is more justifiable at lower testing rates. In some tests conducted at higher rates the post-knee region has a slight upward slope.

15.81. However, Currey's data gives a value of 15.5. These comparisons are a little tenuous; due to the different test conditions, materials, definition of the stress examined and so on. I can find no reasonable explanation of why my data and that of Currey (1975) are so divergent on this value but in agreement on the coefficient of stiffness. Part of the explanation could be the difference in environmental conditions of these tests. In the derivation of equation 3.045, P was the negative exponent of stress in the relationship of creep stress and time-to-rupture (equation 3.035). It has been reported by Currey (1965) and by Rimnac *et al.* (1993) that bone creeps at a higher rate at more elevated temperatures. It is reasonable to assume that it will also fail more quickly, thus P will be larger. It may therefore be expected that my tests conducted at approximately body temperature would produce a larger P value than those of Currey conduced at laboratory temperature. However, I do not consider that such a change in temperature could account for the difference between 56.8 and 15.5 (especially considering that the antler results show the opposite trend). Similar, but perhaps more tenuous, comparisons can be made for bovine ulna and antler using the values obtained from creep tests by Mauch *et al.* (1992). In that paper the value obtained for the P (of equation 3.033) was 16.7 for bovine ulna, 26.9 for specimens from the base of a red deer antler and 21.0 for those from the antler tip. For antler my data implies a value of P = 17.0. In this case, as with the bovine bone tests, my experiments were conducted at a higher temperature. However, here my value of P is considerably lower.

I have shown that the relative size of the values of P of the extended NTDF model, for bone and antler, from published data on creep tests and those derived from the comparison of the tensile data with a model based on creep data are incompatible. This may indicate the application of the model to the results obtained from antler is not be justified. This could be due to the considerable difference in the knee and ultimate stresses in antler (whereas they are similar in normal bone).

It is noteworthy that the material stiffness in bending and in tension used together improve the predictive power of the relationship further. In my derivation of equation 3.045, from equation 3.044, they were assumed to be equal. Thus comparison of equation *d* (A9.003) with equation 3.044 may be more justifiable. However, the relative size of the exponents is not that predicted by the model. This indicates that the agreement of the results from bovine bone with an equation of the form of 3.045 maybe partly fortuitous.

In section 3.2.4 I introduced Sedlin's rheological model for bone. In that section I reported that his model implied that the knee stress of bone would increase with an increase in the applied strain rate. I will now examine how the experimental results fit the predicted form of relationship. Using equations 2.011 and 2.012 the stress on the first

Saint-Venant body can be shown to be equal to the applied stress with that experienced by the dashpot subtracted.

$$\sigma_{St\,V} = \sigma_{applied} - \eta\,\dot{\varepsilon} \qquad (4.031)$$

Motion of the first Saint-Venant body is impeded until a certain stress is reached. I assume that the motion of this first body, represents the knee in the stress-strain curve of the real material. Thus equation 4.031 implies that the knee stress predicted by this, basically visco-elastic, model is linearly related to strain rate. If this was the case logging the values would produce a J or banana shaped curve, as exhibited slightly by figure 4.012. Thus these quantities have been re-analysed using un-logged data values for strain rate and the other variables. This analysis is presented in table A9.004. In some cases the totally non-logarithmic equations have a higher predictive power of the knee stress than those containing a logarithmic term. Equations *a* and *e* in table A9.004 have an R^2 value at least 12% greater than the equivalent equations containing the logarithmic form of cross-head speed (equations *a* and *e* table A9.002). The R^2 values increase for all the regression equations that can be directly compared (*a*, *b*, *e* and *f* of table A9.004). This increase is larger for the antler specimens than it is for the bone ones. However, similar analysis of Currey's data for 35 specimens of bovine femoral bone, showed a reduction in the R^2 value obtained using a non-logarithmic form of strain rate to approximately a third of that obtained when the logarithm of strain rate was used. The reason for the conflicting nature of these results is unknown. These results suggest that the dependence of knee stress on testing rate for antler specimens is described more accurately by a linear relationship and that for bovine bone specimens by an exponential relationship. This difference in the form of the relationship suggests a number of possibilities three of which are: first, the processes that result in the knee region are different in the two materials; second, if the processes are the same then their relationship to loading rate is different (These possibilities are discussed in more detail in chapter 9.); third, this observation is an artefact. Perhaps a more extensive study is required, using a greater range of testing rates.

In this section I have shown that the knee stress of both bovine femoral bone and red deer antler are significantly dependent on the cross-head speed at which the specimens are stretched. My quantitative results are slightly at odds with those in the literature, but the qualitative results are in agreement. The form of the relationship of knee stress to testing rate appears to be different for the two materials.

4.2.6.7. RESULTS: THE EFFECT OF CROSS-HEAD SPEED ON ULTIMATE STRESS

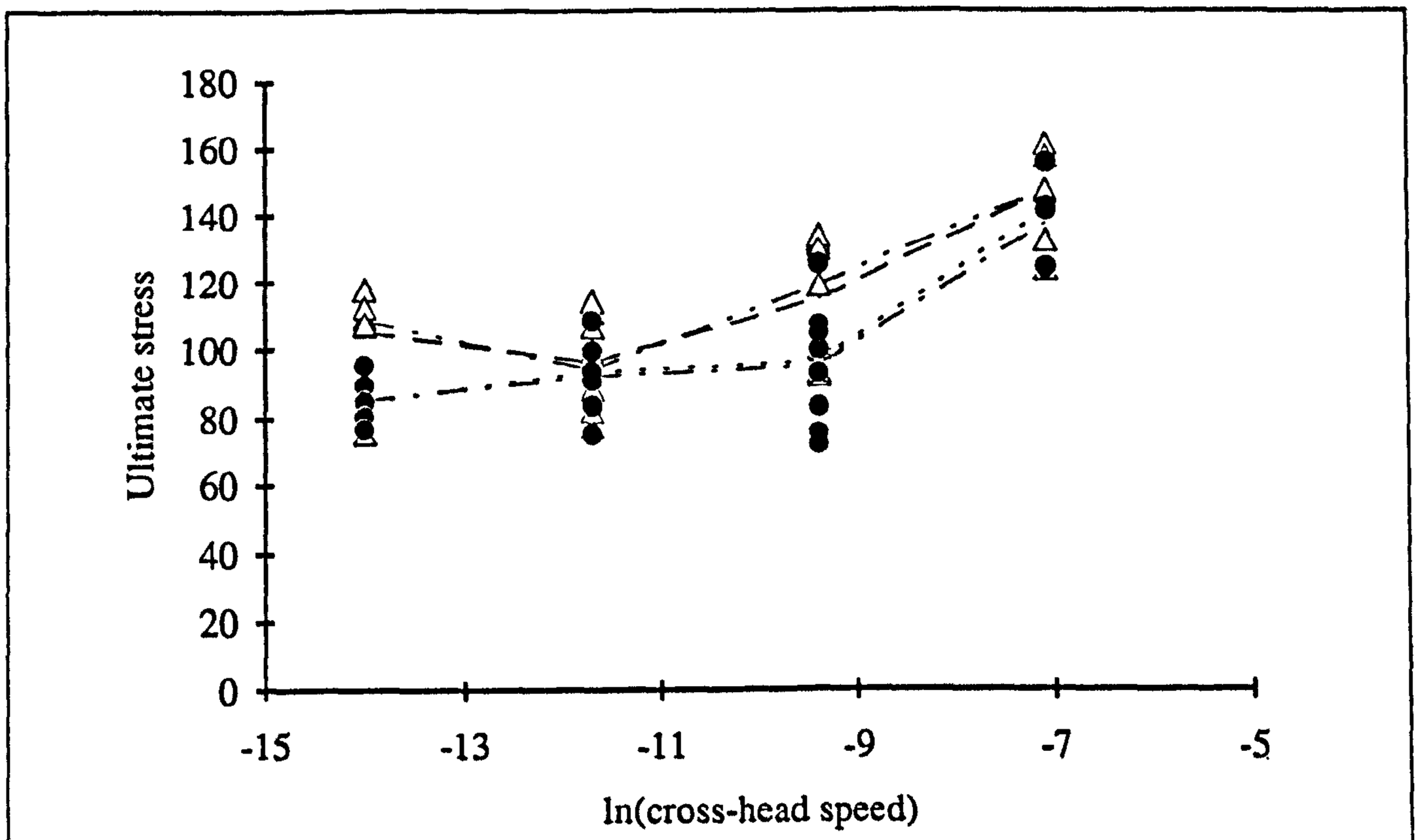

Units:

σ_{ult} Ultimate stress, MPa

$\dot{x}$ Cross-head speed, m s^{-1}

Comments:

For full key see figure 4.009

Figure 4.013

Relationship of the ultimate stress of bovine femoral bone and red deer antler to the cross-head speed of the test

The relationships between the ultimate stress and the cross-head speed of the tests conducted on bovine femoral bone and red deer antler are shown in figure 4.013. The tend is for the ultimate stress to increase at the higher rates. However, this is not a clear cut relationship, the median and mean value lines of both materials show that the trend is not uniform. This is also shown by the predictive power of the regression equations for both antler and bone when only the cross-head speed is used (see table A9.005 equations *a* and *e*). In both of these equations the R^2 values are less than 50%. As in the analysis of knee stress, the addition of the material stiffness (whether tensile or bending) as a variable reduces the unexplained variation by about half: increasing R^2 values to more than 70%. Despite the apparent non-linearity of the relationships shown in figure 4.013, the cross-head speed is a very highly significant predictor of the ultimate stress in all but two of the equations shown in table A9.005. The exceptions are equations *k* and *l* where the *p* values associated with the rate term is 0.090 (non-significant) and 0.008 (highly

significant) respectively. These two equations are for the bovine bone data and include the tensile material stiffness as an explanatory variable. The reduced significance of the rate term in these equations can be attributed to the dependence of E_t on the cross-head speed. It was shown above that for bone there is a significant relationship between the tensile material stiffness and the cross-head speed. On the other hand there is no evidence for such a rate-stiffness relationship in the antler data.

One feature of the data that is especially noticeable in figure 4.013 is that the separation between the ultimate stress of bone and that of antler is not as clear as that for the values of knee stress (figure 4.012). The greatest statistical difference between the ultimate stress of the materials is at the lowest cross-head speed used. One-way analysis of variance was conducted on the data for specimens tested at each cross-head speed, using the type of material as the test grouping. This gave the following results, presented in order of increasing speed: $p = 0.009$, 0.542, 0.036 and 0.274. This shows that the ultimate stress of bone and antler are significantly different at two of the four testing speeds. There is no statistical indication that they are different at the other two speeds. The examples of tensile loading curves given in figure 1.012 show that despite the difference in the shapes of these loading curves, or mechanical response, these materials have similar ultimate stresses. This could be interpreted as meaning that the differences between these materials, at a structural or chemical level, play no part in the final failure stress only in the path that is taken to reach it.[16]

Many of the comparisons and forms of analysis possible with these ultimate strength data are the same as those performed on the values of the knee stress. In every equation relating the ultimate stress to the cross-head speed, with or without other variables, the coefficient or exponent of the rate is higher than that in the corresponding equation for knee stress. (The associated t value is also higher.) However, the R^2 values of the equations do not show such a uniform change when the different stresses are analysed.

In the papers reviewed in the previous chapter relationships of ultimate stress to the rate of testing for a number of materials were given. Considering antler first, Currey (1989) obtained an exponent of 0.050 for reindeer antler (table 3.003). This value is similar to, but lower than, those I obtain in equations of compatible form (c, d, i and j of table A9.005) This may be due to higher temperature used in my study, which would result in a higher creep rate. This suggests that the time dependence of antler specimens

---

[16]A poor analogy is that of a modified dashpot. The modification is the addition of a rigid element that will fail on attaining certain value of stress. The viscosity of the dashpot will determine the mechanical response but not the failure stress. The modifying element determines the failure stress only.

may be greater at higher temperatures. However, such an explanation appears to be contradicted in the case of bovine femoral bone. The exponents are considerably lower in my study than those obtained from Currey's (1975) data (table 3.002).

The equations relating failure stress to the cross-head speed for the bovine specimens can be compared with those derived from the NTDF model. Equation *k* (table A9.005) is of the same form as the predicted equation 3.045, both are repeated below. First the predicted relationship

$$\ln(\sigma_{ult}) = \ln(E) + \frac{1}{P+1}\ln(B_N\,(p+1)) + \frac{1}{P+1}\ln(\dot{\varepsilon}) \qquad (4.032)$$

and then the experimental one, rearranged into the same order

$$\ln(\sigma_{ult}) = 1.00\,\ln(E_t) + 1.80 + 0.0175\,\ln(\dot{x}) \qquad (4.033)$$

Equation 4.032 (3.045) was derived from the NTDF model, and some assumptions. One assumption was that the material stiffness used in the normalisation of the relationship and that measured in tension could be equated. Similar remarks to those made in section 4.2.6.6 above can be applied to such a comparison. Clearly the agreement of the exponent of material stiffness in the model and in the regression equation fitted to the bovine bone experimental data is apparently exact. E_t is a very highly significant predictor of the ultimate stress. The reason for this level of significance could be that the stiffness measured during the test is accounting for some of the effect of cross-head speed.

Using the theoretical equation 4.032 and the regression equation 4.033 a value of P can be obtained. Equating the extreme right-hand terms of both equations results in a value of P = 56.14. This value is considerably greater than the value of P obtained from creep tests of human bone by Caler and Carter (P = 15.81) and from Currey's bovine bone data (P = 14.79). When this method is used to find a value of P for the antler specimens an answer of 13.95 is obtained. The disagreement between the values of P obtained from creep data and my tensile tests may be due to a number of causes: I have extended the model too far, comparisons between different environmental conditions may be invalid or the variable P may not be compared in these two situations due to assumptions made in the original model.

The comparison between the theoretical and experimentally determined exponent of stiffness for bovine bone shows them to be very similar. This raises the question why is this not the case for antler. The coefficient for this material is less than 0.5 (equation *i*, table A9.005). If the argument that the normalising stiffness and that measured in tension can not be equated is followed, and thus equation *j* is used in a comparison with equation

3.044, the value of P obtained is 1.03. The disparity between the various values of P obtained here by various routes and those in the literature, could be due to a number of causes. For example the non-constant strain rate, or the use of an apparently poor relationship of strain rate and material stiffness in that model (see section 4.2.6.5). Yet another (and I think more likely) explanation is that I am pushing this simple model too far.

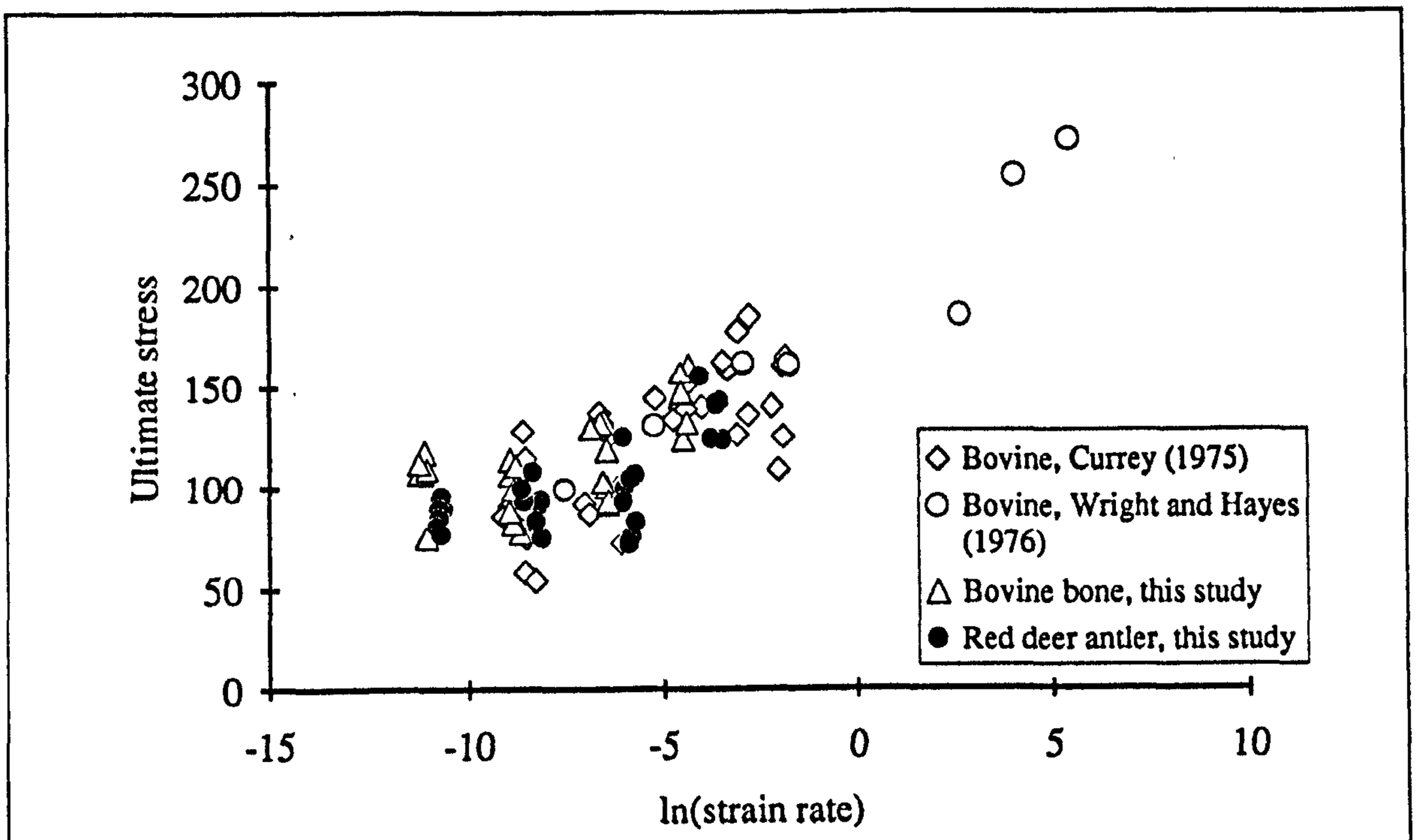

Units:

σ_{ult} Ultimate stress, MPa

$\dot{\varepsilon}$ Strain rate, s^{-1}

Figure 4.014

The ultimate stress and strain rate values for specimens of bovine bone and antler from this study and those by Wright and Hayes (1976) and Currey (1975)

In the previous section (4.2.6.6) I examined the results for knee-stress using non-logged data. The justification was based on comparisons with Sedlin's model. The relationship of the knee stress and the sliding of the Saint-Venant bodies is quite obvious. However, the relationship between the ultimate stress and the movement of these bodies is less clear. The shape of the stress strain response of antler suggests it could be viewed as a material with a multitude of such bodies. If it is assumed that the number of Saint-Venant bodies is large, but finite, then the maximum applied stress possible is that required to set all the bodies in motion. As in the previous section the externally applied force required to produce motion in the Saint-Venant bodies is related to the strain rate. The form of this relationship is assumed to be linear. Regression equations based on such a linear relationship are presented in table A9.006. When the totally un-logged equations

are compared with those in the previous tables it is noticeable that the explanatory power of the un-logged equations is greater. This is especially noticeable when equations *a* and *e* of table A9.006 are compared with equations *a* and *e* in table A9.005. As in the previous case, this observation may be an artefact due to the small number of cross-head speeds used. It was shown in figure 3.002 that the results of Wright and Hayes (1976) which cover a greater range of testing rates appear more linear on such a plot. To show the relationship between the results of Wright and Hayes (1976), Currey (1975) and those obtained in this study I have plotted them together in figure 4.014. To make the results more compatible I have used a value of strain rate rather than cross-head speed for my results. The strain rate I used is that measured during the initial section of the loading curve. (The difference between the measures of strain rate used in the published studies was presented in section 4.2.6.2. Figure 4.014 gives the impression that the relationship is of a double logarithmic form. This is due to the curved appearance of the plot resulting from the results of Wright and Hayes combined with my results for the slowest strain rate.

4.2.6.8. RESULTS: THE EFFECT OF CROSS-HEAD SPEED ON KNEE STRAIN

In this section I examine data set TB1 and TB2 (see appendix 4) for evidence of a relationship between the cross-head speed used for the tensile testing of bone and antler and the value of the knee strain. The method used to determine the value of knee strain for each specimen is described above in section 4.2.6.1.

Figure 4.015 shows that the dependence of the knee strain of the antler specimens on the cross-head speed is greater than the dependence of the knee strain of the bovine specimens on the same quantity. This observation is supported by statistical analysis, which indicates there is about a five-fold difference in the strength of the relationships. There is also a difference in the significance of the relationships. The knee strain of antler has a very highly significant relationship with the cross-head speed ($p < 0.001$ for the rate term in equation *a* table A9.007). The equivalent relationship for bone, *e*, is non-significant, but only just: $p = 0.051$. For the antler specimens the addition of material stiffness as another explanatory variable improves the predictive power of relationships, especially when the stiffness is that measured in tension. The exponent in the fully logarithmic equations (*d*, *i* and *j*) is less than that obtained by Currey (1989) for reindeer antler (0.063).

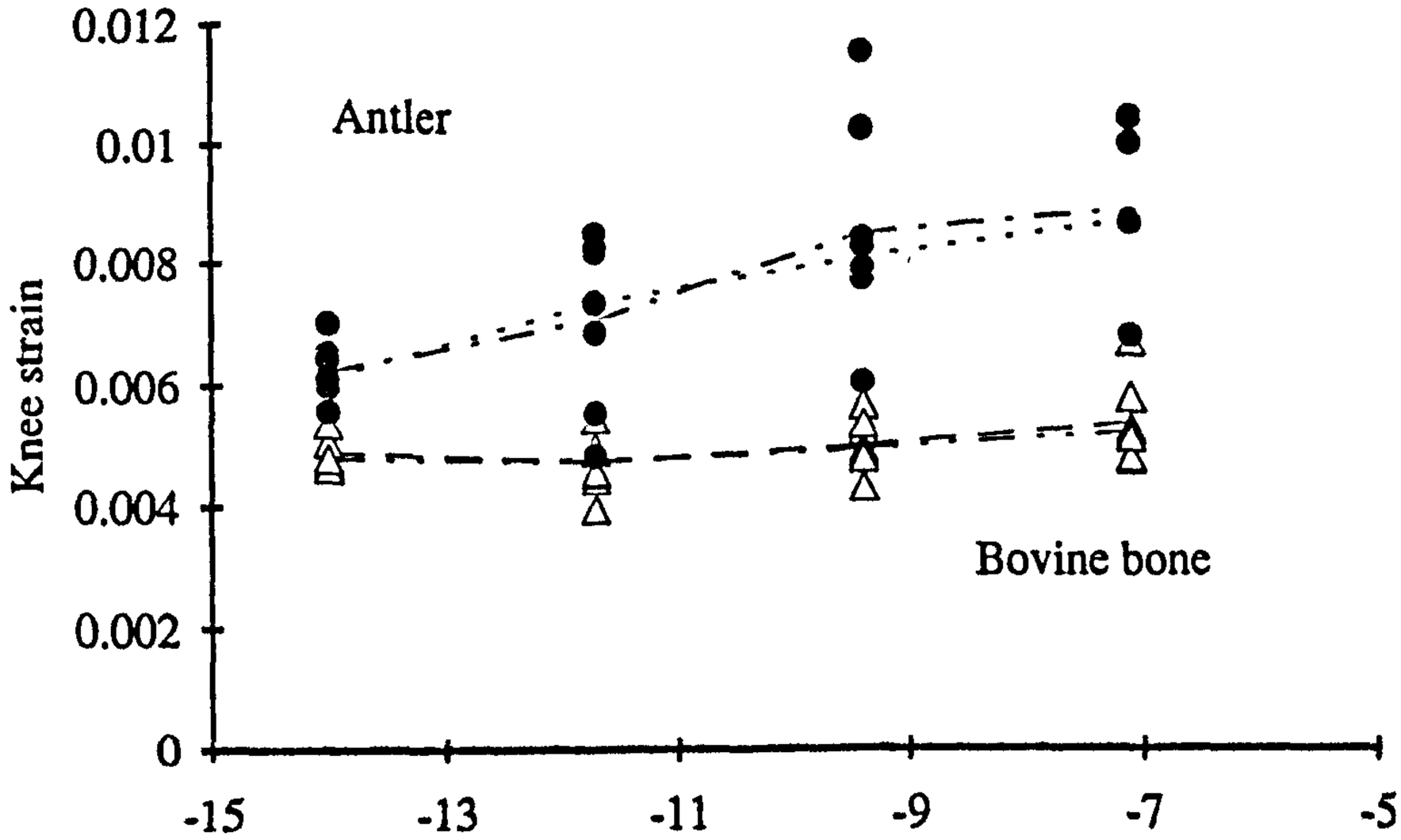

Units:

ε_K Knee strain

$\dot{x}$ Cross-head speed, m s^{-1}

Comments:

For full key see figure 4.009

Figure 4.015

The results obtained for knee strain at four cross-head speeds for specimens of bovine femoral bone and red deer antler

The plot of knee strain against rate for bovine bone data is almost horizontal. The R^2 value of the relationships based on cross-head speed alone is low (equations *e* and *g*). The rate term is not significant at the 5% level ($p = 0.051$ and $p = 0.059$). When E_b was used as a second explanatory variable (equations *f* and *h*) this only slightly increased the predictive power of the equation. It also resulted in the rate term becoming less significant ($p = 0.122$ and $p = 0.132$). In these two equations the stiffness terms are non-significant. (In the case of the variables examined previously, σ_K and σ_{ult}, the process of introducing the material stiffness as another variable cut the unexplained variation in half.) A similar result is obtained when the tensile material stiffness is used. This result would suggest that the knee strain for bone can be considered as a constant at these cross-head speeds. This could be interpreted as implying that the initiation of the failure of bone, expressed as the knee region of the curve, is determined by strain and not stress.

The suggestion that the initiation of the failure of bovine bone may be triggered by achieving a certain strain level rather than a certain stress level, may have parallels in a comparison of the TDF to the NTDF models. In the earlier model the time-to-rupture

was considered to be a function of time and stress alone, while in the later model it was a function of normalised stress, which can be regarded as pseudo-strain, and time. However, before too much weight is given to the idea that the knee strain is constant, it should be noted an examination of Currey's 1975 data shows a greater dependence of this quantity on the testing rate. The reason for this difference is unclear. In figure 4.011 a plot of the stress-strain relationship predicted by the NTDF model was produced. This plot, and the equations on which it was based, imply that the knee-stress of bone should be fully determined by the initial stiffness and the loading rate. This (as shown by table A9.007) has not been found to be the case with the experimental data for bovine bone. This could indicate that the NTDF model is unable to accurately predict the occurrence of the knee in the loading curve. This is not surprising as the purpose of the original model was to predict the failure stress, not the stress-strain response of the material, and the equations I used to extend the model contain a number of assumptions. Inaccuracies in some of these assumptions may be the cause of the inability of the model to predict the relationship of the knee strain to the cross-head speed for bovine bone.

Sedlin's rheological model (figure 3.009) can be used to predict a possible form for the relationship of knee strain values to testing rate. This relationship can be derived by considering the model in two parts. The first part considered is the dashpot and the spring that is in series with the Saint-Venant elements (spring 2 figure 3.009). The first Saint-Venant body moves at a set level of stress. Therefore stress, and thus strain, in the spring when the Saint-Venant body starts to move are also constant. Thus the extension of this part of the model when the knee occurs is independent of testing rate and has a constant value. The second part of Sedlin's model: the single spring (spring 1), displays a strain that is proportional to the applied load. It was shown in equation 2.012 that the applied load, before the motion of the elements, is a linear function of strain rate and strain. This interpretation of Sedlin's model predicts the knee strain is linear function of strain rate. This can be analysed further: I noted above that spring 1 displays a strain that is proportional to the applied load. However, considering the extreme case: if it is assumed that the time-dependent effect is small, then the dashpot can be replaced with a slider element[17] suggests that the load on the Saint-Venant bodies and the strain are simply related by the stiffness of the spring. On considering both these situations, I suggest that Sedlin's model predicts that the knee strain of cortical bone is approximately linearly related to the rate of loading and the stiffness of the bone. (The situation is clouded by the relationship of stiffness to loading rate and so on.) The regression equations that result from analysis of the experimental data using this predicted form of relationship are given in table A9.008. The regression equations in table A9.008 can be compared with those in table A9.007. This comparison shows that the explanatory power of the rate term alone has fallen for antler (table A9.007*a* and table A9.008*a*) but

---

[17]See section 3.2.1 or Tanabe *et al.* (1991a).

increased for bone (table A9.007*e* and table A9.008*e*). The same trend is reflected by comparison of the other equations. The lack of consistency may be due to the small number of rates used. However, it should also be noted that Sedlin's model was developed for cortical bone and not for antler. Therefore, the increase in the predictive power of equation based on his model for the bone data, compared to the decrease for the antler data, could imply that Sedlin's model of bone should not be applied to antler.[18]

4.2.6.9. RESULTS: THE EFFECT OF CROSS-HEAD SPEED ON ULTIMATE STRAIN

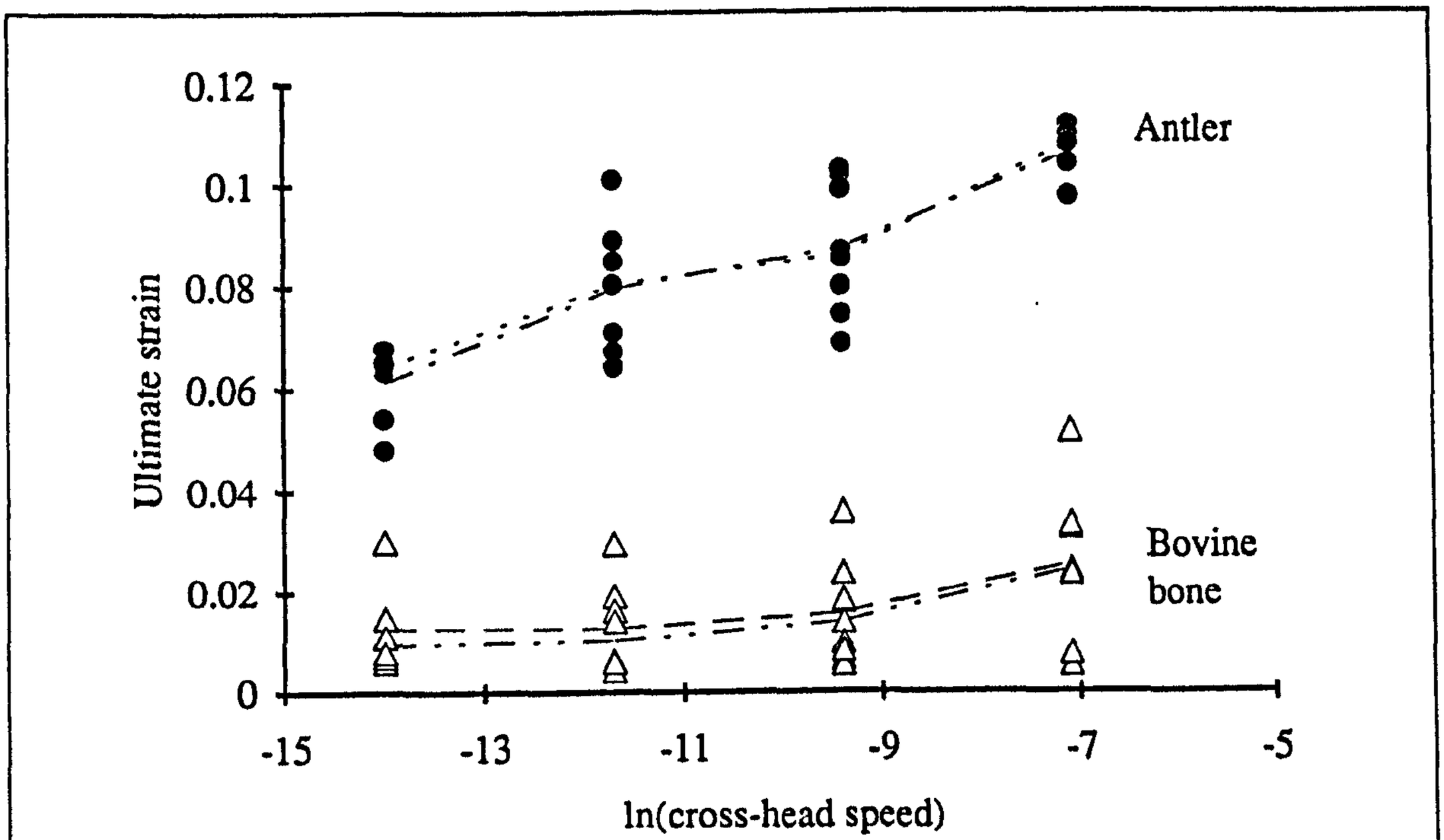

ε_{ult} Ultimate strain

$\dot{x}$ Cross-head speed, m s^{-1}

Comments:

For full key see figure 4.009

Figure 4.016

The ultimate stain values of specimens of bovine femoral bone and red deer antler tested at four cross-head speeds

As with the previously examined quantities, the ultimate strain of the antler specimens are more dependent on the cross-head speed than the corresponding results for bone. The ultimate strain values obtained from these tensile tests are several times greater then value of knee strain. The average multiplication factor is 11.0 for antler and

---

[18]In section 4.2.6.6 it was noted that Sedlin's model fitted the knee stress of bone more accurately than a logarithmic relationship and *vice-versa* for the antler data.

3.2 for bone. There is also a clear separation between the results for each material (shown to be very highly significant by one-way analysis of variance). The exponent of rate obtained for the antler specimens is greater than that obtained by Currey (approximately 0.08 as opposed to 0.04).

In their graphical representation of tensile curves of bovine tibial bone (figure 3.001) Crowninshield and Pope show most of the features reported in previous sections: increased stiffness with rate, increased knee stress with rate and an increase in knee strain. However, they also depict a marked decrease in ultimate strain with rate, as opposed to the increase found here.

The increase of ultimate strain with testing rate can be explained by the ideas of damage accumulation. In a previous section damage was expressed as $D = 1 - (E_M/E_U)$ (equation 2.114). Although damage is equal to unity at the instant after failure, at the instant before failure it is less than unity (as suggested in section 2.3.3.8). Finding the size of this discontinuity may hold the key to determining when the material will fail. I will consider two failure criteria: First, that failure occurs when a certain level of damage is reached; the *maximum damage criterion*. Second, that failure occurs when a certain effective stress is reached; the *maximum effective stress criterion*.[19]

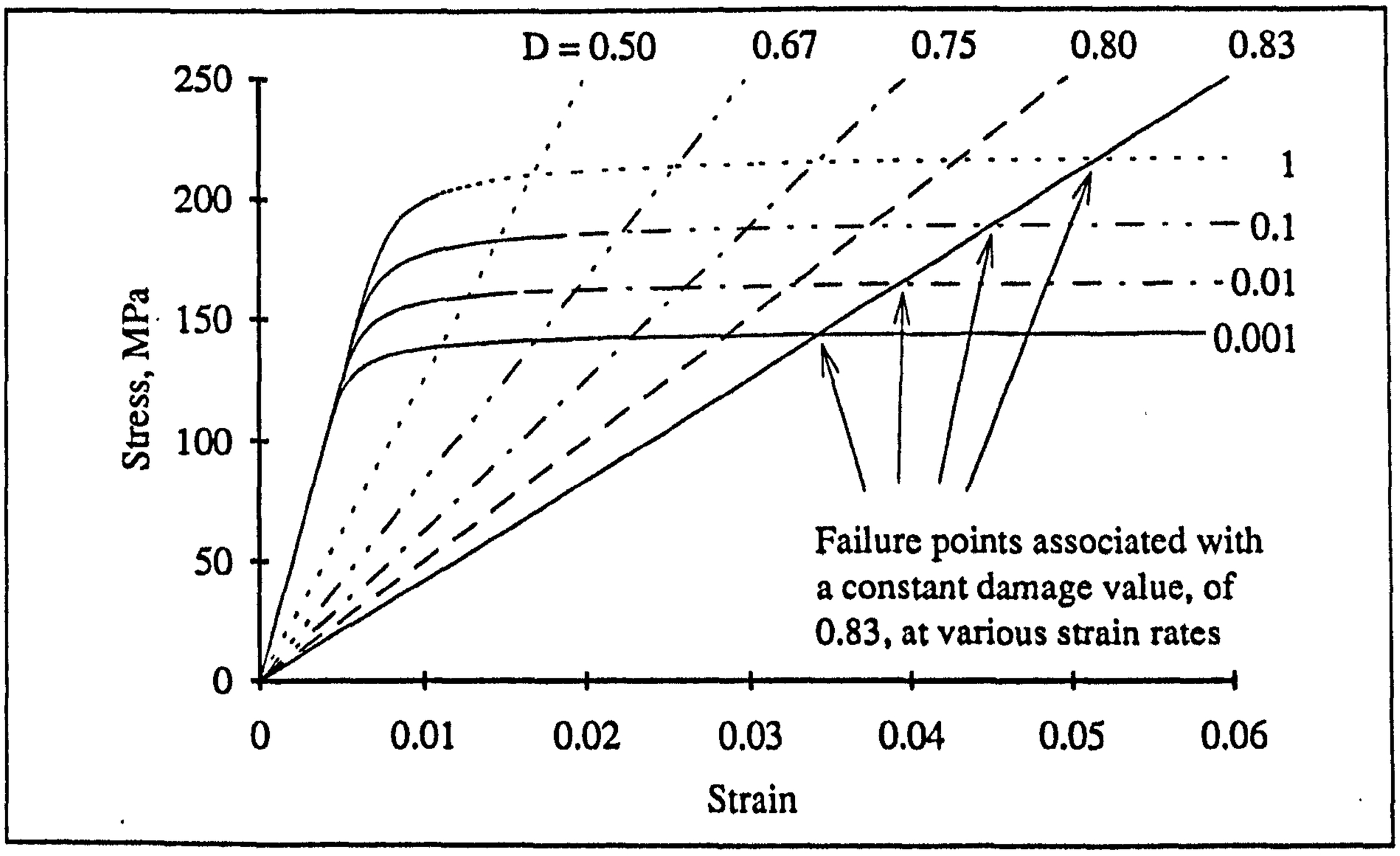

Figure 4.017

Prediction of the ultimate failure of bone, based on a constant ultimate damage criterion

---

[19]In this section no account is taken of the effect of cracks or flaws in the material. The effect that such discontinuities have on the failure of materials is considered in chapter 5. Thereafter the ideas of *fracture mechanics* will also be applied to bone and antler.

An expression for the maximum damage criterion can be formed from by combining equation 2.114 and my extension of the NTDF model. Equation 2.114 implies that if the damage at failure is constant then so is the ratio of $(\sigma_{ult}/\varepsilon_{ult})$ to E_t. The loci of stress and strain values that fulfil this condition for a few values of damage, D, are shown in figure 4.017 superimposed on the predicted stress-strain relations for bone (figure 4.011). Using the constant damage criterion, failure of the bone is predicted to occur where the damage line and loading curve intersects.

A mathematical form of relationship of ultimate strain to strain rate shown in figure 4.017 can be obtained by manipulation of equation 4.019 (using the same assumptions as in that case). Remembering that the numerical values are those relating to human bone obtained by Caler and Carter (1989).

$$\frac{1}{B_N E_N^{\,P} (P + 1)} \frac{\sigma^{P+1}}{\dot{\sigma}} = D \qquad (4.034)$$

The rate term in equation 4.034 is converted from one of stress to one of strain, by substituting $\dot{\varepsilon} E_N = \dot{\sigma}$ into the equation. This results is

$$\frac{1}{B_N E_N^{\,P+1} (P + 1)} \frac{\sigma^{P+1}}{\dot{\varepsilon}} = D \qquad (4.035)$$

Using $D = 1 - (E_M/E_U)$ and assuming the normalising stiffness and the undamaged stiffness to be the same (a reasonable assumption for the behaviour of the model), equation 4.035 can be rearranged to give

$$\frac{1}{B_N (P + 1)} (1 - D)^{P+1} \varepsilon^{P+1} \frac{1}{\dot{\varepsilon}} = D \qquad (4.036)$$

This equation can then be re-expressed as

$$\varepsilon = \frac{\left(D \dot{\varepsilon} B_N (P + 1)\right)^{1/(P+1)}}{(1 - D)} \qquad (4.037)$$

Thus if the material fails when a certain level of damage is reached, in other words D_{ult} is constant, the ultimate strain will be related to the strain rate in the following way

$$\varepsilon_{ult} = C \dot{\varepsilon}^{1/(P+1)} \qquad (4.038)$$

Where C is a constant that is defined by the material properties. Thus the maximum damage criterion predicts that the ultimate strain increases exponentially with an increase in testing rate. The values of B_N and P given by Caler and Carter (1989) can be substituted into equation 4.038 to obtain a prediction of ultimate strain if the amount of damage at failure is known or estimated. However, equation 4.038 can also be used as a prediction of the form of a suitable regression equation for the relationship of ultimate

strain to cross-head speed. The value of the coefficient of strain rate, using Caler and Carter's value of P, is 0.0595, which is considerably less than those obtained from experiments on bovine bone (equations *g* and *h* of table A9.009 and *c* and *d* of table A9.009).

As an alternative to the maximum damage criterion I suggested that a material may fail at a constant value of the effective stress: the maximum effective stress criterion. (The effective stress is defined as the stress that would be experienced by a specimen of undamaged material that has mechanical properties equivalent to the damaged specimen. The value of effective stress is therefore at least that of the nominal stress.) An analogue of a material that fails in this way could be a bundle of identical isolated fibres: the failure of one fibre has no effect on the strength of the others. Failure of each individual fibre will occur when they experience a certain load, say 10 N. Thus a bundle of 1000 undamaged fibre will support 10 kN. In the analogy some damage can be induced within the bundle of fibres by cutting some of the fibres, the situation then changes. If only 500 intact fibres remain the load they can support is reduced to 5 kN. However, in both cases the failure strain will be the same. If the failure strain is constant at failure, then the value of ultimate damage must be variable. The relationship of failure strain to effective stress is shown graphically in figure 4.018.

The maximum effective stress criterion, like the maximum damage criterion can be presented graphically and mathematically. Here I will concentrate on the graphical presentation. This presentation, like that of the previous criterion, shows the loci of predicted failure points. The intersection of these loci with the loading curves indicates the point of ultimate failure. The first task is to define a function that describes the effective stress in terms of the measured strain. For this task I return to the basic damage equations.

$$D = 1 - \frac{E_M}{E_U} \tag{4.039}$$

This can be re-expressed as a relationship of measured stress (nominal) to effective stress

$$D = 1 - \frac{\sigma}{\sigma_{eff}} \tag{4.040}$$

Thus

$$\sigma_{eff} = \varepsilon E_U \tag{4.041}$$

Equation 4.041 implies that loci of effective stress values, when plotted on stress-strain axis will be a straight line. The slope of this line will be the slope of the stress-strain relationship for the undamaged material. So if the effective stress at failure is constant then the ultimate strain is directly related to the initial material stiffness. The ultimate

strain is independent of the stress-strain relationship in the knee and post knee-regions of the loading curve (in the analogy when and how many fibres are cut). I have shown this graphically in figure 4.018. By using the predicted curves of figure 4.011, and assuming that the material stiffness is constant at 25 GPa (the value used in the production of the curves) I have superimposed a number of loci for difference effective stress values. Gordon (1976) presents a discussion of the theoretical strength of material's based on the strength of atomic bonds.[20] He gives an approximate rule for theoretical strength (for metals) as being E/6. If it is assumed that this forms an upper limit to the effective stress, it also forms an upper limit of strain. Substituting E/6 for the effective stress in equation 4.041 gives an upper strain limit of 0.167 (or 1/6). It is tempting to compare this value with those obtained for bone and antler. However, I consider that this is taking the idea of effective stress too literally. This approach may be applicable to the bundle type of material described in the above analogy, where there is a clear relationship between effective stress and the forces on the atomic bonds. Unfortunately, bone and antler are more complex; they are not composed of independent fibres. In chapter 5 an explanation of why structures fail at loads that are less than such a theoretical one is introduced.

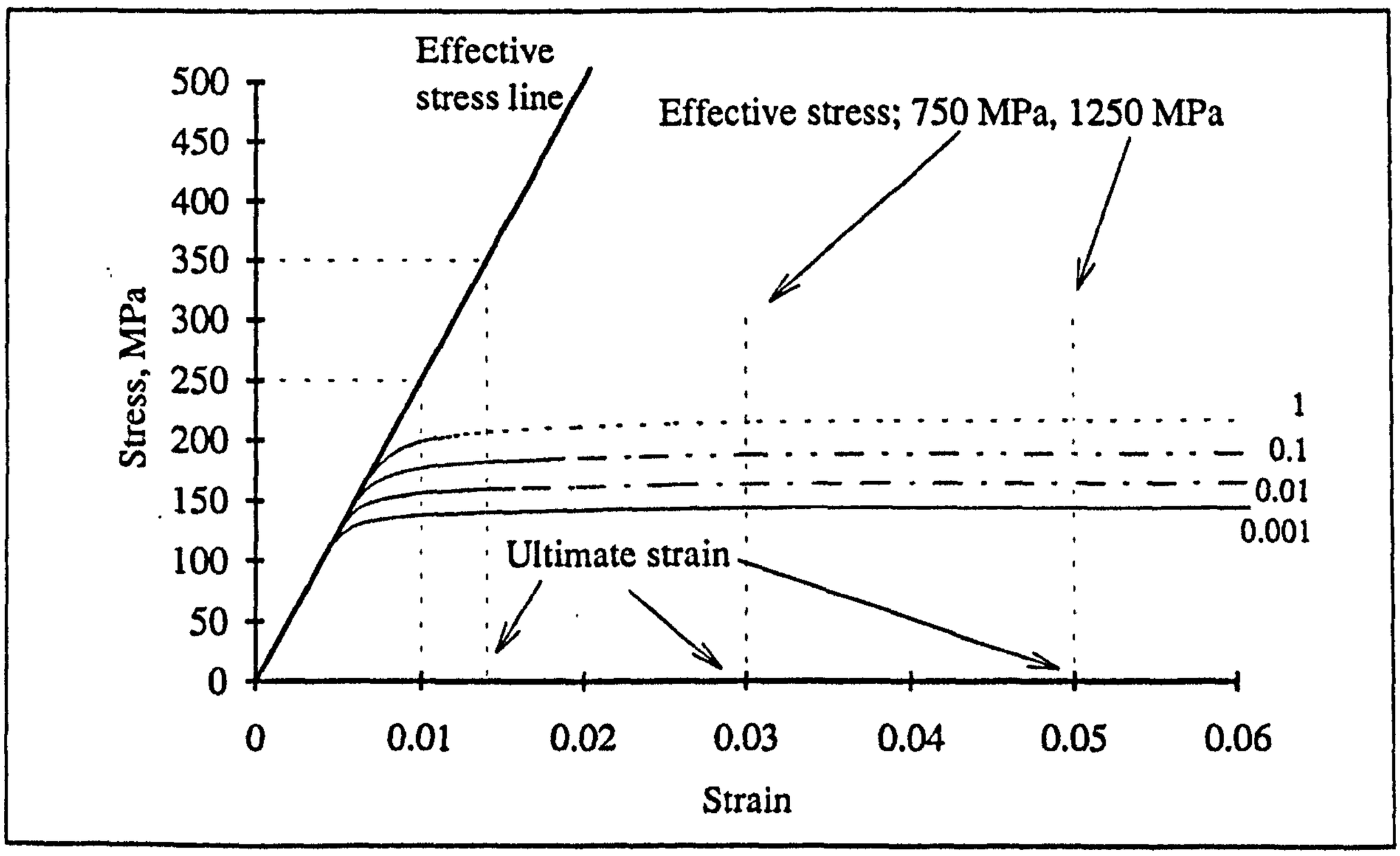

Figure 4.018

The predicted ultimate strain superimposed on the predicted stress-strain response of bone at four strain rates: 1, 0.1, 0.01 and 0.001 s^{-1}

[20]His discussion forms an introduction to the work of Griffith and the detrimental effect of cracks, introduced here in chapter 5. The strength of the atomic bonds is a determining factor of the surface energy of a material.

The maximum effective stress failure criterion, as presented above, predicts that the ultimate strain will be constant. This assertion was based on the assumption that the material stiffness was constant. If it is assumed that the material stiffness increases with strain rate, it can be shown that the model predicts that the ultimate strain will decrease with strain rate.[21]

The models of ultimate strain presented above are based on a number of assumptions that I have already questioned. Despite these shortcomings the observation that one predicts an increase in the ultimate strain with testing rate and the other a constant or declining value, can be compared with the experimental results presented in figure 4.016. Such a comparison shows there is more agreement between the experimental results and the constant damage level failure criterion. However, if Crowninshield and Pope's results are considered (figure 3.001) the opposite opinion would be reached. It is tempting to suggest that antler results appear to be consistent with the maximum damage criterion, while those for bone (being less rate dependent and more variable) are consistent with the maximum effective stress criterion. I consider that the failure criteria based on a maximum effective stress, is a more intellectually acceptable one. An argument in support of this position can be based on a consideration of a damaged material that is not loaded. It would appear irrational to suggest that an unloaded material could fail at any level of damage less than $D = 1$. Perhaps the maximum effective stress criterion is incorrect for the same reason that the use of a maximum (nominal) stress failure criterion was found to be incorrect by Griffith in 1920 (Griffith, 1920, see chapter 5). He showed that the presence of a crack in a material disproportionally decreased its failure stress. The most likely situation is a compromise between the various failure criteria. Such a compromise is discussed in chapter 9, after more evidence has been presented.

An analytical section that is related to this one is 4.2.6.11 where I examine the effect of cross-head speed on two estimates of the ultimate damage. However, before I do that there is another feature of the stress-strain plot that has not been examined yet: the final slope.

---

[21]This raises the question of how the stiffness increases? If it is due to the accumulation of less damage what stiffness should be used to asses damage? See sections 4.2.6.5 and 4.2.6.11.

4.2.6.10. RESULTS: THE EFFECT OF CROSS-HEAD SPEED ON THE FINAL SLOPE

The most noticeable result shown in figure 4.019 (shown below) is that the cross-head speed does not have a statistically significant effect on the final slope in any of the regression equations given in tables A9.011 and A9.012 for either material. However, the material stiffness in tension is a significant variable in equations *a* and *b* of the latter table. This observation disagrees with that made by Currey for reindeer antler (Currey, 1989).

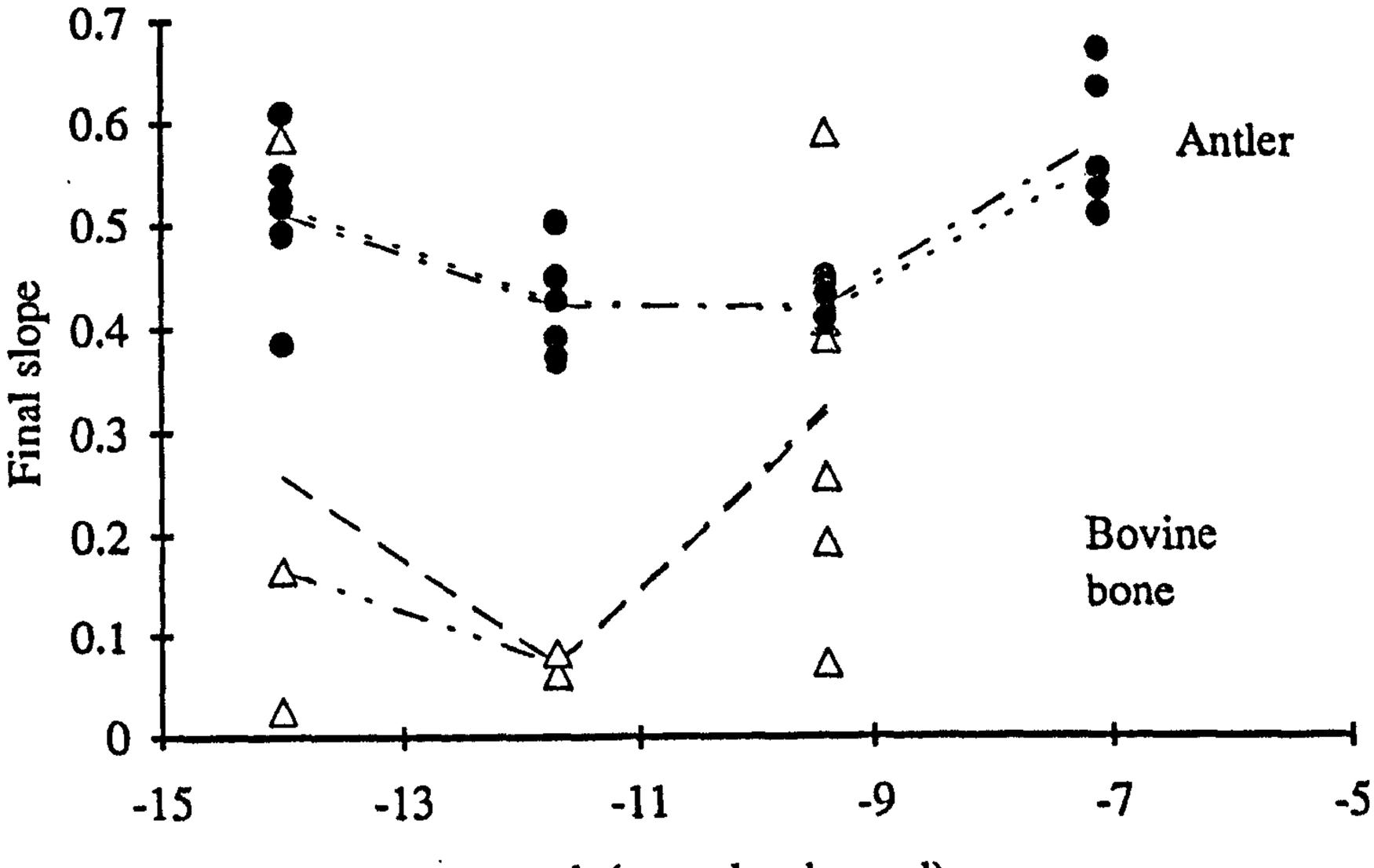

Units:
S Final slope, GPa
$\dot{x}$ Cross-head speed, m s^{-1}
Comments:
For full key see figure 4.009

Figure 4.019

The ultimate stain values of specimens of bovine femoral bone and red deer antler tested at four cross-head speeds

In these results for final slope there is, as in many of the others, a division between those for bovine bone and those for antler. This is not surprising when the shapes of their stress-strain curves are examined (figure 1.012). In this data set (compared to the previous ones) there are fewer results available from bovine specimens. There are two reasons for this: first a number of bone specimens only attained a very limited amount of post-knee strain thus preventing the fitting of a regression line (this may account for the higher values obtained for some bone specimens). Second, in some

cases at the highest cross-head speed, such as that shown in figure 1.012b, the post-knee region of the stress-strain curve for bovine bone exhibited a distinct change in slope. The reason for this feature is unknown. It could be a result of damage being accumulated at a faster rate at the higher stresses attained at these higher cross-head speeds. Perhaps this damage accumulation has some property similar to inertia. This inertia could result in an elongation rate of the specimen that is greater than the cross-head of the machine will permit, so the load falls. The falling load would these reduce the damage rate (and the energy available for damage growth). The specimen is therefore able to sustain further elongation. The stress needed for the specimen to extend at the same rate as the machine increases as the inertia of the damage is depleted. This explanation parallels that of the self regulating mechanism that I proposed in the model which compared creep and tensile behaviour in section 3.3.3.2.

There is a complicating factor in the analysis of the post-knee behaviour. The effects studied start to occur at the same time that the machine-specimen interaction results in an increase in strain rate. Thus the stress-strain behaviour in the knee region is probably partly determined by the test machine used. Thus I will not pursue an investigation of this inflection in the loading curve; as it may be an artefact. However, a similar effect has been observed by other workers (for example by Sedlin in 1965, see figure 3.008) and when specimens of an aluminium alloy similarly shaped to the bone specimens used in this work were tested the effect was not observed. To clarify this matter an investigation using a closed loop machine, in both strain and stress control is required.

4.2.6.11. RESULTS: THE EFFECT OF CROSS-HEAD SPEED ON ULTIMATE DAMAGE

In previous sections a mathematical description of damage has been presented. This equation has been repeated at various points in the text and is repeated again here:

$$D = 1 - \frac{E_M}{E_U} \qquad (4.042)$$

In a previous section (for example 4.2.6.9) I also assumed that when unloaded the material when unloaded will display a linear stress-strain relationship, returning to its original length. Thus the value of E_M at failure can, using the same assumptions, be expressed as $\sigma_{ult}/\varepsilon_{ult}$. (This quantity is the same as Currey's (Currey, 1989) final stiffness, shown in figure 3.006.) The value of E_U to be used has to be chosen. There are two options: the material stiffness in three point bending, E_b, or the stiffness measured from the initial region of the loading curve, E_t. I will examine both of these options and

then discuss the merit or otherwise of each. The equations and nomenclature I will use are given below (the value of 1000 in the equation is to account for the stress values being given in MPa and the stiffnesses in GPa). First, the ultimate damage calculated by using the tensile stiffness.

$$D_t = 1 - \frac{\sigma_{ult}}{1000\,\varepsilon_{ult}\,E_t} \qquad (4.043)$$

Second, the ultimate damage, using the bending stiffness.

$$D_b = 1 - \frac{\sigma_{ult}}{1000\,\varepsilon_{ult}\,E_b} \qquad (4.044)$$

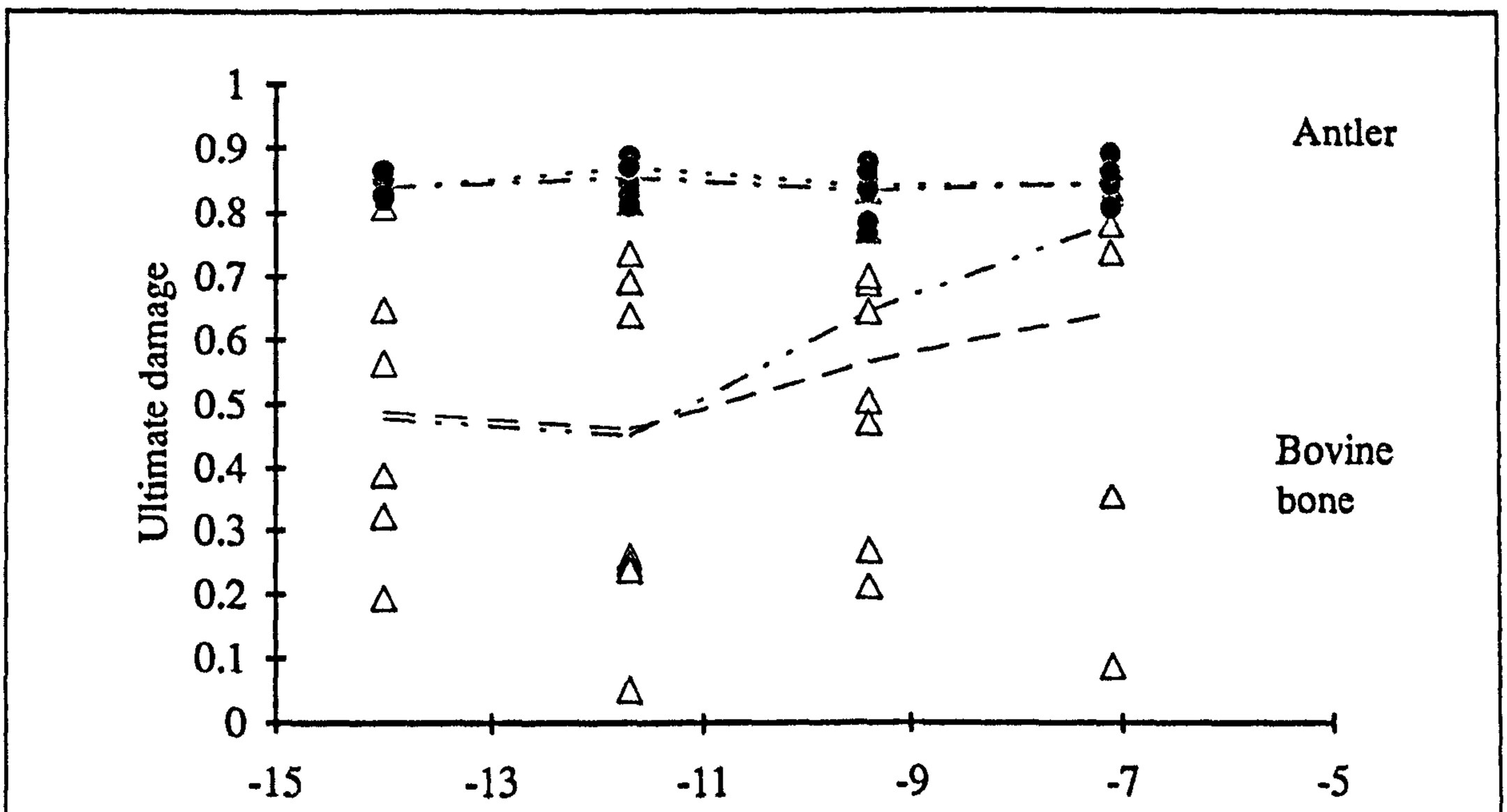

D_t Ultimate damage, using a prediction based on the material stiffness in tension.

$\dot{x}$ Cross-head speed, m s^{-1}

Comments:

For full key see figure 4.009

Figure 4.020

The ultimate damage values of specimens of bovine femoral bone and red deer antler tested at four cross-head speeds, obtained by using equation 4.043

Figure 4.020 shows that there is a difference in the range of ultimate damage values (as defined here) for specimens of bovine bone and red deer antler. The antler specimens display a very uniform value of ultimate damage, while those of bone show a larger range of values. Some of the bone specimens sustain about the same amount of damage as those of antler before failure. To emphasise this point a section of the plot shown in figure 4.020 is repeated in figure 4.021. (In the second case the symbols for the

bovine results are plotted on top of those for antler.) The most important aspect of these results could be that none of the antler specimens display a low level of ultimate damage.

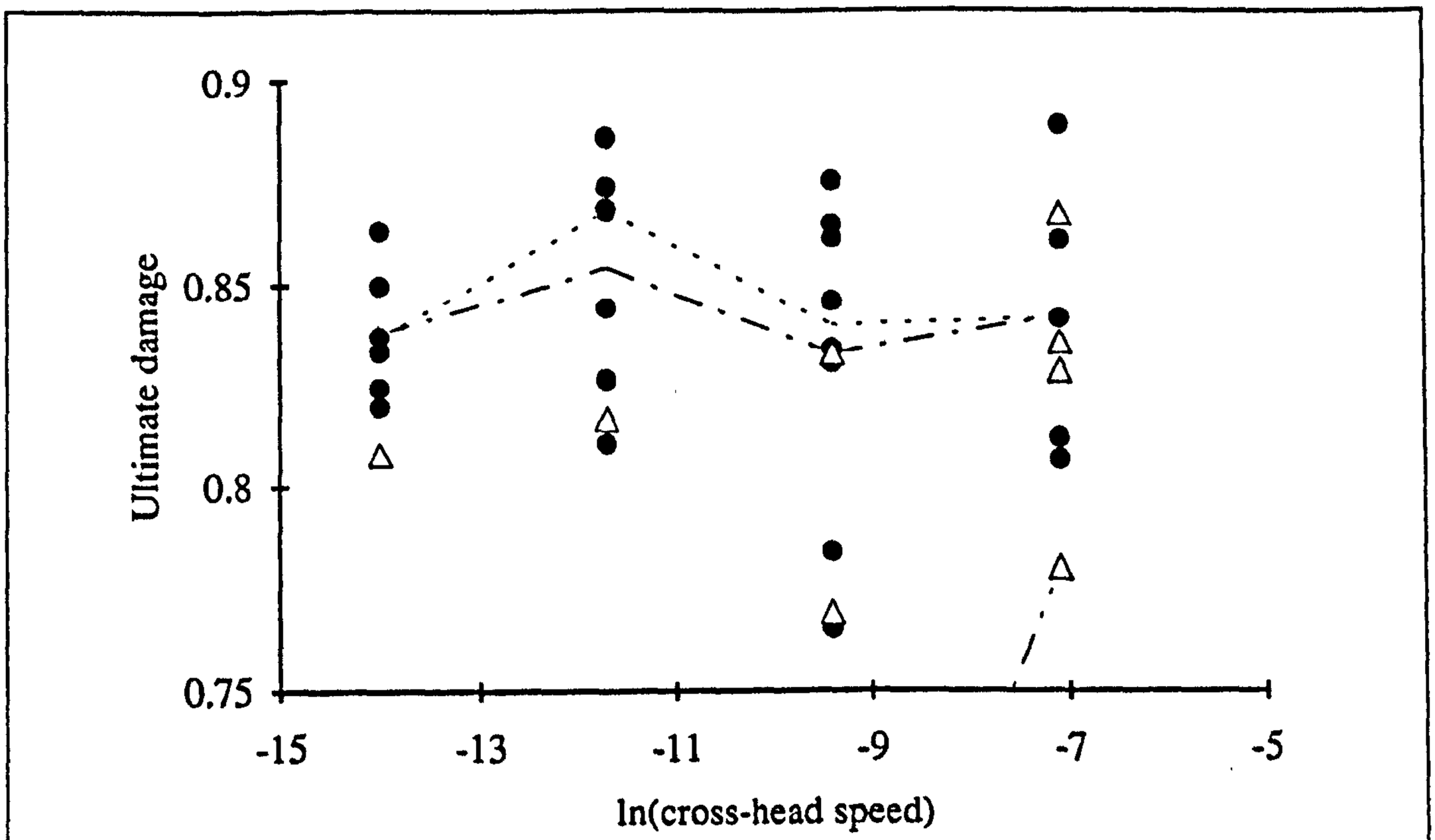

D_t Ultimate damage, using a prediction based on the material stiffness in tension.

$\dot{x}$ Cross-head speed, m s^{-1}

Comments:

This plot does not contain all the points in data set TB1. For full key see figure 4.009

Figure 4.021

The ultimate damage values of specimens of bovine femoral bone and red deer antler tested at four cross-head speeds, obtained by using equation 4.043

From the results presented here it would appear that the use of a constant damage criterion is valid for antler, but not for bone. If the non-constant ultimate damage of bone is due its brittle behaviour (or susceptibility to cracks and flaws), the ultimate damage level exhibited by antler may be the upper-bound of that attainable by the more highly mineralised bone, if stress concentrations are avoided. However, the values of ultimate damage for antler may be closely grouped not for structural or physical reasons but for reasons of mathematics and definition. From examination of figure 4.017, it can be seen that the same increment in strain will result in a large increment in damage at low damage levels and a small one at high levels. Thus a range of ultimate strains falling at higher values will imply a smaller range of damage values than the same range of strain values grouped around a lower value of strain. This effect is seen when the strains shown in figure 4.016 are compared with the damage values given here. Thus the mathematical form of the damage expression means that for high failure strains the results will tend to be forced into the upper range on values, but never reaching unity. For example, to reach

a value of unity an idealised material must have an infinite post-knee strain, but to reach a value of 0.8 the post knee strain have to only be five times the pre-knee strain. Thus to attain a higher damage value the material must display considerably more post-knee strain. It is this effect that constrains the antler results to a limited range of damage values. Such a constraint may remove any dependence on strain rate, or at least reduce the ability of regression analysis to detect it. However, this effect can not explain why there are no low damage values for the antler specimens tested here.

The regression equations relating the ultimate damage to the cross-head speed used during the tests are given in tables A9.013 and A9.014. The bending stiffnesses have been used as additional variables as in the previous cases. However, in the work presented here the ultimate damage is calculated using a measure of material stiffness. Thus it may be expected that these two quantities are highly correlated, unless damage is truly a constant. For example, I would expect these quantities to be related if the value of the final slope, $\sigma_{ult}/\varepsilon_{ult}$, was constant. To examine this I have repeated the calculation of damage, using the mean value of the final slope (of bone or antler as appropriate) in place of the value for each specific specimen. The variation in the damage values resulting from this calculation is due only to the variation in the material stiffness. The regressions shown in tables A9.013 and A9.014 have been repeated using these new damage values. The values of the R^2 and the t values of these regressions are shown in the square brackets next to or below those relating to the regression equation shown. Those regressions that include the material stiffness in tension, table A9.014, show that it is not the final stiffness that is constant, if it was the R^2 values would be in the range of 90 to 100%.

Another possible way to calculate damage is to use the material stiffness in bending (equation 4.044). The bending stiffness was measured under standard conditions. Thus it may provide a better measure of the properties of the undamaged material then the tensile stiffness. The latter is dependent on loading rate. Thus if the calculation of damage is based on tensile stiffness it is arguable that an investigation of the effect of cross-head speed on damage is flawed. This would clearly be the case if the change in initial slope was caused by the accumulation of damage.

It can be seen in figure 4.022 that damage calculated on the bases of the material stiffness in bending has resulted in some spurious results. A number of values of ultimate damage for the bovine bone specimens are negative. This result, when taken at face value, implies that for these specimens the material has improved its mechanical properties. However, there are a number of explanations for this anomaly. The primary candidate is that the material stiffness in tension is poorly predicted by the material stiffness in bending. Thus for a specimen that fails at a small post-knee strain it is

possible that its final stiffness is greater than its bending stiffness. This situation will produce a negative damage value.

From the results presented here it appears that using the material stiffness in the pre-knee region of the loading curve gives the best estimate of damage. However, there is still the effect of strain rate on this stiffness to be considered. Therefore, I suggest that an estimate of the stiffness under an instantaneous load, may be more applicable. An examination of this aspect of my results could be an area suitable for further investigation.

D_b Ultimate damage, using a prediction based on the material stiffness in bending.

$\dot{x}$ Cross-head speed, m s^{-1}

Comments:
For full key see figure 4.009

Figure 4.022

The ultimate damage values of specimens of bovine femoral bone and red deer antler tested at four cross-head speeds, obtained by using equation 4.044

The results obtained from the two measures of damage studied here can be summarised in a few main points. The level of damage attained by antler specimens is relatively high, very uniform and statistically not dependent on the testing rate. The calculated damage levels of the bovine bone specimens, are scattered from very low values up to those of antler, but not beyond, and show no statistical relationship to the testing rate.

The scatter of the ultimate damage values for bovine bone compared to those of antler is consistent with results presented in previous (and following) sections. In the discussion of the behaviour of bovine bone and antler during impact testing (section 1.4.2.3) I reported that bovine bone is more brittle than antler. This can be attributed to bone's greater sensitivity to stress concentrations. Such stress concentrations can be caused by scratches (as a result of poor preparation), changes in the cross-sectional shape of the specimen and internal features such as blood vessels and so on. This would result in a more localised final failure process. This results in a reduction in the ultimate strain and ultimate damage obtained in such a flawed specimen. The theory of fracture mechanics and the notch sensitivity of bone and antler are presented in chapters 5, 6 and 7, and evidence of the relationship of final strain and distribution of the failure process in provided in chapter 8 in on the video of appendix 9.

4.2.6.12. RESULTS: THE EFFECT OF CROSS-HEAD SPEED ON WORK INPUT

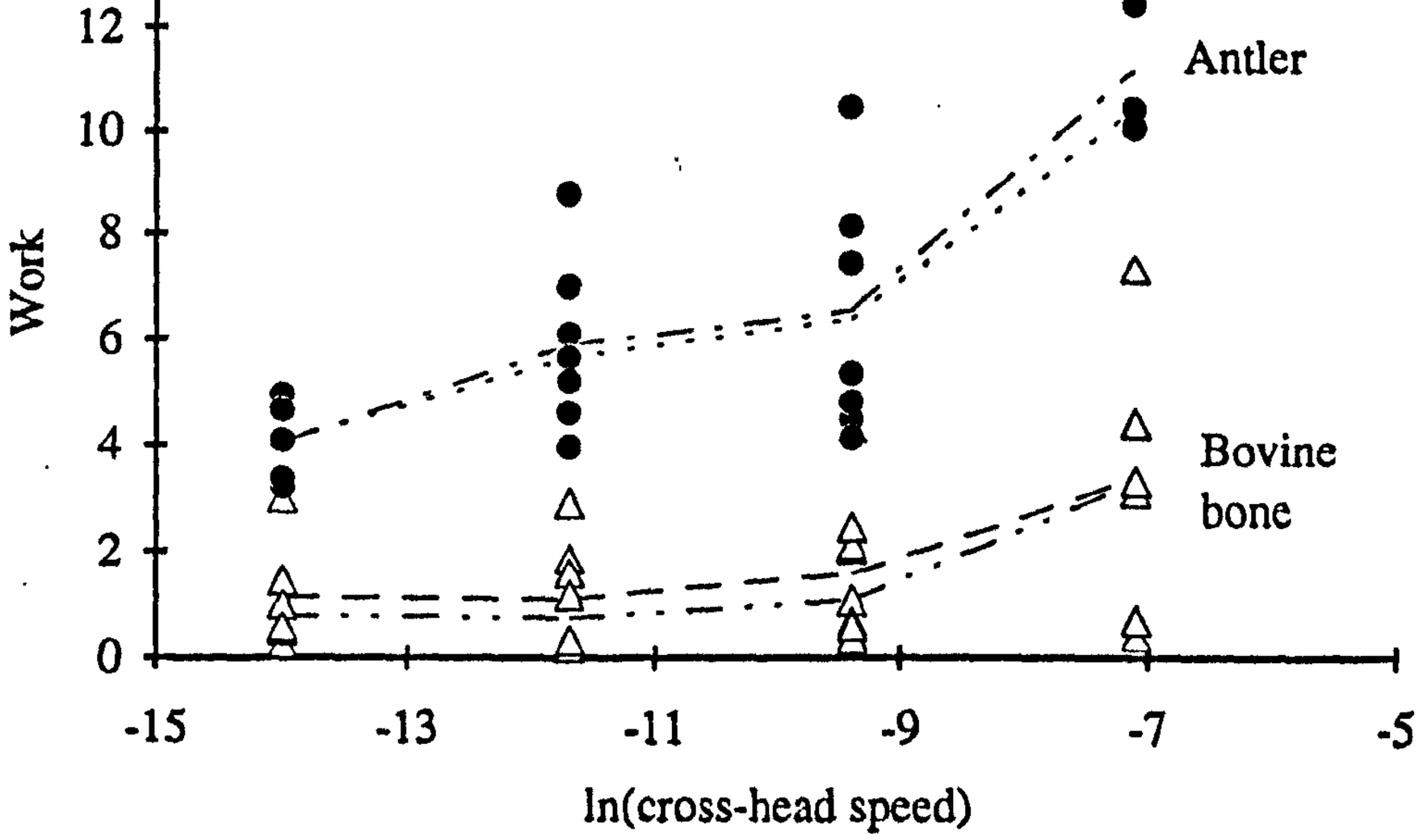

Units:

W Work, area under the loading curve, MJ m^{-3}

$\dot{x}$ Cross-head speed, m s^{-1}

Comments:

For full key see figure 4.009

Figure 4.023

The average work per unit volume supplied to the gauge length of tensile specimens of bone and antler up to final failure (area under the stress-strain curve)

The plots in figure 4.023 show the dependence of the area under the loading curve on the testing rate. It has been shown that the stiffness of the material in the initial part of the loading curve is not very rate dependent, but that the knee stress, ultimate stress and ultimate stress all increase with increasing loading rates. Thus it is not surprising that the work supplied to the specimen up to the point of failure, W, is also rate dependent. In all but two cases (equations *c* and *d*) the rate is a significant variable. For the results from the antler specimens the cross-head speed is a very highly significant variable in every equation of table A9.017 and A9.018. (In equations *a* to *d* of table A9.017 the constant term in the last equation (*d*) is the only factor that is not very highly significant.)

The antler specimens require a greater energy input to break them than that required by the bone specimens. This is the same result as that of the impact tests described in chapter 1. This difference is the result of antler's ability to sustain larger strains, not larger forces. In the tensile tests the ultimate strain values of antler are higher than those of bone. In the impact tests the deformation of the antler specimens was far in excess of those of the bovine bone specimens.

It is possible to produce a model prediction of the relationship of work to testing rate by integration of the predicted stress-strain relationships obtained from the extended NTDF model. (This relationship is given in section 4.2.6.5 and shown in figure 4.011). This could be done either algebraically or by approximation from the data that make up the curves. The latter method is the same as that used for the experimental data. However, as both approaches would require an estimate of the failure strain and I consider that such a calculation may extend the model too far, this idea is not pursued.

It was previously stated that the force needed to extend a visco-elastic material (or Sedlin's rheological model) depends on the rate of that extension. Thus, as work can be expressed as the product of force and distance that the force moves, the work needed to extend a visco-elastic material by a certain length depends on the extension rate. It therefore appears that both the damage and the visco-elastic approaches can be used to explain the rate dependence of work. The relationship between damage (or visco-elasticity) and the value of work given here is complicated. One of the main problems is that the proportion of this work that is recoverable is unknown. In the damage models I have used so far I have assumed that the material will return by a linear relationship to its original length, like an idealised elastic-damage material (figure 2.013b). However, figure 1.011 suggests this is not the case. This aspect of the behaviour of bone and antler is examined experimentally as a supporting investigation to the notch sensitivity tests in chapter 7 (the resilience tests of sections 7.4.3.1 and 7.7.1.1).

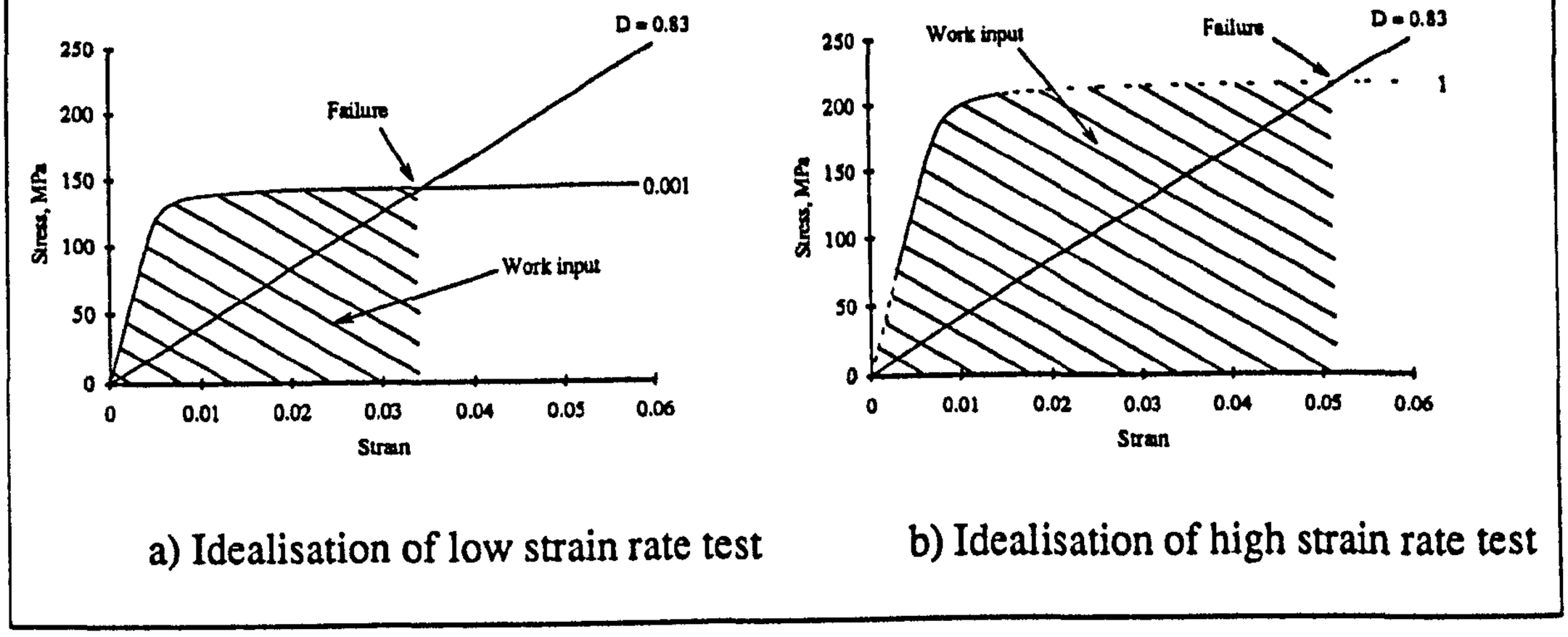

a) Idealisation of low strain rate test

b) Idealisation of high strain rate test

Figure 4.024

A idealisation showing how the work input to a specimen is dependent on testing rate if failure occurs at a constant damage level

The most important aspect of the results obtained here is not the high degree of dependence on cross-head speed of the work input to the antler specimens, but the contrast of this result with those presented above for the values of ultimate damage. Thus the damage sustained by an antler specimen is not significantly dependent on the cross-head speed, but the faster it is loaded the more energy is needed to produce that amount of damage. This clearly has implications for the interpretation of the results of the impact tests described in chapter 1, and (allowing for the differences between environmental conditions) the use of antlers by deer during the rut. This appears to agree with the idea that the production of damage is dependent on stress (or strain by the NTDF model) and time. The less time that is available for the failure process the higher stress (or strain) input needs to be to produce failure. A higher stress or strain input equates with a higher energy input. This is shown in a rather idealised way in figure 4.024. The curves in this figure have been adapted from those on figure 4.017.

4.2.6.13. RESULTS: THE EFFECT OF SPECIMEN SIZE ON VARIOUS MECHANICAL QUANTITIES

In the preceding sections the effect of cross-head speed on a number of variables has been considered. These variables are: material stiffness, knee stress, ultimate stress, knee strain, ultimate strain, ultimate damage and work input. In section 4.2.6.3 it was shown that the size of a specimen affects the rate at which it is stretched in an open loop controlled testing machine. In the experiments examined here two sizes of specimen were used, one set was approximately 4 mm wide and the other 5 mm wide. All other dimensions were similar. To asses the effect of specimen size on the results obtained, all

the regression equations were repeated using an additional variable that indicated if the specimen was 4 or 5 mm wide. The regression equations are not given, but their R^2 values are given in parentheses in the same tables as the results of the initial analysis (appendix 9). If the results indicate that the inclusion of a specimen size variable changes the predictive power of the regression equations there are two possibilities: First, it could be an effect of specimen size *per se*. Second, it could be an artefact caused by the machine-specimen interaction (see appendix 7). On examination of the results no dramatic change or consistent trend of changes was observed for any of the variables studied. However, if the results for bone and antler are examined separately a more consistent trend is seen in some cases. (For example see table A9.001.) This finding suggests that any distortion of the results of tests at one cross-head speed due to the machine-specimen interaction, may be ignored when it is compared to the difference caused by the different cross-head speeds used (figures 4.005 and 4.006). Thus I conclude that the effects of cross-head speed demonstrated in this chapter are due to the rate-dependent properties of the test material and not to an interaction with the equipment used to test it.

4.2.7. SUMMARY OF THE RESULTS FROM TENSILE TESTS ON BONE AND ANTLER CONDUCTED AT FOUR CROSS-HEAD SPEEDS.

The results obtained from this study of the effect of cross-head speed on the mechanical response of antler and bone during tensile testing are summarised in table 4.007. The results clearly show that the mechanical properties of these materials are rate dependent.

Some of the results obtained from the examination of various quantities measured from the stress-strain curves of the bone and antler specimens tested in this study can be summarised graphically. This is done in figures 4.025 and 4.026. The lines shown on the plot connect the origin to the mean knee stress and strain values, and then to the mean ultimate stress and strain values. This is done for the specimens tested at each cross-head speed. The boxes represent the limits of one standard deviation from the mean values. These figures show the general trends that have been examined in more detail above. It will be noted that as shown in figure 4.012 and figure 4.013 the knee stress and ultimate stress values for bovine bone at the lowest cross head speed do not have the lowest mean value. No reasonable explanation for this apparent anomaly has been found.

Variable (section)	Material tested in tension	
	Reindeer antler	Bovine femoral bone
Material stiffness, E_t (4.2.6.5)	E_t has a non-significant dependence on cross-head speed. E_t has a very highly significant dependence on E_b.	E_t has a very highly significant dependence on cross-head speed. E_t has a greater dependence on E_b than on cross-head speed.
Knee stress, σ_K (4.2.6.6)	Cross-head speed is a very highly significant predictor of σ_K. The additional variable E_b is more significant than the speed.	Same as for antler.
Ultimate stress, σ_{ult} (4.2.6.7)	Cross-head speed is a very highly significant predictor of ultimate stress.	Same as for antler
Knee strain, ε_K (4.2.6.8)	Cross-head speed is a very highly significant predictor of knee strain.	The dependence of ε_K on cross-head speed is just below the significance level of used in this study.
Ultimate strain, ε_{ult} (4.2.6.9)	Cross-head speed is a very highly significant predictor of ultimate strain.	Cross-head speed is a significant predictor of ultimate strain.
Final slope, S (4.2.6.10)	As for bovine bone, but the additional variable E_t was significant.	No statistical dependence of S on cross-head speed was found.
Ultimate damage, D_{ult} (4.2.6.11)	No statistical dependence of D_{ult} on cross-head speed was found.	As for antler.
Work, W (4.2.6.12)	Cross-head speed is a very highly significant predictor of work input.	As for antler.
Comments: It has been shown that in all cases where a significant relationship was found between the cross-head speed and a variable (such as knee stress or ultimate strain) the relationship was a positive one; a higher testing rate resulting in a higher value of the variable.		

Table 4.007

The effect of cross-head speed on various mechanical properties of bovine bone and antler measured in tension

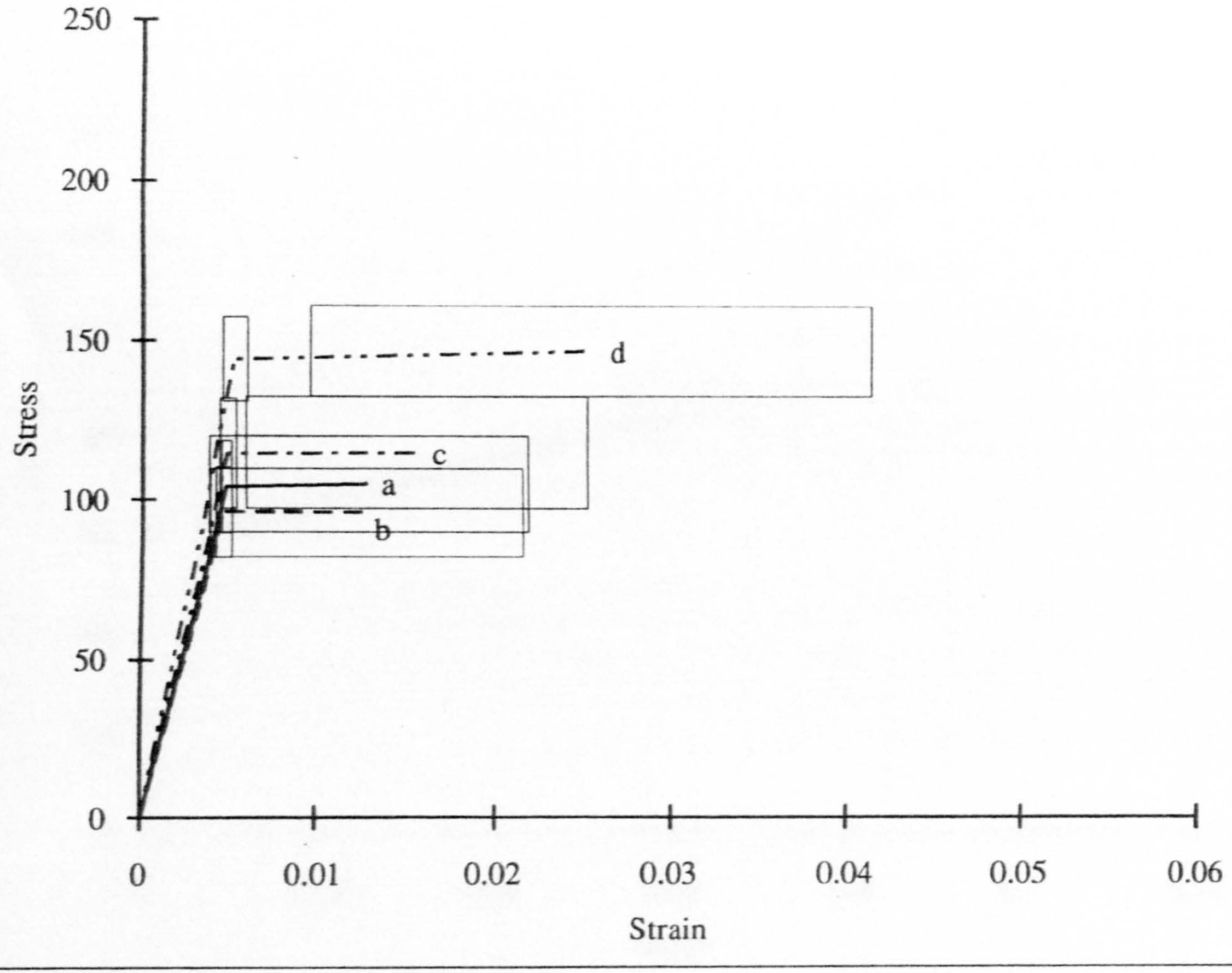

Units:

σ Stress, MPa

ε Strain, unitless

Comments:

The idealised stress-strain relationships shown have been produced by connecting the mean values of the stress and strain at the knee and at failure (as defined in this study). The boxes placed around these values indicate the area of possible values that are within one standard deviation of the mean value. The cross-head speeds are: a, 8.33×10^{-7}; b, 8.33×10^{-6}; c, 8.33×10^{-5} and d, 8.33×10^{-4} m s^{-1}. The axes have been chosen so they are consistent with those of Crowninshield and Pope (1974) (see figure 3.001)

Figure 4.025

Idealised stress-strain relationships for bone at four cross-head speeds (based on mean values)

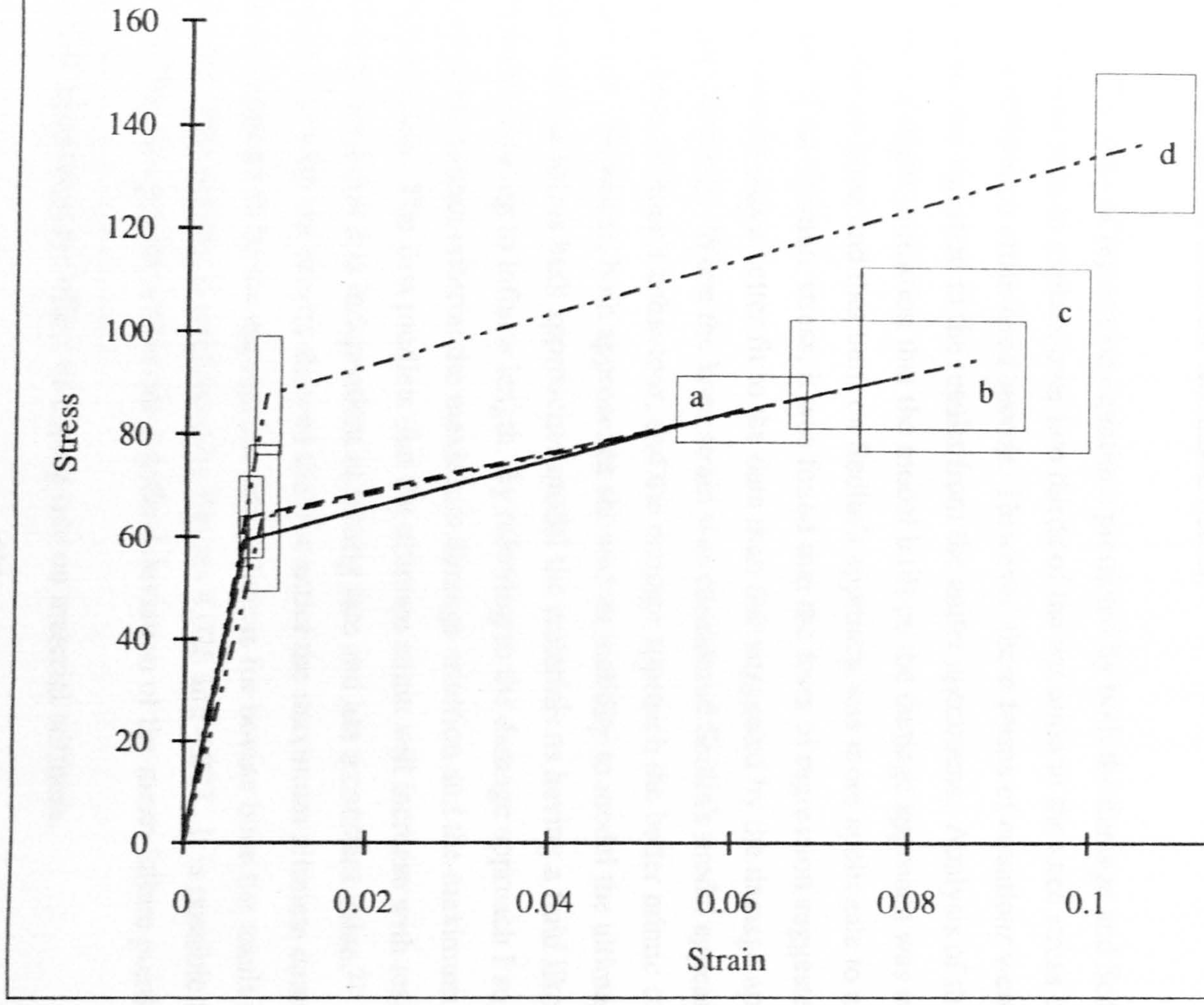

Units:

σ Stress, MPa

ε Strain, unitless

Comments:

The idealised stress-strain relationships shown have been produced by connecting the mean values of the stress and strain at the knee and at failure (as defined in this study). The boxes placed around these values indicate the area of possible values that are within one standard deviation of the mean value. The cross-head speeds are: a, 8.33×10^{-7}; b, 8.33×10^{-6}; c, 8.33×10^{-5} and d, 8.33×10^{-4} m s^{-1}.

Figure 4.026

Idealised stress-strain relationships for antler at four cross-head speeds (based on mean values)

In the previous sections I have examined and developed a number of ways of modelling and thus possibly explaining the time dependence of certain of the quantities examined. These models have been based on two basic approaches. The first is the *rheological model* for bone proposed by Sedlin in 1965. The second approach uses the ideas of *damage accumulation* as first proposed by theoretically by Kachanov in 1958 and the similar but experimentally derived approach of Caler and Carter (1989). The most important model is perhaps that I developed from a combination of the NTDF model of Caler and Carter and a simple scalar definition of damage (section 4.2.6.5 equations 4.019 to 4.025). This combination has extended the NTDF model from one that only predicts the failure stress in a tensile test to one that predicts the stress-strain response. This model although mimicking the stress-strain response reasonably well fails to model the increase in stiffness during the loading period, the task for which it was developed. However, a visco-elastic model (or that of Sedlin) is able to display such an increase. The application of both models to the knee and post-knee behaviour was also examined. In the cases where the examination, of the various quantities studied, used ideas derived from each model one approach was not found to be clearly superior in the accuracy of its modelling. However, in several cases differences were observed between the two approaches, these are discussed below.

The form of regression equations predicted by both the damage and Sedlin's models were able to explain over two thirds of the variation in the knee stress of bone tested at difference cross-head speeds. However, these forms of equations were less able to explain the variation in the results from the antler specimens. Analysis of the data provided a slight indication that the model built on the damage approach was more applicable to bone and that built on Sedlin's approach was more applicable to antler. In the case of the ultimate stress, it was found that the form of regression suggested by Sedlin's model was a better fit to the data than that suggested by the damage approach, for both materials. When the knee strain was considered Sedlin's model appears the better mimic of bone's behaviour, and the damage approach the better mimic of antler's behaviour. However, both approaches showed an inability to model the ultimate strain. In their initial forms both approaches model the materials as having a fluid like behaviour: flowing to infinite length. By referring to the damage approach I suggested two possible failure criteria: the maximum damage criterion and the maximum effective stress criterion. The first predicts that the ultimate strain will increase with testing rate and the second that it is independent of testing rate and has a constant value.[22] Comparison with the results showed that for antler the maximum ultimate damage criterion appears to be the appropriate one, whereas for bovine bone the result is less clear cut. This finding is reinforced by figures 4.026 and 4.027. It is possible to draw a vertical line that passes within one standard deviation of the mean failure points of bone.

---

[22]This is neglecting the effect of testing rate on material stiffness.

Such a line would describe the maximum effective stress criterion. It is also possible to draw a line that passes through the origin and within one standard deviation of the mean failure points of bone. This line would describe the maximum damage criterion. In the case of the antler specimens only the line associated with the maximum damage criterion can be so drawn. This finding is supported by the analysis in section 4.2.6.11 where the ultimate damage value is examined directly. The values for antler are high and consistent (these two facts are interrelated). In contrast the ultimate damage of the bovine bone specimens displays a considerable range of values.

Another aspect of antler's and bone's behaviour that was examined is the final slope of the tensile loading curve. The difference between this quantity for the two materials is shown diagrammatically in figures 4.025 and 4.026. It was found that this slope showed no statistically significant relationship to the rate at which the specimen was tested. This quantity was the least rate dependent of all of those examined. This finding is surprising for the bovine bone, for the impression gained during testing was of an increase in this slope at higher testing rates. This impression is reinforced by the slopes in figure 4.026. This anomaly may arise from the inability to obtain a justifiable value from bone specimens tested at higher rates due to a non uniform post-knee region.

The final quantity examined for rate dependence was the area under the loading curve, or the work input to the specimen up to the point of final failure. This quantity was found to be at least significantly dependent on testing rate for both materials. I suggested that this rate dependence could be modelled by both the damage approach and Sedlin's model. It was shown that the rate dependence of this quantity need not be contradictory to the maximum effective stress failure criterion. This observation accords with the idea that damage takes time to accumulate. The more quickly the ultimate damage level is reached the more energy the process requires and consumes.[23] The balance of energy required to that consumed has not been determined at this stage.

From an overview of the results in this chapter it appears that Sedlin's model is able to mimic the behaviour of bone and antler up to and including the knee region, while that of damage accumulation and the maximum damage criterion models the post-knee region. Therefore I propose that a new rheological model could be constructed which combined these approaches. This combination is based on a number of related observations on the two original approaches. Some of which are listed here:

a) Sedlin's model is a visco-elastic model that has been adapted by the addition of a plastic element.

---

[23]Another measure of work that results from a combination of the area under the curve and the concept of an effective stress is commented on in chapter 10.

b) No discrimination between an elastic-plastic or an elastic-damage material can be made on evidence from the loading curves alone.

c) To discriminate between elastic-plastic and elastic-damage materials unloading information is also required.

d) From the evidence of figure 1.010 and the resilience tests described in chapter 7, the post-knee unloading behaviour of bone and antler appear more like those of a damage material than a plastic one.[24]

e) The use of a plastic element in Sedlin's model did not introduce an ultimate strain criterion only an ultimate stress level.

f) To enable the concept of damage to model the behaviour of bone the idea of rate dependence was introduced. This is a departure from the ideas as set out in section 2.3.3.7 where the idealised damage (and idealised yield) was visualised as occurring a specific value of stress.

g) The amount of damage can be expressed in terms of effective stress of effective area reduction.

The basis of the new rheological model proposed here is to replace the plastic element in Sedlin's model with a *failure element*. The failure of this element would result in the modelling of the knee region (point b). However, this would not provide a failure criterion, nor would it model the unloading behaviour. If only one damage element was used this would also result in a shape knee. To overcome these discrepancies between the model and reality, the failure element has been combined with a spring and dashpot to form a *time dependent damage body* (figure 4.027a). To obtain a more progressive response a series of such bodies is proposed. For the purposes of representation only three such elements are shown in figure 4.027b. It is assumed that the whole damage body fails, and can thus be removed from the model, when the load on the failure element reaches a set level. This level (signified by D and a number) is not the same for each element. If it was (assuming the springs and dashpots are the same) the elements would all fail at the same time. The effect of placing the damage element in parallel with a dashpot is to introduce time dependence to the rate at which damage is accumulated. The faster the element is loaded the smaller is the proportion of the load transferred through the failure element. Placing the failure element in series with a spring also defines the elongation at which they fail, due the springs linear relationship of load and extension.[25]

The overall extension of the solid will depend in the relative stiffnesses of spring 1 and the damage bodies at the rate in question. (In the same way that the knee strain predicted

---

[24]In section 3.2.4.1 an adaptation of Sedlin's model proposed by Piekarski to 'allow for the possibility that in cyclic loading some reversible plastic deformation can occur' was introduced.

[25]If it is assumed that the same failure elements are used in models of antler and bone, then the use of springs of lower stiffness in the damage bodies of the antler would result in a higher failure strain and a more curved loading response as in the real material.

by Sedlin's model depends on rate.) Clearly in the model proposed here, as in Sedlin's model, the reduction in stiffness resulting in the knee region can be modelled. However, unlike Sedlin's model but like the damage approach and similar to real bone this reduction in stiffness is permanent, due to the removal of the failed damage bodies. Similarly, unlike Sedlin's model but like the damage approach and real bone, this model will return to its original length on reloading. The dashpot elements of the proposed model will produce a hysteresis loop in a loading-unloading test. Such behaviour is exhibited by a visco-elastic material, antler, bone and Sedlin's model but not a pure damage material. As more damage elements fail the load applied to the other elements will increase thus their extension under the same externally applied load will be greater. This may account for the increased width of the hysteresis loop in the post-knee and the deformation noted in figure 1.011. The delayed recovery exhibited by this model and by the natural materials may explain the observation of a high initial stiffness on reloading: the stress-strain resonance in the initial sections of the re-loading curve is due to a combination of that test and delayed recovery from the previous test.

The final point listed above refers to the relationship of damage to effective stress. In the model presented here a similar relationship is quite obvious. The removal of failed elements is equivalent to the reduction in effective area associated with the idea of damage accumulation. As in the case of the visco-elastic models described previously and the concept of effective area, the failure of the damage elements in the model should not be equated to the failure of structures within the real material; the model is of behaviour only.[26] However, equating the failure of elements with the effective stress is a useful tool in visualising the final failure process. I noted above that when a damage body fails the load placed on the others is increased. When this occurs the other elements will extend (due to the dashpots this will not be instantaneous), this action can result in two possibilities: first all the elements can sustain this extra load. In this case for further damage to occur the externally applied load (or deformation) has to be increased. This will be referred to as a *stable damage increment.* Second, the redistribution of load results in another element failing. This will be referred to as an *unstable damage increment.* This second scenario will result in the further extension of the specimen without any increase in the applied load. When the load due to the second failure is redistributed then the two possibilities are available again. Final failure will occur when the last damage body fails. The two possibilities suggested above imply this final failure may be reached by two routes: progressive failure of the elements or a catastrophic chain

---

[26]It is tempting to suggest that by using several sets of damage bodies in series the effect of failures at different points along the specimen could be modelled. Such a graphical approach has parallels with the use of a finite element mesh. Hayhurst *et al.* (1984) describe such a mesh: when the damage level in a mesh element surpassed a predetermined value it was effectively removed from the mesh. By this method they modelled creep crack propagation.

reaction of failures. Clearly mechanical response in the knee and post-knee region of the model proposed in figure 4.027b depends on the distribution of failure loads between the failure eliminates. Very simplistically, if there is little difference between the values of failure load of the different failure elements then the failure process is more likely to be unstable. However, if the difference between the failure loads is large then the material is likely to be more stable.[27]

Examination of the tensile stress-strain responses of antler and bone especially the slope of the post-knee region suggests that the process of stable damage increments dominates in antler but that the unstable damage process dominates in bone. I proposed such instability or 'inertia' in the damage processes of bone as the reason for the inflection in the post-knee region of the loading curve of bovine bone at high rates. The cause of this inflection can be visualised as an initially unstable damage process resulting in the extension and consequent drop in load. The load decreases until the damage process reverts to a more stable one. In some cases a reduction in the applied load was observed just prior to failure of the bovine bone specimen. This observation is also in harmony with the idea of an unstable damage process.

Considering the evidence produced thus far I suggest that the time-dependent damage model proposed in figure 4.027 combines the advantages of Sedlin's rheological model and the damage approach while avoiding their disadvantages. This new model appears to be able to mimic all the aspects of the behaviour of antler and bone examined so far.

In the derivation of his model Sedlin used creep tests. I examine the behaviour of antler and bone under a creep loading in the next section. The model I have proposed will be re-examined in the light of the results of those tests. The creep tests may also provide some information on the way damage is accumulated is accumulated: are the processes in antler and bone stable or unstable?

---

[27]Clearly the number of elements involved effects the nature of the relationship of the failure stresses. Only a few elements have been shown in figure 4.027 perhaps in a mathematical representation an integral representation could be used for an infinite number of such bodies. In a previous footnote it was suggested that using springs of different stiffnesses in the damage bodies may assist in modelling the difference between bone and antler. Due to the load-extension relationship of the springs this would also affect the distribution of the failure loads.

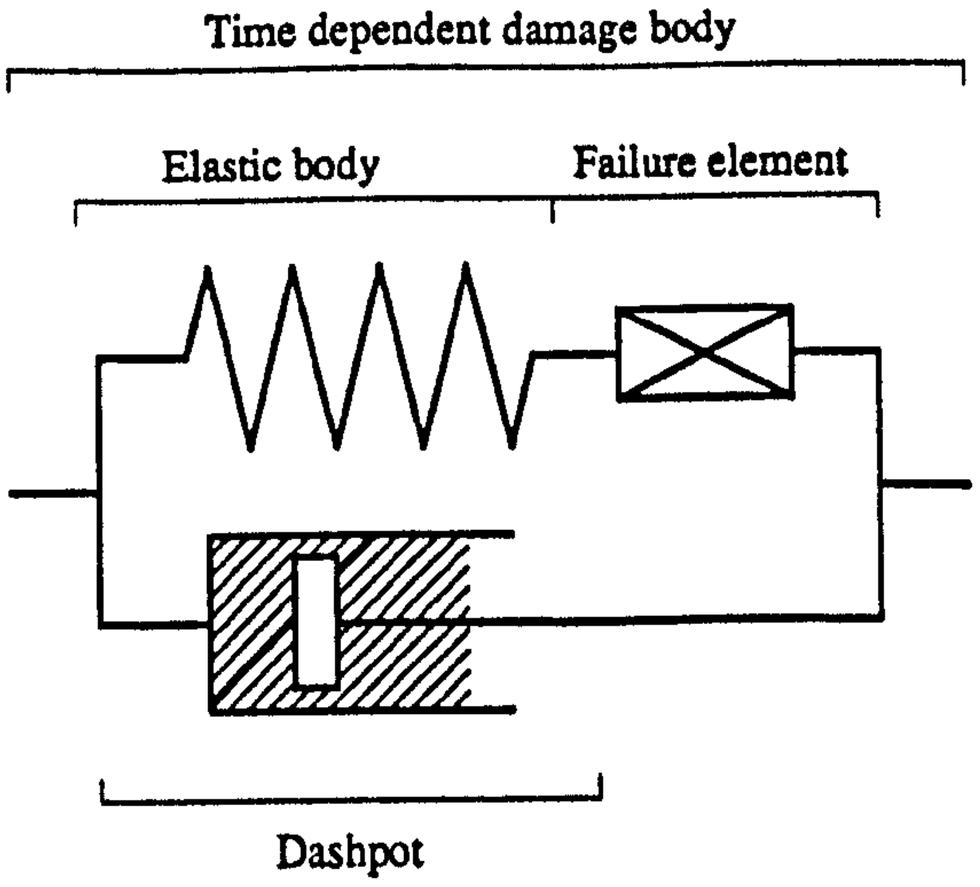

a) Proposed model of time dependent damage body

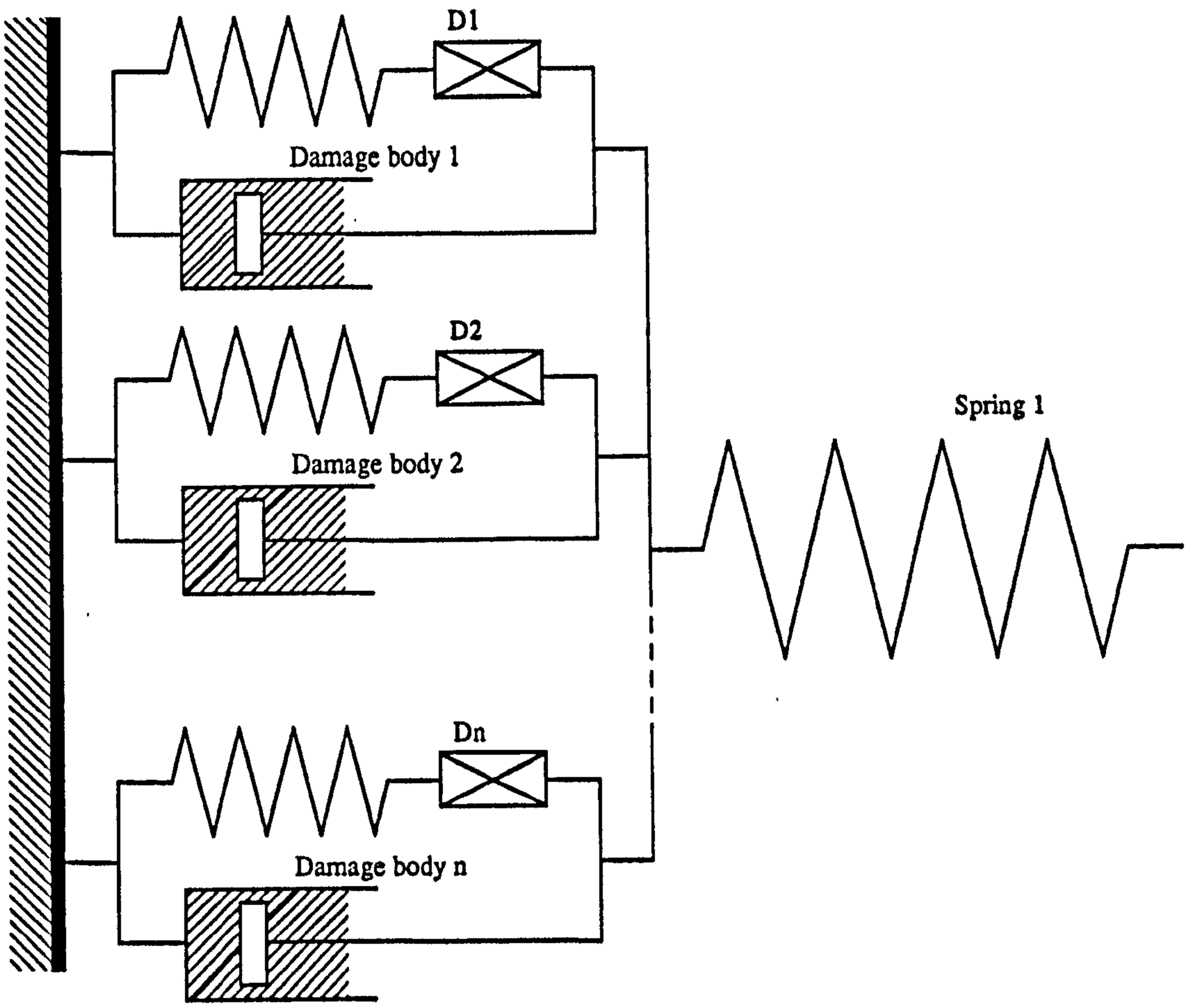

b) Proposed time-dependent damage model for bone and antler

Figure 4.027

Proposed time-dependent damage model for bone

4.3. TIME-DEPENDENT BEHAVIOUR: CREEP-RUPTURE TESTS

The work described here was conducted after the tests described in the paper by Mauch, Currey and myself (1992). That paper is presented in appendix 6. One of the aims was to improve on the technique used for those tests and thus obtain more data from each specimen. It was hoped that these improved tests would answer some of the questions raised by Mauch *et al.* The main differences in the experimental technique followed here is use of an environmental chamber, and the attachment of an extensometer to the specimen so that strain was monitored throughout the test.[28]

The creep experiments will be described, then their results analysed using the approaches and ideas outlined in the previous chapters. I shall then try to relate the results to the previously described tensile tests. As a result of the limited availability of antlers, the creep tests of antler were conducted on specimens from reindeer, whereas material from red deer antlers was used in all the other types of tests conducted on antler. However, the work presented in this thesis can be considered in conjunction with the works by Mauch *et al.* (1992) and Currey (1989). If this is done data from tensile and creep tests of antler specimens from both species are available. In both sets of tests (tensile and creep) I used bovine bone from the mid-diaphysis of the femora of young animals, about one to one and half years old, thus enabling direct comparisons to be made.

4.3.1. EXPERIMENTAL DESIGN

One of the aims of this set of experiments was to obtain data that could be fitted to Caler and Carter's NTDF model (equation 3.035). This simply requires values of, creep stress, time-to-rupture and some measure of normalising stiffness for each specimen. I intended to use the stiffness of the specimen measured, by way of an extensometer, during the loading period of the tests as the normalising factor. Thus for the first set of specimen tested (antler) the stiffness was not measured in three-point-bending. With hindsight this was an unfortunate omission from the test procedure. As the combination of a higher loading rate (8.33×10^{-4} m s^{-1}), the relatively slow data acquisition rate of about 37 Hz and the r shaped curve of the stress-strain response of antler, resulted in some of these stiffnesses being indeterminable due to lack of data points. Also the design of the test equipment has the effect of softening the test machine (the possible effects of which have already been explained at some length). This

---

[28]It was the requirement of a system to record stress-strain-time data that resulted in the construction of the AJS/BBC data collection system (see appendix 1).

oversight was rectified in the case of the bovine bone. To obtain more information on the factors affecting the creep behaviour of bone and antler the calcium content was determined for each specimen, by the technique explained in appendix 3.

4.3.2. TEST MATERIAL

The materials from which the test specimens were manufactured are listed in table 4.008. The specimens manufactured from the bones described in table 4.008 were used exclusively for creep testing. Data for some specimens are unavailable. The main reasons for this are the rejection of specimens before commencement of the tests due to poor quality, failure of the equipment or my poor use of it. The last categories include such things as wrong cross-head speed, poor clamping of the specimen and so on. No data were rejected because it did not fit the model that was applied to it.

Bone type	Comments	Identification numbers (Data used)	Data Sets
Reindeer antler	Naturally cast from a male of unknown age, (the size of antler (0.76 m) indicates at least several years old). Stored in laboratory conditions.	30/08/90/01 - 30/08/90/89 (36)	CA1
Femur	Bovine femur, from an 18 month old animal. Stored in freezer for four weeks before sectioning.	10/01/91/01 - 10/01/91/39 (33)	CB1

Table 4.008

Source, storage and usage test material

4.2.3. SPECIMEN PREPARATION FOR THE CREEP-RUPTURE TESTS

All the specimens were prepared in a similar way to the tensile specimens described in appendix 2. However, there are a number of differences: First, a datum corner was not employed (as it was in most of the later tests). Second, the antler specimens were not tested in three-point-bending. The bovine specimens were tested in bending to a load approaching 2 N using a cross-head speed of 8.33×10^{-6} m s^{-1}. The machine deflection during these tests was taken into account (using the method reported in appendix 2). The specimens were machined into the waisted shape similar to that shown in figure 4.001. The nominal width used was 4 mm.

4.3.4. SPECIMEN TESTING: EQUIPMENT AND METHODS

The test equipment used was adapted from that I built for the experiments described in Mauch *et al.* (1992). The basic arrangement is shown in figure 4.028. The test equipment consisted of the addition of a lever system to the Instron 1122 testing machine. This lever system permitted the application of a constant load to the specimen, by supporting a predetermined mass. The force on the specimen was measured directly using the Instron's load cell, thus removing any problems in its calculation due to the mass of the loading system itself or friction in the bearings. The main adaptations of the equipment between its use by Mauch and in these tests were:

a) The stiffness of the loading arm was increased (and the wire supporting the mass changed to a metal rod). This enabled a higher loading speed to be used. The arm of the testing rig and the wire supporting the mass act like a spring, and the sudden movement (or deceleration) of the cross-head sets up oscillations in the applied load (due to the inertia of the mass used to apply this load). Such perturbations in the load level are undesirable. It was found that they were reduced to an acceptable level with this stiffening at a maximum cross-head speed of 8.33×10^{-4} m s^{-1} [50 mm min^{-1}].

b) Enclosing the specimen and jaws within a tank, containing water that was maintained at a pre-set temperature. Thus regulating two factors that can effect the mechanical response of bone: humidity and temperature (see section 1.4.4.2). The use of such a tank required the manufacture of some new jaws. These were of a simple design, basically two roughened plates, forming a sandwich around the specimen. The closing force was applied by two M6 bolts. I constructed these jaws from aluminium, brass and stainless steel. (The jaws were painted mat black to limit the amount of corrosion and reduce stray light during photography.) The tank was constructed of perspex™ (PMMA) with a glass front. The sides and base of the tank were painted matt black to aid photography. Water was pumped to the tank through flexible tubing. The temperature of the feeder tank was regulated such that the temperature in the test tank was maintained to within one degree of 37°C. The water used was obtained from the normal piped supply and did not have physiological salts added. To reduce possible bacterial or fungal growth in the water a small amount of thymol was added. (This tank and jaw arrangement were adapted for use during tensile tests where it was fixed to the base of the machine rather than the creep rig.) A diagram of these jaws has already been given in figure 4.002.

c) The extension and thus strain exhibited by the specimen was measured using an Instron extensometer with a nominal gauge length of 10 mm. Two different extensometers were used, one that could measure a 10% length increase (for bone specimens) and one that could measure a 50% increase (for the antler specimens). These extensometers were waterproofed as described in section 4.2.4.

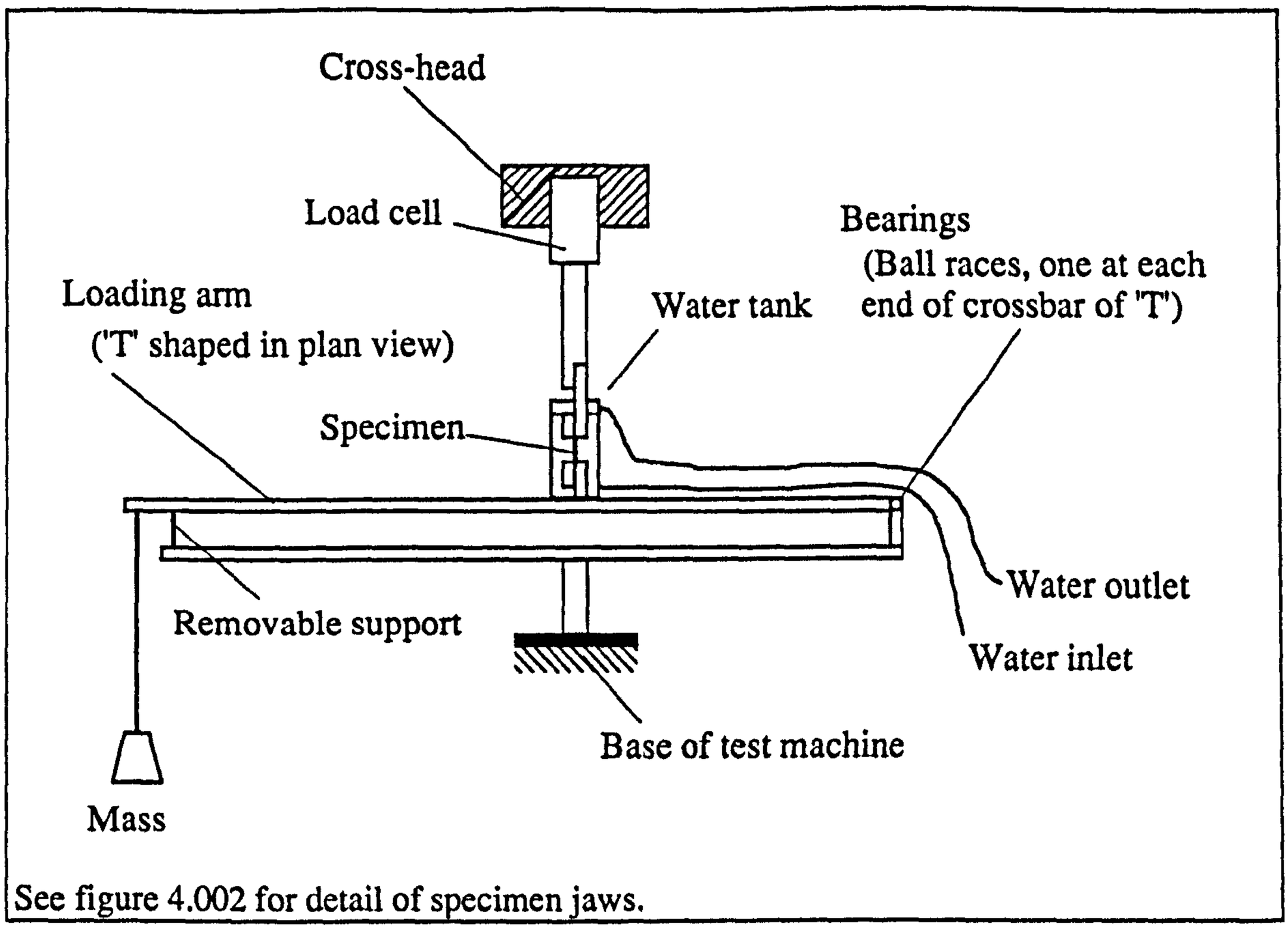

Figure 4.028

The basic diagram of the creep rig used for the testing of antler and bone specimens

Stress (load), strain and time data were recorded using the AJS/BBC data collection system described in appendix 1. The sampling rate was reduced at various times during the test. The main reason for this was the limited memory storage available in the data collection system. Also the rate at which changes occur generally decreases with time.

The tests were conducted in the following way. First the specimen, with the extensometer attached was placed in the jaws as in the tensile test. The data collection system was started. Then the cross-head was set in motion at a speed of 8.33×10^{-4} m s^{-1}. The load was monitored by way of the data collation system's display. When the load had become constant and a sufficient gap was observed between the loading arm and the support the cross-head was stopped and the support removed. The test then continued until the specimen failed (unless the data storage system became full or prolonging the test was not considered worthwhile). (Clearly for those tests that were discontinued no rupture data is available.) The same procedure was used for both materials.

4.3.5. RESULTS OBTAINED FROM CREEP-RUPTURE TESTS ON BONE AND ANTLER (DATA SETS CA1, CA2, CB1 AND CB2)

In this section the results obtained from the creep tests performed on specimens of bone and antler will be described and analysed. Information on how to obtain the data sets used in this analysis is given in appendix 4.

4.3.5.1. THE MECHANICAL QUANTITIES STUDIED

In section 2.3 some of the parts of, and specific points on, a creep rupture curve were labelled (figure 2.009). However, some of those values are difficult to determine or are not required in the normal analysis of creep-rupture curves, for example the points of intersection of the primary and secondary stages, or the secondary and tertiary stages, of creep. Similarly other quantities not given in figure 2.009 can be of interest. In figure 4.029, the same curve is repeated showing the derivation of various quantities. The quantities that have been measured for specimens of both materials tested and the nomenclature I will use is listed below.

a) E_b, *Material stiffness in three-point-bending:* this was determined for the specimens of bovine bone, before they were reduced in their central section.

b) E_t, *Material stiffness in tension:* this was determined from fitting a regression line to the stress-strain data obtained during the loading period of the test.

c) σ_0, *Creep stress:* the load exerted on the specimen during the test normalised by the specimens initial cross-section, quoted in MPa. The value of the load used was recorded by the load cell, thus avoiding errors due to friction in the bearings and so on. As the area used is the initial one this can be interpreted as both the initial nominal stress and the initial true stress.

d) t_R, *Time-to-rupture:* calculated by subtracting the time at which the loading started from the time associated with the last data point before the specimen failed.

e) ε_0, *Instantaneous strain:* this value of strain used as an approximation to the instantaneous strain, was that associated with first occurrence of the creep stress.

f) ε_1^*, *Steady state instantaneous strain:* this is the value of strain resulting from the substitution of $t = 0$ into the regression equation relating strain to time during the secondary creep stage.

g) ε_3, *Steady state rupture strain:* this value of strain when $t = t_R$ is substituted into the regression equation relating strain to time during the secondary creep stage.

h) ε_R, *Rupture strain:* this is greatest value of strain obtained before failure.

i) $\varepsilon_{0\rightarrow R}$, *Creep strain:* this is an estimate of the total time dependent strain, calculated from $\varepsilon_R - \varepsilon_0$.

j) $\varepsilon_{1\bullet\rightarrow 3}$, *Steady state creep strain:* this is time dependent strain that would be attained by the specimen if it maintained its minimum creep rate for the full duration of the test.

k) $\varepsilon_{1\bullet\rightarrow R}$, *Approximate creep strain:* this is an estimate of the time dependent strain that would be attained by the specimen when the steady state approximation is used in the primary region only.

l) $\dot{\varepsilon}_{0\rightarrow R}$, *Average creep rate:* the total time dependent strain, divided by the time-to-rupture. This quantity is shown in figure 4.029 as the slope of the line of long dashes. Due to the size of the numbers that are involved all creep rates are expressed in units of micro-strain per second, $\mu\varepsilon\ s^{-1}$. (Thus the average creep rate values given are derived using the calculation $\dot{\varepsilon}_{0\rightarrow R} = (\varepsilon_R - \varepsilon_0) \times 10^6 / t_R$.)

m) $\dot{\varepsilon}_{1\bullet\rightarrow 3}$, *Steady state creep rate:* this is creep rate during the secondary region of the creep curve. This is shown in figure 4.029 by the thin solid line. The value of this quantity was obtained by fitting a regression line to the discrete data points.

n) $\dot{\varepsilon}_{1\bullet\rightarrow R}$, *Approximate creep rate:* the average creep rate if the primary region is approximated using the steady state line. This is the slope of the line consisting of short dashes in figure 4.029.

o) $\dot{\varepsilon}_{total}$, *Total strain rate:* this is the value of the total strain accumulated during the test divided by the time-to-rupture, ε_R / t_R.

p) Ca, *Calcium content:* this was determined for material removed from the specimen after testing by the method described in appendix 3.

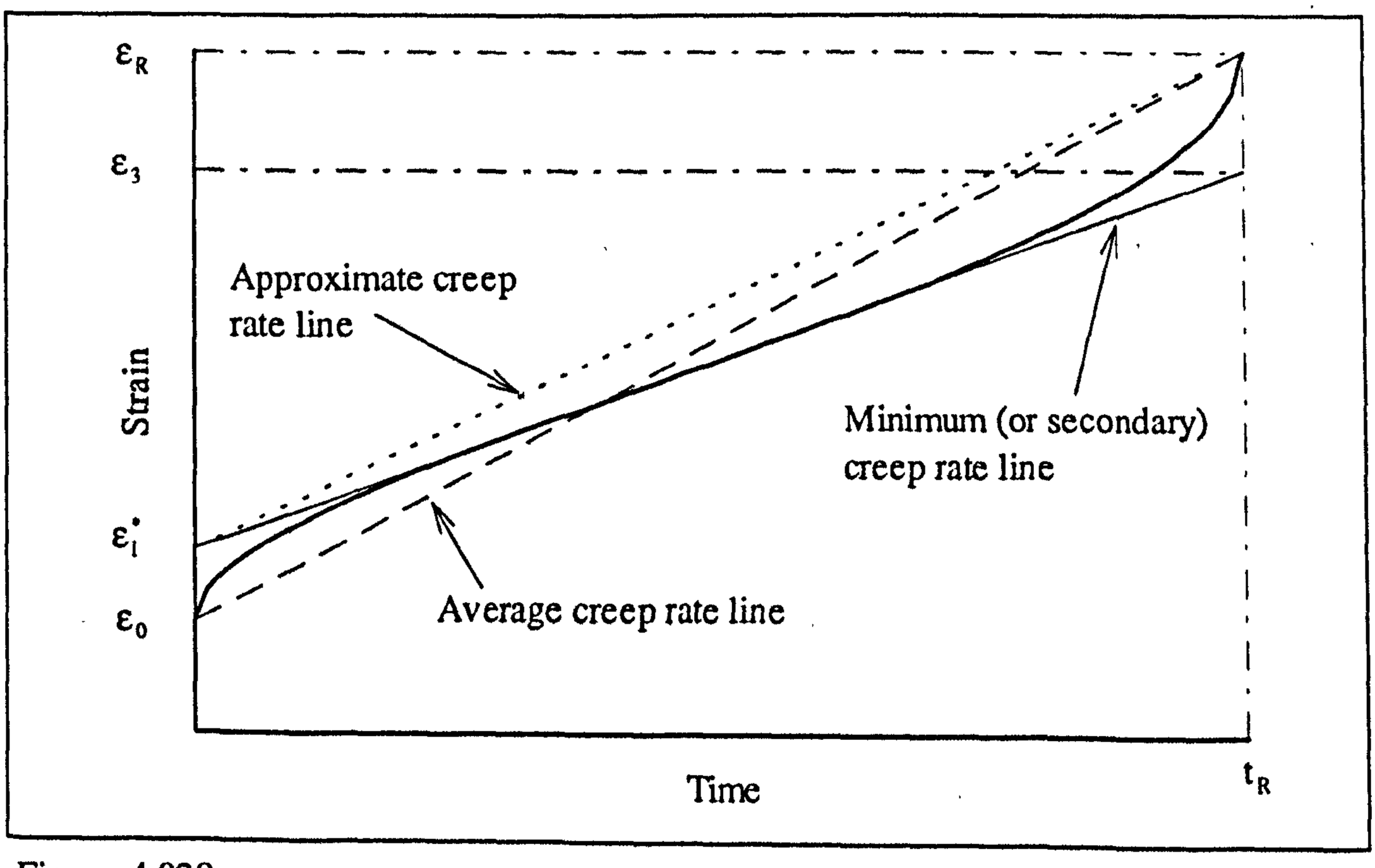

Figure 4.029

An idealised creep-rupture curve and accompanying nomenclature

The values obtained for the various quantities listed above have been examined using regression analysis. The results have been divided into two main data sets, one containing the results from the tests on antler, the other those on bone. These two data sets are referred to as CA1 for the antler data and CB1 for the bone. From each of these data sets another smaller one has been derived. These smaller sets (CA2 and CB2) contain those data from specimens for which a value of (almost) all the variables are available. Thus using these *core data* comparisons between different explanatory variables can be made based on the results from the same specimens. Along with those having incomplete data sets, specimens were excluded from this reduced data set if they failed within 20 seconds, $t_R < 20$. The choice of this limit was based on a number of factors. First, recommendations for creep testing of plastics, for example BS 4618 (1970) which states

> The load should be applied as smoothly and as quickly as possible. The strain response immediately afterwards is affected by the loading path, and in the absence of complex evaluation procedures the earliest strain measurements should be ignored. If the period required to apply the load lasts for a time t_1, any strain measurements taken before $10t_1$ (measured from the start of loading) should be ignored.

In many cases the loading period was approximately half a second. However, due to the design of the loading rig, more compliant specimens took longer to load (in some cases several seconds). Thus if data such as the steady state creep rate was to be used the total time of the test would need to be more than ten times the loading period. Also, for a number of specimens that entered or approached the knee region of the tensile curve during the loading period, the strain-time response did not exhibit much dependence on the ending of the loading phase. Thus the stress-strain-time relationships of these specimens displayed little apparent difference to a tensile test. (This observation fits the model that I developed to link creep and tensile tests, section 3.3.3.2. This topic will be returned to later.) When the data is plotted all the data points will be shown (data sets CA1 and CB1). The data set the points belong to will be indicated by the symbols used.

In figures 4.030 to 4.033 I have produced graphs of the measured value of strain against time. These were produced directly from the raw data. (The time values are those recorded. The loading occurred at $t > 0$ as the equipment was started at different times. This difference was accounted for when the time-to-rupture and other time quantities were calculated.) There are some clear differences between the shapes of the curves, and the relative amounts of primary, secondary and tertiary creep. This is an important observation that will be discussed at various points in the following sections.

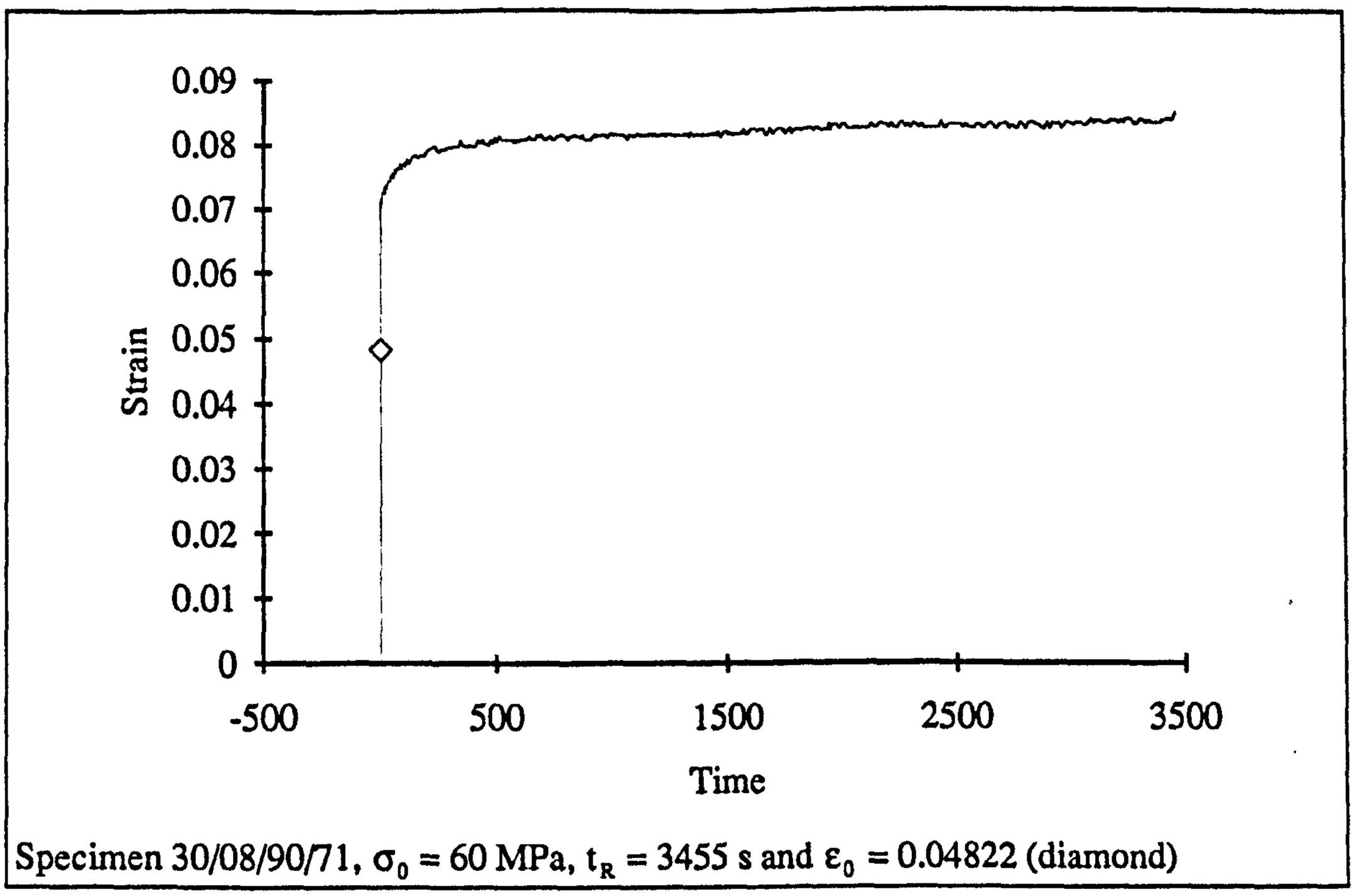

Specimen 30/08/90/71, $\sigma_0 = 60$ MPa, $t_R = 3455$ s and $\varepsilon_0 = 0.04822$ (diamond)

Figure 4.030

Creep curve, strain-time for a specimen of reindeer antler

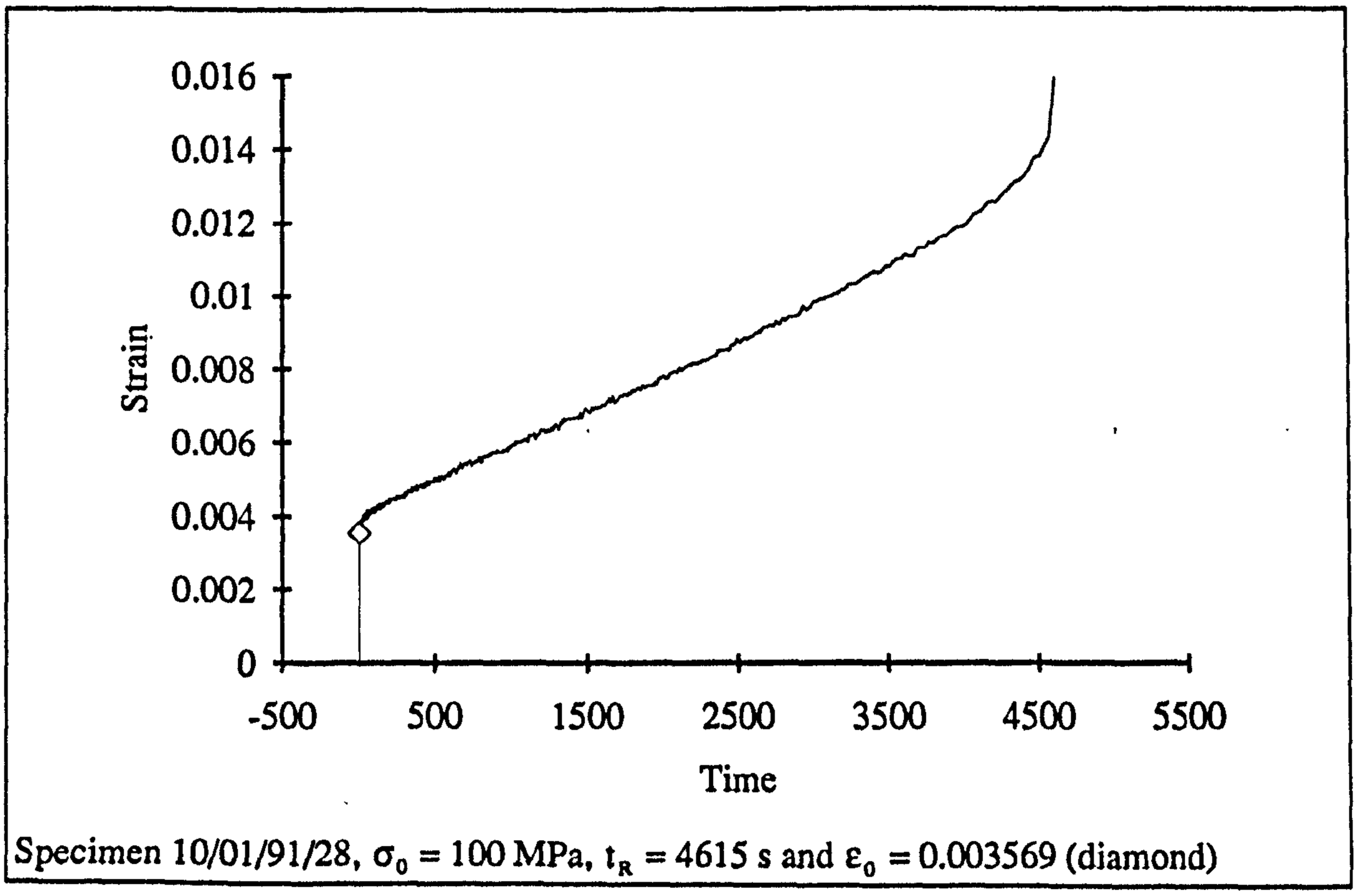

Specimen 10/01/91/28, $\sigma_0 = 100$ MPa, $t_R = 4615$ s and $\varepsilon_0 = 0.003569$ (diamond)

Figure 4.031

Creep curve, strain-time for a specimen of bovine femoral bone

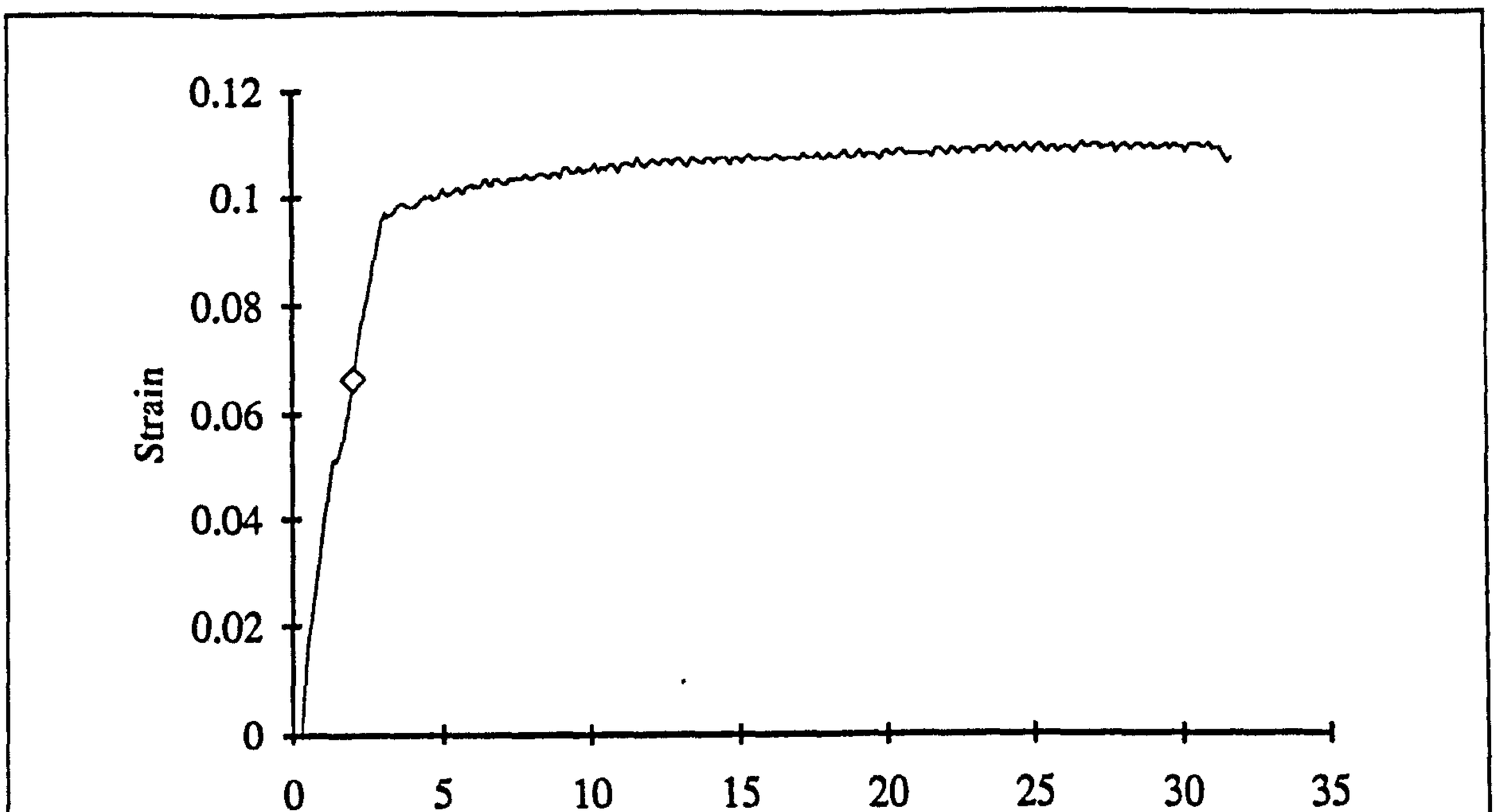

Specimen 30/08/90/67, $\sigma_0 = 62$ MPa, $t_R = 31.5$ s and $\varepsilon_0 = 0.066390$ (diamond)

Figure 4.032

Creep curve, strain-time for a specimen of reindeer antler

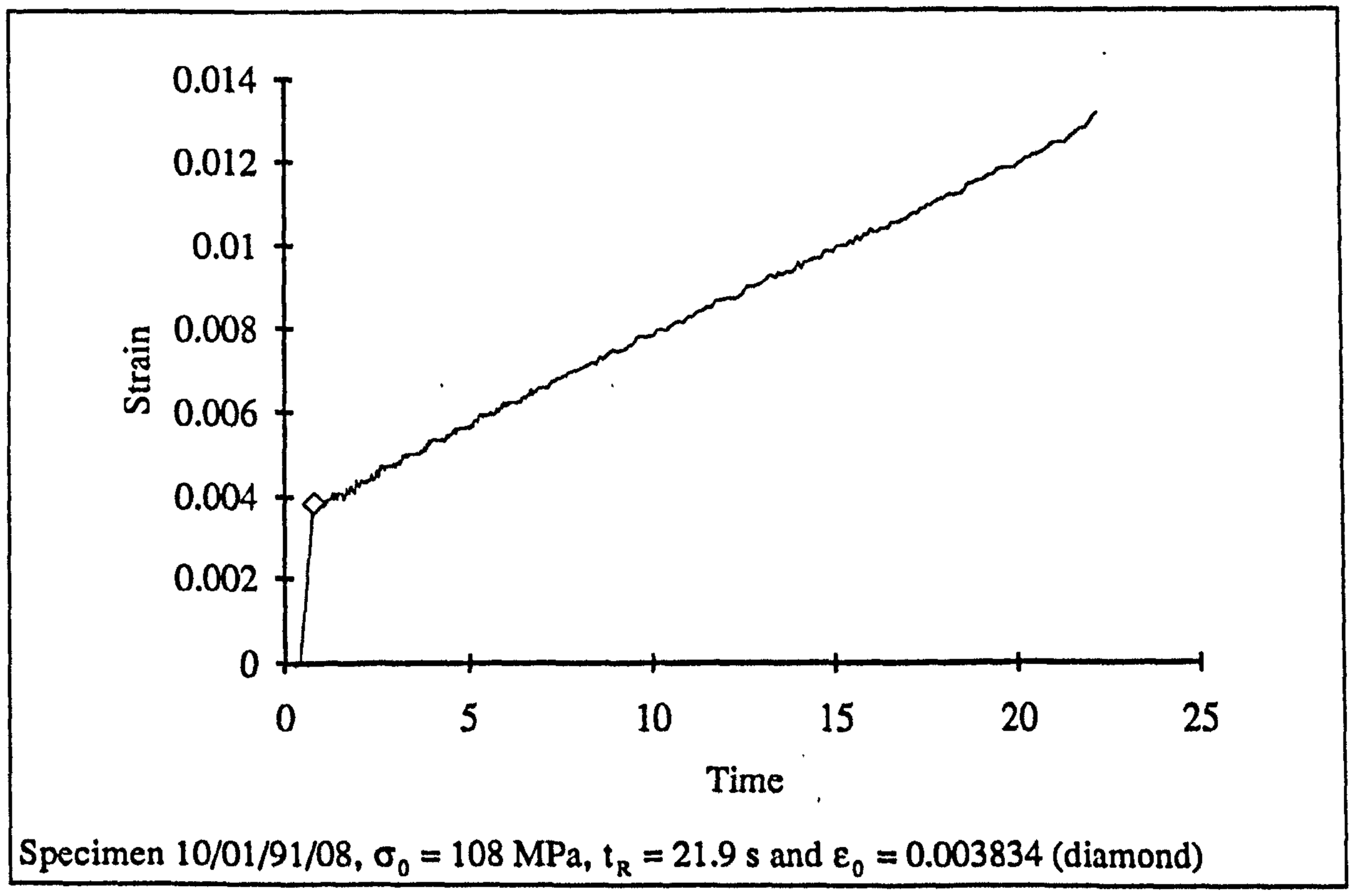

Specimen 10/01/91/08, $\sigma_0 = 108$ MPa, $t_R = 21.9$ s and $\varepsilon_0 = 0.003834$ (diamond)

Figure 4.033

Creep curve, strain-time for a specimen of bovine femoral bone

4.3.6. CREEP-TESTS: A VISCO-ELASTIC APPROACH

One of the limitations of visco-elastic models that was outlined above is their inability to model failure. However, it may be possible to use such an approach for the initial and secondary regions of the creep curves obtained in this study. In chapter 2 the equation of the creep compliance of a three element solid was given (2.023), and in appendix 5 the more general equation is presented. Both of these equations are repeated below. First for the three parameter solid

$$J(t) = \frac{1}{q_0}\left[1 + \frac{q_1 - p_1 q_0}{q_1} e^{(-q_0 t)/q_1}\right] \qquad (4.045)$$

and then the more general case

$$J(t) = \frac{\varepsilon(t)}{\sigma_0} = C_0 + C_1 e^{-\alpha_1 t} + C_2 e^{-\alpha_2 t} + \ldots \qquad (4.046)$$

One method of finding the value of the coefficients in equation 4.046 depends on the compliance tending towards a constant value. (As it should for a visco-elastic solid.) For in that case as t becomes large the equation becomes

$$J(t) \cong \frac{1}{q_0} \qquad (4.047)$$

When the value of the creep compliance at this time is estimated the equation can be re-expressed as

$$1 - J(t)\, q_0 = \frac{q_1 - p_1 q_0}{q_1} e^{(-q_0 t)/q_1} \qquad (4.098)$$

The left hand side of this equation is known. As a result of this the equation can be solved, by plotting the logarithm of the left hand side against time, t. The gradient would be the exponent and so on. This approach can not be used for the data I obtained, because these specimens did not show a trend towards a constant length as would be expected for a visco-elastic solid, but a constant creep rate as would be expected for a visco-elastic fluid. Therefore fitting an equation for a visco-elastic solid to the data is not only problematical, but also valueless. From examination of the creep rates of both materials it appears that the bone specimens display a more fluid like behaviour than the antler ones, as shown in figure 4.030 to 4.033. It was noted in section 3.2.3 that in his study Currey (1965) did not load his specimen in the 'plastic-range'. On unloading his specimens they recovered most of their time dependent deformation. Thus Currey's test results are more in keeping with a visco-elastic solid than a visco-elastic fluid. This suggests that bone's behaviour is dependent on the applied stress: at low stresses solid and at high stresses fluid.

4.3.6.1. THE TRANSITION FROM A VISCO-ELASTIC SOLID TO A VISCO-ELASTIC FLUID LIKE MATERIAL: RELATIONSHIP TO THE DAMAGE APPROACH

The suggestion of two types of behaviour, made above, is supported by the work of Fondrk *et al.* (1988) (section 3.3.3.1). These workers, although only using short term tests and reusing specimens, produced a value of a creep-threshold above which a constant creep rate was obtained and below which the creep rate was so low a constant extension could be assumed. I have already pointed out similarities between their paper and the damage approach. If this transition is considered as a change between a brittle (the solid region) and a ductile (the fluid region) behaviour, there are obvious comparisons between the behaviour of bone and the behaviour of metal as described by Kachanov (shown graphically in figure 2.011). At the higher values of creep stress the failure behaviour is ductile and at lower stresses it is a combination of ductile and brittle processes. It has already been suggested by Carter and Caler (1983) that data from tests on human bone fit the equation for the purely brittle behaviour, and I have pointed out that the form of the equation is the same as that for ductile behaviour. I also noted that published data on cyclic failure may also show such a transition (section 3.3.1 and figure 3.011). The modelling of a transition from a visco-elastic solid to a visco-elastic fluid at high stresses is the whole basis of Sedlin's rheological model for bone (figure 3.009). Unfortunately I have insufficient data from creep tests at low stresses to reproduce a very convincing experimental equivalent of Kachanov's plot for the materials tested here. However, the results for antler, shown below in figure 4.034, appear to show such a transformation. To obtain better evidence that such a transition occurs in the creep rupture behaviour, as well as in the nature of the creep behaviour, and that there are related, a larger number of long term (low creep stress) tests are needed. If the strain is recorded during such creep-rupture tests it is possible to examine the possible relationship between a Kachanov like brittle-ductile rupture transition and a visco-elastic like solid-fluid transition. Such an investigation could consolidate (or demolish) the argument proposed here.

4.3.7. CREEP-RUPTURE RESULTS: GENERAL CORRELATION APPROACHES

In this section I will produce the plots suggested in the work by Conway (1967), and listed in table 2.001. I will follow his recommendation on which variable to plot on the ordinate and abscissa axis, although in most cases the dependent variable is plotted on the abscissa axes. Regression equations were fitted to the antler and bovine bone data using the variables as they are plotted. This procedure is then repeated with the addition

of other variables that are assumed to have some normalising effects on the data. Where it is relevant I will refer to the damage approach to creep-rupture. A later section will deal with some of the aspects of damage not discussed in this section. In the following sections I also extend some of the analysis to explore relationships suggested by this initial study.

4.3.7.1. LOGARITHMS OF CREEP STRESS, $\ln(\sigma_0)$, AND TIME-TO-RUPTURE, $\ln(t_R)$

This is the first plot suggested by Conway (table 2.001). It is also the same plot as that presented (idealistically) in the work on creep rupture by Kachanov (figure 2.011). The data points in figure 4.034 show that there is a clear distinction between the stress needed to make a specimen of bovine femoral bone and one of reindeer antler rupture at the same time. The same observation was made for bovine ulnae and red deer antler by Mauch *et al.* (1992). As in that paper the relationship of $\ln(\sigma_0)$ to $\ln(t_R)$ that I have obtained for bovine bone is very weak and the would-be coefficient term is non-significant ($p = 0.081$ equation *d*). This situation is not much improved by the addition of other variables. The relationship of stress and time for the antler specimens (equation *a*) is stronger than that of bone and the would-be coefficient is highly significant ($p = 0.003$). The strength of the relationship for antler is improved by the addition of the stiffness in tension as an additional variable.

Figure 4.034 uses the same axes as that for the behaviour of metals given by Kachanov (figure 2.011). When these plots are compared, the results from the antler specimens appear to fit the two regions of behaviour commonly seen in metals and modelled in Kachanov's work. A transition appears to occur in the antler data at a time-to-rupture of about 400 seconds ($\ln(t_R) \cong 6$). Thus the use of a single regression line may be an over simplification of the situation. For metals the change in slope of such a plot signifies a change in the rupture process. This raises the question: could this change in the slope of the antler data signify a change in failure process? Could such a change be related to the idea of a creep threshold for bone suggested by Fondrk *et al.* (1988)? However, before these two approaches are equated too closely, it should be noted that the impression of a change in slope is very dependent on the point on the extreme right and the data relating to those points obtained from specimens that ruptured at times less than 20 seconds. If this suggestion that antler results arise from different rupture processes is correct the application of a model for combined brittle and ductile rupture could be more effective than the use of either, the brittle or the ductile, model individually.

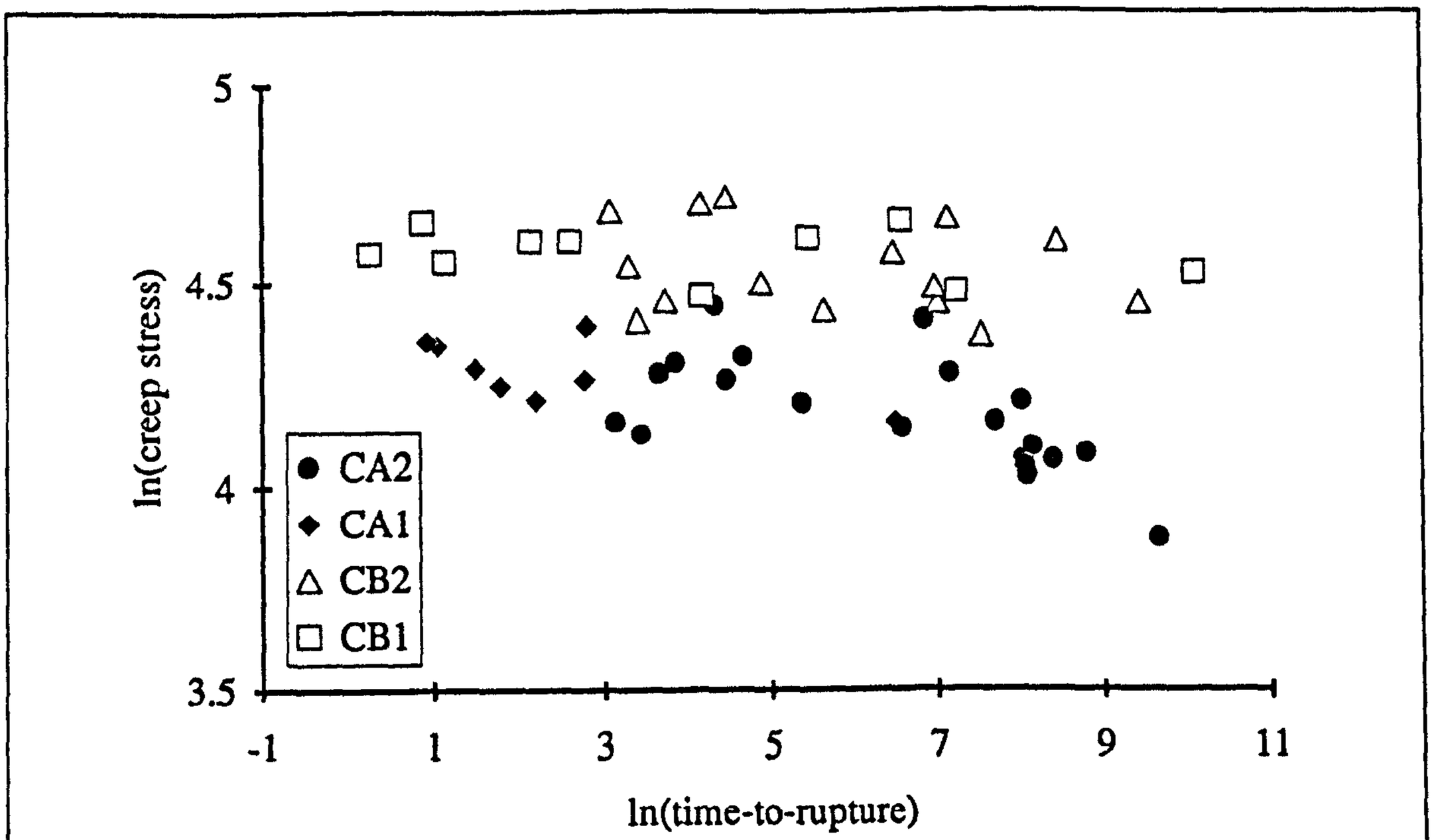

Units:

σ_0 Creep stress, MPa

t_R Time-to-rupture, s

Comments:

CA1 and CA2 are the data sets of antler results. CA2 is the core of data on which the regression analysis is conducted. The same arrangement holds for the bovine data sets CB1 and CB2.

Figure 4.034

The relationship of the creep stress and the time-to-rupture for reindeer antler and bovine femoral bone

For equation *a*, the relationship of time-to-rupture and creep stress, the would-be coefficient of stress I obtained from the antler specimens was -9.35. This value is lower than that obtained by Mauch *et al.* for specimens from the base or tip of a red deer antler (-14.9 and -21.0 respectively).

The predictive strength of the relationship of stress and time-to-rupture obtained for the bone specimens, equation *d*, (the equivalent for antler is equation *a*) is considerably weaker than that obtained by Caler and Carter (1989) for human bone as calculated by Mauch *et al.* (1992). (As is the predictive strength of the relationship obtained from the latter workers own tests on bovine ulna.) The coefficient of the stress term in equation *d* (-4.28) is very similar to that obtained by Mauch *et al.* (-4.2) for bovine bone, but lower than the recalculated value of Caler and Carter (-15.2). Both of the lower values are associated with non-significant stress variables.

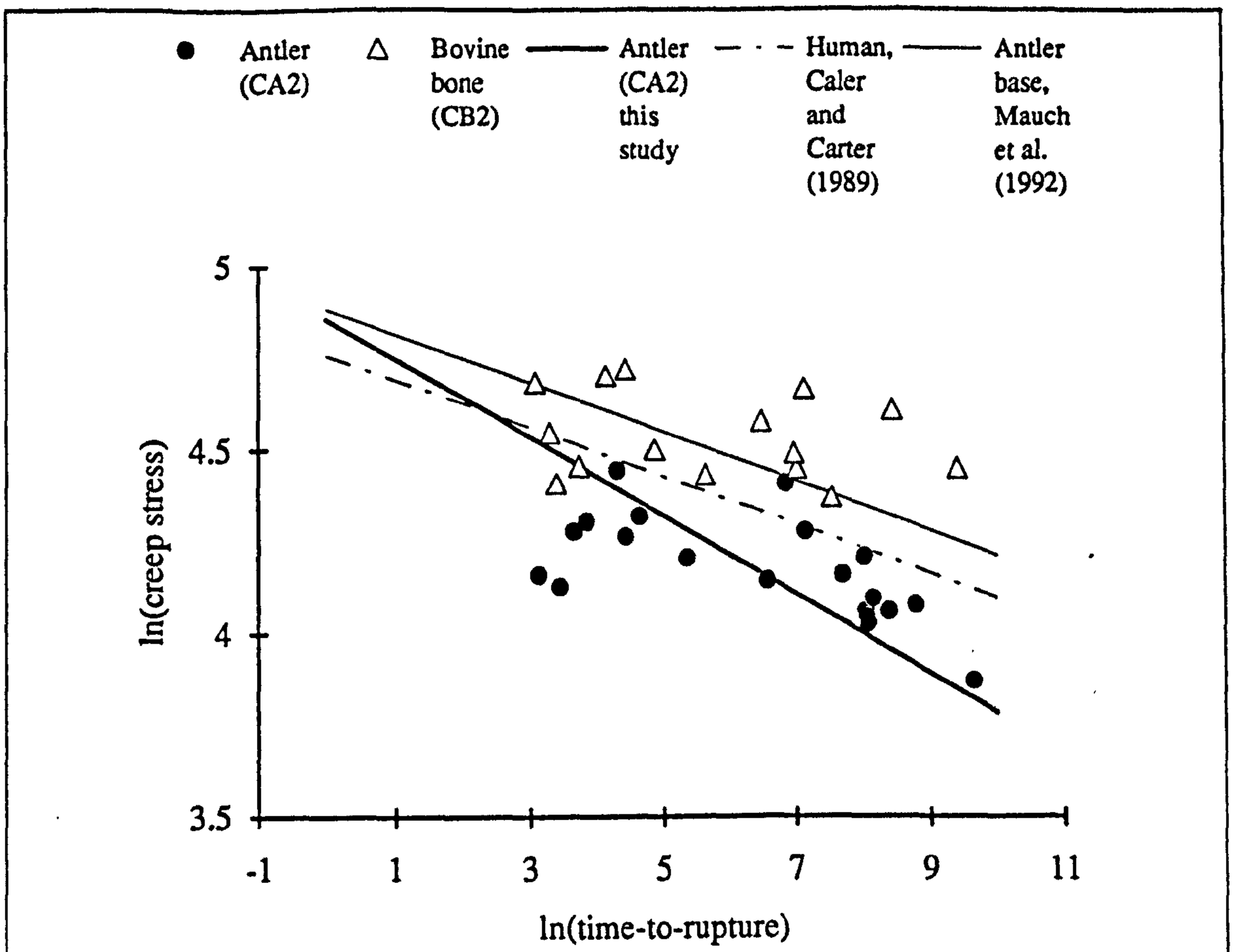

Units:

σ_0 Creep stress, MPa

t_R Time-to-rupture, s

Comments:

For full key see figure 4.034

Figure 4.035

The significant relationship of the creep stress and the time-to-rupture for antler and bovine bone, showing the regression equations obtained in this and other studies

A poor correlation between the logarithmic values of the creep stress and the time-to-rupture was observed in both materials (this was especially poor bovine bone). This implies that Carter and Caler's TDF model can not reasonably be applied to these results. The reason the relationship for the results given here (and those of Mauch *et al.*) are so poor compared to those of Caler and Carter's work is unknown. The significant regression equations quoted by Mauch *et al.* can be drawn on a plot of the data obtained in this thesis (figure 4.035). Figure 4.035 shows that the results I have obtained in this study are comparable to those obtained by other workers, even if the relationship between the variables is not as strong as that obtained by others.

The introduction of the NTDF model by Caler and Carter and the results of Mauch *et al.* suggest that the inclusion of an additional variable, such as E_b or E_t, should

improve the predictive power of the relationships. This is shown to be the case for the antler specimens but not for the bovine bone ones (table A9.019). (Although with the addition of the material stiffness in bending the lack of significance of the creep stress term is decreased.) The reason for this unexpectedly negative result is unknown. In both cases the use of calcium content as an additional variable had little effect.

4.3.7.2. CREEP STRESS, σ_0, AND TIME-TO-RUPTURE, $\ln(t_R)$

As in the case of the logged data, figure 4.036 shows that the stress needed to achieve the same time-to-rupture for these two materials is different. As would be expected the antler results, although no longer logged, show a stronger relationship between the two variables and the additional ones (see table A9.020). In most cases the strengths of the relationships are lower than the comparable one for the logged stress data.

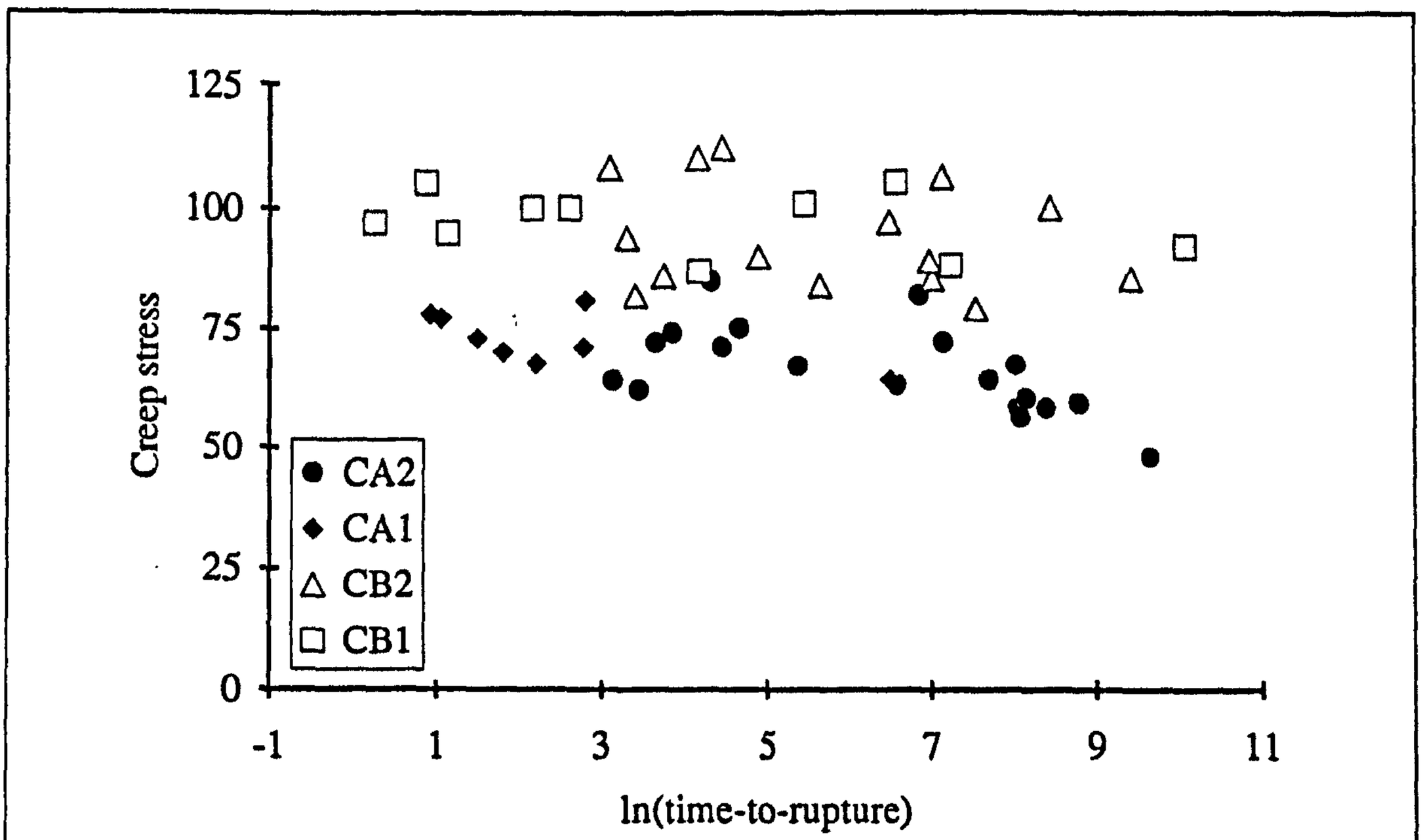

Units:

σ_0 Creep stress, MPa

t_R Time-to-rupture, s

Figure 4.036

Relationship of creep stress to time-to-rupture for reindeer deer antler and bovine femoral bone specimens

4.3.7.3. LOGARITHM OF STRESS AND LOGARITHM OF ELONGATION AT RUPTURE: PART 1, $\ln(\sigma_0)$ AND $\ln(\varepsilon_R)$

In this study I have used a number of different measures of elongation, or strain, at rupture. Some of these measures include the extension attained by the specimen during loading. While some only contain the extension gained after the load has been applied. Other measures are based on extrapolations of the strain-time data. This enables the removal of the effect of some regions of the curve; tertiary creep for example. All of these measures of strain are related to those shown in figure 4.029. In this case (part 1) I examine the effect of creep stress on the total extension attained by the specimens of bone and antler during the creep tests, ε_R.

When the values of rupture strain are used for the 'elongation at rupture' it is the bovine specimens that show the strongest relationship between the variables considered. The coefficients are almost ten times greater in the case of bone (equations *a* and *d*). The predictive power of these equations is also stronger in the case of the bovine bone specimens. This latter observation is true for both the core data (CA2 and CB2) and the full data sets (CA1 and CB1). It is interesting that in most cases both E_b and Ca have a detrimental effect on the predictive power of the relationship. The strongest predictive equations for each material (*b* and *f*) use the material stiffness measured during the test as a second variable. In both equations the stiffer the material is the smaller its predicted rupture strain is. This trend within the materials agrees with that seen between the materials.

There is a difference in the areas of the plot where the data points for each material are grouped. (The axes have be chosen so comparisons can be drawn with the other measures of elongation at rupture examined in the following sections.) The mean values of rupture strain are 0.07968 for the antler specimens and considerably less, 0.01063, for those of bovine bone.

The separation of the data for bone and antler (CB2 and CA2) into two groups can be examined by using one-way analysis of variance on each of the variables. This analysis was conduced on the logarithmic form of ε_R and σ_0, as plotted. The analysis shows that the separation is statistically very highly significant, in both cases $p < 0.001$. In the case of $\ln(\varepsilon_R)$ the value of F is 248.55.[29] (In the following sections these values are compared with those describing the separation of the materials when other measures of elongation at rupture are used.)

---

[29]This F value is compared with those obtained for other measures of 'elongation at rupture', using same number of specimens and thus degrees of freedom.

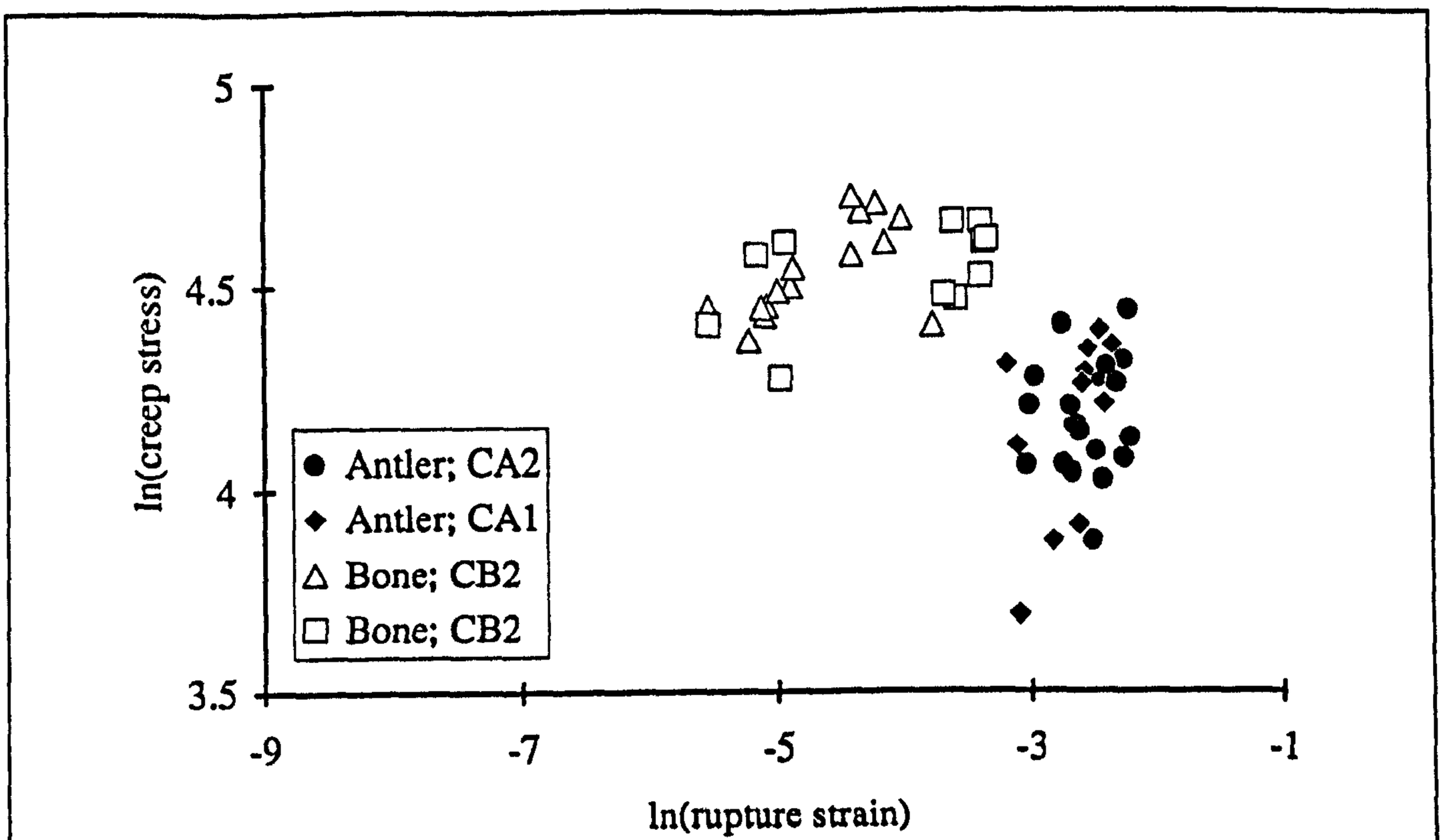

Units:

σ_0 Creep stress, MPa

ε_R Rupture strain, unitless

Figure 4.037

Relationship of the strain at rupture and the creep stress for antler and bone

Examination of the graph shows that the rejection of one point from data set CB2 would improve the strength of the relationship between $\ln(\sigma_0)$ and $\ln(\varepsilon_R)$. However, this point is not dissimilar from a number of others in the full data set, CB1, so I did not exclude it in the analysis.

4.3.7.4. LOGARITHM OF STRESS AND LOGARITHM OF ELONGATION AT RUPTURE: PART 2, $\ln(\sigma_0)$ AND $\ln(\varepsilon_{0\rightarrow R})$

One effect of using creep strain in place of the rupture strain is to reduce the separation of the results for antler and bovine bone. One-way analysis of variance still gives the difference between the logarithm of the elongation term for CA2 and CB2 as being very highly significant one, as $p < 0.001$. However, the value of F has now fallen to 88.74. The results for bone are more widely spread than those of antler. Those for antler while still being closely grouped, have been shifted towards those of bone. This is mainly due to antlers lower material stiffness and thus greater instantaneous strain. (This lower stiffness and greater strain, will result in a longer loading period that may exaggerate the effect.)

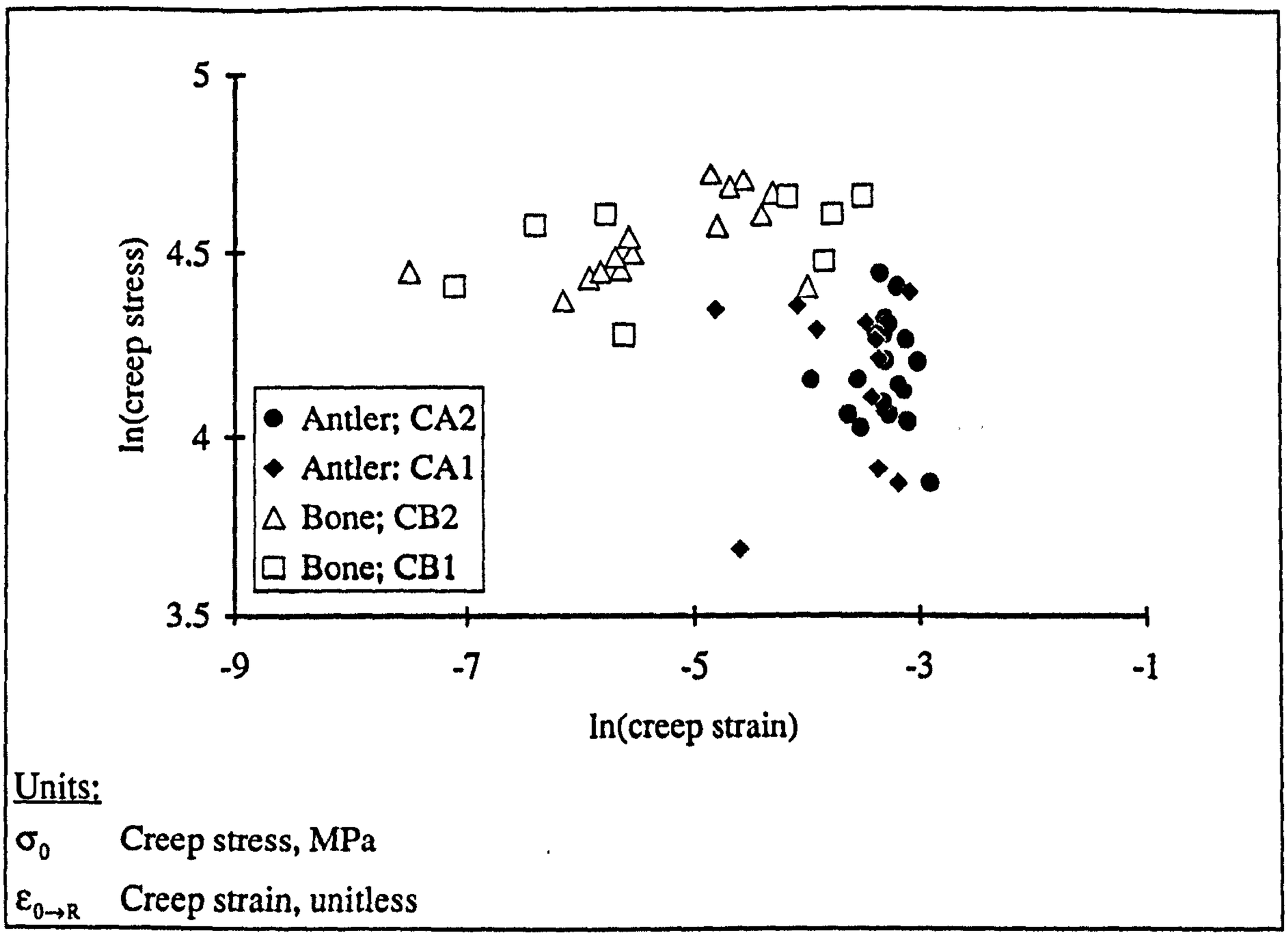

Units:

σ_0 Creep stress, MPa

$\varepsilon_{0\rightarrow R}$ Creep strain, unitless

Figure 4.038

Values of creep strain and creep stress for specimens of antler and bone

In the previous section it was shown that a decrease in the rupture strain was associated with an increase in stiffness, for both materials. When the creep strain is considered this is not found to be the case (equations *b* and *f*): in one case there is a positive relationship with stiffness and in the other it is negative. However, in equation *b* the coefficient of the stiffness term is not significantly different from zero and likewise in equation *f*, so this apparent anomaly is not statistically important. The difference in the form of the relationships for creep strain and rupture strain, is most probably due to the relationship between stiffness and the strain obtained during the loading period, as this strain is included in one case and excluded in the other. This relationship will be a strong one due to the small range of creep stresses used. Thus it would appear that the instantaneous strain, ε_0, is very dependent on which material is being tested, and the strains gained under conditions of constant load are dependent on other factors.

The equations in table A9.022 show that the creep strain of the bovine bone specimens is more dependent on creep stress than the creep strain of the antler specimens are. The coefficients of calcium content in equations *c* and *g*, (although non-significant) are of the same sign. This agrees with the differences between the materials themselves, the lower creep strain being exhibited by the more mineralised tissue.

4.3.7.5. LOGARITHM OF STRESS AND LOGARITHM OF ELONGATION AT RUPTURE: PART 3, $\ln(\sigma_0)$ AND $\ln(\varepsilon_{1*\rightarrow R})$

In the measure of elongation considered here the strain accumulated in the primary creep stage is excluded, and use is made of the steady state creep approximation. The separation of the 'elongation at rupture' of bone and antler is no longer statistically significant, $p = 0.156$ ($F = 2.11$). When compared with the higher levels of significance associated with the difference in the strains of antler and bone in the previous sections, this result implies that a considerable amount of that previously recorded variation is due to the behaviour of the materials in the primary region.

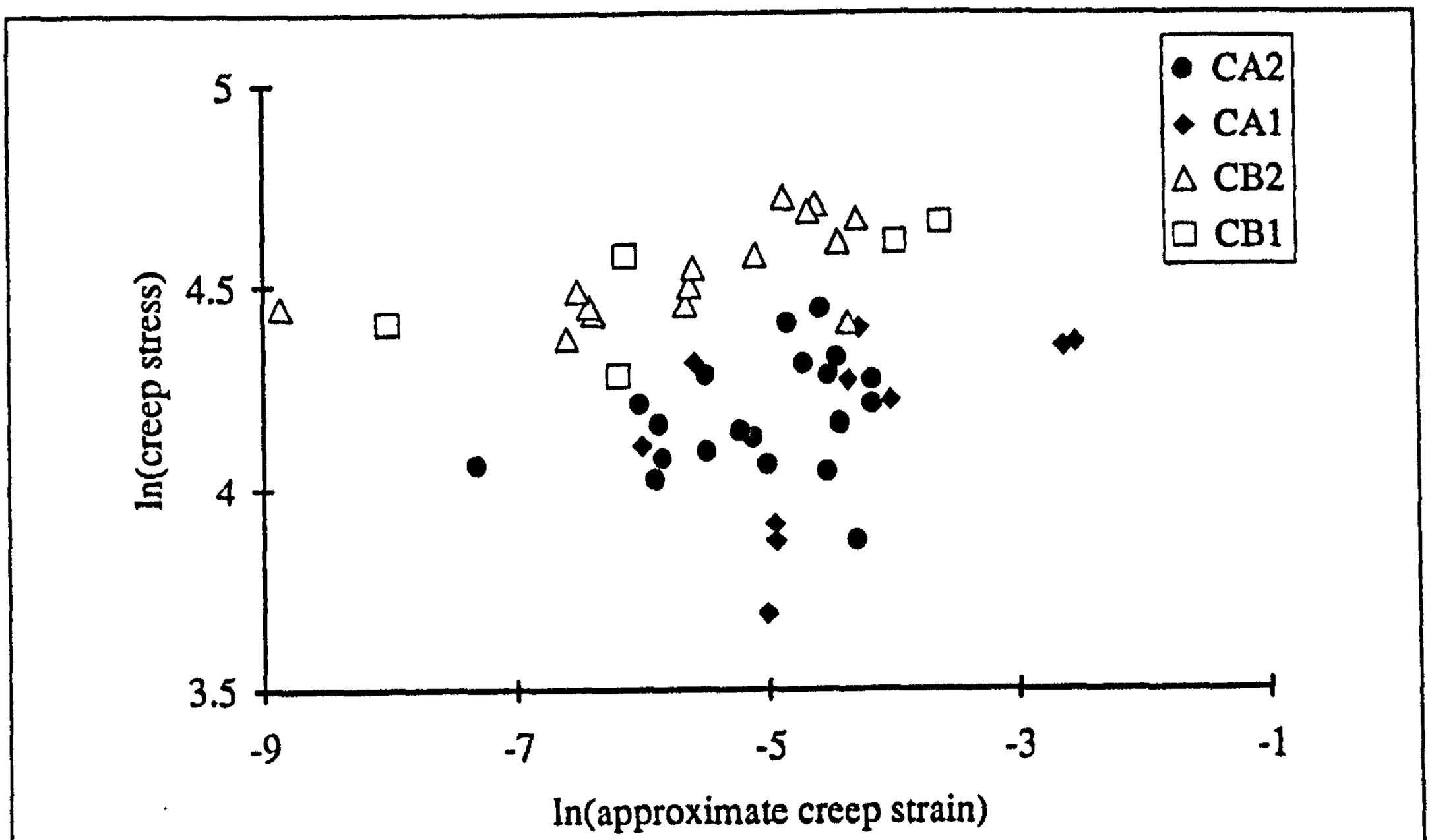

Units:

σ_0 Creep stress, MPa

$\varepsilon_{1*\rightarrow R}$ Approximate state creep strain, unitless

Comments:

For full key see figure 4.038

Figure 4.039

Approximate creep strain and the creep stress for specimens of antler and bovine bone

The predictive power of the relationships given in table A9.023 has increased over those in table (A9.022), and some of those in table (A9.021) in which other measures of elongation were used. As in those cases it is the increase in predictive power with the addition of the stiffness in tension in the equations for the antler data that is most noticeable, especially between equations *a* and *b*.

As in table A9.022 the coefficient of $\ln(E_t)$ in equations *b* and *f* of table A9.022 are again of opposite sign, and again they are not significant. The addition of calcium content as an explanatory variable, does not add to the overall explanatory power of the equations of both materials. However, the value of the coefficient is very similar in each case -11.4 in equation *c* and -11.3 in equation *g*, although non-significant. Thus such an analysis may only result in adding a factor by which some of the difference between the groupings of data, bone and antler, may be removed. This may provide no more insight than simply using a number to label the data as coming from a bone or antler specimen.

4.3.7.6. LOGARITHM OF STRESS AND LOGARITHM OF ELONGATION AT RUPTURE: PART 4, $\ln(\sigma_0)$ AND $\ln(\varepsilon_{1*\rightarrow 3})$

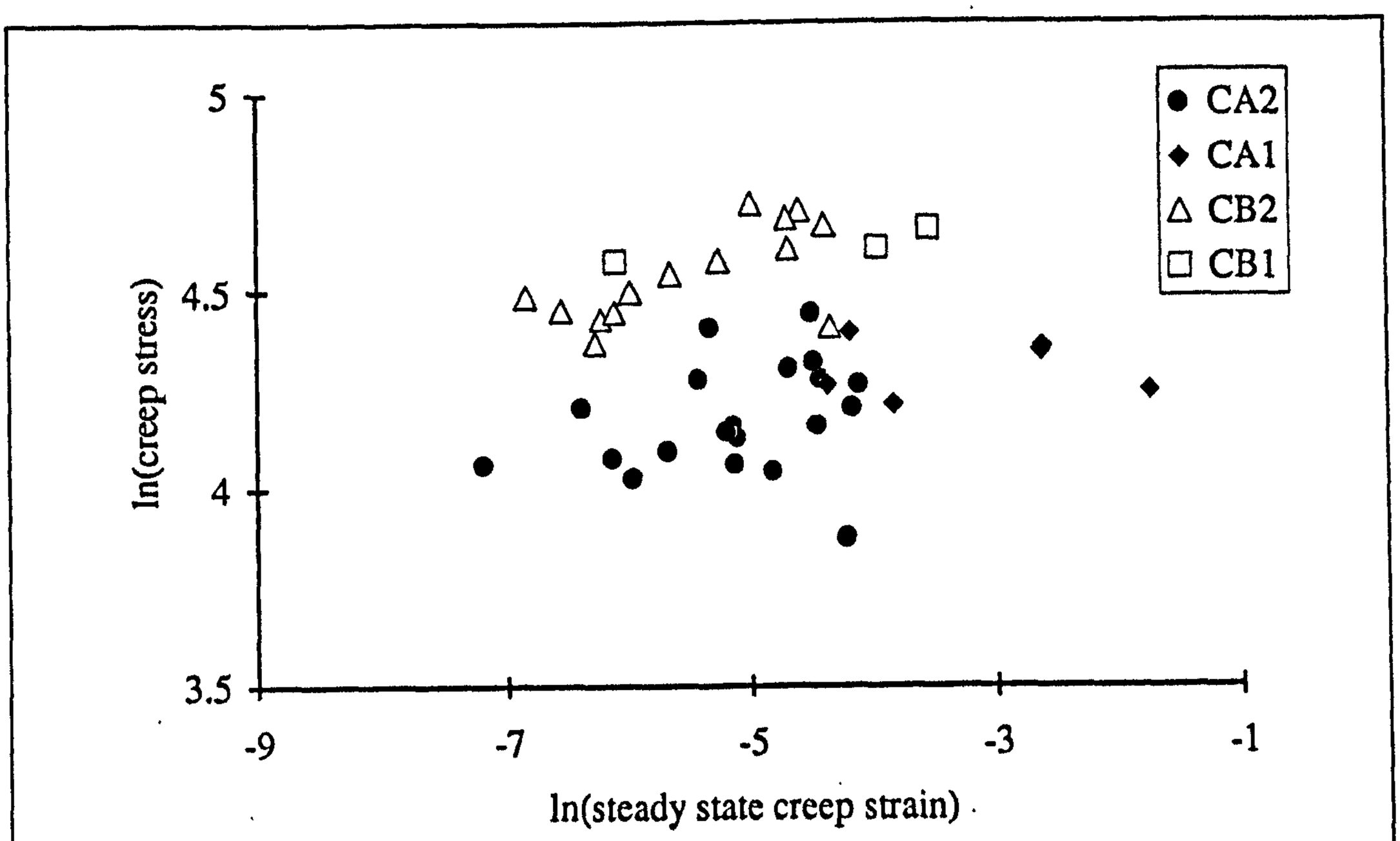

Units:

σ_0 creep stress, MPa

$\varepsilon_{1*\rightarrow 3}$ Steady state creep strain

Comments:

For full key see figure 4.009

Figure 4.040

Steady state creep strain and creep stress for specimens of antler and bone

When the steady state creep strain is considered as the 'elongation at rupture', the values obtained for bovine bone all fall within the range of those obtained for the specimens of red deer antler, and there is no statistical evidence to support the hypothesis that the values for those materials are different, $p = 0.249$ ($F = 1.38$).

Comparison of the equations in table A9.023 and A9.024 shows that the use of an estimate of the strain accumulated in the tertiary region in place of the recorded value has no uniform effect on the significance of creep stress as an explanatory variable for the regression equations of either material. However, the use of an estimate increased the power of the regressions in all but the first equation. I find this surprising because I consider that the nature of the final failure process combined with a low sampling rate could result in considerable scatter in the measured tertiary strain.

One interesting observation is the higher strength of the regression equation presented here as equation *f* (table A9.024) compared to that of equation *f* table A9.023. In the equation presented here the material stiffness in tension is a highly significant variable, $p = 0.009$, whereas in the earlier one it is non-significant. The only difference is that the strain measure now uses an extrapolated estimate of the strain in the tertiary region rather than the actual value. This could be interpreted as indicating that the strain in the tertiary region is not related to the tensile stiffness of the bovine specimens.

4.3.7.7. LOGARITHM OF STRESS AND LOGARITHM OF ELONGATION AT RUPTURE: GENERAL OBSERVATIONS

The overall impression given by analysis of the logarithm of creep stress and the logarithm of various measures of elongation at rupture used here, is that the relationship between those quantities is not very strong. The addition of other variables such as the stiffness measured during the loading period, E_t, increases the predictive power of the relationship in some cases.

The most interesting result is a by-product of the main analysis. This is the observed changes in the separation between the values of the 'elongation at rupture' of antler and bone. This separation is dependent on the definition of the 'elongation at rupture' that is used. If the rupture strain is used, in other words the total deformation up to the point of rupture, all the antler specimens display a greater value than the bone specimens (figure 4.037). However, ignoring the strain exhibited by the specimens during loading blurs the difference in the results for the two materials (figure 4.038). When the 'elongation at rupture' is estimated from the steady state creep-rate, there is no statistical evidence for a difference between the results from antler and bone. This observation is a result of the contrasting creep behaviour of antler and bone. This contrasting behaviour is highlighted by the shapes of the creep curves of bone and antler. Some of these creep curves are shown in figures 4.030 to 4.033. In figures 4.030 to 4.033 the variation in the proportion of the total strain that falls within the primary, secondary and tertiary regions appears to be dependent not on the stress or time-to-

rupture, but on the test material examined. The distribution of strain between these regions can be examined quantitatively, by expressing the various strains as a percentage of the rupture strain. This calculation has been performed on the core data (CA2 and CB2) and is presented in table 4.009.

Strain	Reindeer Antler		Bovine femoral bone	
	Percentage of rupture strain, ε_R		Percentage of rupture strain, ε_R	
	Mean	s.d.	Mean	s.d.
ε_0	50.24	16.13	42.61	17.56
ε_1^*	90.10	5.83	49.87	22.05
$\varepsilon_{1*\rightarrow 3}$	9.64	5.77	42.58	20.48
ε_3	99.75	1.88	94.88	10.85

Table 4.009

The mean values of various strains measured during creep tests of antler and bone expressed as a percentage of the total strain

The results in table 4.009 show that the measured instantaneous strain, ε_0, accounts for about half the total deformation of both materials. The value of ε_0 for antler may be an overestimate (relative to that of bone) due to the longer loading period for this more compliant material. When the percentage of the total elongation of each material that can be attributed to the steady state instantaneous strain, ε_1^*, is examined a clear difference is seen. For the antler specimens this measure contains about 90% of the total strain. However, less than half of the total elongation of bovine bone specimens is described by this measure. The corollary of this is that antler specimens gain only about 10% of their rupture strain during the steady state region of their creep behaviour, while bone gains about 40%. The difference between the materials is again highlighted when steady state rupture strain, ε_3, is examined. A glance at figure 4.029 shows that the difference between ε_3 and ε_R is a measure of the strain in the tertiary creep region. The results in table 4.009 imply that antler exhibits only a very limited amount of tertiary creep. Bovine femoral bone exhibits an average of about 5% of its total elongation in this tertiary region. The standard deviation values in table 4.009 imply that the antler specimens are more consistent in their behaviour than these of bovine bone.

The examinations of the relationship of elongation at rupture and creep stress has revealed few significant correlations between these quantities. However, it has highlighted a difference between the creep behaviour of bone and antler. Antler exhibits a higher (or similar depending of the measure used) elongation at rupture than bone, although it is subjected to a lower stress.

4.3.7.8. ELONGATION AT RUPTURE AND THE LOGARITHM OF THE TIME-TO-RUPTURE: PART 1, ε_R AND $\ln(t_R)$

Conway (1967) suggests that values of the elongation at rupture and the time-to-rupture should be plotted against each other (table 2.001). It is a reasonable assumption that if the rate of extension is constant for all specimens then those that fail first will display a smaller elongation at the time of rupture. However, specimens do not creep at the same rate. Thus how are the elongation at rupture and the time-to-rupture related, if at all?

As in the previous analysis where I used the 'elongation at rupture' as a variable, here I use a number different measures of this quantity. The results are presented in the same way: figures here regression equations in appendix 9.

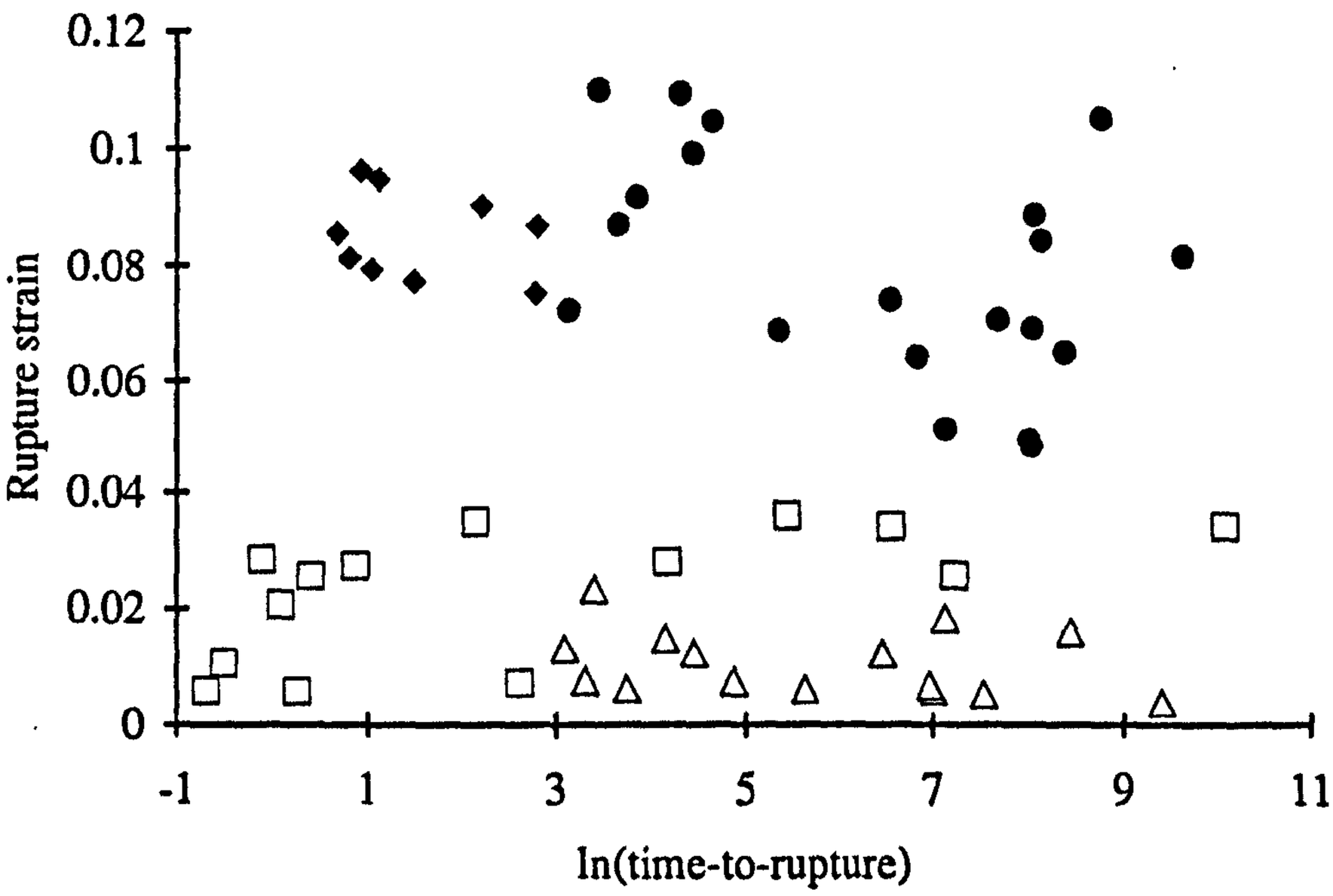

Units:

ε_R Rupture strain, unitless

t_R Time-to-rupture, s

Comments:

For full key see figure 4.038

Figure 4.041

Rupture strain and time-to-rupture for specimens of antler and bovine bone

As in previous sections the main impression gained from figure 4.041, is one of the difference in rupture strain between the two materials, rather than a relationship between the variables. The graph indicates a slight relationship between the variables for

antler and no relationship for bone. This is expressed quantitatively by the R^2 values associated with the various regression equations given table A9.025.

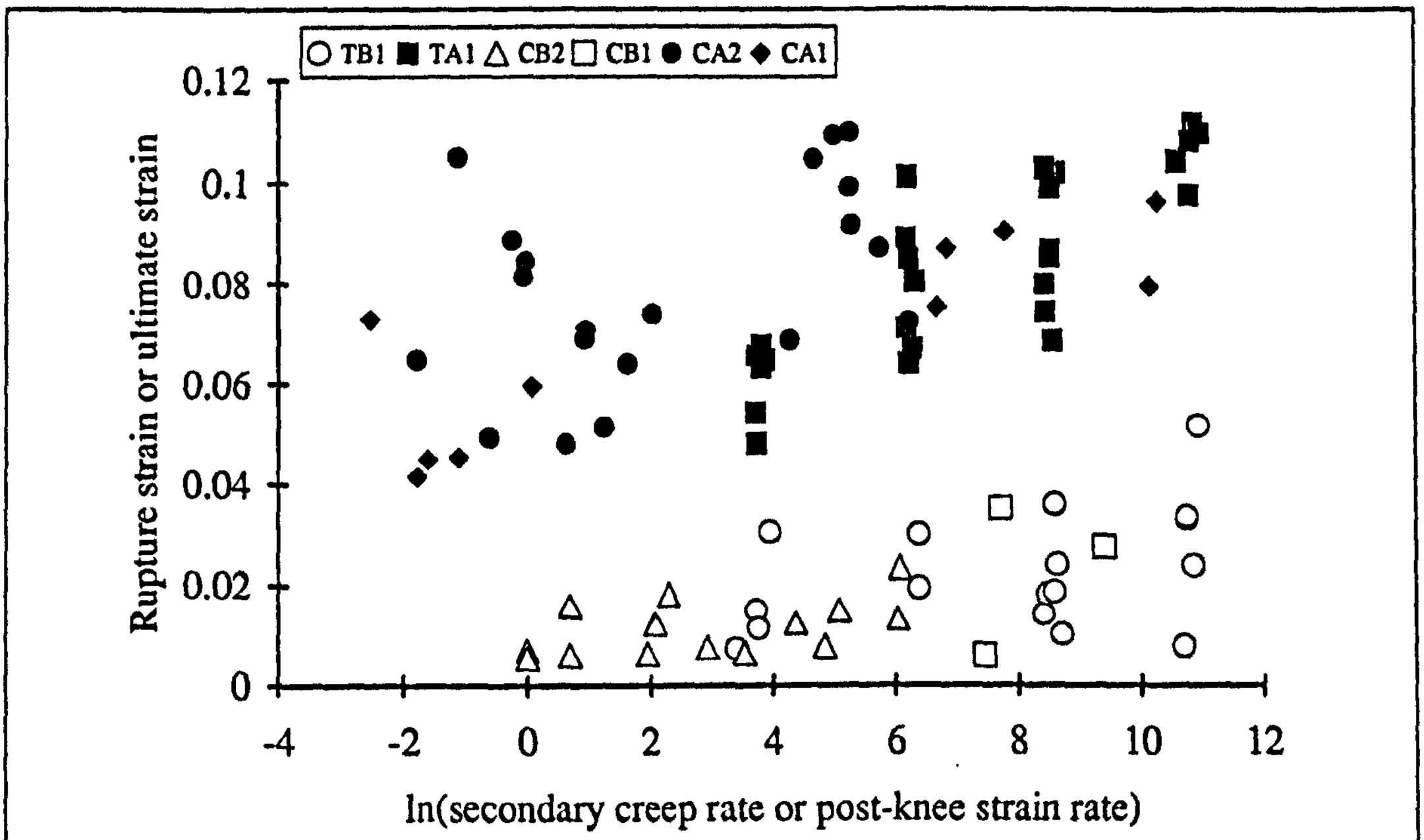

Units:

ε_R Rupture strain (creep test), unitless

ε_{ult} Ultimate strain (tensile test), unitless

$\dot{\varepsilon}_{1*\rightarrow 3}$ Steady state creep rate (creep test), $\mu\varepsilon\ s^{-1}$

$\dot{\varepsilon}_{pk}$ Post-knee strain rate (tensile test), $\mu\varepsilon\ s^{-1}$

Comments:

The different test materials are identified by solid (antler) of open (bovine bone) shapes. The key shows the data sets that have been used, indicated by the type of shape. The strain, or creep, rate units used here are consistent with those in later sections. However, they are different from the units used above. (For example see figure 4.008.)

Figure 4.042

Relationship of the strain at failure to the extension rate in both creep and tensile tests of antler and bone

The regression equations show that the addition of E_t as an explanatory variable improves the predictive power of the relationship for the antler data. Although it has occurred in the equations of previous tables the greater significance of the additional variable, in equation *b*, is very noticeable. In this case the *p* values associated with the two values are, in the order of their appearance in the equation, 0.088 and 0.021. Thus the strain at rupture has a non-significant relationship to the time-to-rupture, but has a significant relationship to the material stiffness in tension. The greatest statistical significance of the rupture strain, in the equations given, is that in equation *a* for antler, and *f* or *g* for bovine bone. However, this variable is only significant in the first equation.

Thus there is no strong statistical evidence for a relationship between the total strain at rupture and the time-to-rupture for either material.

The most obvious result shown in figure 4.041 is that the rupture-strain of antler is greater than that of bovine bone. A similar result was also noted in values of the ultimate strain reached during tensile tests. The similarity between the strain values for each material can be seen by comparing figure 4.041 with figure 4.016. The figure showing the tensile test results suggests a trend; the separation between the ultimate strain values of bone and antler increases at higher cross-head speeds or extension rates. The plot of the creep results suggests another trend; the greater the time-to-rupture the smaller the separation between the results. As the values of the rupture strains do not vary much, a shorter time-to-rupture suggests a higher creep rate. Thus these two trends may be similar. In the model suggested in section 3.3.3.2 a comparison was drawn between idealised creep tests and the behaviour of a material in the post-knee region of a tensile test. It was suggested that if the post-knee region was horizontal then this was essentially a creep test with $\sigma_0 = \sigma_K$. This idealisation suggests that the relationship of rupture strain to secondary creep rate in a creep test, could be the same as that for the ultimate strain to the post-knee strain rate in a tensile test. I have therefore plotted these quantities in figure 4.042. The tensile data used comes from data sets TB1, for bovine bone, and TA1 for antler. The data from creep tests is from the same data sets as used in the other parts of this section. Figure 4.042 shows that not only are the ranges of the final strains in each type of test similar for each material, but also the trend of increasing final strain with extension rate is similar in both types of test.

Perhaps the extreme example of this trend (of the failure strains of antler being greater than those of bovine bone especially at higher testing rates) offered in this work are the images of the impact tests in section 1.4.2.3. In such impact tests the extension rate of the tensile surface can be assumed to be higher than in the tensile and creep tests described here. Under such test conditions the antler specimens displayed a sharp curvature, suggesting a very high surface strain, without failing. However, the bovine specimens failed at a very low curvature. This evidence when considered together highlights the rate dependent nature of the failure strain of bone and antler.

The observations made in this section raise the interrelated questions: Why is the failure strain of these materials rate dependent? Does this provide any insight to the failure process? One argument, which has already been proposed, that may answer both these questions is that failure occurs by the accumulation of damage in the form of small cracks or voids. The accumulation of this damage is perceived as a function of both the applied stress and the time it is applied for. Thus at low extension rates there is more time for damage to accumulate and thus the failure has a more brittle nature, and

consequently a smaller extension at failure. At higher extension rates damage has less time to accumulate, the stress is larger and thus the final strain is also greater. This argument is essentially that of the maximum damage criterion of section 4.2.6.9. However, (as pointed out in section 4.2.6.9) this argument neglects the work of Griffith (1920) on the effect of cracks on the failure stress, and thus indirectly strain, in a solid. I consider that the failure mechanism identified by Griffith has an important role in the failure of bone (and possibly antler). This role is to modify the ideas of the damage approach as argued here. This modification is discussed in more detail (in chapter 9) after the work of Griffith has been introduction in chapter 5.

The agreement of the data obtained from both tensile and creep tests, as presented here, is perhaps not surprising. I mentioned in section 4.3.5.1 that during some of the creep tests conducted at the higher end of the range of stresses used examination of the strain rate data showed little alteration on attaining the creep stress. It was also noted that such tests produced a stress-strain curve that was very similar to that obtained during a tensile test.

4.3.7.9. ELONGATION AT RUPTURE AND THE LOGARITHM OF THE TIME-TO-RUPTURE: PART 2, $\varepsilon_{0\rightarrow R}$ AND $\ln(t_R)$

In this case, the measure used for elongation at rupture is the creep strain, $\varepsilon_{0\rightarrow R}$. The relationship between this measure of elongation at rupture and the time-to-rupture is non-significant. Equation *b* stands out from the others, the addition of the material stiffness in bending has dramatically improved the predictive power of equation *a*, but this variable is still not a statistically significant one. When the results for creep strain are compared with those of rupture strain (section 4.3.7.6 above), it appears that it is the strain gained during the loading period that results in the relationship of rupture strain to time-to-rupture. Intuitively this is reasonable as the strain gained during the loading period is (approximately) the product of the creep stress and the material compliance (the reciprocal of its stiffness). The relationship of the strain gained during the loading period and the time-to-rupture are dealt with in a later section, as such a relationship is basically the same as the NTDF model.

The main results of the examination of creep strain and the logarithm of the time-to-rupture are: There is no significant relationship between creep strain and the time-to-rupture, but there is a difference in the amount of creep strain the two materials accumulate. It was suggested in section 3.3.3.2 that creep-strain is analogous to the post-knee strain of a tensile test. Such an action, with the data examined in this section, would suggest that the post-knee strain is not dependent on testing rate. If the ultimate strain of

a tensile test is used as an approximation to the post-knee strain, then the evidence from experimental tests contradicts the model's predictions. (Clearly, the ultimate strain and post-knee strain are not the same. However, I consider further analysis of this point is not relevant here.)

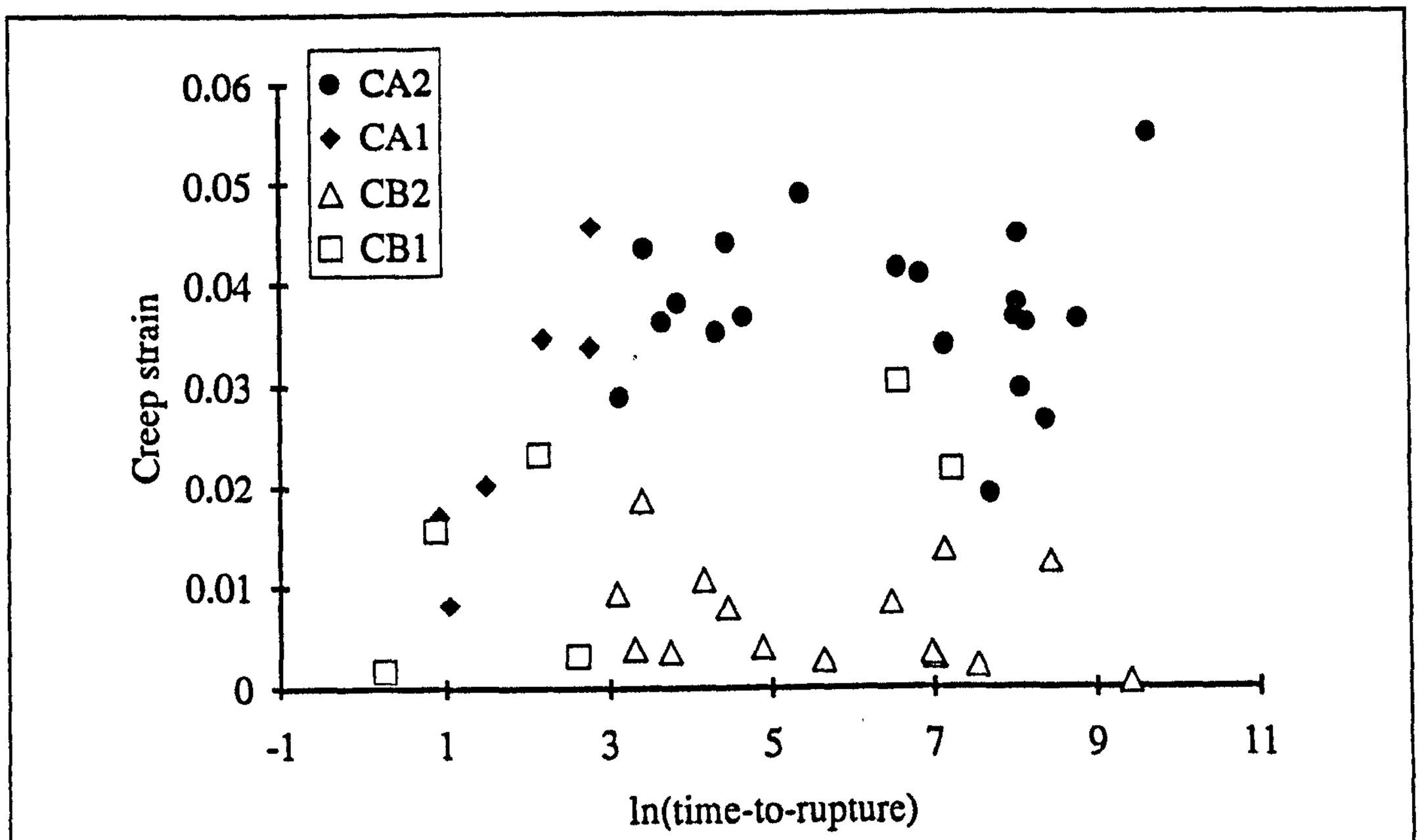

Units:

$\varepsilon_{0\rightarrow R}$ Creep strain, unitless

t_R Time-to-rupture, s

Comments:

For full key see figure 4.038

Figure 4.043

Creep strain and time-to-rupture

4.3.7.10. ELONGATION AT RUPTURE AND THE LOGARITHM OF THE TIME-TO-RUPTURE: PART 3, $\varepsilon_{1*\rightarrow R}$ AND $\ln(t_R)$

Figure 4.044 shows the data points for the approximate creep strain at rupture, $\varepsilon_{1*\rightarrow R}$, and the time-to-rupture from the complete data sets, CA1 and CB1. This measure of elongation at failure is derived by subtracting from the strain at rupture the strain value obtained by the backward extrapolation of the creep curve to the start of the loading period (see figure 4.029). Thus in those cases where the strain rate alters little between the loading and creep sections of the tests the backward extrapolation line passes close to the origin. This effect has produced two data points with high values of approximate creep strain. Due to their low values of time-to-rupture these points are not within the

core data sets (CA2 and CB2), which are used for the regression analysis presented in table A9.027.

Unlike the data set examined in the previous section (4.3.7.9), here the results for antler show some relationship between the variables. Again the strongest relationship is that in which material stiffness in tension is the second variable. In all three of the equations given for antler (*a*, *b* and *c* table A9.027) the strain term is, at least, significant. However, the bovine specimens display a lack of significance of the elongation term in describing the time-to-rupture.

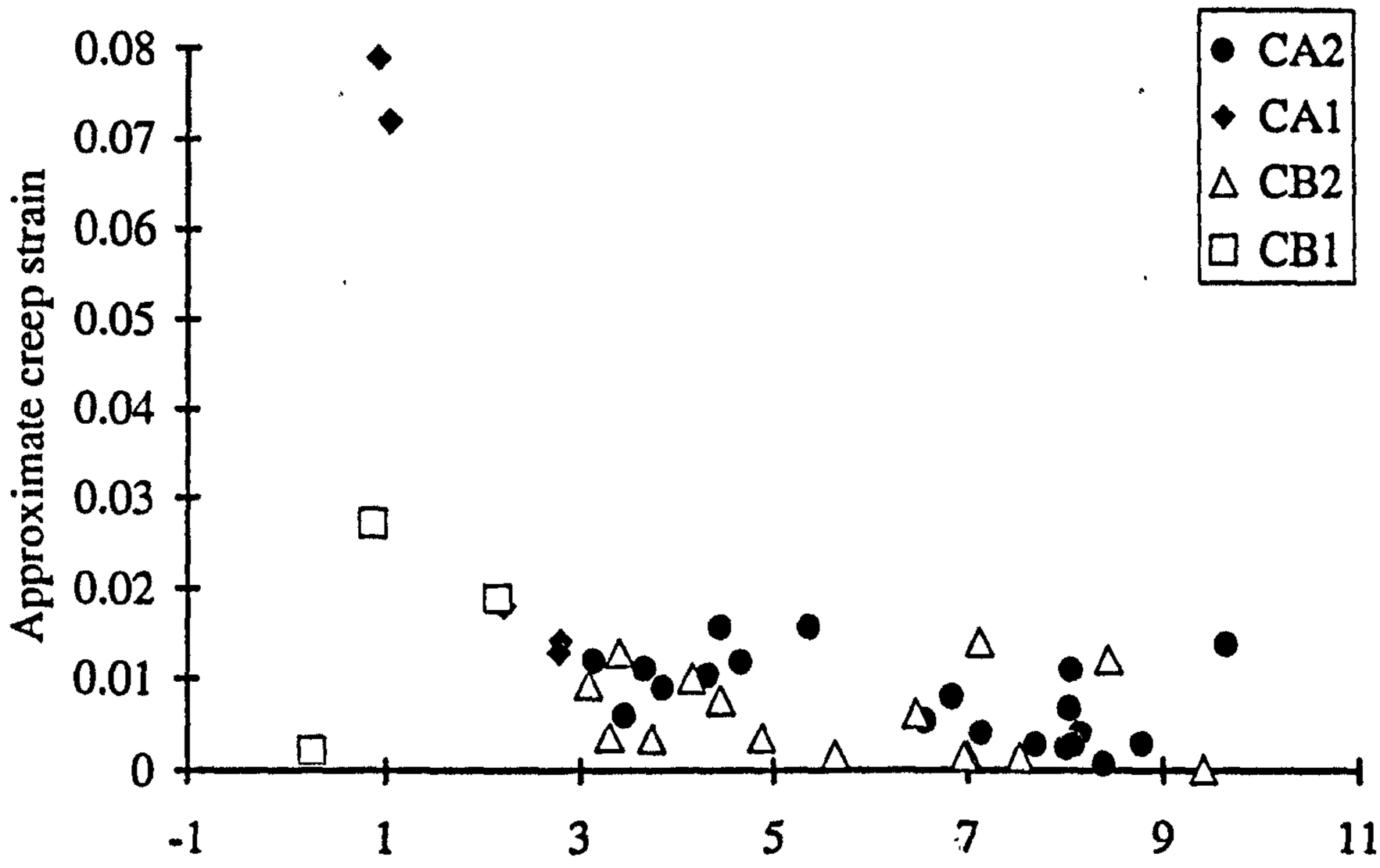

Units:

$\varepsilon_{1*\rightarrow R}$ Approximate creep strain, unitless

t_R Time-to-rupture, s

Comments:

For full key see figure 4.038

Figure 4.044

Approximate creep strain and time-to-rupture

Using one-way analysis of variance on both of the variables plotted in figure 4.044, provides no statistical evidence that the values are different for the different materials (data sets CA2 and CB2). For the approximate creep strain $p = 0.895$ and for the time-to-rupture $p = 0.320$.

4.3.7.11. ELONGATION AT RUPTURE AND THE LOGARITHM OF THE TIME-TO-RUPTURE: PART 4, $\varepsilon_{1*\rightarrow 3}$ AND $\ln(t_R)$

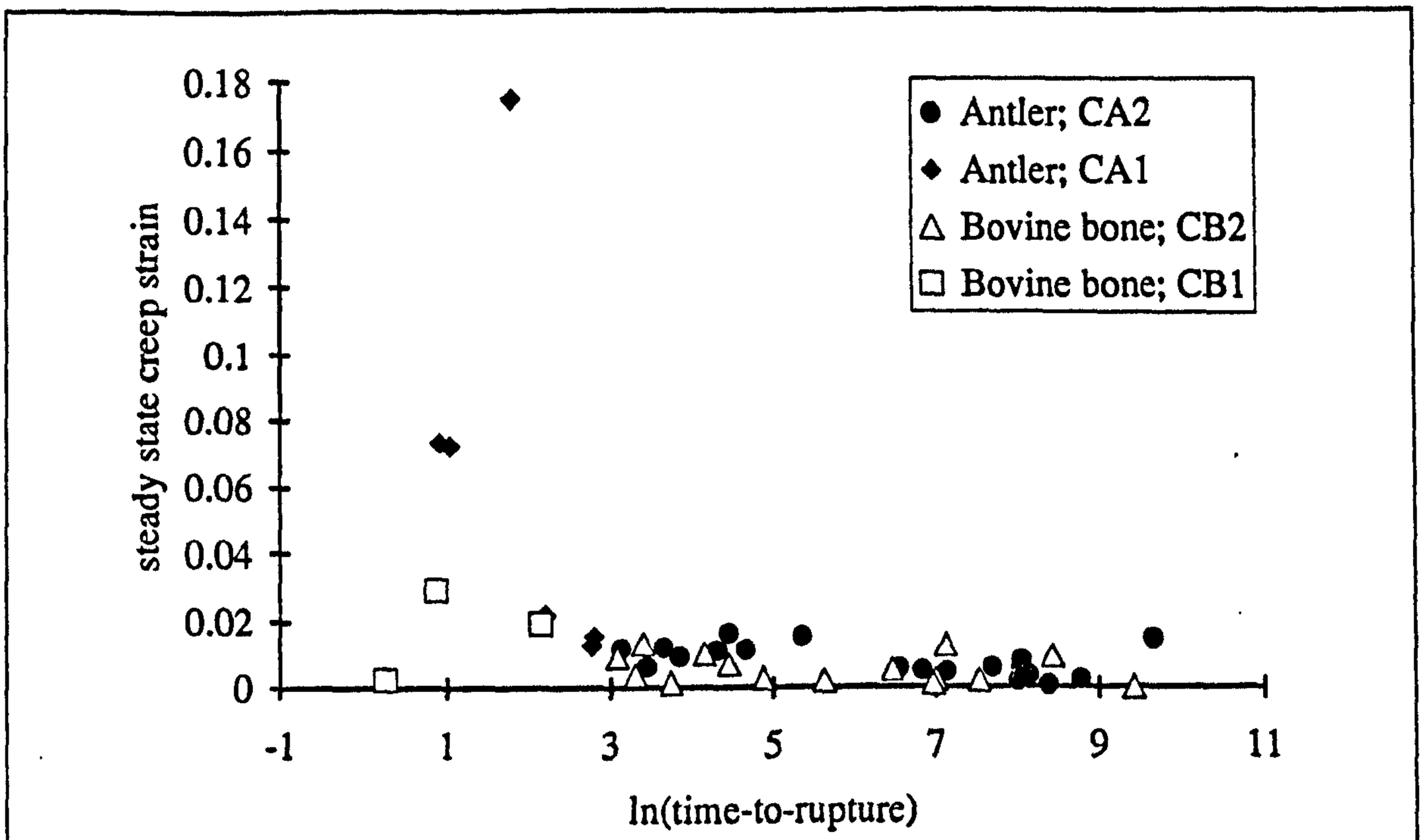

Units:

$\varepsilon_{1*\rightarrow 3}$ Steady state creep strain, unitless

t_R Time-to-rupture, s

Comments:

For full key see figure 4.038

Figure 4.045

Steady state creep strain and time-to-rupture

The results shown in figure 4.046 and in table A9.028 display no marked difference to those in the previous section. There is no clear separation between the data sets CA2 and CB2. Again the explanatory power of the equations for the antler specimens is greater than that for the bone ones.

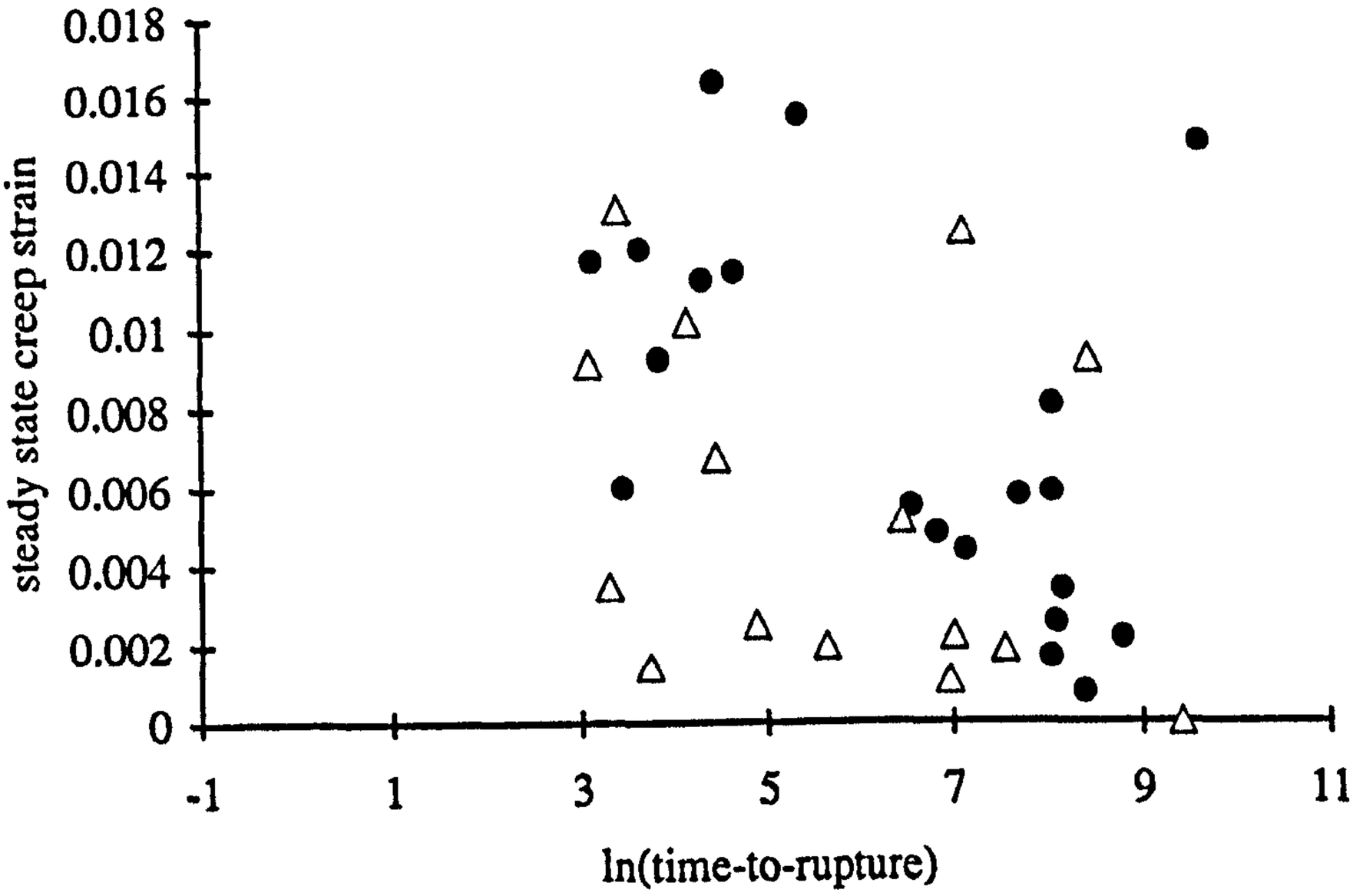

Units:

$\varepsilon_{1*\rightarrow 3}$ Steady state creep strain, unitless

t_R Time-to-rupture, s

Comments:

For full key see figure 4.038

Figure 4.046

Steady state creep strain and time-to-rupture, core data CA2 and CB2 only

4.3.7.12. ELONGATION AT RUPTURE AND THE LOGARITHM OF THE TIME-TO-RUPTURE: PART 5, SUMMARY

Examination of the various measures of elongation at rupture and the time-to-rupture for the bovine bone specimens has shown a general lack of a significant relationship between these quantities. The antler specimens however show a significant relationship in a number of cases. One exception is equation *a* table A9.026 (referred to in section 4.3.7.9), as I reported in that section, this may be due to the exclusion of the instantaneous strain, ε_0, a quantity similar to that used by Caler and Cater to predict the time-to-rupture.

The increase in the predictive power of the relationship of elongation at rupture to the time-to-rupture resulting from the use of the material stiffness in tension as an additional explanatory variable, is most noticeable in the analysis of the antler specimens. This is probably a result of the bigger range of material stiffnesses exhibited by antler. The equations predict that the stiffer the antler specimen the longer it will take to rupture. If the elongation rates were the same, the closer the material stiffness of antler gets to that

of bovine bone, the smaller is the difference in their rupture times. The measure of elongation used effects the form of the dependence on E_t. The greater the difference between the elongations associated with bone and antler, the greater the difference a small increase in stiffness would make to the predicted elongation value of antler. For example, see equation *b* in table A9.025 and equation *b* in table A9.028. This appears to support the idea that the material stiffness is a useful normalising factor, possibly even between materials. However, it should be remembered that there is a relationship between stiffness and elongation, especially when the strain obtained in the loading period is included in such a measure (as in section 4.3.7.8 where rupture strain was used). It has already been shown that the strain attained by antler in the loading and primary creep stages (Where E_t can be considered as directly relevant) are larger than those of bovine bone.

The most important result shown in this investigation of the elongation at rupture and the time-to-rupture, is the comparison with the tensile test data in section 4.3.7.8. The best way to compare the tensile and creep tests is to examine the elongation at rupture and the extension rate. This form of analysis was suggested by the assumptions made in the model proposed in section 3.3.3.2 to link creep and tensile tests. This model was based on assimilating the post-knee region of a tensile test with the post-loading section of a creep test. The results when plotted together appear to coincide. The faster the material is extended the greater its failure strain will be. I suggested that this finding fitted, and could be explained by, the theory of damage accumulation. This theory can also be applied to the more general result from the antler data that there is a decrease in the elongation at rupture when that rupture takes longer to occur. In Kachanov's work (2.3.3) two extreme cases were introduced: ductile and brittle failure. Ductile failure was shown to dominate at high stresses and was related to short times to rupture. Brittle failure occurs at low stresses and is associated with long term tests. This was shown in figure 2.011. It was pointed out in section 2.3.3 that in a ductile failure the elongation is large and in a brittle failure it is small. So it can be argued that Kachanov's damage model suggests that a failure that takes a long time will be associated with a small elongation, and a quick failure with a large elongation. This is what has been found in the tests on antler, but not in those of bone specimen. The explanation for this may be found in figure 4.034 where a transition from brittle to ductile behaviour was suggested for antler and not for bone. These pieces of evidence appear to support each other. However, I only suggest that there may be such a change in antler's behaviour, as I do not consider the evidence is strong enough for any more than a suggestion. There is also the danger that I am falling into the same trap as I have criticised others for doing, of applying a model and using agreement of the data with that model to justify its use.

4.3.7.13. LOGARITHM OF CREEP STRESS AND THE LOGARITHM OF ELONGATION RATE: PART 1, $\ln(\dot{\varepsilon}_{1\star\rightarrow3})$ AND $\ln(\sigma_0)$

In this section, and the sections up to 4.3.7.15, I examine the next correlation of creep-rupture data suggested by Conway (1967).[30] As in the previous cases, I examine a number of different measures of the rate variable. The results are summarised in section 4.3.7.16. This time these measures are of elongation rate, and are the slopes of the lines shown in figure 4.029.

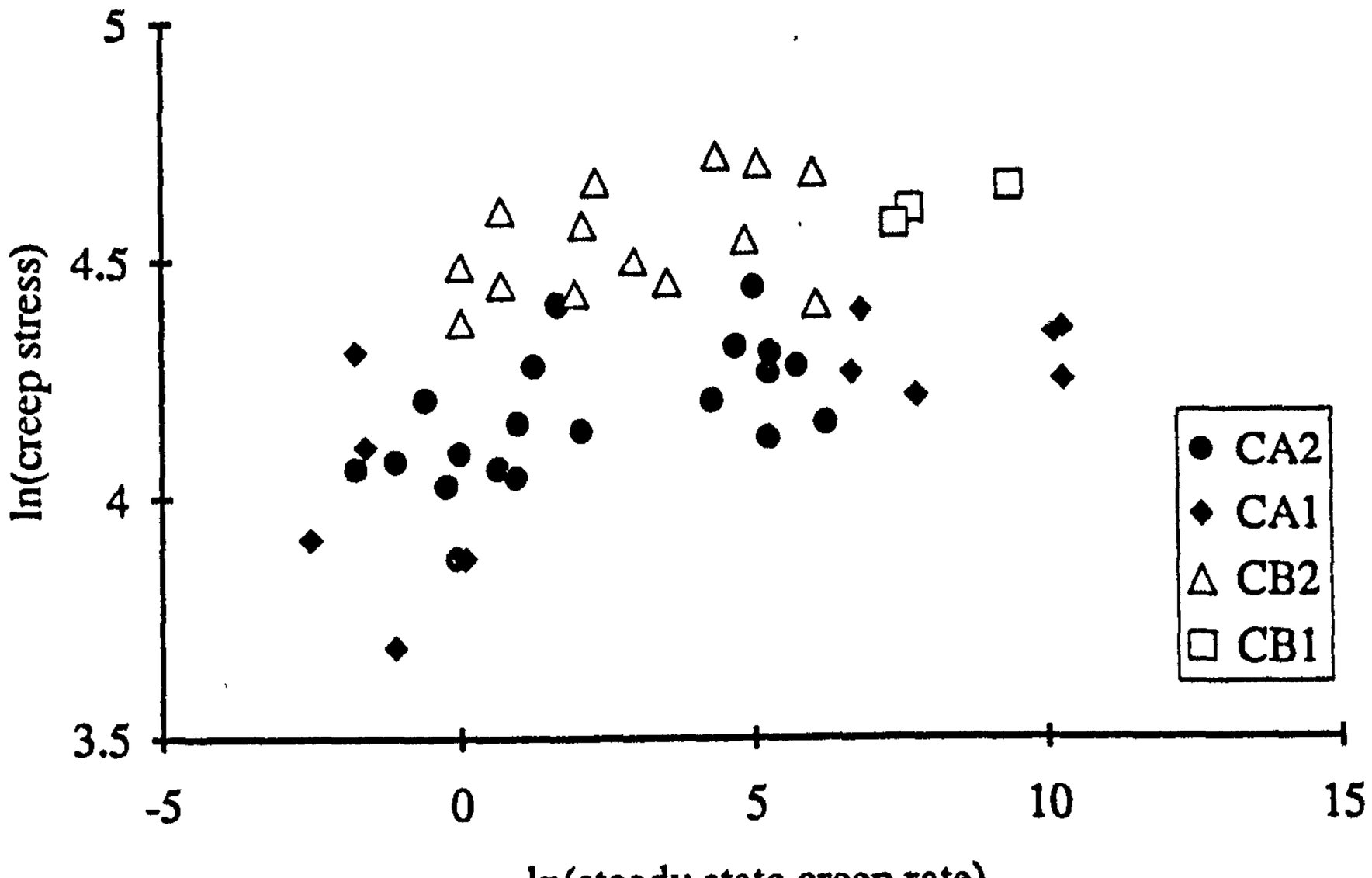

Units:

σ_0 Creep stress, MPa

$\dot{\varepsilon}_{1\star\rightarrow3}$ Steady state creep rate, $\mu\varepsilon\ s^{-1}$

Comments:

For full key see figure 4.038

Figure 4.047

Creep stress and steady state creep rate

Figure 4.047 shows the relationship between the applied creep stress and the creep rate measured during the secondary region of the creep curve, or steady state creep rate. The bovine bone specimens require a higher creep stress to attain the same creep rate as those made of antler.

---

[30]I have plotted the variables in the way he suggests, even if it appears wrong in some cases.

The relationship between the variables as shown in figure 4.047 does not appear to be very strong. The relationship for the set of data from all the antler specimens, CA1, is very dependent on those specimens not included in the core data. Including those with a high creep rate, resulting in rupture at times less than 20 seconds, and those with such a low creep rate that were rejected due to missing data.

The relationship between the steady state creep rate and a number of variables are expressed quantitatively by the equations in table A9.029. The results for antler show stronger relationships than those for bovine bone. When the creep stress is the only variable considered it is found to be a highly significant variable in the case of antler, but non-significant in the case of bone (equation *a* for antler and *d* for bone). The weak predictive power of the relationship between the creep stress and the steady state creep rate for the bovine data appears to undermine the use of the damage approach as explained in chapter 3. This is because such a relationship is the first stage in the development of the equations that relate time-to-rupture to the creep stress. The section on rupture as a result of unlimited flow (section 2.3.3.1) contains the assumption that the relationship for the initial strain rate could be expressed as

$$\dot{\varepsilon}_0 = B_1 \sigma_0^{\,m} \tag{4.049}$$

or in logarithmic form

$$\ln(\dot{\varepsilon}_0) = \ln(B_1) + m \ln(\sigma_0) \tag{4.050}$$

As Kachanov ignored the primary creep stage in the development of his damage theory, I consider this equation (4.050) is the theoretical equivalent of the experimentally derived relationships *a* and *d* in table A9.029. In Kachanov's work the values from the theoretical equation, B_1 and m, were used in the derivation of an equation for the prediction of the time-to-rupture by a purely ductile process. This value was then used in the prediction of failure by other processes.

In their examination of the relationship of creep rate to creep stress, Fondrk *et al.* (1988) obtained a very good relationship when the results of a number of tests on the same specimen were considered, but when all the results were pooled the strength of the relationship decreased, (this paper was reviewed in section 3.3.3.1). However, the results of their pooled data are still greater than those obtained here. This may be due to the reuse of their specimens.

4.3.7.14. LOGARITHM OF CREEP STRAIN AND THE LOGARITHM OF ELONGATION RATE: PART 2, $\ln(\dot{\varepsilon}_{1*\rightarrow R})$ AND $\ln(\sigma_0)$

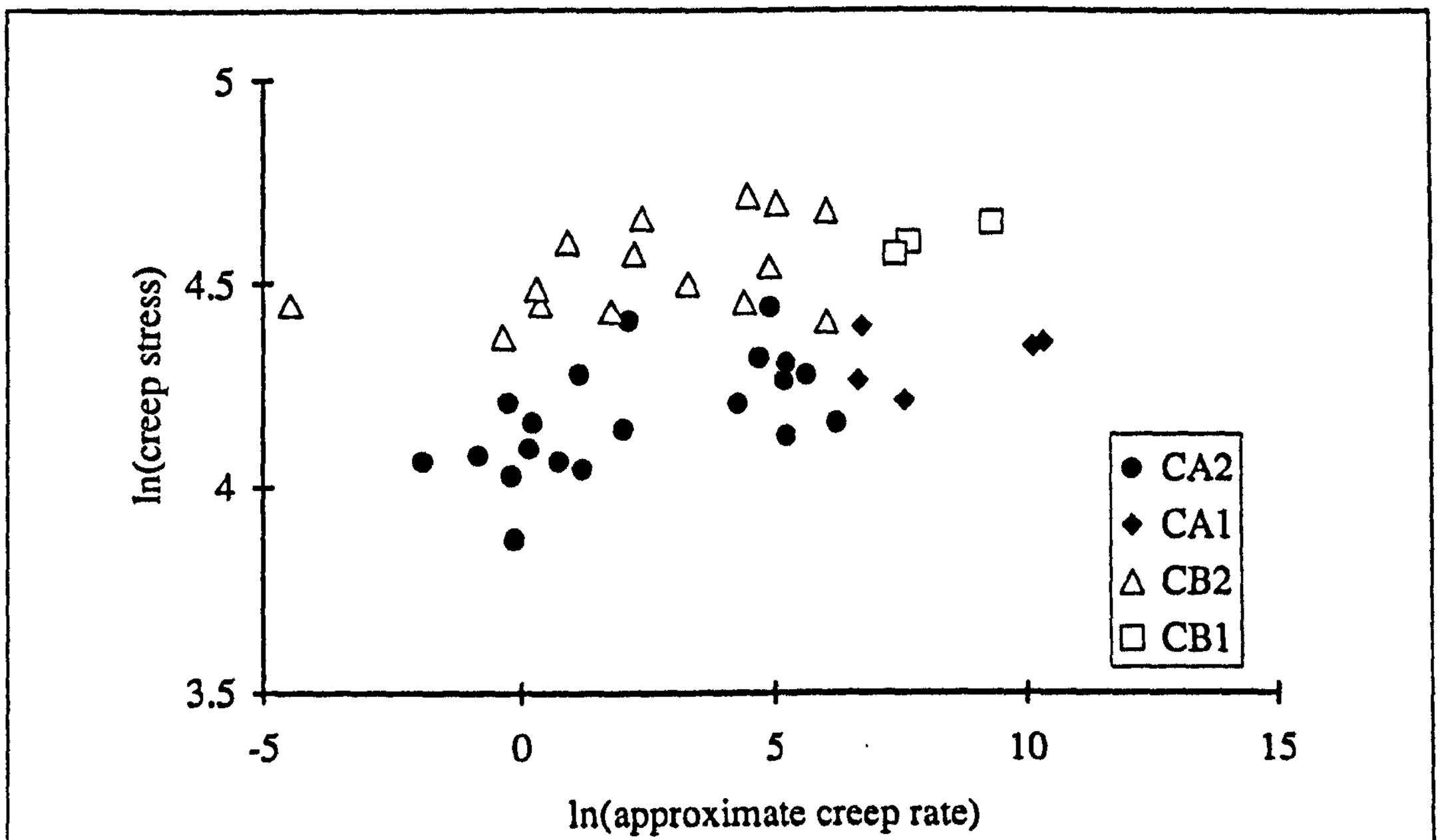

Units:

σ_0 Creep stress, MPa

$\dot{\varepsilon}_{1*\rightarrow R}$ Approximate creep rate, $\mu\varepsilon\ s^{-1}$

Comments:

For full key see figure 4.038

Figure 4.048

Creep strain and approximate creep rate

The results shown in figure 4.048 are little different from those for the steady state creep rate. The stress term is significant in the regressions of the antler data and not significant in those for bovine bone (table A9.030). The regression equations indicate that increasing the amount of calcium decreases the strain rate for both materials. However, the calcium content is a non-significant variable. The creep rates for the specimens of each material are similar and the creep stress different.

4.3.7.15. LOGARITHM OF CREEP STRESS AND THE LOGARITHM OF ELONGATION RATE: PART 3, $\ln(\dot{\varepsilon}_{0\rightarrow R})$ AND $\ln(\sigma_0)$

As in the analysis of the other measures of elongation rate presented in the previous sections, the main feature of these data in the separation between the creep stress applied to the materials. Again the relationships are stronger for the antler specimens (see table A9.031).

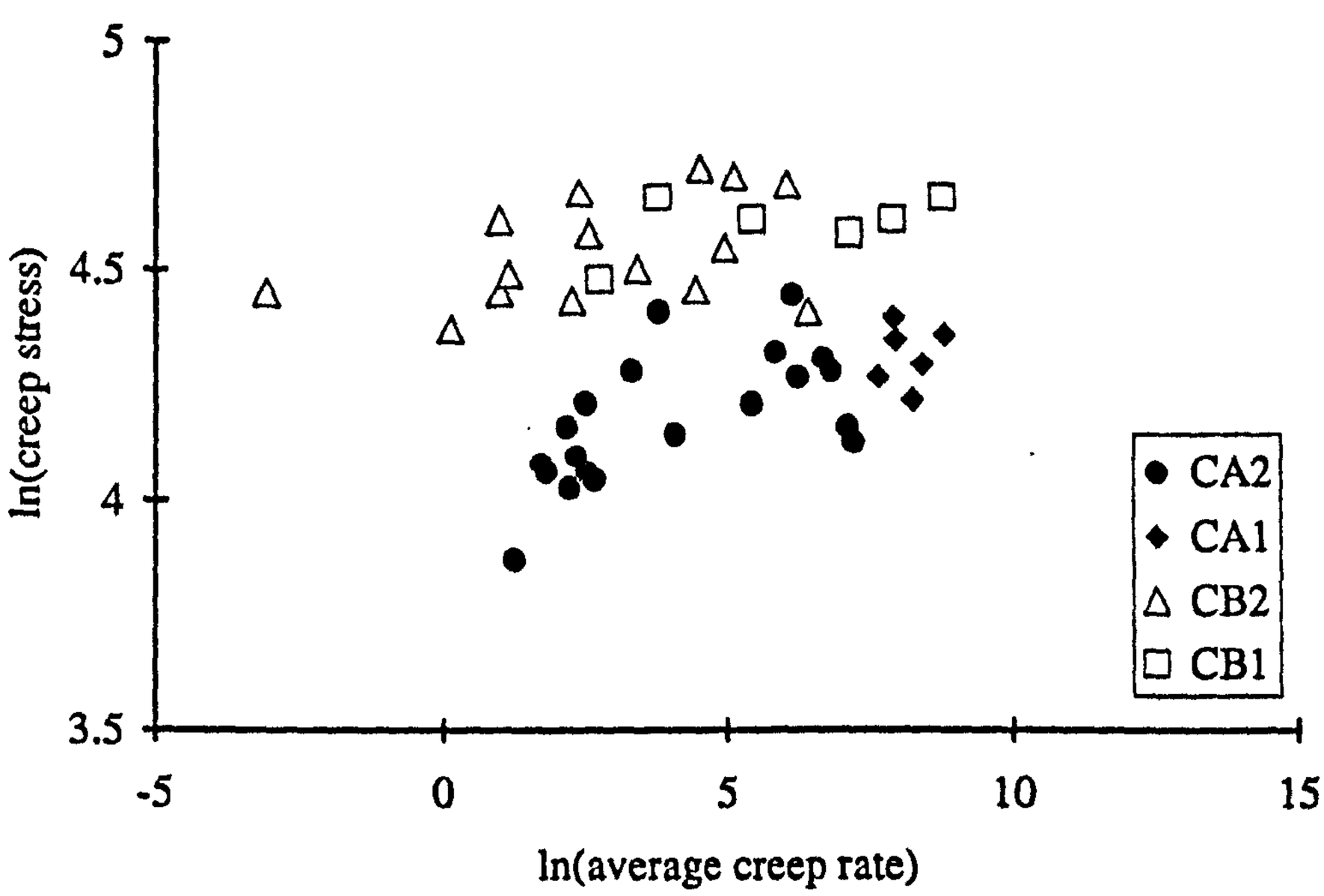

Units:

σ_0 Creep stress, MPa

$\dot{\varepsilon}_{0\rightarrow R}$ Average creep rate, $\mu\varepsilon\ s^{-1}$

Comments:

For full key see figure 4.038

Figure 4.049

Creep stress and average creep rate

4.3.7.16. LOGARITHM OF CREEP STRAIN AND THE LOGARITHM OF ELONGATION RATE: PART 4, SUMMARY

One result of this study is the observation that to attain the same elongation rate as antler bovine bone requires a greater creep stress. When considered in the light of the creep analogue tensile model,[31] this observation is consistent with the results for the tensile tests of antler and bone examined in section 4.2.6.6. The bovine bone specimens exhibit a higher knee stress than the antler specimens.

[31]This model is formulated in section 3.3.3.2.

Another result of this study is the poor relationship between the two main variables: elongation rate and creep stress. This relationship was found to be very poor whichever measure of elongation was used. It was mentioned in section 4.3.7.13 that the relationship of elongation rate to creep stress, is used as the basis of the damage concept formulated by Kachanov. Therefore, the lack of such a relationship demonstrated by the experimental data examined here casts considerable doubt on the application of the damage model in that form. Similarly a visco-elastic approach would predict a relationship of creep strain to creep stress, if the material is a solid. In the theoretical section on visco-elasticity a linear dependence on stress was assumed. From the evidence of a transition from an apparently solid to a fluid like material a higher power relationship would be expected. However, by definition a fluid will not attain a stable length during a creep test. Considering this fact and the lack of a failure criterion in visco-elasticity, modelling a relationship between the elongation at rupture and the applied stress is not straightforward.

This apparent lack of relationship between creep stress and elongation rate is probably due to the influence of other variables that have not been examined here. For example a simplistic consideration of porosity suggests that the stress on the material will be greater than the calculated one if the material contains more pores (blood vessels and so on). Likewise the structure of the materials is variable. However, it was envisaged that such variations would also be exhibited in the various measures of stiffness used. An attempt was made to use the material stiffness as a normalising variable, but this approach gave only limited success.

4.3.7.17. LOGARITHM OF TIME-TO-RUPTURE AND THE LOGARITHM OF ELONGATION RATE: PART 1, $\ln(t_R)$ AND $\ln(\dot{\varepsilon}_{1\bullet\rightarrow 3})$

The data for only 14 bovine bone specimens are presented in figure 4.050. This is because one of the values of creep rate was so low that it was effectively zero, thus its logarithmic value could not be obtained.

From figure 4.050 and the regression equations of the data given in table A9.032 there is clearly a very highly significant relationship between the time-to-rupture and the steady state creep rate. The *p* values associated with the creep rate in equations *a* (for antler) and *d* (for bovine bone), where it is the only explanatory variable, are both less than 0.001. The R^2 values associated with these equations, 93.0% and 82.8%, indicate that this single variable explains nearly all the variation in the time-to-rupture of specimens of bone and antler subjected to a creep test. Another notable point about the data sets for bone and antler is that they fall in the same region of the graph. This can be

illustrated by comparing the slope and intercept of the regression equation fitted to the data shown in figure 4.050. The values of the slope are -0.762 for antler and -0.773 for bone, and those of the intercept are 8.14 for antler and 7.68 for bovine bone. The data produced in this study can also be compared with that produced by Rimnac *et al.* (1993) for bovine femoral bone at 37°C. Their data are plotted with mine in figure 4.051, their data displays the same form of relationship.

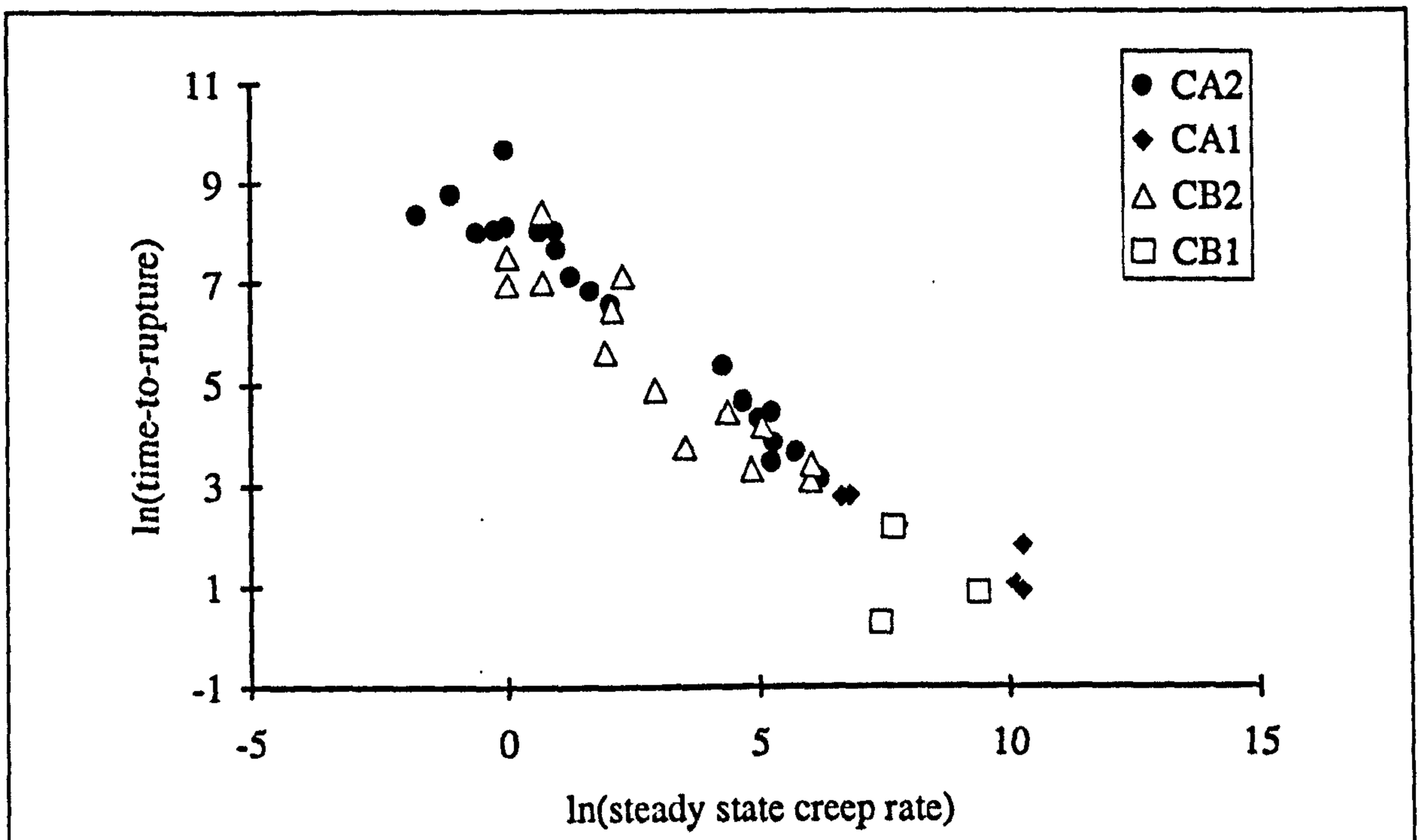

Units:

$\dot{\varepsilon}_{1*\rightarrow 3}$ Steady state creep rate, $\mu\varepsilon\ s^{-1}$

t_R Time-to-rupture, s

Comments:

For full key see figure 4.038

Figure 4.050

Steady state creep rate and time to rupture

Previously I reported (section 2.3.1) that Conway considered one of the most common relationships in creep-rupture to be the inverse proportionality between the time-to-rupture, t_R, and the secondary creep rate, $\dot{\varepsilon}_{1*\rightarrow 3}$. I pointed out that such a plot implies that the quantity $\varepsilon_3 - \varepsilon_1^*$ (or $\varepsilon_{1*\rightarrow 3}$) is constant. I did this by using the definition of steady state creep rate (equation 2.029) repeated here

$$\dot{\varepsilon}_{1*\rightarrow 3} = \frac{\varepsilon_3 - \varepsilon_1^*}{t_R} \text{ or } \frac{\varepsilon_{1*\rightarrow 3}}{t_R} \qquad (4.051)$$

Equation 4.051 was then rewritten in logarithmic form as

$$\ln(\dot{\varepsilon}_{1*\rightarrow 3}) = \ln(\varepsilon_{1*\rightarrow 3}) - \ln(t_R) \qquad (4.052)$$

Equation 4.052 would appear to imply that the relationship of creep rate to time-to-rupture should always have a slope of negative unity. However, if the quantity $\varepsilon_{1*\rightarrow 3}$ is also a function of creep rate (and thus by association possibly creep stress) then some other slope could be obtained.[32] Figure 4.052 shows that this is the case. Using the evidence of figure 4.052 it would appear that the relationship of steady state creep strain to steady state strain is of the form

$$\ln(\varepsilon_{1*\rightarrow 3}) = A + B \ln(\dot{\varepsilon}_{1*\rightarrow 3}) \qquad (4.053)$$

Regression analysis of the data shown in figure 4.052 shows that this form of relationship is statistically significant for bone and very highly significant for antler. The resulting equations are: for antler

$$\ln(\dot{\varepsilon}_{1*\rightarrow 3}) = -5.67 + 0.238 \ln(\dot{\varepsilon}_{1*\rightarrow 3}) \qquad R^2 = 55.7\% \qquad (4.054)$$

and for bone

$$\ln(\dot{\varepsilon}_{1*\rightarrow 3}) = -6.13 + 0.227 \ln(\dot{\varepsilon}_{1*\rightarrow 3}) \qquad R^2 = 25.7\% \qquad (4.055)$$

If equations 4.052 and 4.053 are combined the result is

$$\ln(\dot{\varepsilon}_{1*\rightarrow 3}) = A + B \ln(\dot{\varepsilon}_{1*\rightarrow 3}) - \ln(t_R) \qquad (4.056)$$

Thus converting this to the form of the regressions in table A9.032 gives

$$\ln(t_R) = A - (1 - B) \ln(\dot{\varepsilon}_{1*\rightarrow 3}) \qquad (4.057)$$

The values of B given above 0.238 for antler and 0.227 for bone, agree very well with the values of (1-B) in the regressions of table A9.032: 0.762 and 0.773 for antler and bone. Therefore the slope of the plots shown in figure 4.050 and 4.051, is closely related to the relationship of steady state creep strain and the steady state creep rate. The deviation from a slope of negative unity is due to the rate dependence of the steady state creep strain.

---

[32]In figure 4.042 it was shown that the total strain exhibited by the specimen at rupture was related to the extension rate.

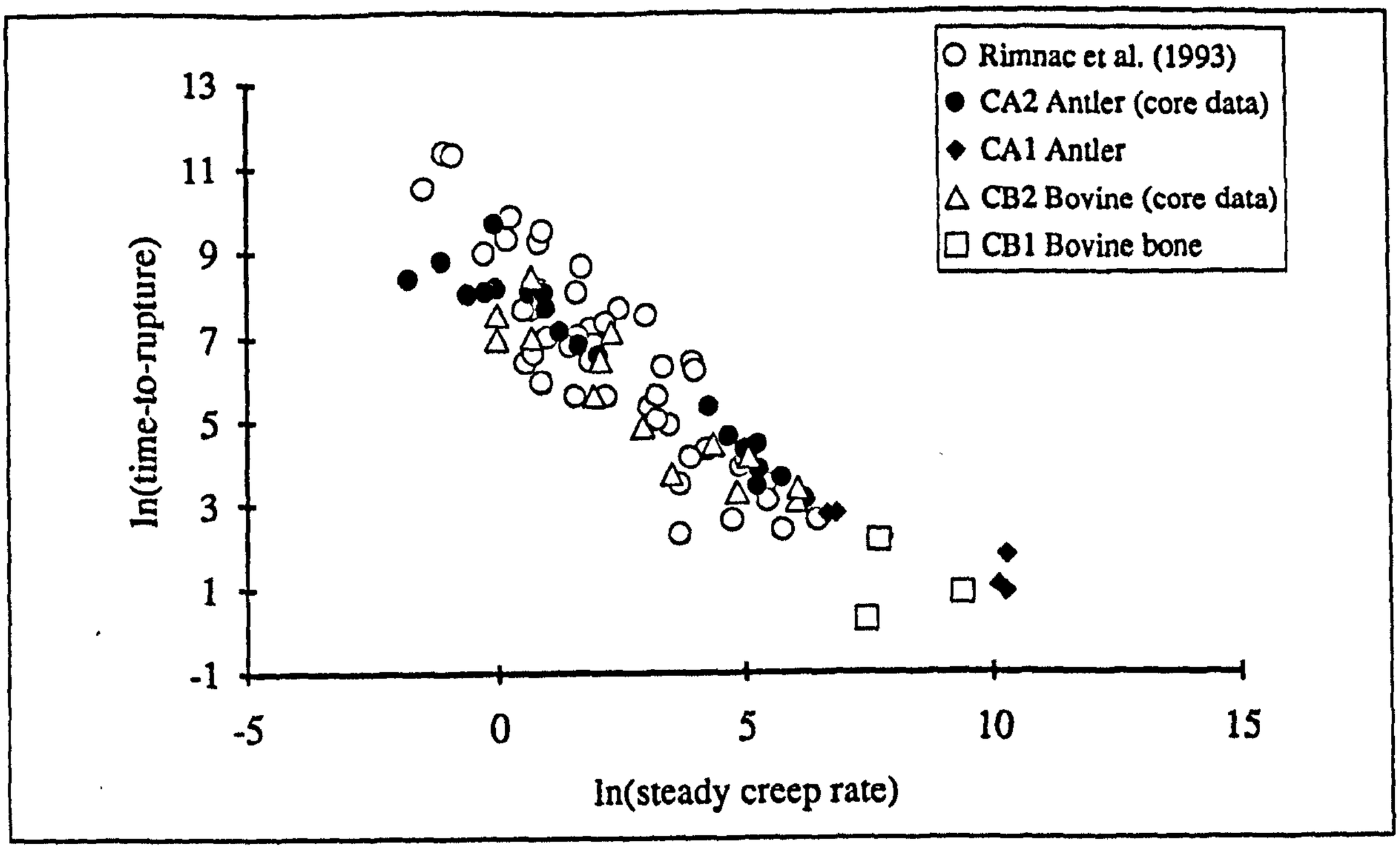

Figure 4.051 Reproduction of figure 4.050 with additional data.

Steady state creep rate and time-to-rupture, data from this study and Rimnac *et al.* (1993)

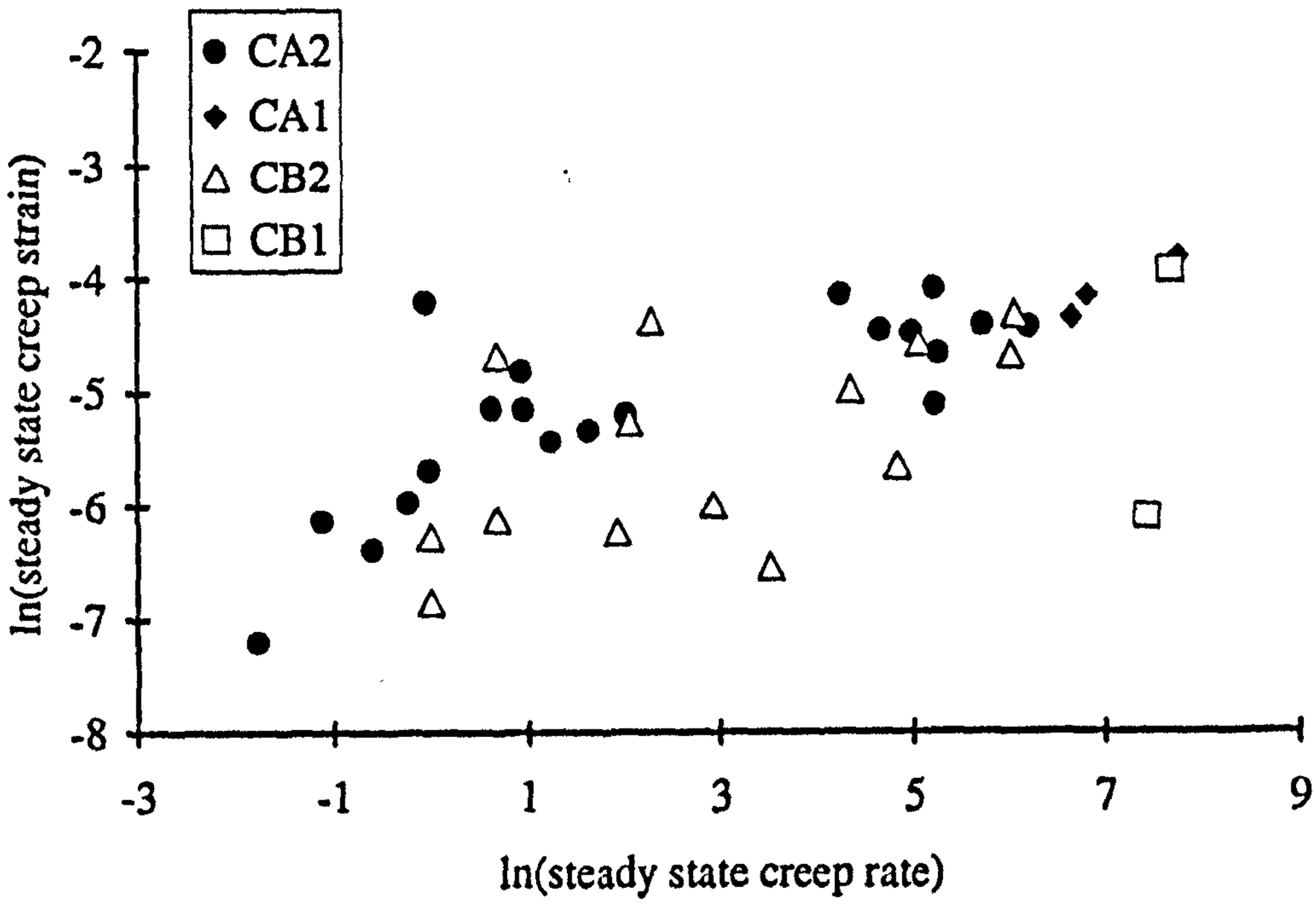

Units:

$\dot{\varepsilon}_{1*\rightarrow 3}$ Steady state creep rate, $\mu\varepsilon\ s^{-1}$

$\varepsilon_{1*\rightarrow 3}$ Steady state creep rate, unitless

Comments:

For full key see figure 4.038

Figure 4.052

Steady state creep rate and steady state creep strain

4.3.7.18. LOGARITHM OF TIME-TO-RUPTURE AND THE LOGARITHM OF ELONGATION RATE: PART 2, $\ln(t_R)$ AND $\ln(\dot{\varepsilon}_{1*\rightarrow R})$

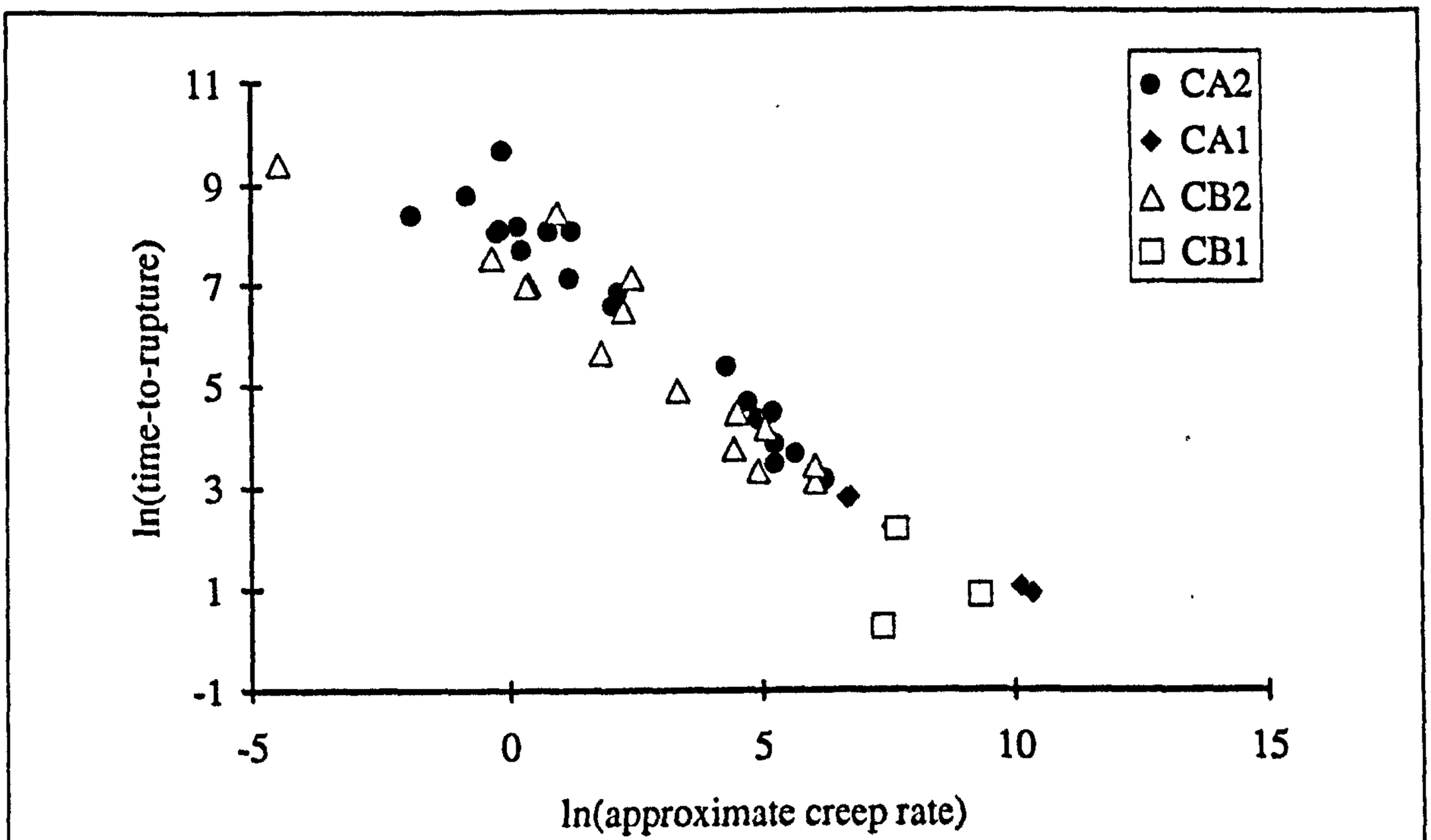

Units:

$\dot{\varepsilon}_{1*\rightarrow R}$ Approximate creep rate, $\mu\varepsilon\ s^{-1}$

t_R Time-to-rupture, s

Comments:

For full key see figure 4.038

Figure 4.053

Approximate creep rate and time-to-rupture

When the approximate creep rate is used as the only explanatory variable of the time-to-rupture (equations *a* and *d* table A9.033) the difference in the slopes of the regressions lines for bone and antler increases slightly (-0.772 for antler and -0.656 for bovine bone) compared to those where the steady state creep rate is the variable used, as in the previous section (table A9.032). The explanatory power of the relationship is still very high, and is increased slightly for the bovine results over those in the previous section. It has already been shown (table 4.009) that the distribution of strain between the various regions of the creep curve is different for bone and antler. Therefore, the rates calculated from those strains will also change. The point that appears on the extreme left hand side of the plot is that which had a steady state creep rate that was so low that it was approximated to zero, as reported previously. Re-analysis of the data without this point gives an equation of similar predictive power. However, this new equation has a different intercept and a slope closer to that of the antler data (-0.760).

The addition of the tertiary creep has had little effect on the predictive power of the regression equations compared to the when the steady state creep rate was used.

4.3.7.19. LOGARITHM OF TIME-TO-RUPTURE AND THE LOGARITHM OF ELONGATION RATE: PART 3, $\ln(t_R)$ AND $\ln(\dot{\varepsilon}_{0\rightarrow R})$

The measure of creep rate used here, that of the average creep rate over the whole period of the test has increased the division between the two materials. It has also resulted in an increase in the explanatory power of the relationships, with those of antler only a few per cent short of being fully explained. The lowest R^2 % value for the antler data (CA2) shown in table A9.034 is 98.7%, while the lowest for bovine bone is 88.4%. The division between the materials is a result of the previously mentioned difference in the shape of the creep curves.

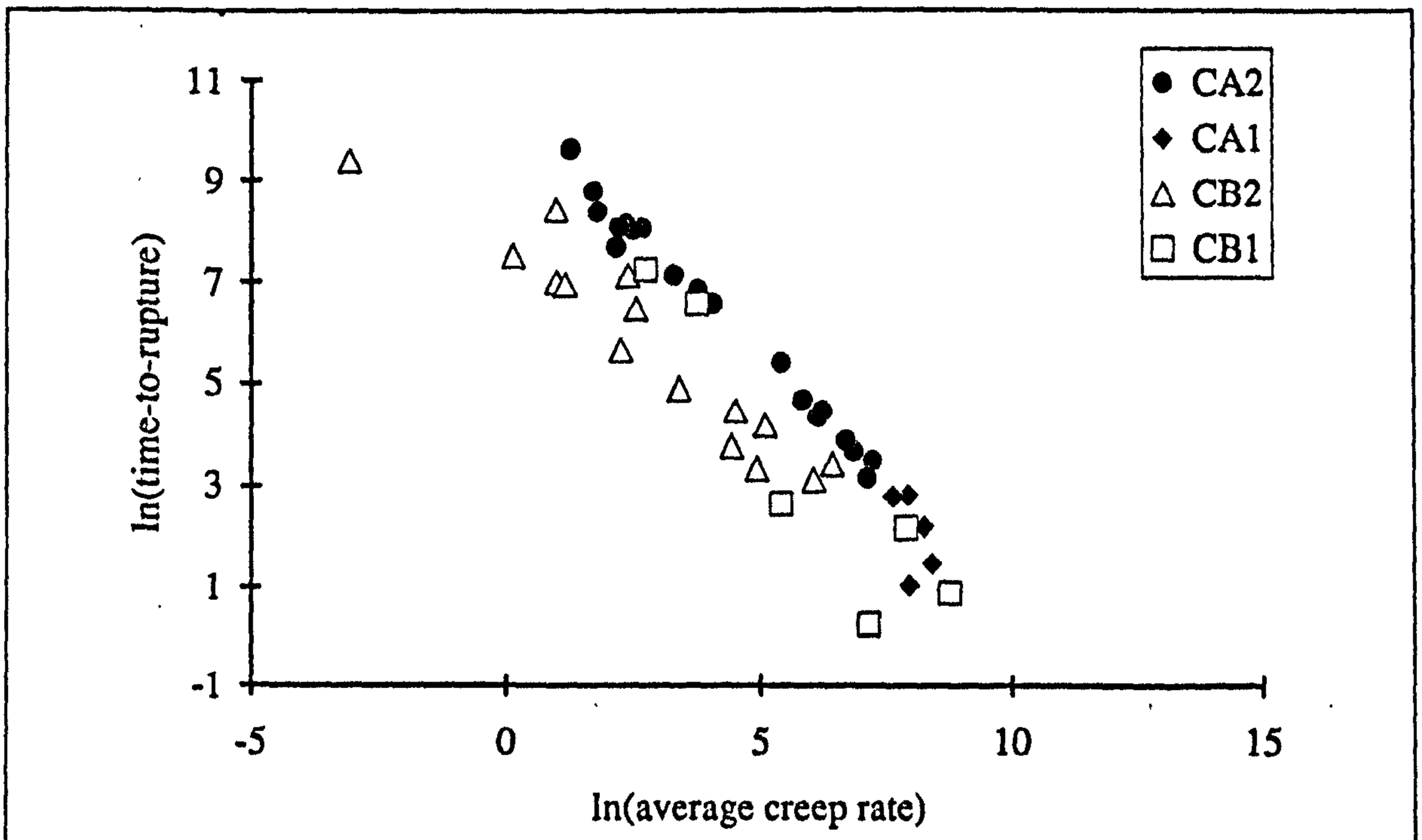

Units:

$\dot{\varepsilon}_{0\rightarrow R}$ Average creep rate, $\mu\varepsilon\ s^{-1}$

t_R Time-to-rupture, s

Comments:

For full key see figure 4.038

Figure 4.054

Average creep rate and time-to-rupture

4.3.7.20. LOGARITHM OF TIME-TO-RUPTURE AND THE LOGARITHM OF ELONGATION RATE: PART 4, SUMMARY

In sections 4.3.7.17 to 4.3.7.19 the relationship of the logarithms of the time-to-rupture and the elongation rate have been examined. A different measure of elongation has been used in each section. The most obvious result of this examination is the very strong relationship between these two variables, stronger than any other relationship for creep data examined so far. The strength of this relationship increases as more of the time dependent strain is taken into account in the variable. It is tempting to follow this trend to the extreme, and use a measure of the average total strain rate. In other words the total strain at rupture divided by the time-to-rupture. Indeed this gives very powerful predictive relationships. The R^2 value for regression equation equivalent to *a* in the tables A9.032 to A9.034 above is 94.9% for antler and for bone (equation *d*) 98.9%. However, further study of this relationship is not useful. This regression equation basically proves that rupture strain is constant, in the same way as the analysis in section 4.3.7.17 shows that the steady state creep strain is almost constant for the specimens of each type of material. The plot of the total strain rate follows the trend seen in figures 4.053 and 4.054, the data for both materials fall on two increasingly separated lines.

If the slope of the plots of the logarithms of time-to-rupture and elongation rate were negative unity this would indicate that the elongation at rupture were constant. However, this is not the case, as the elongation at rupture is dependent on the elongation rate (for example figure 4.052). The similarity of slope for the time-to-rupture and elongation rate plots for antler and bone suggests a similar rate dependence of the elongation term for both materials. The rate dependence of the rupture strain of creep tests and the ultimate strain of tensile tests was shown in figure 4.042. The evidence of that figure suggests this dependence is similar whether the extension rate is applied by external means (a tensile test) or is due to internal changes in response to an external load (a creep test). This supports the idea of assimilating these two types of test.

Another notable result is that in some cases the data sets for bone and antler not only have the same slope but appear to fall on the same line. In such cases the values of the elongation at rupture are not only a rate-modified value, but this value is the same for both materials. This observation is related to those made previously on the effect of using different measures of extension rate used (sections 4.3.7.13 to 4.3.7.16).

4.3.7.21. CLOSING REMARKS ON THE GENERAL CORRELATION APPROACHES SUGGESTED BY CONWAY (1967) AS APPLIED TO DATA FOR ANTLER AND BOVINE BONE

The analysis presented in sections 4.3.7.1 to 4.3.7.20 is based on the plots of creep-rupture data suggested by Conway (1967), presented here in table 2.001. I have extended this analysis to include other explanatory variables, and in some cases other approaches. For example figure 4.034 that shows the logarithms of creep stress and time-to-rupture uses the same axes as figure 2.011 that shows the two failure regimes modelled by Kachanov. I suggested that the antler data shows a transition that may be equated to the transition noted in Kachanov's approach: at the lower stresses a brittle rupture at the higher a ductile rupture. In support of this I cited the creep threshold proposed by Fondrk *et al.* (1988) for bone. Although the evidence for such a transition is slim, other results have been reported that appear to support this idea. However, the proposal that there are two different failure mechanisms occurring within the creep tests of antler could be (to paraphrase Witringham quoted at the start of this thesis) introducing a false maxim as data and building further inquiries upon these. I consider further experiments at lower stresses are required to clarify this proposal. (Clearly such tests will be of considerable duration.) The regression analysis of the data in figure 4.034 showed the relationship between the stress and time-to-rupture variables to be weaker than those in the literature it was compared with. Perhaps further experimentation, such as a study of porosity and structure, would explain more of the variance.

The other implications of the results obtained from the analysis presented in this section will be considered together with those of the other forms of analysis applied to these creep tests in section 4.3.10. Therefore I only highlight the main results in table 4.010.

Variables (section)	Material tested in creep	
	Reindeer antler	Bovine femoral bone
Creep stress Time-to-rupture (4.3.7.1 - 4.3.7.2)	There is a highly significant relationship between these two variables. Lower stresses result in a longer time-to-rupture.	The relationship of these variables is non-significant.
Creep stress Elongation-at-rupture (4.3.7.3 - 4.3.7.7)	The nature of the relationship depends on the measure of elongation used, but it is non-significant in all cases.	The nature of the relationship depends on the measured used, but in all cases it is significant and the elongation is greater at higher stresses.
elongation at rupture Time-to-rupture (4.3.7.8 - 4.3.7.12)	The relationships were significant in each case except where the measure of elongation was the creep strain.	All the relationships were non-significant.
Creep stress Creep rate (4.3.7.13 - 4.3.7.16)	Significant or highly significant relationship, this depends on the measure used. At higher stresses there is a higher the creep rate.	All relationships were non-significant.
Time-to-rupture Creep rate (4.3.7.1 - 4.3.7.2)	Very highly significant negative relationship, whichever strain rate measure was used.	As for antler.

Table 4.010

Summary of the main results obtained from creep tests of antler and bone by the general correlation approaches based on the suggestions of Conway (1967)

4.3.8. CREEP-RUPTURE RESULTS: THE DAMAGE APPROACH

In the first part of this section I shall examine the results of the creep-rupture tests on specimens of bovine femoral bone and reindeer antler, with reference to the damage approach as outlined in section 2.3.3. However, in the previous section (4.3.7) equations of the same form as some of those contained in the damage approach have been fitted to the data and damage models have been referred to. Where it is appropriate I therefore refer to those earlier sections rather than repeating the analysis here. Later in this section I examine the creep-rupture data using a variety of normalising variables similar to those used by Caler and Carter (1989) and Mauch, Currey and Sedman (1992).

4.3.8.1. KACHANOV'S 'RUPTURE BY AN IDEALISED DUCTILE PROCESS'

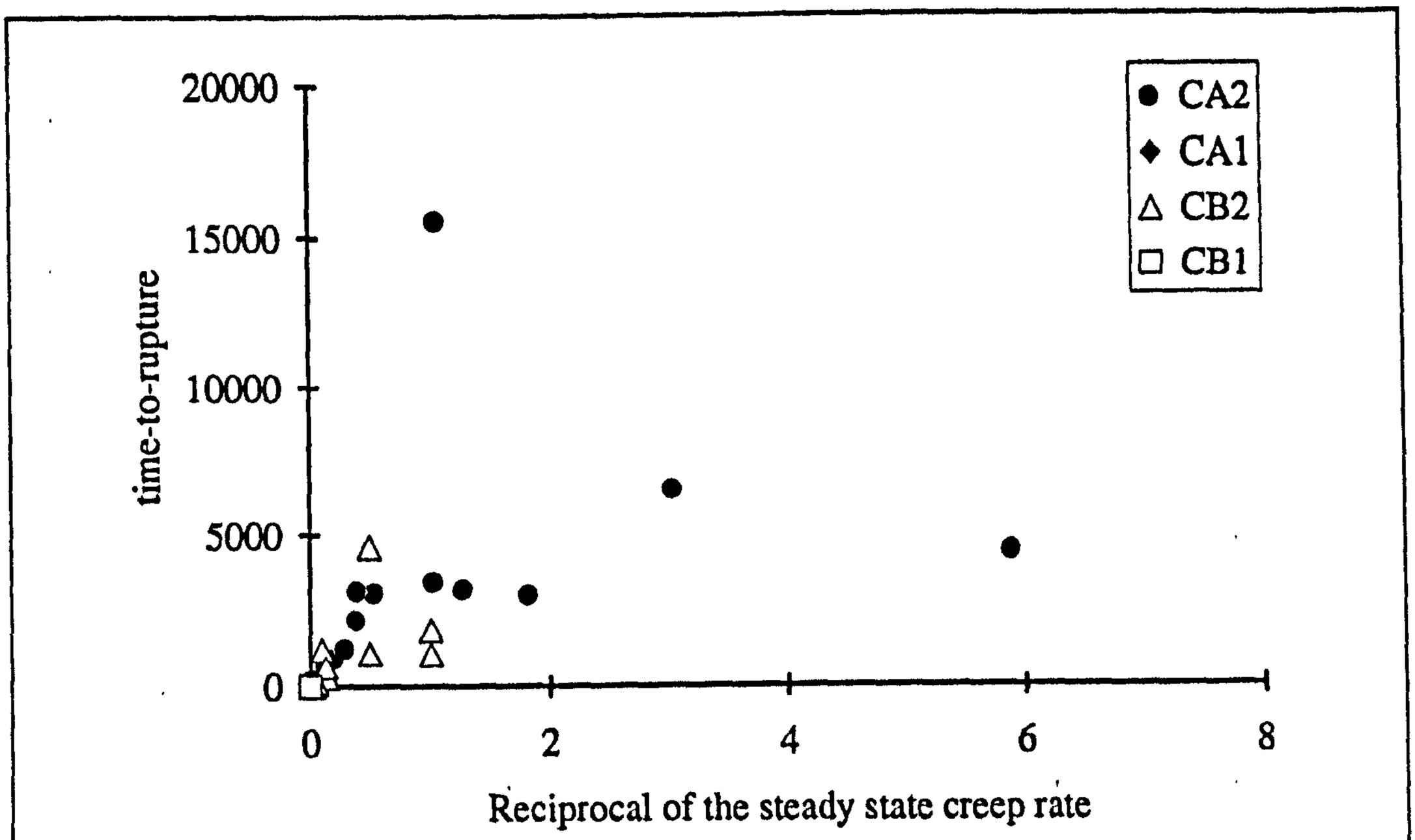

Units:

t_R Time-to-rupture, s

$1/\dot{\varepsilon}_{1\bullet\rightarrow3}$ Reciprocal of the steady state creep rate, s

Figure 4.055

The time-to-rupture and the reciprocal of the steady state creep rate

In the presentation of Kachanov's (or Hoff's) prediction of the time-to-rupture due to a purely ductile creep process (section 2.3.3.1) a number of equations were derived. One such equation that related the time-to-rupture to the initial applied stress has already been examined in section 4.3.7.1. However, in section 2.3.3.1 I showed that Kachanov's

equation could be expressed in a different form in which the rupture time is linearly related to the reciprocal of the initial steady state strain rate

$$t_1 = 1/(m\,\dot{\varepsilon}_0) \qquad (4.058)$$

Therefore, in the following plots and analysis I have used the time-to-rupture and the reciprocal of the measured steady state creep rate. If the data fit equation 4.058 a plot of time-to-rupture and the reciprocal of the steady state creep rate will form a line of gradient 1/m. Figure 4.055, shows that the data are very bunched near the origin so this region has been enlarged in figure 4.056. (If logarithms were taken of each variable the data would be more pleasingly distributed on the plot. However, the form of the relationship would not be so clear as such a plot would permit power terms to be included in the relationship.)

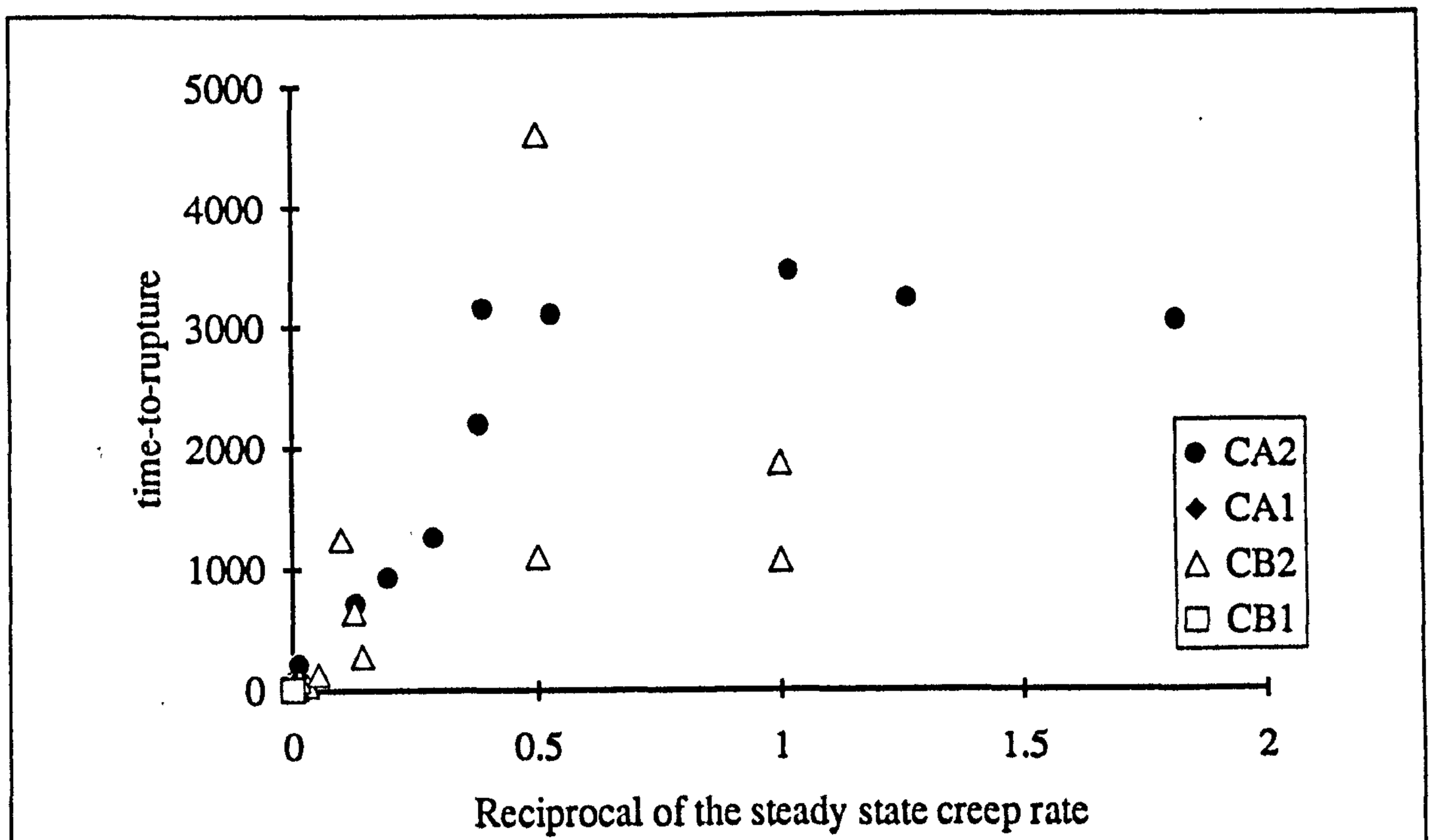

Units:

t_R Time-to-rupture, s

$1/\dot{\varepsilon}_{1*\rightarrow 3}$ Reciprocal of the steady state creep rate, s

Comments:

Curtailed axes, so some of the data points fall outside the region of the graph.

Figure 4.056

The time-to-rupture and the reciprocal of the steady state creep rate

Regression analysis of the data (table A9.035) shows only weak relationships between the two main variables. Thus the data obtained from creep tests of reindeer antler and bovine femoral bone do not fit the equation predicted for creep-rupture by a purely ductile process. The use of equation 4.058 rather than equation 2.038 (which

predicts the time-to-rupture as a function of stress) may give more insight to the failure process. I noted in section 3.3.1 that the equations that Kachanov gives for failure by a purely ductile process (2.039) and that for a purely brittle process (2.047) are of a similar form.[33] Thus fitting experimental data to one of these equations is the same as fitting the data to the other equation, but obtaining a different set of constants. Carter and Caler (1983) fitted their data to an equation that they said was the same as Kachanov's purely brittle rupture equation. However, the form of the equation they referred to was essentially the same as Kachanov's equation for failure by a purely ductile process. I noted in section 3.3.1 that due to the limited extension of specimens of bone at rupture the assumption of brittle behaviour is reasonable. The lack of agreement with the equation used here provides no evidence in favour of failure by a purely ductile process. The failure by an idealised brittle process is considered next.

4.3.8.2. KACHANOV'S 'RUPTURE BY AN IDEALISED BRITTLE PROCESS'

The equation that Kachanov gives for the prediction of time-to-rupture by a purely brittle process (equation 2.047) is based on the applied stress. This equation suggests a logarithmic relationship between the time-to-rupture and the creep stress. This relationship was examined in section 4.3.7.1 and it was shown that the data I have obtained were not well described by it. However, other workers have obtained such a relationship for bone. I do not know why my results do not show such a relationship; there does not appear to be any procedural or experimental artefact that can account for it, although a number of candidates have been examined. I consider that my results are, within experimental error, a true report of what happened to the material. I suggest that a large amount of the variation is due to variation in the material itself. I have no reasonable method for normalising this effect out of the analysis, as not all the specimens were tested in three-point-bending, nor was the tensile stiffness available for all the specimens.[34]

The variation between different specimens could be viewed as similar to the effect of testing a standard material at different temperatures; the creep rate is no longer simply determined by the creep stress. Therefore, if the only externally applied variable, stress, is not directly related to the behaviour of the material, a comparison between different aspects of the material's behaviour may be more beneficial. Such comparisons make up

---

[33] $t_1 = \frac{1}{m B_1 \sigma_0^{\,m}}$ (2.039) $\qquad t_2 = \frac{1}{B_2 (n+1) \sigma_0^{\,n}}$ (2.047)

[34] An assessment of the structure and porosity could have been made. This was not done as it was considered that the results may not justify the time required to determine these variables.

the bulk of the correlations suggested by Conway (1967) and conducted above. Such an approach can also be applied here. I consider that the equations that predict failure under the two idealised situations can be combined. This can be done by rearranging one to form an expression for the creep stress that is then substituted into the other. This operation will enable the prediction of the time-to-rupture by a purely brittle process to be expressed as a function of creep rate. This manipulation of the equations is conducted as follows:

$$t_1 = \frac{1}{m B_1 \sigma_0^{\,m}} \tag{4.059}$$

Equation 4.059 can be written as

$$\sigma_0 = (m B_1 t_1)^{\frac{-1}{m}} \tag{4.060}$$

This equation (4.060) can then be substituted into the equation 2.047 (the equation for time-to-rupture by a brittle process). This will give

$$t_2 = \frac{(m B_1 t_1)^{\frac{n}{m}}}{B_2 (n + 1)} \tag{4.061}$$

The time to fail can now be expressed in terms of the creep rate by using the following equation

$$t_1 = \frac{1}{m \dot{\varepsilon}_0} \tag{4.062}$$

The final result of this operation is

$$t_2 = \frac{\left(m B_1 \frac{1}{m \dot{\varepsilon}_0}\right)^{\frac{n}{m}}}{B_2 (n + 1)} = \frac{B_1^{\,n/m} \dot{\varepsilon}_0^{\,-n/m}}{B_2 (n + 1)} \tag{4.043}$$

It was noted in section 2.3.3.3 that $m \geq n$ (for metals).. This equation 4.063 conforms with the regression equations that were found to fit the data most accurately out of the various equations that comprised the 'general correlation approaches' of section 4.3.7. The strong power of this form of regression equation (R^2 values of over 90% in many cases) is not proof that the failure is purely brittle, but is certainly consistent with it. An equation of the same form to that I have derived from Kachanov's work (4.043) was used by Rimnac *et al.* (1993) (equation 3.056) to relate their creep results to those arising from the damage concept (see section 3.3.3). The interrelationship of the various approaches, experimental and analytical, presented in this thesis (either from my own work of published studies) is discussed in chapter 9.

4.3.8.3. KACHANOV'S 'RUPTURE BY AN COMBINED IDEALISED BRITTLE AND DUCTILE PROCESS'

In section 2.3.3.3 I presented Kachanov's prediction for the time-to-rupture by a combined ductile and brittle process. The equation he gave (2.061) is repeated here

$$\frac{t_3}{t_1} = 1 - \left(1 - \frac{(m - n)}{m}\ \frac{t_2}{t_1}\right)^{\frac{m}{m-n}} \qquad (4.064)$$

where

t_1 = time-to-rupture by a purely ductile creep process

t_2 = time-to-rupture by a purely brittle creep process

t_3 = time-to-rupture some combination of ductile and brittle creep processes.

In the two preceding sections I have used the relationship of the creep rate to describe the time-to-rupture by the two idealised modes. These could be substituted into equation 4.064 to obtain another possible form of regression equation. However, it was noted in section 4.3.7.1 that there was only a slight suggestion of a transition in the behaviour of the antler specimen. This conclusion was reached by comparing the creep results obtained in this study (figure 4.034) with the form of relationship predicted by Kachanov's equations (figure 2.011). Using this evidence and the agreement with the brittle failure equation and the disagreement with the ductile failure model, I suggest that the application of Kachanov's combined failure model will be of little benefit. However, if creep tests are conducted at lower loads, and the relationship of creep stress to time-to-rupture suggests a transition then this model may be useful.

4.3.8.4. ODQVIST'S CORRECTION TO KACHANOV'S APPROACH

In a previous section (2.3.3.5) I introduced Odqvist's correction to Kachanov's approach. I suggested that if the elongation at rupture was constant, the time-to-rupture would be related to the creep rate and the value of the 'instantaneous plastic strain'. Regression equations of this form fitted the data poorly. Odqvist introduced a correction to account for the creep that occurs in the primary stage. In creep curves shown in figures 4.030 to 4.033 the position of the diamonds marks the value of the instantaneous strain. These figures show (as do the values in table 4.009) that the behaviour of bone specimens is similar to that modelled by Kachanov: no primary creep region. The antler specimens behave in a way that may be modelled more accurately by Odqvist's correction: considerable primary creep. Unfortunately, I have been unable to confirm this observation by fitting the data to Odqvist's model. Another way of accounting for

the differences between the primary creep behaviour of antler and bone was suggested in the NTDF model applied in the following sections.

4.3.8.5. THE NTDF MODEL APPROACH: PART 1 NORMALISED BY BENDING STIFFNESS

In section 3.3.1 I reported that Carter and Caler (1983) consider part of the formulation of the TDF model to be equivalent to the model proposed by Kachanov. Kachanov's model was corrected by Odqvist to include the deformation that occurs in the primary region. A modification to the TDF model, which has a similar underlying effect, resulted in the NTDF model (described in section 3.3.2). This model is based on the relationship of time-to-rupture and the creep stress normalised by a measure of the material stiffness. There are a number of different possibilities available for the normalising stiffness. Some of these normalising factors are examined in this and subsequent sections.

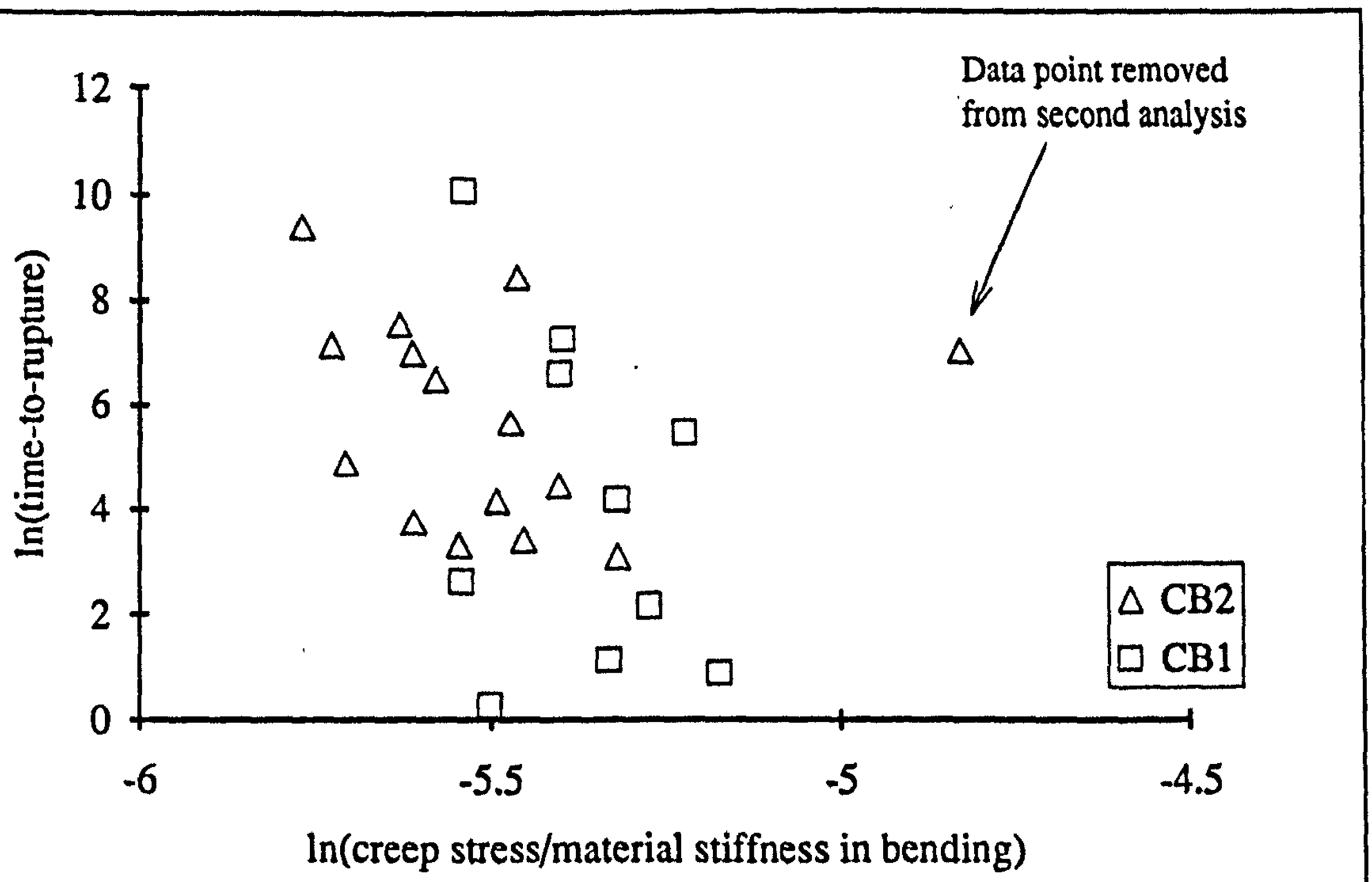

Units:

σ_0/E_b Creep stress/material stiffness in bending (or normalised stress), unitless

t_R Time-to-rupture, s

Figure 4.057

Relationship of time-to-rupture and the stress normalised by bending stiffness

In this section I consider the normalisation used by Mauch, Currey and Sedman (1992): the material stiffness in bending, E_b. Unfortunately, as I reported previously this measure is unavailable for the antler data. The normalised stress is obtained by dividing the creep stress by the stiffness, both expressed in the same units. Thus the resulting quantity is not only dimensionless, but also unitless.

The data I obtained is plotted in figure 4.057, and the associated regression equations given in table A9.036. The predictive power of the equations is reduced by the inclusion of the outlying data point shown in figure 4.057. When this point is removed, the regressions for the remaining 14 values of data set CB2 are those shown in table A9.037. The plot of the data has also been repeated this time with the addition of the regression lines described in the paper by Mauch *et al.* (1992) (see appendix 6), which have been appropriately converted.

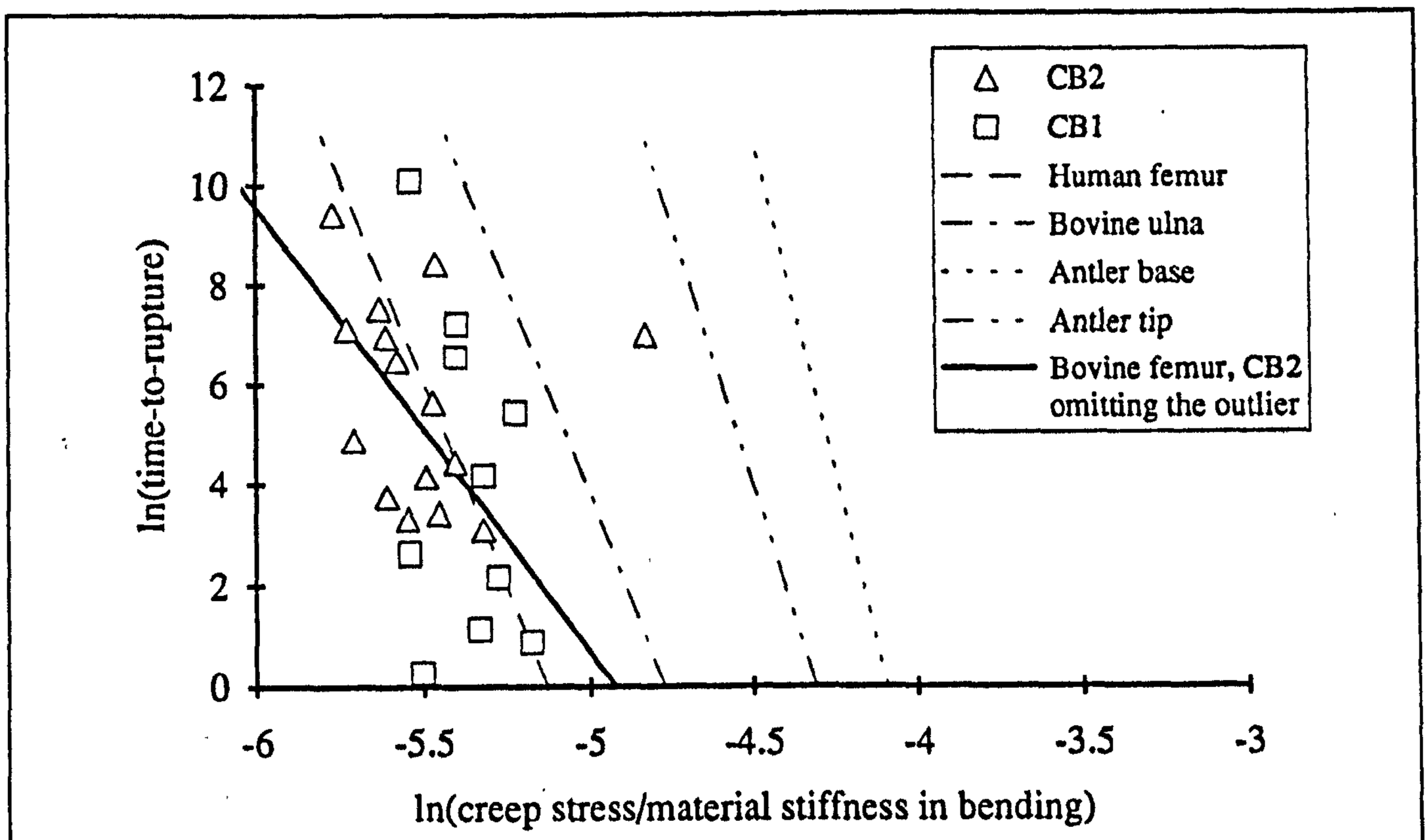

Units:

σ_0/E_b Creep stress/material stiffness in bending, unitless

t_R Time-to-rupture, s

Comments:

The data sets CB1 and CB2 are from the creep tests on bovine femoral bone conducted in this study. The dashed regression lines come from data in Mauch *et al.* (1992). These data are from their own work (antler and bovine) and from that of Caler and Carter (1989) (see appendix 6). The normalisation used by Caler and Cater was the tensile stiffness not the bending stiffness (see section 3.3.2).

Figure 4.058

Time-to-rupture and normalised creep stress

Figure 4.058 shows the results I have obtained and the regression lines calculated from this data. It also shows the regression lines given by Mauch *et al.* (1992) for their own data and that of Caler and Carter (1989). All the coefficients given by Mauch *et al.* are significant. In the equivalent results presented here (equation *a* of table A9.036 and *a* of table A9.037) only the coefficient (or would-be exponent) in the regression equation for the core data with the outlier removed is significant. Its value, 8.86, is approximately half that quoted for bone (human and bovine) and a little over a third of that quoted for antler by Mauch *et al.* Examination of the plot appears to show that for the full set of data without the outlier, the regression line from Caler and Carter's work fits the data better than that based on the core data (CB2) without the outlier. However, regression analysis of the larger data set (CB1 without the outlier) changed the equation only a small amount $\ln(t_R) = -41.0 - 8.39 \ln(\sigma_0/E_b)$.

The observation that the regression line obtained by Caler and Carter (1989) from tests on human bone conducted at physiological temperature passes through my data while that obtained by Mauch *et al.* for tests at room temperature on bovine ulna pass to the right of the main body of results add weight to a statement made in the latter paper:

> Comparing the results of Caler and Carter from the human femur with ours from bovine bone, it is clear that the bovine ulna specimens took, at any particular value of σ/E, a much longer time to fracture than the human specimens. However, this difference is not important. Compared with the experiments of Carter and Caler, our experimental method involved different specimen temperatures. . . It would be surprising if the fracture process were not in some way temperature sensitive.

This assertion is also supported by a recent paper by Rimnac *et al.* (1993) (section 3.3.3) who find that temperature has a significant effect on the creep rate of bovine femoral bone. However, as Rimnac *et al.* do not give the stiffness of their specimens, an exact comparison between their work and mine can not be made. The overall impression gained from figure 4.058 for the bovine and human bone results is that there is a stronger agreement between the results from specimens tested at the same temperature, as opposed to those obtained from the same species.

4.3.8.6. THE NTDF MODEL APPROACH: PART 2 NORMALISED BY TENSILE STIFFNESS

It was reported in the description of the experimental design (section 4.3.4) that the extensometer was used to monitor extension of the specimens during the creep tests. The original reason for monitoring strain was to obtain a value of the material stiffness measured during the loading period. This stiffness could then be used as a normalising factor. The result of this normalisation is shown in figure 4.059. As in the work of

Mauch *et al.* (1992) (appendix 6 figure 3), the clearest result here is the separation between the data for of reindeer antler and those for bovine bone.

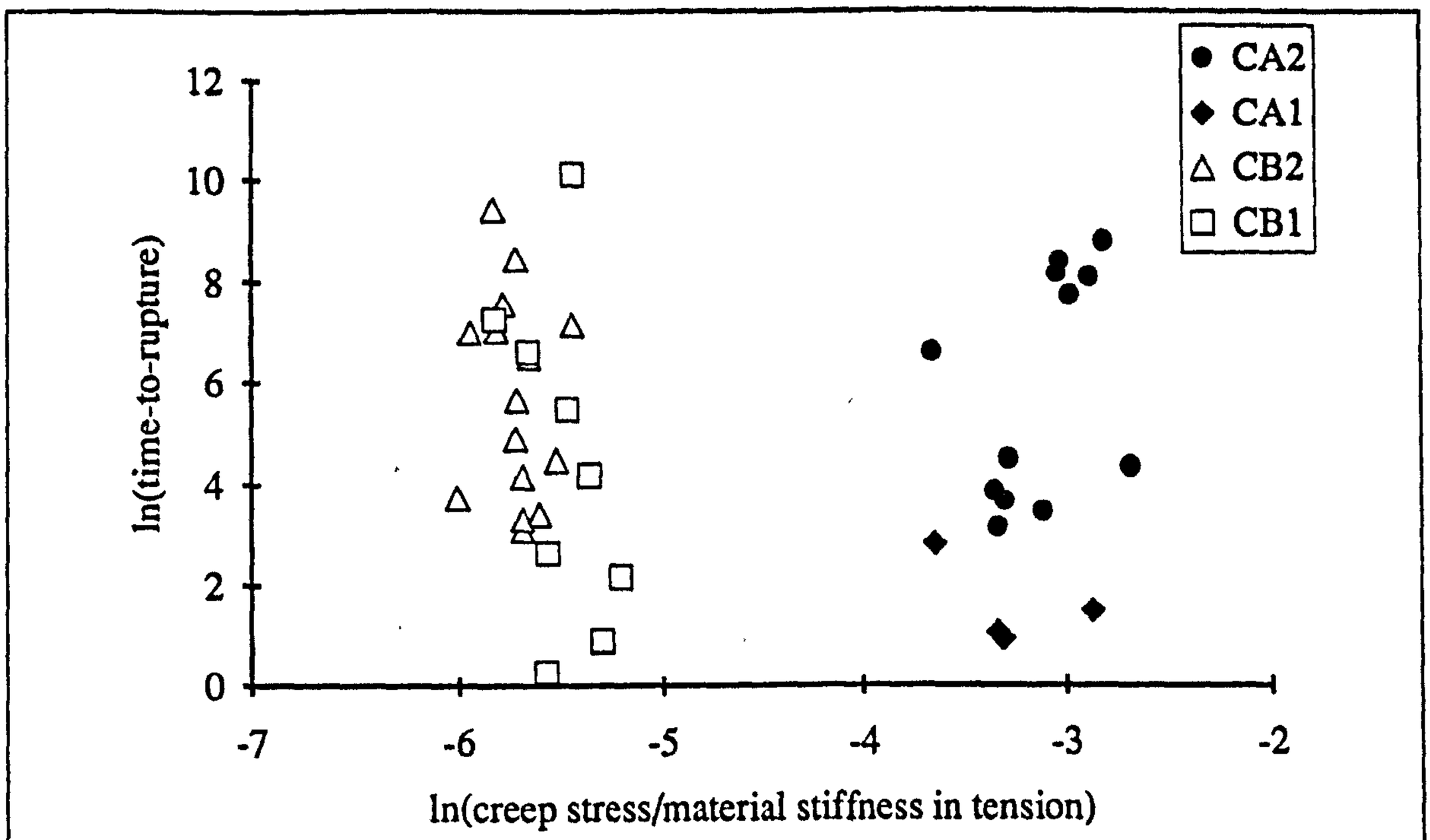

Units:

σ_0/E_t Creep stress/material stiffness in tension, unitless

t_R Time-to-rupture, s

Comments:

For full key see figure 4.038

Figure 4.059

Time-to-rupture and stress normalised by tensile stiffness

The regression equations of the data shown in figure 4.059 are presented in table A9.038. These equations show the same result as the figure. The normalised stress and time-to-rupture values for each material show little correlation with each other. This result is surprising, considering the results in the literature. I do not know the reason for the lack of a clear relationship within my own data. One interesting result is that of equation *b*, where the inclusion of the material stiffness measured in tension has increased the explanatory power of the relationship. Due to the nature of logarithms, regressing the logarithm of the stress normalised by the modulus is the same as regressing the two variables separately, because

$$\ln(\sigma_0/E_t) = \ln(\sigma_0) - \ln(E_t) \qquad (4.065)$$

Therefore equation *b* suggests that it may be better to use a fraction of the stiffness as the normalising factor rather than using it directly. One result of the relationship shown in

equation 4.065 is that some of the equations in table A9.038 are the same as those in table A9.019. (For example equation *b* of table A9.038 can be equated with equation *b* of table A9.019, the difference being due to rounding errors.) However, the most important point of these two regression equations of the antler data are that they suggest that the stress should be multiplied by the stiffness rather than being divided by it. The trend shown by the antler data is for an increase in stiffness to be related to a decrease in the time-to-rupture.

The interrelationship of the equations in this section and those of section 4.3.7.1 can be viewed as connecting the approaches of Conway, Kachanov, Odqvist with that of Caler and Carter. Thus the poor agreement of this equation with the experimental data of this study is disappointing. When the excellent fit of this type of model to experimental results obtained by Caler and Carter, and the fit obtained of Mauch *et al.* are considered (see appendix 6) it appears that the use of the material stiffness measured during the loading period of the creep test may be an inadequate normalising factor. Considering the evidence from other workers, other relationships and evidence in this thesis I do not consider that the poor fit of this interpretation of the NTDF model to these data is grounds for its rejection. However, it may be grounds for questioning the experimental technique, especially the value of material stiffness. It has been pointed out in appendix 7 that a soft testing machine can affect the measured stiffness of a material. The design of the creep rig had a considerable softening effect on the test machine.

4.3.8.7. THE NTDF MODEL APPROACH: PART 3 INSTANTANEOUS STRAIN

The interpretation of σ/E as 'some measure of the initial strain' was suggested by Mauch *et al.* Therefore, another pair of explanatory variables suggest themselves, ε_0 and ε_1^*. In this section I examine the relationship of $\ln(t_R)$ and $\ln(\varepsilon_0)$.

As observed in the analysis of $\ln(t_R)$ and $\ln(\sigma/E_t)$, the results for bone and antler are displaced from each other along the horizontal axis. This indicates that to rupture at the same time the antler specimens must be subjected to a larger instantaneous strain than the bovine femoral specimens. The results, especially those of antler, show considerable scatter. Despite this scatter they still reinforce the findings of Mauch *et al.*: specimens of antler (reindeer or red deer) take longer to fail than those of bovine bone (correspondingly femoral or ulna). The difference in the relationships of time-to-rupture to the instantaneous strain could be due to the difference in the calcium content of the two materials. However, the coefficient of the calcium term is different in equations *c* and *g*.

Thus statistically there may be an improvement if calcium is used as a variable in analysis of the pooled data, but it may be acting as little more than a label as to which specimens are bone and which are antler.

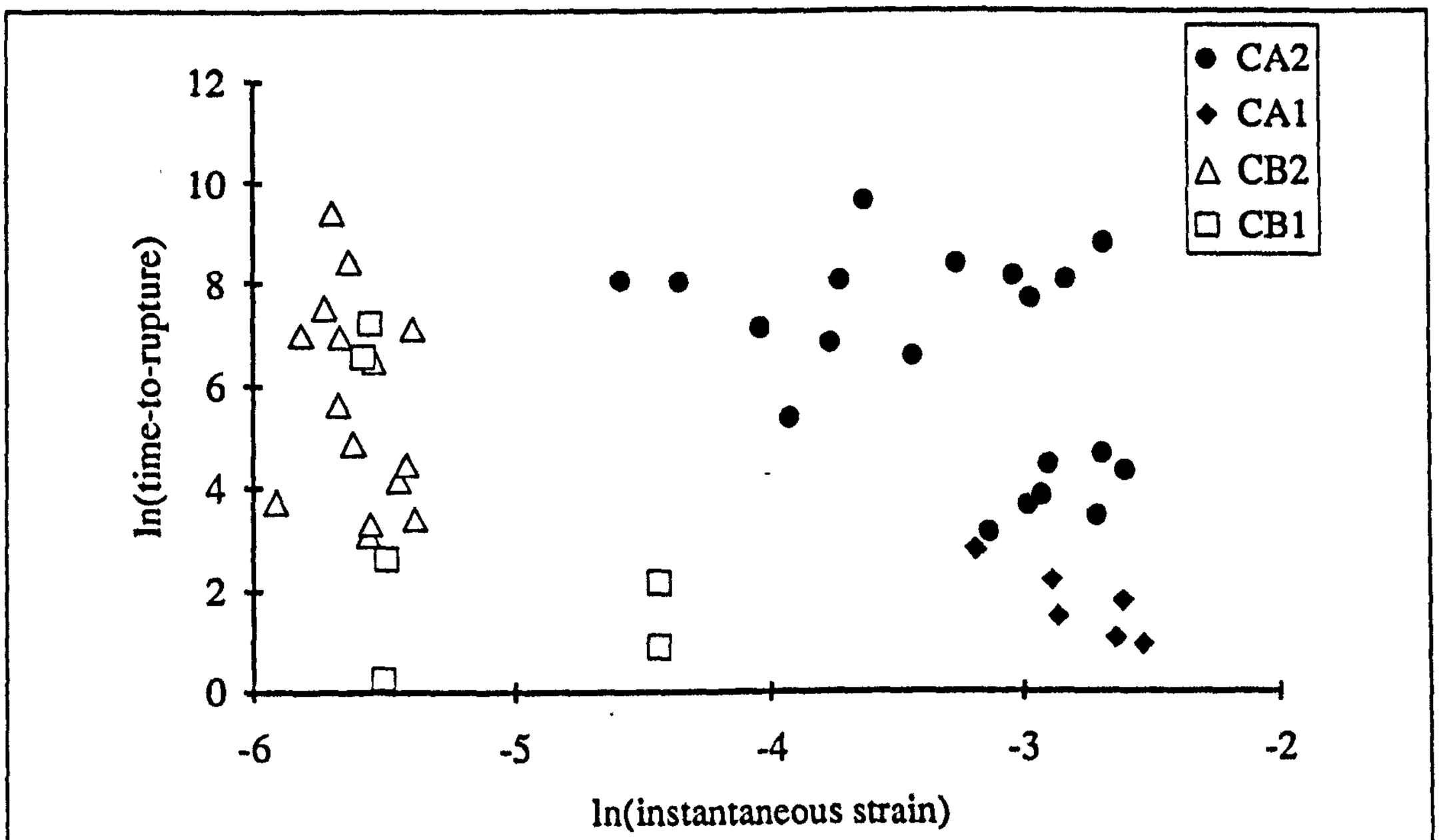

Units:

ε_0 instantaneous strain, unitless

t_R Time-to-rupture, s

Figure 4.060

Time-to-rupture and instantaneous strain

4.3.8.8. THE NTDF MODEL APPROACH: PART 4 STEADY STATE INSTANTANEOUS STRAIN

In this section I examine the second alternative to the normalisation of the creep stress by the material stiffness made possible by the use of an extensometer. This quantity is the steady state instantaneous strain, obtained by the backward extrapolation of the steady state region of the creep curve (see figure 4.061).

Figure 4.061 shows the data points for both the full and core data sets. This is similar to the approach in section 4.3.7.11. However, logarithmic values of both quantities are used here. Figure 4.061 has been repeated (in figure 4.062) with only the core data sets (CA2 and CB2). The regression equations for the core data are given in table A9.040.

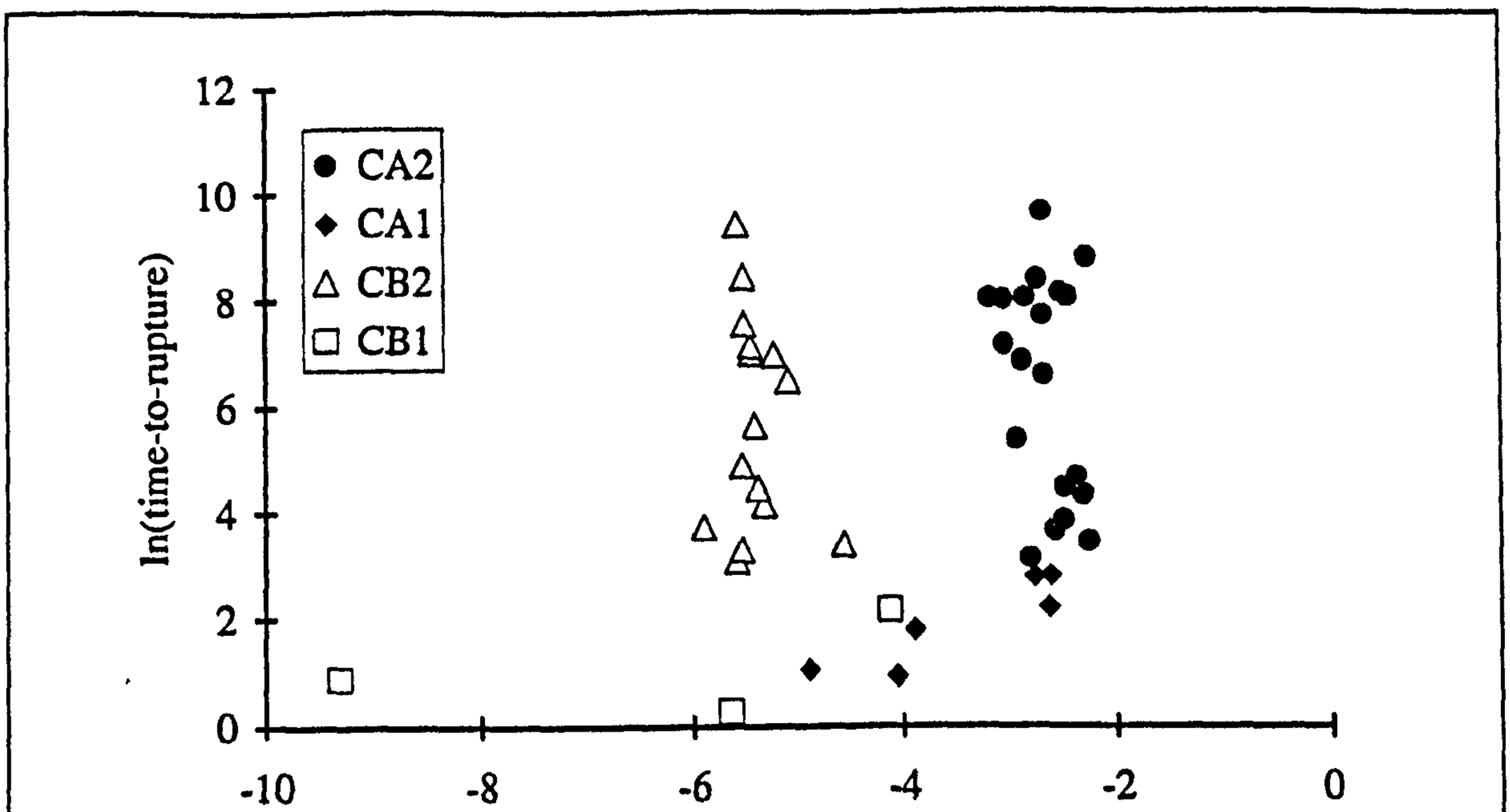

Units:

ε_1^* steady state instantaneous strain, unitless

t_R Time-to-rupture, s

Figure 4.061

Time-to-rupture and the steady state instantaneous strain

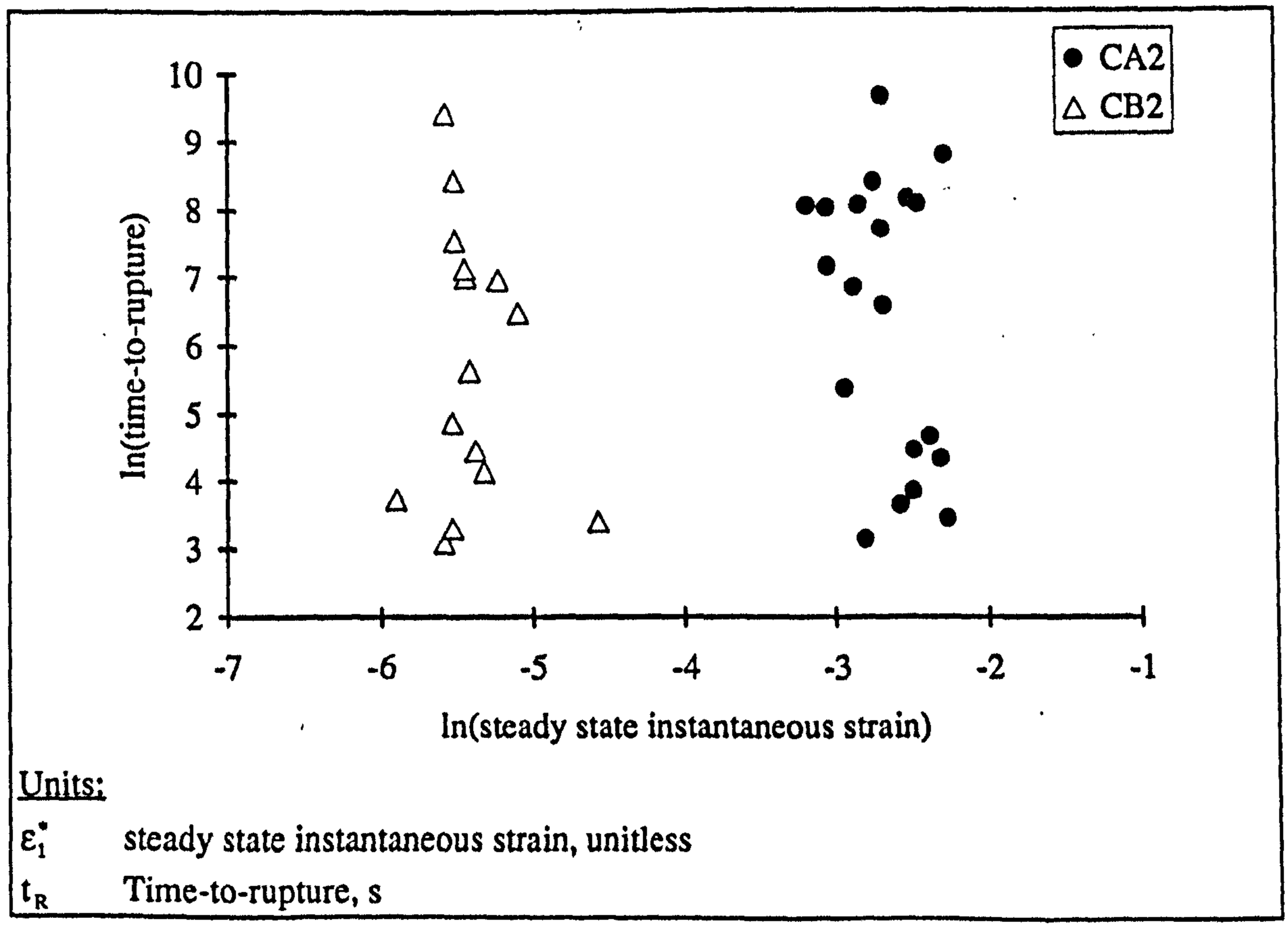

Units:

ε_1^* steady state instantaneous strain, unitless

t_R Time-to-rupture, s

Figure 4.062

Time-to rupture and the steady state instantaneous strain

The results for the core data for each material are clearly separated. However, the regression analysis in table A9.040 shows that there is no significant relationship between the steady state instantaneous strain and the rupture time. (The *p* values associated with the strain term in equations *a* and *d* are 0.144 and 0.651 respectively.) The separation between the results for bovine bone and antler displayed here is more a reflection of their different elastic properties than their different creep behaviour, but as Conway pointed out (section 2.3.1), the pre-rupture behaviour is likely to affect that associated with rupture.

4.3.8.9. THE NTDF MODEL APPROACH, PART 5: SUMMARY

It is evident that the NTDF model, in its various forms, is not compatible with the data presented here. This is probably a result of a number of factors; one of these is the inadequacy of the normalising factor. With hindsight, constant rate tensile tests to a low stress level, as used by Caler and Cater (1989) may have been a better approach. Due to the lack of agreement with the NTDF model, it cannot be used as evidence in determining the failure mode.

The only clear result obtained from the analysis of the application of the NTDF model is the obvious difference between the bone and antler. This evidence reinforces a question raised by Mauch *et al.*: if the use of a normalising factor improves the relationship for each material separately, why does it not improve the overall relationship and bring the data sets together? The key to the difference in behaviour of antler and bone may be in the rate at which damage is accumulated. This is examined in section 4.3.9.

4.3.8.10. SUMMARY OF THE DAMAGE APPROACH

In sections 4.3.8.1 to 4.3.8.9 I have examined the application of the equations derived from the damage approach to the creep rupture data obtained from tests on specimens of bone and antler. Unfortunately the data I have obtained do not readily conform to these forms of equation. This result is somewhat surprising considering some of the results published in the literature. I have attributed some of this lack of conformity to the lack of an adequate normalising factor. Without knowing the cause of the low predictive power of the relationships, the possibility that the application of these equations is not justifiable must be considered. By implication this result erodes the evidence for the creep behaviour of bone being due to a damage process. However, this

lack of supporting evidence cannot be used as evidence against the idea of a damage process.

4.3.9. CREEP-RUPTURE RESULTS: MODELLING THE CREEP CURVE USING CONSTITUTIVE DAMAGE EQUATIONS

In section 2.3.3.6 I asked whether creep deformation is independent of the damage parameter. I reported that a pair of constitutive equations had been developed by Hayhurst and other workers in various of papers, over a number of years.[35] The constitutive equations relate the strain rate to the amount of damage within the material, and the rate of damage accumulation to the amount of damage already accumulated by the material. A large amount of literature has been produced by Professor D. R. Hayhurst and his co-workers.[36] Unfortunately, as I become aware of this literature at a late stage in this study, I have not been able to review more than a few papers. I have therefore based this section around a single paper by Dunne, Othman, Hall and Hayhurst (1990) entitled *Representation of Uniaxial Creep Curves Using Continuum Damage Mechanics.* Because my creep-rupture tests were conducted before I was aware of this paper, the experimental design is not ideal for the application of the methods expounded in the paper. Therefore I view this section, although containing many interesting results, as preliminary to further research.

In figures 4.030 to 4.033, creep-rupture curves were shown for both bovine bone and reindeer antler. From these few images it was clear that bovine bone and antler exhibit different strain-time curves when under constant load. This appearance was reinforced numerically by determining the percentage of the total creep strain assigned on average to the different regions of the creep curve (table 4.009). The bovine specimens appear to extend rapidly during the loading period, and when the creep stress is reached, the extension rate is drastically reduced. The extension rate then appears almost constant until shortly before failure. It appears that bovine femoral bone exhibits only a slight primary creep region (relative to the secondary region). For antler specimens almost the opposite is true; on attaining the creep stress they continue to extend at a high rate displaying a considerable primary creep region. This primary region gradually evolves into a steady state region (or region of minimum creep rate). Rupture occurs without any noticeable increase in creep rate.

---

[35]Many of these papers are concerned with creep rupture of metallic components or specimens, some of which contain notches. A number of the papers contain photographs of damage in the form of intergranular voids within the metal's structure.

[36]I would like to express my thanks to Professor Hayhurst for supplying a number of recent reprints.

The shape of the strain-time response during a creep-rupture test is important because it is a reflection of damage accumulation (assuming the material is an elastic damage one). In the TDF and NTDF models one of the basic assumptions was that damage is accumulated uniformly during the period of a creep test. Damage and strain are related so the difference in the shape of the creep curves raises the question: whether this is a reasonable assumption. In section 3.3.3 I reported Currey's (1989) remark that the high power of stress in the TDF model implies that the damage rate in antler at stresses only fractionally above the knee stress imply damage rates several orders of magnitude greater than that at yield. Currey remarks that it is unlikely that the ability of antler to sustain stresses considerably above the knee stress is due to the ability of antler to absorb more damage. In section 3.3,3.2 I suggested that if a tensile test and a creep test could be compared, different shapes of the strain time response during the creep test would predict a different stress-strain response during a tensile test. Examination of the creep curves in figures 4.030 to 4.033 qualitatively answers some of these questions: the shape of the antler creep curve is that which I predicted would result in the type of post knee behaviour exhibited by antler is a tensile test. More rigorous examination of these curves enables expansion of some of these arguments. For example if equation 2.114 is used for damage, repeated here

$$D = 1 - \frac{E_M}{E_U} \tag{4.066}$$

Assuming a constant damage rate under constant stress would result in the following equation for an ideal creep test constant stress:

$$D = 1 - \frac{\varepsilon_U}{\varepsilon_M} \tag{4.067}$$

If ε_U is assumed to be equal to ε_0 and damage is equal to unity at rupture the strain time response of a constant damage rate creep response can be represented as

$$D = 1 - \frac{\varepsilon_0}{\varepsilon_M} = \frac{t}{t_R} \tag{4.068}$$

Thus

$$\varepsilon_M = \varepsilon_0 \Big/ \left(1 - \frac{t}{t_R}\right) \tag{4.069}$$

Equation 4.069 can be represented diagrammatically as shown in figure 4.063 (plotting $\varepsilon_M/\varepsilon_0$ against t/t_R). If rupture occurs before damage reaches a value of unity (which is the case unless the strain at rupture is infinite) the plot shown in figure 4.063 will bear more resemblance to the creep curves of bovine bone than those of antler, especially in the tertiary region. These observations support the suggestion that it may be the differences in accumulation, distribution or mechanism of damage in bone and antler that results in their different mechanical behaviour. Thus the examination and quantification

of the differences in the creep curves may provide more information on the differences between the materials than the creep stress, creep rate and time-to-rupture relationships examined in the previous sections.

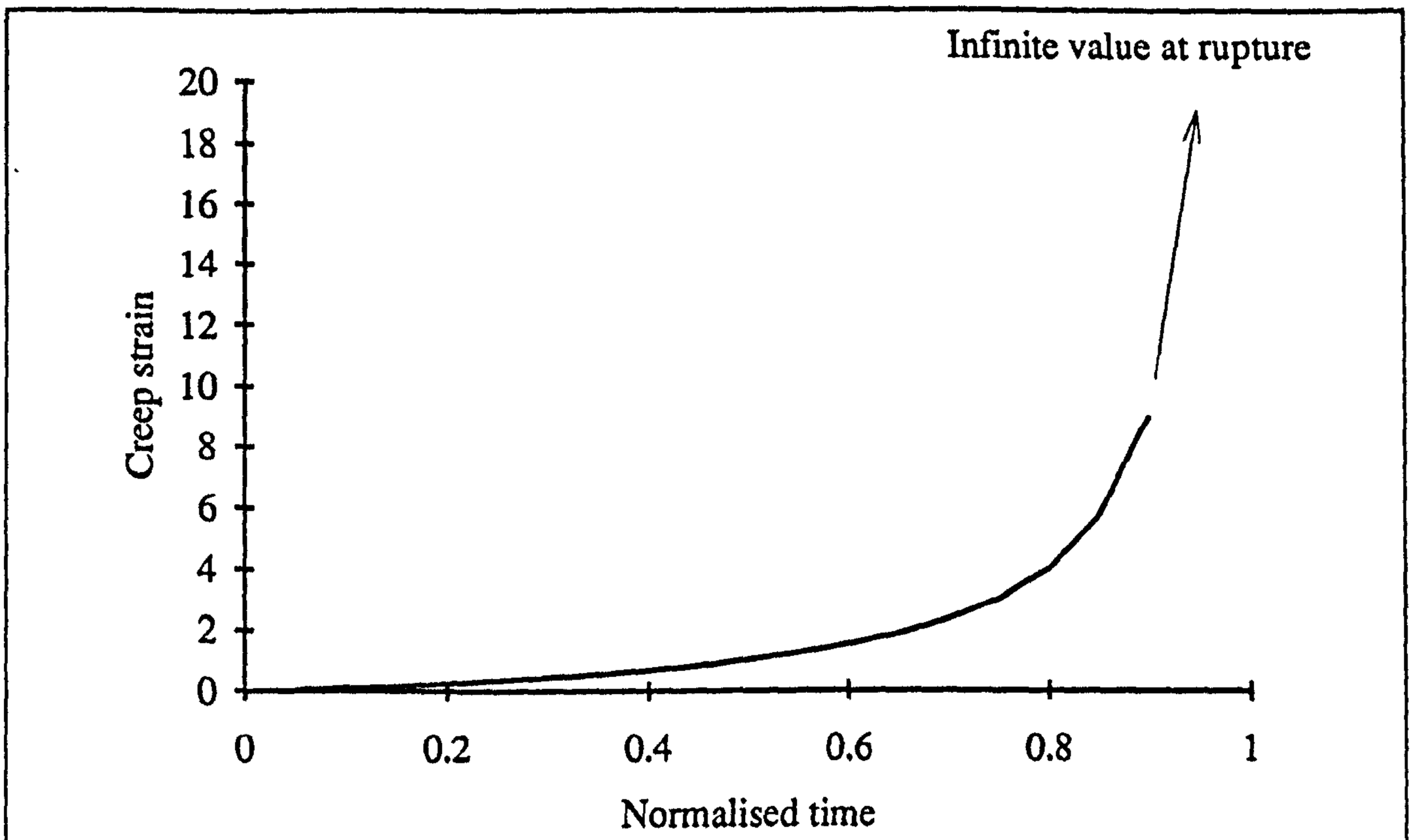

The creep strain is expressed in multiples of ε_0. The time is shown normalised by the time-to-rupture.

Figure 4.063

Prediction of the creep strain during a creep test where damage is accumulated at a constant rate.

Dunne *et al.* (1990) examine constitutive damage equations developed by Hayhurst and co-workers. The equations they examine are those for uniaxial creep, and are given in the following form (in this section I will retain Dunne *et al's* nomenclature for the theoretical equations):

$$\dot{\varepsilon} = K t^{-m} \left(\frac{\sigma}{1 - \omega} \right)^{n} \qquad (4.070)$$

$$\dot{\omega} = A t^{-m} \frac{\sigma^{\nu}}{(1 - \omega)^{\phi}} \qquad (4.071)$$

where (in the authors' words) $\dot{\varepsilon}$ is the strain rate, $\dot{\omega}$ the damage rate, σ the applied stress, t the time, and K, m, n, A, ν and ϕ the material constants (which the authors determined for alloy 800H at 850°C and 2¼ Cr-Mo at 550°C). The authors say that the scalar damage variable, ω, (for which I use D) is introduced into the strain rate equation to model the progressive deterioration and failure of the material, which becomes dominant during tertiary creep. The authors state that the two constitutive equations (4.070 and 4.071)

may be integrated in closed form to obtain the relationship between the creep strain and time. This equation is given as

$$\varepsilon = \frac{K \sigma^n t_f^{1-m}}{(1-m)\left[1-\left(n/(\phi+1)\right)\right]}\left[1-\left[1-\left(t/t_f\right)^{1-m}\right]^{1-\left(n/(\phi+1)\right)}\right] \qquad (4.072)$$

where t_f is the time-to-rupture and is given by

$$t_f = \left[\frac{1-m}{A(\phi+1)\sigma^v}\right]^{1/(1-m)} \qquad (4.073)$$

The authors then state that these equations have been used (by Othman and Hayhurst, 1990) to develop a stress independent two-parameter representation of uniaxial creep. First Dunne *et al.* obtain the expression for the creep-strain at failure, which they do by substituting $t = t_f$ into equation 4.072, giving

$$\varepsilon_f = \frac{K \sigma^n t_f^{1-m}}{(1-m)\left[1-\left(n/(\phi+1)\right)\right]} \qquad (4.074)$$

Dunne *et al.* (1990) then say that equation 4.074 can be normalised to give equation 4.076.

$$\varepsilon/\varepsilon_f = 1-\left[1-\left(t/t_f\right)^{1-m}\right]^{\left[1-\left(n/(\phi+1)\right)\right]} \qquad (4.075)$$

which is expressed in a more concise way as

$$\upsilon = 1-\left[1-\tau^{1-m}\right]^{\Delta} \qquad (4.076)$$

where υ is the normalised strain, τ the normalised time, and Δ is the material constant group $\left[1-\left(n/(\phi+1)\right)\right]$. The authors then discuss methods of determining the six material constants; K, m, n, A, ν and ϕ. They use a Gauss-Newton optimisation technique to fit their experimental data to equation 4.076 to obtain the constant groups (1 - m) and Δ. They say this can be done for a series of stress levels, thus obtaining a series of values. It has already been shown that the creep behaviour of the biological tissues studied here depend on other variables besides stress. Due to the preliminary nature of the study in this thesis and time limitations, I adopted another approach. First I rearranged equation 4.076 and expressed it in logarithmic form.

$$\ln(1-\upsilon) = \Delta \ln\left(1-\tau^{1-m}\right) \qquad (4.077)$$

Using values of υ and τ obtained from the digitally recorded creep data,[37] I examined the relationship of two quantities using least squares linear regression, of the form

$$\ln(1-\upsilon) = A + B \ln\left(1-\tau^{1-m}\right) \qquad (4.078)$$

---

[37]Although not explicitly stated, it appears that in this paper the normal convention of referring to the time dependent deformation as the creep strain is followed. Thus I used the following calculations $\upsilon = (\varepsilon - \varepsilon_0)/(\varepsilon_R - \varepsilon_0)$ and $\tau = t/t_R$.

In this regression analysis all the data points, from ε_0 to ε_R, were used.[38] The regression analysis was repeated for a range of values of m, from 0 to 1 in increments of 0.01. On inspection of the results, a number of possible methods of determining the values of the constants were available. One method was to choose the equation with the highest R^2. This would be the equation for which the value of m used (out of the values considered) produced the equation (of the form 4.078) that fitted the experimental data most accurately. However, for many of the specimens, the R^2 value was quoted at 100%, or the highest value, for a range of values of m. Another obvious method, and that adopted in this study, was to examine the value of the constant, A, in the regression equation. Comparing equation 4.007 with equation 4.078 shows that there is no such constant in the equation given by Dunne *et al.* The value of A that I obtained from these regression equations changed in a regular way depending on the size of m. The constant becomes smaller as the value of m decreases, eventually becoming negative within the range of values of m associated with the highest values of R^2. Thus I used this change in sign to estimate the value of m (of equation 4.077). This was done by averaging the values of m that produced the smallest positive and negative values of A. The value of Δ was obtained from the average of the B values from the same equations. The results thus obtained for these two constants can be examined with reference to a number of the variables or mechanical properties examined above. After I have conducted such an examination, I will return to the paper by Dunne *et al.* and examine how to derive further constants contained in equation 4.079.

The results presented here have been derived from the same set of experiments presented in the previous sections (data sets CA1, CA2, CB1 and CB2). However, I will use only that data obtained from curves where the R^2 values associated with the regression equations from which m and Δ were obtained are greater than 80%. This limit was chosen so that the data set included a reasonable number of antler and bovine bone specimens. To increase this number, some of the data set included in CA1 and CB1 but not in CA2 or CB2 are included. Therefore, the data examined here is presented in separate data sets CA3 and CB3 (see appendix 4). Due to the preliminary nature of this study, only a limited regression analysis of the data is presented, the majority of the results being presented only graphically.

Having obtained a set of constants for both bovine bone and antler, it is possible to compare them. The mean values are presented in table 4.011. These values can then be used to construct a representative normalised creep curve for each material. These curves one for antler and one for bone are shown in figure 4.064.

---

[38]In the derivation of the various quantities and parameters considered here I have maintained the same units as used previously: time in seconds, stress in MPa and so on.

Material	m		Δ		n
	mean	s.d.	mean	s.d.	
Reindeer antler	0.8690	0.0830	0.7895	0.2315	15
Bovine femur	0.4668	0.1914	0.7473	0.2685	17

Table 4.011

The mean values of the two parameters, m and Δ, obtained from creep curves of Reindeer antler and bovine femoral bone specimens

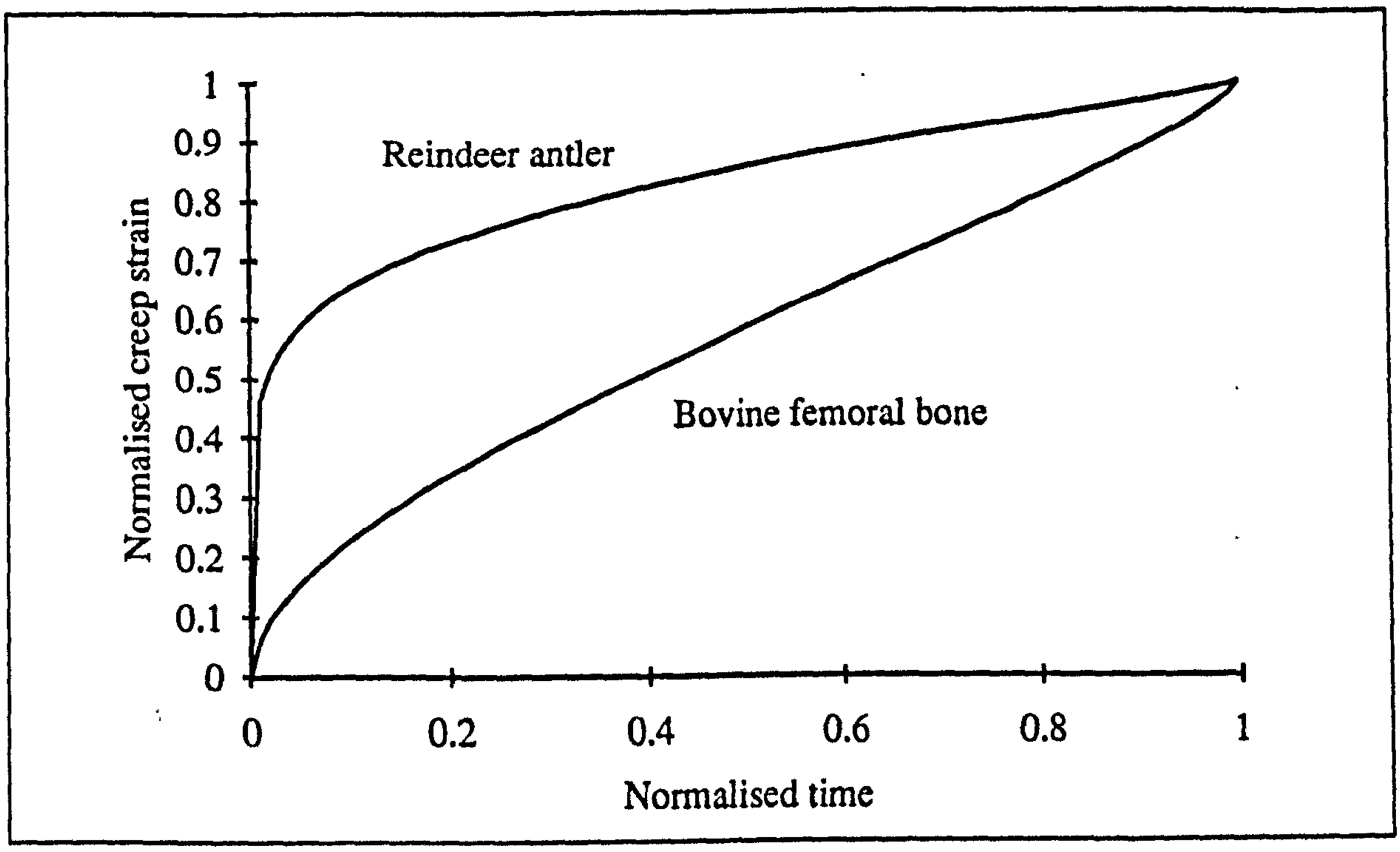

Figure 4.064

Normalised creep curves obtained by substituting the mean values from table 4.011 into equation 4.076

The plots of the mean curves shown in figure 4.076, compare well with those shown in figures 4.030 to 4.033 (remembering that they are a normalised representation of the curve after ε_0, indicated by the diamond, has been reached).

Figures 4.065 *a* and *b*, show an envelope of curves produced by the addition (and subtraction) of the standard deviation to one of the parameters whilst the other remains at its mean value. The effect of increasing the value of m is to increase the sharpness of the curvature of the first curve (that in the primary region), while an increase in Δ reduces the curvature in the tertiary region. Thus a material with a high value of m generally has a more dominant primary region than one with a lower value. A material with a low value of Δ has a more dominant tertiary region compared to a material with a high value of Δ.

The situation is not always as clear cut as this may suggest. If the two constants are viewed as being responsible for two types of curve, Γ shaped for m and J shaped for Δ, the overall shape is clearly a result of both constants.[39] For example, the amount of curvature in the later stages of the curve will depend on the severity of both the Γ and J shapes. This viewpoint raises other questions: is it misleading to divide the creep curve into three regions? Are the two parameters m and Δ related to different processes occurring during the initial and final stages of the creep rupture test? From examination of the curves and equations above, clearly the secondary or steady state region is that where the effect of the Γ and J shaped curve balance out.[40] It is difficult to establish if the processes are different in the initial and final stages of the creep test or if they are simply occurring at a different rate, perhaps due to the increase in the effective stress.

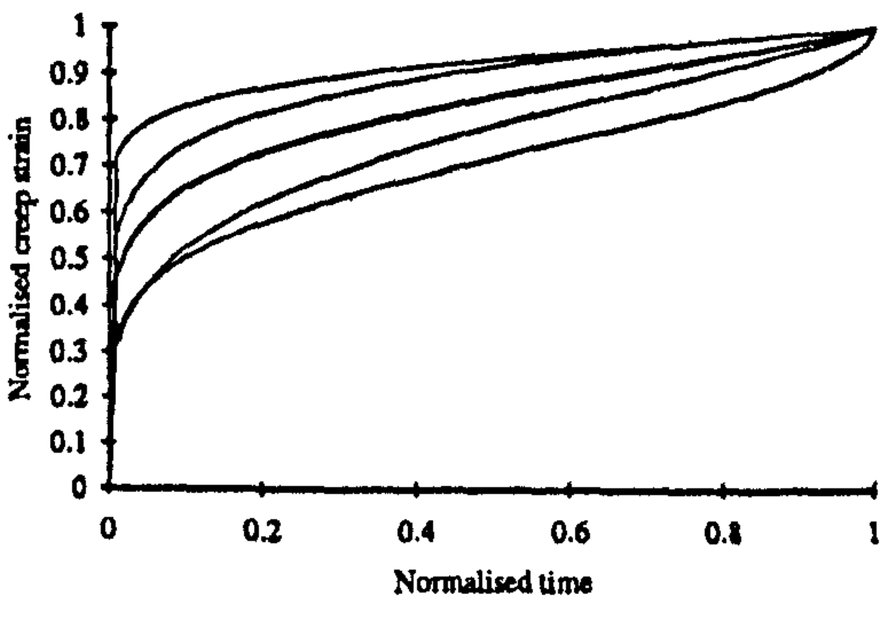

a) Reindeer antler

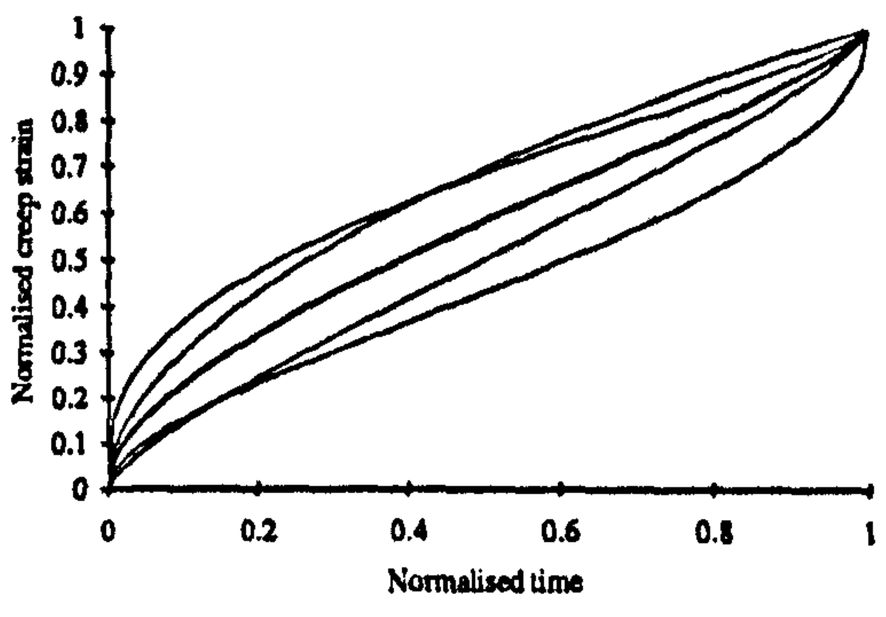

b) Bovine femoral bone

Curves of the normalised creep strain for bone and antler. The central curve (the thicker line) was derived by substituting the mean values of the constants in to equation 4.076. The other curves results from adding or subtraction the value of the standard deviation to one of these constants. Only one constant was changed in each case.

Figure 4.065

Reconstructed average normalised creep-strain curves and their standard deviations

Although figure 4.064 shows a distinct difference between the model creep curves of antler and bovine bone, calculated using the mean values of m and Δ, figure 4.065 *a* and *b* show that statistically there is a considerable range of possible shapes of the creep curve for both materials. It is with the hope of gaining more insight into the variation of these constants that their values have been compared with other variables. Some of these variables are others from this analysis and others are external to this analysis such as

---

[39]Mathematically the situation is more complex, the equation is of a power form not the addition of two curves. However this view is sufficient for my purposes.
[40]A similar idea was mentioned to me by Dr Robert Ker (University of Leeds), with respect to the creep-rupture tests of tendon, which displays only a limited secondary region.

calcium content. In the first figure the values of m and Δ are plotted against each other. It is clear from figure 4.066 as it is from table 4.011 that the values of Δ for the two materials are similar while those of m are different, the m values for antler being generally higher. It is also interesting that the data for bovine bone appear to be randomly scattered, while those for antler show a relationship between these quantities ($R^2 = 86.3$). As the value of Δ decreases, the value of m increases. Thus the shape of the later sections of the creep curve vary less than figure 4.065*a* implies. This inter-relationship of m and Δ is important as it supports the observations made on inspection of the creep curves that the secondary/tertiary region for antler specimens of antler displays little variation within the same specimen and between specimens. (The values of ε_3 are very similar to those of ε_R and to each other, see table 4.009.) This raises the question why the results for bone, obtained in the same way, are less consistent. I suggest that this is due to the more brittle nature of the bovine bone.

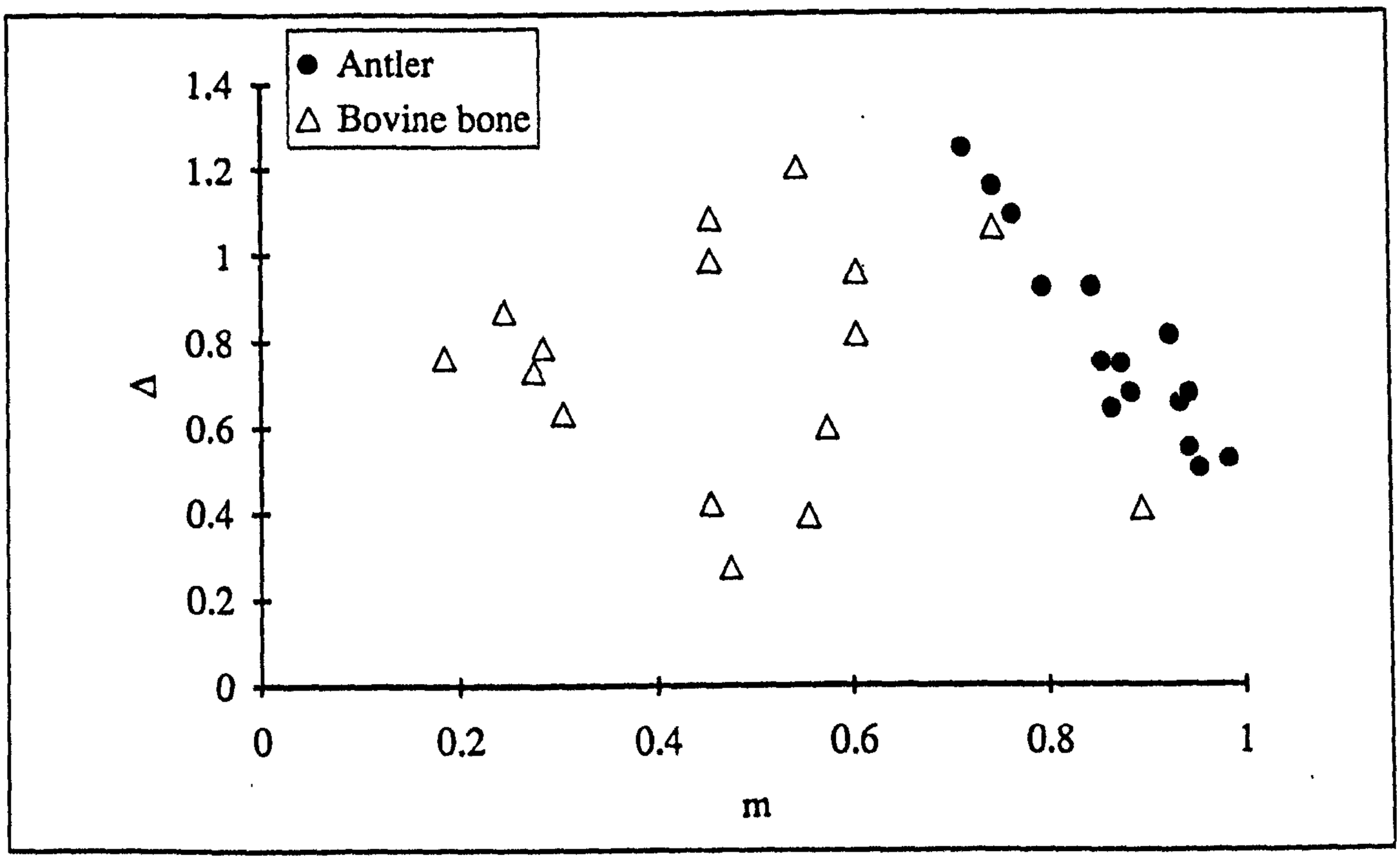

Figure 4.066

The relationship of m and Δ obtained from creep-rupture tests of reindeer antler and bovine femoral bone specimens

If it is assumed that the calcium content of the bone is acting (in a similar way to particulate reinforcement in industrially manufactured composites) to reduce the creep strain of the material, the degree of such reinforcement may change the shape of the strain response. (If this argument is followed, papers such as *Particle Reinforcement Of Ductile Matrices Against Plastic Flow and Creep* by Bao *et al.* (1991), which contains a theoretical study of the effect of particle volume fraction and shape and packing morphology, could provide some insight.) An examination of how these constants relate

to the mineral content of the materials is therefore the logical progression. This is shown in figures 4.067 and 4.068. However, although the use of calcium content produces a clear division between the results for the two materials, there is no relationship between the variables for the data from one material. This implies that other factors, such as the difference in the structure of the materials, play an important role in determining the materials mechanical response.

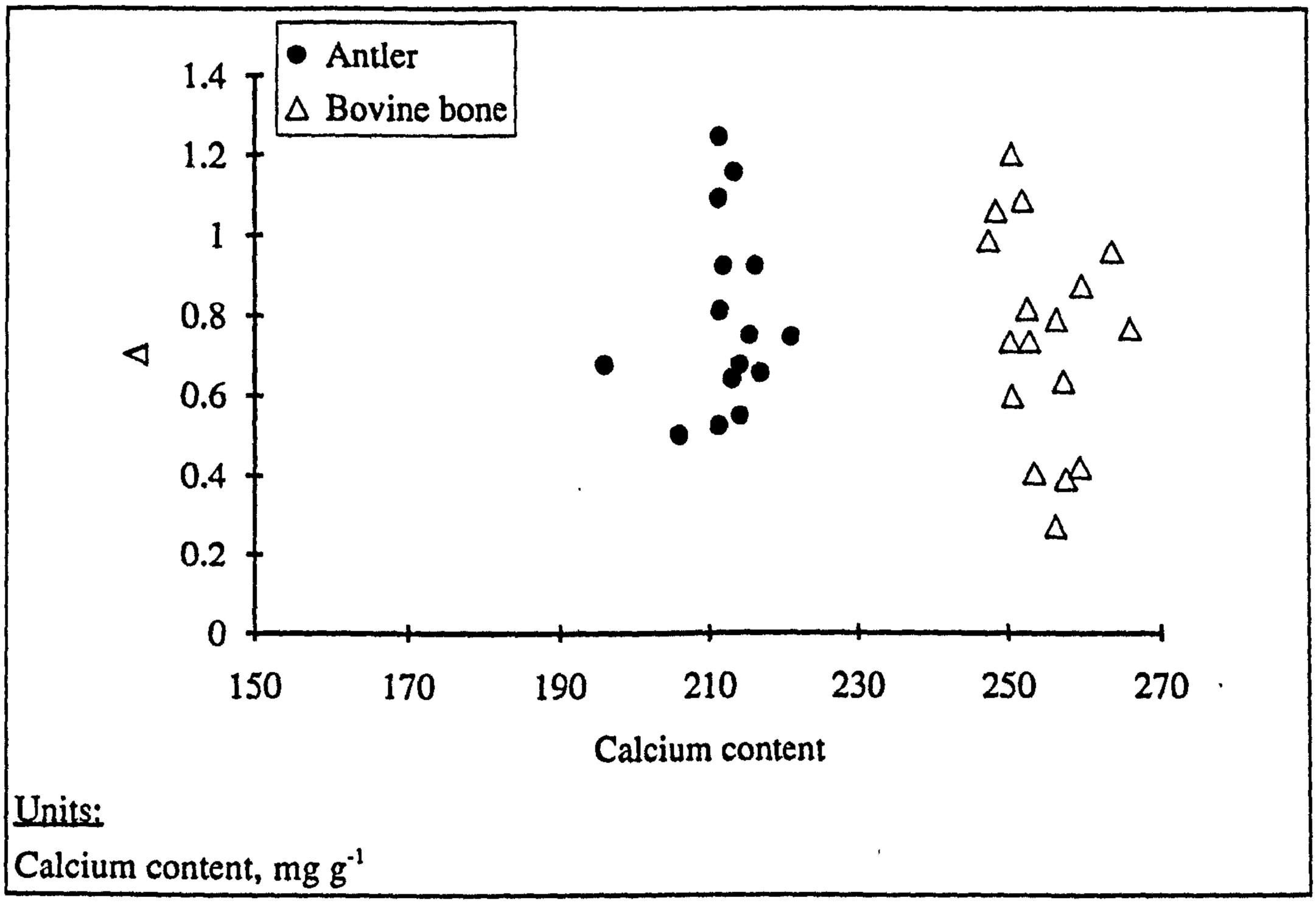

Figure 4.067

The relationship of the values of Δ from equation 4.076 to the calcium content of the specimens

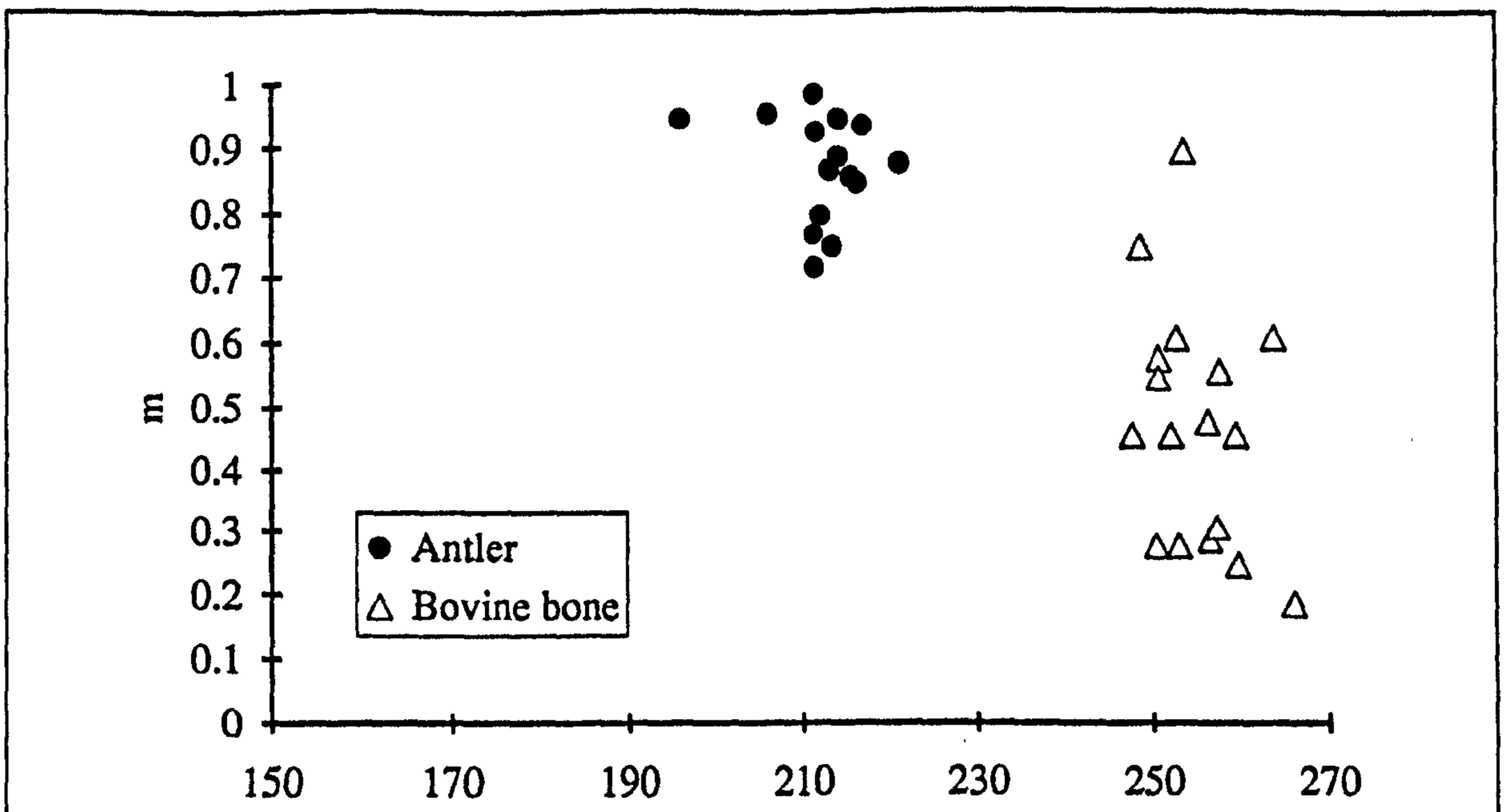

Units:

Calcium content, mg g^{-1}

Figure 4.068

The relationship of the values of m from equation 4.076 to the calcium content of the specimens

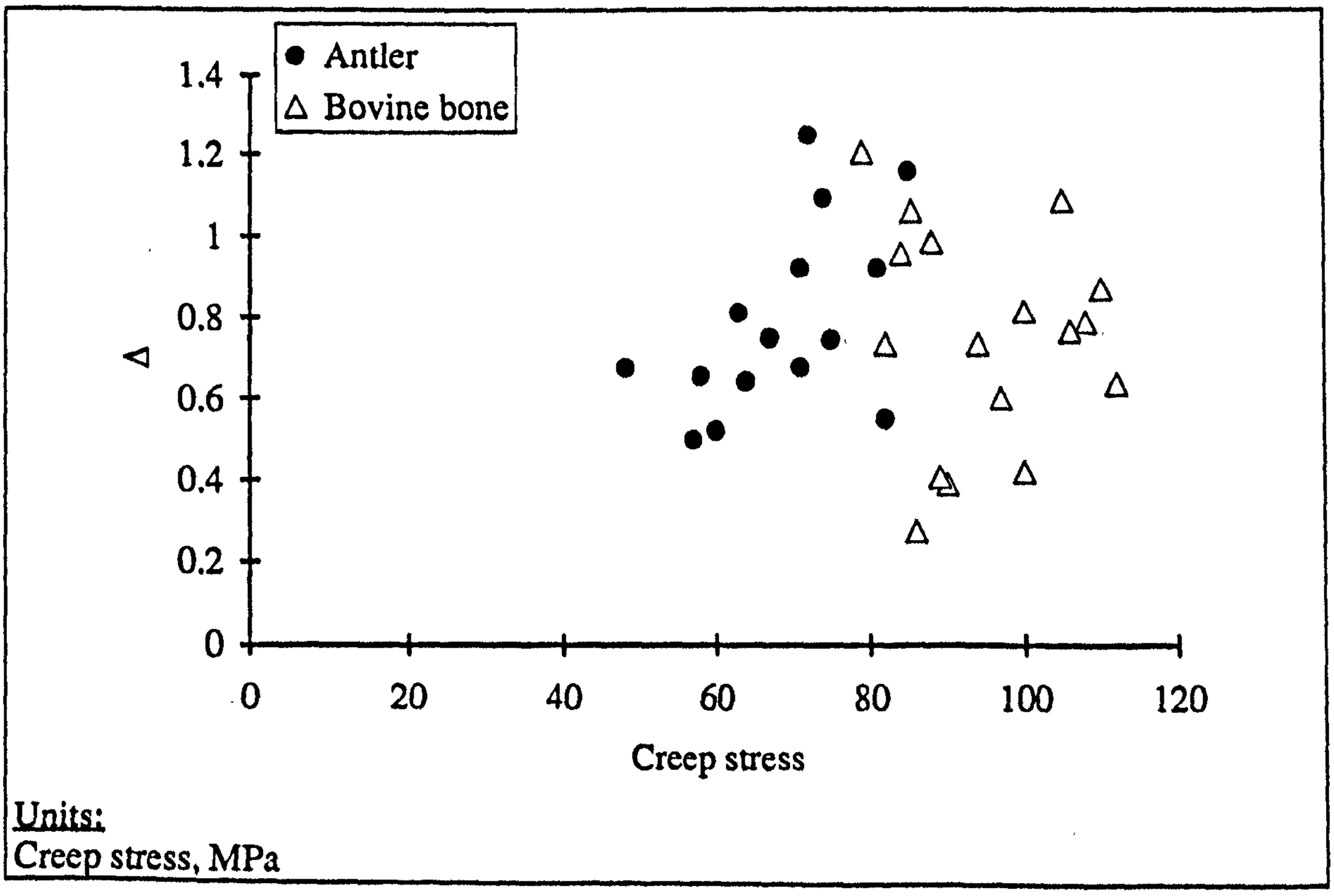

Units:

Creep stress, MPa

Figure 4.069

The relationship of Δ to creep stress

I will now return to the derivation of the values of the parameters within the two constitutive damage equations (4.070 and 4.071) examined by Dunne *et al.* (1990). After explaining how to derive the values of m and Δ (for which I used a different method), Dunne *et al.* continue to derive the other variables. The next group they examine, $K\,\sigma^n$, comes from rearranging equation 4.074 in the following form.

$$K\,\sigma^n = \varepsilon_f\,(1 - m)\left[1 - \left(n/(\phi + 1)\right)\right]/t_f^{(1-m)} \qquad (4.079)$$

I will rewrite this using the previous equations

$$K\,\sigma^n = \frac{\varepsilon_f\,(1 - m)\,\Delta}{t_f^{(1-m)}} \qquad (4.080)$$

Dunne *et al.* (1990) say that 'the values determined for the three groups $(1 - m)$, $\left[1 - \left(n/(\phi + 1)\right)\right]$ and $K\,\sigma^n$ for each stress level may then be used as starting values for the optimization scheme that optimizes with respect to three constants groups'. They point out that although the first two constants have been determined for each stress level, they are assumed to be independent of stress.[41] They state that because this is not the situation in practice, an average is used. The relationship of m and Δ to the creep-stress used in the tests on reindeer antler and bovine bone examined here are presented in figures 4.069 and 4.070. Figure 4.070 appears to show a relationship between m and the stress level, which is consistent for both materials. However, there is only a very limited amount of overlap in the values of creep stress used for the tests on antler and those on bovine bone.

Figure 4.070 indicates that as the creep stress increases, the value of m decreases for both materials. This implies that as the stress increases, the proportion of the total creep-strain that occurs in the primary region decreases. Thus the response is not linear with respect to stress (this was indicated in section 4.3.6). Before too much significance is attached to this result, the possibility that it is an artefact of the experimental technique should be considered. It has already been reported that due to the design of the creep rig, a longer time is required for a higher stress to be reached. Thus more creep can be accumulated before the creep stress is attained, reducing the measured creep-strain. However, this does not account for the data points falling in a line (as bone is stiffer, its loading period is shorter). This result, the relationship of m and creep stress, is an area that needs further consideration, experimental and analytical. An obvious requirement is for creep tests on bovine bone to be conducted over a stress range that encompasses the stresses used for tests on antler. Also more consideration of whether m merely helps to describe the creep curve, or relates to the processes that produce the curve is needed.

---

[41]The authors reduce the second constant to $\left[n/(\phi + 1)\right]$.

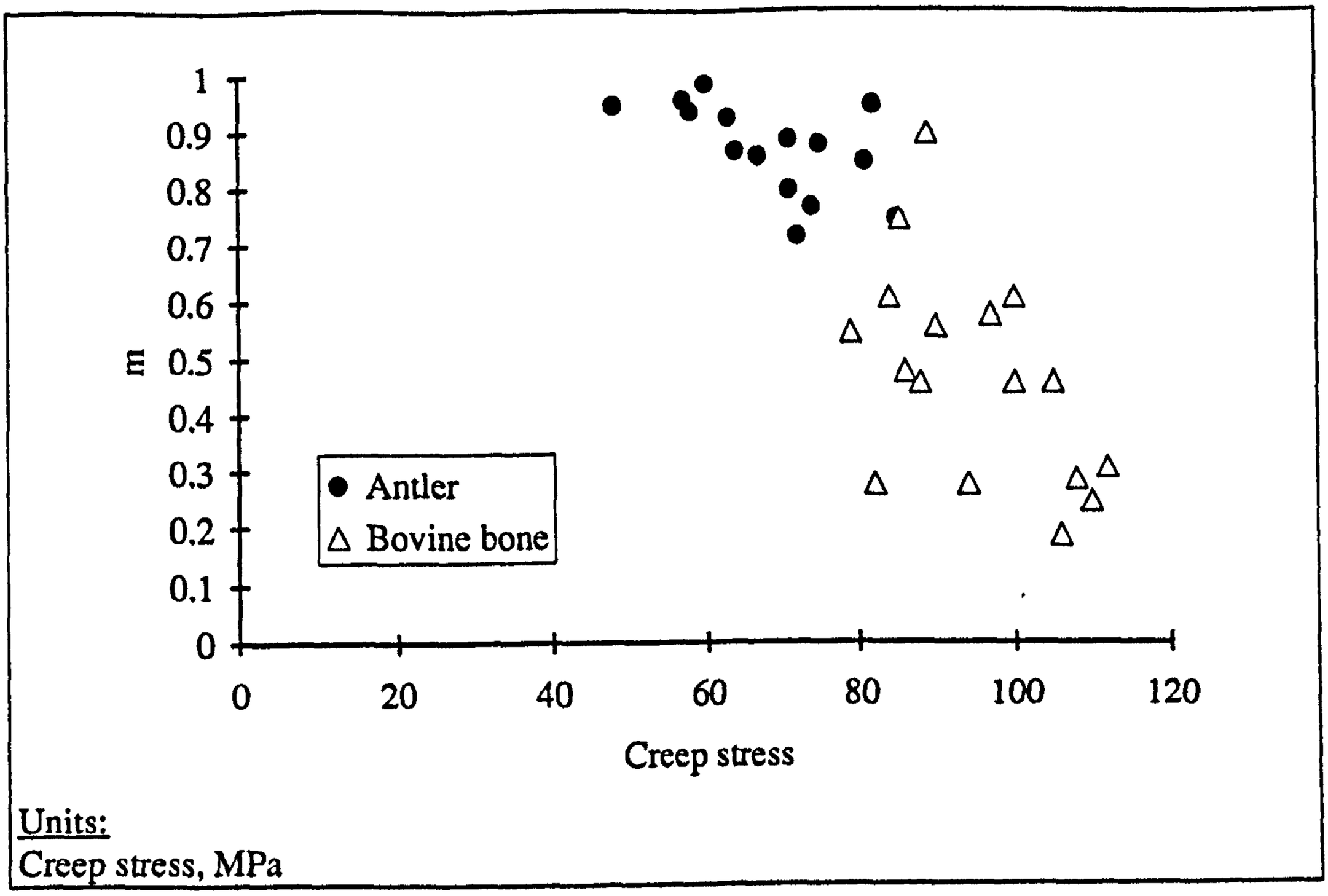

Figure 4.070

The relationship of Δ to creep stress

The values of K and n can be derived, in a similar way to the method used by Dunne *et al.* The first step is to express equation 4.081 in logarithmic form.

$$\ln\left(K\,\sigma^{n}\right) = \ln\left(\frac{\varepsilon_f\,(1 - m)\,\Delta}{t_f^{(1-m)}}\right) \tag{4.081}$$

Thus

$$\ln(K) + n\ln(\sigma) = \ln\left(\frac{\varepsilon_f\,(1 - m)\,\Delta}{t_f^{(1-m)}}\right) \tag{4.082}$$

The value of the right hand term can be calculated from the values already obtained from the experimental data. When this was done, the equations shown in table 4.012 were obtained. The stress term in the regression equation for the antler data is significant but that in the equation for the bovine bone data is not significant. Values of the constants can be obtained from these equations (and the other constants obtained by following the method of Dunne *et al.*). However, due to the lack of significance shown in the second regression equation of table 4.012, and other factors, such as the material variability and the limited number of tests, I believe that the reliability that can be placed on such results decreases very rapidly as the number of assumptions and extrapolations increases. This is because the derived value of these constants is dependent on the value of other derived constants.

Type of specimens	Regression equations and t values and derived values. (Data sets CA3 and CB3)	R^2 %	
CA3 15	$\ln\left(\frac{(\varepsilon_R - \varepsilon_0)(1 - m)\Delta}{t_R^{(1-m)}}\right) = -18.4 + 2.84 \ln(\sigma)$ t: -3.67 2.40 $n = 2.84$ $K = 1.021\times10^{-8}$	25.3	*a*
CB3 17	$\ln\left(\frac{(\varepsilon_R - \varepsilon_0)(1 - m)\Delta}{t_R^{(1-m)}}\right) = -16.7 + 1.72 \ln(\sigma)$ t: -1.55 0.73 $n = 1.72$ $K = 5.588\times10^{-8}$	0.0	*b*

Table 4.012

Regression equations for the calculation of n and K

As stated above, I am unwilling to derive the full set of constants as described by Dunne *et al.* (1990) from the results I have obtained from creep tests of specimens of reindeer antler and bovine femoral bone. However, I consider that this multi-parameter approach gives more insight into the way damage accumulates in the two materials and how this affects the material properties. Thus I consider that this is one direction in which the study of the mechanical properties of bone (not limiting the study of the two materials investigated here) could be extended. Using the approach of Dunne *et al.* has produced a number of parameters, some of these are similar for the two materials and some are different. If other variables were considered, such as porosity, structure and a more detailed mineral analysis, perhaps the factors that govern or modify these parameters (and thus mechanical response) could be more accurately determined.

The analysis presented here has confirmed an observation made previously; that is the difference in the shape of the creep curves of bone and antler. I consider that the shape of the creep curve reflects the damage within the specimen. If equation 2.114 is used again (with its accompanying assumptions) to represent the level of damage, the development of damage during the creep test can be represented as

$$D = 1 - \frac{\varepsilon_U}{\varepsilon_M} \qquad (4.083)$$

The predicted value of normalised creep strain is assumed to be represented by the same equation used to calculate the values for the individual specimens

$$\varepsilon_{\text{normalised creep}} = \frac{\varepsilon_M - \varepsilon_0}{\varepsilon_R} \qquad (4.084)$$

Thus damage can be modeled as

$$D = 1 - \frac{\varepsilon_0}{\varepsilon_{\text{normalised creep}}\ \varepsilon_R + \varepsilon_0} \qquad (4.085)$$

I performed this calculation using the normalised creep strain values obtained from the mean constants (as shown in figure 4.064) while the value of the instantaneous strain and rupture strain were the mean values obtained from the same specimens (data set CA3 and CB3). As the values of the normalised strain and damage both fall in the same range (0 to 1) they are plotted together in figure 4.071. The curves show that the rate of damage accumulation (thus calculated) is initially slower in bovine bone than in antler. The damage rate decreases with time for both materials. This decrease is very dramatic for the antler specimens. After this decrease has occurred, the damage rate associated with antler is less than that associated with the bovine bone. It should also be noted that this approximate representation of damage predicts that both materials rupture before damage reaches unity. This procedure implies that bone sustains more damage before failure than antler (contrary to the results in section 4.3.6.11 for the tensile tests). When this figure is compared to figure 4.063, the assumption of linear damage accumulation is clearly more valid for the bovine bone specimens than for the specimens of antler.

Figure 4.071

Plots of the mean normalised strains and the level of damage associated with these strains (also based on mean values)

4.3.9.1. CLOSINGS REMARKS ON THE MODELLING THE CREEP CURVE USING CONSTITUTIVE DAMAGE EQUATIONS

I opened the section with the question of whether the creep deformation is independent of the damage parameter. If this is the case damage will be accumulated at a constant rate. Using the scalar measure of damage, I have shown that the creep response of bovine bone is closer than that of antler to what would be expected in such a situation. The predicted curve is dominated by an upward curve prior to failure. This curve was compared to the tertiary region of the experimental tests on bovine bone.

Having used a basic damage parameter and the assumption of a constant damage rate and found that the predicted creep behaviour was at odds with the experimentally observed behaviour, I have examined another relationship of damage and creep strain was examined. These equations (4.070 and 4.071) were obtained from a study by Dunne *et al.* (1990) and are repeated here.

$$\dot{\varepsilon} = K t^{-m} \left(\frac{\sigma}{1 - \omega} \right)^{n} \tag{4.086}$$

$$\dot{\omega} = A t^{-m} \frac{\sigma^{v}}{(1 - \omega)^{\phi}} \tag{4.087}$$

I was unable to obtain all the constants for both equations. However, I did obtain values of m and Δ; these are presented in table 4.011. The values of Δ for each material were similar: 0.79 for antler and 0.75 for bone (one way analysis of variance did not show a statistically significant difference $p = 0.639$). However, the values of m were found to be different and this difference was statistically very highly significant ($p < 0.001$). The important result contained in the values of m and Δ may not only be the similarity in the values of m for antler and bone or the difference their values of Δ, but that the values of m and Δ for antler are similar and those for bone are different. (This is a direct result of the shape of the creep curves of the two materials. Applying this observation to those creep tests is thus a circular argument.) If it is possible to extrapolate this result to tensile tests, the balance of the parameters in the case of antler may be consistent with the idea of stable damage increments. However, as I stated above, I consider this to be only a preliminary study of these parameters.

Obtaining values of m and Δ has permitted the modelling of an average creep curve for both materials. From this curve I was able to construct a plot showing the development of damage with respect to time for such an average creep test. (To construct the plot I used the simple definition of damage used throughout this thesis.) The plot showed that the average antler specimen accumulates damage very rapidly in the initial region $t/t_R < 0.05$, more rapidly than bone. After the initial region the rate of damage

accumulation for an antler specimen is lower than that of bovine bone. At failure the average bovine bone specimen displays more damage than that of antler. This finding may hold the key to the differences between the behaviour of antler and bone. How these findings relate to the findings obtained from the tests of the time-dependence of antler's and bone's behaviour is examined in section 4.4.

4.3.10. CREEP-RUPTURE RESULTS: CLOSING REMARKS AND CONCLUSIONS

In the analysis of the creep data I consider the most important finding to be the difference in the shape of the creep curves of antler and bone. The analysis of single explanatory variables from these curves, for example the time-to-rupture or the creep rate are unable to adequately define this difference. (Similarly the values of knee stress, or ultimate stress, do not fully express the differences in the tensile response of these materials.) I know of no previous investigation of the creep behaviour of antler where the strain has been monitored throughout the duration of the test.[42] The differences in the shapes of these curves and the information I have derived from them show that when subjected to a creep loading, bovine bone accumulates strain rapidly during the loading period, but on reaching the creep stress the rate of accumulation of strain dramatically decreases. The creep strain rate remains relatively constant until the point of rupture is approached; the rate then increases. Bone behaves in almost the classic fashion displaying primary, secondary and tertiary stages. Antler however behaves differently; it too displays extension during the loading period, but there is no marked decrease in the strain rate when the creep stress is reached. A decrease in the creep rate does occur after the creep stress has been reached, but this it is a more gradual process compared to that of bone. The antler specimens tested here failed to display a marked tertiary region. This difference is demonstrated in four plots of experimental data in figures 4.030 to 4.033, in a normalised representation of the creep curves in figure 4.064, and numerically in table 4.009.

Two methods of modelling the shape of the creep curves were examined. The first, visco-elasticity (section 4.3.6), was abandoned as the shape of the curves suggested a fluid like material. The derivation of the equations was not possible by the methods explained and attempted here. As pointed out in a number of places above, a visco-elastic model can not predict failure. A second method modelling the creep curves using constitutive damage equations was also examined. It was hoped that this second method would not only model the shape of the curves, but would also provide further insight into

---

[42]The only published work on the creep behaviour of antler I am aware of is that by Mauch *et al.* (1992) presented in appendix 6.

the nature of the failure in the two materials or at least help pinpoint the differences. Although the equations contained within this analysis were able to fit the experimental data adequately in most cases, a derivation of the full set of constants was not possible. However, of the two methods, the damage approach as applied here was better able to model and explain the behaviour of the two materials.

If individual variables are unable to express the overall picture, they do however provide detail. The analysis of these individual variables has highlighted some differences and similarities between these materials. For example, for specimens that rupture at the same time, the bovine bone specimens were able to sustain a higher creep loading than the antler specimens were. A similar finding was previously reported by Mauch *et al.* (1992). Much of the analysis applied to the data derived from the creep rests was analysed using an approach suggested by a theory or previous experimental study of one or other of the materials. Unfortunately, in many cases these analyses were inconclusive. The poor predictive power of many of the relationships appears to stem from the material's variability. The only externally applied quantity is creep stress, which was not as strongly related to the recorded behaviour as it is in some published studies. However, when some of the recorded variables were compared with each other, the predictive strengths of the relationships were higher. This was especially the case when the time-to-rupture and the creep rate were examined. With hindsight this situation could have been improved upon if a greater number of standardising variables had been used.

The examination of the creep-rupture data using the regression equations suggested by the various damage approaches (whether that approach was Kachanov's original equations or Caler and Carter's NTDF model) was unable to provide strong evidence for or against such an approach. With perhaps one exception; the case where I converted Kachanov's prediction for failure by a purely ductile process from an equation expressed in terms of creep stress to one in terms of creep rate. Because the predictive power of this equation was so low compared to that for his prediction of failure by a purely brittle process, I consider that failure by the ductile process can be rejected. I have shown that Kachanov's creep stress-based predictive equations for failure by these processes are essentially the same. The rejection the ductile process thus implies (as assumed by Carter and Caler (1983)) that the failure of bone is by a predominantly brittle process.

4.4. CLOSING REMARKS ON THE TIME-DEPENDENT PROPERTIES OF BONE AND ANTLER.

The most obvious finding of this chapter, so obvious that stating it is almost unnecessary, is that both antler and bone display time-dependent mechanical responses. I suggested in section 4.2 that a study of the time dependence of these materials during tensile testing may help to elucidate the nature of the failure process and whether it is also time-dependent.

In the attempt to examine and understand the nature of the time-dependence of antler and bone, two possible explanations were examined: first that this behaviour was related to visco-elasticity and second that the time dependence was due to the gradual accumulation of damage. The first possibility was based on a model suggested for the mechanical properties of bone by Sedlin in 1965. The damage approach was a combination of the ideas from the original damage theory of Kachanov and some that have previously been applied to bone. Data derived from tensile tests conducted at four cross-head speeds was examined using regression analysis. The forms of the regression equations used were those suggested by the two possible explanations for time-dependent behaviour. In an attempt to examine the possibility that the progressive development of damage could be responsible for the rate dependence of the stiffness of antler and bone, I manipulated the NTDF model to provide a predicted stress-strain response for bone. This displayed this method's ability to predict the knee region and its inability to mimic the change in stiffness. The application of the term visco-elastic to bone is based on the ability of this theory to model the change in stiffness, but it fails to describe the knee region. As a result of this and other forms of analyses I suggested that the mechanical response of antler and bone is due to a combination of a visco-elastic type behaviour and a damage process. I suggested that the visco-elastic type behaviour dominates in the pre-knee region and that the damage process is responsible for that knee and thus influences the mechanical response in the post-knee region. (In chapter 8 some convincing evidence that the knee and post-knee region are dominated by the damage process is presented.) On the basis of this suggestion I constructed a mechanical analogue to mimic the behaviour of these materials. I consider that the mechanical response of the material, and more specifically how it fails, will be dependent on the way in which the damage is accumulated, whether in stable or unstable damage increments.

In the second half on this chapter the behaviour of specimens of bone and antler subjected to creep rupture tests was examined. It has already been proposed that there is a close link between creep tests and tensile tests, this was confirmed by some the results of these tests. It was found that the behaviour of bovine bone was very similar to the idealised behaviour used to form the linking model (shown in figure 3.013 of section

3.3.3.2) On reaching the creep stress, bone exhibits an almost constant creep rate until failure. Using the ideas of section 3.3.3.2, this implies that the almost horizontal post knee-behaviour in a tensile test of bone is due to the same process. It was suggested in section 3.3.3.2 that in order for the post-knee region of a tensile test to have an upward slope like that of antler, the creep rate of the material would have to reduce with time. In this situation, maintaining a constant creep rate would require a greater load to be applied, the corollary being if the material is extended at a constant rate it applies more force on the extending device. It was clearly shown that antler displays a substantial reduction in creep rate. The creep rate is initially almost as fast as that during the loading period; it then reduces by a gradual process to only a small fraction of this initial rate. Thus the creep curves can be used to model the tensile curves. However, such modelling casts little light on what causes this difference and how it relates to the failure process.

The cause of the different mechanical responses of bone and antler and the nature of the failure process are inextricably linked. I consider that the balance between the visco-elastic like and damage like behaviour holds the key both the mechanical response and the final failure process. The visco-elastic like behaviour can be viewed as regulating the accumulation of damage. In antler the visco-elastic behaviour dominates. This idea conforms to the lower stiffness and curved loading line of antler in the pre-knee region and its greater slope in the post-knee region, compared to that of bovine bone. It has been noted that using the measure applied here, antler displays more damage at failure than many of the bone specimens. This implies that the regulation of the damage is not in the form of a restriction on the amount of damage but a reduction of the effect that this damage has. This idea is supported by the lack of evidence for the classical tertiary behaviour in a creep test of antler. Specimens of bovine bone have also been noted as displaying increases in length associated with decreases in load. This occurs in both the immediate post-knee and immediate pre-failure section of some tensile tests. (However, due to the machine-specimen interaction these observations should be treated with caution.) This behaviour I have attributed to some kind of unstable damage increments. When this idea is associated with the lower and more variable ultimate strain and damage values exhibited by bovine bone it suggests the possibly of some failure localisation effect in bone. In the next few chapters I shall introduce and examine the effect of an artificially induced failure localisation, in the form of a crack or machined notch in a material. The way antler and bone react to such a notch may give further insight as to the nature of the damage moderating process.

5

NOTCH SENSITIVITY AND FRACTURE MECHANICS OF BONE AND ANTLER: A THEORETICAL BACKGROUND

> The worst sin in an engineering material is not lack of strength or lack of stiffness, desirable as these properties are, but lack of toughness, that is to say, lack of resistance to the propagation of cracks.

J. E. Gordon (1976)

The New Science of Strong Materials

5.1. INTRODUCTION

To cut a sheet of domestic glass all that is needed is to score the surface and to apply a small bending moment to the sheet, or light blows near to the scratch. This will result in the scratch becoming a crack that extends and cleaves the sheet in two. The force required seems disproportionally small when compared to that needed to fracture glass that has not been scratched; for the scoring has only slightly reduced the local thickness. The two sections of the cleaved sheet can be placed next to each other and the external dimensions of the original sheet obtained. Other materials will not respond in such a drastic fashion when scratched, mild steel for example. Many of these materials deform considerably before fracturing, thus the fragments when reunited do not reproduce the original shape; an extreme example of this is chewing gum.

The term *notch sensitive* is applied to materials that behave in a similar manner to that described for glass. They exhibit a decrease in strength due to the presence of the notch that is disproportionately large, compared to the slight reduction in cross-sectional area. Materials for which the strength is purely determined by the cross-sectional area and the applied load, the strength decreasing in proportion to any induced notch, are described as *notch insensitive*. Why do materials behave like this? What relevance has this behaviour to bone and antler? In this chapter and subsequent ones I answer these questions: first, by summarising how the general field of *fracture mechanics* has developed, concentrating on linear elastic fracture mechanics (LEFM). Second, by describing how this technique has been applied, by others, to bone and antler. Third, by reporting the experiments I have conducted for this thesis, the results and their implications.[1]

5.2. THEORETICAL AND HISTORICAL OUTLINE OF LINEAR ELASTIC FRACTURE MECHANICS

The idea that a sharp change in cross section could produce a *stress concentration* (a region where the stress is of a greater value than would be calculated by dividing the load by the cross section at that level) was formally introduced by Inglis (1913a). In this famous paper he calculated the stress concentrations around an elliptical hole and various related shapes within a perfectly elastic material. Gordon (1976) points out that this paper appeared after the Admiralty had conducted some experiments to measure the strength of ships. Their investigation included the strain gauging of H.M.S. Wolf in 1903; no stress greater than 80 MPa was found. As this is only about a fifth of the

---

[1]The initial inspiration for these experiments came from a meeting with Dr Peter Purslow, and from his paper (Purslow, 1991).

strength of the steel used, the question still remained: why were ships breaking in two? Gordon also observed that none of the strain gauges were placed near an opening in the hull, such as a hatch. The relevance of this observation will become clear after my review of the paper by Inglis.

5.2.1. STRESSES IN A PLATE DUE TO THE PRESENCE OF CRACKS AND SHARP CORNERS (INGLIS, 1913a)

A report in *Engineering* (1913)[2] describes the presentation to the Institution of Naval Architects given by Inglis, of his paper entitled *Stresses in a Plate Due to the Presence of Cracks and Sharp Corners*. The pertinent points of the paper are clearly explained in the report in the following way

> The author has worked out completely the distribution of the stresses round an elliptical hole in a tie-bar. He finds that if the ellipse has its major axis transverse to the line of pull, the [tensile] stress reaches its maximum value at the extremities of this major axis, where the stress attains to a value given by the relation
>
> $$p = p_0 \left(1 + \frac{2a}{b}\right)$$
>
> where p_0 denotes the average value of the stress in the unpierced portion of the tie-rod, and a and b one-half respectively of the major and minor axis. In the case considered the stress at the extremities of the minor axis is a compression having the value p_0.

The account of the paper given in *Engineering* continues by pointing out that

> If the two axes of this ellipse are equal, it degenerates into a circle, and the maximum stress becomes three times the mean. If, on the other hand, the minor axis is 1/1000 of the major axis, the ellipse approximates to a mere crack in the plate; and if the major axis be perpendicular to the line of the pull, the maximum stress becomes 2001 p_0.

The equation given above is commonly rewritten as

$$\sigma_{tip} = \sigma_{-} \left[1 + 2\sqrt{a/\rho}\right] \qquad (5.001)$$

Where σ_{tip} is the tensile stress at the tip of the ellipse (in the direction tangential to the curvature of the tip), σ_{-} the tensile stress at a distance not effected by the hole and ρ is radius of curvature at the tip of the ellipse. The magnitude of ρ is defined by Knott (1973) as being equivalent to the radius of the circle that passes through the tip and two

---

[2]This report is referenced in this thesis as 'Inglis, 1913b' as I do not know the identity of the writer.

adjacent points. Inglis (1913a) includes 5.001 equation (in a slightly different form using a ratio of the stresses) and says

> This formula will accordingly apply to a cavity of any shape, the length of cavity being 2a and the ends having a radius of curvature ρ; provided that the cavity near its ends merges smoothly into an ellipse.

The report in *Engineering* says that it was pointed out during the meeting (by Stromeyer), that if the mathematical view of cracks was correct, as soon as one crack appeared the 'matter became dangerous'. However, in his published paper Inglis (1913a) did point out that 'in ductile materials some easing off of the local stresses at the end of a crack will be effected by plastic yield of the substance'. How this may occur will be discussed later.

The exact solutions for the stresses around a crack (given in curvilinear co-ordinates) are presented by Inglis in the second section of his paper. One solution being for the 'case of a plate subjected to a tensile stress R in all directions, the plate having an elliptical hole defined by $a = a_0$'. Another solution, which is the most well known, is 'case of a plate subjected to a tensile stress R in the direction $\beta = \pi/2$, the plate having an elliptical hole defined by $a = a_0$'. In the latter case only the initial derivation and the important solution are given, these are the values of stresses at the surface of the hole (the values of this quantity at certain points have been given above).[3]

The occurrence of stress concentrations is very important in explaining why cracks and scratches weaken materials. It shows that the stress level at a specific point within the material is not simply dependent on the cross-sectional area and the applied load, but also the shape of the object or the flaws within it and, as will be shown later, the material from which the object is made. The paper by Inglis extends this idea to other shapes including 'a square hole with rounded corners' which (to a non-naval architect like myself) sounds like a hatch.

---

[3]Knott (1973) presents a more complete solution for the stresses at the surface of an elliptical hole in a plate under simple tension. Solutions to both cases are given by Timoshenko and Goodier (1982), articles 62 and 63. They also report that the radial stress case was solved by G. Kolossof in his doctoral dissertation, Dorpat, 1909.

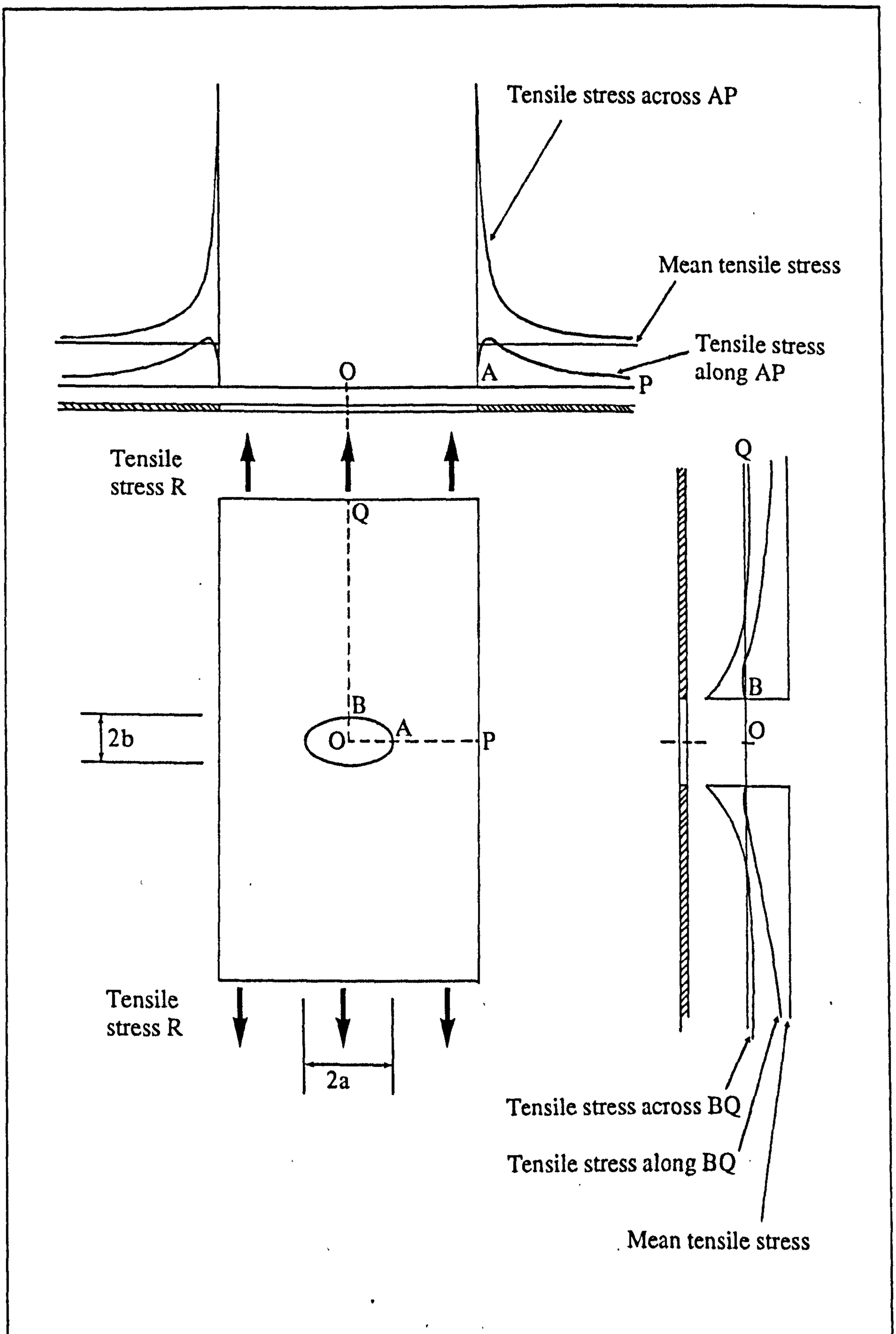

Figure 5.001 Adapted from figures 1 and 2 in Inglis (1913a)

Stress distributions along and across the vertical and horizontal axes the origin of which is the centre of an elliptical crack with an aspect ratio of 3:1

5.2.2. THE ENERGY BALANCE APPROACH

In this section I will examine the energy balance approach to fracture propagation. This examination is divided into two parts, for historical reasons. The first section (5.2.2.1) contains a review of Griffith's original paper (Griffith, 1920) and gives the background to the energy approach. However, the approach and equations now in use, although regularly cited as coming from this original paper, are based on a correction produced by Griffith four years later. Therefore this examination of the original paper will be brief, and the newer explanation is examined in section 5.2.2.2.

5.2.2.1. THE PHENOMENA OF RUPTURE AND FLOW IN SOLIDS (GRIFFITH, 1920)

Using both the mathematical solutions given by Inglis (for the stresses in the 'case of a plate subjected to a tensile stress R in all directions, the plate having an elliptic hole defined by $a = a_0$') and his own experimental results, Griffith (1920) developed a 'theoretical criterion of rupture'.[4] This formed part of a larger research project to discover the effect of surface treatments, such as filing or grinding, on the strength of metallic machine parts subjected to alternating or repeated stresses. Under such conditions the load that these materials could sustain is smaller than the range in which they behave elastically, the strength being dependent on the size of the scratches. Thus a new theory was needed to replace the maximum tension hypothesis,[5] for as he pointed out;

> The general conclusions were that the scratches ordinarily met with could increase the maximum stresses and strain from two to six times, according to their shape and the nature of the stresses, and that these maximum stresses and strains were to all intents and purposes independent of the absolute size of the scratches. Thus, on the maximum tension hypothesis, the weakening of, say, a shaft 1 inch in diameter, due to a scratch one ten-thousandth of an inch deep, should be almost exactly the same as that due to a groove of the same shape one-hundredth of an inch deep.
>
> These conclusions are, of course, in direct conflict with the results of alternating stress tests.

As the predicted increase in stress did not, in itself, explain the greater weakness of scratched materials, a new explanation was needed. Griffith tackled this problem by developing a theory based on the balance of the energies involved in the fracture process. This approach is best explained in his own words:

---

[4]In the description of his original paper Griffith's own nomenclature will be used, this is different from the nomenclature in common usage today.

[5]The maximum tension hypothesis says that failure will occur when the certain tensile stress is reached.

> According to the well-known "theorem of minimum energy," the equilibrium state of an elastic solid body, deformed by specified surface forces, is such that the potential energy of the whole system is a minimum. The new criterion of rupture is obtained by adding to this theorem the statement that the equilibrium position, if equilibrium is possible, must be one in which rupture of the solid has occurred, if the system can pass from the unbroken to the broken condition by a process involving a continuous decrease in potential energy.

He continued by pointing out that the energy associated with the new surfaces has also to be accounted for. For the theoretical application of this concept he examined a cracked plate. This was a flat homogeneous isotropic plate of uniform thickness. The plate was loaded so that at all points away from the area of the crack the principal stresses, in the plane of the plate, are parallel and perpendicular to the crack. He designated these stresses as: P; directed out of the plane, Q; the principal stress parallel to the crack and R; the principal stress perpendicular to the crack. The crack is represented by the limiting ellipse or focal line (the crack being so slender that the minor axis of the ellipse has almost no length). By using the solution given by Inglis for the stress around an elliptical hole Griffith derived an equation for the increase in strain energy due to the introduction of the crack, in the case where Q = R (and P = 0, in the case of plane stress). For a very narrow crack its length is the same as the focal length of the ellipse, 2c. In this case the increase in strain energy is

$$W = \frac{(3 - p)\,\pi\, c^2\, R^2}{8\,\mu} \qquad (5.002)$$

where

W = the increase in strain energy due to the crack

$p = 3 - 4\,\sigma$ in the case of plane strain, or $\frac{3 - \sigma}{1 + \sigma}$ for plane stress

c = the length of half the focal line (or half of the crack length)

μ = the modulus of rigidity of the material.

It was found that this equation also satisfied the condition of R = 0 (and P = 0, in the case of plane stress) and the case that of all the stresses in the plane being equal to zero. Griffith said that rupture is thus determined entirely by the stress R, perpendicular to the crack.

The change in energy of the system was determined by combining the energy due to the new crack surfaces, with the calculated increase in strain energy. He defines the potential energy of the surface of the cracks, per unit thickness of the plate as

$$U = 4\,c\,T \qquad (5,003)$$

where

U = the potential energy of the surfaces

T = the surface tension of the material

Thus the total decrease in the potential energy of the system, due to the presence of the crack, is give as

$$W - U = \frac{(3 - p)\,\pi c^2 R^2}{8\,\mu} - 4\,c\,T \qquad (5.004)$$

By differentiation the point at which the energy absorbed and that released are in balance is determined, and an equation for the stress at this point obtained. The equation presented in the original paper (Griffith, 1920) is not the same as that normally produced in books and articles relating to fracture mechanics. Unlike the commonly used solution Griffith's original solution for plane stress contains a Poisson's ratio term σ.

$$R = \sqrt{\frac{2\,E\,T}{\pi\,\sigma\,c}} \qquad (5.005)$$

in this case

σ = Poisson's ratio

E = Young's modulus, which is also expressed as $2\,(1 + \sigma)\,\mu$.

In the next section the equation that is now used in place of equation 5.005 is introduced. However, both equations possess the most important feature of the predictions based on the energy balance approach: the stress required to propagate a crack is proportional to the reciprocal square root of the crack length.

5.2.2.2. THE ENERGY BALANCE APPROACH: THE MODERN INTERPRETATION

The equation now used in fracture mechanics that is widely attributed to 'Griffith, (1920)' results from a correction he made to the above energy term in 1924, (Berry 1972, Atkins and Mai 1988). For this reason the exact method and nomenclature used by Griffith will, henceforth, be abandoned. In its place I will use a distillation of the explanation and symbols that are in common usage. When I use the term *Griffith equation* (or similar wording) this will refer to the, standard, corrected form of the equation, given in this section (equation 5.021).

As Griffith pointed out, the introduction of a crack into a flat sheet can be described in terms of the changes in energy. This approach can be explained as follows, let the total energy, U_t, of the system be defined as;

$$U_t = U_o + U_e + U_s - F \qquad (5.006)$$

Where; U_o is the elastic energy of the loaded system without a crack, U_e is the energy released due to the crack, U_s the surface energy due to the crack, and F is the external

work supplied to the system. When no external work is supplied, unstable crack propagation can occur only if the increase in crack length releases more stored energy than will be consumed in the production of the new surfaces. The case normally examined is that of an infinite plate of thickness t, subjected to uniaxial stress σ, through fixed ends.[6] The amount of strain, or potential, energy released on the introduction of a central transverse, through-the-thickness, crack of length 2a, is

$$U_o = - \frac{\sigma^2 \pi a^2 t}{E^*} \tag{5.007}$$

where E^* is the Young's modulus of the material under conditions of plane stress and $E^* = E/(1 - \nu^2)$ for conditions of plane strain, ν is the Poisson's ratio of the material. Thus, with no external work, equation 5.006 may be rewritten as;

$$U_t = U_o - \frac{\sigma^2 \pi a^2 t}{E^*} + 4 a t \gamma_s \tag{5.008}$$

In equation 5.008 γ_s is the surface free energy of the material. If the equilibrium condition, $\partial U_t / \partial a = 0$ is now used equation 5.008 becomes

$$0 = - \frac{2 \pi \sigma^2 a t}{E^*} + 4 t \gamma_s \tag{5.009}$$

The U_o term has become zero, as it is not dependent on the crack length. This equation is rearranged to give the now familiar formula for the stress level at this equilibrium condition. As the energy balance of the system is in equilibrium any attempt to increase the load and thus the available energy within the system, will result in catastrophic crack propagation. Similarly, a decrease in the load level will result in a reduction of the energy available to the crack, so it will not extend. The equilibrium stress level is thus referred to as the critical stress level, σ_{cr}

$$\sigma_{cr} = \sqrt{\frac{2 E^* \gamma_s}{\pi a}} \tag{5.010}$$

Clearly this equation can be rearranged to give the *critical crack length*, the maximum stable crack at a given stress level. Any increase in the length of the crack above this critical length will result in crack propagation and failure of the structure.

Equation 5.009 can be viewed in a different manner, for it may also be expressed as

---

[6]Due to the fixed end conditions there is no external work, F = load × distance moved. Some texts use an edge crack length a, here I use an internal crack length 2a, thus some of the initial parts of this derivation may appear to be incorrect by a factor of two if compared with such texts.

$$\frac{2\pi\sigma^2 a t}{E^*} = 4 t \gamma_s \tag{5.011}$$

When equation 5.011 is divided by 2t, it is the same as that which is obtained by examining a single edge crack in a plate of unit thickness.[7]

$$\frac{\pi\sigma^2 a}{E^*} = 2\gamma_s \tag{5.012}$$

From above this may also be expressed as

$$-\partial U_e/\partial a = \partial U_s/\partial a \tag{5.013}$$

Because $2\gamma_s$ is a constant this means that $-\partial U_e/\partial a$ is also a constant. As this analysis is based on the energy within the material, this term being negative implies that energy is released from the system. So the term *potential energy release rate* is used, and this quantity is given the symbol G.[8]

$$G = -\frac{dU_e}{da} \tag{5.014}$$

$$G = \frac{\pi\sigma^2 a}{E^*} \tag{5.015}$$

In the phrase (and quantity) *potential energy release rate* the rate is with respect to the crack length (Knott 1973). When this quantity is used it is important to remembered that it is commonly defined for a unit thickness. (To avoid confusion, I consider that it may be better to view this rate as being with respect to crack area, which in the case of a single edge crack will be A = ta, and for a central crack A = 2ta. Such a view would remove the need to divide by 2t, as was done above.) If the potential energy release rate for a crack equals its surface energy, the crack will propagate. Under these conditions it is said to have reached its critical value.

$$G_c = 2\gamma_s = \frac{\pi\sigma_{cr}^2 a}{E^*} \tag{5.016}$$

This condition is shown graphically in figure 5.002.

---

[7]If an imaginary cut is made perpendicular to the internal crack of length 2a, through its mid-point, this crack can be viewed as two edge cracks of length a. In this way a mental model of how the internal and edge crack equations relate to each other can be formed.
[8]G is also called the *elastic energy release rate* (Ewalds and Wanhill, 1986) or the *strain energy release rate* (Smith, 1991).

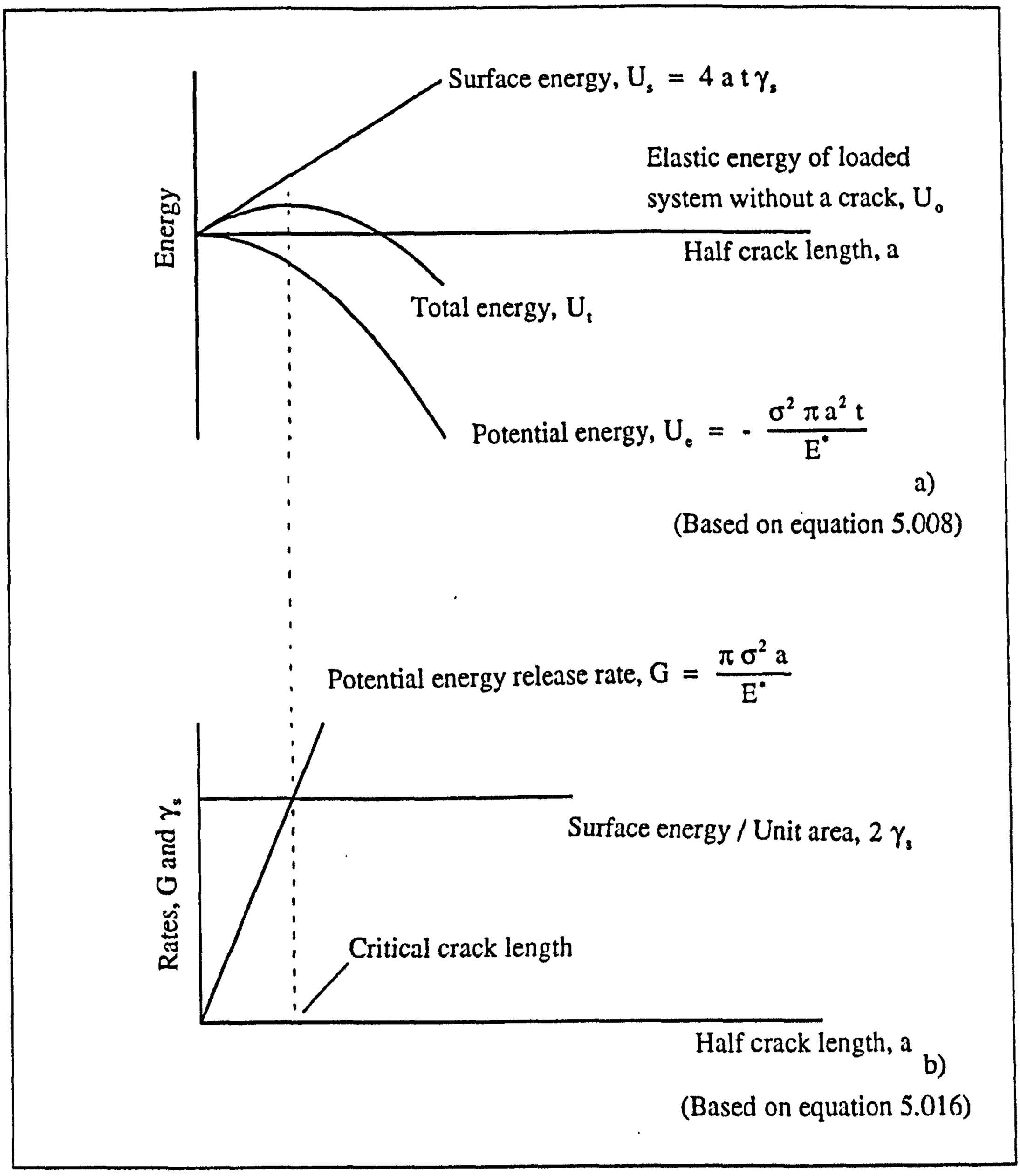

Figure 5.002

Variation of energy with crack length for an internal (through the thickness) crack of length 2a in a sheet of thickness t.

This energy approach was first applied to the fracture of glass. Griffith (1920) used this material for experimental verification of his theory. The values of $\sigma \sqrt{a}$, which he obtained from experiments, were on average 10 per cent below that predicted from values of Young's modulus, surface free energy and so on.[9] Atkins and Mai (1988) point out that for glass the process zone of irreversible flow at the crack tip is extremely small

[9]The equation he was using was, of course, that contained in 1920 paper, not the later 1924 correction.

and therefore the *work-of-fracture*, R, has, for all practical purposes, the same value as twice the surface free energy.[10] So in the case of glass

$$R = 2\gamma_s \tag{5.017}$$

Atkins and Mai (1988) state that the surface energies of many other materials, when estimated from equation 5.010, were found to be substantially greater than theoretical values. A study of the thermodynamic basis for these and other energy approaches has been conducted by Stevens and Guiu (1991). This includes an examination of the effect of energy dissipating processes, such as plastic deformation, on the energy balance. Stevens and Guiu state that the observation that small-scale yielding increased the critical crack extension force, led Irwin (1948) and Orowan (1952) to propose, independently, that this effect could be accounted for by the addition of the work of plastic deformation to the surface energy. The modification of the above equation is shown below, using γ_p to represent this work;

$$\sigma_{cr} = \sqrt{\frac{2\,E^*\,(\gamma_s + \gamma_p)}{\pi\,a}} \tag{5.018}$$

A value of ratio of plastic work to the surface free energy is given by Atkins and Mai (1988); they say $\gamma_p/\gamma_s \approx 1000$ (no specific material is named). Thus the surface free energy is only small constituent of the work-of-fracture. Honeycombe (1981) in his book on steels, says that it has been found that $\gamma_p >> \gamma_s$, as the surface free energy term is so small in this case he ignores it, and thus expresses the condition for crack spreading in a crystalline solid, such as iron, as

$$\sigma_{cr} = \sqrt{\frac{E^*\,\gamma_p}{\pi\,a}} \tag{5.019}$$

It is now common to combine the plastic work and the surface energy into one term;

$$R = 2\,(\gamma_s + \gamma_p) \tag{5.020}$$

So equation (5.018) can be expressed as

$$\sigma_{cr} = \sqrt{\frac{E^*\,R}{\pi\,a}} \tag{5.021}$$

Equation 5.021 is commonly referred to as the *Griffith equation* (in modern texts on fracture mechanics). The importance of this equation is that it expresses the relationship between the applied stress and the crack length for an elastic material. The work-of-

[10]There is an inconsistency in the way different workers define these quantities. In the work by Atkins and Mai, the surface free energy is defined with respect to both surfaces and the work-of-fracture with respect to one surface. This definition is also used by Knott (1973), and is the one used in this thesis.

fracture, R, may be viewed as a crack resistance force (Smith, 1991) and is considered to be a material property.

Sometimes the symbol, G, is used in place of, R. The former is the *potential energy release rate*, with respect to the crack area (see above). It is only under the conditions associated with equilibrium fracture that these two quantities are equal, the energy absorbed by the fracture process balancing that released, thus $R = G_c$ (as shown in figure 5.002). If the work available is greater than that required, $R < G$, the result is an unstable fracture. Atkins and Mai provide a table of 'representative toughness values for various materials' a small part of which is given in table (5.001). (The original table contains over 70 engineering and non-engineering materials, so I have chosen common materials that display an almost logarithmic scale of work-of-fracture values.)

Material	Work-of-Fracture R, kJ m^{-2}	Young's modulus E, GPa
Bulk soda glass	0.01	70
Cast iron	0.2 - 3	130-180
Steel (hardened and tempered)	2	210
Medium carbon steel	14	210
Lead	30	14
Boron-epoxy composite across the fibres (V_f = 25 %, intermittent bonding)	200	95
Bone[11]	2	13.5

Table 5.001 After Atkins and Mai (1988)

Work-of-fracture and Young's modulus values for some common materials and 'bone'

It is interesting that these results imply that at the same crack length a specimen of medium carbon steel can sustain a load 65 times that sustainable by bulk soda glass. (This is assuming the materials are behaving perfectly elastically.) By the same arguments, at the same stress level the medium carbon steel can sustain a crack 4200 times longer than that which will cause the bulk soda glass to fail, at the same stress. Here is the answer to the question posed in the introduction to this chapter; less work is required to propagate a crack in glass. In the introduction the cause of this difference in work was alluded to, the plastic deformation around the travelling crack tip. Clearly if the fragments can be fitted together to form the original shape there has been only a very limited amount of plastic deformation, a brittle fracture.

---

[11]The source, literary or experimental, of these values is not given, nor is the type of bone. However, I have included them for the purposes of general comparison.

5.2.3. THE STRESS INTENSITY FACTOR APPROACH

As Knott (1973) phrases it, in this method;

> We concentrate on a crack tip region which is small compared with the body as a whole but sufficiently large with respect to atomic dimensions for us to be reasonably happy with the application of linear elastic theory.

This approach was originally developed by Irwin in 1957a. In the conclusion of his paper entitled *Analysis of stresses and strains near the end of a crack traversing a plate* he says

> The stress field near the end of a somewhat brittle tensile fracture, in situations of generalized plane stress or plane strain, can be approximated by a two-parameter set of equations. The most significant of these parameters, the intensity factor is $(E\,G/\pi)^{1/2}$ for plane stress where G is the force tending to cause crack extension.

It was reported above that Inglis (1913a) obtained a comparatively simple analytical solution of the stresses for a number of situations based on an elliptical hole in a stressed plate. The solutions he gave were in curvilinear co-ordinates one being for the 'case of a plate subjected to a tensile stress R in all directions, the plate having an elliptical hole defined by $a = a_0$'. Atkins and Mai (1988) use the solution, for the stresses in the line of the crack (ellipse) for that situation to demonstrate the derivation of the stress intensity factor, their approach is followed here.

For a sharp crack, $a >> b$, the stresses σ_{yy}, σ_{xx} and τ_{xy} in the line of the crack (represented by the major axis of the thin ellipse, which also forms the x-axis of the Cartesian co-ordinate system) are as follows;

$$\sigma_{yy} = \sigma_{\infty} \coth \xi \tag{5.022}$$

$$\sigma_{xx} = \sigma_{\infty} \left\{1 - \left[1 + 4\,e^{-\xi}\right] \sin 2\xi + \left[2\,e^{\xi} \sinh 2\xi - 1\right] \cosh 2\xi\right\} \tag{5.023}$$

$$\tau_{xy} = 0 \tag{5.024}$$

Where $x = c \cosh \xi$ (where 2c is the focal length of the ellipse). To examine the stresses in relation to a point, the distance r ahead of the crack, let

$$r = (x - a) \tag{5.025}$$

so the distance may be expressed as,

$$r = c \cosh \xi - a \tag{5.026}$$

In the case of a slender ellipse $a >> b$, $c \equiv a$, so the above equation becomes

$$r = a(\cosh \xi - 1) \tag{5.027}$$

which may be rearranged to give

$$\cosh \xi = \frac{r}{a} + 1 \tag{5.028}$$

Using the hyperbolic relationship $\cosh^2 x - \sinh^2 x \equiv 1$, and substituting into it equation 5.028 gives

$$\sinh^2 \xi = \left(\frac{r}{a} + 1\right)^2 - 1 = \frac{r^2 + 2ar + a^2}{a^2} - \frac{a^2}{a^2} \tag{5.029}$$

This simplifies to

$$\sinh^2 \xi = \frac{r}{a}\left(\frac{r}{a} + 2\right) \tag{5.030}$$

So

$$\sinh \xi = \sqrt{\frac{r}{a}}\sqrt{\frac{r}{a} + 2} \tag{5.031}$$

Thus, using equations 5.022 and 5.031 the stress (across the crack tip) is expressed as;

$$\sigma_{yy} = \sigma_\infty \coth \xi = \sigma_\infty \frac{\cosh \xi}{\sinh \xi} = \sigma_\infty \frac{\frac{r}{a} + 1}{\sqrt{\frac{r}{a}}\sqrt{\frac{r}{a} + 2}} \tag{5.032}$$

Atkins and Mai say that if the strong intensification of the stress in the region of the crack tip controls fracture (and because there is a rapid fall-off of stress away from the edge of a slender ellipse) it is reasonable to rewrite the above equation (5.032) as an expression in r/(2 a) of which only the first few terms will be important as the remote stresses will not be influencing matters. Then

$$\sigma_{yy} = \frac{\sigma_\infty \sqrt{a}}{\sqrt{2r}}\left[1 + \frac{3}{2}\left(\frac{r}{2a}\right) - \frac{5}{8}\left(\frac{r}{2a}\right)^2 + \frac{7}{16}\left(\frac{r}{2a}\right)^3 \ldots\right] \tag{5.033}$$

This equation becomes a better approximation when more terms are used. The product of the applied stress and the half-crack length in the above equation, $\sigma_\infty \sqrt{a}$, is grouped into one parameter, which is the fundamental parameter of LEFM. Atkins and Mai (1988) point out that it has become customary to also include $\sqrt{\pi}$ within this parameter to obtain

similarity with the Griffith equation and that it is represented by the symbol K. So for a thin slit in a large sheet equation 5.033 has become:

$$\sigma_{yy} \approx \frac{\sigma_{\infty}\sqrt{\pi a}}{\sqrt{2\,\pi\,r}} = \frac{K}{\sqrt{2\,\pi\,r}} \qquad (5.034)$$

K is called the *stress intensity factor* (SIF). The zone over which the first term of the series is an adequate approximation for σ_{yy} is called the K-dominant region of the stress field. K incorporates the applied stress and the half-crack length and describes the stress field adjacent to the crack tip, whereas the stress concentration factor K_t only gives the magnification of stress at one point.

5.2.3.1. THE SHAPE CORRECTION FACTOR

Atkins and Mai cite Irwin's realisation in 1957 (Irwin, 1957b) that for other geometries the local crack tip stresses in the line of the crack could also be expressed using the same 'first term of a series' approximation, but with a 'shape correction factor' Y. This correction factor would take account of the method of loading, size and shape of the cracked body. Thus $K = Y\,\sigma\,\sqrt{\pi\,a}$ is used in place of $K = \sigma_{\infty}\,\sqrt{\pi\,a}$, as in practical situations the stress is applied to a region that can not be approximated to an infinite distance from the crack, nor is the structure infinite, but has some definable shape.

5.2.3.2. OPENING MODES

So far the only type of cracking that has been specifically discussed is that due to tensile stress across the crack that results in its splitting open and extending along its own axis, this is referred to as mode I cracking. There are two other modes that are defined: first, mode II or shearing along the length of the crack. Second, mode III that is described as, twisting across the crack face. Fractures that occur in practical situations are normally some combination of these modes, producing a so called *mixed mode* fracture. The main modes are illustrated in figure 5.003.

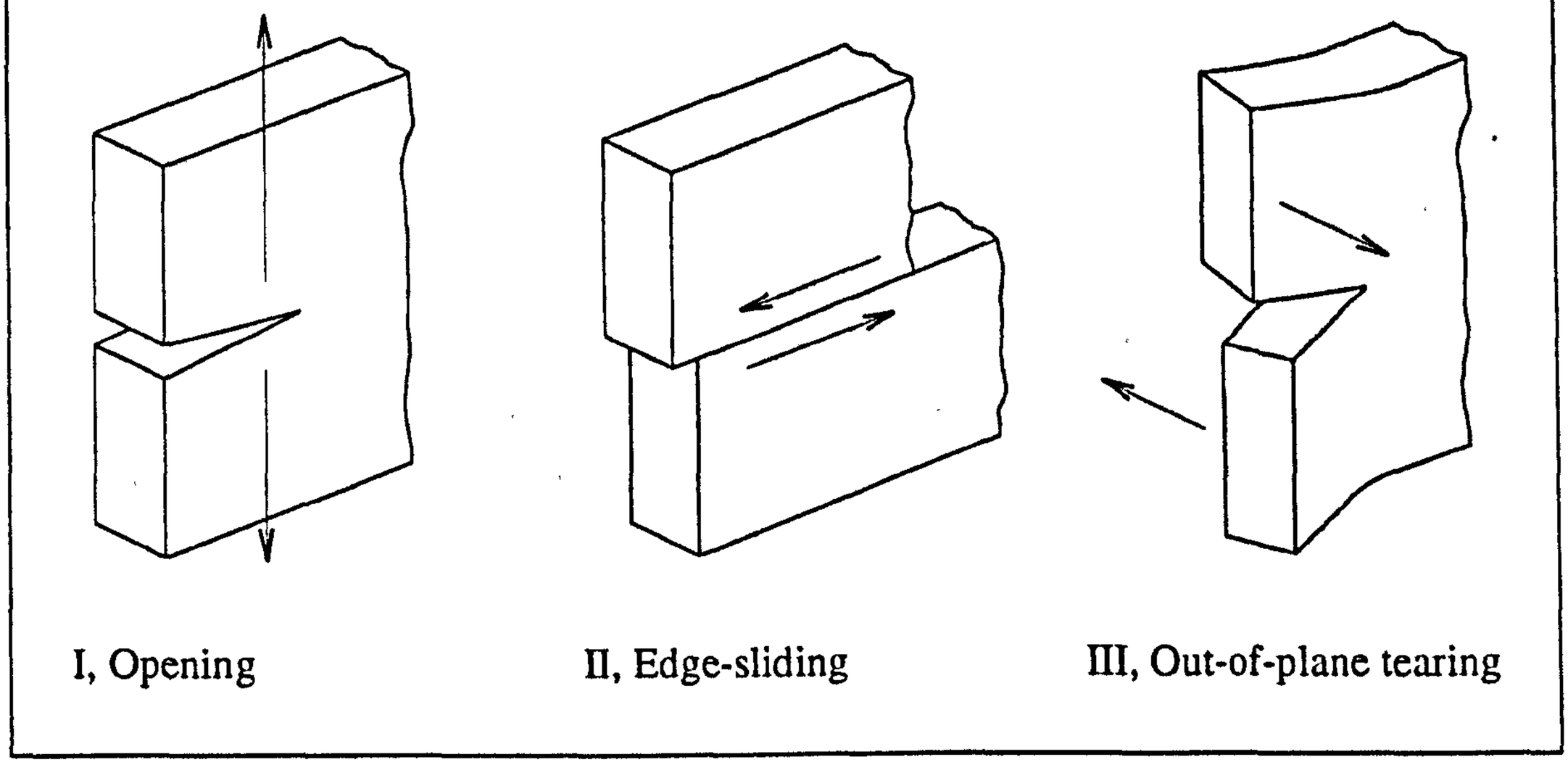

Figure 5.003

The three opening modes defined in fracture mechanics

5.2.3.3. THE CRITICAL STRESS INTENSITY FACTOR.

It was stated above that K is a description of the stress field around a notch or crack, but what is the relevance of this to fracture? This can be seen when the equation containing the shape correction factor is rearranged;

$$\sigma = \frac{K}{Y\sqrt{\pi a}} \qquad (5.035)$$

Thus the right hand side of this equation can be substituted for stress in the equations for the energy balances, and release rate G can be expressed in terms of K. Atkins and Mai say

> In other words K of the propagating crack could serve to characterise a material's resistance to crack propagation, and would be an alternative parameter to R. Fracture events themselves take place in the process zone, so we anticipate that a K-characterisation of fracture events will be successful provided that the process zone is small and lies wholly within the 'K-dominated' region of the actual crack tip stress and strain field, i.e. the region in which the first term of the series is a sufficiently good approximation.

This theory is supported by experimental findings. Tests on similar specimens of the same material, with varying crack lengths do indeed show that K, calculated from $Y\sigma\sqrt{\pi a}$, is constant during crack propagation. Experiments conducted on the same material but using different geometries and hence shape correction factors also give the same results.

By substituting of the length of a starter crack (a machined notch for example) and the stress σ_{cr}, at which the crack starts to move, into equation 5.035 a reasonably constant value of K is obtained. This is called the *critical stress intensity factor*[12] and is given the symbol K_C. This quantity is a constant for a material,[13] thus it and the appropriate shape correction factor, can be used to predict the stress at which a test piece, or structure, will fail. Alternatively by knowing the critical stress the length of the (critical) crack, which will result in failure, can be determined. The critical stress intensity factor is thus a more suitable parameter than the material's yield or ultimate failure stress for predicting and explaining fracture of materials that behave in a linear elastic manner. When the crack is propagating in a stable manner the above equation can be expressed as

$$\sigma_{cr} = \frac{K_C}{Y\sqrt{\pi a}} \qquad (5.036)$$

Thus the stress needed to fracture a cracked elastic material is proportional to the reciprocal square root of the crack length. Thus the effect of doubling the crack length is to quarter the theoretical strength. This explains the disproportionate reduction in strength of materials containing cracks.

5.2.3.4. THE SUBSCRIPTS USED FOR K_c UNDER DIFFERENT OPENING MODES AND STRESS, OR STRAIN, STATES.

The critical stress intensity factor for a material will depend on the opening mode that is employed. Thus subscripts are used to distinguish them. For opening mode I (concentrated on here) K_{IC} is used, likewise the other modes are denoted by K_{IIC} and K_{IIIC}. Atkins and Mai (1988) point out that there is some inconsistency in the literature over the use of K_C and K_{IC}. Both being applied to opening mode I but the former is used for plane stress conditions at the crack tip and the latter for plane strain conditions.[14] The plane strain critical stress intensity factor K_{IC} is the lower limiting value and is obtained in fractures of thick sheets. This is shown in figure 5.004, (after Smith, 1991). As the plane strain value is lower this is the one normally quoted for a material, as it provides a conservative bound on the resistance of the material to fracture and thus provides a margin of safety for structures where it is used as a design parameter. Hence the standard experimental methods of obtaining K_C try to produce conditions of plane strain.

---

[12]Atkins and Mai (1988) point out that the *critical stress intensity factor* is some times called the *fracture toughness*, but here I will follow their nomenclature.
[13]This is not exactly true, for it is only a constant, and minimum value, for the material under conditions of plane strain. Thus it is these conditions that are normally used in the standard test methods, for example BS 5447 (1977).
[14]Plane stress and plane strain are defined in the glossary are the rear of this thesis.

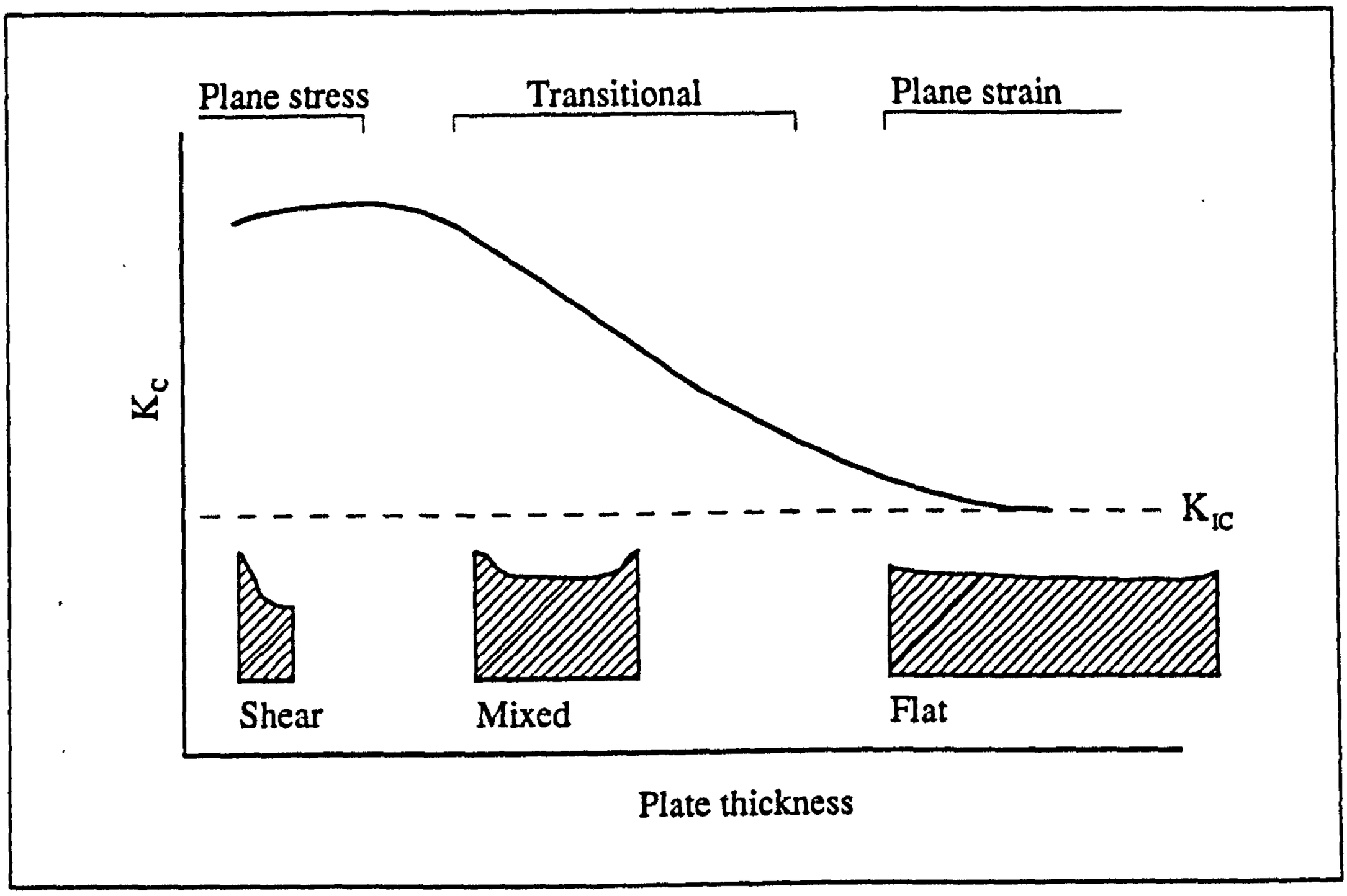

Figure 5.004

The change in K_c and type of fracture with thickness of the specimen

5.2.3.5. THE RELATIONSHIP OF K_c TO R AND G_c

If the equation for the critical stress intensity factor for an infinite plate is compared to the Griffith equation it can be seen that

$$R = {K_c^2}/{E'} \qquad (5.037$$

Equation 5.037, following the nomenclature given above, can be expressed as

$$R = {K_c^2}/{E} \qquad (5.038)$$

for plane stress, and for the case of plane strain as

$$R = \frac{K_{IC}^2 \left(1 - \nu^2\right)}{E} \qquad (5.039)$$

For equilibrium fracture this equation can also be used to describe the critical potential energy release rate, as the work-of-fracture equals this rate under those conditions. The relationship between R and G has already been referred to in section 5.2.2.2. It was stated that it is only under the conditions associated with equilibrium fracture that these two quantities are equal, the energy absorbed by the fracture process balancing that released, $R = G_c$. Thus G_c may be substituted for this variable in the equations above.

5.2.3.6. CRACK SHARPNESS

A specimen that contains a blunt crack or machined notch, as opposed to a sharp one, normally requires a greater fracture load. Thus the value of K_c is also a function of the bluntness of the crack. If K_c is plotted against the crack tip radius ρ, a graph similar to figure 5.005 may be produced. The value of K_c falls with decreasing ρ, until the critical value of the tip radius is reached, ρ_c, at this and sharper crack tips K_c is constant.

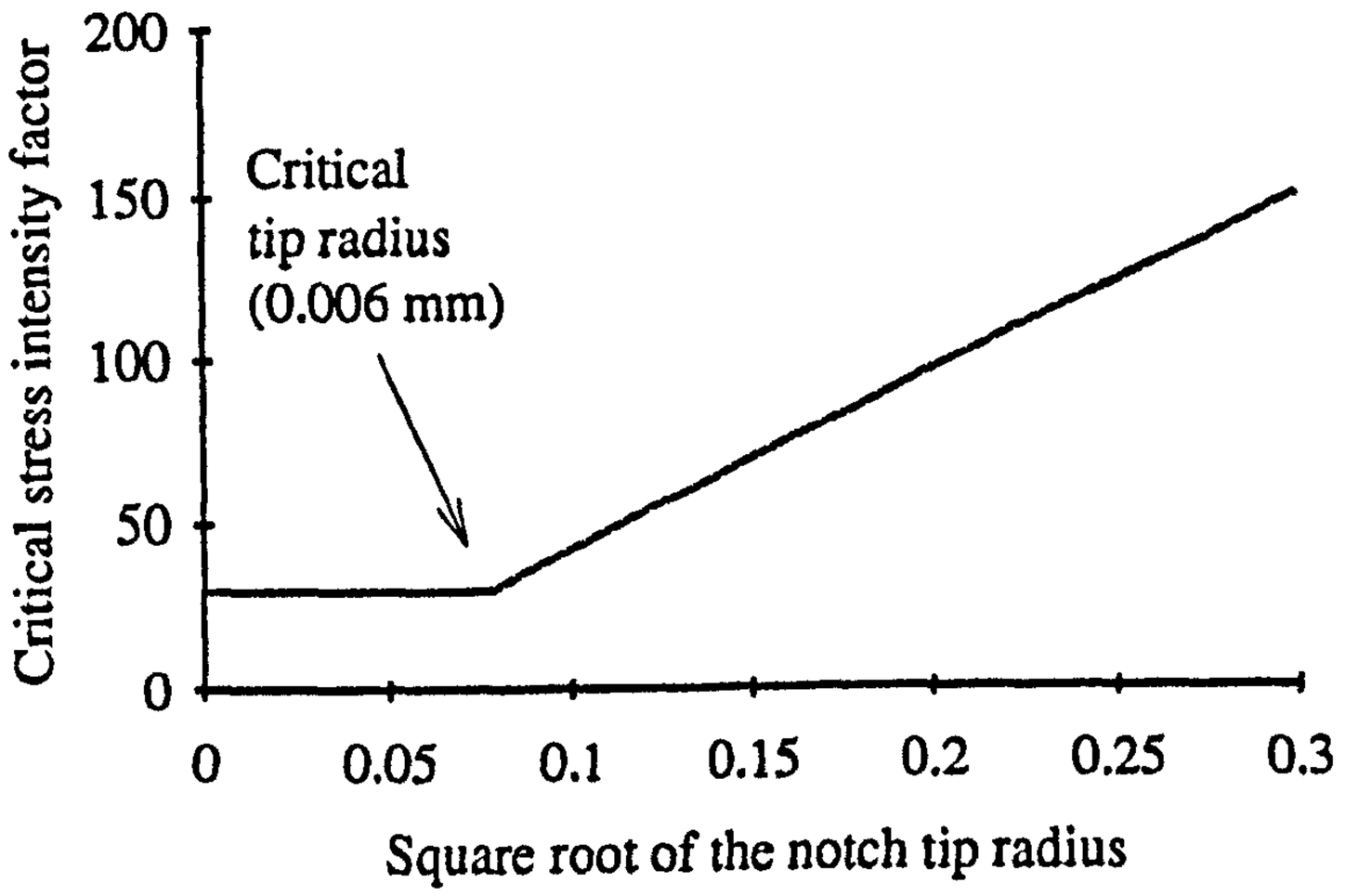

Note: Data for high-strength steel. K_c in MPa $m^{0.5}$ and $a^{0.5}$ in $mm^{0.5}$

Figure 5.005 After Knott (1973)

Relationship of the critical stress intensity factor and the square root of the notch tip radius

5.2.3.7. THE CRACK TIP PROCESS ZONE SIZE

In the stress intensity factor approach, as in the case of the energy approach, some account needs to be taken of the behaviour of real materials. From an examination of equation (5.034) it would appear that at the crack tip the stress is infinite, if an infinitely sharp crack is assumed. This implies that at any load level the crack will always propagate. A property of many materials that permits them to sustain loads when they are cracked is plastic deformation or damage at the crack tip. This deformation results from the stresses near the crack tip being greater than the yield stress of the material. In this explanation the idea of yield and plasticity, as in metals, will be used but the process zone could be due to some other form of failure induced by the high stresses at the crack tip. The form the process zone takes will depend on the material's structure. A simple method to approximate the extent of the plastic zone (used in the study of metals) is to find the distance ahead of the crack at which the largest principal stress first reaches the

uniaxial yield stress of the material (see figure 5.006). This criterion has, as Smith (1991) points out, some deficiencies since yielding is associated with shear stresses, but it has the advantage of simplicity. Thus a useful first approximation of the region's width, r_y, in line with the crack, is the portion of this line where the calculated stresses exceed the yield stress. From equation 5.034 the distance at which the yield stress, σ_Y, is reached is given by

$$\sigma_Y = \frac{K_I}{\sqrt{2\,\pi\,r_y}} \tag{5.040}$$

This equation may be rearranged to give the width of this region as

$$r_y = \frac{1}{2\,\pi}\left(\frac{K_I}{\sigma_Y}\right)^2 \tag{5.041}$$

It is clear from the above equations that as the stress intensity factor increases so will the plastic zone size. (The SIF itself increases with the applied load.) If this region has yielded no stress above the level of the yield stress can exist in this zone, so the theoretically higher stress in the zone is unattainable, likewise the associated strain energy can not be acquired by this region of the material. As the load is unchanged this discrepancy should be accounted for; it can be quantified as follows. Assuming unit thickness, σ is the force per unit length. The total elastic force under the curve $\sigma = K_I/\sqrt{2\,\pi\,r}$ in the region of the yield zone is

$$\int_0^{r_y} \sigma\,dr = \int_0^{r_y} \frac{K_I}{\sqrt{2\,\pi\,r}}\,dr \tag{5.042}$$

The force per unit length, σ_Y, sustained by the plastic or damage process acts over the length of the process zone. The above equation also equates to

$$K_I\,\sqrt{2\,r_y/\pi} = 2\,\sigma_Y\,r_y \tag{5.043}$$

Atkins and Mai (1988) say that it is thus customary to argue that the yield zone should thus extend to 2 r_y which they call d_y

$$d_y = \frac{K_I^{\,2}}{\pi\,\sigma_Y^{\,2}} \tag{5.044}$$

This zone may be shown schematically as a circular area diameter d_y ahead of the crack tip (as in figure 5.006), or of radius d_y centred on the crack tip since the zone is found to spread back to the flank of the crack. Smith (1991) says;[15]

---

[15]Smith (1991) uses different nomenclature. I have changed his symbol from r_p to d_y.

Irwin assumed that the crack tip extended to the centre of the plastic zone so that the effective crack length is $a + d_y/2$. If the plastic zone is small relative to the crack, then it may be corrected for by using this effective crack length in SIF calculations.

This is shown diagrammatically in figure 5.006.

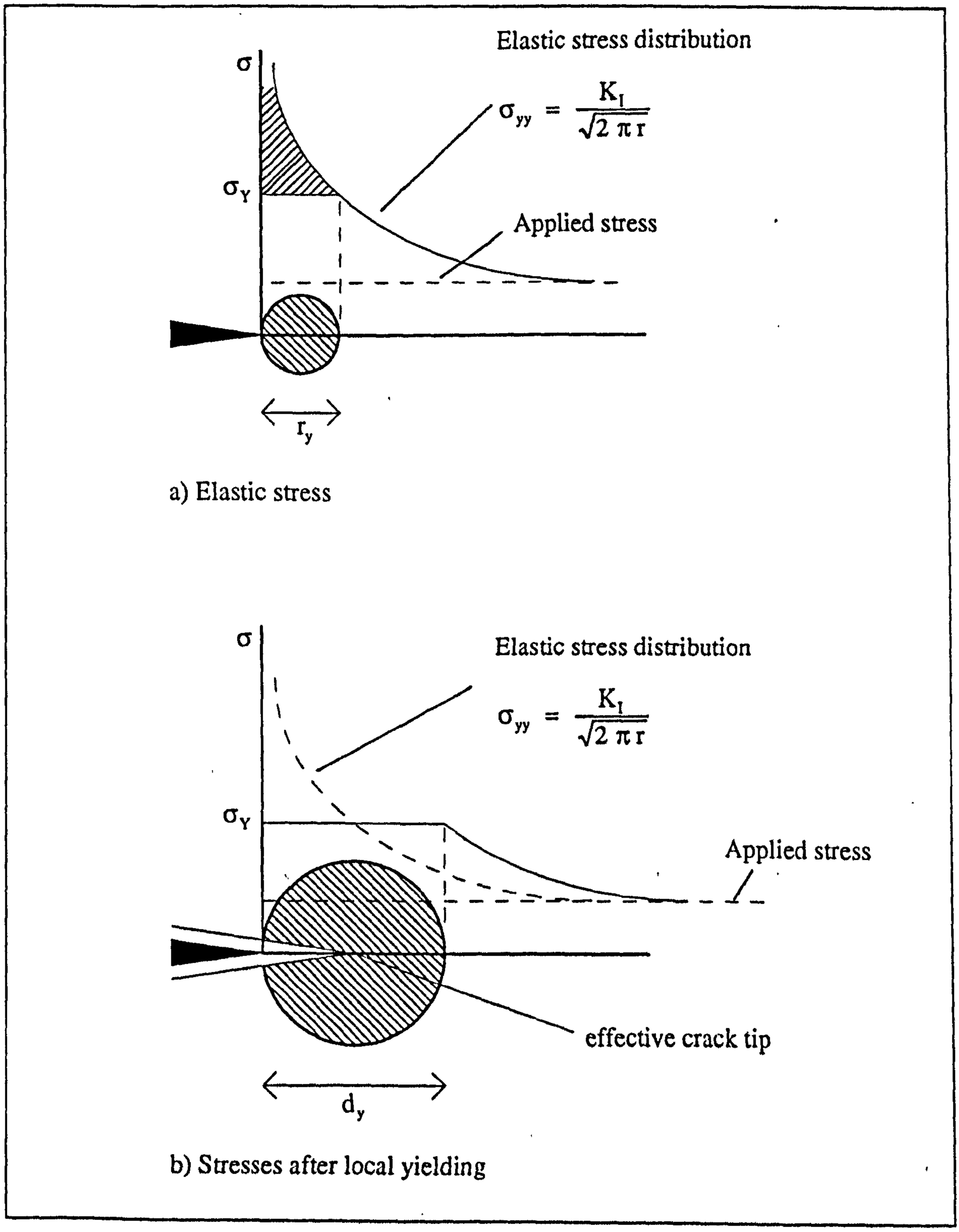

Figure 5.006

Approximations to the crack tip process zone

It has already been mentioned that the plastic zone size will increase with an increasing stress intensity factor. This implies that if the SIF reaches its critical value this correlates with the maximum size of the process zone. Thus it also implies that during equilibrium crack growth the process zone is of constant size. Also mentioned above is the dependence of the critical stress intensity factor on the state of stress and strain in the material. A related complicating factor is that in thick sheets undergoing plane strain deformation the constraints placed on the flow stress, result in a smaller process zone. To account for both these effects Atkins and Mai give the formulae

$$\left(d_y\right)_{cr} \text{ plane strain } = \left(\frac{1}{3}\right)\left(\frac{1}{\pi}\right)\left(\frac{K_{IC}}{\sigma_Y}\right)^2 \qquad (5.045)$$

$$\left(d_y\right)_{cr} \text{ plane stress } = \left(\frac{1}{\pi}\right)\left(\frac{K_C}{\sigma_Y}\right)^2 \qquad (5.046)$$

As $K_C > K_{IC}$ this results in the plane strain crack tip zone being less than one-third the size of that for plane stress conditions.

For many materials the process zone size is proportional to the crack tip radius. Sharp cracks produce a small zone of highly strained material, while blunt cracks produce a larger zone but lower strains. In the extreme of these cases, the former zone may be too small to contain an inclusion or flaw, while in the latter case the zone could incorporate many inclusions but none may be strained sufficiently to assist crack extension. So it would appear very sharp cracks have to be blunted by plastic flow (or some other process), before the process zone size will be large enough to include flaws that are strained sufficiently. This explains the horizontal section of the plot in figure 5.005. Atkins and Mai say that once initiated, a crack tends to propagate with its own characteristic *natural bluntness* ρ_c (and thus a constant process zone size, SIF and so on). They also comment that this leads to the concept of critical crack opening displacement. During fracture the crack tip opening displacement (COD, $\delta_c \approx 2\,\rho_c$) can be used as an alternative to R and K_c. (A standard for this test exists for metallic components tested in bending, BS5762 (1979), and a description of the method can be found in Atkins and Mai (1988).)

In practice if the calculated size of the plane stress process zone (d_y for Irwin) is of the same order as the plate thickness, then plane stress conditions are normally assumed. If the length of the calculated plane stress d_y is about 10 per cent, or less, of the plate thickness then plane strain is assumed (Smith 1991).

5.2.3.8. THE SHAPE OF THE CRACK TIP PROCESS ZONE

In the initial analysis of the process zone at the crack tip, only the length of the zone was estimated by a very simple yield criterion. Two more sophisticated criteria are in common usage, the Tresca and Von Mises criteria. These are expressed in terms of the principal stresses $\sigma_1 > \sigma_2 > \sigma_3$. (A description of these criteria can be found in the glossary at the back of this thesis.) The shape of these process zones is shown in figure 5.007, and mathematical derivation of these shapes can be found in Smith (1991). It is noticeable that the zones are similar in shape, the Tresca criterion producing a larger yield zone. (However, Ewalds and Wanhill (1986) show a kidney shaped yield zone for the Von Mises criteria under plane stress conditions. Smith also adopts the kidney shape in a later diagram, redrawn here as figure 5.008a.)

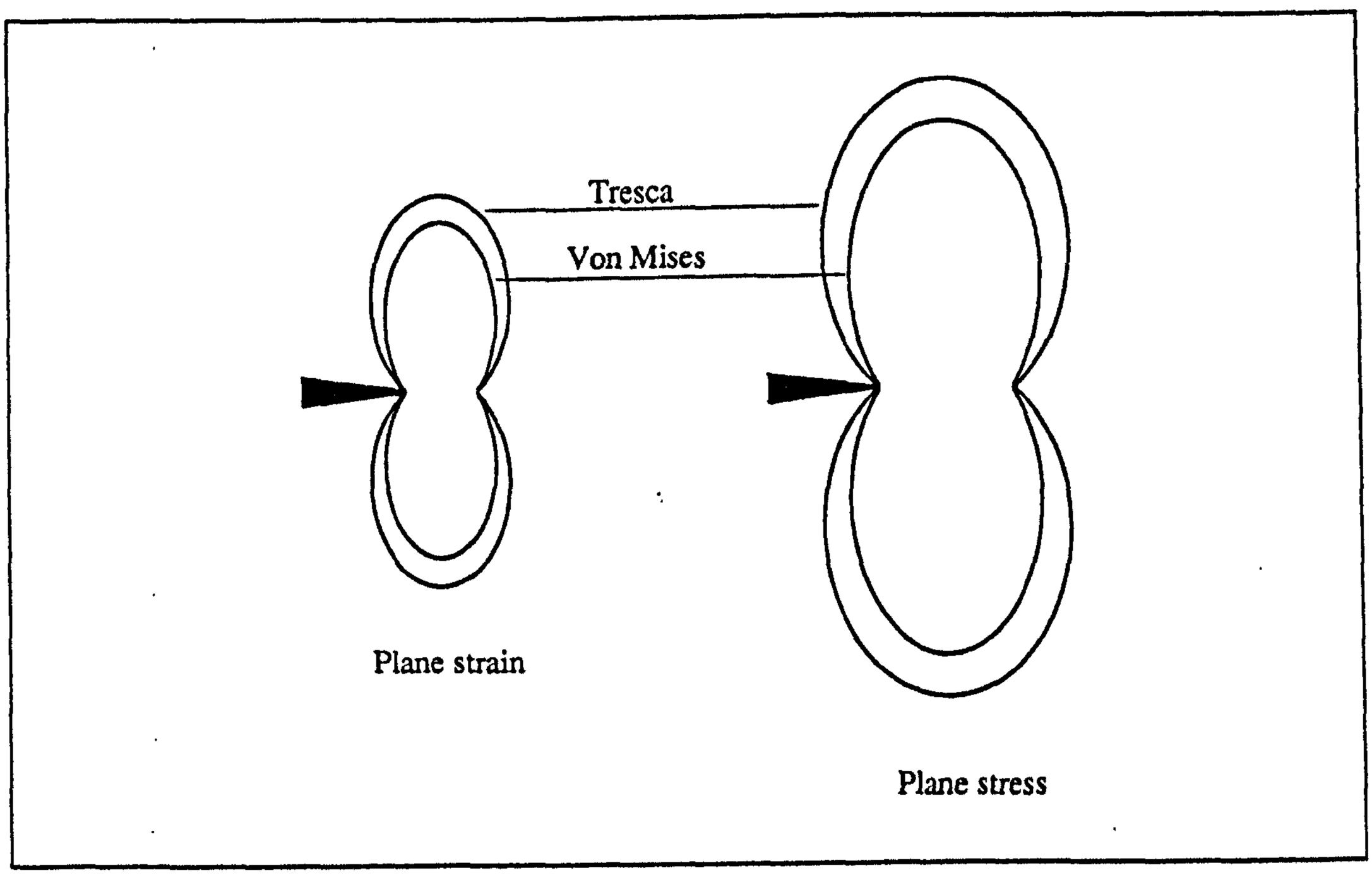

Figure 5.007 After Smith (1991)

Plastic zone shapes for plane strain and plane stress

There is a variation in the size of the zone depending on the conditions of stress and strain within the material, as in the simple model. Plane stress producing a larger yield zone. The ratio of plane strain to plane stress zone length, in the line of the crack is $1 : (1 - 2\nu)^2$. There is a variation in conditions of stress and strain through the thickness of a material. This is due to the changes in constraints, from the materials surface to its interior, resulting in plane stress at the surface and plane strain deeper in the material. Consequently the process zone will change in size through a section of the material, the largest being at the surfaces (see figure 5.008). This is the reason for the thickness of the

material effecting the value of K_c as shown in figure 5.004 above. (The exact form of the transition from plane stress to plane strain shown in figures 5.008a and b is different. In one case the transition is gentle and in the other it is more angular, the true nature of the transition is not important here.)

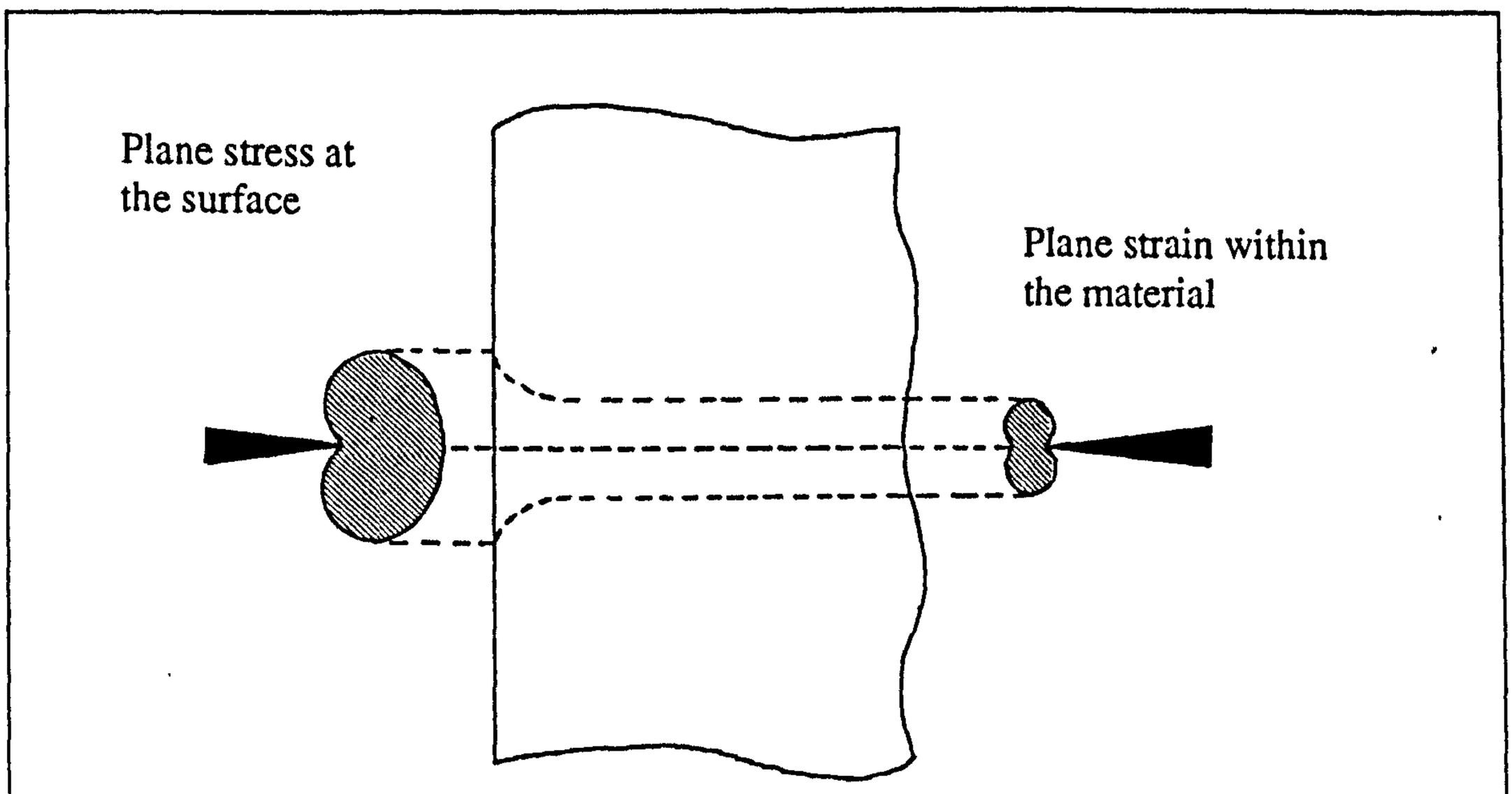

a) After Smith (1991)

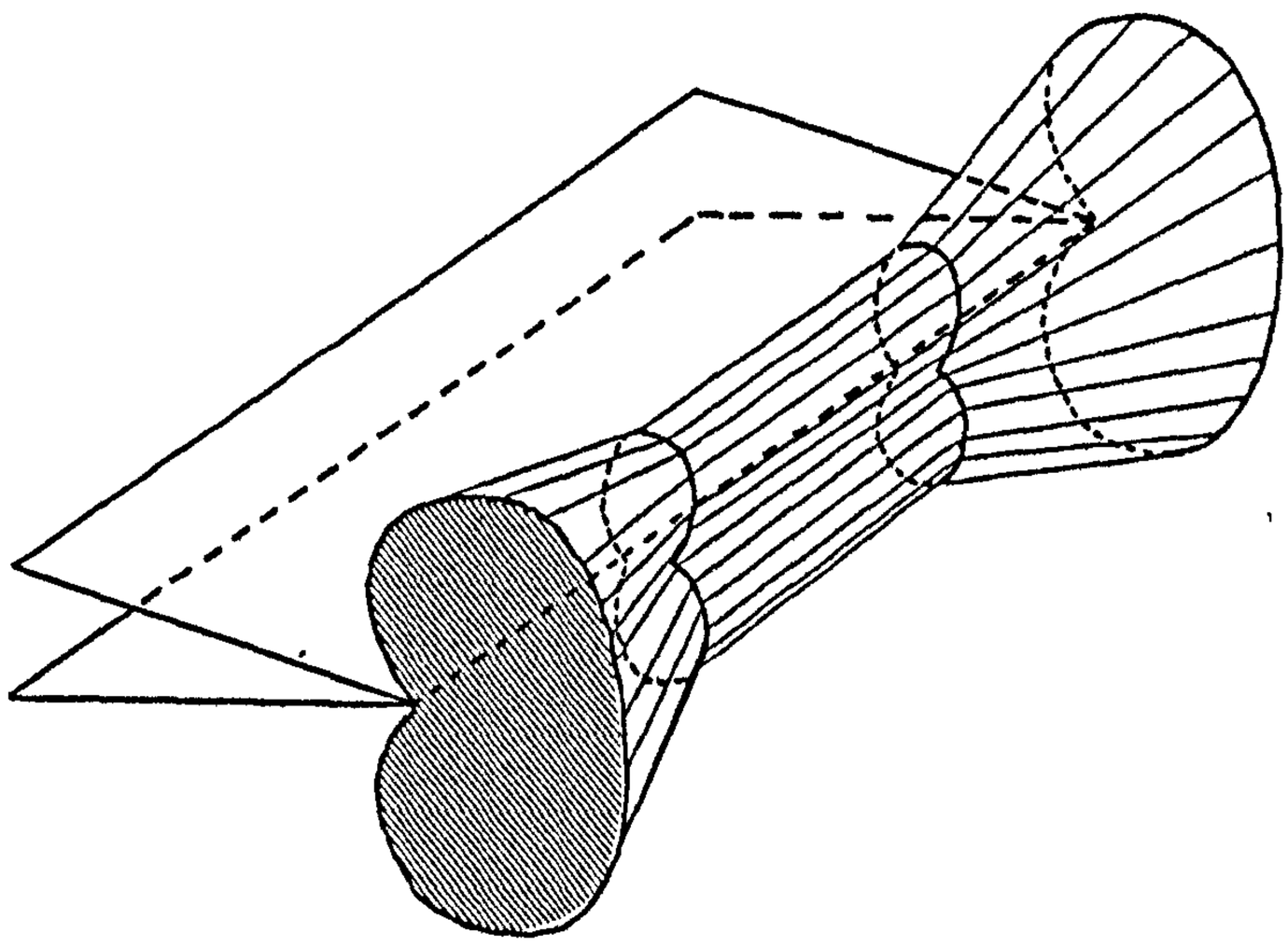

b) After Ewalds and Wanhill (1986)

Figure 5.008

Two pictorial representations of the plastic zone in a thick plate

5.2.3.9. THE DUGDALE STRIP YIELD MODEL OF PLASTIC DEFORMATION AROUND THE CRACK TIP

Dugdale assumed that plastic deformation occurs in a strip ahead of the crack tip (Smith, 1991). The arrangement is shown in figure 5.009. The plastic zone is modelled as spreading a distance $|c - a| = \Delta_y$ ahead on the crack. In the first part of the analysis the crack is supposed to extend completely through the plastic zone, and thus has length 2c. By considering the elastic stress distribution immediately ahead of the plastic zone, the relationship between σ, a and c can be derived. The mathematics of this derivation can be found in Knott (1973). The first step is to use the Westergaard function, which relates the stress at a distance to the length of the crack and the size and position of a pair of point forces that are opening the crack. The loading over the plastic zone is then viewed as the integral of a set of forces equal to the yield stress, which are negative as they are closing the crack (Smith, 1991). So by integration over the plastic zone a value for the stress intensity factor is obtained. The next step is to find the stress that would need to be applied to an elastic crack of length 2c to obtain the same stress intensity factor. These two equations are then combined. Assuming that the external stress σ is much less than the yield stress an approximation for the length Δ_y of the plastic zone

$$\Delta_y = a \frac{\pi^2 \sigma^2}{8 \sigma_Y^2} = \frac{\pi}{8} \left(\frac{K_I}{\sigma_Y} \right)^2 \qquad (5.047)$$

The Dugdale zone size is a little larger than that predicted by the Irwin model but has the same dependence on the stress intensity factor and the yield stress.

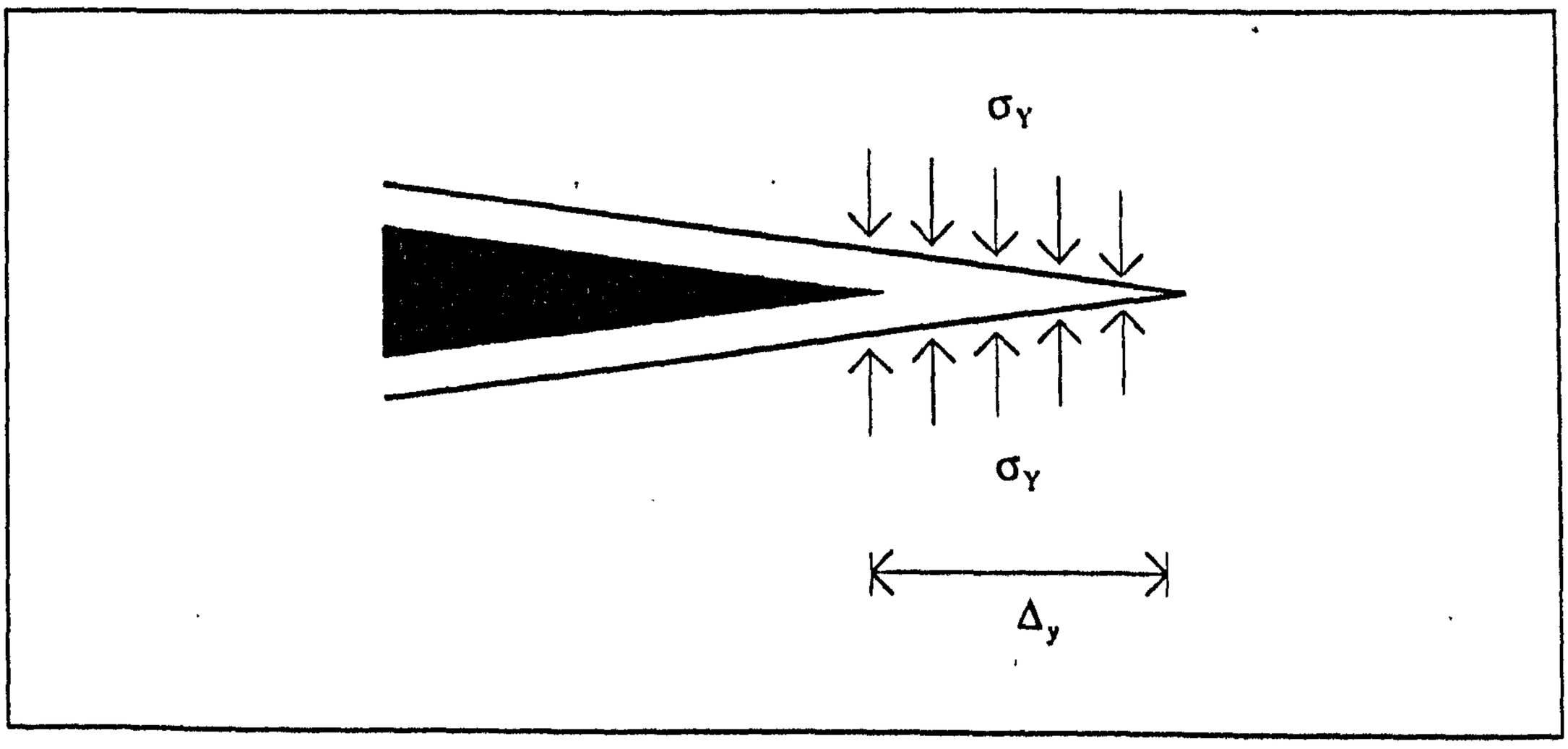

Figure 5.009

The Dugdale strip yield model

5.2.4. SOME LIMITATIONS OF LINEAR ELASTIC FRACTURE MECHANICS

The theory of linear elastic fracture mechanics as described above contains a number of assumptions, which place severe limits on the validity of its application to various situations. Some important restrictions are

a) The material tested has to behave (away from the zone of the crack) in a perfectly linear elastic manner.

b) Any plastic deformation that occurs at the crack tip is contained within a small volume. For the theory, or the corrected theory, to still hold this plastic deformation must be contained well within the K-dominant region of the stress field.

c) The crack is self-similar, this means it extends along its own axis. This has been assumed in all the above analysis.

Unfortunately many materials and the cracks in them do not satisfy these requirements. Even so in some cases LEFM may be used as a first approximation and no worthwhile improvement gained by using a more complicated approach. For materials inadequately described by this linear elastic model other theories have been developed. These include ones based on a non-linear elastic response to load and others in which consideration is given to large amounts of plastic deformation. Some of these approaches are outlined below.

5.3. FRACTURE MECHANICS OTHER THAN L.E.F.M.

As indicated above, LEFM was developed to describe crack growth and fracture in a linear elastic material. Some modifications have be applied to the theory to enable it to encompass materials that exhibit a small amount of plasticity or damage at the crack tip. However, when the amount of plasticity increases the validity of the LEFM theory is questionable, and others are required. These form the part of the body of work referred to as elastic-plastic fracture mechanics (EPFM). When the plasticity is very widespread another set of theorems is applied, those of plastic collapse. Ewalds and Wanhill (1986) show the applicability of these techniques graphically, their diagram is redrawn in figure 5.010.

Another reason for questioning the applicability of LEFM to some materials is not the production of plastic or damaged regions, but their non-linear elastic response to loads. Theories to account for this behaviour will be refer to here as non-linear elastic fracture mechanics (NLEFM). Most of the fracture mechanics research performed on

bony tissue has used standard bone, not antler, and has used LEFM. (A later section contains a review of the way LEFM has been implemented and the justifications given for its use.) Antler has an initially non-linear loading curve. Thus the use of the linear elastic approach appears inappropriate, if not wholly inaccurate.

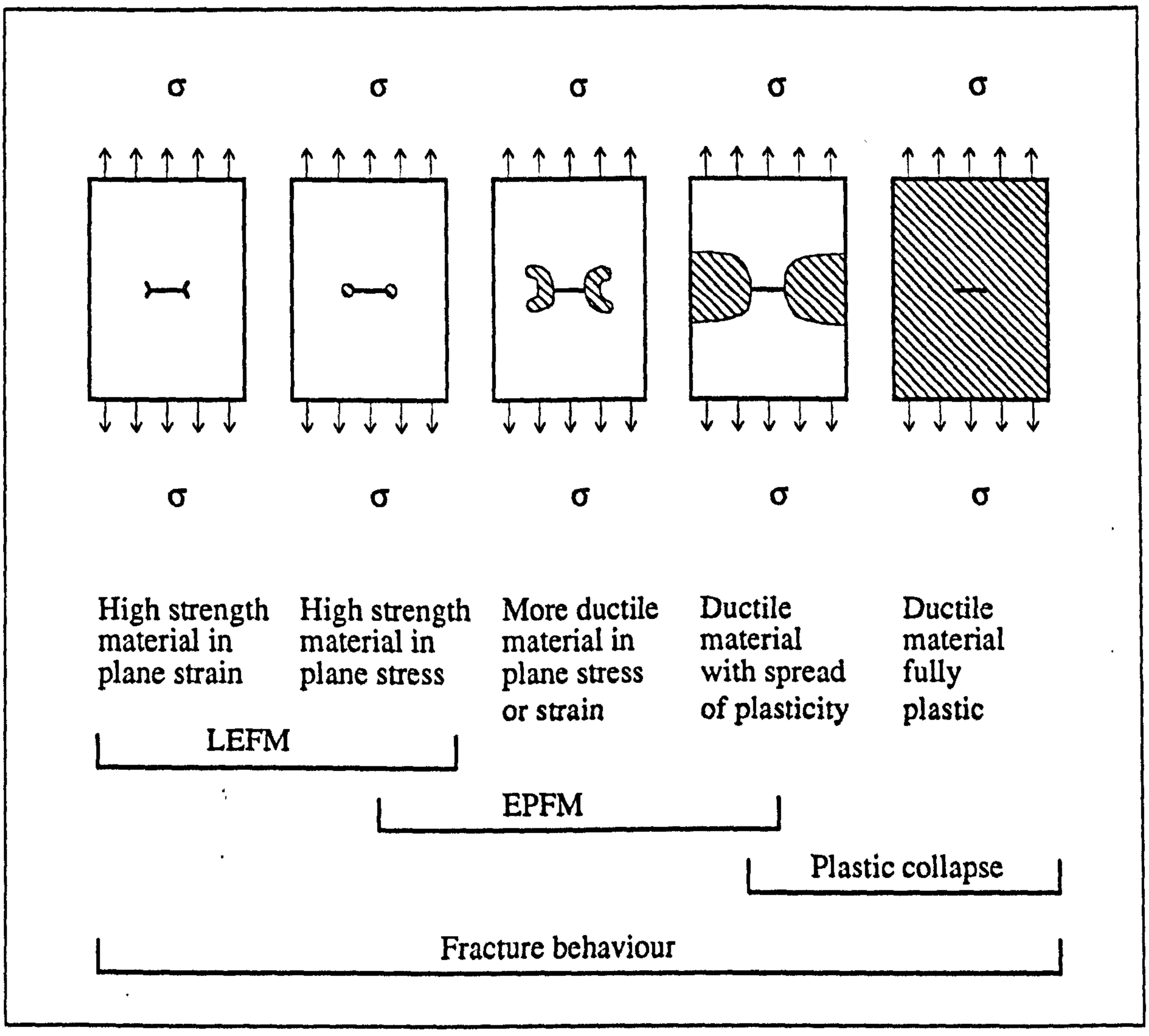

Figure 5.010. After Ewalds and Wanhill (1986)[16]

The ranges of applicability of LEFM and EPFM for describing fracture behaviour

In this section two methods from EPFM and two from NLEFM will be described. As will become clear this distinction is a bit artificial, except in the case of the Gurney approach which is based on non-linear elasticity with no plastic deformation. The EPFM methods are examined first.

---

[16]Ewalds and Wanhill use the term 'high strength' with reference to metals, here it can be considered to imply a brittle material.

5.3.1. CRACK OPENING DISPLACEMENT

This approach was introduced by Wells in 1961 (Ewalds and Wanhill, 1986). Wells argued that the stress at the crack tip radii a critical value, and that if this is so it is the plastic strain in the region of the crack tip that controls fracture. One measure of this plastic strain is the displacement of the crack surfaces (from each other), especially at or close to the crack tip. Thus this displacement can be used as a criterion for fracture (in the same way as the SIF in LEFM). In 1966 Burdekin and Stone formed an expression to describe the crack opening displacement, δ. This expression was based on the Dugdale strip yield model (Ewalds and Wanhill, 1986). Thus showing that it was related to the SIF for the conditions of LEFM. (This also helps to explain the relationship between the stress intensity factor and the crack tip radius already mentioned in section 5.2.3.6.) The COD derived via the Dugdale model is expressed as

$$\delta = \frac{K_I^2}{E \sigma_Y} \tag{5.048}$$

While that derived using the Irwin circular plastic zone is

$$\delta = \frac{4}{\pi} \frac{K_I^2}{E \sigma_Y} \tag{5.049}$$

More details on the derivation of these are provided by Ewalds and Wanhill (1986) and Smith (1991). From the comments made in the sections above it will be realised that for the propagating crack the COD will be a constant. A standard procedure for using this method for the testing of metallic materials is given in BS 5762 (1979).

5.3.2. THE J INTEGRAL

The J integral is parameter used to characterise fracture in EPFM. However, it has its basis in same approach as used to obtain similar parameters in LEFM. In this section I will only give a very brief description of this quantity, as I do not use it in my work. However, a more lengthy explanation and possible method of application are provided in appendix 8. I have included appendix 8 as, with hindsight, I consider that this approach may be more applicable to the study of antler, and possibly bone, than the approaches I have used. I am unable, due to lack of time, to pursue this approach. Therefore I would like to suggest that the application of the J integral to antler and bone is an area for future study.

The J integral is similar to the potential energy release rate, G, described in section 5.2.2.2. For condition of linear elasticity these quantities are equivalent. The J integral is defined as the rate of change of potential energy per unit thickness with respect

to crack length. In the energy balance equation (6.006) no distinction was made between energy stored by linear or non-linear elasticity. In previous chapters it has been show that the behaviour of a material (whether it is: elastic, elastic-plastic or even elastic-damage) is unknown until the material is unloaded. Likewise the energy that will be released by the material is unknown. One of the assumption in the derivation of the J integral is that the material is not unloaded. Therefore the nature of its unloading behaviour is disregarded, and an approach similar to the energy balance used for linear-elastic materials is used.

5.3.3. THE GURNEY APPROACH

The Gurney approach to the determination of the specific work-of-fracture, R, for non-linear elastic materials is best explained graphically. This is not just for ease of explanation, but also because this method is commonly applied in a graphical manner. If a crack is produced in a specimen of an elastic material the stiffness of the specimen will decrease, but the structure will remain elastic. Thus if an elastic material is loaded then unloaded and a crack within it having extended, the locus of the load-deformation point will enclose an area that is equivalent to the energy lost. If the area of the new crack surface is known R can be calculated.

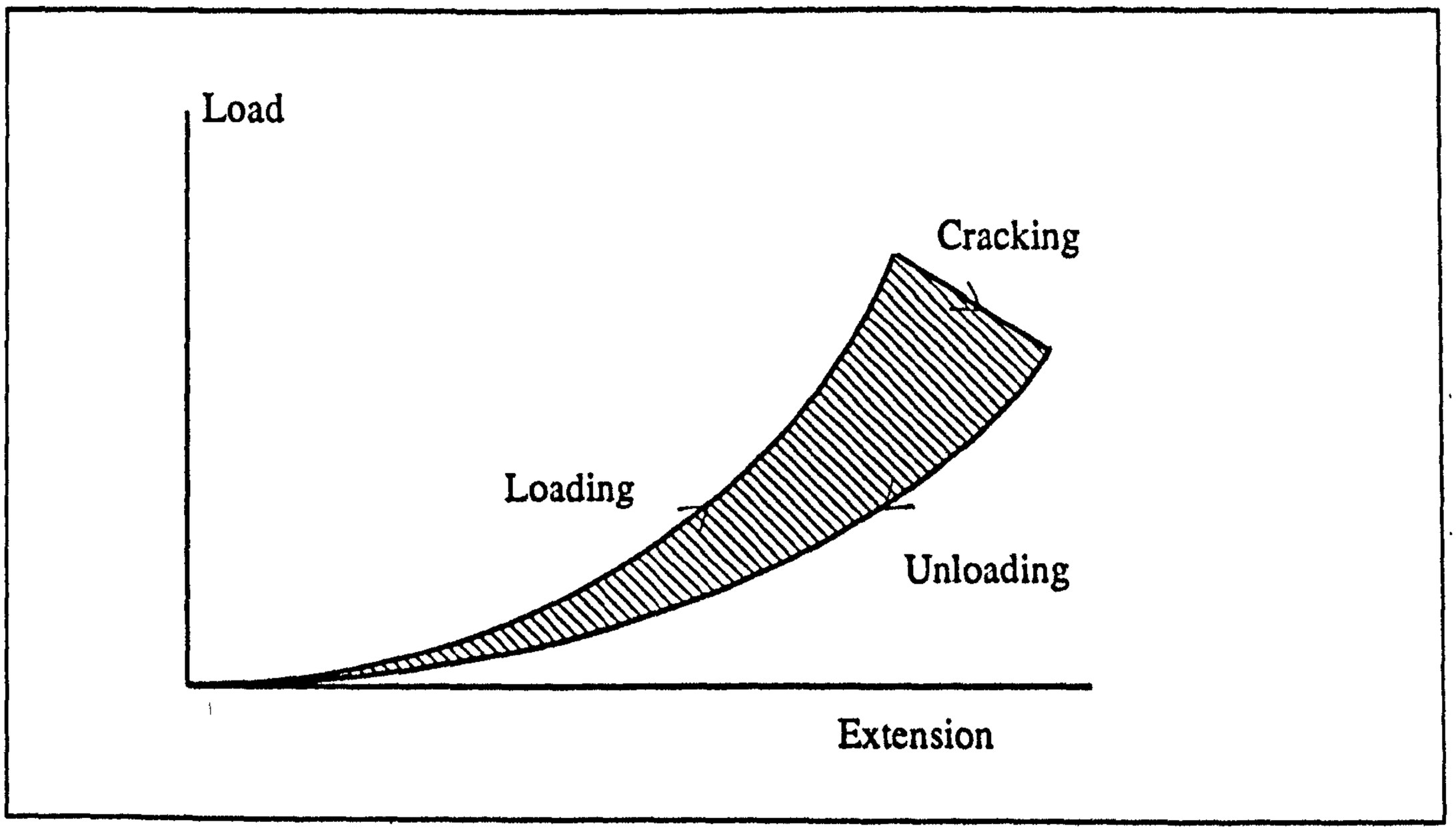

Figure 5.011 After Atkins and Mai (1988)

Fracture toughness determination for highly extensible solids using the Gurney approach

5.3.4. PURSLOW'S APPROACH TO NON-LINEAR ELASTIC FRACTURE

Purslow (1991) investigated the way in which the shape of the stress-strain relationship affects the dependence of fracture stress, and fracture strain, on crack length. For this study he used the non-linear elastic stress-strain relationship: $\sigma = k\,\varepsilon^n$. This gives J, linear or Γ shaped curves depending on the value of n used. He investigates two situations, one where the material is notch-sensitive and the other where it is notch-insensitive. In the notch-sensitive case he defines the border of the energy-free zone around the notch (in a single edge notched specimen) by a semicircle, the radius of the semicircle is equal in length to the notch. For the notch insensitive case (in which the material could be considered as acting like a mass of independent longitudinal fibres, although the model assumes a homogeneous, isotropic material) he uses a rectangular energy-free zone. The width of this rectangular zone is the same as the crack length, and it spreads along the whole length of the specimen. These two arrangements are shown in figure 5.012.

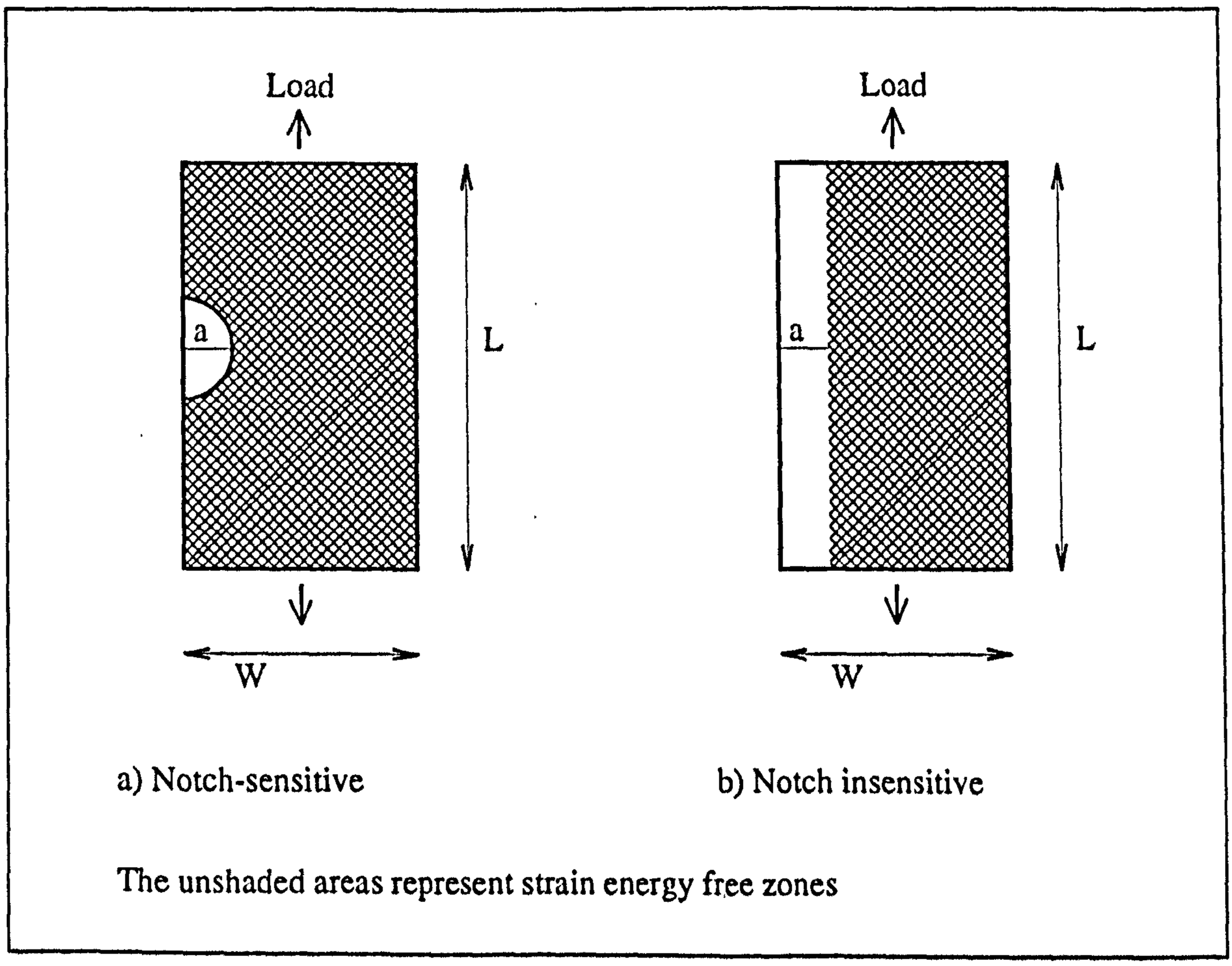

a) Notch-sensitive

b) Notch insensitive

The unshaded areas represent strain energy free zones

Figure 5.012

SEN specimens of a notch-sensitive and a notch insensitive non-linear material

The total strain energy in the specimens at the instant of failure is given by

$$U = \left(\int_0^{\varepsilon_f} \sigma \, d\varepsilon \right) \times \text{shaded volume} \qquad (5.050)$$

Where ε_f is the macroscopic failure strain. So for the notch sensitive case, using t for the specimen thickness, this will be

$$U = k \frac{\varepsilon_f^{n+1}}{n+1} t \left(W L - \frac{\pi a^2}{2} \right) \qquad (5.051)$$

and for the notch insensitive case

$$U = k \frac{\varepsilon_f^{n+1}}{n+1} t L (W - a) \qquad (5.052)$$

Purslow expresses the specific work-of-fracture as

$$R = - \left| \frac{d U}{d A} \right|_u \qquad (5.054)$$

where A is the crack area (= at). So by differentiation of equations 5.051 and 5.052 he obtains expressions for the work-of-fracture in both situations. For the notch-sensitive case he gives

$$R = k \frac{\varepsilon_f^{n+1} \pi a}{n+1} \qquad (5.055)$$

and by substitution he obtains the related equation

$$R = k \frac{\sigma_f^{(n+1)/n} \pi a}{n+1} \qquad (5.058)$$

Likewise for the notch insensitive case, by differentiation of equation 5.052 Purslow acquires the relationship

$$R = k \frac{\varepsilon_f^{n+1} L t}{n+1} \qquad (5.056)$$

Purslow uses the above equations to predict the form of the log-log relationships between the failure stress and the crack length, and that between failure strain and crack length, making the assumption of a constant fracture toughness. Unfortunately on examination of the derivation of equations 5.055 and 5.056, I find them to be incorrect.[17] The form of Purslow's log-log relationship is unaffected by these errors, but the corrected equations are given here for completeness and for their later utilisation. The first error appears in the equations for the notch sensitive case. It occurs during the conversion of the expression from one in terms of strain to one in terms of stress. This conversion should be as follows:

---

[17]I would like to apologise to Dr Peter Purslow for not spotting these errors in the draft copy of this paper (Purslow, 1991) which he kindly gave me.

$$R = k \frac{\varepsilon_f^{n+1} \pi a}{n+1} \tag{5.057}$$

Using his stress-strain relationship

$$\sigma_f = k \varepsilon_f^n \tag{5.058}$$

which is the same as

$$\left(\frac{\sigma_f}{k}\right) = \varepsilon_f^n \tag{5.059}$$

and

$$\left(\frac{\sigma_f}{k}\right)^{1/n} = \varepsilon_f \tag{5.060}$$

Multiplication of the two equations above (5.059 and 5.060) implies

$$\varepsilon_f^{n+1} = \left(\frac{\sigma_f}{k}\right)^{(n+1)/n} = \sigma_f^{(n+1)/n} k^{-(n+1)/n} \tag{5.061}$$

Thus (5.057) can be rewritten as

$$R = k \frac{\left(\sigma_f^{(n+1)/n} k^{-(n+1)/n}\right) \pi a}{n+1} = \frac{\sigma_f^{(n+1)/n} k^{-1/n} \pi a}{n+1} \tag{5.062}$$

This may be simplified to

$$R = \frac{\sigma_f^{(n+1)/n} \pi a}{k^{1/n} (n+1)} \tag{5.063}$$

Purslow says (equation 7 of Purslow 1991) for constant R

$$\sigma_f \propto \left(\frac{n+1}{a}\right)^{n/(n+1)} \tag{5.064}$$

This is not correct as there is another term that depends on n. He continues by examining the linear case, n = 1. Which gave $\sigma_f \propto a^{-0.5}$, this is still true for the corrected equation. By substituting n = 1 into the new equation (5.063) the following relationship is obtained

$$R = \frac{\sigma^2 \pi a}{k\, 2} \tag{5.065}$$

In the linear case k = E, the Young's modulus. So the equation may be rewritten as

$$\sigma_f = \sqrt{\frac{2 E R}{\pi a}} \tag{5.066}$$

This is similar to the Griffith equation (5.021), the difference being the inclusion of the $\sqrt{2}$ term.[18]

---

[18]The factor of $\sqrt{2}$ is not due to confusing the definition of the R with γ, see section 5.2.2.2. I suggest that it is due to the assumed shape of the energy-free zone.

The error in equation (5.056) is that the t term should have been removed during the differentiation stage. (It can be seen that the erroneous form of the equation is not dimensionally correct.) This error has no influence on the conclusions drawn in the paper. Purslow's description of the predicted log-log relationships for the notch-sensitive case mentioned above are still correct. These predictions are: for failure stress

$$\ln(\sigma_f) = k_1 - m \ln(a) \qquad (5.067)$$

where $m = n/(n + 1)$. The prediction for failure strain is

$$\ln(\varepsilon_f) = k_2 - p \ln(a) \qquad (5.068)$$

where $p = 1/(n + 1)$, and where k_1 and k_2 are constants.

Purslow suggests the applicability of his theoretical analysis can be tested by measuring σ_f and ε_f as functions of the crack length, a, for materials whose response to stress is adequately described by $\sigma = k \varepsilon^n$. Then comparing how well these results fit the straight line plots predicted by the logarithmic relationships, given above. He follows this procedure using three rubbers that give approximately J shaped stress-strain curves. The values of the gradient in the log-log relationship of the experimental data are similar to those obtained by substituting a measured value of n into the theory. He does however point out a criticism of the simplified model for the notch-insensitive case. This is, that notch-insensitivity usually only occurs in anisotropic composite structures, and not in the homogeneous isotropic material of the model.

The paper is concluded with a short comment on what the derived relationships imply for a material with an r shaped loading curve. In that case an increase in the crack length will produce a large decrease in the fracture strain but only a small decrease in the fracture stress. Antler is then mentioned as a biological tissue that possesses such a loading curve. In a later chapter this theory is applied to the results I have obtained from suitable tests on antler.

5.4. SUMMARY

In this chapter I have introduced some of the theories that comprise the area of study commonly called fracture mechanics. The theories originally produced for idealised linear elastic materials have (in the seventy or so year history of the subject) been modified and adapted, so that they can be used to explain, model and predict the fracture of real materials (usually metals). The concept that underpins these theories, is that it requires energy to produce new fracture surfaces, this energy is (generally)

obtained from the strain energy stored in the material through which the crack is propagating. The energy available to drive the crack is dependent on the applied stress, the material stiffness and the length of the crack. For a certain stress level the crack has to reach a specific length before fracture can occur, the critical crack length. Likewise for a certain crack length a specific stress level has to be attained for the fracture to propagate. The relationship between crack length and stress at failure is dependent on the material. This dependence has resulted in the definition of a number of material properties for linear elastic materials; *work-of-fracture*, the *critical potential energy release rate* and the *critical stress intensity factor*. Similar quantities have been defined for non-linear elastic material. These quantities describe the resistance of the material to the propagation of a crack. The more energy that is consumed during the fracture process, the *tougher* or less *notch sensitive* the material is.

I have already reported some of the differences in the mechanical properties of bovine bone and antler, and how these may relate to their intended biological function. In chapter 7 I will analyse some experiments I have conducted to assess the notch sensitivity of red deer antler and bovine bone. That analysis is based on the theories that have been presented here. However, before I consider my own results I will examine a number of the published studies of the *notch sensitivity* or *fracture mechanics* of bone and antler.

6

NOTCH SENSITIVITY AND FRACTURE MECHANICS OF BONE AND ANTLER: PUBLISHED STUDIES

6.1. INTRODUCTION

The fracturing of normal mammalian bones has been studied using a number of approaches. These can be broadly divided into two areas: first, a biological, or medical, type of approach where the fracture properties of whole bones have been investigated, normally under laboratory test conditions. In some cases the conditions used are an attempt to mimic those encountered *in vivo*. (There is also a large body of more clinically related study, based on naturally occurring fractures in patients.) Second, a material science approach where interest has concentrated on the failure properties of the material rather than those of the whole structure. The study undertaken in this thesis falls in the second category. Thus most of the works reviewed will also fall in this second category. As this study contains a comparison between bovine bone and antler, published work on both these materials will be reviewed. There is however only a limited amount of literature available on the fracturing of antler. For information on the fracture properties of antler I have been restricted almost exclusively to the doctoral thesis of Watkins (1987).

6.2. EARLY STUDIES

The effects of stress concentrations in whole bones were discussed by Currey (1962). He divided the stress concentrators into three main types, which he reports as

> (a) surface discontinuities;
> (b) differences in the elastic moduli of adjacent parts, due to bone being made up of two very different materials, collagen and apatite;
> (c) internal discontinuities.

He considered the internal discontinuities to be the most noteworthy. These were classified as cylindrical blood-channels, canaliculi, osteocyte lacunae and non-cylindrical blood-channels. For each of these discontinuities a value of the stress concentration factor is given, these were arrived at by use of standard engineering tables. Currey then discussed the effect of such stress concentrations on impact fractures. The approach he used was similar to the approach Griffith used in formulating his equation (see section 5.2.2). Currey's analysis was based on the strain energy storage at the instant before the bone failed. If the ultimate stress is constant it will be achieved at a lower load in a bone containing a stress concentrator, than in one without such a flaw. The lower load will thus produce a lower value of stored strain energy. Currey continued by describing how a crack would extend in a bone without such internal flaws. The idea that these flaws may also act as crack arrestors, by blunting the advancing crack, was also presented.

The first experimental demonstration that existence of a surface notch significantly lowers the energy required to fracture a specimen of bone was published Bonfield and Li (1966). They obtained this result by examining the impact strength of notched and un-notched specimens of bovine bone. They tested two specimen orientations: first longitudinal and second transverse, both relative to the long axis of the bone. The specimens were approximately 32 mm × 5 mm × 5 mm, with a 0.76 mm deep 45° V-notch at their midpoint. (Original values are in inches.) The authors report that:

> The results on notched impact specimens which required a smaller impact energy for fracture than unnotched specimens demonstrate that bone is very sensitive to the presence of surface defects. From these results it may also be concluded that most of the energy absorbed in fracture is required to initiate a crack of a critical size, with the subsequent propagation of the crack absorbing relatively little energy.

These tests were conducted at different temperatures between -196 and 900°C. From examination of their graphs it appears that for longitudinal specimens at 25°C, the introduction of the notch reduces the required energy for fracture from between 0.282 and 0.113 J [2.5 and 1 in lbs] to less than 0.011 J [0.1 in lbs].

Felbeck and Atkins (1984) point out that it is often said that such impact data reflect the toughness (or resistance to cracking) of materials under dynamic conditions. These authors continue by saying this data is only a qualitative indication of crack resistance and that it is preferable to use quantitative concepts, such as those I have presented in the previous chapter. In the following sections I review of some published studies of bone and antler in which the results were obtain by the application of these concepts. The studies are divided into groups depending on the test method and thus the type of specimen used, these include: three-point-bending specimens, *single edge notch* (SEN) specimens, *compact tension* (CT) specimens and *centre notch cylindrical* (CNC) specimens.

There are a number of directions in which specimens of bone, from long bones or antlers, have been tested. There are two commonly used directions: first, specimens can be manufactured so the plane of the crack is parallel to the long axis of the bone producing a *longitudinal fracture*. Second, the specimens can be prepared so that the plane of the crack perpendicular to the long axis of the bone. This arrangement will produce a so-called *transverse fracture*. A great deal of work has been published on the former direction. These include studies concerned with variables such as strain rate, specimen size, density and so on. Due to the large amount of this literature and extant reviews[1] only some of the investigations relevant to this study are discussed here. A

---

[1]For example, the reviews presented by Charalambides (1988), Bonfield (1987) and Behiri (1982).

more extensive review of results from transverse fracture experiments is included for comparison with the results obtained in my work.

6.3. THREE-POINT-BENDING SPECIMENS

Pope and Outwater (1972) examined energy required to propagate a crack. They called this the 'fracture energy'. The examination of this quantity was accomplished by a variety of methods, including restrained three-point-bending of whole bones.[2] These bones, femurs and tibia of rhesus monkeys, dogs and humans, had a starter crack cut in them so the crack propagated in a transverse direction. The energy was measured from the area under the load deflection curve and divided by the area of fracture surface formed.[3] This is essentially the Gurney method described above. The relevant part of their table of results is given below. The energy values have been converted from lbf in/in^2 to SI units.[4]

Animal	Bone	Mean fracture energy (as given)	Mean fracture energy k J m^{-2}	Number of tests
Rhesus Monkey	Tibia	10.45	1.83	5
Rhesus Monkey	Femur	10.29	1.80	9
Bovine (aged)	Femur	7.81	1.37	3
Canine	Tibia	10.73	1.88	9
Canine	Femur	10.79	1.89	8
Human (preserved)	Tibia	2.26	0.40	5
Human (preserved)	Femur	2.01	0.35	6

Table 6.001 After Pope and Outwater (1972)

The mean fracture energy for pre-cracked whole bones in three-point-bending

---

[2]They state 'the specimens were then broken under three point bending, the specimen being freely supported at one metaphysis while being built-in at the other'.
[3]They do not state if they considered this to be one or both surfaces.
[4]The data in the table have no accompanying units. The nomenclature list in the paper gives the units of the mean fracture energy as lbf/in^2, but in the text the units of lb/in./in.^{2} are also quoted. Neither of these are dimensionally correct as they should have units of work divided by area W/L^2 or, as work has units of force multiplied by distance, units of $F\,L/L^2$. Thus, due to this lack of clarity, the units that I have assigned to the published values could thus be erroneous.

There are a number of problems associated with the use of whole bone specimens; the main one is the lack of repeatability of the test due to variations in the specimen shapes, sizes and material properties. Another problem is how to accurately measure the fracture area of such an irregular shape. These problems can be reduced by using specimens of a standardised shape machined from whole bones. Specimens are normally standardised within a study, if not between studies. This standardised approach is more common than the testing of whole bones, and is the one I have used. Thus a number of such specimen types and sets of results reported in the literature will be reviewed here.

6.3.1. THE TATTERSALL TAPPIN SPECIMEN GEOMETRY

A commonly used specimen geometry for the investigation of the work-of-fracture of bone is similar to that used by Tattersall and Tappin (1966), who examined standard engineering materials and not bone or antler. The basic specimen geometry is shown in figure 6.001. The argument for use of such a geometry is based on the Griffith energy balance. If the energy released by a small extension in the crack length is insufficient to propagate the crack further, the crack growth will be halted, unless external work is supplied to keep the crack moving. In the case of such a stable crack it is possible to measure the energy required to produce a known area of crack surface. When the total energy necessary to cause fracture is normalised by the area of one fracture surface the value obtained is the work-of-fracture, R (see section 5.2.2.2). Tattersall and Tappin state that a stable crack can be realised by limiting the amount of energy stored in the specimen and the test machine at the moment of fracture initiation. This can be achieved in two ways: first by using a hard testing machine.[5] Second by shaping the specimen so that only a small load is required to initiate crack growth. The latter option will reduce the strain energy within the specimen, and may be achieved by the introduction of a stress concentration, or by reducing the area of the first region to fail. In the case of the Tattersall Tappin specimen geometry this is achieved by reducing the centre cross section so that only a triangular section remains, as shown in figure 6.001. The specimen is tested in a three-point-bending rig. The apex of the remaining triangle of material is placed so that it is under tensile loading. The crack starts at this apex, as the crack advances it will become broader, due to the specimen shape. The broadening of the crack front helps to sustain stable crack growth, as the energy required to force the crack through the same depth of material increases with crack length.

---

[5]A *hard machine* does not deform under load. Thus it stores no strain energy. Using a hard machine reduces the energy available to propagate the crack. Thus the crack is more likely to be stable. The effect of a compliant or open loop machine of tensile tests is described in appendix 7.

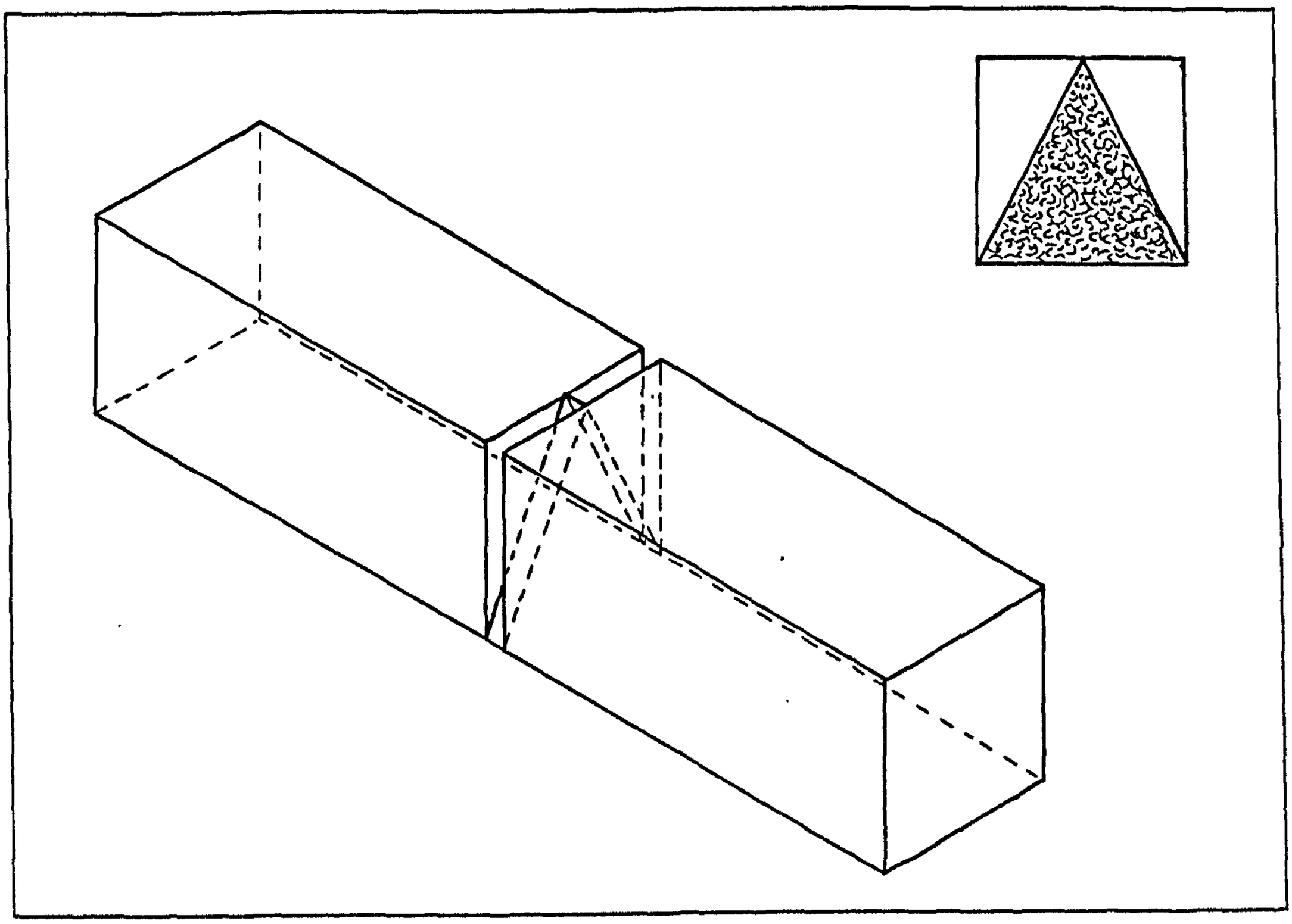

Figure 6.001 After Tattersall and Tappin (1966)

The basic shape of the specimen used by Tattersall and Tappin

There is some inconsistency in the nomenclature used in the literature relating to this test specimen and the results obtained from it. In their paper Tattersall and Tappin use the equation

$$-\frac{\partial U}{\partial A} = \gamma \qquad (6.001)$$

The authors state that U is the elastic energy stored in the structure, A is the area of the fracture surface and γ is the 'surface energy'. This statement agrees with the theory I presented in section 5.2.2.2. However, Tattersall and Tappin then appear to use the term 'work of fracture' in place of *surface energy*. For example, they say that having measured the amount of work consumed in the test, that

> This amount of work was divided by the area of the fracture faces to give the values quoted for the work of fracture.

Their use of this engineering nomenclature is confused further, for when they refer to their so called 'work of fracture' results they say 'from the results on alumina, the value of γ for a test that ...'. Thus I consider that Tattersall and Tappin have used the terms *work of fracture* and *surface energy* interchangeably, both meaning the value of $\gamma_s + \gamma_p$ as defined in section 5.2.2.2. Thus to convert the values presented in their paper into what is commonly defined as *work-of-fracture* the quoted values should be multiplied by two.

The inconsistency of nomenclature contained within Tattersall and Tappin's paper has been transmitted to the area of bone research. This is demonstrated by Currey (1979a) who stated that 'the work of fracture was calculated as the total work done on the specimen divided by twice the area of the broken ligament'. Unfortunately other workers are not always as clear. Therefore some care is required when comparing results. I have attempted to present the corrected values in this review.

Piekarski (1970) reported values (in units of kg cm/cm^2) of the work-of-fracture for stable and unstable crack growth in wet bovine femoral bone. He says these values were measured using the Tattersall and Tappin method. He does not state which definition of area he used. However, he does use the symbol γ as being equal to his results and when referring to the Griffith equation uses $\sigma = (2\,\gamma E/\pi\, a)^{0.5}$. He states '$\gamma$ is the surface energy (or the work of fracture)'. Piekarski's statement is clearly inconsistent (see equation 5.017). Thus the values he gives of the work-of-fracture are half what they should be, using the normal definition. The original and corrected values of this quantity are shown in table 6.002 (I used g = 9.81 m s^{-2}). The most notable result is not the size of the work-of-fracture, but their relative size; there is more than a sixty-fold difference between the energy consumed by stable and catastrophic propagation.

Rate of crack propagation m s^{-1}	Work-of-fracture (as given, γ) kg cm/cm^2	Work-of-fracture (corrected, R) kJ m^{-2}
1.67×10^{-7}	63.8 (49.3 - 78.9)	125.2
1.67×10^{-6}	60.2 (48.2 - 69.9)	118.1
Catastrophic propagation	0.984 (0.42 - 3.70)	1.93

Table 6.002 After Piekarski (1970)

The work-of-fracture at three rates of crack propagation

Piekarski also considered the effect of stress concentrations. He says that if 'bone were a truly brittle solid the Griffith crack theory could be applied'. Thus he used by the Griffith theory (equation 5.021) together with typical values for the failure stress and Young's modulus, together with his values of the work-of-fracture to obtain a value of the critical crack length. This procedure produced values of a = 76.5 mm for controlled propagation and 1.3 mm for the uncontrolled propagation. Piekarski states:

> Clearly, critical cracks 76.5 mm long cannot exist and the Griffith theory therefore does not apply. This further helps to confirm the suggestions that slow crack propagation is essentially a 'pull-out' type mechanism. Pre-existing cracks 1.3 mm long are feasible but none of the internal discontinuities noted above have orientation dimensions of anything like this size.

However, I would like to point out that in the Griffith equation a is half the crack length, the resultant internal flaws should thus be twice as large, i.e. 153 mm or 2.6 mm. By combining the Griffith equation and the corrected values of the work-of-fracture, together with Piekarski's typical values of stress and material stiffness I obtained the following equation

$$a_{int} = \frac{19.62\times10^{9}\ R}{(98.1\times10^{6})^{2}\ \pi} \qquad \text{Units } \frac{N\,m^{-2}\ J\,m^{-2}}{(N\,m^{-2})^{2}} = m \qquad (6.002)$$

where a_{int} is value of half length of the *pre-existing crack* or what I will call the *intrinsic edge notch* length, of 81.2, 76.6 and 1.3 mm (in the same order as the table).[6] These are the same as those calculated by Piekarski. This confirms that his so called work-of-fracture values are surface energy ones. The corrected work-of-fracture values for the non-catastrophic propagation are considerably larger than those obtained by other workers. The greater size of the work-of-fracture values results in the unreasonable size of the intrinsic notch length. His approximation of the failure stress σ_f = 98.1 MPa also appears to be lower than that obtained by other workers. (When they perform a similar procedure on the results from SEN specimens Bonfield and Datta (1976) use the value σ_f = 120 MPa, if this failure stress was substituted in equation 6.002 it would produce notch lengths of approximately two-thirds Piekarski's values.[7]) Therefore, Piekarski's use of the calculated intrinsic notch length to reject the applicability of the Griffith equation and thus LEFM for the study of bone, is questionable. (His idea that this size should in some way be related to a structural feature is also used by other workers. I will use this approach initially, but discuss it in a later section.)

One cause of the greater work-of-fracture results obtained in Piekarski's work may be the duration of the tests. Piekarski gave no indication of how the crack speed was measured. It may be an average, calculated from the duration of the test and the specimen depth. I have assumed this to be the case and used the data available to calculate an approximate duration for the tests. In the slower stable case, with a specimen depth of 5 mm, the crack speed implies a testing time of nearly eight and a half hours. The long duration of the test could have contributed to the higher energy values associated with the slower tests. Because, as shown above, bone exhibits time-dependent properties such as *creep*, I suggest that some of the energy, calculated from the area under the load deflection plot will be as a result of creep or more probably damage accumulation and not used for forcing the crack through the material.

---

[6]I use the term *intrinsic edge notch* for the calculated value of a (a_{int}) because from the derivation of the Griffith equation, an internal crack, loaded in tension, would have length 2a. This is also more consistent with the SEN specimens used in my own work.
[7]I will retain Piekarski's values in equation (6.002) to enable comparisons between the results of different workers.

Moyle *et al.* (1975) report in a conference proceeding that they used a similar approach to Tattersall and Tappin. In this case the specimens were manufactured from canine femoral bone. (The state of hydration of the specimens is not given.) The orientation of the triangular section was such that the crack propagated in a direction that would be equivalent to it circumnavigating the original bone, not passing through the wall thickness. Moyle *et al.* (1975) refer to the Tattersall and Tappin paper for their method. They, correctly, use only one of the fracture surfaces in their calculation of the work-of-fracture.[8] The values Moyle *et al.* obtained were in a range of 7.8 to 15.5 kJ m^{-2} [44.6 to 88.5 in lbs in^{-2}]. The mean of these values is given as 11.0 kJ m^{-2} [63.0 in lbs in^{-2}] and the standard deviation as 1.0 kJ m^{-2} [5.9 in lbs in^{-2}]. These values fall between the slow and catastrophic values obtained by Piekarski. When I substituted of the mean value into equation 6.002 above I obtained a value of $a_{int} = 7.1$ mm. As in the investigation described previously this calculated value of an intrinsic crack length is of the same order as the bone size. Therefore the work-of-fracture values are either too high or the derivation of this quantity is wrong, misunderstood or meaningless. These authors do note that no account is taken of 'plastic flow, pullout of fibers, etc.'.

The same authors as above, Moyle *et al*, published a very similar piece of work in 1978. The mean value of the work-of-fracture (of 23 specimens) of canine femoral bone is given in table 6.003. The specimens were prepared and tested in the following way. Cylinders of bone were stored in a frozen state before final specimen preparation. It is reported that 'the specimens were irrigated in physiological saline during cutting and were kept in a saline bath during mechanical testing'. The deformation rate used was 4.23×10^{-6} m s^{-1} [0.01 in min^{-1}]. These workers investigated if differences in toughness were correlated with osteone size or fractional area. This was not found to be the case. The authors do however say that the size of the osteones was related to the ability to sustain slow crack propagation. The specimens that failed by slow crack propagation had smaller diameter haversian systems.

The Tattersall and Tappin test procedure was subjected to a more critical analysis by Rogers and Moyle (1988). They re-examine the 6% increase in work-of-fracture on doubling the specimen size reported by Tattersall and Tappin (1966). Rogers and Moyle's examination of three previous studies on bone showed that the species with the smallest specimen area had the highest work-of-fracture their table is shown below.

---

[8]This is not stated in Moyle *et al.* (1975), the evidence is from Moyle and Bowden (1984), which contains the statement; 'it is important to note that twice the measured area, sometimes used in fracture mechanics studies, was not used in this study or in any of the other studies of this type performed in this laboratory'.

Species (Authors)	Specimen areas mm^2	work-of-fracture mean ± s.d. $kJ\ m^{-2}$
Canine (Moyle *et al*, 1978)	1.49 - 5.09	9.0 ± 3.3
Human (Moyle and Bowden, 1984)	5.40 - 12.8	7.8 ± 2.1
Equine (Anderson, 1979)	5.00 - 12.0	7.0 ± 2.0

Table 6.003 After Rogers and Moyle (1988)

Comparison of work-of-fracture with specimen areas for canine, human and equine femoral bone

Moyle and Bowden (1984) provide a load deflection curve and the cross-head speed they used (4.23×10^{-6} m s^{-1}), from which I estimate that their tests took about four minutes to complete. This is vastly shorter than the time I have estimated for Piekarski's tests that showed stable crack growth. This may help to explain the order of magnitude difference between these two sets of results.

Rogers and Moyle (1988) examined size effects by conducting tests on nine groups of specimens, consisting of three sizes of three different materials: Plexiglas®, bovine tibial bone and aluminium. They state that the bovine bone specimens were equilibrated for 45 min at about 38.6°C, within physiological saline and tested in the same conditions. Their results are re-produced below:

Material	Size group	Area ± s.d. mm^2	Work-of-fracture ± s.d. $kJ\ m^{-2}$	Calcium content (wt %)	Void area (%)
Aluminium	1	21.5 ± 1.2	52.2 ± 1.6	-	-
Aluminium	2	11.0 ± 0.9	62.4 ± 18.4	-	-
Aluminium	3	5.61 ± 0.27	63.9 ± 14.8	-	-
Plexiglas®	1	21.6 ± 0.9	0.666 ± 0.071	-	-
Plexiglas®	2	10.3 ± 0.8	0.587 ± 0.069	-	-
Plexiglas®	3	5.32 ± 0.20	0.607 ± 0.070	-	-
Bone	1	11.7 ± 1.9	10.5 ± 2.0	21.3	3.86
Bone	2	5.89 ± 0.69	8.92 ± 1.57	18.2	5.87
Bone	3	3.48 ± 0.68	5.48 ± 1.79	17.8	4.87

Table 6.004 After Rogers and Moyle (1988)

Mean work-of-fracture, calcium content and fractional void area values for aluminium Plexiglas® and bovine tibial bone

Rogers and Moyle found that the work-of-fracture was not dependent on specimen size for Plexiglas® or aluminium. However, for the bone results they concluded that 52.2% of the variance in the work-of-fracture values was accounted for by the difference in specimen area ($R^2 = 0.522, p < 0.001$). To help explain the remaining variation *calcium content* and *void area* of the specimens was also measured. No significant correlation between work-of-fracture and fractional void area or work-of-fracture and calcium content was indicated. They conclude that the work-of-fracture may be affected by the microstructure of the specimen.

> That is, even if work-of-fracture is not dependent on specimen size *per se*, the use of very small specimens from heterogeneous materials may produce inaccurate results due to the fact that the sizes of microstructural constituents are not negligible compared with specimen size and their distribution is non-homogeneous.

Currey, in his paper already mentioned above (Currey, 1979a), reported three mechanical properties of three bone tissues. These are the work-of-fracture, bending strength and modulus of elasticity of antler, bovine femur and fin whale bulla. The work-of-fracture was calculated using the Tattersall and Tappin method, on specimens that were machined and tested wet. Data for mineral content and density were also included. It was noted that antler specimens never broke cleanly in two, but merely cleaved to about half their depth. Part of the corrected table of results is shown in table 6.005. The values obtained by Currey for bovine femoral bone are slightly lower than all the other results reported in this section, with the exception of Piekarski's results for catastrophic failure.

Material	Work-of-fracture kJ m^{-2} (sample size, s.e.)	Mineral content % weight remaining	Density 10^3 kg m^{-3}
Antler	12.37 (5, 1.104)	59.3 (5, 0.49)	1.86
Femur	3.42 (13, 0.414)	66.7 (25, 0.17)	2.06

Table 6.005 After Currey (1979a)

Work-of-fracture of antler red deer (*Cervus elaphus*) and bovine femur (*Bos taurus*)

If the intrinsic notch length is calculated using the data from the studies reviewed above, it is found that in most cases a_{int} is larger than one that could easily be explained by comparison with the structures within the materials tested. These lengths approach the dimensions of the test specimens and in some cases the dimensions of the whole bones. This observation can be interpreted in a number of ways: First, as Piekarski did, as a reason to reject LEFM. Second, if the applicability LEFM to the bulk material is accepted. The observation that the size of the intrinsic edge notch calculated for the failure stress of an un-notched specimen is similar to the dimensions of that specimen

may be used as evidence that the material fails by some other method before brittle fracture can occur.[9] This may imply that bone possesses some method to avoid the stress concentrating effects of small discontinuities, such as channels for blood vessels and the other pores needed to maintain this living tissue. Third, the large size of some of the calculated intrinsic edge notches can be interpreted, as a reason to question the values obtained for the work-of-fracture. This idea has already been mentioned and can also be divided into a number of approaches: is creep or damage increasing the amount of work absorbed by the specimen prior to failure? Is the energy dissipated in only the surface layers of the fracture and what effects do *pull-outs* have if they do occur? A point related to the previous one is what area should the energy be divided by to obtain the work-of-fracture? Should the area be that calculated from the external dimensions of the triangle or should it take the surface topography into account.[10] There is however a more fundamental question regarding the concept of an intrinsic edge notch: what does it mean? This question arises when the background to the Griffith equation is considered (section 5.2.2.2), for it is based on a through-the-thickness crack. Therefore it implies that the intrinsic edge notch has a length that is that calculated from the equation, and a width equal to the material is thickness. Thus comparison of the calculated length with structural components in bone is a questionable activity; the size of such individual structures is independent of the specimen width. This point will be discussed again when other methods of finding the *intrinsic edge notch* are reviewed.

6.3.2. PLAIN NOTCHED BENDING SPECIMEN

Three-point-bending specimens with a plain notch have been used by a number of researchers. In this case, the notch is a straight cut in the material at the tension surface of the test piece, as shown in figure 6.002. Different cross sectional shapes for the notch have been used by different people: some use a straight cut and others a V-notch.

---

[9]A possibly analogous effect is observed in the fracturing of thin and thick sheets of metal, the thin sheet failing by a mainly ductile process (necking) while the thick sheet fails in a mainly brittle fashion (See figure 5.004.). However, this may not be appropriate here, as the notched and un-notched specimens may be viewed as the thin sheet and the whole bone as the thick sheet.

[10]Research into the relationship of the work-of-fracture and the fracture surface topography is being conducted by other workers at York. They are examining the relationship between the work-of-fracture and the fractal dimension of a line on the fracture surface (Currey and Brear, 1992).

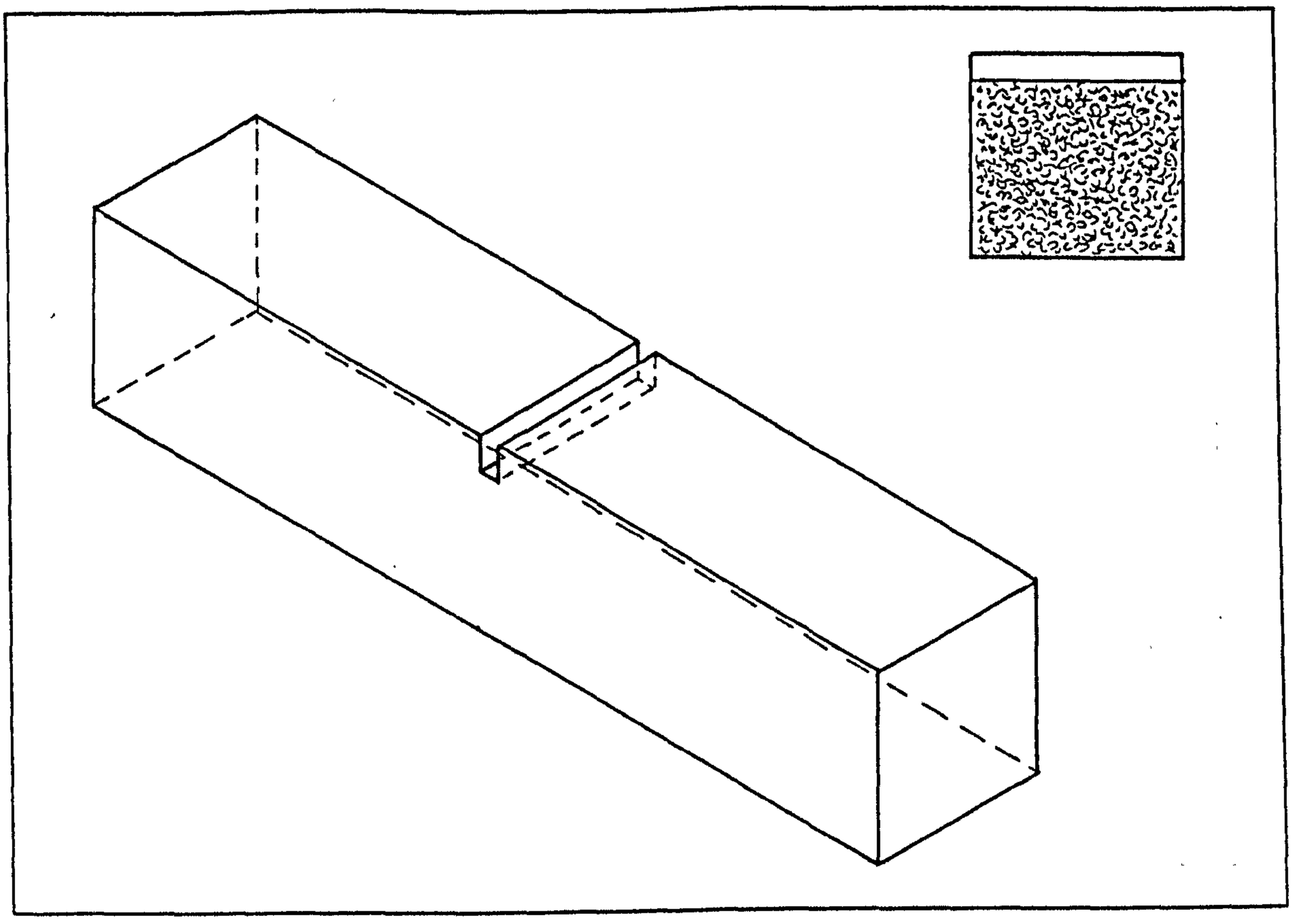

Figure 6.002

Plain notched three-point-bending specimen

Watkins (1987) used plain notched specimens to investigate the work-of-fracture of antler and bovine bone. He states the notch to depth ratio was typically 0.1 - 0.27 for antler and 0.2 - 0.3 for bone, although it was as high as 0.63 for some bone specimens. All the tests were conducted using a cross-head speed of 3.3×10^{-4} m s^{-1} [2 mm/min]. Most specimens were tested on an Instron 4202 machine, but some tibial bone specimens were tested on a harder (Dartec hydraulic) testing machine at the same speed. He does not state what temperature and environmental conditions were used. A similar test procedure to that described above for the Tattersall and Tappin specimen geometry was followed. The loading history was recorded using a chart recorder. The energy absorbed by the specimen was derived from the area under the curve. The work-of-fracture was then calculated by dividing this energy by the fractured area of the test-piece. He found that the crack propagation in antler was far more stable than that in bone. Bone was found to fail catastrophically after an initially linear loading curve, giving a triangular shaped plot, and as he points out this will produce a result that is an overestimate, which can be taken as an upper bound of the toughness values. Like Currey (1979a) he reports that the antler specimens rarely failed completely; instead a hinge tended to form on the compressive face. In the antler specimens the crack path tended to deviate along the test piece rather than remaining perpendicular to its long axis (and hence also the long axis of the antler). The area that was cleaved when this happened was larger than the ligament

area. Watkins says that because the use of the ligament area will result in an overestimate of the work-of-fracture, the actual crack area was used. The results are given in two tables: First for those specimens where the crack travelled at right angles to the beam axis (⊥), giving results representative of the toughness of antler when fractured across the osteones. Second, for the cases where the crack deviated (— or ∠). These tables are combined below in table 6.006. Table 6.006 it is clear the work-of-fracture is lower when the crack is propagating along the specimen, between the osteones.

Specimen	Work-of-fracture $kJ\ m^{-2}$	Crack path
Reindeer	13.5	⊥
Reindeer	14.0	⊥
Reindeer	16.8	⊥
Sika	13.7	⊥
Sika	13.1	⊥
Sika	11.5	⊥
Sika	13.4	⊥
	Mean ± s.d. 13.7 ± 1.58	
Sika	9.27	—
Sika	10.50	—
Sika	10.80	—
Sika	10.70	∠
Sika	8.50	∠
Sika	12.20	∠
Sika	9.11	—
Sika	9.34	—
Sika	10.40	∠
Sika	7.66	∠
Sika	6.70	—
Sika	7.40	∠
	Mean ± s.d. 9.39 ± 1.62	

Table 6.006 Data from Watkins (1987) (Tables 4.1 and 4.2 p89 of his thesis)

Work-of-fracture values for antler specimens from reindeer and sika

A comparative study of bovine bone and antler specimens was also performed, by Watkins. In this case it is stated that the antler specimens had been dried, the condition of the bone is not explicitly stated:

Specimen	Work-of-fracture[11] kJ m^{-2}	Sample size
Dried antler	2.14 ± 0.715	10
Femur	2.64 ± 0.814	8
Tibia	3.10 ± 1.480	9

Table 6.007 After Watkins (1987)

Work-of-fracture of dried antler and bone specimens

In the above tests (table 6.007) all the failures were catastrophic. Some non-linearity was noted in the loading curve but it was very slight. A comparison of these bone results and the non-dried antler results is made, in which Watkins points out that even when the toughness of bone is accepted at its upper bound value, bone has only a fifth of the toughness of antler. His values for the work-of-fracture of bone and those for antler from the first table are similar to those of Currey (1979a). Both these sets of data show that antler requires more energy to fracture it than bone. Watkins data also demonstrate the detrimental effect drying has on the work-of-fracture of antler, and thus the need to test this material under standard conditions.

The studies reviewed so far (in section 6.3) have used bending specimens to obtain a value of the energy consumed by the fracturing process. The experimental and analytical approach of these papers is based on Griffith's idea of an energy balance controlling the stability of fracture. Section 5.2.3 contained an introduction to another way of quantifying the fracture behaviour of a material. This is the stress intensity factor approach, in which the stress field ahead of the crack is the quantity examined. This approach has been applied to bone using different types of specimens. A study by Robertson *et al.* (1978) who used a plain notched bending specimen is reviewed here.

Robertson *et al.* (1978)[12] used V-notched specimens in experiments on bovine femora. They also introduced a fine 'pre-crack' at the root of the notch in some specimens, by either sawing or slowly bending the specimen. The experiments were conducted in Ringers solution at 37°C. In this case the values of the critical stress intensity factor (referred to in the paper as fracture toughness) K_{IC} were reported. The calculation used to obtain these values was taken from Srawley and Brown (1964) and includes a shape correction factor. Their results are shown below.

---

[11]The form of the tolerances is not given but if there is consistency within the work they are s.d.

[12]The authors of this paper are named as Diane Margel Robertson, David Robertson and Craig R. Barrett, but reference is made to a thesis by a D. R. Margel-Robertson.

Strain rate s^{-1}	K_{IC} No pre-crack MPa $m^{0.5}$	K_{IC} Wire-sawn MPa $m^{0.5}$	K_{IC} Natural crack MPa $m^{0.5}$
7.3×10^{-5}	6.70	5.8	5.92
7.3×10^{-5}	5.07	5.54	4.89
7.3×10^{-5}	4.87	5.07	4.41
7.3×10^{-5}	4.37	5.04	4.14
7.3×10^{-5}	4.07	4.56	3.97
2.9×10^{-5}	4.47	5.00	5.12
2.9×10^{-5}	3.70	4.64	5.07
Mean (s.d.)	4.75 (0.975)	5.09 (0.447)	4.79 (0.681)

Table 6.008 After Robertson *et al.* (1978)

The critical stress intensity factor of bovine femora bone as a function of pre-cracking

Robertson *et al.* analysed the above results stating that 'the K_{IC} values are not at the 95% level significantly different, indicating that the existence of a pre-crack is not particularly crucial'. This result suggested to them that the major effort in bone fracture goes towards propagation rather than initiation of the crack. The authors point out this is in contradiction to the results of Bonfield and Datta (1976) and Pope and Outwater (1972) who consider fracture initiation to be the main energy absorbing activity. Therefore this interpretation of their results also directly contradicts the original work of Bonfield and Li (1966).

Robertson *et al.* also report some experiments using strain rates of 7×10^{-6} s^{-1} to 3×10^{-2} s^{-1}, although they do not say how these strain rate values were arrived at. The results are shown graphically and display a degree of scatter. However, Robertson *et al.* do state that a significant correlation was found between K_{IC} and the strain rate of the test (the latter is logged). The equation they obtain is

$$K_{IC} = 8.177 + 0.7028 \log \dot{\varepsilon} \qquad (6.003)$$

The standard error of the estimate was given as 1.175 MPa $m^{0.5}$. The values of K_{IC} ranged between *ca.* 3 and 8 MPa $m^{0.5}$ with an average of 5.7 $\pm$ 1.4 MPa $m^{0.5}$. By definition of the critical stress intensity factor is a material constant, in the same way as Young's modulus is. In the same way that changes in the material stiffness with strain rate, imply that Young's modulus is inappropriate, this relationship implies that the concept of a critical stress intensity factor may be equally inappropriate, in this

situation.[13] This relationship appears to be consistent with the increase in failure stress displayed by tensile specimens of bone at increasing cross-head speed reported in chapter 4.

Robertson *et al.* give a value of what they call the critical crack length, which they define as 'a measure of the largest flaw which a material can tolerate before unstable fracture occurs'. This explanation is consistent with that normally given for the critical crack size, in as far as it goes. However, the critical crack size is a function of the stress placed on the material: if the stress is small a large crack can be sustained, if the stress is large then only a small crack will be tolerated. In LEFM the function relating the critical crack size and the stress, is normally expressed by the Griffith equation (5.021). The authors say 'the critical crack was measured at the first readily distinguishable point at which $d\sigma/d\varepsilon = 0$'. They do not give the values of stress associated with the critical crack lengths they recorded, only the average value of the critical crack length 'resolved perpendicular to the tensile stress axis' this was 0.36 mm. I suggest that due to the method used to obtain this quantity, it may be assumed that, very approximately, the stress at the crack tip (neglecting concentrating effects) is the same as the tensile failure stress of the material. Therefore this quantity may be similar to the intrinsic edge notch.

6.3.3. CONCLUSIONS FROM THE REVIEW OF THE USE OF THREE-POINT-BENDING SPECIMENS

The important results contained within the studies that have used three-point-bending specimens reviewed here can be summarised as follows.

a) The work-of-fracture of bone is rate dependent: unstable fracture propagation appears to consume less energy.

b) Antler has a higher work-of-fracture than bone (within the same study).

c) Antler prefers to split longitudinally: this direction requires less energy.

d) Dry antler requires less energy than fracturing damp or wet antler.

e) There is some variation depending on the size of the specimens used. However, there is considerably more variation between the results obtained by different experimenters.

f) The critical stress intensity factor appears to be independent of the type or existence of a pre-crack.

g) The critical stress intensity factor increases with testing rate.

---

[13]Such changes are not uncommon. In their table of *representative toughness values for various materials* Atkins and Mai (1988) state 'caution: values can depend markedly on rate, temperature and environment'.

Points a and g appear to be contradictory, as the work-of-fracture and the critical stress intensity factor are related in such a way that if one increases so should the other (see equation 5.051).[14]

6.4. SINGLE EDGE NOTCH SPECIMENS (SEN)[15]

The single edge notch, or SEN, specimen is very simple in design. They are a flat strip with a notch cut in one side. This specimen is then subjected to tensile loading until failure. This specimen is normally used to find the critical stress intensity factor and the critical potential energy release rate (which as mentioned above is equal to the work-of-fracture under equilibrium conditions). A few researchers have used such a specimen geometry to examine bone; of whom the most relevant, known, ones are Melvin and Evans (1973)[16], Bonfield and Datta (1976) and Moyle and Gavens (1986). In all these cases transverse fracture was examined.

The first paper I will examine is that of Melvin and Evans (1973). These workers state that

> Single edge notch specimens, nominally one inch long, one inch wide and 0.090 inches thick were machined from fresh bovine femoral bone. The specimens were kept moist during machining and storage with saline solution.

These specimens were used to obtain a measure of K_{IC} for longitudinal and transverse cracks at cross-head speeds of 8.5×10^{-6}, 8.5×10^{-5} and 8.5×10^{-4} ms^{-1} [0.02, 0.2 and 2 inches/min]. The authors say that the slowest cross-head speed produced 'slow stable crack growth which in most cases is followed by rapid crack propagation'. For the longitudinal cracks stable propagation extended for up to 6.5 mm ('as far as quarter of an inch or more'). However, for the transverse fracture the crack extends only a millimetre and 'then propagates rapidly by bifurcation at that point with two cracks running diagonally away from the plane of the notch'. The authors calculated values of the stress intensity factors associated with the initiation of the slow crack growth. They give the mean values as 3.21 MPa $m^{0.5}$ [2925 psi $(in)^{1/2}$] for 12 longitudinal fractures and 5.58

---

[14]I do not consider that the change in material stiffness associated with a change in testing rate can account for this difference.

[15]In the review of papers in this and following sections I have retained the authors nomenclature in many cases. Thus for fracture stress both σ_{ft} and σ_f are used, I consider these interchangeable. However, the use of K_C and K_{IC} may not be interchangeable, see figure 5.004.

[16]Although, they refer to their specimens as single edge notch specimens, Melvin and Evans specimens are not standard as the loading pins are not on the centre line of the specimen.

MPa $m^{0.5}$ [5080 psi $(in)^{1/2}$] for 12 transverse fractures. Melvin and Evans report that tests performed at the two higher testing rates produced values for the stress intensity factor associated with the propagation of stable fracture are similar to each other but 10% greater than those quoted for the slower rates. The authors measured the length of the stable crack and state that 'based on the extended crack length K_{IC} was calculated for those specimens which exhibited rapid crack propagation'. For longitudinal fracture the mean value is given as 5.05 MPa $m^{0.5}$ [4598 psi $(in)^{1/2}$], and for the transverse fracture as 7.69 MPa $m^{0.5}$ [6998 psi $(in)^{1/2}$]. Melvin and Evans report that 'no significant increase in K_{IC} with increasing crosshead rate was noted'. I consider that these last two values should be treated with caution or at least viewed as an upper bound. The catastrophic nature of the crack propagation implies a surplus of available energy. Thus the application of an equation based on an assumed energy balance will imply a consumption of energy by the cracking process that is greater than the true value. However, the calculated value for fast fracture is smaller than that calculated for slow fracture.[17] Thus there is an anomaly: in stable crack growth the resistance to fracture increases with cross-head speed, while the resistance to a fast fracture is less than that to a slow one. This point is returned to in section 6.5.2.

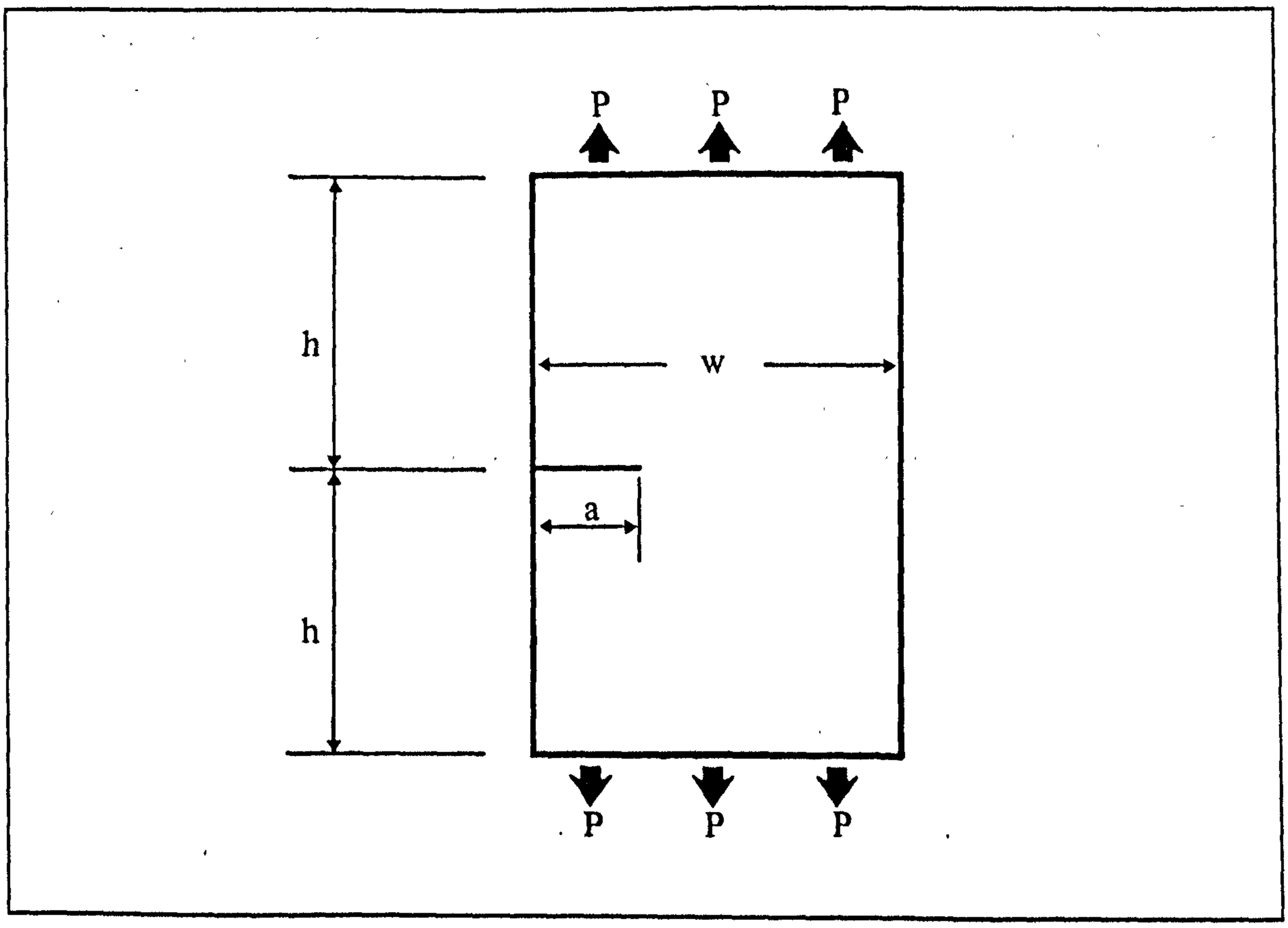

Figure 6.003

Single edge notch (SEN) specimen

[17]A comparable, but less extreme, result to that obtained by Piekarski (1970), see table 6.002, but contradicting that of Robertson *et al.* (1978), see equation 6.003.

Melvin and Evans (1973) also conducted compliance tests and derived values of G_{IC} in the two test directions. These values ranged from 1.38 to 3.08 kJ m^{-2} (7.9 to 14.6 in.-lb/in.^{2}) for the longitudinal direction and 3.13 to 5.53 kJ m^{-2} (17.9 to 31.6 in.-lb/in.^{2}) for transverse propagation. These authors also stated that moisture dramatically affects the value of K_{IC}. They examined this variable by testing one specimen 'moist' and one 'thoroughly dry'. The moist one had a K_{IC} 60% greater than the dry one. These early experiments have been repeated, expanded and improved upon by other workers.

Bonfield and Datta (1976) used SEN specimens that were attached to the machine by pin joints, and were thus free to rotate when tested. These authors realised that because of edge effects a correction should be included when calculating the stress intensity factor. They employed the correction due to Brown and Srawley (1966) for the conditions in which the ends are free to rotate.[18] Rooke and Cartwright (1976) say this is accurate to within 1% for all $h/b \geq 1$ and $a/b \leq 0.6$.

$$Y = 1.12 - 0.23(a/w) + 10.6(a/w)^2 - 21.7(a/w)^3 + 30.4(a/w)^4 \qquad (6.004)$$

The specimens Bonfield and Datta studied were produced from the compact bone of bovine tibia. This enabled relatively large specimens to be manufactured with a gauge length of 25.4 mm, a width of 18 mm and a thickness of 2 mm. The specimen shoulders, 21 mm wide, were reinforced on each side by pieces of steel sheet. The steel was bonded to the bone using quick setting epoxy resin. The connecting pins passed through the metal and the bone. Two series of specimens were prepared. In the first series the notches used were 0.38 mm wide, and had lengths of between 1.25 mm and 14 mm. The tip radius for these notches was 0.38 mm, they were thus key-hole shape. For the second series the notch length was kept constant at 6 mm and the tip radius changed from 0.19 mm to 1.25 mm. During preparation the specimens were immersed in or kept moist with Ringer's solution. The tests were performed at room temperature, 'at a constant rate of 3×10^{-4} s^{-1} to fracture'.[19] The stresses required to fracture the specimens were recorded, and the results given are repeated in table 6.009. These results are plotted in figure 6.004. Figure 6.005 shows a graph of fracture stress and the square root of the notch length. According to the theory of LEFM this relationship should be a linear one.

---

[18]This is not exactly as stated in Bonfield and Datta (1976) for they include $\sqrt{\pi}$ within the function, thus their first constant is 1.99, and so on.

[19]I assume that this 'rate' was calculated using the specimen gauge length and the cross-head speed of the machine. The problems with this method at explained in appendix 7.

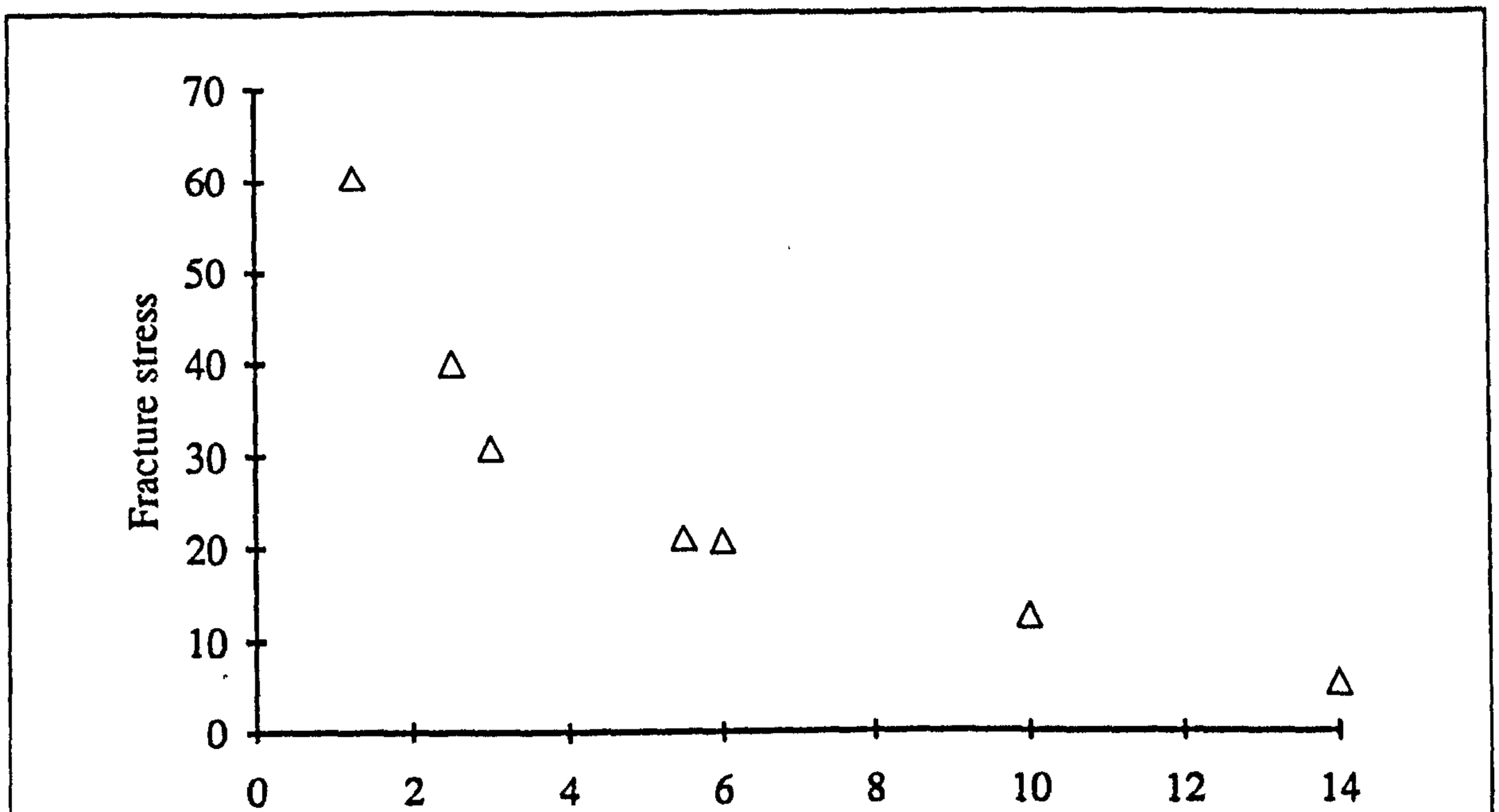

Units:

a Notch length, mm

σ_{fr} Fracture stress, MPa

Figure 6.004 After Bonfield and Datta (1976)

Fracture stress at various notch lengths (data in table 6.009)

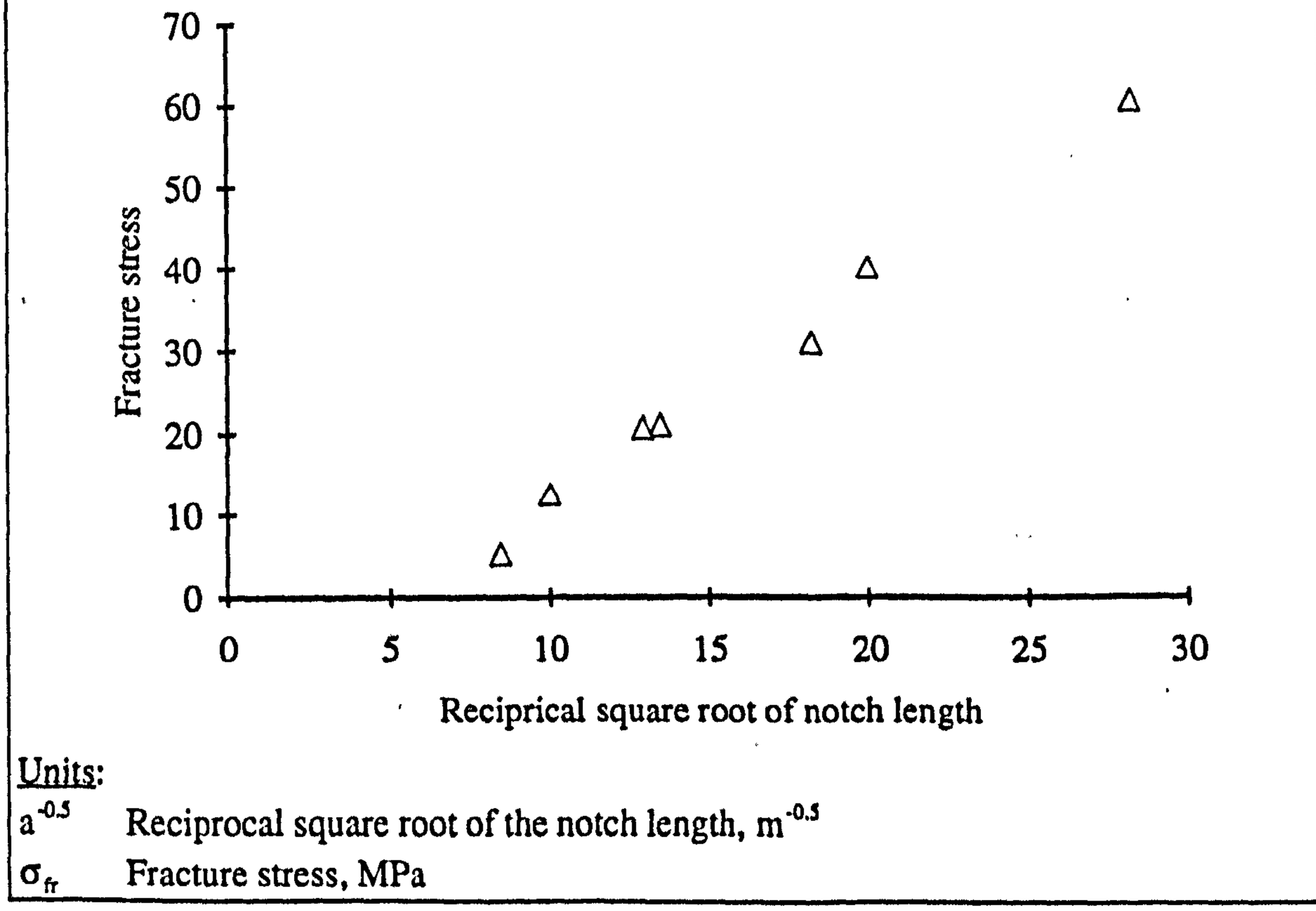

Units:

$a^{-0.5}$ Reciprocal square root of the notch length, $m^{-0.5}$

σ_{fr} Fracture stress, MPa

Figure 6.005 Data derived from Bonfield and Data (1976)

Fracture stress and the reciprocal square root of the notch lengths

Notch length, a mm	1.25	2.5	3.0	5.5	6.0	10.0	14.0
Fracture stress, σ_{fr} MPa	60.3	40.0	30.8	21.0	20.7	12.5	5.3

Table 6.009 After Bonfield and Datta (1976)

Fracture stress of bovine tibia specimens with various notch lengths

Bonfield and Datta state that the above results satisfy an equation of the form:

$$\sigma_{fr} = A\, a^{-0.5} - B \qquad (6.005)$$

where A and B are constants, equal to 2.60 MPa $m^{0.5}$ and 13.5 MPa respectively.[20] They state that an un-notched specimen, tested under identical conditions, had a mean failure stress of about 120 MPa. Bonfield and Datta extrapolate the equation to this value and obtain a measure of the 'intrinsic crack or flaw length', of 370 μm if it is an edge crack, and 740 μm if it is an internal one. (These values changed when they applied a shape correction: A = 2.20 MPa $m^{0.5}$, B = 6.0 MPa, the intrinsic flaw now has a predicted value of 340 μm or 680 μm.) As I stated above in my discussion of Piekarski's paper (section 6.3.1) the concept of an intrinsic edge notch should be considered with some reference to how it was obtained. In this case the edge crack referred to is less than 0.5 mm long, but due to the thickness of the specimens used it is 2.0 mm wide. Consideration of the specimen thickness implies that the idea of relating the calculated value of the intrinsic edge notch to specific structural features within bone is misconceived. I suggest that when the heterogeneous structure of bone is considered, the idea that the calculated length can be viewed as a single edge notch in an otherwise uniform material is questionable. (However, it should be remembered that the effect of this heterogeneity will also be present in the SEN specimens.) Thus I suggest that the intrinsic edge notch should be viewed as an indication of the global effect of various additional internal discontinuities within the tensile specimen.

Bonfield and Datta's results for tests on specimens that had notches of the same length, but different tip radii are shown below.

Tip radius mm	0.19	0.38	0.54	0.75	0.94	1.25
Fracture stress, σ_{fr} MPa	25.4	25.5	24.8	27.3	24.6	26.5

Table 6.010

Fracture stress and notch tip radius for bovine tibia SEN, specimens

[20]Using the data they provide I obtained a different equation $\sigma_{fr} = 2.69\, a^{-0.5} - 15.6$

Bonfield and Datta (1976) concluded from these results that the fracture stress was approximately independent of the crack tip radius and pointed out that this is not consistent with the Inglis theory. They observed no cracks around the machined crack tip, but said that 'the presence of sub-microscopic cracks of constant radius of curvature is not precluded'.[21] They also calculated the critical stress intensity factor K_{IC} for each test, which resulted in values of 2.2 to 4.6 MPa $m^{0.5}$. However, this range of values is not consistent with the failure stresses and dimensions given in their paper.[22] Consequently the values they calculated from the erroneous stress intensity factors are also wrong. For an elastic solid the critical stress intensity factor and the surface energy are related, via Young's modulus.[23] They substituted the upper and lower limits for E (27.3 and 19.0 GPa), together with their higher value for critical stress intensity factor into $\gamma = K_{IC}^2/2\,E$. By this operation they obtained values of γ from 3.9×10^2 to 5.6×10^2 J m^{-2}. They point out that the presence of non-elastic deformation means that these values are an over-estimate. In a review of this experiment Bonfield (1981 and 1987) states[24]

> This suggests that, somewhat fortuitously, in the various cases, fracture probably propagated from a similar sub-microscopic crack at the periphery of the machined radius and therefore could be considered as approximating to the ideal condition of an atomically-sharp crack tip.

Notch length, a mm	1.25	2.5	3.0	5.5	6.0	10.0	14.0
Fracture stress, σ_{fr} MPa	60.3	40.0	30.8	21.0	20.7	12.5	5.3
K_{IC}, MPa $m^{0.5}$	4.3	4.4	3.9	4.6	5.1	7.6	9.1
R, J m^{-2} (using E = 27.3 GPa)	0.69	0.72	0.55	0.79	0.95	2.11	3.06
R, J m^{-2} (using E = 19.0 GPa)	1.00	1.03	0.80	1.14	1.36	3.03	4.40

Fracture stress of bovine tibia specimens with various notch lengths as provided by Bonfield and Datta (1976), with recalculated values of the stress intensity factor and work-of-fracture

Table 6.011

Fracture properties of bovine tibial specimens with various notch lengths

Moyle and Gavens (1986) conducted a series of tests very similar to, but more extensive than, those of Bonfield and Datta. They used a total of 80 specimens, 75 of

---

[21]Chapter 8 contains evidence for the existence of such small cracks.
[22]This anomaly was pointed out by Moyle and Gavens (1986). I recalculated the values using their stated dimensions, failure stresses and shape correction factor. The values I obtained are listed in table 6.011.
[23]See section 5.2.3.5 and equations 5.017 and 5.020.
[24]He uses identical wording in each paper.

which contained a notch. The specimens were obtained from frozen bovine tibiae. They were initially cut with a diamond saw, with tap water irrigation. The surfaces were then ground on 600 grit silicon carbide paper. A vertical mill was used for machining the specimens to the required shape with a gauge length of 25.4 mm and a width of 15.9 mm. Holes were drilled in the shoulder section and steel plates were bolted to these to permit pin loading. The edge cracks had a length of 4, 6, 8, 10 or 12 mm. The tip curvature was produced by a drill of 2.38 mm [3/32 in] or 1.59 mm [1/16 in] diameter, or by a 0.79 mm [1/32 in] diameter end mill. For each combination of crack length and tip radius they tested five specimens. The specimens were tested using an Instron closed-loop hydraulic testing machine. Loading was applied at a constant rate using a stroke controlled ramp function having a deformation rate of 7.5×10^{-6} m s^{-1}. The specimens were not allowed to dry at any time during the preparation of testing. Besides the fracture stress, these authors determined the calcium content and fractional void area. The results are shown in table 6.012.

Nominal crack length mm	Fracture stress mean ± s.d. MPa	Actual crack length mean ± s.d. mm
4	54.18 ± 9.29	4.17 ± 0.18
6	39.25 ± 7.41	6.19 ± 0.33
8	28.11 ± 5.15	8.08 ± 0.19
10	14.52 ± 2.49	10.23 ± 0.18
12	8.12 ± 1.92	12.15 ± 0.12
15 specimens in each test group		

Table 6.012 After Moyle and Gavens (1986)

Fracture stress and actual crack length for each nominal crack length

Nominal crack tip radius of curvature mm	Fracture stress mean ± s.d. MPa	Actual crack tip radius of curvature mean ± s.d. mm
0.40	27.76 ± 19.16	0.46 ± 0.032
0.79	28.43 ± 16.40	0.82 ± 0.032
1.19	30.32 ± 18.16	1.21 ± 0.026
25 specimens in each test group		

Table 6.013 After Moyle and Gavens (1986)

Fracture stress and actual crack tip radius of curvature for each nominal crack tip radius

Their initial analysis of the stress level at which the specimen failed was based on the Inglis equation[25]

$$\sigma = \sigma_{\infty}\left[1 + 2\sqrt{a/\rho}\right] \qquad (6.006)$$

Moyle and Gavens performed regression analysis, and determined that this relationship was significant. However, this significance was found to be due to the crack length term and no significant relationship was found between the fracture stress and crack tip radii. They state 'there is no significant effect of the crack tip radius on the fracture stress'. Moyle and Gavens indicate that 89% of the variance in fracture stress is due to crack length. This agrees with the findings of Bonfield and Datta above. The next step Moyle and Gavens used in their analysis was a comparison with the Griffith equation. The regression analysis produced the same form of equation as for Bonfield and Datta above (equation 6.005), this time A = 7.12 and B = 54.21 MPa ($F = 428.47$, $p<0.0001$, $R^2 = 0.85$). Moyle and Gavens claim this is a reasonable result, because a zero failure stress implies an edge crack of 17.3 mm, which is approximately the width of the specimen. However, I would like to point out that if this logic is accepted it implies the equation (the values of A or B, or both) is dependent on the specimen size. Because to obtain an edge crack the same width as a specimen 30 or 10 mm wide, at zero stress, will require other equations. Substituting a 10 mm long crack into the equation gives a failure stress of 16.99 MPa, and 30 mm gives a value of $\sigma_f = -13.1$ MPa. Thus according to Moyle and Gavens logic their equation is valid only for specimens of the same width as those from which it was derived.

Moyle and Gavens substitute the mean failure stress obtained from the un-notched specimens, 112.7 MPa, into their regression equation to predict an *'intrinsic flaw size'*. This proved to be 1.82 mm for an edge crack or 3.64 mm for an internal crack. Clearly if the form of the equation is dependent on the specimen width, this implies a similar dependence in the case of the intrinsic flaw size.[26] The authors state

> There are no naturally occurring voids present in the bone the size of the intrinsic flaw. In plexiform bone, due to its lamellar structure, the vascular canals lie circumferentially around the bone. The crack produced in the specimens propagates parallel to these canals and they may act as extension of the crack tip.

---

[25]See section 5.2.1.

[26]I have already suggested that the measure referred to as the 'intrinsic flaw size' (or in my words intrinsic edge notch) should not be considered as a single crack. If this were done here the largest dimension of the intrinsic edge crack is not that determined from the experimental results, 1.82 mm, but that determined by the thickness of the specimen, 2 mm. This topic will be returned to again as more evidence for the true meaning of the intrinsic edge notch emerges.

By assuming a Young's modulus of 20 GPa and equating A with $\sqrt{2\,E\gamma/\pi}$ in the Griffith equation Moyle and Gavens (1986) obtained a work-of-fracture, 2γ, value of 7.96 kJ m^{-2}. They also calculate K_{IC} using the same shape correction factor as above, equation (6.004). However, they do point out that, because the crack tip is blunt the values determined should only be considered as an estimate. The mean value they obtained was, $K_{IC} = 11.2 \pm 2.6$ MPa $m^{0.5}$, with a range of 6.3 to 15.9 MPa $m^{0.5}$. They found no significant correlation between fracture stress and calcium content.

Lakes *et al.* (1990) performed tests on specimens of mature bovine Haversian bone, obtained from the mid-diaphyses of fresh frozen tibiae. They state that the preparation method followed was the same as that used by Bonfield and Datta (1976).[27] Specimens of the same size were used, but in this case they contained notches of between 0.25 and 16 mm long. The results were examined using linear elastic fracture mechanics, but Lakes *et al.* also include a discussion of crack tip yielding and Cosserat elasticity.[28] Their experimental results are given only in graphical form, but the authors also include an equation of the same format as (6.005) where A = 2.2 MPa $m^{0.5}$ and B = 6.0 MPa. They say that in this case the equation embodies a shape correction factor. The statistical significance level of this curve is not given. (This equation is identical to that given by Bonfield and Datta (1976). Lakes *et al.* are not very explicit, but it may be that the same results are reproduced).[29] Using the ideas of LEFM they examined the relationship of the critical stress intensity factor to the failure stress. They took the shape correction factor into account. This showed that in the case of short notches the experimental data deviate from the theoretically expected values. It is pointed out that for short notches, the root radius cannot be neglected. Thus they also examine the stress concentration factor by considering the notch to be half an ellipse and comparing them with the results predicted by the Inglis formula, for consistency given here as

$$\sigma_f = \frac{\sigma_{ult}}{1 + 2(a/\rho)^{1/2}}\,Y \qquad (6.007)$$

where σ_f is the stress at which fracture occurs and σ_{ult} the ultimate strength of an un-notched specimen. The authors reported that such a model underestimates the strength of

---

[27]Bonfield is one of the co-authors of Lakes *et al.* (1990).

[28]Cosserat elasticity is described as 'a continuum theory which incorporates some of the internal degree of freedom of structural materials'. This permits the redistribution of stresses (from those predicted by classical elasticity) thus reducing stress concentrations.

[29]Lakes *et al.* say 'the LEFM curve, based on energy considerations, is obtained by curve fitting of the analytical curve to the experimental data as described by Bonfield and Datta (1976). The empirical relationship is: σ_{cr} (in MPa) = 2.2 a (in m)$^{-1/2}$ - 6.0'. However, they do point out during the experimental methods section that the notch lengths in their paper are different to those of Bonfield and Datta.

a notched bone specimen by more than a factor of two.[30] In the conclusions of the paper they state that 'bone in the presence of a notch is tougher than was expected on the basis of the theory of elasticity'.

In their analysis of the 'plastic zone' Lakes *et al.* use the Dugdale model (section 6.2.3.9). They point out that the influence of plastic deformation is to effectively blunt the crack. When they substituted values for crack length and stress into the equation for the size of the plastic zone,[31] they obtained an answer of $\Delta_y = 0.5$ mm. This is less than the root radius of the notches machined in the specimens. From this Lakes *et al.* conclude 'the crack tip blunting effect of plastic deformation is therefore minimal in the present experiments'. I have presented (in chapter 4) some evidence that the knee in the tensile loading curve is due damage accumulation not plasticity. Therefore I disagree with the idea that the crack tip process zone of a crack in bone is composed of plastically deformed material. Thus I not only question the conclusion drawn by Lakes *et al.* but also the direct application of the yield strip model to the analysis of bone.

These three studies (Bonfield and Datta, 1976; Moyle and Gavens, 1986 and Lakes *et al*, 1990) can be compared, as their test conditions were almost identical. (If an approximation of the strain rate in the second study is made, by dividing the stated deformation rate by the gauge length, the same value as given in the other works is obtained.) Unfortunately only limited raw data is supplied in the last study. In the first study the values of the corrected stress intensity factors range from 3.9 to 9.1 MPa $m^{0.5}$, and in the second study it ranges from 6.3 to 15.9MPa $m^{0.5}$. The higher stress intensity factors appear to result from the higher stresses in the second study. By substituting a crack length of 4 mm into the equivalent equation (6.005) in both studies, the difference is demonstrated: Bonfield and Datta's (1976) equation predicts σ_{fr} 27.6 MPa, (or with the shape correction factor 28.78 MPa) and that of Moyle and Gavens predicts a value of 58.4 MPa. Because the difference in specimen dimensions is small, the variation in shape correction factor will not account for this difference. In his 1987 review *Advances in the fracture mechanics of cortical bone* Bonfield compares his result for the intrinsic flaw length with those of Moyle and Gavens. He also notes their higher values of K_{IC} and points out that in the work by Moyle and Gavens the crack path contained a bifurcation whereas in his work the crack followed a single relatively straight path. He implies this could be the reason for the difference in the values. However, I suggest that as the failure is catastrophic the maximum stress attained will be that needed to initiate the crack, and therefore this stress will be independent of the crack's later bifurcation. Perhaps the bifurcation indicates that there was a greater energy storage within the test equipment

---

[30]It is unclear how the experimental values were determined.

[31]These values were a = 1 mm, σ = 64 MPa and σ_Y = 100 MPa.

used by Moyle and Gavens. Is his review Bonfield cites some more workers who have followed a similar experimental technique, which he reports in the following way.

> Another recent study by Silva and Fortes (1987), also on SEN specimens of bovine tibial bone corresponds more closely to the Bonfield and Datta results with
>
> $$\sigma_{Fr} = 4.77\, a^{-1/2} - 39.51 \text{ MN m}^{-2}$$
>
> with a mean K_c of 5.9 ± -0.72 MN $m^{-3/2}$.

Another interesting comparison can be made when the two sets of data are plotted on the same graph. Due to the different specimen widths I have normalised the notch lengths, a, by the width, w. The resulting values are shown in figure 6.006. It is very noticeable that the data from Bonfield and Datta (1976) shows a clear curve as would be expected from a material obeying the equations of LEFM. However, the mean values from Moyle and Gavens (1986) display an almost linear relationship between crack length and failure stress. Unfortunately the data for individual specimens is not provided by Moyle and Gavens, so a full re-analysis is not possible. However, I have conducted a number of regressions on their mean values. (One value is given for each of the five notch lengths.) From these I obtained the equations shown in table 4.016. Similar results are quoted by Moyle and Gavens, but they do not compare the results. As mentioned above, Moyle and Gavens found a strong relationship between the failure stresses and the notch length. They report that '89% of the variance in fracture stress is attributable to variance in crack length'. They also report 'a plot of the fracture stress Vs the inverse square root of the crack length...($F = 428.47$, $p < 0.0001$, $r^2 = 0.85$)'. They say the latter result 'substantiates the applicability of a relationship similar to the Griffith equation'. However, the function containing the reciprocal square root of notch length explains less of the variance in failure stress than the linear relationship. I suggest this observation produces a degree of doubt as to the applicability of LEFM to describe the relation of failure stress and notch length in bone, at least for their data set.

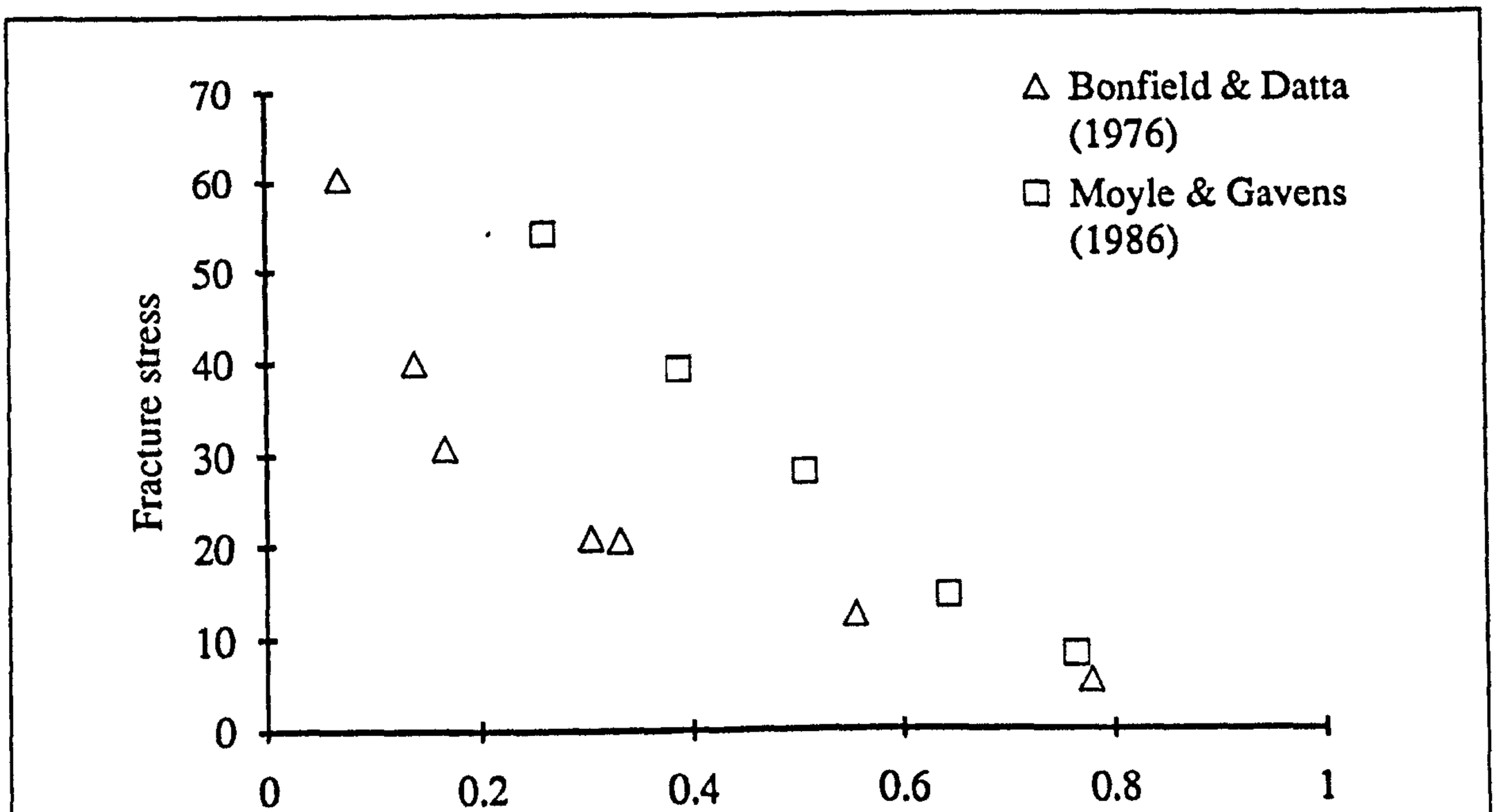

Units:

a/w Normalised notch length, unitless

σ_f Fracture stress, MPa

Figure 6.006

The fracture stress at various normalised notch lengths obtained by Bonfield and Datta (1976) and Moyle and Gavens (1986)

	Regression equations, *p* and t values.[32] The stress is in units of MPa and the length, a and w, are in metres.	R^2 %	
5 mean values	$\sigma_f = -55.6 + 7.24\ a^{-0.5}$ *p*: 0.005 0.001 t: -7.59 11.75	97.2	*a*
5 mean values	$\sigma_f = 76.6 - 92.9\ (a/w)$ *p*: 0.000 0.001 t: 22.61 -14.92	98.2	*b*

Table 6.014

Regressions of the mean failure stresses at various notch lengths for the data supplied by Moyle and Gavens (1986)

[32]These regressions were obtained by analysing the published data using Minitab. R^2 values have been adjusted for degrees of freedom.

O'Connor (1976) is another worker who has used SEN specimens, to investigate the fracture mechanics properties of bovine bone. These specimens were oriented longitudinally with respect to the long axis of the bones from which they came. Between the shoulders the specimens had a gauge length of 37 mm and a cross-sectional area, away from the notch, of 1 mm by 2 mm.[33] The notches had a tip radius of 0.38 mm and a range of lengths from 0.2 to 1.2 mm. The test conditions are not given, but other, tensile, tests in the same thesis were performed using an 'Instron floor-model testing machine' and

> To prevent drying the specimen (and lower clamp) was mounted in a Ringers bath, submerging the specimen up to the region of the strain gauges. Tests were performed in an Instron environmental chamber which enables the maintenance of a constant temperature (±0.1°C).

The results for nearly 80 SEN specimens are reported. In her analysis she appears to follow the procedure used by Bonfield and Datta (1974b). Unfortunately the reference she gives bears no relevance to fracture mechanics. O'Connor says the data for each bone is fitted to the equation, $\sigma_{fr} = A\, a^{-0.5} + B$. I consider that this equation contains a typographical error, for when she refers, in a pervious section, to the paper from which it she says it comes, the equation takes the form of $\sigma_{fr} = A\, a^{-0.5} - B$. The latter equation is the same as reported in Bonfield and Datta (1974b and 1976), and mentioned above. No values of B given in her table 5.5 are less than zero. A range of intrinsic flaw sizes is presented, where the half-crack length is 310 ± 90 μm or 110 ± 40 μm. The method given for the calculation of these values, was to substitute either the maximum stress for an un-notched specimen obtained in her work 112 MPa, or a value of 172 MPa from the literature, respectively, along with the experimentally derived values of A and B into the relationship of fracture stress to crack length, $\sigma_{fr} = A\, a^{-0.5} + B$. However, on substituting the values of the intercept stress B and slope A from her table (5.5, p228) and the chosen stress levels into given equation, I obtain different crack lengths from those in the table (differences also occurred when the, assumed, correct relationship was used). From the data for the second specimen O'Connor obtains a value of 440 μm, whereas I obtain a value of 290 μm, I consider that this amount of discrepancy could not be due to rounding errors in her calculations, nor is this error consistent throughout the set of data.

O'Connor also determined values of K_{IC} in three ways. However, there is some lack of clarity in how the values were determined in some cases. Because, there appears to be an algebraic error in the derivation of her equation 5.6. She combines the following equations (the nomenclature has been altered here to that used in this work).

---

[33]The values given by O'Connor are 0.1×10^{-3} by 0.2×10^{-3} m. However, the scale bar on photos of the specimens and the sizes given in tables of results, indicate that they should be ten times this value.

$$\sigma_{fr} = A\, a^{-0.5} + B \qquad (6.008)$$

and

$$K_{IC} = \sigma_{fr}\, (\pi\, a)^{0.5} \qquad (6.009)$$

Arriving at

$$K_{IC} = (\sigma_{fr} - B)\, a^{0.5}\, \pi^{0.5} \qquad (6.010)$$

or

$$K_{IC} = A\pi^{0.5} \qquad (6.011)$$

The last two equations appear to imply that $\sigma_{fr} = (\sigma_{fr} - B)$. The only logical explanation I can see for this is that O'Connor has viewed the intercept stress B as some sort of error term or datum quantity that should be subtracted from the measured value of the fracture stress hence σ_{fr} is replaced by $(\sigma_{fr} - B)$. However, I can not find where she provides any such logic for this transformation. The mean value she gives for K_{IC} using equation 6.011 (from the data in table 5.5) is 3.1 ± 1.1 MPa $m^{0.5}$. For comparison the results derived from the standard equations were also presented $K_{IC} = \sigma_{fr} \sqrt{\pi\, a}$ and $K_{IC} = Y\, \sigma_{fr} \sqrt{\pi\, a}$. The shape correction factor is that already mentioned for pin jointed SEN specimens (equation 6.004). However, the photographs she supplies of some of these specimens show that they do not posses a hole for such pin mounting, nor did I find any evidence for it in the text. The values she gives for bovine bone are: without the correction 3.1 ± 1.7 MPa $m^{0.5}$, and 4.3 ± 1.7 MPa $m^{0.5}$ with the correction.[34] O'Connor points out that the critical stress intensity factor represents an intrinsic property of the material and thus should be independent of crack length, but says this parameter varies with the value of $a^{-0.5}$, and provides a plot of these two quantities. The plot shows that the longer the crack the higher the value of the stress intensity factor obtained. This should not be the case as the critical stress intensity is supposed to be independent of specimen geometry. (It is not stated which of the methods of calculation was used for the critical stress intensity values shown in the plot.)

Due to the apparent numerical and typographical errors, and the general lack of clarity in O'Connor's work (or my ignorance when trying to understand it), I urge considerable caution when drawing conclusions from her work. This is unfortunate as her study obviously involved a great deal of effort and is one of the few that use SEN specimens, especially within such well controlled environmental conditions.

---

[34]O'Connor (1976) table 5.7.

6.4.1. SUMMERY OF THE USE OF SEN SPECIMENS

A number of studies of the fracture behaviour of bone using SEN specimens have been reviewed. There are a number of findings that could be relevant to this study of the fracture of bone and antler. These are

a) K_{IC} of a 'moist' specimen is greater than that of a 'thoroughly dry' one. In other words dry bone is more brittle.

b) Some sets of results support the application of LEFM (Bonfield and Datta, 1976). However, I suggest others can be used to question it. For example the results of Moyle and Gavens (1986). (See figure 6.006.)

c) The data is normally fitted to an equation of the form $\sigma_{fr} = A\, a^{-0.5} - B$. This implies the fracture stress id greater, by B, than that predicted by the Griffith equation.

d) The fracture stress does not appear to be dependent on the notch tip radius, contrary to the elastic theory.

e) It has been suggested (by Bonfield) that the fractures may propagate from a sub-microscopic crack.

f) The intrinsic flaw size has been compared to the internal structures of bone. I consider this to be a meaningless exercise.

g) The crack tip process zone is viewed as a plastic zone. I consider this to be incorrect. (The evidence to support my opinion is presented in chapters 7 and 8.)

6.5. COMPACT TENSION SPECIMENS (CT)

After pointing out that the testing of SEN specimens is arranged to produce an approximately linear stress-stain behaviour and a catastrophic fracture, Bonfield (1987) says

> These conditions become limiting if a deeper insight into the mechanics of fracture is required, i.e. for example, to differentiate between the nucleation and propagation of a crack and to determine the interaction of a crack front with microstructural features. For this type of study, it is desirable to control the crack velocity, so that the progress of the crack through the bone can be monitored. This type of experiment is difficult with SEN and CNC specimens, but is possible with a compact tension (CT) specimen geometry.

The ability to produce stable crack propagation is a result of the geometry of the CT specimen. This geometry is shown in figure 6.007 and described below.

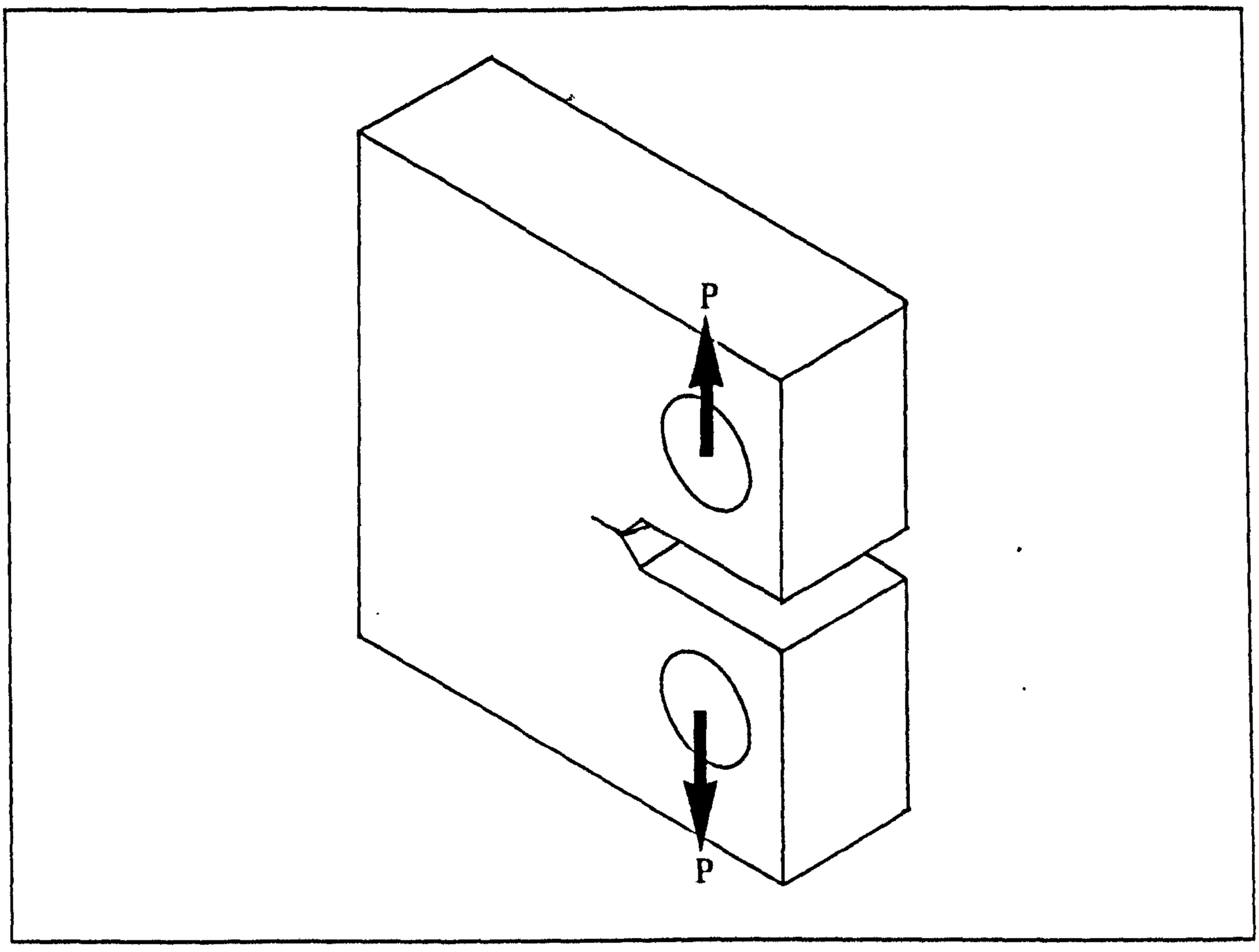

Figure 6.007

Compact Tension (CT) Specimen

The CT specimen can be likened to two identical cantilever beams projecting from the same wall and positioned on top of each other. The two beams are bent apart by equal forces applied near the end of each beam, the force on the top beam is directed upwards and that on the lower it is downwards, see figure 6.008. For such a beam the deflection, at a point A, δ_A is described by

$$\delta_A = \frac{P a^3}{3 E I} \qquad (6.012)$$

where: P is the applied load, a is the length of the beam and I is the second moment of area. If the beams are increased in length, analogous to an increase in crack length, the load required to maintain a constant deflection, δ_A, will decrease. Therefore the energy stored in the beams will also decrease. This analogy shows how for the compact tension specimen the stored energy will also decrease when a crack extends. The dimensions of the specimen will determine the relationship of this reduction in energy to crack extension, and will also determine the initial energy level. Specimens of this general form are sometimes referred to as 'double cantilever beam' or DCB specimens.

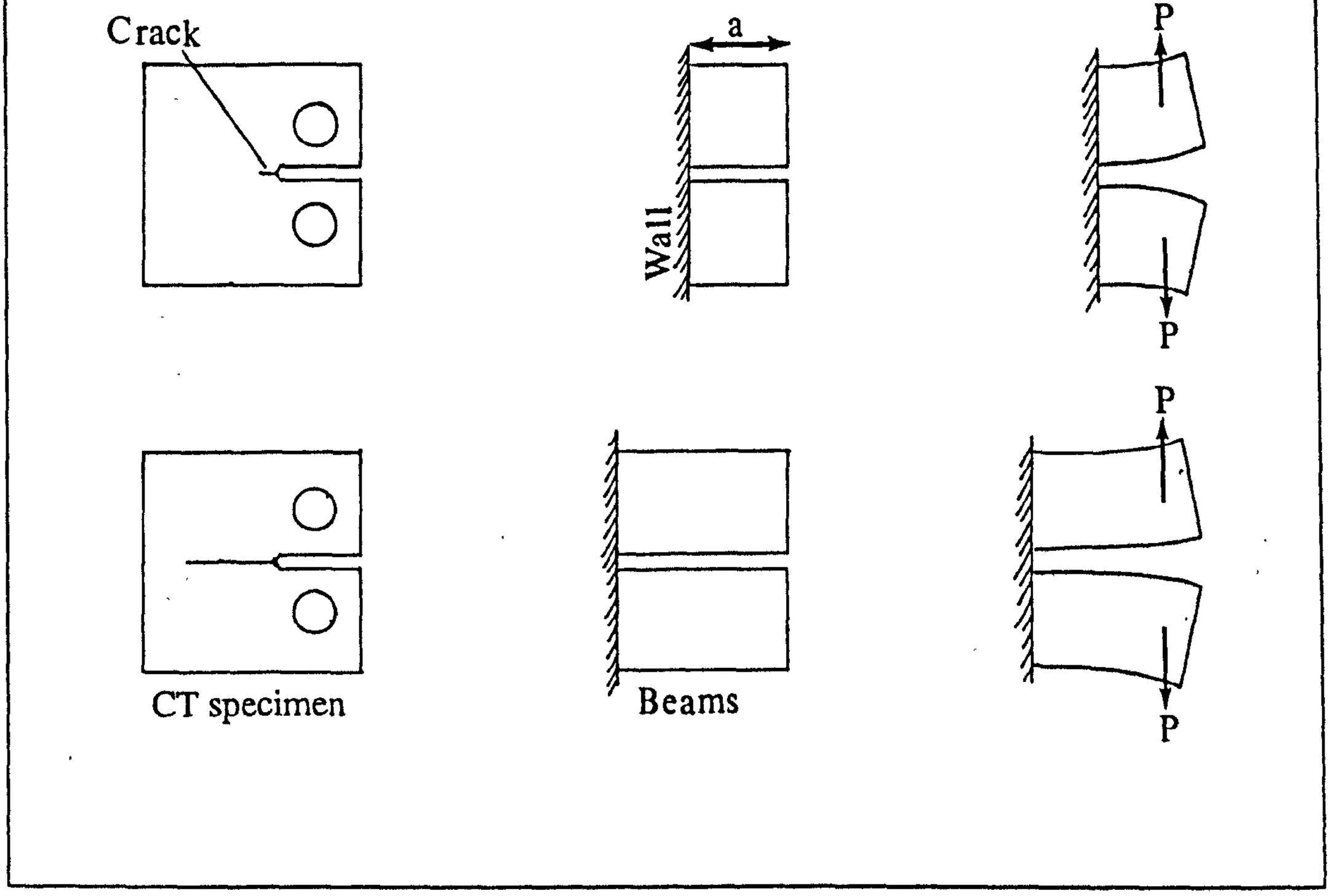

Figure 6.008

An analogy of the CT specimen using cantilever beams

Standards covering specimen geometry and testing conditions exist for the testing of metallic materials, for example B.S. 5447 (1977). This British Standard gives ratios for the recommended specimen dimensions and the related values of the shape correction factor. It also contains information on the testing method to be followed. Due to the stability of crack growth that can be obtained with this type of geometry, it is possible to obtain many results from the same specimen. This is achieved by recording the load and related crack length during propagation. As Bonfield (1987) points out this has the advantage of examining the propagation of a natural crack. Because an artificially machined one may not be of the critical sharpness, ρ_c, and thus could give erroneous values of K_{IC} (as reported in section 5.2.3.6). Another advantage of CT specimens is that because the results that are obtained from small specimens are valid, the crack can be made to propagate longitudinally or transversely through the bone material. Because of their greater relevance to my work, the tests conducted with transverse cracks will be examined first. Unfortunately there are very few published works that use this orientation. This is most probably due to the greater ease of propagation of a crack in the longitudinal direction.

6.5.1. THE USE OF CT SPECIMENS TO INVESTIGATE CRACKING IN DIRECTIONS OTHER THAN LONGITUDINAL

The only people I am aware of who have used CT specimens oriented so that the crack runs transverse to the long axis of the bone are Behiri and Bonfield (1989), who state they are the first to do so. In this study they examine the orientation dependence of the fracture mechanics of cortical bone. The specimens were stored in Ringer's solution at - 20°C until they were tested. The paper only states that they were loaded at room temperature, the degree of saturation or otherwise of the specimen is not given. Due to the equipment used I assume they were tested in the open air. Initially they performed tests on CT specimen oriented so the starter crack was at 0°, 15°, 30°, 45°, 75° and 90° to the axis of the bone. When these specimens were deformed at a constant cross-head speed of 1.7×10^{-7} m s^{-1} they found that regardless of the orientation of the introduced notch, the subsequent fracture path followed the same direction that is parallel to the long axis of the bone. When they increased the cross-head speed to 3.3×10^{-7} m s^{-1} a similar result was obtained for all orientations apart from 90° where the crack bifurcated. To force the fracture to follow the desired path they modified the specimen geometry. This modification was in the form of grooves 0.5 mm deep and of a V-shape cross section, machined in the two large faces of the specimen, so that they formed a continuation of the starter notch. They loaded the specimens at 1.7×10^{-7} m s^{-1} noting the load as the crack reached various lengths.[35] The specimens typically exhibited stable crack growth except for those at 90°, which developed catastrophic failures, after a stable initiation of the crack. With these data they calculated various values of the critical stress intensity factor. (Due to the modification to the specimen geometry they also used a different equation for the SIF.) They used this procedure on each of the ten specimens tested at the six orientations given above. Changing the angle of the crack from 0 to 90° decreased the crack velocity from about 3.37×10^{-5} to 2.33×10^{-5} m s^{-1}. This change in orientation increased the value of the average stress intensity factor from 3.2 to 6.5 MPa $m^{0.5}$. Behiri and Bonfield (1989) state that if the effect of the decrease in crack velocity is taken into account these results suggest that the ratio of the stress intensity factors in these two perpendicular directions would be greater than two.

The procedure for obtaining a value of the critical stress intensity factor for bone, by used of grooved CT specimens has been assessed by Norman *et al.* (1992). They accomplished this by comparison with un-grooved specimens. They used the fact that the stress intensity factor is a material property (and thus should be the same whichever specimen geometry was used) to find which dimensions should be used in the shape

[35]Examination of 'a load-deflection plot typical for most of the specimens tested throughout the orientation range' implies the tests lasted about half an hour. Unless preventative measures were taken the specimen could have been subjected to drying effects.

correction factor for the grooved specimens. (As they needed to compare results the fracture direction they used was longitudinal in all cases.) They state

> The equation obtained for K_c for the grooved specimens is consistent with the earlier work of Bonfield and Behiri (1989) for modified compact tension specimens.

6.5.2. THE USE OF CT SPECIMENS TO INVESTIGATE CRACKING IN THE LONGITUDINAL DIRECTION

Wright and Hayes (1977) were the first to use CT specimens to examine the fracture behaviour of bone. They studied longitudinal crack propagation in specimens from bovine femora, which they kept moist during testing by using a spray bottle. The aim of this work was to determine experimentally the applicability of linear elastic fracture mechanics to bone, and how this was affected by dry density, bone microstructure and specimen thickness. This was done by deducing values of the critical stress intensity factor and the critical potential energy release rate. This investigation also included an examination of the effects of microstructure and dry density of the bone and specimen thickness. The compliance calibration method was used to experimentally derive an equation relating specimen's compliance to the length of the machined crack.[36] This equation was then used to obtain estimates of the load induced crack length, during the tests. The compliance expression given is

$$C = 240.1 - 2392.9\left(\frac{a}{W}\right) + 9385.7\left(\frac{a}{W}\right)^2 - 15885.9\left(\frac{a}{W}\right)^3 + 10177.2\left(\frac{a}{W}\right)^4 \qquad (6.013)$$

This regression has a very good fit, $R^2 = 0.997$, to the compliance values obtained from ten specimens using nine slot lengths for each specimen. However, Wright and Hayes report that considerable scatter existed in the compliance values at each slot length. It was found that the residuals were related to values for the dry density of each specimen. Thus the above prediction of the crack length was improved by taking account of the differences in dry density. The dry density was calculated by cutting a section from the specimen this was then dried in a desiccator, before it was weighed. Its dimensions were then measured with a micrometer. Wright and Hayes determined the failure load and crack length from the intersection of the loading curve and a secant line that had a slope that was 4% lower than that of the linear section of the loading curve. (Thus as the

---

[36]This uses the fact that as the crack in the specimen becomes larger the stiffness of the specimen decreases (compliance is the reciprocal of stiffness), thus by producing cracks of various known length and recording the specimen compliance a relationship between these two quantities can be established. This can be expressed as a polynomial function of crack length or the ratio of crack length to width of the specimen.

loading line curves over, it will intersect the secant line when the load is 96% of what it would have been, if it not deviated from the linear section of the loading line.) This method, they say, is that prescribed by the 'ASTM Tentative Method (1970)'. Using these values and a shape correction factor, they obtain a single value of the critical stress intensity factor of each specimen. Values of G_c, the critical potential energy release rate, were determined by differentiating the compliance equation and using

$$G_c = \frac{P}{2B^2} \frac{\partial C}{\partial a} \qquad (6.014)$$

where:C is the specimen compliance and P is the maximum load.

Wright and Hayes tested 40 specimens and presented their results for the thickness, density, critical stress intensity factor and the critical potential energy release rate in tabular and graphical form. The plot given below was produced from their table of results.

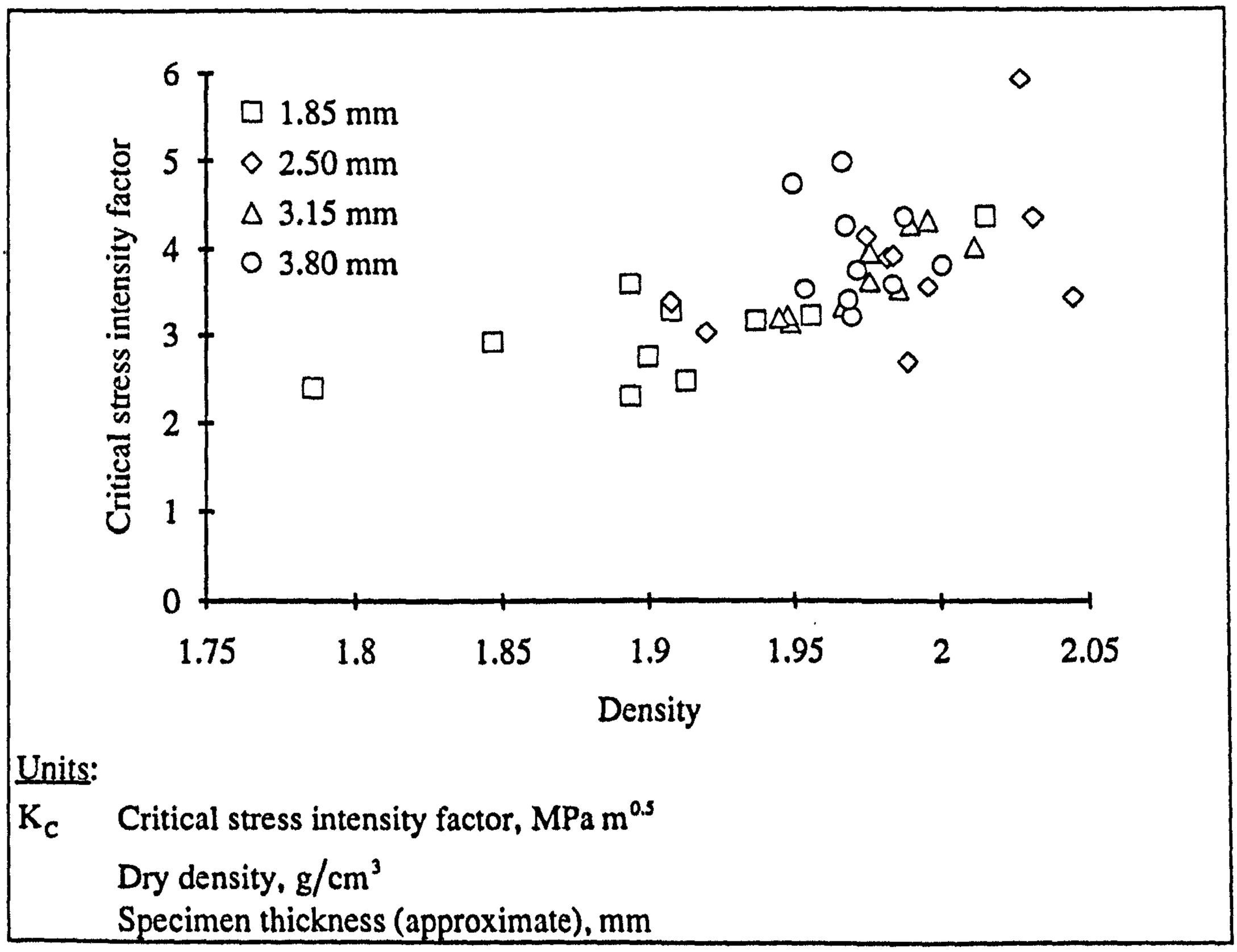

Units:

K_c Critical stress intensity factor, MPa $m^{0.5}$

Dry density, g/cm^3

Specimen thickness (approximate), mm

Figure 6.009 After Wright and Hayes (1977)

Critical stress intensity factor plotted against dry bone density for forty fracture test specimens

The authors state that the critical stress intensity factor values were significantly dependent on the density. Figure 6.009 shows the lower values of K_{IC} were associated with lower densities. Because the fracture in all the specimens was in the same type of bone (primary compact) the authors were unable to determine any effect due to microstructure on the critical stress intensity factor. After correction for density (the 1.85 mm thick specimen group had a lower density) no statistically significant interaction between thickness and K_{IC} was found ($p = 0.58$). The mean value of the critical stress intensity factor was 3.62 MPa $m^{0.5}$ (s.d. = 0.73 MPa $m^{0.5}$).

Wright and Hayes also examined the relationship between K_{IC}, in Pa $m^{0.5}$, and G_C, in J m^{-2}, initially they used the regression

$$K_{IC}^2 = A\,G_C + B \qquad (6.015)$$

For which they obtained the values $A = 9.42\times10^9$ and $B = 1.61\times10^{12}$. They also tested the null hypothesis that the regression line passes through the origin. The hypothesis could not be rejected ($p > 0.05$). Thus the equation could be rewritten without the second constant . A plot of the data (obtained from their table of results) is shown below.

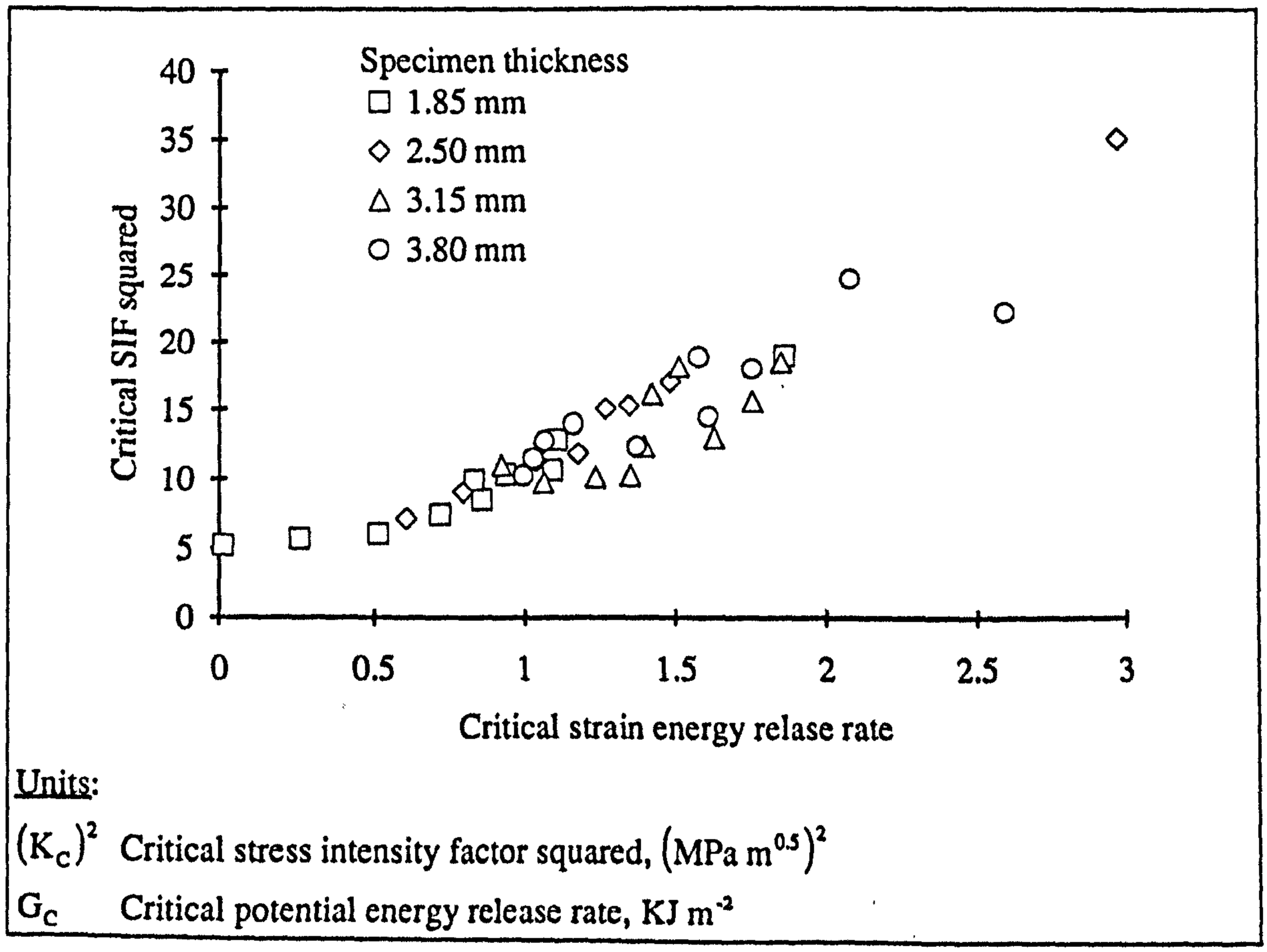

Units:

$(K_C)^2$ Critical stress intensity factor squared, $(MPa\ m^{0.5})^2$

G_C Critical potential energy release rate, KJ m^{-2}

Figure 6.010 Data from Wright and Hayes (1977)

Critical stress intensity factor plotted against critical potential energy release rate

From the results of critical stress intensity factor and critical potential energy release rate Wright and Hayes obtained a value of an effective modulus E^*, defined as[37]

$$K_{IC}^2 = E^* G_C \qquad (6.016)$$

They compared this value with one predicted by substituting published compliance coefficients into an equation for the theoretical effective modulus for a transversely isotropic material, published by Sih *et al.* (1965). The experimentally obtained value was 9.42 GPa and the theoretical was 10.40 GPa. They say the agreement between these values provides strong support for the use of either fracture mechanics parameter, K_{IC} or G_C, to quantitatively describe crack propagation in bone.

Another variable of fracture mechanics tests that has been studied, using the advantage of stable crack growth given by CT specimens, is the velocity of the crack. Two papers on this subject are examined here: Bonfield *et al.* (1978) and Behiri and Bonfield (1980).

Bonfield *et al.* (1978) examined the effects of cross-head speed, and thus crack velocity, on the standard fracture mechanics parameters for longitudinal cracks in test pieces of bovine femur. The cross-head speeds ranged from 1.7×10^{-6} to 33×10^{-6} m s^{-1}. They state that 'the specimens were deformed "wet" in an Instron testing machine'. However, the picture of a specimen shows the surface darkened with carbon 'to improve contrast' so the crack can be seen. This coating may have precluded the use of sprays at least on that surface. (The test they show, by way of an example, took about 400 seconds and used a cross-head speed of 17×10^{-6}, this combined with the values of crack velocity given implies some tests lasted over quarter of an hour. Unless spraying or some other method was used to prevent it, drying would most certainly occur.) The compliance calibration method was used to establish values of G_c at various points during crack propagation, for which the load and crack length had been recorded. The compliance calibration curve was constructed for cracks between 7 and 18 mm long and the specimen width was 26 mm. Values of the critical stress intensity factor were calculated for the same crack lengths, using the appropriate shape correction factor. For cracks longer than 18 mm they noted that the crack velocity decreased. A table of results for one specimen is provided in the paper, and reproduced here in table 6.015.

---

[37]See section 5.2.3.5 for more information on this relationship.

a mm	P kg	$\delta C/\delta a$ N^{-1}	G_c kJ m^{-2}	K_{IC} MPa $m^{0.5}$
9.0	21.0	2.6	2.760	4.0
11.0	19.0	3.8	3.300	4.3
12.0	*17.2*	*4.4*	*3.130*	*4.4*
13.0	*15.2*	*5.05*	*2.810*	*4.2*
14.0	*14.0*	*5.3*	*2.50*	*4.3*
15.0	12.4	6.0	2.220	4.3
16.0	10.8	7.0	1.960	4.3
17	9.0	7.7	1.500	4.2
18	7.0	20.0[38]	2.360	3.8
Cross head speed = 1.7×10^{-5} m s^{-1} Measured time for crack growth from a = 9 mm to a = 18.0 mm, is 172 s. Average crack velocity, from the above, = 5.2×10^{-5} m s^{-1}. Width (W) = 26.0 mm. Thickness (B) = 2.0 mm. The figures in italics indicate values within limits 0.45 < a/w < 0.55.				

Table 6.015 After Bonfield *et al.* (1978)

Derivation of G_c and K_c from experimental measurements of P and a

Bonfield *et al.* (1978) report that an increase in cross-head speed of a factor of 20 increased the resultant crack velocity from 2.1×10^{-5} to 2.7×10^{-4} m s^{-1}, and that an increase of crack velocity in this range produced a systematic increase in G_c from 0.920 to 2.780 kJ m^{-2}. This variation is significant compared to the scatter in values measured at a given cross-head speed. This variation also larger than that related to density found by Wright and Hayes (1977). Thus the variation appears to be due to the increase in cross-head speed and not either of these other two factors. Over the same range of crack velocities K_{IC} increased from 2.4 to 5.3 MPa $m^{0.5}$. Bonfield *et al.* also used the values of the critical stress intensity factor and the critical potential energy release rate to calculate a value of Young's modulus. For this they used the relationship

$$K_{IC} = \frac{E}{1 - \nu^2} G_c \qquad (6.017)$$

They point out that this equation is theoretically only correct for elastically isotropic materials (in plane strain). Into equation 6.017 they substituted a value of 0.2 for the

---

[38]In the published table this value is given as 2.0 not 20.0, it would appear, from the other data in the table, that an error in positioning the decimal point has occurred. This is in more accord with statements in their text and similar results in Behiri and Bonfield (1980), where on increasing a from 16.5 to 18.5 results in a change in $\delta C/\delta a$ of 7.5 to 22 N^{-1}.

Poisson's ratio term, and using the slope of plot of the average values of G_C and K_{IC} for each of the five cross-head speeds used they obtained a value of $E \approx 8.4$ GPa. The authors use the similarity of this derived E to those obtained experimentally as an indication of the validity of the method used to calculate G_C and K_{IC}.

Behiri and Bonfield (1980) adopted a very similar approach, to that of Bonfield *et al.* (1978). In this later work specimens of bovine tibias were machine to the same dimensions as a the earlier work. A similar table of results to that shown in table 6.015 is given. In this later study the range of cross-head speeds was larger: 1.7 to 84×10^{-7} m s^{-1}. Within this range crack velocity increased from 1.75 to 23.6×10^{-5} m s^{-1}, G_C from 1.736 to 2.796 kJ m^{-2} and K_{IC} from 4.46 to 5.38 MPa $m^{0.5}$ (from these values Behiri and Bonfield calculated $E \approx 11.5$ GPa, using the same assumptions as above). At higher cross-head speeds it was found that the fracture travelled too quickly to measure its speed by the method that was used. This also meant that values of the critical stress intensity factor could not be ascertained, as this requires crack length and load data. To obtain some data from these tests to enable comparison with the lower rates, they measured the area of the load-deflection curves and divide this by twice the fracture surface area to give what they called W, the *fracture energy*.[39] Table 6.016 combines the results of these two papers.

It is interesting that the values for the crack velocity in femoral bone are a lot lower than that for tibial bone tested at similar cross-head speeds. The critical stress intensity factor is also affected. The dependence of the critical potential energy release rate and the critical stress intensity factor on crack velocity in both investigations is presented in the later paper. However, no explanation for these differences is proposed in the later paper (Behiri and Bonfield, 1980).

---

[39]W is similar, in its calculation and relation to the process of fracture, to the surface energy γ (or R/2) calculated for the case of a specimen in three point bending. This is assuming the fracture is stable and the load returns gently to zero.

Bone (bovine)	Cross-head speed $\times 10^{-7}$ m s^{-1}	Average crack velocity $\times 10^{-5}$ m s^{-1}	Average G_c kJ m^{-2}	Average K_{IC} MPa m$^{0.5}$	Average W kJ m^{-2}
Femur	17	2.1	0.920	2.4	-
Femur	33	2.2	1.149	2.7	-
Femur	84	3.2	1.260	3.4	-
Femur	170	5.3	2.500	4.2	-
Femur	330	27[40]	2.780	5.2	-
Tibia	1.7	1.75	1.736	4.46	0.764
Tibia	3.3	1.95	1.753	4.61	1.314
Tibia	8.4	3.60	1.806	5.02	1.345
Tibia	17.0	7.60	2.110	5.04	1.562
Tibia	33.0	12.60	2.254	5.23	1.900
Tibia	84.0	23.55	2.796	5.38	2.125
Tibia	170.0	-	-	-	0.125
Femur data from Bonfield *et al.* (1978) Tibia data from Behiri and Bonfield (1980)					

Table 6.016

Average values of G_C and K_{IC} obtained for various crack velocities in specimens of bovine bone

6.5.3. SUMMERY OF THE RESULTS OF PUBLISHED EXPERIMENTS USING CT SPECIMENS

Using a CT specimen permits the examination of stable crack growth. Thus the use of these specimens is perceived to be more consistent with the ideas of LEFM. They also permit the derivation of a range of values from one specimen. The papers reviewed have contained a number of important point.

a) The resistance to crack propagation is dependent on the fracture direction.

b) For the same deformation rate, the fracture rate depends on the orientation of the specimen.

c) The critical stress intensity factor (or resistance to fracture) increases with dry density of the bone.

---

[40]In the published table from which this data is taken this value is given as 2.7 not 27, but within the discussion section of the paper it says the crack velocity increased from 2.1×10^{-5} to 2.7×10^{-4}, this appears to be more in keeping with the other data in the table and the graphical representation of the results.

d) The critical stress intensity factor and the critical potential energy release rate are related in the manner predicted by LEFM.

e) Specimen thicknesses ranging from 1.85 to 3.80 appear to have no effect on the stress intensity factor.

f) An increased deformation rate results in an increased crack velocity and potential energy release rate.

6.6. CENTRAL NOTCH CYLINDRICAL SPECIMENS (CNC)

Another specimen geometry that has been used to examine bone, is the *centre notch cylindrical* (CNC) specimen. This is a cylindrical tube produced from the shaft of the bone, containing a longitudinal crack centrally machined in the wall of the tube. The loading of the specimen is in the form of a sudden increase in internal pressure. This pressure change is produced by a shock tube. The resulting fracture is unstable.

The only study I am aware of that uses CNC specimens is that by Bonfield and Datta (1974b). The reason for its inclusion in this review is that the results of their study are often referred to as a justification for the use of the LEFM theory. However, it should be noted that the test rate used here is several orders of magnitude greater than those achieved with a standard tensile testing machine. The authors estimate a strain rate, in an un-notched specimen of 7 s^{-1}. This test is essentially an impact test. The values of K_{IC} and γ obtained are significantly less than those obtained by the same authors at lower rates: $K_{IC} = 0.23$ MPa $m^{0.5}$ and $\gamma = 2.0$ J m^{-2} .

6.7. JUSTIFICATIONS GIVEN IN THE LITERATURE FOR APPLYING LEFM TO BONE

Although, as has been shown, a number of different workers have applied the theory of LEFM to bone, few have attempted to justify its application. Most authors do not attempt any justification. While others couch their justification in terms that still leave room for doubt. Those that do provide a justification, either imply or explicitly state that the rationale for using linear elastic fracture mechanics is based on two observations. First, that the loading line of bone is basically linear and the behaviour elastic. Second, that Bonfield and Datta (1974b), using CNC specimens, obtained a linear relationship between the failure stress σ_f and $a^{-0.5}$, as is predicted by LEFM. The second observation, is supported by Bonfield and Datta's 1976 paper, in which they used SEN specimens. This form of justification of the 'suitability' or 'applicability' of applying

LEFM is given by Bonfield *et al.* (1978), Bonfield (1981) and Bonfield (1987). However, I reported above that tests similar to those of Bonfield and Datta (1976) were conducted by Moyle and Gavens (1986), and that these later tests appear to be at odds with the earlier work. The more recent results do not show any improved explanation of variations in the fracture stress, when the relationship from LEFM is used in place of that base simply on the remaining cross-sectional area (or more accurately the crack length).

The most thorough, though unpublished, justification for the application of LEFM to bone, is given by Charalambides (1988) in the literature review of her thesis entitled *Comparison of Fracture in Cortical Bone and Analogue Composites.* She not only gives the argument shown above, but also considers three others: First, are the plane strain conditions satisfied? Second, is the process zone small enough that LEFM may still be applied. Third, what is the effect of the anisotropy of bone? These arguments will be similarly treated here and the references expanded upon.

As explained above (section 5.2.3.4) the state of the stress conditions within the structure affect the stress intensity factor. The conditions of plane strain (under which it is normal to test as the SIF is a minimum) are associated with specimens over a certain thickness. Below this thickness the SIF is a function of the specimen thickness (see figure 5.004). Wright and Hayes (1977) that the thickness of CT specimens (from 1.85 to 3.80 mm) had no significant effect on the critical stress intensity factor. Behiri (1982) reports a similar finding for a range of 0.5 to 2.0 mm, in addition he reports that all the fracture surfaces produced were 'very square' that would also imply that testing had been carried out within the plane strain domain.[41]

As stated in section 5.2.4 LEFM is only valid if the size of the process zone at the crack tip is small. Charalambides refers to two values, the smallest dimension and the size of the plastic zone. The ratio of these must exceed 2.5 or 4.[42] These values she attributes respectively to ASTM (1980) and Brown and Srawley (1966). To clarify these ratios I examined these given in BS 5447 (1977), the standard for testing plane strain fracture toughness of metallic materials. This document states that the crack length and the thickness should at least be no less than

$$2.5\left(\frac{K_{IC}}{\sigma_Y}\right)^2 \qquad (6.018)$$

---

[41]However, he reports one thickness effect, that is specimens under 0.5 mm thick proved difficult to align with the result that they underwent mode III type failure. Thus he recommends that no specimen of less than 1 mm thick should be tested.

[42]For the size of the plastic zone she uses the symbol r_p but this is not defined.

To take account of underestimates in the value of the SIF, or some other validity criterion not being met, it is recommended by BS 5447 (1977) that the smallest dimension should be at least

$$4\left(\frac{K_{IC}}{\sigma_Y}\right)^2 \tag{6.019}$$

Inserting the critical values into equation (5.044) for the Irwin process zone (plane stress conditions).

$$(d_y)_{cr} = \frac{K_{IC}^2}{\pi \sigma_Y^2} \tag{6.020}$$

This implies that the smallest dimension, shown here as b, should be

$$b \geq 2.5\pi(d_y)_{cr} \qquad \text{or} \qquad b \geq 4\pi(d_y)_{cr} \tag{6.021}$$

For the two conditions given above. This fits with the practical rule given in section 5.2.3.7 that if d_y is 10 per cent or less of the plate thickness (or $b \geq 5(d_y)_{cr}$ assuming thickness to be the smallest dimension), plane strain is assumed. Robertson *et al.* (1978) in their fracture study of bovine femoral bone in three-point-bending, calculated a 'plastic zone' radius r_y of about 0.017 mm, and they state

> Since this is small with respect to crack length, it is felt that the use of linear elastic fracture mechanics to describe the fracture toughness of bone is justified.

They do not give the size of their specimens, but they are likely to be a few millimetres in the smallest dimension. To calculate this value they used the equation

$$r_y = \frac{1}{2}\left(\frac{\sigma_c}{\sigma_Y}\right)^2 a. \tag{6.022}$$

where σ_c is the 'gross fracture stress', in Robertson *et al's* case this was taken as the outer fibre stress. This equation they obtained from Weiss and Yukawa (1964) who derived it by substituting the equation for the SIF into the following equation (previously given as equation 5.041)

$$r_y = \frac{1}{2\pi}\left(\frac{K}{\sigma_Y}\right)^2 \tag{6.023}$$

This equation is a single case from the solutions of the stresses around a crack. These are the stresses that would open the crack, they thus act across the plane of the crack. Weiss and Yukawa say that

> Fracture mechanics represents a good mathematical model as long as the gross fracture stress is small compared to the yield strength of the material.

Presumably this is the statement that Robertson *et al.* base their justification on. However, I consider that they have made a conceptual mistake in using this equation as a justification for the application of LEFM to bone. Weiss and Yukawa have chosen their words carefully, they do not say that a small fracture stress compared with the yield justifies its use but that failure to comply with this requirement implies that LEFM is not a good model. Weiss and Yukawa also add some refinements to their statement. They point out that the stresses and strains within the 'plastic-zone' must also be considered. Heed should be taken of the fact that the equation is based on assumptions of linear elasticity, and the stress fields around a crack in such a solid. Thus it forms a criterion for the rejection of, not justification for LEFM.

Lakes *et al.* (1990) use the Dugdale model of the process zone (section 5.2.3.9). They consider an edge notch 1 mm long, using values of $\sigma = 64$ MPa and $\sigma_Y = 100$ MPa, thus obtaining a value of $\Delta_y = 0.5$ mm. This result (combined with the equations above) would seem to imply that either plane stress should be assumed, or specimens more than 5 mm thick are required. It should be noted that (as in the case of Robertson *et al.* above) the size of this zone has been obtained using an equation from LEFM; thus the validity of this method of justification is questionable.

All of the justifications (and calculations) based on the on the process zone size, which purportedly show plane strain conditions or only limited departure from the theoretical elastic stress distribution at the crack tip, contain the assumption that the process zone in bone can be equated with the plastic zone in an idealised elastic-plastic material. One of the main themes of this thesis is that bone is not an elastic-plastic material but a time-dependent damage material (see chapter 4). Therefore, I consider that the application of LEFM to bone and antler can not be justified by using equations that assume the process zone is formed from plastically deformed material.

Charalambides (1988), also includes a section on the anisotropy of bone within her justifications section. She points out that the anisotropy of bone was known before fracture mechanics was applied, and that the fracture properties having now been studied in several directions. However, she expands the subject no further. I would like to reiterate that the original theory is based on a homogeneous anisotropic linearly elastic material. This anisotropy reduces the applicability of the theory of LEFM.

Another form of justification, that has already been mentioned (section 6.5.2), is given by Bonfield *et al.* (1978) in which they calculated a value of the transverse Young's modulus from the experimental results of K_{IC} and G_C. The agreement of this value with the ones measured directly, they say suggests that the method they used (standard LEFM equations with a shape correction factor) is a valid basis for the calculation of the SIF.

6.8. NON-LINEAR OR NON-ELASTIC THEORIES OF FRACTURE APPLIED TO BONE AND ANTLER

The only explicit application of non-linear or non-elastic theories to the fracture of bone or antler that I have found is that by Watkins (1987).[43] He obtained values of the work-of-fracture using the Gurney approach, outlined above (section 5.3.3). He performed tests using a form of compact tension (or DCB) specimens, on antler and bovine tibiae for comparison. In both series of tests Watkins forced the crack to run between the osteones. The reindeer antler specimens he used were 1 to 2 mm in thickness, 30 to 40 mm deep and 60 mm long, and those made from bovine bone were larger being $4 \times 40 \times 80$ mm. To keep the crack running centrally in the bone specimens a notch was machined down each side (the antler specimens were too thin to cut grooves in). The resultant cracking was between the osteones and thus longitudinal with reference to the original bone. The specimens were loaded at 3.33×10^{-5} m s^{-1} until the crack had progressed approximately 3 mm, (the actual distance was recorded). The specimens were loaded and unloaded a number of times to obtain more data. His results are reproduced below. Like Piekarski (1970), Watkins records a lower value of work-of-fracture for an unstable fracture compared to the values for stable ones.

Type of fracture	Work-of-fracture kJ m^{-2}	n
Stable fracture	2.38 ± 0.90	5
Unstable fracture	0.66 ± 0.24	7

Table 6.017 After Watkins (1987)

Work-of-fracture of bovine tibia specimens

Specimen	Work-of-fracture kJ m^{-2}	Crack path	n
Reindeer i	5.62 ± 0.917	—	6
Reindeer ii	6.86 ± 1.110	—	6
Reindeer iii	7.00 ± 1.090	—	5
Reindeer iv	13.30 ± 2.620	∠	5
Reindeer v	13.10 ± 2.680	∠	5
Reindeer vi	11.30 ± 1.580	∠	5

Table 6.018 After Watkins (1987)

Work-of-fracture of reindeer antler specimens

---

[43]I have said this is the only explicit application of a non-linear theory to bone and antler, as Watkins says his reason for using it is the questionable validity of LEFM for these materials. However, other techniques that have been used are also implicitly valid for non-linear elastic materials, such as the Tattersall and Tappin test.

Watkins found the crack growth to be 'slow and controllable' in antler but 'fast and catastrophic' in bone. The crack propagation in the antler specimens was far more stable. In some cases the fracture in antler deviated from the shortest path across the specimen, it was noted that this resulted in an increase in the work-of-fracture. The toughness of antler between the osteones is 2 to 3 times that of bone tested in the same direction.

6.9. CONCLUDING OBSERVATIONS

The previous sections of this chapter contain descriptions of some published investigations of the fracture properties of bone and antler. These investigations have studied different bones and used different specimen geometries and test conditions. The authors have also placed the emphasis of their work on different findings. (Nearly all the workers have assumed that LEFM is applicable to the materials studied. It is this approach I will discuss here.)

There is a large degree of variation between the results obtained in the different studies reviewed. There is also some flexibility in the equations used and in their interpretation. However, possible reasons for these variations are contained within the results. For clearly the experimentally obtained value of the critical stress intensity factor (for example) is affected by a number of variables. Some of these are given in table 6.019.

In the previous sections I have questioned the validity of the interpretation of one commonly applied equation and the results obtained from it. That is the concept of an intrinsic flaw or what I have called the *natural edge crack*. I suggest that this has no relation to an individual structure present in the untested bone, but that the natural edge notch is some measure of the global effect of the additional flaws present throughout the structure of the un-notched specimen at the time of failure. Therefore the area of the natural edge crack will be dependent on the specimen width. For example, if it is viewed as an expression of the global effect changes in structure,[44] then a wider specimen would exhibit a larger amount (but the same proportion) of this change in structure. I use the term 'changed structure', as the notched specimens that are used to derive the relationship between failure stress and notch length are composed of the same material, they are not homogeneous. Therefore they will also be weakened (or strengthened) by the same internal structures as the un-notched specimens.

---

[44]For example, if there were small which cracks emanated from the osteocyte lacunae.

Variable	Effect	Source of evidence
Bone density	Increasing density results in an increase in the obtained K_{IC}.	Wright and Hayes (1977) Behiri and Bonfield (1984)[45]
Bovine bone or antler	Antler has a higher work-of-fracture	Currey (1979a) Watkins (1987)
Type of bone: femur or tibia	Bovine tibial bone has a higher K_{IC} than femoral bone.	Bonfield *et al.* (1978) Behiri and Bonfield (1980)
Strain rate, cross-head speed or crack velocity	At moderately slow rates an increase in the rate of the fracture process results in an increase in K_{IC}	Robertson *et al.* (1978) Melvin and Evans (1973) Bonfield *et al.* (1978) Behiri and Bonfield (1980) Watkins (1987)
	When the rate is near to or is catastrophic, the value of K_{IC} falls. There is also a decrease in the measured value of the work-of-fracture.	Piekarski (1970) Behiri and Bonfield (1984)[46] Watkins (1987)
Fracture direction	The preferential fracture direction is longitudinal.	Watkins (1987) Behiri and Bonfield (1989)
Notch tip radius	The fracture properties do not appear to be dependent on the notch tip radius.	Bonfield and Datta (1976) Moyle and Gavens (1986) Robertson *et al.* (1978)
Moisture content	Dry bone or antler has a lower work-of-fracture than the wet material	Melvin and Evans (1973) Watkins (1987)

Table 6.019

The effect of a number of variables on the fracture properties of bone

A number of justifications for the application of LEFM have been given in the literature, those that I am aware of have been mentioned in section 6.7, where some comments were made on them. The literature also contains a number of criticisms of or reasons to reject this approach, or the principles on which it is based. That due to Piekarski (1970) has been mentioned. Another is mentioned by Lakes *et al.* (1990), when discussing SEN specimens with short notches they say that it may be appropriate to view the notch as having a non-zero root radius of curvature they continue:

---

[45]Quoted in Bonfield (1987).
[46]Quoted in Bonfield (1987).

> The notch may be considered as half an ellipse and the Inglis formula
>
> $\sigma_{fr} = \sigma_{ult} / \left[1 + 2(c/r)^{1/2}\right] Y$ is applied for an elliptical hole. Here, σ_{ult} is the ultimate tensile strength of a un-notched specimen, c is the notch length, and r is its radius of curvature. Such a model underestimates the strength of bone in the presence of a notch by more than a factor of two.

The reports that the experimentally obtained values of K_{IC} are independent of notch tip radii, casts doubt on the appropriateness of using the LEFM approach.

The critical stress intensity factor is defined as a material property, like Young's modulus. Thus the rate dependence of this quantity decreases the ability to justify using this quantity. The dependence of this, supposedly, material property on other factors implies that it should not be quoted without some reference to the test conditions.

Perhaps what I am trying to say, and it is a question that does not appear to be asked within the literature on bone or antler, can best be expressed in the words of Harris *et al.* (1988) in their paper *Strength and toughness of fibre composites.*

> There is of course no reason why a function of the form $K_c = Y \sigma (\pi a)^{1/2}$ cannot be calculated for any type of behaviour; the important question is whether the value of the function so calculated has any significance.

In the sections that follow I do calculate this function, among others, and then discuss if it has any significance for specimens of reindeer antler and bovine bone. Further investigation of the fracture mechanics of bone and especially antler may provide more detailed information on the failure mechanisms of these materials. When the information from the notch sensitivity tests is combined with that from the other mechanical tests it may be possible to produce a better description of the failure process of bone and antler.

7

NOTCH SENSITIVITY AND FRACTURE MECHANICS OF BONE AND ANTLER: EXPERIMENTAL RESULTS

All bones are relatively brittle compared with soft tissues, and their work of fracture seems to be less than that of wood. This brittleness limits the structural risks which a large animal can accept. As we have already pointed out in connection with ships and machinery, the length of the Griffith crack is an absolute, not a relative distance. That is to say, it is just the same for a mouse as it is for an elephant. Furthermore the strength and stiffness of bone are much the same in all animals. This being so, it rather looks as if the largest size of animal which can be regarded as moderately safe is somewhere round about the size of a man or a lion. A mouse or a cat or a reasonably fit man can jump off a table with impunity; it is distinctly doubtful if an elephant could. In, fact elephants have to be very careful; one seldom sees them gambolling or jumping over fences like lambs or dogs.

J. E. Gordon (1978)

Structures or why things don't fall down

7.1. INTRODUCTION

The initial objective of my own fracture mechanics tests was to investigate the application of Purslow's (1991) approach to predicting the failure characteristics of antler. His study was more concerned with the notch sensitivity of non-linear elastic materials than with the derivation of fracture criterion, such as K_{IC}, G_{IC} or J_{IC}, so the tests I present here will be referred to as *notch sensitivity tests*. Purslow gives relationships between failure stress σ_f, or failure strain ε_f, and the ratio of the notch length to the specimen width a/w, for materials whose stress-strain response is described by $\sigma = k\,\varepsilon^n$. A full explanation of Purslow's theory is given in chapter 5, above. The initial objective of my work was expanded to include tests on bovine bone and other forms of analysis, including the application of equations from linear elastic fracture mechanics (LEFM). To help distinguish between materials that display some notch sensitivity and materials that are notch sensitive in the manner described by LEFM, I will introduce the term *classically notch sensitive*, by which I mean that the relation between the failure stress and the notch length is that predicted in LEFM ($\sigma_f \propto a^{-0.5}$). Material can therefore be placed in three groups: first those which are notch insensitive (their strength being dependent on the minimum cross-sectional area only); second, the *classically notch sensitive* materials, third, materials that are notch sensitive, in that their strength is not solely dependent on their cross-sectional area, but is also dependent on the length of any notch or discontinuity within the specimen. This last group can be envisaged as the general case of which LEFM is just one specific example.

The tests used to assess the notch-sensitivity of bone and antler were also used to obtain some recordings, photographically and on video tape of the optical changes, in the form of whitening at the notch tip, that occur in both bovine bone and antler when the specimen is loaded. Due to the importance of these optical changes, and similar observations made during tensile and creep tests, this result is examined separately in chapter 8. However, some of the quantitative results are examined in this chapter, with reference to their possible effect on the fracture behaviour.[1]

Another aspect of the fracture of bone and antler that is examined is the rate dependence of this process. To examine the effect of the loading rate on the fracture of antler and bone, specimens were extended at four different cross-head speeds. The materials and cross-head speeds used here are the same as those used in the examination of the rate dependence of the tensile properties of bone and antler presented in chapter 4.

---

[1]To avoid confusion between the macroscopic crack (fracture mechanics) and the microscopic cracks (damage), I will use the terms *fracture* and *microcrack* respectively. This results in some slight changes in nomenclature. For example the *crack tip process zone* become the *fracture tip process zone*.

Analysis of the results of these notch sensitivity tests produced some relationships that may help to explain or at least describe the notch sensitivity of these materials (for the specimen geometry used). In this chapter the analysis was conducted using regression equations as in chapter 4. However, not all the regression equations are quoted, as occasionally the form of the equation is not relevant only the predictive power of one variable compared to another. The main findings of this analysis of the notch sensitivity of bone and antler and some comparisons with un-notched behaviour are presented in section 7.10. In chapter 9 the results of notch sensitivity tests presented here and those given in the literature (reviewed in chapter 6) are combined with the results of creep, tensile and impact tests, to create an overall picture of the failure of bone and antler.

7.2. SPECIMEN GEOMETRY, TEST MATERIAL, PREPARATION TESTING AND SOME INITIAL FINDINGS

This section contains some information on the type of specimen that was used (and why) and the materials examined. Some initial test results are examined. The results of these initial tests, originally designed to indicate the size of the notch tip radius to be used in the following tests, demonstrated that improvements were required in the specimen preparation technique.

7.2.1. FACTORS THAT DETERMINED THE SPECIMEN GEOMETRY

Because of the original objectives of this work, it was decided, in discussion with Dr Peter Purslow,[2] that the same specimen geometry as that used in the creep and tensile tests could be adapted for use in these tests. There were three important factors that contributed to this decision.

a) Purslow's approach was developed around tensile specimens containing a single edge notch (SEN); this dictated the shape of the specimen.

b) Tests were also to be performed on un-notched specimens. (This was to permit comparisons to be made. These tests also enabled predictions of the un-notched behaviour of the notched specimens to be made.) Therefore, the failure load of these un-notched specimens had to be within the working range of the available load cell and clamping system (0 to 1000 N); this determined the maximum cross-sectional area of the specimens.

c) An appropriate width to thickness ratio was required. This was governed, to some degree, by the radius of curvature and thickness of the compact bone in the antlers

---

[2]Muscle and Collagen Research Group, University of Bristol Veterinary School.

used. Due to the previously successful results, during creep tests, and my experience in their production, I decided to retain the specimen size of approximately 4 by 1.25 mm (in the gauge section) and augment these with larger sizes of about 5 or 6 mm by 1.25 mm.

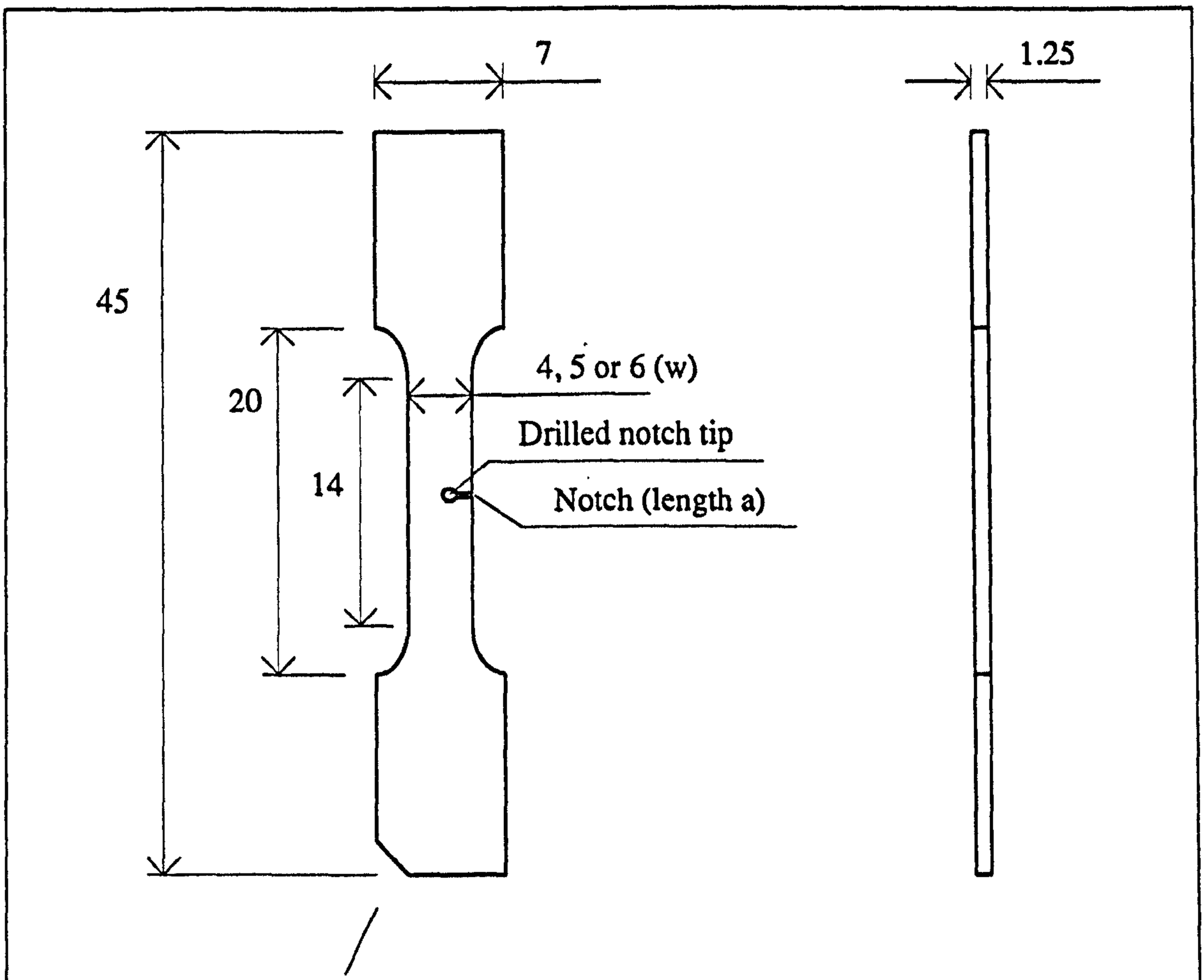

Note: This is not a true radius, as the flare at the reduced cross-section is more gradual. The specimen is viewed in its *natural* orientation, the largest surface seen here was that closest to the surface of the original bone.

Figure 7.001

Basic shape and dimensions of the SEN specimens used in this study

7.2.2. TEST MATERIAL

All the antler specimens used for notch sensitivity tests were prepared from the appendages of red deer. Of the four antlers used two were from the same animal, although only the data from one of this pair is analysed here, (see table 7.001).[3] The bone specimens were mostly manufactured from bovine femoral bone. However, some bovine tibial bone was also used. More information on the material used is given in tables 7.001 and 7.002.

Antler type	Comments	Identification numbers (data used)	Data Sets
Red deer	Un-cast antler, from young stag shot 1989, clean of any velvet.	13/03/91/01 - 13/03/91/46 (13) (23)	NA1 NA2
Red deer	Un-cast, animal assumed to be young because of small number of tines, clean of any velvet.	04/06/91/01 - 04/06/91/113 (93)	NA3
Red deer	Distal end sawn off, assumed un-cast, no velvet on antler when received. This antler is from the same animal as that below. Both were in the same condition.	10/11/91/01 - 10/11/91/104 (30) (19)	NA4 NA5 (TA1)
Red deer	See above. Used to produce notch sensitivity, tensile and impact specimens. The notch sensitivity data are not analysed here, but images of these tests are presented in chapters 8, appendix 11 and on accompanying video tape.		(IA1)

Table 7.001

Source, storage and usage of antler test material, used for notch sensitivity tests

[3]The notch sensitivity tests conducted using material from the second antler were used to obtain images of the optical effects. These images are discussed in chapter 8, appendix 11 and presented in the accompanying video recording.

Bone type	Comments	Identification numbers (data used)	Data Sets
Femur (1)	Approximately 18 months old, epiphysis un-fused. Collected fresh from butcher, then stored in freezer for four days before it was cut into slabs.	19/08/91/01 - 19/08/91/33 (27)	NB1
Femur (2)	Approximately 18 months old, epiphysis un-fused. Collected fresh from butcher, then stored in a freezer for four days before it was cut into slabs.	19/08/91/34 - 19/08/91/58 (21)	NB1
Femur (3)	Approximately 18 months old, epiphysis un-fused. Collected fresh from butcher, then stored in freezer for four days before cutting into slabs.	10/09/91/01 - 10/09/91/24 (16)	NB2
Femur (4)	Unknown age, only diaphysis obtained, stored in freezer for indeterminate time.	03/10/91/01 - 03/10/91/34 (32)	NB3
Tibia (1)	Approximately 18 months old, epiphysis un-fused. Collected fresh from butcher, then stored in freezer for 19 days before cutting into slabs.	03/10/91/35 - 03/10/91/52 (16)	NB3
Tibia (2)	Approximately 18 months old, epiphysis un-fused, fresh cut into slabs same day as obtained.	03/10/91/53 - 03/10/91/75 (17)	NB3
Femur (5)	Approximately 18 months old, epiphysis un-fused. Collected fresh from butcher, then stored in freezer for 4 days before cutting into slabs.	28/10/91/01 - 28/10/91/39 (31) (3)	NB4 NB5 (TB1)
Femur (6)	Approximately 18 months old, epiphysis un-fused. Collected fresh from butcher, then stored in freezer for 8 days before cutting into slabs.	01/11/91/01 - 01/11/91/52 (13)	NB5 (TB1)

Table 7.002[4]

Source, storage and usage of bovine bone test material, used for notch sensitivity tests

7.2.3. SPECIMEN PREPARATION

The method used to prepare the specimens was essentially the same as that described in section 4.2.3 (for the preparation of the tensile specimens of the same materials, including the determination of E_b). The difference between the two methods

[4]The numbers in the bone type column are used to label which bones the specimens were obtained from to permit examination of this variable, especially in data set NB3.

was the addition of a notch in this case. The notches used took three forms: first those with a drilled tip; second those where the tip was that produced by the saw used to cut the notch; third those that were sharpened with a razor blade. The first type of notch is shown diagrammatically in figure 7.001. Before testing the dimensions of the notch were measured using a travelling microscope, with a graduated eye piece for the smaller dimensions. These measurements were performed on both sides of the specimen (except in the case of specimens for the initial tests).

This method of preparing the specimens was developed in response to the results of the initial tests described below. A full description of the method used to prepare all the specimens, including figures, is given in appendix 2. When the method of specimen preparation is at variance with the method given in that appendix it will be noted in the main text.

7.2.4. SPECIMEN TESTING

Because different variables were investigated the method of testing was not exactly the same for all specimens. However, these changes mostly consisted of using different cross-head speeds and methods of data collection. Some of the common test features are summarised below. Any variations will be noted where relevant.

a) An Instron 1122 was used in all tests.

b) The load transducer was an Instron tensile load cell, rated by the manufacturer at 100 kg full scale (approximately 9810 N).

c) The strain (or more correctly extension) transducer was either a 10 or a 50% static extensometer produced by Instron, both of which had a nominal 10 mm gauge length. These had been waterproofed as described in section 4.2.4.

d) The mechanical data (stress, strain and time) were recorded using the AJS/BBC data collection system described in appendix 1.[5]

e) All specimens were clamped in the same jaws that were used for the tensile and creep tests (chapter 4). In this case, as for the tensile tests, the bottom jaw was fixed to the base of the test machine.

f) All specimens were tested while completely submerged in tap water at a temperature within one degree of 37°C.

g) In all except the initial tests the orientation of the specimens was consistent. The specimens were tested in what I have defined as their natural orientation. (See section 4.2.3 or appendix 2.)[6]

---

[5]The exceptions to this being the first set of tests presented here and a set that were designed to produce video images for conference presentation (see appendix 11). These both used chart recorders to obtain the load-time response of the specimens (rather than load-extension).

7.2.5. INITIAL TESTS ON SEN SPECIMENS OF ANTLER, DEFINITIONS, RESULTS AND ANALYSIS (DATA SET NA1)

This section contains a description of the initial tests conducted on SEN specimens of antler, and an analysis of the results. The results obtained from these tests determined the specimen preparation methods used for the tests that followed. These initial tests also influenced the experimental design of the later tests. The definitions of various quantities calculated from the results of these tests and some of the methods of analysis used in this section are also used in the examination of later tests on both antler and bovine bone.

7.2.5.1. INITIAL TESTS: THE FIRST SEARCH FOR A CRITICAL NOTCH TIP RADIUS

When I initially discussed this work with Dr Purslow, we decided that tests should be conducted to investigate and account for two basic variables, specimen width and notch length. However, I considered that before such an investigation could be undertaken an appropriate notch tip radius had to be found. So, in the initial series of tests (the results of which are contained in data set NA1) 13 specimens, 8 from the base of the antler and 5 from the tip, were prepared. The specimens were about 4 mm wide, with notches having a variety of tip radii. The holes used to produce the notch tips ranged in diameter from 0.19 mm to 1.78 mm. These specimens were prepared in a similar way to that described above in appendix 2. However, there were two differences: first, a datum corner was not employed; second, the notch dimensions were measured on one surface only. The notches in the specimens from the antler base were prepared first, and these specimens had been tested, and preliminary analysis conducted, before those from the tip were fully prepared.[7] The procedure used for these initial tests was also slightly different from that described above; the Instron's chart recorder was used to monitor the load with respect to time. No extension or strain measurements were taken. The specimens were fractured using a cross-head speed of 8.3×10^{-5} m s^{-1} [5 mm min^{-1}].

It was stated in section 5.2.3.6 that the tip radius, above a critical size, can affect the value of the stress intensity factor in a linear elastic material. As the tip radius, ρ, increases in size above its critical value, ρ_c, the stress intensity factor associated with fracture growth also increases. If the tip radius is less than its critical value the

---

[6]Some of the images in chapter 8 appear to contradict this. However this results from the camera being, deliberately, mounted up-side-down.

[7]The specimens were taken from the extremes of the antler to highlight any possible changes due a variation in the material's mechanical properties through the length of the structure.

corresponding stress intensity factor (assuming the relevant conditions are satisfied) is a constant and minimum value, K_{IC}. I hoped that a range of tip radii would enable me to obtain a plot for antler (similar to figure 5.005) from which the value of ρ_c could be determined. Once such an estimate of ρ_c had been obtained I planned to conduct all further tests using a tip radius that was smaller than this critical value. If such a smaller notch tip radius is used it can be assumed that the values of the stress intensity factor obtained were more likely to be the critical, and minimum, values. (The assumption that LEFM is valid is implicit in this approach. However, it has already been shown that the stress-strain response of antler is non-linear, so this approach must be viewed as a first approximation only.)

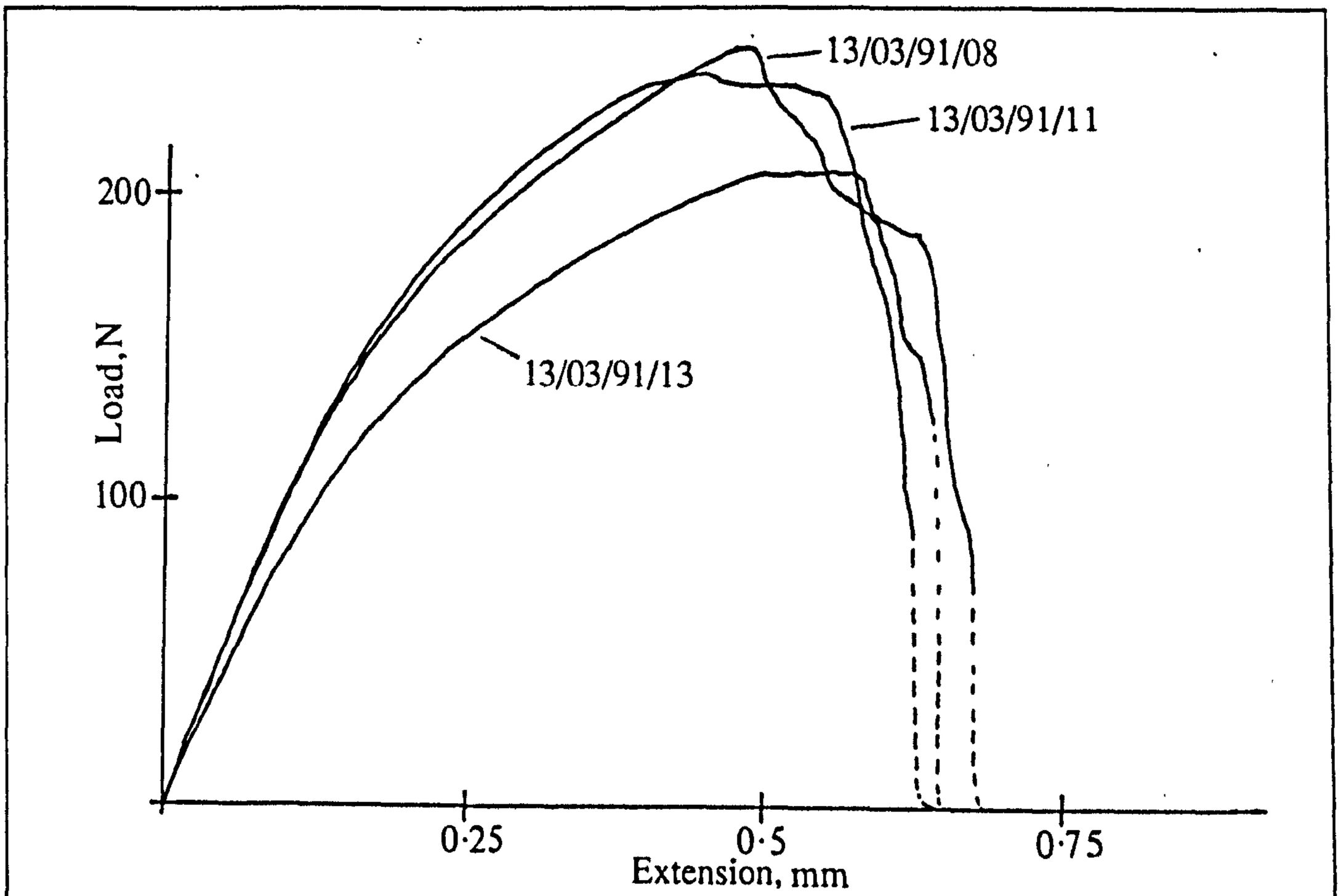

Redrawn from the original chart recordings

Figure 7.002

Load-time plots obtained during the initial tests of SEN specimens of antler (NA1)

Figure 7.002 contains some stress-time plots obtained from the tests of SEN specimens of antler examined here. There are a number of important features shown in this figure that are difficult to quantify. However, they could have a profound relationship with the fracture process. These features may also provide some information of how the fracture process should be described and quantified. The two most important features are: the obvious curvature of the loading line and the controlled propagation of the fracture.

The pronounced curvature of the loading line is not surprising considering that a similar behaviour is obtained for un-notched specimens. However, if such curvature were to occur in a material that in the un-notched state displayed a linear response (until it started to fail), the application of fracture theories would have to be questioned. This is because such curvature could indicate that the material is starting to fail by a non-fracture process, for example yielding. In the case of antler, where both un-notched and notched specimens show a curved loading line, it is unclear if the curvature in the response of the notched specimens is due solely to the normal mechanical response of the material, or to a combination of the normal mechanical response and the tensile failure process.

The slow fracture propagation, and the convoluted path the fracture takes across these specimens is shown (for some similar specimens) in chapter 8. Clearly, the rip-like fracture propagation implies that energy still has to be supplied to the fracture after its initiation. The amount of energy available to propagate a fracture is, as explained previously, dependent on the specimen geometry and the test machine used. Therefore, this observation is not of much significance in its own right. However, I show later that bovine bone specimens of the same shape, tested under the same conditions, behave quite differently. This slow ripping process would suggest that antler has some mechanism that avoids catastrophic fracture under the conditions that would cause such a self propagating fracture in bovine femoral bone. This mirrors the observations made during the impact test described in chapter 1.

The first analysis of the results was performed (immediately after the tests) on the data from the eight specimens cut from the base of the antler. To ascertain whether stress intensity factor was affected by the radius of the notch, the maximum load value and the relevant dimensions were substituted into the equation for K_{IC}. The shape correction factor used in that primary analysis of the data was the same as that used by Bonfield and Datta (1976) (equation 6.004), which assumes the specimen is loaded by way of pin-jointed ends. However, the specimens used in this work were clamped at their widened ends. I thus considered that this pin-jointed shape correction factor was inappropriate.

Rooke and Cartwright (1976) report the correction factor obtained by Harris (1967) for an edge notch in a sheet which does not bend as

$$Y = \frac{5}{\sqrt{20 - 13(a/w) - 7(a/w)^2}} \qquad (7.001)$$

Although using equation 7.001 may give a better approximation to the test conditions, the antler specimens do bend (as examination of the photographic and video evidence has shown). I therefore proposed that <u>if LEFM is valid for specimens of antler</u>, the true shape correction factor will fall between that for the unbending sheet and that for the pin

jointed specimens.[8] A graph of these shape correction factors is given in figure 7.003. I assumed that the pin-jointed correction factor formed the upper bound and that for the unbending sheet the lower bound. Intuitively, I would expect the true shape correction factor to fall closer to that for the unbending sheet, equation 7.001. As it was unclear which shape correction factor was more appropriate, some of the data analysis is accomplished by examining the stress intensity factors calculated alone and then containing each of these correction factors. As the values obtained for the SIF depend on the shape correction factor used, and they are experimentally determined quantities, a nomenclature other than K_{IC} will be employed: K^{I}_{IQ}, K^{P}_{IQ}, K^{U}_{IQ} and K^{*}_{IQ} (these are defined below).

7.2.5.2. THE DEFINITIONS OF K^{I}_{IQ}, K^{P}_{IQ}, K^{U}_{IQ} AND K^{*}_{IQ}

The values obtained from experimental tests are not necessarily the true values of K_{IC} as it was defined in chapter 5. The difference could be due to many things, for example specimen thickness (and thus stress conditions), specimen size and so on. There is also the more fundamental question of whether the critical stress intensity factor is valid for the material that is being examined. I will therefore introduce some other nomenclature for the experimentally derived values. I consider three forms of derivation of the *so called critical stress intensity factor*. These use the same original form but in two cases a shape correction factor is applied. I used the term 'so called critical stress intensity factor', because this quantity is by definition a material property and constant; however by using different shape correction factors different values will result. Clearly, even if LEFM is truly applicable at least two of the three calculated forms of the critical stress intensity factor will be incorrect. The various values of the stress intensity factor obtained in this work are determined as follows.

a) The *infinite sheet* stress intensity factor, K^{I}_{IQ}. This equation is from the original theory (see chapter 5), and contains no shape correction factor. Repeated here as

$$K^{I}_{IQ} = \sigma_f \sqrt{\pi a} \qquad (7.002)$$

b) The *un-flexing* finite sheet SIF, K^{U}_{IQ} (from equations 7.002 and 7.001)

$$K^{U}_{IQ} = \frac{5}{\sqrt{20 - 13\left(\frac{a}{w}\right) - 7\left(\frac{a}{w}\right)^2}} \sigma_f \sqrt{\pi a} \qquad (7.003)$$

---

[8]This logic was also applied to the examination of SEN specimens of bovine bone, for which it appears to be more justifiable.

c) The *pin-jointed* finite sheet stress intensity factor, K_{IQ}^{P} (from equations 7.002 and 6.004)

$$K_{IQ}^{P} = \left(1.12 - 0.23\left(\frac{a}{w}\right) + 10.6\left(\frac{a}{w}\right)^{2} - 21.7\left(\frac{a}{w}\right)^{3} + 30.4\left(\frac{a}{w}\right)^{4}\right) \sigma_f \sqrt{\pi a} \qquad (7.004)$$

Where σ_f is the failure stress, taken as the maximum value of the nominal stress, a is the notch, or fracture, length and w the specimen width (see figure 7.001).

d) The symbol K_{IQ}^{*} will be used when the stress intensity factor referred to is, or could be, any of K_{IQ}^{I}, K_{IQ}^{P}, K_{IQ}^{U} individually or collectively. (Remember that the general term 'stress intensity factor' is also abbreviated to SIF.)

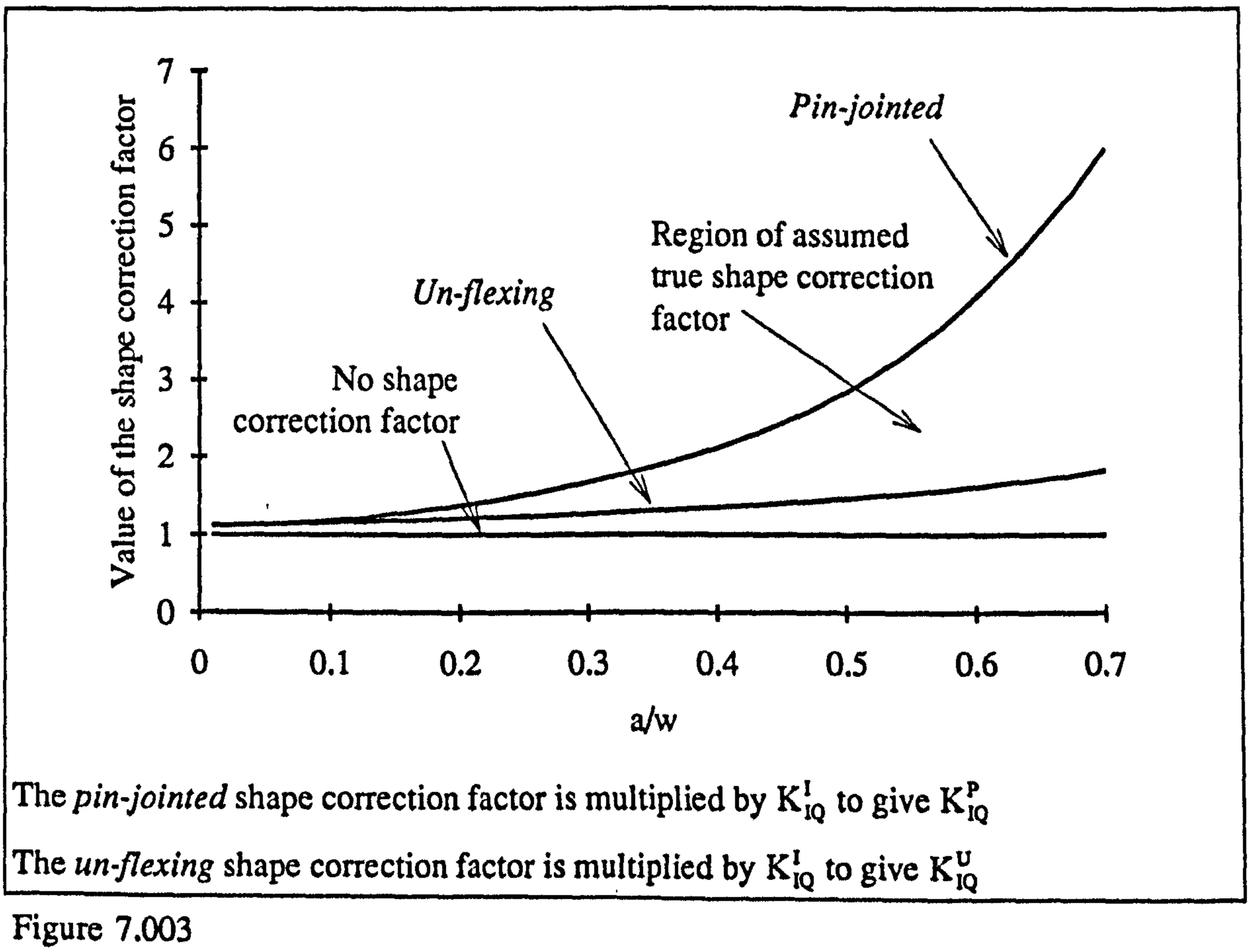

Figure 7.003

Values of the pin-jointed and un-flexing shape correction factors over a range of values of the ratio of notch length to specimen width, for SEN specimens

7.2.5.3. INITIAL TESTS: RESULTS

Antler specimen	Antler tip or base	Bending stiffness E_b GPa	Square root of tip radius $\rho^{0.5}$ $(10^{-2})m^{0.5}$	Failure stress σ_f MPa	Notch length a mm	Width w mm	Stress intensity factor K_{IQ}^P MPa $m^{0.5}$
13/03/91/04	Base	10.45	1.77	68.79	0.93	3.94	5.42
13/03/91/05	Base	9.73	2.17	53.66	1.15	3.98	5.25
13/03/91/08	Base	9.85	2.98	57.66	1.43	3.91	7.48
13/03/91/09	Base	9.48	2.16	61.99	1.15	3.93	6.11
13/03/91/10	Base	10.21	1.37	60.42	0.88	3.94	4.52
13/03/91/11	Base	8.88	1.94	52.33	1.19	3.92	5.36
13/03/91/12	Base	8.53	1.94	57.71	1.13	3.94	5.54
13/03/91/13	Base	7.86	1.00	48.58	0.75	3.93	3.19
Mean	Base	9.38	1.92	57.64	1.07	3.94	5.36
s.d.		0.89	0.59	6.29	0.21	0.02	1.23
13/03/91/96	Tip	7.57	1.94	58.20	1.06	3.97	5.24
13/03/91/97	Tip	6.26	1.94	40.79	1.06	3.97	3.67
13/03/91/98	Tip	7.70	1.03	46.82	0.81	3.94	3.28
13/03/91/99	Tip	7.48	0.97	48.71	0.78	3.99	3.27
13/03/91/100	Tip	6.64	1.32	47.96	0.78	3.97	3.22
Mean	Tip	7.13	1.44	48.49	0.90	3.97	3.74
s.d.		0.64	0.47	6.26	0.04	0.02	0.86
Mean	Both	8.51	1.73	54.12	1.01	3.95	4.73
s.d.		1.37	0.58	7.59	0.21	0.02	1.34

Comments;

The units of the square root of the notch tip radius are given as $(10^{-2})m^{0.5}$. The meaning of this can be clarified by taking the example of a 2 mm diameter drilled hole, the radius ρ = 1 mm = 0.001 m, thus $\rho^{0.5}$ = 0.0316 $m^{0.5}$. I have then expressed this as $\rho^{0.5}$ = 3.16 $(10^{-2})m^{0.5}$.

Table 7.003

Data Obtained from the Initial set of tests on notched antler specimens (Set NA1)

The data from the initial tests described above and the calculated values of the stress intensity factor with the pin-jointed shape correction factor are given in table 7.003. (Information on how to obtain the full data sets is given in appendix 4.) Other quantities were derived from this data, these are analysed, along with those in the table, in the following sections. A few results are apparent just by visual inspection of table 7.003. For example there is a considerable difference between the stress intensity factor, K_{IQ}^{P}, obtained for the material from the tip of the antler compared with that from the base. There also appears to be a relationship between K_{IQ}^{P} and the square root of the notch tip radius.

7.2.5.4. INITIAL TESTS: ANALYSIS OF THE RESULTS (DATA SET NA1)

The main method of analysis used here is linear regression, using one or more explanatory variables.[9]

Analysis of the first set of results obtained, those from the specimens at the base of the antler, showed a very strong correlation between K_{IQ}^{P} and $\rho^{0.5}$, $R^2 = 91.4\%$ (figure 7.004). With the additional data from the specimens from the antler tip this fell to $R^2 = 80.1\%$. These correlations were initially assumed to correspond to the relationship of the SIF to the tip radius, as expected (figure 5.005). No constant value of K_{IQ}^{P} was obtained at the sharper notch tips; thus it appeared that the critical notch tip radius was smaller than all of those used here. However, further analysis showed that this result is, unfortunately, erroneous.

The strong correlation of K_{IQ}^{P} and the tip radius appears to be due to one, poorly planned, stage of the specimen preparation (shown graphically in figure 7.005). During the drilling of these specimens the same datum was used to locate the edge of the specimen on the drilling machine (figure A2.001, appendix 2). The table of the milling machine was not moved between the drilling of the different specimens. Thus the centre of the hole was the same distance from the edge of the specimen. This resulted in a larger drill not only giving a larger tip radius but a longer notch. This error produced an undesirable correlation between $\rho^{0.5}$ and a/w, $R^2 > 90\%$ (*h* and *i* table 7.004). The shape correction factor is supposed to remove any correlation with a/w. However, it was found

---

[9]The statistical analysis was performed using Minitab release 7. All values of R^2 quoted for the results obtained in this work are adjusted for the number of degrees of freedom, as defined by Minitab (1989). The t values are quoted are those given by this package. Appendix 12 contains a table relating the Student's t values to *p* values for the levels of significance used in this study.

that there was a strong correlation between K_{IQ}^{P} and a/w (for the specimens from the base of the antler $R^2 = 80.7\%$). Therefore, the correlation between K_{IQ}^{P} and $\rho^{0.5}$ may have arisen due to these interrelations.

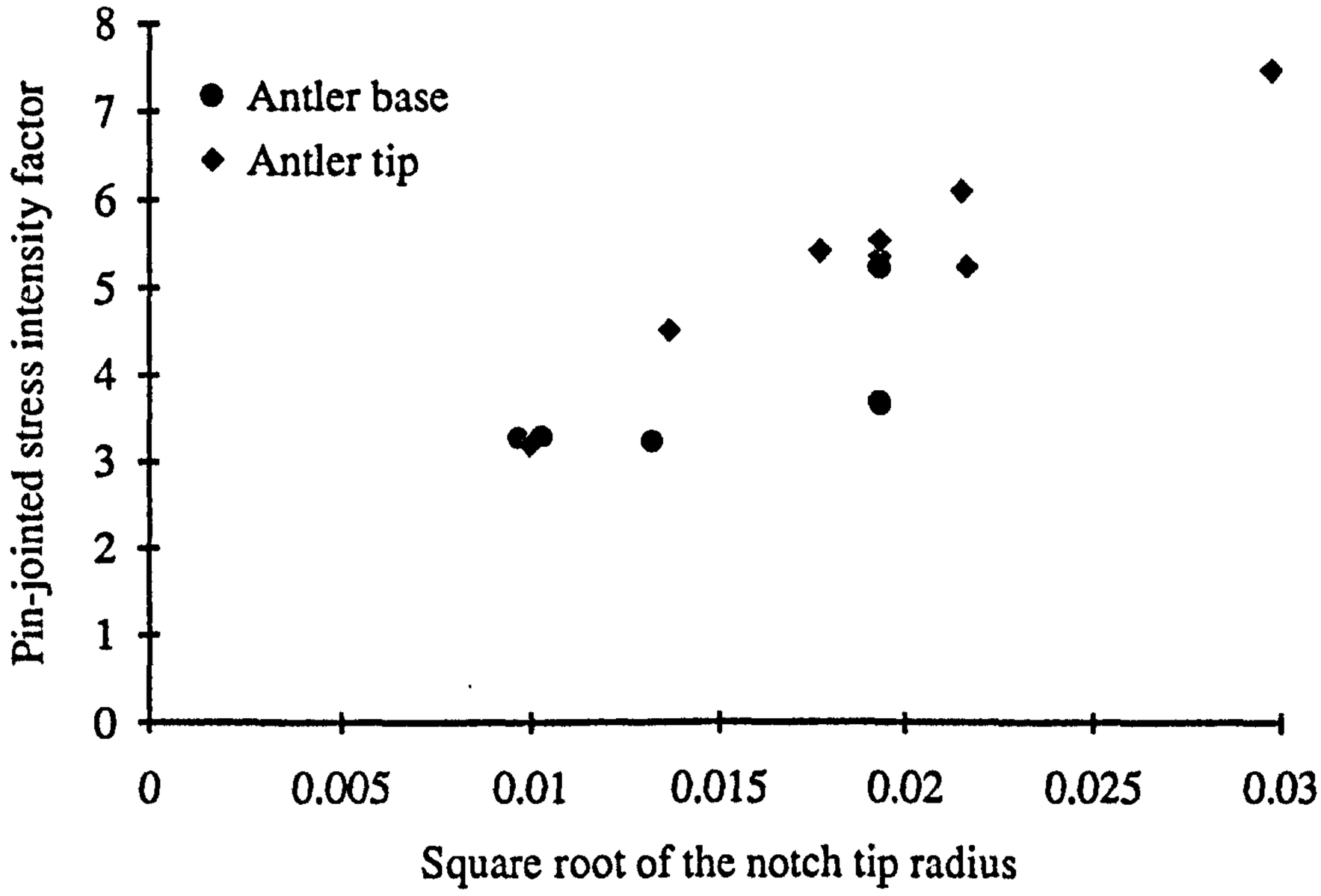

Units:

K_{IQ}^{P} *Pin-jointed* critical stress intensity factor, MPa $m^{0.5}$

$\rho^{0.5}$ Square root of the initial notch tip radius, $m^{0.5}$

Comments:

The symbolism used in reference to the graph is the same as those used in the tables of regression equations presented in this chapter. For example in the regression equations the symbol K_{IQ}^{P} is used for the pin-jointed critical stress intensity factor and it will be analysed in units of MPa $m^{0.5}$.

Figure 7.004

The values of the pin-jointed critical stress intensity factor and the square root of the notch tip radius

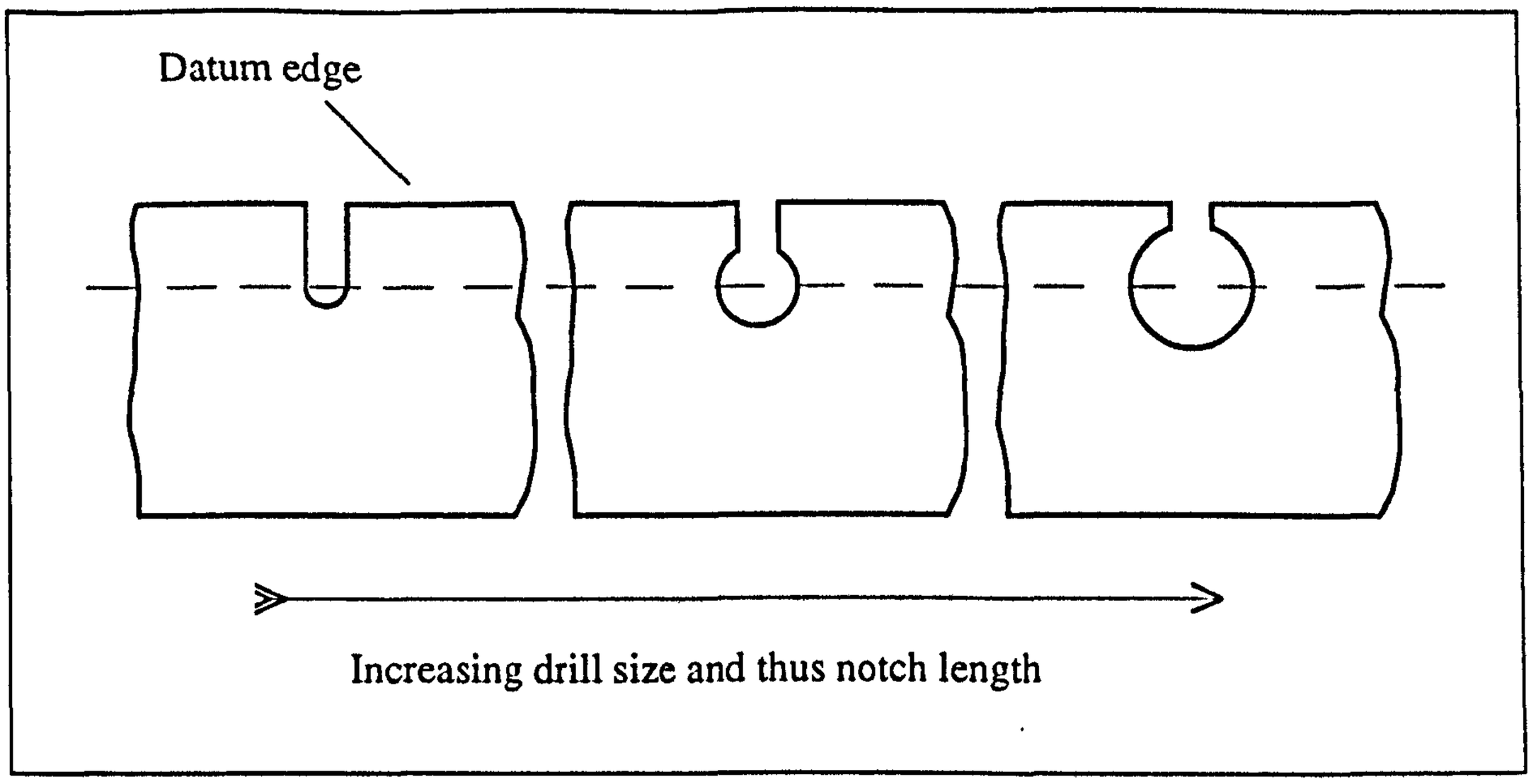

Figure 7.005

The source of the relationship between notch length and tip radius in data set NA1

The regression equations mentioned above, between K_{IQ}^{P} and $\rho^{0.5}$, are shown in the table 7.004. The regression equations are arranged in pairs. The first equation is for the data from the specimens manufactured from the base of the antler, and the second for the full set of data. The aim of this arrangement is to clearly display changes occurring in the relationships due to the inclusion of material from the antler tip. The structure and thus mechanical properties of this additional material may be different. From the results in table 7.003 clearly the material from the tip of the antler is less stiff than that from its base. This difference in mechanical properties would be very noticeable if the antler were still in velvet (see section 1.2.3).

The purpose of a shape correction factor is to remove any correlations between the SIF and the specimen geometry. Equations *c* and *d* of table 7.004 show that this has not been achieved by using the shape correction factor for the condition of pin-jointed ends. It is unclear, at this stage, if this shape correction factor has helped to remove any of the correlation between the SIF and a/w. To assess the shape correction factor's effectiveness the relationship of these variables without such a factor was also investigated. Table 7.005 contains the same form of regressions as equations *a* to *j* of table 7.004, but this time no shape correction factor is involved in the calculation of the SIF, K_{IQ}^{I}.

Source of antler specimens	Regression equations and t values (Data set NA1)	R^2 %	
8 base	$K_{IQ}^{P} = 1.51 + 201\ \rho^{0.5}$ t: 3.28 8.70	91.4	*a*
8 base 5 Tip	$K_{IQ}^{P} = 1.10 + 210\ \rho^{0.5}$ t: 2.03 7.03	80.1	*b*
8 base	$K_{IQ}^{P} = - 0.21 + 20.4\ (a/w)$ t: - 0.21 5.50	80.7	*c*
8 base 5 Tip	$K_{IQ}^{P} = - 1.03 + 22.7\ (a/w)$ t: - 1.19 6.70	78.5	*d*
8 base	$K_{IQ}^{P} = - 0.71 + 0.647\ E_b$ t: - 0.15 1.29	8.8	*e*
8 base 5 Tip	$K_{IQ}^{P} = - 1.02 + 0.676\ E_b$ t: - 0.56 3.18	43.2	*f*
8 base	$K_{IQ}^{P} = 0.11 + 191\ \rho^{0.5} + 0.169\ E_b$ t: 0.07 7.71 1.03	91.5	*g*
8 base 5 Tip	$K_{IQ}^{P} = - 1.35 + 173\ \rho^{0.5} + 0.363\ E_b$ t: - 1.92 8.06 4.03	91.7	*h*
8 base	$K_{IQ}^{P} = - 0.78 + 149\ \rho^{0.5} + 4.4\ (a/w) + 0.222\ E_b$ t: - 0.26 1.18 0.35 0.94	89.7	*i*
8 base 5 Tip	$K_{IQ}^{P} = - 2.21 + 98.1\ \rho^{0.5} + 8.47\ (a/w) + 0.362\ E_b$ t: -2.12 1.39 1.10 4.06	91.8	*j*
8 base	$(a/w) = 0.101 + 8.97\ \rho^{0.5}$ t: 4.79 8.48	91.0	*k*
8 base 5 Tip	$(a/w) = 0.102 + 8.81\ \rho^{0.5}$ t: 7.49 11.73	91.9	*l*
Units: K_{IQ}^{P}, MPa $m^{0.5}$. $\rho^{0.5}$, $m^{0.5}$. E_b, GPa. w, mm. a, mm.			

Table 7.004

Regression equations of the pin-jointed stress intensity factor and a number of explanatory variables and related relationships

Source of antler specimens	Regression equations and t values (Data set NA1)	R^2 %	
8 base	$K^I_{IQ} = 2.01 + 64.7\ \rho^{0.5}$ t: 5.24 3.22	57.3	*a*
8 base 5 Tip	$K^I_{IQ} = 16.8 + 78.7\ \rho^{0.5}$ t: 4.71 4.02	55.8	*b*
8 base	$K^I_{IQ} = 1.70 + 6.00\ (a/w)$ t: 2.38 2.33	38.9	*c*
8 base 5 Tip	$K^I_{IQ} = 0.948 + 8.21\ (a/w)$ t: 1.61 3.62	50.2	*d*
8 base	$K^I_{IQ} = -0.06 + 0.362\ E_b$ t: -0.04 2.22	35.9	*e*
8 base 5 Tip	$K^I_{IQ} = 0.136 + 0.341\ E_b$ t: 0.20 4.33	59.7	*f*
8 base	$K^I_{IQ} = 0.16 + 51.5\ \rho^{0.5} + 0.233\ E_b$ t: 0.16 2.90 1.98	71.3	*g*
8 base 5 Tip	$K^I_{IQ} = 0.035 + 53.8\ \rho^{0.5} + 0.244\ E_b$ t: 0.08 3.98 4.28	82.9	*h*
8 base	$K^I_{IQ} = -0.78 + 149\ \rho^{0.5} + 4.4\ (a/w) + 0.222\ E_b$ t: -0.26 1.18 0.35 0.94	89.7	*i*
8 base 5 Tip	$K^I_{IQ} = 0.142 + 63.1\ \rho^{0.5} - 1.05\ (a/w) + 0.244\ E_b$ t: 0.20 1.33 -0.20 4.07	81.0	*j*
Units: K^I_{IQ}, MPa $m^{0.5}$. $\rho^{0.5}$, $m^{0.5}$. E_b, GPa. w, mm. a, mm.			

Table 7.005

Regression equations of the results from the initial tests on antler specimens (Set NA1)

Table 7.005 shows that similar trends to those for K^P_{IQ} (equations *a* to *d* table 7.004) are exhibited by K^I_{IQ} (equations *a* to *d* table 7.005). However, the coefficient of determination is lower for each of the comparable equations in the second table. It can therefore be concluded, from the results of these initial tests, that the inclusion of the pin-jointed shape correction factor has increased the undesired correlation between the SIF

and specimen geometry. The coefficient of determination of the relationships between the SIF and E_b is greater when the shape correction factor is not included. So:

a) The inclusion of the pin-jointed shape correction factor has increased the undesired correlation between the SIF and specimen geometry.

b) The inclusion of the pin-jointed shape correction factor has decreased the correlation between the SIF and E_b, a measure of the material's stiffness.

The second observation 'b' is intriguing. We have seen that material stiffness plays a considerable role in determining some of antler's other mechanical properties, such as knee stress and failure stress (chapter 4). A relationship between the SIF and the material stiffness is also predicted by some of the theory of LEFM. The theory of LEFM contains an equation that provides a relationship between these quantities, (equation 5.037, $K_c^2 = E^* R$). This equation implies that a stronger correlation may exist between the value of the stress intensity factor squared and the material stiffness, than that between the non-squared values examined above. If a linear correlation existed between the SIF squared and the material stiffness, it would suggest that the specific work-of-fracture of the material is independent of the material's stiffness. Regression analysis of the material stiffness and SIF squared, using both uncorrected form and that containing the pin-jointed shape correction factor was performed. It was found that the coefficient of determination falls, or remains the same, when compared with the regression of the SIF (not squared) and material stiffness (*f* in tables 7.004 and 7.005). The coefficients of determination become 38.0% and 58.4% (in the same order of presentation as the tables). The decrease in R^2 is smaller in the cases where no shape correction factor is used.

The importance of the material stiffness in predicting the calculated fracture parameter, SIF, can also be demonstrated by comparing equations *a* and *b* with equation *h* in table 7.004. It appears that the reduction in the coefficient of determination from the first to the second equations (*a* to *b*) is due to the difference in bending stiffness of the specimens from the tip and the base of the antler. It is also clear from equation *e* and *f* of the second table, where in the second equation a greater range of material stiffness values are included in the analysis.

Before any importance is attached to these SIF results it should be remembered that they have been obtained by applying equations from LEFM to a material that is non-linear and probably non-elastic. The correlation between the stress intensity factor and the notch tip radius may be spurious, because the tip radius is not an independent variable. The importance of the material stiffness in determining the nominal fracture stress of these antler specimens is highlighted in table 7.006, which shows the best subset regressions for a number of variables. This table demonstrates that not only is the stiffness the best single predictor ($R^2 = 65.3\%$), but any combination with the other variables considered reduces the explanatory power of the relationship.

Predictors of the failure stress on SEN antler specimens					
(a/w)	$\rho^{0.5}$	w	d	E_b	R^2 %
				X	65.3
	X				7.0
			X	X	63.0
		X		X	62.1
X	X			X	65.1
		X	X	X	59.5
X	X		X	X	61.3
X	X	X		X	61.1
X	X	X	X	X	55.8

Units:

σ_f, MPa. $\rho^{0.5}$, $m^{0.5}$. E_b, GPa. d, mm. w, mm. a, mm.

Comments:

This table shows the variables (indicated by X) that give the highest value of the coefficient of determination, when the variables listed along the top line are used to explain the nominal failure stress, σ_f in MPa, of the SEN antler specimens in data set NA1. The table shows the two best combinations of one, two then three and so on explanatory variables.

Table 7.006

The variables that give the best subsets regressions of the failure stress 13 notched specimens of antler (Data set NA1)

7.2.5.5. INITIAL TESTS: CONCLUSIONS DRAWN FROM THE ANALYSIS OF THE INITIAL TESTS ON SEN SPECIMENS OF ANTLER (DATA SET NA1)

Unfortunately an appropriate tip radius for future use was not found from these tests. However, analysis of the results has highlighted some relationships that could be important when attempting to obtain an accurate understanding of the failure and fracture processes of antler, tested under the conditions used here. These are listed below:

a) There is a strong correlation between the critical stress intensity factor containing the shape correction, K^P_{IQ}, for a pin-jointed specimen and the square root of the notch tip radius, $\rho^{0.5}$.

b) The correlation referred to in a) was reduced when the SIF considered did not contain a shape correction factor, K^I_{IQ}. Thus the correlation would appear to be an artefact.

c) There was a correlation between the SIF and the geometry of the specimen, this was stronger in the case of the SIF that contained the pin-jointed shape correction factor, K_{IQ}^{P}, than in the case of the uncorrected SIF K_{IQ}^{I}.

d) A very strong correlation between the square root of the notch tip radius and the specimen geometry exists. This means the effects of specimen geometry and notch tip radii are not separable. Because, the relationship between the SIF and one of the variables may be due to this variable's interaction with the other one, with which the SIF is truly correlated. This finding casts some doubt over any generalisations that may be based on the previous conclusions a), b) and c).

e) A correlation between the SIF and the material stiffness was found. This correlation decreased with the application of the pin-jointed stress correction factor.

f) The importance of the material stiffness as a predictor of the failure stress (and thus by implication the SIF) was also shown. Of the variables considered material stiffness was by far the best predictor, it explained 65.3 % of the variation in the failure stress. The addition of other variables was found to be detrimental to the amount of variance explained.

Assistance in the solution of the conundrum highlighted in d), is sought by the analysis of the next series of tests, in which sharp and blunt notches were investigated.

7.3. TESTS ON THE NOTCH SENSITIVITY OF ANTLER USING SEN SPECIMENS WITH SHARP AND BLUNT NOTCHES (DATA SET NA2)

In this section the results of tests performed on SEN specimens of red deer antler, containing notches the tip of which either drilled or sharpened with a razor blade are presented. One aim of these tests, like the initial ones, is to establish whether there is a difference in the fracture behaviour of specimens containing notches of different tip radii. By using a razor blade to sharpen the notches, a greater difference in tip radii could be examined. Another aim of these tests was to examine the various applications of equations that were later applied to data sets containing larger numbers of specimens. By the application of these techniques it was hoped that any further insight to the failure of antler would be gained and flaws in the preparation or testing of the specimens would be highlighted.

7.3.1. EXPERIMENTAL PROCEDURE

In this second series of exploratory (or initial) tests (data set NA2), 23 specimens were used. These specimens were produced from the mid-portion of the same antler used for the production of the specimens for the initial tests (data set NA1). The nominal width of these specimens was 4 mm. Nine of the specimens were produced according to the method given in appendix 2 (the largest tip radius, ρ, was measured as 0.40 mm and the smallest as 0.08 mm). Another twelve SEN specimens contained notches that were cut without the specimen having been drilled. These twelve notches were then sharpened by manually forcing a razor blade a short distance into the material at the tip of the machined notch. These sharpened notches will be referred to as *cut* (as opposed to drilled). One consequence of the size and shape of these cut notch tips, is the lack of a measurable value of the tip radius. The two remaining specimens were tested in the un-notched state. Testing was carried out as described in section 7.2.4. As in the initial tests, all the specimens were fractured using a cross-head speed of 8.3×10^{-5} m s^{-1} [5 mm min^{-1}].

7.3.2. RESULTS

As stated in the introduction to this section (7.3) the data contained within data set NA2 comes from tests that are preliminaries to the examination of larger data sets. These results influenced the experimental design of these later tests. Therefore the actual analysis of these results is less important than the conclusions that were drawn from it. The methods used for the analysis of the data from set NA2 were repeated on the data from the larger and better designed experiments. The results of this repeated analysis were essentially the same. However, I give more credence to the data and results of the later experiments (NA3, NA4 and NA5). (Their greater reliability is due to the larger data sets, improved experimental design and better specimen preparation.) Therefore in this section I give the conclusions drawn from the analysis of data set NA2 alone, and their implications. (To show that these conclusions are not unsubstantiated some of the analysis of data set NA2 is presented in appendix 10.)

a) There is no apparent effect of notch tip radius, cut or drilled, on the fracture load or the stress intensity factor. Thus no value of the critical fracture tip radius (as defined in LEFM) was found. As a result of this a range of tip radii was used in all the subsequent tests, unless this variable was to be specifically excluded.

b) The use of the un-flexing and pin-jointed shape correction factors greatly increased the correlation of the SIF and the specimen geometry, for these SEN specimens. The more unrestrained the specimens are assumed to be, the stronger the relationship is.

c) The corollary of point b is that a reduction in the correlation of material stiffness and the SIF results from inclusion of this shape correction factor. The reduction was grater when the pin-jointed shape correction factor was used.

d) It is unclear if the best linear relationship to explain the failure stress with respect to load is based on a or a/w (the notch insensitive case) or $a^{-0.5}$ (the notch sensitive case in LEFM).

e) Purslow's logarithmic approach (section 5.3.4) for relating failure stress to notch length was found to explain the failure stress to a lesser extent than the linear relationships of a, a/w or $a^{-0.5}$. The exceptions to this were the relationships of a and a/w when only the specimens with a drilled notch tip were considered.

f) The material stiffness, as measured in three-point-bending, is a very important factor in determining the failure stress of the SEN specimens produced from antler.

g) The coefficients in regression equations obtained by augmenting the logarithmic equations from Purslow's approach with the logarithm of material stiffness are very similar to the Griffith equation, in form and in the value of the coefficients.

Another result obtained from these tests (that has not been reported above) was the observation of changes in the optical properties of the material. These changes took the form of a *whitened* area encompassing the tip of the machined notch or travelling fracture. This observation is discussed in chapter 8.

The observations made in this section are reinforced by these resulting from the analysis of larger and better designed data sets. This analysis is presented in the following sections.

7.4 NOTCH SENSITIVITY OF ANTLER (DATA SET NA3)

The previous tests (sets NA1 and NA2) do not support the theoretical and experimentally observed result that for classically notch sensitive materials the tip radius affects the critical stress intensity factor. Therefore I was unable to determine a value for, or even the existence of, the critical notch tip radius. Thus I decided to conduct these tests on specimens that contained notches with drilled tips. This decision was based on a number of factors, two of which are: first, the variability of the notch lengths of drilled specimens could be controlled more easily than those sharpened by using a razor blade; second, the notch tip was better defined (and thus the notch length was easier to measure) when the specimen was drilled. To help identify any effects that may be related to the tip radius, more than one drill size was used for the production the specimens within each set of tests.

The tests discussed in this section were performed on specimens from a single red deer antler. The specimen geometry and methods of preparation have already been outlined in section 7.2.3 (and appendix 2). Therefore in this section I will concentrate on the aims and results of these tests.

7.4.1. AIMS AND EXPERIMENTAL DESIGN

The main aim of these tests was to examine the application of some of the predictions and quantities involved in fracture that have been presented in chapter 5. The predictions or models examined were: Purslow's original theory; my adaptations of it and some basic LEFM. The main quantity resulting from the theory of LEFM examined is the calculated values of the stress intensity factor at failure. This investigation was accomplished by using SEN specimens. Two geometrical quantities of the specimens were altered: specimen width (4 and 6 mm) and notch tip radius (0.37, 0.33 and 0.20 mm).

The fracture mechanics approache used here (and in the analysis of data sets NA1 and NA2) is based on the supposition of linear elasticity. Purslow's approach is also based on the assumption of elasticity, albeit a specific non-linear form. Therefore it is necessary to ascertain a measure of antler's elasticity if the results obtained using either of these approaches are to be accepted or rejected. This assessment of antler's elasticity was performed by examining the *resilience* of the material.[10] Resilience is the energy under the unloading curve expressed as a percentage of the energy under the loading curve. A fully elastic material (linear or non-linear) will have a resilience of 100%. The resilience was determined from the first loading-unloading cycle. The first cycle was used to avoid any errors due to changes induced in the material by mechanical loading, such as the *work hardening* that occurs in carbon steels. (Other cycles were undertaken to examine this change in properties but these are not discussed in this thesis.)

Purslow's approach assumed a constant value of n, for each material, in the equation $\sigma = k \varepsilon^n$. The theoretical prediction of the failure stress contains some function of n in every term. A number of tests were conducted to ascertain whether the value of n for antler is constant, and if it is predictable from the examination of other known mechanical properties. These tests used standard tensile specimens loaded until they fail.

---

[10]In this examination of resilience I am mimicking the experimental procedure used by Purslow (1991).

The resilience and tensile tests required an extra four groups of specimens (2 sets 4 mm wide and two sets 6 mm wide). Specimens were assigned to each group after they had been tested in three-point-bending so that each of the ten groups contained an even spread of samples of different material stiffnesses.

Calcium content was determined all the specimens (by the method in appendix 3) after they had been mechanically tested. For three specimens, because of a mistake, a result is not available. Two of these specimens were among the un-notched specimens that were loaded until they failed. The other specimen, for which a value of the calcium content was not obtained, was a 6 mm wide notched specimen, drilled with drill III. To enable better comparisons to be drawn between the regressions, for the notched specimens, which contained calcium as a predictor and those which do not, all the data for this specimen were removed from the data set. Complete sets of data for some other specimens were either unavailable or have been removed from the data set (hence the uneven group sizes in the analysis here). Grounds for rejection were: inability to obtain the standard specimen shape from the slab of bone as cut from the antler; lack of usable stress-strain data. The latter cause of rejection was usually due to mistakes during testing, although in some cases it was due to corrupted data.

A comparison between various properties of each group of specimens (for which the data will be examined) is provided in table 7.007. It can be seen that apart from the desired differences between the groups, tip radius, width and by implication notch length, they are reasonably consistent in the properties presented here.

	Nominal specimen width 4 mm			Nominal specimen width 6 mm		
		s.d.	n		s.d.	n
Drill I approximate notch tip radius 0.37 mm	w = 3.87	0.04	13	w = 5.91	0.05	10
	ρ = 0.36	0.01	13	ρ = 0.37	0.00	10
	E_b = 10.59	2.99	13	E_b = 10.75	2.45	10
	a = 1.36	0.51	13	a = 2.15	0.80	10
	Ca^{++} = 227.33	8.19	13	Ca^{++} = 231.84	3.98	10
Drill II approximate notch tip radius 0.33 mm	w = 3.86	0.05	7	w = 5.91	0.04	10
	ρ = 0.33	0.01	7	ρ = 0.33	0.01	10
	E_b = 10.34	2.00	7	E_b = 10.93	2.54	10
	a = 1.30	0.39	7	a = 1.76	0.51	10
	Ca^{++} = 229.29	7.30	7	Ca^{++} = 227.23	4.97	10
Drill III approximate notch tip radius 0.20 mm	w = 3.86	0.04	9	w = 5.93	0.03	10
	ρ = 0.20	0.01	9	ρ = 0.20	0.01	10
	E_b = 10.79	3.03	9	E_b = 10.93	2.56	10
	a = 1.47	0.46	9	a = 1.68	0.65	10
	Ca^{++} = 229.04	9.14	9	Ca^{++} = 228.89	6.06	10
Resilience tests	w =3.86	0.04	11	w = 5.88	0.05	10
	E_b = 11.22	2.68	11	E_b = 11.25	2.82	10
	Ca^{++} = 225.97	7.27	11	Ca^{++} = 231.42	6.59	10
Tensile	w = 3.88	0.06	6	w = 5.96	0.05	6
	E_b = 10.58	2.46	6	E_b = 10.45	1.98	6
	Ca^{++} = 228.52	5.10	5	Ca^{++} = 224.26	6.46	5

Units:

w	Specimen width, mm.
ρ	Machined notch tip radius (measured), mm.
E_b	Material stiffness (modulus) in three-point-bending, GPa.
a	Notch length, mm.
Ca^{++}	Concentration of calcium ions in dry mass of defatted bone by weight, mg g^{-1}.

Table 7.007

Various mechanical and geometrical properties of the specimens, in each of the test groupings, for which the data is used in the analysis presented here (Data set NA3)

7.4.2. TEST METHOD

The test method used is that described in section 3.2.4. The cross-head speed used was 8.3×10^{-5} m s^{-1} [5 mm min^{-1}]. The mechanical response of the specimen was captured using the AJS/BBC data collection system. A Canon EOS 600 (a 35 mm single lens reflex camera) was used to capture the occurrence of optical changes occurring during the mechanical testing of the specimens.[11] Some images obtained using a video system during similar tests are provided in chapter 8.

7.4.3. RESULTS

In this section I shall examine the numerical results. However, there was another perhaps more important result; a zone of whitened material was observed at the tip of the notch when the specimens were loaded. This result is discussed in more detail in chapter 8, where it is shown that this whitened appearance is related to the occurrence of the knee region in a tensile test. Thus it appears that the region of material ahead of the notch undergoes the same process as occurs during the knee of the tensile test. This is analogous to the behaviour of metals for which the knee and the fracture tip process zone are both due to plastically deformed material. Further investigation of this 'whitening' phenomenon, and some discussion of is significance for the fracture process is contained in section 7.5. Here I consider the numerical results obtained from tests of SEN specimens of red deer antler (data set NA3).

7.4.3.1. RESULTS: RESILIENCE

In the theoretical introduction to both the Griffith's approach and what I have referred to as Purslow's approach it was pointed out that both theories are based on the assumption that the material to which it is applied is elastic. In the first case the material is linear-elastic, the stress-strain relationship is described by the function $\sigma = E\,\varepsilon$, and in the second the stress-strain relationship is described by the function $\sigma = k\,\varepsilon^n$. For an elastic material, linear or non-linear, all the energy supplied during loading is recovered when the material is unloaded. Therefore a simple method of assessing the degree of elasticity of a material is to examine these quantities. The ratio of the work recovered to the work supplied is called resilience. The value of resilience contains no information on the linearity or otherwise of the elasticity.

---

[11]These pieces of equipment were used separately. The method of interconnecting them, described in appendix 1, had not yet been developed.

Resilience tests were performed on 21 specimens. Values of resilience were obtained from the digital stress-strain data. The areas under the loading and unloading stress-strain curve were calculated by using the trapezium rule on every successive pair of points. (These areas are shown diagrammatically in figure 7.006.) The two values obtained were then expressed as a percentage ratio, $\Re$. A number of the stress-strain plots resulting from these tests are shown in figure 7.007.

$$\Re = \frac{\text{Area b}}{\text{Area a} + \text{Area b}} \times 100\%$$

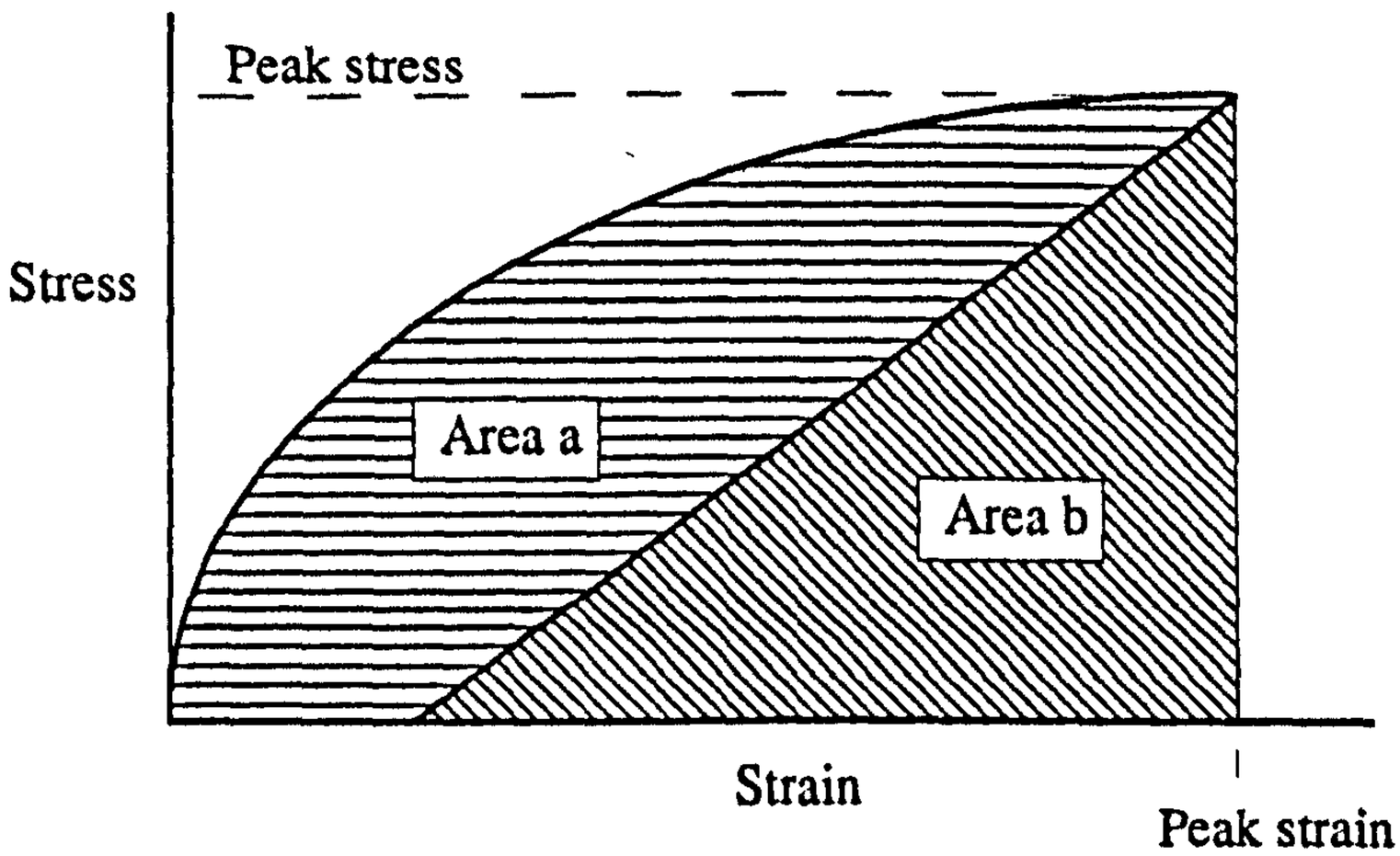

Figure 7.006

An idealised representation of the areas used in the calculation of resilience

The values of resilience obtained from the specimens of antler examined here are shown in figure 7.008 plotted against the value of peak stress. These are the variables plotted by Purslow (1991) for rubber. However, the usefulness of such a plot is dubious, as it can be seen from figure 7.007 (and 4.2.6.6) that antler specimens exhibit a wide range of knee stresses. Therefore, if the analogy of an elastic-plastic material is used, some specimens may still be elastic ($\Re = 100\%$) while others may be behaving plastically ($\Re < 100\%$) at the same stress. It appears that antler specimens have a more uniform value of knee strain than knee stress (see figure 4.026). Therefore the resilience should be more closely related to the strain level than it is to the stress level. To examine this idea I have plotted the resilience values against peak strain in figure 7.009. The shapes of the plots in figures 7.008 and 7.009 suggest a logarithmic relationship between the resilience and the measured mechanical variable. This relationship is shown in figure 7.010.

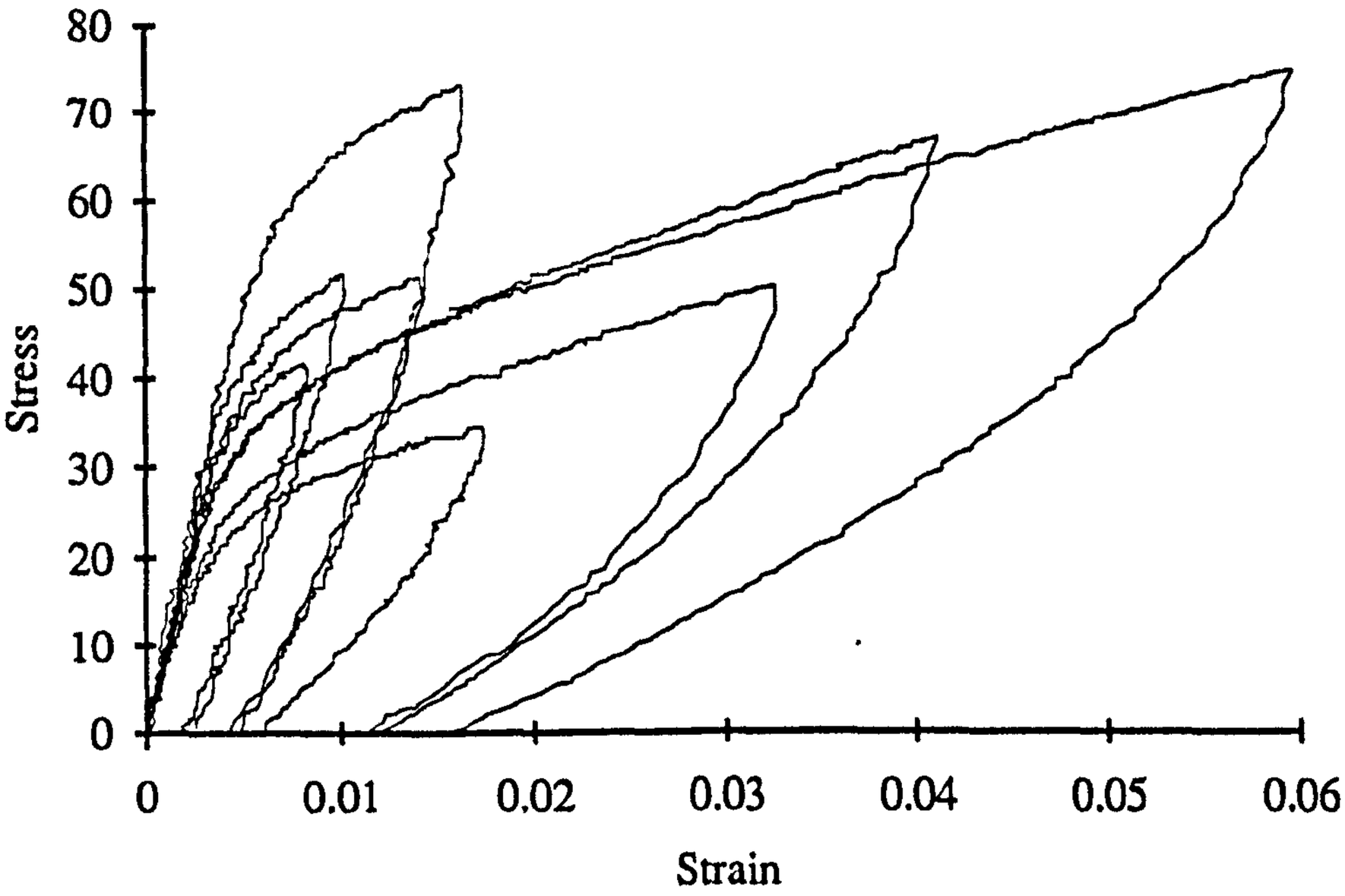

a) Loading-unloading plots from resilience tests on 8 specimens of red deer antler.

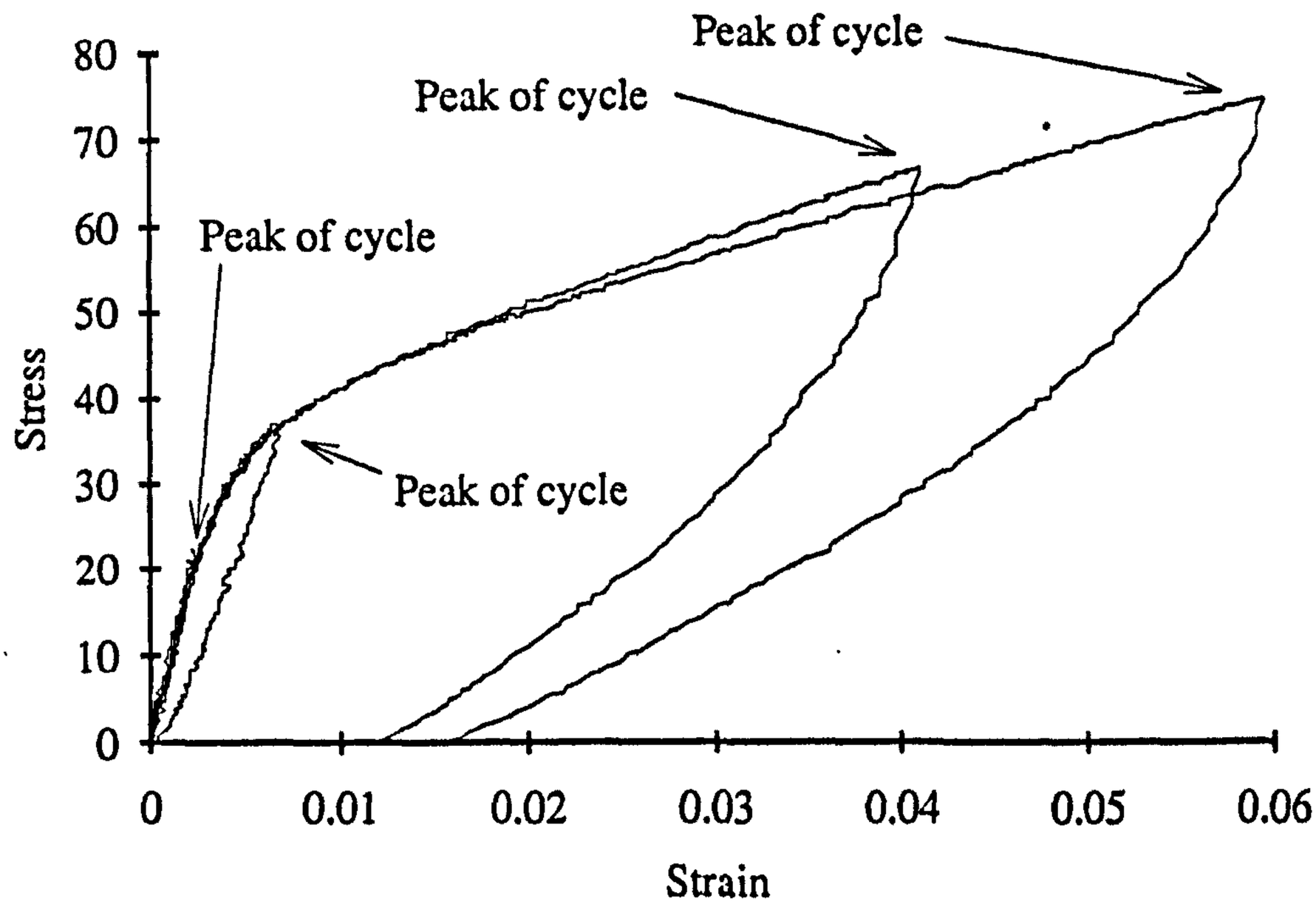

b) Loading-unloading plots from resilience tests on 4 specimens of red deer antler that have a similar stress-strain response.

Units:

σ	Stress, MPa
ε	Strain, unitless

Figure 7.007

Some plots of the actual stress-strain relationships obtained from SEN specimens of red deer antler

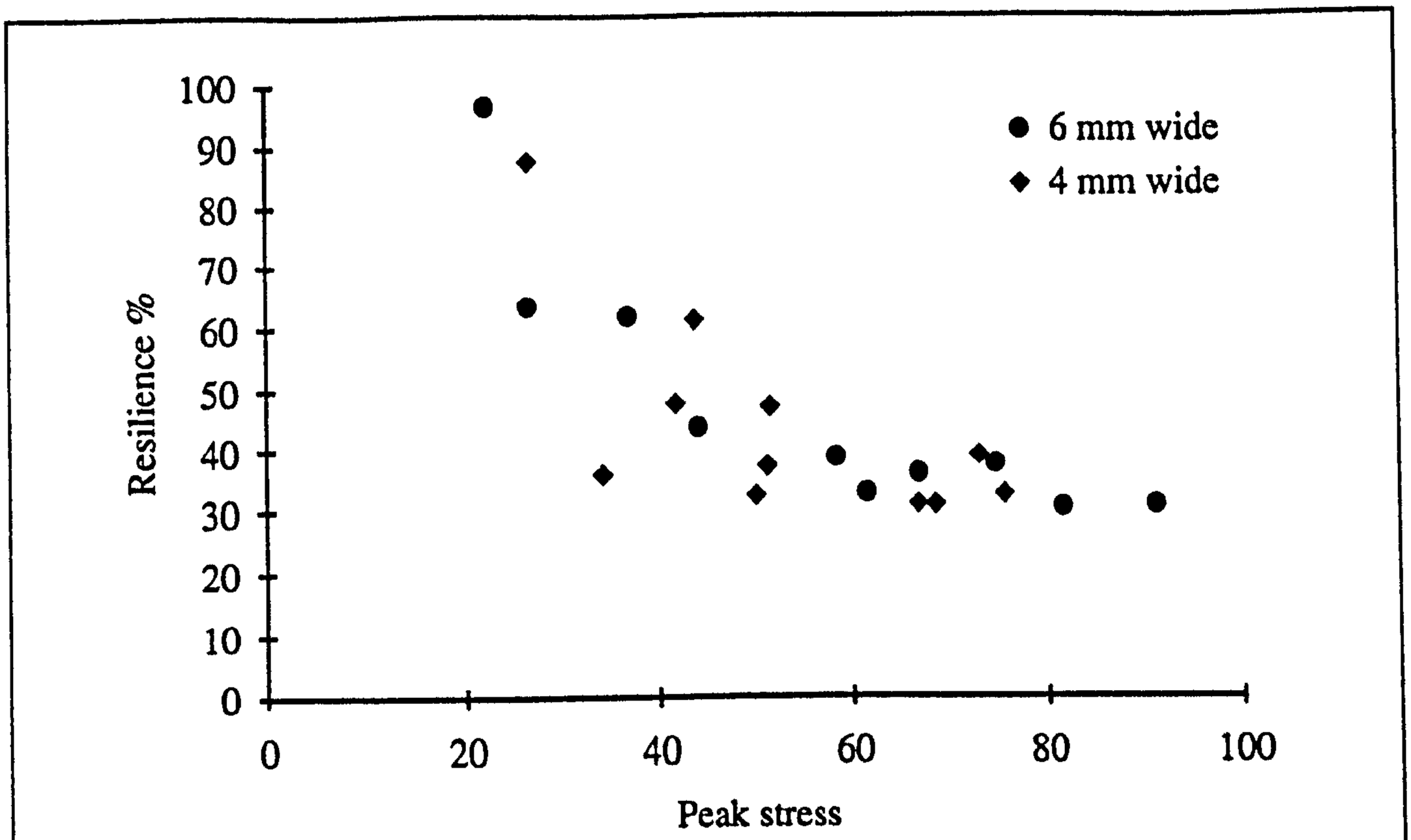

Units:

$\Re$ Resilience, unitless.

σ_{peak} Peak stress in first loading cycle, MPa

Figure 7.008

Resilience versus peak stress

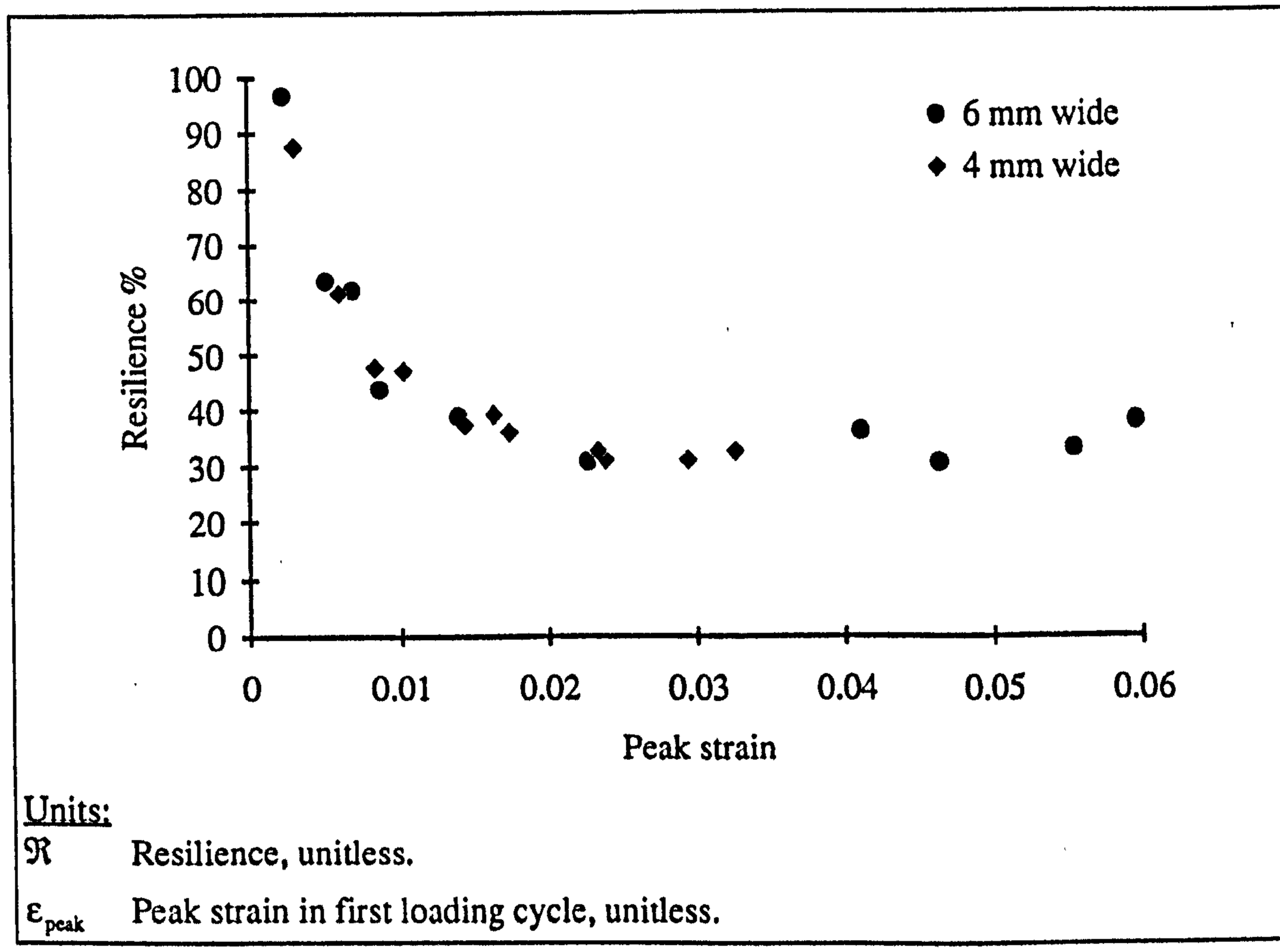

Units:

$\Re$ Resilience, unitless.

ε_{peak} Peak strain in first loading cycle, unitless.

Figure 7.009

Resilience versus the peak strain

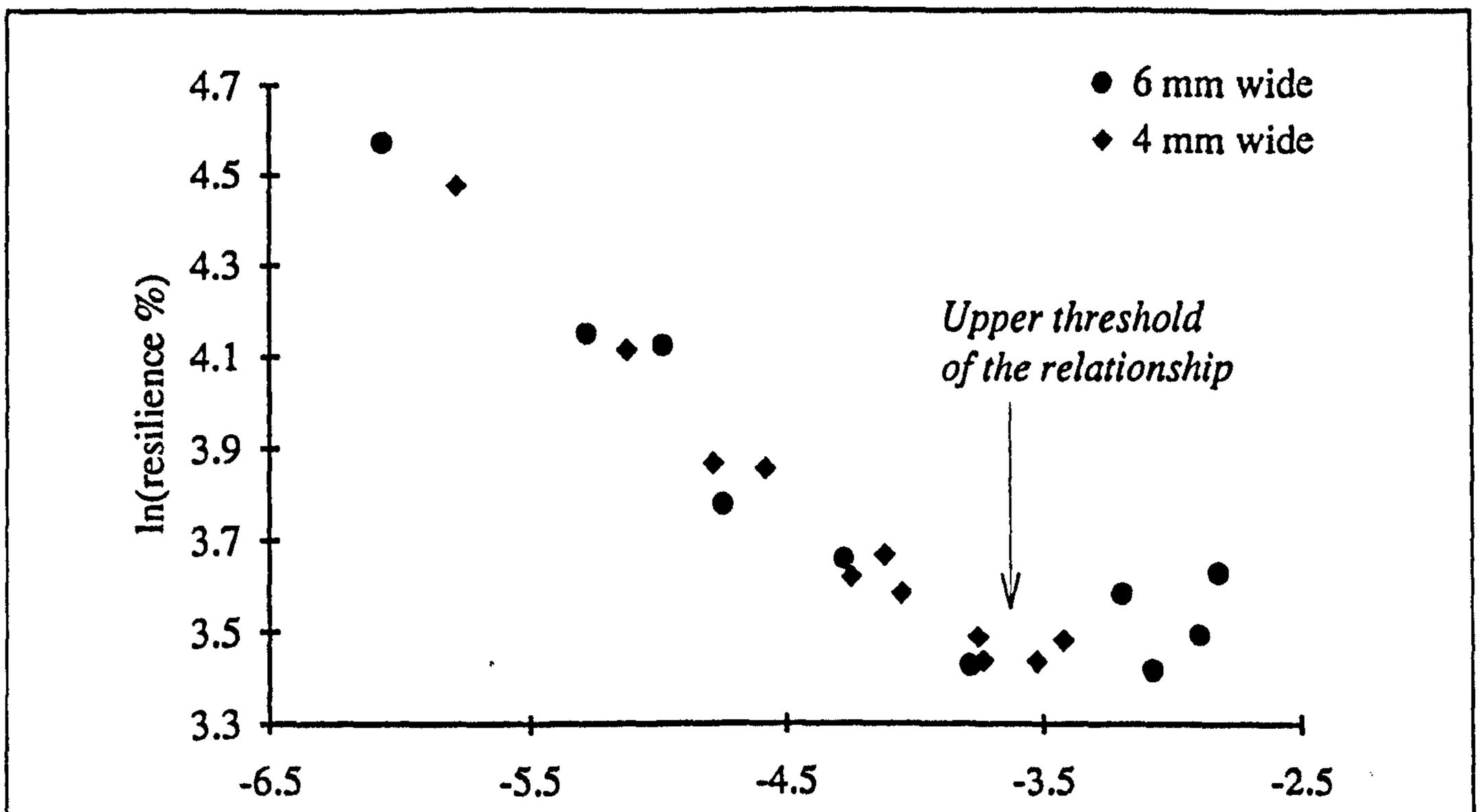

Units:

$\Re$ Resilience, unitless.

ε_{peak} Peak strain in first loading cycle, unitless.

Figure 7.010

Resilience versus the peak strain

Type of antler specimens	Regression equations and t value of resilience and the peak stress or strain shown in figures 7.009 and 7.010. (Data set NA3)	R^2 %	
11, 4 mm 10, 6 mm	$\ln(\Re) = 6.68 - 0.744 \ln(\sigma_{peak})$ t: 16.58 - 7.29 Full data set	72.3	*a*
11, 4 mm 10, 6 mm	$\ln(\Re) = 2.34 - 0.337 \ln(\varepsilon_{peak})$ t: 14.88 - 9.22 Full data set	80.8	*b*
9, 4 mm 6, 6 mm	$\ln(\Re) = 1.59 - 0.490 \ln(\varepsilon_{peak})$ t: 15.40 - 22.12 Data for peak strains up to the upper threshold only	97.2	*c*
Units: $\Re$, Ratio. σ_{peak}, MPa. ε_{peak}, ratio			

Table 7.008

Regressions of resilience and the measured mechanical properties

The graph of the logarithmic relationship of the experimentally determined values of resilience and peak strain is shown in figure 7.010. This logarithmic relationship is not followed at the higher values of strain shown. This departure from the relationship I have indicated in figure 7.010 and call the *upper threshold of the relationship*. By removing six data points with strains higher than this upper threshold the predictive power of the regression fitted to the data was improved. Both of these relationships are given in table 7.008 (equation *b* and *c*). They may also be expressed in the following way:

$$\Re = 10.38\ \varepsilon^{-0.337} \qquad \text{(full data set)} \qquad (7.005)$$

$$\Re = 4.90\ \varepsilon^{-0.490} \qquad \text{(reduced data set)} \qquad (7.006)$$

These equations (7.005 and 7.006) are not theoretically based nor are they universal. They produce meaningless values of $\Re > 100\%$ at strains lower than 0.001 (equation 7.005) and 0.002 (equation 7.006). These strain values can be seen as the lower threshold of the relationships, or the upper limit of the fully elastic behaviour. By substituting the mean value of material stiffness in tension, E_t, into the above equations and assuming linear elasticity, an approximation of the stress at which the material departs from elastic behaviour can be made. The mean value of $E_t = 9.63$ GPa was obtained from the tests on the un-notched specimens. The results of this substitution imply that the behaviour departs from elasticity at 10 or 19 MPa, depending on which equation is used. As the data obtained at high strains have less relevance to the departure from elasticity than the lower strains, equation 7.006 is more justifiable. Thus the higher value of stress would appear to be the better estimate of the limit of full elasticity.

The procedure used to find the limit of full elasticity can not, reasonably, be used to find the stress equivalent of the upper threshold of the equation, due to the departure from elasticity (and the linearity implicit in the value of E_t). The specimens with high values of peak strains generally have high values of peak stress. Thus an examination of figures 7.008 compared with figure 7.010, suggests that the upper threshold will fall at approximately 60 MPa. It is unclear what the upper threshold of the relationship corresponds to in the mechanical sense. Figure 7.009 suggests that the resilience reaches an almost constant value on attaining this upper threshold. Perhaps this corresponds to the results of ultimate damage (section 4.2.6.10). If it is assumed that the unloading line was linear and did return to the origin, examination of figure 4.017 shows that for a similar increase in strain the change in resilience is smaller at higher strains than at strain close to the knee region. (I consider that the non-linearity and the residual strain on unloading will compound this effect.)

The mechanical response of a notched specimen can now be examined with reference to the upper limit of fully elastic behaviour. The mean nominal failure stress of

the notched specimens is approximately 40 MPa and all are above 20 MPa. Thus the bulk of the material is stressed above the limit of fully elastic behaviour. By comparing the value of 40 MPa with the plotted values in figure 7.008, it can be seen that the resilience of the bulk material is approximately 50%. The loss of elasticity in the material will result in a reduction in the strain energy available to drive or initiate a fracture, compared to that in a similarly loaded material that has retained its elasticity. This loss of elasticity therefore helps to toughen antler. This implies that the results obtained from the various fracture relationships examined here should be treated with scepticism.

The loss of elasticity within antler before fracture will affect the measured values of the fracture parameters. For example the measured value of the work-of-fracture (although not generally considered here) may be greater than the energy needed simply to partition the material. The additional work is dissipated within the bulk material due to this non-elastic response. (If this is the case the size and geometry of the specimen away from the region of the fracture will affect the measured value of the work-of-fracture.)

During these tests it was observed that on unloading the strain values did not return immediately to the origin. The return path was curved as shown in figure 7.007. On the complete removal of the load the strain continued to decrease with time. When some of the specimens were reloaded it was clear that there was an increase in the width of the loading un-loading loops obtained in the post-knee region (relative to those in the pre-knee region). This implies an increase in the proportion of time-dependent behaviour in the post-knee region. This widening of the hysteresis loop and the associated decrease in the material stiffness are consistent with the ideas I suggested in chapter 4 and encapsulated in my proposed rheological model (figure 4.027). I suggested that as the proportion of post-knee strain increases the material behaves in a more time-dependent manner than it does in the pre-knee region. The damaging behaviour suggested in chapter 4 is also consistent with the loss in resilience of the material. In the rheological model I suggested the removal of the damage body reduces the amount of recoverable work available.[12]

In this experiment the same cross-head speed was used for all the tests: loading-unloading, notched and un-notched. Considering the results in chapter 4, I suggest that using different cross-head speeds would produce difference quantitative results, although

---

[12]It is tempting to suggest that the better correlation of the resilience values with the peak strain rather than the peak stress, is another facet of the behaviour that make the NTDF model superior to the TDF model. This is based on the idea that it is the damaging process that consumes the energy. However, I do not consider I have the time or data to pursue this suggestion.

similar qualitative results (provided the difference in cross-head speeds used was not excessive, impact for example).

The results of the resilience tests on antler show that it should not be regarded as a fully elastic material at strains above 0.002 (or a stress of about 19 MPa). These values are less than these associated with the knee of an un-notched specimen of this material tested at the same cross-head speed. This loss of elasticity can be regarded as a toughening mechanism, as it will reduce the energy available to propagate a fracture. I suggest that the consumption of work that results in this loss of elasticity is due to a combination of visco-elastic-like and damage behaviour, as proposed in section 4.2.7.

7.4.3.2. RESULTS: WHAT ARE THE VALUES OF N AND K, WITHIN THE EQUATION $\sigma = k\,\varepsilon^n$ FOR RED DEER ANTLER?

Purslow assumed the following stress-strain relationship in his theory and investigation of various rubbers

$$\sigma = k\,\varepsilon^n \tag{7.007}$$

To apply his theory I have assumed that the stress-strain relationship for antler is described by the relationship of equation 7.007. To examine the validity of this assumption, and to obtain values of the coefficients in the relationship equation 7.007 was converted to logarithmic form

$$\ln(\sigma) = \ln\left(k\,\varepsilon^n\right) \tag{7.008}$$

$$\ln(\sigma) = \ln(k) + n\ln(\varepsilon) \tag{7.009}$$

Equation 7.009 was then used as the basis of a regression analysis of the stress and strain values obtained from tensile tests of un-notched antler specimens, which were loaded until they failed. With digital data this conversion presents no difficulty, the logarithmic value of each stress value can be plotted against the logarithmic value of each corresponding strain point. The gradient of the resulting plot will give the value of n and the intercept the value of ln(k). This was the procedure followed for the data from the tensile test specimens. The gradient of the logged data was found by fitting a least squares regression line, a procedure available within the plotting package to which the analysis program was linked.[13] (The range of values used for fitting this line were the

---

[13]Simpleplot produced by Bradford University Software Services Ltd. This package uses $\log_{10}$ not ln so the value of k was calculated accordingly.

stress-strain points that satisfied the inequality, $0.001 \leq \varepsilon \leq \varepsilon_{ult}$.) It can be seen that the data points do not fall on a straight line, indicating that a more complex function may be required to give a better fit. However, I have used Purslow's relationship in this thesis as a first approximation. Clearly a more accurate relationship should not only account for the shape of the loading curve, but also the unloading curve (the loss of elasticity). The twelve values of n that were obtained have a mean of 0.39 and standard deviation of 0.05.

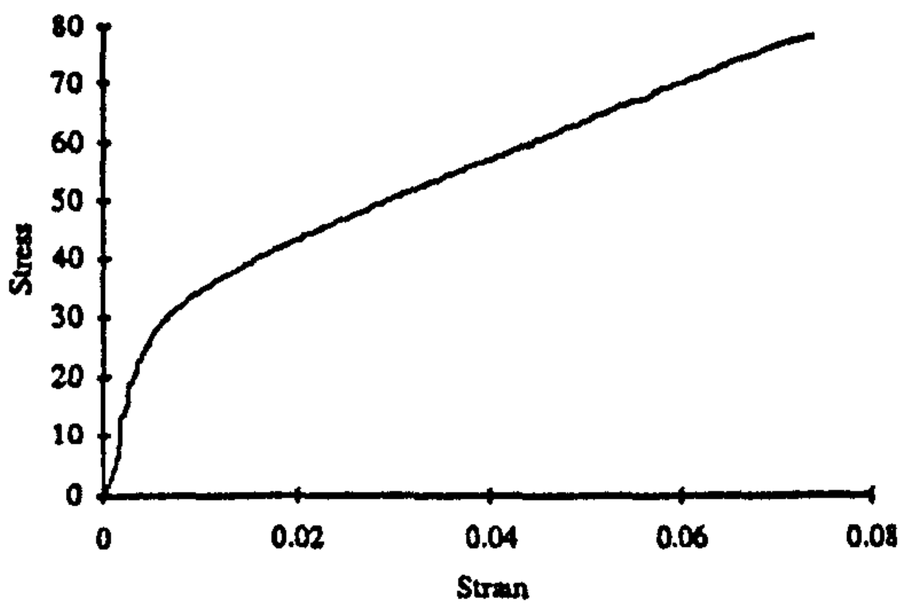

a) Stress-strain response of red deer antler

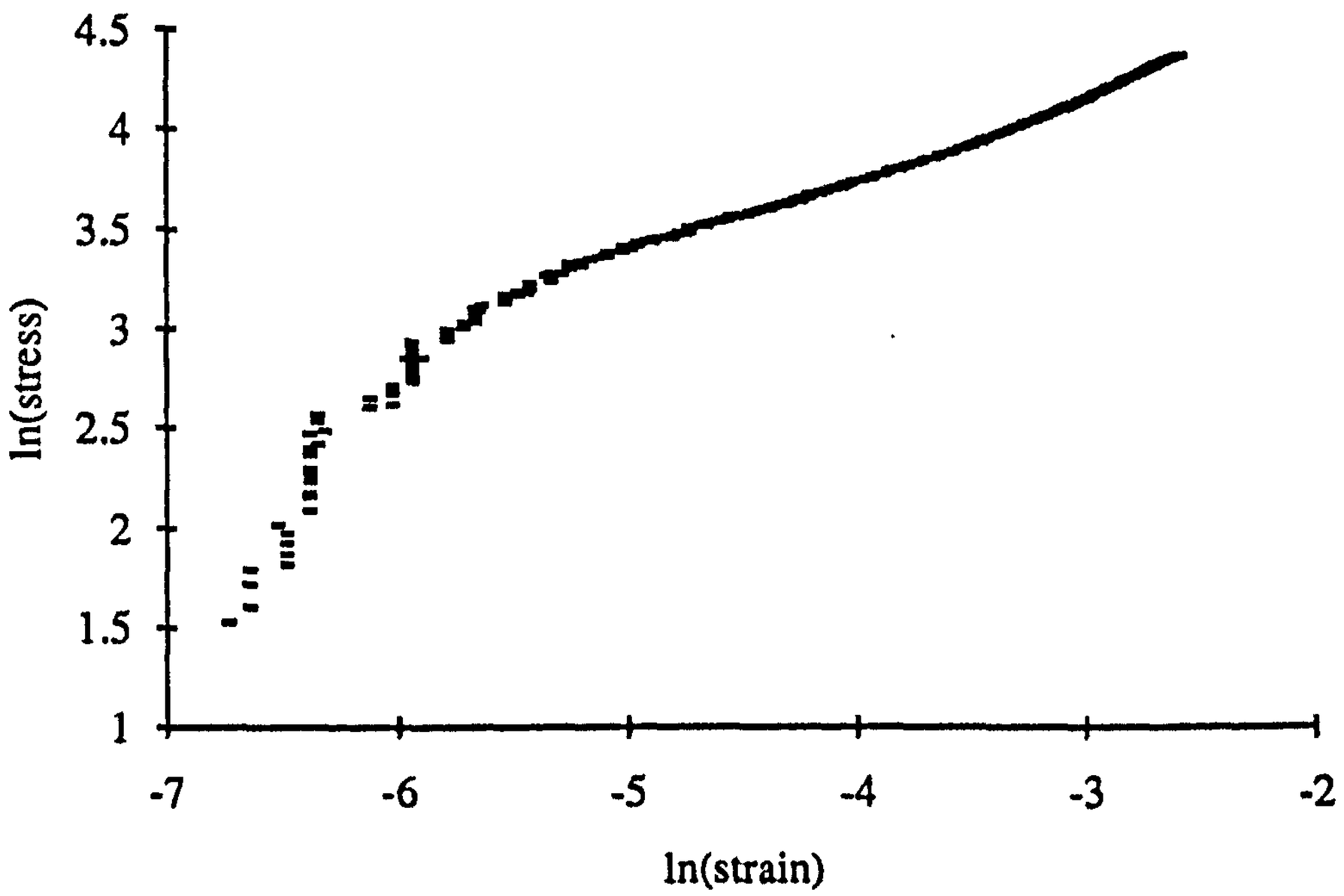

b) Logarithmic plot of stress-strain data for a specimen of red deer antler

Figure a shows the stress-strain response of specimen (04/06/91/62) using normal axes (a line connects the data points). Figure b shows the same data points for which $\varepsilon \geq 0.001$, expressed in logarithmic form. In the second figure the points are plotted and no connecting line is used.

Units:

σ	Stress, MPa
ε	Strain, unitless

Figure 7.011

Logarithmic plot of the stress-strain data for an un-notched specimen of red deer antler

To enable Purslow's approach to be justifiably applied to the value of n for the material is required. I consider that the values obtained for n are too variable for it to be

regarded as a material constant. Therefore relationships between n and other explanatory variables were sought, so that a predicted value of n could be obtained for each specimen. An obvious candidate for such a predictive variable is the stiffness of the material from which the specimen is made. A theoretical basis for such a relationship of the material's stiffness to n can be postulated by considering a specimen under tensile loading. This relationship is developed in the following way

$$\sigma = k \varepsilon^n \tag{7.010}$$

Equation (7.010) predicts that the secant modulus, E_s, (in tension) at any time, t, will be

$$E_s = \frac{\sigma}{\varepsilon} = \frac{k \varepsilon^n}{\varepsilon} = k \varepsilon^{n-1} \tag{7.011}$$

$$\ln(E_s) = \ln(k) + (n - 1) \ln(\varepsilon) \tag{7.012}$$

Therefore if the secant modulus is measured at a constant value of strain for each specimen, this equation becomes

$$\ln(E_s) = \ln(k) + n C_1 - C_1 \tag{7.013}$$

Which may also be expressed as

$$n = C_2 \ln(E_s) - C_2 \ln(k) + 1 \tag{7.014}$$

where C_1, $C_2 = 1/C_1$ are constants.

Equation (7.014) suggests that a modified linear relationship should exist between the values of n and the logarithmic value of the secant modulus. The modification is due to the third variable k. However, this third variable may be non-trivial, for it is obvious that in the linear case, n = 1, k has the same value as the secant modulus. In these tests k was found to have a mean value of 243.1 MPa and a standard deviation of 28.1 MPa. In the data examined here the secant modulus was obtained by dividing the (corresponding) stress by the strain value preceding that at which $\varepsilon \geq 0.004$. A quantity that will be referred to as the tensile modulus, E_t, was also obtained. The method used to obtain E_t was to fit a regression line to what appeared to be the initially straight section of the loading curve. For most specimens this covered the range 0 to 20 MPa. Unfortunately, it is not possible to derive either of these material stiffnesses from the data collected during the testing of notched specimens. Thus the material stiffness in three-point-bending is the only value of stiffness available as a possible predictor. The later relationship on which the use of this predictor is based is a bit tenuous, so the use of calcium as another predictor has also been examined.

Width of antler specimens	Regression equations and t values for the values of n and material stiffness obtained from tensile tests of red deer antler.	R^2%	
6, 4 mm 6, 6 mm	$n = 0.578 - 0.0242\ E_s$ t: 16.29 - 5.49	72.6	*a*
6, 4 mm 6, 6 mm	$n = 0.545 - 0.0163\ E_t$ t: 25.42 - 7.61	83.8	*b*
6, 4 mm 6, 6 mm	$n = 0.573 - 0.0176\ E_b$ t: 10.63 - 3.50	50.6	*c*
6, 4 mm 6, 6 mm	$n = 0.744 - 0.175\ \ln(E_s)$ t: 12.75 - 6.14	76.9	*d*
6, 4 mm 6, 6 mm	$n = 0.704 - 0.143\ \ln(E_t)$ t: 20.51 - 9.31	88.6	*e*
6, 4 mm 6, 6 mm	$n = 0.814 - 0.182\ \ln(E_b)$ t: 6.87 - 3.61	52.2	*f*
Units: n, unitless. E_s, GPa. E_t, GPa. E_b, GPa.			

Table 7.009

Relationship of n to the material stiffness

When the regression equations in table 7.009 were repeated using calcium as an additional predictor of n, the values of R^2 increased in all but two cases (the equivalents of *a* and *d*). In one the improvement was more than an additional 15% of the total possible. However, on further analysis it was found that this increase was due to the exclusion from the regression of two data sets. The exclusion of these two points was a result of not obtaining a calcium content value for these specimens. The removal of these two data points from the data set produced a greater increase in the power of the relationships of the form shown in table 7.009 than the increase obtain by their exclusion due to the use of calcium as an additional variable. This finding indicates that the inclusion of calcium as an explanatory variable reduces, the overall explanatory power of the regression equation. This finding and examination of the graph of this data (figure 7.012) cast some doubt on the robustness of predictions of n based on the material stiffness and calcium content. Table 7.009 clearly shows that the stiffness in tension is a better predictor of n than the secant modulus, which is in turn is better than the bending modulus. However, the first two forms of modulus are not available for the notched

specimens, so the relationships shown by equation *c* or *f* will have to be used as a predictor of n for these specimens.[14]

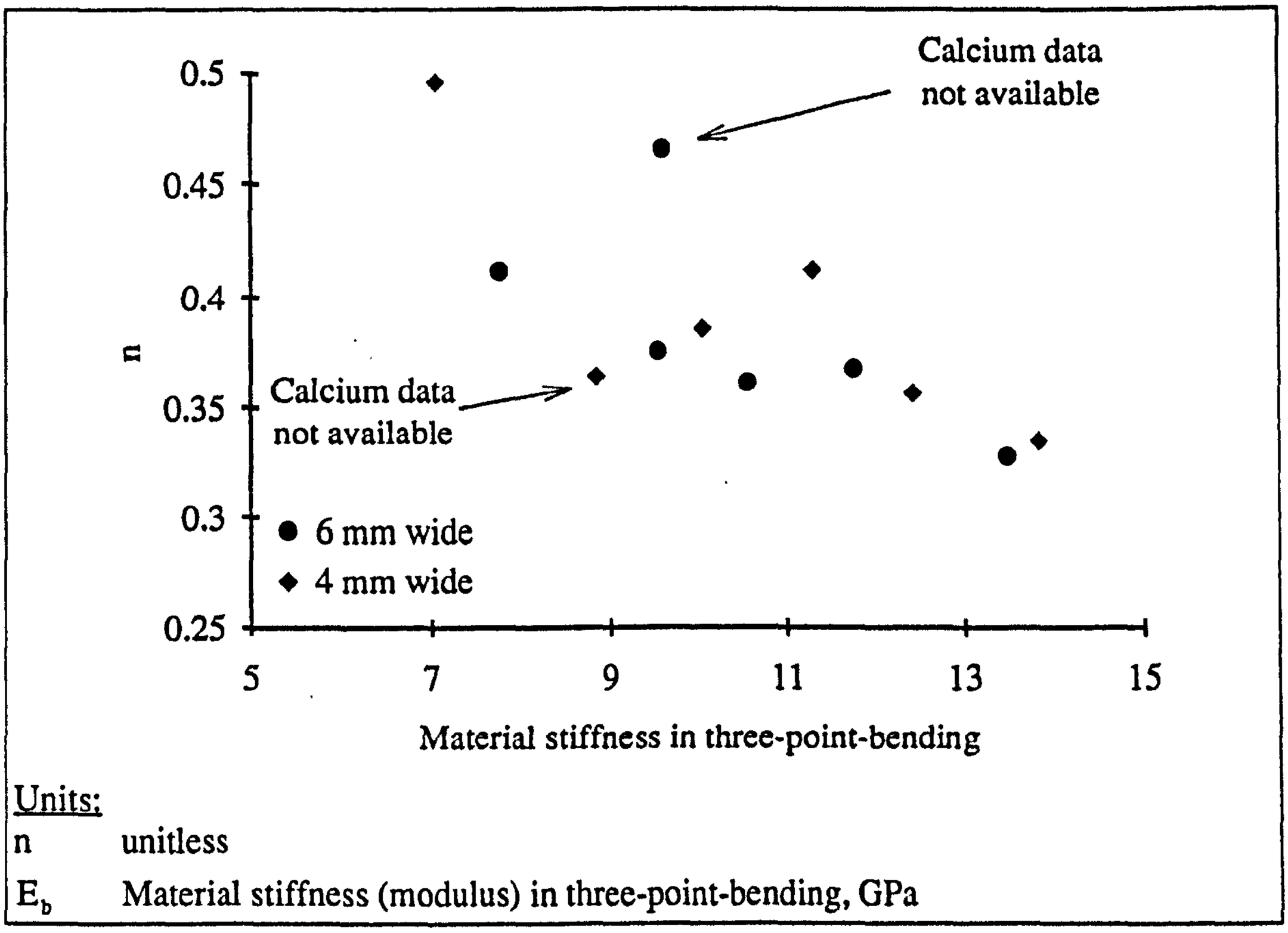

Units;

n	unitless
E_b	Material stiffness (modulus) in three-point-bending, GPa

Figure 7.012

The relationship of n (in the equation $\sigma = k \varepsilon^n$) and the material stiffness

An investigation of how the value of k in the equation $\sigma = k \varepsilon^n$ may be correlated with the available predictors or n itself, failed to provide any significant relationships. This initially appears a somewhat surprising result, due to the comments above about k being directly related to the material stiffness if n = 1. However, n is not equal to unity nor is it constant. The effect of the different values of k and n is shown in figure 7.013, which is a plot of the relationship of stress and strain modelled by the equation $\sigma = k \varepsilon^n$. It can be seen that this relationship appears to describe the stress-strain relationship during loading quite adequately, except for the lack of a definite knee region.[15] The two curves that have the steepest initial slope are those with the lowest values of n, not those with the highest values of k. This observation conforms with the regression equations in table 7.009 and implies that the value of k is not as important as

---

[14]With hindsight it is possible to say that porosity or micro-hardness values, for example, should have been obtained. However, this would have required more time than was available.

[15]However, it does not describe the unloading curves shown in figure 7.007. These unloading curves and the associated loss of elasticity are discussed in the previous section.

that of n in determining the shape of the relationship at the lower strain values (for the range of values of n and k considered here).

The result of this investigation to find the values of *n* and *k* in the relationship $\sigma = k \varepsilon^n$ (when it is used to describe the tensile stress-strain response of un-notched specimens of antler) showed that neither n or k are constant. The mean values are n = 0.39 and k = 343.1 MPa. It was found that the values of n are related to the material stiffness measured in tension, and similarly but less significantly related to the materials bending stiffness. The lack of a consistent value of n or k clearly complicates an examination of the applicability of Purslow's equations. It also implies that the fracture behaviour of antler is likely to be variable.

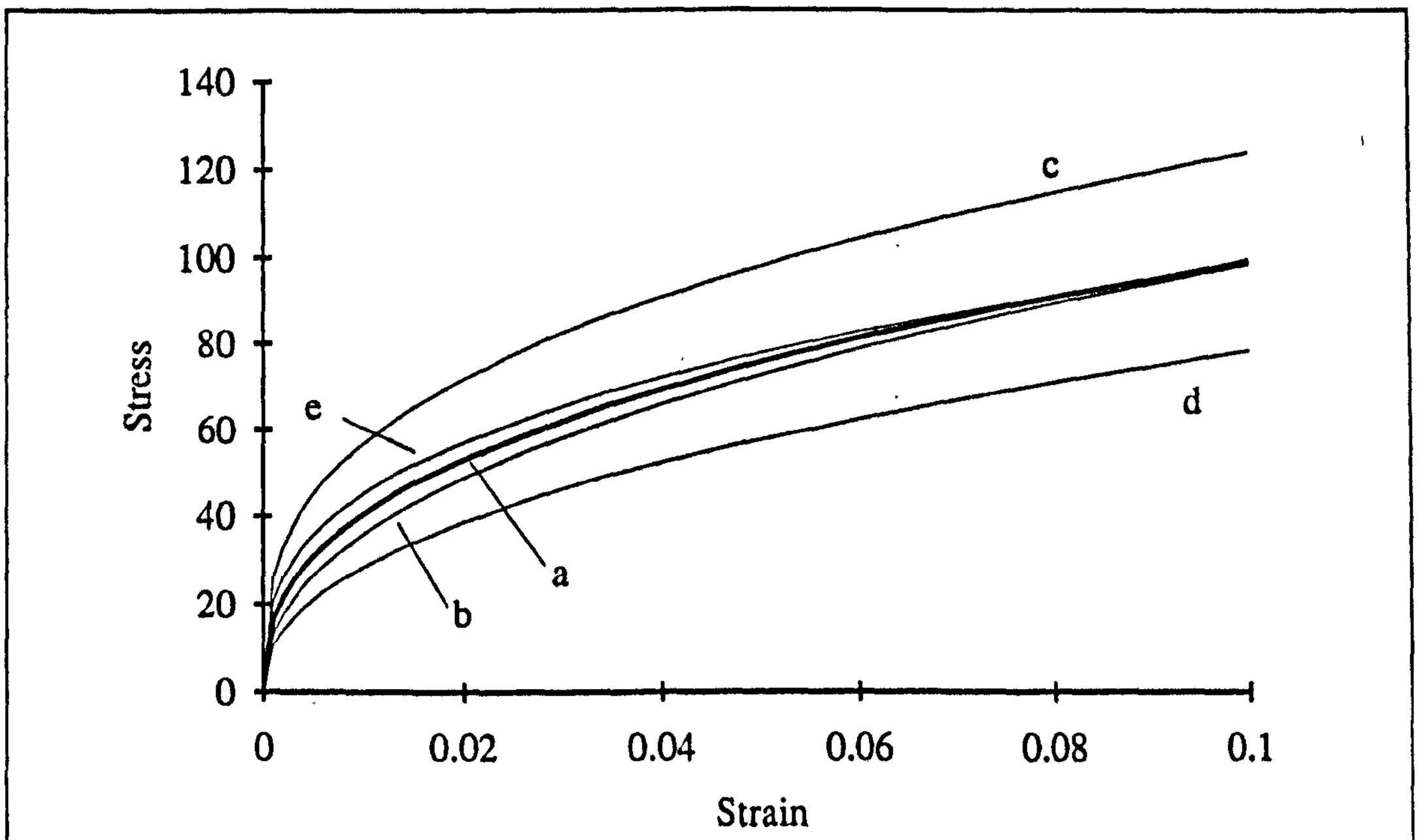

Units:

σ	Stress, MPa.		
ε	Strain, unitless.		

Comments:

a	k = 243.10 MPa	n = 0.39	(k mean, n mean)
b	k = 271.15 MPa	n = 0.44	(k mean + s.d., n mean + s.d.)
c	k = 271.15 MPa	n = 0.34	(k mean + s.d., n mean - s.d.)
d	k = 215.05 MPa	n = 0.44	(k mean - s.d., n mean + s.d.)
e	k = 215.05 MPa	n = 0.34	(k mean - s.d., n mean - s.d.)

Figure 7.013

The stress strain relationship of red deer antler predicted using the equation $\sigma = k \varepsilon^n$ and the experimentally determined values of k and n

7.4.3.3. RESULTS: FAILURE STRESS AND NOTCH LENGTH

In this section I examine the data obtained from the SEN specimens of antler. For this I use the equations predicted for the classically notch sensitive material (LEFM) and for the notch insensitive material. Figure 7.014 shows the values of the failure stress (load divided by the un-notched cross-section[16]) of the notched specimens plotted against the ratio of the notch length and the specimen width (a/w). The line drawn on the plot is from the mean failure stress (86.5 MPa) of the un-notched specimens (also included in the figure) to the point where the notch length is the same as the specimen width and thus the failure stress will be zero. Most of the data points for the notched specimens fall below this line, indicating some degree of notch sensitivity. Figure 7.015 shows the same stress data for the notched specimens this time plotted against $a^{-0.5}$. Neither of these plots convey a very convincing correlation (R^2 of 22.5% and 14.4% respectively).

Some of the variation on the values of the failure stress of the notched specimens can be attributed to the variation in the mechanical response of the different specimens. From previous observations it is known that the strength of an un-notched specimen is dependent on some of its material properties (see 4.2.6.7). By examining the relationship of the predictors available for both the notched and un-notched specimens to the ultimate stress of the un-notched specimens, I hoped to obtain an equation that could be used to normalise out some of this specimen-dependent variability. This normalisation used equation *e* in table 7.009 that describes the results from the tests of un-notched specimens (shown in figure 7.016). This equation permitted a prediction to be made of the strength that the notched specimens would have attained if the notch had not been present, σ_{pred}. The actual strength attained by each of the specimens was then expressed as a ratio with the predicted value for that specimen, σ_f/σ_{pred}.

---

[16]The failure stress calculated using the reduced cross-sectional area is referred to as the ligament stress. In all other cases the failure stress is the nominal stress calculated using the full width and thickness of the specimen.

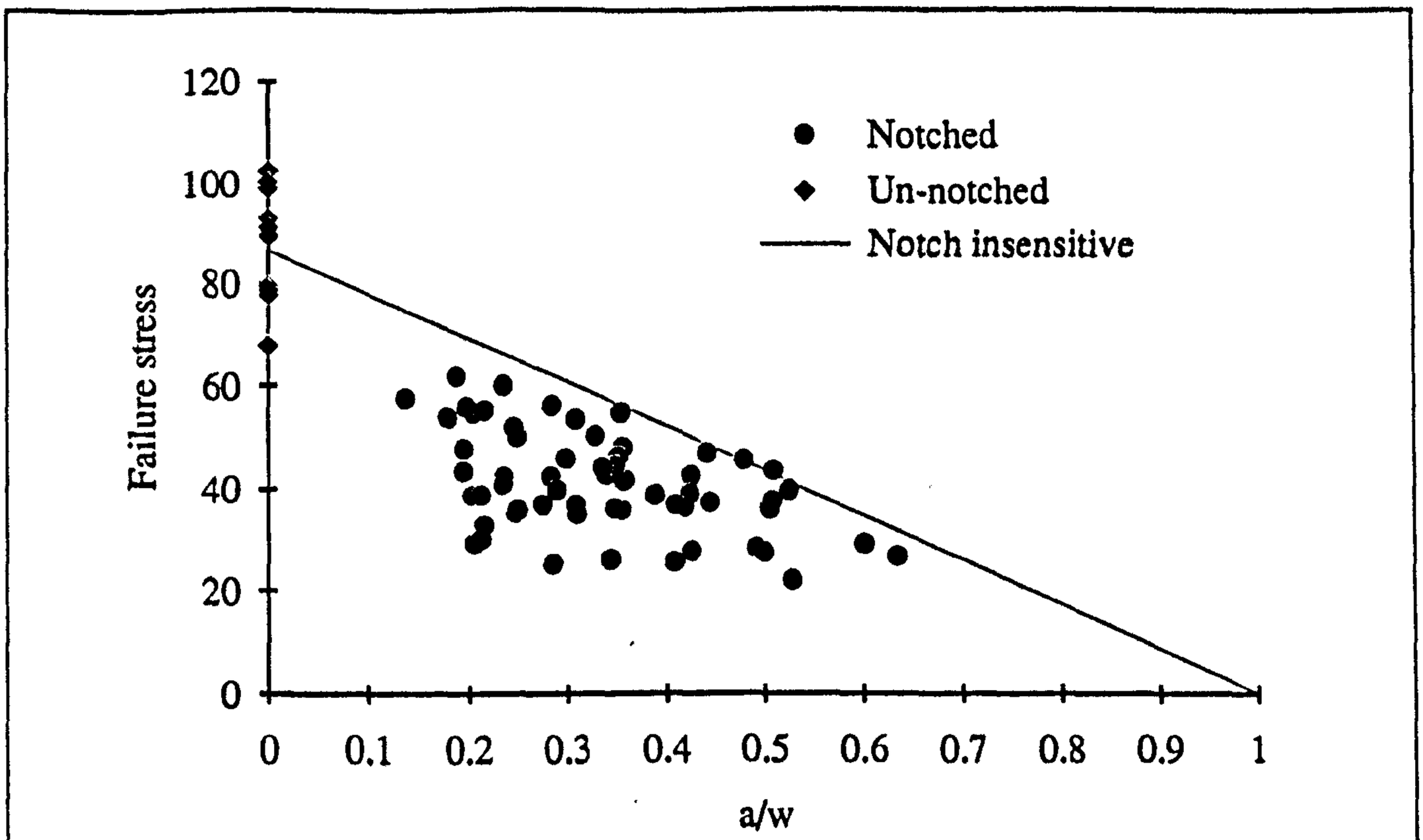

Units:

σ_f Stress at failure, MPa

a/w notch length/specimen width, unitless

Figure 7.014

Failure stress and a/w for notch and un-notched specimens of red deer antler

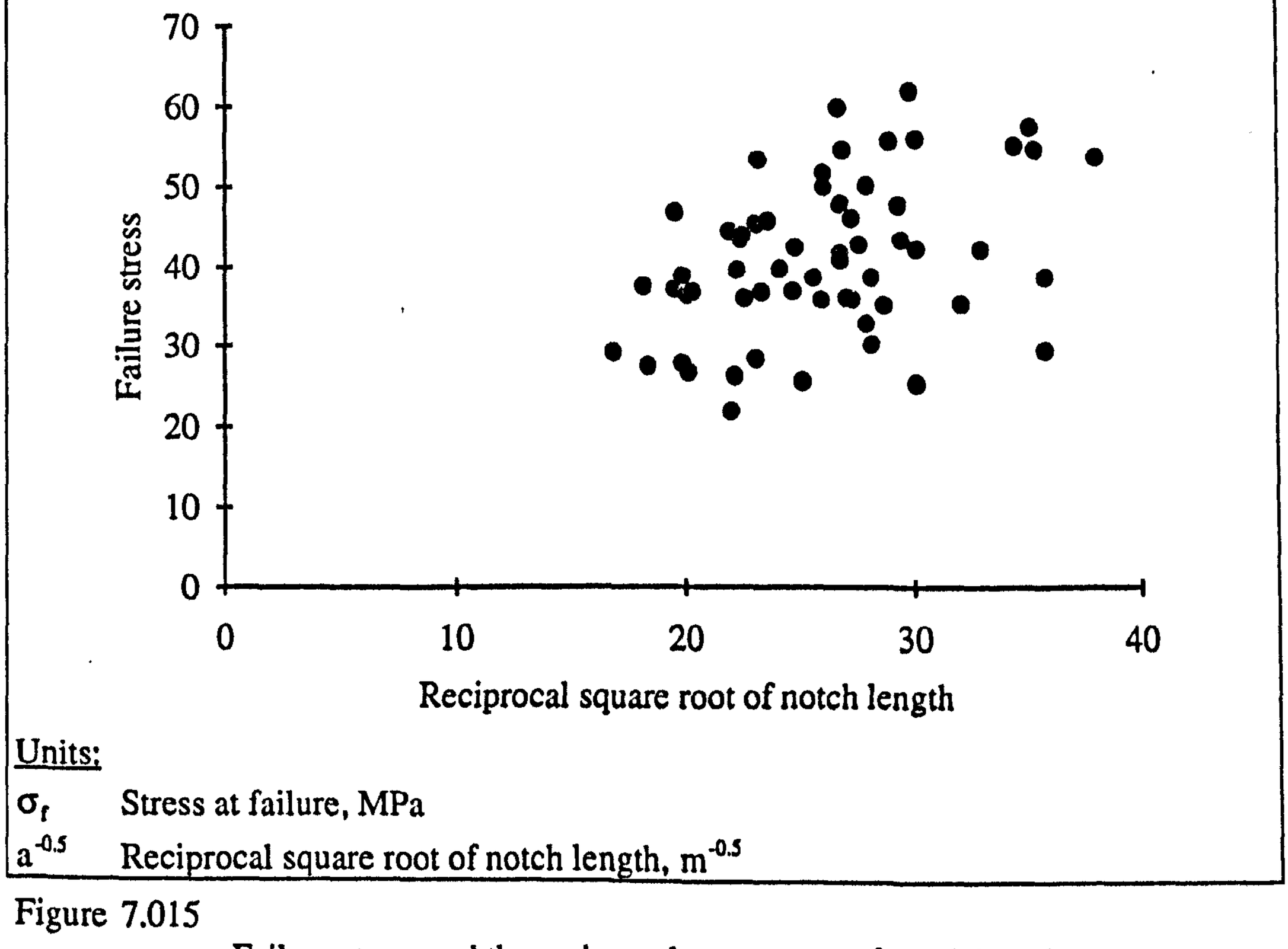

Units:

σ_f Stress at failure, MPa

$a^{-0.5}$ Reciprocal square root of notch length, $m^{-0.5}$

Figure 7.015

Failure stress and the reciprocal square root of notch length

Type of antler specimen	Regression equations and t values (data set NA3)	R^2 %	
59 SEN	$\sigma_f = 54.6 - 40.5\ (a/w)$ t: 16.03 - 4.23	22.5	*a*
59 SEN	$\sigma_f = 20.1 - 0.797\ a^{-0.5}$ t: 3.17 3.33	14.8	*b*
12 Tensile	$\sigma_{ult} = 45.3 + 3.91\ E_b$ t: 3.32 3.07	43.4	*c*
10 Tensile	$\sigma_{ult} = 41.1 + 4.25\ E_b$ t: 2.80 3.17	50.2	*d*
10 Tensile	$\sigma_{ult} = -93 + 3.78\ E_b + 0.615\ Ca^{++}$ t: - 0.82 2.77 1.19	52.6	*e*
59 SEN	$(\sigma_f/\sigma_{pred}) = 0.634 - 0.508\ (a/w)$ t: 22.05 - 6.27	39.8	*f*
59 SEN	$(\sigma_f/\sigma_{pred}) = 0.198 + 0.0102\ a^{-0.5}$ t: 3.52 4.82	27.7	*g*
Units: σ_f, MPa, a/w, ratio. $a^{-0.5}$, $m^{-0.5}$. σ_{pred}, MPa.			

Table 7.010

Predictive equations of the failure stress and the ratio of failure stress to predicted stress

In table 7.010 the apparent improvement in predicting the variation of the failure stress of the un-notched specimens between equations *c* and *e*, due to the inclusion of calcium content as a predictor (R^2 = 43.4% to 52.6%) is exaggerated. This is due to the exclusion of two data points from the analysis. These points are those for which calcium values are not available. The regression with these two points rejected, without using calcium as a predictor is shown in relationship *d*. A graph of this data is provided in figure 7.016. (This is the same as the problem reported for the same data set in section 7.4.3.2.)

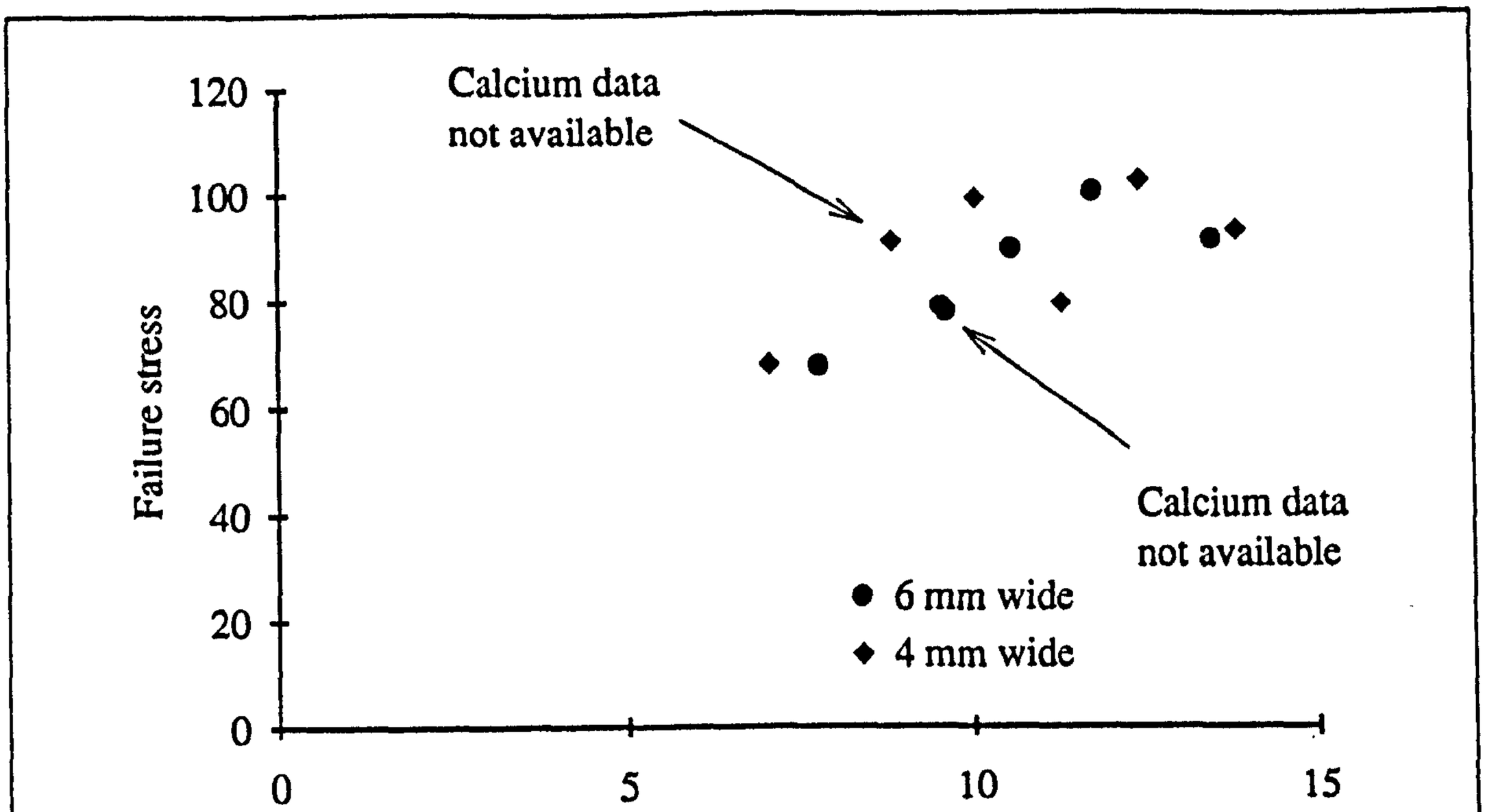

Units:

σ_f Failure stress, MPa.

E_b Material stiffness in bending, GPa.

Figure 7.016

Failure stress and material stiffness for un-notched specimens of antler (Data set NA3)

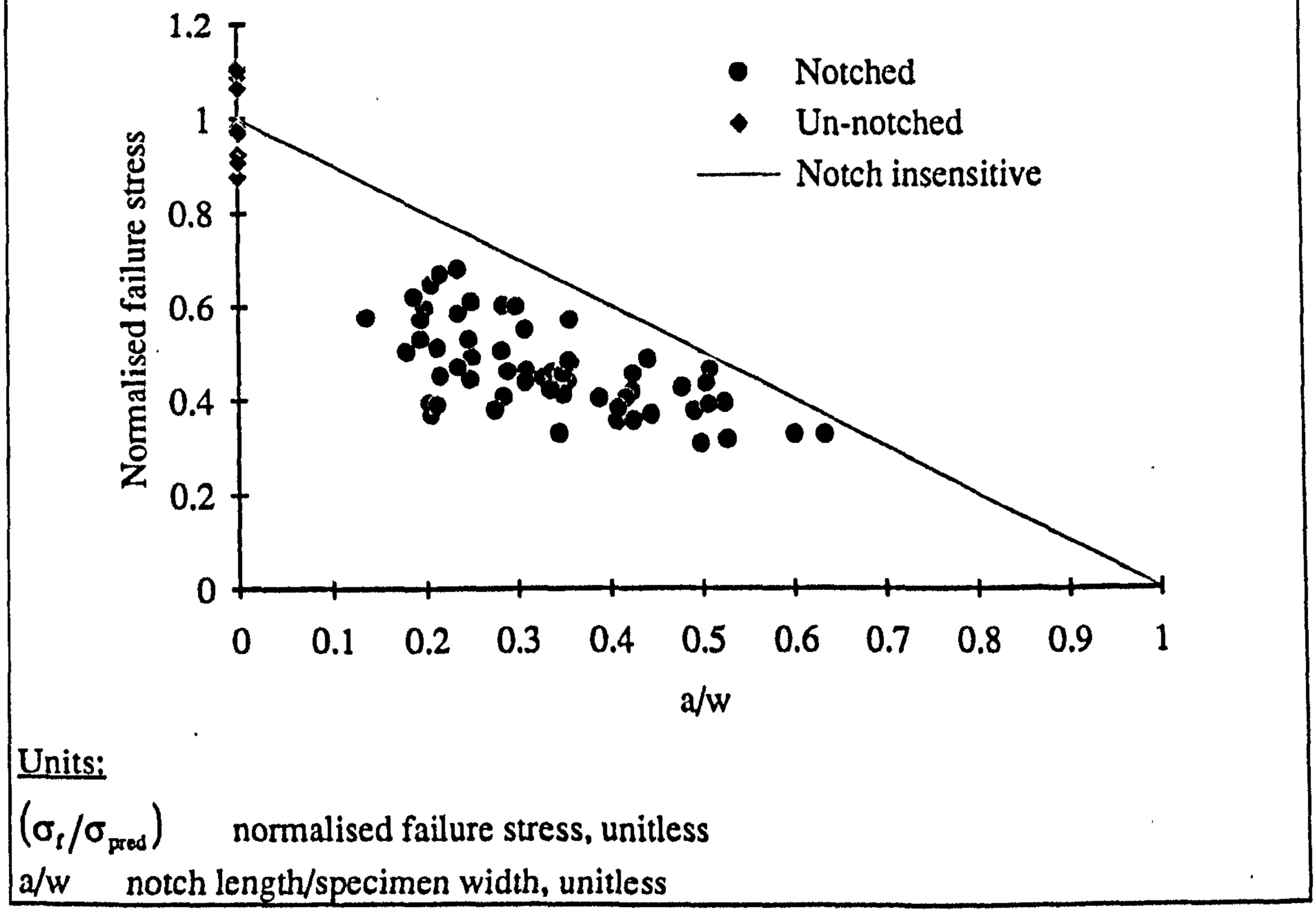

Units:

(σ_f/σ_{pred}) normalised failure stress, unitless

a/w notch length/specimen width, unitless

Figure 7.017

Normalised failure stress (σ_f/σ_{pred}) and a/w for specimens of red deer antler

Table 7.010 shows that some improvement in the correlation of the failure stress to the notch length is obtained by using the predicted stress ratio. The use of the predicted failure stress (derived using equation *e* table 7.010) to normalise the failure stress for the notch specimens has resulted in all the data points falling below the notch insensitive line. Thus indicating that the material is notch sensitive, and those points that fall close to, the equivalent of, this line in figure 7.014 did so because they are composed of antler that is inherently stronger than the average material (whether or not a specimen made from it contains a notch).

The predictive power of the equation used to derive the predicted stress itself is quite poor (*e* table 7.010). Therefore, using the bending modulus and the calcium content of the specimens directly, as separate explanatory variables, was also examined (table 7.011). The results from this analysis are presented in table A10.004. The table shows that this more direct approach explains the failure stress more accurately than the predicted stress method. The inclusion of calcium has little effect on the predictive qualities of the equations. (This is not due to the calcium content and the material stiffness being strongly related to each other, $R^2 = 1.1\%$.) The inclusion of the notch tip radii in equations *d* and *e* of table 7.011, decreased the value of the coefficient of regression by about one per cent. The regression equations in table 7.011 show that the failure stress of the SEN specimens of antler examined here is almost equally significantly dependent on the material's stiffness as it is on the notch length.

The aim of this analysis was to determine the relationship of the failure stress to notch length in SEN specimens of antler: is the relationship one of a notch-sensitive or notch insensitive material? The results in tables 7.010 and 7.011 show that a/w is a better predictor of the failure stress than using $a^{-0.5}$. The former variable is also more significant in each set of comparable equation. Taken at face value this implies that antler is behaving in a way that is more similar to a notch insensitive material than it is to a classically notch sensitive one. However, in this section I have shown that antler specimens containing a notch are less strong than would be suggested if the material were notch insensitive. One method that is available to explore this observation in more detail is to examine the ligament stress; which for a notch insensitive material is constant.

Type of antler specimen	Regression equations and t value of the nominal failure stress of SEN specimens of red deer antler	R^2%	
59 SEN	$\sigma_f = 30.9 - 42.8\,(a/w) + 2.28\,E_b$ t: 7.49 - 6.14 7.19	59.0	*a*
59 SEN	$\sigma_f = -6.60 + 0.876\,a^{-0.5} + 2.30\,E_b$ t: - 1.06 4.85 6.67	51.7	*b*
59 SEN	$\sigma_f = -4.5 - 43.9\,(a/w) + 2.18\,E_b + 0.161\,Ca^{++}$ t: - 0.16 - 6.28 6.70 1.29	59.4	*d*
59 SEN	$\sigma_f = -38.6 + 0.896\,a^{-0.5} + 2.21\,E_b + 0.142\,Ca^{++}$ t: - 1.23 4.94 6.22 1.04	51.8	*e*

Units:

σ_f	Stress at failure, MPa
E_b	Material stiffness (modulus) in three-point-bending, GPa
w	Specimen width, mm
a	Notch length, mm
$a^{-0.5}$	Reciprocal square root of notch length, $m^{-0.5}$
Ca^{++}	Calcium ion concentration in dry mass of defatted bone by weight, mg g^{-1}

Table 7.011

The relationships between the failure stress and various mechanical and geometrical properties of SEN antler specimens

7.4.3.4. RESULTS: LIGAMENT STRESS

Another way to investigate the relation of failure stress to notch length is to calculate the ligament failure stress. This will be defined as the load at failure divided by the ligament area or

$$\sigma_{lig} = \frac{\sigma_f\, w}{w - a} \qquad (7.015)$$

This approach is somewhat similar to those already used, as this equation can be manipulated to give

$$\sigma_f = \sigma_{lig} - \sigma_{lig}\,(a/w) \qquad (7.016)$$

For a notch insensitive material the ligament stress will be, by definition, a constant. Therefore, if antler is notch insensitive the ligament stress at failure should show no relationship with a/w or a, and should be the same as the value obtained from the un-

notched specimens. For the 59 specimens containing notches the mean value of the ligament stress at failure was 62.4 MPa (s.d. 13.33) this is almost 30% less than the mean value for the un-notched specimens (86.5 MPa). So, it appears that the notch does have an effect greater than that due to the simple reduction in cross-sectional area. This is supported by equation *c* of table 7.012 where the ratio of notch length to specimen width is shown to be a highly significant predictor of the ligament stress.

In equation *c* of table 7.012 the material stiffness is shown to be a very highly significant predictor of ligament strength. Analysis showed that the correlation of the ligament stress at failure and the material stiffness measured in three-point-bending is the best correlation of a failure stress (ligament or nominal) and a single predictor obtained in this data set (NA3) it has an $R^2 = 45.8\%$ for the 59 specimens. This may be because the ligament stress is already related to the specimen geometry, due to the manner of its calculation.

Type of antler specimen	Regression equations and t value	R^2%	
59 SEN	$\sigma_{lig} = -8.46 + 0.803\,\sigma_{pred}$ t: - 0.85 7.21	46.8	*a*
59 SEN	$\sigma_{lig} = -40.9 + 3.35\,E_b + 0.294\,Ca^{++}$ t: - 0.94 6.55 1.51	47.0	*b*
59 SEN	$\sigma_{lig} = -36.2 - 32.7\,(a/w) + 3.33\,E_b + 0.227\,Ca^{++}$ t: - 0.90 3.21 7.02 1.25	54.5	*c*

Units: σ_{lig}, MPa. σ_{pred}, MPa. E_b, GPa. a/w, unitless $a^{-0.5}$, $m^{-0.5}$. Ca^{++}, mg g^{-1}.

Comments:

In equations *b* and *c* the inclusion of calcium produces a slight improvement in the predictive power of the relationship, but this predictor has little significance.

Table 7.012

The ligament stress of red deer antler SEN specimens

In this section I have shown that antler is notch sensitive. The ligament strength of a specimen containing a notch is on average 30% less than the strength of specimens that do not contain a notch. This reduction in strength is related to the size of the notch and to the stiffness of the material. The effect of changing material stiffness has a similar

effect on the ligament stress as it does on the strength of un-notched specimens: a higher stiffness results in a higher failure stress.

7.4.3.5. RESULTS: FAILURE STRAIN AND NOTCH LENGTH

In this section I report the results of analysis of the relationship of the *failure strain*, ε_f, to some of the other fracture parameters. The concept of strain in relation to notched specimens should be treated with caution. In these tests the term strain is used to describe the extension of a portion of the specimen (approximately 10 mm), containing the notch, divided by the initial length of that portion of the specimen. This definition is essentially the same as that given in section 2.2.1.1 for nominal strain. However, in section 2.2.1.1 the definition was applied to a uniform rod, whereas here the material contained a discontinuity in the form of a notch. If the material is notch sensitive this notch will have the effect of concentrating the stress and thus strain at its tip. Due to this discontinuity the strain measure used here should be viewed as an average over the length considered. If the material is notch insensitive the failure strain will be the same for a notched or un-notched specimen.

The failure strain used here was, in nearly all cases, the strain recorded when the maximum value of stress was first reached. In some cases the slope of the stress-strain curve reduced dramatically before this point (but had not become negative). In these cases the value of the strain at which this change occurred was used. It was shown in section 4.2.6.9 (figure 4.016) that all the un-notched specimens of red deer antler failed at a strain greater than 0.04 at any of the cross-head speeds used. (At the same speed as used in these test the lowest value of strain was greater than 0.06.) The result for the un-notched specimens from the data set considered here (NA3, produced from the same antler as the notched specimens) show a similar result: for these twelve un-notched specimens the mean ultimate strain was 0.077 (s.d. 0.011) and the smallest value was 0.06. In the light of the results from un-notched specimens, the observation that no notched specimen failed at a strain greater than 0.04 shows that the material is notch sensitive. Further examination of the results for the un-notched specimens, section 4.2.6.8, shows that the knee strain of the un-notched antler specimens is also more than the failure strains of these notched specimens.

There is one important difference that should be considered when comparing the failure strain of notched specimens with the strains of un-notched specimens. The failure strain of the notched specimens, as defined here, is not necessarily the maximum value obtained during the test, but that which it assumed to be associated with the initiation of fracture. Many of the antler specimens exhibited a progressive, almost a slow ripping

type, fracture propagation. This is in stark contrast to the fast fracture associated with brittle materials. (This was demonstrated by the plots in figure 7.002.) Also, the measure of strain used is an average, over about 10 mm, so the effect of high strains around the notch is smoothed out.

A similar search for significant explanatory variables of failure strain, to that conducted for explanatory variables of failure stress, was carried out. (The variables investigated included: notch length, specimen width, the ratio of these, the notch lengths to the power of negative one half, specimen thickness, tip radius, gauge length, modulus in three-point-bending, calcium content and the logarithmic value of some of these quantities.) This search revealed no reasonable predictor of the failure strain. The best (but still non-significant $p = 0.088$) correlation with a single variable was obtained with the calcium content of the specimen. This is shown in figure 7.018.

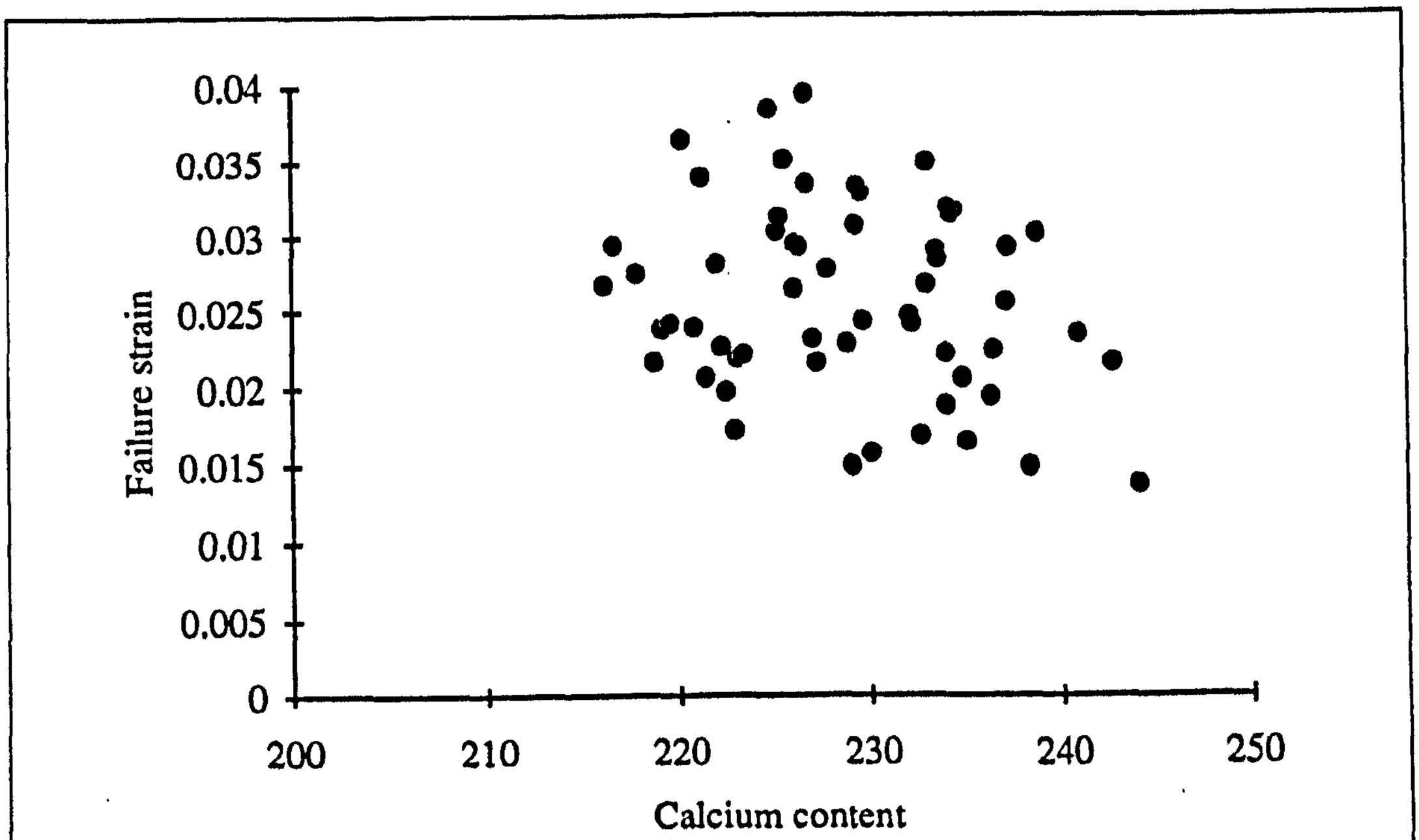

Units:

ε_f Failure strain.

Ca^{++} Calcium content, mg g^{-1}.

Figure 7.018

The relationship between failure strain and calcium content

It can be seen that there is a very slight trend towards larger failure strains at the lower calcium contents. In the examination of the data from the creep tests (section 4.3.7.3 to 4.3.7.6) the regression equations relating the logarithm of the elongation at rupture (for all measures examined) to the logarithm of creep stress and the logarithm of calcium content displayed a similar result. (A similar result is reported by Currey (1990)

for pooled data from bones obtained from a variety of species.) A higher calcium content was related to a lower extension at failure. However, the important observation is that already made regarding the size of these failure strains. These strains, which are associated with the point at, or before, the maximum stress was reached in a SEN specimen of red deer antler are less than those associated with either the knee or failure of un-notched specimens of the same material. However, from the analysis of resilience tests (section 7.4.3.1) the strain values obtained suggest that there is some non-elastic deformation present.

The clear result here is that the strain at which failure starts in a notched specimen of antler is less than that in an un-notched specimen. This is an indication that antler is a notch-sensitive material. As a notch sensitive material it can be expected that there will be a concentration of stress and thus strain at the notch tip. In chapter 8 I present photos and video images that show such a concentration, and thus reinforce this conclusion. This suggests that the strain in the bulk of the material, away from the notch, is lower than the measured value. Thus the main sections of the specimens are more likely to behave in an elastic manner that the failure strain values indicate.

7.4.3.6. RESULTS: PURSLOW'S APPROACH AND OTHER LOGARITHMIC EQUATIONS

In Purslow's approach (section 5.3.4) logarithmic equations that related the failure stress (or failure strain) to the notch length were suggested. The coefficients of these equations were determined by the value of n in the assumed stress-strain relationship $\sigma = k \varepsilon^n$. (See equation 5.067 and 5.068.) Under this heading I will also examine some other forms of logarithmic equation. These are based on Purslow's approach and are similar to those of the more classical Griffith approach. I have already shown that these two approaches predict a very similar relationship of failure stress to notch length when the stress-strain is linear, n = 1 (equations 5.021 and 5.066). An important feature of these equations is that when n = 1 they both predict that the failure stress is dependent on the square root of the material stiffness (in this theoretical case Young's modulus) as well as fracture length. In section 5.3.4 the effect of assuming n = 1 on the predicted relationship of failure stress to notch length was examined by substituting this value in to equation 5.063. This equation is repeated here and converted into a logarithmic prediction of failure stress in the following equations.

$$R = \frac{\sigma_f^{(n+1)/n} \pi a}{k^{1/n} (n + 1)} \qquad (7.017)$$

$$\sigma_f = \left(\frac{\pi a}{k^{1/n} (n + 1) R} \right)^{n/(n+1)} \tag{7.018}$$

$$\ln(\sigma_f) = \frac{n}{n + 1} \ln(R) + \frac{1}{n + 1} \ln(k) + \tag{7.019}$$

$$\frac{n}{n+1} \ln(n + 1) - \frac{n}{n + 1} \ln(\pi) - \frac{n}{n + 1} \ln(a)$$

The results obtained from the tests of SEN specimens of red deer antler have therefore been analysed in a number of related ways. First, n is assumed to be a constant. Thus the equation that this analysis is based on is that given by Purslow (1991) to relate the failure stress to the notch length (equation 5.067). This first approach results in equation *a* of table 7.013. However, when Purslow examined his data, he did so using a normalised form, the normalising factor being specimen width. I adopt this normalisation in my second approach (equation *b*). However, a more general case can be examined, as the logarithm of a fraction may be split into two logarithms:

$$\ln(a/w) = \ln(a) - \ln(w) \tag{7.020}$$

The third form of regression equation I use relates the logarithm of failure stress to the logarithms of notch length and specimen width. The next three equations presented in table 7.013 are repetitions of the first three, but include the material stiffness as an additional variable. The final group of three equations use a predicted value of (n + 1) as the additional variable. The rationale for using this variable is based on equation 7.019 above, and the apparently random values of k (see section 7.4.3.2). Thus it appears that equation 7.019 can be simplified to

$$\ln(\sigma_f) = C_3 + C_4 \ln(n + 1) + C_5 \ln(a) \tag{7.021}$$

Where n is predicted by equation *f* of table 7.007 above, which is repeated here

$$n_{pred} = 0.814 - 0.182 \ln(E_b) \tag{7.022}$$

Using more complex equations (for example based on substituting the predicted value of n into the n/(n+ 1) terms in equation 7.019) produce little or no improvement in predictive power over this form of equation (7.021). The strong correlation between the predicted value of n and the material stiffness prevented the examination of the effect of using both explanatory variables.

As the predicted value of n is a relatively simple function of the material stiffness in three-point-bending it is not surprising the coefficients of determination in the regression equations are little altered when a function of either the material stiffness or a function of n is the second variable considered. In each of the three types of equation examined the use of the material stiffness rather than the predicted value of n gave a relationship with very slightly high predictive power. The material stiffness was a very highly significant predictor in every case. It was also a slightly more significant variable than the predicted value of n in each of the equivalent equations (*d* to *g*, *e* to *h* and *f* to *i*). The inclusion of calcium content as an additional variable in equations *a* to *f* of table 7.013 improves the correlations only slightly (the equations are not presented here), R^2 values become (in the order as shown in the table) 19.5%, 26.2%, 24.9%, 57.9% 63.4% and 63.1%.

The results shown in table 7.013, if viewed in the context of linear elasticity, appear to suggest that the failure stress of antler is more dependent on length of the machined notch than a classically notch sensitive material. For a notch insensitive material the coefficient of the length term would be -1, and for the classically notch sensitive material -0.5, in this case the values obtained are about -0.3. This result appears to be at odds with the earlier finding that the relationship of failure stress to notch length was better described by the notch insensitive model. However, if it is assumed that the material exhibits non-linear elasticity of the form Purslow uses this result may be explained. In his theory Purslow proposes that the value of the coefficient is -n/(n + 1). The mean value I obtained for n from un-notched specimens was 0.39. Thus the coefficient predicted by Purslow's equation is -0.28, which is not too dissimilar to the values I have obtained experimentally especially in equation *d*. I said this may explain the experimental values because I consider there are too many assumptions and approximations in the application of this approach to antler. The main problem is the variability between the mechanical responses of the different antler specimens.

In Purslow's approach a prediction of the failure strain was also included. The data for the specimens tested here did not comply with his predicted relationship, nor was any reasonable correlation with other factors found (as already suggested above, section 7.4.3.5). If the variability of the mechanical response of antler is ignored and this relationship of stress to notch length is accepted at face value, the question arises; what does this relationship mean? In his paper Purslow shows a diagram of the effect of an increasing notch length in material with either a J or ſ shaped stress-strain response. This shows that the material with the ſ shaped stress-strain response will exhibit a proportionally greater decrease in the strain at failure when a notch is present than would a material with a J shaped stress-strain response. The reverse in true when stress is considered. This idea will be returned to in the main conclusion section of this chapter.

Type of antler specimen	Regression equations and t value	R^2%	
59 SEN	$\ln(\sigma_f) = 3.79 - 0.259 \ln(a)$ t: 85.32 - 3.26	14.2	*a*
59 SEN	$\ln(\sigma_f) = 3.30 - 0.331 \ln(a/w)$ t: 33.76 - 4.07	21.6	*b*
59 SEN	$\ln(\sigma_f) = 3.31 - 0.332 \ln(a) + 0.324 \ln(w)$ t: 15.09 - 3.97 2.22	19.8	*c*
59 SEN	$\ln(\sigma_f) = 2.29 - 0.291 \ln(a) + 0.646 \ln(E_b)$ t: 11.56 - 5.18 7.66	57.4	*d*
59 SEN	$\ln(\sigma_f) = 1.80 - 0.350 \ln(a/w) + 0.634 \ln(E_b)$ t: 9.06 - 6.27 8.08	62.9	*e*
59 SEN	$\ln(\sigma_f) = 1.88 - 0.357 \ln(a) + 0.295 \ln(w) + 0.638 \ln(E_b)$ t: 8.05 - 6.24 2.96 8.06	62.6	*f*
59 SEN	$\ln(\sigma_f) = 5.42 - 0.291 \ln(a) - 4.94 \ln(n_{pred} + 1)$ t: 25.09 5.17 7.62	57.1	*g*
59 SEN	$\ln(\sigma_f) = 4.87 - 0.350 \ln(a/w) - 4.85 \ln(n_{pred} + 1)$ t: 23.65 - 6.26 - 8.04	62.7	*h*
59 SEN	$\ln(\sigma_f) = 4.96 - 0.358 \ln(a) + 0.296 \ln(w) - 4.87 \ln(n_{pred} + 1)$ t: 19.49 - 6.23 2.96 - 8.02	62.3	*i*
Units: σ_{lig}, MPa. σ_{pred}, MPa. E_b, GPa. w, mm. a, mm.			

Table 7.013

Various logarithmic relationships of failure stress to notch length

7.4.3.7. RESULTS: LEFM APPROACH, THE CRITICAL STRESS INTENSITY AND SHAPE CORRECTION FACTORS

In this section I examine the results of substituting the values obtained from tests on SEN specimens of red deer antler into the equations obtained from the stress intensity factor approach to LEFM. I have already shown that antler should not be considered elastic or linear at the stresses considered here. However, the substitution of the experimental values into these equations for this material produces results that can be compared with those I have obtained for bovine bone. Thus this approach, although clearly not a justifiable technique for examining antler, may cast light on the results and thus the behaviour of bovine bone.

The mechanical and geometric values obtained from this set of tests (NA3) were substituted into the expressions for the various critical stress intensity factors used in this work K^{I}_{IQ}, K^{U}_{IQ} and K^{P}_{IQ} (these were defined in section 7.2.5.2). Based on the analysis of the initial tests I have already stated that the reduction of the restraints on the specimen increases the value of the SIF and decreased the correlation of the SIF with the material's modulus. The reduction in the assumed restraints also increased the correlation of the stress intensity factors with the specimen geometry (as in the initial tests). The relationships of the SIF to E_b and the SIF to a/w are shown graphically in figures 7.019 to 7.020, and statistically in table 7.015.

Type of antler specimens	K^{I}_{IQ}, MPa $m^{0.5}$ mean (s.d.)	K^{U}_{IQ}, MPa $m^{0.5}$ mean (s.d.)	K^{P}_{IQ}, MPa $m^{0.5}$ mean (s.d.)	
59 SEN	2.83 (0.64)	3.72 (0.92)	5.56 (2.3)	*a*

Table 7.014

Values of the various stress intensity factors as used in LEFM, applied to notched specimens of antler (set NA3)

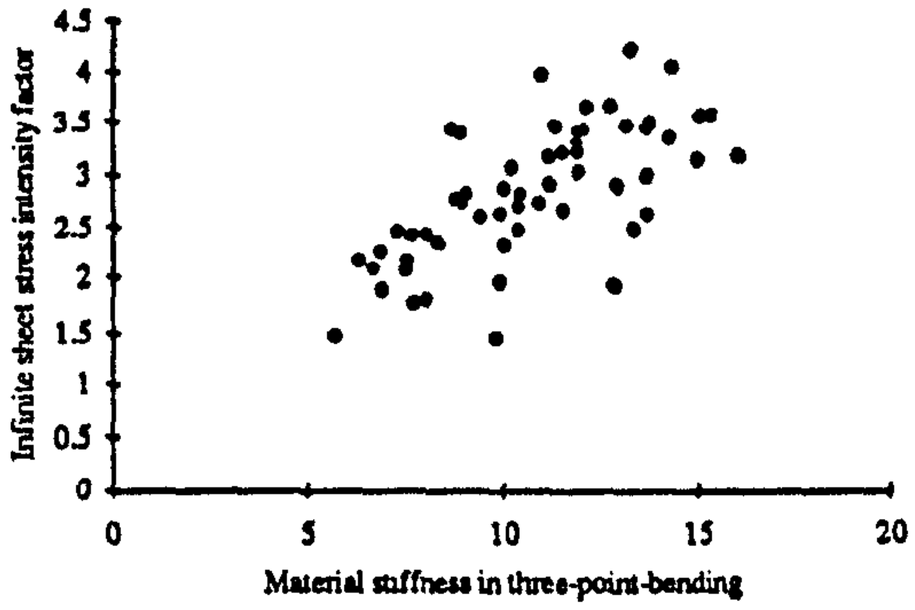

a) Infinite sheet stress intensity factor

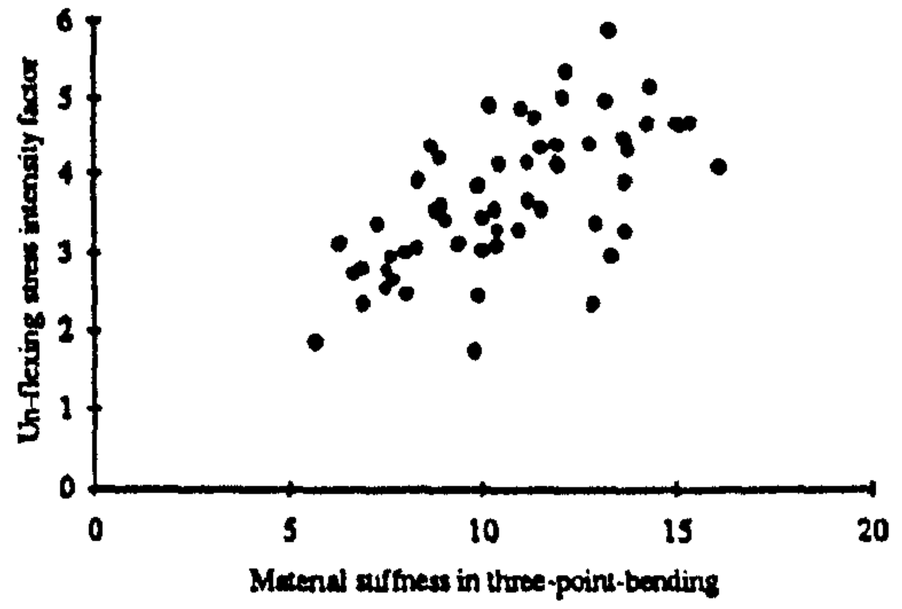

b) Un-flexing sheet stress intensity factor

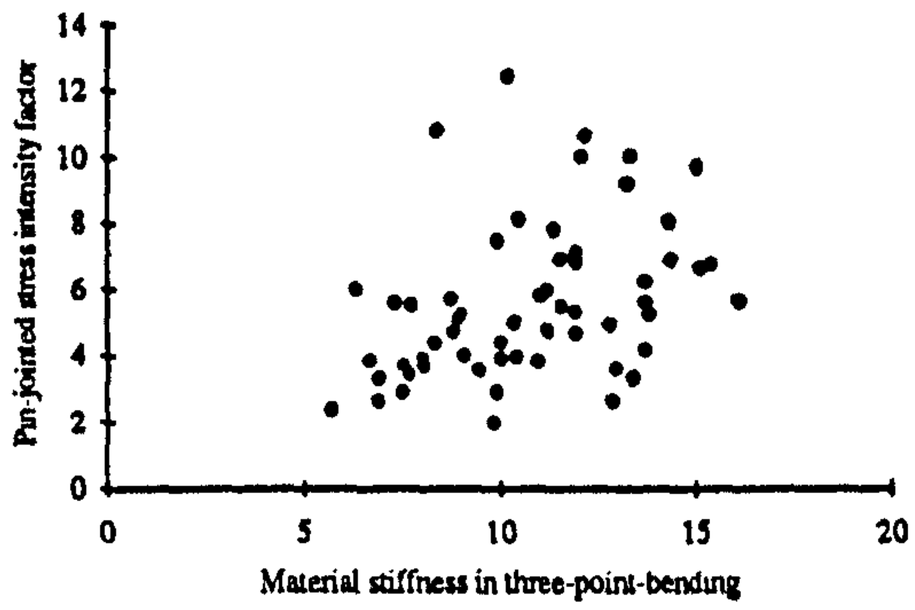

c) Pin-jointed stress intensity factor

Decreasing assumed restraints on the specimen (infinite sheet to un-flexing sheet to pin-jointed) decreases the correlation of the calculated critical stress intensity factor and the material stiffness. The critical stress intensity factor is supposedly a material property thus its correlation with another material property is not surprising.

<u>Units:</u>

a) K^{I}_{IQ}, MPa $m^{0.5}$. E_b, GPa.

b) K^{U}_{IQ}, MPa $m^{0.5}$. E_b, GPa.

c) K^{P}_{IQ}, MPa $m^{0.5}$. E_b, GPa.

Figure 7.019

<u>The relationships of the calculated critical stress intensity factors (K^{I}_{IQ}, K^{U}_{IQ} and K^{P}_{IQ}) and the material stiffness</u>

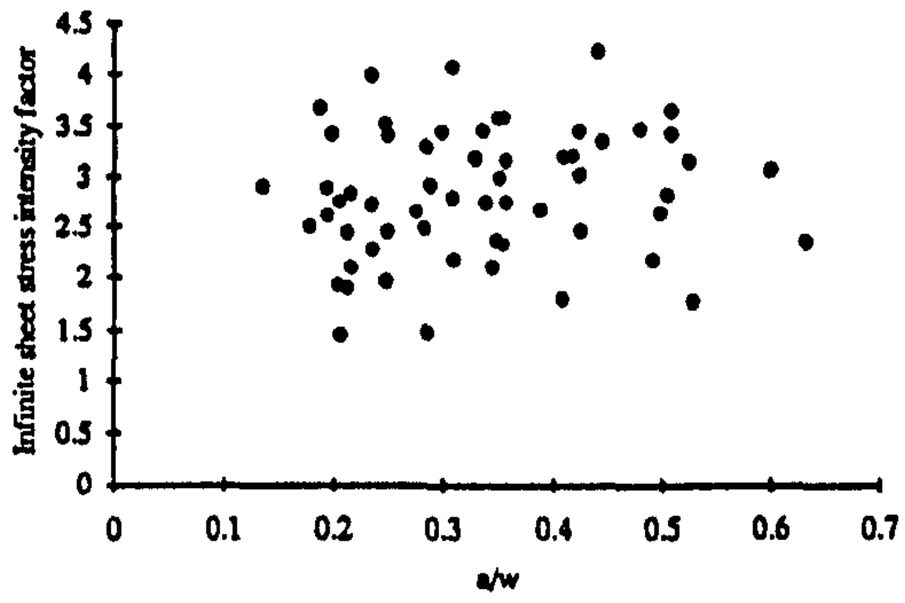

a) Infinite sheet stress intensity factor

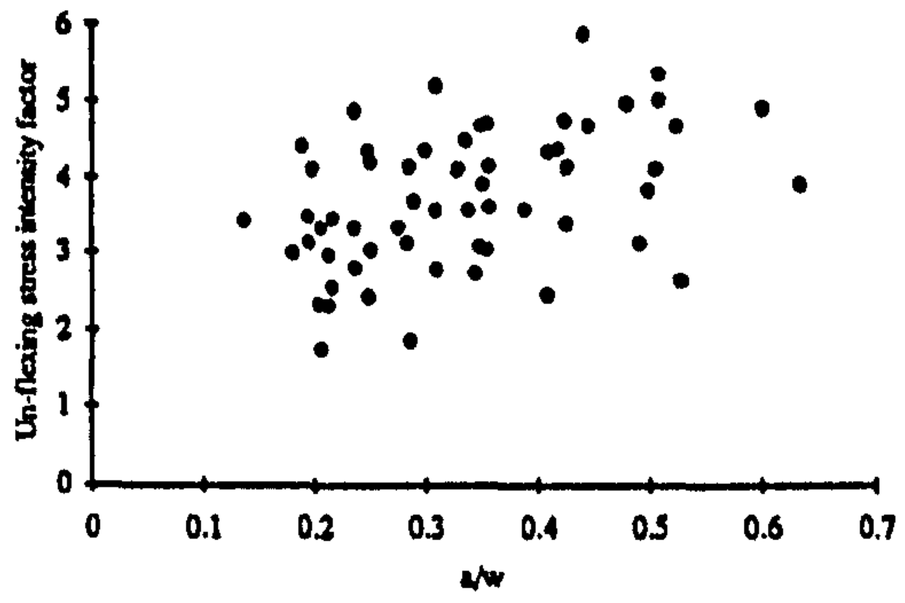

b) Un-flexing sheet stress intensity factor

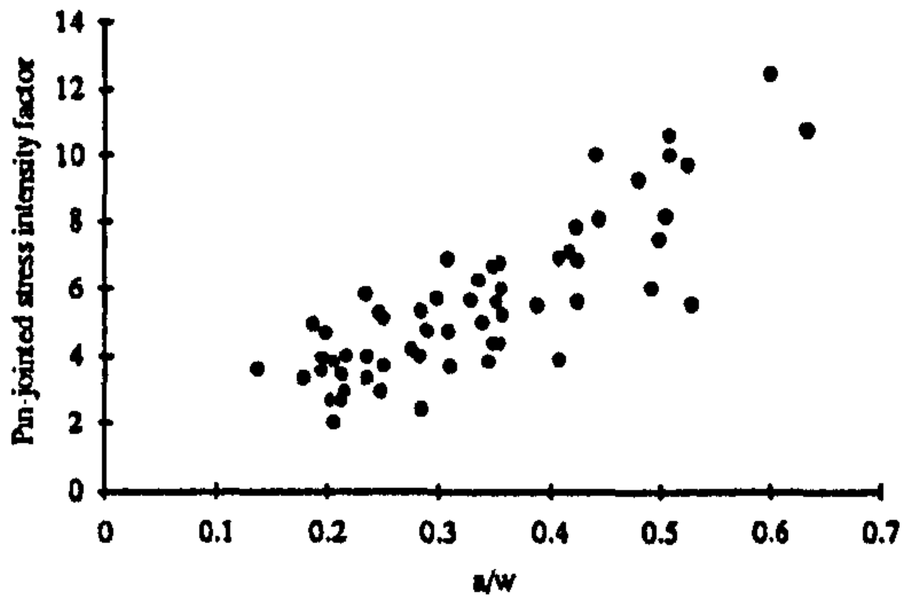

c) Pin-jointed stress intensity factor

A decrease in the assumed restraints on the specimen prompts an increase in the correlation of the calculated critical stress intensity factor and the specimen geometry (this is shown in figures a, b and c). The critical stress intensity factor is supposedly a material property thus its correlation with a geometrical factor is undesirable.

Units:

a) K^{I}_{IQ}, MPa $m^{0.5}$. a/w, ratio.

b) K^{U}_{IQ}, MPa $m^{0.5}$. a/w, ratio.

c) K^{P}_{IQ}, MPa $m^{0.5}$. a/w, ratio.

Figure 7.020

The relationships of the calculated critical stress intensity factors (K^{I}_{IQ}, K^{U}_{IQ} and K^{P}_{IQ}) and the ratio of notch length to specimen width

Type of antler specimens	Regression equation and t values	R^2 %	
59 SEN	$K^{I}_{IQ} = 1.00 + 0.170\ E_b$ t: 3.76 7.00	45.3	*a*
59 SEN	$K^{U}_{IQ} = 1.27 + 0.228\ E_b$ t: 3.17 6.24	39.6	*b*
59 SEN	$K^{P}_{IQ} = 1.86 + 0.345\ E_b$ t: 1.52 3.11	13.0	*c*
59 SEN	$K^{I}_{IQ} = 2.56 + 0.773\ (a/w)$ t: 10.03 1.07	0.3	*d*
59 SEN	$K^{U}_{IQ} = 2.55 + 3.47\ (a/w)$ t: 7.79 3.71	18.0	*e*
59 SEN	$K^{P}_{IQ} = - 0.024 + 16.6\ (a/w)$ t: - 0.05 11.47	69.3	*f*
Units: K^{*}_{IQ}, MPa $m^{0.5}$. E_b, GPa. a/w, ratio.			

Table 7.015

Relationship of various calculated critical stress intensity factors to the material stiffness or the ratio of the notch length to the specimen width

7.4.3.8. RESULTS: EFFECT OF NOTCH TIP RADIUS

In the analysis all the data from these experiments (NA3) I have not mentioned the effect of notch tip radius. To analyses the effect of notch tip radius on the mechanical properties examined I repeated all the regression equations using the notch tip radius as an additional variable. The inclusion of the tip radius was in the form of $\rho^{0.5}$ in the linear predictions or in the form $\ln(\rho)$ in the logarithmic ones. In every case it was found that the inclusions of this additional variable reduced the value of R^2. I therefore conclude that, as shown in the initial tests, the notch tip radius has no effect on the measures of failure behaviour examined here.

7.4.3.9. RESULTS: EFFECT OF SPECIMEN WIDTH

No evidence was found to suggest a significant difference between the properties of the nominally 4 and 6 mm wide un-notched specimens. However, it is clear from equation *f* of table 7.013 that the specimen width has a highly significant effect on the failure stress. In the theoretical equations of LEFM the fracture is considered to be within an infinite sheet. When this theory is applied to the data from experimental tests a shape correction factor is used to account for the specimens smaller size and different geometry. This could be one explanation for the dependence on specimen width. Another explanation could be that the failure process is not that envisaged in classical fracture mechanics, but is similar to the failure of un-notched specimens. The use of such a fracture mechanics approach may be further complicated by the non-linear non-elastic nature of the material.

7.4.4. SUMMARY OF FINDINGS AND CONCLUSIONS DRAWN FROM DATA SET NA3

The data examined in this section were obtained from notched and un-notched specimens obtained from a single red deer antler. The un-notched specimens were used to examine the aspects of the material's mechanical behaviour that are important in the application of the theories of fracture mechanics. A number of important results emerged from the analysis of this behaviour and the application of the various approaches used to investigate the fracture of antler. Some of these results although of limited importance in this aspect of the study of antler and bone have ramifications for the wider study of these materials.

a) Antler appears to be elastic at strains less that 0.002. Above this value of extension the energy supplied to the material was not recovered on unloading. (However, I suggest this could depend on cross-head speed.)

b) The unloading path is not linear nor does it pass through the origin.

c) The resilience of antler is more strongly correlated with the maximum strain than it is with the maximum stress.

d) The function $\sigma = k \varepsilon^n$ can be used as a reasonable model of the loading stress-strain response of antler. Although this equation is obviously superior to a linear relationship it has only a limited ability to model the knee region. (The advantage in finding a more appropriate relationship is reduced by the lack of elasticity exhibited by this material.)

e) The values of n and k for antler are not constant. The relationship of n to the material stiffness is very highly significant. A significant predictor of k was not found.

f) Antler is notch sensitive.

g) The most reasonable model for the relationship of the failure stress of a SEN specimen of antler to the notch length appears to be one based on Purslow's approach (the equation he suggested with the addition of a material stiffness term).

$$\ln(\sigma_f) = 1.80 - 0.350 \ln(a/w) + 0.634 \ln(E_b) \qquad (7.023)$$

However, there are a considerable number of approximations and assumptions contained within the application of Purslow's approach. The explanatory power of this relationship is only a few percentage points greater than that provided by either the classically notch sensitive approach or the notch insensitive approach. Thus the exact form of this relationship is still open to debate.

h) When the ligament stress was examined it was estimated that the introduction of a notch had, on average, reduced the strength of the specimens by 30%.

i) The strain associated with the initiation of the failure of the material (normally the maximum stress), calculated for a section of the specimen containing the notch was less than that associated with the knee, or failure, of un-notched specimens, but more than that estimated as the limit of pure elasticity

j) The critical stress intensity factor approach has been applied to the SEN specimens of antler. The application of this approach does not appear to be justifiable due to the material's non-linear and non-elastic response to tensile loading. It was found that the stress intensity factor that did not contain a shape correction factor was the least correlated with the geometry of the specimen, a/w. It was also found that this uncorrected stress intensity factor was the most highly correlated with material stiffness (of the three examined). This may be a result of applying an inappropriate theory, for as I quoted Harris *et al.* (1988) as saying (at the end of chapter 6), there is no reason why such a function cannot be calculated for any type of behaviour; the important question is whether the value obtained has any significance. The relationship of the calculated stress intensity factor and the material stiffness suggests that this calculation does not give a single value that could be considered as a material property. (If this fact was used to justify the rejection of this approach for the examination of antler. This approach would also have to be rejected as a method to examine the fracture of bovine bone. In a later section I will show that the same relationships of the three critical stress intensity factors with the geometrical factor or the material stiffness are displayed by bovine bone.)

k) The effect of specimen width on the fracture behaviour was unclear. The relationship between the width and the failure stress suggests that a shape correction factor may be required. However, the determination of such a quantity, whether it is justifiable or not, is not considered here.

The results of these tests have provided little quantitative information on the fracture behaviour of antler. However, they have provided some qualitative information

on the fracture process. I consider the most interesting result to be the apparent departure from elastic behaviour before the initiation of fracture propagation. This will deduce the amount of energy that will be released from the material by the propagation of a fracture. Therefore it increases the amount of energy that will be required from external sources. Griffith (1920) (see section 5.2.2.2) gave the equation

$$U_t = U_0 + U_e + U_s - F \qquad (7.024)$$

The energy released due to fracture propagation is U_e. For the specimens examined here, the fracture was not catastrophic, but took the form of a slow rip with a convoluted fracture surface. During this fracture process the test machine was still in motion, so work was still being supplied to the specimen. Therefore it can be assumed that the energy required by the fracturing process was considerably more than that available due to the propagation of the fracture. Later it will be shown that this situation is not true for specimens of bovine bone.

At the beginning of this section I suggested that a more important result than the numerical values examined here was the observation of a whitened zone at the notch tip. In the next section I examine the results of a set of experiments designed to obtain more information, both qualitative and quantitative, on this whitened zone.

7.5. NOTCH SENSITIVITY OF ANTLER (NA4): PROCESS ZONE CORRECTION TO NOTCH LENGTH

In the previous section I noted that a zone of whitened material was observed at the tip of the notch. In this section I examine what implications this whitened zone may have for the fracture process. More specifically I will examine the size of the whitened zone ahead of the machined notch tip, at the instant of the first observed fracture propagation. The optical changes in this zone indicate that the material is undergoing a similar process to that which occurs during the knee region of a tensile test. (The evidence to support this statement is provided in chapter 8, appendix 11 and in the images recorded on the accompanying video tape.) I have suggested that the knee region in the stress-strain curve obtained during a the tensile test is due to damage accumulation in the form of numerous microcracks. I conclude that the process zone at the notch tip in a SEN specimen of antler is composed of similarly damaged, not plastically deformed, material (as exhibited by elastic-plastic materials; those normally considered in the theoretical explanation of fracture mechanics, as in chapter 5). Examination of the notch tip process zone may reveal more information on the failure processes of antler. An examination of this process zone may help to explain the lack of dependence of the

failure stress on the notch tip radius. For example, the existence of cracks ahead of the machined notch has already been proposed as an explanation of the lack of a relationship between the notch tip radius and the mechanical behaviour of bone (Bonfield, 1981 and 1987, see section 6.4).

7.5.1. AIMS AND EXPERIMENTAL DESIGN

The experiments in this series of tests (NA4) were conducted on SEN specimens of red deer antler. These experiments overlap the previous tests and those of set NA5. They are also replicated using bovine bone as the test material in data set NB4 (section 7.8). The main aim of these tests, NA4, was to examine the size and implications of the zone of whitened material observed at the notch tip just before fracture initiation. Chapter 8 contains some pictures of this phenomenon, obtained using a high speed video system. The information used here, the length of the whitened zone at the instant of failure, was obtained from examination of the video tape recordings.

The experimental design was based on an examination of antler specimens of constant nominal width (4 mm) and small range of notch lengths (nominally 2 mm), but possessing a range of notch tip radii.[17] (The mean values of the measured tip radii for the various drills used are: 0.89, 0.75, 0.70, 0.66, 0.66, 0.48, 0.48, 0.40, 0.36, 0.32 and 0.19 mm.)

7.5.2. EXPERIMENTAL PROCEDURE

Specimen preparation and testing were performed according to the protocol in appendix 2. The specimens were obtained from the same antler as that used to obtain specimens for the investigation of tensile properties at different cross-head speeds (data set TA1 described in chapter 4) and SEN specimens at different cross-head speeds (data set NA5). The material stiffness in three-point-bending was obtained for each specimen, as described before; using a cross-head speed of 8.3×10^{-6} m s^{-1}. All the tensile tests of the SEN specimens were conducted at cross-head speed of 8.3×10^{-5} m s^{-1}. These tensile tests were recorded on high speed video tape, at a rate of 1000 images per second. The test protocol used for making a video recording of the tests is the same as that used in the case of the un-notched specimens. The SEN specimens were tested in the natural orientation, that is, one similar to their position in the original structure (section 4.2.3).

---

[17]The small range of notch lengths used removes a considerable amount of variance due to this factor. Therefore it prohibits the rigorous examination of the effect of this variable on quantities such the stress intensity factor.

7.5.3. DATA ANALYSIS AND RESULTS

In the theoretical section on fracture mechanics it was stated that the mathematically predicted stress (based on the assumption of a purely elastic material) at the fracture tip was not reached, as real materials cease to be elastic at stresses smaller than the predicted one (5.2.3.7). In the theoretical section it was assumed (in keeping with the literature on the subject) that the material becomes plastic at a certain stress, thus limiting the value of the maximum attainable stress. Therefore to enable an energy balance approach like Griffith's, which was based on the mathematical predictions of stress, to remain valid a modification accounting for this plastic behaviour must be incorporated. In section 5.2.3.7 such a modification, due to Irwin, was introduced. His modification assumes that an *effective fracture length* can be used in place of the actual fracture length. This effective length is defined as the length of the machined notch with the addition of half the length of the process zone in the line of the fracture, or $a + r_y$.

The determination of the process zone size in the theoretical section was based on the application of the stress intensity factor approach. I have suggested that this is not valid for antler. However, the correlation of optical changes with the occurrence of the knee region of the tensile test suggests another method of determining the size of this zone; simply measuring its length. (The method used to obtain this measurement is given below.) This measurement enables a modification, similar to Irwin's, to be applied to the data analysed here. The data are examined in a similar way to the previous sets of data. However, the predictive equations are repeated. In the second equation the notch length is augmented by, r_w, half the measured length of the whitened zone. ($r_w = d_w/2$, where d_w is the length of the whitened zone measured from the machined notch tip in the line of the notch, on the video frame preceding that on which fracture propagation is first visible). This nomenclature has been adopted in place of r_y and d_y as the whitened zone does not consist of plastically deformed material. This measurement is shown diagrammatically in figure 7.021. The additional length, r_w, was used in all stages of the calculation of the second of each pair of equations. (Thus the values of the notch length to specimen width ratio and the shape correction factors will all be modified.) The equations will not be presented in full. Instead, tables indicating which explanatory variables are considered, whether they are significant and the resulting R^2 values are given. If the effective notch length accounts for the effect of the process zone, then the explanatory power and significance of the length term quantity should increase.

The approximate length of the white zone was obtained from two estimates: first its length relative to the tip radius of the notch; second its length relative to the width of the reduced section. These relative lengths were then multiplied by the measured dimensions of the relevant feature. The two estimates of the zone length were averaged

to give one value for each specimen. Approximations had to be made as to the edge of the area, these edges are not clear cut, nor is the whitened zone a regular shape. This process was aided by examining the video images of both the real-time recordings and those re-recorded at 30 frames per second (the original rate was 1000 frames per second). The frame in which the fracture is first seen was located by using the rewind and jog facilities of the video tape player. In some cases it was necessary to take into account the change in shape of the drilled hole.

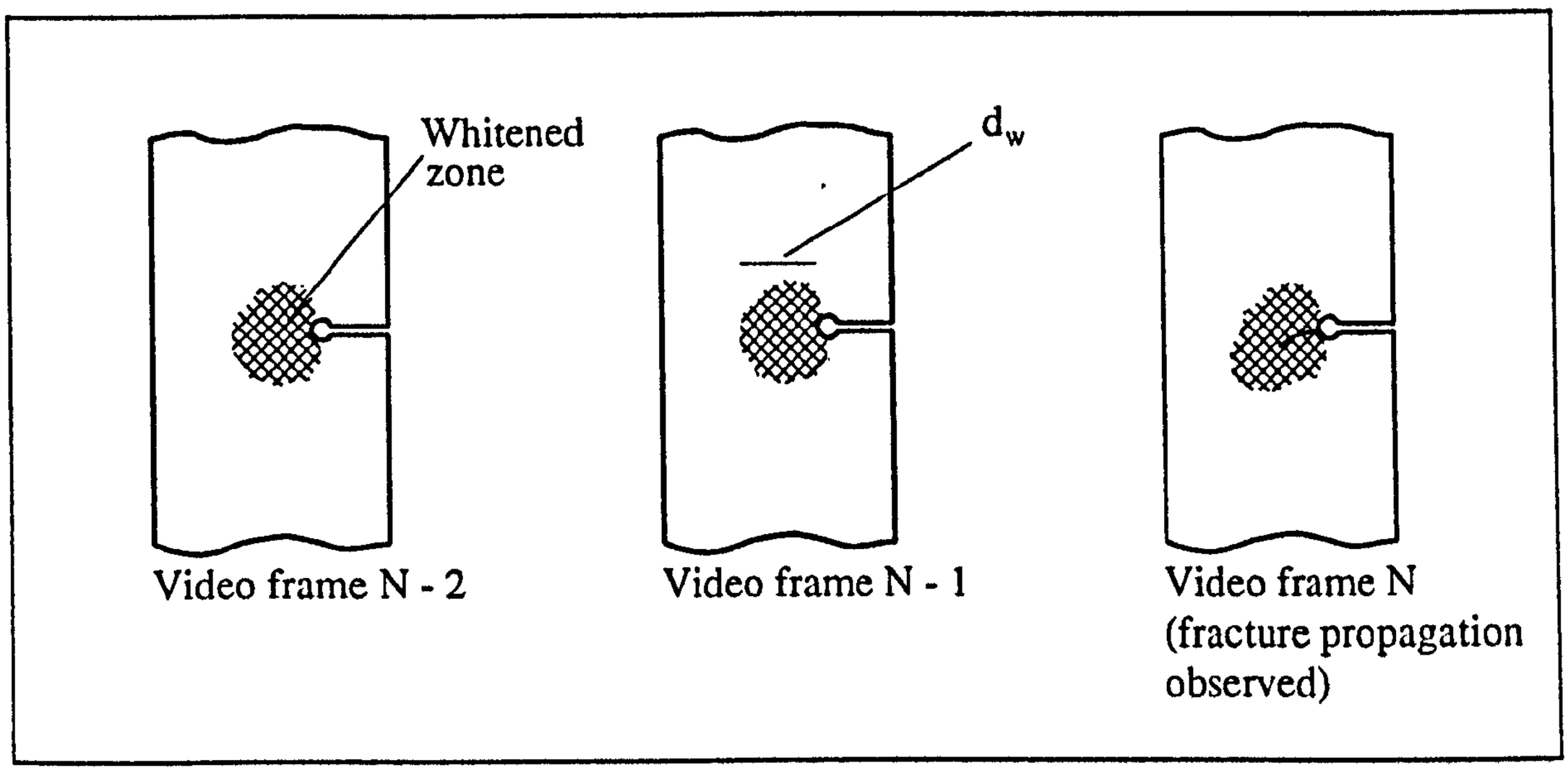

Figure 7.021

A diagrammatic representation of the whitened zone at the notch tip measured on the video frame prior to that on which the first fracture propagation was observed

7.5.3.1. RESULTS OBTAINED USING THE MEASURED NOTCH LENGTH AND IRWIN'S EFFECTIVE FRACTURE LENGTH: FAILURE STRESS

In this section the results of regression analysis of the relationship of the failure stress and the length of the machined notch are examined. As in the analysis of data set NA3 the classically notch sensitive and notch insensitive cases are examined. Each regression was repeated, in the second case the length term included half the length of the whitened zone. The regression equations are not given, as the important feature is whether the effective notch length is a better predictor than the machined notch length. This in turn may indicate if the fracture process of antler can be numerically, and thus possibly descriptively, described using such a modification to the various theories of fracture mechanics. Some of the results are presented in table 7.016. This table indicates which explanatory variables are used, if they are significant and the coefficient of determination, or $R^2\%$ (adjusted for degrees of freedom). It should be remembered that the range of values of the machined notch length was limited and the specimen width effectively constant.

Predictors of the failure stress, σ_f					R^2%	
(a/w)	$(a + r_w)/w$	$a^{-0.5}$	$(a + r_w)^{-0.5}$	E_b		
NS	-	-	-	-	2.1	*a*
-	NS	-	-	-	0.9	*b*
-	-	NS	-	-	2.5	*c*
-	-	-	NS	-	0.7	*d*
HS	-	-	-	VHS	67.5	*e*
-	NS	-	-	VHS	51.5	*f*
-	-	HS	-	VHS	67.0	*g*
-	-	-	NS	VHS	51.7	*h*

Units:

σ_f	Stress at failure, MPa
E_b	Material stiffness (modulus) in three-point-bending, GPa
w	Specimen width, mm
a	Notch length, mm
$a^{-0.5}$	Reciprocal square root of notch length, $m^{-0.5}$
r_w	Half the length of the whitened zone, mm

Table 7.016

The significant of the measured notch length and that augmented by the addition of half the length of the whitened zone as predictors of failure stress

Table 7.016 shows that the addition of half the length of the whitened zone decreases the predictive power of the notch length as an explanatory variable of failure stress (*a* and *b*; *c* and *d*). The overall low predictive power of this variable is probably due to the limited range of notch lengths used. From the analysis presented in previous sections it is known that the material stiffness has a significant effect on the value of the failure stress, therefore this variable is also included (*e*, *f*, *g* and *h*). The inclusion of this variable helps to account for over half of the total variation. Thus the notch length has a greater possibility of explaining the remaining variance. Both the classically notch insensitive and classically notch sensitive forms of relationships based on the machined notch length have a higher coefficient of determination, R^2%, than the equivalent relationship based on the effective fracture length. The addition of half the length of the whitened zone has reduced the R^2% values by about a quarter in each case. When the significance of the length variable is considered in the last four equations the result is reinforced. Without the correction the notch length is a highly significant predictor of failure stress in both forms of relationship. The effective fracture length is not a significant predictor of the failure stress. The regression equations indicate that this length correction, based on the measure of effective fracture length does not increase the

accuracy of the predictive equations. This suggests the analogy with Irwin's correction for a plastic zone is invalid. A similar conclusion is reached if the logarithmic form of the variables is examined. These results are shown in table 7.017.

Predictors of the logarithm of the failure stress, $\ln(\sigma_f)$				R^2%	
$\ln(a)$	$\ln(a + r_w)$	$\ln(E_b)$	$\ln(w)$		
NS	-	-	-	1.3	*a*
-	NS	-	-	0.9	*b*
HS	-	VHS	-	67.9	*c*
-	NS	VHS	-	54.9	*d*
HS	-	VHS	NS	66.7	*e*
-	NS	VHS	NS	53.2	*f*
Units: σ_f, MPa. E_b, GPa. w, mm. a, mm. r_w, mm.					

Table 7.017

The significant of the measured notch length and that augmented by the addition of half the length of the whitened zone as predictors of failure stress in logarithmic form

As with table 7.016, table 7.017 shows that using the effective fracture length in place of the machined notch length reduces the significance of the length variable as a predictor of the failure stress.

7.5.3.2. POSSIBLE EXPLANATIONS FOR, AND IMPLICATIONS OF, THE LOWER DEPENDENCE ON IRWIN'S EFFECTIVE FRACTURE LENGTH THAN ON THE NOTCH LENGTH.

Using the addition of some fraction of the length of the whitened zone as a correction to the notch length appears to be a sensible procedure. However, the evidence presented above indicates that either this procedure is not valid for this material or that some other function of the whitened zone length should be used. It must also be remembered that the method used to obtain this length is not a rigorous mathematical one as expounded in section 5.2.3.7 (almost impossible with such an ill-defined and variable material) but an experimental one.. Thus the measured length is open to variability in the material and in the accuracy of the estimates on which it is based. No consideration has been given to the state of stress or strain within the material, or to what depth below the surface these optical changes are related to. (If the analogy with a plastic zone is valid than the zone's dimensions will be larger at the surface of the material. See figure 5.008.)As such these results are somewhat preliminary ones.

Irwin's effective fracture length is based on the assumption that the notched material is an elastic-plastic one, so the maximum tensile stress that can be sustained ahead of the notch is the yield stress. It has already been reported that antler is not an elastic-plastic material; its equivalent to yield is a damaging process. This damaging process is attributed to the formation of innumerable small cracks. This damage modifies the stress-strain relationship of the specimen. The stress-strain plots of many damage materials are indistinguishable from those of elastic-plastic material until they are unloaded. Therefore transposing Irwin's correction from one type of material to the other appears valid, up to the time of the first fracture propagation; as until then there is no unloading. However, it has already been shown that the load-deformation plot of antler is different to that of the ideal elastic-plastic material. For when antler enters and passes the knee region of the plot (at which whitening occurs), the load it can sustain continues to increase, although at a lower rate with respect to deformation. Thus the stress in the whitened zone ahead of the notch will not be that predicted by the mathematical solution based on a perfectly elastic solid, nor will it display a single limiting value.[18] Using the evidence from the tensile tests it would appear that the stress in the whitened zone may vary between that associated with the knee stress to that associated with failure. It can be assumed that the stress at the notch tip will still be more than that a small distance ahead of the notch tip. (Some of the images in chapter 8 show strains in the region of the notch tip far greater than those recorded in tensile tests. Thus such an extrapolation may not be valid.)

If the material in the process zone fails when it reaches a certain strain, then increasing the load required to reach this strain will increase the energy required to initiate fracture. This logic suggests that the material would be tougher if it did not display the reduction in stiffness associated with the whitened, or damaged, zone. However if this damaging process (and thus loss of elasticity) did not occur, more of the strain energy in the specimen would be available to propagate the fracture. Therefore a balance exists between increasing the energy required to initiate fracture and reducing the stored energy available to propagate the fracture once it has formed. It is logical to suggest that the size of the whitened zone may indicate where the point of balance falls in a particular test configuration.

---

[18]In this simple analogy the triaxial nature of the stress field ahead of the notch is not considered.

7.5.3.3. RESULTS: THE SIZE OF THE WHITENED ZONE

In the previous section it was found that transposing Irwin's effective notch length to antler was only of limited success. In this section the size of the whitened zone will be examined a separate variable.

The strongest relationships between one of the various measured variables and the length of the whitened zone is that with the notch tip radii ($R^2\% = 57.3$). It has already been stated that the notch tip radius does not appear to affect the mechanical response of a notched antler specimen. (This is contrary to the behaviour predicted, and observed, for a notched linear-elastic material, as reported in chapter 5.) Therefore, if the whitened zone length is important in the mechanical response and failure of a specimen, the relationship between these two dimensions is surprising, as it implies that the length of the whitened zone (and thus, presumably, the amount of damage) will also have no relationship to the mechanical response of the material.

When viewed in isolation it is not surprising that the radius of the notch tip and the length of the whitened zone are related. For a round hole in a perfectly elastic sheet, under simple tension, the size of the hole affects the severity of the stress gradient in the material at the edge of the hole; the smaller the hole, the smaller is the distance from the edge of the hole to the point at which the stress falls to a value equal to, for example twice the applied stress.[19] Thus the distance at which the stress required for a specimen of antler to display whitening may similarly be positively related to the notch tip radius. This would also imply that a larger applied stress would result in a wider whitened zone, this was found to be true. The regression equations are given in table 7.018. An argument that suggests that the size of the whitened zone, and thus the effective fracture length, depends on the notch tip radius would also suggest that the notch tip radius would affect the mechanical response of the specimen. Indeed the significant relationship between fracture stress and the zone length may indicate such an effect. However, it is not obvious that this is the determining factor. Is the larger whitened zone caused by the higher stress, or do the larger whitened zones reduce the notch sensitivity of the material and therefore increase the stress required to fracture it?

---

[19]The equation for the tensile stresses in an elastic sheet with a round hole, across a line perpendicular to the line of the applied load at a distance r from the centre of the hole is

$$\sigma = \frac{\sigma_{applied}}{2}\left(2 + \frac{a^2}{r^2} + 3\,\frac{a^4}{r^4}\right).$$ The equivalent for an ellipse can be determined from the paper by Inglis (1913), I do not consider this worthwhile here. (See section 5.2.1.)

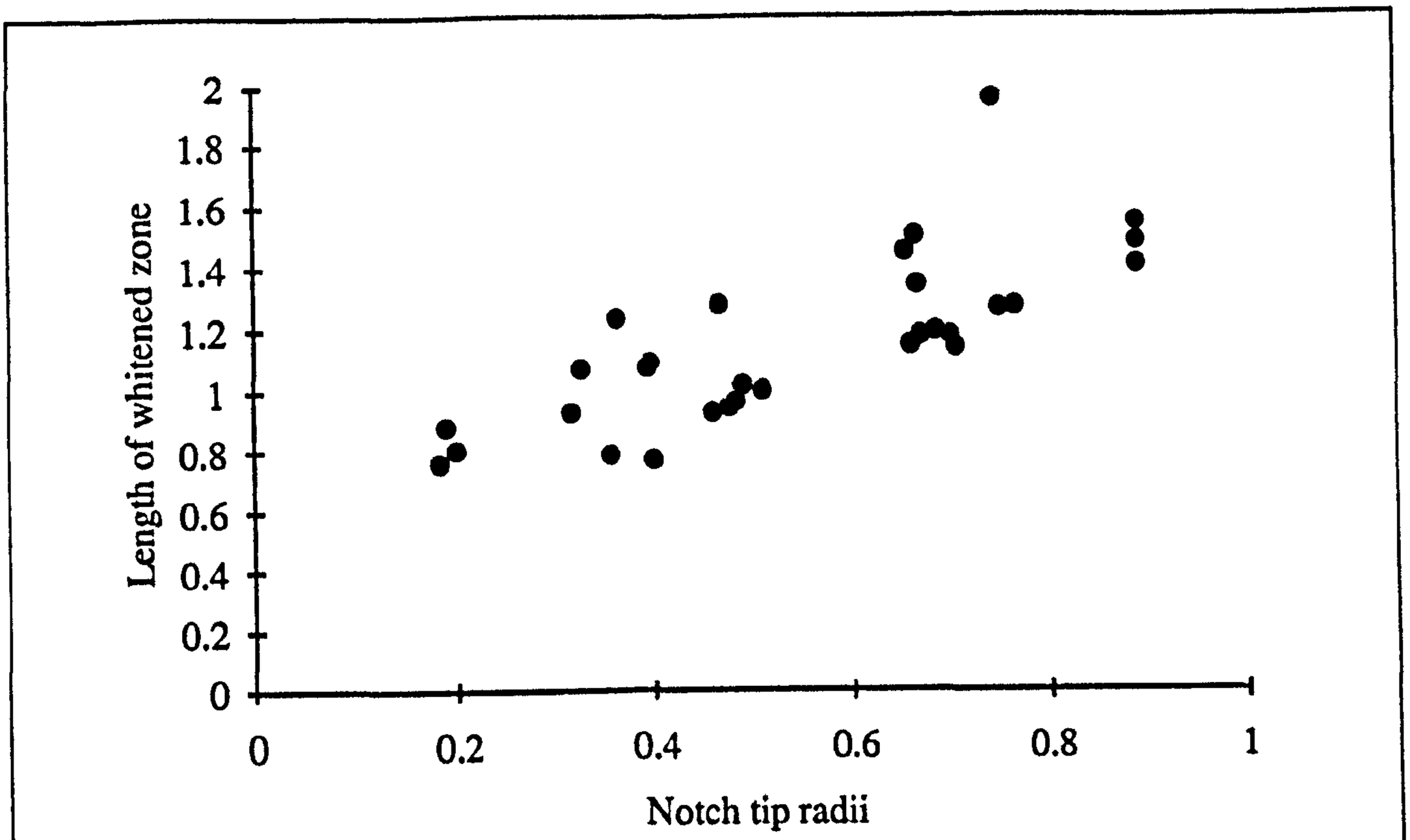

Units:

d_w The length of the whitened zone, mm

ρ Machined notch tip radius (measured), mm

Figure 7.022

The relationship of the estimated length of the whitened zone and the measure notch tip radius

Antler specimens	Regression equations and t values of the data shown in figure 7.022	R^2 %	
30	$d_w = 0.608 + 0.999\ \rho$ t: 6.61 6.32	57.3	*a*
30	$d_w = 0.123 + 0.934\ \rho + 0.0117\ \sigma_f$ t: 0.61 6.44 2.67	65.0	*b*
Units: d_w, mm. ρ, mm. σ_f, MPa.			

Table 7.018

Relationship of whitened zone length to tip radius for specimens of red deer antler

It has already been shown that the material stiffness in three-point-bending is a significant predictor of the failure stress of SEN specimens of antler and that this stress is also dependent on the length of the notch. In table 7.019 regression equations obtained for the logarithmic forms of these quantities are given. Although both the notch tip radius and the length of the whitened zone are non-significant predictors of the failure stress the length of the whitened zone is more significant (equations *a* and *b* table 7.018).

(Examination of the data highlighted a number of relationships that although apparently logical and statistically significant in themselves may be misleading due to spurious interactions, such as relationships between notch length and tip radius. Therefore the analysis presented here is limited to those relationships that appear to be less prone to such errors.) It appears that neither the length of the whitened zone nor the notch tip radius are significant predictors of the failure stress of antler specimens.

Antler specimens	Regression equations and t values	R^2 %	
30	$\ln(\sigma_f) = 2.63 + 0.739 \ln(E_b) - 0.932 \ln(a) - 0.0036 \ln(\rho)$ t: 8.79 7.52 - 2.66 - 0.07	66.7	*a*
30	$\ln(\sigma_f) = 2.60 + 0.730 \ln(E_b) - 0.861 \ln(a) - 0.0234 \ln(d_w)$ t: 9.41 6.97 - 2.49 0.25	66.7	*b*
30	$\ln(\sigma_f) = 2.59 + 0.736 \ln(E_b) - 0.857 \ln(a) + 0.0020 \ln(\rho) + 0.0138 \ln(d_w)$ t: 8.49 7.44 - 2.35 0.04 0.82	66.2	*c*
Units: d_w, mm. ρ, mm. σ_f, MPa. a, mm. E_b, GPa.			

Table 7.019

Predictive equations of the failure stress using the notch tip radii and whitened zone length as explanatory variables

7.5.4. CONCLUSIONS ON THE USE OF A CORRECTION APPLIED TO THE MACHINED NOTCH LENGTH, BASED ON THE WHITENED ZONE LENGTH

As far as I am aware these are the first measurements of the size of such a whitened zone at a notch tip in antler (or bone) that have been analysed to see if this phenomenon will provide any quantitative information on the fracture process. This analysis has produced the rather surprising result that the length of the whitened zone does not appear to be significantly related to the failure stress of the material. However a strong correlation was found between the length of the whitened zone and the radius of the notch tip from which it emanated. This result is not surprising, when the distribution of tensile stress in an elastic plate containing a hole is considered. However, these two observations are incompatible when antler is considered in the light of the fracture mechanics theory presented in chapter 5. It is possible that an explanation to this conundrum could be related to the non-classical form of antler's notch sensitivity. I

suggest that the damage ahead of the machined notch tip is the factor that controls the initiation of fracture. This damage is one of the factors that alters the stress field, from that which would be predicted for an elastic specimen of the same dimensions. This may explain the lack of correlation between failure stress and notch tip radius.

I have noted in the analysis of the previous data set that the behaviour of the SEN specimens of antler tested here is not that associated with a classical notch sensitive material. The results in this section may hold another explanation for this, or at least another reason to question its applicability. If the size of the white zone is considered to be related to the ideas of a plastic zone in LEFM, the application of that theory is not justifiable due to the size of this zone. From the results reported above clearly this zone extends over a considerable section of the specimen; in some cases about 50% of the remaining ligament. Therefore, the question of whether these specimens are truly fracturing or failing by the accumulation of damage within the ligament has to be considered. This aspect of the results and how this and the other findings relate to the failure of antler is discussed in chapter 9. The idea that the failure mechanism of these SEN specimens of antler is not a pure fracture process raises a question: is the fracture behaviour of antler observed here dependent on the size of the specimen that is used? (Perhaps in the same way that a tensile specimen of steel may yield and fail by that process while a large structure made of the same material; say a ship or storage tank may fail by brittle fracture.) I consider that this is likely, but I have no time to investigate this suggestion.

7.6. NOTCH SENSITIVITY OF ANTLER (NA5): THE EFFECT OF CROSS-HEAD SPEED

In the previous section I examined the size of the whitened zone at the notch tip in relation to the initiation of the fracture. I attributed this whitening to the same behaviour that occurs during the knee region of a tensile loading test. In chapter 4 it was shown that both the knee strain and knee stress of antler specimens are dependent on the cross-head speed used for the test. Similarly the creep tests examined in the same chapter suggest that the accumulation of damage is rate dependent. Therefore if the initiation of fracture is controlled in some way by the amount of damage present (as suggested in section 7.5.4) it would be logical to assume that the initial fracture process is also dependent on the cross-head speed. A pursuit of this logic is the basis of this section

7.6.1. AIMS AND EXPERIMENTAL DESIGN

The main aim of these tests was to examine the effect of cross-head speed on the failure of antler specimens containing long and short notches. Two specimen widths were examined, nominally 4 and 5 mm. These specimens were prepared from the same antler as the specimens of set NA4 (and TA1). (The specimens of all three groups were prepared as one batch, and divided into the test groupings after their bending stiffness had been determined.) The specimens were prepared as explained in appendix 2. The tips of the notches were not drilled. They were simply cut with the Exact diamond edged band-saw. The depth of the cuts used was intended to produce notch to specimen width ratios (a/w) of approximately 0.4 and 0.1. The purpose of this was to highlight any effects of notch length. However, limiting the range of notch lengths in such a way reduces the validity of examining the power of notch length as a predictive variable. Thus the regression equations in this section can not be used as evidence for or against the use of a notch insensitive or classically notch sensitive relationship of fracture stress to notch length.

7.6.2. EXPERIMENTAL PROCEDURE

Testing was performed in the same way as for the specimens in data set NA4. However, there was one exception, the specimens were tested at four different cross-head speeds: 8.3×10^{-4} (5 specimens), 8.3×10^{-5} (7 specimens), 8.3×10^{-6} (3 specimens) or 8.3×10^{-7} m s^{-1} (4 specimens).[20] This series of tests, on SEN specimens of red deer antler, was also recorded using the high speed video equipment (see chapter 8), the testing of these specimens being interspersed with those of set NA4 and TA1 (described above).

7.6.3. RESULTS

The results will be presented in a similar format as those already given. To demonstrate the effect of cross-head speed the logarithmic value of this speed in metres per second will be used. As already stated the relationship between this quantity and the strain rate experienced by an un-notched test specimen is not straightforward (see appendix 7). For a notched specimen the idea of strain rate is not normally applied (deformation rates are some times considered in terms of fracture opening rates, for example). Therefore the arguments for its use in the case of un-notched specimens are

---

[20]These are the same speeds used in the study of the effect of testing rate on the mechanical behaviour of un-notched specimens described in section 4.2.

not easily transposed to the analysis of notched specimens. However, I found that the natural logarithm of the cross-head speed was a good predictor of the mechanical response.

7.6.3.1. RESULTS: THE EFFECT OF CROSS-HEAD SPEED ON THE FAILURE STRESS

Antler specimens	Regression equations and t values	R^2 %	
19 SEN	$\sigma_f = 73.5 - 58.7\ (a/w)$ t: 13.03 - 3.29 One-way analysis of variance of standardised residuals with cross-head speed resulted in *p:* 0.001, highly significant.	35.3	*a*
19 SEN	$\sigma_f = 37.5 + 0.570\ a^{-0.5}$ t: 4.57 2.55 One-way analysis of variance of standardised residuals with cross-head speed resulted in *p:* 0.004, highly significant.	23.5	*b*
19 SEN	$\sigma_f = 47.5 - 61.0\ (a/w) + 2.28\ E_b$ t: 2.40 - 3.49 1.37 One-way analysis of variance of standardised residuals with cross-head speed resulted in *p:* < 0.001, very highly significant.	38.4	*c*
19 SEN	$\sigma_f = 14.5 + 0.581\ a^{-0.5} + 1.93\ E_b$ t: 0.62 2.61 1.05 One-way analysis of variance of standardised residuals with cross-head speed resulted in *p:* 0.001, very highly significant.	23.9	*d*
Units: σ_f, MPa. w, mm. a, mm. $a^{-0.5}$, $m^{-0.5}$, E_b, GPa.			

Table 7.020

Predictions of fracture stress using the equation for a classically notch sensitive material and a notch insensitive material

In table 7.020 the regression equations for the data obtained from 19 specimens tested at the four different cross-head speeds stated above are presented. The R^2 % values are approximately the same as those for the previous sets of data. However, in this case the values of a and a/w do not cover a complete range but fall into two groups. Thus these equations can not be used to distinguish which function of notch length best describes its relationship to the failure stress. The main point of interest here is the effect

of cross-head speed. The standardised residuals of the regressions were examined.[21] Figure 7.023a shows the data used to obtain equation *a* of table 7.020 the line of which is also shown in the figure. The standardised residuals of this equation are then plotted against the cross-head speed in figure 7.023b. This last figure clearly shows the dependence of the standardised residuals on the cross-head speed used during the test. Therefore the cross-head speed appears to be an important factor in determining the failure stress of these notched antler specimens. This observation is reinforced by the one-way analysis of variance of standardised residuals of the regressions.[22] The results of such one-way analysis of variance are shown in table 7.020.

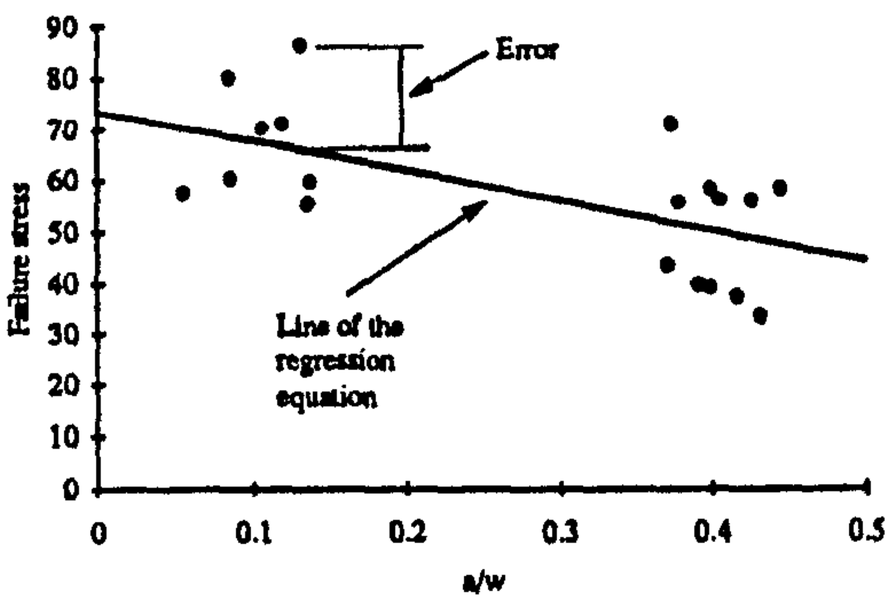

a) Relationship of failure stress and ration of notch length to specimen width

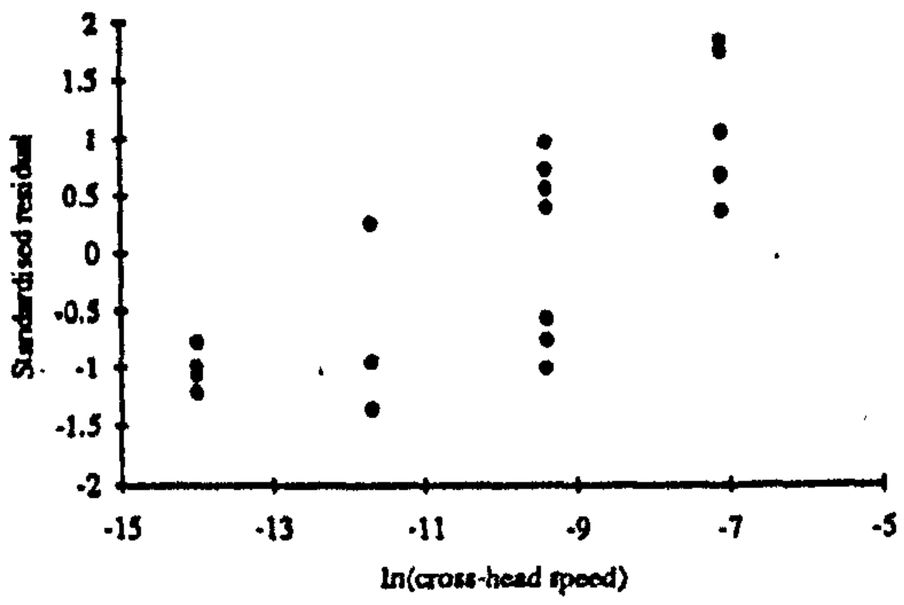

b) Relationship of the standardised residuals (of a) and the cross-head speed

Units:

σ_f	Failure stress, MPa.
	Standardised residual, unitless.
a/w	Ratio of notch length to specimen width, unitless

Figure 7.023

The data, regression line and error for the relationship of failure stress to the ratio of notch length to specimen width (equation *a* table 7.020) and the relationship of the standardised residuals to cross-head speed

It was noted above that the cross-head speed does not necessarily possess a direct relationship with the loading rate or strain rate at the notch tip. However, I found that when the standardised residuals are plotted against the natural logarithms of the different cross-head speeds an apparently linear relationship is produced. This suggests the use of

---

[21]The standardised residuals (or error between the real values of the quantity whose variance is being explained and the value predicted by the regression equation, divided by the standard deviation of these differences) were calculated using the main regression command in Minitab.

[22]Using one-way analysis of variance on the residuals of the regression equation indicates if the cross-head speed is a significant factor in explaining the values of the residuals. The *p* value alone gives no indication if this significance is due to a trend, but simply that there is a difference between the values when grouped in this way.

such a logarithmic expression for cross-head speed as an additional variable in multiple regression analysis. Therefore, I will now repeat the previous regressions using the cross-head speed as another explanatory variable (table 7.021).

Antler specimens	Regression equations and t values (see appendix 12 for table of t and *p* values for the levels of significance used).	R^2 %	
19 SEN	$\sigma_f = 111 - 68.2\ (a/w) + 3.49\ \ln(\dot{x})$ t: 13.22 - 5.84 4.99	73.1	*a*
19 SEN	$\sigma_f = 69.7 + 0.754\ a^{-0.5} + 3.80\ \ln(\dot{x})$ t: 8.08 4.95 4.80	66.7	*b*
19 SEN	$\sigma_f = 74.3 - 73.6\ (a/w) + 3.79\ E_b + 4.06\ \ln(\dot{x})$ t: 9.42 - 11.03 5.90 9.94	91.4	*c*
19 SEN	$\sigma_f = 32.4 + 0.800\ a^{-0.5} + 3.51\ E_b + 4.34\ \ln(\dot{x})$ t: 2.77 7.07 3.79 7.21	81.8	*d*
Units: σ_f, MPa. a/w, unitless $a^{-0.5}$, $m^{-0.5}$. E_b, GPa. $\dot{x}$, $m\ s^{-1}$			

Table 7.021

The effect of cross-head speed as a modification to the equations describing a notch insensitive material or a classically notch sensitive one

The results presented in this section clearly show that the failure behaviour of antler, as examined here, is rate dependent. When the strength of this relationship is compared with that of ultimate stress and cross-head speed exhibited by un-notched specimens (equations *a* and *b* table A9.005) it is noticeable that a change in cross-head speed affects the un-notched strength more strongly than it does the notched strength. This observation appears to agree with the idea that the failure of SEN specimens of antler is controlled by a time-dependent damage process.

7.6.3.2. RESULTS: THE EFFECT OF CROSS-HEAD SPEED ON LIGAMENT STRESS

The ligament stress was defined above (section 7.4.3.4) as the stress calculated from the failure load and the cross sectional area of the notched section of an SEN specimen. Figure 7.024 shows how this quantity is related to cross-head speed. The mean values are given in table 7.022.

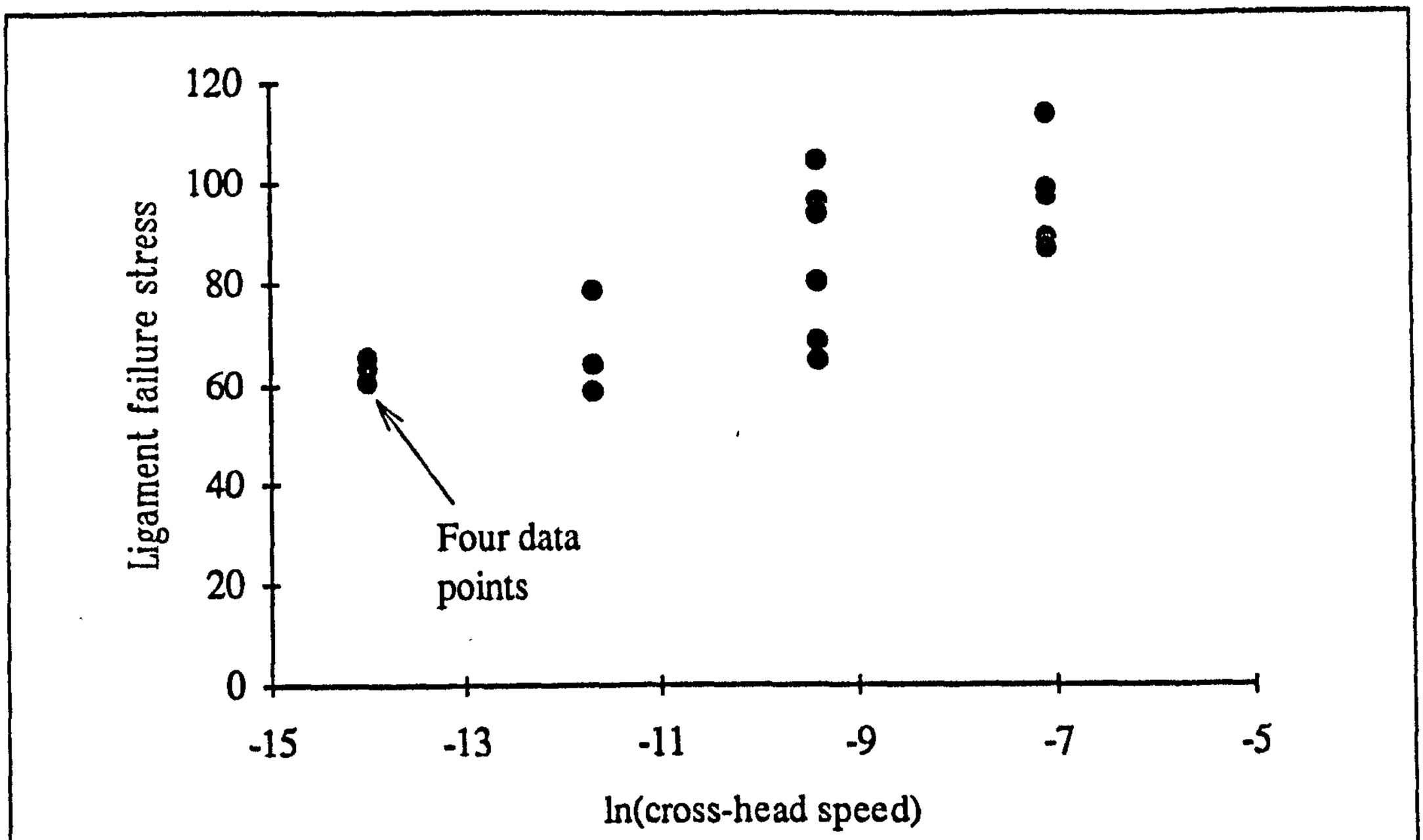

Units:

σ_{lig} Ligament stress, MPa.

$\dot{x}$ Cross-head speed, m s^{-1}.

Figure 7.024

The relationship of ligament stress to cross-head speed

Cross-head speed m s^{-1}	σ_{lig} Mean value (s.d.) MPa	Number of specimens
8.3×10^{-7}	63.86 (2.19)	4
8.3×10^{-6}	67.00 (10.26)	3
8.3×10^{-5}	82.59 (15.76)	7
8.3×10^{-4}	97.29 (10.40)	5

Table 7.022

Mean values of the ligament stress at different cross-head speed

In table 7.023 the powers of a number of parameters to explain the variation in the ligament stress, individually and in combination are presented. In this case the two best individual variables, and then the best two pairs of variables and so on. The R^2 % values given are those adjusted for the degrees of freedom.

Predictors of the ligament stress, σ_{lig}, for SEN specimens of red deer antler (data set NA5)						R^2 %
E_b	ln($\dot{x}$)	a/w	$a^{-0.5}$	w	d	
-	X	-	-	-	-	53.5
X	-	-	-	-	-	10.1
X	X	-	-	-	-	86.4
-	X	X	-	-	-	52.3
X	X	-	-	X	-	85.8
X	X	X	-	-	-	85.8
X	X	X	-	X	-	85.0
X	X	-	X	X	-	85.0
X	X	X	-	X	X	83.8
X	X	X	X	X	-	83.8
X	X	X	X	X	X	82.5
Units: σ_{lig}, MPa. E_b, GPa. d (thickness), mm. w, mm. a, mm. $a^{-0.5}$, $m^{-0.5}$. $\dot{x}$, $m\ s^{-1}$.						

Table 7.023

The combinations of various explanatory variables that give the best predictions of the ligament stress

It is clear from table 7.023 that of the predictors investigated those that best explain the variations in the ligament stress at failure are the material stiffness and the cross-head speed of the test, with the latter in logarithmic form (R^2 = 86.4%). The equation is given in table 7.024. Both predictors are very highly significant. This equation is similar to equation *b* in table A9.005, were the effect of material stiffness and cross-head speed on the ultimate stress of un-notched antler specimens was examined. When the ultimate stress results of the un-notched tests are compared with the ligament stress values for the SEN specimens, it is noticeable that the relationship with E_b is similar (6.14 for SEN and 6.76 for un-notched), but the relationship with rate is lower in the case of the SEN specimens (5.85 as opposed to 7.70). The use of variables along with the material stiffness and the cross-head speed results in a reduction of the predictive power of the relationship.

Antler specimens	Regression equation and t values	R^2 %	
19 SEN	$\sigma_{lig} = 67.3 + 5.85\ \ln(\dot{x}) + 6.14\ E_b$ t: 5.87 9.84 6.50	86.4	*a*
Units: σ_{lig}, MPa. $\dot{x}$, m s^{-1} E_b, GPa.			

Table 7.024

The equation relating the variables which have the greatest predictive power of this examined in table 7.023

7.6.3.3. RESULTS: FAILURE STRAIN, NOTCH AND PROCESS ZONE LENGTH, THE EFFECT OF CROSS-HEAD SPEED

This set of data provides better correlations between the failure strain and other explanatory variables, than the previous data sets (NA1, NA2, NA3 and NA4). The material stiffness, measured in three-point-bending, was found to be the most significant predictor. Some regression equations are given in table 7.025, in each case the material stiffness is significant (by the definition used in this thesis, see appendix 12). In equations *b* and *c* the notch length term was also significant. In none of the equations examined was the cross-head speed found to be a significant predictor of the failure strain.

Antler specimens	Regression equations and t values	R^2 %	
19 SEN	$\varepsilon_f = 0.0574 - 0.0158\ (a/w) - 0.00211\ E_b + 0.000440\ \ln(\dot{x})$ t: 5.43 - 1.77 - 2.45 0.81	32.7	*a*
19 SEN	$\varepsilon_f = 0.0470 + 0.000216\ a^{-0.5} - 0.00213\ E_b + 0.000565\ \ln(\dot{x})$ t: 4.52 2.15 - 2.59 1.06	37.8	*b*
19 SEN	$\ln(\varepsilon_f) = -1.46 - 0.155\ \ln(a) - 0.876\ \ln(E_b) + 0.0171\ \ln(\dot{x})$ t: - 1.76 - 2.25 - 2.52 0.87	38.5	*c*
Units: ε_f, Unitless. E_b, GPa. w, mm. a, mm. $a^{-0.5}$, $m^{-0.5}$. $\dot{x}$, m s^{-1}.			

Table 7.025

Relationship of the failure strain to notch length measures, material stiffness and cross-head speed

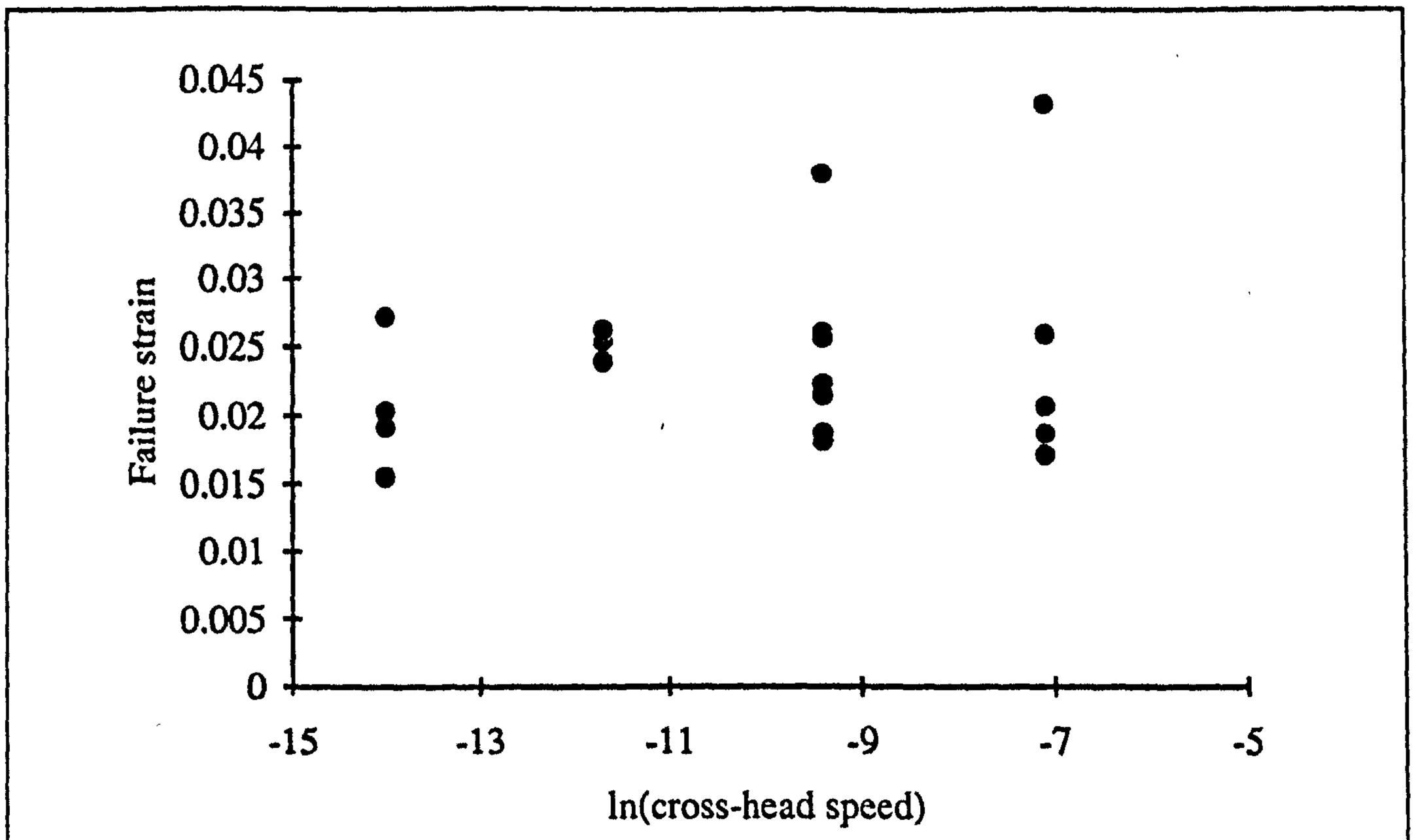

Units:

ε_f Failure strain, unitless.

$\dot{x}$ Cross-head speed, m s^{-1}.

Figure 7.025

Relationship of failure strain to cross-head speed

The analysis of the results in the form of logarithmic values supplies little additional information on the fracture process. However, it provides further equations that can be compared with the un-notched results obtained from specimens of the same antler. This comparison is discussed in the conclusion to this chapter.

7.6.3.4. RESULTS: PURSLOW'S APPROACH, THE EFFECT OF CROSS-HEAD SPEED

In this section the results of regression analysis performed on the logarithmic values of a number of variables are presented. This analysis is based on the approach outlined in section 5.3.4 and based on the work of Purslow (1991). In this case the cross head-speed is included as another variable. The regression equations are given in table 7.026. The value given in parenthesis in the $R^2\%$ column is that obtained when the regression is performed without the inclusion of the cross-head speed as a variable. (Despite the use of only extreme values of a/w it is noticeable that the coefficient of the notch length term is very similar to that obtained from data set NA3 in table 7.013a.)

Antler specimens	Regression equations and t values	R^2%	
19 SEN	$\ln(\sigma_f) = 4.66 - 0.260 \ln(a) + 0.0651 \ln(\dot{x})$ t: 32.74 - 5.33 4.74	69.2 (30.3)	*a*
19 SEN	$\ln(\sigma_f) = 4.30 - 0.265 \ln(a/w) + 0.0671 \ln(\dot{x})$ t: 30.54 - 5.63 5.05	71.4 (30.1)	*b*
19 SEN	$\ln(\sigma_f) = 4.11 - 0.263 \ln(a) + 0.399 \ln(w) + 0.0680 \ln(\dot{x})$ t: 8.15 - 5.43 1.13 4.91	69.8 (26.1)	*c*
19 SEN	$\ln(\sigma_f) = 2.80 - 0.282 \ln(a) + 0.805 \ln(E_b) + 0.0762 \ln(\dot{x})$ t: 7.69 - 9.35 5.27 8.80	88.5 (33.4)	*d*
19 SEN	$\ln(\sigma_f) = 2.53 - 0.280 \ln(a/w) + 0.757 \ln(E_b) + 0.0774 \ln(\dot{x})$ t: 6.85 - 9.33 4.96 8.89	88.4 (32.0)	*e*
19 SEN	$\ln(\sigma_f) = 2.67 - 0.282 \ln(a) - 0.135 \ln(w) + 0.783 \ln(E_b) + 0.0768 \ln(\dot{x})$ t: 6.11 - 9.16 0.59 4.87 8.61	88.0 (29.2)	*f*
Units: σ_f, MPa. E_b, GPa. w, mm. a, mm. $a^{-0.5}$, $m^{-0.5}$. $\dot{x}$, $m\ s^{-1}$.			

Table 7.026

Relationship of the failure stress to the notch length, the material stiffness and the cross-head speed

7.6.3.5. RESULTS: EFFECT OF CROSS-HEAD SPEED ON THE WHITENING AT THE NOTCH TIP

One important aspect of the effect of the cross-head speeds used was the lack of whitening at the lowest speed. Whitening was not observed in any SEN specimen of antler tested below 8.33×10^{-5}, whereas it was observed in all specimens tested at or above this speed. As the results for the length of the whitened zone are only available at the two highest speeds analysis of these results is of little value. However, one-way analysis of variance showed that there was no significant difference between the results obtain at these two speeds. Although no whitening was observed prior to failure of the specimens loaded at the lower cross-head speeds such an effect was observed around the tip of the propagating fracture in a few cases. If the size of the whitened zone does indicate the amount of damage that occurs within a specimen this result presents a paradox. Damage is time-dependent and its existence reduces the specimen's strength. Thus there should be more damage within the specimens tested at lower cross-head

speeds (which failed at lower stresses). However, the existence of whitening when used as an indication of damage contradicts this position. In chapter 8 it will be shown that a similar result is obtained for the optical changes associated with the knee region in tensile tests. Explanations of this finding are proposed in chapter 8. Here it is sufficient to suggest that the amount of whitening displayed by a certain amount of damage appears to reduce as the time since the formation of that damage increases. However, it is also suggested in chapter 8 that a smaller amount of whitening at the lower cross-head speed may be a reflection of a more visco-elastic-like behaviour than a damage-like behaviour. I have already suggested that the mechanical behaviour of antler may be due to the combination of these two behaviours. These observations, and similar ones made for bovine bone, are discussed in chapter 8.

One important consequence of the rate dependence of the whitened zone is that it casts doubt on the use of the length of this zone as a quantitative correction to notch length in the search for a fracture parameter. The use of such a measure is clearly undermined if several cross-head speeds are used. The consequence of this time dependence within the experiments conducted at one cross-head speed is unknown.

This section ends the analysis of the notch sensitivity of antler; in the following sections similar analysis is conducted on the results obtained from SEN specimens of bovine bone. The conclusions drawn from the analysis of both materials are presented in section 7.10, where the similarities and differences of these materials are examined. Later, in chapter 9, these conclusions are combined with these from other types of test to obtain a wider picture of the failure behaviour of bone and antler.

7.7. NOTCH SENSITIVITY OF BOVINE BONE (DATA SETS NB1, NB2 AND NB3)

The first set of data analysed from tests on bovine bone contains data from experiments that were originally separate investigations. However, I have combined them here to form a data set comparable to the one containing data from antler specimens reported above, set NA3 examined in section 7.4 (specimen width, type of notch, etc.). The reasons these tests on bovine bone, were conducted as separate investigations are mainly those of material availability, and parallel investigations. For example the development of a system for recording the instant that a photograph was taken with reference to the stress-strain data.[23] This fragmentary approach to experimentation unfortunately produced some spurious effects and a poor (overall) experimental design.

---

[23]An error in the earthing of this system resulted in the loss, and thus replication, of a set of experiments.

The main aim of the tests examined here is to examine the application of the equations from LEFM to the results obtained from SEN specimens of bovine bone. Those equations are based on certain assumptions as to the material properties and the failure process. Thus non-conformity of the experimental data with those equations could indicate a difference between the assumed and actual behaviour of the material. Such a difference may also be due to differences between the theoretical test conditions and those encountered in practice. The equations from Purslow's approach and related logarithmic relationships will also be examined. These later approaches contain fewer assumptions as to the nature of the relationship of failure stress to notch length. As in the case of the tests on antler (NA3) the effect of the notch tip radius on the mechanical response of the specimen is also examined.

The overall experimental design is very similar to that used for antler in section 7.4. The specimens of bovine bone were prepared in the same way as the antler specimens, except the middle size drill (drill II approximately 0.33 mm in radius) was replaced with a larger one to give a greater range of tip radii. One of the main differences between this and the other series of tests, and a contributory factor to potentially spurious effects, is that both bovine femoral and tibial bone was used. Another source of possible spurious effects is that some individual bones were used for only a limited number of the various test configurations. However, the greatest problem arises from an inconsistency in the three-point-bending tests. For the first set of experiments here (data set NB1) the cross-head speed used was 3.33×10^{-5} m s^{-1} (the same as during the antler tests, data set NA3), but in the later two sets this was decreased to 8.33×10^{-6} m s^{-1}. This difference in testing rate combined with the time-dependent properties of the material appears to have produced a higher value of material stiffness in the first case. This could also be due to the different bones studied. (Due to the mix of the specimens from the original data sets this has resulted in the specimens that were machined to a nominal width of 4 mm, having an average bending stiffness greater than their 6 mm wide counterparts, as shown in table 7.027.) Because it is not definitely known why the specimens examined in the initial set of tests had a higher bending stiffness, that quantity should be viewed critically. The lack of a reliable measure of material stiffness in three-point-bending prevents its use as a normalising factor, or method of reducing the unexplained variation within the regression analysis. (Which would enable the relationship of, for example, the failure stress and the notch length to be more confidently determined.) However, the large number of specimens within this data set: 129, 88 of which are notched, increases the significance of those relationships that do exist. Information on the experimental groups examined and the source of their constituent samples is given in table 7.028.

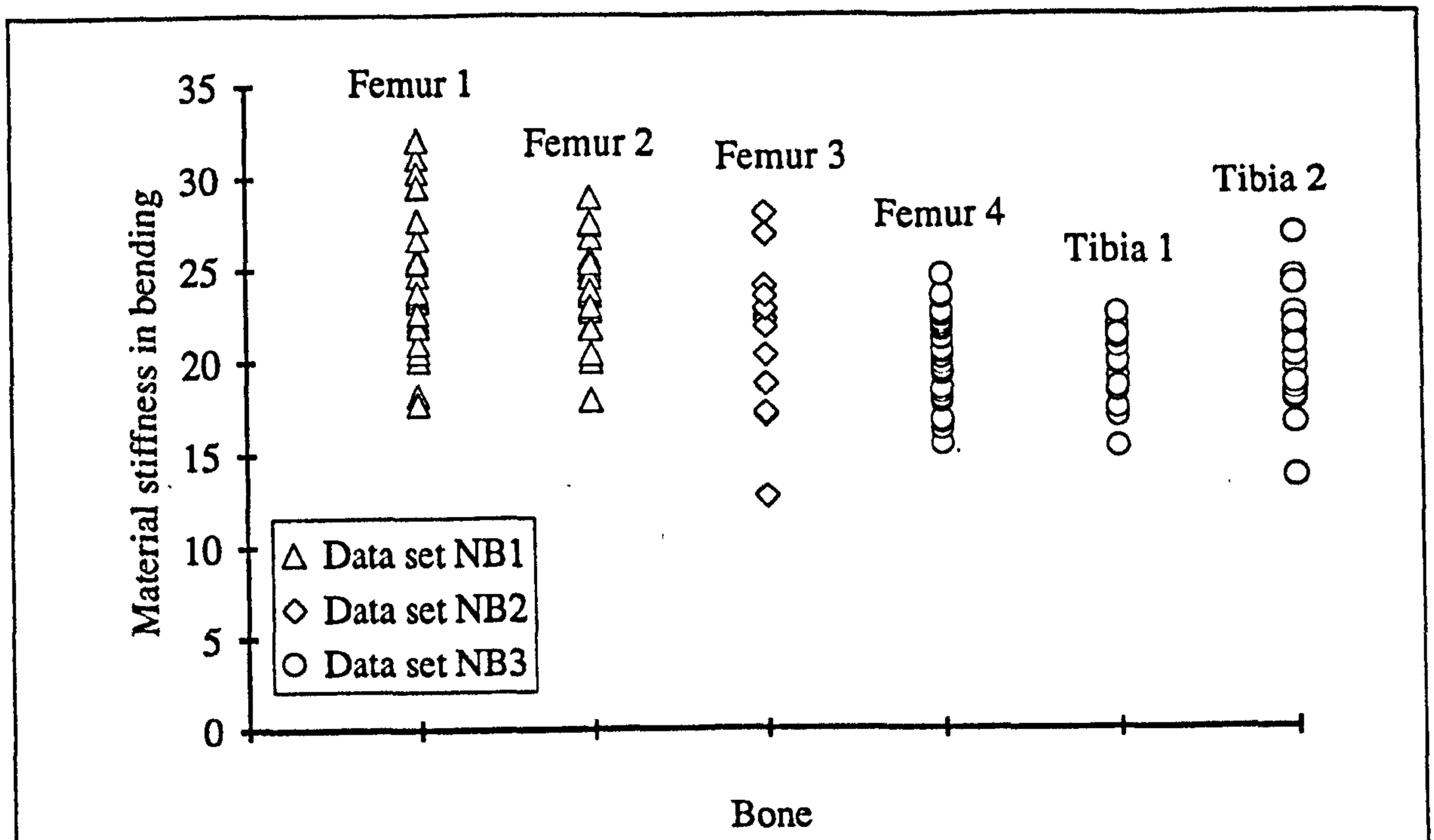

Units:

E_b Material stiffness in three-point-bending, GPa.

Comments:

See table 7.002 for information on the source and storage of the bones.

Figure 7.026

The measured bending stiffness, E_b, of the specimens from the different bones used

Group	Original data set, bone type (see table 7.002)						*Total*
	NB1 Femur 1	NB1 Femur 2	NB2 Femur 3	NB3 Femur 4	NB3 Tibia 1	NB3 Tibia 2	
4 mm, ℜ	2	1	-	-	2	2	*7*
4 mm, tensile	7	2	-	-	2	4	*15*
4 mm, Drill I	7	6	-	-	2	-	*15*
4 mm, Drill III	7	5	-	-	2	1	*15*
4 mm, Drill IV	4	7	-	-	1	2	*14*
6 mm, ℜ	-	-	-	5	2	2	*9*
6 mm, tensile	-	-	-	8	2	-	*10*
6 mm, Drill I	-	-	6	7	1	2	*16*
6 mm, Drill III	-	-	5	6	1	2	*14*
6 mm, Drill IV	-	-	5	6	1	2	*14*
Total	*27*	*21*	*16*	*32*	*16*	*17*	*129*

Comments:

Tensile refers to tests conducted on un-notched specimens

Table 7.027

The distribution of specimens in each test grouping from the different bones

	Nominal width 4 mm			Nominal width 6 mm		
		s.d.	n		s.d	n
Drill IV approx.	w = 3.88	0.03	14	w = 5.90	0.02	14
notch tip radius	ρ = 0.48	0.01	14	ρ = 0.50	0.00	14
0.49 mm	E_b = 23.14	3.38	14	E_b = 20.61	2.49	14
	a = 1.74	0.33	14	a = 2.27	0.69	14
Drill I approx.	w = 3.87	0.04	15	w = 5.92	0.04	16
notch tip radius	ρ = 0.38	0.01	15	ρ = 0.38	0.00	16
0.38 mm	E_b = 23.48	3.29	15	E_b = 20.37	3.40	16
	a = 1.63	0.35	15	a = 1.91	0.79	16
Drill III approx.	w = 3.87	0.02	15	w = 5.92	0.03	14
notch tip radius	ρ = 0.19	0.01	15	ρ = 0.20	0.00	14
0.20 mm	E_b = 23.76	3.31	15	E_b = 20.77	2.98	14
	a = 1.33	0.48	15	a = 1.70	0.68	14
Resilience	w = 3.88	0.04	7	w = 5.82	0.08	9
	E_b = 20.77	4.30	7	E_b = 19.73	3.68	9
Tensile	w = 3.87	0.04	15	w = 5.82	0.15	10
	E_b = 22.92	3.85	15	E_b = 20.74	2.06	10

Units:

w Specimen width, mm.

ρ Notch tip radius, mm.

E_b Material stiffness in bending, GPa.

a Notch length, mm.

Comments:

The drill numbering and the notch tip radius sizes are not in the same order. This is because the labelling of drills I and III are the same as those described in section 7.4.1, drills II of that section has been replaced by one of a larger diameter.

Table 7.028

The mean values of some geometrical and physical properties of the specimens in each test grouping

7.7.1. RESULTS

The presentation of the results of these tests on SEN specimens of bovine bone mirrors that used for the results of SEN specimens of antler in section 7.4.3. However, in that section there was more bias towards Purslow's approach to fracture, whereas here the bias is towards LEFM.

7.7.1.1. RESULTS: RESILIENCE TESTS

It was noted in section 7.4.3.1 that both Griffith's and Purslow's approaches to fracture are based on the ideas of energy stored within the material. Therefore it is important to determine if the energy supplied to the material is available for the fracture process.

Figure 7.027 shows the stress-strain plots of some resilience tests performed on bovine femur specimens. The results obtained from these and other specimens are shown in figures 7.028 to 7.030. The bone type and nominal specimen width are indicated in the plots. A feature shown in figure 7.028 is the maintenance of a high degree of resilience up to high stress levels (about 100 MPa). This corresponds with the so called knee stress of bovine bone. In the literature on bone the initial section of the tensile loading plot is often referred to as the elastic region. This value is greater than the stress values associated with a reduction in resilience in antler specimens. As higher values of stress are attained the resilience decreases in an apparently non-regular way. Figure 7.029, a graph of the same resilience values but this time plotted with reference to peak strain, shows one distinct specimen that reached a high strain value. (This high level of strain was achieved only once during the resilience tests, due to the other specimens failing before they were unloaded.) The data from this extreme specimen implies that the resilience may reach a threshold level, or that the data could be better represented by a logarithmic relationship (as in the case of the antler specimens). The predictive strength of the double logarithmic relationship of resilience to peak strain was found to be quite strong, $R^2 = 76.3\%$ (table 7.029), if a factor signifying if the specimen is from a femur or a tibia is added then this value is increased to 82.0%. The former equation can be expressed as

$$\Re = 3.56\,\varepsilon^{-0.569} \qquad (7.026)$$

This equation would suggest that a resilience of over 100% would be obtained at stresses less than 0.0028. Using the mean value of 24 GPa for the material stiffness in tension (obtained from 39 un-notched specimens tested at the same cross-head speed in data sets

NB1, NB2 and NB3) a corresponding value of stress can be obtained. The resulting value is 67 MPa. Therefore this method indicates that the bovine bone specimens studied here depart from elastic behaviour when the stress level reaches about 67 MPa. There is of course some variation between specimens. This value is a few megapascals more than the average nominal failure stress for the notched specimens (65 MPa, n = 88). Therefore I consider that the material in the SEN specimen of bovine bone, which is not adversely affected by stress concentrations, is behaving in an elastic (or very nearly elastic) fashion until the failure stress is reached. This result does not, on its own, support the use of LEFM for the study of bovine bone. Perhaps what is more important, it does not provide grounds for the rejection of LEFM. However, it does imply that only a small increase in the local stress at failure, due to the concentrating effect of the notch may result in non-elastic behaviour. (The calculated value of ligament stress is greater than the value associated with the elastic limit.) The extent and degree to which such non-elastic behaviour affects the validity of LEFM (as explained in chapter 5) are considered in the later sections when more evidence on the nature of this non-linearity has been presented.

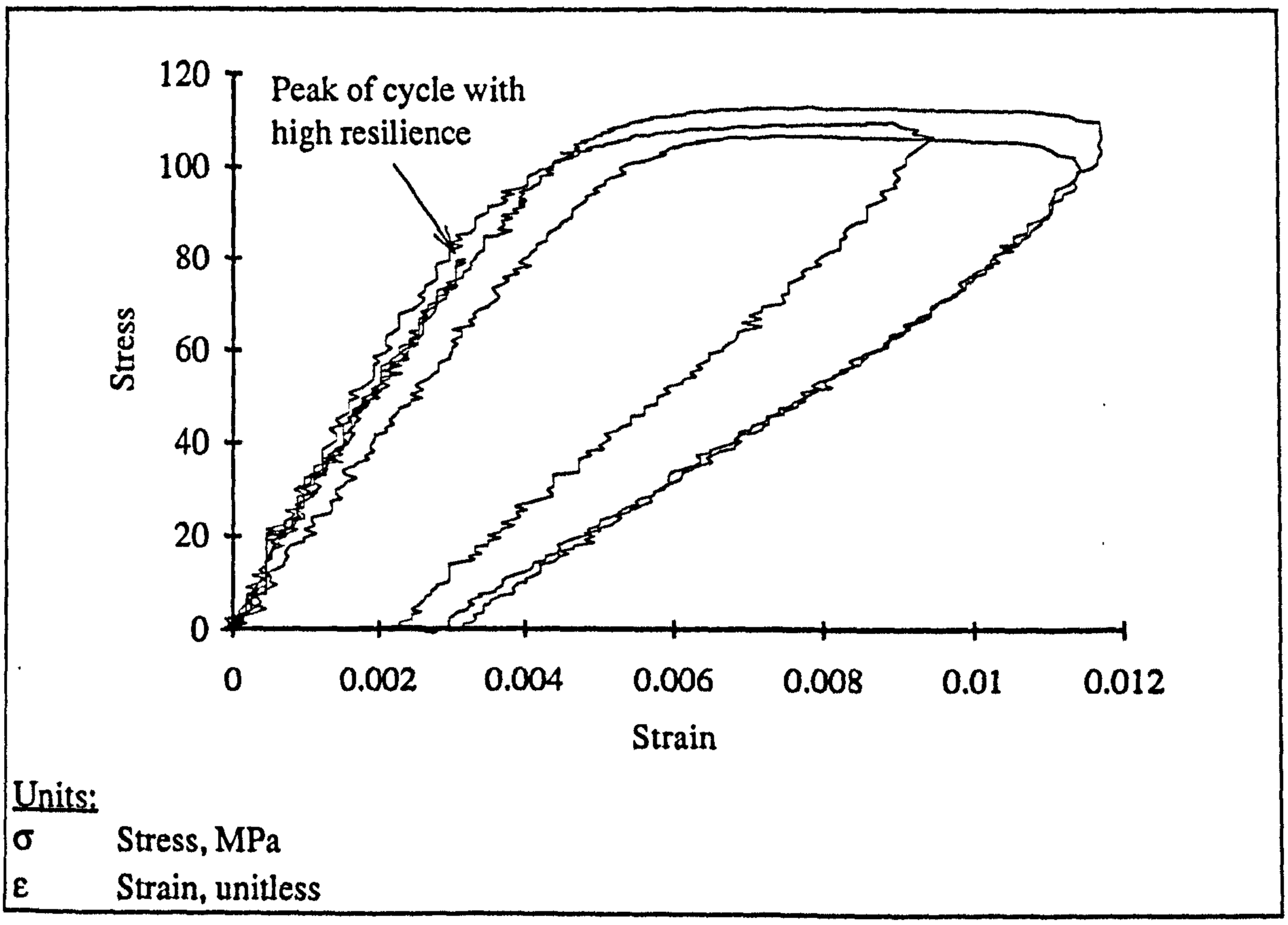

Figure 7.027

Loading cycles from the resilience tests of four specimens of bovine femoral bone

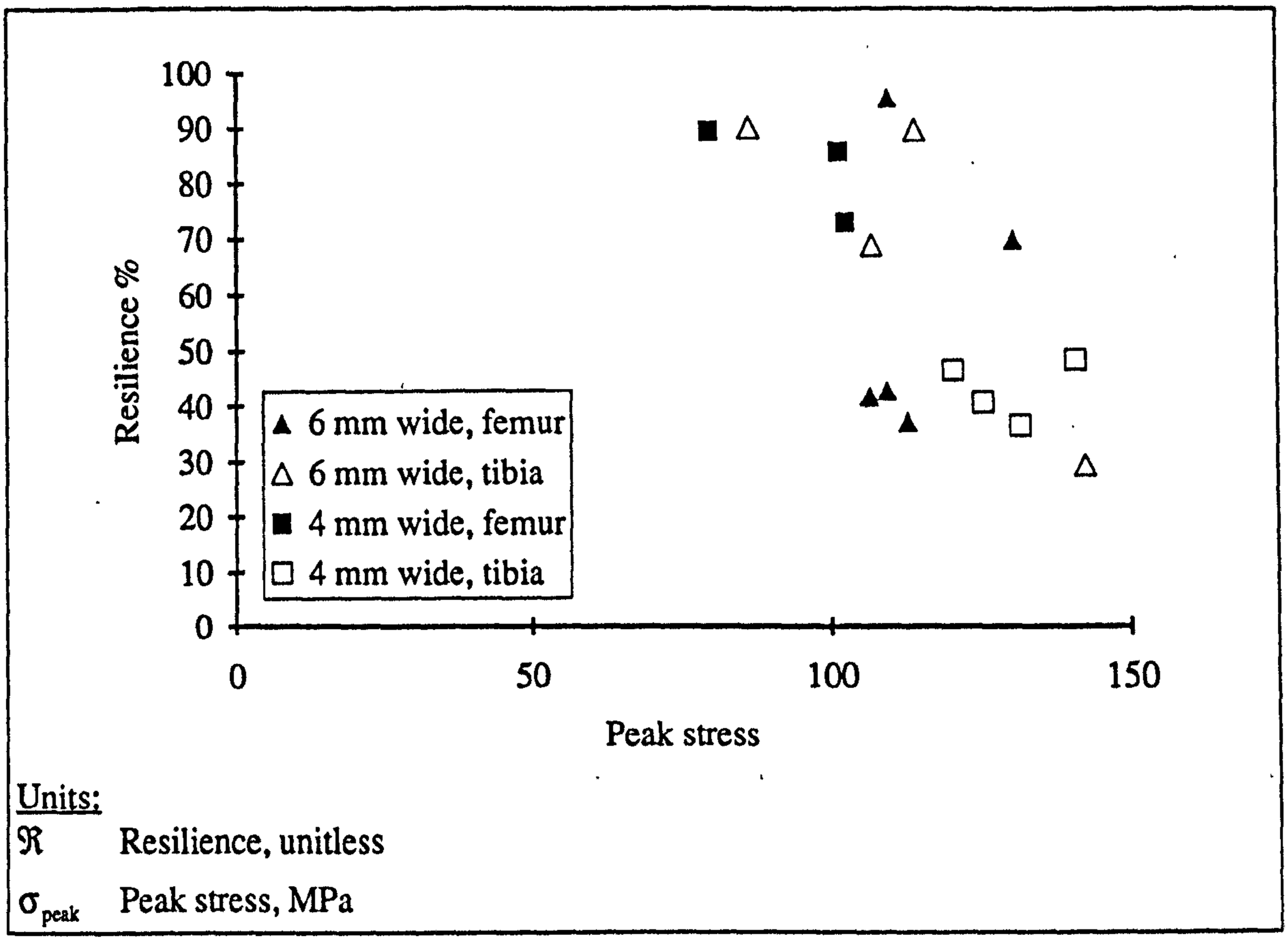

Units:

$\Re$ Resilience, unitless

σ_{peak} Peak stress, MPa

Figure 7.028

The relationship of resilience to peak stress for 16 specimens of bovine bone

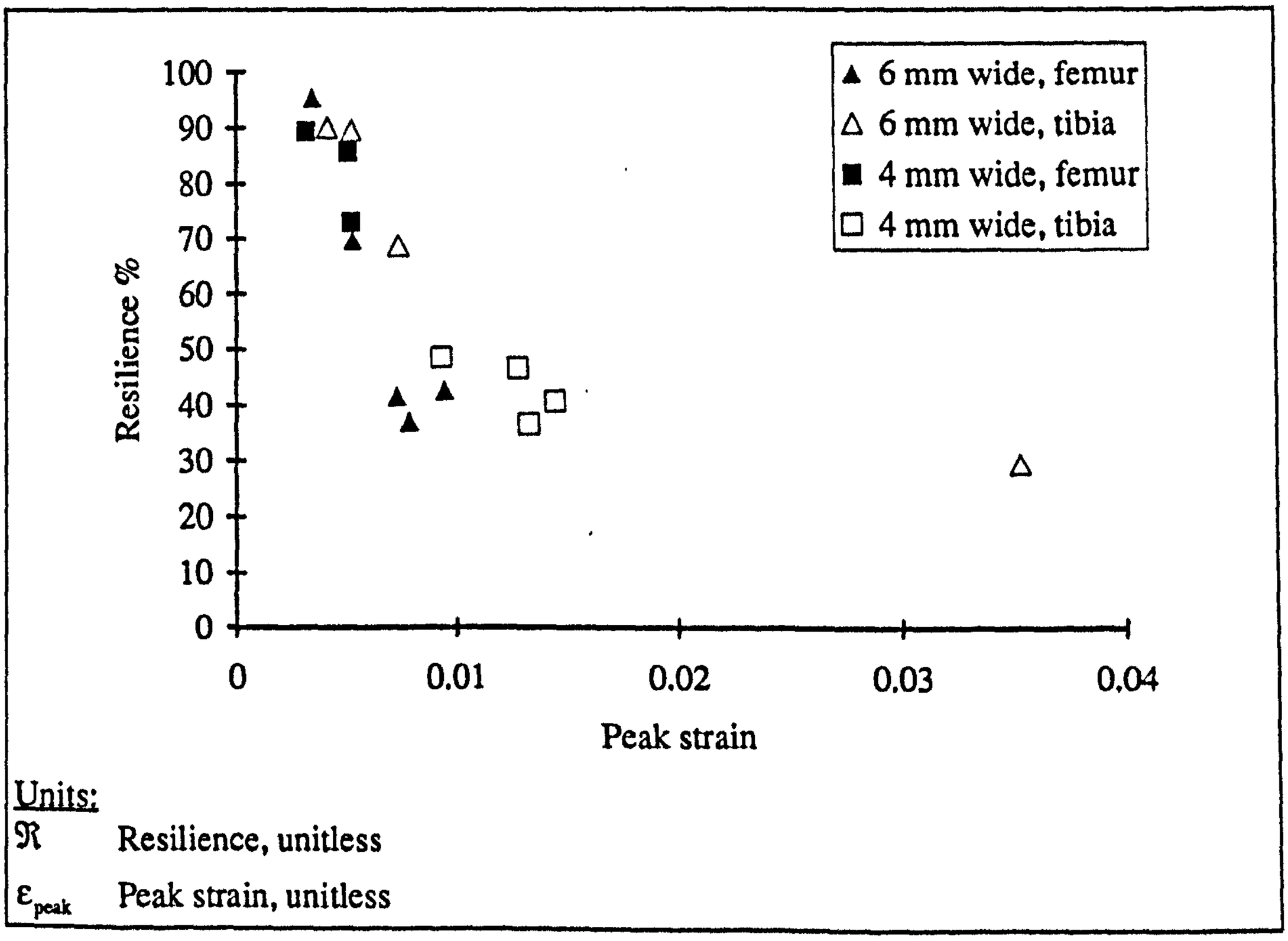

Units:

$\Re$ Resilience, unitless

ε_{peak} Peak strain, unitless

Figure 7.029

The relationship of resilience to peak stress for 16 specimens of bovine bone

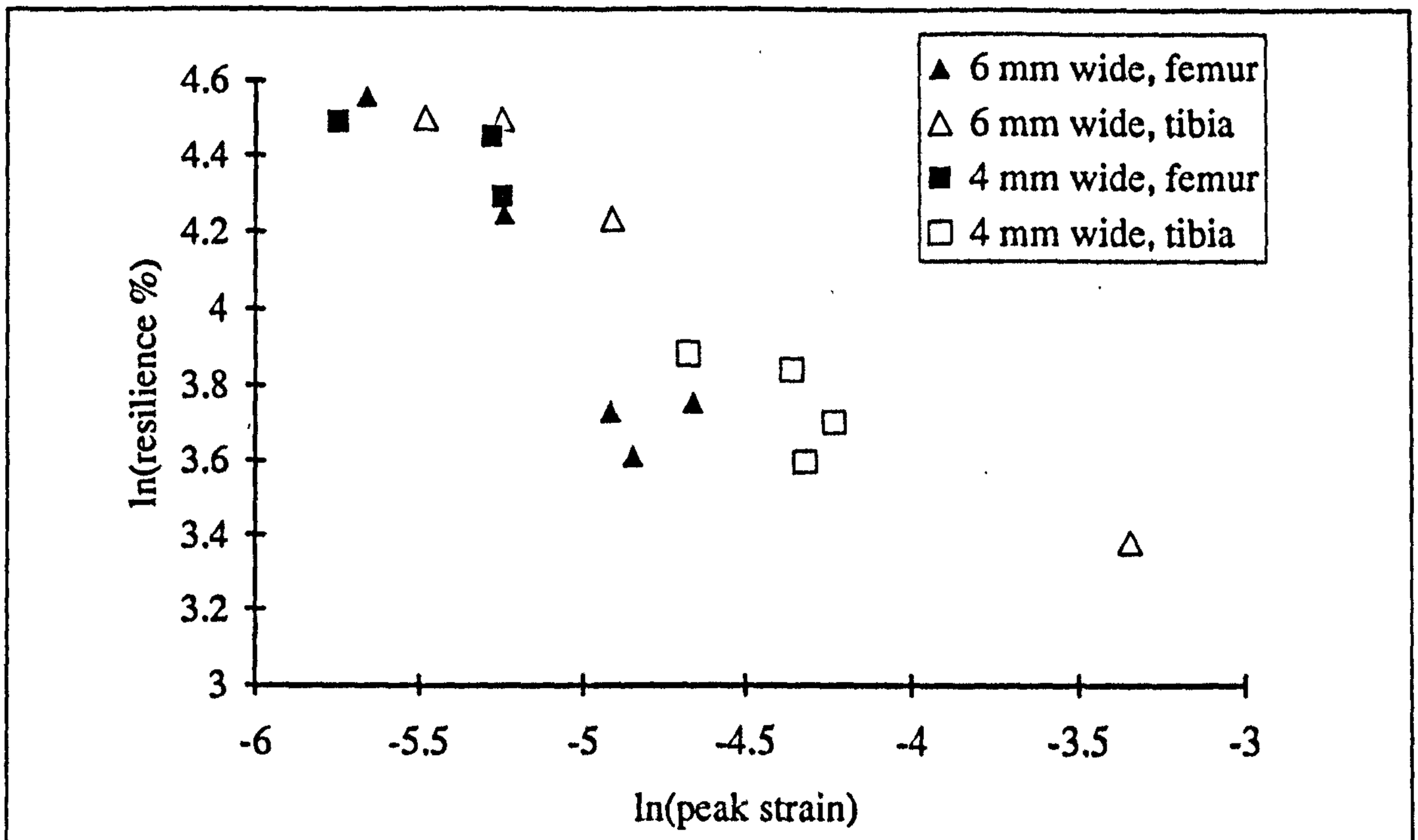

Units:

$\Re$ Resilience, unitless

ε_{peak} Peak strain, unitless

Figure 7.030

The logarithmic relationship of resilience to peak strain for 16 specimens of bovine bone

Bovine specimens	Regression equations and t values	R^2%	
Tensile 16	$\ln(\Re) = 11.7 - 1.61 \ln(\sigma_{peak})$ t: 4.85 - 3.17	37.6	*a*
Tensile 16	$\ln(\Re) = 1.27 - 0.569 \ln(\varepsilon_{peak})$ t: 3.18 - 7.02	76.4	*b*
Units: $\Re$, ratio. σ_{peak}, MPa. ε_{peak}, ratio.			

Table 7.029

Regressions of resilience and the measured mechanical properties

7.7.1.2. RESULTS: IS N CONSTANT?

In previous sections I have used an equation presented in a paper by Purslow (1991) to describe the stress-strain curve of antler, the equation was $\sigma = k\,\varepsilon^n$. It was found that for antler the value of n was not constant. In this section I consider if this is the case for bone.

The stress-strain relationship obtained from a tensile test of bovine bone, appears to be very similar to that of elastic-brittle or elastic-plastic materials. Purslow's equation appears to be of the wrong form to fit this very angular curve well. Purslow used his relationship of stress to strain to determine the energy stored within a notch sensitive and totally notch-insensitive specimen. Therefore, an important consideration is whether or not the material away from the notch in a bovine specimen experiences a stress (or strain) sufficiently high for that material to enter the knee or curved section of the loading curve.

The mean failure stress of the notched bovine bone specimens (both tibia and femur) is 65.06 MPa (s.d. 18.93, n = 88). This value can be compared to the stresses obtained from the un-notched specimens and the estimated limit of elasticity. The mean knee stress for the un-notched specimens in this data set is 117.7 MPa (s.d. 16.13, n = 32, data from tensile and resilience tests). In the previous section it was shown that bovine bone is essentially elastic up to a stress of 67 MPa. These results appear to indicate that on average the bulk of the material in a notched specimen is still in the equivalent of the initial stage of a tensile loading curve, and within a range that can be considered to be essentially linear. In section 4.2.6.9 I showed that the initial section of the loading line was curved, but that this curvature was so slight I was unable (by the method used) to determine an equation to model it. Therefore, I consider that it is reasonable to assume that the value of n is unity, for the stresses experienced by the bulk of the SEN specimens.

The assumption the bovine bone behaves in a linear-elastic fashion away from the notch in the SEN specimens, suggests that Purslow's approach and the theory of LEFM should merge, for as explained in section 5.3.4. However, I will fit the data to the same forms of logarithmic equation used by Purslow and those I have developed from them. This analysis permits the form of the relationship between the crack length and the failure stress to be studied, rather than simply fitting the data to the theoretical equations.

7.7.1.3. RESULTS: NATURE OF THE FRACTURE

The most obvious difference between the fracture of bovine bone and antler, is perhaps the nature of the failure. It was reported above that in antler specimens the crack propagates by a slow rip or tearing process. Compared to this the failure of bovine bone specimens appears to be almost explosive. The route the fracture takes across a bovine specimen is more direct than that taken by a crack in antler, and the surface appears to be less fibrous. Evidence of this difference is provided in chapter 8 and the accompanying video. The loading response preceding this failure was more linear than that displayed by antler specimens (examples are given in chapter 8). The load deformation behaviour was that which would be expected for a brittle material. This type of response is not at odds with LEFM. However, the catastrophic nature of the crack suggests that any values relating to the energy required to fracture the specimen will be an overestimate.

In the analysis of the fracture of antler it was shown that antler was able to absorb more energy during the fracture than was released due to the propagation of the fracture. In the case of bovine bone it appears that the main resistance to failure by fracture may come from the greater load needed to initiate the crack rather than a toughening mechanism. Even a casual glance at the loading curves shows that the area under the curve for bovine bone specimens is far smaller than that under the curve for the antler specimens examined above. (Loading curves from comparable tests are provided in chapter 8.) This implies that less energy is required to fracture bone. This finding agrees with the results of the impact tests described in chapter 1, and the results available in the literature reviewed in chapter 6.

From an examination of the curvature of the loading curves just prior to failure exhibited by specimens of tibial bone, the general impression was gained that tibial bone was behaving in a manner that could be described as between that of femoral bone and antler (the emphasis being very strongly towards femoral bone).

As in the case of the antler tests, a whitened zone was seen at the notch tip prior to crack propagation. Due to the speed of the crack propagation there is no physical evidence to suggest this behaviour occurred around the tip of the travelling crack. However, the impression I gained during the testing of these specimens, from visual observations, was that this did occur.

7.7.1.4. RESULTS: FAILURE STRESS, NOTCH LENGTH AND NOTCH TIP RADIUS

Bovine specimens	Regression equations and t values	R^2%	
88 SEN tibial & femoral	σ_f = 101 - 98.4 (a/w) t: 20.42 - 7.68	40.0 (42.2)	*a*
71 SEN femoral	σ_f = 101 - 105 (a/w) t: 19.08 - 7.66	45.2 (50.4)	*b*
17 SEN tibial	σ_f = 104 - 77.4 (a/w) t: 10.48 - 3.06	34.3 (41.8)	*c*
88 SEN tibial & femoral	$\sigma_f = 2.14 + 2.52\ a^{-0.5}$ t: 0.24 7.11	36.3 (35.5)	*d*
71 SEN femoral	$\sigma_f = 0.47 + 2.48\ a^{-0.5}$ t: 0.05 6.31	35.7 (35.0)	*e*
17 SEN tibial	$\sigma_f = 11.0 + 2.57\ a^{-0.5}$ t: 0.70 4.17	50.6 (51.3)	*f*
Units: σ_f, MPa. $a^{-0.5}$, $m^{-0.5}$. a/w, ratio.			
Comments: The figure within parentheses in the R^2% column is the value of R^2% when the values of the materials stiffness in three-point-bending is used as an additional variable.			

Table 7.030

The failure stress and notch length data fitted to the equations for a notch insensitive material and a classically notch sensitive material

Figures 7.031 and 7.032 show the values of failure stress of the notched specimens and the commonly compared expressions for notch length, one for the classically notch insensitive material and the other for the classical notch sensitive material. Table 7.030 shows the corresponding regression equations, as in the case of antler data described above the inclusion of the material stiffness improves the predictive quality of the relationship, the values being shown within brackets in the same table. (The equations are not given in full due to possible spurious effects resulting from differences in the determination of the material stiffness.) No reliable predictor of the failure stress of the un-notched specimens was found. Thus a prediction of the failure stress of the specimens, had they not contained a notch, is not available as a normalising

factor (as it was in the case of the comparable antler specimens). The regression equations relating the ultimate stress and the material stiffness in bending and in tension are given in table 7.031. The stiffness in bending is not a significant variable in the prediction of the ultimate stress of these bovine bone specimens (contrary to the observations in section 4.2.6.7). However, the material stiffness in tension (measured from the slope of the initial region of the loading curve) is a very highly significant predictor of the ultimate stress (as would be expected from section 4.2.6.7). (The data sets in table 7.031 are different sizes as data are not available for two specimens.)

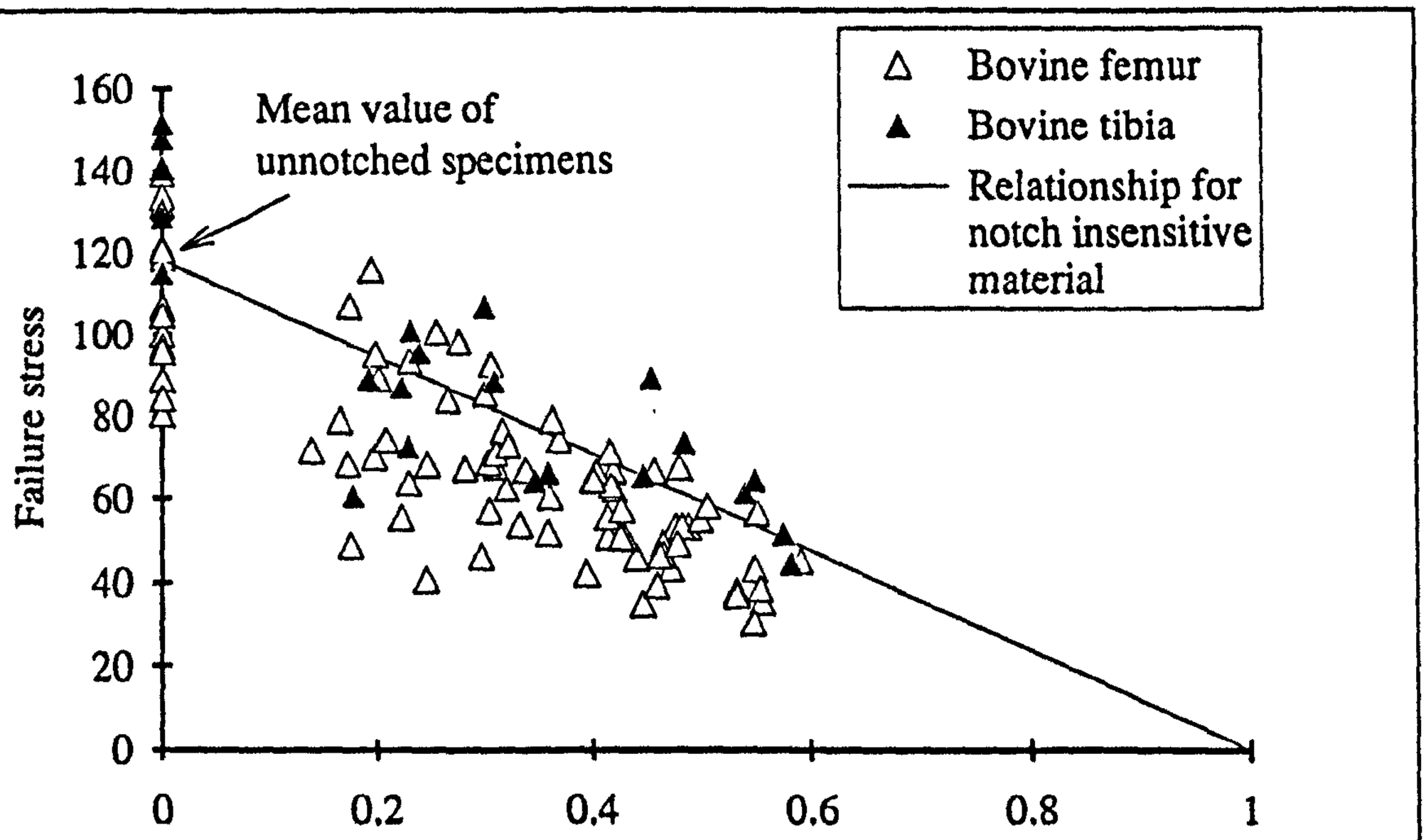

Units:

σ_{ult}	Ultimate stress (un-notched specimens), MPa
σ_f	Failure stress (notched specimens), MPa
a/w	Ratio of notch length to specimen width, unitless.

Figure 7.031

The failure stress of notched specimens and the ultimate stress of un-notched specimens of bovine bone in relation to the ratio of notch length to specimen width

Figure 7.031 shows the relationship of the failure stress to a/w, the ratio of notch length to specimen width. The line shown on the plot connects the mean ultimate stress of the un-notched specimens with zero stress at a/w = 1. If it is assumed that the distribution of failure stresses for the notched specimens is the same as that for the un-notched specimens, (due to some random distribution of mineral content and porosity for example) then if the results for the notched specimens fall on the line that would imply the material was notch insensitive. The plot shows that most of the results fall below the line, indicating a degree of notch sensitivity.

Bovine specimens	Regression equations and t values	R^2 %	
Tensile 25	$\sigma_{ult} = 119 - 0.04\ E_b$ t: 4.38 - 0.03	0.0	*a*
Tensile 23	$\sigma_{ult} = 45.9 + 3.15\ E_t$ t: 2.52 4.11	42	*b*
Units: σ_{ult}, MPa, E_b, MPa. E_t, MPa.			

Table 7.031

Relationship of the ultimate stress of un-notched specimens to the material stiffness measured in bending or during the test

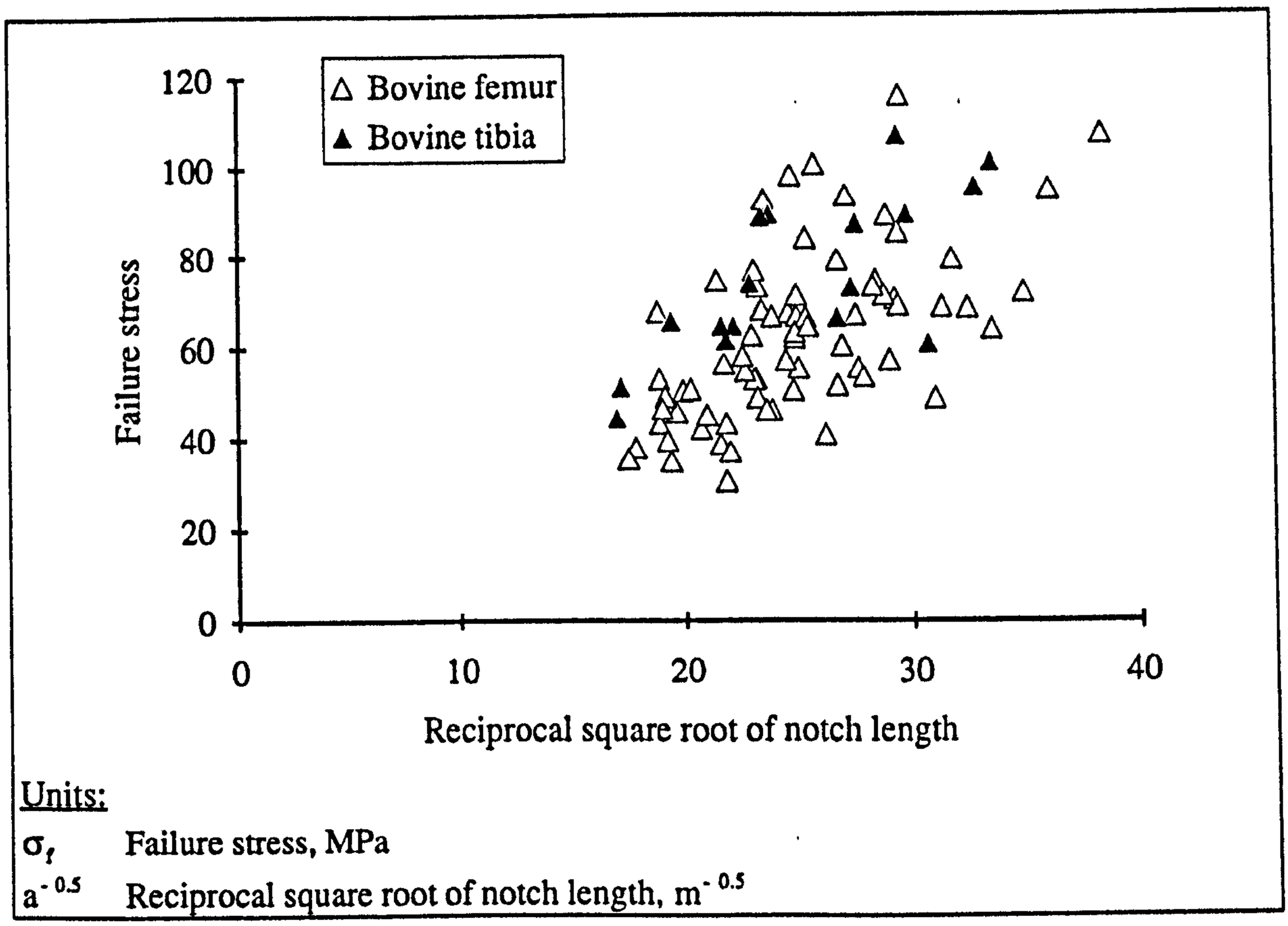

Units:

σ_f Failure stress, MPa

$a^{-0.5}$ Reciprocal square root of notch length, $m^{-0.5}$

Figure 7.032

Relationship of failure stress to notch length using the relationship predicted by LEFM

Figure 7.032 shows the relationship of the failure stress of 88 SEN specimens of bovine bone to $a^{-0.5}$. For a classically notch sensitive material this is, by definition, a linear relationship. This relationship is encapsulated in the Griffith equation (5.021), repeated here

$$\sigma_{cr} = \sqrt{\frac{E^* R}{\pi a}} \qquad (7.027)$$

Using the nomenclature of this section the Griffith equation can be rearranged as

$$\sigma_f = \left(\frac{E^* R}{\pi}\right)^{0.5} a^{-0.5} \qquad (7.028)$$

It is clear from figure 7.032 and equation *d* of table 7.030 that although such a relationship is exhibited by the experimental data there is a considerable amount of noise or unexplained variation in the results. There are innumerable possible causes of this noise. One of which, the variation of mechanical properties between specimens was considered in a similar analysis of antler specimens, section 7.4.3.3. This was partly compensated for by using the normalising factor of the material stiffness in three-point-bending. This normalising factor is unavailable in this case. Another possible source of variation is the size of the notch tip radii. These are indicated in figure 7.033.

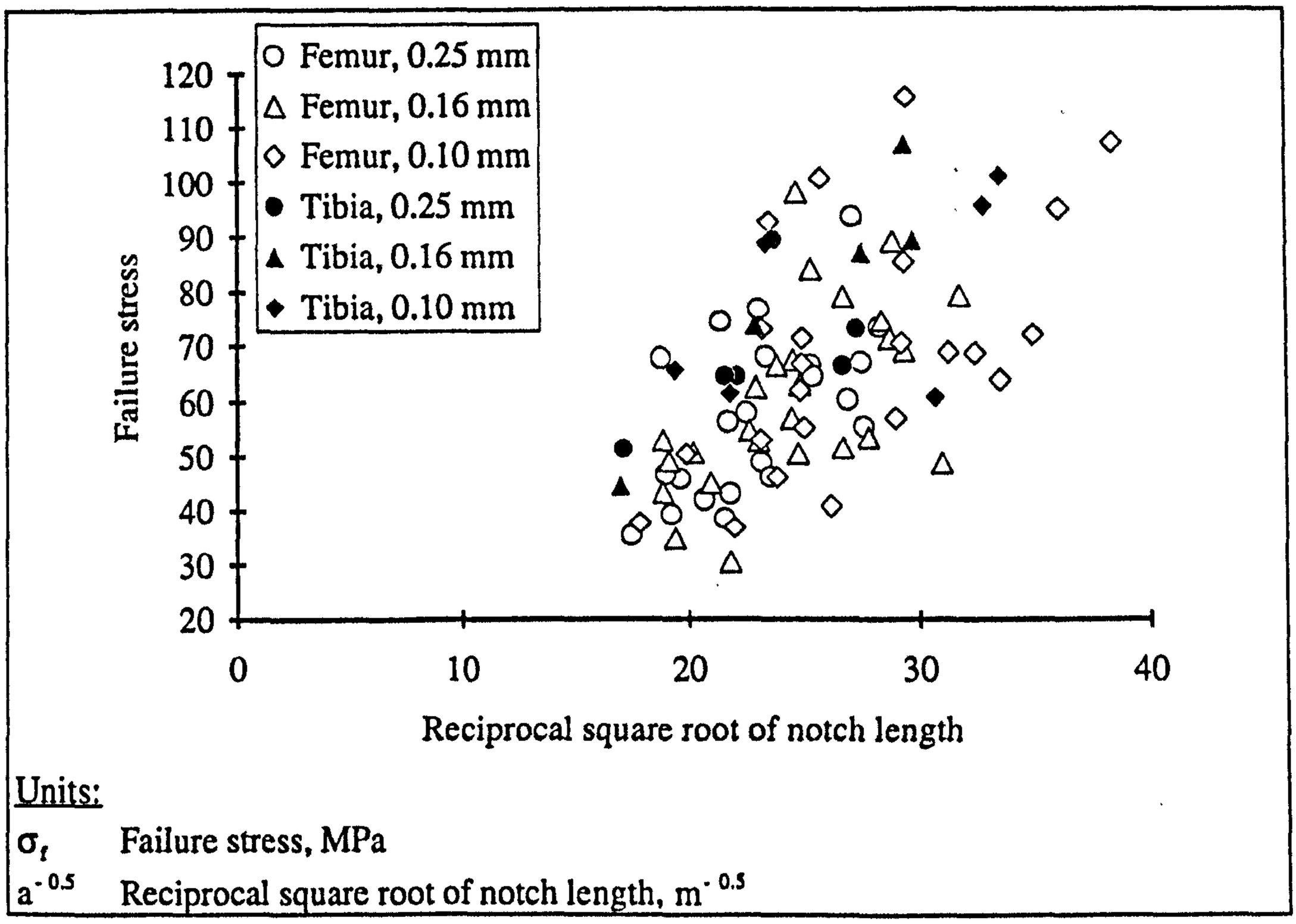

Units:

σ_f Failure stress, MPa

$a^{-0.5}$ Reciprocal square root of notch length, $m^{-0.5}$

Figure 7.033

Relationship of failure stress to notch length using the relationship predicted by LEFM, indicating the different bone types and approximate notch tip radius

Figure 7.033 shows the same data as figure 7.032. In this case the drill used to produce the notch tip is indicated by the symbol plotted. There is no clear pattern to these results. This visual result, and its accompanying statistical analysis, appear to show that the size of the notch tip radius has no significant influence on the failure stress of the SEN specimens of bovine bone. This is contrary to the predictions encapsulated in the

Inglis equation, but in agreement with the findings in the literature (see chapter 6). The considerable variation in the ultimate stress values of the un-notched specimens suggests that the apparent lack of influence of the tip radius should be treated with caution. (In a later section where a normalising function is available this aspect of the results is examined again, for a limited range of notch lengths.)

Non-compliance with the predictions of Inglis equations has implications for the application of LEFM and the investigation of the failure processes. The first implication for the LEFM approach is clearly seen when the derivation of the Griffith equation is examined (section 5.2.2.2). Griffith used Inglis solution for the stresses around an elliptical hole to derive the terms in his energy balance. Therefore, the non-compliance with the predictions of the Inglis equation, which is a direct result of these solutions brings into question the applicability of Griffith's equation and thus LEFM. The observation that the notch tip radius exerts no significant influence on the failure stress can also be interpreted as showing that the tip radii used are all sharper than the critical tip radius; a suggestion so unlikely as to be almost ludicrous. Alternatively it may be that, as suggested by Bonfield (1981 and 1987), 'fracture probably propagated from a similar sub-microscopic crack at the periphery of the machined radius'. This, or these, sub-microscopic cracks could perhaps be caused during machining or be the result of slicing through vascular or cellular spaces at the machined notch tip. However, from the occurrence of optical changes at the notch tip prior to failure and the realisation that bone is more akin to a time-dependent damage material than to an elastic one. I suggest that these sub-microscopic cracks may be related to the formation of damage ahead of the notch. It could be that the true critical notch tip radius is in the same order as the microcracks that form this process zone. (Clearly there are complicating factors, as already outlined in the analysis of the test on antler, such as the reduction in the stress experienced by the crack due to the damage within the process zone, and the microcracks will not be through-the-thickness cracks, and so on.) This aspect of the notch sensitivity results will be returned to again, because the interpretation of the process zone as a zone of damaged material helps to explain a number of observations in the literature and provides insight of the failure processes that occur in bone as it fails. In the following section more evidence in support of this interpretation is provided.

There is another observation that questions the applicability of the theory of LEFM to these results. Table 7.030 shows that the values of the failure stress of these SEN specimens of bovine bone are described more accurately by assuming the material is notch insensitive than by assuming it is classically notch sensitive. This observation is rather surprising considering the widespread application of this theory to bone. (Although a similar finding was reported by Moyle and Gavens 1986.) Another way to

examine notch sensitivity that may cast more light on this result is to examine the values of the ligament stress. This is done in the following section.

7.7.1.5. RESULTS: LIGAMENT STRESS

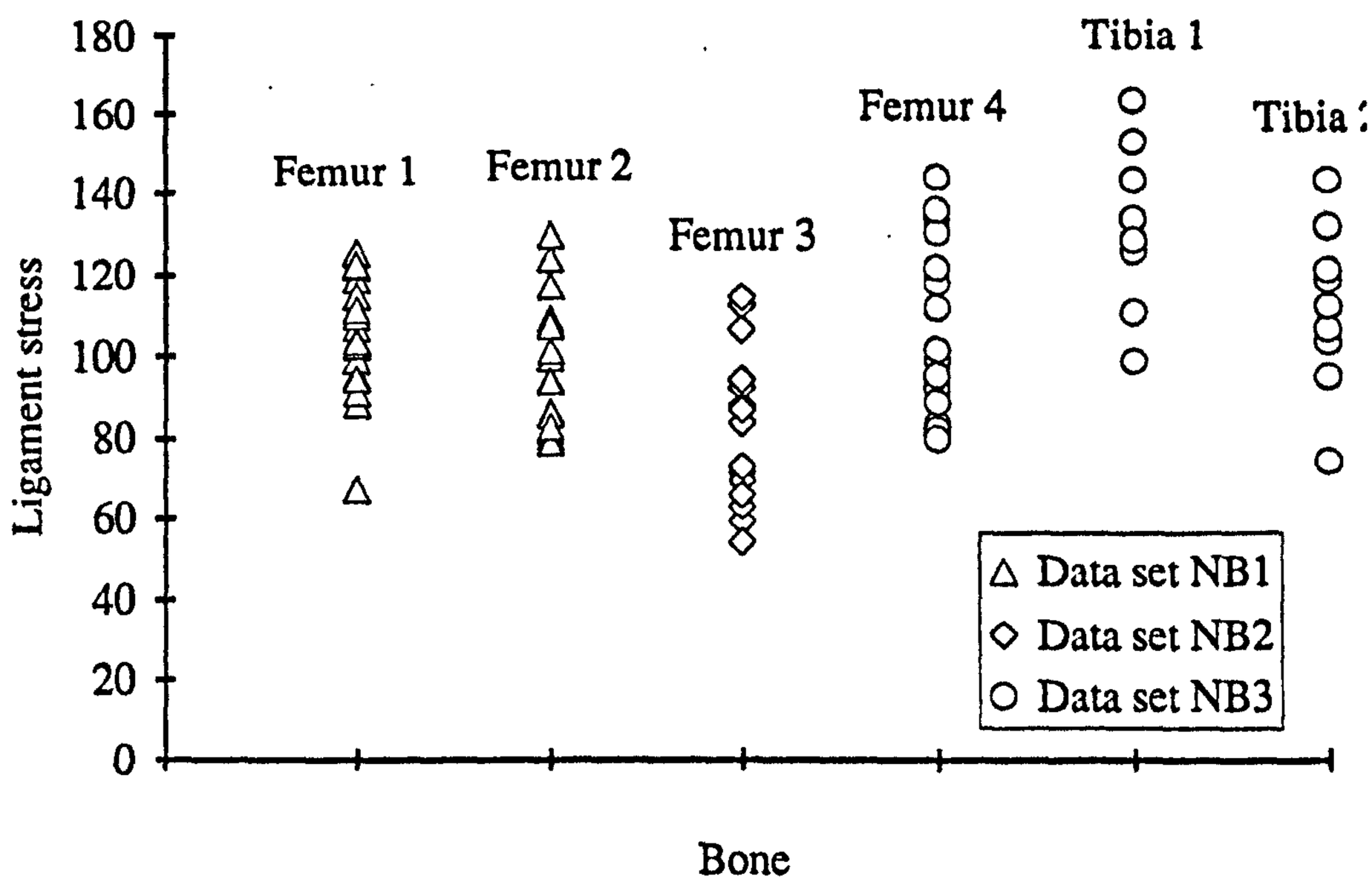

Units:

σ_{lig} Ligament stress, MPa

Comments:

See table 7.002 for information on the source and storage of the bones.

Figure 7.034

The values of the ligament stress for the specimens obtained from the different bones used in these tests

For a notch insensitive material the ligament stress is a constant and therefore independent of notch length, tip radius and so on. Thus examination of the values obtained for this quantity may give additional information on the sensitivity of bone to notches. The ligament stress values reinforced the observation of differences between the results from the different bones tested. A factor that simply labelled the sample as being from a femur or a tibia being the best single predictor of the ligament stress from a group of possible factors, $R^2 = 15.4\%$. (These factors were: tibia or femur, data set, material bending stiffness, specimen width, specimen thickness, notch length, notch tip radius, ratio of notch length to specimen width and the reciprocal of the square root of the notch length.) The second best single predictor was specimen thickness. When the values of the ligament stress are plotted against the different bones this variation becomes more

obvious. This is done in figure 7.034. This result would appear to indicate that bone is notch insensitive if no strong relationship of σ_{lig} to a/w exists for example. However, on examination of figures 7.034 and 7.035, it would be difficult to claim that the ligament stress maintains a constant value, without some normalising factor to clean up some of the noise. The results obtained from the values of the ligament stress are inconclusive. Combinations of the various predictors listed above can be used, such as specimen width and thickness. However, due to the poor experimental design these are also dependent on the bone from which the specimen was cut. Thus the source of the variation in σ_{lig} is unclear. The ligament stress values appear to be very close to those of the un-notched specimens tested at the same cross-head speed. The results are shown in table 7.032.

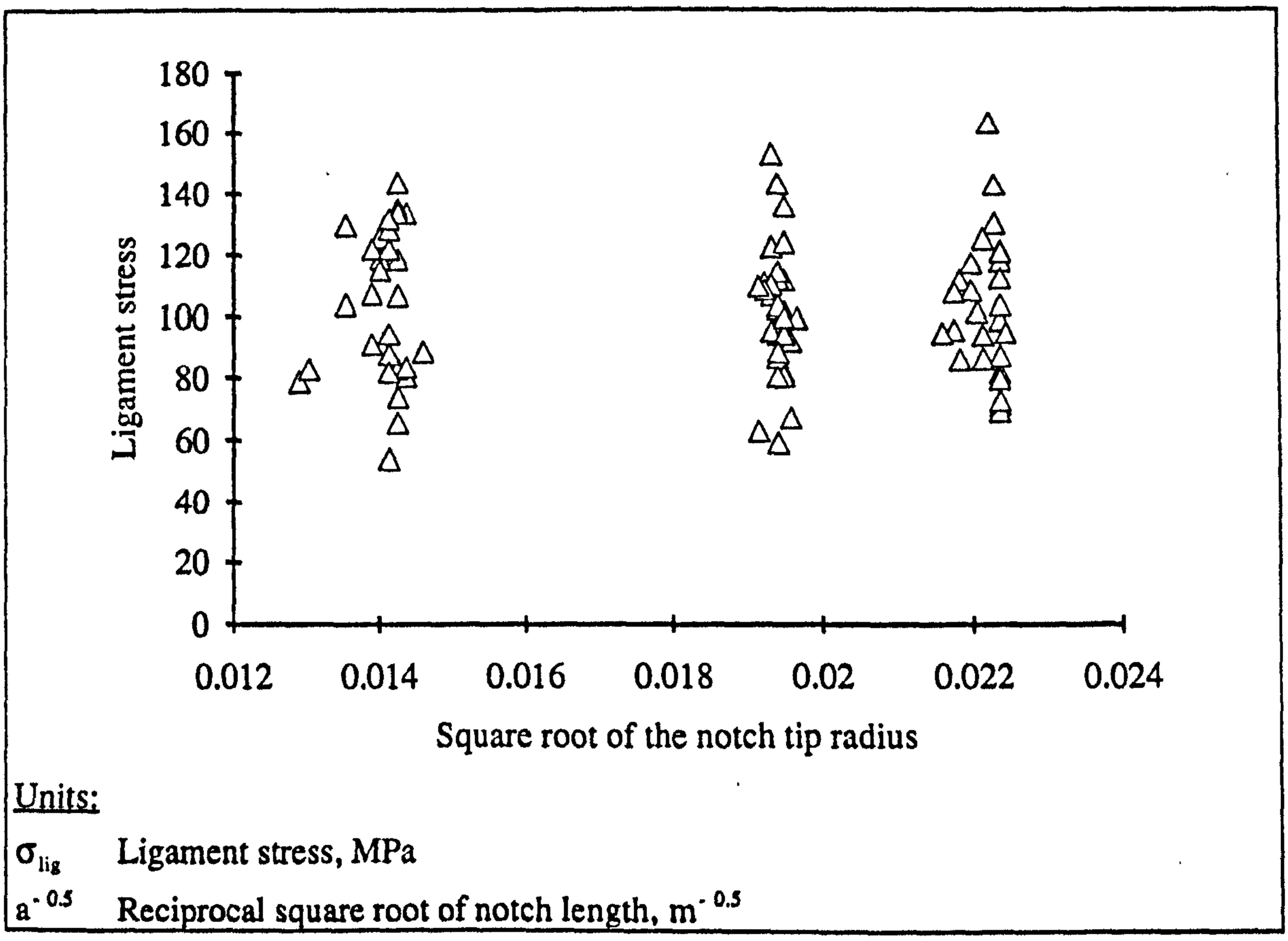

Figure 7.035

The values of the ligament stress and the square root of the notch tip radius

	Mean	s.d.	number of specimens
σ_{ult} (un-notched)	118.29	19.77	25
σ_{lig} (notched)	102.96	22.34	88

Table 7.032

Mean values of the ligament stress of the SEN specimens and the ultimate stress of the tensile specimens in this data set (NB1, NB2 and NB3)

This suggests that the mean value of the ligament stress is 13 % less than the mean value of the un-notched specimens. One-way analysis of variance showed the difference between the two groups of results to be statistically highly significant. Although as a direct measure this comparison is of little more value than proof that the material is notch sensitive. (For this being the case the value of the ratio will depend on the size of the notch.) If it is assumed that the specimens are, as intended, replicates of the antler specimens in section 7.4. This value suggests that the introduction of a machined notch has a proportionally larger effect on the failure stress of antler than it does on bovine bone. This observation will be returned to in chapter 9, where the ideas of damage accumulation and fracture mechanics are combined to give an explanation of the final failure of bone and antler.

7.7.1.6. RESULTS: FAILURE STRAIN AND NOTCH LENGTH

Due to extensometer slippage or failure of the water-proofing there are only 75 results for the failure strain of notch bone specimens. The type of bone, tibia or femur, was found to be the single most important factor in determining the failure strain of a notch specimen in these data sets. This again suggests a difference exists between the two types of bovine bone used here.

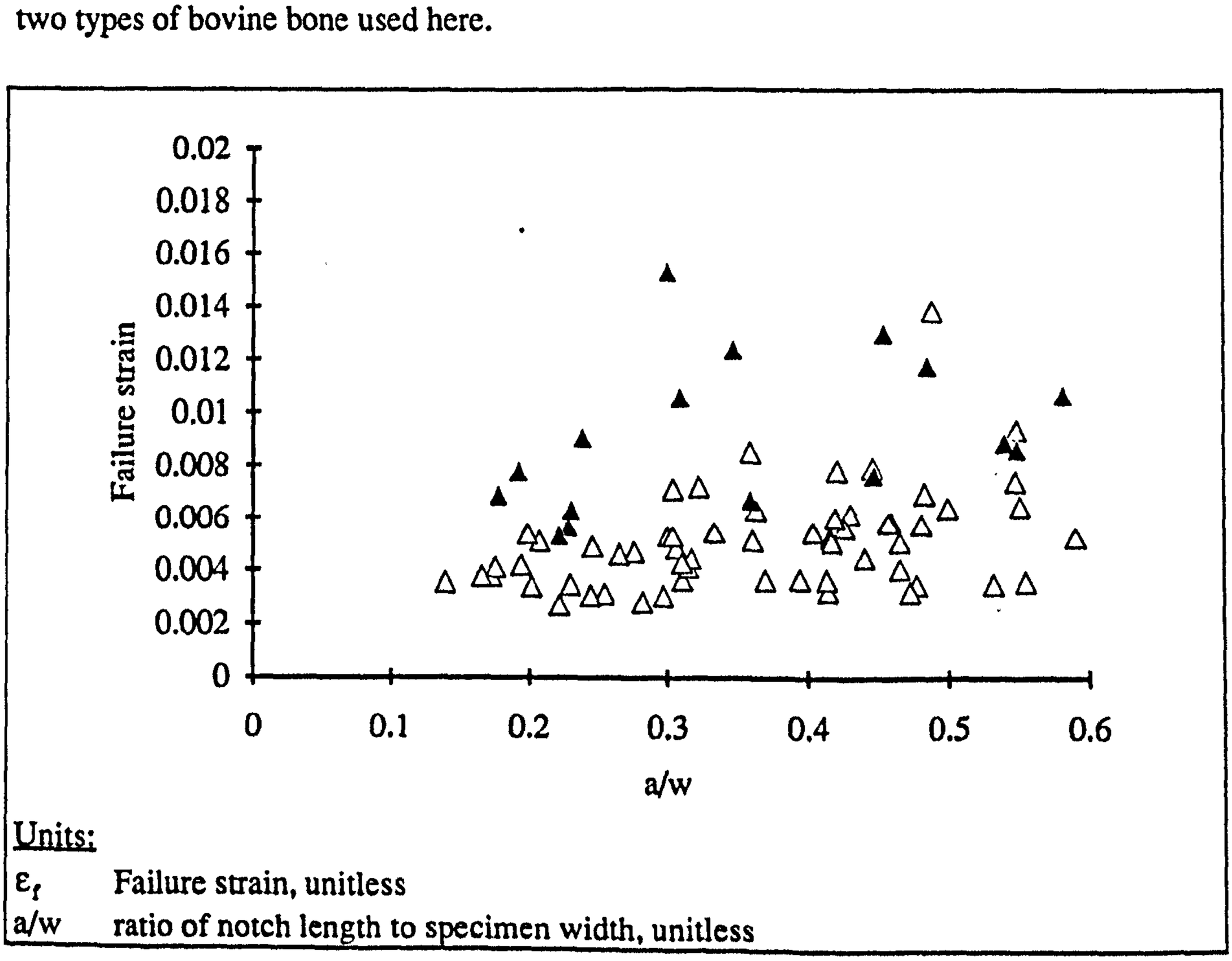

Units:

ε_f Failure strain, unitless

a/w ratio of notch length to specimen width, unitless

Figure 7.036

Failure strain and a/w of notched specimens of bovine bone

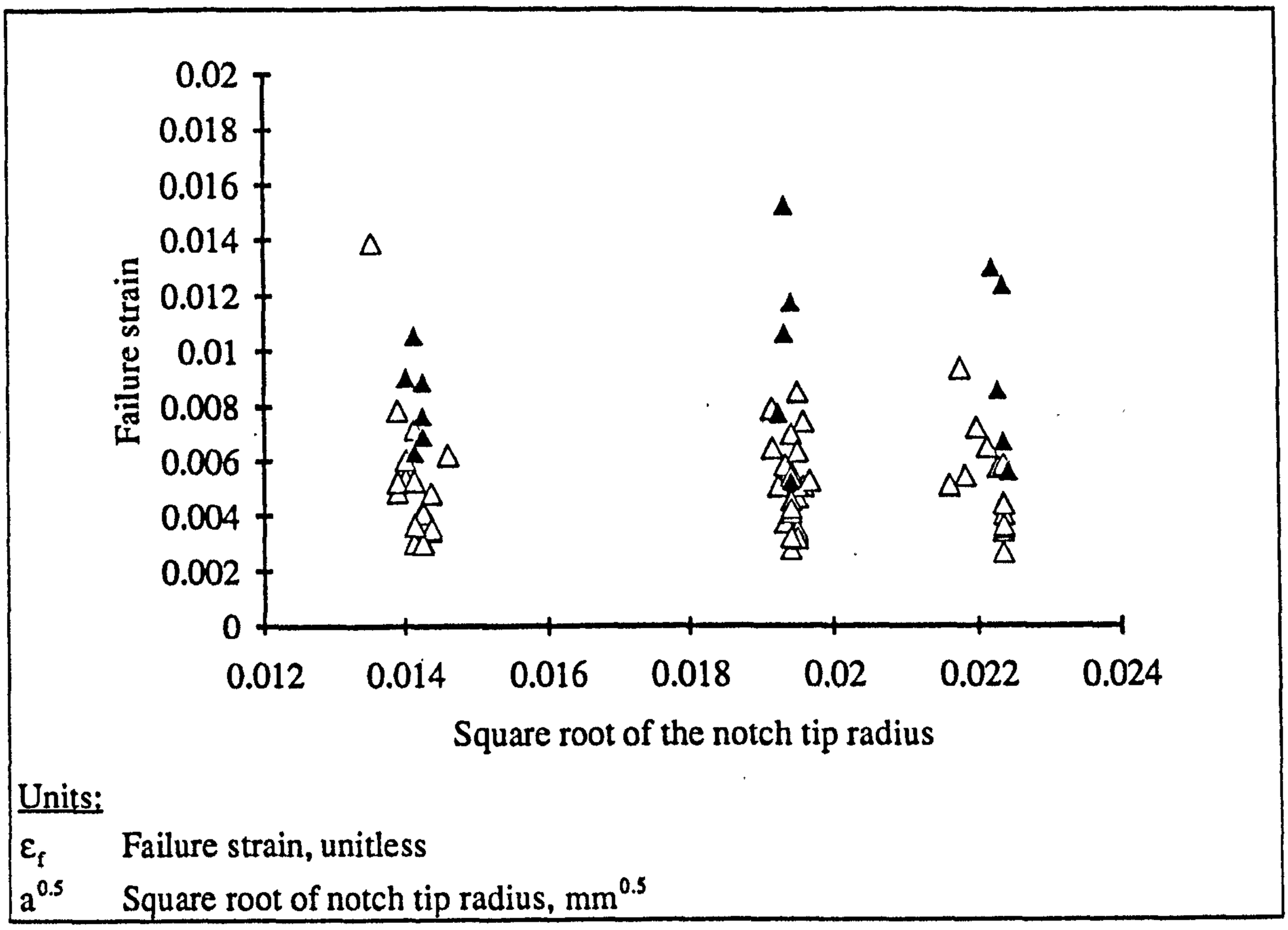

Units:

ε_f Failure strain, unitless

$a^{0.5}$ Square root of notch tip radius, $mm^{0.5}$

Figure 7.037

Relationship of failure strain and the square root of notch tip radius for bovine bone

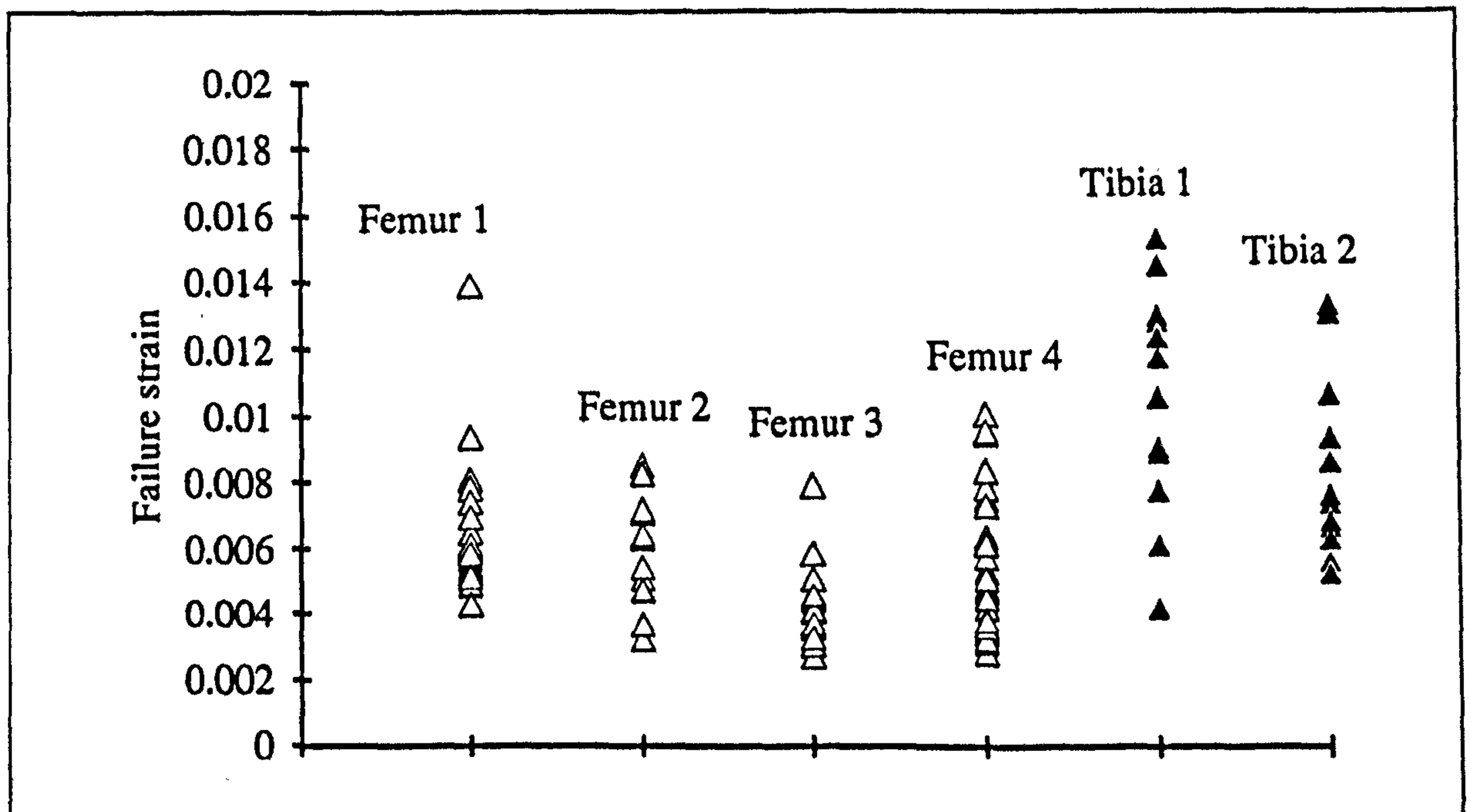

Units:

ε_f Failure strain, unitless

Comments:

See table 7.002 for information on the source and storage of the bones.

Figure 7.038

The relationship of failure strain to the bone from which the specimen was obtained

The effect of notch tip radius appears to have no effect on the ultimate strain. In this data set specimens were obtained from a number of different bones, and it was found that the bone from which the specimen was obtained seems to influence the failure strain.

The values of the failure strain exhibited by the SEN specimens of bovine bone range up to the mean value obtained for the un-notched tensile specimens taken to failure ($\varepsilon_{ult} = 0.015$, s.d. = 0.012). (It may be remembered that in the comparable tests on antler the failure strain of the SEN specimens and the ultimate strain of the un-notched specimens did not overlap.) This could be interpreted in two similar ways: first, the notched specimens are failing by a similar process to the un-notched specimens, and this process is damage accumulation. Second, the un-notched specimens are failing by a similar process to the notch specimens, and this process is fracture. From the data presented here it is not possible to support either argument. However, this idea is one of the pieces of the jigsaw that is finally assembled in chapter 9, where its relationship to the results of other tests is considered.

7.7.1.7. RESULTS: PURSLOW'S AND OTHER LOGARITHMIC APPROACHES

The same type of investigation as performed for antler (in section 7.4.3.6) is represented here, except that the value of n is assumed to be a constant in all cases. The use of these logarithmic equations enables an exponential relationship that best fits the data to be found rather than fitting the data to the theoretical LEFM relationship. This may provide more evidence as to which theoretical equation describes the data best; thus shedding light on the failure process. The data is shown in a pooled form and then the results from the different types of bone are examined separately. It was very noticeable during the analysis that the addition of the values for the bending modulus has only limited effect on the predictive power of the relationships, in some cases beneficial in other detrimental. This is probably due to the spurious effects already mentioned. However, it was noted in chapter 4 that this variable was more significant in the case of antler than it was in the analysis of the bovine results in standard tensile tests. The R^2% values given in brackets in table 7.033 are those obtained when E_b was used as an additional variable.

Bovine specimens	Regression equations and p values	R^2%	
88 SEN tibial & femoral	$\ln(\sigma_f) = 4.39 - 0.506 \ln(a)$ t: 103.89 - 7.40	38.2 (37.6)	*a*
88 SEN tibial & femoral	$\ln(\sigma_f) = 3.61 - 0.490 \ln(a/w)$ t: 47.16 - 7.19	36.8 (39.7)	*b*
88 SEN tibial & femoral	$\ln(\sigma_f) = 4.02 - 0.544 \ln(a) + 0.244 \ln(w)$ t: 22.24 - 7.81 2.06	40.2 (41.1)	*c*
71 SEN femoral	$\ln(\sigma_f) = 4.39 - 0.526 \ln(a)$ t: 91.68 - 6.76	38.9 (38.7)	*d*
71 SEN femoral	$\ln(\sigma_f) = 3.54 - 0.527 \ln(a/w)$ t: 42.50 - 7.08	41.3 (47.2)	*e*
71 SEN femoral	$\ln(\sigma_f) = 3.88 - 0.527 \ln(a) + 0.326 \ln(w)$ t: 19.97 - 7.45 2.56	43.5 (46.9)	*f*
17 SEN tibial	$\ln(\sigma_f) = 4.52 - 0.444 \ln(a)$ t: 71.47 - 4.53	54.9 (56.6)	*g*
17 SEN tibial	$\ln(\sigma_f) = 3.93 - 0.345 \ln(a/w)$ t: 27.10 - 2.74	28.8 (34.2)	*h*
17 SEN tibial	$\ln(\sigma_f) = 4.81 - 0.415 \ln(a) - 0.192 \ln(w)$ t: 15.61 - 4.02 - 0.96	54.7 (54.2)	*i*
Units: σ_f, MPa. a, mm. w, mm.			

Table 7.033

The relationship of failure stress to some geometrical properties of SEN specimens of bovine bone

In the equations shown in table 7.033 the coefficient of the notch length term is approximately equal to 0.5 (in some it is above, while in others it is below). This suggests that the equations conform to that predicted for a classically notch sensitive material. Therefore this, by implication, suggests that the failure of these SEN specimens is due to a brittle fracture of the type described by LEFM. These suggestions are examined in the conclusion to this chapter where it is put in the context of other results.

7.7.1.8. RESULTS: THE LEFM APPROACH, THE CRITICAL STRESS INTENSITY AND SHAPE CORRECTION FACTORS

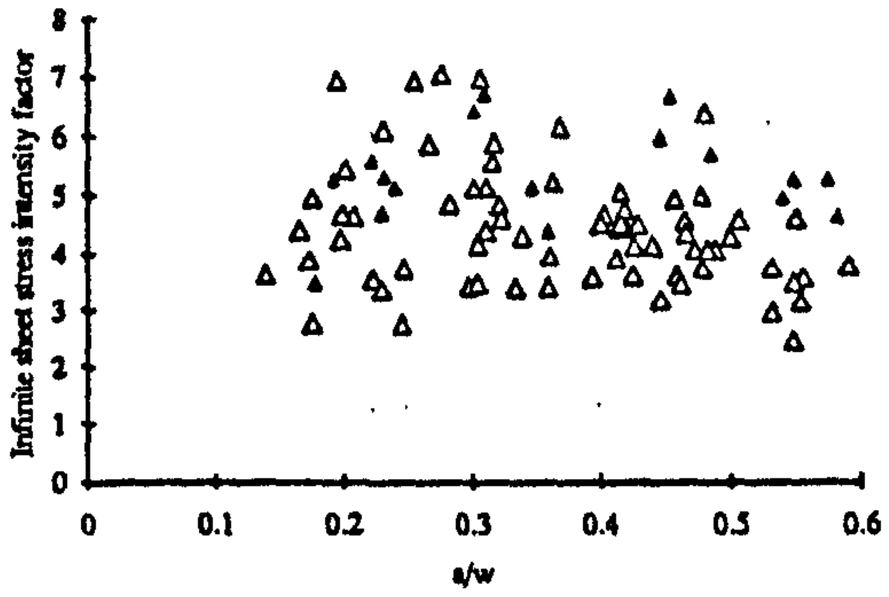

a) Infinite sheet stress intensity factor

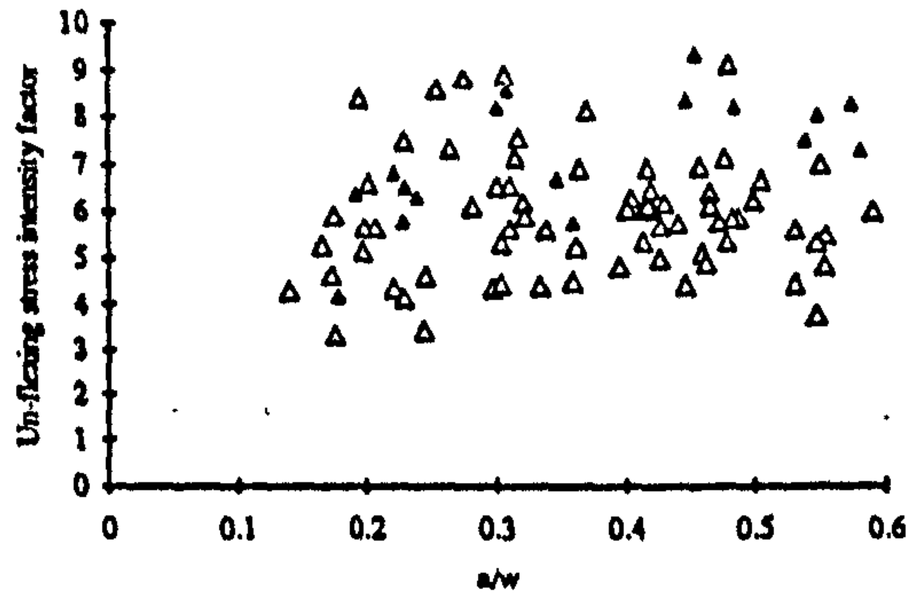

b) Un-flexing sheet stress intensity factor

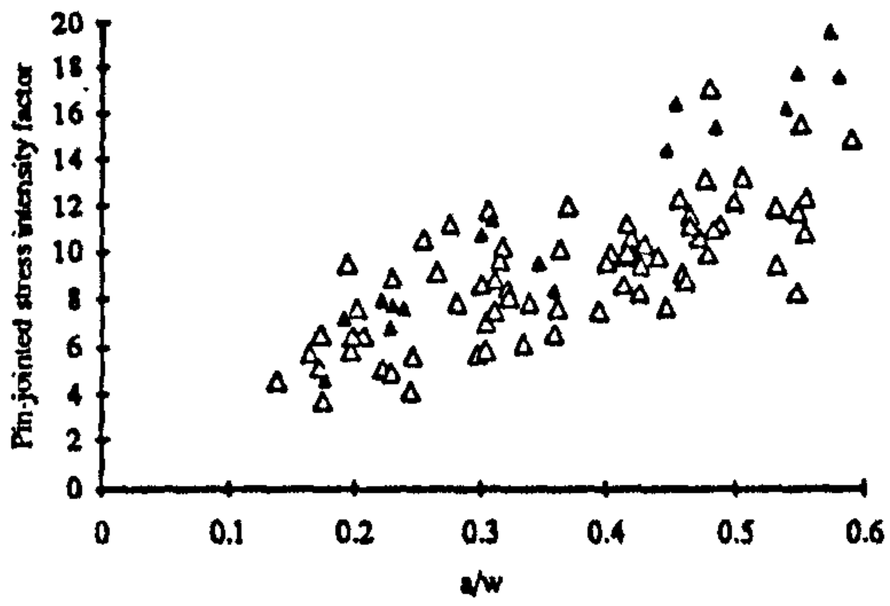

c) Pin-jointed stress intensity factor

A decrease in the assumed restraints on the specimen prompts an increase in the correlation of the calculated critical stress intensity factor and the specimen geometry (this is shown in figures a, b and c). The critical stress intensity factor is supposedly a material property thus its correlation with a geometrical factor is undesirable.

Units:

a) K^{I}_{IQ}, MPa $m^{0.5}$. a/w, ratio.

b) K^{U}_{IQ}, MPa $m^{0.5}$. a/w, ratio.

c) K^{P}_{IQ}, MPa $m^{0.5}$. a/w, ratio.

Figure 7.039

The relationships of the calculated critical stress intensity factors (K^{I}_{IQ}, K^{U}_{IQ} and K^{P}_{IQ}) and the ratio of notch length to the width of specimens of bovine bone

The numerical value obtained from the equations describing three *stress intensity factors* defined in section 7.2.5.2 was calculated for each of the 88 notched specimens. The values of the infinite sheet SIF were examined first. It was found that the best single predictor of the infinite sheet SIF (from those readily available in the data set) was the type of bone the specimen was made from tibia or femur. (The next best single predictor was the width of the specimen.) Thus the data was examined in two parts depending on

bone type (table 7.034). Repeating all of the analysis of section 7.4.3.7 on these bovine data is of little use as the value of the materials stiffness in three-point-bending was found to be a poor predictor of the basic SIF, probably due to the differences in the measurement of this value mentioned above.

Figure 7.039 shows the relationship of the various measures of the experimentally determined stress intensity factor, K^{*}_{IQ}, and the ratio of the notch length to specimen width. The regression equations for each material are shown in table 7.034. As in the case of the antler specimens (section 7.4.3.7) the use of the pin-jointed shape correction factor has clearly induced a relationship between the SIF and a/w. In that case a/w is a very highly significant predictor of the SIF for both materials (equations *c* and *f*). However the results obtained for the two materials, femoral and tibial bone, differ on the form of SIF for which a/w is not a significant explanatory variable. The femoral bone specimens display a result that agrees with the theoretical one, the un-flexing sheet shape SIF being the only one that is not significantly dependent on a/w. The sign of the coefficients of a/w in equation *a* and *c* (where a/w is at least a significant explanatory variable) are also in keeping with the theoretical predictions. In a previous section (7.2.5.2) I predicted, from examination of the specimen's deformation during the test that the true shape correction factor (and thus SIF) may fall between that of the un-flexing sheet and the pin-jointed sheet. If this were the case the coefficient of a/w in equation *b* would be less than zero. However, as it is non-significant it is not possible to be certain on this account.

The SIF for the tibial specimens shows a different and stronger trend to that of the femoral bone specimens. In their case it is the un-corrected or infinite-sheet SIF that has no significant relationship with a/w ($p = 0.601$). (This result agrees more with that obtained for antler than it is to that of femoral bone.) Equation *f* clearly shows that the application of a pin-jointed shape correction factor is not valid in this case. The constant 0.182, is not significantly different from zero. Thus the value of K^{P}_{IQ} is almost entirely dependent on a/w and can therefore be disregarded.

Bovine specimens	Regression equations and p values	R^2 %	
71 SEN femoral	K^{I}_{IQ} = 5.30 - 2.37 (a/w) t: 13.59 - 2.34	6.0	*a*
17 SEN tibial	K^{U}_{IQ} = 5.74 + 0.45 (a/w) t: 11.43 0.35	0.0	*b*
71 SEN femoral	K^{P}_{IQ} = 2.93 + 16.9 (a/w) t: 4.06 9.01	53.4	*c*
17 SEN tibial	K^{I}_{IQ} = 5.07 + 0.78 (a/w) t: 8.81 0.53	0.0	*d*
71 SEN femoral	K^{U}_{IQ} = 5.12 + 5.75 (a/w) t: 7.16 3.16	36.0	*e*
17 SEN tibial	K^{P}_{IQ} = 0.182 + 31.5 (a/w) t: 0.20 13.68	92.1	*f*
Units: K^{*}_{IQ}, MPa $m^{0.5}$.	a, mm. w, mm.		

Table 7.034

Relationship of the critical stress intensity factor and some geometrical properties of the SEN specimens of bovine bone

An examination of the relationship between the SIF and the material stiffness is difficult to justify for this data set (as explained above). However, in the analysis of another set of SEN specimens of bovine bone (see table 7.046), it was shown that the relationship between K^{*}_{IQ} and the material's bending stiffness was most significant when $K^{*}_{IQ} = K^{I}_{IQ}$. The same result was exhibited by the antler specimens of data set NA3. This (combined with the relationships between the various SIF and a/w) demonstrates that the use of a shape correction factor has a detrimental effect on the predictive power of the stress intensity factor approach. This suggests there is some inconsistency between the theoretical and the experimental situation. The possible implications of this observation are considered in section 7.10.10.

It has already been shown that the notch tip radius has no apparent effect on the failure stress of these SEN specimens of bovine bone. Thus it is not surprising that figure 7.040 shows it has no apparent effect on the infinite sheet SIF. This result is not one that is predicted by LEFM and the related theories. Considering the definition of the SIF this implies that the stress field ahead of the notch is not dependent on the notch tip radius.

There are a number of possible explanations of this observation. First the stress field is dependent on the notch tip but the critical stress intensity factor is not an appropriate method for expressing this dependence. Another possible explanation, and when other evidence is considered the probable explanation, is the machined and measured notch tip radius is not the one responsible for failure. The true notch tip (as proposed above) is a result of stress induced microcracking within the process zone at the notch tip. In section 7.8 a more thorough consideration is given to the size of this process zone.

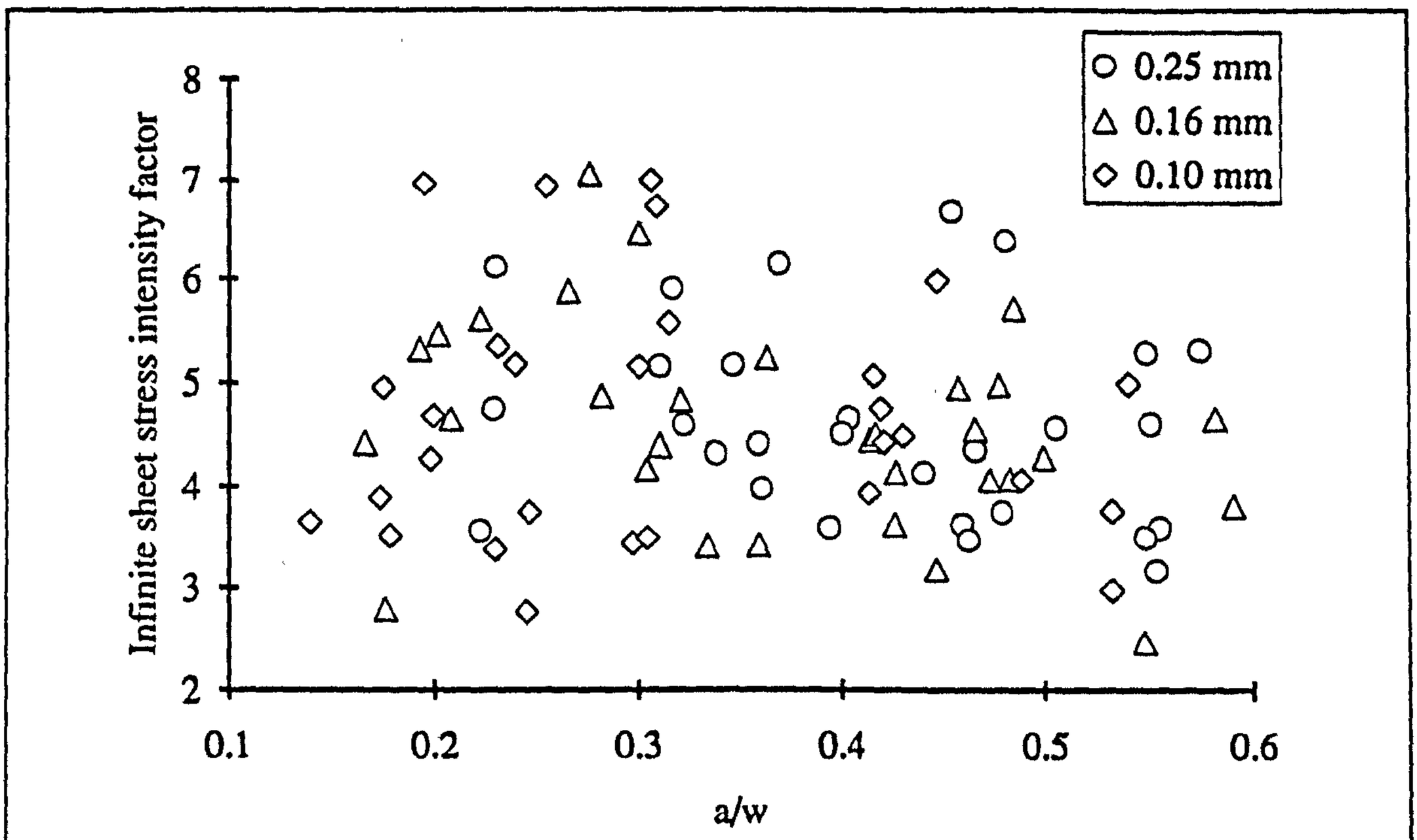

Units:

$K^{\bullet}_{IQ}$ Infinite sheet stress intensity factor, MPa $m^{0.5}$

a/w Ratio of notch length to specimen width, unitless

Figure 7.040

Relationship of the infinite sheet stress intensity factor, $K^{\bullet}_{IQ}$, to the ratio of notch length to specimen width, a/w, with the data classified as to the approximate notch tip radius

The general impression gained from these tests on SEN specimens of bovine bone is that this material is notch sensitive and this notch sensitivity appears to be modelled by Griffith's relationship of crack length to fracture stress. However, although the results are modelled by this equation that does not mean the fracture process is that on which the equation is based. Agreement between the values of the critical stress intensity factor obtained in this study with those in the literature, suggests that the results obtained here are not overtly dependent on the specimen geometry (when the appropriate shape correction factor is applied).

7.7.2. SUMMARY OF THE RESULTS CONTAINED IN DATA SETS NB1, NB2 AND NB3

The analysis of the 88 SEN specimens of bovine bone and accompanying tensile and resilience test results has produced a number of findings.

a) The failure of these specimens was catastrophic.

b) The loading line was reasonably linear.

c) The resilience of bone is, as may be expected from the low slope of the post-knee region, more strongly related to strain than stress.

d) The limit of full elasticity was estimated as being associated with a strain of 0.0028 and a stress of 67 MPa.

e) The SEN specimens failed at a (mean) stress slightly below the (mean) stress estimated to be the limit of full elasticity. Thus suggesting that the material of SEN specimens away from the notch was still behaving elastically.

f) Fitting the data to the equations associated with the notch insensitive and classically notch sensitive materials suggested that the material was more like a notch sensitive one.

g) The observation noted in f) was qualified by an examination of the ligament stress that clearly showed that bovine bone is notch sensitive.

h) Examination of the failure strains of the notched specimens showed they were not markedly different from those of the un-notched specimens.

i) Regressing the failure stress and notch length data in logarithmic form produced relationships that were essentially the same as the relationship produced by LEFM.

j) The calculated values of three forms of stress intensity factor were examined for the instant of failure. These results showed that the pin-jointed critical stress intensity factor was (as originally assumed) an inappropriate correction factor for these specimens. If the calculation used did not include a shape correction factor, or it did contain that associated with an un-flexing sheet, the values of the SIF obtained were similar to these presented in the literature.

k) No evidence was found to suggest that the tip radius of the notch has an effect on the fracture behaviour.

If it is assumed that the essentially linear-elastic properties of the test material, the catastrophic nature of the fracture and the agreement with a classically notch sensitive stress to crack length relationship, can be used to justify the application of LEFM a question remains; why is there no dependence on notch tip radius. This is explained, as it was for the case of the antler specimens, by the existence of a damage zone ahead of the notch. In the next section I examine (as I did for antler in section 7.5) the size of the whitened zone in relation to the failure stress and the tip radius.

7.8. NOTCH SENSITIVITY OF BOVINE FEMORAL BONE (NB4): PROCESS ZONE CORRECTION TO NOTCH LENGTH

This section mirrors section 7.5. In the earlier section the material studied was red deer antler, whereas here the concern is with the results from SEN specimens of bovine femoral bone. In this section the size of the whitened zone ahead of the machined notch tip, at the instant of the first fracture propagation, is investigated. As is the case for antler, the optical changes observed in tensile tests of bovine bone are related to the knee region of the loading curve. As in the case of the antler specimens, I attribute the whitening of the bovine specimens to the accumulation of damage (in the form of microcracking). The knee region of an un-notched tensile specimen of bovine bone is more severe than that displayed by antler. The overall impression is that the loading curve is only slightly different to that of the ideal elastic-plastic or elastic-damage material. The knee stress and the ultimate stress have essentially the same value. It was postulated in section 7.5 that antler's ability to sustain stresses more than its knee stress may explain the failure of the effective fracture length, as measured in this thesis, to improve the predictive power of the regression equations over those obtained using just the machined length. Irwin's effective notch length is based on the assumption that the test material is elastic-plastic. Thus consideration of the load deformation response of both bone and antler implies that application of Irwin's effective fracture length to the results obtained from bovine bone may be more useful than it was for the antler results.

7.8.1. AIMS AND EXPERIMENTAL DESIGN

The experiments in this series of tests (NB4) were conducted on SEN specimens of bovine femoral bone. The main aim of these tests is to examine the size and implications of the zone of whitened material observed at the notch tip just before fracture initiation. The method used to measure the length of the whitened zone is the same as that used for the antler specimens (section 7.5).

The experimental design in this set of tests was the same as that used to obtain data set NA4. Specimens were prepared such that they were of similar width (4 mm) and possessed a small range of notch lengths (nominally 2 mm). The mean ratio of notch length to specimen width was 0.54 (s.d. 0.05). Specimens were prepared with a range of notch tip radii, using the same drills that were used to prepare the antler specimens. The mean values of the notch tip radii used are: 0.90, 0.77, 0.71, 0.68, 0.67, 0.51, 0.50, 0.40, 0.38, 0.33, 0.20 for the drilled specimens and 0.09 mm for those sawn without drilling. The holes drilled in the bone specimens appeared cleaner, than those in antler, having

fewer burrs and a sharper outline. This may explain the larger measured radii obtained for this material.

7.8.2. EXPERIMENTAL PROCEDURE

The experimental procedure was the same as that described in section 7.5.2 for the corresponding tests on antler.

7.8.3. DATA ANALYSIS AND RESULTS

The data from these tests on bovine bone are analysed in essentially the same way as those for antler in section 7.5.3.

7.8.3.1. RESULTS OBTAINED USING THE MEASURED NOTCH LENGTH AND IRWIN'S EFFECTIVE FRACTURE LENGTH: FAILURE STRESS

Table 7.035 contains the results of analysis conducted to find the best combinations of predictors of the failure stress. The table indicates which explanatory variables are used, if they are significant and the coefficient of determination, or $R^2\%$, (adjusted for degrees of freedom).

The results given in lines *a* and *b*, *c* and *d* of table 7.035 demonstrate that the addition of half the length of the whitened zone decreases the predictive power of the notch length as an explanatory variable of failure stress. This finding is the same as that made for antler, but is far more noticeable. Here the length variable changes from a very highly significant predictor to a non-significant variable.

A similar result is obtained when the material stiffness in three-point-bending is used as an additional variable. The significance of the machined notch length is lower (highly significant in place of very highly significant), but the effective notch is non-significant in each case. This result is also obtained when the variables are expressed in logarithmic form table 7.036. In this case the relationship of fracture stress to notch length is not restricted to the classical relationships.

Predictors of the failure stress, σ_f					R^2%	
(a/w)	$(a + r_w)/w$	$a^{-0.5}$	$(a + r_w)^{-0.5}$	E_b		
VHS	-	-	-	-	33.1	*a*
-	NS	-	-	-	0.2	*b*
-	-	VHS	-	-	35.8	*c*
-	-	-	NS	-	2.2	*d*
HS	-	-	-	S	45.1	*e*
-	NS	-	-	HS	24.7	*f*
-	-	HS	-	S	47.1	*g*
-	-	-	NS	HS	24.8	*h*

Units:

σ_f	Stress at failure, MPa
E_b	Material stiffness (modulus) in three-point-bending, GPa
w	Specimen width, mm
a	Notch length, mm
$a^{-0.5}$	Reciprocal square root of notch length, $m^{-0.5}$
r_w	Half the length of the whitened zone, mm

Table 7.035

The best subset predictors of the failure stress of SEN specimens of bovine femoral bone

Predictors of the logarithm of the failure stress, $\ln(\sigma_f)$				R^2%	
ln(a)	$\ln(a + r_w)$	$\ln(E_b)$	ln(w)		
VHS	-	-	-	34.7	*a*
-	NS	-	-	0.9	*b*
HS	-	HS	-	48.4	*c*
-	NS	HS	-	27.5	*d*
HS	-	S	NS	50.8	*e*
-	NS	S	NS	27.9	*f*

Units:

σ_f, MPa. E_b, GPa. w, mm. a, mm. r_w, mm.

Table 7.036

The best subset predictors of the failure stress in logarithmic form

The results presented in table 7.035 and 7.036 clearly show that the effective fracture length (as defined here) is not an appropriate form of correction to the notch length, but has a considerable detrimental effect on the power of the regression equations.

Irwin's effective fracture length was developed so that LEFM could be extended to materials that displayed more plastic deformation at the fracture tip than is permitted in the normal application of LEFM.

One of the basic quantities derived in LEFM is the critical stress intensity factor, which by definition, should be a material constant. This quantity is examined in the next section.

7.8.3.2. RESULTS OBTAINED USING THE MEASURED NOTCH LENGTH AND IRWIN'S EFFECTIVE FRACTURE LENGTH: THE CRITICAL STRESS INTENSITY FACTOR

The data obtained from these tests on bovine bone were substituted into equations describing the three SIF equations used in this thesis. This process was performed twice: once using the machined notch length and once using the effective notch length.

Notch length	K^{I}_{IQ} mean (s.d.)	K^{U}_{IQ} mean (s.d.)	K^{P}_{IQ} mean (s.d.)	
a	3.77 (0.67)	5.75 (0.95)	12.67 (2.38)	*a*
$a + r_w$	4.31 (0.84)	8.02 (1.64)	23.61 (5.84)	*b*

Units:

K^{I}_{IQ} *Infinite-sheet* critical stress intensity factor, MPa $m^{0.5}$.

K^{U}_{IQ} *Un-flexing* critical stress intensity factor, MPa $m^{0.5}$.

K^{P}_{IQ} *Pin-jointed* critical stress intensity factor, MPa $m^{0.5}$.

Table 7.037

Values of the various stress intensity factors as used in LEFM calculated using the length of the machined notch and a length based of Irwin's effective notch length (Data set NB4)

As noted above, the values obtained for the SIF should be constant. In each case the standard deviation of this quantity increases when it is calculated using the effective notch length in place of the machined notch length. Therefore the values calculated using the effective notch length are further from the ideal of a constant value. This observation shows that the machined notch length is the more satisfactory of the two measures of notch length. The mean calculated values of the SIF are also increased by using the effective notch length. This is due to two factors, first the notch length in the basic equation for the infinite sheet SIF is greater. Second, in those cases where a shape

correction factor is used the ratio $(a + r_w)/w$ is clearly greater than a/w and thus the numerical value of the correction is greater (see figure 7.003).

Analysis of the data from SEN specimens of antler showed that there was a correlation between E_b and the calculated SIF, K^*_{IQ}. It was found that the strength of this relationship and also the predictive power of the relationship depended on which value of SIF was examined. This finding has been repeated with these specimens of bovine bone the results are presented in table 7.038. The use of the effective notch length reduces the correlation between these two supposedly material properties. This is further evidence to suggest that using this additional length is not a useful procedure. The relationship of the different stress intensity factors to the material stiffness shown here can be compared to their relationship to the geometry of the specimen shown in section 7.7.1.8. This comparison will be returned to in the conclusion of the chapter; section 7.10.10.

Notch length	K^I_{IQ} Significance (p)	K^U_{IQ} Significance (p)	K^P_{IQ} Significance (p)	
a	HS (0.002)	HS (0.005)	NS (0.225)	*a*
$a + r_w$	HS (0.004)	NS (0.056)	NS (0.519)	*b*

Table 7.038

<u>The significance of bending stiffness as a predictor of the calculated critical stress intensity factor (Data set NB4)</u>

7.8.3.3. COMMENTS ON THE LOWER DEPENDENCE ON IRWIN'S EFFECTIVE FRACTURE LENGTH THAN ON THE UNCORRECTED NOTCH LENGTH

Each of the tables above (7.035 to 7.038) shows the same result; the effective notch length, $a + r_w$, appears to be less satisfactory as a measure of the true notch length than the machined length is. The effective notch length is a less significant predictor of failure stress. It also generates greater variability in the critical stress intensity factor a supposedly constant quantity.

As in the case of the antler specimens, the application of a correction to the machined notch tip appears to be a logical procedure. I will not repeat the comments made in section 7.5.3.2, but most of them apply to bovine bone as well as to antler. One exception to this is clearly the idea that the damage zone may not be equivalent to a plastic zone are different due to the increased stress possible in the damage zone of antler. The load deformation plots of bovine bone suggest that such an argument cannot be

applied in this case. In the section analysing the antler tests it was found that the whitened zone size was dependent on the notch tip radius. It was also found that the existence of the zone was rate dependent. So further discussion of this zone is reserved until those aspects have been examined.

7.8.3.4. RESULTS: THE SIZE OF THE WHITENED ZONE

The strongest relationships between one of the various measured variables and the length of the whitened zone is that with the notch tip radii ($R^2\% = 26.6$). With the additional variables of notch length, fracture stress and material stiffness in bending this value was raised to 41.0% (although the notch length and the failure stress were non-significant). In section 7.5.4 I stated that the existence of a relationship between the whitened zone length and the notch tip radius was not surprising. This was based on a consideration of the effect that radius has on the severity of the changes in stress distribution as the distance from a hole in an elastic plate loaded in tension increases. It is therefore surprising that the relationship between these two quantities is lower when the results of bovine bone are considered than when those of antler are considered.

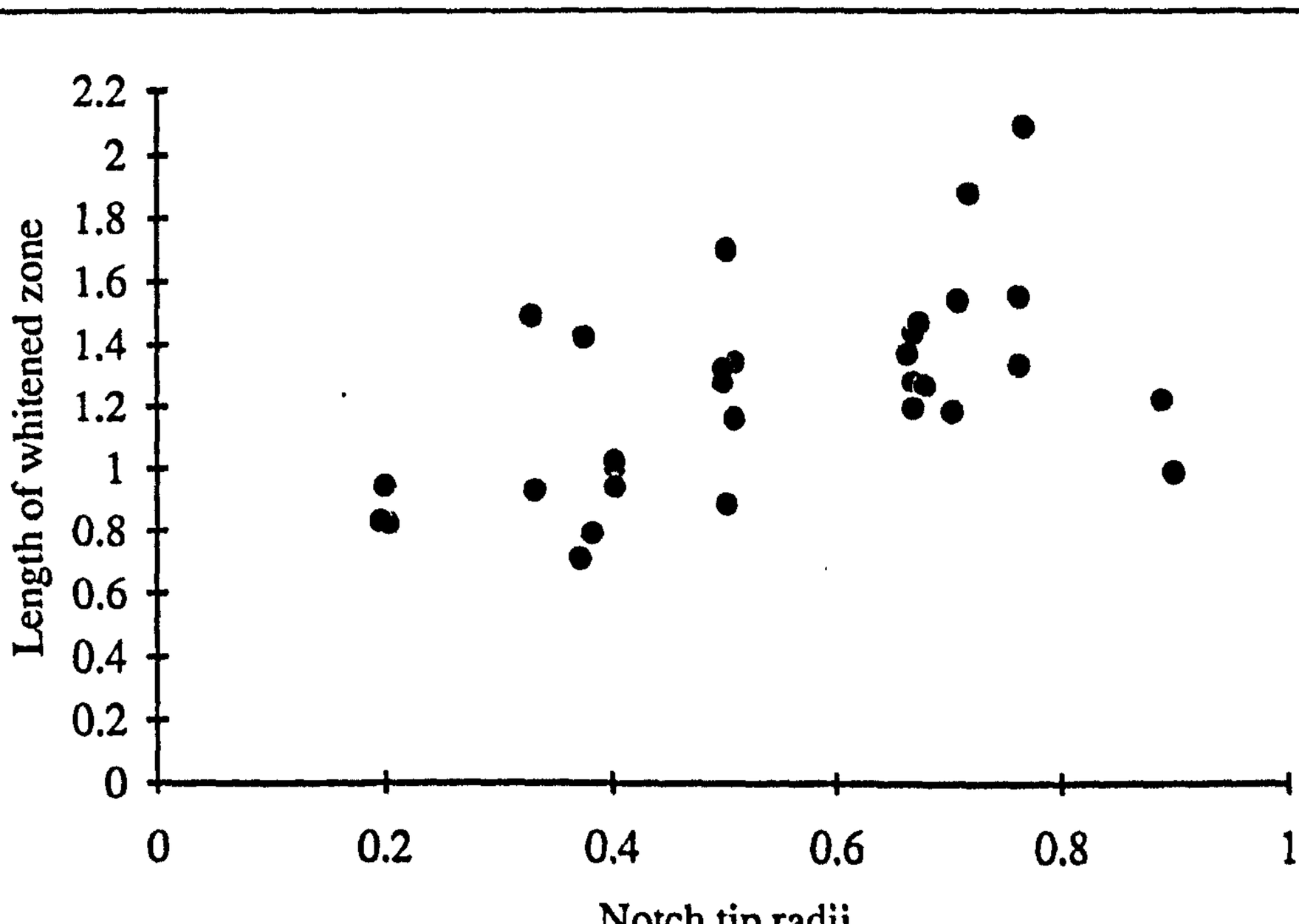

Units:

d_w The length of the whitened zone, mm

ρ Machined notch tip radius (measured), mm

Figure 7.041

Relationship of the length of the whitened zone to the notch tip radius

Bovine specimens	Regression equations and t values	R^2 %	
31 SEN femoral	$d_w = 0.756 + 0.884\ \rho$ t: 5.09 3.45	26.6	*a*
31 SEN femoral	$d_w = 0.480 + 0.658\ \rho + 0.00859\ \sigma_f$ t: 1.89 2.16 1.34	28.5	*b*
31 SEN femoral	$\ln(\sigma_f) = 3.15 + 0.463\ln(E_b) - 0.752\ln(a) + 0.148\ln(\rho)$ t: 5.23 2.73 - 2.16 2.05	53.7	*c*
31 SEN femoral	$\ln(\sigma_f) = 2.59 + 0.566\ln(E_b) - 0.608\ln(a) + 0.288\ln(d_w)$ t: 4.21 3.50 - 1.75 2.60	57.2	*d*
Units: d_w, mm. ρ, mm σ_f, MPa.			

Table 7.039

Relationships between whitened zone length, tip radius, failure stress, notch length and material stiffness

An examination of equations *c* and *d* in table 7.039 shows that by the definition used here the notch tip radius is just classified as a significant predictor of the failure stress ($p = 0.05$). However, the length of the whitened zone is more significant ($p = 0.015$). The equations can be rewritten as

$$\sigma_f = 23.34\ \frac{E_b^{0.463}\ \rho^{0.148}}{a^{0.752}} \qquad (7.029)$$

$$\sigma_f = 13.33\ \frac{E_b^{0.566}\ d_w^{0.288}}{a^{0.608}} \qquad (7.030)$$

Equations 7.029 and 7.030 appear to be very similar to the equations predicted by both Griffith (5.021) and Purslow (for the case where n = 1) (the radius and whitened zone length terms are non-significant). This impression is not only given by the power of the (non-significant[24]) notch length term but the power of the (highly significant) stiffness term. In the Griffith equation (equation 5.021) or Purslow's approach with n = 1 the predicted power of stiffness in such a relationship is 0.5. This is an important result, but has no direct relationship to the analysis of the size of the damage zone, so it will be discussed in the conclusion of this chapter.

---

[24]This non-significance is probably due to the limited range of notch lengths used.

7.8.4. CONCLUSIONS ON THE USE OF A CORRECTION APPLIED TO THE MACHINED NOTCH LENGTH, BASED ON HALF THE WHITENED ZONE LENGTH

Using the same logic as applied to elastic-plastic materials, the existence of a zone of damaged material at the notch tip will reduce the stress in that region. Therefor it also seems logical that it will affect the fracture process. Following the ideas of Irwin I have augmented the measured length of the machined notch with half the length of the whitened zone. This was found to be detrimental to the predictive power of the various relationships examined. This finding is similar to that made for the antler specimens examined in a similar way. As is the relationship of whitened zone length to tip radius, however, in this case the length of the whitened zone was found to be significantly related to the failure stress. As in the case of antler, it is impossible to determine if the size of the whitened zone is due to the higher stress, or if the higher stress is due to the size of the whitened zone. As pointed out above perhaps the most important result here is not the size of the damage zone at the notch tip but its existence. This aspect is considered in chapter 8.

In the analysis of the antler results it was shown that the existence of a whitened zone was rate dependent. In the next section this is shown to also be the case for bovine bone.

7.9. NOTCH SENSITIVITY OF BOVINE BONE (NB5): THE EFFECT OF CROSS-HEAD SPEED

In this section the results of tests on SEN specimens of bovine bone conducted at different cross-head speeds are analysed. Apart form the test material these experiments replicate those examined in section 7.6

7.9.1. AIMS AND EXPERIMENTAL DESIGN

The aims and experimental design used for these tests on bovine bone are the same as the comparable tests conducted on antler described in section 7.6.1

7.9.2. EXPERIMENTAL PROCEDURE

Testing was performed at four different cross-head speeds; 8.3×10^{-4} (4 specimens), 8.3×10^{-5} (6 specimens), 8.3×10^{-6} (3 specimens) or 8.3×10^{-7} m s^{-1} (3 specimens). Otherwise the experimental protocol followed in this case was the same as in all but the initial tests. This series of tests was also recorded using the high speed video equipment some of the images are presented in chapter 8. The testing of these specimens was interspersed with those contained in data sets NB4 and TB1.

7.9.3. RESULTS

The results will be presented in the same format as those in section 7.6.3. To demonstrate to effect of cross-head speed the logarithmic value of this speed in metres per second will be used.

7.9.3.1. RESULTS: THE EFFECT OF CROSS-HEAD SPEED ON THE FAILURE STRESS

Bovine specimens	Regression equations and t values	R^2 %	
16 SEN femoral	$\sigma_f = 176 - 173\ (a/w) + 4.58\ \ln(\dot{x})$ t: 12.54 - 11.37 3.56	90.7	*a*
16 SEN femoral	$\sigma_f = 48.7 + 1.61\ a^{-0.5} + 3.84\ \ln(\dot{x})$ t: 2.99 10.38 2.73	89.1	*b*
16 SEN femoral	$\sigma_f = 112 - 157\ (a/w) + 2.44\ E_b + 3.65\ \ln(\dot{x})$ t: 4.84 - 12.32 3.16 3.53	94.5	*c*
16 SEN femoral	$\sigma_f = -19.0 + 1.45\ a^{-0.5} + 3.07\ E_b + 2.72\ \ln(\dot{x})$ t: - 1.07 14.19 4.66 3.00	95.8	*d*
Units: σ_f, MPa. w, mm. a, mm. $a^{-0.5}$, $m^{-0.5}$. E_b, GPa. $\dot{x}$, m s^{-1}			

Table 7.040

The relationship of failure stress to testing rate and notch length

Similar analysis to that conducted on the antler specimens in section 7.6.3.1 demonstrated that the logarithm form of the cross-head speed was a good predictor of the fracture behaviour. I will make only brief comments on the results; as most of them are qualitatively similar to those obtained for the antler specimens. The results will be compared in the conclusion to this chapter.

The equations in table 7.040 (when compared to equation *e* and *f* table A9.005) suggest that changing the cross-head speed by a small amount affects the failure stress of the notched specimens less than it would the ultimate stress of un-notched specimens of bovine femoral bone. Such a comparison is a little dubious as no account is taken of the reduced cross-section of the material. Thus contrasting the ligament stress and the ultimate stress of the un-notched specimens may be more valid.

7.9.3.2. RESULTS: THE EFFECT OF CROSS-HEAD SPEED ON LIGAMENT STRESS

Figure 7.042 shows how the ligament stress is related to cross-head speed. The mean values are given in table 7.041.

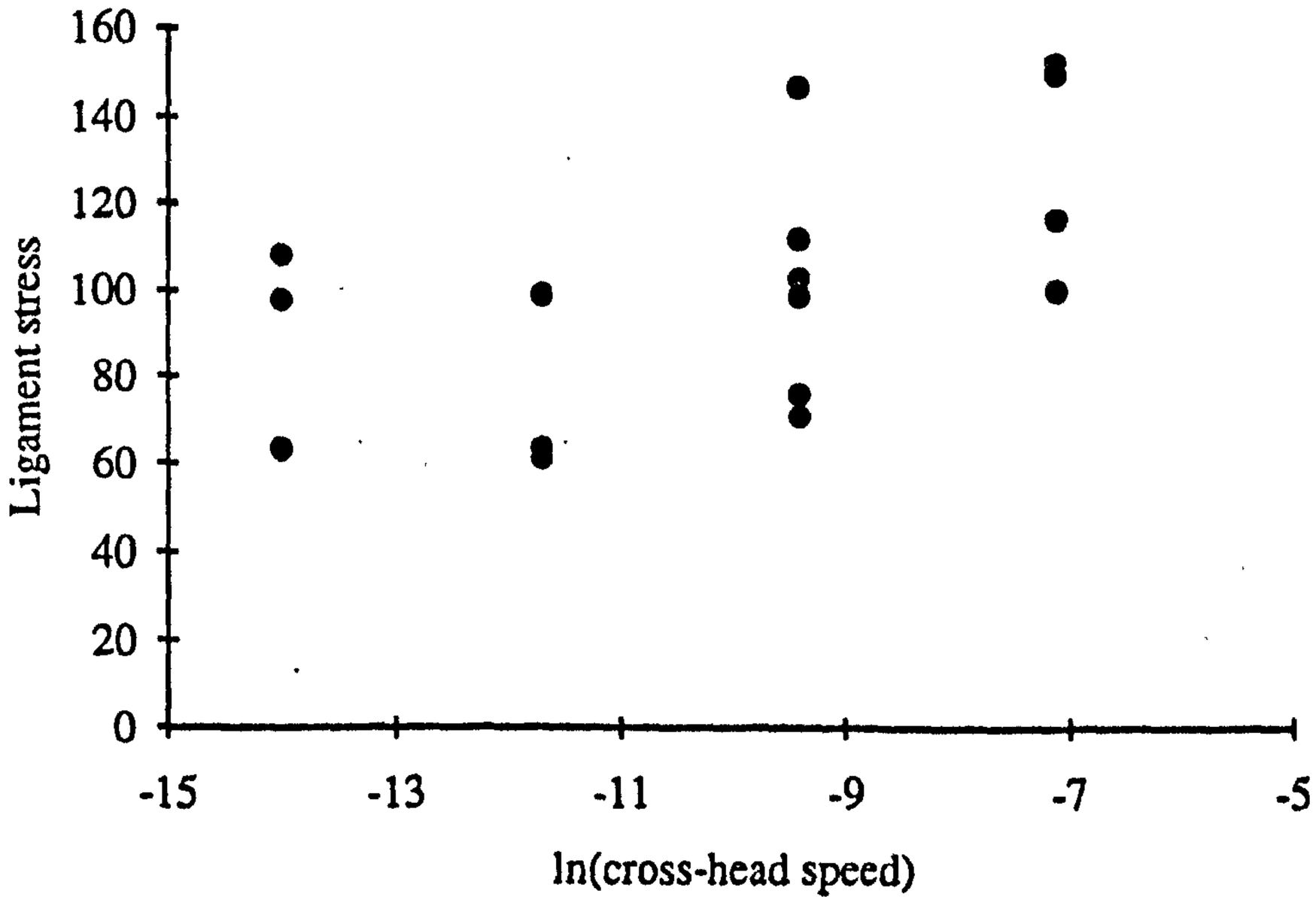

Units:

σ_{lig} Ligament stress, MPa.

$\dot{x}$ Cross-head speed, m s^{-1}.

Figure 7.042

Relationship of ligament stress to cross-head speed

Cross-head speed $m\ s^{-1}$	σ_{lig} Mean value (s.d.) MPa	Number of specimens
8.3×10^{-7}	89.4 (23.1)	3
8.3×10^{-6}	74.2 (21.2)	3
8.3×10^{-5}	100.6 (27.3)	6
8.3×10^{-4}	129.1 (25.6)	4

Table 7.041

Mean values of the ligament stress at each cross-head speed used[25]

In table 7.042 the powers of a number of parameters to explain the variation in the ligament stress, individually and in combination are presented. In this case the two best individual variables, and then the best two pairs of variables and so on. The R^2 % values given are those adjusted for the degrees of freedom.

Predictors of the ligament stress, σ_{lig}, for SEN specimens of bovine femoral bone (Data set NB5)						
E_b	$\ln(\dot{x})$	a/w	$a^{-0.5}$	w	d	R^2 %
X	-	-	-	-	-	61.5
-	-	-	X	-	-	41.5
X	-	-	X	-	-	78.5
X	-	X	-	-	-	75.3
X	X	-	X	-	-	88.7
X	X	X	-	-	-	87.6
X	X	X	X	-	-	88.0
X	X	-	X	X	-	87.9
X	X	X	X	X	-	87.2
X	X	X	X	-	X	86.9
X	X	X	X	X	X	85.8
Units: σ_{lig}, MPa. E_b, GPa. d, mm. w, mm. a, mm. $a^{-0.5}$, $m^{-0.5}$.						

Table 7.042

The best subset predictors of the ligament stress

---

[25]It is interesting that lower value of the mean stress obtained at the second slowest cross-head speed mirrors the results for un-notched specimens. I have no explanation for this apparent coincidence.

Table 7.042 shows an interesting result; the best single predictor of ligament stress is the material stiffness, the best two are E_b and $a^{-0.5}$, the best three predictors are E_b, $a^{-0.5}$ and the logarithmic of cross-head speed. This relationship is shown below in table 7.043 also included is the prediction based only on cross-head speed and material stiffness.

Bovine specimens	Regression equation and t values	R^2%	
16 SEN femoral	$\sigma_{lig} = 26.3 + 3.90 \ln(\dot{x}) + 4.57 E_b + 0.582 a^{-0.5}$ t: 1.23 3.57 5.73 4.70	88.7	*a*
16 SEN femoral	$\sigma_{lig} = 23.5 + 4.03 \ln(\dot{x}) + 5.82 E_b$ t: 0.68 2.28 4.79	70.4	*b*
Units: σ_{lig}, MPa. $\dot{x}$, m s^{-1} E_b, GPa. $a^{-0.5}$, $m^{-0.5}$.			

Table 7.043

Predictive equations of the ligament stress of SEN specimens of bovine bone

7.9.3.3. RESULTS: FAILURE STRAIN, NOTCH AND PROCESS ZONE LENGTH, THE EFFECT OF CROSS-HEAD SPEED

As part of the analysis of failure strain, the procedure used to produce table 7.042 was repeated, interchanging failure strain for failure stress. The single best predictor was the cross-head speed term (R^2 = 2.9%). No significant predictors of failure strain were found.

7.9.3.4. RESULTS: PURSLOW'S APPROACH, THE EFFECT OF CROSS-HEAD SPEED

In this section the regression analysis performed on the logarithmic values of a number of variables is presented. This analysis is based on that in section 7.6.3.4, where results of SEN specimens of antler were analysed. The regression equations are given in table 7.044. The value given in parenthesis in the R^2% column is that obtained when the regression is performed without the inclusion of the cross-head speed as a variable.

Bovine specimens	Regression equations and t values	R^2%	
16 SEN femoral	$\ln(\sigma_f) = 4.62 - 0.432 \ln(a) + 0.0525 \ln(\dot{x})$ t: 18.15 - 7.70 2.14	81.5 (76.8)	*a*
16 SEN femoral	$\ln(\sigma_f) = 4.03 - 0.435 \ln(a/w) + 0.0550 \ln(\dot{x})$ t: 15.71 - 8.32 2.39	83.7 (78.2)	*b*
16 SEN femoral	$\ln(\sigma_f) = 3.42 - 0.430 \ln(a) + 0.885 \ln(w) + 0.0580 \ln(\dot{x})$ t: 4.12 - 8.04 1.52 2.45	83.2 (76.8)	*c*
16 SEN femoral	$\ln(\sigma_f) = 0.971 - 0.368 \ln(a) + 1.15 \ln(E_b) + 0.0308 \ln(\dot{x})$ t: 1.72 - 12.80 6.62 2.51	95.7 (93.9)	*d*
16 SEN femoral	$\ln(\sigma_f) = 0.655 - 0.371 \ln(a/w) + 1.09 \ln(E_b) + 0.0342 \ln(\dot{x})$ t: 1.26 - 13.79 6.67 2.99	96.3 (94.0)	*e*
16 SEN femoral	$\ln(\sigma_f) = 0.646 - 0.371 \ln(a) - 0.381 \ln(w) + 1.09 \ln(E_b) + 0.0343 \ln(\dot{x})$ t: 1.07 - 13.20 1.28 6.19 2.80	95.9 (93.6)	*f*
Units: σ_f, MPa. a, mm. w, mm. $\dot{x}$, m s^{-1} E_b, GPa.			

Table 7.044

The relationship of the failure stress to the notch length and cross-head speed

7.9.3.5. RESULTS: THE EFFECT OF CROSS-HEAD SPEED ON THE CRITICAL STRESS INTENSITY FACTORS

Cross-head speed, m s^{-1}	K^I_{IQ}, MPa $m^{0.5}$ mean (s.d.)	K^U_{IQ}, MPa $m^{0.5}$ mean (s.d.)	K^P_{IQ}, MPa $m^{0.5}$ mean (s.d.)
8.33×10^{-7}	3.21 (1.29)	4.38 (2.11)	7.43 (5.01)
8.33×10^{-6}	2.58 (0.22)	3.45 (0.54)	5.59 (2.34)
8.33×10^{-5}	3.71 (0.76)	5.18 (1.06)	9.25 (2.75)
8.33×10^{-4}	3.97 (0.81)	5.18 (1.64)	7.96 (4.82)

Table 7.045

The mean values of the SIF for bovine femoral bone at different cross-head speeds

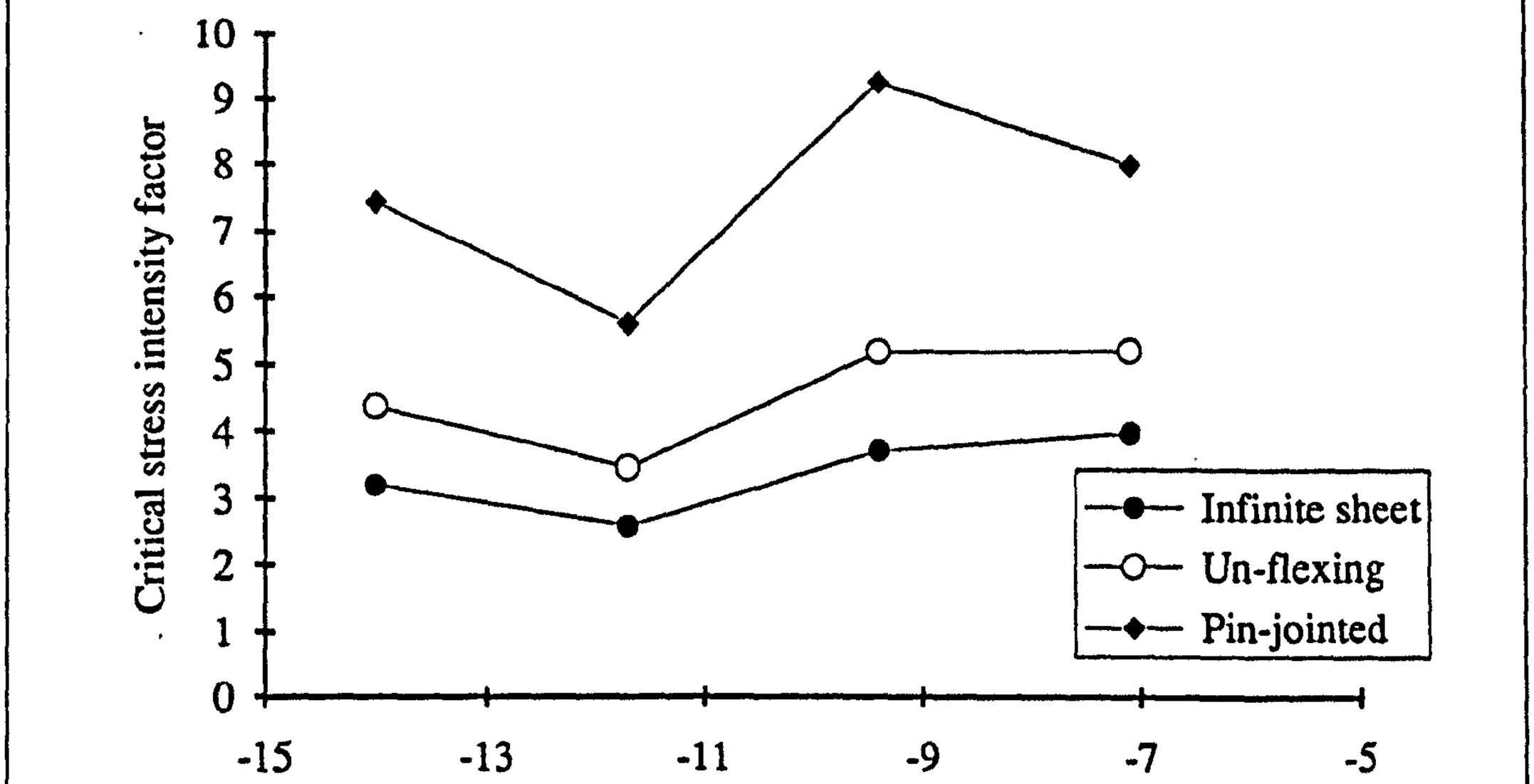

Units:

$\dot{x}$ Cross-head speed, m s^{-1}

K^{*}_{IQ} Critical stress intensity factor, MPa $m^{0.5}$

Figure 7.043

Relationship of the three measures of the critical stress intensity factor to the cross-head speed of the test

Bovine specimens	Regression equations and t values	R^2 %	
16 SEN femoral	$K^{I}_{IQ} = 1.35 + 0.150\ E_b + 0.0917\ \ln(\dot{x})$ t: 0.94 2.97 1.25	43.8 (41.6)	*a*
16 SEN femoral	$K^{U}_{IQ} = 2.88 + 0.153\ E_b + 0.125\ \ln(\dot{x})$ t: 1.02 1.54 0.87	13.1 (14.6)	*b*
16 SEN femoral	$K^{P}_{IQ} = 9.23 + 0.049\ E_b + 0.229\ \ln(\dot{x})$ t: 1.13 0.17 0.55	0.0 (0.0)	*c*
Units: K^{*}_{IQ}, MPa $m^{0.5}$. $\dot{x}$, m s^{-1} E_b, GPa.			

Table 7.046

Relationship of the critical stress intensity factor to the material stiffness and the cross-head speed of the test

There is no statistical evidence for a significant relationship between K^{I}_{IQ} and the cross-head speed. This appears to be due in part to the unexplained low values of fracture stress associated with the second lowest cross-head speed. The cross-head speed in question is that used in all cases except where test rate is the variable under consideration. Thus this low value can be compared with others obtained for bovine femoral specimens in this work. When this was done it was clear that not only is this mean value low compared to the others obtained at the same rate (4.43 MPa $m^{0.5}$ from data sets NB1, NB2 and NB3 or 3.77 MPa $m^{0.5}$ from data set NB4), but that the values obtained here (data set NB5) at a rate ten times faster are lower then the values from the other data sets. This may be due to the different bones used, but the source of this in consistency is unknown.

7.9.3.6. RESULTS: EFFECT OF CROSS-HEAD SPEED ON THE WHITENING AT THE NOTCH TIP

Whitening was observed in only one specimen tested at a cross-head speed below 8.33×10^{-5} m s^{-1}. However, whitening was noted in all specimens tested at or above this speed. This is a very similar finding to that made for the antler specimens (section 7.6.3.5) and the implications are the same so they will not be repeated here. The whitening of bone, and antler, observed during creep, tensile and notch sensitivity tests is examined in chapter 8.

7.10. CLOSING REMARKS ON THE NOTCH SENSITIVITY OF BOVINE BONE AND RED DEER ANTLER

The main impression gained from the notch sensitivity tests that have been examined in this chapter is that bovine bone fractures in manner similar to that described by classical fracture mechanics, whereas the fracture of antler requires a greater amount of energy to be supplied.

The fracture behaviour of bone and antler can be compared by examining the mechanical response of the SEN specimens of the different materials with each other and with response of the un-notched specimens. This comparison has to be rather qualitative as there are few quantities that can be justifiably determined for both materials. One fundamental quantity that is not available for both materials is a measure of the fracture toughness, or the resistance to fracture propagation.[26] Thus a comparison of this property

---

[26]With hindsight the determination of the J integral (see appendix 8) for both materials might have been a profitable, if lengthy process. However, the determination of this

has to be inferred from the available measures. One such measure is an approximation of the energy supplied to the material until the time of fracture initiation. I will consider each aspect of the fracture behaviour in turn, and examine its effect on the fracture behaviour of the notched (and in some cases un-notched) specimens. I will also consider how this effects the justification of applying the theory of linear elastic fracture mechanics (LEFM). However, I will start with a comparison of the mechanical response of the material within these SEN specimens, as inferred from normal tensile and resilience tests conducted on un-notched specimens.

7.10.1. MECHANICAL RESPONSE OF BONE AND ANTLER: LINEARITY

The stress-strain response of both bovine bone and antler display a departure from linearity which I have referred to as the knee region. The response of bovine bone appears reasonably linear either side of this knee, while that of antler is only linear after it. When examining the behaviour of SEN specimens using energy approaches it is necessary to know the equation that governs this stress-strain response so that the energy supplied to and stored within the specimen can be determined. (This is assuming full elasticity.)

Due to the notch in the specimen, it is possible that the bulk of the material is not stressed to the values associated with the knee in the tensile loading curve. This would simplify the required stress-strain relationship. This was found to be the case with the bovine specimens. Therefore, a linear stress-strain response can be assumed for this material. In the case of the antler specimens the stress-strain response was too curved for a linear response to be assumed and a power relationship was used.[27] Because of the shape of the stress-strain responses of these materials, it appears the Griffith's equation is more suited to bovine bone, and Purslow's approach more suited to antler.

7.10.2. MECHANICAL RESPONSE OF BONE AND ANTLER: THE LOSS OF ELASTICITY

The classical approach to fracture mechanics is to consider the material to be elastic. Thus the energy released from the material that is unloaded due to propagation of

---

parameter would be complicated by the variation of the mechanical properties between the different specimens.

[27]With hindsight, the validity of the constants in the power relationship may have been improved by determining them from only the initial section of the loading curve, instead of using all the data up to the final failure.

the fracture is available to assist further fracture growth. Clearly if the energy available for fracture growth can be reduced in some way, the material will appear tougher.[28] It was estimated that the bulk of the material in the bovine bone specimens was essentially fully elastic at the time of fracture. However, it was estimated that only 50% of the energy supplied to the SEN specimen of antler was available to help propagate the fracture. This suggests that the energy balance approach to modelling fracture may be valid for bone but it is not valid (without some modification) for antler. Thus the use of Griffith's equation for bone may be valid, but the use of Purslow's approach to fracture to model the behaviour of antler is questionable.

7.10.3. NATURE OF THE FRACTURE OF BONE AND ANTLER: THE STRESS-STRAIN RESPONSE UP TO FRACTURE INITIATION

In this section the differences in the stress-strain[29] response of the notched specimens of bovine bone and antler are reviewed.

7.10.3.1. SHAPE OF THE STRESS-STRAIN RESPONSE OF SEN SPECIMENS

When the stress-strain responses of the SEN specimens of bone and antler up to the point of fracture initiation are examined[30] the behaviour that would be expected from an examination of the material properties (the response of un-notched specimens) is exhibited. The response of bone is relatively linear and that of antler very curved. This reflects the almost linear-elastic response of the bovine material up to the failure stress, and the non-linear non-elastic response of the antler specimens.

7.10.3.2. AREA UNDER THE STRESS-STRAIN RESPONSE OF SEN SPECIMENS

If the values of the failure stress and strain of notched specimens of bone and antler are compared, clearly the area under the stress-strain plot for the antler specimens is larger. Thus the energy supplied up to the point of failure is also larger. This energy can be estimated by using the equation

---

[28]I say 'appear tougher' because this will not increase the energy needed to separate the two surfaces, only decrease the energy that is available to do so. This opens the rather philosophical question of what is meant by 'toughness': is it the energy needed to separate the material surfaces, or the energy that has to be supplied to the structure to do so.
[29]See comments in section 7.4.3.5 about the use of 'strain'.
[30]Examples from this data set are given in chapter 8.

$$U \approx \frac{\sigma_f \varepsilon_f}{2} \qquad (7.031)$$

This has been done for data sets NA4 and NB4, in which the specimens are considered to be of comparable geometry. The values obtained were: for antler approximately 570 kJ m^{-2} (mean values from 30 specimens), and for bovine femoral bone 160 kJ m^{-2}. Because of the curvature of the loading response of the antler specimens this method will underestimate the value for that material proportionally more than it will underestimate the value for bovine bone.[31]

The amount of energy supplied to the SEN specimens of antler is clearly greater than that supplied to the bovine specimens. As there is a loss of elasticity, the amount of this supplied energy that is available for the fracture process is reduced. However, from the evidence above of a resilience of about 50% for the antler specimens this still suggests that they have more internally stored energy available to propagate a fracture. This indicates that the actual process of separating the fracture surfaces of an antler specimen requires more energy than it does in the case of a bovine one.

7.10.3.3. LIGAMENT STRESS OF SEN SPECIMENS COMPARED TO THE ULTIMATE STRESS OF TENSILE SPECIMENS

In section 7.4.3.4 (data set NA3) I noted that the mean ligament stress of the SEN specimens of antler was about 30% less than the mean ultimate stress of un-notched specimens of the same antler. When a similar comparison of the stress results of notched and un-notched specimens of bovine bone was conducted it was noted that the reduction was only 13%. These values are 'ball-park figures', due to the dependence of specimen geometry, etc. This could indicate two things: first both materials are notch sensitive. Second, the notch sensitivity of antler appears, by this measure, to be greater than that of bone.

In his paper Purslow (1991) suggests that for a material with a J shaped loading curve an increased notch length will result in a large decrease in the failure stress, but only a small decrease in strain. On the other hand, a similar increase in notch length in a material with an Γ shaped curve will result in a small decrease in failures stress and a large decrease in failure strain. These are more extreme than the curves considered here, but the arguments are the same. Thus the comparison of failure stresses conducted here although appearing to contradict this suggestion is only one side of the argument. The strains are commented on in the next section.

---

[31]The actual areas have been calculated using the trapezium rule but the data are not supplied or analysed here.

7.10.3.4. FAILURE STRAIN OF SEN SPECIMENS COMPARED TO TENSILE SPECIMENS

A comparison of the failure strains of notched bone and antler specimens to the ultimate strain of un-notched specimens showed that the difference in the results was more marked for the antler specimens. The results from notched and un-notched for the antler specimens did not overlap. The values of failure strain from the notched specimens of bovine bone ranged up to the mean value of the strains obtained by the un-notched specimens.

In section 7.7.1.6 I suggested that the similarity of the failure strains of notched and un-notched specimens of bovine bone could be due to a similarity in the failure processes. In an examination of metals the difference between brittle fracture (as described by LEFM) and failure by yielding, or plastic flow, is quite clear. In the brittle fracture of metals the material is cleaved with essentially no other deformation. In the plastic flow of metals, as in the case of tensile specimens, a neck may occur and the whole structure may be plastically deformed. In the case of failure by damage accumulation, as proposed in this thesis for the failure of bone and antler, this distinction is less easily made. The evidence of the other results reviewed here, suggested that the notched specimens of bovine bone fail by a fracture rather than a damage process. Based on the similarity in the failure stresses, I suggest that the (un-notched) tensile specimens may fail by a combination of a damage and a fracture process. The damage that is accumulated by an un-notched specimen of the material may in some circumstances act in the same manner as the machined notch. This suggestion is returned to in chapter 9 where the evidence of other experiments conducted for this thesis and reported in the literature is combined.

7.10.4. NATURE OF THE FRACTURE OF BONE AND ANTLER: THE WHITENED ZONE

Perhaps the most interesting and important result of these tests is the region of whitened material that occurs around the tip of the notch. I have attributed the whitening to the occurrence of damage in the form of microcracking.[32] The existence of such a zone will reduce the stress within the region of the notch tip and therefore increase the external work that has to be applied to fracture the material. In other words the damage zone toughens the material. Not only does the reduced stiffness of this region reduce the stress in the region of the fracture tip, but the production of this damage consumes energy that would otherwise be available to assist in the propagation of the fracture.

---

[32]The evidence for this is presented in the next chapter.

An attempt was made to correct the length on the machined notch to account for the reduction in stress at its tip. It was hoped such a correction would improve the mathematical modelling of the fracture process This attempted correction was unsuccessful. This may be because the apparent time-dependence of the appearance of the whitened zone is at odds with that assumed time-dependence of the damage zone.

7.10.5. NATURE OF THE FRACTURE OF BONE AND ANTLER: CATASTROPHIC FAILURE OR SLOW RIP

The fracture propagation of the SEN specimens of antler tested here took the form of a slow ripping process. (This can be seen in the accompanying video.) However, the fracture of bovine bone was catastrophic. The fracture behaviour of a specimen is very dependent on that specimen's geometry, the test machine used and so on. However, the vastly different behaviour, and the consistent test conditions in this case, permit some degree of comparison.

The slow ripping of the antler specimens, and the requirement of more externally supplied energy, (compared to the self propagating fracture of bovine bone) I interpret as indicating antler's greater resistance to fracture propagation.

7.10.6. NATURE OF THE FRACTURE OF BONE AND ANTLER: THE FRACTURE ROUTE AND FRACTURE SURFACES

The route of the fracture in specimens of bovine bone was relatively straight; passing from the notch to a nearby point on the opposite edge of the specimen. (In some of the 6 mm wide specimens the fracture bifurcated before reaching the second edge. This produced a triangular fragment.) The route taken by the fracture in the antler specimens appeared to be dependent on the structure of the material; reflecting the almost fibrous construction of the material. The fracture of antler was more akin to that associated with wood than with a homogeneous material.

The feature of fractured specimens that is usually examined, with scanning electron microscopes and similar devices, is the topography the fracture surfaces. Such a study has only been conducted on a few of the specimens tested for this thesis. The results are not presented here, as the relatively large-scale features can be seen in the images presented on the accompanying video tape. The fracture surfaces of the antler specimens are much more fibrous than those of the bovine bone specimens. (However, the comparison of surface roughness depends on the magnification used. As noted in

section 6.3.1, some work has been conducted in this laboratory to quantify this effect using fractal analysis.) The more fibrous fracture surfaces of antler suggest the occurrence of fibre pull-out and other mechanisms commonly seen in industrial fibre composites.[33]

7.10.7. NATURE OF THE FRACTURE OF BONE AND ANTLER: RELATIONSHIP OF FAILURE STRESS TO NOTCH LENGTH

An investigation of the failure stress in relation to the length of the machined notch showed that for bovine bone this relationship is that predicted by LEFM. The fracture stress of bone is related to the reciprocal square root of the fracture length. A similar relationship for antler implied that the failure stress was related to the reciprocal of a higher root (approximately $a^{-0.26}$).

7.10.8. NATURE OF THE FRACTURE OF BONE AND ANTLER: THE EFFECT OF NOTCH TIP RADIUS

The overall conclusion about the effect of notch tip radius on the fracture behaviour is that it is non-significant. This lack of an effect, contrary to the predictions of elastic theory, I attribute to the existence of a damage zone at the tip of the machined notch.

7.10.9. NATURE OF THE FRACTURE OF BONE AND ANTLER: THE RATE DEPENDENCE OF THE FRACTURE BEHAVIOUR

The dependence of the failure stress of SEN specimens on the cross-head speed was examined in a number of ways. In the case of the logarithmic equations it was found that either on its own, or with additional variables, the cross-head speed was a significant predictor of the failure stress for the bovine bone specimens. However, in the case of antler it was a very highly significant predictor. The strength of the relationship was also greater in the case of the antler specimens. Thus the failure process of antler can be interpreted as being more time-dependent. This may be due to the occurrence of damage related energy dissipating events occurring to a greater extent in antler than in bone. The

---

[33]An investigation of the 'pull-out' type mechanisms in antler has not been conducted for this thesis. This aspect of the material is discussed in the thesis by Watkins (1987) referred to in chapter 1.

accumulation of damage is rate dependent. So if this damage process is modifying the fracture behaviour it is not surprising that the fracture behaviour is also time-dependent.

There is a slight paradox in the relationship of cross-head speed to fracture stress. The fracture stress increases with an increase in cross-head speed. If the damage process consumes energy that would normally be available for fracture, there should be a lower energy consumption at a higher rate. Thus fracture should occur at a lower stress. This difference in stress can be interpreted as a difference in the resistance to fracture. Therefore I will refer to this paradox as the *fracture resistance versus rate* paradox; this is examined in chapter 9.

The cross-head speed was also found to affect the whitened zone at the notch tip. This zone was only observed at the higher of the four cross-head speeds used. Thus indicating it may not be a fully justifiable measure of the extent of the damaged material. (This is considered in more detail in chapter 8.)

7.10.10. QUANTIFYING THE FRACTURE BEHAVIOUR OF BONE AND ANTLER: THE CRITICAL STRESS INTENSITY FACTOR AND OTHER PARAMETERS

In this chapter I have examined the application of the critical stress intensity factor to the data for bone and antler. A number of problems with this approach have been highlighted. (Those concerned with the shape correction factor will not be reviewed here.) The most important and the least expected (but with hindsight not surprising) effect is the correlation with material stiffness.

The relationship of the stress intensity factor to the material stiffness, and the generally good fit of Griffith's equation suggests that the work-of-fracture of bone may be a more consistent and justifiable quantity to use than the calculated value of the SIF. This may have implication for the justification of fracture mechanics that (essentially) uses the critical stress intensity factor and the value of the work-of-fracture to obtain a value of the material stiffness and thereby justify LEFM (see section 6.7).

7.10.11. IS BONE A CLASSICALLY NOTCH SENSITIVE MATERIAL?

A fundamentally important question that this chapter may be able to answer is whether or not bovine bone is a classically notch-sensitive material. Generally the results indicate that this assertion can not be rejected. However based on my own results and

those in the literature (see chapter 6), I consider that there should be several caveats to this.

a) The fracture behaviour of bone is time dependent.

b) The fracture tip process zone is composed of damaged material.

c) The concept of a critical stress intensity factor, is not fully justifiable. If it is used the stiffness of the material should also be determined and quoted (or some normalisation conducted). There is also the question of what effect the damage zone will have on accuracy of the stress intensity factor as a description of the stress field ahead of the notch.

7.10.12. COMMENT ON THE USE OF SEN AS OPPOSED TO CT SPECIMENS

In section 6.5 I reported Bonfield's (1987) explanation of the advantages of using CT specimens. However, I consider that there may be some disadvantages with the use of such specimens, if as I suggest the fracture process is modified by the occurrence of time dependent damage. The main question is one of finding the correct rate at which specimens should be tested. I suggest that the use of a slow controlled fracture, although giving material science type information on the behaviour of bone could, due to rate dependence, be somewhat divorced from the real situation However, I do appreciate the introduction of additional energy that is associated with catastrophic failure, and the need to conduct tests the results of which can be viewed as being accurate even if the conditions are non-physiological. (As, indeed, nearly all of my tests are far from being mimics of the physiological situation.)

8

OPTICAL CHANGES OBSERVED DURING THE MECHANICAL TESTING OF BONE AND ANTLER

All useful composites sustain increasing damage as they are progressively strained. This allows them to relieve the excessive stresses that would accrue if a mechanism of this type were not available.

Howard, I. C. and Fond, M. S. (1986)

Size effects in the fracture of notched fibre-reinforced plastics.

in *Size Effects in Fracture.*

8.1. INTRODUCTION

This chapter describes and shows some of the images of the optical changes observed and recorded during the mechanical testing of bovine bone and antler. (The mechanical aspects of some of these tests have already been described in preceding chapters. Many of the images are of specimens in data sets NA4, NA5, NB4 and NB5.) Some of these images and their implications were presented at the eighth meeting of the European Society of Biomechanics, in Rome, 21-24 June 1992. The meeting abstract and a description of the video that formed part of that presentation are included in appendix 11 of this thesis. (The video itself is bound separately.)

An optical change is defined, in this thesis, as an alteration in the material's appearance that is evident to the naked eye. (Having used such a definition it should point out that to obtain data from these observations they were recorded.) I do not include in my definition of optical changes the variations in the appearance of a material caused by staining, photo-elasticity or other such techniques. However, changes produced by staining will be discussed.

In the initial sections of this chapter I shall mention some optical effects that have been observed in engineering and biological materials, by other workers. I then describe the equipment I used to obtain images of the optical changes occurring in specimens of bovine bone and antler during creep, tensile and notch sensitivity tests. Some of these recorded images are then presented. Finally I consider the likely causes of the observed optical changes and what information these observations provide regarding the mechanical response and failure of bone and antler.

8.2. OPTICAL CHANGES IN ENGINEERING MATERIALS

Optical changes occurring in a number of engineering materials and some biological ones have been reported in the literature. Only two such reports, one of a polymer the other of a glass reinforced plastic (GRP), will be mentioned in this section.[1]

Clear photographic evidence of mechanically induced optical changes in a polymer is presented by Tse *et al.* (1991) in their study of poly(vinyl chloride) (PVC)

---

[1]Photos possessing a similar appearance are provided by a number of other authors, such as Schulte (1986) and Williams (1990), but these were produced using x-rays rather than visible light. Some trial experiments using x-rays to examine bone and antler were conducted as part of this thesis, but these proved unsuccessful due partly to the power of the x-ray source (decollimated x-ray crystallography equipment).

blended with experimental chlorinated polyethylene (CPE) resins. These materials were used because of their matching refractive indices, and when blended they produce a translucent material. The specimens Tse *et al.* used contained a semicircular edge notch (1 mm in radius). These were subjected to tensile loading at an extension rate of 1.67×10^{-6} m s^{-1} [0.1 mm min^{-1}]. The region of the optical changes, at the notch, was photographed with a travelling optical microscope used in transmitted light mode (the specimen was positioned between the observing instrument and the light source). The images in the paper show a very dark *zone* where the changes have occurred. The boundary of the zone is rather indistinct. When the specimens were sectioned the zone was visible through the cross-section of the material. These workers report one of their results for such a notched specimen in the following way:

> The first visible damage was stress-whitening due to a cavitation mechanism that occurred near the linear limit of the stress-displacement curve.

Images of optical effects observed in centrally notched specimens of glass reinforced plastic - chopped strand mat and cross-ply laminated - are provided by Howard and Found (1986). The images were obtained using reflected light (like a standard domestic photograph). The authors point to the optical changes as evidence of differences in loading of the ligaments and of the central sections immediately above and below the notch. The ligaments have a whitened appearance, the regions above and below the hole appear more translucent.

8.3. OPTICAL CHANGES IN BIOLOGICAL MATERIALS

In the case of biological materials, which fall under the classification of *hard tissues*, there are only a few published accounts of mechanically induced optical changes. One of these is Currey's (1977) study of nacre[2] in tension, which includes images of the tension surface of a three-point-bending specimen, subjected to a regime of loading and unloading. This loading resulted in bright lines, like an aerial view of waves, appearing perpendicular to the long axis of the specimen.

There are few published or reported observations of optical changes in bone or antler. The only ones of which I am aware are those of Burstein *et al.* (1973) and Watkins (1987) (and secondary references to these, or the experiments they describe, such as that in 1974 by Currey and Brear). These reports only describe the observed

[2]Nacre, or mother of pearl, is one of the characteristic skeletal structures of molluscs, occurring in cephalopods, gastropods and bivalves (Currey 1977).

effects, providing no recorded images. Burstein *et al.* (1973) report observations made during tensile testing of bone.

> When the specimen began its plastic deformation the test section became lighter if viewed by reflected light and darker if viewed by transmitted light.

They do not state what type of bone this account refers to, nor do they describe the test conditions. (In the same paper they report results for mechanical tests on human and bovine material.) The existence of, what they refer to as, 'plastic strain' indicates the specimens were not dry.[3]

A more detailed description of optical effects, this time in antler, is given by Watkins (1987), who reports observations he made during short beam tests. These tests (performed to examine the material's shear properties) used beams with a span-to-depth ratio of 5:1. The depths were between 3 and 4 mm. Load was applied at two cross-head speeds; 3.3×10^{-5} m s^{-1} [2 mm min^{-1}] and 8.3×10^{-6} m s^{-1} [0.5 mm min^{-1}]. No statement about the hydration state of the specimen is given. Watkins reports his observations as follows:

> During the test it was noticed that several transversely orientated white opaque regions developed on the tensile face, further loading would cause one of these regions, about 0.1 mm long, to develop into a crack. Unloading the specimen and examining it under a binocular microscope showed no evidence of compression creases on the top face, only the opaque cracks on the tensile face were visible. Further loading would cause one of the cracks to extend to 0.25 - 0.50 mm in length, when the crack would then suddenly extend breaking the specimen transversely.

Watkins does not pursue this finding.

Some unpublished investigations conducted with the aim of obtaining clear photographic images of the optical changes occurring in bone have been conducted by Kevin Brear.[4] He used specimens of bovine bone, approximately 3.6 mm wide by 1 mm thick, some of which contained small drilled holes. The specimens were stored in water, and then tested in air. The tests were conducted as soon as possible to avoid drying effects. The load was applied by an Instron 1122 machine (the same one used in this thesis), using a cross-head speed of 8.33×10^{-5} m s^{-1} [5 mm min^{-1}]. No direct method of strain measurement was used. The images were recorded using a manually operated Chinon 35 mm single lens reflex camera (SLR), with motor wind. This system permitted up to two frames to be captured each second. The specimen was strongly illuminated from the opposite side to the camera. Strips of paper were lightly placed on the sides of the specimen to prevent light from directly entering the camera. The images Kevin

---

[3]Professor John Currey has told me that the tests, which he witnessed, were conducted on wet bovine bone.

[4]Mr Kevin Brear is the technician to Professor Currey, in whose laboratory the experimental work of this thesis was conducted.

obtained show areas of the specimen becoming darker as the test progresses. This was especially evident near the hole in the drilled specimens. It was not possible to accurately correlate these optical changes with the load or extension data.

8.4. EQUIPMENT USED TO RECORD THE OPTICAL CHANGES OCCURRING IN BOVINE BONE AND ANTLER

The method used by Brear (described above) could not easily be adapted to the test conditions under which I wished to record optical events. There are a number of reasons for this. First, I wanted to record the strain directly using an extensometer.[5] This piece of equipment either obscured the bone from the camera, or cast shadows over the specimen if it was mounted on the illuminated side. It also complicated the attachment of material to reduce stray light, as used by Brear. Second, I intended to conduct all of my testing in a temperature controlled water bath (it was hoped this would avoid drying artefacts in the optical, as well as the mechanical, results). This further restricted the positioning of lights and screening material (due to the corners of the tank, inlet and outlet pipes, internal reflections and so on). To avoid these problems I illuminated the specimens from the same side as the camera, painting the inner surface of the base and three walls of the tank matt black to reduce reflections and stray light. The changes observed and recorded were thus the reverse of those recorded by Brear. In my case the reduction in transmitted light was expressed as an increase in reflected light. Hence the term *whitening* or *whitened zone* is used to describe the observed optical changes.

In this work two media were used to record the optical changes. The first medium was a standard 35 mm black and white film, normally Ilford HP5, although some slower Ilford FP4 was also used.[6] Both film types were loaded into standard cassettes (36 frames per cassette) and used with a single lens reflex (SLR) camera. The second medium was video tape. The recording was initially performed using a high speed machine and tapes, before downloading at a slower speed to standard domestic video tapes. Clearly the type and level of illumination were different for each medium. I shall now describe these systems in more detail.

---

[5]The mechanical test equipment used for each type of test reported here has already been described in the relevant chapter 4 or 7.
[6]HP5: ASA 400. FP4: ASA 125.

8.4.1. 35 mm SINGLE LENS REFLEX CAMERA

Chronologically the first system used to record the whitening was a Canon EOS 600 (a 35 mm SLR) with a Canon compact-macro lens (EF 50 mm 1:2.5). When used with manually set focus, aperture and exposure, this system was able to capture a maximum of five images per second. Initially no precise correlation between the stress-strain data and the recording of the images was readily obtainable. The only method available was to note the number of the data point at which the photograph was taken, or to take the photograph at a predetermined data point number. The data point number was displayed on the monitor screen, and was incremented with each new set of stress and strain values captured. This was only practical when both the data collection system and the camera were running at a low frequency. This system is shown schematically in figure 8.001. Some later adaptations to the (AJS/BBC) data collection system permitted accurate correlations to be easily made; a signal obtained from making connections to the flash contacts was recorded synchronously with the mechanical data. The adaptations to the data collection system are described in detail in appendix 1. This improved system received only limited use, as soon after its construction and testing I become aware of the availability of a high speed video system.

During the initial photographic recordings the illumination of the specimen was by lighting units designed for microscopes, comprising a low voltage bulb and a focusing lens. However this was improved upon in later tests by using a fibre optic light source. This was a Schott KL 1500-T, which directs light from a 150 watt, 15 volt bulb, along two separate flexible bundles of optical fibres. This provided more light, thus permitting shorter exposures to be used.

8.4.1.1. METHOD OF OPERATION OF THE 35 mm SLR CAMERA

The general approach was to take a single photograph of the specimen before it was loaded. This negative was labelled using the camera's data back. (This device permits numbers, say time, data, frame number, etc., to be imprinted directly on the negative. Only the first frame of each film was labelled as continual use of the data back reduced the maximum frequency of the camera.) The specimen was then loaded. Occasionally photographs were taken before the optical events were observed. However, most photographs were taken when I observed these changes.

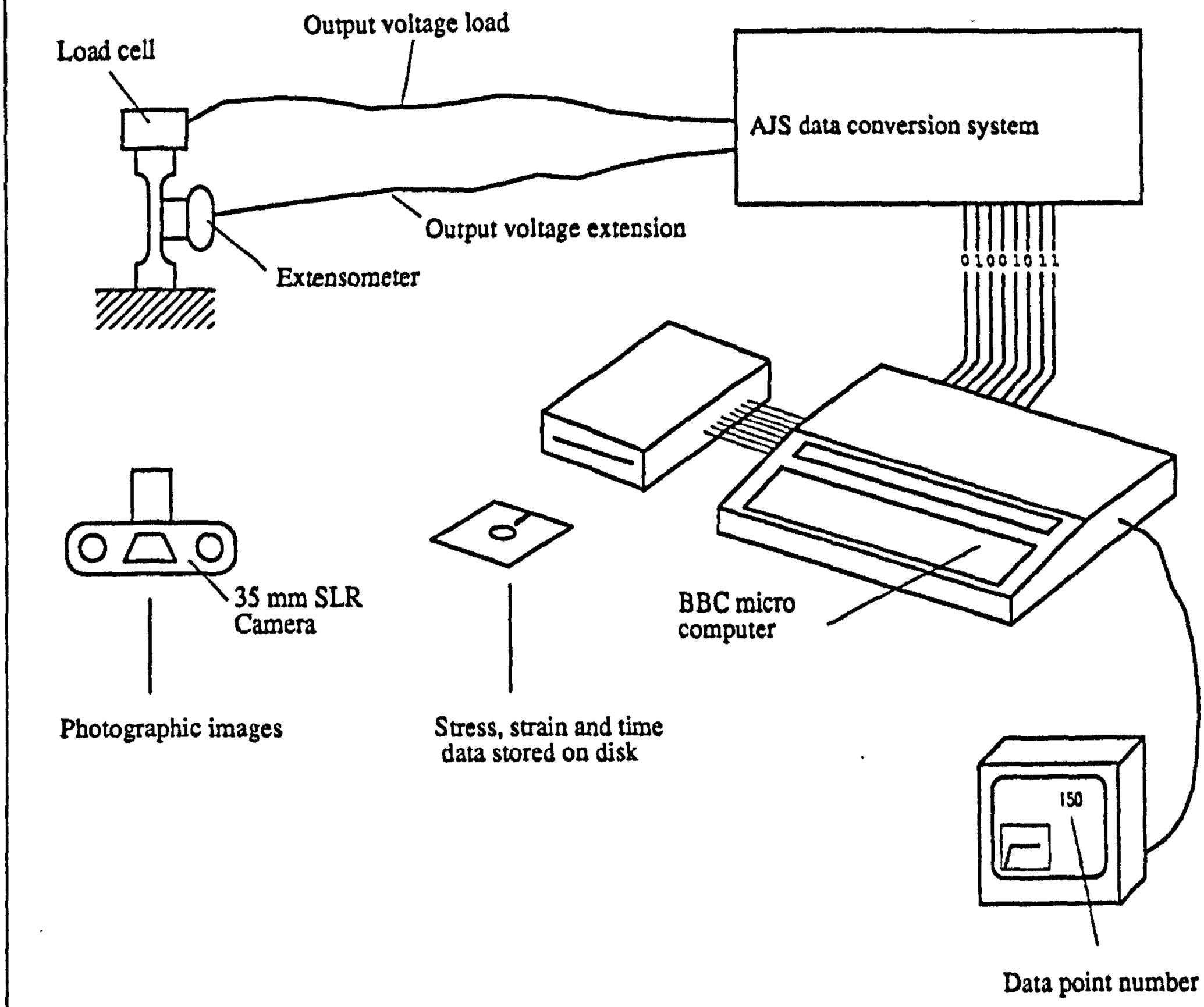

Figure 8.001

The arrangement of the various parts of the test equipment during the initial tests using a 35 mm SLR camera

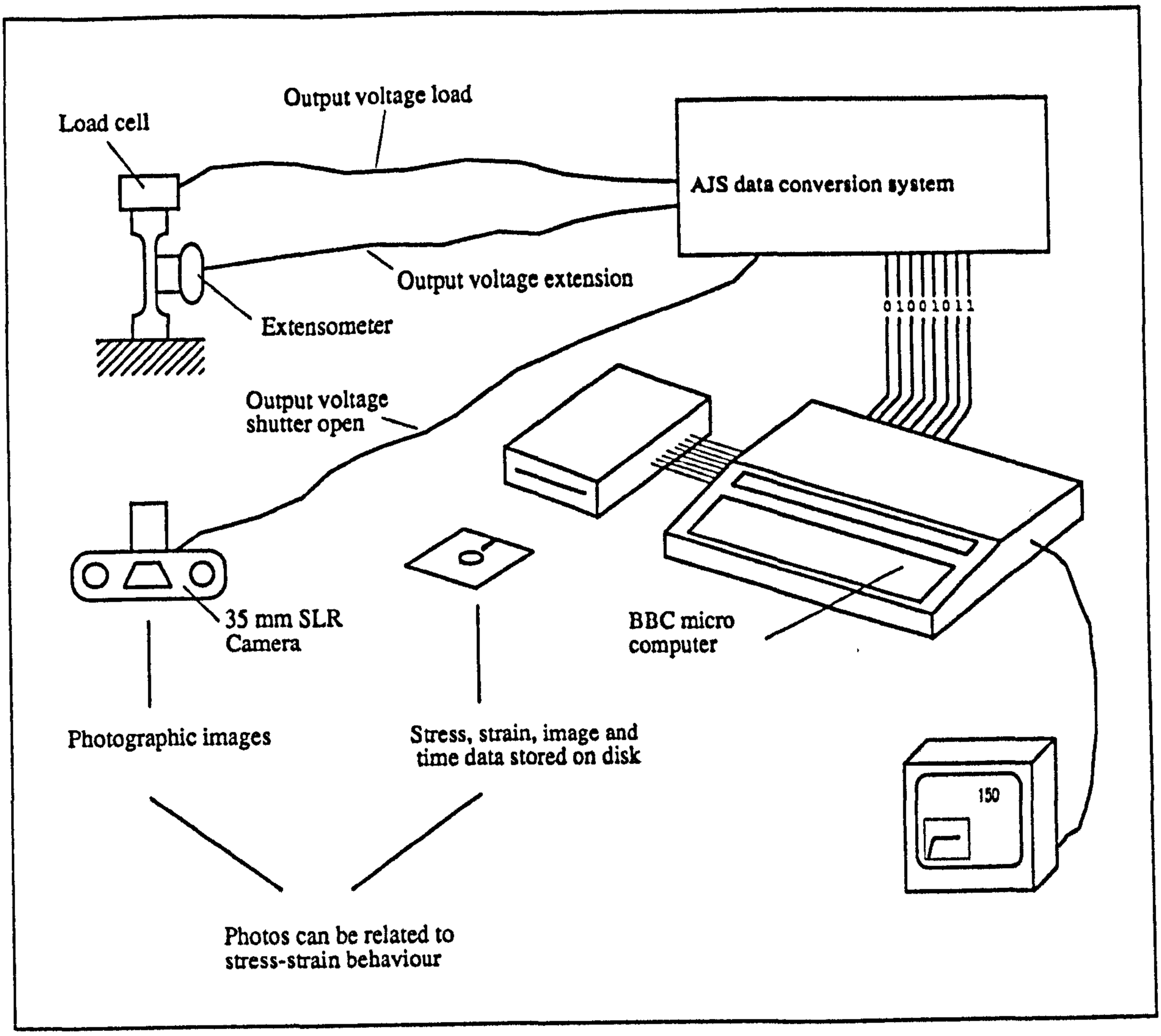

Figure 8.002

The arrangement of the various parts of the test equipment during tests in which the times of the images were obtained with a 35 mm SLR camera were recorded by the AJS/BBC data collection system

8.4.2. HIGH SPEED VIDEO RECORDER

After completion of the creep tests (described in chapter 5) and before embarking on the notch sensitivity tests contained in data sets NA4, NA5, NB4 and NB5, I became aware of a high speed video system available for loan from my grant-giving body, SERC.[7] This system was based around a Kodak Ektapro video recorder, which enables frames to be recorded at a number of pre-set speeds between 30 and 1000 frames per second inclusive. When operating at its maximum frame rate the Ektapro video tapes retain a maximum of about 30 seconds of recording, this increases *pro rata* as the frame rate decreases. (The method of recording allowed more than one image to be displayed on each frame. These images could be either higher aspect ratio pictures obtained at a

[7]I thank Mr Pete Goodyer of the Science and Engineering Research Council, for granting my request to borrow this equipment, and his very clear instructions on how best to use it.

greater frequency, of up to six times the frame rate, overlaid pictures from a second camera, or both. One format of the last configuration is shown by pictures of the impact specimens, figures 1.014 to 1.017 of chapter 1.) The images recorded by the Ektapro system can be replayed by the system at 30 frames per second. Alternatively they may be stepped through individually or at one, two, three or four frames per second, in either direction. These replayed images may be recorded onto the VHS tapes, for future analysis. Data may be added to each frame: time (both actual and from the start of recording), frame number, frame rate and the state of the system (record, stop, play, rewind and so on). One such frame is shown in figure 8.007. Additional equipment supplied (by SERC) with the high speed video and camera, included, a television monitor, Panasonic 6200 VHS video tape recorder and a Mitsubishi P71B video printer. This system in shown schematically in figure 8.003, and a photograph of the experimental arrangement is shown in figure 8.004.

Apart from a greater flexibility in the type of pictures it can capture, a video system has other advantages over using normal film and an SLR camera. It permits better judgement of the appearance of the recorded image, before the commencement of a test. This system also enables the picture of the specimen to be constantly monitored during the test, and those frames that have been recorded can be examined immediately. Hence the best light levels, camera position and focus can be readily found, thus reducing the number of preliminary experiments, saving time and materials.

8.4.2.1. METHOD OF OPERATION: FIRST VIDEO SYSTEM CONFIGURATION

The test procedure used was as follows: the specimen was placed in the jaws within the water tank, with the extensometer attached if desired. The appropriate cross-head speed for the test was selected and the (AJS/BBC) data collection system primed for use, so that only one further key stroke was required to initiate data storage. The VHS recorder was then started in recording mode, thus enabling a *real time* recording to be made of the whole test. The Ektapro system was then put in recording mode and the (AJS/BBC) data collection system activated. The last operation was to set the cross-head of the Instron into motion. After the test, the equipment was turned off in the reverse order. The high speed recording was then, if required, downloaded to the VHS tape at 30 frames per second, and any especially interesting frames were examined and stored at slower speeds. Hard copies of some images were obtained using the video printer. The high speed tapes were then reused to record the next test. Correlation of the images with the stress and strain data was obtained by using the instant of complete rupture as a datum time in both data sets.

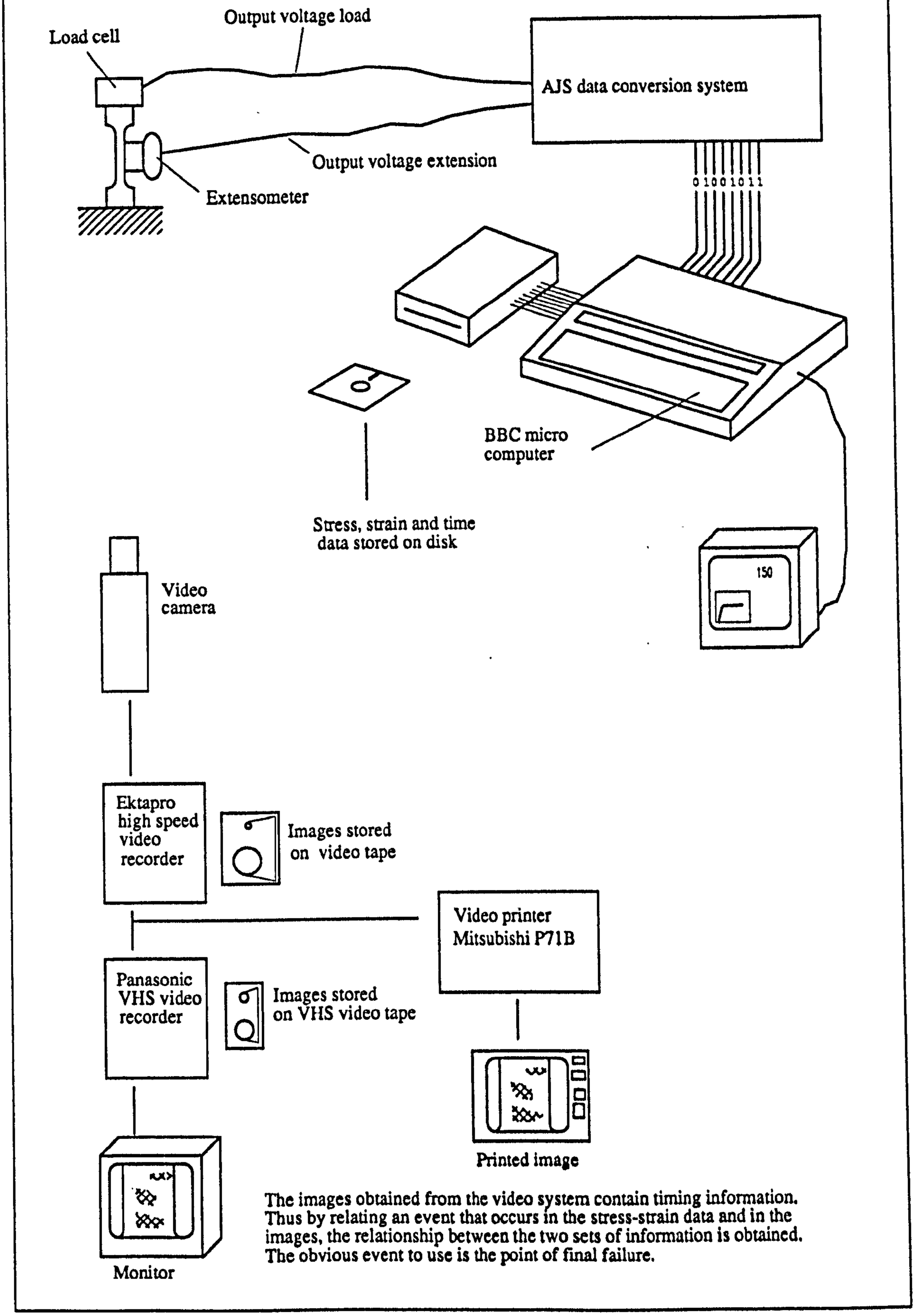

Figure 8.003

The arrangement of the various parts of the test equipment during tests in which the images were obtained by using one video camera

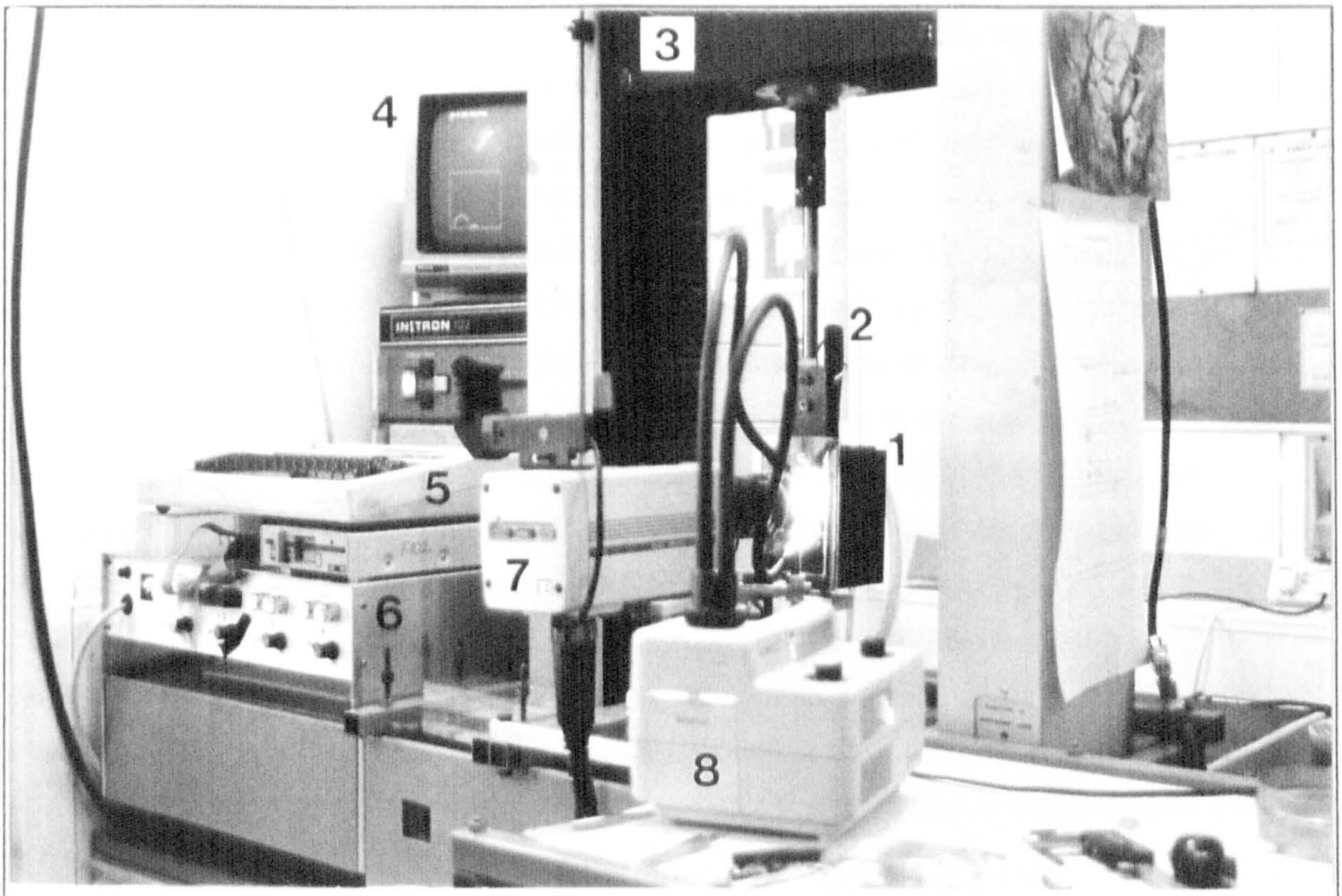

1) Environmental chamber 2) Tube containing extensometer 3) Cross-head
4) Monitor (load-extension) 5) BBC micro computer 6) AJS data system
7) Video camera 8) Light source

Figure 8.004

The arrangement of the mechanical and optical test equipment for the experiments using one video camera (the first video system configuration)

8.4.2.2. METHOD OF OPERATION: SECOND VIDEO SYSTEM CONFIGURATION

Some additional equipment was obtained when the system was borrowed for the second time. Two cameras were now connected to the high speed video recorder. This permitted synchronous recording of the mechanical response and the optical changes. Originally I envisaged this additional camera was used to record the stress-strain, or more correctly the load-deformation, output as displayed on a cathode ray oscilloscope.[8] This would provide a direct correlation between the mechanical and optical behaviour of the material in the same frame. Using a cathode ray oscilloscope would also enable tests to be performed at speeds greater than those realistically permitted by the low sampling rate

---

[8]The basic loading and mechanical data collection system would be the same as that used to obtain the initial results of this whole study (described in chapter 1), the Polaroid camera being replaced by the video.

of the (AJS/BBC) data collection system, (8.33×10^{-4} m s^{-1}). Unfortunately the image on the oscilloscope screen was not bright enough to be recorded at frame rates close to the desired 500 or 1000 frames per second. The alternative system used was a standard flat bed chart recorder[9] into which the load signal was fed (via the in-house amplifier normally used with the oscilloscope); the other axis was time. By overlaying the images from these two cameras the recorded frames contained an image of the specimen and an image of the load-time plot, thus correlation of the two types of data was inherent in this system. A Umatic SP video tape machine[10] was also added to the equipment and used in the same way as the VHS recorder already mentioned. This enabled a higher quality recording to be made which was also easier to edit and copy with less loss of quality. (A result of such editing and copying is shown in the video tape submitted as part of this thesis.) Printouts were obtained in the same way as above, but also by using another video printer, a Mitsubishi CP50B. (The second camera and Mitsubishi CP50B printer were used to obtain the images of the impact specimens presented in chapter 1.) A diagrammatic representation of the arrangement of the experimental equipment is shown in figure 8.005.

---

[9]The Instron's own chart recorder was not used as the pen is positioned part way round the paper feed roller. Thus a two dimensional image would contain some distortion.
[10]A near broadcast quality analogue machine, using 0.75 inch tapes running at 3.75 inches per second.

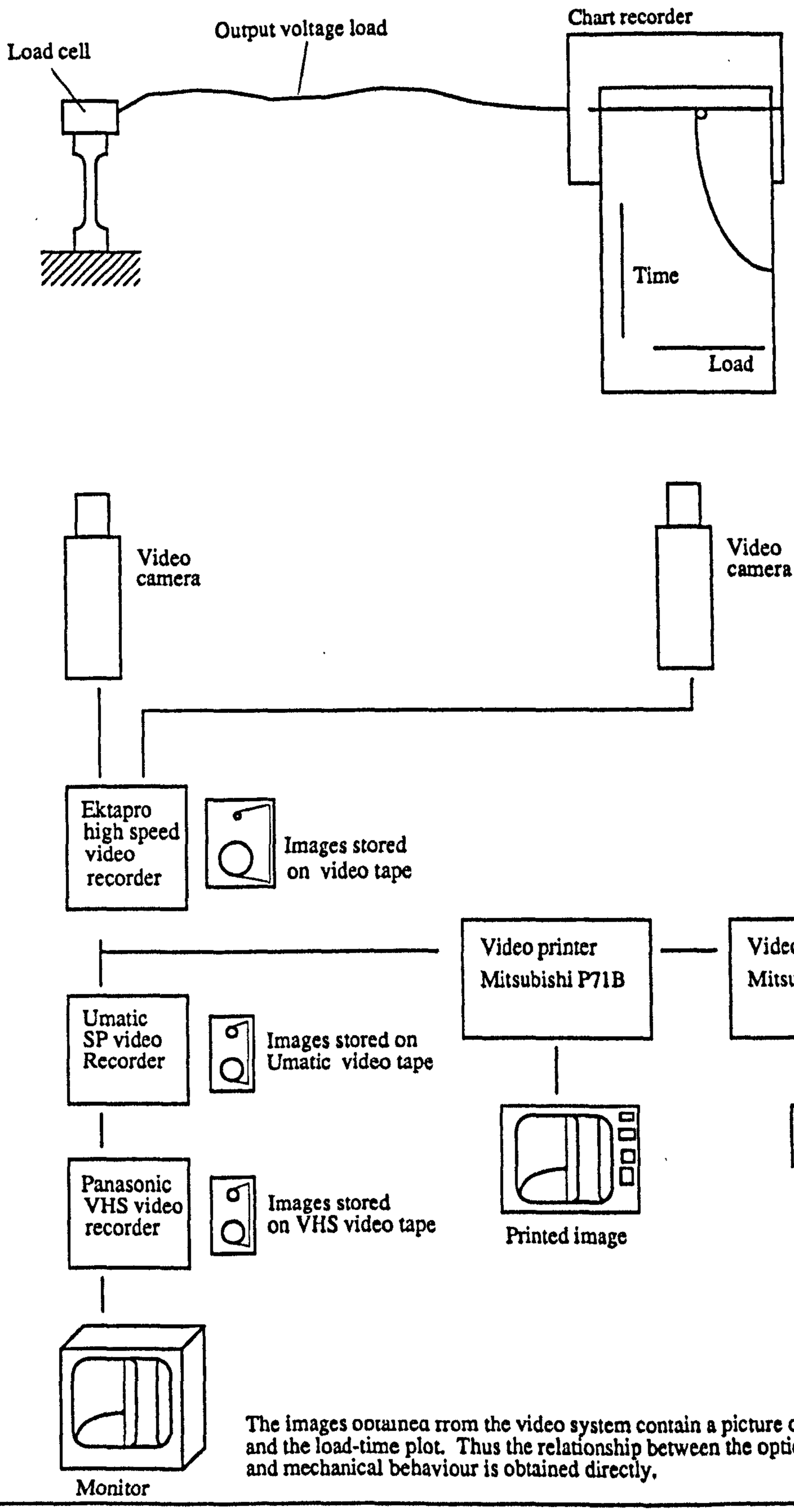

Figure 8.005

The arrangement of the various parts of the test equipment during tests in which the images were obtained by using two video cameras

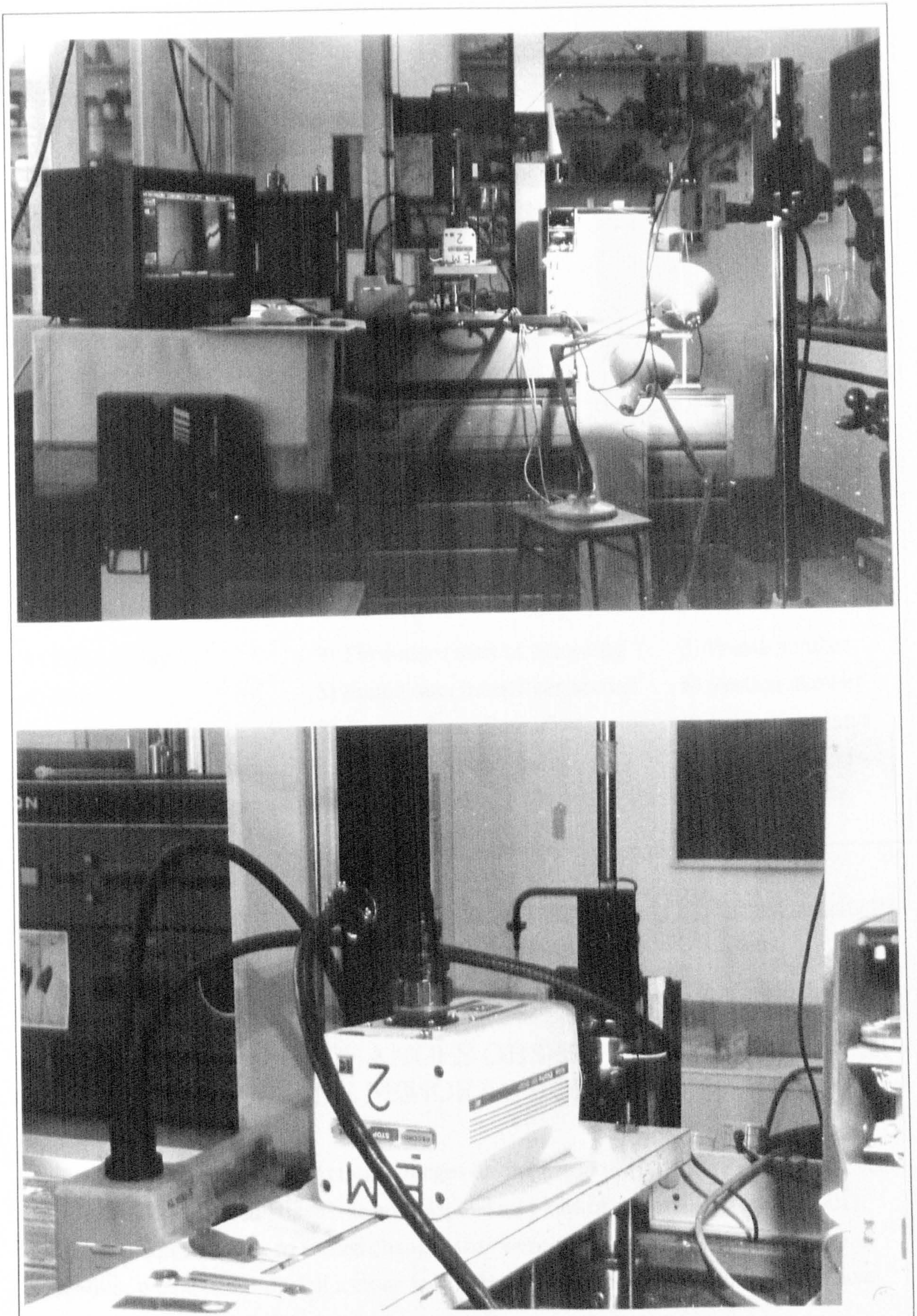

Figure 8.006

The arrangement of the mechanical and optical test equipment for experiments using two video cameras (the second system configuration)

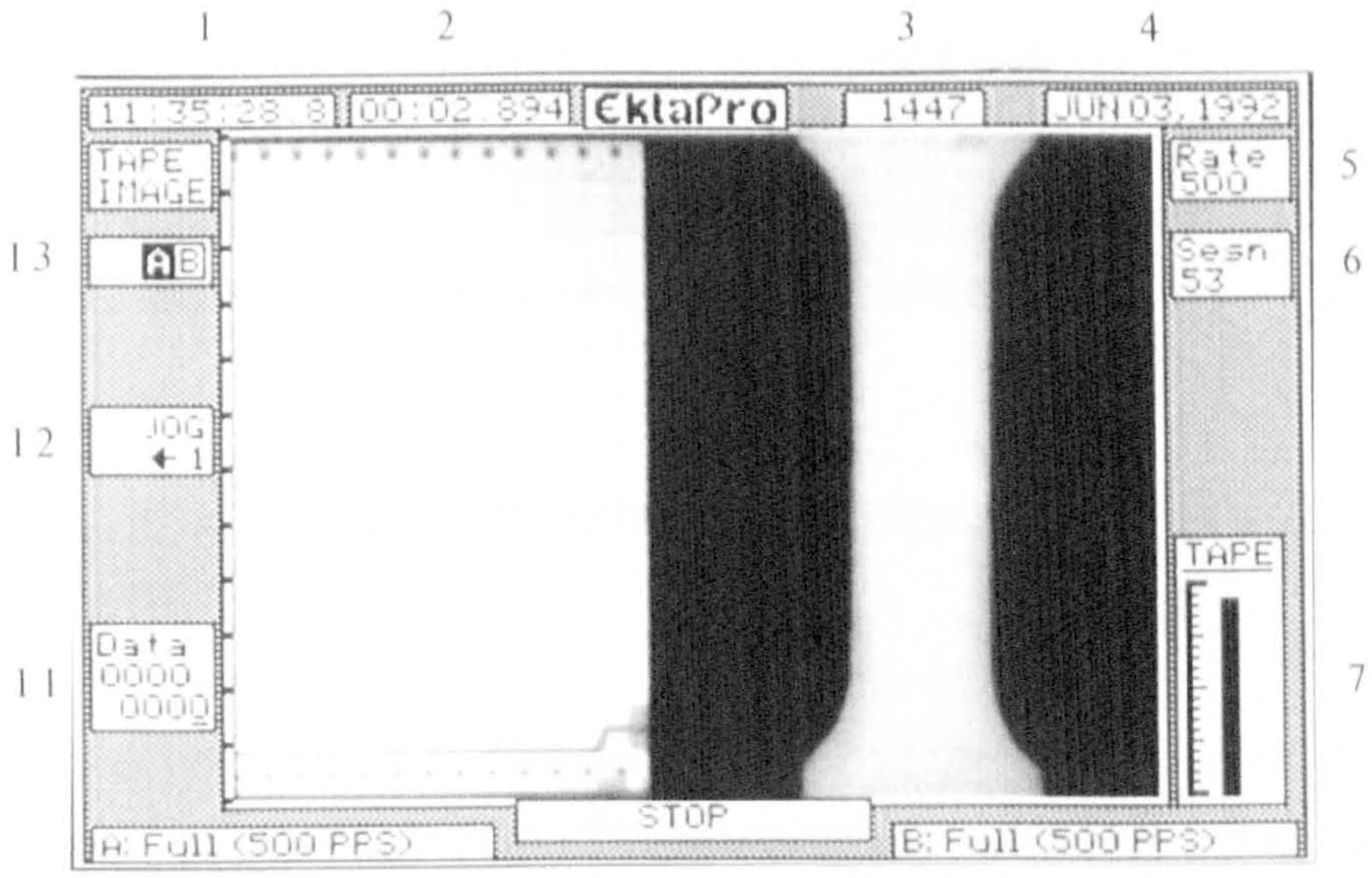

1) Time of day
2) Time since start of recording
3) Frame number
4) Date
5) Frame rate, frames per second
6) Session number
7) Tape remaining
8) Camera B configuration
9) Recording status
10) Camera A configuration
11) ADC input (not used)
12) Jog and step rate
13) Image overlay arrangement

Figure 8.007

A sample frame from the Kodak Ektapro, showing the position of the frame rate, frame number, time and other information

8.5. OPTICAL CHANGES OBSERVED DURING CREEP TESTING (OF BOVINE FEMORAL BONE)

All the recordings of optical changes during creep testing used the canon 35 mm SLR camera (described above), as an independent piece of equipment (figure 8.001). The initial aim was only to record changes that were observed, as it was not known if whitening would occur during a creep test. The mechanical results of these tests have already been presented in chapter 4.

The first observation of whitening occurred during the creep testing of bovine bone specimens (CB1). No whitening was noticed during the previous creep tests on reindeer antler (CA1). However, this may be a consequence of not specifically looking

for such changes, which may have occurred, unobserved. Optical changes were first observed in a bovine femoral bone specimen (10/01/91/19), which was subjected to a stress of about 84 MPa. Failure occurred at a strain of 0.023 after 30 seconds. By examination of the creep test results presented in chapter 4 it can be seen that this specimen was not unusual in its mechanical response. Unfortunately these optical changes were not captured on film; notes taken at the time simply state that the whitening was seen and that the specimen fractured through the region where they occurred.

8.5.1. THE APPEARANCE AND RECORDED IMAGES OF THE OPTICAL CHANGES

The second observation of whitening was during the testing of another bovine femoral bone specimen (10/01/91/14). The whitened zones took the form of three narrow, approximately elliptical areas, the long axes of which were perpendicular to the long axis of the specimen. These areas were seen to extend with time until failure occurred, which for this specimen, happened to coincide with the position of the knife edge of the extensometer. The first successful photographic recording of the optical changes during a creep test of bovine bone was during the test of specimen 10/01/91/17. (This is the first recording of such an event in bone during a creep test, that I am aware of.) Some of the images obtained are shown below in figure 8.008. In this case the whitened zones formed striations across the specimen, the fracture occurring in the most striated region. The optical changes disappear after fracture. (Unfortunately no initial photograph was taken of this specimen.) The disappearance of the striations is not due to the fractured ends of the specimen moving out of the focal plane of the lens. The bottom section of the specimen is rigidly fixed (as was the camera), and this effect was also observed with the 'naked-eye'.

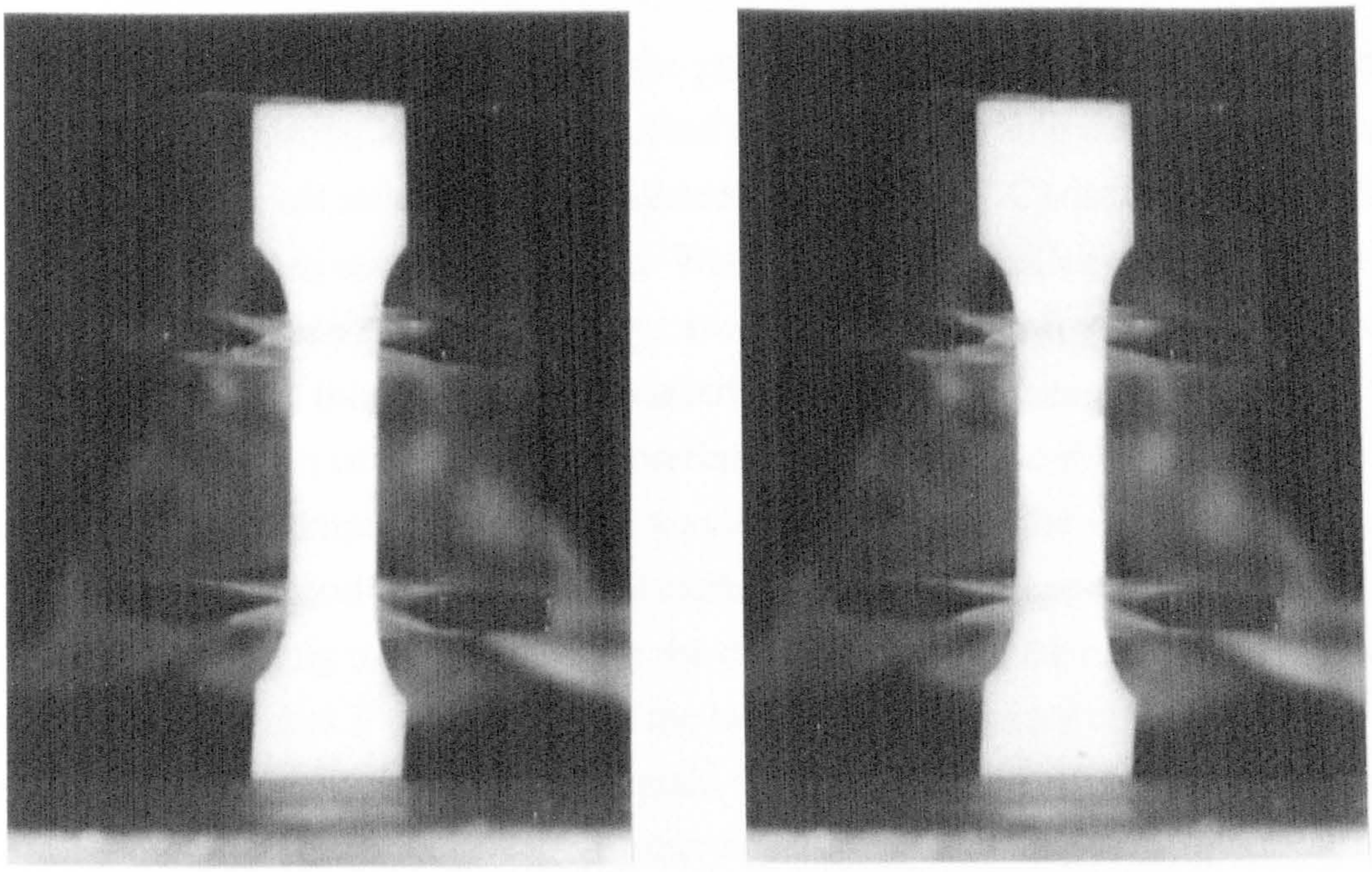

Specimen 10/01/91/17

Figure 8.008

Optical changes recorded during the creep testing of a bovine femur specimen

8.5.2. THE RELATION OF THE OPTICAL CHANGES TO THE MECHANICAL STATE OF THE CREEP SPECIMENS

An attempt was made to correlate the photographs with the mechanical state of the specimen. This was achieved, as described above, by recording the number of the data point that had most recently been recorded by the (AJS/BBC) data collection system, as stated above this was not very practical. When optical changes were observed, the camera was operated at a higher frequency. Due to the power term used to reduce the sampling frequency as the creep test progressed, the camera frequency could exceed that of the data collection system. Thus any correlation became vague if not confused. However, the general impression I gained was that the extent of the whitening increased most rapidly in the period just before final rupture. Therefore it appears that the occurrence of whitening may be related to the tertiary region of the creep curve. It is tempting to propose that if this is the case the lack of such a tertiary region in the response of the antler specimens could explain why no whitening was observed in that material. Clearly this is an area where further experimentation may be beneficial.

8.6. OPTICAL CHANGES OBSERVED DURING TENSILE AND LOADING-UNLOADING TESTS

Initially the same recording equipment as that in the creep tests was used to record the optical changes occurring during tensile tests; an SLR camera used independently (figure 8.001). A few tests were then successfully performed using the same camera but with the improved data collection system (figure 8.002). One result from the improved data collection system is shown in figure 8.009. These recordings of the tests provided some qualitative information. However, most of the results presented here are from the tests for which a video recording system was used, from which more quantitative data was obtained.

The first set of experiments recorded on video tape, used one camera and the (AJS/BBC) data collection system (figure 8.003). Only a small length, about 6 mm, of the gauge section was viewed and recorded on video tapes. The same arrangement was used for the notched tests (for comparison with which these tensile tests were under taken; the two types of tests being interspersed). The mechanical data from these tests has already been presented in chapter 4 (data sets TA1 and TB1). All the specimens were loaded at a constant cross-head speed until failure occurred. Such a test will be referred to as a *tensile* test. It may be remembered that these data sets contain results from specimens tested at different cross-head speeds, and the specimens were of two widths 4 and 5 mm.

In the second set of experiments recorded on video tape (which have not been described previously), two cameras were used (figure 8.005). In these tests only one width of specimen, 4 mm, was examined using a cross-head speed of 8.33×10^{-5} m s^{-1}. Two loading regimes were studied: tensile tests and *loading-unloading* tests. These loading-unloading tests followed the same mechanical regime as that used for the resilience tests described in chapter 7. However, in this case the specimens were put through this loading-unloading process until they failed. The loading was not at any particular frequency or even at regular intervals as it was under manual control, although the same cross-head speed was used in all the loading and unloading phases of these tests. In the following sections I examine the results of these two types of test: tensile and loading-unloading.

8.6.1. TENSILE TESTS

The first successfully recorded images of whitening during a tensile test were of a bovine femoral bone specimen. These were captured using the Canon 35 mm SLR camera connected to the improved AJS/BBC data collection system (figure 8.002). Figures 8.009 and 8.010 show some of the images of whitening obtained along with the mechanical response of the specimen. The load was applied using a cross-head speed of 8.33×10^{-5} m s^{-1} [5 mm min^{-1}]. (This specimen, 03/10/91/16, has a larger cross-sectional area than the majority used in this thesis; being 5.55 mm wide and 1.24 mm thick.) The images show the striated appearance of the specimen before failure. The last 13 photographs were taken at a rate of about five frames per second. (The raw data for this specimen is used by way of example in appendix 1, which describes the data acquisition equipment in more detail.)

Figure 8.009 shows that optical changes occur between various points on the stress strain curve. However it also demonstrates the limitations of this method of recording the images. First, the frequency of the images is quite low. This results in the instant of the first whitening being only crudely approximated. Second, the limited length of the film used means that some events may be lost, as in this case where the fracture was not recorded. These limitations were partly overcome by use of the video system.

Both configurations of the video system were successfully used to record whitening in both antler and bovine bone specimens. Images obtained from the second configuration (two cameras and the chart recorder) are shown in figures 8.010 and 8.011.

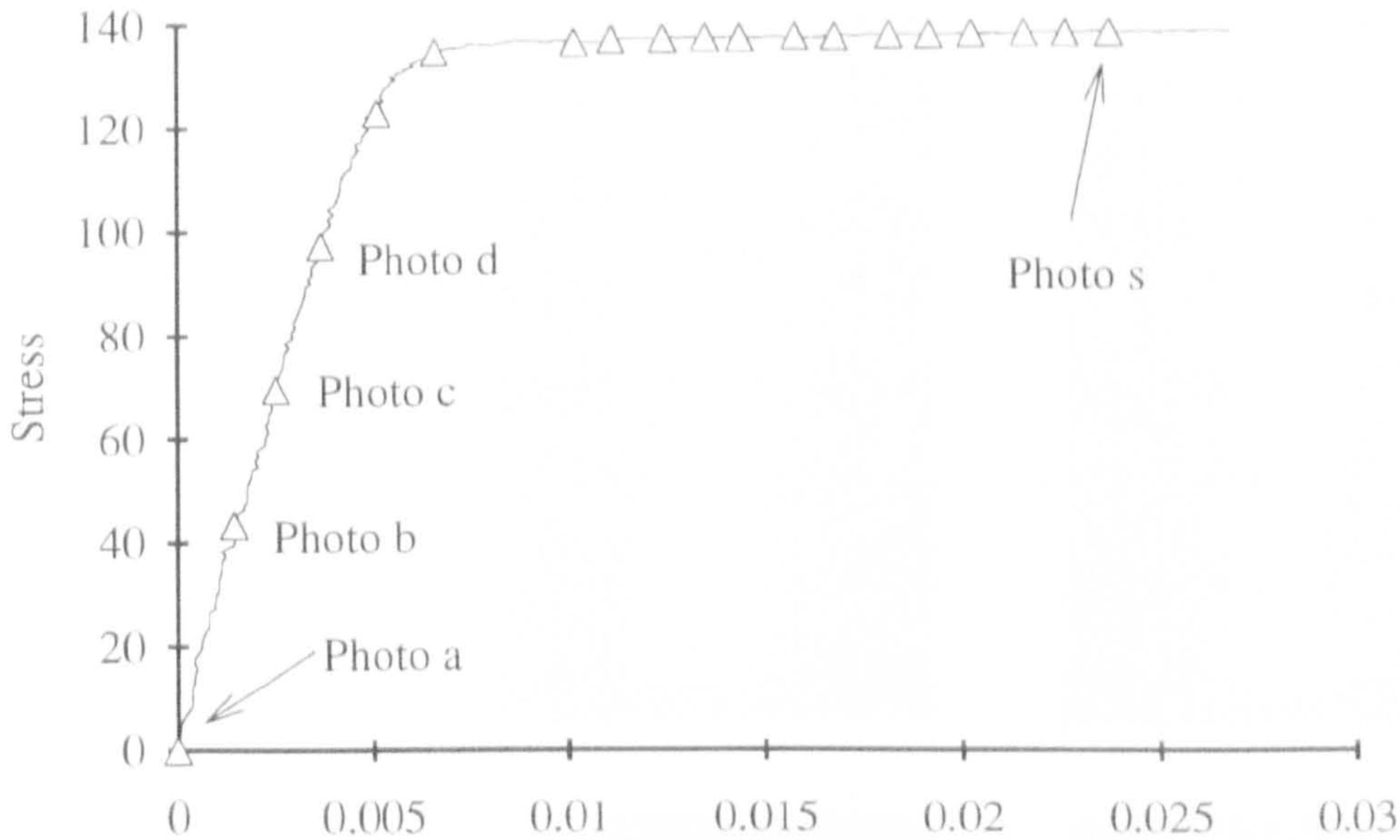

Units:

σ Stress, MPa

ε Strain, unitless

Comments:

The triangles indicate the relationship of the photos to the stress-strain behaviour. Some of the photos are reproduced below.

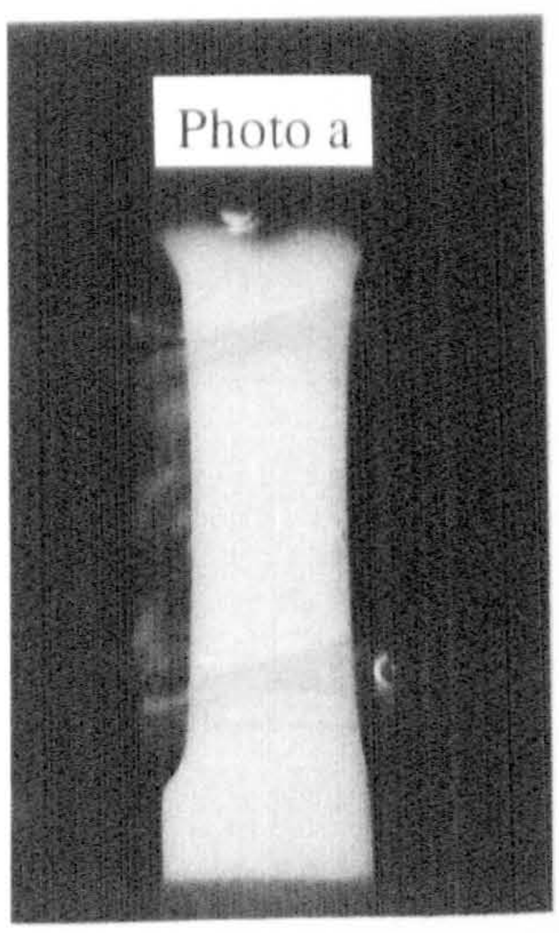

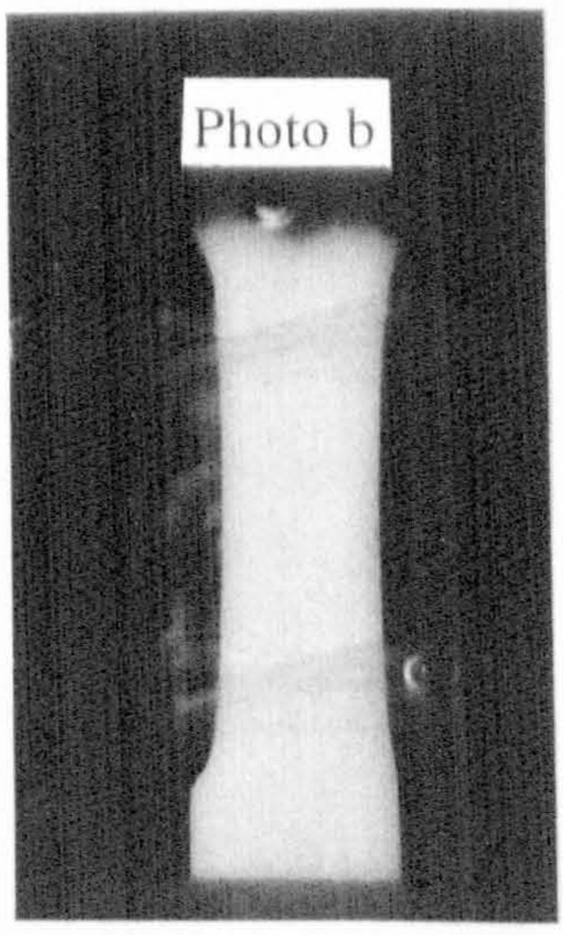

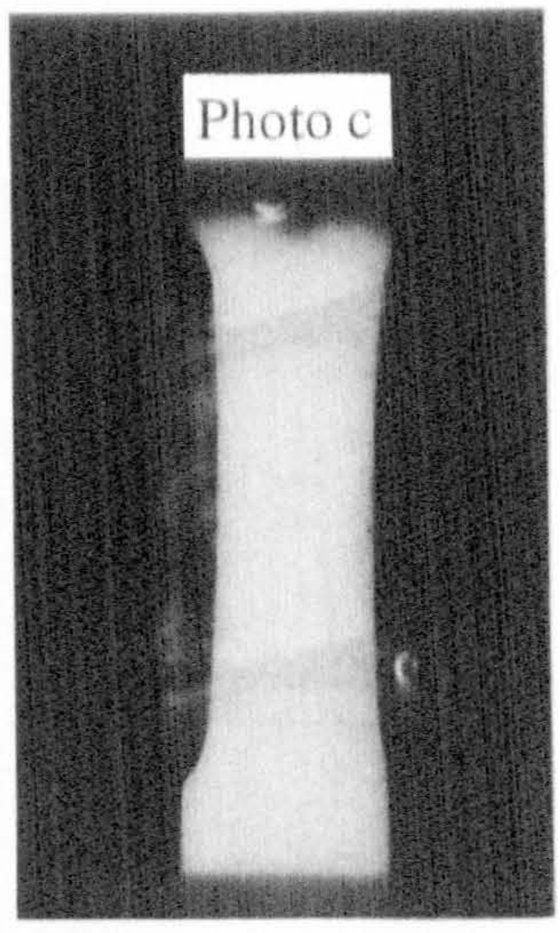

Specimen 03/10/91/16

Figure 8.009 Continued in figure 8.010

Optical changes occurring in a specimen of bovine femoral bone during a tensile test (photographic recording)

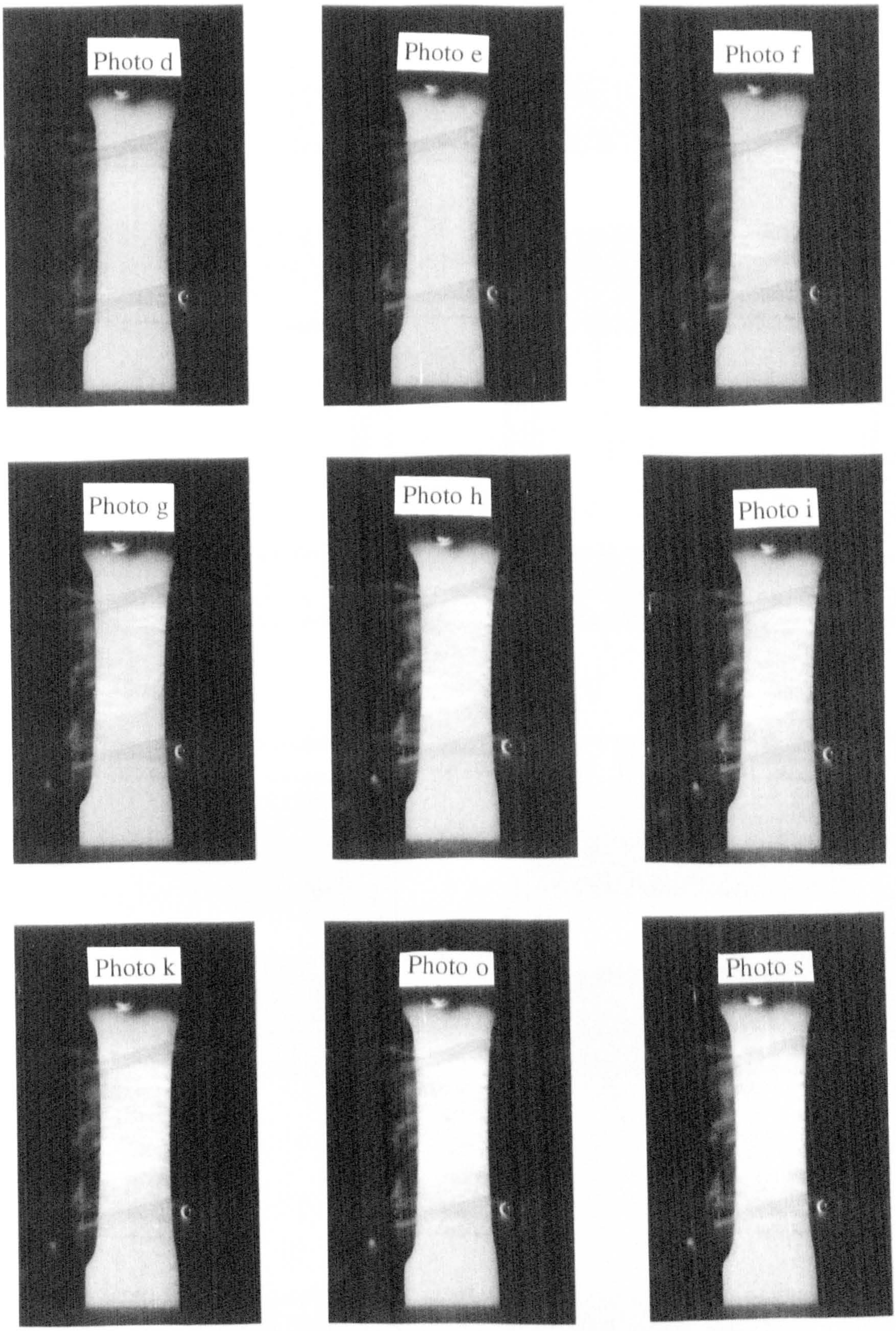

Figure 8.010 Continued form figure 8.009

Optical changes occurring in a specimen of bovine femoral bone during a tensile test (photographic recording)

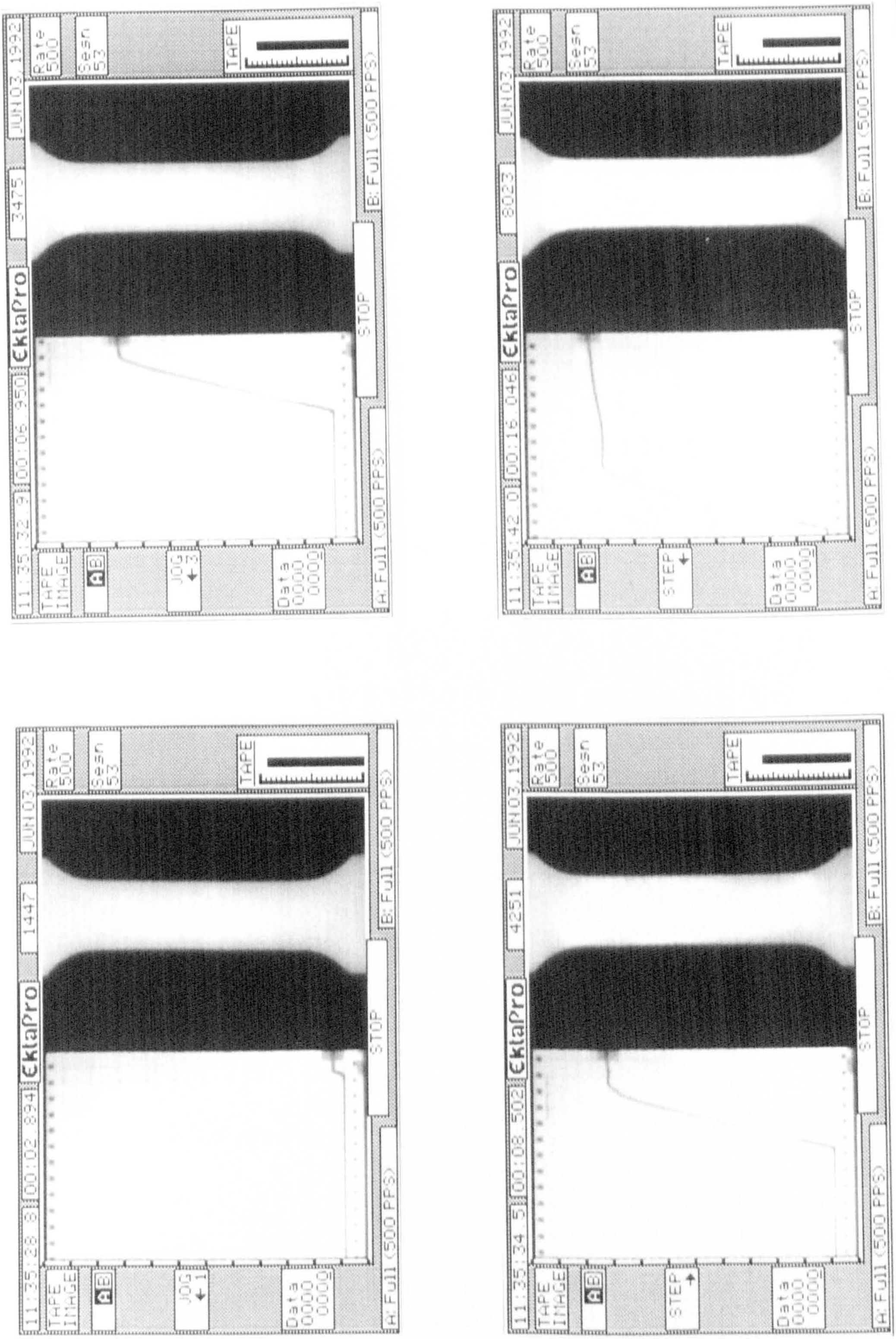

Figure 8.011

Optical changes occurring in a specimen of bovine femoral bone during a tensile test (synchronous video recording)

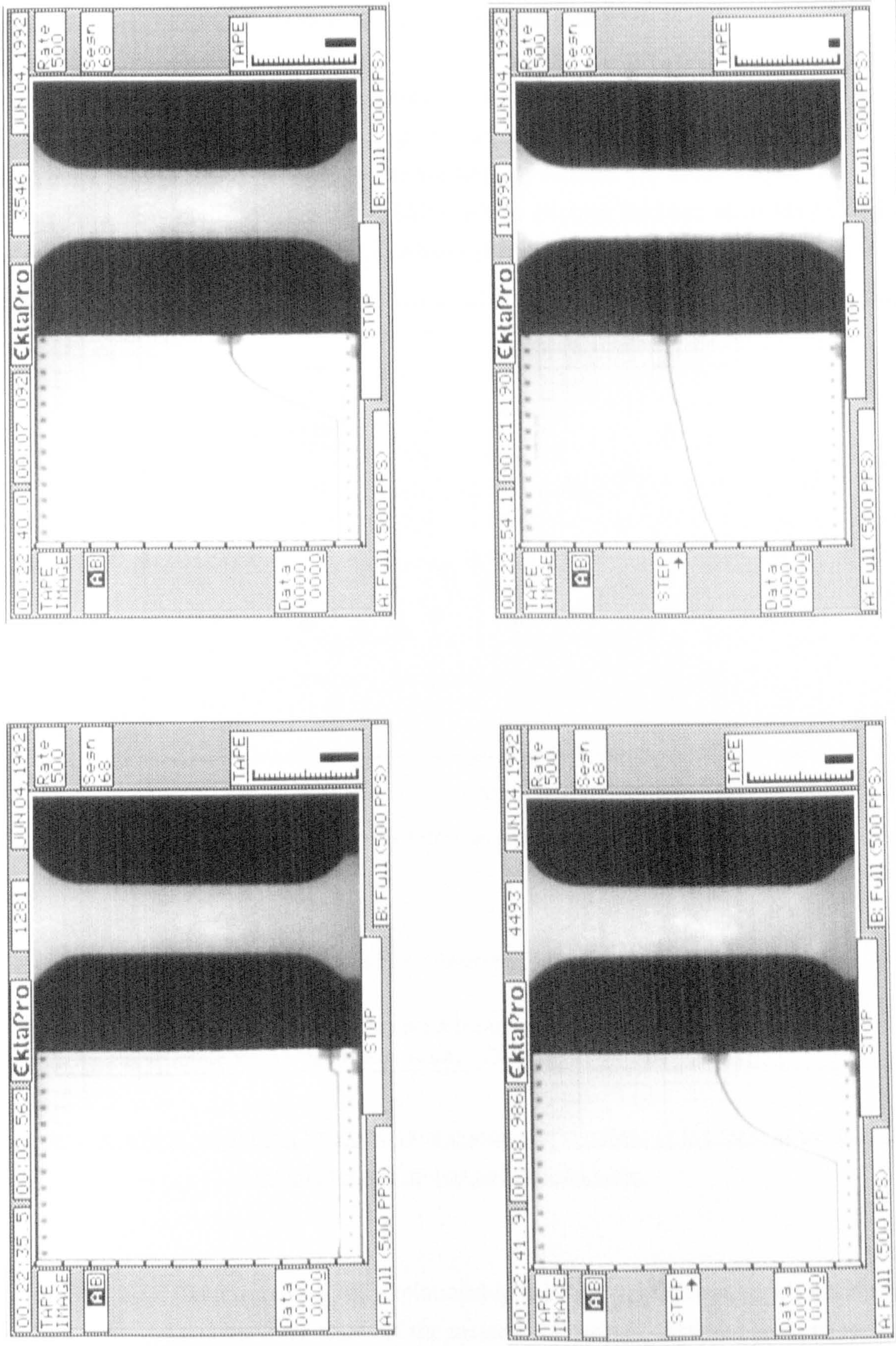

Figure 8.012

Optical changes occurring in a specimen of red deer antler during a tensile test (synchronous video recording)

8.6.1.1. THE RELATION OF THE OPTICAL CHANGES TO THE MECHANICAL RESPONSE OF THE TENSILE SPECIMENS

In this section I examine the relationship of the optical changes to those in the mechanical response during tensile testing. It is clear from figures 8.009 to 8.012 (and the accompanying video) that these events are strongly related. On initial inspection this is also shown convincingly in the figure 8.013, which displays the knee stress (as defined in section 4.2.6.1) and the stress value at which whitening was first observed.

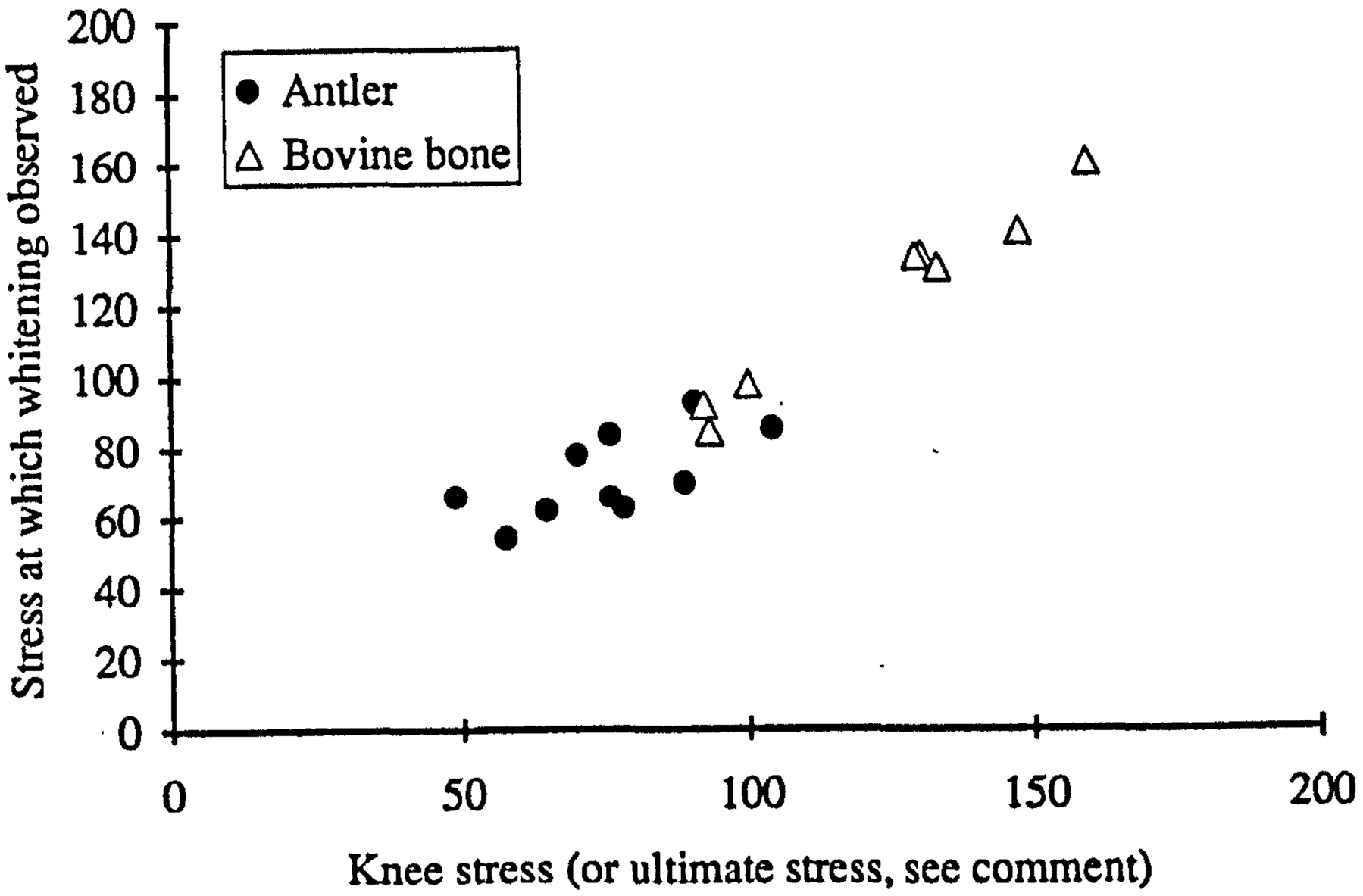

Units:

σ_K Knee stress, MPa

σ_w Stress at which whitening was first observed, MPa

Comments:

A number of the bovine specimens showed a limited or irregular post-knee region. In those cases the ultimate stress value was used. (Data sets TA1 and TB1)

Figure 8.013

The stress at which whitening was observed compared to values of the knee stress during tensile tests of antler and bovine bone

Figure 8.013 appears to show a relationship between the stress at which whitening was first observed and the knee stress of the material. However, this data contains factors that could undermine its usefulness. One factor is that the data was obtained from tests conducted at three cross-head speeds (hence the large range of stress values).[11] Another

[11]Specimens were tested at four speeds but no whitening was observed at the lowest speed.

is the use of the ultimate stress in place of the knee stress. The use of this substitution for some of the bovine bone specimens is justified by the low slope in the post-knee region. This feature of the stress-strain response highlights another problem with this data, if the knee and post-knee stresses are similar a relationship between the whitening and the value of the knee stress does not imply that the whitening occurs at the knee, only that it does not occur before it.

An examination of the strain at which whitening was first observed and the knee strain of the same specimens as examined in figure 8.013 showed that generally the strain associated with whitening was greater than that calculated for the knee. However, the correlation between the two sets of data was poorer than that for the stress values. I consider that this may be a result of only examining a small section of the gauge length. Thus some of the localised events may occur out of the field of view. Another effect of having most of the screen filled with only a small section of the specimen was the lack of a datum, or region of material, with which the changes could be contrasted. There is also the possibility that the optical and mechanical events have been incorrectly synchronised. The synchronisation process relied on the appearance of the ultimate failure in the images and in the mechanical data. (In some cases the fracture was not in the field of view and thus the sudden recoil of the specimen was used as the point of fracture.)

In the second set of video recordings (those using two cameras) the problems mentioned above were avoided, as the full gauge length was recorded. These tests were conducted without using an extensometer. The quantity that is most compatible with the specimen's strain is its extension, which may be approximated from the cross-head speed and the time (assuming a rigid machine, see appendix 7). However, all the specimens had the same nominal dimensions, and all testing was conducted at 8.33×10^{-5} m s^{-1}, so such a normalisation is not needed for a comparative study. Figure 8.014 shows the relationship of the appearance of whitening to the mechanical response. This relationship was obtained by viewing the video recordings while covering the side of the monitor showing the mechanical response, so that only the specimen was visible. When whitening was observed the card covering the mechanical response was removed, and the point reached on the load-time plot noted. It can be seen from the five bovine femoral bone and five red deer antler results shown in figure 8.014 that the whitening is clearly associated with the knee region of the loading curve. (The numbers associated with the load-extension lines are the video session numbers.)

The whitening of bovine bone specimens that attained a high ultimate strain, was more widely and more evenly distributed than the whitening in specimens that failed at lower strains. This is demonstrated by contrasting the first and second, with the last set of images recorded on the accompanying video and in appendix 11 (session numbers 36,

71 and 53). It is noticeable in figure 8.014 that the bovine bone specimen that attained the greatest extension at failure also attained the highest load. The load can be normalised to stress giving: σ_{ult} = 104 and 112 MPa for the first and second specimens (sessions 36 and 71) and 178 MPa for the last specimen (session 53). Perhaps this difference in ultimate strain (extension) is related to the difference in ultimate stress. One possible explanation for the low stress and strain values exhibited by most of the specimens is the existence of a flaw in the material (or one due to poor preparation). This flaw may behave rather like a notch; concentrating the stress and thus optical effects. Such a stress concentration would result in failure at a lower applied stress and the localisation of the failure process combined with this lower stress would result in a strain response more akin to that of a brittle material. This argument suggests that there should be a relationship between the ultimate strain value and the knee, or ultimate, stress for specimens of bovine bone. Although my tensile results do show such a relationship they can not be justifiably used to support this suggestion as the tests were conducted at different cross-head speeds, and both quantities were shown to be rate dependent. Perhaps this argument forms part of the explanation of this rate dependence; the rate dependence of one quantity (say strain) being a result of its dependence on the other truly rate-dependent quantity (say stress), and not on the testing rate directly. Such an idea is consistent with the *maximum damage criterion* I proposed in section 4.2.6.9.

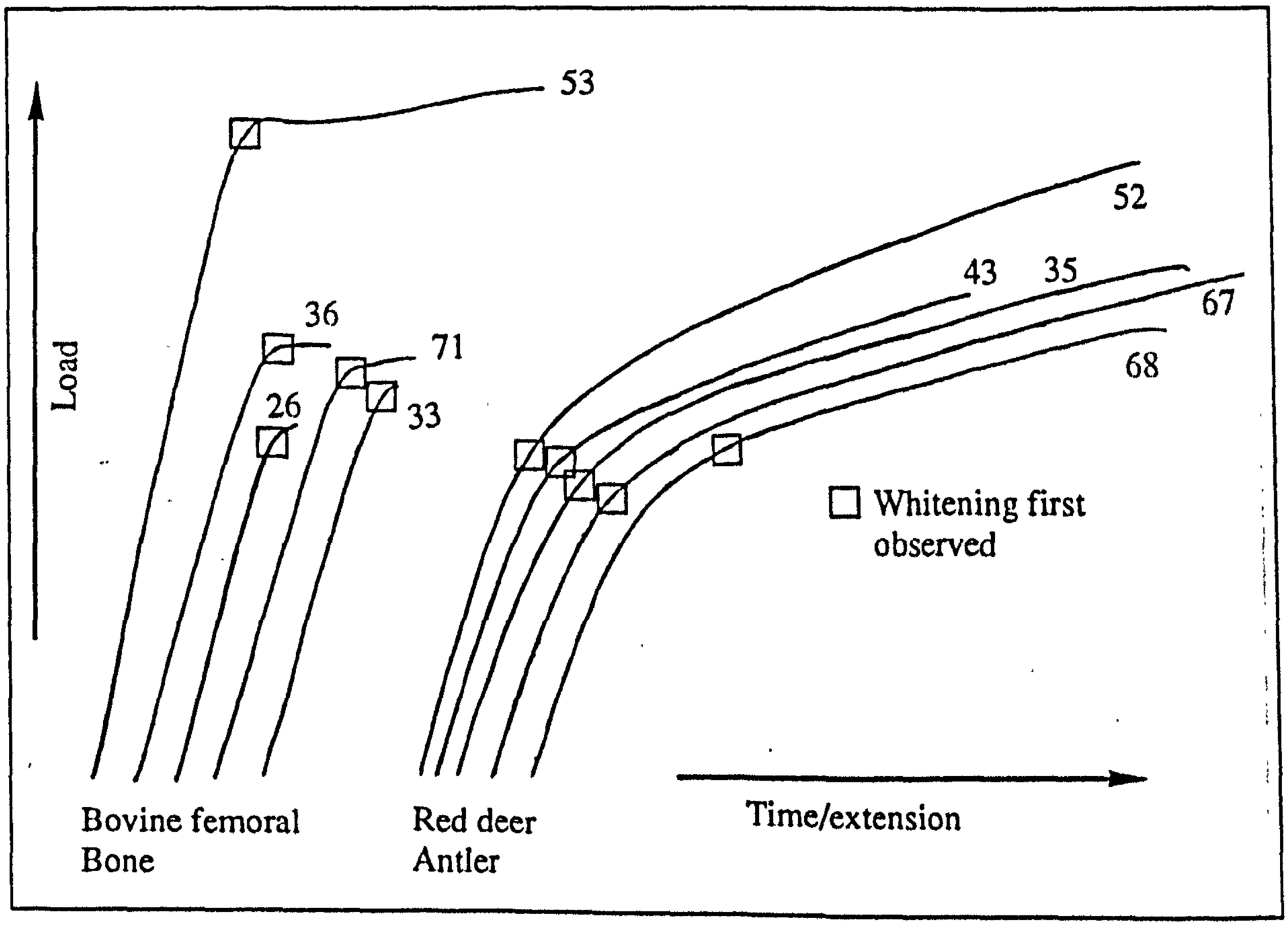

Figure 8.014

The point at which whitening was observed during tensile tests of bovine femoral bone and red deer antler specimens

Antler specimens, in comparison to those of bovine bone, maintained a more mottled appearance throughout the tensile tests. The edges of the initial blotchy regions of whitening in antler were more diffuse than those in bovine bone, on further loading these regions expanded and combined until the whole gauge length was white. This suggests that the process that results in whitening occurs throughout the whole material before it fails. This observation combined with the larger strains exhibited by the antler specimens agrees with the comments in the previous paragraph regarding the localisation of failure in bovine bone.

8.6.2. LOADING-UNLOADING TESTS

In loading-unloading tests the observations made in the tensile tests were present along with other effects that help to reinforce the location of the optical events on the stress-strain curve. No optical changes were noticed while the loading-unloading cycles were within the pre-knee region of the loading curve. Whitening was observed when the loading regime entered the knee region on the curve (as in the tensile tests). Unloading the specimens reduced the intensity of, and area affected by, the optical changes. This reduction lagged behind the changes in the applied load for both materials, but more noticeably in antler. When fully unloaded the specimens, especially those of antler, retained a vestige of the whitening effect. It was noted that this residual effect decreased with the elapse of time; simultaneously the residual strain decreased. Therefore it appears likely that the optical changes correspond more accurately with the strain exhibited by the specimen rather than the stress applied to it. This effect is shown by the images in the accompanying video, and in figures 8.015 to 8.022.

Upon reloading, the whitening was seen to re-intensify especially when the loading curve surpassed its previous value. Without a more accurate method of assessing the level of whitening it is difficult to say if it is the attainment of the previously greatest value of stress or strain that is important. When the mechanical response passes that attained on the previously greatest cycle not only does the whitening reappear (in the same regions of the specimen), but the mechanical behaviour assumes a response similar to that which would be expected if no unloading had occurred. (Much in the same way that an elastic-plastic material does in its post-yield region.)

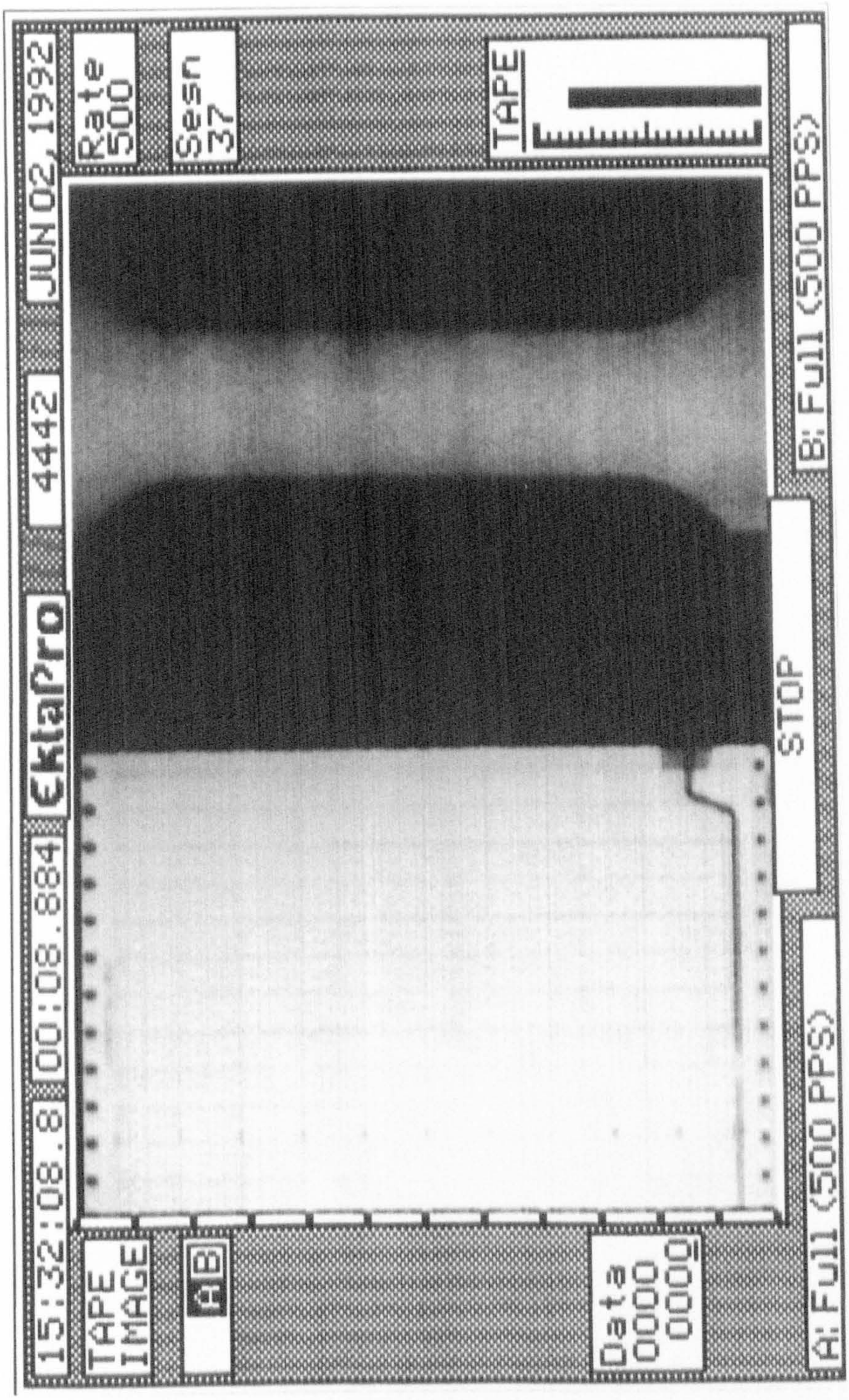

Figure 8.015 Part of a series from figure 8.015 to 8.022

First print from a series of frames showing a loading-unloading test of a specimen of red deer antler

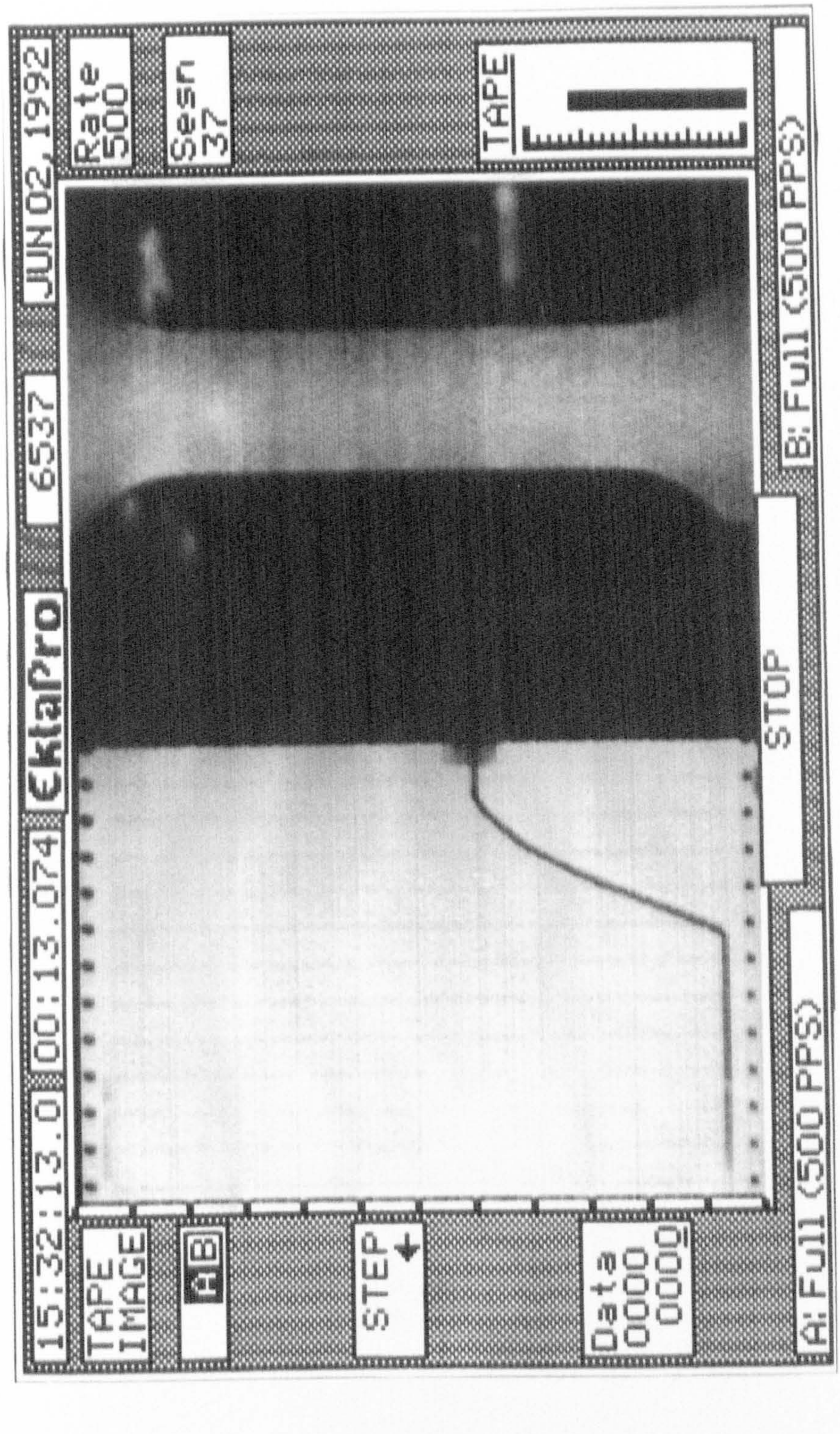

Figure 8.016 Part of a series from figure 8.015 to 8.022

Second print from a series of frames showing a loading-unloading test of a specimen of red deer antler

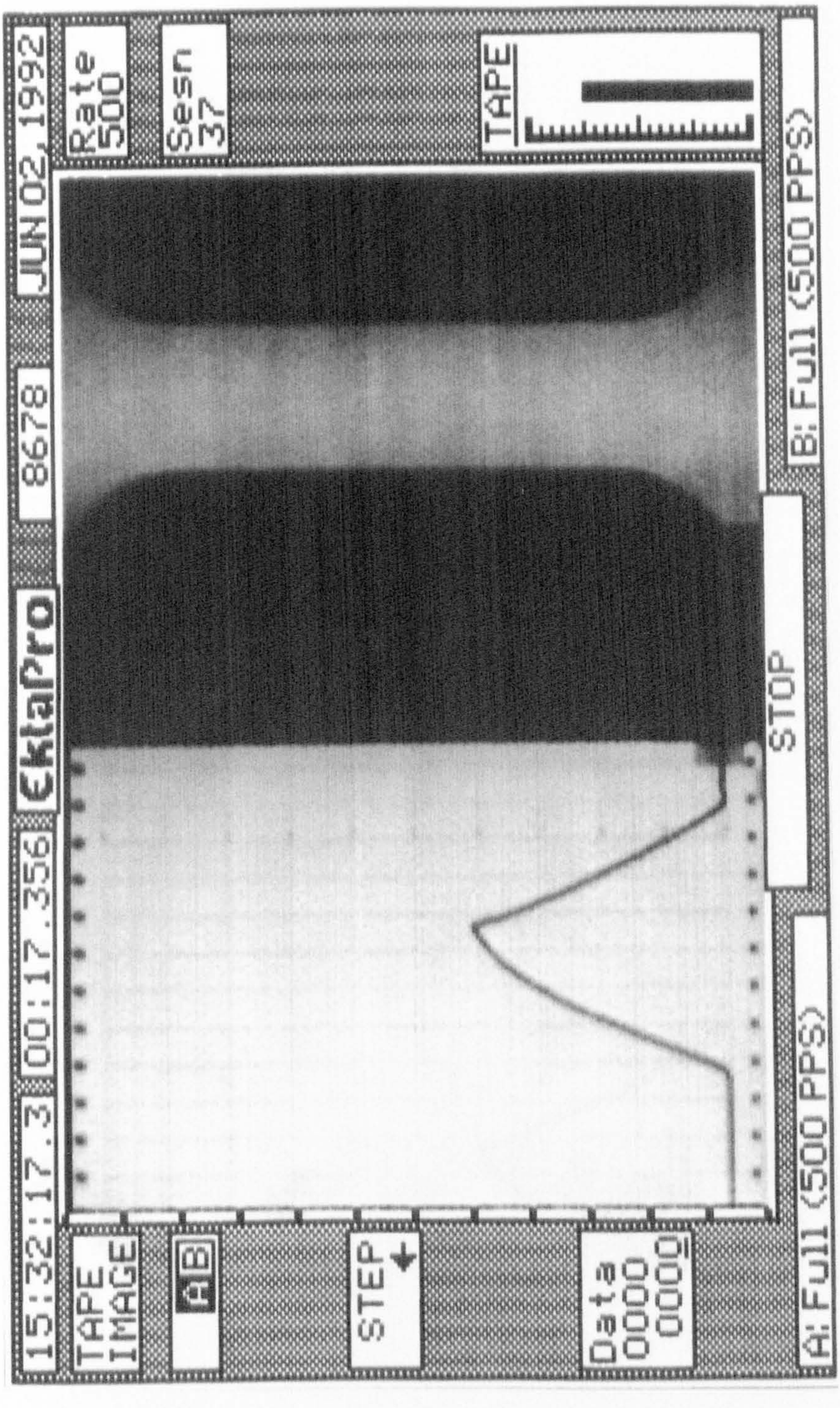

Figure 8.017 Part of a series from figure 8.015 to 8.022

Third print from a series of frames showing a loading-unloading test of a specimen of red deer antler

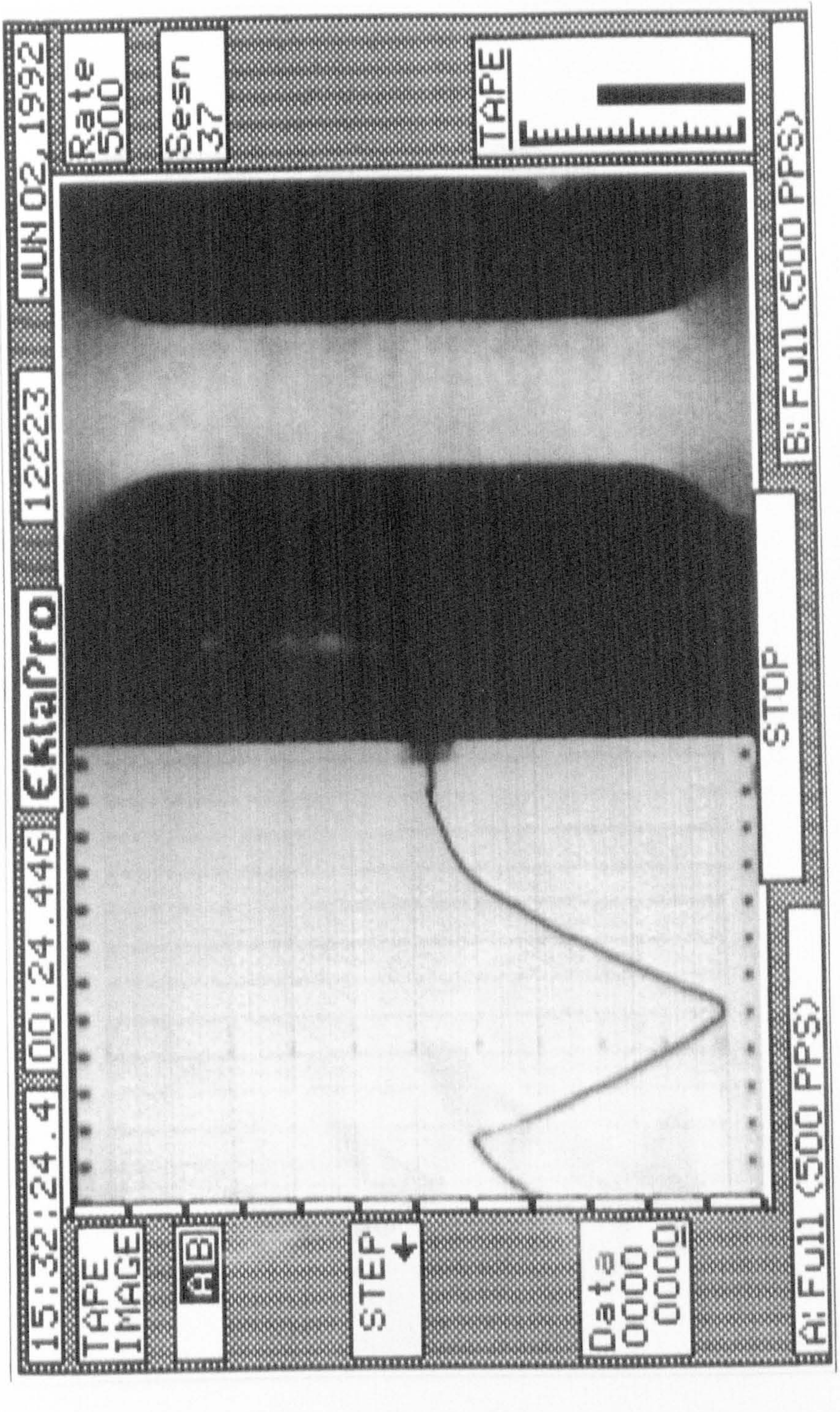

Figure 8.018 Part of a series from figure 8.015 to 8.022

Fourth print from a series of frames showing a loading-unloading test of a specimen of red deer antler

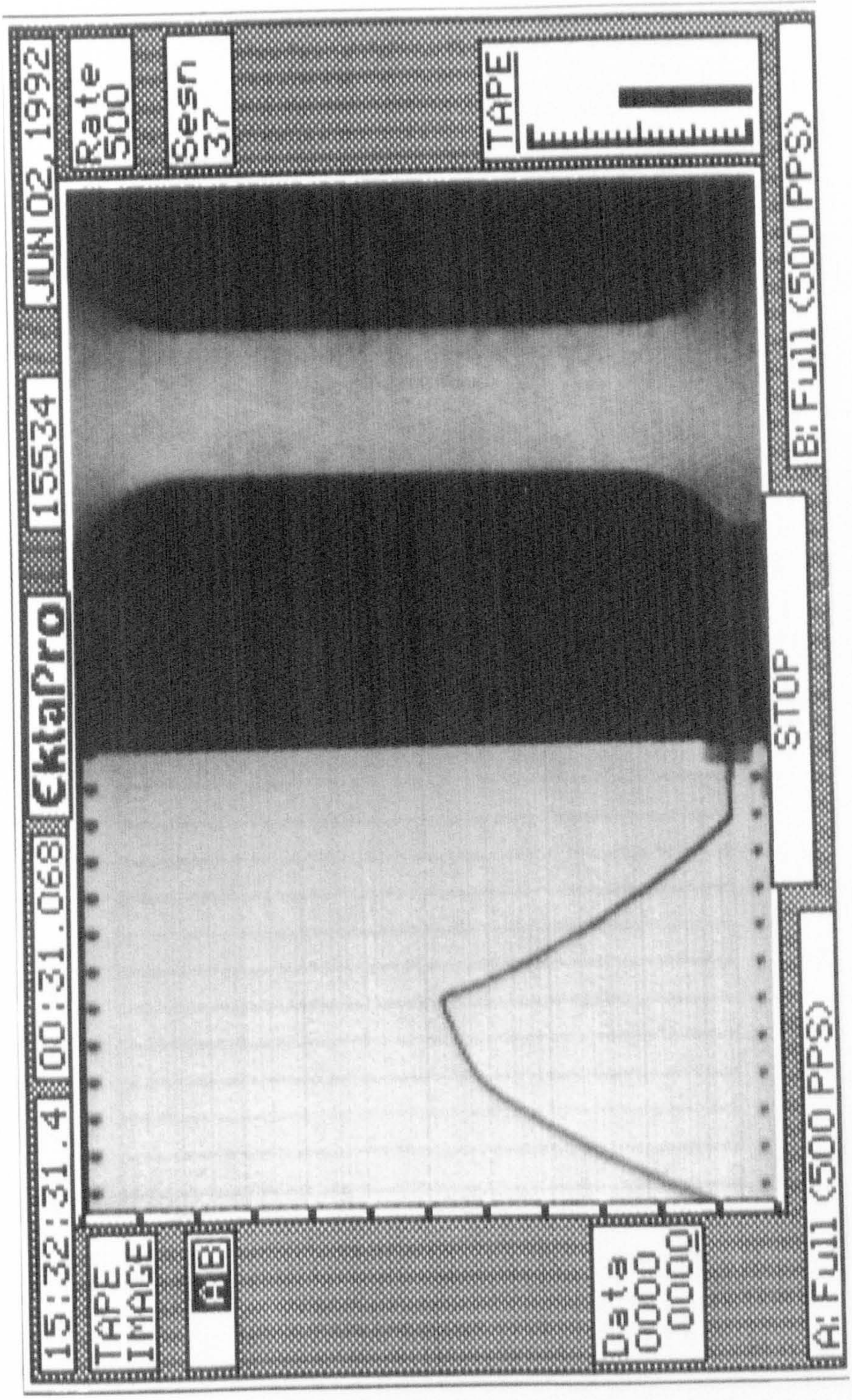

Figure 8.019 Part of a series from figure 8.015 to 8.022

Fifth print from a series of frames showing a loading-unloading test of a specimen of red deer antler

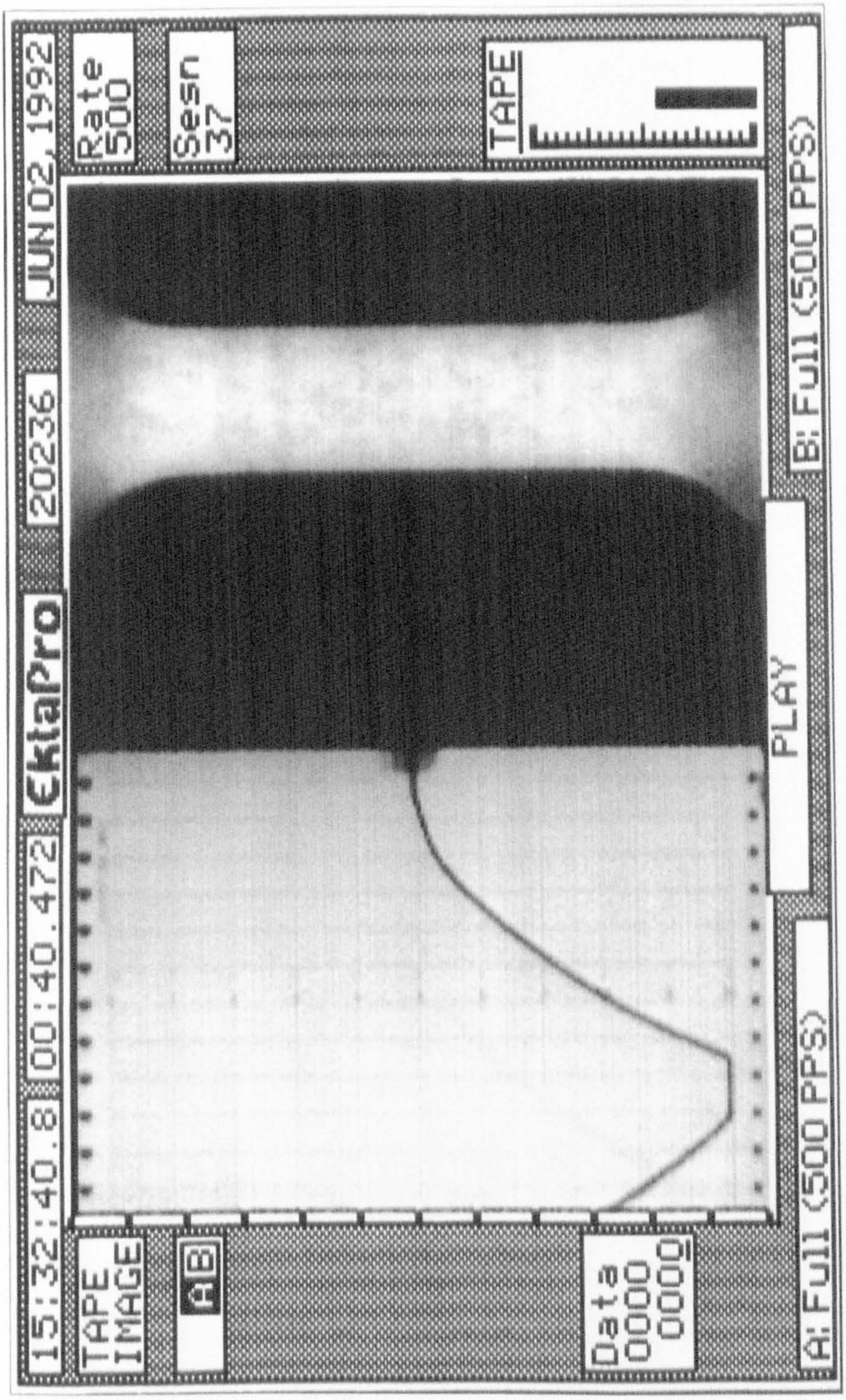

Figure 8.020 Part of a series from figure 8.015 to 8.022

Sixth print from a series of frames showing a loading-unloading test of a specimen of red deer antler

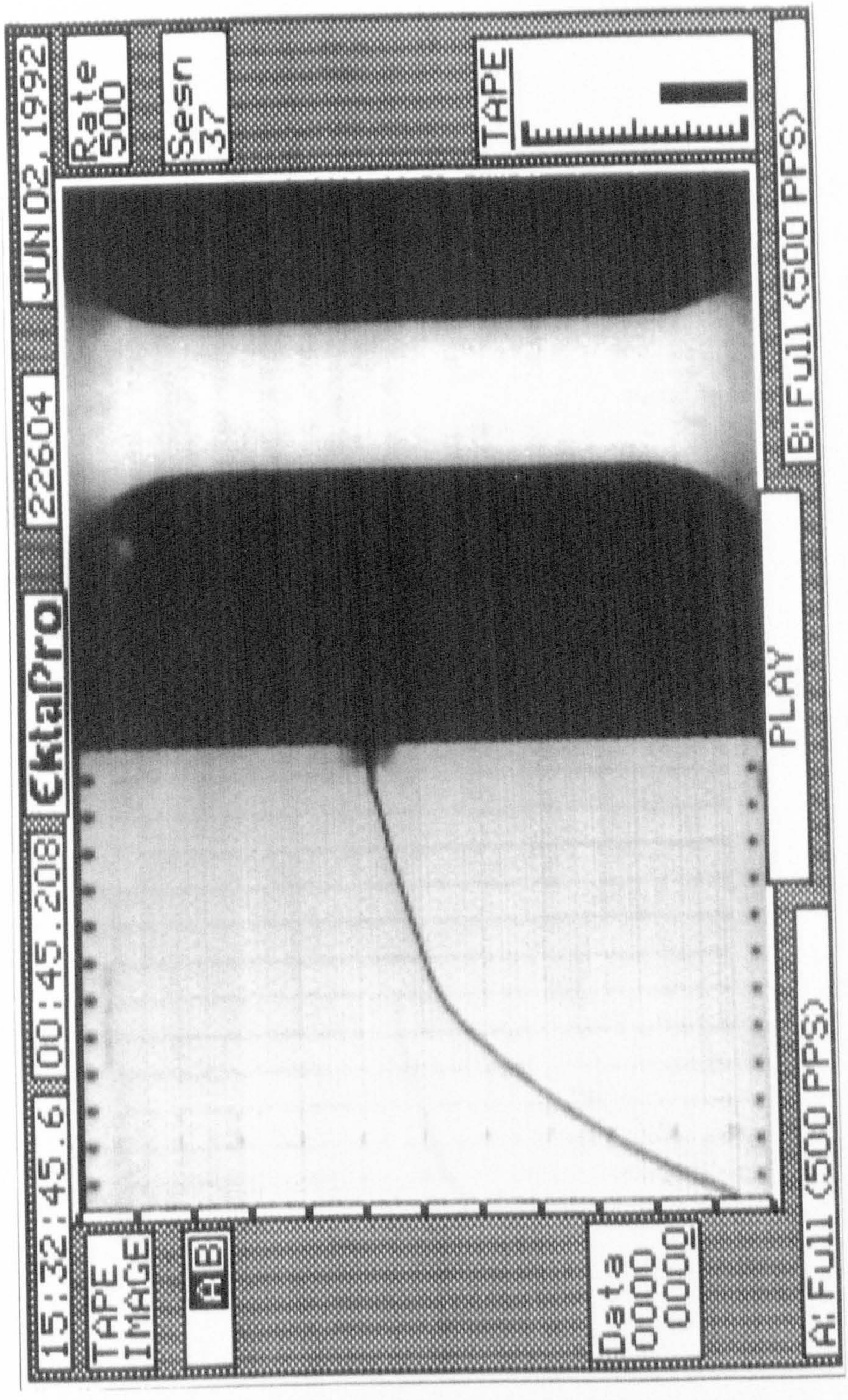

Figure 8.021 Part of a series from figure 8.015 to 8.022

Seventh print from a series of frames showing a loading-unloading test of a specimen of red deer antler

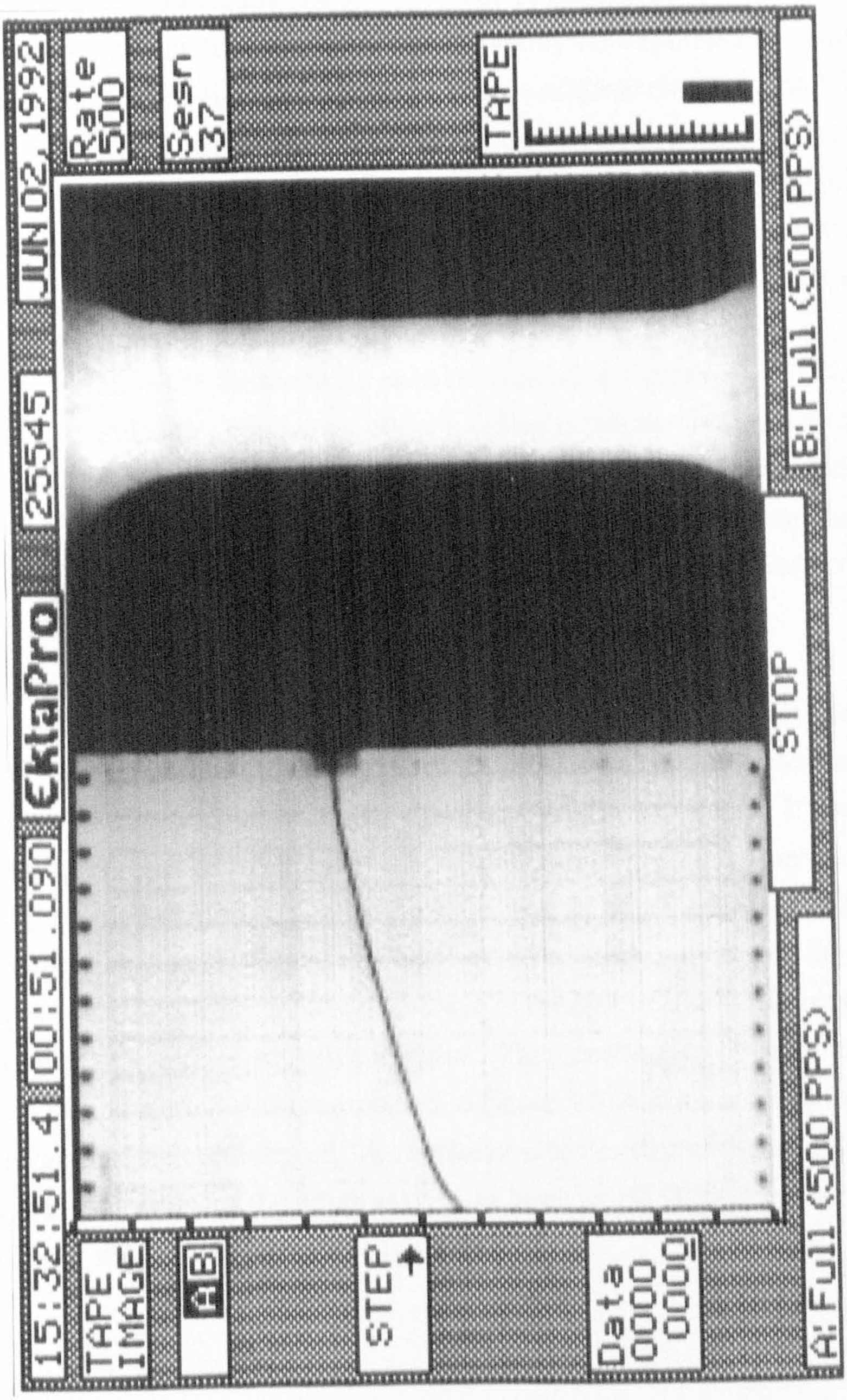

Figure 8.022 Part of a series from figure 8.015 to 8.022

Eighth print from a series of frames showing a loading-unloading test of a specimen of red deer antler

8.7. OPTICAL CHANGES OBSERVED DURING NOTCH SENSITIVITY TESTING

The effect of a machined notch (or other lack of homogeneity) is to concentrate the stress, and thus strain at the tip of such a discontinuity (as explained in chapter 5). (Unless the material is notch insensitive, which neither of these materials are.) It was observed that whitening is concentrated around the discontinuity as shown below and in appendix 11. This effect was captured with each arrangement of recording equipment previously described. However, the results presented here are from the tests recorded using the first configuration of video equipment (figure 8.003). The mechanical aspects of these tests have already been examined in sections 7.5, 7.6, 7.8 and 7.9. To demonstrate the extremes of the notch tip radii the following figures are of SEN specimens of bone and antler containing either a drilled notch tip created with the largest drill used in data sets NA4 and NB4 (from which the specimens come), or a notch that was cut with the Exakt diamond saw (as described in appendix 2). (The mechanical data for these specimens is within data set NA5 and NB5.) These four tests were conducted at a cross-head speed of 8.33×10^{-5} m s^{-1}.

In chapter 7 (and especially in section 7.4.3.5) I pointed out that the idea of strain in relation to notched specimens is perhaps not the ideal measure. The images in following figures clearly demonstrate why this measure is questionable. If the previous evidence is accepted, that whitening is related to the knee in the tensile curve, then this suggests that areas that exhibit such whitening are more highly loaded and deformed than areas that do not show such a response. Therefore these images show that the stresses and strain around the notch are greater than those in the bulk material. This is what would be expected for a notch sensitive material. This localisation of strain is most clearly shown when figure 8.036 is compared to figure 8.034, which shows the same specimen before loading commenced. A comparison of the size of the notch suggests that the strain in the region of the notch may be as large as 100%, clearly the averaged strain is far lower than this remarkably high value.

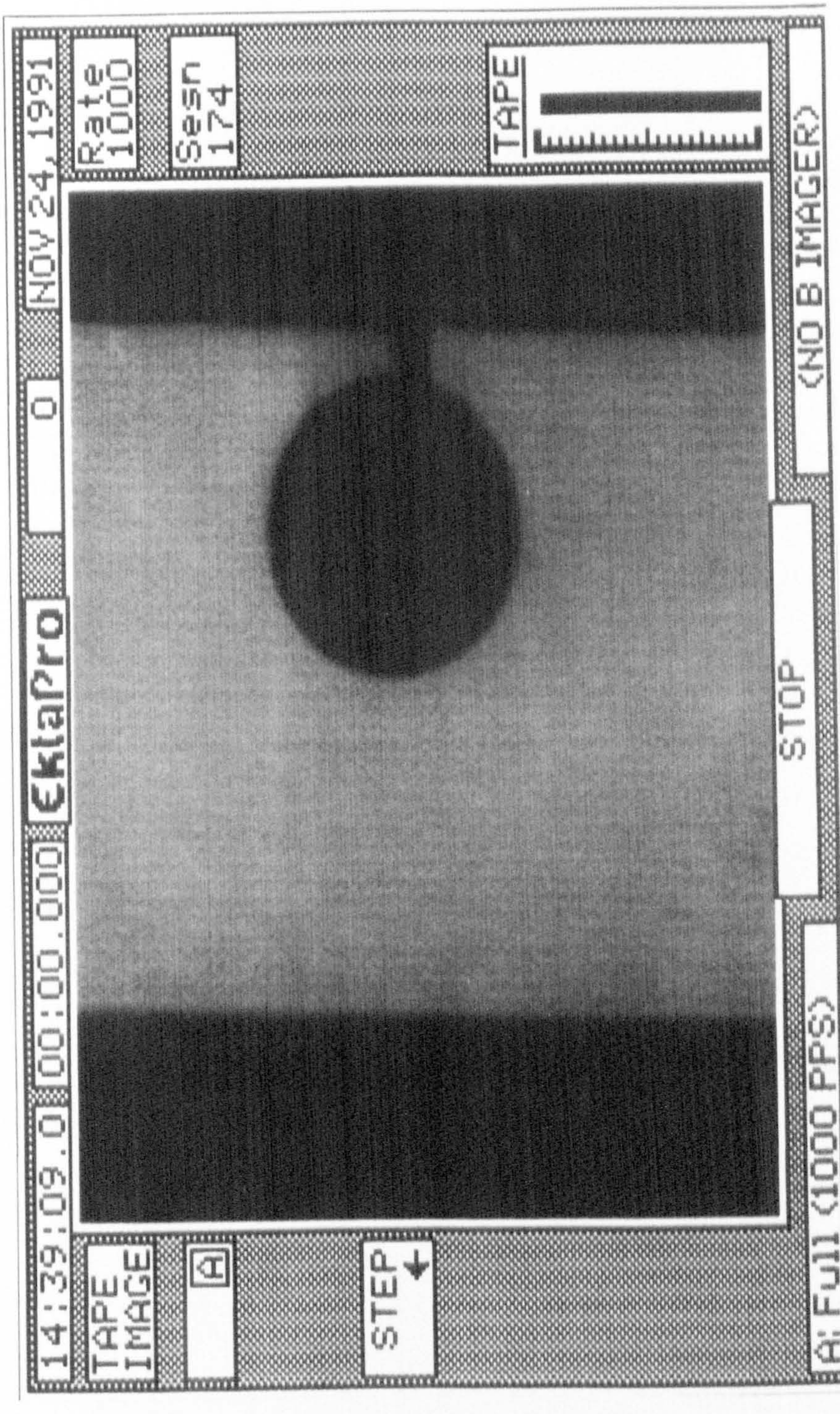

Specimen 10/11/91/01

Figure 8.023 Part of a series from figure 8.023 to 8.027

First print from a series of frames showing a test of an SEN specimen of red deer antler with a large notch tip radius

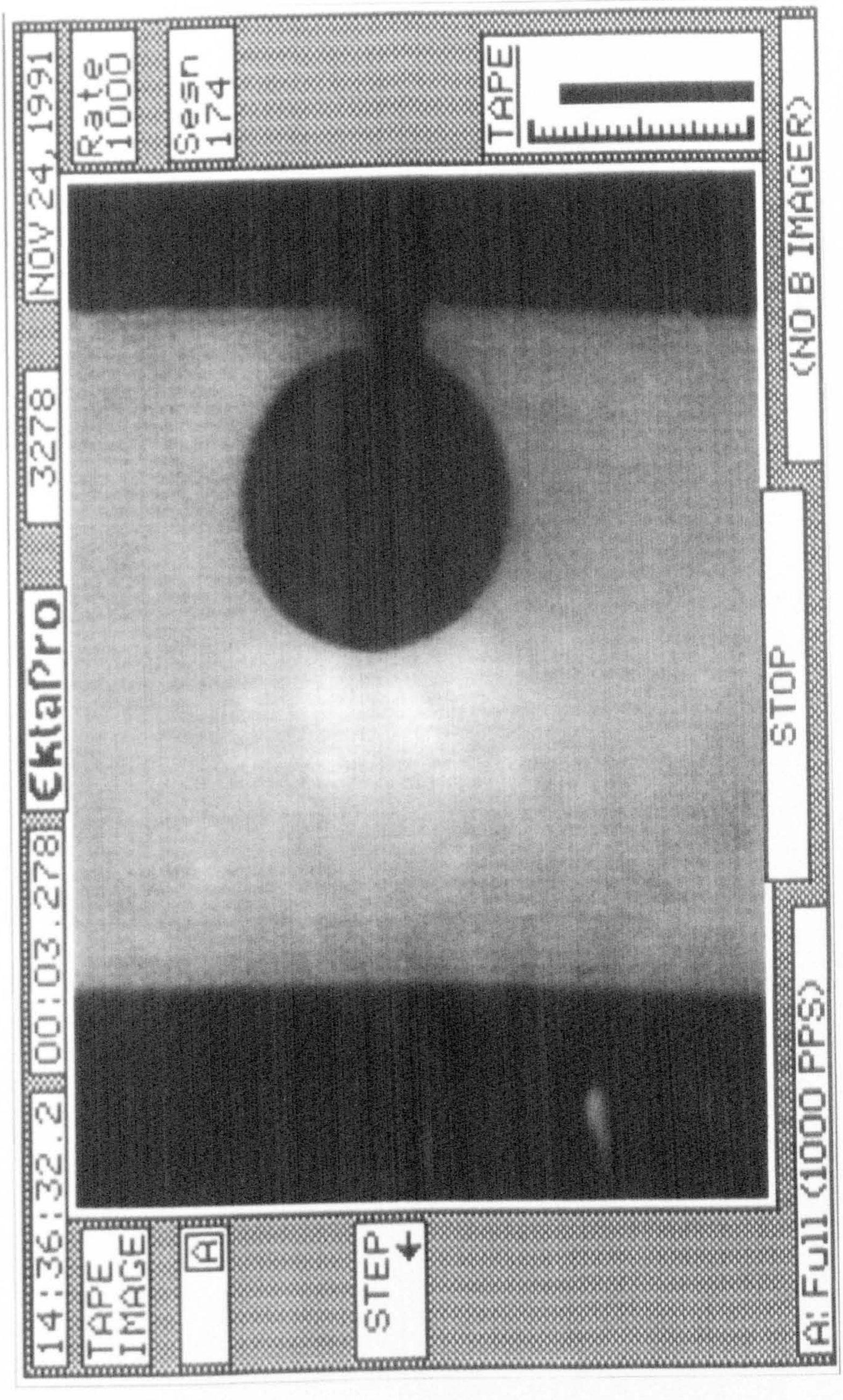

Specimen 10/11/91/01

Figure 8.024 Part of a series from figure 8.023 to 8.027

Second print from a series of frames showing a test of an SEN specimen of red deer antler with a large notch tip radius

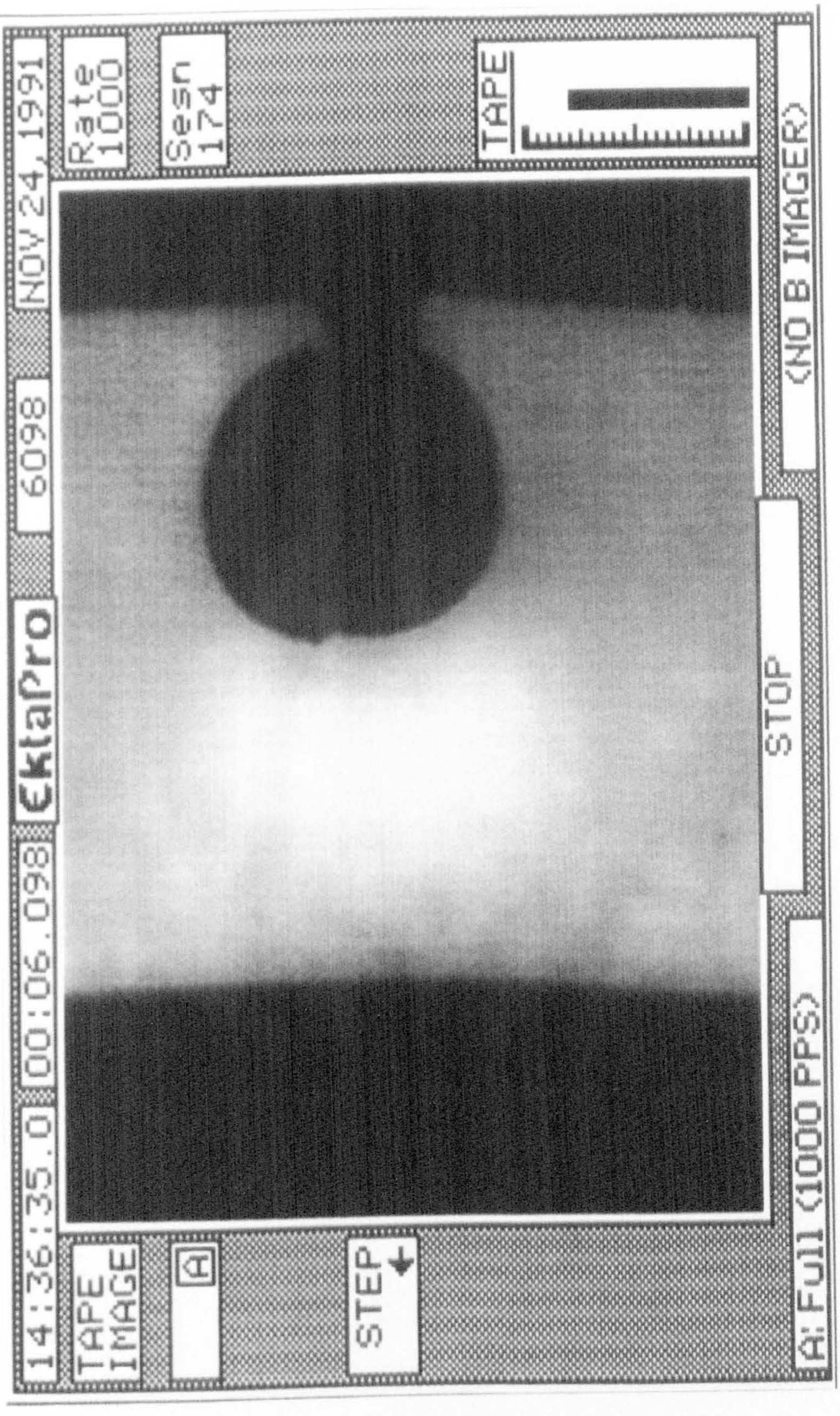

Specimen 10/11/91/01

Figure 8.025 Part of a series from figure 8.023 to 8.027

Third print from a series of frames showing a test of an SEN specimen of red deer antler with a large notch tip radius

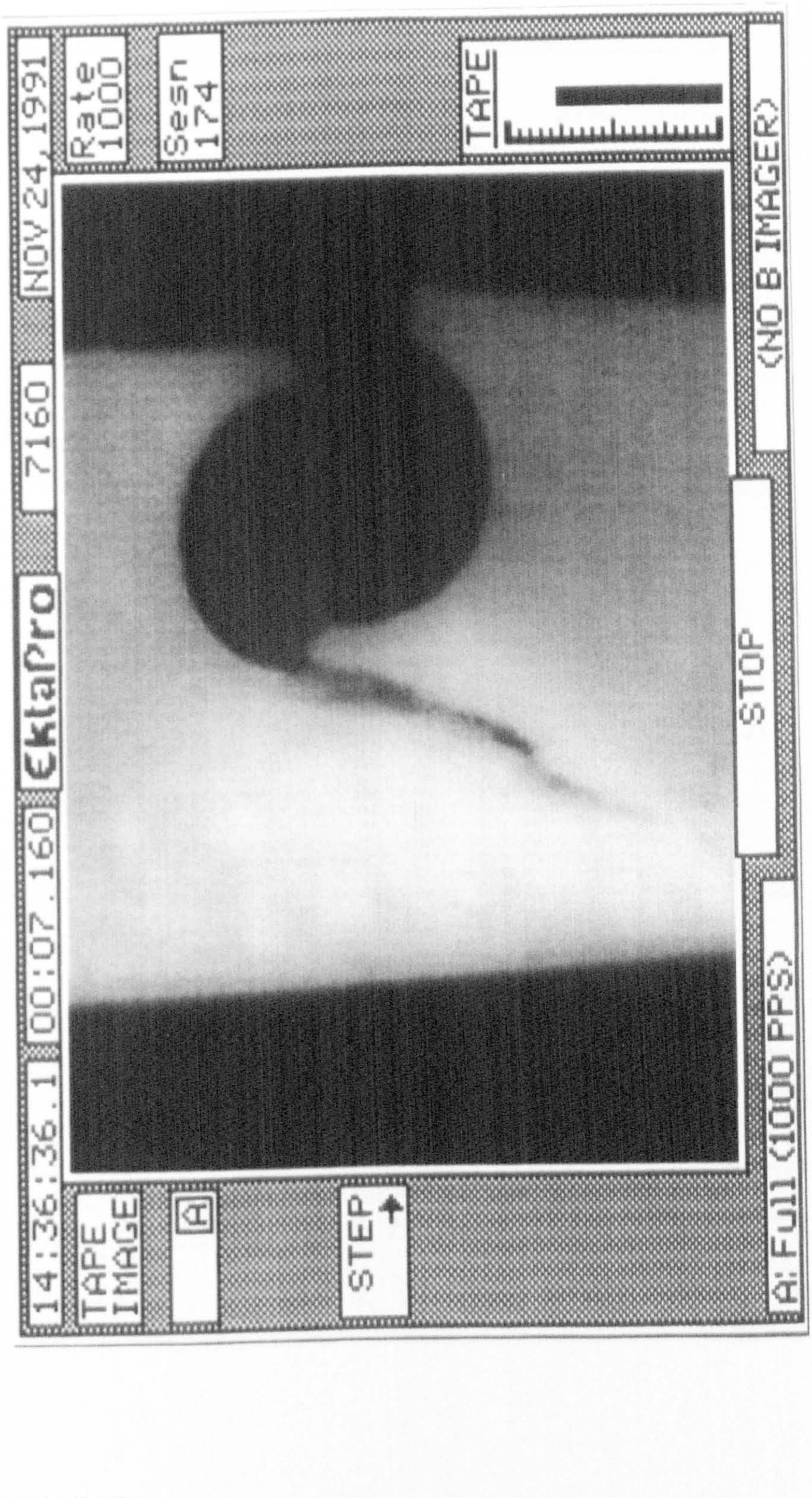

Specimen 10/11/91/01

Figure 8.026 Part of a series from figure 8.023 to 8.027

Fourth print from a series of frames showing a test of an SEN specimen of red deer antler with a large notch tip radius

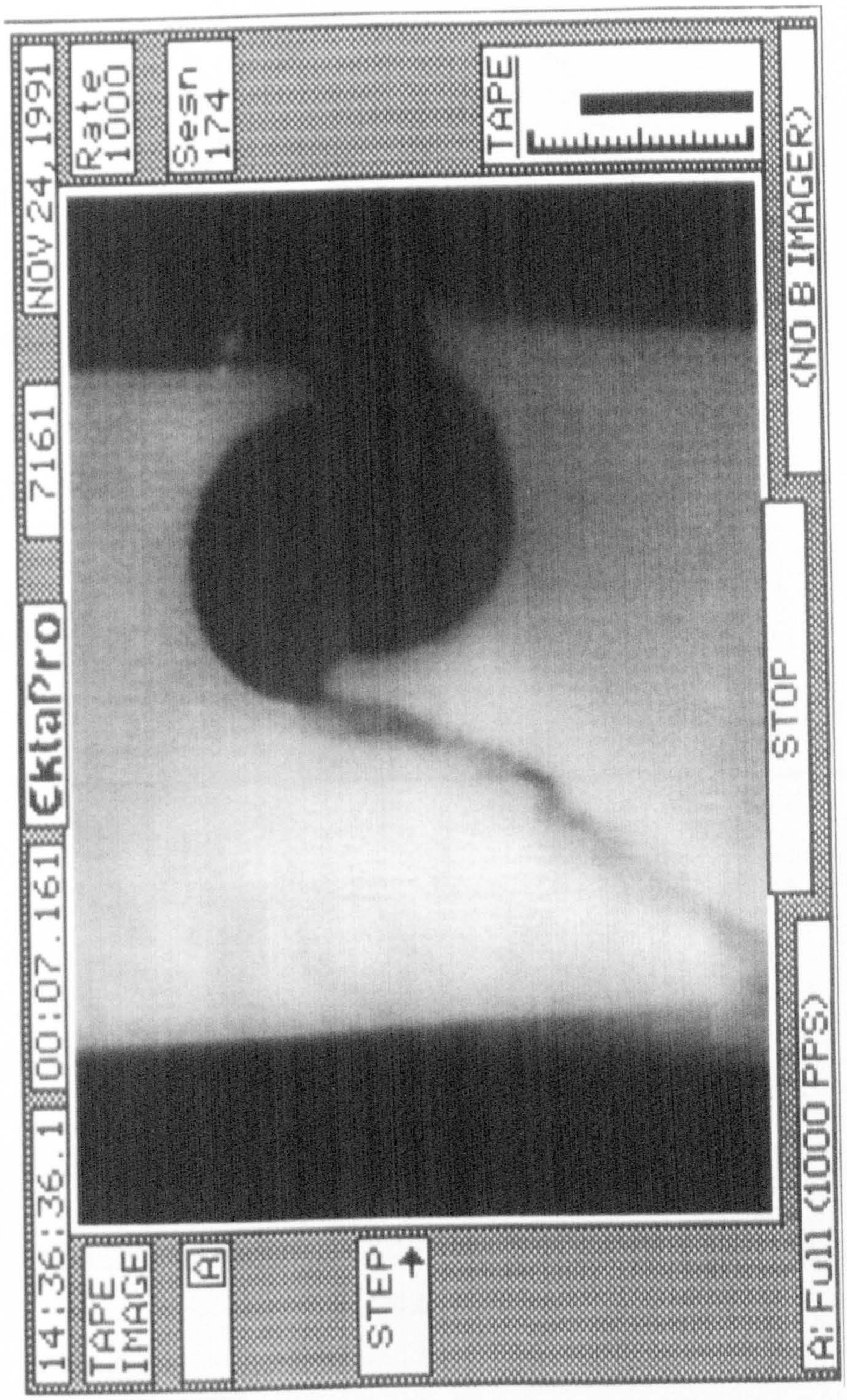

Specimen 10/11/91/01. First image of total failure

Figure 8.027 Part of a series from figure 8.023 to 8.027

Fifth print from a series of frames showing a test of an SEN specimen of red deer antler with a large notch tip radius

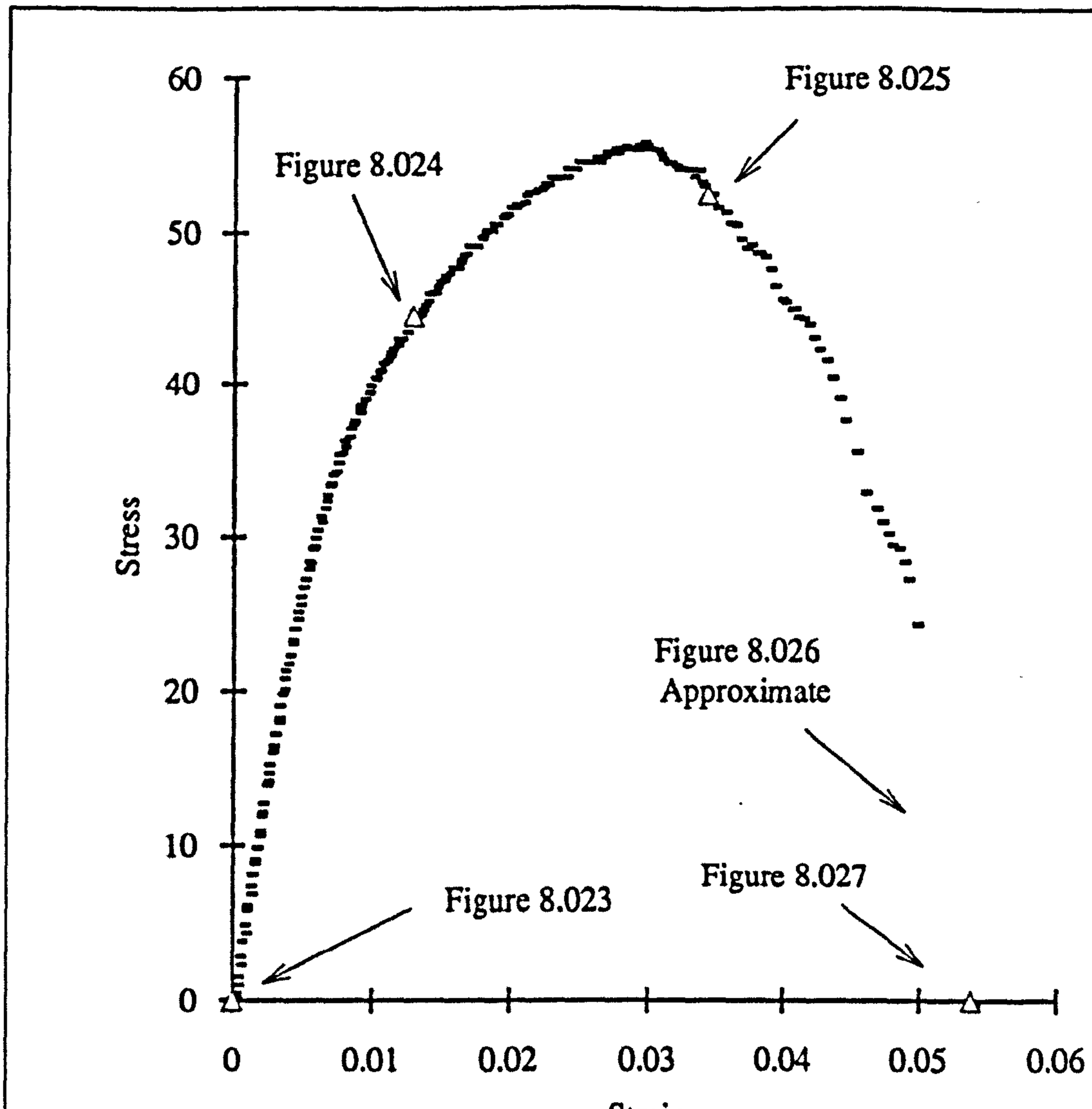

Units:

σ Stress, MPa

ε Strain, unitless

Comments:

Specimen 10/11/91/01. See notes in text regarding the definition of strain.

Figure 8.028

The positions of the images in figures 8.023 to 8.027 relative to the mechanical behaviour of the specimen

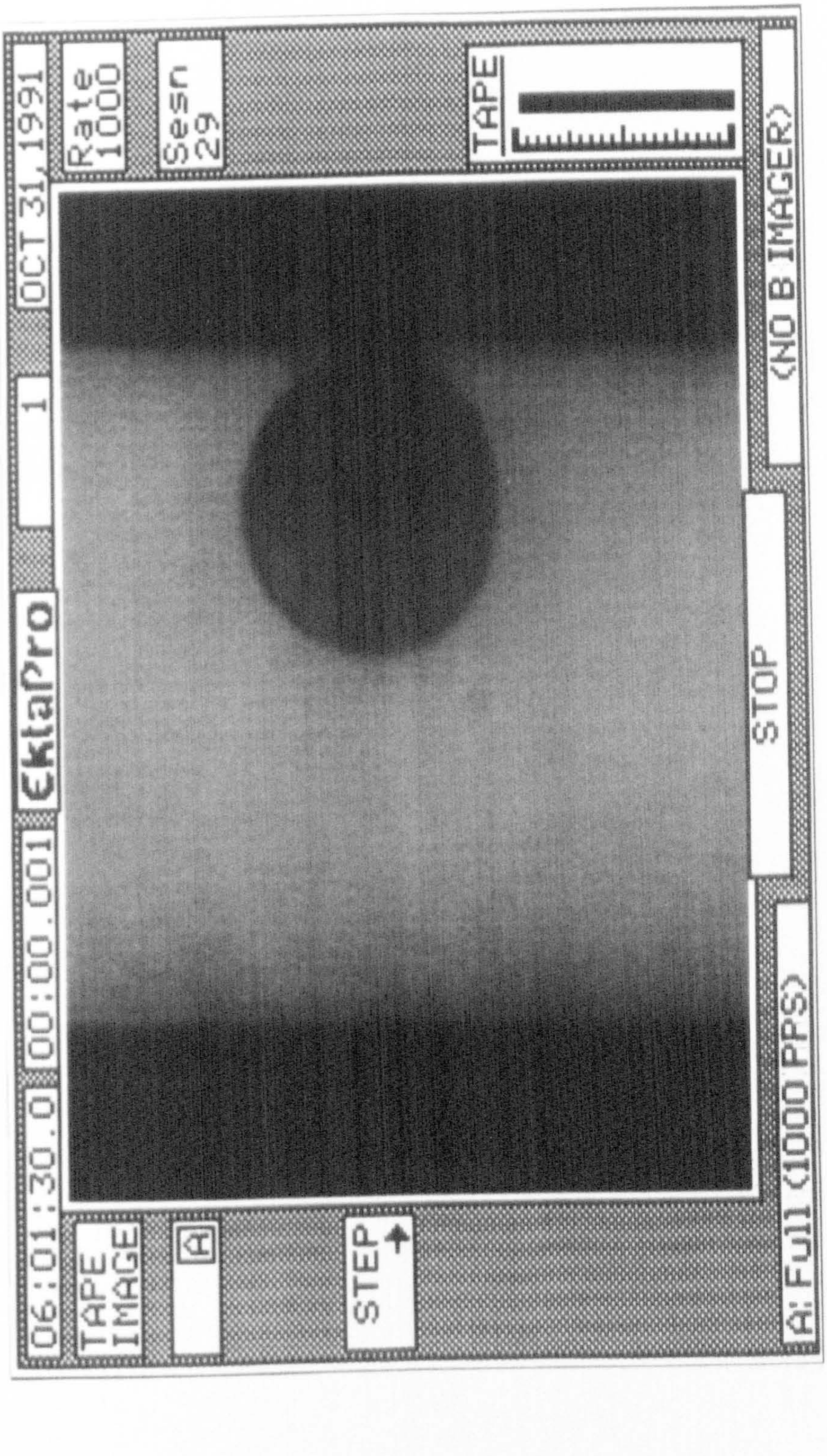

Specimen 28/10/91/32

Figure 8.029 Part of a series from figure 8.029 to 8.032

First print from a series of frames showing a test of an SEN specimen of bovine femoral bone with a large notch tip radius

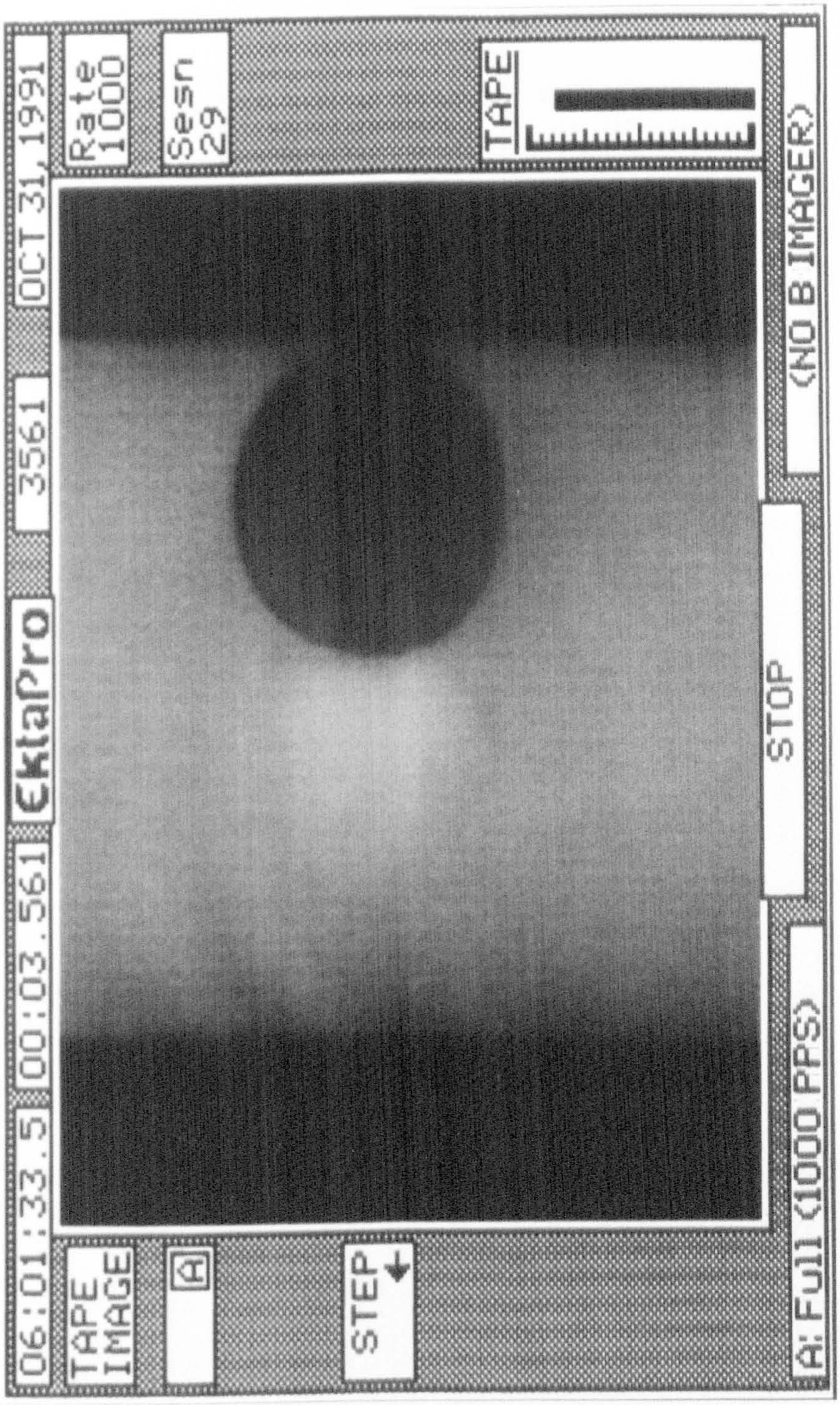

Specimen 28/10/91/32

Figure 8.030 Part of a series from figure 8.029 to 8.032

Second print from a series of frames showing a test of an SEN specimen of bovine femoral bone with a large notch tip radius

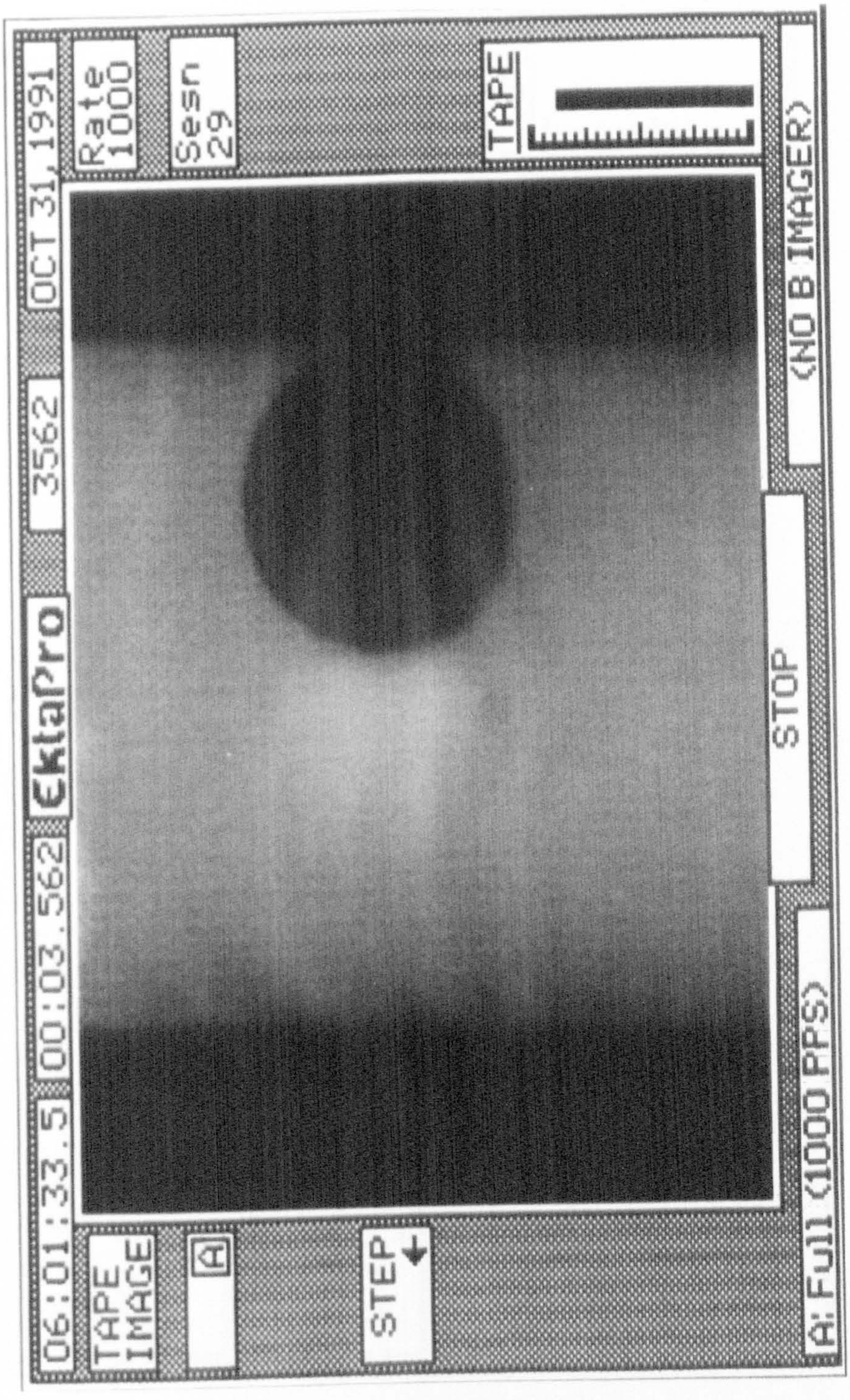

Specimen 28/10/91/32

Figure 8.031 Part of a series from figure 8.029 to 8.032

Third print from a series of frames showing a test of an SEN specimen of bovine femoral bone with a large notch tip radius

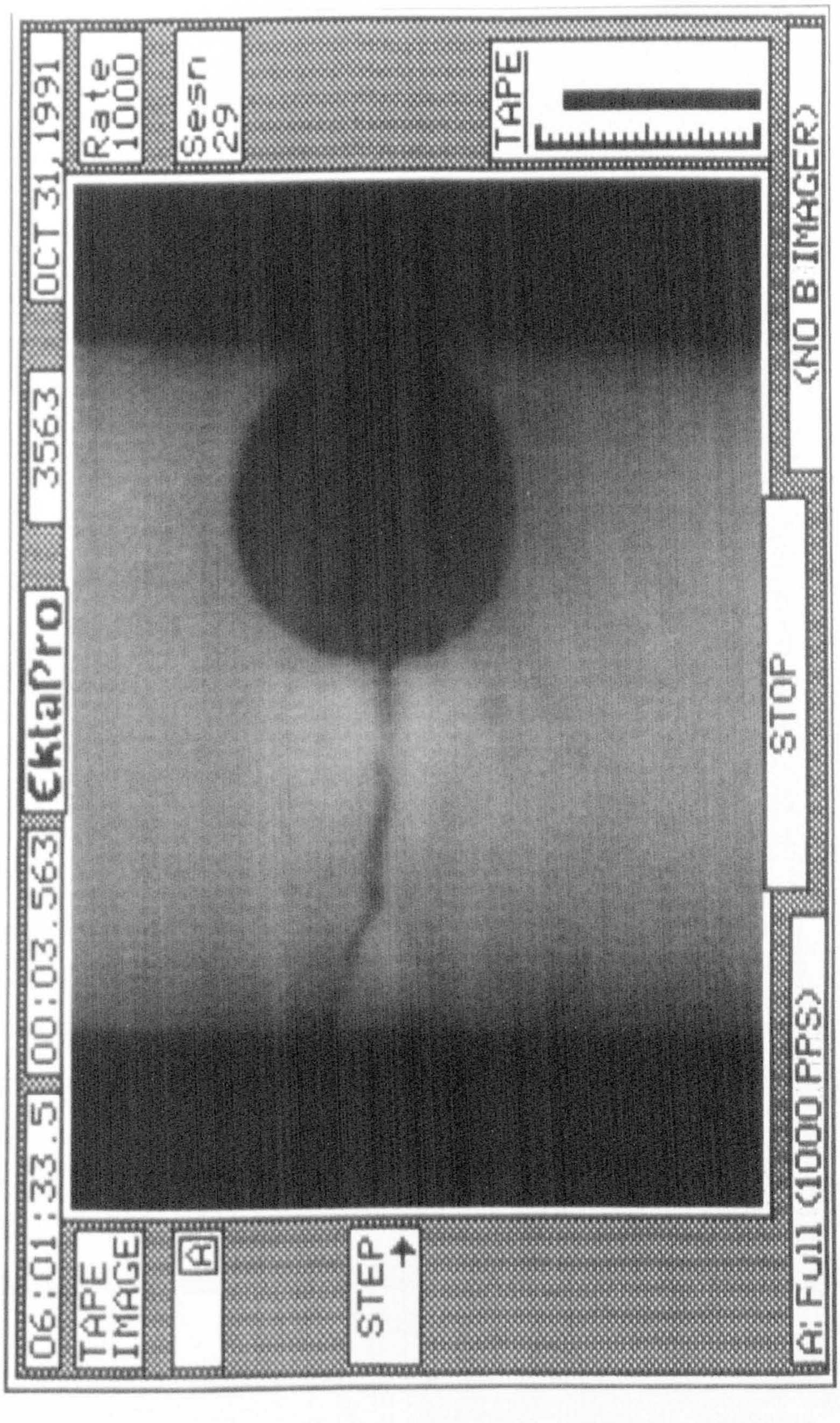

Specimen 28/10/91/32 First image of total failure

Figure 8.032 Part of a series from figure 8.029 to 8.032

Fourth print from a series of frames showing a test of an SEN specimen of bovine femoral bone with a large notch tip radius

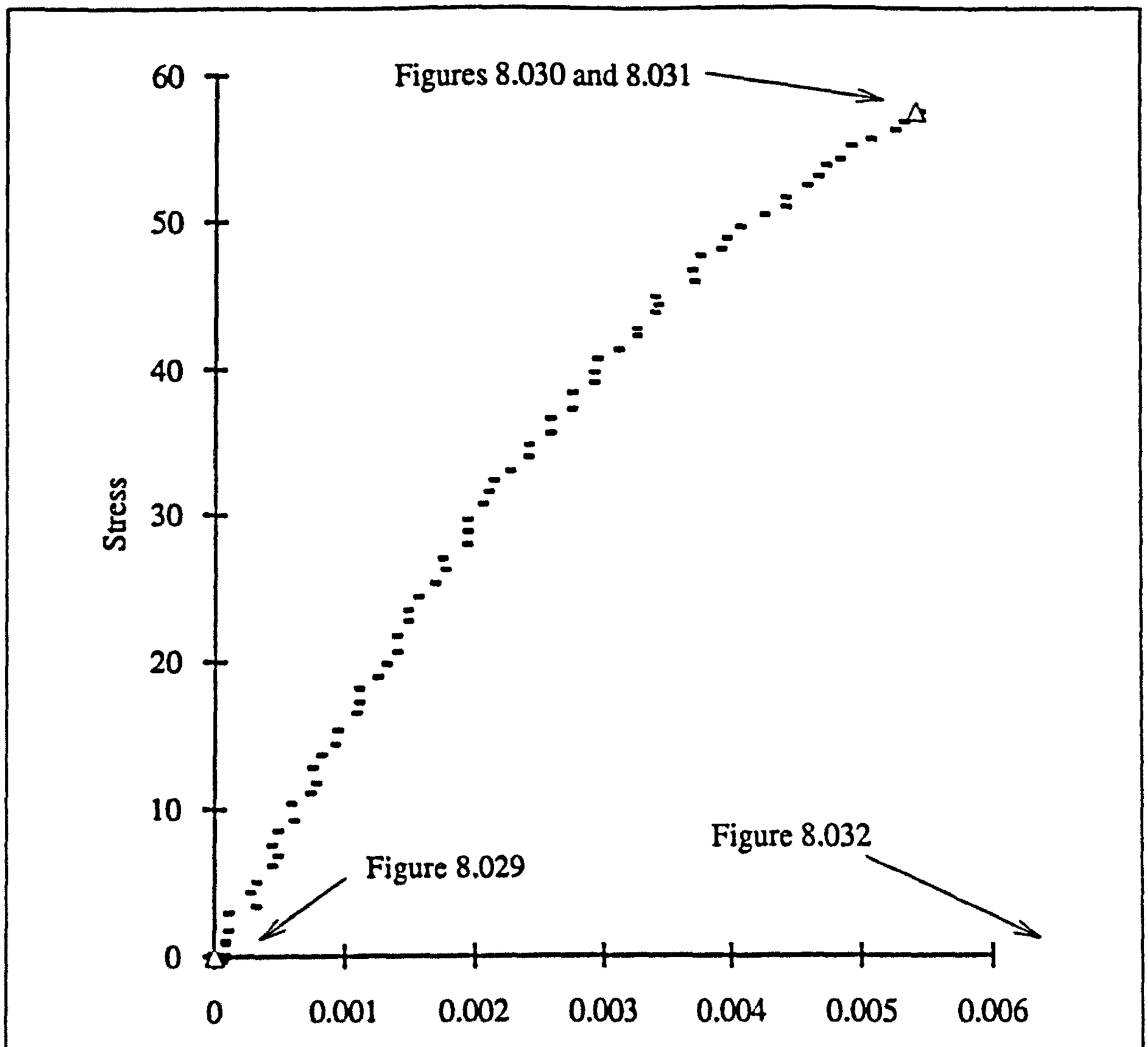

Units:

σ Stress, MPa

ε Strain, unitless

Comments:

Specimen 28/10/91/32.

Figure 8.033

The positions of the images in figures 8.029 to 8.032 relative to the mechanical behaviour of the SEN specimen of bovine bone

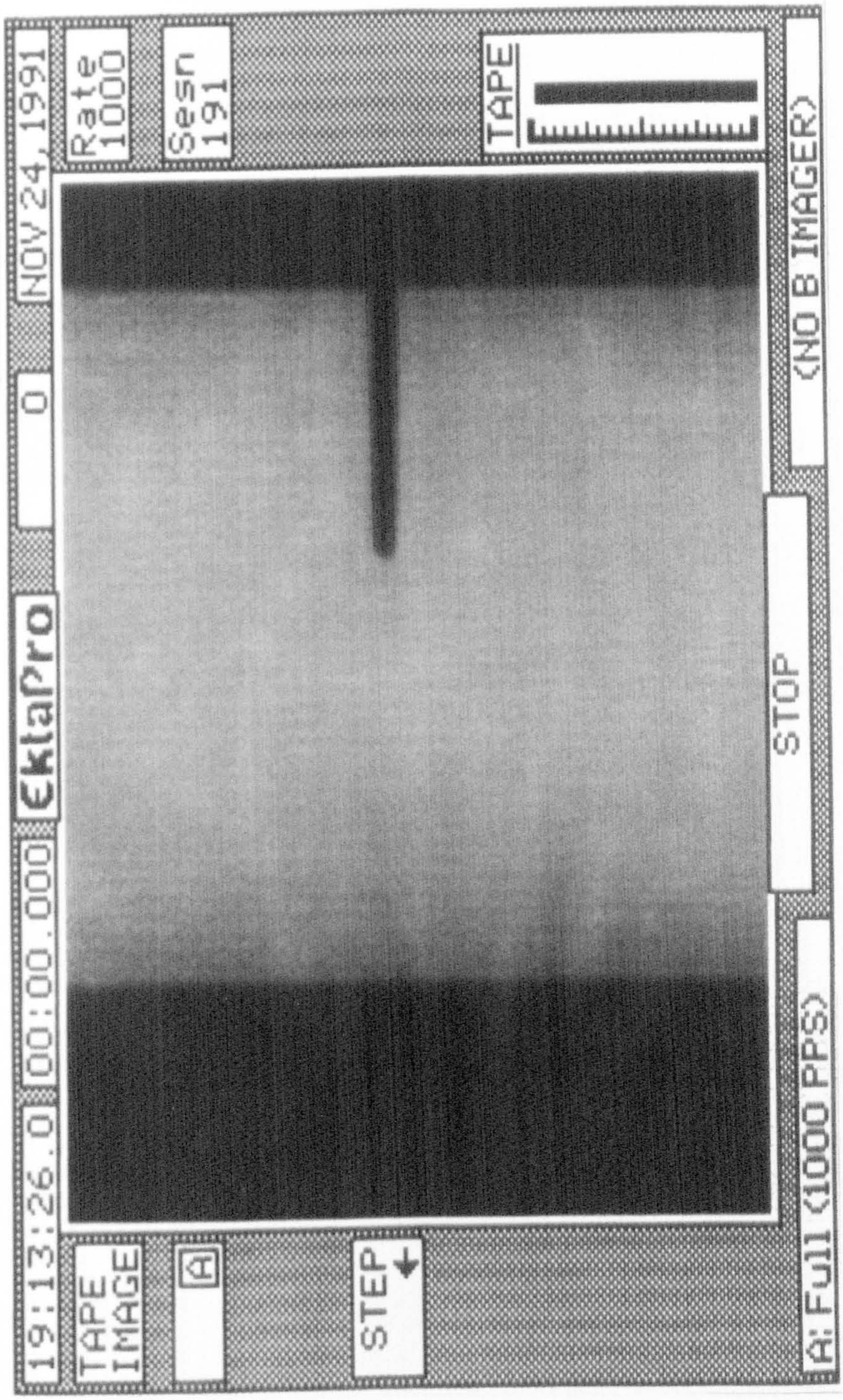

Specimen 10/11/91/14

Figure 8.034 Part of a series from figure 8.034 to 8.036

First print from a series of frames showing a test of an SEN specimen of red deer antler with a small notch tip radius

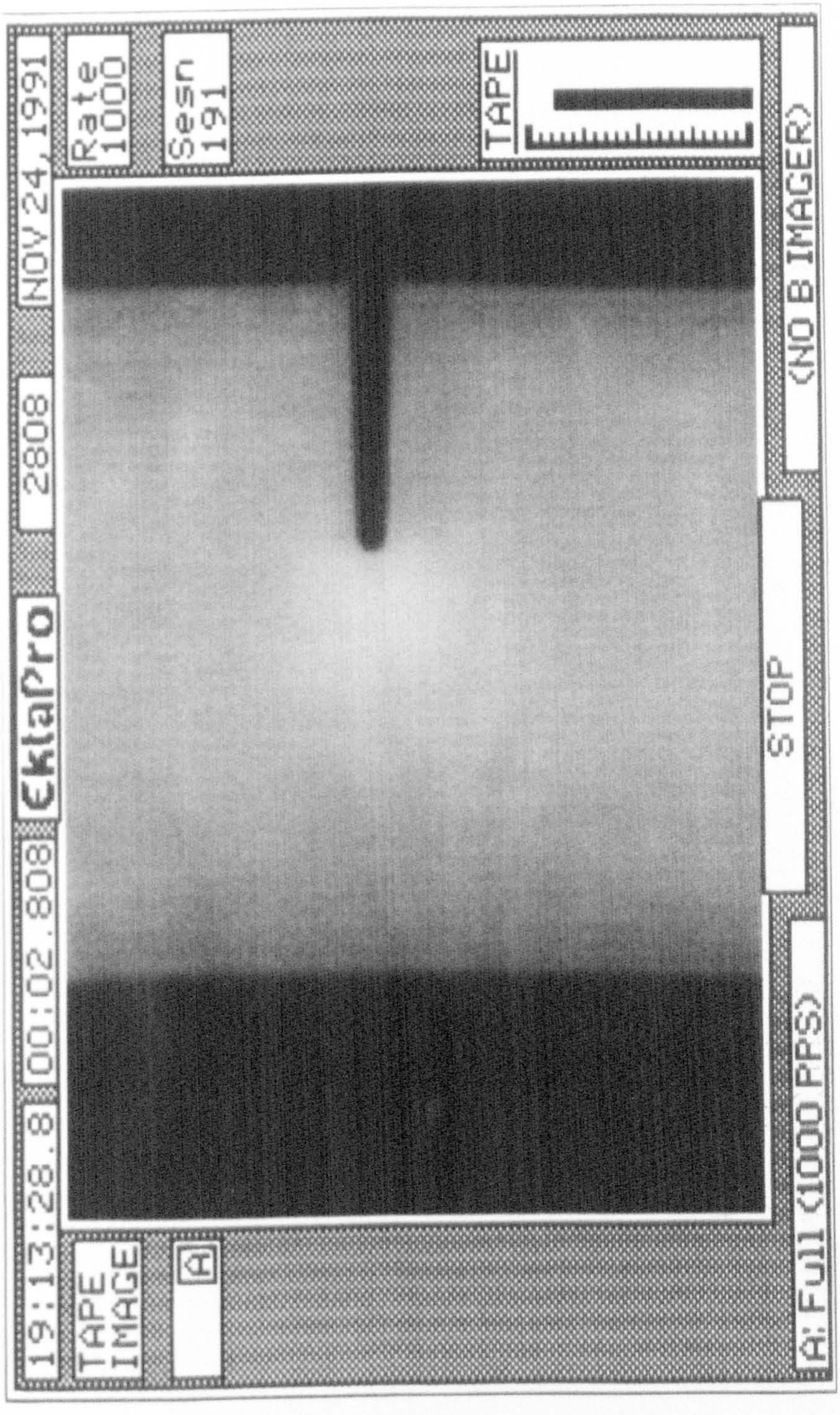

Specimen 10/11/91/14

Figure 8.035 Part of a series from figure 8.034 to 8.036

Second print from a series of frames showing a test of an SEN specimen of red deer antler with a small notch tip radius

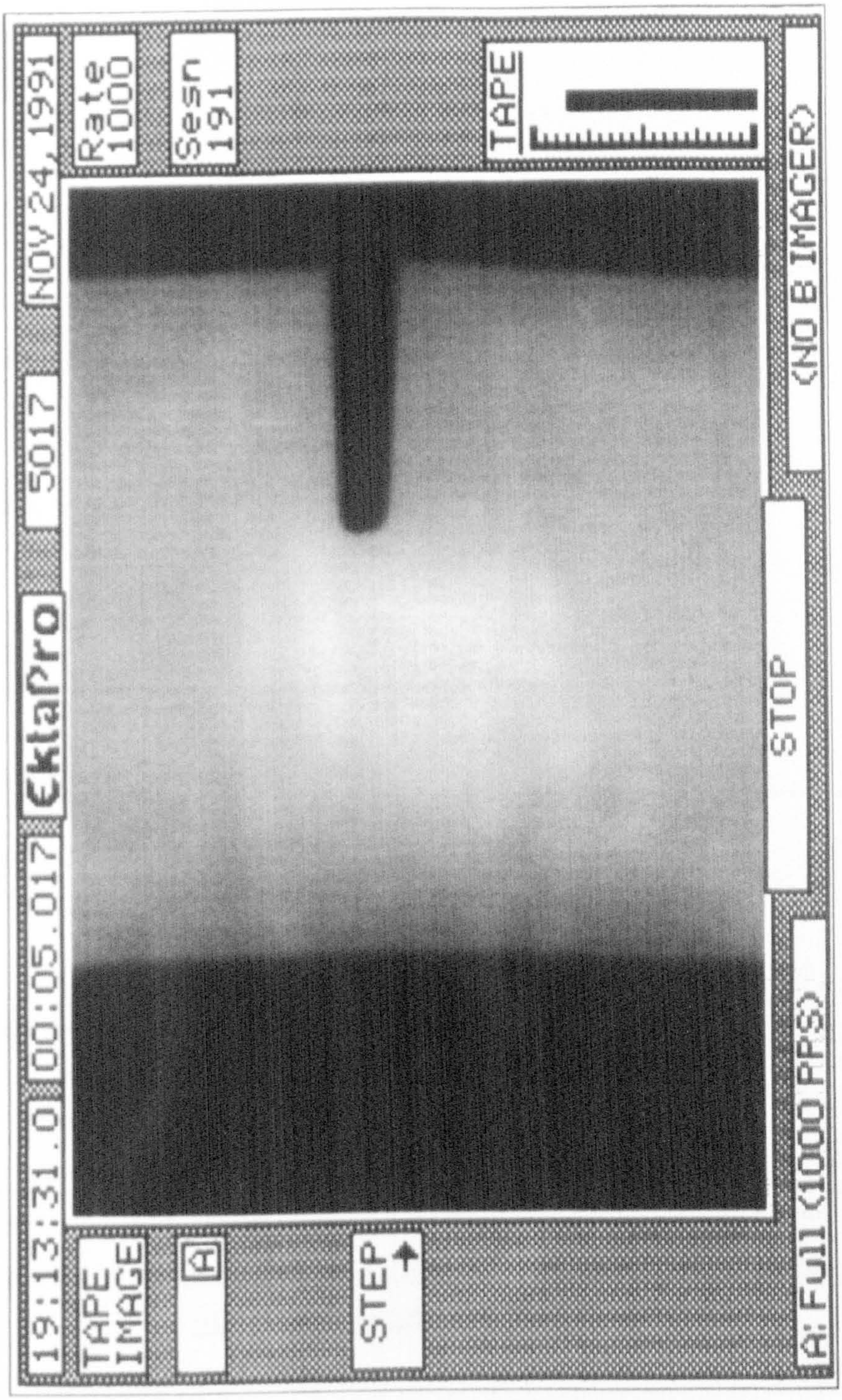

Specimen 10/11/91/14. Total failure occurs when time = 6.746 seconds

Figure 8.036 Part of a series from figure 8.034 to 8.036

Third print from a series of frames showing a test of an SEN specimen of red deer antler with a small notch tip radius

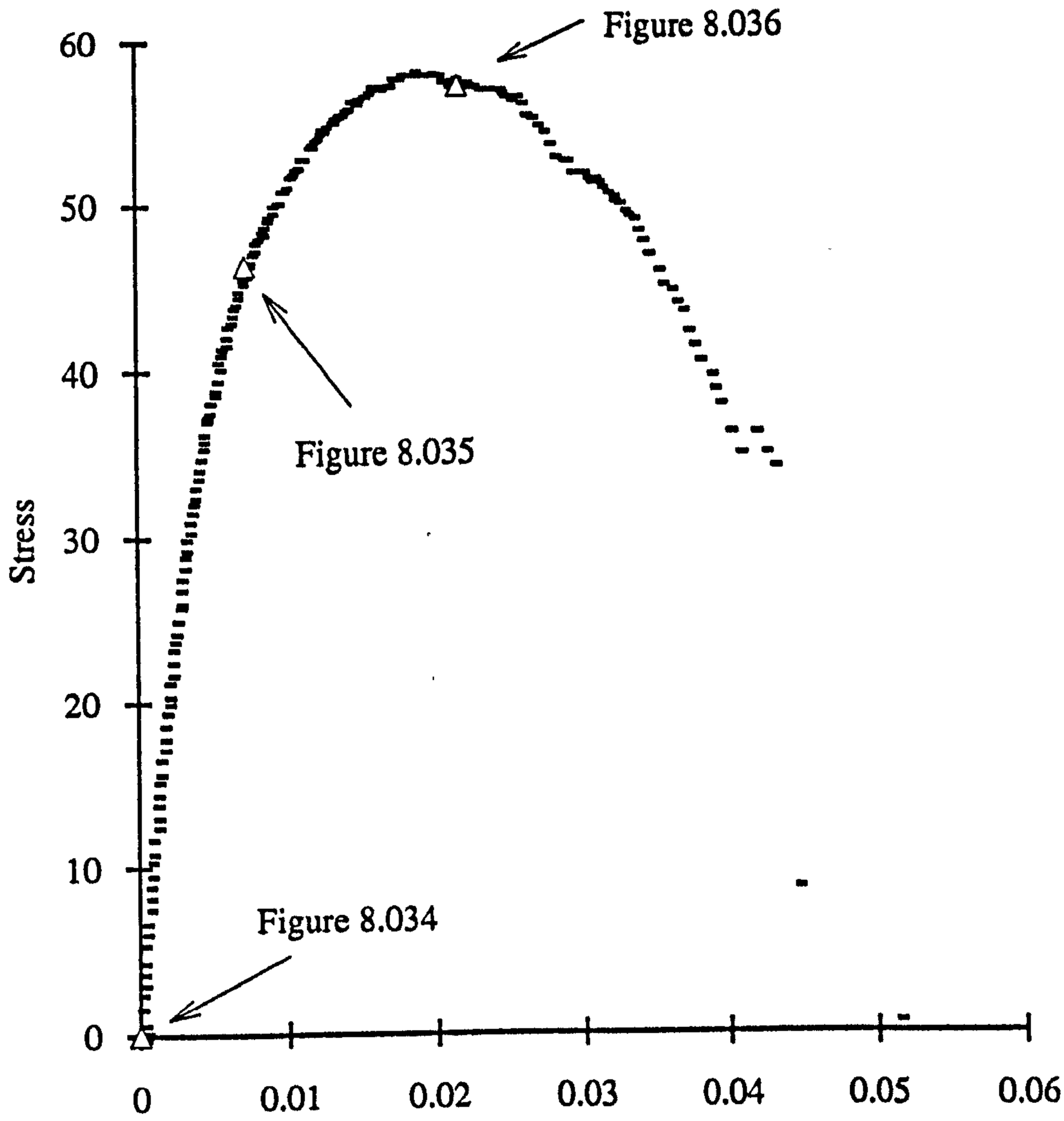

Units:

σ Stress, MPa

ε Strain, unitless

Comments:

Specimen 10/11/91/14.

Figure 8.037

The positions of the images in figures 8.034 to 8.036 relative to the mechanical behaviour of the SEN specimen of red deer antler

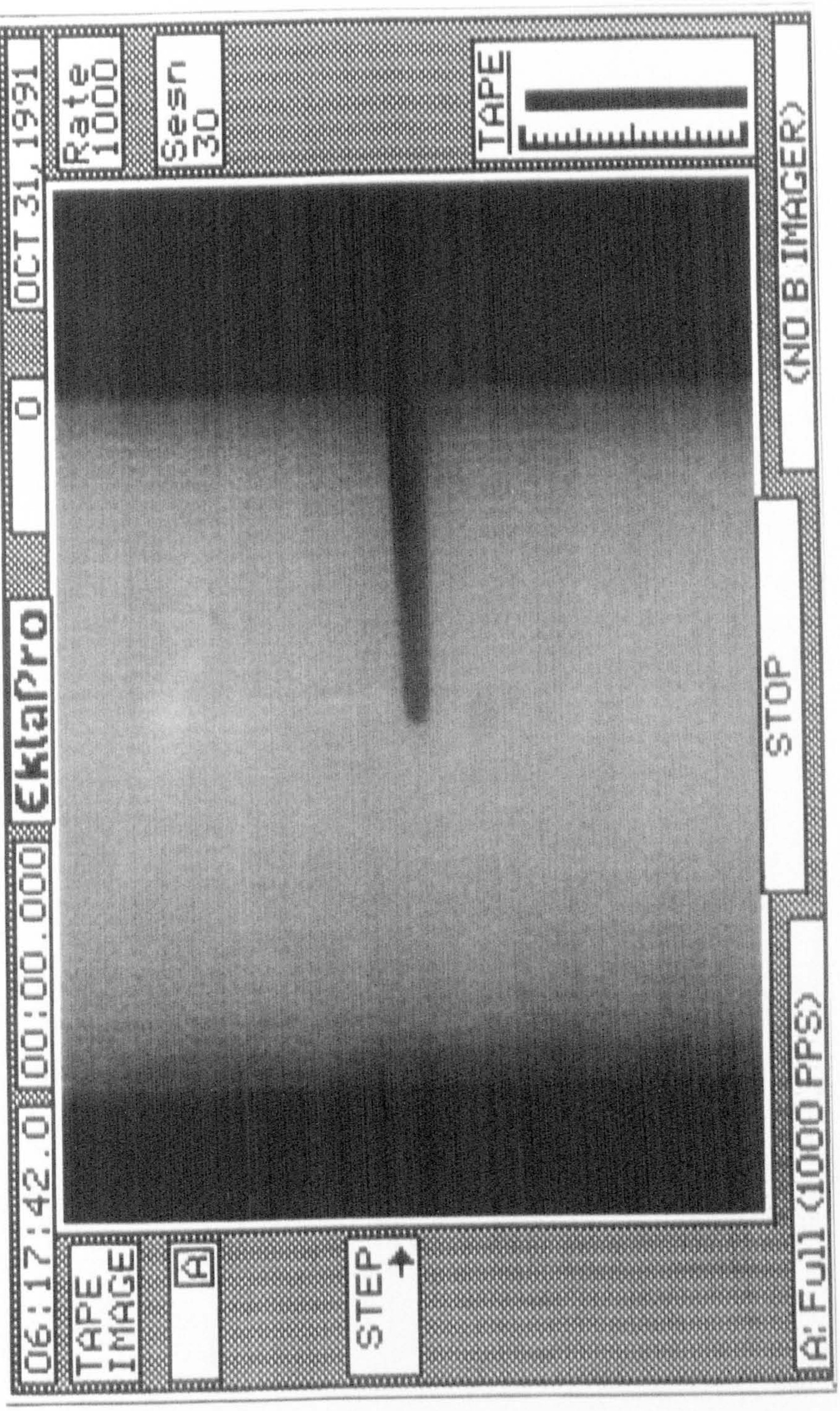

Specimen 28/10/91/28

Figure 8.038 Part of a series from figure 8.038 to 8.040

First print from a series of frames showing a test of an SEN specimen of bovine femoral bone with a small notch tip radius

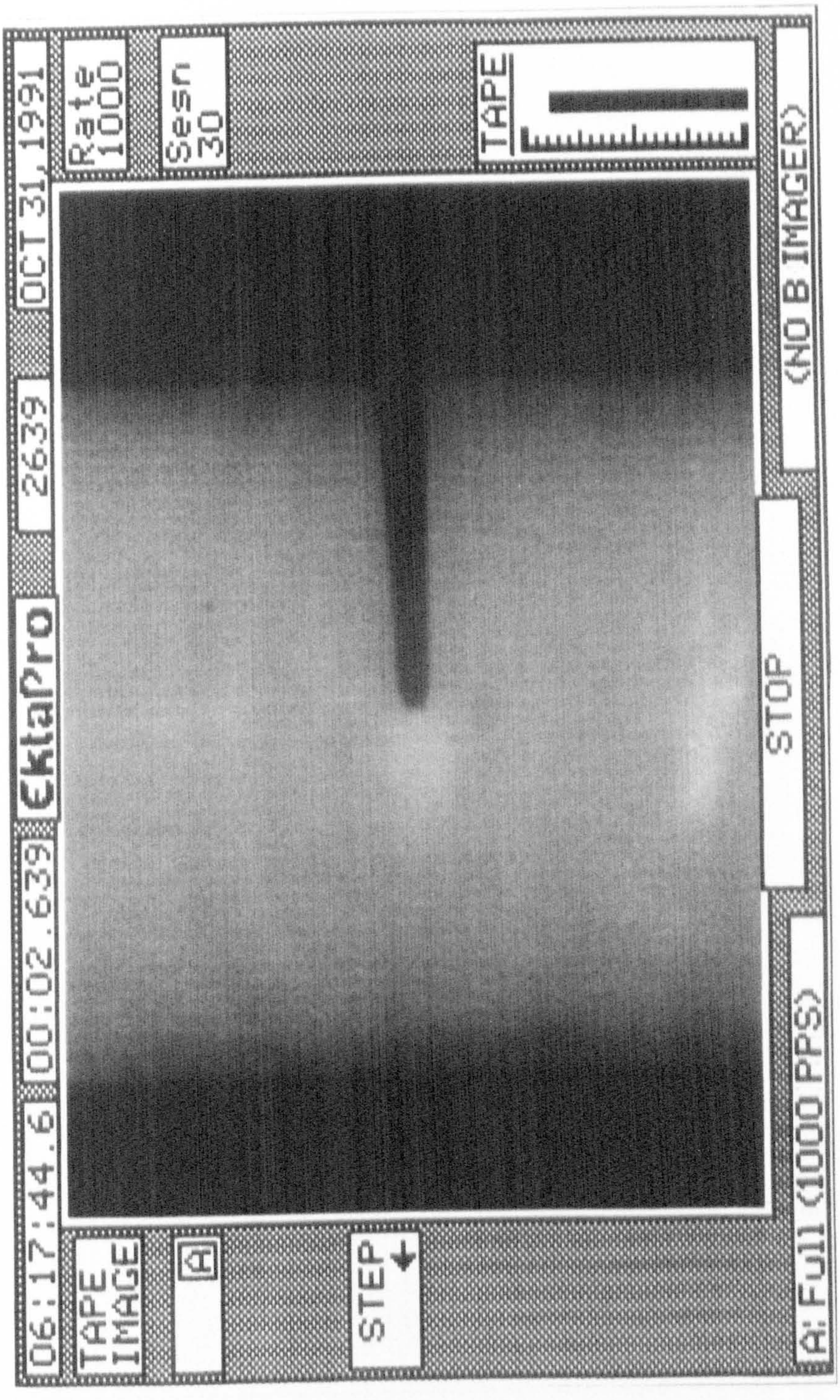

Specimen 28/10/91/28

Figure 8.039 Part of a series from figure 8.038 to 8.040

Second print from a series of frames showing a test of an SEN specimen of bovine femoral bone with a small notch tip radius

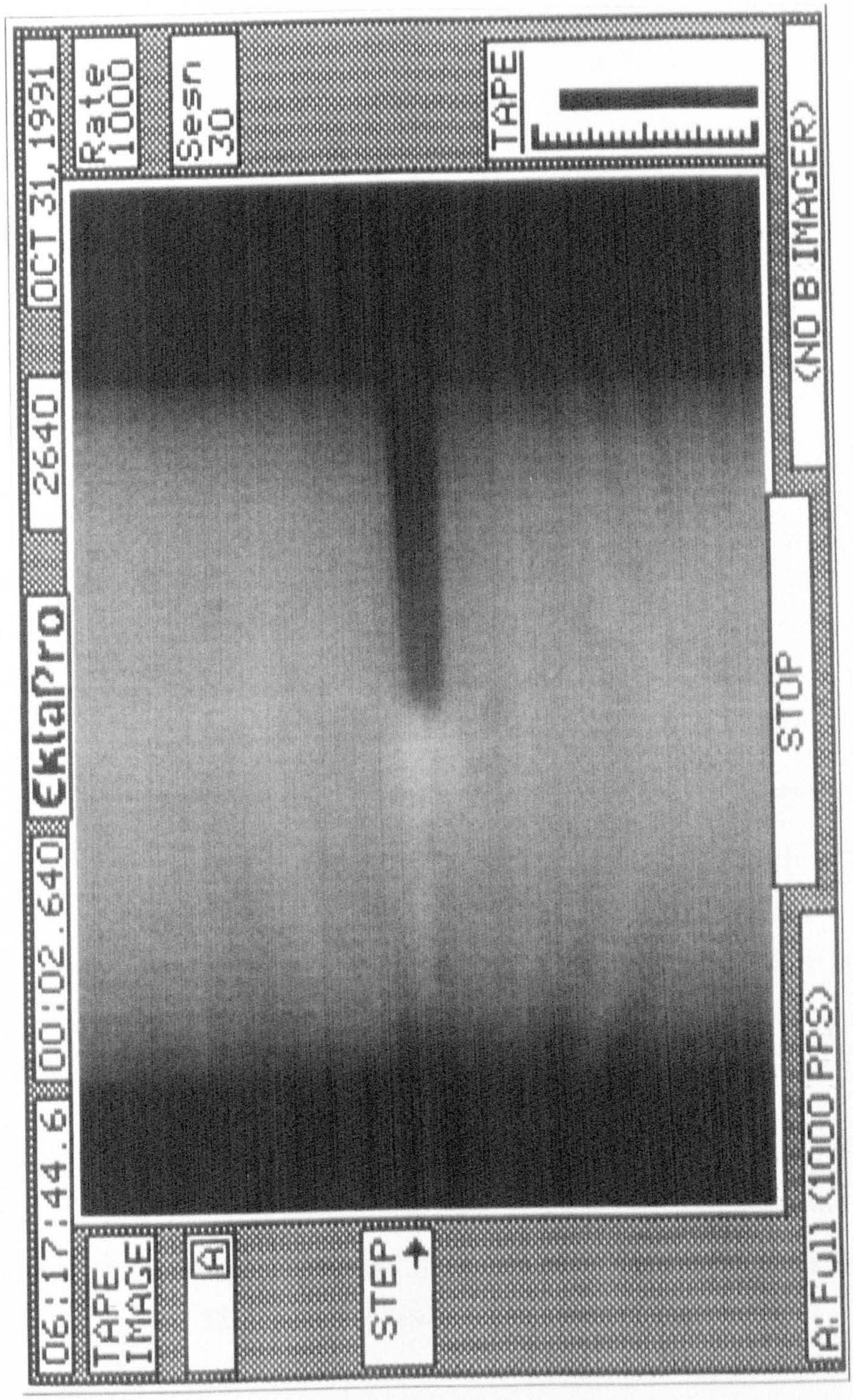

Specimen 28/10/91/28. First image of total failure.

Figure 8.040 Part of a series from figure 8.038 to 8.040

Third print from a series of frames showing a test of an SEN specimen of bovine femoral bone with a small notch tip radius

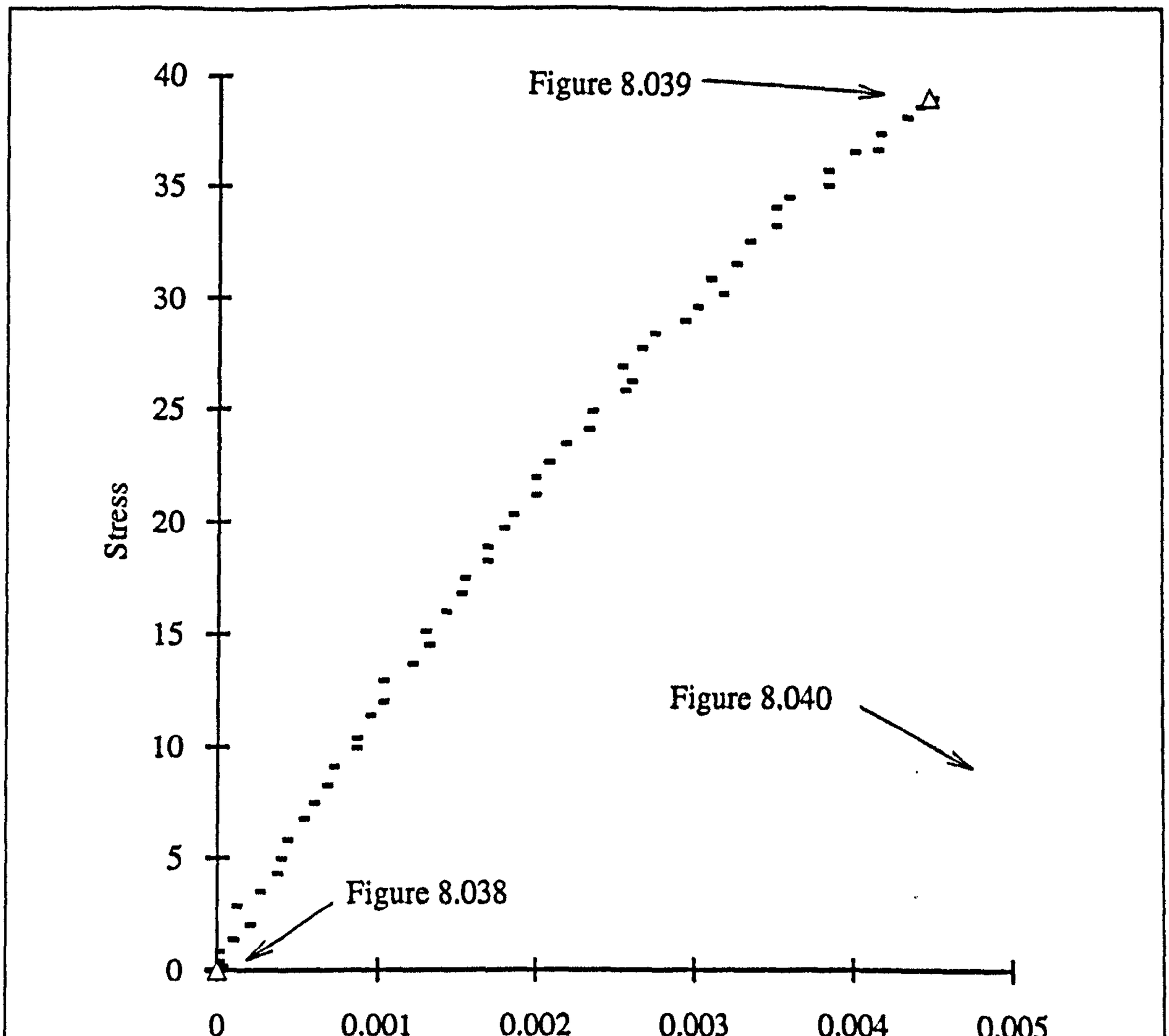

Units:

σ Stress, MPa

ε Strain, unitless

Comments:

Specimen 28/10/91/28.

Figure 8.041

The positions of the images in figures 8.038 to 8.040 relative to the mechanical behaviour of the SEN specimen of red deer antler

8.7.1. THE RELATION OF THE OPTICAL CHANGES TO THE STRUCTURAL AND MECHANICAL STATE OF THE NOTCHED SPECIMENS

During my comparison of the mechanical response of the notched specimens and their optical response (by a similar procedure to that used to create figure 8.028 and so on) it became apparent that the onset of whitening corresponded to the increased deviation from a linear response. This correlation was more noticeable in the antler specimens. This finding was only qualitative as the determination of the point at which the deviation from linearity increases was based on visual inspection and was not quantified. (For example the first whitening observed on the video recording of specimen 10/11/91/01 corresponded with a stress of 28 MPa. The mechanical response of which is shown in figure 8.028.)

The whitening appears to spread over a greater area of the antler specimens compared to those of bovine bone. However, when the length of the whitened zone at the time of the first observed fracture propagation was examined this difference was not apparent (see figure 8.042).[12] The length of the whitened zone was determined by the method explained in section 7.5.3. The suggestion of a larger whitened zone in the case of the antler specimens may be due to two factors: first, the zone is larger in the direction perpendicular to the crack; second, the increased size of the whitened zone in the antler specimens occurs after the initiation of the fracture. The second explanation is demonstrated in figures 8.043 to 8.050. Due to the slow ripping type of fracture in antler the whitened zone traverses the specimen more gradually than it does in the case of the bovine specimens. The loading-unloading tests have shown that when these materials are unloaded they may still retain some residual whitening. One consequence of the unloaded material (such as that through which a crack has passed) returning to its original appearance was a *shooting star* effect, where a bright spot was seen to travel across the specimen trailing the crack behind it. This explanation raises the question why does this not appear to occur during the fracture of bovine bone; this question is examined in section 8.9.2.4 and in chapter 9, where evidence from the mechanical tests is also considered.

From the images and mechanical responses shown in figures 8.023 to 8.041 it is apparent that the fracture of bovine bone is catastrophic. The minimum average speed of the fracture tip in the SEN specimens of bovine bone examined here is 2 m s^{-1}. This value was arrived at due to the complete lack of an image showing the travelling crack in bovine bone. The a frame rate used in the testing of specimens in data sets NB4 and NB5

---

[12]While figure 8.042 shows the length of the whitened zone at the time of fracture initiation is similar for bone and antler; it also displays a relationship between this length and the notch tip radius. Thus relationship is examined in section 7.5 for antler and 7.8 for bovine bone.

was 1000 frames per second. (These data sets contain information on 47 specimens. The same finding is true for those specimens rejected from these data sets.) If the minimum ligament width is assumed to be 2 mm then the speed is simply derived. In the SEN specimens of bovine bone the fracture traverses the material by a reasonably direct path, the overall fracture angle deviating by less than 45° from the line of the machined notch. Some wider specimens demonstrated bifurcation of the crack as it approached the un-notched surface. After fracture occurred the now unloaded bone returned reasonably quickly to its original optical appearance.

I mentioned above a *shooting star* effect exhibited by some antler specimens; this is shown to some degree by discrete images of figures 8.043 to 8.050 These figures are from a test at a cross-head speed of 1.67×10^{-3} m s^{-1} [100 mm min^{-1}]. However, this effect was also observed at lower cross-head speeds, including those where no whitening was seen prior to fracture initiation. The time required for the fracture to traverse an antler specimen could be several seconds. Even at this faster cross-head speed the fracture took about 0.1 s to traverse the specimen. These images also demonstrate (at the level of magnification and resolution of the video images, see comments at the end of section 6.3.3) that the route the fracture took was less direct than that in bovine bone specimens. In some antler specimens the fracture ran a short distance, then appeared to be diverted; continuing its propagation in a longitudinal direction.

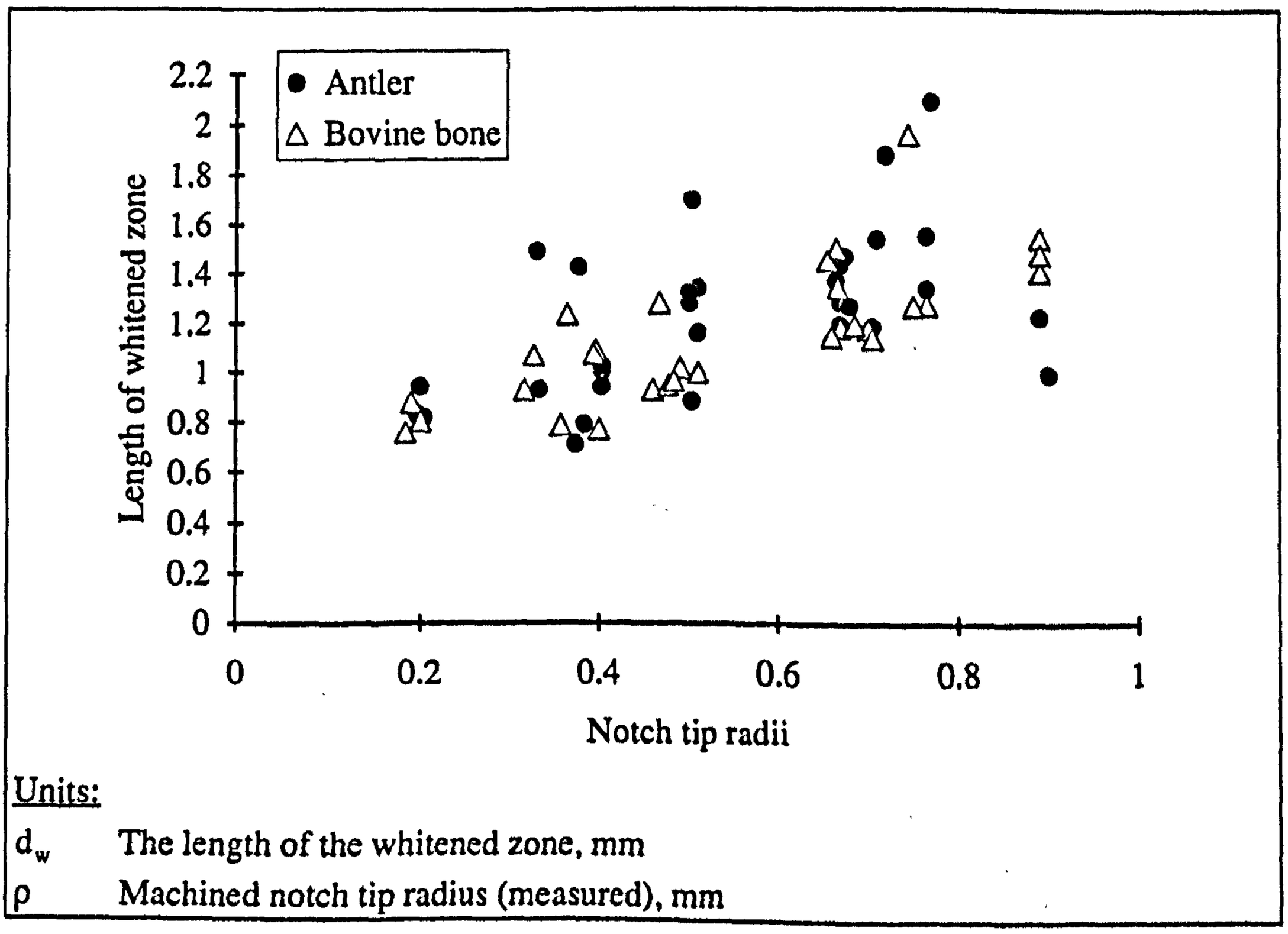

Units:

d_w The length of the whitened zone, mm

ρ Machined notch tip radius (measured), mm

Figure 8.042

Relationship of the length of the whitened zone to the notch tip radius

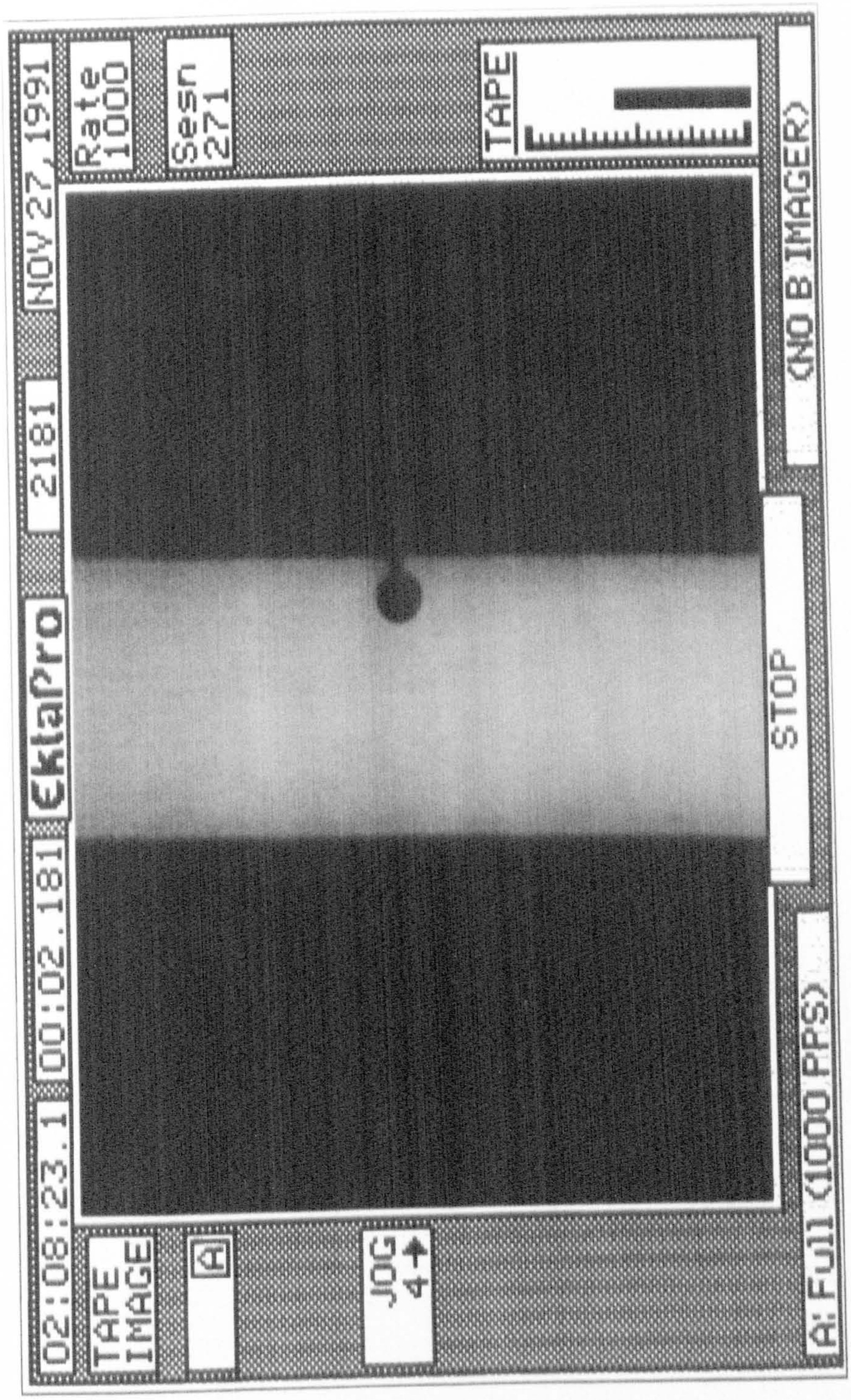

Figure 8.043 Part of a series from figure 8.043 to 8.050

First print from a series showing the *shooting star* effect of the moving whitened zone in specimen of antler

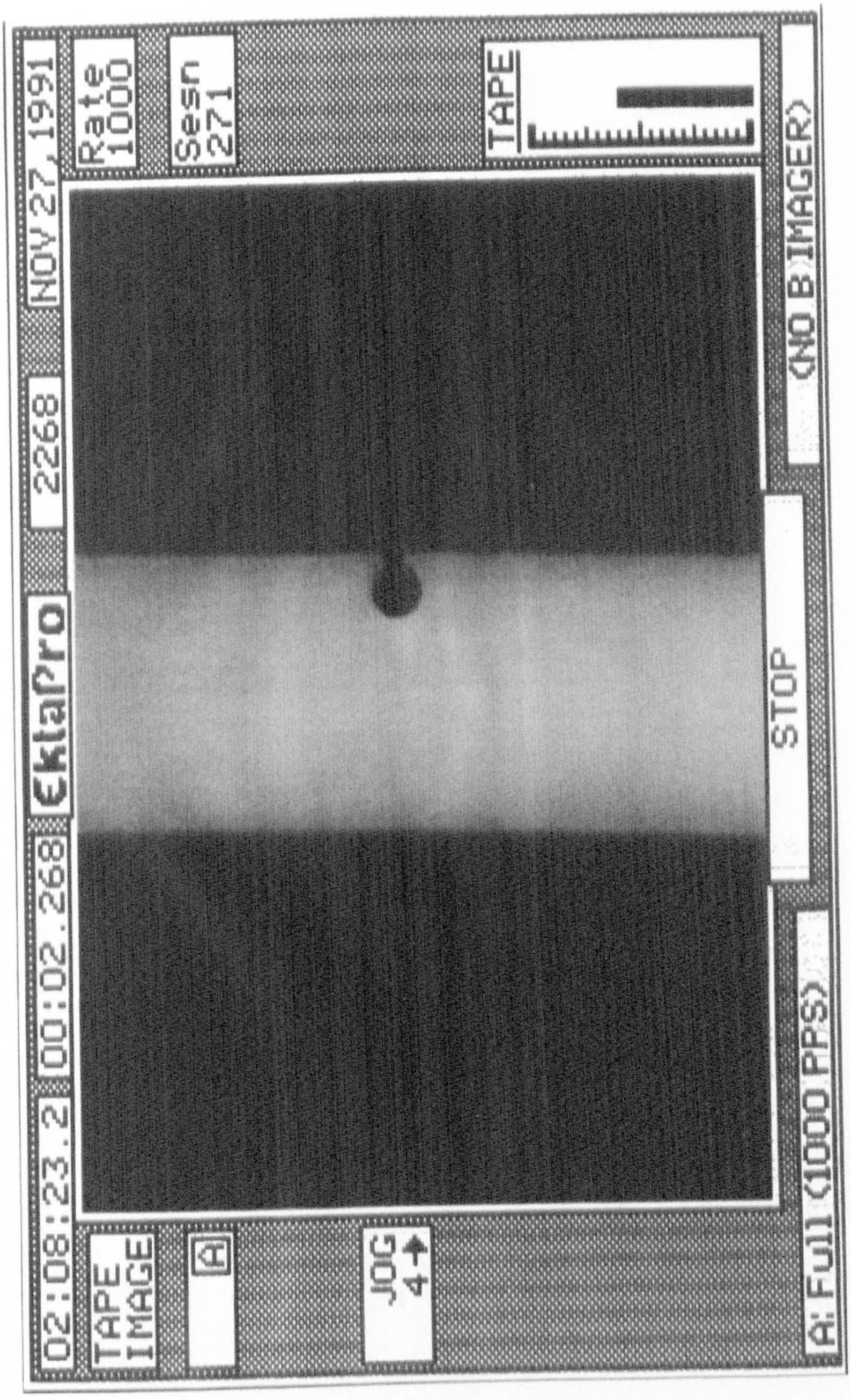

Figure 8.044 Part of a series from figure 8.043 to 8.050

Second print from a series showing the *shooting star* effect of the moving whitened zone in specimen of antler

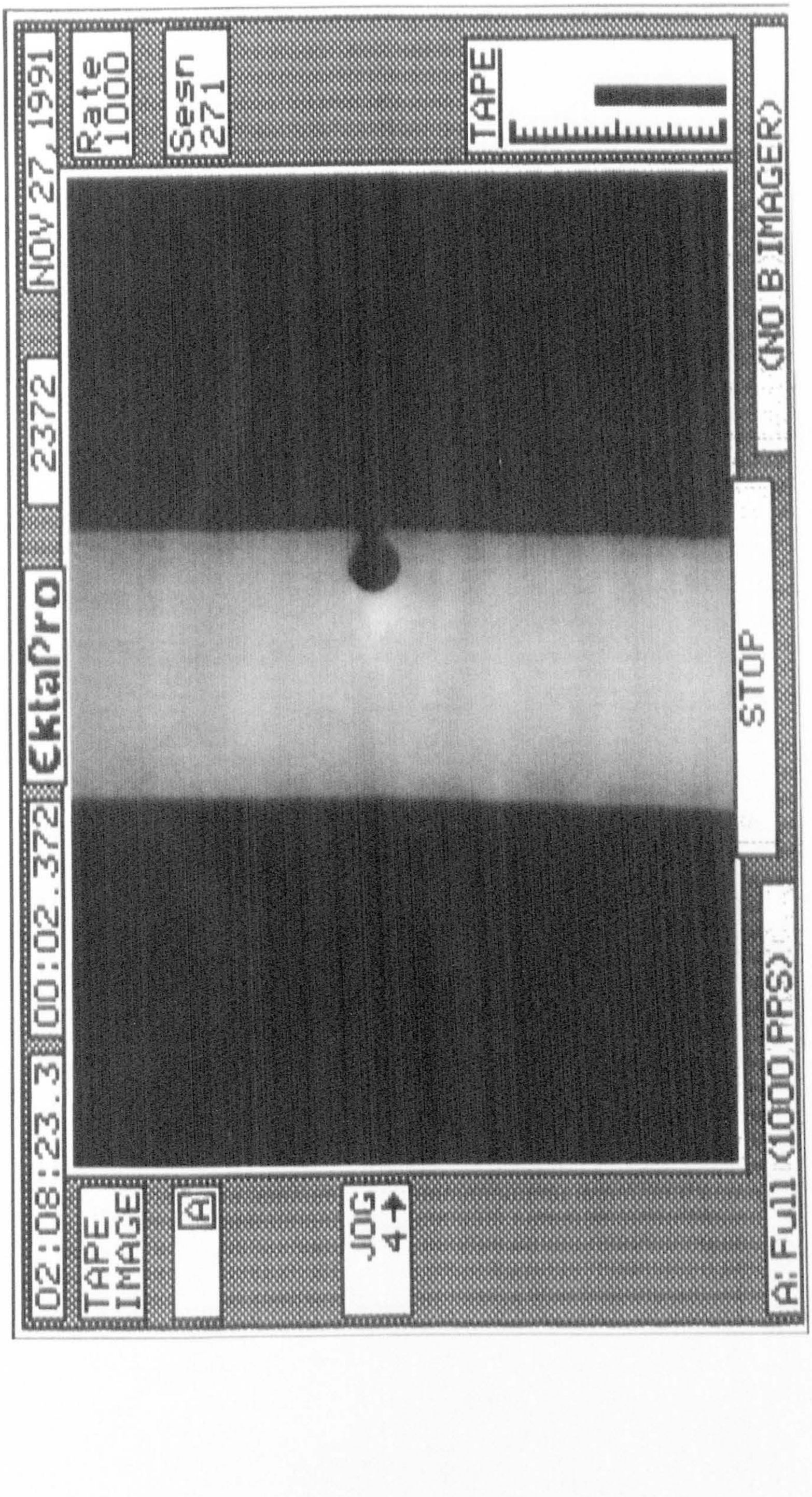

Figure 8.045 Part of a series from figure 8.043 to 8.050

Third print from a series showing the *shooting star* effect of the moving whitened zone in specimen of antler

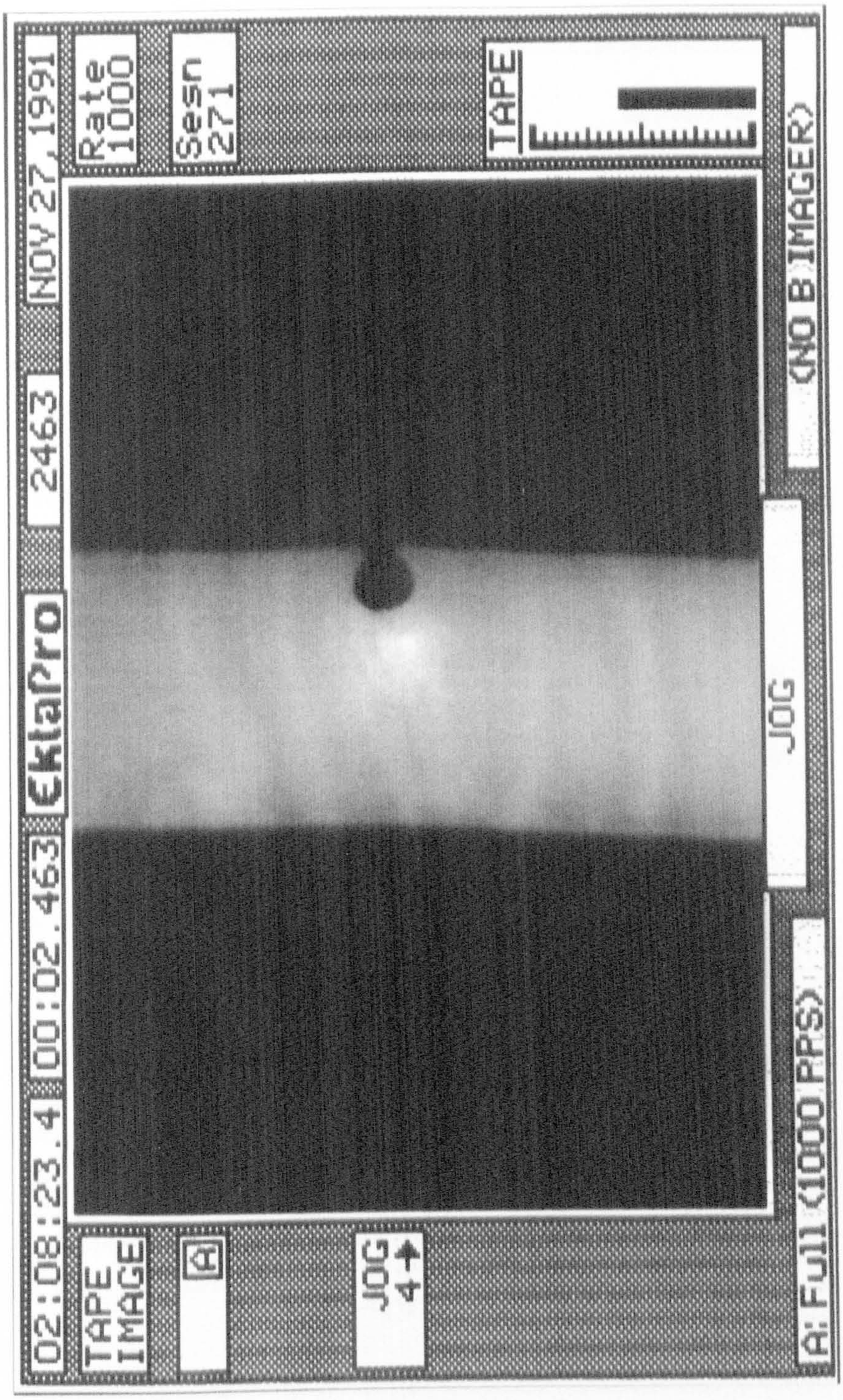

Figure 8.046 Part of a series from figure 8.043 to 8.050

Fourth print from a series showing the *shooting star* effect of the moving whitened zone in specimen of antler

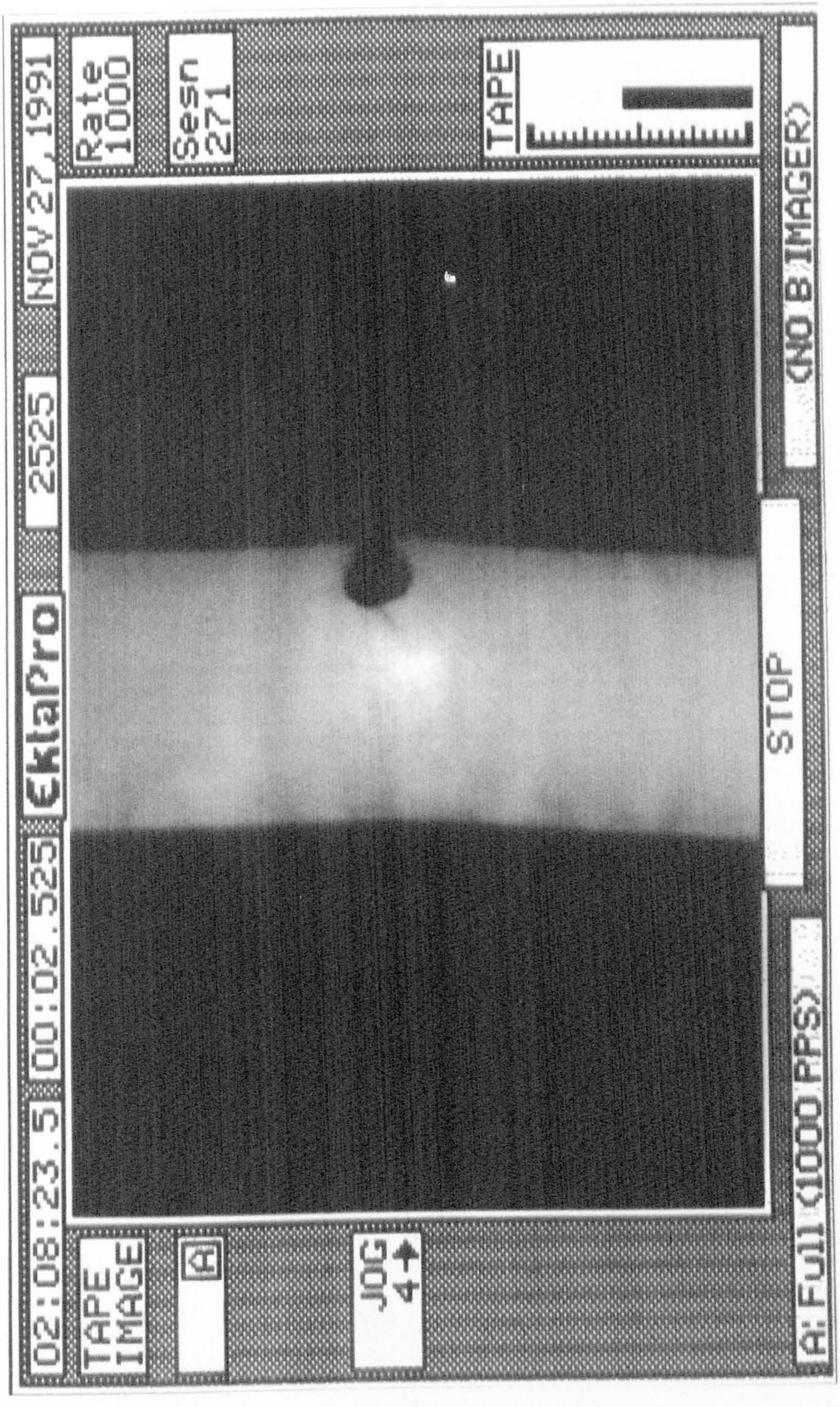

Figure 8.047 Part of a series from figure 8.043 to 8.050

Fifth print from a series showing the *shooting star* effect of the moving whitened zone in specimen of antler

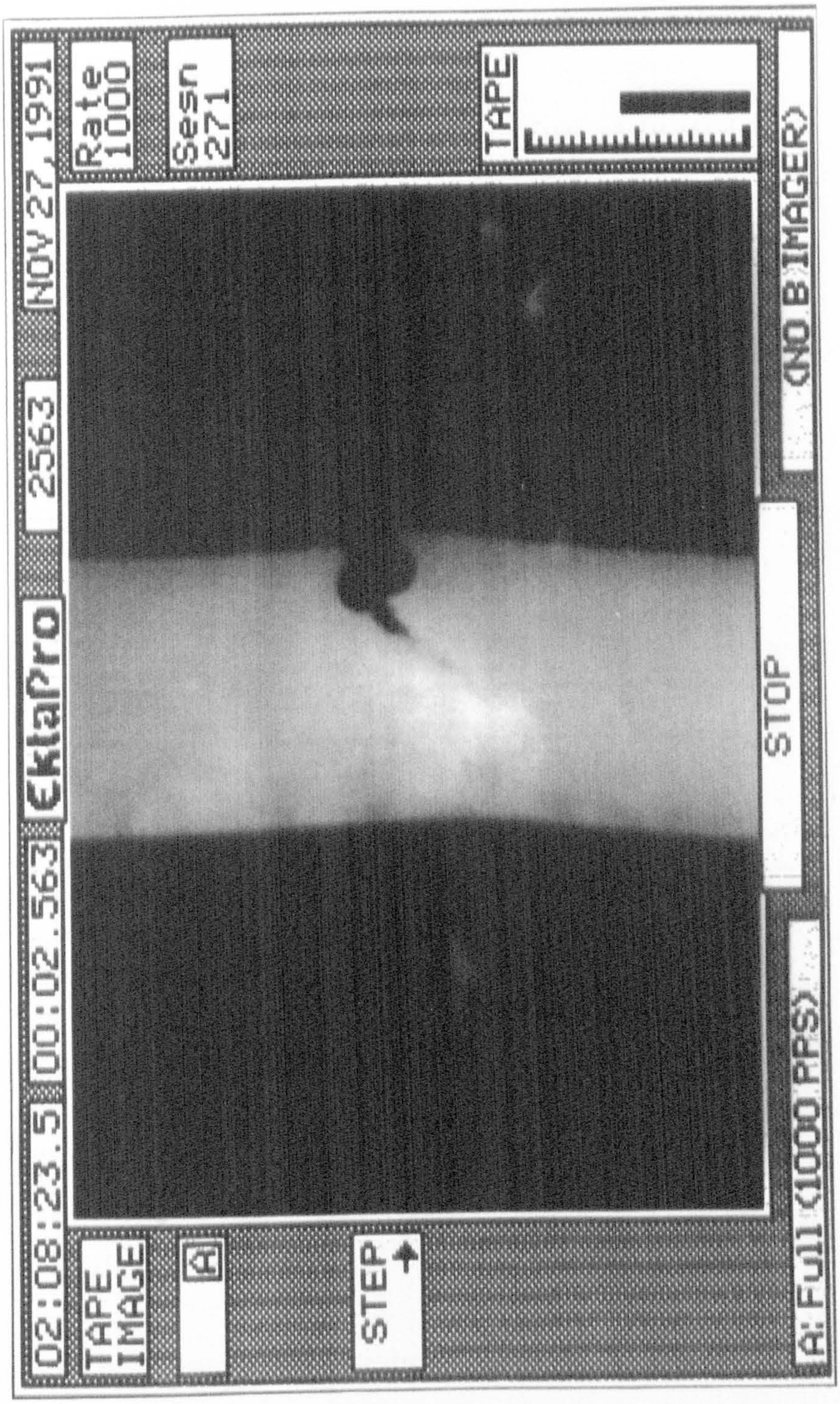

Figure 8.048 Part of a series from figure 8.043 to 8.050

Sixth print from a series showing the *shooting star* effect of the moving whitened zone in specimen of antler

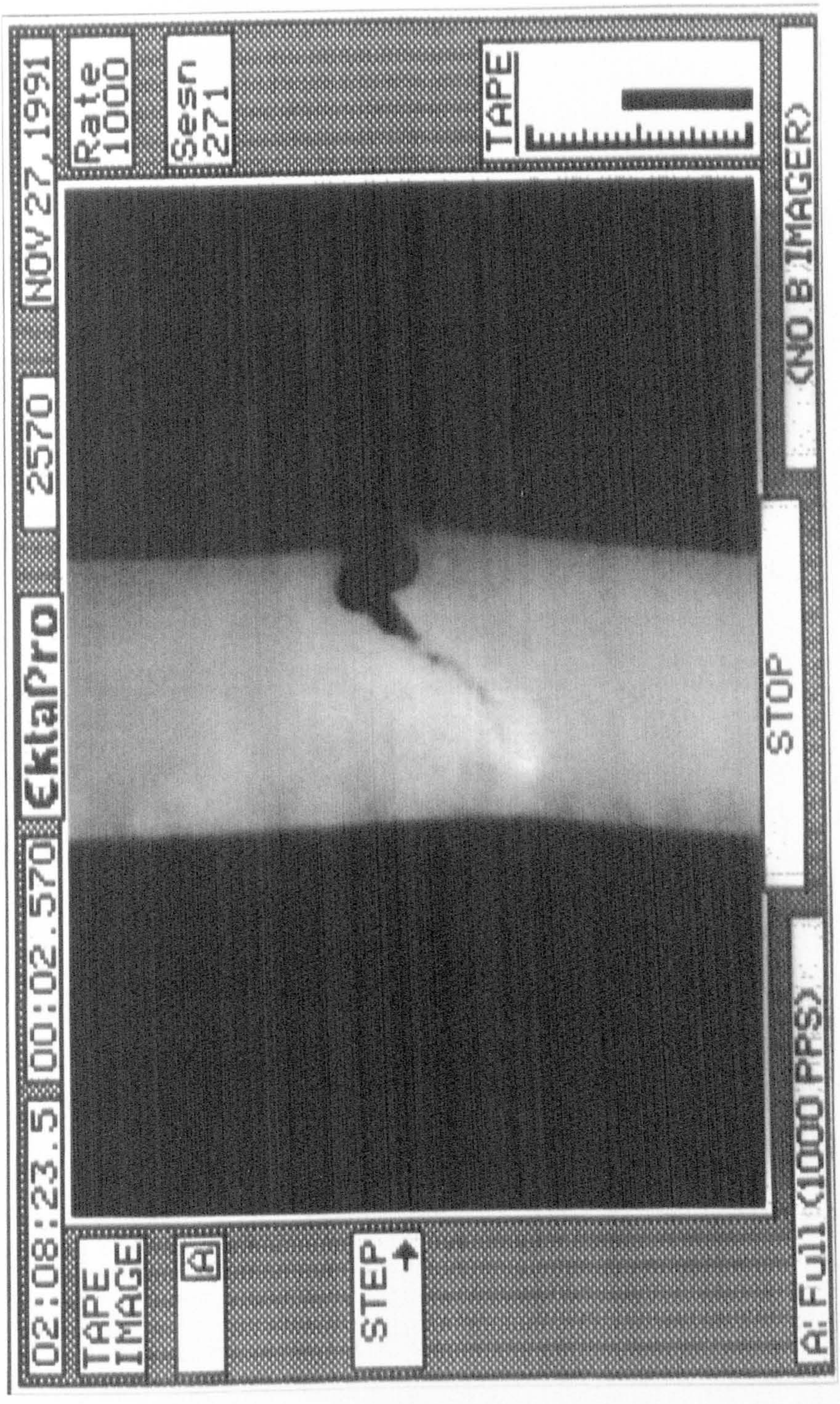

Figure 8.049 Part of a series from figure 8.043 to 8.050

Seventh print from a series showing the *shooting star* effect of the moving whitened zone in specimen of antler

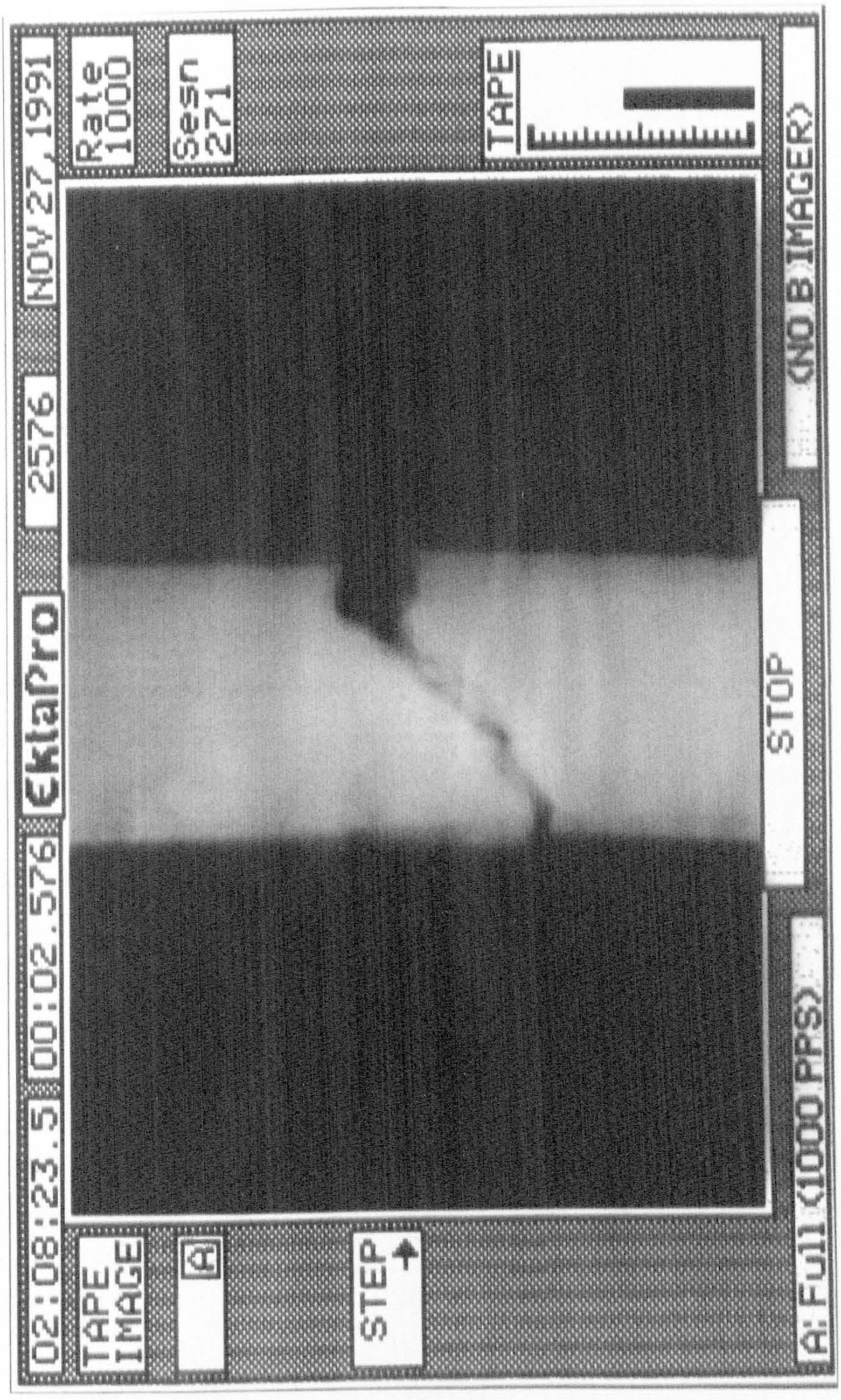

Figure 8.050 Part of a series from figure 8.043 to 8.050

Eighth print from a series showing the *shooting star* effect of the moving whitened zone in specimen of antler

8.8. THE EFFECT OF CROSS-HEAD SPEED ON THE OBSERVED OPTICAL CHANGES

I have already reported, in section 7.6.3.5 for antler and section 7.9.3.6 for bovine bone, that the whitening of tensile specimens of both materials is dependent on the cross-head speed used. The cross-head speeds have been used in those tests were: 8.33×10^{-7}, 8.33×10^{-6}, 8.33×10^{-5} and 8.33×10^{-4} m s^{-1} [0.05, 0.5, 5 and 50 mm min^{-1}]. In addition to those tests I have also conducted some at higher rates on antler only. These higher rates were: 1.67×10^{-3}, 3.33×10^{-3}, 8.33×10^{-3} and 1.67×10^{-2} m s^{-1} [100, 200, 500 and 1000 mm min^{-1}].

At speeds below 8.33×10^{-5} m s^{-1} the whitening that did occur was very indistinct. Whitening at this speed was only observed for a few bovine specimens, only one of which is within the data sets examined in chapter 7. Whitening was not noticed in any of the specimens tested at the slowest speed. The whitening appeared brighter at higher cross-head speeds. I consider this is a real effect, not an artefact due to more gradual changes being more difficult to perceive. The effect of this possible artefact was reduced by viewing the real-time and downloaded images at different speeds (fast forwards, rewind or examination of individual frames). After I have discussed the most probable cause of the observed whitening, I will propose an explanation for the time dependence of this effect.

8.9. CAUSES AND IMPLICATIONS OF THE WHITENING OF BONE AND ANTLER

In this section I suggest some possible causes and implications of the effect of the whitening of bone and antler. The implications I am concerned with here are those that may provide a greater understanding of the mechanical response and failure process of these materials.

8.9.1. THE CAUSES OF WHITENING

The occurrence of mechanically induced optical changes (as defined above) is well known in amorphous polymers,[13] and composites as described in section 8.2. Comparisons can be drawn between these changes and the changes observed in bone and antler. The causes of the optical changes are different in these two engineering materials.

---

[13]One manifestation of this is may be observed when a clear (so called) plastic rule is bent over the edge of a desk.

In polymers the optical effect is referred to as *crazing*. Crazes are thin crack-like domains that form under tension (Atkins and Mai, 1988). They are 'useful indicators of impending failure in polymer products in service: they impair clarity, reflect light and are particularly obvious in transparent materials' (Powell, 1983). Although they appear as shiny cracks in an otherwise clear solid, crazes differ from cracks as they are filled with mechanically transformed polymer, which has a different refractive index to that of the bulk material (Atkins and Mai, 1988). This material takes the form of load-bearing fibrils (10 to 20 nm in diameter) that bridge the space between the new surfaces. A true crack would not possess any load-bearing elements. Consequently a craze is less dangerous than a crack, due to its smaller disrupting effect on the stress field in the material. Crazes are induced by stress concentrations. Atkins and Mai say that these stress concentrations may be due to inclusions or surface defects (and their formation is sensitive to the presence of solvents). Crazes are the precursors of cracks within the polymer. These cracks are generated by the progressive degradation of the craze material, until a void develops within it. Such voids grow into cracks, which advance through the bulk of the material by the formation of craze at their tips; until complete fracture of the specimen occurs.

The optical changes observed in composite materials are attributed to crack and void formation (Gordon, 1976). The exact form of these cracks will depend on the type of composite under examination: continuous fibres in a matrix (aligned or random), short fibres in matrix (aligned or random), particles in a matrix, lamellar structures and so on. The optical changes may be associated with a complex combination of some, or all, of the following types of cracks: fibre or particulate debonding, fibre failure, microcracking, microvoiding or, on a larger scale, delamination. Optical changes in GRP are described in passing by Gordon (the main discussion being on the fracture mechanism of the material).

> Whenever a fibre-glass article has suffered from a blow. . . the material in that region, though not broken, usually turns white. This whiteness is due to the reflection of light from the surface of the many internal cracks. Material in this condition is not much weaker than it was before, although it has already absorbed a good deal of energy, simply in providing all those internal surfaces.

It was proposed by Burstein *et al.* (1973) that the optical changes they observed in bone are due to 'pull-out which creates voids and crazes'. The production of internal fractures or voids in bone and antler is supported by the work of Dr Peter Zioupos of the same laboratory as myself.[14] Such new surfaces would scatter light, which previously

---

[14]By loading the materials into the knee region while immersed in a bath of florescent strain (fluorescein), and then viewing them with a laser confocal microscope, the mechanically induced internal fractures have been observed. These flaws are especially clear in specimens containing a notch or hole.

would have been transmitted, thus inducing whitening in reflected light conditions and darkening in transmitted light conditions, as has been observed and reported here. The introduction of such fractures, within the material, would result in a reduction of the mechanical integrity of the structure. Therefore the occurrence of optical changes agrees with the previously proposed idea that the mechanical responses of bone and antler are a result of damage accumulation. On unloading the specimen tends to return to its original length thus closing the cracks. Hence there is a reduction in the amount of whitening. In section 3.3.3.1 I quoted Fondrk *et al.* (1988); they attributed the time-dependent recovery of the residual strain at the end of a loading-unloading cycle to the 'incomplete closure of submicroscropic cracks', for this idea they refer to a published work on polymers. If the whitening in bone and antler is due to cracking, this argument explains the closer correlation of the optical changes with strain than with stress (suggested in section 8.6.2).

I propose, but possess no convincing evidence in support of the hypothesis, that the lack of whitening at low cross-head speeds is due to a combination of: the lower rate of crack formation and the greater time available for water to enter the fractures. I suggest that this water reduces the difference in refractive index between the fractures voids and the surrounding material. The combination of these effects is to reduce the density of light scattering surfaces. This hypothesis could be investigated using the staining method of Zioupos mentioned above. If it is true, specimens loaded quickly will contain less stained fractures than those loaded slowly, while exhibiting more whitening.

If the ingress of water is the mechanism by which the whitening effect is reduced, it may help to explain why on reloading whitening does not increase markedly until a value of strain larger than that previously obtained is reached. The fractures already incurred will merely be pulled apart slowly, permitting water to enter gradually. I propose that when the previous strain level is surpassed new fractures are produced. The surfaces of these new fractures would separate more rapidly thus optical changes are more readily observed. In chapter 4 I suggested that the mechanical response of bone and antler may be due to a combination of a visco-elastic like behaviour and a damage behaviour. Clearly the presence of cracks agrees with the idea of damage. Perhaps the lack of an optical effect at lower cross-head speeds is due to the visco-elastic like behaviour. At these speeds the material (or this idealisation of it) may have time to extend by a visco-elastic mechanism rather than by microcracking. (Such a hypothesis if true suggests that modifications are needed to the model of bone I proposed in sections 4.2.7.)

The occurrence of microcracking can be verified to some extent by monitoring the acoustic emission during tensile and loading-unloading tests.[15] The detection of acoustic emission supports the idea that the knee region is due to a large number of discontinuous events, such as microcracks. Acoustic emission of bovine metatarsal specimens under tensile loading to failure has been studied by Fisher *et al.* (1986). Two cross-head speeds were used in their study 3.33×10^{-6} and 3.33×10^{-4} m s^{-1} [0.2 and 20 mm min^{-1}], which they convert into strain rate values of 0.0001 s^{-1} and 0.01 s^{-1}. They observed no acoustic emission during the initial linear section of the loading curve. This lack of acoustic emission continued until failure was imminent. This result, when compared to those of Wright *et al.* (1981) and the findings of Peter Zioupos, indicates some lack of sensitivity in their equipment. However, Fisher *et al.* do report one finding that concurs with the optical effects noticed during the creep tests, and reported above.

> When a tensile test specimen was loaded in tension to 88% of its ultimate stress (the presence of the first event) and then the load level was held constant, acoustic emissions continued to be emitted for 7.2 s and despite no further increase in load, the bone failed.

Wright *et al.* (1981) examined acoustic emission (AE) of bovine bone specimens in tension. They tested three groups of specimens decalcified, deproteinised and a control group.

> Acoustic emission from the control specimens tended to initiate just prior to the yield point and continued during yielding. Significant AE counts occurred again just prior to fracture. No emissions occurred in the elastic region and few occurred in the major portion of the 'plastic' region between yield and fracture.

A similar increased level of emission in the knee region of mechanical response, compared with the post-knee region, has also been noticed by Peter Zioupos. This supports the proposal that the initial whitening could be due to the formation of microcracks, and the increase in whitening is perhaps a result of the increase in the number (or possibly size) of these fractures. (Clearly the size is limited by the fracture mechanics type response to less than the *critical* size.)

The optical changes described above are considered to be another manifestation of the events that result in acoustic emission. Similarities can be drawn with the results of an investigation of polystyrene (PS) by Koenczoel *et al.* (1986) in which they monitored load, acoustic emission and optical changes with time. The method they used to monitor the optical changes, due to crazing, was far less arbitrary than that in this thesis. In their system a photocell and light source were inclined at 45° to the axis of the specimen, which was placed between them. The output of the photocell was used as a direct

---

[15]A few initial acoustic emission investigations of loading tests, with no unloading, have been conducted by the author and Dr Peter Zioupos. This work has since been continued and extended by the latter researcher.

measure of the amount of crazing. Koenczoel *et al.* found that the initial reduction in transmitted light was not accompanied by any detectable AE. However, the reduction in transmitted light occurred in the region of the loading curve where it departed from a linear relationship. At higher strains an increased rate of reduction of transmitted light is associated with the onset of AE.

Another piece of evidence concerning the behaviour in the knee region of bone is supplied by Currey and Brear (1974). They used stain-induced changes in the appearance of bone, to show whether, and how, it had 'yielded'. This they accomplished by variously loading beam specimens, either by three or four-point-bending, impact or compression tests. In the last form of test the specimens were buckled, to obtain a tensile surface. After being tested the specimens were placed in stain for a few hours. In those three-point-bending specimens that had 'yielded' characteristic lines of stain passed from the surface to the interior of the bone, on the tensile side of the specimen. The tension surface has a striped appearance, the lines of stain being perpendicular to the specimen's long axis.

The existence of 'microscopic damage in bone' due to cracking has been demonstrated by Burr and Stafford (1990). They used (and evaluated the validity of) a bulk-staining method, on portions of rib from an unembalmed 70 year old male. These portions were then sectioned. They report that the *in vivo* sections of the rib possessed between 1 and 8 cracks. They do not state the size or shape of these cracks, but do provided a picture of one of these cracks. The crack appears in conjunction with a secondary osteone. The crack length is approximately the same as the osteone diameter. (So an approximation to the length of the crack would be a few hundred micrometers. Table 1.001.)

In their work *Compact Bone Fatigue Damage: a microscopic examination,* Carter *et al.* (1977a) conducted flexural fatigue tests (at room temperature) on specimens of wet bovine femoral bone. They examined material from regions of the specimens that had been subjected to tensile, or compressive, stress. They summarise their observations in the following way.

> Microscopic examination of flexural fatigue specimens prior to complete failure established that fatigue fracture is caused by the progressive accumulation of diffuse structural damage. The microdamage observed on the tension side consisted primarily of separation (or debonding) at cement lines and interlamellar cement bands. Tensile cracks in interstitial bone were also observed.

They report and provide images of 'fibrous bridging through cement bands'. This comment invites analogies with the crazing of polymers. The damage modes they observed in compressive regions were different, comprising oblique cracks and longitudinal splitting. This supports their finding as a real effect and not an artefact of

the examination method. They give no dimensions of the cracks in the tensile region, but do provide a series of three photographs at different magnifications. The 'osteon debonding' crack shown is very approximately 400 μm long by 4 μm wide and curves around the debonded structure. Carter *et al.* do not provide any information similar to that given for the fatigue tests for the monotonic flexural tests, apart from saying that the gross fracture morphology is similar.

Considering the evidence described above, I attribute the whitening in bovine femoral bone and antler to the formation of microcracks within the material. The exact nature of these fractures is still uncertain.[16]

8.9.2. THE IMPLICATION OF THE EVENTS THAT CAUSE WHITENING

Acceptance that whitening is caused by microcracks has implications for the interpretation of the mechanical behaviour of bone and antler. The production of microcracks provides a physical explanation for why the mechanical response conforms to that associated with a damage material, albeit not an idealised one. I consider that the most important feature of the production of microcracks is that the process consumes energy. This type of energy consuming process is an important feature in industrially produced composites for the same reason that it is important in bone: it toughens the material.

In this section I shall examine some of the implications of microcracking during creep, tensile, loading-unloading and notch sensitivity tests. Some of these implications have already been mentioned in the sections that discuss the mechanical aspects of these tests.

8.9.2.1. MICROCRACKING IN CREEP TESTS

As reported above, optical changes were observed during the creep testing of some specimens of bovine bone. Such effects were not observed during the testing of specimens of reindeer antler. This could be due to my lax observation in these early tests. However, the optical changes in the bovine bone specimens occurred in the tertiary creep period, a feature which antler does not display. Therefore, this lack of observed whitening in the antler specimens may not be an artefact.

---

[16]This area of investigation is being conducted by Dr Peter Zioupos by the methods already mentioned. Therefore I will not pursue this topic here.

The whitening of bovine bone in the tertiary stage of the creep test suggests that in this section of its behaviour the extension and thus final failure is caused, at least in part, by the accumulation of cracks. Therefore, whitening adds to the evidence that the creep-rupture of bovine bone is not 'a result of unlimited flow' (section 2.3.3.1). This supports the comment made by Carter and Caler (1983) that their experimentally derived equations are equivalent to the equations given by Kachanov for failure by a brittle process; a statement that I questioned in section 3.3.1. Clearly the accumulation of microcracks during a creep test supports the application of the concepts of damage to the results of these tests.

The lack of observed whitening during the primary and secondary stages of creep tests on bovine bone specimens may be explained in at least two ways: first, the deformation in these stages is not due to microcracking; second, the microcracks do occur but they are not observed. I consider that the second explanation is more reasonable. I have reported that tensile specimens that are extended at low cross-head speeds do not exhibit whitening (in the recorded video images). In figure 4.042 I showed that secondary creep rate of less than half a dozen bovine specimens was greater than the strain rate at which whitening was observed in a tensile test. Therefore I suggest that during the secondary creep stage whitening is not observed due to the ingress of water into the microcracks. During the tertiary creep stage, by definition, the creep rate increases thus water has not time to enter the cracks: whitening is seen. This argument is closely connected to the damage accumulation rate examined in section 4.3.9. The damage in bone is not accumulated instantaneously, nor at a constant rate. I will not pursue this line of argument further, but suggest that a study using equipment similar to that of Koenczoel (1986) (mentioned above) may be very informative.

8.9.2.2. MICROCRACKING IN TENSILE TESTS

In the case of tensile tests the main implication of the assertion that whitening is caused by microcracking is that the knee region is due to the accumulation of damage (in the form of these cracks) not to plastic flow. This supports my use (in section 4.2.6.5) of the damage equations to describe the knee in the mechanical response of bovine bone. As in the creep tests, the accumulation of microcracks reduces the stiffness of the material (as modelled by the damage approach).

8.9.2.3. MICROCRACKING IN LOADING-UNLOADING TESTS

The whitening effects observed during the initial loading section of a loading-unloading test are, obviously, the same as those in a tensile test. I have already suggested that the decrease in whitening on unloading is due to the closure of the microcracks, and that the whitening on reloading is less distinct than that observed in the first cycle until the envelope of the previous mechanical response is surpassed. I attributed this to the mechanism of crack opening. I suggest that in the initial crack formation the surfaces separate very rapidly thus providing a period of time before water fills the void. When pre-existing cracks are reopened the surfaces will separate more gradually permitting water to enter them.

The idea that water is pumped in and out of the microcracks in response to the externally applied mechanical loading, may be extended to provide an explanation of some aspects of the mechanical response of bone and antler. This extended argument is very speculative. First I consider that it is reasonable to attribute the time-dependent recovery of the residual strain to such a mechanism. Furthermore, I suggest that it may explain the hysteresis loop of the loading-unloading response in the post-knee region. This situation can be visualised as the elasticity of the material being resisted by the viscous action of the water. When viewed in this way it is almost impossible to avoid comparisons with the models of visco-elastic material presented in section 2.2.1.3.[17] However, this type of direct comparison between spring and dashpot models and physical structures can be misleading (as I have already pointed out by reiterating the comments made by Sedlin in 1965, in section 3.2.4).

8.9.2.4. MICROCRACKING IN NOTCH SENSITIVITY TESTS

In section 7.10.4 (Nature of the fracture of bone and antler: the whitened zone) I pointed out that the production of microcracks around the tip of the notch acts as a toughening mechanism, reducing the notch sensitivity of the materials. In chapter 4 I showed that antler was able to accumulate this damage (expressed as strain) more rapidly than bovine bone was able to accumulate damage. This may be part of the explanation of why bovine specimens fracture catastrophically while those of antler fail in a stable manner. For when the fracture starts to travel in bovine bone there may be insufficient time for damage to accumulate ahead of it; thus no stress shielding effect is produced. If this is the case the fracture is truly brittle, and the fracture behaviour may conform to that encapsulated in the Griffith equation (5.021) (assuming linear-elasticity and so on).

---

[17]Such an analogy suggests an interesting experiment: what happens if the specimens are loaded and unloaded in liquids of different viscosities?

Evidence in support of this idea is provided by the post-test straining experiments of Currey and Brear (1974). These workers state

> from preliminary observations we have made, it seems that the amount of yielding of the type indicated by this staining seems to decrease as the strain rate increases. Impact specimens seem not to show the staining, and specimens loaded at a rate of 0.5 s^{-1} show the effect much less strongly than specimens loaded at a strain rate of 0.01 s^{-1}.

If the microcracks are interpreted as damage then this is the result that would be expected for a material that requires time (and stress) to accumulate damage. The straining tests of Currey and Brear mirror some aspects of my whitening results. For example they note staining at the tip of cracks, and state 'the stain would appear at the root of slots cut into the surface, but not elsewhere'.

The implications of damage occurring at the notch tip have been discussed in chapter 7. The most important is that such a damage zone toughens the material, by relieving the stresses in that region, and in so doing consumes energy. Another consequence of this is that the concept of the critical stress intensity factor as a material property is undermined. The fracture behaviour of bone and antler is thus more analogous to that of composite materials than to that of metals. Such an analogy may be made by using the description of the fracture given by Williams (1990); who says that during crack propagation

> the energy absorbed in creating the new surface is manifest in the zone of highly deformed material surrounding the crack tip. In metals, polymers and other reasonably homogeneous materials the deformation processes are mostly shear yielding, or plastic flow, so the zone is termed the 'plastic zone'. In reality, of course, this is not always so and in polymers, for example, we can have the inhomogeneous process of crazing occurring in the zone, or in toughened polymers there can be second-phase particle cavitation or debonding. These lead to well-defined stress-whitened zones at the crack tip, and in polymers it is more common to talk of the yielded or 'damaged' zone than a 'plastic' zone.

8.10. CONCLUSIONS

During the mechanical testing of bone and antler optical changes were observed. These were related to the changes in the mechanical response of the materials. The cause of both changes is the accumulation of damage in the form of microcracks. This evidence that the mechanical properties of bone and antler are modified by a damage process and not by plasticity, demands that the description and interpretation of their mechanical behaviour should reflect this fact.

9

CONCLUSIONS AND SOME OF THEIR POSSIBLE IMPLICATIONS

> Pooh sat down on a large stone, and tried to think this out. It sounded to him like a riddle, and he was never much good at riddles, being a Bear of Very little Brain.

Milne, A. A. (1974)
Winnie-the-Pooh.

9.1. INTRODUCTION

In this chapter I discuss the interrelationship of the results I have obtained from the different tests conducted on specimens of bovine bone and antler. The tests I have used include impact, tensile, creep and notch sensitivity tests. On the basis of these results I propose an explanation for the mechanical response of bone and antler to tensile loading.

I present my main conclusion first. In later sections I highlight some results that either agree, disagree or qualify this main conclusion. These results are gleaned from my own studies and those within the literature. It is hoped that the examination of the results obtained by others using different tests, or test conditions, will help to confirm or refute the proposed explanation of the mechanical behaviour. In some cases the ideas I present here may even help to explain the published results.

9.2. MAIN CONCLUSION: BONE AND ANTLER FAIL BY DAMAGE ACCUMULATION

Many conclusions can be drawn from the experimental work described in the preceding chapters. However, some of these are implications, or side effects, of the most fundamental conclusion. This cardinal conclusion is that specimens of bovine bone and antler tested in tension, under quasi-static conditions, depart from an idealised linear-elastic response due to a combination of the progressive accumulation of damage (in the form of microcracks) and some anelasticity[1] (viscoelastic like behaviour). The ultimate failure of these materials is due to the accumulated damage and a fracture process. The proportions in which these difference processes (damage, anelasticity and fracture) are combined depends on a number of factors. The three main factors considered here are: First, the material under consideration (bone or antler). Second, the region of the behaviour that is being examined (pre-knee, knee or post-knee). Third, the rate at which the material is loaded (cross-head speed). (Other factors include the temperature and the state of hydration of the specimen.)

My main conclusion includes the phrase 'tested in tension, under quasi-static conditions'; in later sections I will examine the application of the same idea to the results I have obtained, and those in the literature, for bone tested under other conditions. However, first I consider the various stages of the tensile response. The emphasis is placed on the knee and post-knee behaviour, as these were to be the original focus of this

[1]'Anelasticity' is defined here, as it was by Currey (1965) as 'a recoverable strain appearing over a period of time'. In this chapter this strain is considered to be only the time-dependent portion of the strain, and not that caused by the formation of damage, or elasticity.

thesis. Within each stage the different response of the two materials is considered, as are the consequences of the testing rate (cross-head speed) used. Initially I shall give no consideration to the role played by the material's structure.

9.2.1. THE MECHANICS OF THE PRE-KNEE REGION

In my main conclusion I referred to the departure from linear-elastic behaviour. Clearly such departure could be due to two changes, or a combination of them: a change to non-linear elasticity or the loss of elasticity. From the results obtained in this study I conclude that this departure is caused by both non-linearity and the loss of elasticity. For a specimen of bovine bone this departure is slight. Due to the formation of slight hysteresis loops during the loading-unloading cycles and the increase in stiffness of bone at higher testing rates, I concur with the generally held view that for normal bone the departure from linear elasticity is due to the time dependence of the response. As a result of this time dependence, bone has often been considered to be a viscoelastic material (see section 3.2).

The stress-strain response of antler in the pre-knee region is curved. Due to the low estimate of the limit of fully elastic behaviour (obtained from extrapolation of resilience test results) the departure of this material from linear-elastic behaviour also appears to be dominated by non-elastic rather than a non-linear response. I consider this curvature, or departure from a linear response, may be due to different processes or different amounts of the same processes that occur in bovine bone. I suggest that it is a damage accumulation process that dominates the departure of antler from a linear-elastic response.

The effect of increasing the tensile testing rate is to increase the measured stiffness of bovine bone. This effect is consistent with the ideas that the departure from linear-elastic behaviour is due to an anelastic response. However, the antler specimens that were tested under the same conditions did not show such an increase in their stiffness (section 4.2.6.5). I suggest this is consistent with the proposal that the stress-strain response is determined mainly by a damage process. In support of this argument I use the results of the creep tests (section 4.3). Those tests showed that antler accumulates most of its creep strain (due to damage and time-dependent elasticity) very rapidly, whereas for bovine bone the accumulation of creep strain occurs at a proportionately lower, and more constant, rate (see figure 4.064). Thus the reason for the curvature, and lack of time dependence, of the pre-knee stiffness of antler during a tensile test could be that damage (expressed as strain) is sustained so rapidly that the time dependence of its accumulation can be neglected at the test speeds used here. The extreme case would be if the creep

strain was described by a step function. Considering a tensile test of such a material to be a result of a number of step load inputs suggests that the rate at which these steps are applied has no effect on the material stiffness (this is clearly an idealisation). To produce a curved stress-strain curve the size of the steps would have to increase as the stress became larger. This idealisation is shown in figure 9.001 (I have used a uniform increment to the strain response at each level, clearly a power relationship would give a different curve.) When this idealisation is considered it should be remembered that the creep curves on which it is based were conducted at relatively high stresses.

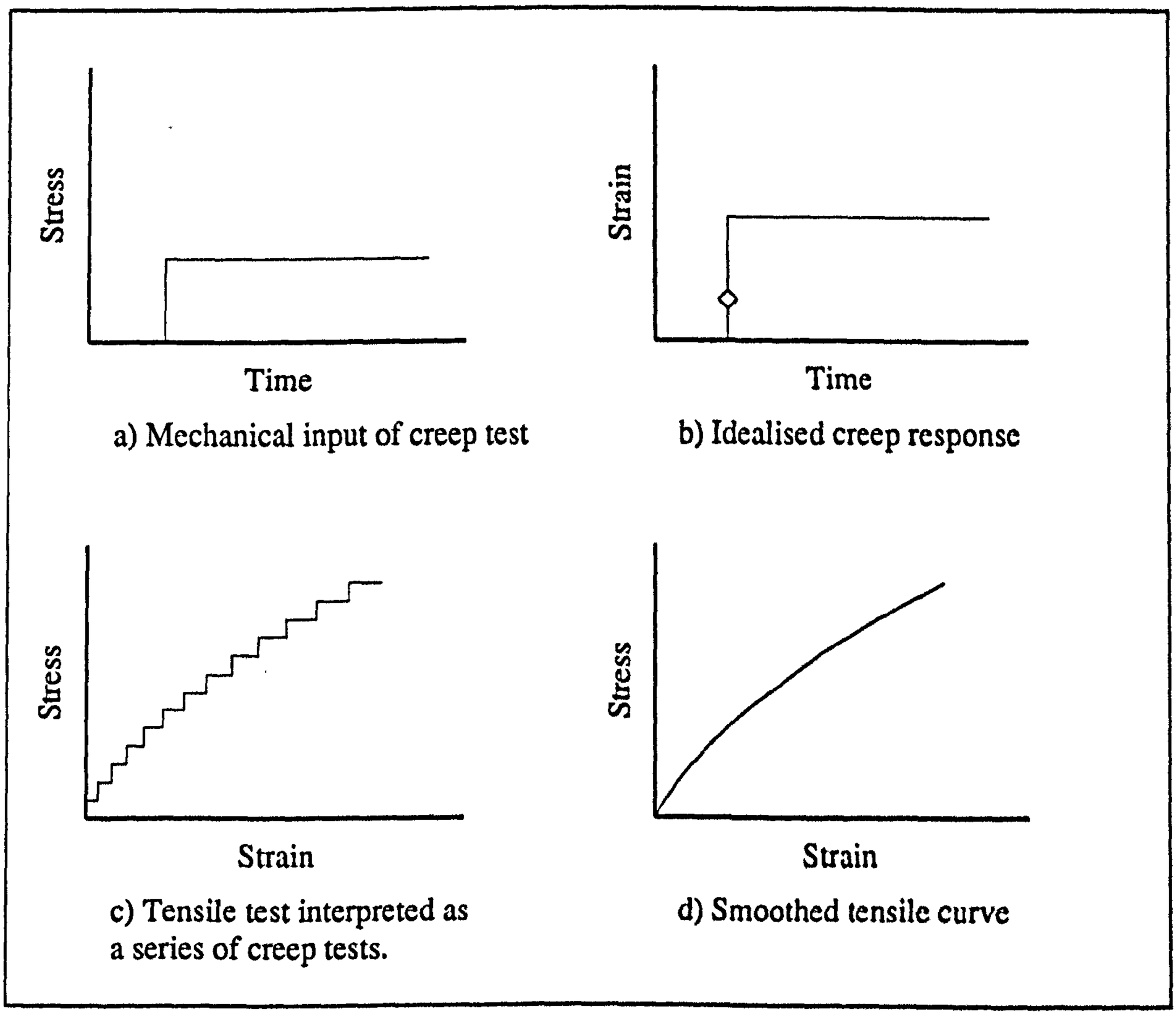

Figure 9.001

<u>The modelling of the tensile response of antler based on the idea of instantaneous damage accumulation</u>

The idea that the pre-knee behaviour is due to a balance of different processes is represented in figure 9.002. The triangular plot shows the relative proportions of the three processes suggested in the main conclusion: damage, anelasticity and fracture. Each side of the triangle represents one process. If only one process affects the behaviour then the points representing this behaviour will fall at the appropriate apex. If the aspect of the

behaviour being examined is considered to be equally due to two processes then the points will fall of the intersection of the 50% line propagating from the appropriate axes, similarly for other proportions and three variables. I have used a qualitative estimate to determine where the points representing the mechanical behaviour should fall on the plot. The cloud of points is used in the place of an individual value to represent the material variability and the approximate nature of the results. Clearly fracture plays no part in the pre-knee behaviour, this form of plot is used here to summarise the suggestions, and so that comparisons can then be made with other stages of the stress-strain response.

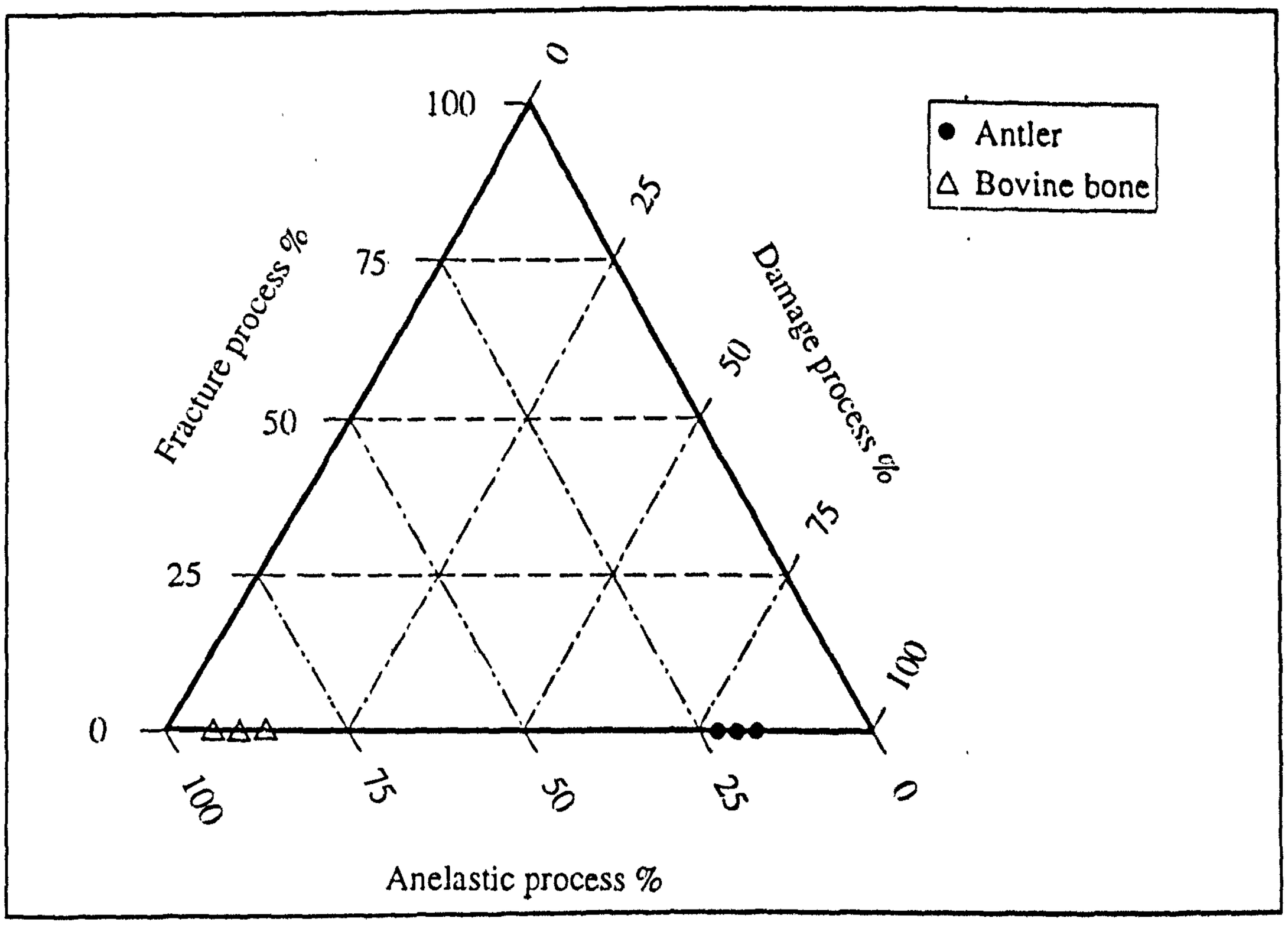

Figure 9.002

The qualitative balance of damage, anelasticity and fracture in the pre-knee region

9.2.2. THE MECHANICS OF THE KNEE REGION

I have proposed in chapters 5 and 8, as have others (most notably Carter, Caler and co-workers see section 3.3) that the knee region of the loading curve is due to the accumulation of damage in the from of microcracking. In the light of the conclusions I have drawn about the pre-knee region it may be more accurate to say that it is due to the rapid increase in the rate of damage accumulation. It has been shown that not only does this event occur after the onset of non-linear non-elastic stress-strain behaviour, but that it is associated with the occurrence of optical changes that are considered to be a direct result of the formation of microcracks within the material. In section 3.3.3.2 I proposed a

model for the existence (and rate dependence) of the knee in bovine bone. In that model I drew analogies between the behaviour in creep and tensile tests. No consideration was given to the mechanism (or combination of processes) which produced these behaviours. The model suggested that the knee was formed when the creep rate of the specimen (due to the load placed upon it) approached the extension rate of the test machine. This model was able to explain the rate dependence of the knee-stress of bone. However, there was one fundamental assumption in the model, that I have since shown to be more justifiable for bovine bone than for antler; that was the assumption of a constant creep rate. The creep rate for antler is initially high and then falls rapidly to only a small proportion of the initial rate. When this behaviour is substituted into the model the effect is similar to that suggested above and shown in figure 9.001. I suggest this is the reason for the extended curvature, and poor distinction between the pre-knee, knee and post-knee behaviour of antler.[2] This explanation, based on the different damage accumulation rates, is also consistent with the lower strength of the cross-head speed as a predictor of knee stress in antler, its lower significance and the weaker relationship (smaller coefficient).

The knee strain values of antler were very highly significantly dependent on rate, while those of bovine bone were only just significant. This latter observation appears easier to explain. At higher testing rates the material becomes stiffer. Thus the strains associated with the higher stresses at which the damage increases sufficiently to produce the knee are more consistent. It could be that it is the more curved stress-strain response of antler that results in its knee strain being rate dependent. For such a curved response a small increase in stress will be related to a proportionally larger increase in strain than it would be in the case of bovine bone.

Thus I generally agree with the work of Carter and Caler (1983) and the interpretation of it by Currey in 1989 (see section 3.3.1 and 3.3.3). The knee region is due to damage that is accumulated as a function of stress and time. However, I suggest that the simple damage accumulation function they use is unable to model the response of antler adequately. It is this difference in the rate at which damage is accumulated in bone and antler that defines their stress-strain response in the knee region of the loading curve.

---

[2]This idea could be confirmed or refuted by conducting creep tests on antler specimens at low stresses. This was not done in this study as I was primarily interested in creep-rupture, and such low stresses would result in a long time-to-rupture. However, test to examine the initial creep response need only last for a relatively short time. I suspect that (unlike the work of Fondrk *et al.* (1988) on bone) no creep threshold will be found.

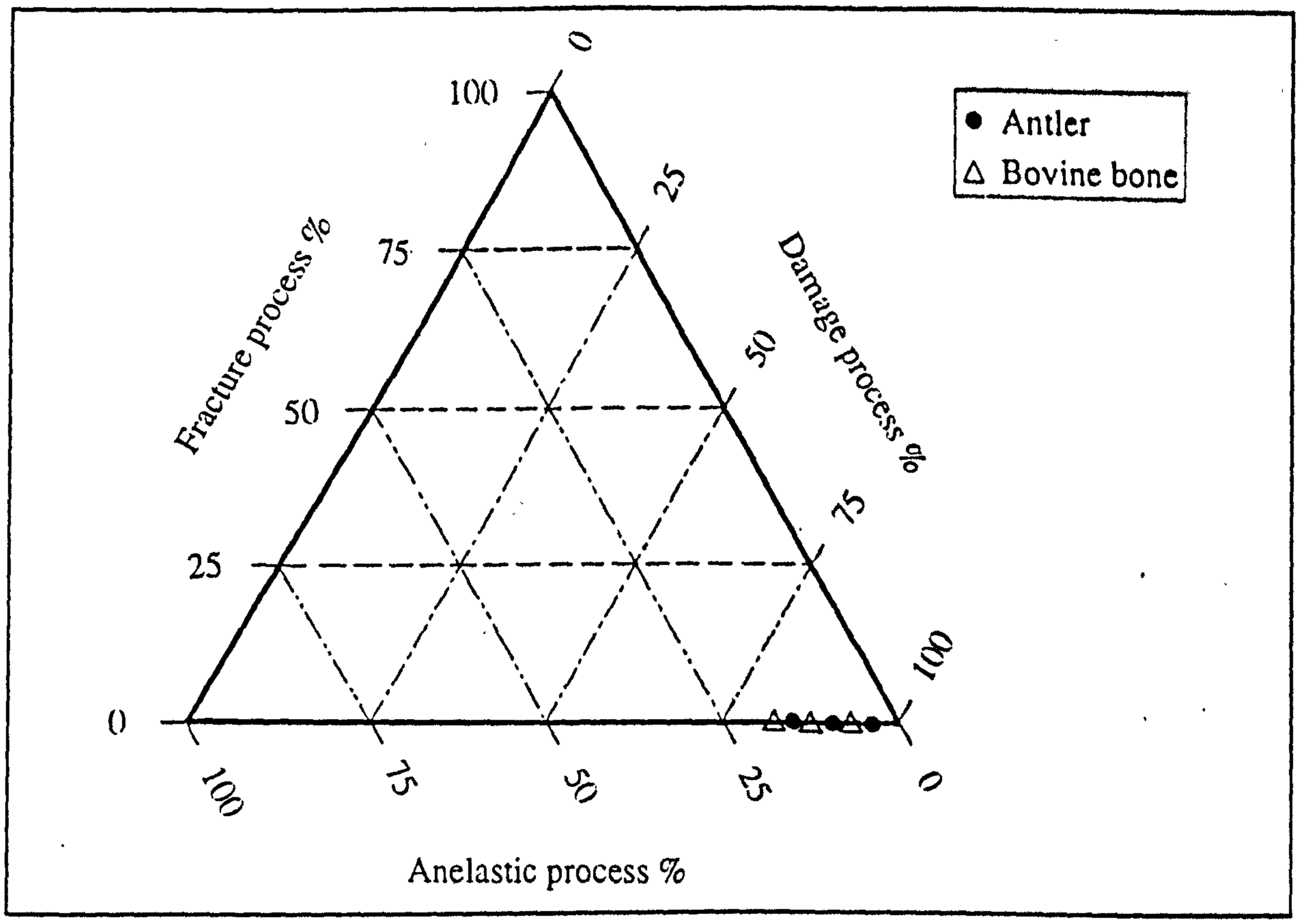

Figure 9.003

The qualitative balance of damage, anelasticity and fracture in the knee region

9.2.3. THE MECHANICS OF THE POST-KNEE REGION

I consider that the post-knee behaviour of bone and antler are simply an extension of the behaviour that occurs in the knee. Bone specimens having achieved a creep rate equivalent to the extension rate of the machine exhibit only a slight increase in load. If the creep rate of the bone specimen falls below the extension rate of the machine the load on the specimen will increase; so it will creep faster. If the creep rate of the specimen exceeds that of the machine, the load on the specimen will fall. As a result of which it will creep at a lower rate. This self regulatory mechanism for producing a horizontal post-knee region is based on the idea of constant extension and creep rates.[3] This has been shown to be a reasonable assumption of bone. However, antler does not display such a constant creep rate (or damage accumulation rate); nor does it display a horizontal post-knee region. The argument in this chapter is that these two facts are related and causal. I consider that the post-knee behaviour of antler is essentially the same as its behaviour in the pre-knee and knee regions of the loading curve. However, due to the constant slope of the post-knee region it would appear that the relationship of extension (size of the idealised step creep response) to load is constant in the post-knee region.

---

[3]This suggests a simple experiment of using a variable cross-head speed in the post-knee region.

(This could explain the lack of a relationship between the applied stress and the strain reported in sections 4.3.7.3 to 4.3.7.7.) The idea that the damage in antler is accumulated in an almost instantaneous manner (damage being essentially a function of stress only) is consistent with the finding that the slope of this region is not significantly dependent of the cross-head speed (when it is used as the only predictor).

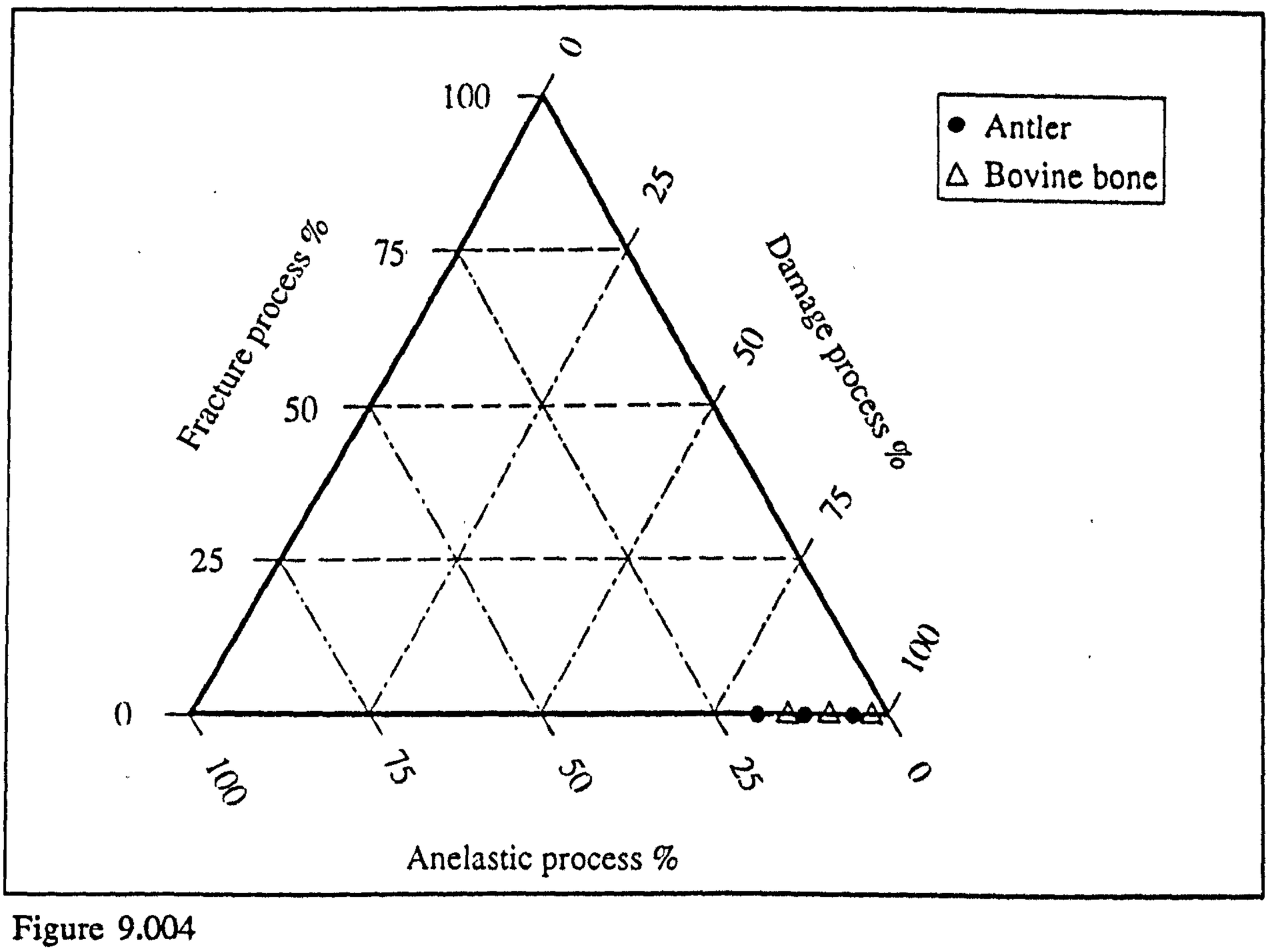

Figure 9.004

The qualitative balance of damage, anelasticity and fracture in the post-knee region

I have attributed the behaviour in the post-knee region to the continued accumulation of damage. In a similar way to how Sedlin (1965) attributed the post-knee region to plastic deformation. In section 3.2.4.1 I pointed out that one of the shortcomings of Sedlin's model was the lack of a failure process. Similarly my models of bone's behaviour[4] initially contained no termination point, although in section 4.2.6.9 I introduced two theoretical failure criteria. The process of final failure is examined in the next section.

[4]One built on the comment of Fondrk *et al.* (1988) (section 3.3.3.2), and the other by extending the equations of Caler and Carter (1989) (section 4.2.6.5)

9.2.4. THE MECHANICS OF FINAL FAILURE

I propose that the final failure of bone and antler is due to the combination of two processes: damage accumulation and fracture. These processes are very much interlinked; both are concerned with the effect of the growth of the fracture surfaces. (By implication they both consume energy.) In one case the total fracture surface is increased by the addition of more microcracks, and in the other it is increased by the propagation of one macrofracture.

A general (and rather obvious) statement can be made to the effect that: bone and antler fail when they can no longer sustain the accumulated damage, or the applied stress. There are many possible mechanisms that may result in the transition from a damaged to a failed material. As an aid to discussion, and a basis of later argument, I will propose two such possibilities. The first I refer to as *damage coalescence* and the second as *damage related fracture*. These are outlined below with the aid of two idealised materials. At this stage I am giving no consideration to the structure or other properties of bone and antler. Thus, these idealised materials are homogeneous and initially elastic.

9.2.4.1. HYPOTHETICAL MATERIAL *A*: FAILURE BY DAMAGE COALESCENCE

One possible explanation for the mechanism of the transition from a damaged to a failed material is based on the assumption of a high, presumably uniform, microcrack density in the failure region. In the theoretical description of damage accumulation (section 2.3.3.8) I suggested that the material fails before the continuity falls to zero. Lorrain and Loland (1983) in a general description of the damage approach suggested that a maximum sustainable damage level, for an elementary volume, occurs when 'the effective stress equals the local cohesive strength of the material'. This viewpoint can be extended to the whole specimen; failure occurring as a result of the production of many small cracks within the material. Final failure occurs when either the material between these cracks becomes more highly stressed and fails, or the cracks coalesce. Such coalescence could result from: a rapid increase in crack production (and thus crack density), crack extension or a combination of both of these. This is shown in a pictorial way in figure 9.005.

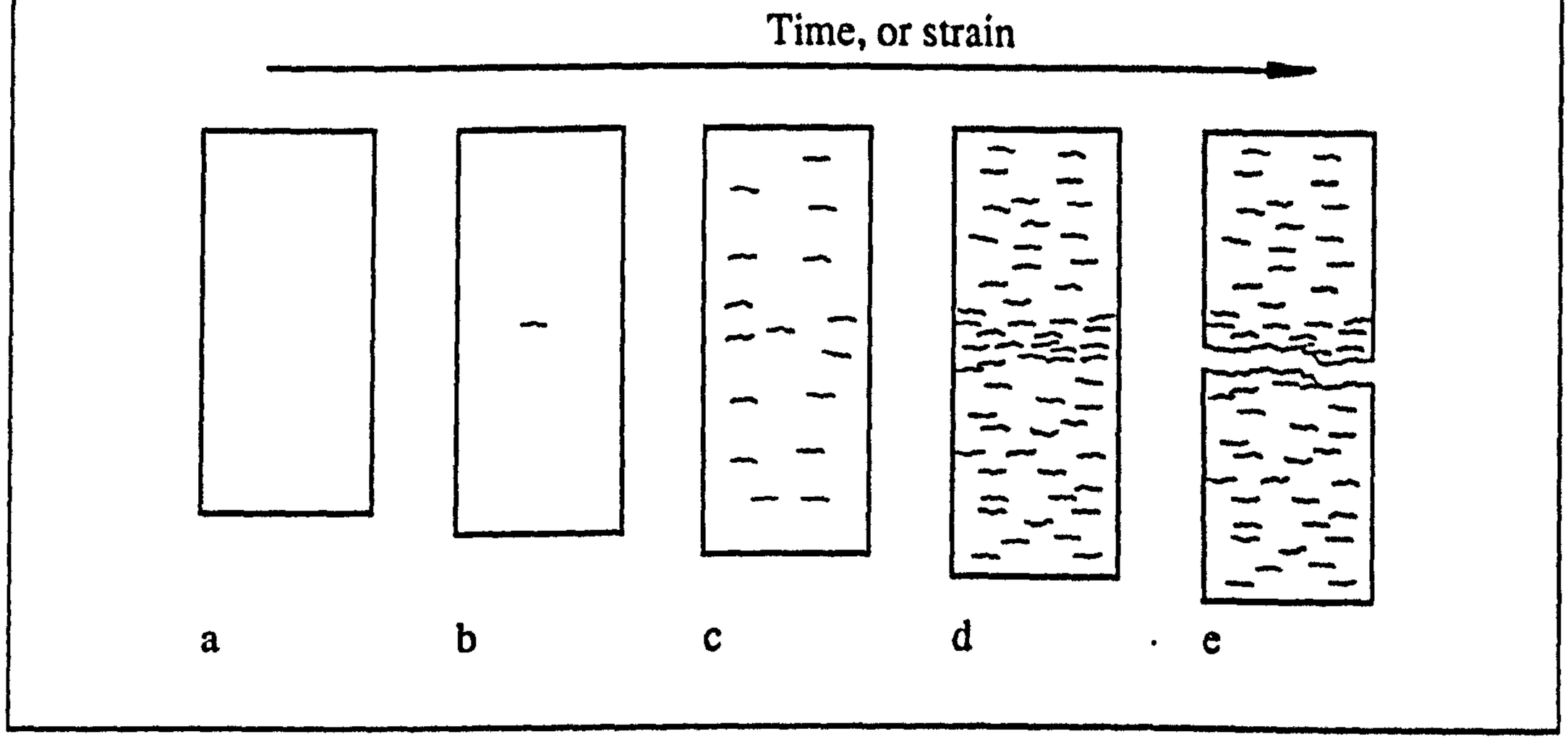

Figure 9.005

Failure of a hypothetical material by damage coalescence

9.2.4.2. HYPOTHETICAL MATERIAL *B*: FAILURE BY DAMAGE RELATED FRACTURE

The second possibility for a mechanism for the transition from a damaged material to a failed one is based on the ideas of notch sensitivity. (These ideas were described in chapter 5.) Failure, of this hypothetical material, occurs when the damage in one region of the specimen has an effect equivalent to the 'critical crack' (as defined in fracture mechanics). As in the case of a 'critical crack', this would result in catastrophic crack propagation across the remaining cross-section. The production of such an equivalent critical crack could be a result of a number of processes. I consider some of the main processes to be: a localised zone of damage, the coalescence of cracks or the growth of a single crack (perhaps within the damage zone). In the last two possibilities the effective critical crack may be viewed as essentially that defined in LEFM. However, the first possibility is different, having more in common with the stimulation of crack growth by a volume of crazed material in a polymer (as described at the end of section 8.9.1). The production of such a zone in a loaded specimen will change the energy stored within that specimen, in a similar but less dramatic way to the introduction of a crack (as noted above crazes are less dangerous than cracks). The equivalent of the notch tip radius can be assumed to be some function of the damage distribution. (Clearly the realism of an analogy between a volume of microcracked material and a craze, is dependent on the scales used. I am assuming a small volume of cracked material, rather like the striations reported in section 8.6.1, is equivalent to the craze; rather than the individual microcracks.) This hypothetical failure process, failure by damage related fracture, is shown pictorially in figure 9.006. I have not included what could be referred to as the

background damage, or damage in the bulk of the material. This background damage will reduce the stiffness of the specimen, and thus the energy available to propagate the fracture. (This important toughening mechanism was discussed in section 7 and 8.) The amount of background damage will determine the amount of strain in the post-knee region, and the energy available to propagate the fracture.

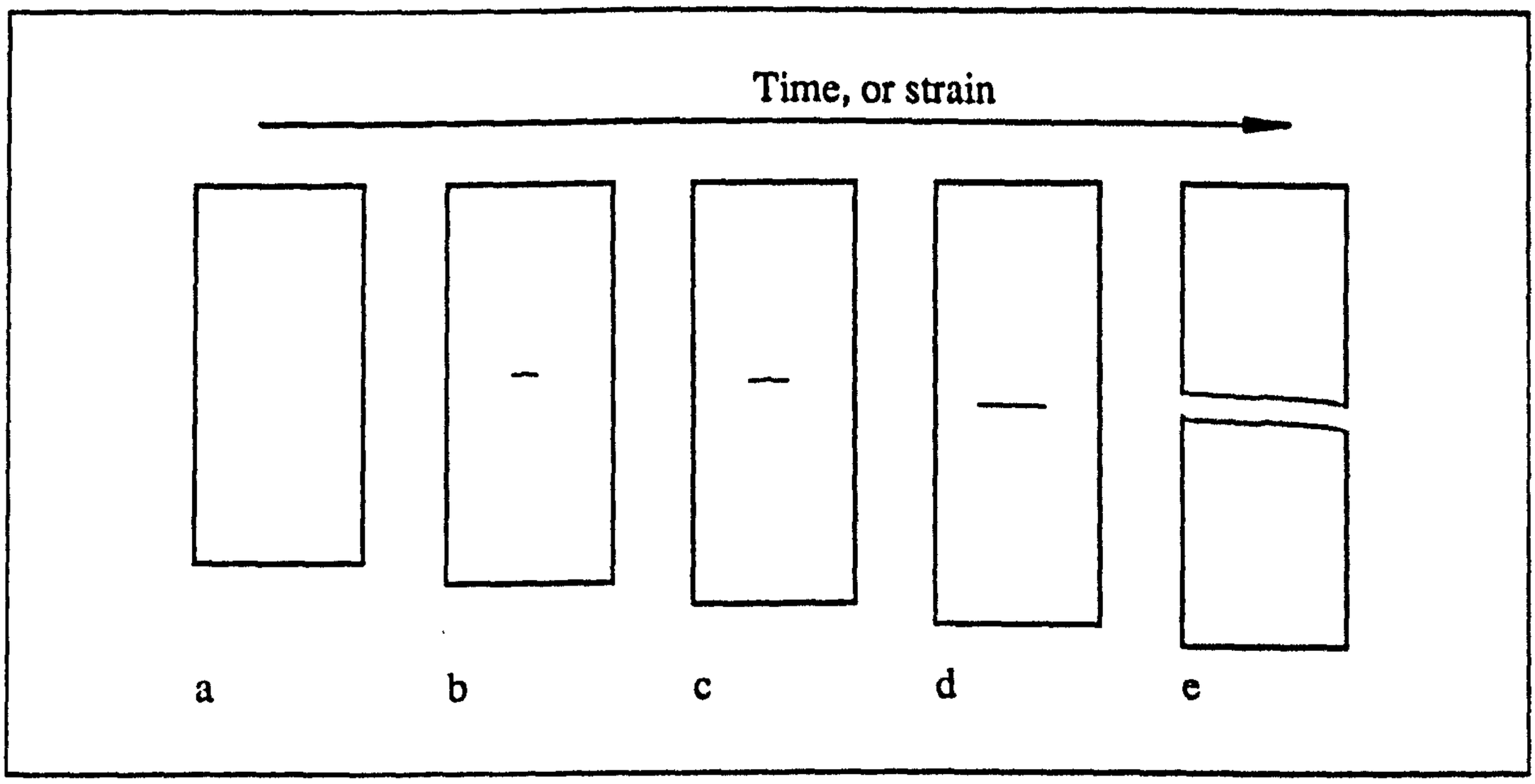

Figure 9.006

Failure of a hypothetical material by damage related fracture

9.2.4.3. BONE AND ANTLER: FAILURE BY A COMBINED PROCESS

I consider that the true failure mechanism of bovine bone and antler fall between the two mechanisms postulated above for the hypothetical materials *A* and *B*. The true mechanism is a combination of these two processes. The relative importance of these two processes within the failure mechanism depended on a number of factors. The most important of these are: The material, bone or antler, and the rate at which it is tested (or in the case of a creep test the applied load).

The failure of antler, under a quasi-static tensile loading, occurs by a mechanism that has a greater similarity to the damage coalescence process than to damage related fracture. However, it appears that the final failure process of bovine bone has more in common with the damage related fracture process. I base this consideration on several pieces of evidence.

a) During tensile testing the damage is more widespread in antler than in bovine bone. (This is indicated by the optical changes.) The damage in bone is usually localised in striations. (See chapter 8)

b) The bovine specimens that failed at low strains (thus exhibiting only a limited post-knee region), normally displayed only a small amount of localised whitening. The fracture when it occurred generally passed through this region. Due to the catastrophic crack propagation I can not say that the fracture was initiated within this region, but that would be the reasonable conclusion.

c) Bone behaves in a more brittle manner than antler; the tensile failure is catastrophic, the failure strain is more variable (from essentially the knee strain to about 0.005), the fracture route is less contorted and the fracture surfaces appear smoother (see chapter 8).

d) Tensile specimens of antler regularly attain a high level of damage before failure and consume more work (see sections 4.2.6.11 and 4.2.6.12).

e) Notch sensitivity tests showed that the failure of SEN specimens of bovine bone conforms with Griffith's equation (5.021) (see chapter 7).

f) Notch sensitivity tests of antler combined with the resilience tests showed that despite the introduction of a notch of considerable size, the bulk of the material still underwent a damaging (and hence toughening) process. Fracture propagation was controlled by, and associated with, the further accumulation of damage. This suggests that fracture growth in antler may be by damage coalescence.

Previously I suggested that the rate at which a specimen is loaded may determine the type of process that results in the ultimate failure of bone and antler. An argument based on the time dependence of the damage accumulation was proposed by Carter and Caler (1983) (see section 3.3). The basis for this argument is that damage takes time to accumulate. As a generalisation, the more rapidly a material is loaded the briefer the time available for damage formation at each stress level. Therefore, by the critical crack length argument, the failure process is more biased towards the fracture type approach at these higher rates. This would suggest the calculated value of the *intrinsic edge notch* should decrease with loading rate. This idea can be examined by combining regression equations obtained from tensile and notch sensitivity tests conduced at the four different cross-head speeds used in this study, as follows

$$\sigma_f = 48.7 + 1.61\, a^{-0.5} + 3.84 \ln(\dot{x}) \qquad \text{(b, table 7.040)} \qquad (9.001)$$

$$\sigma_{ult} = 182 + 6.49 \ln(\dot{x}) \qquad \text{e, table A9.005)} \qquad (9.002)$$

The value of the intrinsic edge notch is obtained by substituting the experimentally obtained value of the ultimate stress (tensile test) into the equation relating failure stress to notch length. In this case both are functions of cross-head speed. Thus

$$a^{-0.5} = \frac{133.3 + 2.65 \ln(\dot{x})}{1.61} \qquad (9.003)$$

which simplifies to

$$a = \frac{1}{(82.8 + 1.65 \ln(\dot{x}))^2} \qquad (9.004)$$

Equation 9.004 suggests that the intrinsic edge notch is smaller at higher cross-head speeds. At the slowest cross-head speed used in this work, 8.33×10^{-7} m s^{-1}, the suggested value is 0.28 mm, at the highest speed from which the data was obtained, 8.33×10^{-4} m s^{-1}, the value suggested is 0.20 mm. It should be remembered that this measure is not the size of an actual crack but the dimension of an edge crack that has the same effect (from a fracture mechanics viewpoint) as the damage accumulated in a tensile specimen. In some of my previous description of the quantity I referred to it as some measure of the global effect of damage. However, as the strain reached at failure is not included in its calculation it may be better to view it as a measure of the fatal region of localised damage. (The accumulation of strain in the post-knee region clearly increases the overall amount of damage.) The strain at failure is examined in the next section.

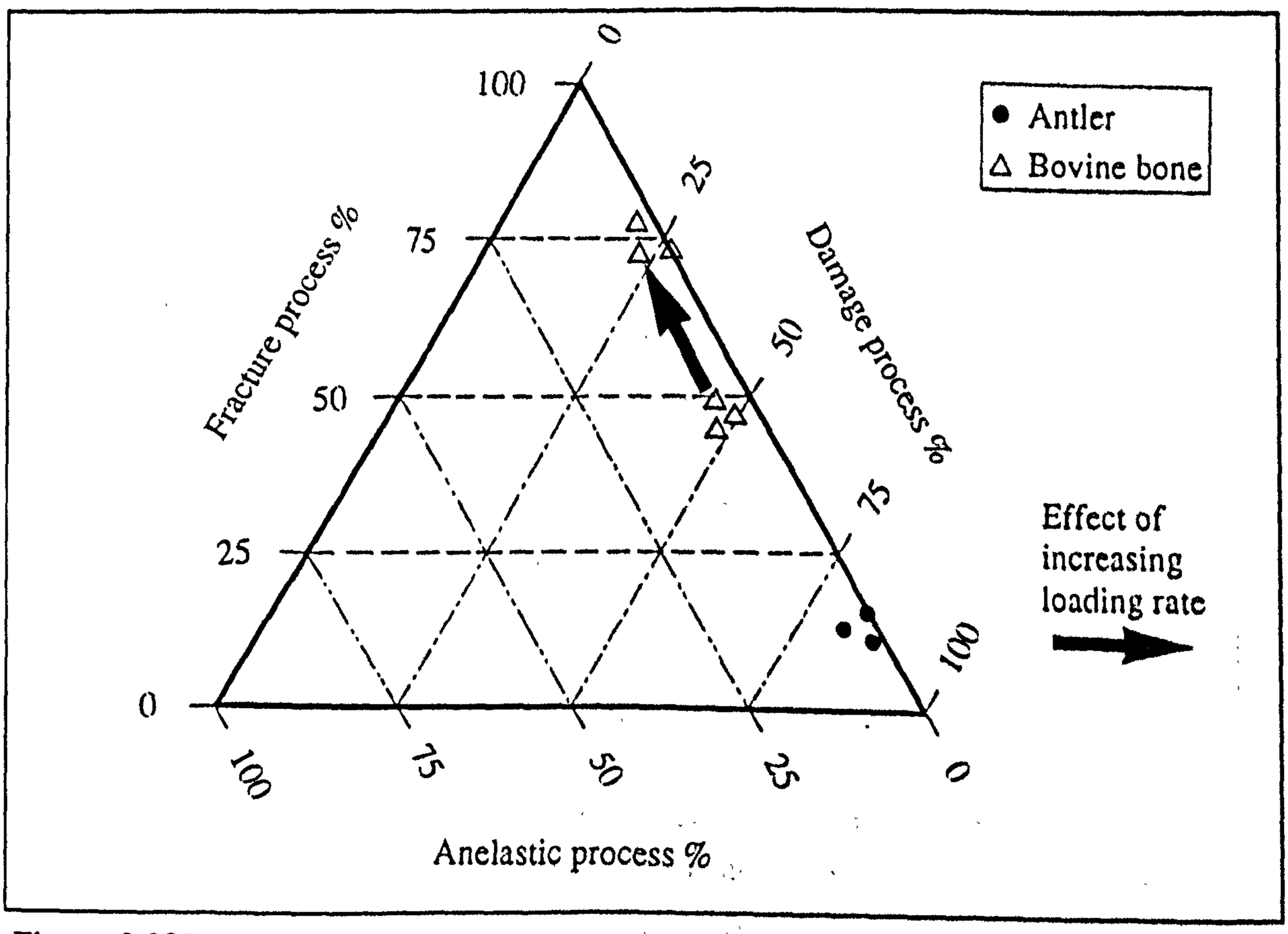

Figure 9.007

The qualitative balance of damage, anelasticity and fracture in the final failure process

In this section I have used the generalisation that, the more rapidly the material is loaded the briefer the time available for damage formation at each stress level. Clearly the exact form of the time and stress dependence of damage accumulation, determines the degree to which the testing rate will influence the mechanism of final failure. I consider that it is this difference that is responsible from the difference in the mechanical behaviour of the materials examined here

9.2.4.4. THE DETERMINATION OF THE POSITION OF THE FINAL FAILURE ON A SCALE OF TIME, STRESS OR STRAIN

It was reported in section 4.2.7 that the point of final failure of antler tested at different cross-head speeds was consistent with the idea of a maximum damage criterion. This is consistent with the ideas presented here that the failure of antler is by damage coalescence and is an almost rate-independent behaviour. In section 4.2.7 the large variability in the ultimate strain of bone tested at different cross-head speeds was highlighted. This variability prevented the acceptance of the maximum damage criterion over the maximum effective stress criterion, or vice versa. I consider that this is consistent with the idea that failure is due to the localisation effect of damage related fracture. The ultimate strain is determined by the amount of background damage that is accumulated. This is shown experimentally by the more widespread whitening in those bovine bone specimens that attain a high value of ultimate strain. (As in the case of antler damage occurring in the bulk of the material will reduce the energy available for fracture propagation. Thus it is tempting to suggest that specimens that reach a high value of strain fail by a combined damage coalescence and damage related fracture process. For those specimens that fail at low strains the failure is due, almost exclusively, to a damage related fracture process.)

It may be possible to construct an argument for the relationship of ultimate strain to testing rate, based on the rate dependence of the accumulation of background damage. However, I consider that there are too many possibilities to make this a justifiable exercise on the limited data presented here.

9.2.5. STRUCTURAL CONSIDERATIONS

In the preceding section, the proposed failure mechanisms took no account of the structure of bone and antler. The structure of a material has an important, if not decisive, role in determining the mechanical behaviour and final failure. In the section on linear elastic fracture mechanics (section 5.2) the importance of the energy required to extend a

crack as controlling feature of the whole fracture process was reported. The energy needed to fracture a specimen is one of the variables that can be altered in industrial composite materials, by altering the overall structure or the size of the structural components. Beaumont (1990) gives two general categories of toughening mechanism in such industrial materials

> The first category includes processes that occur along the crack plane in the crack wake, such as crack bridging: fibre pull-out in a cracked matrix is a good example; so is rubber particle stretching in a rubber-toughened epoxy. These mechanisms exert a direct influence on the crack tip stress intensity, K_I, and on the local crack propagation resistance of the material. The second category mechanism influences toughness by means of events occurring in a process zone, such as phase transformation in, for example, ZrO_2/Al_2O_3 composites, crazing in rubber-toughened polystyrene, and fibre-matrix debonding in glass-epoxy composites.

I consider that these mechanisms, identified in industrial materials, are similar to those demonstrated by the biological tissues examined here. I consider that there is an additional one in the case of SEN specimens of antler; the loss of elasticity in the bulk of the material, by background damage. I consider that such a mechanism also plays an important role in tensile specimens of both bone and antler. For in tensile specimens the fracture, or ripping process, generally occurs after the knee region. Therefore the materials are definitely damaged and have consumed energy (see sections 7.4.3.1 and 7.7.1.1 on resilience testing).

The existence of a phenomenon similar to the fibre pull out has been noted in the literature on the fracture of bone, for example by Piekarski (1970). Watkins (1987) in his examination of antler states that:

> the major toughening systems in antler are fibre pull-out and delamination of lamellae, in simple terms, it contains many weak interfaces which effectively toughen the material.

I consider that it is the failure of such weak interfaces, a damaging process, that toughens both materials. The existence of pull-out type structures on the fracture surface is only one facet of this energy consuming process. I consider that, as with the failure of an elastic-plastic or composite material, much of the energy is consumed by processes occurring away from the fracture sight. This is demonstrated by the optical changes in the tensile specimens of both materials.

A toughening mechanism used in industrial composites is the debonding of fibres. (This mechanism has been transposed to models of bone where the osteones or Haversian systems are seen as the fibres and are pull out of the bulk of the material, for example Krajcinovic *et al.* (1987), see section 3.3.3.3.) The debonding of the fibres ahead of the fracture is a result of the stress in that region. The process is referred to as the Cook-

Gordon mechanism. Examination of Inglis solution for the stress around an elliptical hole shows that the tensile stress in the line of the crack is greatest at a short distance ahead of the crack (see figure 5.001). Thus if this stress falls across a weak boundary (or material), such as the fibre-matrix interface, local failure can result. This local failure can result in a blunting of the crack or a 'T-shaped crack-stopper' as Gordon (1976) calls it. This process is shown in figure 9.008.

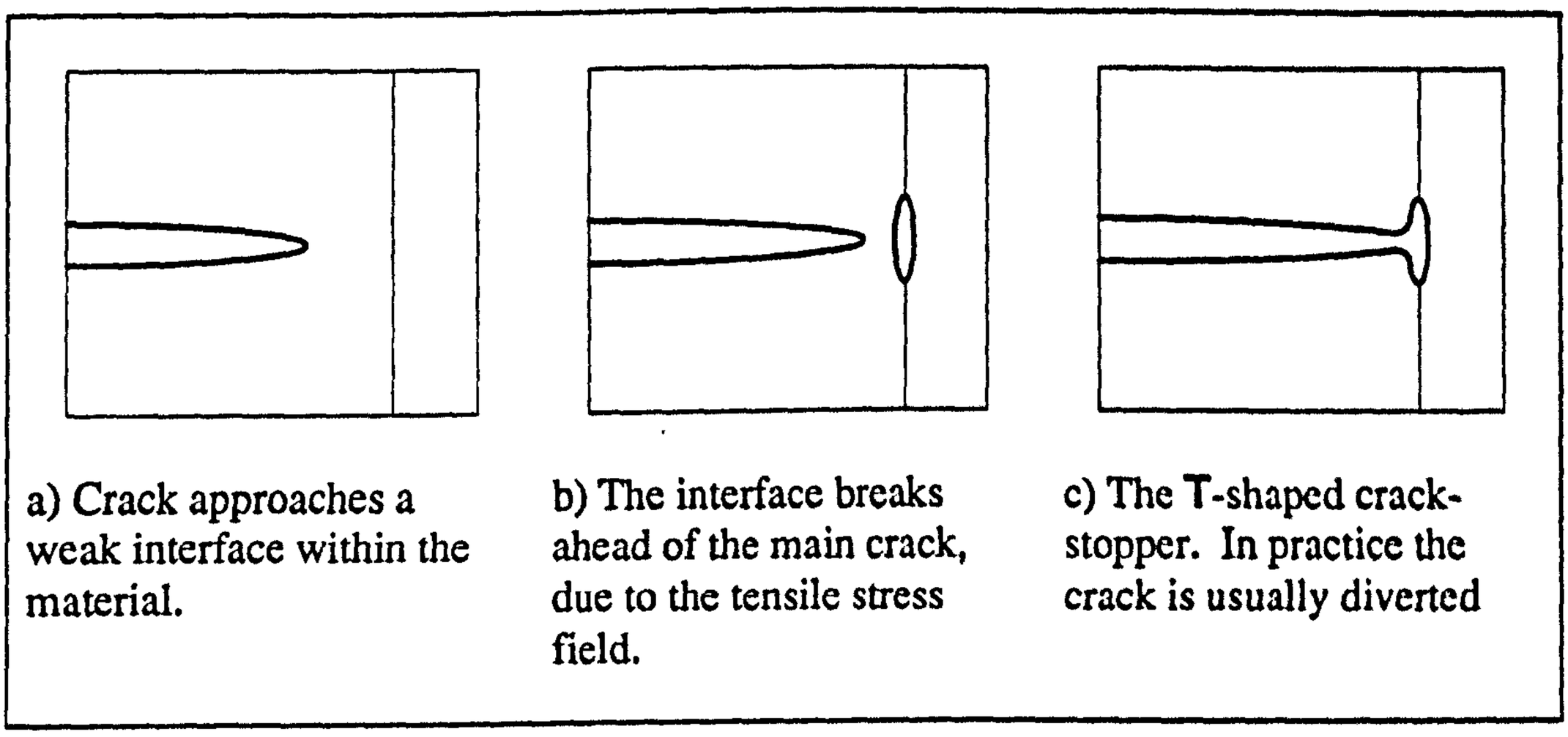

a) Crack approaches a weak interface within the material.

b) The interface breaks ahead of the main crack, due to the tensile stress field.

c) The T-shaped crack-stopper. In practice the crack is usually diverted

Figure 9.008 After Gordon (1976)

Cook-Gordon crack stopping mechanism

The assumption that the Cook-Gordon crack stopping mechanism is used by antler is supported by the way that the fracture propagates more easily along the grain of the material.

In chapter 4 I proposed a time-dependent damage model for bone, perhaps a better analogy would be a mesh of elements. The elements of the bovine model redistributing the load locally when an element fails. However, in antler the load is redistributed more widely thus there is a greater resistance to fracture.

I suggest that it is the more irregular structure of antler, compared to that of bone, combined with the Cook-Gordon mechanism that permit it to sustain large amounts of damage without failing. Antler is able to encapsulate microcracks without apparently experiencing the same detrimental effect that this density of flaws would have in a homogenous elastic material, or for that matter bone. An analogy for the structure of antler (that was suggested to my by Dr Peter Zioupos) is that it is like a mass of noodles; holes do not have the effect you would expect in a continuous material. Straining in one region results in diffuse damage occurring locally and in more remote regions. This analogy can be extended to bone, which appears to behave more like cold noodles; there

is more stress transfer between different elements and the reaction to a hole is more like that expected for a homogeneous material. This analogy is similar to two findings I referred to in chapter 1. The first finding, that reported by Turner (1981), was that the mineral in bone was contiguous in form (section 1.2.5), and the second is due to Watkins (1987) who postulated that in antler the mineral is contained within fibres that he considered were not bonded together (section 1.3.5). Further investigation of the interaction of structure and damage accumulation is being conducted within this laboratory. Therefore, I will end my discussion of this aspect of bone and antler here.

9.3. IMPLICATIONS AND QUALIFICATIONS OF THE CONCEPT OF FAILURE BY DAMAGE ACCUMULATION

The acceptance of the evidence that the failure of bone and antler is due to the progressive accumulation of damage, and that how it progresses depends on the material examined, invites a reconsideration and examination of other aspects of the mechanical response of these materials. Some of the important aspects and their implications are examined below.

9.3.1. LOADING-UNLOADING CURVES OF BOVINE FEMORAL BONE

In figure 1.011 I showed the loading-unloading trace of a specimen of bovine bone emphasising the reduction in stiffness after the knee region. This is clearly consistent with the ideas of damage accumulation. In chapter 8 I suggested that the hysteresis loop and some of the time-dependent mechanical response could be due to the pumping action of the damage cracks.

9.3.2. THE DIFFERENT IMPACT ENERGIES OF BONE AND ANTLER

During impact testing energy is transferred from the impact hammer to the specimen. How this energy is stored, or consumed, by the test material is a determining factor of how much energy is available to separate the fracture surfaces. In metals research this test is used to examine, or demonstrate, the brittle-ductile transition that occurs in steels as the temperature of the test piece is increased. For example, at lower temperatures (below 0°C) a larger proportion of the fracture surface of a steel specimen is a result of brittle fracture rather than ductile fracture. As explained in chapter 5, fracture of a material by a brittle process has a lower energy consumption, than that associated with plastic deformation.

I consider that the brittle-ductile transition of steel is an analogous situation to the impact testing of bone and antler described in chapter 1. The ability of antler to sustain a greater impact loading than bone without failing is due to its ability to consume more of the impact energy, like a ductile metal. However, in the case of antler the energy is consumed by the accumulation of damage not by plastic flow. The consumption of the energy in this way reduces that stored in the material. As a result of this there is less energy available to initiate and propagate cracks. It appears that the bovine bone impact specimens behave more like those of a brittle material, storing the energy that is then available to drive cracks through the material. (The suggestion of only a limited amount of damage being accumulated by impact specimens of bone is supported by the lack of post test staining reported in similar specimen by Currey and Brear (1974) reported in section 8.9.2.4.)

Again, it is antler's ability to accumulate damage far more rapidly than bone can, that is the underlying cause of its greater impact strength.

9.3.3. NOTCH SENSITIVITY AND FRACTURE MECHANICS OF BONE AND ANTLER: COMMENTS ON PUBLISHED STUDIES

The are many implications arising from the acceptance of a damage related failure mechanism for the fracture mechanics of bone and antler. Many of these have already been described in chapter 7. That chapter was mostly concerned with the events leading up to fracture. In this section I shall examine some of the implications of damage accumulation for the process of fracture propagation in bovine bone. I concentrate on bone because I consider that it is the rate dependence of the damage accumulation in this material that may be able to explain some of the results in the literature. Much of this explanation is based on the idea of a fracture with a damage zone at its tip. As the damage in bone is stress and rate-dependent, I suggest that the size of this damage zone is also stress and rate-dependent. I suggest, and use the arguments of rate dependence and my recordings of optical changes in support of the idea, that damage zone at the tip of a self propagating fracture is smaller than that at the tip of a controlled fracture of around a machined notch before fracture initiation.

The apparent lack of a damage zone in impact specimens of bone agrees with the idea that this zone is rate-dependent. I suggest that this approach may be able to solve an apparent paradox in the fracture mechanics results reported in chapter 6. The existence of this paradox appears to be independent of the test method used.

a) Three-point-bending: The concept of a time-dependent damage zone may be able to account for the differences in the work-of-fracture values obtained by Piekarski (1970), see table 6.002. The high values obtain during stable crack propagation could reflect the energy consumed by the damage zone. The small work of fracture at the catastrophic crack propagation rate could reflect the smaller size of the damage zone in that case. This argument is at odds with the result of Robertson *et al.* (1978) referred to in the same section (equation 6.003). They found that the calculated value of the stress intensity factor increased with rate. This agrees with Piekarski's results for stable fracture.

b) Single edge notch specimens (SEN): The fracture resistance versus rate paradox also occurred in the tests (using SEN specimens) of Melvin and Evans (1973) (reviewed in section 6.4).

c) Compact tension specimens (CT): The increasing resistance to stable fracture in the longitudinal direction with testing rate was reported by Bonfield *et al.* (1978) and Behiri and Bonfield (1980). Behiri (1982) gives a similar statement in his conclusions. In addition he says that catastrophic fractures produced lower values of the critical stress intensity factor.

d) Values of the critical stress intensity factor about one tenth of these obtained from CT specimens with stable fracture rates were obtain from CNC specimens by Bonfield and Datta (1974).

I would like to suggest a simple explanation for the paradox. At low fracture velocities the fracture propagates by the damage coalescence process. The more time that is available the more damage that is accumulated. The higher the microcrack density (or volume), the less energy needed to propagate the fracture. Increasing the cross-head speed reduces the amount of damage. Thus more energy is supplied to propagate the fracture. When the fracture is travelling at some critical rate, the formation of damage ahead of it becomes negligible. The stress-shielding effect is lost and the fracture behaves more like that associated with a classical brittle material.

Some evidence in support of this idea is given by the video images. Clearly some simple post-test straining experiments on CT specimen would conform this suggestion. Another way such a change from a damage dominated fracture process to the classical fracture mechanics may be expressed is in the form of the fracture surface. It is reasonable to expect fracture surfaces produced by crack coalescence to be rougher than

those due to fast fracture. A very clear difference between the surfaces of stable and self propagating fractures was given (in his conclusions) by Behiri (1982)

> With controlled crack propagation, a relatively rough fracture surface was produced by the passage of the crack around intersecting osteons (or lamellae) together with some osteon pull-out.
>
> With catastrophic crack propagation, the crack moved indiscriminately through the microstructural constituents of bone and the fracture surfaces were relatively smooth.

9.3.3.2. IMPLICATIONS OF THE RATE DEPENDENT DAMAGE ZONE AT THE FRACTURE TIP IN BONE

There are a number of implications of the existence of a rate dependent damage zone at the fracture tip. Some of these have already been discussed, such as the toughening effect and the undermining of the critical stress intensity factor as a material property. Both of these effects have parallels in the fracture mechanics of composite materials (Williams, 1990). There are however other possible side effects that have been misinterpreted by viewing bone as an elastic-plastic material. One of these is the interpretation of a flat fracture surface as indicating conditions of plain strain, as required by LEFM and especially the critical stress intensity factor. It is reasonable to assume that the preferred direction of the damage cracks will be that in which the plane of the crack is perpendicular to the principal tensile stress. This implies that they would occupy planes parallel with the machined notch. Thus if the fracture propagates by crack coalescence it is unlikely to show the slanting fracture or lip effect associated with plain stress conditions (see figure 5.004). Thus I suggest that the accumulation of damage may account for 'very square' fracture surfaces that Behiri (1982) found, and the lack of an effect of thickness on the critical stress intensity factor found by Wright and Hayes (1977) both reported in section 6.7.

Previously I suggested that another implication of the time dependence of the fracture tip damage zone, mentioned above was that fast fracture propagation was similar to the behaviour described by Griffith while slow fracture propagation was not. Therefore, I question the use of results obtained from tests exhibiting catastrophic fracture propagation to justify the application of LEFM to situations where the fracture is stable. It is interesting that the two sets of experiments that are widely used to justify the application of LEFM to bone (as explained in section 6.7) are ones that generated catastrophic fractures. In that by Bonfield and Datta (1974) CNC specimens were used (see section 6.6), and in a later paper by the same authors (Bonfield and Datta, 1974) SEN specimens were used.

9.4. REITERATION AND CLOSING REMARKS

In the previous section of this chapter I have examined the various sections of the tensile loading response of bone and antler. I consider that this analysis supports my main conclusion: specimens of bovine bone and antler tested in tension, under quasi-static conditions, depart from an idealised linear-elastic response due to a combination of the progressive accumulation of damage (in the form of microcracks) and some anelasticity (viscoelastic like behaviour). The ultimate failure of these materials is due to the accumulated damage and a fracture process. To this main conclusion another should be added: the difference in the departure of bone and antler from an idealised linear-elastic response is due to the difference in the way that they accumulate and distribute the accumulated damage. Bone fails by a damage related fracture process, and antler by a damage coalescence process. As a result of my findings, I suggest that bone (and antler) should be referred to not as an elastic-plastic or viscoelastic material, but as a time-dependent-damage material.